Δελτίο της Ελληνικής Γεωλογικής Εταιρίας
Bulletin of the Geological Society of Greece

Τόμος XLVII, No1

Volume XLVII, No1

13° Διεθνές Συνέδριο της Ελληνικής Γεωλογικής Εταιρίας
Έρευνα και Εκμετάλλευση Ορυκτών Πόρων

13th International Congress of the Geological Society of Greece
September 5-8 2013, Chania, Crete, Greece

13th International Congress of the Geological Society of Greece
Exploration and Exploitation of Mineral Resources

Χανιά/Chania
2013

ΔΕΛΤΙΟ ΤΗΣ ΕΛΛΗΝΙΚΗΣ ΓΕΩΛΟΓΙΚΗΣ ΕΤΑΙΡΙΑΣ

Τόμος XLVII, No 1

BULLETIN OF THE GEOLOGICAL SOCIETY OF GREECE

Volume XLVII, No 1

13ο Διεθνές Συνέδριο της Ελληνικής Γεωλογικής Εταιρίας

Έρευνα και Εκμετάλλευση Ορυκτών Πόρων

13th International Congress of the Geological Society of Greece

Exploration and Exploitation of Mineral Resources

13th International Congress of the Geological Society of Greece
September 5-8 2013, Chania, Crete, Greece

ΕΠΙΜΕΛΕΙΑ ΕΚΔΟΣΗΣ

ΜΑΝΟΥΤΣΟΓΛΟΥ ΕΜΜΑΝΟΥΗΛ

ΠΥΛΙΩΤΗΣ ΙΩΑΝΝΗΣ

Πολυτεχνείο Κρήτης

EDITORS

MANOUTSOGLOU EMMANOUIL

PYLIOTIS IOANNIS

Technical University of Crete

Χανιά/Chania 2013

ΕΛΛΗΝΙΚΗ ΓΕΩΛΟΓΙΚΗ ΕΤΑΙΡΙΑ
ΔΙΟΙΚΗΤΙΚΟ ΣΥΜΒΟΥΛΙΟ

Πρόεδρος:	Λέκκας Ευθύμης
Αντιπρόεδρος:	Ζαμπετάκη-Λέκκα Αλεξάνδρα
Γενικός Γραμματέας:	Γαλανάκης Δημήτρης
Ειδικός Γραμματέας :	Αντωναράκου Ασημίνα
Ταμίας:	Μωραΐτη Ευγενία
Έφορος:	Κράνης Χαράλαμπος
Μέλη:	Γκανάς Αθανάσιος
	Λουπασάκης Κώστας
	Ντρίνια Χαρά

GEOLOGICAL SOCIETY OF GREECE
BOARD OF DIRECTORS

President:	Lekkas Efthymios
Vice President:	Zampetaki-Lekka Alexandra
General Secretary:	Galanakis Dimitrios
Excecutive Secretary:	Antonarakou Asimina
Treasurer:	Moraiti Eugenia
Trustee:	Kranis Haralambos
Members:	Ganas Athanassios
	Loupasakis Constantinos
	Drinia Hara

ΤΑ ΣΥΝΕΔΡΙΑ ΤΗΣ Ε.Γ.Ε.

1ο ΔΙΗΜΕΡΟ, ΑΘΗΝΑ, 1983, Δελτίο XVII
2ο ΔΙΗΜΕΡΟ, ΑΘΗΝΑ, 1984, Δελτίο XIX
3ο ΣΥΝΕΔΡΙΟ, ΑΘΗΝΑ, 1986, Δελτίο XX
4ο ΣΥΝΕΔΡΙΟ, ΑΘΗΝΑ, 1988, Δελτίο XXIII
5ο ΣΥΝΕΔΡΙΟ, ΘΕΣΣΑΛΟΝΙΚΗ, 1990, Δελτίο XXV
6ο ΣΥΝΕΔΡΙΟ, ΑΘΗΝΑ, 1992, Δελτίο XXVIII
7ο ΣΥΝΕΔΡΙΟ, ΘΕΣΣΑΛΟΝΙΚΗ, 1994, Δελτίο XXX
8ο ΣΥΝΕΔΡΙΟ, ΠΑΤΡΑ, 1998, Δελτίο XXXII
9ο ΣΥΝΕΔΡΙΟ, ΑΘΗΝΑ, 2001, Δελτίο XXXIV
10ο ΣΥΝΕΔΡΙΟ, ΘΕΣΣΑΛΟΝΙΚΗ, 2004, Δελτίο XXXVI
11ο ΣΥΝΕΔΡΙΟ, ΑΘΗΝΑ, 2007, Δελτίο XXXX
12ο ΣΥΝΕΔΡΙΟ, ΠΑΤΡΑ, 2010, Δελτίο XLIII

THE CONGRESSES OF G.S.G.

1st MEETING, ATHENS, 1983, Bull. XVII
2nd MEETING, ATHENS, 1984, Bull. XIX
3rd CONGRESS, ATHENS, 1986, Bull. XX
4th CONGRESS, ATHENS, 1988, Bull. XXIII
5th CONGRESS, THESSALONIKI, 1990, Bull. XXV
6th CONGRESS, ATHENS, 1992, Bull. XXVIII
7th CONGRESS, THESSALONIKI, 1994, Bull. XXX
8th CONGRESS, PATRAS, 1998, Bull. XXXII
9th CONGRESS, ATHENS, 2001, Bull. XXXIV
10th CONGRESS, THESSALONIKI, 2004, Bull. XXXVI
11th CONGRESS, ATHENS, 2007, Bull. XXXX
12th CONGRESS, PATRAS, 2010, Bull. XLIII

ΟΡΓΑΝΩΤΙΚΗ ΕΠΙΤΡΟΠΗ

Πρόεδρος: Μανούτσογλου Εμμανουήλ (Καθ.), Πολυτεχνείο Κρήτης

Αντιπρόεδρος: Μαρκόπουλος Θεόδωρος (Καθ.), Πολυτεχνείο Κρήτης

Γραμματέας: Βαφείδης Αντώνιος (Καθ.), Πολυτεχνείο Κρήτης

Ταμίας: Στειακάκης Εμμανουήλ (Επικ. Καθ.), Πολυτεχνείο Κρήτης

Μέλη: Αγιουτάντης Ζαχαρίας (Καθ.), Πολυτεχνείο Κρήτης

Αλεξόπουλος Απόστολος (Αν. Καθ.), Ελληνική Γεωλογική Εταιρία

Αντωναράκου Ασημίνα (Επικ. Καθ.), Ελληνική Γεωλογική Εταιρία

Βοζινάκης Κωνσταντίνος, Περιφέρεια Κρήτης, Περιφερειακή Ενότητα Χανίων

Ζαμπετάκη-Λέκκα Αλεξάνδρα (Καθ.), Ελληνική Γεωλογική Εταιρία

Γαλανάκης Δημήτριος (Δρ) Ελληνική Γεωλογική Εταιρία

Γαλετάκης Μιχαήλ (Επικ. Καθ.), Πολυτεχνείο Κρήτης

Καραχάλιος Στέφανος (Δρ), Περιφέρεια Κρήτης-Περιφερειακή Ενότητα Λασιθίου

Κόκκινου Ελένη (Επικ. Καθ.), Ανώτατο Εκπαιδευτικό Ίδρυμα Κρήτης

Κομνίτσας Κωνσταντίνος (Καθ.), Πολυτεχνείο Κρήτης

Κρητικάκης Γεώργιος (Δρ), Πολυτεχνείο Κρήτης

Κριτσωτάκης Μαρίνος (Δρ), ΓΕΩΤΕΕ - Παράρτημα Κρήτης

Λέκκας Ευθύμιος (Καθ.), Ελληνική Γεωλογική Εταιρία

Μωραϊτη Ευγενία (Δρ), Ελληνική Γεωλογική Εταιρία

Οικονόμου Νικόλαος (Δρ), Πολυτεχνείο Κρήτης

Παναγόπουλος Γεώργιος (MSc), Πολυτεχνείο Κρήτης

Παπαδόπουλος Νικόλαος (Ερευνητής), Ίδρυμα Τεχνολογιας & Έρευνας

Παπανικολάου Κασσιανή (Δρ), Ινστιτούτο Γεωλογικών και Μεταλλευτικών Έρευνών – Παράρτημα Ρεθύμνου

Πασαδάκης Νικόλαος (Αν. Καθ.), Πολυτεχνείο Κρήτης

Ρεπούσκου Ευτυχία (Δρ), Πολυτεχνείο Κρήτης

Σιμιτζής Βασίλης, Οργανισμός Ανάπτυξης Δυτικής Κρήτης

Σουπιος Παντελής (Αν. Καθ.), Ανώτατο Εκπαιδευτικό Ίδρυμα Κρήτης

Φασουλάς Χαράλαμπός (Δρ), Μουσείο Φυσικής Ιστορίας Κρήτης

ORGANIZING COMMITTEE

President:	Manoutsoglou Emmanouil (Prof.), Technical University of Crete
Vise President:	Markopoulos Theodore (Prof.), Technical University of Crete
Secretariat:	Vafeidis Antonios (Prof.), Technical University of Crete
Treasurer:	Steiakakis Emmanouil (Assis. Prof.), Technical University of Crete
Members:	Agioutantis Zacharias (Prof.), Technical University of Crete
	Alexopoulos Apostolos (Assoc. Prof.), Geological Society of Greece
	Antonarakou Asimina (Assist. Prof.), Geological Society of Greece
	Economou Nikolaos (Dr), Technical University of Crete
	Fasoulas Charalampos (Dr.), Natural History Museum of Crete
	Galanakis Dimitrios (Dr.) Geological Society of Greece
	Galetakis Michael (Assist. Prof.), Technical University of Crete
	Karachalios Stefanos (Dr.), Prefecture of Crete, Regional Union of Lassithi
	Kokkinou Eleni (Assist. Prof.), Technological Educational Institute of Crete
	Komnitsas Konstantinos (Prof.), Technical University of Crete
	Kritikakis George (Dr.), Technical University of Crete
	Kritsotakis Marinos (Dr.), GEOTEE - Regional Branch of Crete
	Lekkas Efthymios (Prof.), Geological Society of Greece
	Moraiti Eugenia (Dr.), Geological Society of Greece
	Panagopoulos George (MSc), Technical University of Crete
	Papadopoulos Nikolaos (Assist. Res.), Foundation for Research & Technology-Hellas
	Papanikolaou Kassiani (Dr.), Institute of Geology & Mineral Exploration-Regional Branch of Rethimno (IGME)
	Pasadakis Nikolaos (Assoc. Prof.), Technical University of Crete
	Repouskou Eftychia (Dr.), Technical University of Crete
	Simitzis Vasileios, Organization for the Development of W. Crete (OADYK)
	Soupios Pantelis (Assoc. Prof.), Technological Educational Institute of Crete
	Vozinakis Konstantinos, Prefecture of Crete, Regional Union of Chania
	Zampetaki-Lekka Alexandra (Prof.), Geological Society of Greece

ΕΠΙΣΤΗΜΟΝΙΚΗ ΕΠΙΤΡΟΠΗ/SCIENTIFIC COMMITTEE

Η Οργανωτική Επιτροπή ευχαριστεί θερμά τους κριτές για τη συμβολή τους στην κρίση όλων των εργασιών. Κάθε εργασία κρίθηκε από δύο κριτές για την απόκτηση Πρακτικών υψηλού επιστημονικού επιπέδου. Η Οργανωτική Επιτροπή δεν έχει ευθύνη για το περιεχόμενο και τις απόψεις που εκφράζονται στις εργασίες από τους συγγραφείς.

The Organizing Committee expresses sincere thanks to the reviewers for their contribution in evaluating and approving of the submitted papers. Each paper has passed through two reviewers, producing Proceedings of high scientific level. The Organizing Committee is not responsible for the content and the views expressed by the authors in the papers.

Agioutantis Zacharias (Prof.), Aidona Elina (Dr.), Alexakis Dimitrios, Alexopoulos Apostolos (Dr.), Anastassakis Georgios (Prof.), Antonarakou Assimina (Assist. Prof.), Argyraki Ariadne, Avramidis Pavlos (Assist. Prof.), Bathrellos George (Dr.), Baziotis Ioannis, Bellas Spyridon (Dr.), Bouzinos Antonios (Dr.), Chatzipetros Alexandros, Christanis Kimon (Prof.), Christaras Basile, Christidis George (Prof.), Danelian Taniel (Prof.), Diamanti Nectaria (Dr.), Dokou Zoi (Dr.), Dotsika Elissavet, Drinia Hara, Economou-Eliopoulos Maria (Prof.), Economou Nikos, Exadaktylos George (Prof.), Fassoulas Charalampos, Fermeli Georgia (Dr.), Fikos Ilias (Dr.), Filippidis Anestis (Prof.), Galetakis Michael, Ganas Athanassios, George Stavroulakis (Prof.), Georgiou Pantazis (Dr.), Godelitsas Athanasios, Hasiotis Thomas (Assist. Prof.), Hatzipanagiotou Konstantinos, Iliopoulos George (Dr.), Iliopoulos Ioannis, Kafousia Nefeli, Kaklis Triantafillos (Dr.), Kalaitzidis Stavros, Kallioras Andreas (Dr.), Kamperis Evangelos (Dr.), Kanellopoulos Christos, Kantiranis Nikolaos (Dr.), Kaplanidis Andreas (MSc), Karakitsios Vasileios, Karakostas Vassilis (Assoc. Prof.), Karatzas George (Prof.), Karymbalis Efthimios (Assist. Prof.), Katsanou Konstantina, Kilias Adamantios, Kiratzi Anastasia (Prof.), Klonari Aikaterini, Kokkalas Sotiris (Dr.), Kokkinou Eleni, Komnitsas Konstantinos, Kondopoulou Despina (Prof.), Kontakiotis George, Koskeridou Efterpi (Assist. Prof.), Koufos George, Koukis George (Em. Prof.), Koukouvelas Ioannis (Prof.), Koukouzas Nikolaos (Dr.), Kourgialas Nektarios (Dr.), Koutsovitis Petros, Kritikakis George, Lambrakis Nikolaos (Prof.), Lampropoulou Paraskevi (Dr.), Lekkas Efthymios, Loupasakis Constantinos (Dr.), Manoutsoglou Emmanouil (Prof.), Marinos Vassilis (Dr.), Mattas Christos, Melfos Vasilios, Mitropoulos Panagiotis (Prof.), Moraetis Daniel (Dr.), Mountrakis Demosthenis, Mourtzas Nikos (Dr.), Mouslopoulou Vasiliki (Dr.), Nikolakopoulos Konsantinos, Papadimitriou Eleftheria (Prof.), Papadopoulos Nikos Papoulia Joanna (Dr.), Papoulis Dimitrios, Parcharidis Issaak, Partsinevelos Panagiotis (Assist. Prof.), Pasadakis Nikos, Pe-Piper Georgia (Dr.), Perdikatsis Vasilios (Em. Prof.), Perraki Maria, Pomoni Fotini (Prof.), Pomonis Panagiotis (Assist. Prof.), Psomiadis Emmanouil, Rigakis Nikolaos, Rigopoulos Ioannis (Dr.), Rondoyanni Theodora (Assoc. Prof.), Roumelioti Zafeiria, Rozos Dimitrios (Assoc. Prof.), Sabatakakis Nicholas, Sakellariou Dimitris, Saroglou Haralambos, Scordilis Manolis, Serpetsidaki Anna (Dr.), Skianis Georgios, Skilodimou Hariklia, Skourlis Konstantinos (Dr.), Skourtsos Emmanuel (Dr.), Sokos Efthimios (Dr.),Soulios George, Soulis Konstantinos (Dr.), Soupios Pantelis, Spanoudakis Nikolaos (Dr.), Spyridonos Evangelos, Stamatis Georgios (Prof.), Stamboliadis Elias, Stavropoulou Maria (Assist. Prof.), Steiakakis Emmanouil, Stouraiti Christina (Dr.), Triantafyllou George (Dr.), Tsakalakis Konstantinos (Prof.), Tsangaratos Paraskevas, Tsiambaos George (Prof.), Tsikos Harilaos (Dr.), Tsikouras Basilios (Assist. Prof.), Tsouchlaraki Androniki Tsourlos Panagiotis (Dr.), Tsourou Theodora (Dr.), Vafidis Antonis (Prof.), Vallianatos Filippos (Prof.), Vargemezis George (Dr.), Voudouris Konstantinos, Voudouris Panagiotis, Voulgaris Nicholas (Assoc. Prof.), Xypolias Paraskevas, Zagana Eleni, Zambetakis-Lekkas Alexandra (Prof.).

ΧΟΡΗΓΟΙ/SPONSORS

Υπό την αιγίδα του

ΥΠΟΥΡΓΕΙΟΥ ΠΕΡΙΒΑΛΛΟΝΤΟΣ, ΕΝΕΡΓΕΙΑΣ ΚΑΙ ΚΛΙΜΑΤΙΚΗΣ ΑΛΛΑΓΗΣ

Under the Aegis of the

MINISTRY OF ENVIRONMENT, ENERGY AND CLIMATE CHANGE

και την χορηγία των

TECHNICAL UNIVERSITY OF CRETE

and the sponsorship of

GEOTECHNICAL CHAMBER OF GREECE

EARTHQUAKE PLANNING AND PROTECTION ORGANIZATION

HELLENIC CENTRE FOR MARINE RESEARCH

METKA S.A.

TITAN CEMENT COMPANY S.A

HELLENIC PETROLEUM S.A.

ΠΡΟΛΟΓΟΣ

Υπό τις τρέχουσες παγκόσμιες οικονομικές συνθήκες, η συμβολή της πρωτογενούς παραγωγής στην οικονομική ανάπτυξη της κάθε χώρας είναι ζωτικής σημασίας. Το σύνολο των επιστημονικών μεθοδολογιών και των αποτελεσμάτων τους που σχετίζονται άμεσα ή έμμεσα με την ανίχνευση και των εντοπισμό ορυκτών πόρων αποκτούν ιδιαίτερη σημασία αφού συμβάλλουν στην εκμετάλλευση των ορυκτών πόρων που με την σειρά της ως αναπόσπαστο τμήμα της πρωτογενούς παραγωγής μπορεί να συμβάλλει ουσιαστικά στην οικονομική ανάπτυξη της χώρας μας.

Το 13ο συνέδριο της Ελληνικής Γεωλογικής Εταιρίας με τίτλο «Έρευνα και Εκμετάλλευση Ορυκτών Πόρων» διοργανώθηκε με επιτυχία από την Σχολή Μηχανικών Ορυκτών Πόρων του Πολυτεχνείου Κρήτης και την Ελληνική Γεωλογική Εταιρία με την συνδρομή του Ιδρύματος Έρευνας και Τεχνολογίας (ΙΤΕ), του Ινστιτούτου Γεωλογικών και Μεταλλευτικών Έρευνών-Παράρτημα Κρήτης, του Μουσείου Φυσικής Ιστορίας, του Ανώτατου Τεχνολογικού Ιδρύματος Κρήτης, της Περιφέρειας Κρήτης-Περιφερειακή Ενότητα Χανίων και του Οργανισμού Ανάπτυξής Δυτικής Κρήτης (ΟΑΔΥΚ). Το συνέδριο φιλοξενήθηκε στις εγκαταστάσεις του Μεσογειακού Αγρονομικού Ινστιτούτου Χανίων (ΜΑΙΧ) και του Πολυτεχνείου Κρήτης.

Το σύνολο των εργασιών που κατατέθηκαν υποβλήθηκαν σε επιστημονική κρίση από δυο εξωτερικούς κριτές, ακολουθώντας τη διαδικασία που είναι διεθνώς καθιερωμένη στα επιστημονικά περιοδικά. Σε ειδικές περιπτώσεις πραγματοποιήθηκε κρίση της εργασίας και από τρίτο κριτή.

Οι επιστημονικές εργασίες ομαδοποιήθηκαν σε θεματικές ενότητες και παρουσιάστηκαν στις αντίστοιχες Συνεδρίες και ακολούθως στους τόμους των Πρακτικών του Συνεδρίου, που αποτελούν μετά από αυτήν την διαδικασία εργασίες υψηλού επιστημονικού επιπέδου.

Από την θέση αυτή θα ήθελα ευχαριστήσω θερμά όλους όσους συνέβαλλαν στην επιτυχή διοργάνωση αυτού του συνεδρίου: τους συναδέλφους της Οργανωτικής και Επιστημονικής Επιτροπής για την αμέριστη βοήθεια και συνδρομή τους, το Μεσογειακό Αγρονομικό Ινστιτούτο Χανίων (ΜΑΙΧ) και το Πολυτεχνείο Κρήτης για την φιλοξενία και άριστη συνεργασία τους, τους προπτυχιακούς και μεταπτυχιακούς φοιτητές καθώς και το υπόλοιπο προσωπικό της Σχολής μας για την βοήθεια τους σε όλα τα επίπεδα, το Δήμο Χανίων για την συνδρομή του, καθώς και τους χορηγούς μας που μας επέτρεψαν όχι μόνο την πραγματοποίηση του Συνεδρίου αλλά και την έκδοση του Πρακτικών του. Τέλος θα ήθελα να ευχαριστήσω ιδιαίτερα τους ακούραστους και πάντα παρόντες συνεργάτες της διοργάνωσης αυτής τους κ.κ. Δαλιάνη Δημήτρη και Ηλία Γιαννούλα που επιμελήθηκαν την διαδικτυακή επικοινωνία μας.

Εμμανουήλ Μανούτσογλου

Πρόεδρος της

Οργανωτικής επιτροπής

PROLOGUE

Under the current global financial conditions, the contribution of primary production to the economic development of each country is vital. All the research methodologies and research results which associate directly or indirectly with the exploration of mineral resources are of particular importance since they contribute to the exploitation of mineral resources. This is an integral part of primary production which can contribute significantly to the economic growth of our country.

The 13th Congress of the Greek Geological Society entitled "Exploration and Exploitation of Mineral Resources" was successfully organized by the School of Mineral Resource Engineering of the Technical University of Crete and the Greek Geological Society with the contribution of the Foundation for Research and Technology – Hellas, the Institute of Geology and Mineral Exploration (Branch of Crete), the Natural History Museum of Crete, the Technological Educational Institute of Crete (Branch of Chania), the Prefecture of Crete (Chania Region), the Organization for the Development of W. Crete and the Technical University of Crete.

All submitted papers were peer-reviewed by two external reviewers, according to internationally established procedures also adopted by scientific journals. In special cases papers were peer-reviewed by a third reviewer.

The papers were then grouped into thematic sessions and were presented during the congress. Finally, the papers were included in the Proceedings of the Congress documenting this high-level scientific work.

From this position I would like to thank all those who contributed to the successful organization of this conference: colleagues of the Organizing and the Scientific Committee for the continuous assistance and support, the Mediterranean Agronomic Institute of Chania (MAICh) and the Technical University of Crete for their hospitality and excellent cooperation, undergraduate and graduate students as well as the rest of the staff of our School for their help at all levels, the Chania Prefecture for their assistance, as well as our sponsors who enabled us to complete a very successful Congress and also publish the volumes of the proceedings. Finally I would like to especially thank Mr. Dimitris Dalianis and Mr Ilias Giannoulas, the tireless and ever-present collaborators who maintained our online conference management system.

Emmanouil Manoutsoglou

President

of the Organizing Committee

ΔΟΜΗ ΤΩΝ ΠΡΑΚΤΙΚΩΝ / SCHEME OF THE PROCEEDINGS

ΤΟΜΟΣ 1 / VOLUME 1

Εναρκτήριες Ομιλίες/Opening Lectures

Παλαιοντολογία, Στρωματογραφία και Ιζηματολογία/Palaeontology, Stratigraphy and Sedimentology

Γεωμορφολογία/Geomorphology

Πετρολογία και Ορυκτολογία/Petrology and Mineralogy/

ΤΟΜΟΣ 2 / VOLUME 2

Τεκτονική και Γεωδυναμική/Tectonics and Geodynamics

Υδρολογία και Υδρογεωλογία/Hydrology and Hydrogeology

Γεωχημεία και Βιογεωχημεία/Geochemistry and Biogeochemistry

Περιβαλλοντική Γεωλογία/Environmental Geology

Γεωεπιστήμες στην Εκπαίδευση και Γεώτοποι/Geosciences in Education and Geosites

ΤΟΜΟΣ 3 / VOLUME 3

Γεωφυσική και Σεισμολογία/Geophysics and Seismology

Φυσικές Καταστροφές Natural Hazards

Τηλεπισκόπηση και ΓΣΠ/Remote Sensing and GIS

Θαλάσσια Γεωλογία/Marine Geology

ΤΟΜΟΣ 4 / VOLUME 4

Κοιτασματολογία, Μεταλλευτική Τεχνολογία και Οικονομική Γεωλογία/Ore Geology, Mining Technology and Economic Geology

Τεχνική Γεωλογία και Γεωτεχνική Μηχανική/Engineering Geology and Geotechnical Engineering

Γεωθερμία/Geothermics

Έρευνα και Εκμετάλλευση Ορυκτών Πόρων/Exploration and Exploitation of Mineral Resources

Βιομηχανικά Ορυκτά και Πετρώματα/Industrial Minerals and Rocks

Ενεργειακές Πρώτες Ύλες/Energy Resources

ΠΕΡΙΕΧΟΜΕΝΑ/CONTENTS

ΤΟΜΟΣ 1 / VOLUME 1

Opening Lectures/Εναρκτήριες Ομιλίες

Palaeontology, Stratigraphy and Sedimentology/Παλαιοντολογία, Στρωματογραφία και Ιζηματολογία

Geomorphology/Γεωμορφολογία

Petrology and Mineralogy/Πετρολογία και Ορυκτολογία

Εναρκτήριες Ομιλίες
Opening Lectures

Μαριολάκος Η.Δ.: Μεταλλευτική και μεταλλουργική δραστηριότητα των προϊστορικών κατοίκων του Αιγιακού και πέρι-Αιγιακού χώρου: Μια γεωμυθολογική προσέγγιση……2

Μπαζιώτης Ι. και Taylor L.A.: Είμαστε μόνοι στο συμπάν; Οι μετεωρίτες δίνουν απαντήσεις;..……...……..……32

Παλαιοντολογία, Στρωματογραφία και Ιζηματολογία
Palaeontology, Stratigraphy and Sedimentology

Agiadi K., Koskeridou E., Triantaphyllou M. and Karakitsios V.: Paleobathymetry of a Pliocene Voutes coast (Heraklion, Crete)……...…..…52

Athanasiou M., Triantaphyllou M., Dimiza M., Gogou A., Bouloubassi I., Tsiolakis E. and Theodorou G.: Early-Middle Miocene from Kotaphi hill section (Nicosia, Cyprus): Preliminary biostratigraphy and paleoceanographic implications……...…..……62

Chatziapostolou A., Siavalas G., Kalaitzidis S. and Christanis K.: Geological study for a wetland restoration: The case of the drained Mouria Lake (W. Peloponnese)…….……...72

Codrea V., Solomon Al., Fărcaş C. and Barbu O.: On some local restricted Maastrichtian environments of the "Haţeg Island" (Transylvania, Romania)…….82

Drinia H.: Climatic vs tectonic control on the Early Late Miocene tectono-stratigraphic deposits of the Pre-Apulian Zone, Western Greece……..……92

Drinia H., Antonarakou A. and Louvari M.A.: Foraminiferal biostratigraphy and palaeoenvironmental analysis of the basal part of Kalamavka formation (Late Miocene, Ierapetra Basin, Eastern Crete) ……...……..102

Drinia H., Antonarakou A., Mihalakopoulos S. and Tsiolakis E.: Eastern Mediterranean foraminiferal palaeoecological response to Mid-Late Pliocene climatic regime: A preliminary note….112

Filippidi A., Stathopoulou E.T. and Theodorou G.: Taphonomical observations on the pygmy hippopotamus site in Aghia Napa, Cyprus…….122

Karakitsios V. and Chatzicharalampous E.: Biostratigraphy and sedimentology of the Ionian Zone Ammonitico Rosso in the Mavron Oros area (NW Epirus, Greece) - Paleogeographic implications……..……...……136

Karakitsios V., Roveri M., Lugli S., Manzi V., Gennari R., Antonarakou A., Triantaphyllou M., Agiadi K. and Kontakiotis G.: Remarks on the Messinian evaporites of Zakynthos Island (Ionian Sea, Eastern Mediterranean)…… ……..……146

Karditsa A. and Poulos S.E.: The application of grain size trend analysis in the fine grained seabed sediment of Alexandroupolis Gulf……..……...….157

Kontakiotis G., Antonarakou A. and Zachariasse W.J.: Late Quaternary palaeoenvironmental changes in the Aegean Sea: Interrelations and interactions between North and South Aegean Sea.……167

Koskeridou E., Thivaiou D. and Giamali Ch.: Molluscan assemblages in a highly variable setting in littoral bottoms of the Lower Pleistocene of Rhodes (Greece)… ……178

Kostaki G., Kilias A., Gawlick H.J. and Schlagintweit F.: ?Kimmeridgian-Tithonian shallow-water platform clasts from mass flows on top of the Vardar/Axios ophiolites…….....184

Kostopoulou S., Triantaphyllou M.B., Dimiza M.D., Gogou A., Bouloubassi I., Rousakis G., Parinos C., Diamantopoulou An., Geraga M. and Lykousis V.: Preliminary results of high resolution paleoceanography and paleoclimatology during sapropel S1 deposition (South Limnos Basin, North Aegean Sea)…… ……...……..194

Mantzouka D., Sakala J., Kvaček Z. and Karakitsios V.: Palaeobotanical study of Polichnitos region, southern part of Lesbos Island, Greece (preliminary results on angiosperm wood)……..204

Moforis L., Kostopoulou S., Panagopoulos G., Pyliotis I., Triantaphylou M., Manoutsoglou E. and Zelilidis A.: Sedimentation processes and palaeographic evolution of Makrilia Pliocene deposits, SE Crete…….……216

Zoumpouli E., Pomoni-Papaioannou F., Zelilidis A. and Iliopoulos G.: Biostratigraphical and sedimentological study of an Upper Cretaceous succession in the Sami area (central area of Kefallinia, W. Greece)…… ……..……...……...226

Γεωμορφολογία

Geomorphology

Aidona E., Kazakis N., Mavroidaki K. and Voudouris K.: Magnetic susceptibility as a tool for the discrimination of anthropogenic and lithogenic history of topsoils: preliminary results from the broader area of Thessaloniki city…….……236

Griffiths H.M., Kalivas D.P., Petropoulos G.P. and Dimou P.: Mapping erosion and deposition changes in the protected wetlands of the Axios River Delta, N. Greece using remote sensing and GIS……..245

Ifandi E., Tsikouras B. and Hatzipanagiotou K.: Contribution to the evolution of the Perama Cave (Ioannina, NW Greece)…….……255

Ilia I., Rozos D. and Koumantakis I.: Landform classification using GIS techniques. The case of Kimi municipality area, Euboea Island, Greece……...……..264

Kokinou E., Panagiotakis C. and Kinigopoulos Th.: Retrieval of similar topographic areas....275

Kokinou E., Skilodimou H.D. and Bathrellos G.D.: Morphotectonic analysis of Heraklion Basin (Crete, Greece)……..285

Michail M. and Chatzipetros A.: Morphotectonic analysis of faults in Sperchios Basin (Fthiotis, Central Greece)…..……295

Papoulia M., Karymbalis E., Gaki-Papanastassiou K. and Maroukian H.: Assessment of the susceptibility of the coast of Astypalaea Island (S.E. Aegean Sea) to sea level rise……305

Perrou Th., Kaza I., Efthymiadis V., Karymbalis E. and Chalkias C.: Recent coastline changes of fan-deltas in the Western Gulf of Corinth, Central Greece……..…….315

Psomiadis E., Migiros G. and Antoniou V.: Geomorphological quantitative analysis of Sperchios River Basin area (Central Greece) utilizing geographical information systems…….325

Skentos A., Liosis N. and Pavlopoulos K.: Geomorphological mapping of Messogia plain (East Attica, Greece)……..…… ……335

Valkanou K., Karymbalis E., Papanastassiou D., Gaki-Papanastassiou K. and Giles P.: Analysis of relationships among coastal alluvial fans and their contributing catchments in North Evoikos Gulf (Central Greece)…….……344

Πετρολογία και Ορυκτολογία
Petrology and Mineralogy

Baziotis I., Asimow P.D., Koroneos A., Poli G. and Ntaflos T.: Multi-stage history of compound mantle xenoliths from Western USA: Implications for metasomatic processes in the deep mantle……357

Christidis G.E and Koutsopoulou E.: Thermal behaviour of stevensite at temperatures up to 800°C…….…….366

Drakoulis A., Koroneos A., Soldatos T. and Papadopoulou L.: Mineralogy and chemistry of amphiboles and thermobarometry of Papikion Mt pluton, Rhodope, Northern Greece……...373

Karampatsou G., Markopoulos Th., Repouskou E. and Triantafyllou G.: Minerological and physico-chemical properties of the building materials of Koule castle, Heraklion, Crete…….383

Kougemitrou I., Economou G., Giovanopoulos J., Baziotis I., Leontakianakos G. and Stathopoulos V.: A mineralogical study of pigments used in two Iakovidis paintings: Verification of artwork authenticity using Raman micro-spectroscopy method……..392

Mposkos E. and Perraki M.: Metamorphic record in metalherzolite pockets within the Virsini metaharzburgite from the Kechros HP metamorphic complex in Eastern Rhodope, Greece…….397

Papoulis D., Komarneni S., Toli D., Panagiotaras D. and Bakalis S.: Synthesis and characterization of four new halloysite–TiO_2 nanocomposites…….…….407

Pipera K., Koroneos A., Soldatos T., Poli G. and Christofides G.: Origin of the High-K Tertiary magmatism in Northern Greece: Implications for mantle geochemistry and geotectonic setting……..416

Stamatakis M.G. and Mitsis I.: The occurrences of Mg-hydroxycarbonates in serpentinites of the western section of the South Aegean volcanic arc (West Attica peninsula-Northeastern Argolis peninsula), Greece……...……..427

Thabet I., Kilias A., Koroneos A. and Kamh S.: Petrography and zircon morphology of syntectonic granitoids rocks of Hafafit area, South Eastern Desert (Egypt)…..……438

Tsikouras B., Etiope G., Ifandi E., Kordella S., Papatheodorou G. and Hatzipanagiotou K.: Petrological implications for the production of methane and hydrogen in hyperalkaline springs from the Othrys ophiolite, Greece……..…449

Vallianatos F., Michas G., Papadakis G., Kyriakopoulos K. and Vasilakopoulos V.: A Non-Extensive statistical physics approach to the characterization of the pyroclastic deposits of the Kos volcanic center……458

Voudouris P., Constantinidou S., Kati M., Mavrogonatos C., Kanellopoulos C. and Volioti E.: Genesis of alpinotype fissure minerals from Thasos Island, Northern Greece - Mineralogy, mineral chemistry and crystallizing environment..... ……468

Voudouris P., Psimis I., Mavrogonatos C., Kanellopoulos C., Kati M. and Chlekou E.: Amethyst occurrences in Tertiary volcanic rocks of Greece: Mineralogical and genetic implications……..…..477

Voudouris P., Xinou A., Kanellopoulos C., Kati M., Mavrogonatos C., and Lyberopoulos P.: A new occurrence of pyrophanite from the amphibolite-hosted skarn in Western Kimmeria, Xanthi, Northern Greece……..487

ΤΟΜΟΣ 2 / VOLUME 2

Tectonics and Geodynamics/Τεκτονική και Γεωδυναμική

Hydrology and Hydrogeology/Υδρολογία και Υδρογεωλογία

Geochemistry and Biogeochemistry/Γεωχημεία και Βιογεωχημεία

Environmental Geology/Περιβαλλοντική Γεωλογία

Geosciences in Education and Geosites/Γεωεπιστήμες στην Εκπαίδευση και Γεώτοποι

Τεκτονική και Γεωδυναμική
Tectonics and Geodynamics

Bradley K.E., Vassilakis E., Weiss B.P. and Royden L.H.: A re-assessesment of the shallow paleomagnetic inclintions of the Western Cyclades, Greece……498

Chousianitis K., Ganas A., Papanikolaou M., Argyrakis P., Drakatos G. and Makropoulos K.: Time series analysis of the NOANET CGPS stations……..……..508

Ganas A., Oikonomou I.A. and Tsimi C.: NOAfaults: a digital database for active faults in Greece……..…….518

Kalisperi D., Rigakis I., Makris J.P., Romano G. and Vallianatos F.: Continuous magnetotelluric observations in Western Crete as a tool for the study of the Hellenic subduction Zone...……..……...…531

Kamberis E., Sotiropoulos S., Marnelis F. and Rigakis N.: Thrust tectonics in the central part of the External Hellenides, the case of the Gavrovo thrust……..540

Kilias Ad., Vamvaka A., Falalakis G., Sfeikos A., Papadimitriou E., Gkarlaouni Ch. and Karakostas B.: The Mesohellenic trough and the Thrace Basin. Two Tertiary molassic Basins in Hellenides: do they really correlate?..... ……....551

Kkallas Ch., Papazachos C.B., Scordilis E.M. and Margaris B.N.: Re-examining the stress field of the broader southern Aegean subduction area using an updated focal mechanism database……..…….563

Mariolakos I.D. and Manoutsoglou E.: The geotectonic evolution of Olympus Mt and its mythological analogue……..574

Mountrakis D., Kilias A., Pavlaki A., Fassoulas C., Thomaidou E., Papazachos C., Papaioannou C., Roumelioti Z., Benetatos C. and Vamvakaris D.: Neotectonic analysis, active stress field and active faults seismic hazard assessment in Western Crete……..……582

Mouslopoulou V., Moraetis D., Benedetti L., Guillou V. and Hristopulos D.: Paleoearthquake history of the Spili fault, Crete, Greece……..…….595

Panagopoulos G., Giannakakos E., Manoutsoglou E., Steiakakis E., Soupios P. and Vafidis A.: Definition of inferred faults using 3D geological modeling techniques: A case study in Tympaki Basin in Crete, Greece……605

Papoulis D., Romiou D., Kokkalas S. and Lampropoulou P.: Clay minerals from the Arkitsa fault gouge zone, in Central Greece, and implications for fluid flow…….....616

Ring U., Gessner K., Thomson S. and Markwitz V.: Along-strike variations in the Hellenide Anatolide orogen: A tale of different lithospheres and consequences……..……625

Rondoyanni Th., Lykoudi E. and Kalogeras E.: Coseismic surface displacement variability in relation to lithology……637

Sakellariou D., Mascle J. and Lykousis V.: Strike slip tectonics and transtensional deformation in the Aegean region and the Hellenic arc: Preliminary results…….……..…647

Simou E., Karagkouni V., Papantoniou G., Papanikolaou D. and Nomikou P.: Morphotectonic analysis of Kozani Basin (Western Macedonia, Greece)…… ……657

Thabet I., Kilias A. and Kamh S.: Microstructural finite strain analysis of the Hafafit granitoids domes South Central Eastern desert of Egypt…….667

Υδρολογία και Υδρογεωλογία
Hydrology and Hydrogeology

Angelakopoulou E., Koumantakis I., Vasileiou E. and Stathopoulos N.: Groundwater quality characteristics of the Anavisos Basin……682

Antonakos A. and Nikas K.: Delineation of recharge areas of the aquifer systems of Corinthia prefecture by the use of isotopic evidence……...692

Katsifa M., Koumantakis I., Stathopoulos N. and Vasileiou E.: Environmental pressures to the water resources in the wider area of Roditsa, in Sperchios River Delta of Eastern Central Greece……702

Kazakis N., Voudouris K., Vargemezis G. and Pavlou A.: Hydrogeological regime and groundwater occurence in the Anthemountas River Basin, Northern Greece…..……..……711

Kourgialas N.N. and Karatzas G.P.: Flood and groundwater management for the mountain plateau of Omalos based on geoinformatics techniques……..……721

Kyriazis D., Zagana E., Stamatis G., Fillippidis F. and Psomiadis E.: Assessment of groundwater pollution in relation to heavy metals of the alluvial aquifer of Thriasion Plain (NW Attica)…..…731

Lappas I., Tsioumas V. and Zorapas V.: Spatial-temporal analysis, variation and distribution of precipitation in the water district of Central-Eastern Greece……..….740

Matiatos I. and Alexopoulos A.: Analysis of temporal hydrochemical and isotopic variations in spring waters of Eastern Peloponnesus (Greece)……...……..750

Pavlou A., Soulios G., Dimopoulos G., Tsokas G., Mattas C., Kazakis N. and Voudouris K.: Groundwater quality of the coastal aquifers in the eastern part of Thermaikos Gulf (from Aggelochori to Kallikrateia)…..……..761

Soulios G., Mattas C., Kaklis T., Sotiriadis M., Voudouris K. and Dimopoulos G.: Is the construction of a sanitary landfill acceptable in a karstic area? The case of the sanitary landfill site in Fokida, Central Greece……...…….771

Stathopoulos N., Rozos D. and Vasileiou E.: Water resources management in Sperchios River Basin, using SWOT analysis……...779

Tsangaratos P., Pizpikis T., Vasileiou E., Pliakas F., Schuth C. and Kallioras A.: Development of multi-criteria decision support system (DSS) coupled with GIS for identifying optimal locations for soil aquifer treatment (SAT) facilities……...789

Vasileiou E. and Koumantakis I.: The role of Kefalovruso and Amourio springs in the hydrodynamic conditions of Potamia Elassona Basin……..801

Γεωχημεία και Βιογεωχημεία
Geochemistry and Biogeochemistry

Giouri K., Papadopoulos A., Bourliva A., Tzamos E., Papadopoulou L. and Filippidis A.: Trace element content and morphological characteristics in microscale of commercially available clays used as cosmetic products……...812

Iordanidis A. and Garcia-Guinea J.: Analytical geochemistry in the service of medicine: An experimental study of urinary stones from Northern Greece……..818

Kafousia N., Karakitsios V., Mattioli E. and Jenkyns H.C.: Chemostratigraphy of the Toarcian oceanic anoxic event from the Ionian Zone, Greece……825

Kilias S.P., Chatzitheodoridis E. and Lyon I.: Molecular, chemical and morphological evidence for hematite biogenicity at the Quaternary Cape Vani Mn-(Ba-Fe) deposit, Milos, Greece……..834

Moraetis D. and Mouslopoulou V.: Preliminary results of REE-Y sorption on carbonate rocks……843

Nioti D., Maravelis A., Tserolas P. and Zelilidis A.: TOC and $CaCO_3$ content in Oligocene shelf deposits on Lemnos Island and their relation with depositional conditions……852

Pyliotis I., Hamilaki E., Pasadakis N. and Manoutsoglou E.: Comparative evaluation of Rock-Eval and elemental analysis to determine organic carbon content in sediment samples……..…862

Pyliotis I., Zelilidis A., Pasadakis N., Panagopoulos G. and Manoutsoglou E.: Source rock potential of the Late Miocene Metochia formation of Gavdos Island, Greece……871

Rallakis D., Siavalas G., Oskay R.G., Tsimiklis D. and Christanis K.: Maturity of dispersed organic matter in bituminous formations of the Ionian Zone (Epirus region, NW Greece)……880

Περιβαλλοντική Γεωλογία
Environmental Geology

Aidona E., Pechlivanidou S. and Pennos Ch.: Environmental magnetism: Application to cave sediments……...….892

Argyraki A., Kelepertzis E., Fligos G., Athanasiou E., Gardiakos K. and Kourgia V.: Geochemical mapping of urban soils in Athens, Greece - Preliminary results……...…901

Argyraki A., Paraskos F., Marmara M., Papadopoulou K. and Maglaropoulou A.: Comparative geochemistry of three urban streams in Athens: Kifissos-Podoniftis-Pikrodafni……..…..910

Filippidis A., Godelitsas A., Kantiranis N., Gamaletsos P., Tzamos E. and Filippidis S.: Neutralization of sludge and purification of wastewater from Sindos industrial area of Thessaloniki (Greece) using natural zeolite……..920

Georgiadis I.K., Papadopoulos A., Filippidis A., Godelitsas A., Tsirambides A. and Vogiatzis D.: Removal of malachite green dye from aqueous solutions by diasporic Greek raw bauxite……927

Giouri K., Vavelidis M. and Melfos V.: Occurrence of arsenic in waters and sediments of the Palea Kavala River, NE Macedonia, Northern Greece……....934

Kanellopoulos C. and Mitropoulos P.: Geochemical effect of the rock chemistry and the anthropogenic activities on groundwater: The case study of NW Euboea, Greece……942

Katsimicha D., Pentari D., Pantelaki O. and Komnitsas K.: Effect of wet milling on the adsorption capacity of a greek natural zeolite used for the removal of heavy metals from solutions…..953

Kokinou E., Belonaki C., Sakadakis D. and Sakadaki K.: Environmental monitoring of soil pollution in urban areas (a case study from Heraklion city, Central Crete, Greece)……963

Koutsopoulou E., Katsanou K., Papoulis D., Zagana E. and Tsolis-Katagas P.: Environmental assessment of contaminants in a downstream area of a landfill……972

Samara T. and Yoxas G.: Drastic method to map groundwater vulnerability to pollution using nitrate measurements in agricultural areas……..……981

Zotiadis V. and Argyraki A.: Development of innovative environmental applications of attapulgite clay……..…992

Γεωεπιστήμες στην Εκπαίδευση και Γεώτοποι
Geosciences in Education and Geosites

Fassoulas C., Staridas S., Perakis V. and Mavrokosta C.: Revealing the geoheritage of Eastern Crete, through the development of Sitia Geopark, Crete, Greece……1004

Galani L., Theodorakopoulou K., Skentos A., Kritikos G. and Pavlopoulos K.: GIS as an educational tool: Mapping cultural sites in greek space-time…..……...1017

Leontakianakos G., Vrachas C., Baziotis G., Baziotis I., Soultati G. and Fermeli G.: Theoretical approach of teaching lithosphere in junior high school: A critical review of the content and objectives defined by the curriculum of the Ministry of Education…….……1024

Tsangaratos P., Perraki M. and Ilia I.: Developing an interactive application embodied in the geosciences educational procedure……...1031

ΤΟΜΟΣ 3 / VOLUME 3

Geophysics and Seismology/Γεωφυσική και Σεισμολογία

Natural Hazards/Φυσικές Καταστροφές

Remote Sensing and GIS/Τηλεπισκόπηση και ΓΣΠ

Marine Geology/Θαλάσσια Γεωλογία

Γεωφυσική και Σεισμολογία
Geophysics and Seismology

Angelis G.L., Stephanopoulos P., Papamarinopoulos St.P.: Geoelectric prospecting in University Campus region for detection of possible geological discontinuities, Rio, Patra, Greece…..……1042

Apostolopoulos G., Pavlaki C., Perleros V. and Amolochitis G.: Geophysical investigation and its geological interpretation in the frame of an intergrated survey prior to a dam construction in Plati River Valley, Rethymno, Greece…….….1052

Baskoutas I. and Papadopoulos G.: Qualitative precursory pattern before several strong earthquakes in Greece……...1061

Benekos G., Parcharidis I., Foumelis M. and Ganas A.: Ground deformation measurements over Lake Trichonis based on SAR interferometry…...……1071

Bouranta E., Vallianatos F., Hatzopoulos J.N., Papadopoulos I. and Gaganis P.: Microtremor HVSR study of site effects in the urban area of the town of Mytilene, Lesvos (Greece) - Preliminary results……1081

Ghaib F.A., Abdulla H. and Anwar H.: Resistivity investigation for well-site definition around Barika Village, Southeast Sulaimany city, Iraqi Kurdistan region……1090

Gkarlaouni Ch., Papadimitriou E., Lasocki S., Lizurek G., Karakostas V. and Kilias A.: Stochastic analysis of earthquake activity in two seismogenic fault systems in Greece…….1099

Karagianni E., Paradisopoulou P. and Karakostas V.: Spatio-temporal earthquake clustering in the Western Corinth Gulf……..…1109

Karmis P., Giannoulopoulos P., Sofos F. and Lappas I.: Hydrogeophysical exploration for estimating groundwater reservoirs areas in Southern Rhodes through ERT (Electrical Resistivity Tomography) method……....1118

Kiratzi A.: The 1912 Ganos earthquake: Source constraints using ground motion simulations……..1128

Kiratzi A., Aktar M. and Svigkas N.: The 10 June 2012 M_W 6.0 earthquake sequence in the easternmost end of the Hellenic arc……1138

Kiratzi A., Klimis N., Theodoulidis N., Margaris V., Makra K., Christaras B., Chatzipetros A., Papathanassiou G., Savvaidis A., Pavlides Sp., Roumelioti Z., Sapountzi L., Diamantis I., Lazaridis Th., Petala E. and Mimidis K.: Characterization of site conditions in Greece for realistic seismic ground motion simulations: Pilot application in urban areas……1148

Leptokaropoulos K.M., Papadimitriou E.E., Orlecka–Sikora B., Karakostas V.G. and Vallianatos F.: Modeling seismicity rate changes along the Hellenic subduction Zone (Greece)…….…..1157

Mesimeri M., Papadimitriou E., Karakostas V. and Tsaklidis G.: Earthquake clusters in NW Peloponnese……..1167

Michas G., Papadakis G. and Vallianatos F.: A Non-Extensive approach in investigating Greek seismicity……..1177

Mouzakiotis E. and Karastathis V.K.: Improved earthquake location in the area of North Euboean Gulf after the implementation of a 3D non-linear location method in combination with a 3D velocity model……....1185

Papadakis G., Vallianatos F. and Michas G.: The earthquake intervent time distribution along the Hellenic subduction Zone.....……1194

Papadopoulos I., Papazachos C., Savvaidis A., Theodoulidis N., Vallianatos F. and Tsourlos P.: Results for the shallow structure of the broader region of Chania by HVSR measurements of ambient noise and their validation using simulation of ambient noise and independent geological information……...……1201

Paradisopoulou P., Papadimitriou E., Mirek J. and Karakostas V.: Coseismic stress distribution along active structures and their influence on timedependent probability values…….1211

Pitilakis K., Roumelioti Z., Manakou M., Raptakis D., Liakakis K., Anastasiadis A. and Pitilakis D.: The web portal of the EUROSEISTEST strong ground motion database……..1221

Roumelioti Z., Theodoulidis N. and Bouchon M.: Constraints on the location of the 2008, M_W 6.4 Achaia-Ilia earthquake fault from strong motion data……..….1231

Scordilis E., Kementzetzidou D. and Papazachos B.: Local magnitude estimation in Greece, based on recordings of the Hellenic Unified Seismic Network (HUSN)……..1241

Simyrdanis K., Tsourlos P., Soupios P. and Tsokas G.: Simulation of ERT surface-to-tunnel measurements……...……1251

Soupios P., Papadopoulos N. and Sarris A.: Reconstructing concealed cultural remains through integrated geophysical tomographic methods……...……1260

Stavroulopoulou O., Sokos E., Martakis N. and Tselentis G.A.: Earthquake relocation for Northwestern Greece using 3D crustal model; method comparison and seismotectonic interpretation…….....1269

Tema E.: Detailed archaeomagnetic study of a ceramic workshop at Kato Achaia: New directional data and archaeomagnetic dating in Greece……..1279

Tema E., Pavlides S. and Kondopoulou D.: Late bronze age pottery as indicator of the deposition temperatures of the Minoan pyroclastic products, Santorini, Greece……....1289

Teza E., Scordilis E.M., Papazachos C.B. and Karakaisis G.F.: Near-real-time evaluation of the evolution of a seismic excitation: Application to the January 8, 2013 Lemnos seismic sequence……..…..1298

Triantafyllis N., Sokos E. and Ilias A.: Automatic moment tensor determination for the Hellenic Unified Seismic Network……...……1308

Tsampas A.D., Scordilis E.M., Papazachos C.B. and Karakaisis G.F.: Globally valid relations converting magnitudes of intermediate and deep-focus earthquakes to M_W…….1316

Tzanis A., Vallianatos F. and Efstathiou A.: Multidimensional earthquake frequency distributions consistent with Non-Extensive statistical physics: The interdependence of magnitude, interevent time and interevent distance in North California……..……..1326

Vafidis A., Andronikidis N., Hamdan H., Kritikakis G., Economou N., Panagopoulos G., Soupios P., Steiakakis E. and Manoutsoglou E.: The CLEARWATER project: preliminary results from the geophysical survey in Tympaki, Crete, Greece……..……1338

Vafidis A., Andronikidis N., Hamdan H., Kritikakis G., Economou N., Panagopoulos G., Zanettidis S., Merziotis D., Pateras S., Nikoforakis E. and Blais J.P.: Rock characterization for the foundation of two water reservoirs using geophysical and borehole data……..1345

Vargemezis G., Diamanti N., Fikos I., Stampolidis A., Makedon Th. and Chatzigogos N.: Ground penetrating radar and electrical resistivity tomography for locating buried building foundations: A case study in the city centre of Thessaloniki, Greece……..…….1355

Ventouzi Ch., Papazachos C., Papaioannou Ch., Hatzidimitriou P. and the EGELADOS working group: Obtaining information on the Q-structure of the southern Aegean subduction area by spectral slopes from temporary and permanent networks…….1366

Votsi I., Tsaklidis G., Limnios N., Papadimitriou E. and Vallianatos F.: A Markov model for seismic hazard analysis along the Hellenic subduction Zone (Greece) …….1376

Φυσικές Καταστροφές
Natural Hazards

Diakakis M.: Flood reconstruction using botanical evidence in Rapentosa catchment, in Marathon, Greece……...1388

Diakakis M. and Deligiannakis G.: Changes in flood mortality during the last 50 years in Greece……..….1397

Diakakis M., Katsetsiadou K. and Pallikarakis A.: Flood fatalities in Athens, Greece: 1880-2010……..1407

Pertsinidou C.E., Tsaklidis G. and Papadimitriou E.: Seismic hazard assessment in the Northern Aegean Sea (Greece) through discrete Semi-Markov modeling……..…….….1417

Saroglou H.: Rockfall hazard in Greece……...……1429

Vafidis A., Steiakakis M., Agioutantis Z., Andronikidis N., Kritikakis G., Economou N., Pandi K., Spanoudakis N., Savvaidis A., Margaris B., Theodoulidis N., Lekidis V., Karakostas Ch., Mangriotis M.D., Kalogeras I., Koutrakis S., Rozos D., Loupasakis C., Rondoyanni Th., Tsangaratos P., Dikmen U., Papadopoulos N., Sarris A., Soupios P., Kokkinou E., Papadopoulos I., Kouli M. and Vallianatos F.: "Geo-characterization" of selected areas in Crete, Greece, towards realistic assessment of seismic design actions……..…1439

Τηλεπισκόπηση και ΓΣΠ
Remote Sensing and GIS

Alexakis D.D., Agapiou A., Themistocleous K., Lysandrou V., Sarris A. and Hadjimitsis D.G.: Natural and human hazard assessment of the archaeological sites of Paphos area (Cyprus) with the use of remote sensing and GIS……..1448

Grimpylakos G., Karacostas T.S. and Albanakis K.: Spatial and temporal distribution of rainfall and temperature in Macedonia, Greece, over a thirty year period, using GIS……..1458

Kordouli M., Kavoura Kat., Nikolakopoulos K. and Sabatakakis N.: Landslide inventory using GISMA techniques……...1472

Marsellos A.E., Foster D.A., Min K., Kidd W.S.F., Garver J. and Kyriakopoulos K.: An application of GIS analysis on structural data from metamorphic rocks in Santorini Island……..….1479

Nikolakopoulos G.K., Choussiafis Ch. and Karathanassi V.: Landslide detection using ALOS optical and radar data. A case study from the Ilia prefecture…….1489

Nikolakopoulos G.K., Tsombos I.P., Photiades A., Psonis K. and Zervakou A.: Using remote sensing multispectral data and GIS techniques for the geological mapping of Halki Island…….1500

Raspini F., Loupasakis C., Rozos D. and Moretti S.: Basin and local scale detection of ground subsidence through persistent scatterer interferometry: The Anthemountas Basin (Northern Greece) case study…….1510

Stefouli M., Vasileiou E., Charou E., Stathopoulos N., Perrakis A. and Giampouras P.: Remote sensing techniques as a tool for detecting water outflows. The case study of Cephalonia Island……...1519

Tsangaratos P. and Koumantakis I.: The value of geological data, information and knowledge in producing landslide susceptibility maps……...1529

Tsangaratos P. and Rozos D.: Producing landslide susceptibility maps by applying expert knowledge in a GIS - based environment……..1539

Θαλάσσια Γεωλογία
Marine Geology

Kapsimalis V., Talagani P., Panagiotopoulos I.P., Kaberi H., Rousakis G., Kanellopoulos Th.D., Iliakis S. and Hatzianestis I.: Pollution assessment of the Drapetsona Keratsini coastal seabed……....1552

Petropoulos A., Androni A., Ntamkarelou T. and Anagnostou Ch.: Carbonate and organic carbon content in the recent sediments of Elefsis bay as indicators for the paleoenviromental evolution of the system…….....1562

Poulos S., Ghionis G. and Petrakis S.: Investigating the existence of a "palaeo-foreshore" zone at Molos beach (Kefalos bay, Paros, Greece)… ……..…1572

Tsoutsia A., Kapsimalis V., Poulos S., Paraskevopoyloy V. and Dassenakis E.: Assessment of heavy metals contamination in the coastal sediments of the broader area of Chios harbor (Aegean Sea)……...……....1581

Zananiri I., Mitropoulos D., Zimianitis V., Ioakim Chr., Papadopoulos V. and Efthimiou G.: Marine geology data accessibility in the European Framework: The I.G.M.E. participation in the GEO-SEAS project……...…1590

ΤΟΜΟΣ 4 / VOLUME 4

Ore Geology, Mining Technology and Economic Geology/Κοιτασματολογία, Μεταλλευτική Τεχνολογία και Οικονομική Γεωλογία

Engineering Geology and Geotechnical Engineering/Τεχνική Γεωλογία και Γεωτεχνική Μηχανική

Geothermics/Γεωθερμία

Exploration and Exploitation of Mineral Resources/Ερευνα και Εκμετάλλευση Ορυκτών Πόρων

Industrial Minerals and Rocks/Βιομηχανικά Ορυκτά και Πετρώματα

Energy Resources/Ενεργειακές Πρώτες Ύλες

Κοιτασματολογία, Μεταλλευτική Τεχνολογία και Οικονομική Γεωλογία
Ore Geology, Mining Technology and Economic Geology

Anagnostopoulos I., Lampropoulou P., Tzevelekou Th., Stivanakis V., Kastanaki A. and Papamantellos D.: Utilization trials of lignite solid byproducts of West Macedonia and Peloponnesus lignite fired power plants for the production of lightweight aggregates……...1600

Anastassakis G.: Relationship between phosphates mineralogy and mineral processing - The case of Greece……..1609

Eliopoulos D.G. and Economou-Eliopoulos M.: Palladium and platinum in hydrothermal systems: The case of porphyry-Cu systems and sulfides associated with ophiolite complexes……..1618

Kalaitzidis S.: National reporting codes for the mineral industry: The case of JORC in Australia…..……1628

Kilias S.P., Naden J., Paktsevanoglou M., Giampouras M., Stavropoulou A., Apeiranthiti D., Mitsis I., Koutles Th., Michael K. and Christidis C.: Multistage alteration, mineralization and ore–forming fluid properties at the Viper (Sappes) Au–Cu–Ag–Te ore body, W. Thrace, Greece……...1635

Perdikatsis V.: Quantitative determination of mineral matter in lignite by X-RAY spectrometry, using the Compton effect……...……...…1645

Trichos D., Alevizos G., Stratakis A., Petrakis E. and Galetakis M.: Mineralogical investigation and mineral processing of iron ore from the Skines area (Chania – West Crete)……..…1652

Τεχνική Γεωλογία και Γεωτεχνική Μηχανική
Engineering Geology and Geotechnical Engineering

Andrianopoulos A., Saroglou H. and Tsiambaos G.: Rockfall hazard and risk assessment of road slopes……1664

Antoniou A. and Spyropoulos I.: The influence of rockmass properties at the plastic zone around a circular tunnel……....1674

Asteriou P., Saroglou H. and Tsiambaos G.: Rockfalls: influence of rock hardness on the trajectory of falling rock blocks…..……1684

Chatziangelou M. and Christaras B.: Rock mass blastability dependence on rock mass quality……..…1694

Konstantopoulou G. and Spanou N.: Stability analysis of construction and demolition waste (CDW) deposits in theabandoned quarry of Profitis Ilias, Kozani, Greece…….…….1706

Kotsanis D., Panagiotopoulos P., Rozos D. and Loupasakis C.: Engineering geological mapping of the Pallini urban area……....1715

Ktena St. and Sabatakakis N.: Correlation between mechanical and petrographic parameters of sandstones……...…..1726

Lekkas E., Alexoudi V. and Lialiaris I.: Reduction of rockfall risk of the Teleferik area of Santorini-Greece……...1731

Loupasakis C., Lalos G. and Rozos D.: Safety assessment and remedial measures design for an extensive rockfall along the main road to Kimi, East Euboea, Greece…….1739

Marinos V. and Goricki A.: The engineering geological behaviour of disturbed and weatherd gneiss in slopes. The case of the "vertical axis" of Egnatia motorway, Komotini - Nymfea, Northern Greece……..….1749

Marinos V., Lazaridou S., Perleros V. and Sotiropoulou K.: Engineering geological behaviour of recent conglomerate deposits in dam foundation. The case of Agiokampos dam in Thessaly, Central Greece…….1759

Minos-Minopoulos D., Pavlopoulos K., Apostolopoulos G., Dominey-Howes D. and Lekkas E.: Preliminary results of investigations of possible ground deformation structures in the early christian basilica, ancient Lechaion harbour, Corinth, Greece…….1769

Mourtzas N.D., Gkiolas A. and Kolaiti E.: Stabilization of the limestone escarpment of the Skete of Osios Nikanoras under wet conditions due to future filling of the Ilarion dam's reservoir……1779

Mourtzas N.D., Gkiolas A., Vakiris D. and Soulis V.: Investigation and mitigation of a failure at the Taxiarches canal of Mornos aqueduct……..…1792

Mourtzas N.D. and Sotiropoulos E.: Palaeotectonic environment and landslide phenomena in the area of Malakasa, Greece…….1805

Pavlaki A., Meladiotis I. and Pavlakis P.: Applicability of the "Lefka Ori" Western Crete region "GeoFactors" Interaction Matrix (GFIM) as a key to understanding the engineering geological condtions……..1820

Profitis E., Kapatos D., Chatzitheodoridis E., Xirouchakis D. and Loupasakis C.: Digital methods for measuring grain size parameters of aggregate–binder mixtures……..….1834

Rozos D., Tsangaratos P., Loupasakis C., Koumantakis I. and Markantonis K.: Assessing areas of slope instability through a spatial decision support system……..1844

Rusi M. and Hoxha P.: CSD correction as a tool for estimating 3d block size distribution…….1854

S**aratsis G. and Stavropoulou M.:** São Paulo cavern-shaft collapse viewed as a trap-door problem……1864

Saroglou H. and Kazilis N.: Engineering geological conditions of Klokova mountain, Greece……...…1872

Sideri D., Modis K. and Rozos D.: Application of geostatistical simulation models in the characterization of complex geological structures…….1882

Steiakakis E., Vafidis A., Manoutsoglou E. and Vavadakis D.: Influence of geological and geotechnical conditions to design of a water reservoir in karst area…….1892

Tsangaratos P. and Benardos A.: Applying artificial neural networks in slope stability related phenomena……1901

Γεωθερμία
Geothermics

Chatzigiannis G. and Kavouridis Th.: The geothermal occurrence of Kapistri, Ierapetra area, Crete……...……1914

D'Alessandro W., Gagliano A.L., Kyriakopoulos K. and Parello F.: Hydrothermal methane fluxes from the soil at Lakki plain (Nisyros Island, Greece)…….1920

Kanellopoulos C.: Various morphological types of thermogenic travertines in Northern Euboea and Eastern Central Greece……1929

Papachristou M., Ungemach P. and Fytikas M.: Geothermal resource management-a reservoir simulation approach - the Paris Basin case……1939

Skianis G.Aim. and Vaiopoulos A.D.: Mapping hydrothermal alteration zones from spectral band ratios: A geostatistical approach based on the stable semivariogram model……1949

Έρευνα και Εκμετάλλευση Ορυκτών Πόρων
Exploration and Exploitation of Mineral Resources

Agioutantis Z., Komnitsas K. and Athousaki A.: Aggregate transport and utilization: Ecological footprint and environmental impacts……1960

Elia C., Konstantopoulos P., Maravelis A. and Zelilidis A.: The tectono-stratigraphic evolution of Eastern Mediterranean with emphasis on Herodotus Basin prospectivity for the development of hydrocarbon fields……1970

Kapageridis I., Apostolikas A., Pappas S. and Zevgolis I.: Use of mine planning software for the evaluation of resources and reserves of a sedimentary nickel deposit……1980

Mpalatsas I., Rigopoulos I., Tsikouras B., and Hatzipanagiotou K.: Evaluation of cretaceous limestones from the Aitoloakarnania province (Western Greece) for their use as road aggregates in terms of their content in swelling clay minerals……1990

Pantelaki O., Bellis G. and Stamboliadis E.: The upgrading amenability of the phosphate deposits of Western Greece……2000

Shehu Ar. and Shehu Ag.: "Extractive Industries Transparency Initiative - EITI" Outlook on the explotation of Albanian mineral resources……2010

Βιομηχανικά Ορυκτά και Πετρώματα
Industrial Minerals and Rocks

Bourliva A., Michailidis K., Sikalidis C. and Filippidis A.: Spectroscopic and thermal study of bentonites from Milos Island, Greece……2020

Galetakis M., Zourbakis V., Koinakis I., Leventakis K. and Alevizos G.: Aggregate production on the Island of Crete, Greece: Current production conditions and future perspective……2030

Leontakianakos G., Baziotis I., Profitis E., Chatzitheodoridis E. and Tsimas S.: Assessment of the quality of calcination of marbles from Thassos Island using Raman spectroscopy and X-Ray Diffraction……2040

Skliros V., Lampropoulou P.G., Tsikouras B., Hatzipanagiotou K., Christogerou A. and Angelopoulos G.N.: Characterization of a new laboratory ceramic product from industrial by-products as raw materials and caustic magnesia as additive……2050

Tseni X., Tsikouras B. and Hatzipanagiotou K.: Suitability assessment of carbonate rocks from the kataraktis passage member of the Olonos-Pindos Zone (Ileia prefecture, Western Greece) for industrial applications……2059

Xirouchakis D.: Correlations between mechanical and geometrical parameters in aggregates: A tool for quality assessment and control……2069

Xirouchakis D. and Bouzinos A.: Geological materials testing and uncertainty calculations: A simple GUM-based algorithm……..……..……..2081

Ενεργειακές Πρώτες Ύλες
Energy Resources

Koukouzas N., Katsimpardi I. and Merachev D.: Simulation of underground coal gasification process in a Bulgarian coal field…..……..……..2090

Mpotziolis Ch., Kostopoulou S., Triantaphyllou M., Maravelis A. and Zelilidis A.: Depositional environments and hydrocarbon potential of the Miocene deposits of Zakynthos Island……..…..2101

Oskay R.G., Inaner H., Karayigit A.I. and Christanis K.: Coal deposits of Turkey: Properties and importance on energy demand……2111

Papanicolaou C., Typou J., Ioakeim J., Kotis Th. and Foscolos A.: The prospect of using Greek lignite in an energy portfolio related to power generation…….2121
Rigakis N., Karakitsios V., Marnelis F. and Sotiropoulos Sp.: Geological solutions concluded by petroleum geochemical data in Western Greece……2131

Δελτίο της Ελληνικής Γεωλογικής Εταιρίας, τομ. XLVII , 2013
Πρακτικά 13ου Διεθνούς Συνεδρίου, Χανιά, Σεπτ. 2013

Bulletin of the Geological Society of Greece, vol. XLVII 2013
Proceedings of the 13th International Congress, Chania, Sept. 2013

ΜΕΤΑΛΛΕΥΤΙΚΗ ΚΑΙ ΜΕΤΑΛΛΟΥΡΓΙΚΗ ΔΡΑΣΤΗΡΙΟΤΗΤΑ ΤΩΝ ΠΡΟΪΣΤΟΡΙΚΩΝ ΚΑΤΟΙΚΩΝ ΤΟΥ ΑΙΓΑΙΑΚΟΥ ΚΑΙ ΠΕΡΙ-ΑΙΓΑΙΑΚΟΥ ΧΩΡΟΥ:

ΜΙΑ ΓΕΩΜΥΘΟΛΟΓΙΚΗ ΠΡΟΣΕΓΓΙΣΗ

Μαριολάκος Η.Δ.[1]

[1] *National and Kapodistrian University of Athens, Faculty of Geology and Geoenvironment, Department of Dynamic, Tectonic and Applied Geology mariolakos@geol.uoa.gr*

Περίληψη

Η ανακάλυψη, η επεξεργασία και η χρήση των μετάλλων είναι η τέταρτη στη σειρά πολιτιστική επανάσταση του Homo sapiens. Η πρώτη είναι η κατασκευή των λίθινων εργαλείων, η δεύτερη η ανακάλυψη και η χρήση της φωτιάς και η τρίτη η ανακάλυψη της Γεωργίας.

Η πέμπτη επανάσταση είναι η ανακάλυψη των κραμάτων.

Με την αναζήτηση μεταλλευμάτων συνδέονται σημαντικοί πρωταγωνιστές της Ελληνικής Μυθολογίας όπως ο Τιτάνας Κρόνος, που πρέπει να δραστηριοποιήθηκε κατά την Μινωική εποχή, ο Κάδμος και ο Θάσος, ο Φρίξος και η Έλλη, οι Αργοναύτες, ο Ηρακλής, ο Προμηθέας.

Ο θεός που ασχολείται με την μεταλλουργία και την επεξεργασία των μετάλλων είναι ο Ήφαιστος, ο οποίος δεν ορίζει μόνον τη φωτιά, αλλά είναι και ο μεγάλος θεός της εξελιγμένης τεχνολογίας της εποχής, αφού είναι ο πρώτος που παράγει κράματα, όπως είναι ο μπρούντζος.

Ένας άλλος μεγάλος Τιτάνας που συνδέεται με την μεταλλουργία, και συγκεκριμένα με αυτή του σιδήρου, είναι ο Προμηθέας, ο οποίος σύμφωνα με τον μύθο, πήρε ή έκλεψε τη φωτιά από τον Όλυμπο ή τον Ουρανό, και την έφερε στον κόσμο. Αυτό θεωρήθηκε «έγκλημα» από τους Ολύμπιους. Έτσι, αποφάσισαν να τον τιμωρήσουν, αλυσοδένοντάς τον σε μια πλαγιά του όρους Καυκάσος.

Η χρήση των μετάλλων άλλαξε το πολιτισμικό, οικονομικό, κοινωνικό, πολιτικό και ναυτιλιακό καθεστώς σε παγκόσμια κλίμακα, ήδη από την προϊστορική εποχή.

Το πλέον τυπικό παράδειγμα είναι η Κρήτη, που ενώ στερείται πρακτικά ορυκτού πλούτου, αυτό δεν την εμπόδισε να γίνει η μεγαλύτερη ναυτική και εμπορική – οικονομική δύναμη του κόσμου. Μια δύναμη που πρέπει να κυριάρχησε για πάνω από 1000 χρόνια τουλάχιστον. Οι Μινωίτες πρέπει να υπήρξαν πρωτοπόροι της εξάπλωσης της οικονομικής και ναυτικής κυριαρχίας σ' ολόκληρο τον κόσμο, από τις Ινδίες μέχρι τη Βόρειο Αμερική, και όλα αυτά μέχρι την μεγάλη έκρηξη του ηφαιστείου της Σαντορίνης, όταν η σκυτάλη πέρασε στους Μυκηναίους, που έφτασαν στο απόγειό τους με τον Ηρακλή και την Αργοναυτική Εκστρατεία.

Η Μινωική και Μυκηναϊκή κυριαρχία, που πρέπει να διήρκεσε πάνω από 2000 χρόνια, τελειώνει με την κατάρρευση του Μυκηναϊκού Πολιτισμού και την επακόλουθη περίοδο, που είναι γνωστή ως «σκοτεινοί αιώνες».

Λέξεις κλειδιά: *χαλκός, κράματα, ναυτιλία, εμπόριο, μινωική εποχή.*

1. Εισαγωγή

Πριν 2,5 εκατομμύρια χρόνια ένα νέο γένος ζωικού οργανισμού εμφανίστηκε στη Γη, το γένος Homo, που εξελίχθηκε ταχύτατα. Μέσα σε 2.000.000 χρόνια περίπου εμφανίστηκαν τέσσερα είδη: ο Homo habilis, ο H.erectus, ο H.neanderthalensis και ο H. sapiens. Σήμερα υπάρχει μόνον το είδος Homo sapiens, δηλαδή το είδος μας.

Το γένος Homo διαφέρει από όλα τα άλλα είδη, επειδή είναι το μόνο που χρησιμοποίησε την νοημοσύνη και τις δεξιότητές του για να κατασκευάσει εργαλεία.

Τα εργαλεία (Εικ. 1) είναι πολύ σημαντικά κατασκευάσματα επειδή αυξάνουν τη δύναμη του ανθρώπου. Ως υλικό χρησιμοποίησε όχι οποιονδήποτε λίθο, αλλά τον σκληρό λίθο, αυτόν που περιέχει λίγο ή πολύ SiO_2.

Τα εργαλεία είναι η πρώτη μεγάλη τεχνολογική επανάσταση του Homo.

Με βάση τα λίθινα εργαλεία η εποχή του Homo μπορεί να διακριθεί σε διάφορες περιόδους, όπως δίδονται στην Εικ. 2.

Στην Εικ. 3 δίδονται οι μεγάλοι σταθμοί της πολιτισμικής εξέλιξης του γένους Homo. Σύμφωνα με τα μέχρι τις μέρες μας αποτελέσματα της επιστημονικής έρευνας, διαπιστώνονται δύο καθοριστικής σημασίας επιτεύγματα του γένους μας που επειδή άλλαξαν την όλη εξελικτική πορεία του ανθρώπινου πολιτισμού, χαρακτηρίζονται ως πολιτισμική επανάσταση.

Μετά την κατασκευή και χρήση των εργαλείων, η *δεύτερη* μεγάλη πολιτισμική επανάσταση είναι η *χρήση της φωτιάς,* που προσδιορίζεται χρονικά πριν 1,5 εκατομμύρια χρόνια.

Η *τρίτη επανάσταση που είναι η ανακάλυψη της Γεωργίας*, έγινε πάρα πολύ αργότερα. Πιο συγκεκριμένα πρέπει να ξεκίνησε πριν 12.000 χρόνια και να ολοκληρώθηκε κατά την *Μεσολιθική Εποχή*.

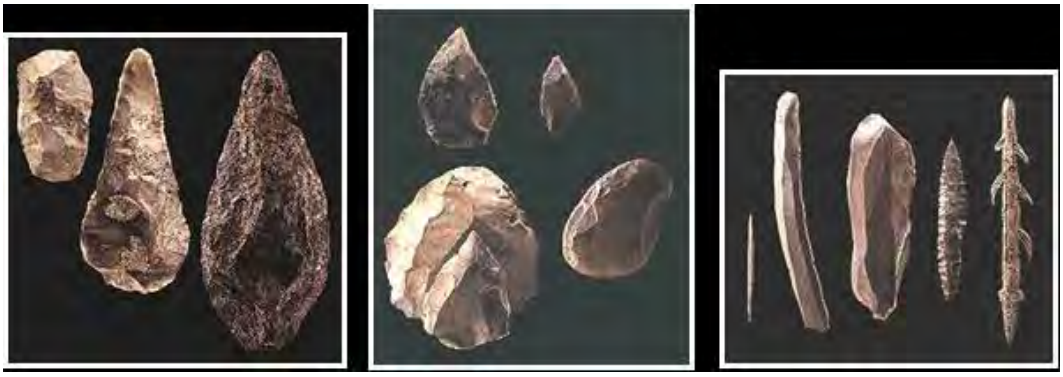

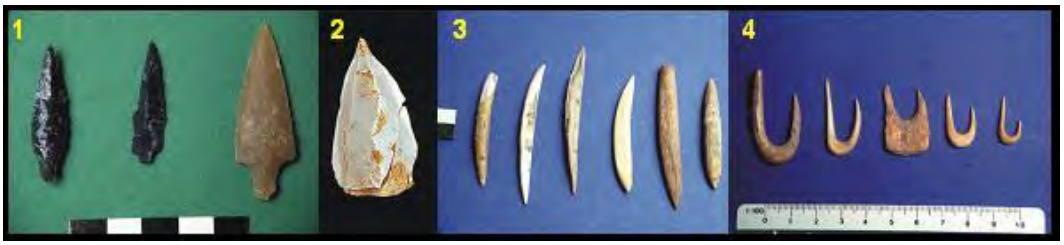

Εικόνα 1 – Λίθινα και οστέινα εργαλεία διαφόρων σταδίων εξέλιξης του λίθινου πολιτισμού. 1. Σαρακηνό Βοιωτίας 2:Βαρχοσκεπή Μποϊλα Ιωαννίνων, 3, 4: Σπήλαιο Κύκλωπας Αλοννήσου.

ΑΠΟ ΤΟ ΒΥΖΑΝΤΙΟ ΣΤΟ ΝΕΟΤΕΡΟ ΕΛΛΗΝΙΣΜΟ						
ΠΕΡΙΟΔΟΣ ΑΝΕΞΑΡΤΗΤΟΥ ΕΛΛΗΝΙΚΟΥ ΚΡΑΤΟΥΣ	1830 – σήμερα					
ΤΟΥΡΚΟΚΡΑΤΙΑ	1453 – 1830					
ΒΥΖΑΝΤΙΝΗ ΕΠΟΧΗ	330 – 1453					
ΕΠΟΧΗ ΣΙΔΗΡΟΥ						
ΡΩΜΑΪΚΗ	146 π.Χ. – 330 μ.Χ.					
ΕΛΛΗΝΙΣΤΙΚΗ	323 – 146 π.Χ.					
ΚΛΑΣΣΙΚΗ	480 - 323 π.Χ.					
ΑΡΧΑΪΚΗ	700 - 480 π.Χ.					
ΓΕΩΜΕΤΡΙΚΗ	1.100 – 700 π.Χ.					
ΕΠΟΧΗ ΤΟΥ ΧΑΛΚΟΥ	ΗΠΕΙΡΩΤΙΚΗ ΕΛΛΑΔΑ	ΚΥΚΛΑΔΕΣ	ΚΡΗΤΗ	ΧΡΟΝΟΛΟΓΗΣΗ		
	ΥΕ	ΥΚ	ΥΜ	1.600 – 1.070 π.Χ.		
	ΜΕ	ΜΚ	ΜΜ	2.100 – 1.600 π.Χ.		
	ΠΕ	ΠΚ	ΠΜ	3.200 – 2.100 π.Χ.		
ΕΠΟΧΗ ΤΟΥ ΛΙΘΟΥ	ΝΕΟΛΙΘΙΚΗ	6.500 – 3.200 π.Χ. (8.500 – 5.200 π.α.σ.)				
	ΜΕΣΟΛΙΘΙΚΗ	9.000 / 8.000 - 7.000 / 6.500 π.Χ. (11.00 – 8.500 π.α.σ.)				
	ΠΑΛΑΙΟΛΙΘΙΚΗ	ΑΝΩΤΕΡΗ ΠΑΛΑΙΟΛΙΘΙΚΗ	35.000 – 12.000 π.α.σ.			
		ΜΕΣΗ ΠΑΛΑΙΟΛΙΘΙΚΗ	100.000 – 35.000 π.α.σ.			
		ΚΑΤΩΤΕΡΗ ΠΑΛΑΙΟΛΙΘΙΚΗ	1.400.000 – 100.000 χρόνια	Ύστερ. ΚΠ	0,3–0,1 εκ. χρόνια	
				Μέση ΚΠ	0,7-0,3 εκ. χρόνια	
				Πρώιμη ΚΠ	1,4-0,7 εκ. χρόνια	
		ΑΡΧΑΪΚΗ ΠΑΛΑΙΟΛΙΘΙΚΗ	2.500.000 – 1.400.000			

Εικόνα 2 – Διάκριση της εποχής του Homo με βάση τα λίθινα εργαλεία.

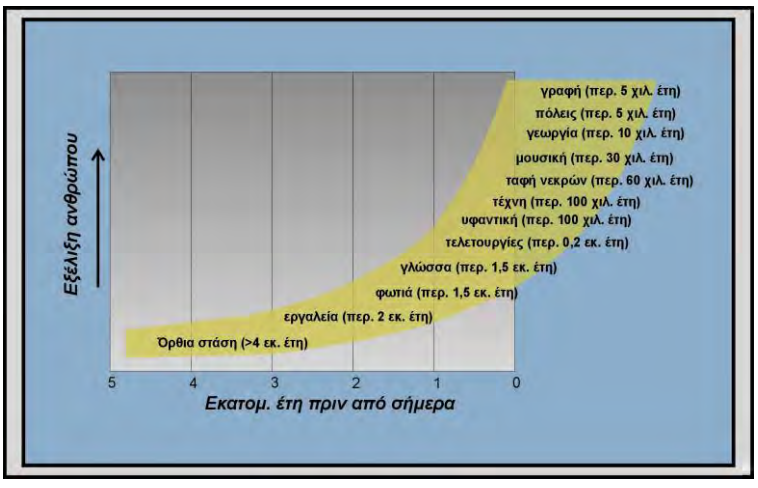

Εικόνα 3 – Η πολιτισμική εξέλιξη του γένους του ανθρώπου και οι σημαντικότερες τεχνολογικές κατακτήσεις.

2. Η εποχή των Μετάλλων - Η 4η Εγάλη Επανάσταση

Μέχρι την 7η χιλιετία π.Χ., και για τα προηγούμενα 2 εκατομ. χρόνια περίπου, ο άνθρωπος στην καθημερινή του ζωή, χρησιμοποιούσε διάφορα εργαλεία που όλα όμως ήσαν λίθινα.

Την περίοδο αυτή, που για την Ελλάδα θεωρείται η έναρξη της Νεολιθικής εποχής (6850 π.Χ.), ο Homo sapiens έχει περάσει τελειωτικά από το στάδιο της *τροφοσυλλογής* στο στάδιο της *τροφοπαραγωγής*.

Από κάποια χρονική στιγμή και μετά όμως, ο άνθρωπος αρχίζει να χρησιμοποιεί και τα *μέταλλα* με πρώτο απ' όλα τον *αυτοφυή χαλκό*. Αυτό συνέβη κάπου στις αρχές της 7ης χιλιετίας π.Χ.

Στη συνέχεια, χρησιμοποιώντας τη φωτιά, αρχίζει την *μεταλλουργική επεξεργασία των μεταλλευμάτων χαλκού*. Αρχικά γινόταν επεξεργασία μόνον *των οξειδίων και των ανθρακικών ενώσεων του χαλκού* και πολύ αργότερα *των θειούχων μεταλλευμάτων* (Εικ. 4).

Η μεταλλουργική επεξεργασία των θειούχων μεταλλευμάτων του χαλκού καθυστέρησε, επειδή δεν είχε ακόμη αναπτυχθεί η *τεχνολογία* της *φρύξης*, που του έδωσε την δυνατότητα να χρησιμοποιήσει και πολλούς άλλους ορυκτούς πόρους. Αυτός είναι και ο κύριος λόγος που καθυστέρησε η αξιοποίηση-εκμετάλλευση των κοιτασμάτων της Κύπρου, που διαθέτει κυρίως μεταλλεύματα θειούχου χαλκού.

Για μεγάλο χρονικό διάστημα λοιπόν παράλληλα με τον λίθο ο άνθρωπος χρησιμοποιούσε και τον χαλκό.

Η πολιτισμική περίοδος αυτή είναι γνωστή ως *Χαλκολιθική*.

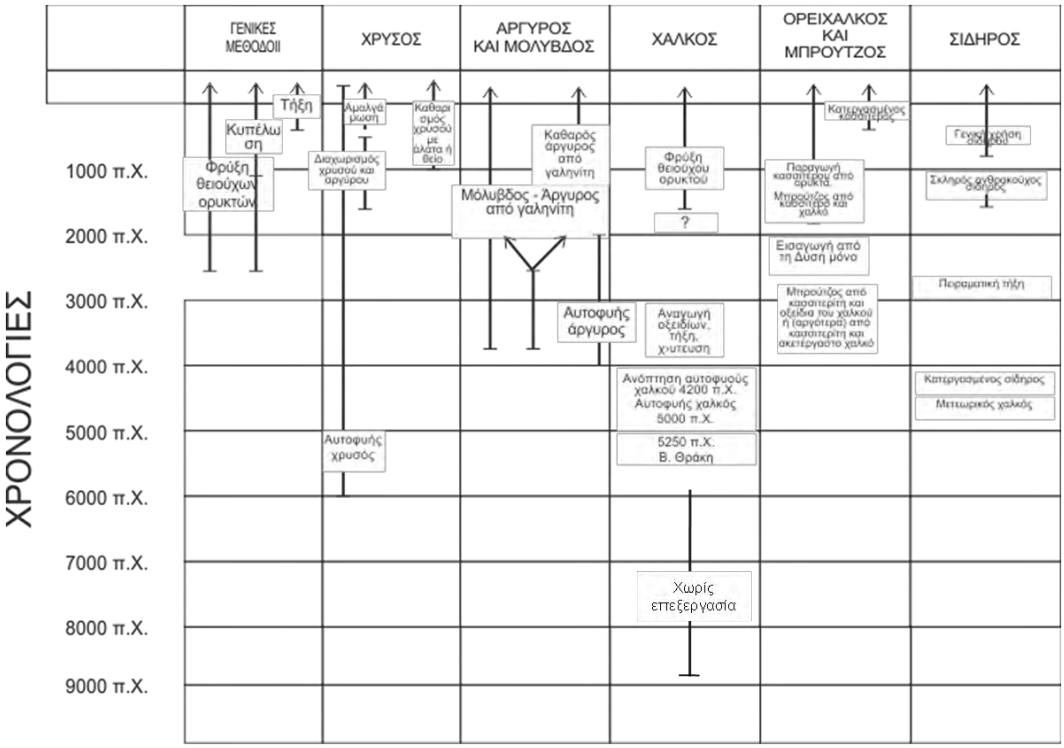

Εικόνα 4 – Χρονολογικός πίνακας της χρήσης και της μεταλλουργικής επεξεργασίας των διαφόρων μετάλλων στον Ελληνικό κόσμο. Ιστορία της Μεταλλευτικής και Μεταλλουργικής δραστηριότητας στον ευρύτερο ελληνικό χώρο (κατά Βασιλόπουλο, με συμπληρώσεις).

Μέχρι τώρα, η Χαλκολιθική εποχή θεωρείται ότι καλύπτει χρονικά το τέλος της Νεολιθικής εποχής, μέχρι και την Πρωτο-Ελλαδική και Πρωτο-Μινωϊκή Εποχή.

Αυτό πρέπει να αναθεωρηθεί για τον Ελλαδικό χώρο, επειδή τελευταία έχει αποδειχτεί ότι η *μεταλλουργική επεξεργασία του χαλκού* έχει ξεκινήσει προς το τέλος της 6ης χιλιετίας π.Χ. (Koukouli & Bassiakos, 2002.). Άρα, η Χαλκολιθική Εποχή αρχίζει κατά το δεύτερο ήμισυ της 6^{ης} χιλιετίας π.Χ. και εκτείνεται μέχρι το τέλος της Νεολιθικής Εποχής.

Η χρήση των μετάλλων και κυρίως η *μεταλλουργική επεξεργασία* τους αποτελεί την *τέταρτη μεγάλη επανάσταση του ανθρώπου*, που διαφέρει όμως πολύ από τις προηγούμενες επειδή, σ' αυτην την περίπτωση, πρόκειται για *τεχνολογική επανάσταση*, αφού ο άνθρωπος παράγει νέα υλικά, νέα μέταλλα που έχουν συγκεκριμένες φυσικομηχανικές ιδιότητες.

Η μεταλλουργία χαλκού, σύμφωνα με τους C.Renfrew και P. Bahn (1991), ξεκίνησε από τρία ανεξάρτητα κέντρα παραγωγής που βρίσκονται βόρεια και ανατολικά από την Μεσοποταμία, ενώ στον Ευρωπαϊκό χώρο υπάρχουν δύο παρόμοια κέντρα: το ένα τοποθετείται στα *βόρεια Βαλκάνια* και το άλλο στην *Ιβηρική* (Εικ. 5).

Επομένως, σύμφωνα με τον προηγούμενο χάρτη, η μεταλλουργική επεξεργασία των χαλκούχων μεταλλευμάτων στον Αιγαιακό και Περιαιγαιακό χώρο, πρέπει να άρχισε γύρω στο 3.500 π.Χ., δηλαδή ξεκίνησε με καθυστέρηση 3.000 χρόνων περίπου, συγκριτικά με τον χρόνο έναρξης στην Μεσοποταμία.

Η άποψη αυτή, όμως μετά τις έρευνες που έγιναν στην περιοχή της Βόρειας Ελλάδας, όπου έχουν βρεθεί μικρές μεταλλουργικές εστίες από το δεύτερο ήμισυ της 6^{ης} ή τις ραχές της 5^{ης} χιλιετίας π.Χ. (Κουκούλη & Μπασιάκος, 2002) δεν ισχύει.

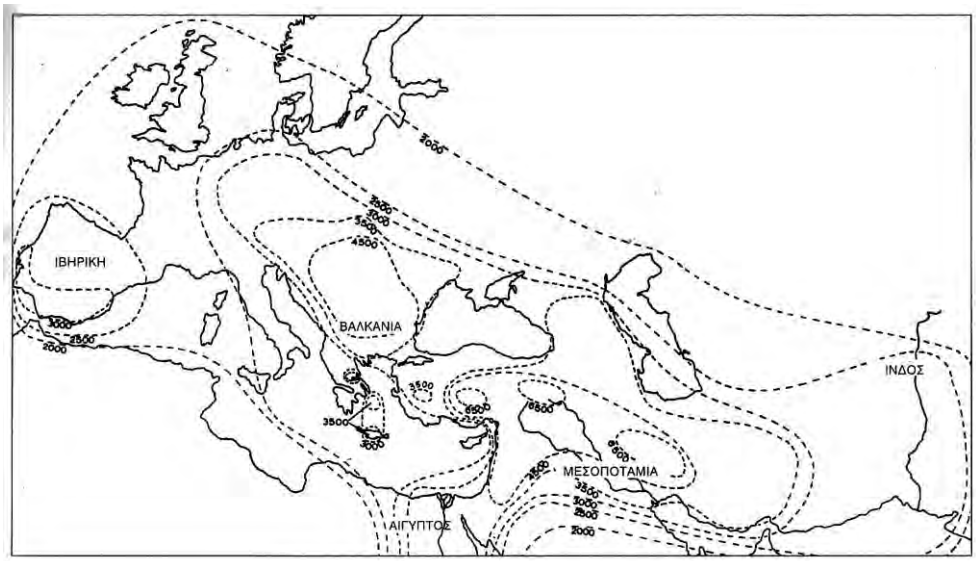

Εικόνα 5 – Οι απαρχές και η εξάπλωση της μεταλλουργίας του χαλκού, κατά C. Renfrew & P. Bahn, 1991. Διακρίνονται τα τρία αρχαιότερα κέντρα μεταλλουργικής επεξεργασίας χαλκού βόρεια της Μεσοποταμίας και το αρχαιότερο της Ευρώπης στα Βαλκάνια.

2.1. Μεταλλουργία Κραμάτων - 5^{η} Πολιτιστική Επανάσταση

Μέχρι και την χαλκολιθική εποχή, ο άνθρωπος εξαρτάτο απόλυτα από την φύση. Αυτό συμβαίνει επειδή τόσο τα πετρώματα που χρησιμοποιούσε για την κατασκευή των λίθινων εργαλείων του, όσο για τη φωτιά και την γεωργική του παραγωγή ακόμα και για τον Χαλκό, προσφέρονται από τη φύση, όπως έχουν, αφού δεν μπορεί να παρέμβει πουθενά ο άνθρωπος.

Όλα αυτά του τα πρόσφερε η *Γαία*, η Μάνα όλων όσων υπάρχουν πάνω στον πλανήτη μας. Ο χαλκός όμως, παρ' ότι χρήσιμος, εν τούτοις παρουσιάζει ορισμένα μειονεκτήματα, επειδή είναι πολύ μαλακός.

Κάποια στιγμή λοιπόν, άγνωστον πως, ο άνθρωπος και μετά από χιλιάδες χρόνια χρησιμοποίησης του χαλκού, ανέπτυξε την τεχνολογία *των κραμάτων*. Πρόκειται για την μεταλλουργική ανάμειξη αρχικά του *χαλκού με το αρσενικό* και στη συνέχεια του *χαλκού με τον κασσίτερο*.

Πίνακας 1 - Συνοπτικός πίνακας των Πολιτιστικών Επαναστάσεων.

Σ υ ν ο π τ ι κ ά

	$1^{η}$ επανάσταση:	Λίθινα Εργαλεία		
	$2^{η}$ επανάσταση:	Φωτιά		
	$3^{η}$ επανάσταση:	Γεωργία – Δήμητρα – Μεσολιθική εποχή		
	$4^{η}$ επανάσταση:	Μέταλλα - χρήση αυτοφυών μετάλλων - Έναρξη $9^{η}$ χιλ. π.Χ.		
		Μεταλλουργική επεξεργασία – $6^{η}$ – $5^{η}$ χιλ. π.Χ.		
		Υπεύθυνος: Ήφαιστος		
→	Μέχρι τώρα:	Pb	Σημείο τήξης :	327 °C
		Ag	Σημείο τήξης :	960 °C
		Au	Σημείο τήξης :	1063 °C
		Cu	Σημείο τήξης :	1083 °C

Άρα: Βάση Χαλκολιθικής εποχής μαζί με την έναρξη της Νεολιθικής (για Ελλάδα 6850 π.Χ.)

→ Άρα, μέχρι τώρα, δηλ. μέσα $2^{ης}$ χιλιετίας π.Χ.:

- Απόλυτος έλεγχος από τη φύση
- Όλα διατίθενται από τη Γαία, τη Μεγάλη Μάνα όλων όσων υπάρχουν πάνω στον πλανήτη μας.

$5^{η}$ επανάσταση:	- Κράματα - Τεχνολογική:
	- Ο άνθρωπος παράγει νέα υλικά
	- Ο άνθρωπος ξεπερνάει τη φύση
	- Μπρούντζο ή κρατέρωμα - αρχικά Cu + As - αργότερα Cu + Sn
	- Ορείχαλκο Cu + Zn
	Υπεύθυνος: **Ήφαιστος**
$5^{η}$ επανάσταση	Υπεύθυνος ο Ήφαιστος που συνέχισε να είναι ο θεός της Μεταλλουργίας όχι της Μεταλλευτικής
$6^{η}$ επανάσταση:	Μεταλλουργία Fe
	Υπεύθυνος: **Προμηθέας**
	- Νέα πυροτεχνολογία
	- Παραγωγή θερμοκρασιών (>1500°C)
	- Άρα πολύ μεγαλύτερη από εκείνη των Ηφαιστείων (~1100°C)
	- Θερμοκρασίες που δεν υπάρχουν στην επιφάνεια της γης
	ΑΡΑ: ο Προμηθέας ξεπερνάει την Γαία και τον παντοδύναμο Δία.

Έτσι παρήγαγε ένα εντελώς νέο υλικό, που είναι γνωστό ως *μπρούντζος* ή *κρατέρωμα*.

Πολύ αργότερα παρήγαγε ένα άλλο κράμα, αυτή τη φορά *χαλκού* και *ψευδάργυρου*, που είναι γνωστό ως *ορείχαλκος*.

Όλα αυτά τα κράματα πλεονεκτούν έναντι του χαλκού, επειδή παρουσιάζουν πολύ μεγαλύτερη σκληρότητα.

Αξίζει να σημειωθεί ότι η τεχνολογία είχε αναπτυχθεί σε τέτοιο βαθμό, ώστε είχαν την δυνατότητα να παραγάγουν κράματα με συγκεκριμένη σκληρότητα.

Από τα μέσα της 2ης χιλιετίας π.Χ. η μεταλλουργία χαλκού αναπτύσσει την μέθοδο της *φρύξης*. Η νέα αυτή τεχνολογία επέτρεψε να χρησιμοποιηθούν και μεταλλεύματα *θειούχου χαλκού* για την παραγωγή χαλκού. Από την περίοδο αυτή και μετά αρχίζει η ουσιαστική ανάδειξη των κοιτασμάτων της Κύπρου με τα πλούσια μεταλλεύματα του *Όρου Τρόοδος, επειδή εκεί αναπτύσσεται μεταλλοφορία θειούχου χαλκού κυρίως*.

2.2. Πότε Άρχισε η Μεταλλευτική Δραστηριότητα;

Πότε ακριβώς άρχισε να χρησιμοποιείται ο χαλκός, είναι δύσκολο να προσδιοριστεί. Παρά ταύτα, υπάρχουν ορισμένα αρχαιολογικά ευρήματα που δείχνουν ότι η πρώτη χρήση, χωρίς σχεδόν επεξεργασία, πρέπει να έγινε στο Β. Ιράκ κάπου μεταξύ 8700 έως 9000 π.Χ., δηλαδή από τη Μεσολιθική Εποχή.

Ο *χρυσός* εμφανίστηκε γύρω στο 6000 π.Χ., ενώ ο *άργυρος* γύρω στο 4000 π.Χ. Τεχνουργήματα από *μόλυβδο* έχουν βρεθεί στο Catalhoyouk που έχουν χρονολογηθεί γύρω στο 3500 π.Χ.μ ενώ ο κασσίτερος εμφανίζεται πολύ αργότερα, στις αρχές της 2^{ης} χιλιετίας π.Χ.

Ο χρυσός έχει χρησιμοποιηθεί ως κόσμημα, ως φυσικό κράμα με άργυρο, που είναι γνωστό ως **ήλεκτρο**. Πολλά κοσμήματα εξάλλου κατασκεύαζαν οι Σουμέριοι ήδη από το 3000 π.Χ.

3. Έλλειψη Μεταλλευμάτων

Μετά την ανακάλυψη της μεταλλουργίας η χρήση όλων των μετάλλων, αλλά ιδιαίτερα του χαλκού, αυξήθηκε τόσο πολύ, ώστε από κάποια χρονική στιγμή και μετά η ζήτηση σε μεταλλεύματα χαλκού και κασσιτέρου στις αναπτυγμένες χώρες της προϊστορικής εποχής πρέπει να αυξήθηκε κατακόρυφα. Σ'αυτή την έλλειψη, πέραν της αυξημένης ζήτησης συνέβαλαν και οι ακόλουθοι δύο ακόμη παράγοντες:

1. Οι παλαιές μέθοδοι μεταλλουργικής επεξεργασίας των μεταλλευμάτων χαλκού, που δεν επέτρεπε ακόμη την εκμετάλλευση των θειούχων μεταλλευμάτων χαλκού, με αποτέλεσμα να μην είναι αξιοποιήσιμα τα τεράστια αποθέματα της Κύπρου, και
2. Η καταστροφή τεραστίων εκτάσεων δασών της Μ.Ασίας, που είχαν χρησιμοποιηθεί στην μεταλλουργική επεξεργασία μεταλλευμάτων του κασσίτερου.

Έχει εκτιμηθεί ότι για την παραγωγή ενός κιλού κασσίτερου έπρεπε να καούν... Έτσι ορισμένοι πιστεύουν ότι ελλείψει ενέργειας μειώθηκε ή και σταμάτησε η παραγωγή κασσιτέρου. Αυτό ανάγκασε τους αναπτυγμένους λαούς της Ανατολικής Μεσογείου να αναζητήσουν πρώτες ύλες εκτός Αιγαιακού και Περιαιγαιακού χώρου. Για να επιτευχθεί όμως αυτό, πρέπει να πληρούνται ορισμένες προϋποθέσεις όπως:

1. Να ξεκινήσει η έρευνα και η αναζήτηση μεταλλευμάτων προς όλες τις κατευθύνσεις, αρχικά γύρω από την Δυτική Μεσόγειο κυρίως και στη συνέχεια εκτός αυτής.
2. Να αναπτυχθεί η ναυτιλία και το εμπόριο, και
3. να αναπτυχθούν νέες τεχνολογίες, αλλά και πολιτικές, διπλωματικές, εμπορικές και άλλες σχέσεις με τους λαούς που ζούσαν στις μεταλλοφόρες περιοχές.

3.1. Οι Πρωτοπόροι της Ναυτιλίας και του Εμπορίου

Οι πρωτοπόροι αυτοί που διαμόρφωσαν τις προϋποθέσεις για την ανάπτυξη της Ναυτιλίας αρχικά και του Εμπορίου στη συνέχεια ή και συγχρόνως, αλλά και την αναζήτηση φυσικών πόρων, όπως εμμέσως περιγράφεται στην Ελληνική Μυθολογία, είναι τρεις Τιτάνες, ο Ωκεανός, ο Άτλας και ο Κρόνος.

3.1.1. Ο Ωκεανός

Ο πρώτος είναι ο *Ωκεανός*, ο οποίος δεν συμμετείχε την Τιτανομαχία, επειδή ίσως είχε φύγει από τον Αιγαιακό χώρο και πήγε δυτικά. Εκεί προφανώς μελέτησε το τεράστιο φυσικο-ωκεανογραφικό σύστημα, τον *Ωκεανό*, που πήρε και τ' όνομά του.

Σύμφωνα με τον *Όμηρο* και τον *Ησίοδο*, ο *Ωκεανός* έχει τα ακόλουθα φυσικό- ωκεανογραφικά χαρακτηριστικά:

1. Είναι ένας *μεγάλος ποταμός*, που περιβάλλει την Γή και δεν σταματάει να ρέει ποτέ (Εικ. 6).
2. Ο ποταμός Ωκεανός είναι:
   - Αψόρροος: δηλαδή παρουσιάζει μια τυρβώδη ροή.
   - Οπισθόρρος: δηλαδή δεν ρέει μόνον προς τα εμπρός, αλλά κατά θέσεις ρέει και προς τα πίσω.
   - Βαθύρροος: ο ποταμός Ωκεανός δεν ρέει μόνο επιφανειακά, αλλά και σε βάθος.
   - Βαθυδίνης: ο χαρακτηρισμός αυτός δεν αφήνει καμιά αμφιβολία, ότι η ροή στο βάθος είναι και αυτή τυρβώδης.

Αν παρατηρήσει κάποιος την Εικ. 6α, τότε διαπιστώνει τα ακόλουθα:

1. Ότι ο ποταμός Ωκεανός αντιπροσωπεύει τα άγνωστα ρεύματα που αναπτύσσονται σε όλους τους Ωκεανούς, όπως για παράδειγμα είναι το *Gulf Stream* το γνωστό *Ρεύμα του Κόλπου* στον Ατλαντικό Ωκεανό.
2. Ότι τα ρεύματα δεν αναπτύσσονται μόνον στην επιφάνεια, αλλά και σε βάθος (βαθύρροος).
3. Ότι ο ποταμός Ωκεανός, δηλαδή τα ρεύματα, περιβάλλουν ολόκληρη τη Γη.

Εικόνα 6 – α) Ο Τιτάνας Ωκεανός και η Τιτανίδα Τηθύς, οι γεννήτορες και των ποταμών, β) τα μεγάλα ρεύματα – ο Ωκεανός πόταμός – ψυχρά και θερμά, επιφανειακά και βαθειά, που περιβάλλουν την Γη. Στον Ατλαντικό διακρίνεται και η πορεία του Ρεύματος του Κόλπου.

Η Εικ. 7 δείχνει πως φαίνεται ο Ωκεανός από δορυφόρο και συγκεκριμένα την πορεία του *Ρεύματος του Κόλπου* από την περιοχή των ακτών της Florida με κατεύθυνση προς Βορειοανατολικά, προς την Ευρώπη. Στην εικόνα αυτή διακρίνονται τα ακόλουθα:

1. η τυρβώδης ροή, δηλαδή ο *αψόρροος χαρακτήρας* του ποταμού και
2. το *οπισθόρροον* της πορείας του.

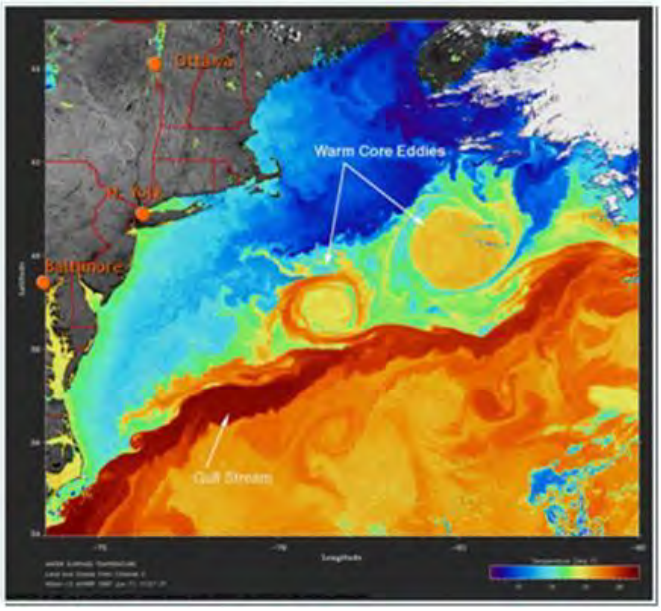

Εικόνα 7 – Δορυφορική εικόνα του Ρεύματος του Κόλπου, όπου διακρίνεται ο αψόρροος και ο οπισθόρροος χαρακτήρας του.

Για να αναπτυχθεί όμως η ναυτιλία και το εμπόριο δεν αρκεί μόνον η γνώση των Ωκεανών πρέπει να είναι γνωστά και τα *εσωτερικά νερά*, οι *μεγάλες λίμνες* και τα *μεγάλα ποτάμια*.

Σχετικά με τα *εσωτερικά νερά* οι Προϊστορικοί Έλληνες γνώριζαν πολύ καλά τόσον τον *Εύξεινο Πόντο* όσο και την *Μαιώτιδα* (την σημερινή Αζοφική) αλλά και την *Βαλτική θάλασσα*, που ήταν γνωστή ως *Σαρματική θάλασσα*. Γνώριζαν ακόμη και την *Κασπία θάλασσα*.

Από τους ποταμούς, που σύμφωνα με τον Ησίοδο είναι παιδιά του *Τιτάνα Ωκεανού* και της *Τιτανίδας Τηθύος*, αναφέρονται πάρα πολλοί και μάλιστα όχι μόνον από τον ευρύτερο Περιαιγαιακό χώρο (αλλά και πάρα πολλοί από χώρους εκτός Ελλάδας, όπως είναι ο *Νείλος*, ο *Ίστρος* (Δούναβης), ο *Βορυσθένης* (Δνείπερος), ο *Ταναΐς* (Δον), ο *Ρας* ή *Ρα* ή *Ρως* (Βόλγας) και πάρα πολλοί άλλοι.

3.1.2. Ο Άτλας

Ο *Άτλας* είναι ο άλλος Τιτάνας που πρέπει να συνέβαλε στην ανάπτυξη της ναυτιλίας. Σύμφωνα με την Ελληνική Μυθολογία, μετά την Τιτανομαχία, στην οποία συμμετείχε, εξορίστηκε από τον Δία στην ΒΔ-ική Αφρική. Εκεί έγινε μεγάλος βασιλιάς και έδωσε τ! όνομά του στο όρος Άτλας, αλλά και στον Ωκεανό που έκτοτε είναι γνωστός ως *Ατλαντικός* (Εικ. 8).

Ο Άτλας ήταν υπεύθυνος για την φύλαξη των χρυσών μήλων των Εσπερίδων. Οι Εσπερίδες κατοικούσαν δυτικά της Αφρικής. Δυτικά της Αφρικής όμως υπάρχει ο Ωκεανός, διάφορα νησιά, όπως οι *Αζόρες*, η *Μαδέρα*, τα *Κανάρια*, τα νησιά του *Πράσινου Ακρωτηρίου* και φυσικά τα *νησιά της Καραϊβικής*. Πέραν αυτών βεβαίως υπάρχει και μία ήπειρος. Κάπου εκεί τοποθετεί ο Όμηρος τον Άδη, εκεί που πήγε ο Οδυσσέας να βρει τις ψυχές κ.λπ.

Οι *Εσπερίδες* επομένως θα πρέπει να κατοικούσαν σε κάποιο απ'αυτά τα μέρη. Θα πρέπει να σημειωθεί ότι, όταν ο Ηρακλής πήγε να φέρει τα μήλα των Εσπερίδων, ο Άτλας ήταν αυτός που τα έφερε από τον Ωκεανό. Συνεπώς πρέπει να γνώριζε τον Ωκεανό και αυτός.

Πέραν όλων αυτών ο Άτλας διεξήγαγε και αστρονομικές παρατηρήσεις που, όπως είναι γνωστό, είναι απαραίτητες για την ανάπτυξη της ναυσιπλοΐας.

α)

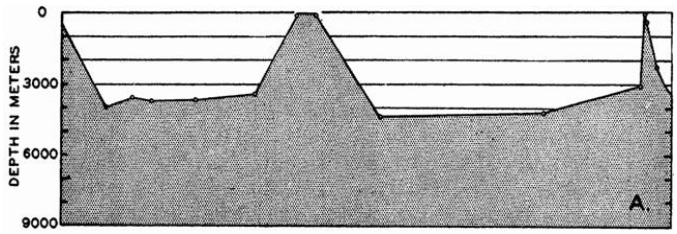

β)

γ)

Εικόνα 8 – α) Ο Βόρειος Ατλαντικός με τα σημαντικότερα ωκεάνια ρεύματα και τα νησιά Αζόρες, Μαδέρα, Κανάρια, Πράσινου Ακρωτηρίου, ως και την Μεσο-Ωκεάνια ράχη, β) τοπογραφική τομή (Α – Δ) εγκάρσια προς τον Ωκεανό (*Stocks and Wüst, 1935*), γ) ο Άτλας μεταφέρει στους ώμους του την Ουράνια σφαίρα.

3.1.3. Ο Κρόνος

Ο *Κρόνος*, ο αρχηγός των Τιτάνων, είναι αυτός που έριξε το θεοκρατικό καθεστώς του πατέρα τους του Ωκεανού, σε συνεργασία με την μητέρα του την *Γαία* και κυριάρχησε στο πολιτισμικό γίγνεσθαι μέχρι την Τιτανομαχία, όπου η γενιά του Δία και του Ποσειδώνα κατατρόπωσαν τους Τιτάνες.

Μετά την ήττα τους και σύμφωνα με μια εκδοχή, ο Κρόνος όπως και ο Άτλας εξορίστηκε και μάλιστα σ' ένα νησί, πολύ μακρυά απ'το Αιγαίο και από την Μεσόγειο. Σε άγνωστους μέχρι τότε τόπους.

Πού βρίσκεται όμως αυτό το νησί;

3.2. Το Νησί της Εξορίας του Κρόνου

Την απάντηση στο τελευταίο ερώτημα δίδει ο Πλούταρχος, ο μεγάλος συγγραφέας που γεννήθηκε στην Χαιρώνεια της Βοιωτίας κατά τον 1ο μ.Χ. αιώνα και ο οποίος πέραν των άλλων, υπήρξε για κάποιο χρονικό διάστημα και Αρχιερέας στο Μαντείο των Δελφών.

Ο πολυγραφότατος Πλούταρχος σε ένα του βιβλίο, που εντάσσεται στα Ηθικά του, και συγκεκριμένα αυτό με τίτλο *"Περί του εμφαινομένου προσώπου τω Κύκλω της Σελήνης"* περιγράφει τον τόπο εξορίας του Κρόνου με τέτοιες φυσικογεωγραφικές λεπτομέρειες, που αν κάποιος πάρει έναν σχολικό γεωγραφικό Άτλαντα, και ακολουθήσει την περιγραφή του, είναι

βέβαιο ότι ακόμα και ένας καλός μαθητής του Γυμνασίου θα καταφέρει να τον προσδιορίσει με ικανοποιητική ακρίβεια.

Από την Εικ. 9 που δίδεται το συγκεκριμένο κείμενο του Πλούταρχου, στο πρωτότυπο και σε μετάφραση, σταχυολογούνται τα ακόλουθα, πολύ συνοπτικά, που είναι και τα πιο σημαντικά σημεία της περιγραφής, επειδή, λόγω χώρου, δεν είναι δυνατόν να αναπτυχθεί με πολλές λεπτομέρειες ολόκληρο το κείμενο. Ο Πλούταρχος μας λέει ότι ο τόπος εξορίας του Κρόνου βρίσκεται *«σ'ένα σημείο ενός από τα τρία νησιά που βρίσκονται δυτικά της Ωγυγίας»*...

Πού βρίσκεται όμως η Ωγυγία;

Σύμφωνα με τον Πλούταρχο *η Ωγυγία βρίσκεται Δυτικά της Βρετανίας σε απόσταση πέντε ημερών ταξίδι με το πλοίο.*

Εάν δεχθούμε ότι ένα ιστιοφόρο πλοίο της εποχής εκείνης, ένα πλοίο δηλαδή παρόμοιο με εκείνο που απεικονίζεται στις τοιχογραφίες του Ακρωτηρίου της Σαντορίνης ή σαν αυτό του ναυαγίου του Uluburun, που είναι νεώτερο του προηγούμενου κατά μερικούς αιώνες, είναι δυνατόν να αναπτύξει ταχύτητα τεσσάρων μιλίων την ώρα (4 m/h) τότε η *Ωγυγία* συμπίπτει με την *Ισλανδία*.

Αυτή η ταχύτητα είναι δυνατόν να αναπτυχθεί κάτω από ευνοϊκές καιρικές συνθήκες, λαμβάνοντας υπ'όψη, επιπλέον, ότι δυτικά από την Βρετανία περνάει ένας κλάδος του Gulf Stream.

Στο συμπέρασμα αυτό καταλήγει κάποιος μετά από τον εξής, πολύ απλό υπολογισμό: 5 ημέρες Χ 24 ώρες Χ 4 μ./ω = 480 μίλια.

Συνεπώς το πλοίο πρέπει να έχει διανύσει μια απόσταση γύρω στα 480 μίλια. Σε μια απόσταση 480 μιλίων δυτικά της Βρετανίας όμως, το μόνο νησί που υπάρχει είναι η *Ισλανδία*.

Ποιά είναι όμως τα τρία νησιά δυτικά της Ωγυγίας (Ισλανδίας);

Τα τρία αυτά νησιά πρέπει να είναι η *Γροιλανδία*, το *Baffin Isl*. και νοτιώτερα η *New Foundland* και ισχυρίζομαι ότι πρέπει να είναι αυτά τα τρία νησιά και όχι άλλα επειδή: (i) είναι τα μεγαλύτερα, (ii) επειδή συμπίπτουν με όσα αναφέρει ο Πλούταρχος (Εικ. 10) και (iii) επειδή δεν υπάρχουν άλλα ανάμεσά τους.

Πού βρίσκεται όμως ακριβώς ο τόπος εξορίας του Κρόνου;

Σύμφωνα με τον Πλούταρχο βρίσκεται σ' ένα σημείο ενός από τα τρία νησιά *«...που ο ήλιος χάνεται μόνον μία ώρα την ημέρα για ένα μήνα...»*. Προφανώς αυτός ο μήνας πρέπει να πέφτει το καλοκαίρι.

Άρα ο τόπος εξορίας του Κρόνου πρέπει να βρίσκεται λίγο νοτιότερα από τον *Πολικό Κύκλο*, δηλαδή λίγο νοτιότερα από τον παράλληλο των 66.5^{o} Βόρειο Πλάτος.

Επειδή από τα τρία αυτά νησιά, η New Foundland βρίσκεται πολύ νοτιότερα, πρέπει να αποκλειστεί αφού ο ήλιος στο νησί αυτό χάνεται πολύ περισσότερες ώρες τους καλοκαιρινούς μήνες. Επομένως ο τόπος εξορίας του Κρόνου πρέπει να βρίσκεται κάπου στις νότιες περιοχές των δύο άλλων νησιών, δηλαδή της Γροιλανδίας και του Baffin Island.

Τί γράφει όμως ακόμη ο Πλούταρχος;

Γράφει τα εξής, κατά την γνώμη μου, συγκλονιστικά για την εποχή εκείνη:

«...δυτικά των τριών αυτών νησιών υπάρχει μία μεγάλη ηπειρωτική χώρα».

Και συνεχίζει:

«...στα παράλια ενός κόλπου της ηπειρωτικής χώρας κατοικούν Έλληνες...»

Ποια όμως μπορεί να είναι αυτή η ήπειρος; Πού μπορεί να βρίσκεται αυτός το Κόλπος; Τί διαστάσεις έχει; Είναι μεγάλος; Είναι μικρός;

941 διάθεσιν. ἐγὼ μὲν οὖν ὑποκριτής εἰμι, πρότερον δ' αὐτοῦ φράσω τὸν ποιητὴν ὑμῖν ••• εἰ μή τι κωλύει, καθ' Ὅμηρον ἀρξάμενος.

Ὠγυγίη τις νῆσος ἀπόπροθεν εἰν ἁλὶ κεῖται',

δρόμον ἡμερῶν πέντε Βρεττανίας ἀπέχουσα πλέοντι πρὸς ἑσπέραν· ἕτεραι δὲ τρεῖς ἴσον ἐκείνης ἀφεστῶσαι καὶ ἀλλήλων πρόκεινται μάλιστα κατὰ δυσμὰς ἡλίου θερινάς. ὧν ἐν μιᾷ τὸν Κρόνον οἱ βάρβαροι καθεῖρχθαι μυθολογοῦσιν ὑπὸ τοῦ Διός, † τὸν δ' ὡς υἱὸν ἔχοντα φρουρὸν τῶν τε νήσων ἐκείνων καὶ τῆς θαλάττης, ἣν Κρόνιον
B πέλαγος ὀνομάζουσι, παρακατῳκίσθαι. τὴν δὲ μεγάλην ἤπειρον, ὑφ' ἧς ἡ μεγάλη περιέχεται κύκλῳ θάλαττα, τῶν μὲν ἄλλων ἔλαττον ἀπέχει, τῆς δ' Ὠγυγίας περὶ πεντακισχιλίους σταδίους κωπήρεσι πλοίοις κομιζομένῳ· (βραδύπορον γὰρ εἶναι καὶ πηλῶδες ὑπὸ πλήθους ῥευμάτων τὸ πέλαγος· τὰ δὲ ῥεύματα τὴν μεγάλην ἐξιέναι γῆν καὶ γίνεσθαι προχώσεις ἀπ' αὐτῶν καὶ βαρεῖαν εἶναι καὶ γεώδη τὴν θάλατταν, ᾗ καὶ πεπηγέναι δόξαν ἔσχε). τῆς δ' ἠπείρου τὰ πρὸς τῇ θαλάττῃ κατοικεῖν Ἕλληνας περὶ κόλπον οὐκ ἐλάττονα τῆς Μαιώτιδος, οὗ τὸ στόμα
C τῷ στόματι τοῦ Κασπίου πελάγους μάλιστα κατ' εὐθεῖαν κεῖσθαι· καλεῖν δὲ καὶ νομίζειν ἐκείνους ἠπειρώτας μὲν αὐτοὺς <νησιώτας δὲ τοὺς> ταύτην τὴν γῆν κατοικοῦντας, ὡς καὶ κύκλῳ περίῤῥυτον οὖσαν ὑπὸ τῆς θαλάσσης· οἴεσθαι δὲ τοῖς Κρόνου λαοῖς ἀναμιχθέντας ὕστερον τοὺς μεθ' Ἡρακλέους παραγενομένους καὶ ὑπολειφθέντας ἤδη σβεννύμενον τὸ Ἑλληνικὸν ἐκεῖ καὶ κρατούμενον γλώττῃ τε βαρβαρικῇ καὶ νόμοις καὶ διαίταις οἷον ἀναζωπυρῆσαι πάλιν ἰσχυρὸν καὶ πολὺ γενόμενον· διὸ τιμὰς ἔχειν πρώτας τὸν Ἡρακλέα, δευτέρας δὲ τὸν Κρόνον.

Ὅταν οὖν ὁ τοῦ Κρόνου ἀστὴρ, ὃν Φαίνοντα μὲν ἡμεῖς, ἐκείνους δὲ Νυκτοῦρον ἔφη καλεῖν, εἰς Ταῦρον παραγένηται δι' ἐτῶν τριάκοντα, παρασκευασαμένους ἐν
D χρόνῳ πολλῷ τὰ περὶ τὴν θυσίαν καὶ τὸν ἀ... ἐκπέμπειν κλήρῳ λαχόντας ἐν πλοίοις τοσούτοις θεραπείαν τε πολλὴν καὶ παρασκευὴν ἀναγκαίαν μέλλουσι πλεῖν πέλαγος τοσοῦτον εἰρεσίᾳ καὶ χρόνον ἐπὶ ξένης βιοτεύειν πολὺν ἐμβαλλομένους. ἀναχθέντας αὖν χρῆσθαι τύχαις, ὡς εἰκός, ἄλλους ἄλλαις, τοὺς δὲ διασωθέντας ἐκ τῆς θαλάττης πρῶτον μὲν ἐπὶ τὰς προκειμένας νήσους οἰκουμένας δ' ὑφ' Ἑλλήνων κατίσχειν καὶ τὸν ἥλιον ὁρᾶν κρυπτόμενον ὥρας μιᾶς ἔλαττον ἐφ' ἡμέρας τριάκοντα· καὶ νύκτα τοῦτ' εἶναι, σκότος ἔχουσαν ἐλαφρὸν καὶ λυκαυγὲς ἀπὸ δυσμῶν περιλαμπόμενον. ἐκεῖ δὲ
E διατρίψαντας ἡμέρας ἐνενήκοντα μετὰ τιμῆς καὶ φιλοφροσύνης, ἱεροὺς νομιζομένους καὶ προσαγορευομένους, ὑπὸ πνευμάτων ἤδη περαιοῦσθαι· μηδ' ἄλλους τινὰς ἐνοικεῖν ἢ σφᾶς τ' αὐτοὺς καὶ τοὺς πρὸ αὐτῶν ἀποπεμφθέντας. ἐξεῖναι μὲν γὰρ ἀποπλεῖν οἴκαδε τοὺς τῷ θεῷ τὰ τρὶς δέκ' ἔτη συλλατρεύσαντας, αἱρεῖσθαι δὲ τοὺς πλείστους ἐπιεικῶς αὐτόθι κατοικεῖν, τοὺς μὲν ὑπὸ

Εγώ βέβαια δεν είμαι παρά ηθοποιός, πριν όμως θα σας αναφέρω τον ποιητή...[152], αν δεν υπάρχει αντίρρηση, αρχίζοντας από τον Όμηρο:

'Η Ωγυγία, νησί που βρίσκεται μακριά στη θάλασσα'[153],

που απέχει δρόμο πέντε ημερών από τη Βρετανία, πλέοντας προς τα δυτικά. Τρία άλλα νησιά, που απέχουν σε ίση απόσταση από εκείνη και μεταξύ τους, βρίσκονται πέρα από αυτή προς το σημείο όπου δύει το καλοκαίρι ο ήλιος. Σ' ένα από αυτά, λένε οι βάρβαροι στον μύθο τους, είχε φυλακίσει ο Δίας τον Κρόνο, κι εκείνος[154], έχοντας φρουρό τον γιο του, είχε εγκατασταθεί δίπλα στα νησιά εκείνα και σε εκείνη τη θάλασσα, την οποία ονομάζουν Κρόνιο πέλαγος. Όσο για τη μεγάλη ήπειρο, από την οποία τριγυρίζεται σε κύκλο η μεγάλη θάλασσα, από τα άλλα νησιά απέχει λιγότερο, από την Ωγυγία όμως γύρω στα πέντε χιλιάδες στάδια και το ταξίδι γίνεται σε πλοία με κουπιά (διότι το πέλαγος διαβαίνεται αργά και είναι λασπουδερό λόγω των πολλών ρευμάτων[155]. Τα ρεύματα βγαίνουν από τη μεγάλη ηπειρωτική χώρα, δημιουργούν προσχώσεις και η θάλασσα είναι πυκνή, γεώδης και θεωρήθηκε πως έχει παγώσει). Από τα ηπειρωτικά μέρη (λένε οι βάρβαροι) τα προς τη θάλασσα κατοικούν οι Έλληνες, γύρω από κόλπο όχι μικρότερο από τη Μαιώτιδα (λίμνη)[156], που το στόμιό του βρίσκεται στην ίδια ευθεία με το στόμιο της Κασπίας θάλασσας. Εκείνοι αποκαλούν και θεωρούν τους εαυτούς τους ηπειρώτες και νησιώτες όσους κατοικούν τούτη τη γη, επειδή περιβρέχεται γύρω γύρω από θάλασσα. Πιστεύουν επίσης ότι με τους λαούς του Κρόνου αναμείχθηκαν αργότερα όσοι έφτασαν με τον Ηρακλή και παρέμειναν και ότι το Ελληνικό στοιχείο, που έσβηνε ήδη εκεί και ήταν υποταγμένο στη βαρβαρική γλώσσα, τους νόμους και τον τρόπο ζωής, αναζωπυρώθηκε, για να το πούμε έτσι, και έγινε πάλι ισχυρό και σημαντικό. Για τούτο τις ανώτερες τιμές έχει ο Ηρακλής, τις αμέσως επόμενες ο Κρόνος.

Όταν λοιπόν ο αστέρας του Κρόνου, τον οποίο εμείς αποκαλούμε, λέει, Φαίνοντα ενώ εκείνοι Νυκτούρο, φτάσει στον Ταύρο μετά από περίοδο τριάντα ετών, αφού προετοιμάσουν επί χρόνο πολύ τη θυσία και τον...[157] στέλνουν, που έχουν ξεχωριστεί με κλήρο, με ανάλογο αριθμό πλοίων, φορτώνοντάς τα με πολλά απαραίτητα και προμήθειες αναγκαίες για ανθρώπους που πρόκειται να ταξιδέψουν στη θάλασσα κωπηλατώντας και να μείνουν στα ξένα χρόνο πολύ. Αφού ανοιχτούν στο πέλαγος, έχουν, όπως είναι λογικό, οι ταξιδιώτες διαφορετική τύχη· όσους σώθηκαν όμως κρατούν στην αρχή στα νησιά που βρίσκονται πέρα, κατοικούνται από Έλληνες και βλέπουν τον ήλιο να κρύβεται για λιγότερο από μια ώρα επί τριάντα μέρες[158]· αυτή είναι νύχτα, που έχει σκοτάδι ελαφρύ και λυκαυγές που φέγγει από τη δύση. Αφού μείνουν εκεί για ενενήντα μέρες, δεχόμενοι τιμές και φιλοφρονήσεις, εφόσον θεωρούνται και αποκαλούνται 'άγιοι', διαπεραιώνονται πια με τη βοήθεια των ανέμων. Εκεί δεν κατοικούν άλλοι πέρα από αυτούς και όσους στάλθηκαν πριν από αυτούς. Πράγματι, ενώ επιτρέπεται σε όσους αφιερώθηκαν στη λατρεία του θεού για τριάντα χρόνια να αποπλεύσουν και να γυρίσουν πίσω, οι περισσότεροι διαλέγουν μετά χαράς να εγκατασταθούν εκεί, άλλοι

Εικόνα 9 – Απόσπασμα από το έργο του Πλουτάρχου «Περί του εμφαινομένου προσώπου τω Κύκλω της Σελήνης» (Ηθικά).

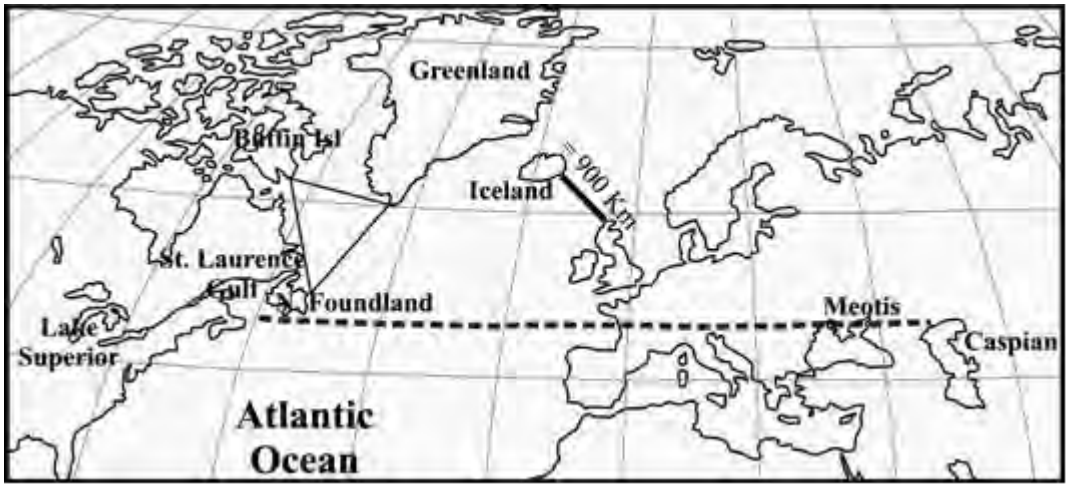

Εικόνα 10 – Οι θέσεις των νησιών που αναφέρει ο Πλούταρχος ότι βρίσκονται δυτικά της Βρετανίας.

Ο Πλούταρχος δίνει και σ' αυτά τα ερωτήματα απαντήσεις.

Ο μεγάλος Κόλπος της μεγάλης ηπειρωτικής χώρας, τα παράλια του οποίου κατοικούνται από Έλληνες βρίσκεται:

«...στην ίδια ευθεία με την είσοδο της Κασπίας Θάλασσας...»
«...Το μέγεθός της είναι το ίδιο με εκείνο της Μαιώτιδας Λίμνης (=Αζοφική)...!»

Από την Εικ. 11 φαίνεται καθαρά ότι στην ίδια ευθεία, δηλαδή στον ίδια παράλληλο με την είσοδο της Κασπίας βρίσκεται μόνον ένας Κόλπος στην μεγάλη ηπειρωτική χώρα. Αυτός ο Κόλπος είναι γνωστός σήμερα ως *St. Lawrence Gulf*, δηλαδή *Κόλπος του Αγ. Λαυρεντίου*. Στο σημείο αυτό σταματάει η περιγραφή του Πλούταχου που αναφέρεται στον τόπο εξορίας του

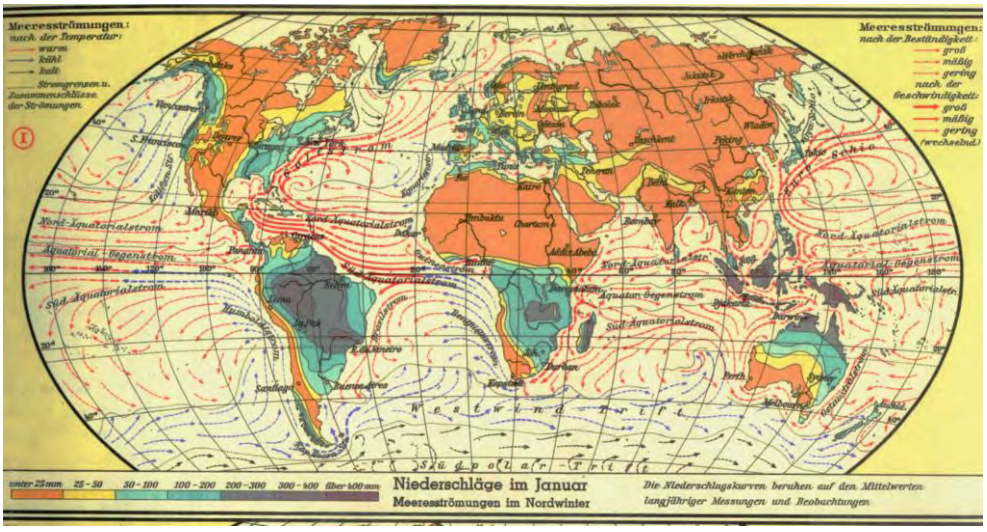

Εικόνα 11 – Τα ρεύματα των Ωκεανών – τα ποτάμια του Ωκεανού – όπως δίδονται στους σημερινούς χάρτες και η θέση του Κόλπου της Μεγάλης Ηπειρωτικής Χώρας του Πλούταρχου, σε σχέση με την είσοδο της Κασπίας και την Μαιώτιδα λίμνη (Αζοφική).

Κρόνου. ο οποίος δέχεται στα νερά του *St. Lawrence River* που ρέει παράλληλα σχεδόν προς τα σύνορα μεταξύ ΗΠΑ και Καναδά αλλά τα νερά του προέρχονται κυρίως από τις *Μεγάλες Λίμνες* και μεταξύ αυτών και από την *λίμνη Superior* (Εικ. 12). Η σημείωση αυτή είναι σημαντική, επειδή δείχνει ότι υπάρχει μία ποτάμια επικοινωνία μεταξύ των Μεγάλων Λιμνών και του Β.Ατλαντικού με εξαίρεση την περιοχή ανάμεσα στην λίμνη *Erie* και *Ontario*, όπου παρεμβάλλονται οι *καταρράκτες του Niagara*.

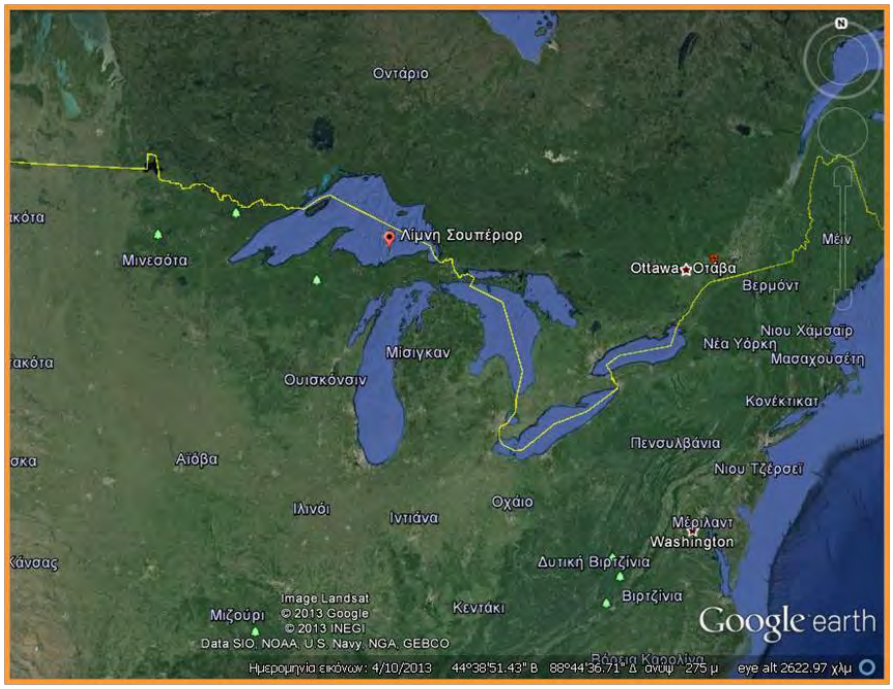

Εικόνα 12 – Η λίμνη Superior και η χερσόνησος Michigan όπου και η εντατική προϊστορική μεταλλευτική δραστηριότητα χαλκού στο χρονικό διάστημα 2500 – 1050 π.Χ. περίπου.

3.3. Γιατί Έφτασε όμως ο Κρόνος στα Πέρατα του Κόσμου;

Γιατί να φύγει από το ηλιόλουστο Αιγαίο και να πάει εκεί που ο ήλιος χάνεται μόνον μια ώρα το καλοκαίρι και συνεπώς τον χειμώνα βγαίνει μια ώρα μόνον και 23 ώρες επικρατεί νύχτα;

Αν υποθέσουμε ότι ο Δίας τον εξόρισε, δεν θα μπορούσε να δραπετεύσει και να πάει σ'ένα πιο ευνοημένο από κλιματική άποψη τόπο;

Πήγε από περιέργεια; Πήγε να ιδρύσει κάποια αποικία; Πήγε ως κατακτητής; Και ακόμη μερικά ερωτήματα.

Για ποιο λόγο ο Πλούταρχος θεώρησε σκόπιμο να περιγράψει όλες αυτές τις δραστηριότητες του Κρόνου και στη συνέχεια του Ηρακλή σ'αυτές τις άγνωστες περιοχές; Χάθηκε να τον εξορίσει κάπου στην Κεντρική Ασία ή κάπου στην Βόρεια Αφρική;

Και πολλά ακόμη ερωτήματα, όπως πότε πήγε; Πώς πήγε; Γιατί πήγε με Έλληνες; Γιατί δεν τους κράτησε κοντά του αλλά τους πέρασε στον μεγάλο Κόλπο της Μεγάλης Ηπειρωτικής Χώρας, που βρίσκεται δυτικά από τον τόπο εξορίας του;

Απαντήσεις σ' αυτά τα πολύ σημαντικά ερωτήματα, καθοριστικής σημασίας κατά την γνώμη μου, δεν δίνει ο Πλούταρχος. Όμως οι έρευνες που έχουν γίνει στην ευρύτερη περιοχή του Michigan, και ο εντοπισμός μιας έντονης μεταλλευτικής δραστηριότητας κοντά στις παράκτιες περιοχές της Λίμνης Superior δίδουν, κατά την γνώμη μου, την απάντηση.

Πολλοί είναι, της γνώμης ότι αυτή η μεταλλευτική δραστηριότητα δεν πρέπει να συσχετίζεται με τους Ευρωπαίους γενικά αγνοώντας "επιδεικτικά" τα όσα γράφει ο Πλούταρχος. Οι πιο πολλοί βέβαια από όσους έχουν ασχοληθεί με το θέμα, μάλλον δεν έχουν ακούσει το όνομα "Πλούταρχος". Πολλοί πάντως που θα πρέπει να τον γνωρίζουν δεν θεώρησαν σκόπιμο να ασχοληθούν με τη συγκεκριμένη περικοπή. Και να σκεφτεί κανείς ότι υπάρχει διεθνής εταιρία που ασχολείται αποκλειστικά με τον Πλούταρχο η International Plutarch Society, που έχει οργανώσει από το 1987 μέχρι σήμερα 9 διεθνή συνέδρια, δεν θεωρήθηκε προφανώς σημαντικό να παρουσιάσουν και να αναλύσουν το περιεχόμενο της περικοπής που αναφέρεται στον Κρόνο, θεωρώντας, ίσως, ότι είναι ασήμαντο το γεγονός ότι πάνω από 4000 χρόνια πριν από τον Κολόμβο άνθρωποι που μιλούσαν Ελληνικά είχαν φτάσει στον κόλπο του St. Lawrence!!!

3.4. Προϊστορικά Μεταλλεία στην Περιοχή του Michigan και στην Λίμνη Superior

Από τα τέλη του 19ου αιώνα, είναι γνωστό ότι στην ευρύτερη περιοχή του Michigan, στα σύνορα με τον Καναδά και στο νησί Royale και γύρω από τη Λίμνη Superior (Εικ. 13) έχουν εντοπιστεί *πανάρχαια μεταλλεία αυτοφυούς χαλκού*, που η καθαρότητά του υπερβαίνει το 99,5%. Πρόκειται δηλαδή για *καθαρό αυτοφυή χαλκό*.

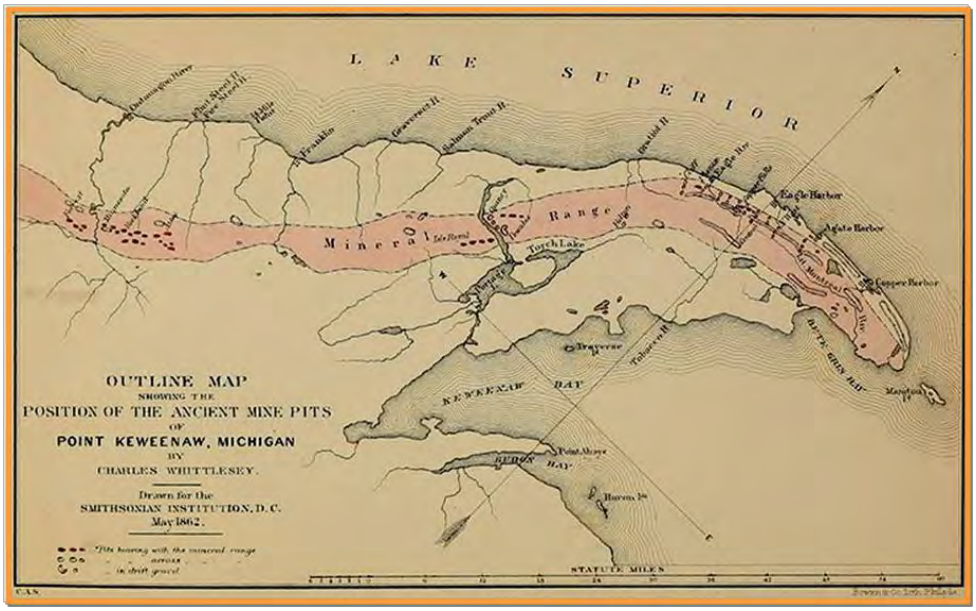

Εικόνα 13 – Η χερσόνησος Keweenan, στην πολιτεία Michigan των Η.Π.Α.

Η συνολική παραγωγή έχει εκτιμηθεί σε 250.000 τόνους, ενώ κατ' άλλους υπερβαίνει τους 500.000 τόνους.

Με βάση ραδιοχρονολογήσεις τα μεταλλεία αυτά λειτούργησαν από το 2500 π.Χ. έως το 1100 π.Χ. περίπου. Υπάρχουν και απόψεις που δέχονται ότι η λειτουργία τους άρχισε γύρω στο 5000 π.Χ., κάτι που φαίνεται δύσκολο να έχει γίνει, εξαιτίας των δυσμενών κλιματικών συνθηκών που πρέπει να επικρατούσαν στην περιοχή την εποχή αυτή, δηλαδή πριν 7000 χρόνια.

Σύμφωνα με τον Πλούταρχο την περιοχή εξορίας του Κρόνου επισκέφτηκε κάποια στιγμή και ο Ηρακλής, ενώ οι άνθρωποι που τον συνόδευαν, μετά από μια περίοδο προετοιμασίας, πέρασαν και στην απέναντι ηπειρωτική χώρα για να αντικαταστήσουν άλλους Έλληνες, που κατοικούσαν εκεί και συγκεκριμένα στα παράλια του μεγάλου Κόλπου που -σύμφωνα με την περιγραφή του Πλούταρχου- πρέπει να είναι ο St. Lawrence Gulf.

Με βάση την χρονολόγηση έναρξης της μεταλλευτικής δραστηριότητας στην λίμνη Superior ο Κρόνος πρέπει να έφτασε στην περιοχή κάπου μεταξύ του 3000 και 2500 π.Χ.

Είναι δυνατόν όμως να δεχθούμε ότι ο Κρόνος είναι ο πρώτος που έφτασε εκεί; Πού γνώριζε ότι εκεί υπήρχαν κοιτάσματα χαλκού;

Προσωπική άποψη είναι ότι πριν από τον Κρόνο -πολύ πριν ίσως- πρέπει να έχουν προηγηθεί άλλοι, ως προπομποί, που θα είχαν στόχο να εξερευνήσουν την περιοχή. Οι άνθρωποι αυτοί όμως για να καταλήξουν τόσο μακριά πρέπει να είχαν εξερευνήσει τις ενδιάμεσες περιοχές και οπωσδήποτε, τουλάχιστον, τις δυτικές παράκτιες περιοχές της Ευρώπης.

Θεωρώ αυτονόητο ότι πρέπει να γνώριζαν και τον Ωκεανό με τα ρεύματά του. Πρέπει να ήσαν συνεπώς πρώτα και κύρια ναυτικοί και μάλιστα όχι μόνον ικανοί, αλλά και ριψοκίνδυνοι, και επί πλέον θα πρέπει να διέθεταν και τα κατάλληλα πλοία.

Ποιός λαός όμως θα μπορούσε να πραγματοποιήσει ένα τέτοιο ταξίδι; Ποιός λαός είχε όλη αυτήν την εμπειρία;

Την εποχή αυτή κυρίαρχοι στη θάλασσα και στο εμπόριο ήταν οι Μινωίτες. Καλοί ναυτικοί όμως ήσαν και οι *Αιγύπτιοι*. Οι *Μεσοποτάμιοι* δεν είχαν ούτε τον στόλο, ούτε το δίκτυο των λιμανιών. Οι *Φοίνικες* δεν είχαν ακόμη κάνει αισθητή την παρουσία τους στο ιστορικό γίγνεσθαι, παρά το γεγονός ότι οι *Χαναΐτες* διέθεταν και στόλο και λιμάνια.

4. Η Κρήτη την Εποχή των Μετάλλων

Στην Κρήτη, όπως είναι γνωστό, έχει αναπτυχθεί ένας από τους σημαντικότερους προϊστορικούς πολιτισμούς.

Το πιο σημαντικό και συγχρόνως περίεργο είναι το γεγονός ότι ενώ στην Κρήτη αναπτύχθηκαν μεγάλες και πλούσιες πόλεις, όπως η *Κνωσσός*, η *Φαιστός*, η *Ζάκρος*, τα *Μάλλια*, κ.ά., με αμύθητο πλούτο, όπως δείχνουν τα ευρήματα σε χρυσό, άργυρο, μεταλλικά εργαλεία, όπλα, πολύτιμους λίθους, ελεφαντόδοντο, κ.λπ., το ίδιο το νησί δεν διαθέτει μεταλλεύματα (Εικ. 14).

Εικόνα 14 – Μεταλλογενετικός χάρτης της Κρήτης.

Πώς αποκτήθηκε λοιπόν όλος αυτός ο πλούτος; Πώς κατασκευάστηκαν αυτά τα ανάκτορα; Πώς έγιναν αυτά τα *υδρευτικά*, *αποχετευτικά*, κ.λπ. έργα, που δεν διέθεταν ούτε τα ανάκτορα των Βερσαλλιών του βασιλιά Λουδοβίκου του ΙΔ, του γνωστού και ως βασιλιά Ήλιου; Είναι δυνατόν να παραχθεί τόσος πλούτος μόνον από γεωργική και κτηνοτροφική δραστηριότητα;

Στην Μινωική Κρήτη όμως ανθούσε η *κεραμεική*, η *σφραγιδογλυφία*, η *μεταλλοτεχνία*, η *χρυσοχοΐα*, και *άλλες τέχνες*.

Αυτό υποδηλώνει πως οι Μινωίτες, παράλληλα με την ναυτιλία και την τεχνολογία, πρέπει να είχαν αναπτύξει και το *διεθνές εμπόριο*. Η άποψη αυτή βασίζεται και στο γεγονός ότι στην Κρήτη έχουν εντοπιστεί και *πολλά λιμάνια*, όπως η *Αμνισσός*, η *Κάτω Ζάκρος*, τα *Μάλλια*, ο *Καμμός*, οι *Γουρνιές*, ο *Μοχλός*, κ.ά.

Σε ποιά άλλη περιοχή της Ανατολικής Μεσογείου έχουν κατασκευαστεί τόσα λιμάνια; Ποιός ο λόγος να κατασκευαστούν λιμάνια, αν δεν τα χρησιμοποιούσαν;

Η Κρήτη λοιπόν διέθετε όλη την υποδομή, για την *κατασκευή*, την *επισκευή*, την *συντήρηση* και τον *ελλιμενισμό πλοίων*. Τα λιμάνια θα μπορούσαν επιπλέον να χρησιμοποιηθούν και ως *εμπορικοί σταθμοί*, για την φύλαξη εμπορευμάτων, κ.λπ. Οι Μινωίτες επομένως είναι αυτοί που θα μπορούσαν να εκμεταλλεύονται όλον αυτόν τον μεταλλευτικό πλούτο της περιοχής και παράλληλα να τον μεταφέρουν και να τον εμπορεύονται.

Υπάρχουν όμως ενδείξεις που θα μπορούσαν να στηρίξουν αυτήν την άποψη;

Ενδείξεις υπάρχουν πολλές.

Πιστεύω όμως ότι η καλύτερη ένδειξη -για μένα απόδειξη- είναι οι συλλογές πολύ αρχαίων χάλκινων αντικειμένων που εκτίθενται στο *Milwaukee Public Museum* της πολιτείας *Wisconsin*. Εκεί λοιπόν, στη συλλογή που είναι γνωστή ως *Old Copper Culture*, ανάμεσα στα άλλα αντικείμενα εκτίθενται και μερικοί *διπλοί πελέκεις*, το σύμβολο της Μινωικής Κρήτης (Εικ. 15).

Εξάλλου από την Εικ. 16, όπου δίδεται η προϊστορική εξέλιξη των γηγενών κατοίκων του *Wisconsin*, καταφαίνεται ότι ο *διπλός πέλεκυς* εμφανίζεται στην περιοχή γύρω στο 1700 π.Χ., που από τους αρχαιολόγους που ασχολούνται με την προϊστορία της περιοχής, αντιστοιχεί στην λεγόμενη *Μέση Αρχαϊκή Περίοδο*. Αξιοσημείωτο είναι το γεγονός ότι ο διπλός πέλεκυς στην Μινωϊκή Κρήτη εμφανίζεται την ίδια ακριβώς εποχή με εκείνη που πρωτοεμφανίστηκε στην ευρύτερη περιοχή της λίμνης Superior.

Εικόνα 15 – Χάλκινος διπλός πέλεκυς, ένας από τους πολλούς που έχουν βρεθεί σε διάφορες θέσεις στις Βόρειες πολιτείες των Η.Π.Α. και εκτίθενται στο Milwaukee Public Museum και αλλού.

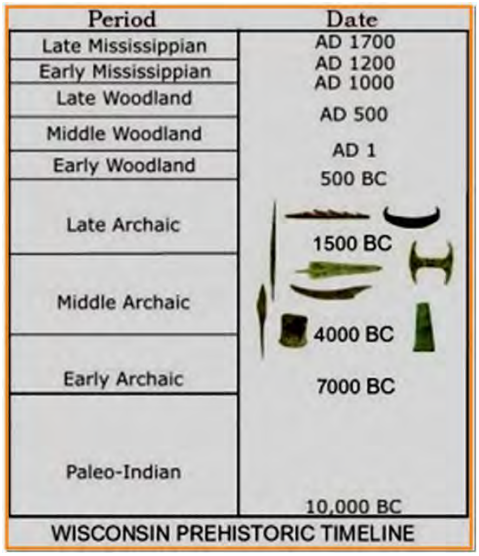

Εικόνα 16 – Πίνακας της προϊστορικής εξέλιξης της πολιτείας Wisconsin των Η.Π.Α.

4.1. Εμπορικές Σχέσεις των Μινωιτών και με Άλλους Μακρινούς Λαούς

Μήπως όμως οι Μινωίτες πέραν των εμπορικών και άλλων σχέσεων με τους προϊστορικούς κατοίκους του Wisconsin και των άλλων περιοχών στην Β. Αφρική και στην Ευρώπη, είχαν και επαφές με χώρες και λαούς της Ανατολής, όπως για παράδειγμα με τις Ινδίες;

Το ερώτημα είναι αυτονόητο, όταν είναι γνωστό ότι την εποχή εκείνη, πολλά υλικά που έχουν βρεθεί σε ανασκαφές, που έχουν γίνει σε όλες σχεδόν τις χώρες της Ανατολικής Μεσογείου, προέρχονται από τις Ινδίες. Εξάλλου, πολλά είδη-υλικά της Μεσογείου έχουν βρεθεί σε αρχαιολογικές ανασκαφές στις Ινδίες.

Όλα αυτά τα *Ινδικής προέλευσης υλικά και αντικείμενα* πρέπει κάποιος να τα μετέφερε από εκεί στην Ανατολική Μεσόγειο, και αντίστροφα από την Μεσόγειο στις Ινδίες. Ας δούμε όμως, κατ' αρχήν, αν και κατά πόσον ήταν δυνατόν ένα πλοίο από την Ανατολική Μεσόγειο να φτάσει στις Δυτικές ακτές των Ινδιών.

Η απάντηση στο ερώτημα δεν είναι μονοσήμαντη. Ας δούμε λοιπόν ποιά είναι τα βασικότερα εμπόδια για ένα πλοίο από την Μεσόγειο να φτάσει στις Ινδίες.

4.1.1. Το Δέλτα του Νείλου

Το μεγαλύτερο φυσικό εμπόδιο είναι το *Δέλτα του Νείλου*, που χωρίζει την Μεσόγειο από την *Ερυθρά Θάλασσα*. Εάν δεν υπάρχει κάποιο κανάλι που να ενώνει την Μεσόγειο με την Ερυθρά Θάλασσα, τότε οποιαδήποτε απευθείας επαφή με τις Ινδίες, διά θαλάσσης, είναι πρακτικά αδύνατη.

Βέβαια, την εποχή εκείνη, δηλαδή πριν 4-5 χιλιάδες χρόνια, το Δέλτα του Νείλου δεν είχε τις διαστάσεις που έχει σήμερα. Αυτό συμβαίνει με όλα τα Δέλτα όλων των ποταμών του Πλανήτη μας. Αλλωστε ο Ηρόδοτος είναι αυτός που λέει ότι...

Για να μπορέσει επομένως να ξεπεράσει το εμπόδιο του Δέλτα, πρέπει να υπάρχει ένα *φυσικό* ή *τεχνητό κανάλι* στο *Δέλτα*. Υπάρχει όμως;

Η απάντηση είναι καταφατική. Τα αρχαία κείμενα αναφέρουν ότι η *6η Δυναστεία των Φαραώ*, που κυβέρνησε την Αίγυπτο από το 2300 έως το 2180 π Χ., είχε κατασκευάσει ένα τέτοιο κανάλι. Τα Μινωικά πλοία και γενικότερα όλα τα πλοία της Ανατολικής Μεσογείου, θεωρητικά, θα μπορούσαν να φθάσουν από την Μεσόγειο στην Ερυθρά Θάλασσα. Για να φτάσουν στις Ινδίες όμως πρέπει: (i) να μπορούν να διαπλεύσουν την *Ερυθρά Θάλασσα* και (ii) στη συνέχεια την *Αραβική Θάλασα*.

4.1.2. Ερυθρά Θάλασσα

Και καθ'οσον αφορά τον διάπλου της Ερυθράς Θάλασσας δεν τίθεται πρόβλημα, αφού δεν παρουσιάζει κάποιες φυσικοωκεανογραφικές ιδιαιτερότητες, που θα δυσχέραιναν την ναυσιπλοΐα. Άλλωστε στα παράλιά της έχουν αναπτυχθεί και διάφορα λιμάνια, τόσο στην Αιγυπτιακή, όσο και στην Αραβική πλευρά, που οπωσδήποτε διευκολύνουν το όποιο ταξίδι.

4.1.3. Η Αραβική Θάλασσα

Στον Ατλαντικό Ωκεανό, όπως αναφέρθηκε, υπάρχουν τα διάφορα ρεύματα που βοηθάνε την ναυσιπλοΐα, εφόσον τα πλοία ακολουθούν την ροή των ρευμάτων. Απεναντίας, εάν ένα πλοίο θελήσει να πλεύσει αντίθετα προς την φορά της ροής του ρεύματος, τότε ο κυβερνήτης θα διαπιστώσει με έκπληξη ότι, ενώ το πλοίο του δείχνει ότι προχωράει, ουσιαστικά δεν έχει μετακινηθεί. Κάτι τέτοιο περιγράφει και ο...

Στην *Αραβική Θάλασσα* βεβαίως παρόμοια ρεύματα δεν υπάρχουν. Εδώ όμως επικρατούν οι *Μουσώνες*, που συνδέονται με τις θερμοκρασιακές συνθήκες και διαφορές που επικρατούν μεταξύ των *ορεινών περιοχών* και της *Αραβικής Θάλασσας* και οι οποίες είναι διαφορετικές κατά την ψυχρή και την θερμή περίοδο του έτους.

4.1.4. Οι θερινοί Μουσώνες

Κατά την θερμή περίοδο του έτους, *οι ορεινοί όγκοι της Κεντρικής Ασίας* θερμαίνονται περισσότερο απ' ότι η *Αραβική Θάλασσα*. Έτσι δημιουργούνται οι *θερινοί μουσώνες*, κατά την διάρκεια των οποίων κυριαρχούν οι *ΝΔ-κοί άνεμοι* (Εικ. 17), που ξεκινούν κατά τον Απρίλη, κορυφώνονται τον Ιούλιο, όταν έχουμε και έντονες βροχοπτώσεις, ενώ από τον Σεπτέμβριο αρχίζει η ελάττωση των θερμοκρασιών και τον Νοέμβριο αρχίζει σιγά σιγά το ψύχος. *Συνεπώς τα ναυτικά ταξίδια από την Ερυθρά Θάλασσα προς την Ινδία είναι σχετικά εύκολα από τον Απρίλιο μέχρι τον Νοέμβριο*.

Εικόνα 17 – Οι θερινοί μουσώνες που ευνοούν την θαλάσσια επικοινωνία μεταξύ της Ερυθράς και των Ινδιών κατά τους μήνες από τον Απρίλιο μέχρι τον Νοέμβριο.

4.1.5. Οι χειμερινοί Μουσώνες

Κατά τους *χειμερινούς μουσώνες* κυριαρχούν οι ΒΑ-κοί άνεμοι (Εικ. 18), επειδή στους ορεινούς όγκους της Κεντρικής Ασίας επικρατεί το ψύχος, ενώ στην Αραβική Θάλασσα οι θερμοκρασίες είναι σαφώς υψηλότερες.

Συνεπώς, την περίοδο μεταξύ του τέλους Δεκεμβρίου και μέχρι τον Απρίλιο, το ταξίδι με πλοίο από τις Ινδίες προς την Ερυθρά Θάλασσα είναι σχετικά εύκολο. Και από εκεί ένα Μινωικό πλοίο θα μπορούσε χρησιμοποιώντας τις τελευταίες τεχνητές διώρυγες του Δέλτα του Νείλου να περάσει στην Μεσόγειο και στην Κρήτη, στο Αιγαίο, στον Εύξεινο κι αλλού.

Εικόνα 18 – Οι χειμερινοί μουσώνες που ευνοούν την θαλάσσια επικοινωνία από το τέλος Δεκεμβρίου μέχρι τον Απρίλιο.

Για να αναπτυχθεί όμως το εμπόριο μεταξύ των Μινωιτών και των Ινδιών πρέπει να πληρούνται δύο επιπλέον προϋποθέσεις:

1. Να υπάρχουν αντίστοιχα *λιμάνια υποδοχής* των εμπορικών πλοίων στις Ινδίες, και
2. *πλοία κατάλληλα* για αυτού του είδους τα ταξίδια.

4.2. Αρχαία λιμάνια στις Ινδίες

Σχετικά με τα λιμάνια, μέχρι τώρα έχουν εντοπιστεί τουλάχιστον τρεις μεγάλες προϊστορικές λιμενικές εγκαταστάσεις στις δυτικές ακτές των Ινδιών.

4.2.1. Το λιμάνι Lothal

Το *λιμάνι Lothal* (Εικ. 19), που βρίσκεται στον *Κόλπο Cambay*, σύμφωνα με τον Ινδό αρχαιολόγο Καθηγητή S.R. Rao, που διεξήγαγε ανασκαφές από το 1955 έως το 1962, έχει χρονολογηθεί ότι

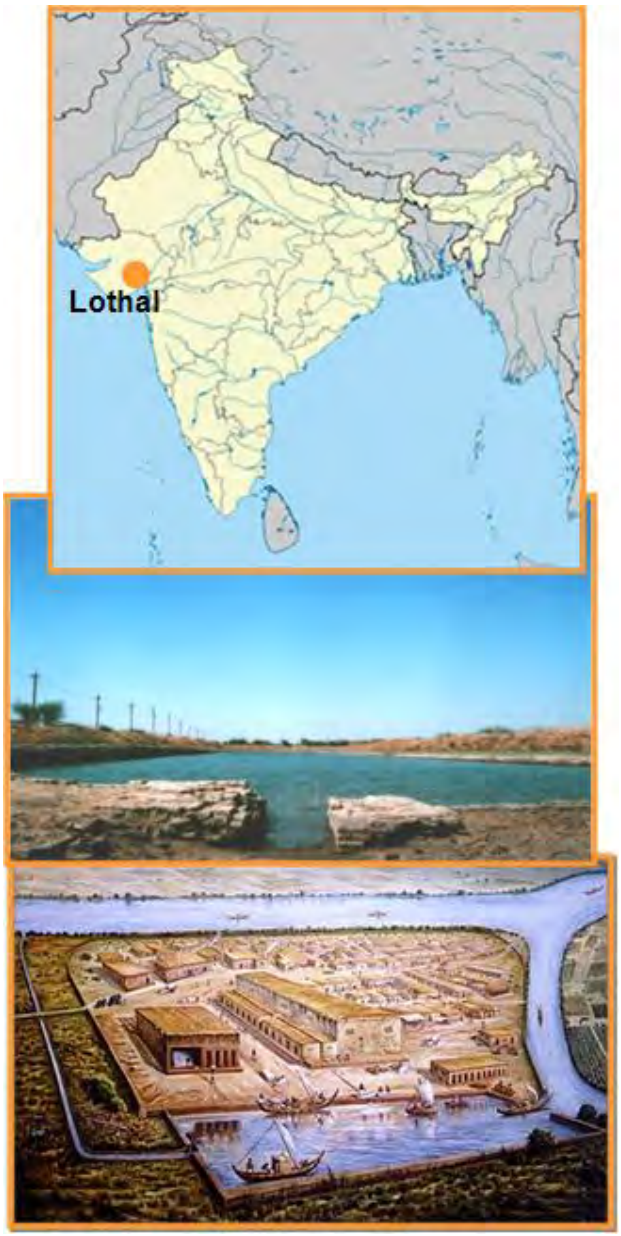

Εικόνα 19 – Το λιμάνι Lothal και η αναπαράσταση της προϊστορικής πόλης (αναπαράσταση: The Archaeological Survey of India).

πρέπει να λειτούργησε τουλάχιστον μεταξύ του 2500 και του 1900 π.Χ. Η χρονολόγηση βασίζεται στις ανασκαφές που έχουν γίνει στην πόλη, η οποία είχε αναπτυχθεί γύρω από το καθ' αυτό λιμάνι.

Πολλά από τα ευρήματα των ανασκαφών, που εκτίθενται στο μουσείο της Lothal, σύμφωνα με ορισμένους μοιάζουν με αντίστοιχα Μινωικά. Ανάμεσα σ' αυτά είναι ελεφαντόδοντο, χάντρες, κ.ά. που μοιάζουν με αυτά που έχουν βρεθεί σε Μινωικά παλάτια.

Πέραν αυτών, έχει βρεθεί και χαλκός καθαρότητας 99.8, που θεωρείται ότι είναι εισαγωγής και μάλιστα ότι προέρχεται από τα προϊστορικά μεταλλεία του Michigan.

4.2.2. Λιμάνι Cambay

Το *λιμάνι Cambay* βρίσκεται λίγο νοτιότερα του προηγουμένου και βορείως της Βομβάης. Το λιμάνι είναι βυθισμένο (Εικ. 20) και έχει χρονολογηθεί την εποχή του μπρούντζου.

Εικόνα 20 – Το βυθισμένο προϊστορικό λιμάνι Cambay.

4.2.3. Λιμάνι Mouziris

Τα δύο προηγούμενα λιμάνια βρίσκονται στις ΒΑ-ικές ακτές της Ινδικής χερσονήσου. Το *λιμάνι Mouziris* βρίσκεται στο ΝΑ-ικό τμήμα αυτής, κοντά στην πόλη *Patanam* και μάλιστα, επειδή βρίσκεται στις εκβολές του *ποταμού Periyar*, είναι ένα φυσικό και καλά προστατευμένο λιμάνι (Εικ. 21).

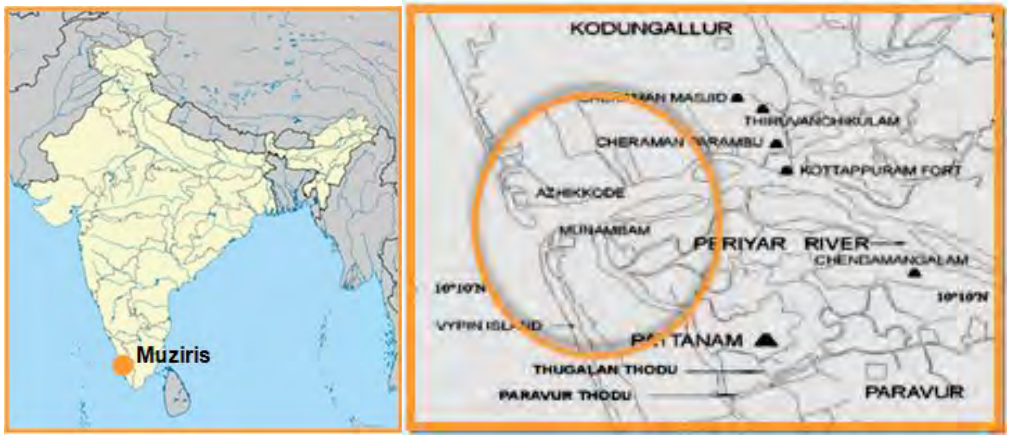

Εικόνα 21 – Η θέση του προϊστορικού λιμανιού Mouziris στο ΝΑ-ικό τμήμα της Ινδικής Χερσονήσου.

Το *λιμάνι Mouziris* ήταν *διάσημο κατά την Ελληνιστική και Ρωμαϊκή εποχή* επειδή από εκεί διακινείτο μεγάλο τμήμα του εμπορίου των μπαχαρικών και κυρίως το πιπέρι, το κάρδαμο, κ.λπ.

Σημειωτέον ότι αναφέρεται σε διάφορα Ινδικά κείμενα, όπως στην *Mahabarata,* που είναι ένα *Σανσκριτικό* κείμενο, αλλά και στο αντίστοιχο *κείμενο των Tamil* που είναι *Patittupatu*. Πέραν αυτών αναφέρεται και σε *Κινεζικά κείμενα*.

Τα κείμενα αυτά βεβαίως δεν αναφέρονται στην προϊστορική εποχή, αλλά στην εποχή του Μεγάλου Αλεξάνδρου και μετά. Επειδή όμως το λιμάνι είναι πολύ παλαιότερο, αν δεν εχρησιμοποιείτο για εμπορικούς λόγους με την Δύση, ποιός ο λόγος ύπαρξής του;

5. Έφτασαν οι Μινωίτες μέχρι τις Ινδίες;

Μετά τα προηγούμενα τίθεται το μεγάλο ερώτημα αν και κατά πόσον ήταν δυνατόν να φτάσουν τα πλοία των Μινωιτών μέχρι τις Δυτικές ακτές των Ινδιών, μία περιοχή που είναι γνωστή και ως *Kerala*.

Η απάντηση της συντριπτικής πλειοψηφίας των ειδικών είναι *απολύτως αρνητική*.

Η άρνηση αυτή μάλιστα πολλές φορές συνοδεύεται και με ένα υπομειδίαμα, που αφήνει πολλά υπονοούμενα.

Κύριο επιχείρημα όλων είναι ότι δεν είναι δυνατόν να έχουν φτάσει μέχρις εκεί τα πλοία των Μινωιτών.

Στην αρνητική αυτή θέση θα ήθελα να παρατηρήσω τα εξής:

1. Όταν κάποιος δεν έχει ασχοληθεί με κάποιο θέμα, η απόρριψη μιας άποψης χρειάζεται κάποια επιχειρήματα.
2. Τα Ινδικά προϊόντα τα βρίσκουμε σε διάφορα μουσεία τόσο Ελληνικά, όσο και σε Αιγυπτιακά, Μικρασιατικά, κ.λπ. Επιπλέον έχουν βρεθεί και στο πλοίο του ναυαγίου του Uluburun.

Μετά από αυτά δεν είναι δυνατόν να αμφισβητηθούν οι εμπορικές σχέσεις μεταξύ των προϊστορικών κατοίκων της Ανατολικής Μεσογείου και των Ινδιών.

Εάν όμως δεν αμφισβητούνται οι εμπορικές σχέσεις, τότε τίθεται το ερώτημα της μεταφοράς των Ινδικών προϊόντων. Πώς έφτασαν όλα αυτά τα προϊόντα στην Μεσόγειο; Ήρθαν *διά ξηράς* ή *διά θαλάσσης ή σε συνδυασμό και των δύο*; Αν ήλθαν *διά ξηράς* τότε ο μόνος τρόπος είναι να έλθουν μέσω Περσίας, Μεσοποταμίας, Μικράς Ασίας και από εκεί να φτάσουν στο Αιγαίο. Αν ήλθαν *διά θαλάσσης* τότε τίθεται το ερώτημα ποιοί ναυτικοί μπορεί να τα έφεραν. Οι ναυτικοί που θα μπορούσαν να τα μεταφέρουν, πρέπει να ήσαν οι Αιγύπτιοι, οι Φοίνικες, οι Αιθίοπες, οι Μεσοποτάμιοι, οι Πέρσες, οι Ινδοί και ίσως και άλλοι.

Απαραίτητη προϋπόθεση είναι να έχουν: (i) *πλοία κατάλληλα* και (ii) *ναυτικές ικανότητες*. Αν υποθέσουμε ότι όλοι αυτοί πληρούν και τις δύο προηγούμενες προϋποθέσεις, υπάρχει κάποια μελέτη που αναφέρει ότι *οι ναυτικές ικανότητες των Μινωιτών ήσαν υποδεέστερες και τα πλοία τους* -συγκριτικά με εκείνα των προηγουμένων- *κατώτερης ποιότητας και επομένως ακατάλληλα*;

Άρα, οι λίγοι που θεωρούμε ότι οι Μινωίτες θα μπορούσαν να έχουν φτάσει μέχρι τις Ινδίες, μάλλον έχουμε δίκιο. Όμως για να γίνει αποδεκτή μια άποψη οι θετικές ενδείξεις πρέπει να γίνουν αποδείξεις. Αυτό σημαίνει έρευνα συστηματική και μάλιστα διεπιστημονική.

5.1. Είναι Δυνατόν να Φτάσουν τα Πλοία των Μινωιτών και των Μυκηναίων Τόσο Μακριά;

Όπως φαίνεται και στην Εικ. 22 τα πλοία των Μινωιτών πρέπει να μοιάζουν με εκείνα που απεικονίζονται στις τοιχογραφίες του Ακρωτηρίου της Σαντορίνης, που δείχνουν μάλλον ένα λιμάνι που έχει κατασκευαστεί σε κάποιο Δέλτα κάποιου μεγάλου ποταμού, που χύνεται στην

Μεσόγειο προφανώς. Το τοπίο, η βλάστηση και η πανίδα που απεικονίζεται, δείχνουν ότι μάλλον πρόκειται για τον Νείλο. Άλλος ποταμός με αυτά τα χαρακτηριστικά στην Μεσόγειο δεν υπάρχει. Εκτός Μεσογείου παρόμοιο τοπίο παρουσιάζουν οι εκβολές στην Κεντροδυτική Αφρική και στις Δυτικές ακτές της Ινδίας. Παρόμοια βλάστηση παρατηρείται και στο Δέλτα του Αμαζονίου αλλά και του Γάγγη, φαίνεται όμως, ότι ανεξάρτητα αν είχαν φτάσει μέχρις εκεί οι προϊστορικοί Έλληνες, όπως δέχονται ορισμένοι, οπωσδήποτε δεν διεξήγαγαν εμπόριο. Όσον αφορά τα Δέλτα άλλων ποταμών, όπως του Δούναβη και των άλλων που εκβάλλουν στον Εύξεινο, ή του Πάδου και του Ροδανού, πρέπει να αποκλειστούν.

Εικόνα 22 – Πλοία της Μινωικής εποχής, όπως απεικονίζονται στις τοιχογραφίες του Ακρωτηρίου της Θήρας.

Όπως αναφέρθηκε, τα πλοία της Μυκηναϊκής εποχής πρέπει να είναι παρόμοια με αυτά του *ναυαγίου του Uluburun* (Εικ. 23). Παρόμοιου τύπου πλοία πρέπει να ήσαν η *Αργώ* αλλά και εκείνο του *Οδυσσέα*. Τα πλοία αυτού του τύπου πρέπει να μπορούν να διαπλεύσουν τον Ατλαντικό προς όλες τις κατευθύνσεις, με την προϋπόθεση ότι οι ναυτικοί γνωρίζουν τα ρεύματα που επικρατούν. Η άποψη αυτή βασίζεται στα ακόλουθα δύο επιχειρήματα:

1. Από τα λεγόμενα του Ομήρου, που λέει σε κάποιο σημείο της Οδύσσειας (λ, 9-15):

«... και αφού πάνω στο πλοίο τα' άρμενα, ένα προς ένα
τα φροντίσαμε
μείναμε καθιστοί – εκείνο γύρευε το δρόμο μόνο του
κυβερνημένο από τον άνεμο.
Όλη τη μέρα, μ' ανοιχτά πανιά, ποντοπορούσε
Ωσότου ο ήλιος έδυσε κι όλοι οι μεγάλοι δρόμοι
βούλιαξαν στο σκοτάδι.
Έφτανε το καράβι πια στα πέρατα του Ωκεανού
με τις βαθειές ροές
όπου των Κιμμερίων ανδρών η χώρα και η πόλη...»
(ΟΕΔΒ, μτφρ. Δ. Μαρωνίτη)

2. Και από το γεγονός ότι ένα ολόκληρο *αλιευτικό πλοίο* και μια *ολόκληρη αποβάθρα από την περιοχή της Fukusima* που αποσπάστηκαν μετά το καταστροφικό tsunami που έπληξε την περιοχή, μετά από ένα χρόνο βρέθηκαν στις δυτικές ακτές της Βόρειας Αμερικής (Εικ. 24). Αυτό συνέβη επειδή τα δύο αυτά, τεραστίων διαστάσεων αντικείμενα, *παρασύρθηκαν από τα ρεύματα του Ειρηνικού Ωκεανού.*

Ανάλογα παραδείγματα βεβαίως, δεν έχουν περιγραφεί από την Αραβική θάλασσα, αλλά οι συνθήκες είναι παρόμοιες αν ένας ικανός καπετάνιος ακολουθήσει τους χειμερινούς ή τους θερινούς Μουσώνες.

Εικόνα 23 – Αναπαράσταση του βυθισμένου προϊστορικού πλοίου από την περιοχή Uluburun της σημερινής Τουρκίας.

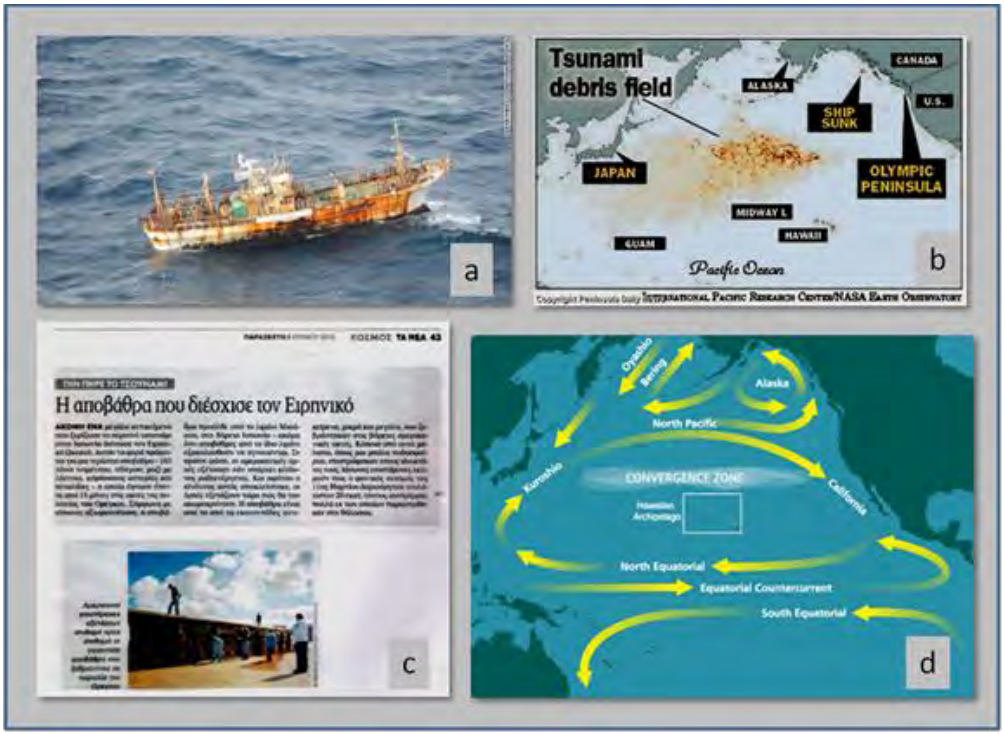

Εικόνα 24 – Δύο εικόνες που επιβεβαιώνουν απόλυτα τα λεγόμενα από τον Όμηρο, τον Ησίοδο και τους Ορφικούς ότι ο Ωκεανός είναι ένας ορμητικός ποταμός που ρέει συνεχώς. a, b: Το ακυβέρνητο αλιευτικό που έφτασε ακυβέρνητο στις δυτικές ακτές των Η.Π.Α., c: η αποβάθρα που διέσχισε τον Ειρηνικό Ωκεανό, d: απλοποιημένος χάρτης ωκεανίων ρευμάτων του Βόρειου Ειρηνικού.

5.2. Μετά τους Μινωίτες, τί;

Μετά την έκρηξη της Σαντορίνης οπωσδήποτε επήλθε μία αποδυνάμωση της Μινωικής παντοδυναμίας και της κυριαρχίας τους στον θαλάσσιο Μεσογειακό χώρο τουλάχιστον, την σκυτάλη παίρνουν οι Μυκηναίοι.

Κατά την διάρκεια της Μυκηναϊκής Εποχής πολλοί είναι αυτί που ενδιαφέρθηκαν για την εξασφάλιση χρήσιμων μετάλλων, όπως:

1. Ο *Φρίξος* και η *Έλλη* που ενδιαφέρθηκαν κυρίως για τον χρυσό των Παραευξείνιων περιοχών και κυρίως της ευρύτερης περιοχής της *Κολχίδας*.
2. Οι *Αργοναύτες* που, κατά την γνώμη μου, η εκστρατεία τους σκοπό είχε την εξασφάλιση πέραν των *μετάλλων* και του *ήλεκτρου* από τις περιοχές της *Βαλτικής Θάλασσας*, το *Σαρματικόν πέλαγος* των Αρχαίων Ελλήνων, οι ακτές του οποίου κατοικούντο από τους γνωστούς κατά την αρχαιότητα *Υπερβορείους*. Σημειωτέον ότι η Αργοναυτική εκστρατεία είναι μάλλον η μεγαλύτερη πανελλήνια εξερευνητική αποστολή της Μυκηναϊκής Ελλάδας, αφού σ'αυτή συμμετείχαν ολόκληρη ηγετική νεολαία όλων σχεδόν των βασιλείων της εποχής.
3. Ο *Ηρακλής*, που ενώ ξεκίνησε κι αυτός με τους Αργοναύτες, κάποια στιγμή τους εγκατέλειψε ή τον εγκατέλειψαν, κι έφυγε να πάει να δραστηριοποιηθεί στην *Ιβηρία* και στην *Κελτία*, αφού είχε προηγηθεί η επίσκεψή του στον *Άτλαντα* της *Αφρικής*, απ'όπου πήρε τα *χρυσά μήλα των Εσπερίδων*.

Βεβαίως ο Ηρακλής δεν περιορίστηκε στον ευρύτερο Περιαιγαιακό χώρο, αλλά επεκτάθηκε και στην Νοτιο-Δυτική Ευρώπη και κυρίως στην Ιβηρική χερσόνησο, και διάφοροι αρχαίοι συγγραφείς, και κυρίως ο Στράβων (.....) όπου ανάπτυξε μία έντονη μεταλλευτική δραστηριότητα και συγχρόνως κατασκεύασε μεγάλα υδραυλικά έργα, κατασκεύασε ή βελτίωσε μεγάλους οδικούς άξονες, ίδρυσε νέες πόλεις (La Corogna, Cadix, Alikante, Βαρκελώνη, Alise St. Reine, Nice, Monaco, κ.λπ.), εγκατέστησε νέες διοικήσεις προφανώς φιλικές προς τους Μυκηναίους, κ.λπ.

Όλα αυτά, προφανώς, για να διευκολύνει την επικοινωνία και την διακίνηση αγαθών, δηλαδή το εμπόριο, μεταξύ της Μυκηναϊκής Ελλάδας και της υπόλοιπης Νοτιο-δυτικής Ευρώπης κυρίως.

Ο Ηρακλής, προτού επεκταθεί στην ΝΔ-ική Ευρώπη, είχε δραστηριοποιηθεί στον ευρύτερο χώρο της *Βόρειας Ελλάδας* και των *Βαλκανίων*, καθώς επίσης και σ'εκείνο του *Εύξεινου Πόντου* και του *Καυκάσου*. Τα *Άλογα του Διομήδη* και η *Χρυσή Ζώνη της Ιππολύτης*, όπως και τα *Βόδια του Γηρυόνη*, του γιου του *Χρυσάωρα*, συμβολίζουν την προσπάθεια του μεγάλου ήρωα να εξασφαλίσει χρυσό για το βασίλειο των Μυκηνών. Στη συνέχεια φαίνεται ότι ο στόχος άλλαξε και άρχισε να ενδιαφέρεται για το νέο μέταλλο που είναι ο *σίδηρος*. Την αλλαγή αυτή δείχνει η εμπλοκή του με τον *Προμηθέα*, που, όπως λέει ο μύθος συμμετείχε στην απελευθέρωσή του στον Καύκασο.

Σε μία άλλη εκδοχή, που θέλει τον Προμηθέα να έχει φυλακιστεί σε κάποιο σπήλαιο του *Ινδοκαύκασου (Hindokash)*, που υψώνεται πάνω από τη σημερινή *Kabul* του *Αφγανιστάν*, ο Ηρακλής έφτασε μέχρις και εκεί και ακόμα πιο πέρα και συγκεκριμένα έφτασε μέχρι την *Άορνο Πέτρα* το σημερινό ..... που βρίσκεται ΒΑ-ικά της Kabul. Πρόκειται για την ίδια περιοχή που 1000 χρόνια αργότερα κατέκτησε ο Μ.Αλέξανδρος.

Όλα αυτά δείχνουν ότι ο Ηρακλής, μέχρι τον θάνατό του, που έγινε πάνω στην Οίτη, αφιερώθηκε στην εξασφάλιση των πρώτων υλών, που αύξησαν τον πλούτο και την κυριαρχία των Μυκηναίων σ' ολόκληρο τον κόσμο, που ξεκινούσε από τον *σημερινό Καναδά* (Πλούταρχος), στην περιοχή της *Λίμνης Superior*, την *χώρα* των *Υπερβορείων* (Ηρόδοτος, Παυσανίας, κ.ά.), την *Δυτική Ευρώπη* (Ιβηρία, Κελτία [Γαλατία], Ιταλία) (Στράβων, Διόδωρος Σικελιώτης, κ.ά.), την *Βόρεια Αφρική* (Αιθιοπία, Λιβύη, Άτλας, κ.λπ.) και τέλος την *Ασία* μέχρι και την *Κοιλάδα του Γάγγη*, όπου ίδρυσε και την πόλη *Παλίμβοθρα* την *αρχαία Παταλιπούτρα*, που σήμερα είναι γνωστή ως *Patna*, πρωτεύουσα του σημερινού Ομοσπονδιακού Κράτους Bihar, των Ινδιών.

Ο Κτησίας (5ος αι. π.Χ.) πάντως αναφέρει ότι στις Ινδίες υπάρχει πολύ *ασήμι* και *αργυρωρυχία* που δεν είναι βαθιά, ενώ τα βαθύτερα των Βάκτρων. Στην Ινδία υπάρχει ακόμα και *χρυσός*. Διευκρινίζει μάλιστα ότι δεν το βρίσκουμε στα ποτάμια ιζήματα, όπως στον *Πακτωλό*, αλλά στα *μεγάλα βουνά*, όπου κατοικούν *γρύπες*, τετράποδα που έχουν μέγεθος όσο ένας λύκος, που δυσκολεύουν την πρόσβαση στο χρυσάφι των βουνών. Πρόκειται δηλαδή για πρωτογενή χρυσό.

6. Μεταλλουργική Δραστηριότητα Θεών και Θεοτήτων

6.1. Ο Ήφαιστος

Ο θεός που ασχολείται με την μεταλλουργία και την επεξεργασία των μετάλλων είναι ο *Ήφαιστος*, ο οποίος δεν ορίζει μόνον τη φωτιά, το *χθόνιον* και το *ηφαιστειακόν πυρ*, αλλά είναι και ο μεγάλος θεός της σύγχρονης τεχνολογίας αφού είναι ο πρώτος που παράγει *κράματα*, όπως είναι ο *μπρούντζος* ή κρατέρωμα και ο ορείχαλκος.

Πέραν αυτών, κατασκευάζει μεταλλικά όπλα και διάφορα αντικείμενα καθημερινής χρήσης, αλλά και *αυτοκινούμενους τρίποδες* με *χρυσούς τροχούς* (Ομ. Ιλ. Σ 368-331).

Άλλοι τεχνολόγοι - μεταλλουργοί είναι ο *Δαίδαλος*, ο *Τάλως* και ο *'Ικαρος*,

Στους τεχνοκράτες της εποχής εντάσσονται και οι *Δάκτυλοι*, οι *Κουρήτες*, οι *Τελχίνες* και οι *Κάβειροι*.

6.2. Προμηθέας: Ο Πρωτοπόρος Τεχνολόγος

Ο *Προμηθέας*, ο γιος του Τιτάνα *Ιαπετού* και της *Ωκεανίδας Κλυμένης* ή της *Ασίας* ή του *Ουρανού* και της *Κλυμένης*, σύμφωνα με τον μύθο, *πήρε τη φωτιά* από τον *'Ολυμπο* ή τον *Ουρανό*, και την έφερε στον κόσμο. Αυτό θεωρήθηκε «έγκλημα» από τους Ολύμπιους. Έτσι, αποφάσισαν να τον τιμωρήσουν, αλυσοδένοντάς τον σε μια πλαγιά του όρους, που σήμερα λέγεται *Kasbek* (5047 m.), που υπάγεται στο ορεινό συγκρότημα του *Καυκάσου* και σήμερα ανήκει στην Γεωργία. Στην ευρύτερη περιοχή του τόπου του μαρτυρίου του Προμηθέα, έχουν ανακαλυφθεί μεταλλεύματα χαλκού, σιδήρου, μολύβδου και ψευδαργύρου.

Πολλοί ερμηνεύουν την προσφορά της φωτιάς προς τον άνθρωπο ως *γνώση*. Αυτό υποδηλώνει ότι ο Προμηθέας τιμωρήθηκε από τους Ολύμπιους θεούς επειδή, χωρίς την άδειά τους, προφανώς, προσέφερε τη γνώση στο ανθρώπινο γένος. Για ποια γνώση μιλάμε όμως; Οι Μυκηναίοι την εποχή τους,, αλλά ήδη οι Πρωτο-Έλληνες από την Πρωτο-Ελλαδική ακόμα και την Μέση Νεο-λιθική Εποχή, είχαν τεράστιες γνώσεις, όχι μόνον στη *γεωτεχνολογία*, αλλά και στην *μεταλλουργική τεχνολογία*. Το μόνο που δεν είχαν οι Μυκηναίοι ήταν η σύγχρονη, για την εποχή εκείνη, *πυροτεχνολογία* για να αποκτήσουν το νέο μέταλλο, τον σίδηρο, και στη συνέχεια την *τεχνολογία σκλήρυνσής* του, με άλλα λόγια την *χαλυβοποίησή* του. Αυτή τη γν'ώση φαίνεται πως απόκτησε ο Προμηθέας και την κράτησε ως μυστικό.

Ποιό όμως μπορεί να είναι το μυστικό που εξόργισε τους Ολύμπιους Θεούς;

Το μυστικό είναι ότι για να παραχθεί η θερμοκρασία των 1535° βαθμών, που είναι απαραίτητη για να εξαχθεί ο σίδηρος από τα μεταλλεύματα του σιδήρου, δεν είναι δυνατόν να ληφθεί από κάποια φυσική πηγή.

Αυτές τις υψηλές θερμοκρασίες τις πέτυχε ο Προμηθέας. Αυτός είναι και ο λόγος που ο Προμηθέας δεν έχει το εργαστήριό του σε κάποιο ηφαίστειο. Γι'αυτό απευθύνεται στον Ήλιο.

Ο Δίας, από τη στιγμή αυτή και μετά, έπαψε να είναι ο κυρίαρχος του κόσμου. Ο Δίας, "Ο πατέρας όλων των θεών και των ανθρώπων", ο παντοδύναμος θεός, ο Αστραπαίος, ο Εγχειρέραυνος, ο Κεραυναίος Δίας, ξεπεράστηκε. Αυτός είναι και ο λόγος του μένους του εναντίον του Προμηθέα.

Αυτός είναι και ο λόγος που ο *Προμηθέας θεωρείται δημιουργός του νέου ανθρώπου*.

Με την *εποχή του σιδήρου αρχίζει η απόλυτη κυριαρχία του ανθρώπου στη φύση*.

7. Η εποχή των Μετάλλων και η Γεωλογική Γνώση

Ο εντοπισμός και η μελέτη των κοιτασμάτων και γενικότερα των ορυκτών πόρων, είναι αντικείμενο της *Κοιτασματολογίας*, που είναι ένας κλάδος της Γεωλογίας.

Η κοιτασματολογική έρευνα προϋποθέτει βαθειά γεωλογική γνώση.

Κατά την γνώμη μου, η προσπάθεια εντοπισμού του καταλληλότερου πετρώματος για την κατασκευή λίθινων εργαλείων πρέπει να ξεκίνησε η *πρώτη γεωλογική έρευνα*.

Με την χρήση των μετάλλων πρέπει να ξεκινάει η *συστηματική γεωλογική έρευνα*. Η αρχή της Χαλκολιθικής εποχής, η οποία, σε αντίθεση με τις επικρατούσες αντιλήψεις, ξεκινάει μαζί σχεδόν με την Νεολιθική εποχή, αντιστοιχεί στο λυκαυγές της γεωλογικής επιστήμης.

Να θυμόμαστε:

1. Ότι στην Ελλάδα η μεταλλουργική επεξεργασία του χαλκού ξεκινάει τουλάχιστον το δεύτερο ήμισυ της 6^{ης} χιλιετίας π.Χ. και συνεπώς η Χαλκολιθική εποχή, με βάση τα ερευνητικά αποτελέσματα των Κουκούλη-Γ.Μπασιάκου, πρέπει να ξεκινάει γύρω στα 1500-1800 χρόνια μετά την έναρξη της Νεολιθικής Εποχής.
2. Ότι οι Μινωίτες, πέραν όλων των άλλων (εμπόριο, ναυτιλία, κ.ά.) πρέπει να είναι από τους πρώτους που ασχολήθηκαν με την κοιτασματολογική έρευνα των ορυκτών πόρων, την μεταλλουργία και την επεξεργασία των μετάλλων.
3. Μετά την έκρηξη του ηφαιστείου της Σαντορίνης (δεύτερο ήμισυ του 17ου αιώνα π.Χ.) την σκυτάλη πήραν οι Μυκηναίοι και οι Μινύες.

8. Αναφορές

Αισχύλος. *Επτά επί Θήβας*, (410-520), ΚΑΚΤΟΣ, τ.24,

Αισχύλος. *Προμηθεύς Δεσμώτης*, (352-375), ΚΑΚΤΟΣ, τ.7.

Andree J. 1922. *Bergban der Vorzeit*, Leipzig.

Ατακτίδης Κ. 1998. Η αρχαία μεταλλουργία της Καβάλας και η Σκαπτή Ύλη του Θουκυδίδη. *Α΄ Πανελλήνιο Σπηλαιολογικό Συνέδριο, 1992, «Άνθρωπος και Σπηλαιοπεριβάλλον». ΥΠ.ΠΟ*., σελ. 149-152.

Bar-Yosef O. 1998. The Natufian culture in the Levant, threshold to the origins of agriculture, *Evol. Anthropol.*, 6 (5), 159–177.

Βαρουφάκης Γ. 2005. *Η ιστορία του σιδήρου από τον Όμηρο στον Ξενοφώντα,* Ελληνικά Γράμματα, 175 σελ., Αθήνα.

Βαρουφάκης Γ. 2005. Μεταλλουργική Μελέτη Χάλκινων Δοκιμίων της Μινωικής Εποχής από τα Κύθηρα, *2nd International Conf. On Ancient Greek Technology, Procceed.*, σελ. 84-88, Εκδ. Τεχν. Επ. Ελλ., Αθήνα, 2006.

Βαρουφάκης Γ. 2008. Ο σίδηρος στα Ομηρικά έπη και Όμηρος ένας ευαίσθητος οικολόγος, *Πρακτ. Συνεδρ. «Επιστήμη και Τεχνολογία στα Ομηρικά Έπη»* (2006), Επιμ. Σ.Α. Παϊπέτη, σελ. 83-88, Πάτρα, 2008.

Bassiakos Y. and Betancourt P.P. 2002. Early Copper Production in Southern Aegean. New Data, *Early Metallurgy in Cyprus the Last Twenty Years 1982 – 2002,* Nicosia.

Bax K. 1981. *Schätze aus der Erde- Die Geschichte des Bergbaus,* Econ Verlag, 359 p., Düsseldorf.

Birks H.J. 1986. Quaternary biotic changes in terrestrial and lacustrine environments, with particular reference to North-West Europe, –In: B.E. Berglund (ed.), *Handbook of Holocene Palaeoecology and Palaeohydrology* (Chichester), 3-65.

Blanco A. and Luzon J.M. 1964. Pre-Roman silver miners at Rio Tinto, *Antiquity,* 43, 124-131.

Catling H.W. 1964. *Cypriot Bronzework in the Mycenaean World,* Oxford, Oxford University Press, Clarendon.

Christ W. 1898. Geschichte der griechischen Literatur bis auf die Zeit Justinians, *C.H. Becksche Verlagsbuch handlung*, 662 s., 1898, Munich.

Constantinou G. 1982. Geological features and ancient exploitation of the cupriferous sulphide orebodies of Cyprus. In I., Muhly, R., Maddin, and V., Karageorghis (eds) *Early metallurgy in Cyprus 4000-500 BC* , 13 -24, Pierides Foundation, Nicosia.

Coghlan, H.H., 1956. Notes on Prehistoric and Early Iron in the Old World (*Occasional Paper on Technology VIII*) (re-printed 1977), Pitt Rivers Museum.

Comendador-Rey B., Reboreda-Morillo, Kockelmann W., Macdonald M., Bell T. and Pantos M. 2006. Η πρώιμη τεχνολογία χαλκού στην «άκρη της γης»: ΝΔ Ιβηρία. *Επιστήμη και Τεχνολογία στα Ομηρικά Έπη, Πρακτ. Διεθνούς Συμποσίου 2006*, Συντ. Σ.Α. Παϊπέτης, 89-104, Πάτρα.

Cunliffe B. 2001. *The extraordinary voyage of Pytheas the Greek,* Penguin Books, London.

Davie O. 1932. The Copper Mines of Cyprus, *The Annual British School of Athens*, 30, London.

Διόδωρος Σικελιώτης. *Βιβλιοθήκης Ιστορικής, Βίβλος Πέμπτη*.- Οι Έλληνες, Κάκτος, Τ. 405, Αθήνα, 1997.

Friedreich J.B. 1851. *Die Realien in der Iliade und Odyssee,* F. Enke Verlag, Erlangen.

Jewell R.L. 2004. *Ancient Mines of Kitchi-Gummi. Cypriot/Minoan Traders in North America,* Published by Jewell Historics, Fairfield, PA, 2008.

Johannessen C.L. and Parker A.Z. 1989. Maize ears sculptured in 12th and 13th century A.D. India as indicators of Pre-columbian diffusion, *Economic Botany*, 43 (2), 164-180.

Jones J.E. 1998. *The Three Washeries at Agrileza in the Laureotiki,* Αργυρίτις Γη, Πανεπιστημιακές Εκδόσεις Ε.Μ.Π., Αθήνα.

Jovanovic B. 1979. The technology of primary copper mining in South-East Europe, *Proceedings of the Prehistoric Society*, 45, 103-109.

Jovanovic B. 1980. The origin of copper mining in Europe, *Scientific American*, 242, 114-120.

Κακαβογιάννη Ο., Ντούνη Κ., Νεζέρη Φ., Γεωργακοπούλου Μ. και Μπασιάκος Ι. 2005. Απόπειρα Τεχνολογικής Προσέγγισης της Παραγωγής Αργύρου και Μολύβδου κατά την Τελική Νεολιθική και Πρωτοελλαδική Ι Περίοδο στα Μεσόγεια, *2nd International Conf. on Ancient Greek Technology, Procceed.,* 77-83, Εκδ. Τεχν. Επ. Ελλ., Αθήνα, 2006.

Κακαβογιάννης Ε.Χ. 1988. *Τα αρχαία μεταλλεία της Λαυρεωτικής*, Αθήνα

Κακαβογιάννης Ε.Χ. 1996. Περί του «τύπου ΙΙ» των αρχαίων ορθογωνίων πλυντηρίων των μεταλλευμάτων της Λαυρεωτικής, *Αρχαιολογικόν Δελτίον*, 44-46, ΥΠΠΟ, Αθήνα.

Kepler J. 1593. *Opera Omnia*. Ed. Dr. Ch. Frisch, Francofurtia. M., 1870.

Koukouli Ch. and Bassiakos I. 2002. Non-slagging copper production of the 5th Millenium: The evidence from the Neolithic settlement of Promachon-Topolnica (Eastern Macedonia, Greece), *Abstracts of 8th Annual Meet. Of Europ. Assoc. of Archeology,* 193-194, 24-29 Sept. Thessaloniki.

Κωνοφάγος Κ. 1980. *Το Αρχαίο Λαύριο* –Εκδοτική Αθηνών.

Κωνοφάγος Κ. 1997. *Η Δημοκρατία της Αθήνας και οι Παραχωρήσεις στους Πολίτες της των Μεταλλείων Αργύρου της Λαυρεωτικής κατά τον 4ο Αιώνα π.Χ.,* 142 σελ.

Κωνσταντίνου Γ. 2005. Η Συμβολή των Χαλκούχων Κοιτασμάτων της Κύπρου στην Ανάπτυξη της Ιατρικής στην Αρχαιότητα, *2nd International Conf. On Ancient Greek Technology, Proceed.*, 114-121, Εκδ. Τεχν. Επ. Ελλ., Αθήνα, 2006.

Λέφκοβιτς Μ. 1997. *Η Μαύρη Αθηνά. Μύθοι και Πραγματικότητα*. (Μεταφρ.Ν. Κυριαζοπούλου). Εκδόσεις «ΚΑΚΤΟΣ», 251 σελ., Αθήνα.

Λουκιανός. Άπαντα. Τόμος 1. *Ηρακλής και Περί του ηλέκτρου ή των κύκνων*. Κάκτος, Αθήνα, 1994.

Μαρίνος Γ. 1958. Το ηφαίστειον του Αχιλλείου, Ανατολικής Όρθρυος, *Δελτ. Ελλην. Γεωλ. Εταιρίας*, ΙΙΙ/Ι, 64-72.

Mariolakos I. 2009. The forgotten Geographic and Physical – Oceanographic Knowledge of the Prehistoric Greeks, *Actas del XIV Congresso de la FIELC*, Athenas, 14-16 de octubre de 2009, Madrid, 2011.

Menzies Gavin 2011. *The Lost Empire of Atlantis: History's Greatest Mystery Revealed*. William Morrow Publ., 374 pp.

Μπασιάκος Ι. and Παπαδόπουλος Ε. 2011. *Πρώιμη παραγωγή χαλκού και αργύρου στα Λιμενάρια Θάσου. Μια τεχνολογική προσέγγιση* (υπό δημοσίευση).

Muhly J.D. 2005. Texts and technology. The beginnings of iron metallurgy in the eastern Mediterranean, *2nd Intern. Confer. on Ancient Greek Technology Proceedings*, 19-31, Tech. Chamber of Greece, Athens, 2006.

Ντάρλας Α. 2005. Οι Παλαιολιθικές Ρίζες της Τεχνολογίας, *2nd Intern. Confer. on Ancient Greek Technology. Proceedings*, 701-707, Εκδ. Τεχν. Επ. Ελλ.

Όμηρος. *Ιλιάς*.

Όμηρος. *Οδύσσεια*.

Παπασταματάκη Δ. 1993. Οι Σκωρίες και η Μεταλλουργία του Χαλκού κατά την Αρχαιότητα, *Δελτίο Ελλ. Σπηλαιολ. Εταιρείας*, XXI, 370-377, Αθήνα.

Παπασταματάκη Αρτ. 2007. Οι αρχαίοι Έλληνες ακολούθησαν την τεχνική της αναγωγικής τήξης για την απόληψη του χαλκού από το μετάλλευμά του, *Χημικά Χρονικά*, 9, 25-28, Αθήνα.

Πλούταρχος. *Περί των εκλελοιπότων χρηστηρίων. Ηθικά*. (μτφρ. ΚΑΚΤΟΣ), τ. 11, 109-243, Αθήνα, 1995.

Πλούταρχος. *Περί του εμφαινομένου προσώπου τω κύκλω της Σελήνης. Ηθικά*. (μτφρ. ΚΑΚΤΟΣ), τ. 24, 85-209, Αθήνα, 1996.

Πλούταρχος. *Περί ποταμών και όρων επωνυμίας* (μτφρ. Δ. Γ. Κουτρουμπάς). Αρχαίοι Έλληνες Γεωγράφοι. Νέα Θέσις, Αθήνα, 1999.

Πλούταρχος. *Περί Ομήρου (Περί του βίου και της ποιήσεως του Ομήρου). Ηθικά*. (μτφρ. ΚΑΚΤΟΣ), τ. 31, Αθήνα, 2012.

Poursat J. 2006. Materials and Craftsmanship in Bronze Age Crete, *Proc. 2nd Intern. Conf. Ancient Greek Technology*, TEE, 44-48, Athens.

Quiring H. 1964. *Die Metallischen Rohstoffe. Ihre Lagerungsverhältnisse und ihre Wirtschaftliche Betdentung, Geschichte a. Vorzeit, Altertum und Mittelalter*. Ed. Emil Kraume; B.4, Ferdinand Enke Verlag, Stuttgart, 1964.

Radivojevic M., Rehren Th., Pernicka E., Sljivar D., Brauns M. and Boric D. 2010. On the origins of extractive metallurgy. new evidence from Europe, *Journal of Archaeological Science*, 37, 2775-2787.

Renfrew A.C. 2006. *Η ανάδυση του πολιτισμού. Οι Κυκλάδες και το Αιγαίο στην 3η χιλιετία π.Χ.* (μτφρ. Δ. Κοκκώνης). Αθήνα.

Renfrew C. and Bahn P. 1991. *Αρχαιολογία. Θεωρίες, Μεθοδολογία και Πρακτικές Εφαρμογές* (Μεταφρ. Α. Καλλέγια). Εκδ. Α. Καρδαμίτσα, 646 σελ., Αθήνα, 2001.

Roberts B.W., Thornton C.P. and Pigott V.C. 2009. Development of metallurgy, *ANTIQUITY*, 83, 1012-1022.

Sandars N.K. 1978. *The Sea People*. (Ελλ. Εκδ. Οι Λαοί της Θάλασσας, μφτρ. Ε. Αστερίου). Εκδόσεις Οδυσσέας, 286 σελ., Αθήνα 2001.

Schaeffer C.F.A. 1965. An ingot god from Cyprus, *ANTIQUITY*, 39, 56-7.

Showleh Taha 2006. Ο Ποταμός Ωκεανός. Επιστήμη και Τεχνολογία στα Ομηρικά Έπη (*Πρακτ. Διεθνούς Συμποσίου 2006, Συντ. Σ.Α. Παϊπέτης)*, 70-74, Πάτρα, 2008.

Skarpelis N. 2003. Ancient Potential Tin Sources in the Aegean, *Acts of the XIVth Congress of Liège*, Belgium, 2-8 September, 2001, 159-164, Basingstoke Press, England.

Sodders B. 1990. *Michigan Prehistory Mysteries*, Avery Color Studios, AuTrain, Michigan.

Solomou S. 1992. *Greek knowledge of India before the fourth century B.C*. A Thesis submitted in partial fulfillment of the Requirements for the Degree of Master of Arts in the Faculty of Graduate Sstudies, Department of Classics, University of British Columbia. Available online at

https://circle.ubc.ca/bitstream/handle/2429/1735/ubc_1993_spring_solomou_stavros.pdf?sequence=3

Sorenson, J L. and Johannessen, C. L., 2006. Biological Evidence for Pre-Columbian Transoceanic Voyages. In. Mair, Victor, H. (ed), *Contact and Exchange in the Ancient World*. 238–97, University of Hawaii Press., Honolulu.

Spedicato, E., 2005. The Deucalion catastrophe. 1. The passage of the Red Sea by Moses and the Phaethon explosion. 2. The Phaethon explosion and some of its affects outside Egypt. The Atlantis Hypothesis. Searching for a Lost Land, *Proceedings of the Intern. Conf., Atlantis*, Melos Island, 2005, 115-129 and 131-143, Athens 2007.

Σταγειρίτη, Α., 1815. *Ωγυγία ή Αρχαιολογία*. (Επανέκδοση. Ελεύθερη Σκέψη, Αθήνα 1996).

Stocks, Theodor, and G. Wüst. 1935. "*Die Tiefenverhältnisse des offenen Atlantischen Ozeans*" . Deutsche Atlantischen Exped. Meteor, 1925–1927, Wiss. Erg., Bd. 3, Teil 1, l., Lief., 31 pp., 1935.

Στράβων: Γεωγραφικά.

Σύνδεσμος Μεταλλευτικών Επιχειρήσεων, 1979. *Ο Ελληνικός Ορυκτός Πλούτος*. 696 σελ., Αθήνα.

Τσαΐμου, Κ. ,1988. *Εργασία και Ζωή στο Αρχαίο Λαύριο σε εγκατάσταση εμπλουτισμού μεταλλευμάτων τον 4ο αιώνα π.Χ.* Διδακτορική Διατριβή, Αθήνα.

Τσαΐμου, Κ.Γ., 1999. Ο χρυσός και ο άνθρωπος. *Ορυκτός Πλούτος*, 1999 (111), 41-54, Αθήνα.

Τσαΐμου, Κ. & Κονοφάγος Η., 1998. *Σύστημα σταθερής πίεσης στον εμπλουτισμό των επίπεδων πλυντηρίων του Αρχαίου Λαυρίου*. Αργυρίτις Γη, Πανεπιστημιακές Εκδόσεις Ε.Μ.Π., Αθήνα.

Tylecote, R.F., 1987. *The early history of Metallurgy in Europe*.

Ζέγγελης Κ.Δ., 1891. *Η επιστήμη της Φύσεως παρ' Ομήρω*. Επανέκδοση Παν/μίου Πατρών 1977, Εισαγωγή Σ. Παϊπέτη.

Δελτίο της Ελληνικής Γεωλογικής Εταιρίας, τομ. XLVII , 2013
Πρακτικά 13ου Διεθνούς Συνεδρίου, Χανιά, Σεπτ. 2013

Bulletin of the Geological Society of Greece, vol. XLVII 2013
Proceedings of the 13th International Congress, Chania, Sept. 2013

ΕΙΜΑΣΤΕ ΜΟΝΟΙ ΣΤΟ ΣΥΜΠΑΝ; ΟΙ ΜΕΤΕΩΡΙΤΕΣ ΔΙΝΟΥΝ ΑΠΑΝΤΗΣΕΙΣ;

Μπαζιώτης Ι. [1,2] και Taylor L.A.[3]

[1] Τμήμα Ορυκτολογίας, Πετρολογίας και Οικονομικής Γεωλογίας, Σχολή Γεωλογίας, Αριστοτέλειο Πανεπιστήμιο Θεσσαλονίκης, 54124, Θεσσαλονίκη, Ελλάδα, ibaziotis@geo.auth.gr; baziotis@metal.ntua.gr

[2] Department of Geosciences, University of Perugia, 06100, Perugia, Italy

[3] Planetary Geosciences Institute, Department of Earth and Planetary Sciences, University of Tennessee, Knoxville, TN 37996, USA

Abstract

The humankind, despite the recent technological achievements, does not yet have the ability to carry out routine trips to nearby celestial bodies. However, space science is a reality. The "Apollo" missions, that took place during the period 1969-1972, included the moon landing, the walk of astronauts and collection of valuable samples. Since then, no similar space journey has been carried out. The possibility for future missions such as the return to the Moon or Mars, or to an asteroid (e.g., Vesta), seems small enough to be implemented in the next decades. Nevertheless, nature has the mechanism and procedures to resolve this problem by sending extra-terrestrial rocks in earth in the form of meteorites. Meteorite fall on Earth is a major event, as it reveals important information about the primordial stages of formation of our solar system, or the creation processes of other planets. However, the big question still remains; whether these rocks host or have traces of past life in turn employs researchers in the last twenty years. McKay et al. (1996) studied the meteorite ALH 84001 originating from Mars, claimed for important discoveries such as structures corresponding to nanobacteria.

In the current paper, we focus on the origin of Martian meteorites, presenting their complete geological history; from the genesis of their protoliths till their falling to the earth. We attempt to shade light in the understanding of meteorite formation using mineralogical-petrological-geochemical data, and the assignment of timing for each event based upon contemporary geochronological data. Recently, studies of the Martian meteorite Tissint, allegedly discovered structures rich in carbon and oxygen. Furthermore, recent field observations from Curiosity rover, indicates the existence of surface water that flowed once in the past at the Martian surface. We conclude that the planet Mars might not be a "dead" planet. But it turns out that many of the meteorites that reach the Earth, have undergone a complex history which is associated with the development of very high pressures and temperatures on the surface of the planet (e.g., Mars) from which they originate, able to destroy any trace of life before them. After all, we should be very sceptic and evaluate all the possibilities before the acceptance for the existence of life out there.

Key words: *Tissint, Mars, planetology, life.*

Περίληψη

Ο άνθρωπος, παρά τα τεράστια άλματα τεχνολογικής ανάπτυξης που έχει κάνει, δε διαθέτει ακόμα τη δυνατότητα για να πραγματοποιήσει ταξίδια ρουτίνας σε κοντινά ουράνια σώματα. Ωστόσο, η θεμελίωση της Διαστημικής Επιστήμης είναι προ-ετών μία πραγματικότητα. Οι Αποστολές Apollo, που έλαβαν χώρα κατά το χρονικό διάστημα 1969-1972, περιελάμβαναν την προσελήνωση, τον περίπατο των αστροναυτών και τη συλλογή πολύτιμων δειγμάτων. Έκτοτε, δεν έχει πραγματοποιηθεί άλλο όμοιο ταξίδι του ανθρώπινου είδους. Η πιθανότητα πραγματοποίησης μελλοντικών αποστολών όπως η επιστροφή στη Σελήνη, ή στον πλανήτη Άρη, ή σε κάποιο αστεροειδή (π.χ. Εστία), φαντάζει αρκετά μικρή ώστε να υλοποιηθεί ακόμα και τις επόμενες δεκαετίες. Παρολαυτά, η φύση, έχει το μηχανισμό και τις διαδικασίες επίλυσης αυτού του προβλήματος, καθώς «στέλνει» εξω-γήϊνα κομμάτια πετρώματος με τη μορφή μετεωρίτη, στη Γη. Η πτώση μετεωριτών στη Γη αποτελεί ένα σημαντικό γεγονός, καθώς αποκαλύπτουν σημαντικές πληροφορίες σχετικά με τα αρχέγονα στάδια σχηματισμού του ηλιακού μας συστήματος, την ηλικία και τη διαδικασία δημιουργίας άλλων πλανητών. Ωστόσο, το μεγάλο ερώτημα, αν φιλοξενούν ή μπορούν να φιλοξενήσουν ίχνη που υποδηλώνουν ζωή απασχολεί τους ερευνητές τα τελευταία είκοσι χρόνια. Η επιστημονική ομάδα υπό την αιγίδα του καθηγητή McKay το 1996 στα πλαίσα μελέτης του μετεωρίτη ALH 84001 με προέλευση τον πλανήτη Άρη, υποστήριξε ότι ανακάλυψε δομές που αντιστοιχούν σε νανοβακτήρια.

Στην παρούσα εργασία εστιάζουμε στους μετεωρίτες με προέλευση τον πλανήτη Άρη, παρουσιάζοντας την ιστορία από τη γέννεση των πρωτολίθων τους, μέχρι και τη στιγμή που προσκρούουν στη γη. Γίνεται προσπάθεια να κατανοηθεί ο τρόπος δημιουργίας ενός μετεωρίτη χρησιμοποιώντας ορυκτολογικά-πετρολογικά-γεωχημικά στοιχεία, και η τοποθέτηση του κάθε γεγονότος στο χρόνο με βάση σύγχρονα γεωχρονολογικά δεδομένα. Σε πρόσφατες μελέτες του μετεωρίτη Tissint, έχοντας επίσης προέλευση από τον πλανήτη Άρη, υποστηρίζεται ότι ανακαλύφθηκαν δομές πλούσιες σε άνθρακα και οξυγόνο. Επίσης πρόσφατες επιτόπιες παρατηρήσεις από το διαστημικό όχημα Curiosity, υποδεικνύουν την ύπαρξη επιφανειακού νερού που έρεε κατά το παρελθόν στην επιφάνεα του πλανήτη Άρη. Με βάση τα προηγούμενα, καταλήγουμε ότι ο πλανήτης Άρης ίσως να μην αποτελεί ένα «νεκρό» πλανήτη. Αποδεικνύουμε όμως ότι πολλά από τα πετρώματα που φθάνουν στη Γη, έχουν υποστεί μία πολύπλοκη ιστορία η οποία συνδέεται με την ανάπτυξη εξαιρετικά μεγάλων πιέσεων και θερμοκρασιών στην επιφάνεια του πλανήτη από τον οποίο προέρχονται, ικανών να καταστρέψουν οποιοδήποτε ίχνος ζωής πριν από αυτές. Αποτέλεσμα αυτού είναι η αξιολόγηση των μελετών να γίνεται με σύνεση πριν αναντίρρητα αποδειχθεί το γεγονός ύπαρξης ζωής.

Λέξεις κλειδιά: *Tissint, Άρης, πλανητολογία, ζωή.*

1. Εισαγωγή

Άρης, ένας από τους Ολύμπιους θεούς που λάτρευε τον πόλεμο, συνάμα είναι και ο πλανήτης που προκαλεί θαυμασμό σε όλο τον κόσμο. Είναι ο κόκκινος πλανήτης και αυτός που αποτελεί τον πλησιέστερο προς τη Γη διαστημικό γείτονα, μετά τη Σελήνη. Μέχρι σήμερα, ο άνθρωπος, δεν είχε την τεχνολογική υποδομή για τη συλλογή πετρωμάτων απευθείας από το έδαφος του πλανήτη Άρη. Ωστόσο, ισχυρές συγκρούσεις άλλων σωμάτων στην επιφάνειά του, προκάλεσαν την αποκόλληση πετρωμάτων διαφόρων μεγεθών, αλλά και λεπτόκοκκης σκόνης. Όλα τα υλικά διέφυγαν και ταξίδευσαν στο αχανές διάστημα για μεγάλο χρονικό διάστημα. Το υλικό αυτό, μετά από το αστρικό ταξίδι εκατομμυρίων ετών φθάνει και διαπερνά την ατμόσφαιρά της Γης. Όταν επιβιώσει της τριβής κατά τη διέλευση από τη γήϊνη ατμόσφαιρα, πεφτει στο έδαφος και πλέον αποτελεί έναν μετεωρίτη.

Ένας μετεωρίτης, όπως γίνεται αντιληπτό, δεν είναι τίποτε άλλο από ένα κομμάτι πετρώματος. Είναι εκείνο το πέτρωμα που έχει διαφύγει δύο καταστροφών, μία στην επιφάνεια του ουράνιου σώματος από το οποίο προέρχεται και μία δεύτερη, κατά την πρόσκρουση στην επιφάνεια της Γης. Όταν ένας πέτρωμα εισέρχεται στην ατμόσφαιρα της Γης, λαμβάνουν χώρα διάφορες διεργασίες, όπως τριβή, υψηλή πίεση, αλλά και χημικές αντιδράσεις με τα περιβάλλοντα αέρια που βοηθούν στο να θερμανθεί, απελευθερώνοντας φως και σχηματίζοντας μία μπάλα φωτιάς, γνωστή και ως μετέωρο. Μετεωρίτες έχουν βρεθεί και σε άλλα ουράνια σώματα του ηλιακού μας συστήματος, όπως στο φυσικό δορυφόρο της Γης, τη Σελήνη και στο πλανήτη Άρη.

Στην παρούσα μελέτη γίνεται προσπάθεια να κατανοηθεί ο μηχανισμός γένεσης ενός μετεωρίτη από τα πρώτα στάδια σχηματισμού του πρωτόλιθού του, μέχρι και τη στιγμή που θα προσκρούσει στη Γη. Παρατίθενται πληροφορίες για τις συνθήκες που επικρατούν στην επιφάνεια του πλανήτη Άρη τη στιγμή πρόσκρουσης ενός αστεροειδούς και της επακόλουθης αποκόλλησης τεμαχίων πετρωμάτων από την επιφάνειά του. Η φυσική των ορυκτών είναι αυτή που αντανακλά την ανάπτυξη εξαιρετικά υψηλών πιέσεων και θερμοκρασιών στην επιφάνεια κατά την πρόσκρουση του αστεροειδούς, λόγω της μετατροπής τους σε άλλες, περισσότερο σταθερές σε ακραίες συνθήκες, ορυκτολογικές δομές. Επιπρόσθετα, χρησιμοποιούνται σύγχρονα γεωχρονολογικά δεδομένα, σε συνδυασμό με ορυκτολογικά-πετρολογικά-γεωχημικά στοιχεία, ώστε να τοποθετηθεί το κάθε γεωλογικό γεγονός στο χρόνο και να αποκαλυφθεί το σύντομο χρονικό διάστημα μεταξύ της αποκόλλησης από την επιφάνεια του Άρη, μέχρι τη στιγμή που πέφτει στο έδαφος ως μετεωρίτης. Απώτερος σκοπός, ωστόσο, της παρούσας εργασίας είναι να παρουσιαστούν εκείνα τα στοιχεία-σημάδια χαρακτηριστικά της ύπαρξης (ή πιθανής ύπαρξης) ζωής. Γίνεται μία ανασκόπηση των εως τώρα ανακαλύψεων που σχετίζονται με βιολογικά ίχνη σε μετεωρίτες. Καταλήγουμε παρόλαυτά ότι θα πρέπει όλα τα στοιχεία να λαμβάνονται με ιδιαίτερη προσοχή καθώς οι μετεωρίες αποτελούν πετρώματα που έχουν υποστεί μία εξαιρετικά πολύπλοκη γεωλογική ιστορία η οποία είναι ικανή να καταστρέψει οποιοδήποτε ίχνος ζωής σε αυτές.

2. Κατηγορίες Μετεωριτών

Οι μετεωρίτες διακρίνονται σε τρεις μεγάλες κατηγορίες: λιθομετεωρίτες, σιδηρομετεωρίτες και λιθο-σιδηρομετεωρίτες (Σχ. 1). Οι λιθομετεωρίτες αποτελούνται κυρίως από πυριτικά ορυκτά και μοιάζουν με πετρώματα που προέρχονται από τον μανδύα της Γης. Αντίθετα οι σιδηρομετεωρίτες αποτελούνται κατεξοχήν από μεταλλικό σίδηρο-νικέλιο. Αναγνωρίζονται εύκολα εξαιτίας του μεγάλου τους βάρους. Οι περισσότερες έρευνες καταλήγουν στο ότι οι σιδηρομετεωρίτες αποτελούν υπολείμματα από τον πυρήνα ενός ουράνιου σώματος το οποίο διαμελίστηκε. Η τρίτη ομάδα μετεωριτών είναι μία ενδιάμεση κατηγορία αποτελούμενη από μεταλλικό υλικό και πυριτικά ορυκτά. Περαιτέρω οι λιθομετεωρίτες διακρίνονται σε δύο κατηφορίες: χονδρίτες και ανονδρίτες. Οι χονδρίτες αποτελούν τον συνηθέστερο τύπο λιθομετεωρίτη. Στο εσωτερικό τους σχηματίζονται μικρές στρογγυλές σφαίρες, που ονομάζονται χόνδροι (chondrules) και αποτελούνται από τα ορυκτά ολιβίνη και πυρόξενο. Οι περισσότεροι χονδρίτες μετεωρίτες έχουν ηλικία γένεσης 4.6 δισεκατομμύρια χρόνια. Μία από τις υποκατηγορίες χονδριτών αποτελούν οι ανθρακώδεις μετεωρίτες (Carbonaceous meteorites), οι οποίοι περιέχουν υψηλές περιεκτικότητες άνθρακα, νερό, και οργανικά συστατικά. Αντίθετα, οι αχονδρίτες, αποτελούνται από ίδια ορυκτά όπως οι χονδρίτες, ωστόσο δε διαθέτουν χόνδρους. Οι μετεωρίτες αυτής της κατηγορίας μοιάζουν με εκείνα τα γήινα πετρώματα που έχουν προέλθει από κρυστάλλωση μάγματος.

Μία ομάδα πετρωμάτων που ανήκει στους αχονδρίτες ονομάζεται σεργκοτίτες (shergottites). Οι σεργκοτίτες ανήκουν στην κατηγορία των αχονδριτών που αντιστοιχούν σε τμήματα του ανώτερου μανδύα του πλανήτη Άρη. Διακρίνονται σε τρεις μεγάλες κατηγορίες: βασαλτικούς, λερζολιθικούς και εκείνους με μεγάλους κρυστάλλους ολιβίνη. Οι βασαλτικοί σεργκοτίτες αποτελούνται από τα ορυκτά πυρόξενο και πλαγιόκλαστο, οι λερζολιθικοί από ολιβίνη και πυρόξενο. Η τρίτη ομάδα σεργκοτιτών αποτελείται από μεγακρυστάλλους ολιβίνη που επιπλέουν μέσα σε μία λεπτόκοκκη κύρια μάζα αποτελούμενη από πλαγιόκλαστο και πυρόξενο. Άλλη ταξινόμηση των σεργκοτιτών στηρίζεται στη χημική σύσταση του πετρώματος και συγκεκριμένα

στα λεγόμενα ασυμβίβαστα στοιχεία και στο ποσοστό ύπαρξής τους μέσα στο αναλυθέν πέτρωμα. Αυτή περιλαμβάνει: (1) εμπλουτισμένης, (2) ενδιάμεσης και (3) αποπλυμένης σύστασης πετρώματα. Στους αχονδρίτες μετεωρίτες με προέλευση τον πλανήτη Άρη, ανήκουν επίσης οι Νακλίτες (Nakhlites) και οι τσασινίτες (Chassignites).

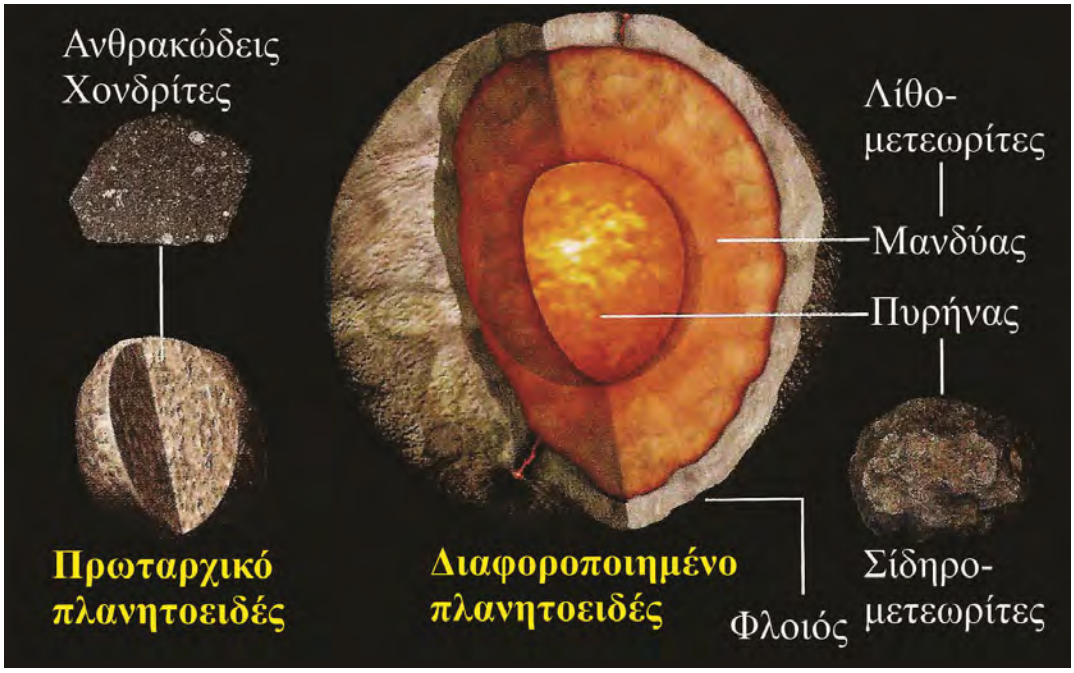

Σχήμα 1 - Σχηματική απεικόνιση που αναπαριστά την προέλευση των μετεωριτών. Οι σιδηρομετεωρίτες προέρχονται από τον πυρήνα, ενώ οι ανθρακώδεις χονδρίτες αποτελούν τμήματα των αρχέγονων πλανητοειδών.

3. Σχηματισμός Μετεωριτών – Το Παράδειγμα του Πλανήτη Άρη

3.1. Πρωτόλιθοι Μετεωριτών

Όπως αναφέρθηκε στο προγούμενο κεφάλαιο, οι μετεωρίτες με προέλευση τον πλανήτη Άρη διακρίνονται σε τρεις κατηγορίες, σεργκοτίτες, νακλίτες και τσασινίτες, το όνομα των οποίων προέρχεται από το όνομα του αρχικού μετεωρίτη που αντιστοιχεί στην κάθε κατηγορία, Shergotty, Nakhla και Chassigny. Η επισταμένη ορυκτολογική-πετρολογική-γεωχημική μελέτη αυτών των πετρωμάτων παρέχει σημαντικές πληροφορίες σχετικά με τον τρόπο γένεσης των πρωτολίθων τους. Η κυρίαρχη, εκ των τριών προαναφερθέντων κατηγοριών είναι εκείνη των σεργκοτιτών μετεωριτών, κι έπεται εκείνη των νακλιτών, γι`αυτό και στη συνέχεια αναπτύσσουμε τα προτεινόμενα μοντέλα σχηματισμού των προτωλίθων τους.

Ο προσδιορισμός των μανδυακών πηγών (αποπλυμένες και εμπλουτισμένες) από τις οποίες προέρχονται οι σεργκοτίτες τοποθετείται στο πλαίσιο δύο ακραίων μοντέλων: 1) βασαλτικών μαγμάτων που προέρχονται από το μανδυά και αφομοιώνουν υλικό φλοιού και 2) βασαλτικών μαγμάτων που προέρχονται από πολλαπλές μανδυακές πηγές. Ακολούθως παρουσιάζονται τα βασικά στοιχεία και ο μηχανισμός δημιουργίας των μοντέλων αυτών.

Τα μοντέλα που έχουν ως βάση την αφομοίωση υλικού, προτείνουν ότι μέσα στον φλοιό βρίσκεται μία επλουτισμένη πηγή ενώ ταυτόχρονα, από την αποπλυμένη πηγή #1 πηγάζουν όλοι οι βασαλτικοί σεργκοτίτες (Σχ. 2α). Οι δύο αυτές πηγές προέρχονται από τα πρώϊμα στάδια διαφοροποίησης του πλανήτη Άρη κατά τη διάρκεια κρυστάλλωσης του αρχικού ωκεανού

μάγματος. Ο ανώτερος μανδύας βρίσκονταν σε αναγωγικές συνθήκες, ενώ ο φλοιός σε ελαφρά οξειδωτικές. Η εφαρμογή αυτού του μοντέλου έχει το πλεονέκτημα της εύκολης ερμηνείας του πρώϊμου διαχωρισμού και της μακρόχρονης απομόνωσης των δύο πηγών (φλοιού και μανδύα). Επιπλέον, στο μοντέλο αυτό παρέχεται η διαδικασία ανάμειξης εμπλουτισμένων και αποπλυμένων συστατικών κατά τη δημιουργία των βασαλτών πριν την τελική ηφαιστειότητα.

Η έτερη κατηγορία μοντέλων, εκείνη που στηρίζεται στις πολλαπλές μανδυακές πηγές, στηρίζεται σε μία αποπλυμένη και μία εμπλουτισμένη πηγή. Αυτές οι δύο πηγές πιθανότατα ήταν απομονωμένες για ένα διάστημα 4 δισ.χρ. Η ανάμιξη αυτών των δύο προήλθε τη στιγμή της τήξης, παράγοντας τις χημικές και ισοτοπικές ενδιάμεσες ποικιλίες των σεργκοτιτών. Το μοντέλο αυτό στηρίζεται στην αρχή ότι οι διαφορετικές πηγές έχουν δημιουργηθεί κατά τη διάρκεια της κρυστάλλωσης του ωκεανού μάγματος σε μεγάλο βάθος. Οι αποπλυμένες πηγές αντιστοιχούν σε σωρειτικές ακολουθίες που δημιουργήθηκαν πριν την κρυστάλλωσης των εμπλουτισμένων.

Χαρακτηριστικά παραδείγματα μοντέλου πολλαπλών μανδυακών πηγών δύο- (Symes *et al*., 2008) και τριών- (Blinova & Herd, 2009) σταδίων απεικονίζονται στο σχήμα 2. Στο μοντέλο των Symes *et al*. (2008) φαίνονται οι περιοχές της μανδυακής πηγής που είναι αποπλυμένη, ενδιάμεση και εμπλουτισμένη σε σύσταση (Σχ. 2β). Τα στοιχεία K, Th, U που είναι ικανά να παράγουν θερμότητα κατά τη ραδιενεργή διάσπασή τους, συγκεντρώνονται σε ύστερο-προϊόντα κρυστάλλωσης και μπορούν να αναμιχθούν με τους αποπλυμένους σωρειτικούς ορίζοντες. Η απομόνωση των πηγών, εξασφαλίζεται μέσω της έναρξης της διαδικασίας τήξης στους προηγούμενους «γόνιμους» αποπλυμένους σωρειτικούς ορίζοντες. Σε αυτό το σχήμα απεικονίζονται σενάρια στα οποία η άνοδος των τηγμάτων διασφαλίζεται με μικρό ποσοστό αφομοίωσης ή κρυστάλλωσης μέχρις ότου τοποθετηθούν σε μαγματικούς θαλάμους στον κατώτερο φλοιό του Άρη. Ακολουθεί η εκκίνηση της κρυστάλλωσης, ενώ η κλασμάτωση δίνει γένεση σε μίγματα τήγματος και κρυστάλλων πριν την τελική τοποθέτησή τους στην επιφάνεια του πλανήτη,. Αυτή η διαδικασία κλασματικής κρυστάλλωσης είναι που κατά τους Symes *et al*. (2008) και Shearer *et al*. (2008) συνδέει τους πλούσιους σε ολιβίνη και πυρόξενο βασάλτες, μέσα σε κάθε διαφορετικής σύστασης ομάδα σεργκοτιτών (αποπλυμένοι και εμπλουτισμένοι).

Στα αρνητικά του μοντέλου αυτού είναι η αδυναμία να προσομοιώσει τη χημισμό των σεργκοτιτών σε σπάνιες γαίες. Αποτέλεσμα αυτού είναι η πρόταση των Blinova & Herd (2009) για ένα, τριών-σταδίων, πετρογενετικό μοντέλο (Σχ. 2γ). Σε αυτό, η πηγή των αποπλυμένων σεργκοτιτών είναι ένα μίγμα σωρειτών ανώτερου μανδύα που προηγουμένως έχει υποστεί τήξη και εξαγωγή τήγματος (μητρικό μάγμα νακλιτών) πριν από 1.3 δισ.χρ. και λιθολογία που προέρχεται από το όριο μανδύα πυρήνα. Αυτές οι δύο πηγές έχουν διαφορετικές αναλογίες Nd/Sm δείχνοντας ότι έχουν εξελιχθεί ανεξάρτητα. Η πηγή με προέλευση τον βαθύ μανδύα μεταφέρθηκε σε μικρότερα βάθη μέσω ενός μανδυακού διάπειρου και υπέστη πολυβαρική τήξη σε ένα εύρος πιέσεων. Ακολούθως, η τήξη του μίγματος του μανδυακού διάπειρου και του μανδυακού υπολείμματος είναι ικανή να αναπαραγάγει τις τιμές σπανίων γαιών των αποπλυμένων σεργκοτιτών. Η εμπλουτισμένη πηγή είναι μία ύστερο-σωρειτική λιθολογία που εντοπίζεται στον ανώτερο μανδύα. Τα μανδυακά διάπειρα είναι οι εκείνες οι περιοχές που παρέχουν την αναγκαία ποσότητα θερμότητας για την εκκίνηση της διαδικασίας μερικής τήξης.

Το πλεονέκτημα της εφαρμογής του μοντέλου πολλαπλών μανδυακών πηγών είναι ότι αποκλείει τη δυσκολία των θερμοδυναμικών και χημικών προϋποθέσεων που τίθενται για την αφομοίωση τμημάτων φλοιούν από τους βασάλτες που προέρχονται από το μανδύα. Ωστόσο, και αυτό το μοντέλο προϋποθέτει συγκεκριμένα χαρακτηριστικά που σχετίζονται με το χρόνο απομόνωσης και ανάμιξης. Για παράδειγμα, η διάδοση θερμότητας στο μανδύα πρέπει να λαμβάνει χώρα σε σχετικά μικρή κλίμακα ώστε να διατηρούνται χωριστά οι δύο μανδυακές πηγές για ένα χρόνικό διάστημα 4 δισ.χρ. Αυτό σημαίνει ότι τα όρια των πηγών είναι θερμικά, δηλαδή επιτρέπεται η μεταφορά θερμότητα όχι όμως και η ανταλλαγή μάζας.

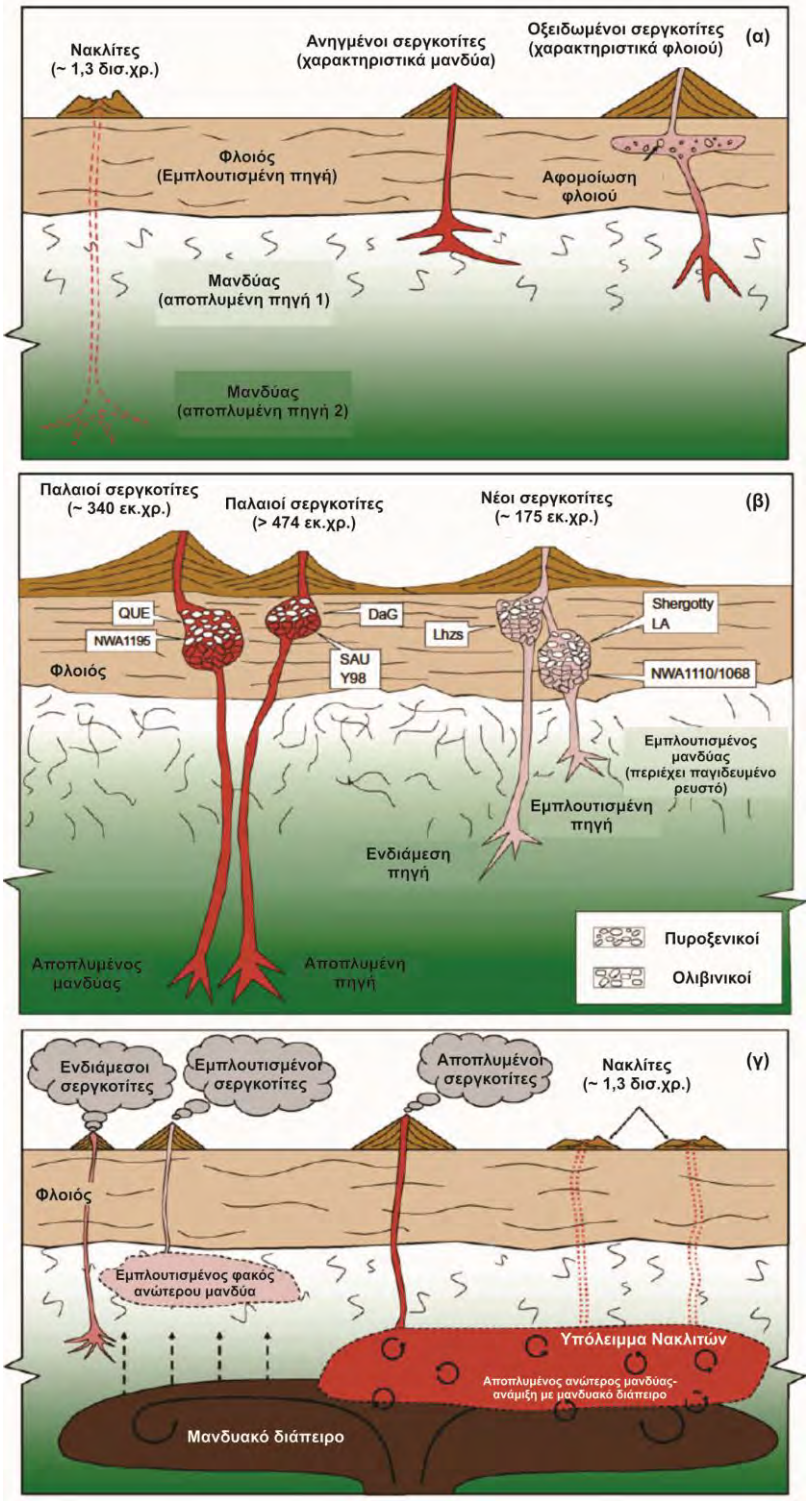

Σχήμα 2 - (α–γ) Μοντέλα προσωμοίωσης μαγματισμού στον πλανήτη Άρη. (α) Μοντέλο αφομοίωσης φλοιού (από Herd *et al*., 2002). (β, γ) Μοντέλα πολλαπλών μανδυακών πηγών (β: Symes *et al*., 2008, γ: Blinova & Herd, 2009).

3.2 Δημιουργία Κρατήρων

Η δημιουργία ενός κρατήρα στην επιφάνεια ενός πλανήτη, και δη του Άρη, αποτελεί μία πολύπλοκη, αλλά εξαιρετικά ταχεία διαδικασία που ολοκληρώνεται σε μόλις λίγα λεπτά. Στην παρούσα ενότητα γίνεται αναφορά στα στάδια δημιουργίας ενός κρατήρα έπειτα από την πρόσκρουση ενός αστεροειδούς (Σχ. 3, 4). Η μέση ταχύτητα πρόσκρουσης των αστεροειδών στην επιφάνεια του Άρη είναι περίπου 10 km/sec. Η σύγκρουση χαρακτηρίζεται από υψηλούς ρυθμούς παραμόρφωσης σε όλες τις κλίμακες παρατήρησης. Κατά την πρόσκρουση αναπτύσσονται πολύ υψηλές θερμοκρασίες και πιέσεις με αποτέλεσμα τα πετρώματα να λιώνουν σε απειροελάχιστο χρόνο. Όταν στερεοποιηθούν, κι ενώ βρίσκονται υπό καθεστώς υψηλών πιέσεων, σχηματίζονται πολύμορφα ορυκτά (π.χ. ρινγκβουντίτης) όπως στον μετεωρίτη Tissint (βλέπε Κεφάλαιο 5, Baziotis *et al*., 2013). Τα στάδια δημιουργίας ενός κρατήρα συνοψίζονται στα ακόλουθα:

1. Πρόσκρουση μεγάλων σωμάτων με πολύ υψηλή ταχύτητα στην επιφάνεια. Προκαλείται απελευθέρωση μεγάλων ποσοτήτων ενέργειας σε πολύ μικρό χώρο (Σχ. 3, #1).
2. Σχεδόν ολοκληρωτική εξάτμιση του αστεροειδούς (Σχ. 3, #2).
3. Ωστικά κύματα διαπερνούν τα πετρώματα προκαλώντας δομικές μετατροπές στα ορυκτά που βρίσκονται στο διάβα τους (φάση συμπίεσης. (Σχ. 3, #3).
4. Έπειτα από τη φάση συμπίεσης, η πίεση ελαττώνεται ελεύθερα υπό τη μορφή μία γιγαντιαίας έκρηξης που προκαλεί τη διαμόρφωση μίας βαθιάς κοιλότητας, η οποία είναι μεγαλύτερη σε διάμετρο από τον αστεροειδή. Σε αυτό το στάδιο τα εκτεταμένα ωστικά κύματα αποδυναμώνονται και η διαμόρφωση του κρατήρα εξαρτάται κυρίως από τη βαρύτητα (Σχ. 4, #4).
5. Υλικό συνεχώς εκτινάσσεται υπό τη μορφή ανεστραμμένου κώνου. Αποτελείται κυρίως από θραύσματα και λειωμένα πετρώματα (Σχ. 4, #5).
6. Μέρος του προηγούμενου υλικού καταρρέει προς το εσωτερικό του κρατήρα σχηματίζοντας στρώματα σχετικά μεγάλου πάχους (Σχ. 4, #6).

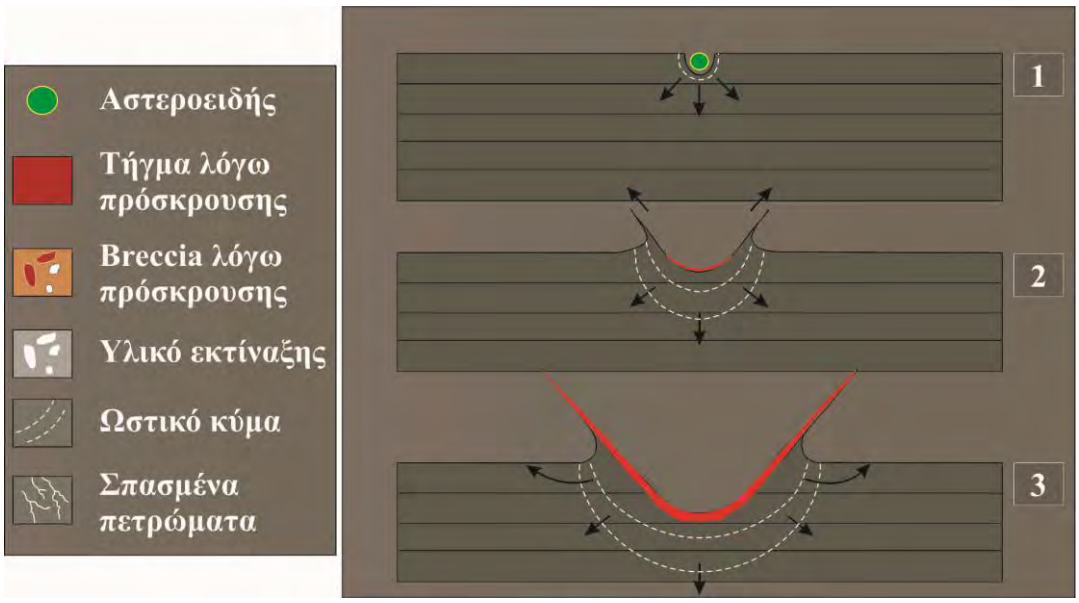

Σχήμα 3 – Στάδια δημιουργία κρατήρων (1-3, βλέπε κείμενο) στον πλανήτη Άρη.

Το στάδιο 3 προς 4, καθορίζει το είδος του κρατήρα. Ανάλογα με τη διάμετρο, διακρίνονται τόσο απλοί όσο και σύνθετοι κρατήρες (Σχ. 4). Στους απλούς κρατήρες το απότομο μέρος του χείλους

του κρατήρα καταρρέει και η αναλογία μεταξύ του τελικού βάθους και της διαμέτρου είναι 1:5. Στους σύνθετους κρατήρες η κατάρρευση είναι πιο εντυπωσιακή, διότι αποτελούνται από μία κεντρικά ανυψωμένη περιοχή, η οποία κατρακυλά προς το εσωτερικό.

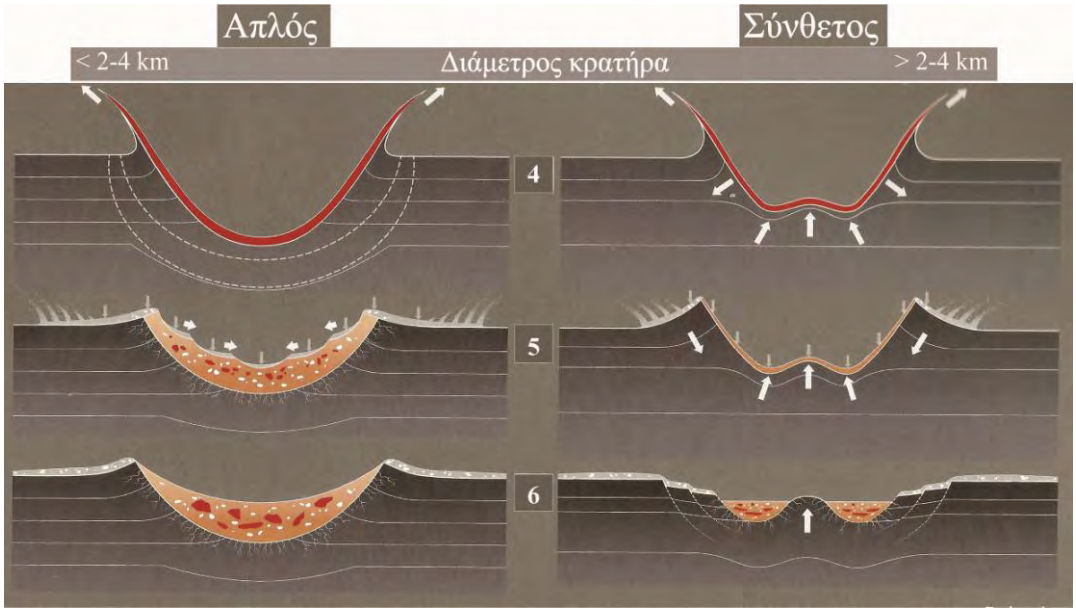

Σχήμα 4 – Στάδια δημιουργία κρατήρων (4-6, βλέπε κείμενο) στον πλανήτη Άρη. Δύο παραδείγματα δημιουργίας απλού (κάτω αριστερή εικόνα) και σύνθετου (κάτω αριστερή εικόνα) κρατήρα με μέγεθος μικρότερο και μεγαλύτερο από 2-4 km, αντίστοιχα. Σύμβολα όπως στο σχήμα 3.

3.3 Περί Χρόνου

Η έννοια προσδιορισμού και τοποθέτησης των γεγονότων στο χρόνο μοιάζει με ένα δισεπίλυτο γρίφο για την περιπτωση των μετεωριτών με προέλευση τον πλανήτη Άρη. Ως «ηλικία» ορίζεται ο χρόνος μεταξύ δύο γεγονότων που έχουν καθοριστεί με συγκεκριμένα χρονόμετρα. Στην πραγματικότητα, τέσσερις διαφορετικές ηλικίες κρύβονται στο εσωτερικό αυτών των πετρωμάτων. Η πρώτη σχετίζεται με με τη χρονολόγηση της κλασμάτωσης στη μανδυακή περιοχή που δημιούργησε την πηγή των ύστερο-τηγμάτων (Moser *et al*., 2013). Η δεύτερη σχετίζεται με την κρυστάλλωση του μάγματος κοντά στην επιφάνεια (όταν πρόκειται για βασαλτικό πέτρωμα) δίνοντας γένεση στον πρωτόλιθο. Η Τρίτη αφορά την ηλικία τήξης κατά την διάρκεια ενός μεγάλου κοσμικού γεγονότος (πρόσκρουση αστεροειδούς) και πιθανότατα αποτελεί το χρόνο εκτίναξης του πετρώματος από την επιφάνεια του Άρη. Η τέταρτη ηλικία είναι εκείνη που σχετίζεται με τον χρόνο παραμονής του μετεωρίτη στην επιφάνεια της Γης. Έτσι λοιπόν, η διαφορά της τρίτης (ηλικία εκτίναξης) με την τέταρτη (ηλικία παραμονής στη Γη) αποτελεί τον χρόνο «ταξιδιού» ενός μετεωρίτη στο διάστημα. Όπως διαπιστώνουμε από το σχήμα 5, υπάρχουν τουλάχιστον 4 διαφορετικοί χρονικοί περίοδοι που σχετίζονται με την ηλικία εκτίναξης μετεωριτών από τον Άρη. Σύμφωνα με τους Fritz *et al*. (2005) οι νεώτερες υλικίες εκτίναξης συνδέονται με τους μετεωρίτες στους οποίους καταγράφονται ψηλότερες συνθήκες πίεσης στο εσωτερικό τους. Το τελευταίο συμβαίνει γιατί οι μετεωρίτες αυτοί έχουν προέλθει από ισχυρότερα κοσμικά γεγονότα, με αποτέλεσμα να συναντούν ταχύτερα την τροχιά της Γης στο διάστημα.

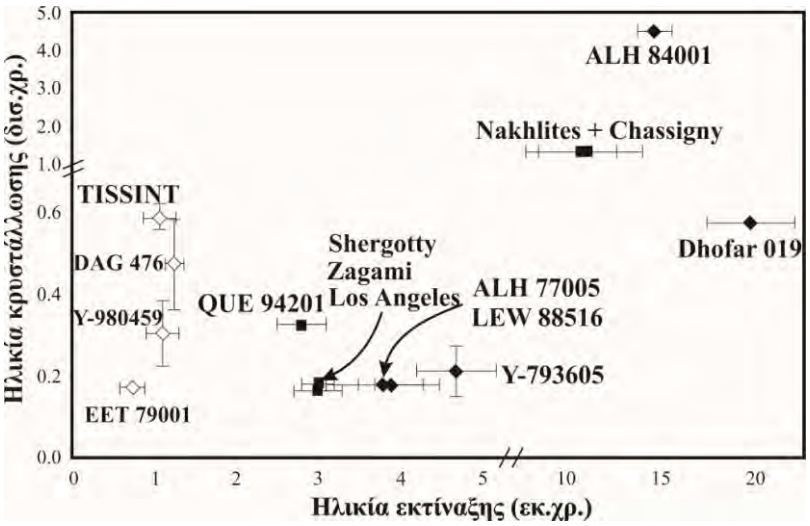

Σχήμα 5 – Ηλικίες εκτίναξης/κρυστάλλωσης για επιλεγμένους μετεωρίτες με προέλευση τον πλανήτη Άρη.

4. Που βρίσκονται οι Μετεωρίτες στη Γη?

Η πτώση μετεωριτών στη Γη αποτελεί ένα σημαντικό γεγονός, καθώς τεμάχη πετρωμάτων από το διάστημα, που πιθανώς προέρχονται από τα αρχέγονα στάδια του ηλιακού μας συστήματος, ανακαλύπτονται από τους ανθρώπους και αποκαλύπτουν σημαντικές πληροφορίες. Υπάρχουν όμως περιοχές της Γης στις οποίες να παρατηρείται μεγάλη συγκέντρωση μετεωριτών? Η απάντηση σε αυτό το ερώτημα, δεν μπορεί να είναι μονοσήμαντη, ωστόσο, είναι καταφατική (Σχ. 6). Η αιτία δεν είναι η μεγαλύτερη συγκέντρωση μετεωριτών στις περιοχές αυτές, αλλά η μεγαλύτερη ευκολία στον εντοπισμό τους.

Σχήμα 6 – Θέσεις πτώσης μετεωριτών στη Γη τα τελευταία 4300 χρόνια. Στο χάρτη απεικονίζονται 34513 σημεία πρόσκρουσης.

Εξαιρετικό παράδειγμα συγκέντρωσης μετεωριτών αποτελεί η περιοχή της Ανταρκτικής. Αποτελεί την καλύτερη «παγίδα» μετεωριτών στη Γη. Αυτό οφείλεται καταρχάς στο ότι οι μετεωρίτες πέφτουν σε πάγο κι όχι σε σκληρά πετρώματα, με αποτέλεσμα να υφίστανται μικρότερη ζημιά. Επίσης, εξαιτίας της φύσης του, ένας μετεωρίτης είναι ένα πέτρωμα, το οποίο

ευκόλως διακρίνεται από το λευκό, χιονοσκέπαστο περιβάλλον της Ανταρκτικής. Παράλληλα, στην περιοχή της Ανταρκτικής υφίσταται μία εξαιρετικά ενδιαφέρουσα διαδικασία συγκέντρωσης μετεωριτών (Σχ. 7).

Σχήμα 7 – Τρόπος μεταφοράς και συγκέντρωσης μετεωριτών στην Ανταρκτική (από Bischoff, 2001).

Κατά τη ροή του πάγου, όταν αυτός συναντήσει ένα εμπόδιο όπως ένα πέτρωμα ή βουνό, έχει την τάση προς τα πάνω κίνησης συμπαρασύροντας τους εγκλεισμένους στο εσωτερικό του, μετεωρίτες, προς την επιφάνεια. Σε πολλές περιοχές όπου ο πάγος είναι παγιδευμένος δίπλα σε μια βουνοπλαγιά, και χωρίς να έχει ροή διαφυγής, μειώνεται σιγά-σιγά σε πάχος εξαιτίας της απόξεσης που προκαλείται από την ηλιακή ακτινοβολία και τους καταβατικούς ανέμους. Τελικά, με το πέρας εκατοντάδων ή και χιλιάδων χρόνων, η απομάκρυνση του πάγου αφήνει μια επιφάνεια γεμάτη με «εξωγήινα» αντικείμενα.

Μία ακόμα περιοχή εντοπισμού μετεωριτών αποτελεί η έρημος του Morocco. Το Morocco κατέχει εξαιρετική θέση για την ανίχνευση και εντοπισμό μετεωριτών εξαιτίας της μεγάλης έκτασης επιφανειών χωρίς εμπόδια που εκτείνονται σε χιλιάδες τετραγωνικά χιλιόμετρα. Το κλίμα αυτών των εκτάσεων χαρακτηρίζεται ως πολύ ξηρό με εξαιρετικά χαμηλό ρυθμό διάβρωσης, συνθήκες ιδανικές για τη μακροχρόνια διατήρηση των μετεωριτών. Ήδη, από τις αρχές της προηγούμενης δεκαετίας, ο αριθμός των μετεωριτών που ανακαλύφθηκαν στην καυτή έρημο του Νότιου Morocco, έχει πολλαπλασιασθεί. Μερικά από τα συλλεχθέντα δείγματα έχουν πολύ υψηλή επιστημονική αξία. Είναι χαρακτηριστικό, ότι το 40% των μετεωριτών με προέλευση τον πλανήτη Άρη, έχουν συλλεχθεί από το Morocco. Ένα από τα σημαντικότερα δείγματα που έχουν ανακαλυφθεί στην έρημο του Morocco αποτελεί το πέτρωμα με κωδικό όνομα NWA 2737, καθώς είναι το δεύτερο μόλις δείγμα από την κατηγορία στην οποία ανήκει. Το επόμενο όμως πέτρωμα είναι ίσως σημαντικότερο από το προαναφερθέν. Το πέτρωμα αυτό ονομάστηκε μετεωρίτης Tissint.

5. Ο Σημαντικότερος Μετεωρίτης της Εποχής μας - Tissint

Πρόσφατα, μόλις στις 18 Ιουλίου 2011, ένας μετεωρίτης έπεσε ανατολικά της περιοχής Tissint, στην κοιλάδα Oued Draa στο Morocco (Σχ. 8). Η συλλογή των θραυσμάτων πραγματοποιήθηκε από νομάδες τρεις μήνες αργότερα, τον Οκτώβριο του 2011. Τα μεγαλύτερα κομμάτια

συλλέχθηκαν από την περιοχή Hmadat Boû Rba'ine και τα μικρότερα (μόλις λίγα γραμμάρια) βρέθηκαν κοντά στα βουνά El Aglâb.

Σχήμα 8 - Μικρό τμήμα του μετεωρίτη Tissint, όπως αυτό ανακαλύφθηκε στο αφιλόξενο έδαφος της περιοχής που κατέπεσε στο Morocco. Το όνομα του μετεωρίτη προέρχεται από το κοντινό ομώνυμο χωριό.

Ο μετεωρίτης Tissint ανήκει στην κατηγορία των σεργκοτιτών με ύπαρξη μεγάλων κρυστάλλων ολιβίνη που «επιπλέουν» σε μία λεπτόκοκκη κύρια μάζα (Irving *et al*. 2012, Baziotis *et al*. 2012). Αποτελεί τον πέμπτο μόλις μετεωρίτη που ο άνθρωπος παρατήρησε κατά την πτώση του και τον συνέλεξε. Έπειτα από τον τέταρτο μετεωρίτη, τον γνωστό Zagami που συλλέχθει στη Νιγηρία το 1962. Η πρώτη πτώση μετεωρίτη που έγινε ορατός και συλλέχθηκε από ανθρώπινο χέρι πραγματοποιήθηκε το 1815 στη Γαλλία. Η επόμενη έγινε πενήντα χρόνια αργότερα, το 1865 στην Ινδία, με την τρίτη να λαμβάνει χώρα το 1911 στην Αίγυπτο. Ο μετεωρίτης Tissint αποτελεί ένα αρκετά φρέσκο πέτρωμα με πολύ μικρό χρόνο παραμονής, έπειτα από την πτώση του, στη Γη. Τούτο είναι αρκετά σπάνιο, καθώς συνήθως οι μετεωρίτες συλλέγονται στη Γη, αιώνες ή και χιλιάδες χρόνια έπειτα από την πτώση τους.

Ο Christopher Herd, καθηγητής από το Πανεπιστήμιο της Alberta στο Edmonton, πρόεδρος της Επιτροπής που επιβεβαίωσε το όνομα και την προέλευση του μετεωρίτη Tissint, έκανε το παρακάτω σχόλιο σχετικά με την πρώιμη ιστορία αυτού του κομματιού πετρώματος: «αυτό το κομμάτι μαγματικού πετρώματος μας λέει πολλά σχετικά με το μάγμα και την προέλευσή του από τον Άρη. Μπορούμε λοιπόν μέσω της γεωχημείας να εμβαθύνουμε στη Γεωλογία του εσωτερικού του πλανήτη». Όπως αναφέραμε πρωτύτερα, οι πλέον διαδεδομένοι μετεωρίτες από τον Άρη, οι σεργκοτίτες, είναι αυτοί που πλεονάζουν. Τεμάχια απο τον μετεωρίτη Tissint βρίσκονται σε συλλογές στην Εθνική Υπηρεσία Αεροναυτικής και Διαστήματος (NASA) της Αμερικής, στο Πανεπιστήμιο της Alberta, της Arizona, του New Mexico, και του Πανεπιστημίου της Washington.

5.1 Γιατί Είναι Σημαντικός ο Tissint?

Ο μετεωρίτης Tissint κατέπεσε στην έρημο του Morocco και συντρίμμια του βρέθηκαν σε μία ακτίνα αρκετών χιλιομέτρων. Ένα παχύ στρώμα υελώδους φλοιού περιβάλει τον μετεωρίτη Tissint, γεγονός που καθιστά το εσωτερικό του τμήμα σχεδόν ανεπηρέαστο από τη γήινη επιμόλυνση. Ο μετεωρίτης αυτός έχει ηλικία γένεσης που αγγίζει τα εξακόσια εκατομμύρια χρόνια (π.χ. Brennecka *et al*., 2012; Grosshans *et al*., 2013; Ferrière *et al*., 2013). Επίσης, περιέχει στο εσωτερικό του θύλακες που έχουν κλείσει μέσα τους σημάδια της ατμόσφαιρας του Άρη, γεγονός που αποδεικνεί την προέλευση από τον εν λόγω πλανήτη (Chennaoui Aoudjehane *et al*., 2012).

Ωστόσο, τι είναι εκείνο που καθιστά ξεχωριστό αυτό το μετεωρίτη? Γιατί η επιστημονική κοινότητα, έχει στραφεί με μεγάλο ενδιαφέρον και μελετά αυτό το εξωγήινο πέτρωμα?

Σε πρόσφατη έρευνα που διεξήχθη στις Ηνωμένες Πολιτείες Αμερικής, ερευνητής του Πανεπιστημίου του Tennessee, στα πλαίσια χρηματοδότησης από τη NASA, ανακάλυψε εκείνα τα δεδομένα που καθιστούν τον μετεωρίτη Tissint το μοναδικό μέχρι στιγμής πέτρωμα που αποκαλύπτει την ταυτότητα προέλευσής του από έναν τεραστίων διαστάσεων κρατήρα του πλανήτη Άρη (Baziotis *et al*., 2013). Σύμφωνα με έρευνες των Shaw & Walton (2013), τα ορυκτά που σχηματίζονται σε συνθήκες πολύ υψηλών πιέσεων, παρέχουν τις απαραίτητες ενδείξεις που σχετίζονται με διεργασίες: (1) δημιουργίας κρατήρων, (2) απομάκρυνσης των πετρωμάτων από την επιφάνεια του μητρικού τους πλανήτη και (3) μεταφοράς των πετρωμάτων στη Γη. Είναι χαρακτηριστικό ότι οι περισσότεροι μετεωρίτες που προέρχονται από τον πλανήτη Άρη, προέρχοναι από κρατήρες διαμέτρου 3 έως 7 km (π.χ. Head *et al*., 2002). Αυτό αποτελεί το πρώτο σημαντικό σημείο στο οποίο ξεχωρίζει ο μετεωρίτης Tissint. Δηλαδή, η προέλευσή του από έναν κρατήρα εξωπραγματικών διαστάσεων συγκρινόμενο με τους αντίστοιχους που έχουν αποδοθεί για την προέλευση των περισσοτέρων μετεωριτών από τον πλανήτη Άρη.

Σύμφωνα με ανεξάρτητες έρευνες που πραγματοποίησε τόσο η ομάδα του καθηγητή Paul DeCarli, ειδικό σε θέματα συγκρούσεων και δημιουργία κρατήρων, αλλά κι εκείνη υπό την αιγίδα του καθηγητή Beck από το Πανεπιστήμιο της Λυόν, έδειξαν ότι τα ορυκτά που σχηματίζονται κάτω από ένα καθεστώς πολύ υψηλών πιέσεων και είναι εγκλεισμένα μέσα σε μετεωρίτες μπορούν να δώσουν πληροφορίες για τη δυναμική των μετεωριτών (Fritz *et al*., 2005; DeCarli, 2013). Μέχρι σήμερα, τα ορυκτά υψηλών πιέσεων που έχουν βρεθεί σε μετεωρίτες που προέρχονται από τον Άρη συνοψίζονται στα ακόλουθα: μασκελυνίτης (maskelynite, προέρχεται από πλαγιόκλαστο-plagioclase), ρινγκβουντίτης (ringwoodite, γ-πολύμορφο του ολιβίνη-olivine, Σχ. 9), ακιμοτοϊτης (akimotoite, πυρόξενος με δομή ιλμενίτη-ilmenite), λινγκουνίτης (lingunite, πλαγιόκλαστο-plagioclase με δομή Na-Ολλανδίτη-Na Hollandite), ματζορίτης (majorite, πυρόξενος-pyroxene με δομή γρανάτη-garnet), τουϊτης (tuite, γ-πολύμορφο του μεριλλίτη-merrilite), στισοβίτης (stishovite, χαλαζίας-quartz με δομή α-TiO_2), και περοφσκίτης (πυρόξενος με δομή περοφσκίτη).

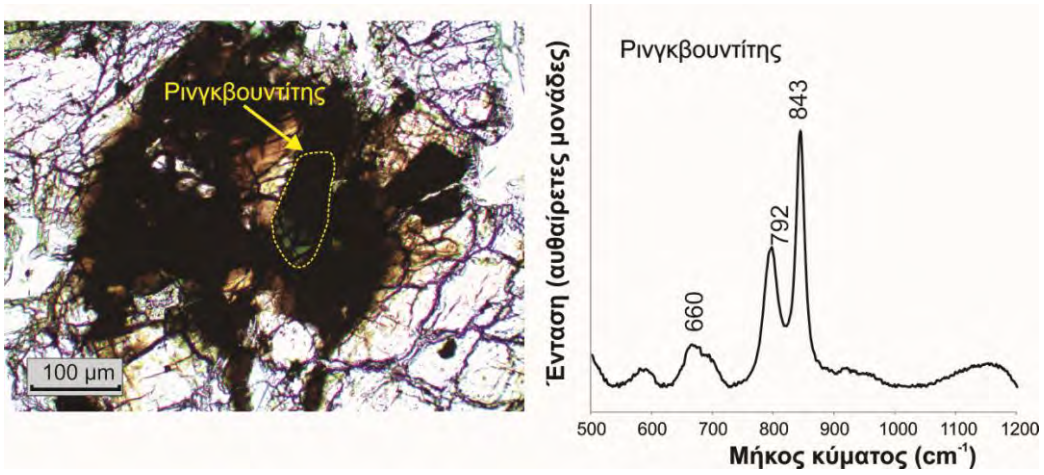

Σχήμα 9 – Αριστερά απεικονίζεται μία εικόνα που έχει ληφθεί από πετρογραφικό μικροσκοπίο. Φαίνεται ένα τμήμα του εσωτερικού του μετεωρίτη Tissint το οποίο έχει υποστεί πολύ υψηλές πιέσεις και θερμοκρασίες έπειτα από την πρόσκρουση αστεροειδούς στην επιφάνεια του πλανήτη Άρη. Το πράσινο ορυκτό, με το κίτρινο περίγραμμα, είναι το ορυκτό ρινγκβουντίτης. Αποτελεί το μεγαλύτερο σε μέγεθος ριγνκβουντίτη που έχει βρεθεί ποτέ σε μετεωρίτη. Η εφαρμογή της μικρο-φασματοσκοπίας Raman απέδειξε τη φύση αυτού του ορυκτού όπως απεικονίζεται στο χαρακτηριστικό φάσμα της δεξιάς εικόνας.

Τα παραπάνω ορυκτά σχηματίζονται σε υψηλές πιέσεις, ενώ εκείνα που παρατίθενται μέσα στην παρένθεση αντιστοιχούν στα αντίστοιχά τους, πρωτογενή ορυκτά χαμηλών πιέσεων. Είναι χαρακτηριστικό ότι, μέχρι σήμερα, όλα τα προαναφερθέντα ορυκτά έχουν βρεθεί σε μεμονωμένες εμφανίσεις μετεωριτών (Πίνακας 1).

Πίνακας 1 - Ορυκτά υψηλών πιέσεων που έχουν βρεθεί σε μετεωρίτες από τον πλανήτη Άρη.

	Rwt	Ak	Maj	Lin/Holl	Tuite	Stv	Pv	Msk
TISSINT	**X**	**X**	**X**	**X**	**X**	**X**	**X**	**X**
DaG 670/735	x				x		x	x
EETA 79001	x							x
Zagami		x		x		x	x	x
Shergotty			x	x		x		x
NWA 4468	x				x			x
GRV 020090	x	x	x		x			x
NWA 856				x		x		x
Y 000047		x						x
Chassigny	x				x		x	x

Συντμήσεις: Rwt, ρινγκβουντίτης; Ak: ακιμοτοίτης; Maj: ματζορίτης; Lin: λινγκουνίτης; Holl: ολλανδίτης; Stv: στισοβίτης; Pv: περοφσκίτης; Msk: μασκελυνίτης.

5.2 Μία Ακόμα Μέγα-καταστροφή στην Επιφάνεια του Άρη?

Όπως αναφέραμε, οι μετεωρίτες με προέλευση τον Άρη, οφείλονται σε πρώτη φάση σε εξαιρετικά μεγάλης ενέργειας συγκρουσιακά γεγονότα ή αλλιώς κοσμικά γεγονότα, που λαμβάνουν χώρα στην επιφάνεια του πλανήτη. Γενικά, ένα κοσμικό γεγονός αποδίδεται στην πρόσκρουση ενός μεγάλου μετεωρίτη, αστεροειδούς ή κομήτη, με ένα άλλο ουράνιο αντικείμενο όπως είναι η Γη, ο Άρης, κάποιος άλλος πλανήτης, δορυφόρος, ή αστεροειδής.

Στην επιφάνεια του Άρη παρατηρούνται πολυάριθμοι κρατήρες, μεταξύ των οποίων, 43.000 εχουν μέγεθος μεγαλύτερο από 5 km. Οι κρατήρες αυτοί έχουν φωτογραφηθεί με τη χρήση των διαφόρων διαστημικών συσκευών που έχουν αποσταλεί από τις υπηρεσίες διαστήματος της Αμερικής, της Ευρώπης και της Ρωσίας. Οι περισσότεροι από τους κρατήρες έχουν λάβει ονόματα επιστημόνων. Κρατήρες μεγάλου μεγέθους συνήθως λαμβάνουν ονόματα πόλεων ή περιοχών που βρίσκονται πάνω στη Γη. Για παράδειγμα, ο μεγαλύτερος γνωστός κρατήρας ονομάζεται «λεκάνη Ελλάς - Hellas Basin» και βρίσκεται στο νότιο ημισφαίριο του κόκκινου πλανήτη. Η διάμετρός του ξεπερνά τα 2.300 km έχοντας ένα βάθος που φθάνει τα 9 km. Δύο ακόμα μεγάλες συγκρουσιακές δομές στην επιφάνεια του Άρη, αποτελούν οι λεκάνες της Αργυρούς και της Ίσιδος. Η λεκάνη της Αργυρούς, με διάμετρο 800 km, βρίσκεται στο νότιο ημισφαίριο και περιβάλλεται από ένα μεγάλο δακτυλίδι βουνών.

Η πλειονότητα των κρατήρων στον Άρη έχει σχηματισθεί κατά το χρονικό διάστημα 4.1 έως 3.8 δισεκατομύρια χρόνια που καλείται «περίοδος ύστερου βαρέως βομβαρδισμού». Κατά τη διάρκεια αυτή της περιόδου, δημιουργήθηκε ένας μεγάλος αριθμός κρατήρων σε όλους τους πλανήτες και δορυφόρους του ηλιακού μας συστήματος, όπως επίσης καταστράφηκαν μικρότερα ουράνια σώματα, άγνωστα τη σημερινή εποχή. Σύμφωνα με την επιστημονική κοινότητα, αποδείξεις εκείνης της περιόδου προέρχονται από τη γεω-χρονολόγηση πετρωμάτων της Σελήνης, η ηλικία των οποίων φανερώνει ότι τα πετρώματα έλειωσαν κατά τη διάρκεια αυτής της μεγάλης περιόδου συγκρούσεων και δημιουργίας κρατήρων. Η «λεκάνη Ελλάς», είναι η δεύτερη μεγαλύτερη και πρώτη ορατή συγκρουσιακή δομή του ηλιακού μας συστήματος. Την πρώτη θέση κατείχε για χρόνια ο κρατήρας που βρίσκεται στο Νότιο πόλο της Σελήνης κι ονομάζεται «λεκάνη Aiken – Aiken Basin». Ωστόσο, πρόσφατα δεδομένα από διαστημικές συσκευές της Εθνικής Υπηρεσίας

Αεροναυτικής και Διαστήματος της Αμερικής δείχνουν ότι στο βόρειο ημισφαίριο του πλανήτη Άρη, η λεκάνη borealis, αποτελεί μία πιθανή συγκρουσιακή δομή με διάμετρο που αγγίζει τα 10.500 km.

Σε όλη την ανθρώπινη και προγενέστερη ιστορία, έχουν καταγραφεί μικρά γεγονότα συγκρούσεων τα οποία έχουν προκαλέσει θανάτους, τραυματισμούς, ή ακόμα και καταστροφές κατοικιών. Μεγαλύτερα γεγονότα, πιο σπάνια ωστόσο, έχουν προκαλέσει κατά τη διάρκεια της μακράς ιστορίας της Γης σημαντική αποδόμηση του φυσικού περιβάλλοντος όπως επίσης και μαζικές εξαφανίσεις οργανισμών. Η μαζική εξαφάνιση των δεινοσαύρων, πριν από περίπου 65 εκατομμύρια χρόνια, αποδίδεται σε ένα τέτοιο καταστροφικό γεγονός. Υπάρχει λοιπόν τρόπος να αντιληφθούμε αν ο μετεωρίτης Tissint προέρχεται από ένα Μεγα-συγκρουσιακό γεγονός, αυτή τη φορά στην επιφάνεια του πλανήτη Άρη?

Η ανακάλυψη των ερευνητών από το Πανεπιστήμιο του Tennessee βασίζεται στην ανίχνευση όλων εκείνων των σημαντικών ορυκτών που σχηματίζονται σε ένα καθεστώς πολύ υψηλών πιέσεων, βρισκόμενα σε ένα και μοναδικό δείγμα, τον μετεωρίτη Tissint. Το μοναδικό παράδειγμα μετεωρίτη με προέλευση τον πλανήτη Άρη, στο οποίο διαστηρούνται ορυκτά πολύ υψηλών πιέσεων οδήγησε στον υπολογισμό των συνθηκών πιέσης και θερμοκρασίας που αναπτύθηκαν κατά τη διάρκεια της πρόσκρουσης ενός μεγάλου ουράνιου σώματος στην επιφάνεια του Άρη. Η ερευνητική προσπάθεια που διεξήχθη στο Ινστιτούτο Πλανητικών Γεωεπιστημών του Πανεπιστημίου του Tennessee έφερε στο φως τα ορυκτά μασκελυνίτης, ρινγκβουντίτης, ακιμοτοϊτης, λινγκουνίτης, ματζορίτης, τουϊτης, στισοβίτης και περοφσκίτης, συγκεντρωμένα όλα σε ένα δείγμα 10 gr. Επιπρόσθετα, πρόσφατα ανακοινώθηκαν δεδομένα από τον ίδιο μετεωρίτη που πιστοποιούν την παρουσία άνθρακα σε μορφή διαμαντιού με μέγεθος μικρότερο από 6 μm (El Goresy *et al*. 2013). Η παρουσία των ορυκτών αυτών δείχνει συνθήκες δημιουργίας σε ένα στενό φάσμα πίεσης και θερμοκρασίας. Ειδικότερα, προγενέστερες μελέτες έχουν δείξει ότι η παρουσία του ορυκτού μασκελυνίτης, δείχνει πίεση σχηματισμού μεγαλύτερη από 40 GPa. Ωστόσο, πρόσφατες έρευνες από τους Καθηγητές Sharp και DeCarli, έδειξαν ότι ο μασκελυνίτης σχηματίζεται σε πολύ χαμηλότερες πιέσεις (Sharp & DeCarli, 2006). Ο Δρ. Ιωάννης Μπαζιώτης, εφαρμόζοντας το μοντέλο της επιστημονικής ομάδας του καθηγητή Fritz (Fritz *et al*., 2005) και χρησιμοποιώντας τις χαρακτηριστικές κορυφές που βρίσκονται στα φάσματα Raman του μασκελυνίτη, κατέληξε σε ένα εύρος πιέσεων που κυμαίνεται από 26 έως 40 GPa. Περαιτέρω, η ανακάλυψη του ορυκτού περοφσκίτης, έδειξε αντίστοιχες συνθήκες πίεσης αλλά για θερμοκρασίες που ξεπερνούν τους 2000 ^{0}C. Επιπλέον, η απουσία των προιόντων αποδόμησης του ορυκτού λινγκουνίτης ώθησε την Επιστημονική ομάδα του Πανεπιστημίου του Tennessee να περιορίσουν τις ανώτερες πιέσεις στα 25 GPa σε θερμοκρασίες που κυμαίνονται στο εύρος 1800 έως 2000 ^{0}C.

Ποια είναι όμως η φυσική σημασία της παρουσίας αυτών των ορυκτών στις εξαιρετικά ακραίες συνθήκες σχηματισμού τους? Αρχικά, κατά τη διάρκεια της μεγάλης πρόσκρουσης, τα ορυκτά που υπόκεινται στο ωστικό κύμα, βρίσκονται σε ένα καθεστώς πολύ υψηλών πιέσεων και θερμοκρασιών. Γεγονός είναι ότι περιοχές του πετρώματος που υφίσταται το μεγάλο συγκρουσιακό κύμα, λειώνουν σχεδόν ακαριαία. Ακολούθως στερεοποιούνται ταχέως, ενόσω το πέτρωμα διατηρείται σε αυτές τις ακραίες συνθήκες πίεσης και θερμκρασίας. Με αυτόν τον τρόπο, τα ορυκτά που σχηματίζονται κατά την στερεοποίηση του λειωμένου υλικού, δείχνουν τις πολύ υψηλές συνθήκες πίεσης και θερμοκρασίας, στις οποίες περιήλθαν. Ποια είναι όμως η διάρκεια που απαιτείται ώστε να σχηματισθούν αυτά τα ορυκτά? Ένα από τα ορυκτά που ανακάλυψε η ερευνητική ομάδα του Πανεπιστημίου του Tennessee ήταν ο ρινγκβουντίτης (Baziotis *et al*. 2013, Liu *et al*. 2013). Η παρουσία του ορυκτού αυτού, λαμβάνοντας υπόψιν το μέγεθός του και το ρυθμό ανάπτυξής του, έδειξε ότι η διάρκεια της πρόσκρουσης δεν ξεπέρασε το ένα δευτερόλεπτο. Περαιτέρω, εφαρμογή μαθηματικών μοντέλων προσομοίωσης σε μία από τις λειωμένες περιοχές που βρίσκονται εντός της μάζας του μετεωρίτη, κατέδειξε την εξαιρετικά ταχεία διεργασία στερεοποίησης αυτού του υλικού. Είναι χαρακτηριστκό ότι η εφαρμογή μοντέλων προσομοίωσης, σε μία περιοχή του πετρώματος κυλινδρικού σχήματος πάχους 350 μικρομέτρων, έδειξε οτι το

κέντρο της στερεοποιείται σε διάστημα 50 μιλισεκόντ και η άκρη της σε μόλις 20 μιλισεκόντ. Εξ`αυτού προκύπτει πως η στερεοποίηση λαμβάνει χώρα με κατεύθυνση από την άκρη προς το κέντρο, σε συμφωνία με την παρουσία των παρατηρούμενων αντίστοιχων ορυκτών. Περαιτέρω, η διάρκεια της πρόσκρουσης, βοήθησε στο να υπολογιστεί το μέγεθος του αστεροειδούς που χτύπησε τον Άρη αλλά και του δημιουργηθέντος κρατήρα. Εφαρμογή πολύπλοκων μαθηματικών εξισώσεων έδειξε ότι το μέγεθος του ουράνιου σώματος που προσέκρουσε στην επιφάνεια του πλανήτη Άρη κυμαίνονταν μεταξύ 10 και 25km, ενώ η διάμετρος του κρατήρα ήταν κατά το μέγιστο 180 km.

Η παρουσία μεγάλων κρατήρων στην επιφάνεια του Άρη είναι γεγονός αδιαμφισβήτητο. Ωστόσο, οι πληροφορίες που παρέχονται από τη μελέτη των περισσότερων μετεωριτών εκφράζουν μεγέθη κρατήρων που κυμαίνονται από 3 έως 7 km. Αντίθετα, η επισταμένη μελέτη του μετεωρίτη Tissint, χρησιμοποιώντας συντηρητικά μοντέλα προσομοίωσης, έδειξε ότι προέρχεται από ένα Μέγα-κρατήρα μεγέθους περίπου 180 km. Ο κρατήρας αυτός δημιουργήθηκε από έναν αστεροειδή, ο οποίος ξεπερνούσε σε μέγεθος τον αντίστοχο που κατέπεσε στη Γη και στον οποίο αποδίδεται η εξαφάνιση των δεινοσαύρων, πριν από περίπου 65 εκατομμύρια χρόνια. Το μέγεθος ενός τέτοιου Μέγα-γεγονότος γίνεται κατανοητό αν φανταστούμε ότι η ενέργειά του ισοδυναμεί με εκατό τρισεκατομμύρια βόμβες TNT ή δύο εκατομμύρια θερμοπυρηνικές βόμβες.

6. Υπάρχουν Σημάδια Ζωής?

6.1. Το παράδειγμα των Διαστημικών Συσκευών-οχημάτων

Στο κεφάλαιο αυτό γίνεται αναφορά σε παλαιότερες (1976, Viking Lander) και πρόσφατες ανακαλύψεις (Curiosity), που μπορούν να συνδέονται με την πιθανότητα ζωής στον πλανήτη Άρη. Επιπλέον δίνονται εκτενή στοιχεία σχετικά με τα πιθανά ίχνη ζωής που φέρουν οι μετεωρίτες με προέλευση τον πλανήτη Άρη, με τελική αναφορά στον μετεωρίτη Tissint.

Η αναζήτηση των επιστημόνων για ίχνη ζωής στον Άρη ξεκίνησε με τις ερευνητικές προσπάθειες της διαστημοσυσκευής Viking Lander το 1976 που παρήχθησαν εντυπωσιακά αποτελέσματα, υπό την καθοδήγηση του ερευνητή Gilbert Levin (Levin και Straat, 1976). Ωστόσο, κατά τη διάρκεια ενός πειράματος φασματοσκοπίας μάζας που διεξήχθη επί τόπου, στη θέση προσγείωσης της διαστημοσυσκευής, με σκοπό την αναζήτηση πολύπλοκων οργανικων ουσιών, κατέρριψε το επιχείρημα, και προέβαλε τη θέση της NASA ότι δεν ανιχνεύθηκε ζωή. Παρόλαυτά, ο Gilbert Levin, ήταν αντίθετος με αυτή την άποψη, και συνέχισε να υποστηρίζει ότι τα πειράματα του 1976 στην πραγματικότητα έδειχναν την παρουσία της μικροβιακής ζωής. Σε πρόσφατη μελέτη με αντικείμενο την επανεξέταση των αποτελεσμάτων από την προσπάθεια του Viking Lander φαίνεται να δικαιώνει την επιστημονική θέση που αρχικά προέβαλε ο Gilbert Levin (Bianchiardi et al, 2012). Το συμπέρασμα είναι ότι η μικροβιακή ζωή στον Άρη μπορεί να σταθεί σε βιώσιμη μορφή, και μάλιστα τα υψηλά επίπεδα του μεθανίου που έχουν εντοπιστεί στην ατμόσφαιρα του Άρη συνάγουν προς αυτή τη κατεύθυνση.

Το Curiosity, ένα μεγαλεπήβολο σχέδιο της NASA με κύριο σκοπό την ανακάλυψη ζωής ξεκίνησε την ερευνητική του προσπάθεια στο αφιλόξενο έδαφος του πλανήτη Άρη τον Αύγουστο του 2012. Το ταξίδι του έχει ως κεντρικό σκοπό την ανακάλυψη της πιθανότητας ζωής στο μακρινό παρελθόν ή σήμερα, στην περιοχή του κρατήρα Gale. Σε πρώτη φάση, η μεγάλη ανακάλυψη του Curiosity επικεντρώνονται στις ισχυρές αποδείξεις ύπαρξης νερού που έρεε άφθονο στο παρελθόν. Οι ερευνητές, ανακάλυψαν απομονωμένες εμφανίσεις τσιμεντοποιημένων βοτσάλων (διαμέτρου 2 έως 30 mm) και κόκκους άμμου με τυπικές δομές που χαρακτηρίζουν ιζηματογενή κροκαλοπαγή (Σχ. 10). Τα αποστρογγυλωμένα βότσαλα μέσα στα κροκαλοπαγή δείχνουν σημαντική ποτάμια διάβρωση. Επιπλέον, οι ορυκτολογικές αναλύσεις έδειξαν οτι επικρατεί το ορυκτό άστριος, γεγονός που αποδίδεται σε ελάχιστη εξαλλοίωση των ιζημάτων αυτών. Σύμφωνα με τους Williams *et al*. (2013), οι κλιματικές συνθήκες κατά τη διάρκεια μεταφοράς του ιζήματος πρέπει να διέφεραν κατά πολύ από το σύγχρονο ψυχρό και ξηρό περιβάλλον, επιτρέποντας την υδάτινη απορροή κατά μήκος πολλών χιλιομέτρων. Επομένως η ύπαρξη νερού που έρεε στην επιφάνεια

του Άρη κατά το παρελθόν επιτρέπει την υποστήριξη της άποψης περί προγενέστερης παρουσίας κατοικήσιμων περιβαλλόντων στον κόκκινο πλανήτη.

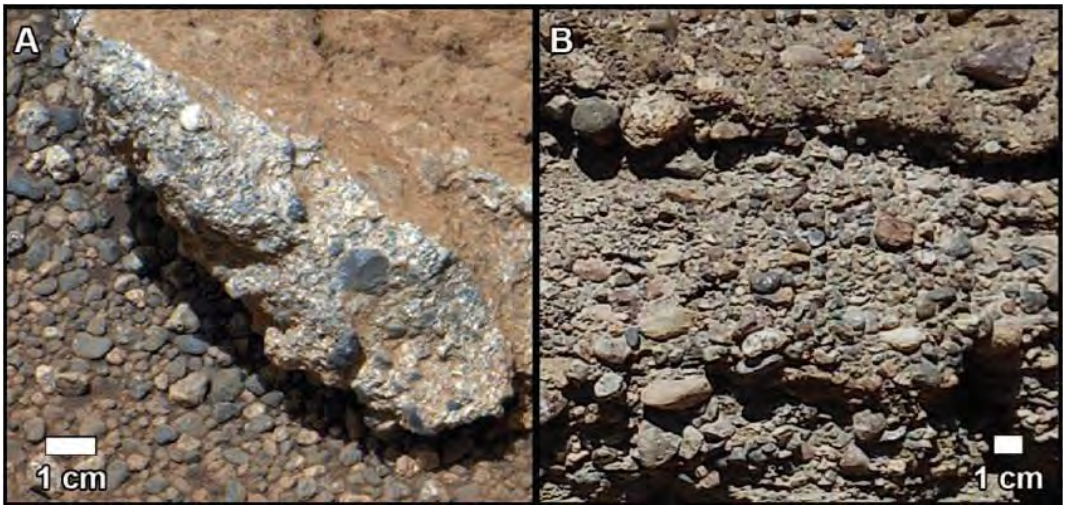

Σχήμα 10 – Σύγκριση κροκαλοπαγών από δύο διαφορετικούς πλανήτες. Α) Φωτογραφία που λήφθηκε από την κάμερα 100-mm Mastcam του οχήματος Curiosity στον πλανήτη Άρη. (Β) Γήϊνοι αποστρογγυλεμένοι κλάστες από αλλουβιακές αποθέσεις, όντας παρόμοιου μεγέθους και σχήματος με εκείνους της φωτογραφίας από τον πλανήτη Άρη (Έρημος Ατακάμα, Χιλή).

6.2. Το παράδειγμα των Μετεωριτών

Με βάση τα προηγούμενα, η απευθείας αναζήτηση των σημαδιών που αποδεικνύουν την «περί κατοικήσιμου θεωρίας» περιβάλλοντος του πλανήτη Άρη μπορεί να αναζητηθεί στους μετεωρίτες. Οι μετεωρίτες που προέρχονται από τον Άρη, κατέπεσαν στη Γη και συλλέχθηκαν γρήγορα μετά την πτώση τους είναι σχετικά σπάνιο να βρεθούν. Η σημαντικότητα τέτοιων πετρωμάτων έγκειται στο ότι αποτελούν δείγματα που δεν έχουν προλάβει να μολυνθούν από το γήινο περιβάλλον. Σε αυτή την περίπτωση, η διείσδυση βακτηρίων στο εσωτερικό του μετεωρίτη μέσω του τετηγμένου υαλώδους περιβλήματος συγκεντρώνει μικρές πιθανότητες. Οπότε, η έρευνα για αυτόχθονα βιολογικά σημάδια καθίσταται ολοένα και πιο σημαντική.

Η πιθανότητα ανίχνευσης ζωής στον πλανήτη Άρη επανήλθε στο προσκήνιο το 1996, με τις έρευνες που διεξήγαγε η επιστημονική ομάδα υπό την αιγίδα του καθηγητή McKay στα πλαίσα μελέτης του μετεωρίτη ALH 84001 (McKay et al, 1996). Ανακάλυψαν υπό-μικροσκοπικά σφαιρίδια ανθρακικών ορυκτών που περιβάλονται από στρώματα σύνθετων οργανικών μορίων πιθανούς βιολογικής προέλευσης. Επιπλέον, οι ίδιοι επιστήμονες ανακάλυψαν ωοειδούς σχήματος νανοσωματίδια που σχημάτιζαν αλυσίδες. συμπεριλαμβανομένων κρυστάλλων μαγνητίτη που καθορίζονται από ορισμένους τύπους γήινων βακτηρίων. Στην πράξη, η υπόθεση των συγγραφέων που δεν έλαβε πλήρους αιτιολόγησης σχετίζεται με τη μορφολογία των μικροσκοπικών κόκκων μαγνητίτη, και οι οποίοι ομοιάζουν με εκείνους που παράγονται από γήϊνα μαγνητοτακτικά βακτήρια. Ωστόσο, το ίδιο σχήμα κρυστάλλων (μεταξύ γήϊνων και εκείνων με προέλευση τον Άρη) δεν υποδεικνύει ίδιο μηχανισμό προέλευσης. Έτσι, Οι δομές αυτές προτάθηκαν αρχικά ως νανοβακτήρια, παρόλαυτά η άποψη επικρίθηκε στο μέγιστο βαθμό καθώς τέτοιοι μικρο-οργανισμοί δε μπορούν να σχηματίσουν αυτόνομες μορφές. Ως εκ τούτου, συνεχίζεται η συζήτηση σχετικά με τον μετεωρίτη ALH 84001 χωρίς να διαφαίνεται μία οριστική απάντηση στον ορίζοντα. Κάποιοι αναφέρθηκαν στο ότι η εργασία των Mckay *et al*. (1996) πυροδότησε μία δημόσια, πολιτική και ερευνητική συζήτηση μέγιστου ενδιαφέροντος για το ενδεχόμενο ύπαρξης ζωής στον Άρη.

Με όλα τα παραπάνω ως το αναγκαίο επιστημονικό υπόβαθρο που σχετίζεται με την υπάρχουσα, καθώς και παρελθούσα ζωή στον Άρη, το δείγμα του νέου μετεωρίτη, Tissint, μελετήθηκε με πολύ μεγάλη προσοχή. Όπως προαναφέρθηκε, ο μετεωρίτης Tissint εκτινάχθηκε κατά τη διάρκεια ενός μεγάλου κοσμικού γεγονότος, που έλαβε χώρα πριν από περίπου ένα εκατομμύριο χρόνια στην επιφάνεια του Άρη. Είναι χαρακτηριστικό ότι αν υπήρχε βιώσιμη μικροβιακή ζωή κάποια εποχή στον Άρη, τότε γιγαντιαίες θύελλες σκόνης θα μετέφεραν ζωντανά κύτταρα, σε άγονες ακόμη και σε αφιλόξενες περιοχές, ίσως σε παρόμοια τοποθεσία με εκείνη από την οποία προέρχεται ο μετεωρίτης Tissint. Η επιστημονική ομάδα υπό την αιγίδα του καθηγητή Wallis, από το Πανεπιστήμιο του Cardiff ανακάλυψε δισκοειδείς και σφαιροειδείς μορφές, με μέγεθος που δεν ξεπερνούν τα είκοσι μικρόμετρα και είναι πλούσιες σε άνθρακα και οξυγόνο (Σχ. 11). Σύμφωνα με τους ίδιους επιστήμονες, τέτοιες δομές δεν είναι δυνατό να ερμηνευθούν με χρήση μη-βιολογικών όρων. Επιπλέον, πρόσφατη ανακοίνωση στο 44ο Διεθνές Συνέδριο για τις Πλανητικές Επιστήμες και τη Σελήνη, από την ερευνητική ομάδα του καθηγητή El Goresy, έδειξε την παρουσία οργανικού άνθρακα (El Goresy *et al*., 2013, Lin *et al*., 2013). Υποστηρίζεται λοιπόν, ότι τελικώς, ο πλανήτης Άρης ίσως να μην αποτελεί ένα «νεκρό» πλανήτη.

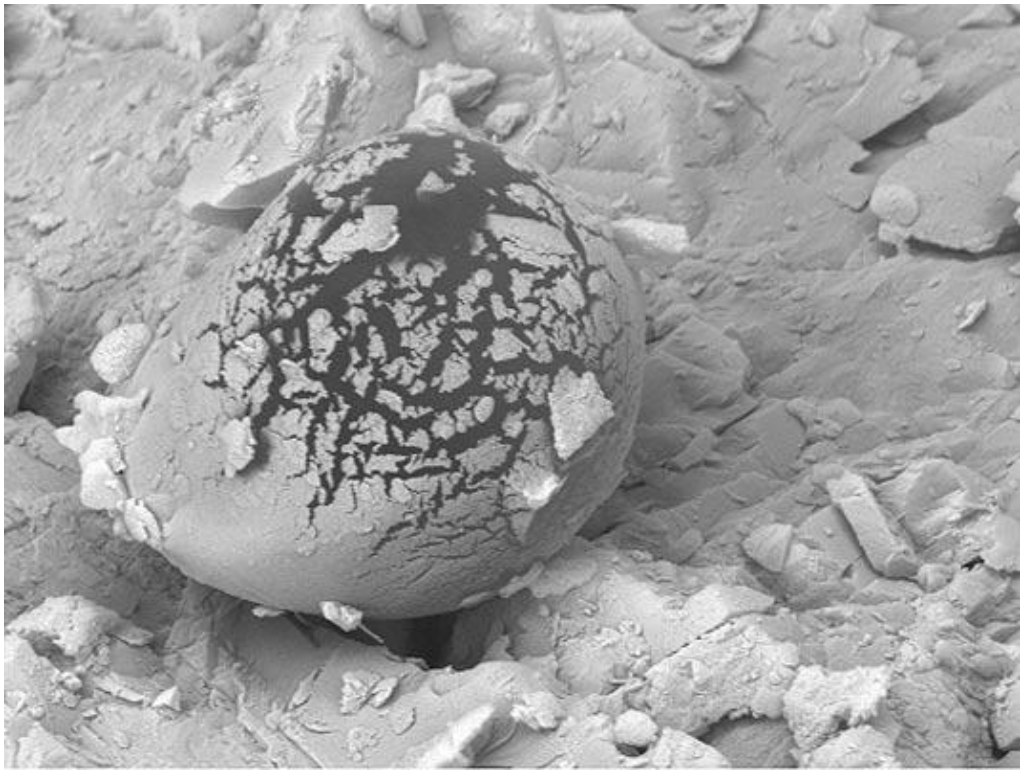

Σχήμα 11 - Μία περίεργη δομή, το «αυγό του Tissint», ανακυλύφθηκε από τον καθηγητή Wallis από το Πανεπιστήμιο του Κάρντιφ στην Αγγλία. Τα σπασίματα στην επιφάνεια της σφαιρικής αυτής δομής αποτελούν σύμφωνα με τον συγγραφέα μία κοιλότητα που περιείχε άνθρακα και οξυγόνο, συστατικά απαραίτητα για την ανάπτυξη ζωής. Η μέγιστη διάμετρος του «αυγού» φθάνει τα 10 μm.

7. Συμπεράσματα

Ο μετεωρίτης Tissint αποτελεί έναν από τους σημαντικότερους μετεωρίτες που έχει ανακαλυφθεί στη Γη. Είναι ο μόνος μετεωρίτης με προέλευση τον πλανήτη Άρη, στον οποίο έχουν βρεθεί όλα εκείνα τα ορυκτά υψηλών πιέσεων, που μεμονωμένα έχουν βρεθεί σε άλλους μετεωρίτες. Επιπλέον, προέρχεται από τον μεγαλύτερο κρατήρα που ως σήμερα έχει αποκαλύψει μετεωρίτης

από τον Άρη. Επομένως, από την ενέργεια, τις υψηλές πιέσεις και θερμοκρασίες που επεκράτησαν κατά τη σφοδρή σύγκρουση, στην επιφάνεια του Άρη, φαντάζει απίθανη η διατήρηση κάθε ίχνους ζωής στο πέτρωμα αυτό. Αναφορικά με το κρίσιμο ερώτημα ως προς το αν υφίσταται το ενδεχόμενο παρουσίας ζωής στον κόκκινο πλανήτη, ο συγκεκριμένος μετεωρίτης πιθανώς να μην παρέχει όλες τις αναγκαίες πληροφορίες, ώστε να απαντηθεί επαρκώς. Η παρουσία ζωής σε άλλο πλανήτη ωστόσο, πλην της Γης, φαντάζει λιγότερο μακρινή σε σχέση με το απώτερο παρελθον. Η Επιστημονική κοινότητα με αποστολή νέων διαστημοσυσκευών (π.χ. Curiosity) και οργάνωση αποστολών, βρίσκεται σε συνεχή αναζήτηση εκείνων των στοιχείων που θα αποδείξουν την παρουσία ζωής στον Άρη. Έτσι πλέον, έχουμε περάσει από το στάδιο των ευχών, σε εκείνο των σταθερών ενδείξεων που θα αποδείξουν οτι δεν είμαστε μόνοι στο Σύμπαν.

8. Ευχαριστίες

Θα ήθελα να ευχαριστήσω θερμά την ερευνήτρια στο Jet Propulsion Laboratory, της California, Liu Yang, για την καθοδήγηση σε θέματα μοντελοποίησης συνθηκών μεταμόρφωσης λόγω shock. Επίσης, ευχαριστώ τον καθηγητή και Πρόεδρο της Οργανωτικής Επιτροπής του 13ου Διεθνούς Συνεδρίου της Ελληνικής Γεωλογικής Εταιρίας κ. Μανούτσογλου, για την πρόσκληση που μου απέστειλε με σκοπό την παρουσίαση του θέματος σχετικά με τους μετεωρίτες.

9. Αναφορές

Baziotis I.P., Liu Y., Mc Sween H.Y., Bodnar R.J. and Taylor L.A. 2012. Tissint Meteorite: A fresh piece of Martian lava with new discoveries, *75th Annual Meeting Met. Soc.*, August 12-17, 2012 in Cairns, Australia, #5250.

Baziotis I.P., Liu Y., DeCarli P.S., Melosh H.J., Mc Sween H.Y., Bodnar R.J. and Taylor L.A. 2013. The Tissint Martian meteorite as evidence for the largest impact excavation, *Nature Comm.*, 4, 1404, doi: 10.1038/ncomms2414.

Baziotis I.P., Liu Y. and Taylor L.A. 2013. Detailed Raman Spectroscopic Study of the Tissint Meteorite: Extraordinary Occurrence of High Pressure Polymorphs in a Single Fresh Piece of Martian Shergottite, *Geoph. Res. Abs.*, 15, EGU2013-5463.

Bianciardi G., Miller J.D., Straat P.A. and Levin G.V. 2012. Complexity analysis of the Viking labeled release experiments, *Int. J. Aeronautical Space Sci.*, 13(1), 14-26.

Bischoff A. 2001. Meteorite classification and the definition of new chondrite classes as a result of successful meteorite search in hot and cold deserts, *Planet. Space Sci.*, 49 (8), 769-776.

Blinova A. and Herd C.D.K. 2009. Experimental study of polybaric REE partitioning between olivine, pyroxene and melt of the Y 980459 composition: insights into the petrogenesis of depleted shergottites, *Geochim. Cosmochim. Acta*, 73, 3471 – 3492.

Brennecka G.A., Borg L.E. and Wadhwa M. 2012. The age of Tissint: Sm-Nd & Rb-Sr isotope systematics, *75th Annual Meeting Met. Soc.*, August 12-17, 2012 in Cairns, Australia, #5157.

Chennaoui Aoudjehane H. *et al*. 2012. Tissint Martian Meteorite: A fresh look at the interior, Surface, and Atmosphere of Mars, *Science*, 338, 785-788.

DeCarli P.S. 2013. Meteorites from Mars via a Natural Two-stage Gas Gun, *Procedia Engineering*, 58, 570-573.

El Goresy, A., Gillet, P., Miyahara, M., Ohtani, L., Ozawa, S., Lin, Y., Feng, L., Escerig, S., 2013. Multiple shock events and diamond formation on Mars, *44th LPSC, The Woodlands,* Texas*,* #1037.

Ferrière L., Brandstätter F., Topa D., Schula T., Baziotis I.P., Münker C. and Koeberl C. 2013. The complex history of Tissint inferred from different types of melt inclusions and isotopic systems, *76th Annual Meeting Met. Soc.*, July 29th - August 2nd, 2013 in Edmonton, Canada, #5194.

Fritz J., Artemieva N. and Greshake A. 2005. Ejection of Martian meteorites, *Meteorit. Planet. Sci.*, 40, 1393-1411.

Grosshans T.E., Lapen T.J., Andreasen R. and Irving A.J. 2013. Lu-Hf and Sm-Nd ages and source compositions for depleted shergottite Tissint, *44th LPSC, The Woodlands,* Texas*,* #2872.

Head J.N., Melosh H.J. and Ivanov B.A. 2002. Martian meteorite launch: high-speed ejecta from small craters, *Science*, 298, 1752–1756.

Herd C.D.K., Borg L E., Jones J.H. and Papike J.J. 2002. Oxygen fugacity and geochemical variations in the martian basalts: implications for martian basalt petrogenesis and the oxidation state of the upper mantle of Mars, *Geochim. Cosmochim. Acta*, 66, 2025–2036.

Irving A.J., Kuehner S.M., Tanaka R., Herd C.D.K., Chen G. and Lapen T.J. 2012. The Tissint depleted permafic olivine-phyric shergottite: petrologic, elemental and isotopic characterization of a recent Martian fall in Morocco, *43rd LPSC, The Woodlands,* Texas, #2510.

Levin G. V. and Straat P.A. 1976. Viking labeled release biology experiment: interim results, *Science*, 194(4271), 1322-1329.

Lin Y. *et al.* 2013. NanoSims analysis of organic carbon from Mars: evidence for a biogenetic origin, *44th LPSC, The Woodlands,* Texas*,* #1476.

Liu Y., Taylor L.A., Baziotis I.P., Mc Sween H.Y., Bodnar R.J., DeCarli P.S. and Melosh H.J. 2013. Impact excavation of Martian meteorites: index from shock formed minerals, *44th LPSC, The Woodlands,* Texas, #1371.

McKay D.S., Gibson E.K., Thomas-Keprta K.L., Vali H., Romanek C.S., Clemett S.J., Chillier X.D.F., Maechling C.R. and Zare R.N., 1996. Search for life on Mars: possible relic biogenic activity in martian meteorite ALH84001, *Science*, 273, 924–930.

Moser D.E., Chamberlain K.R., Tait K.T., Schmitt A.K., Darling J.R., Barker I.R. and Hyde B.C. 2013. Solving the Martian meteorite age conundrum using micro-baddeleyite and lauch-generated zircon, *Nature*, 499, 454-457, doi: 10.1038/nature12341.

Sharp T.G. and DeCarli P.S. 2006. Shock effects in meteorites, *Meteorites and the early solar system II*, 653-677.

Shaw C.S.J. and Walton E. 2013. Thermal modeling of shock melts in Martian meteorites: Implications for preserving Martian atmospheric signatures and crystallization of high-pressure minerals from shock melts, *Meteorit. Planet. Sci.*, 1-13, doi: 10.1111/maps.12100.

Shearer C.K., Burger P.V., Papike J.J., Borg L.E., Irving A.J. and Herd C. 2008. Petrogenetic linkages among martian basalts. Implications based on trace element chemistry of olivine, *Meteorit. Planet. Sci.*, 43, 1241–1258.

Steele A. *et al*. 2012. A reduced organic carbon component in Martian basalts, *Science*, 337, 212-215.

Symes S.J.K., Borg L.E., Shearer C.K. and Irving A.J. 2008. The age of martian meteorite NWA 1195 and the differentiation history of the shergottites, *Geochim. Cosmochim. Acta*, 72, 1696 – 1710.

Wallis J., Wickramasinghe C., Wallis D., Miyake N., Wallis M., Di Gregorio B. and Al Mufti S. 2012. Discovery of biological structures in the Tissint Mars meteorite, *J Cosmology*, 18, 8500-8505.

Williams R.M.E. *et al.* 2013. Martian fluvial conglomerates at Gale Crater, *Science*, 340, 1068-1072.

Δελτίο της Ελληνικής Γεωλογικής Εταιρίας, τομ. XLVII , 2013
Πρακτικά 13ου Διεθνούς Συνεδρίου, Χανιά, Σεπτ. 2013

Bulletin of the Geological Society of Greece, vol. XLVII 2013
Proceedings of the 13th International Congress, Chania, Sept. 2013

PALEOBATHYMETRY OF A PLIOCENE VOUTES COAST (HERAKLION, CRETE)

Agiadi K.[1], Koskeridou E.[1], Triantaphyllou M.[1] and Karakitsios V.[1]

[1] National and Kapodistrian University of Athens, Faculty of Geology and Geoenvironment, Department of Hist. Geology - Paleontology, kagiadi@geol.uoa.gr, ekosker@geol.uoa.gr, mtriant@geol.uoa.gr, vkarak@geol.uoa.gr

Abstract

The fish otolith assemblages identified in the Zanclean sediments of Voutes section (Heraklion, Crete) are analyzed in order to estimate the depth of deposition. The assemblages indicate that Voutes area was in fact a coast inhabited by a neritic fish fauna with significant mesopelagic component, mostly Myctophids. The benthic and benthopelagic group exhibits great diversity. In the late Zanclean, the study area corresponds to a deep neritic environment, which gradually uplifts. At the end of the Zanclean, Voutes area becomes a very shallow coast, as shown by the increased contribution to the assemblage by members of the Gobiid family, as well as the notable presence of Bothidae. Thereafter, the area deepens again, as the shallow benthic-benthopelagic component significantly decreases. This is consistent with the appearance of Pteropods and reaches a peak during the deposition of diatomites at maximum depth. At the upper part of the section, the sea bottom depth decreases again to allow for the deposition of marls with various molluscs remains, where Gadids and Gobiids again reappear. Finally, the upper diatomitic horizon is characterized by a rather poor fish fauna. These observations allow reconstructing the evolution of Voutes coastal area during the latest Zanclean until the Piacenzian.
Key words: *Fish, otoliths, Zanclean, Teleosts, Mediterranean.*

Περίληψη

Στην παρούσα εργασία παρουσιάζεται η παλαιοβαθυμετρική ανάλυση των συναθροίσεων ωτολίθων Ιχθύων, που προσδιορίστηκαν στα ιζήματα ηλικίας Ζαγκλίου στην τομή Βούτες (Ηράκλειο, Κρήτη). Η περιοχή Βούτες αποτελούσε μία ακτή με νηριτική Ιχθυοπανίδα, με υψηλή συμμετοχή μεσοπελαγικών ειδών, κυρίων Myctophidae. Τα βενθικά και βενθοπελαγικά ψάρια εμφανίζουν επίσης μεγάλη ποικιλότητα. Κατά το ανώτερο Ζάγκλιο, η περιοχή μελέτης αντιστοιχούσε σε βαθύ νηριτικό περιβάλλον. Σταδιακά η περιοχή ανυψώθηκε σε πολύ μικρά βάθη, όπως φαίνεται από την αυξημένη συμμετοχή στην πανίδα των Gobidae, αλλά και την παρουσία Bothidae. Στη συνέχεια, η περιοχή βάθυνε ξανά, καθώς παρατηρείται σημαντική μείωση της συμμετοχής των ρηχών βενθικών-βενθοπελαγικών ειδών. Το συμπέρασμα αυτό ενισχύεται από την παρουσία στο επίπεδο αυτό των Πτεροπόδων, αλλά και την απόθεση διατομιτών. Σε ανώτερο τμήμα της τομής, το βάθος της θάλασσας μειώνεται και πάλι, πριν τον ανώτερο διατομιτικό ορίζοντα, ο οποίος ωστόσο εμφανίζει ιδιαίτερα φτωχή συνάθροιση ωτολίθων.
Λέξεις κλειδιά: *Ιχθύες, ωτόλιθοι, Ζάγκλιο, Τελεόστεοι, Μεσόγειος.*

1. Introduction

Crete Island was created during the Late Miocene through the N-S and E-W extensional deformation of the south Aegean, resulting in the formation of multiple tectonic blocks and Late Miocene to Pleistocene sedimentary basins (Meulenkamp et al., 1988; van Hinsbergen and Meulenkamp, 2006). The Neogene sediments overlie a pile of alpine nappe substratum, which includes the metamorphic Plattenkalk and Phyllites - Quarzites Units followed by the Tripolis and Pindos-Ethia, as well as other minor units (Zachariasse et al., 2011).

The present emerged area of the Heraklion basin is a Pliocene graben structure located at the northern part of the central Crete Island, in the southern segment of the Hellenic Arc, between the mountains Psiloritis and Dicti. The alpine basement formations contain a rich melange of Triassic to Eocene sedimentary and metamorphic rocks, overlain by Neogene and Quaternary sedimentary deposits, recording a great diversity of environments and ecosystems (Symeonidis and Konstantinidis, 1967). The Pliocene Heraklion basin occurred in a region marked by a great number of successive paleogeographic Miocene frameworks, in the vicinity of the Messara basin. In the late Late Tortonian the activation of the eastern – western oriented Agia Varvara fault differentiated the two realms, which evolved separately since then (Delrieu et al., 1991).

The Pliocene deposits of the Heraklion basin are the most extensive on the Island. The marine sediments of the lowermost Pliocene generally overlie the late Messinian deposits (Delrieu et al., 1991; Meulenkamp et al., 1979), and consist of whitish marls and marly limestones of deep water origin, reflecting the Pliocene flooding which followed the lago-mare episode immediately after the Mediterranean Salinity Crisis.

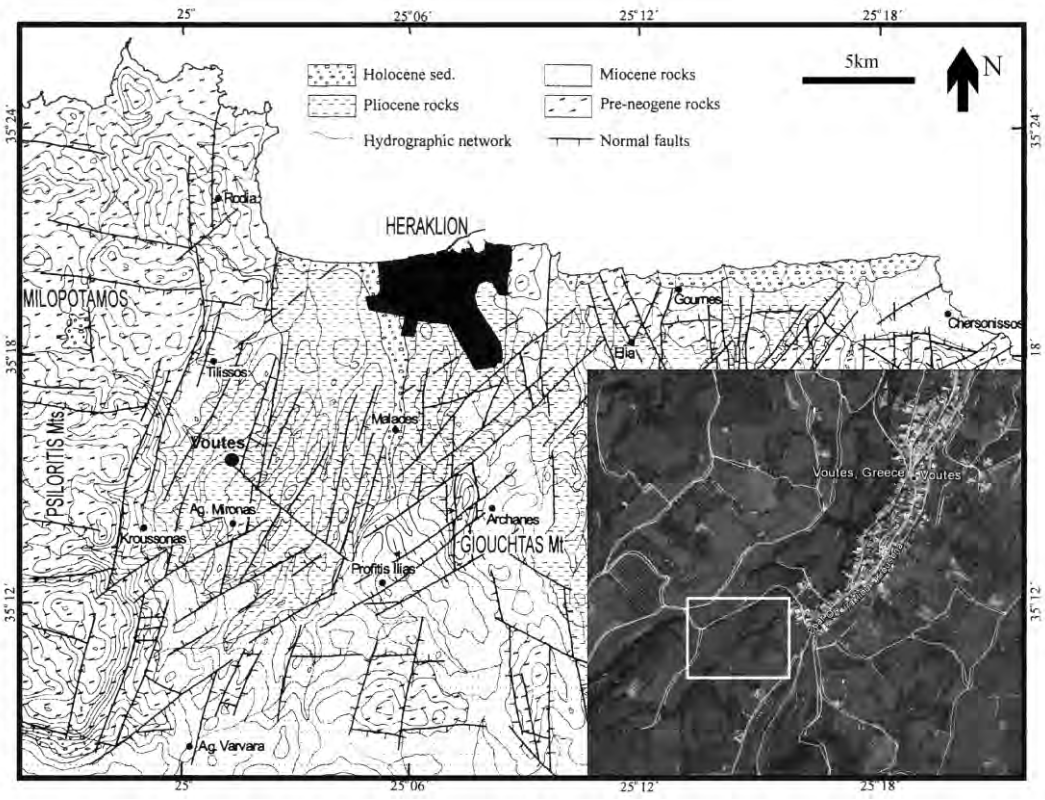

Figure 1 - Heraklion area geological map (Fassoulas, 2001), indicating Voutes village.

Fish otoliths provide a unique tool in the investigation of the fish teleostean paleofaunas, due to their taxon – specific morphology, high frequency with which they are found in sediments of varying environments, and their generally good preservation (Nolf, 1985). In addition, they constitute very valuable paleoecological and paleobathymetrical indicators (Nolf and Brzhobohaty, 1994; Girone, 2000; Agiadi et al., 2010; et al., 2011). In the present study, fish otoliths from the Pliocene sediments of Voutes (Heraklion, Crete) are used as indicators in order to reconstruct the depositional depth.

2. Material and Methodology

The studied Voutes section is located southwest of the village Voutes in central Crete, south of Heraklion city. Geologically it is situated in the western section of the Heraklion basin (Figure 1). The section's sediments may be placed within the Finikia lithostratigaphic group (of Benda et al., 1974 and Meulenkamp et al., 1979) and include more than 60 meters of marls and sandy marls. Strong gravity flows have formed a series of sand lenses, on the lower part of the section, with distinctive sedimentologic attributes and characteristic fauna. The upper part of the section presents three diatomite horizons. On a total, nine (9) sediment samples were taken along Voutes section. Systematic identifications of the fish otoliths found within these samples are presented in Agiadi et al. (2013).

The relevant chronostratigraphic framework (Agiadi et al., 2013) for the evaluation of the results was provided through calcareous nannoplankton biostratigraphy, based on the biozonation scheme of Rio et al. (1990) as this has been incorporated in the magnetobiochronologic framework of Lourens et al. (2004) in Gradstein et al. (2004). The studied interval from Voutes section is assigned to the biozone MNN16, in particular above the highest occurrence of R. pseudoumbilicus and Sphenolithus spp. following the MNN14/15-MNN16 boundary (3.84 Ma, Lourens et al., 2004; Raffi et al., 2006) and just below the top of D. pentaradiatus paracme (3.61 Ma, Lourens et al., 2004), within the latest Zanclean.

The depth of deposition, through the analysis of the fish otolith assemblage, was estimated using the method of Nolf and Brzobohaty (1994) for bathyal and deep neritic assemblages with a significant mesopelagic component, as it was re-adjusted by Agiadi et al. (2010). According to this methodology, based on the modern depth ranges of all the taxa in each sample (Table 1), the number of possible presences for each 50-meter depth interval is calculated and expressed as a percentage of the total number of taxa involved in the analysis. The depth of deposition for each sediment sample is estimated as the maximum percentage in these plots.

The only requirement for the application of this method is that the systematic position of the fossil taxa has a close affinity to their modern analogues. The presence/absence data used includes only those taxa for which present-day bathymetric information is available. This means that higher order identified otolith specimens were completely excluded from analysis. Out of the 43 taxa present in Voutes sediments, only eight are extinct today, Diaphus cavallonis, Myctophum fitchi, Scopelopsis pliocenicus, Pseudophichthys escavaratierensis, Rhynchoconger pantanelli, Parascombrops mutinensis, Gadiculus labiatus and Arnoglossus kokeni. The present-day distributions assigned to these species were those of their most close living relative. To this end, genus level affinity was used, in conjunction with the corresponding present record in the Aegean Sea. These analogies are presented in Table 1. In particular, Scopelopsis pliocenicus has only one living species with a genus-level affinity, Scopelopsis multipunctatus (Hulley, 1990), to which it was assigned. At present, P. splendens is the only Pseudophichthys species occupying the Mediterranean Sea (Bañon et al., 2011). Consequently, P. escavaratierensis was also assigned to P. splendens. Rhynchoconger currently includes seven species, occupying either the Indo-Pacific or the western Atlantic coasts at various depths (Whitehead et al., 1986). In addition, congrids in the present Mediterranean include three species Ariosoma balearicum, Conger conger and Gnathophis mystax (Whitehead et al., 1986).

Table 1 - Present-day bathymetric distribution of the fish taxa identified in Voutes outcrop sediments or their modern equivalent. The data has been acquired from FishBase (Froese and Pauly, 2012).

Taxonomic placement		Bathymetric range (m)	References
Family	**Genus/Species**		
PELAGIC TAXA			
Sternoptychidae	*Maurolicus muelleri*	50->1524	Okiyama 1971
Phosichthyidae	*Vinciguerria poweriae*	50-1000	Yang et al 1996
Myctophidae	*Ceratoscopelus maderensis*	51-1082	Mytilineou et al 2005
	Diaphus adenomus	180-600	Hulley 1990
	Diaphus holti	40-777	Mytilineou et al 2005
	Diaphus metopoclampus (equiv. *D.cavallonis*)	90-1085	Mytilineou et al 2005
	Diaphus rafinesquii	40-1200	Bogutskaya 2007
	Diaphus splendidus	40-750	Hulley 1990
	Diaphus taaningi	40-475	Hulley 1990
	Hygophum benoiti	51-700	Hulley 1990
	Hygophum hygomii	0-800	Hulley 1990
	Myctophum punctatum (equiv. *M.fitchi*)	0-1000	Muus and Nielsen 1999
	Lobianchia dofleini	20-750	Hulley 1990
	Notoscopelus resplendens	0-2000	Hulley 1990
	Scopelopsis multipunctatus (equiv. *S.pliocenicus*)	3-2000	Hulley 1990
Bregmacerotidae	*Bregmaceros* spp.	?-1260m	Castellanos-Galindo et al 2006
BENTHIC AND BENTHOPELAGIC TAXA			
Congridae	*Pseudophichthys splendens* (equiv. *P.escavaratierensis*)	37-1647	Bañon et al 2011
	Modern Mediterranean Congrids (equiv. *R.pantanelli*)	0-700	Whitehead et al 1986
Chlorophthalmidae	*Chlorophthalmus agassizi*	50-1000	Whitehead et al 1986
Moridae	*Laemonema* spp.	200-1200	Whitehead et al 1986
Gadidae	*Gadiculus argenteus* (equiv. *G. labiatus*)	100-1000	Muus and Nielsen 1999
Bythitidae	*Grammonus ater*	reef-associated	Whitehead et al 1986
Carapidae	*Echiodon dentatus*	120-3250	OBIS 2006
Atherinidae	*Atherina boyeri*	coastal, very euryhaline	Maugé 1990
Apogonidae	*Apogon* spp.	reef-associated	Whitehead et al 1986
Epigonidae	*Epigonus denticulatus* (equiv. *Epigonus* sp.)	300-600	Whitehead et al 1986
Acropomatidae	*Synagrops spinosus* (equiv. *P.mutinensis*)	87-544	Mochiuzuki and Gultneh 1989
Sparidae	*Oblada melanura*	?-30	Bauchot and Hureau 1990
	Pagellus erythrinus (equiv. *Pagellus* sp.)	20-200	Bauchot and Hureau 1990
Cepolidae	*Cepola macrophthalma*	15-400	Whitehead et al 1986
Gobiidae	*Aphia minuta*	0-97	Iglesias and Morales-Nin 2001
	Deltentosteus quadrimaculatus	?-333	Mytilineou et al 2005
	Gobius niger	1-75	Whitehead et al 1986
	Gobius paganellus	?-15	Azevedo and Simas 2000
	Lesueurigobius friesii	10-130	Miller 1990
	Lesueurigobius sanzi	47-117	Miller 1990
	Lesueurigobius suerii (equiv. *Lesueurigobius* sp.)	?-337	Mytilineou et al 2005
Citharidae	*Citharus linguatula*	?-200	Nielsen 1981
Bothidae	*Arnoglossus* spp.	15-300	Whitehead et al 1986

All three species exhibit great depth distribution, from a few tens to more than 700 meters, which was thus used as a generalized assessment of the depth distribution of R. pantanelli. There is no living species placed within the genus Parascombrops, nor is there an Acropomatidae representative occupying the Mediterranean Sea at present. From the comparative morphological similarities between the North Atlantic species Synagrops spinosus (Campana, 2004) and the P. mutinensis otoliths of this and previous studies (Agiadi et al., 2011; Agiadi et al., 2013), it may be considered that this is an appropriate modern analogue to the fossil species. The only Gadiculus Mediterranean inhabitant today is G. argenteus (Muus and Nielsen, 1999), which was accepted here as the modern equivalent of G. labiatus. Finally, Arnoglossus spp. depth values encompass the distribution of all six extant Arnoglossus Mediterranean species (Whitehead et al., 1986).

An initial inspection of the depth distribution of the identified taxa in the samples indicated that the paleodepths did not surpass 1000 meters. Consequently, the analyses were conducted until that depth. In addition, Maurolicus muelleri, Vinciguerria poweriae, Ceratoscopelus maderensis, Diaphus metopoclampus, Diaphus rafinesquii, Myctophum punctatum, Notoscopelus resplendens, Bregmaceros sp., Gadiculus argenteus, Scopelopsis multipunctatus and Pseudophthichthys splendens were excluded from the analyses because their modern depth distribution range is great and encompasses almost entirely the 0-1000 meter interval. Their presence were considered only to clarify ambivalent depth estimates.

3. Paleobathymetric Analysis

The paleodepth analysis and estimates are presented in Figures 2 and 3. In sample Voutes b, only three species may be considered, which provided a paleobathymetric estimate between 10-130 meters, *Cepola macrophthalma*, *Deltentosteus* aff. *quadrimaculatus* and *Lesueurigobius friesii*. In Voutes 3 the analysis delivered an estimate of 50-350 meters. However, this range is affected by the 50-meter intervals used in the analysis. After closer examination, it may be observed that the actual paleodepth estimate ought to be that where both *Aphia minuta* and *Diaphus adenomus* could coexist, and that is between 87-100 meters depth. The presence of *D. holti*, *H. hygomii* and *Laemonema* sp. in Voutes 4 leads to a paleodepth estimate between 200-800 meters, with no greater accuracy available for this level. The fish taxa identified in sample Voutes 1 did not allow for any paleobathymetric estimation. In particular, in this sample the following taxa have been identified (Agiadi et al., 2013): Myctophidae indeterminable (ind.), *Bregmaceros* sp., *Laemonema* sp., *Gadiculus labiatus*, Sparidae ind. and Perciformes ind. The great abundance of *Bregmaceros* sp., in conjunction with the presence of Myctophids and deep-water benthopelagic taxa such as *Laemonema* sp., *Gadiculus labiatus* and Perciformes, may indicate a rather deep marine environment, generally exceeding 200 meters.

A mixed fauna is revealed through the paleobathymetric analysis in sample Voutes c. Initially, the graphical results provide an estimate between 300-337 meters, delimited by the maximum depth distribution of *L. suerii*. However, the presence of *Oblada melanura* is problematic. This benthopelagic fish today inhabits rocky bottom of depths up to 30 meters, in the coasts of the eastern Atlantic and the Mediterranean Sea (Bauchot and Hureau, 1990). In addition, reef-associated taxa *Grammonus ater* and *Apogon* sp. (Whitehead et al., 1986) also also present in sample Voutes c. Two faunal units may thus be separated in this level, a deeper neritic unit from an environment reaching depths around 300-337 meters, and a shallow unit from depths between 0-30 meters.

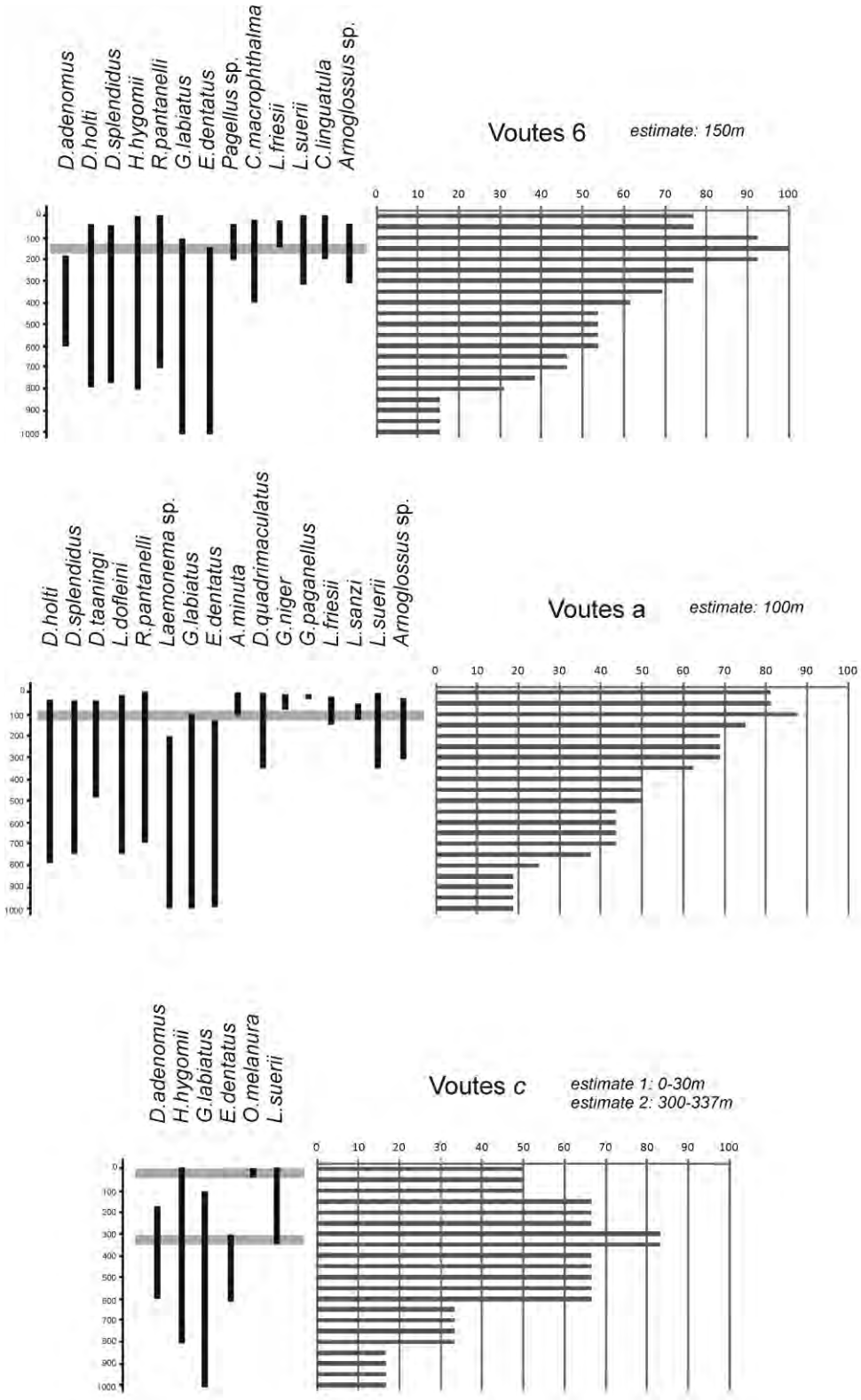

Figure 2 - Paleobathymetric analysis and estimates.

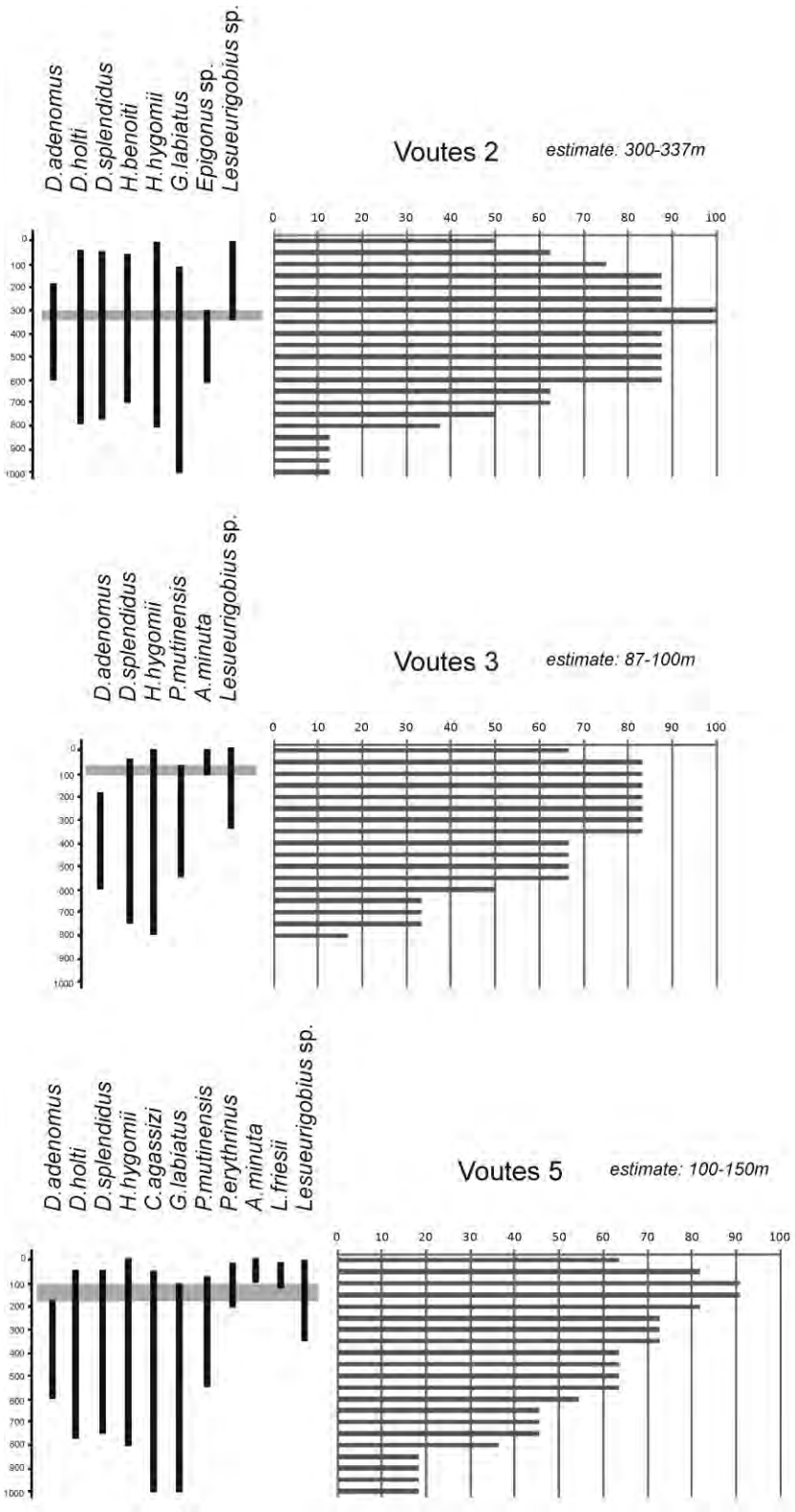

Figure 3 - Paleobathymetric analysis and estimates (continuation).

4. Discussion and Conclusions

The paleobathymetric curve created from the analysis of the fish otolith fauna uncovered in the Voutes outcrop sediments present an interesting input in the paleogeographic evolution of the Central Crete area, namely the Heraklion basin (Figure 4).

Generally, depths throughout this interval do not exceed 350 meters, although the lower part of the section (Figure 2) exhibits much shallower estimates, up to 150 meters. The deeper environments are found on the upper part of the section (Figure 3). However, no specific trend may be safely concluded from the estimated values. Rather several depth variations are visualized (Figure 4). In addition, the lower part of the Voutes outcrop reveals a mixture of the fish faunas from two realms, a deep water probably autochthonous faunal component, and a shallow allochthonous fauna. This is in accordance with the gravity flows observed at the lower part of the section, which seem to have incurred this mixing. Overall, during the late Zanclean, Voutes area was a coast, habitat for a rich shallow neritic Ichthyofauna. The results presented here offer new input on the tectonic – eustatic coupling effect on the paleogeography of central Crete, between 3.84 and 3.61Ma.

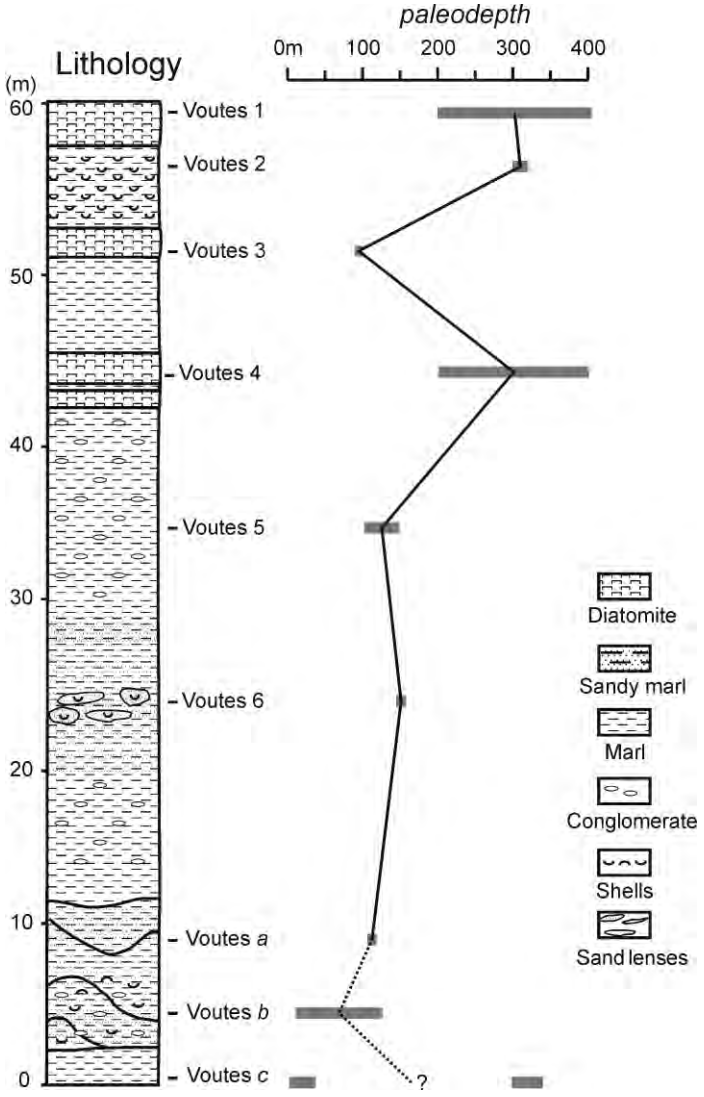

Figure 4 - Voutes section lithology and paleobathymetric curve.

5. Acknowledgments

This research has been co-financed by the European Union (European Social Fund – ESF) and Greek national funds through the Operational Program "Education and Lifelong Learning" of the National Strategic Reference Framework (NSRF) - Research Funding Program: Heracleitus II. Investing in knowledge society through the European Social Fund.

6. References

Agiadi K., Triantaphyllou M., Girone A., Karakitsios V. and Dermitzakis M. 2010. Paleobathymetric interpretation of the fish otoliths from the lower-middle Quaternary deposits of Kephallonia and Zakynthos Islands (Ionian Sea, western Greece), *Rivista Italiana di Paleontologia e Stratigrafia*, 116(1), 63-78.

Agiadi K., Triantaphyllou M., Girone A. and Karakitsios V. 2011. The early Quaternary palaeobiogeography of the eastern Ionian deep-sea Teleost fauna: A novel palaeocirculation approach, *Palaeogeography Palaeoclimatology Palaeoecology*, 306, 228-242.

Agiadi K., Koskeridou E., Triantaphyllou M., Girone A. and Karakitsios V. 2013. Fish otoliths from the Pliocene Heraklion basin (Crete, eastern Mediterranean), *Geobios*, in press.

Azevedo J.M.N. and Simas A.M.V. 2000. Age and growth, reproduction and diet of sublittoral population of the rock goby *Gobius paganellus* (Teleostei: Gobiidae), *Hydrobiol.*, 440, 129-135.

Bañon R., Arronte J.C., Serrano A. and Sánchez F. 2011. First records of purple-mouthed conger *Pseudophichthys splendens* (Anguilliformes: Congridae) from the Galicia Bank (NW Spain). A northward range extension of their distribution in the eastern Atlantic, *Cybium*, 35(3), 262-264.

Bauchot M.L. and Hureau, J.C. 1990. Sparidae, in Quero, J.C., Hureau, J.C., Karrer, C., Post, A., Saldanha, L., eds., *Check-list of the fishes of the eastern tropical Atlantic (CLOFETA)*, JNICT, Lisbon; SEI, Paris; and UNESCO, Paris. Vol. 2.

Benda L., Meulenkamp J.E. and Zachariasse W.J., 1974. Biostratigraphic correlations in the eastern Mediterranean Neogene. Part I: Correlation between planktonic foraminiferal, uvigerinid, sporomorphal and mammal zonations of the Cretan and Italian Neogene, *Newsletter in Stratigraphy*, 3, 205-217.

Bogutskaya N.G. 2007. *Preliminary assignment of coordinates to type localities in the Catalog of Fishes*, Unpublished dbf file.

Campana S.E. 2004. Photographic Atlas of Fish Otoliths of the Northwest Atlantic Ocean, *Canadian Special Publications of Fisheries and Aquatic Sciences*, 133.

Castellanos-Galindo G.A., Rincon E.A.R., Beltran-Leon B., Zapata L.A. and Baldwin C.C. 2006. Check list of gadiform, ophidiiform and lophiidorm fishes from Colombian waters of the tropical eastern Pacific, *Biota Colombiana*, 7(2), 191-209, Bogotà.

Delrieu B., Saint-Martin J.P. and Merle D. 1991. Un modele d'evolution tectonosedimentaire dans le domaine Sud-Egeen au Miocene Superieur: L'accident d'Aghia Varvara (Crete Central, Grece), *Comptes Rendus de l' Academie des Sciences Paris*, 313, 1043-1049.

Fassoulas C. 2001. The tectonic development of a Neogene basin at the leading edge of the active European margin: the Heraklion basin, Crete, Greece, *Journal of Geodynamics*, 31, 49-70.

Froese R. and Pauly D. eds. 2012, *Fish Base*, World Wide Web electronic publication. www.fishbase.org, version (12/2012).

Girone A. 2000. The use of fish otoliths for paleobathymetric evaluation of the Lower to Middle Pleistocene deposits in Southern Italy, *Bull. Societa Palentologica Italiana*, 39(2), 235-242.

Gradstein F., Ogg J. and Smith A. 2004. *A Geological Time Scale*, Cambridge Univ. Press, 610pp.

Hulley P.A. 1990. Myctophidae, In: Quero, J.C., Hureau, J.C., Karrer, C., Post, A., Saldanha, L., eds., *Check-list of the fishes of the eastern tropical Atlantic (CLOFETA)*, JNICT, Lisbon; SEI; Paris; and UNESCO, Paris, Vol. 1, 398-467.

Iglesias M. and Morales-Nin B. 2001. Life cycle of the pelagic goby *Aphia minuta* (Pisces: Gobiidae), *Scientia Marina*, 65(3), 183-192.

Lourens L., Hilgen F., Shackleton N., Laskar J. and Wilson D. 2004. The Neogene Period. In Gradstein E. et al. (eds.) *A Geologic Time Scale 2004*, Cambridge Univ. Press, 409-440.

Maugé L.A. 1990. Atherinidae. In Quero, J.C., Hureau, J.C., Karrer, C., Post, A., Saldanha, L., eds., *Check-list of the fishes of the eastern tropical Atlantic (CLOFETA)*, JNICT, Lisbon; SEI, Paris; and UNESCO, Paris. Vol. 2.

Meulenkamp J.E., Dermitzakis M., Georgiadou-Diakeoulia E., Jonkers H.A. and Boerger H. 1979. *Field Guide to the Neogene of Crete*, Publications of the Geological and Paleontological Department, University of Athens, Athens.

Meulenkamp J.E., Wortel M.J.R., Van Wamel W.A., Spakman W. and Hoogerduyn Strating E. 1988. On the Hellenic subduction zone and the geodynamical evolution of Crete since the late Middle Miocene, *Tectonophysics*, 146, 203-215.

Miller P.J. 1990. Gobiidae. In Quero, J.C., Hureau, J.C., Karrer, C., Post, A., Saldanha, L., eds., *Check-list of the fishes of the eastern tropical Atlantic (CLOFETA)*, JNICT, Lisbon, SEI, Paris; and UNESCO, Paris. Vol. 2.

Mochiuzuki K. and Gultneh S. 1989. Redescription of *Synagrops spinosus* (Percichthyidae) with its first record from the West Pacific, *Japanese Journal of Ichthyology*, 35(4), 421-427.

Muus B.J. and Nielsen J.G. 1999. *Sea fish*, Scand. Fish. Year Book, Hedehusene, Denmark, 340 p.

Mytilineou C., Politou C.Y., Papaconstantinou C., Kavadas S., D'Onghia G. and Sion L. 2005. Deep-water fish fauna in the Eastern Ionian Sea, *Belgian J. Zoology*, 135(2), 229-233.

Nielsen J.G. 1981. Citharidae, in Fischer, W., Bianchi, G., Scott, W.B., eds., *FAO species identification sheets for fishery purposes*, Eastern Central Atlantic; fishing areas 34, 47 (in part). Vol. 2, FAO, Rome.

Nolf D. 1985 Otolithi Piscium, in Schultze, H.P., ed., *Handbook of Paleoichthyology*, vol. 10, 1-145, Stuttgart.

Nolf D. and Brzobohaty R., 1994. Fish otoliths as paleobathymetric indicators, *Paleontologia i evolucio*, 24-25, 255-264.

Biogeographic Information System 2006. OBIS-extracted Depth Data. Harvested by E.Agbayani July 2006 at www.iobis.org.

Okiyama M. 1971. Early life history of the gonostomatid fish *Maurolicus muelleri* (Gmelin), in the Japan Sea, *Bull. Japanese Sea Registry of the Fisheries Research Lab*, 23, 21-53.

Raffi I., Backman J., Fornaciari E., Palike H., Rio D., Lourens L. and Hilgen F. 2006. A review of calcareous nannofossil astrobiochronology encompassing the past 25 million years, *Quaternary Science Reviews*, 25(23-24), 3113-3137.

Rio D., Raffi I. and Villa G. 1990. Pliocene-Pleistocene calcareous nannofossil distribution patterns in the western Mediterranean, In Kastens K.A., Mascle J., et al., eds., *Proceedings of the ODP*, Scientific Results, vol. 107. ODP, College Station TX, 513-533.

Symeonidis N. and Konstadinidis D. 1967. Observations on the Neogenic formations of Central Crete, *Annales Géologiques des Pays Helléniques*, 19, 657-688.

Van Hinsbergen D.J.J. and Meulenkamp J.E. 2006. Neogene supra-detachment basin development on Crete (Greece) during exhumation of the South Aegean core complex, *Basin Research*, 18, 103-124.

Whitehead P.J.P., Bauchot M.L., Hureau J.C., Nielsen J. and Tortonese E., eds., 1984-1986, *Fishes of the North-eastern Atlantic and the Mediterranean*, UNESCO, vol. I (1984), 1-510, vol.II (1986), 511-1007, vol. III(1986), 1008-1473, Paris.

Yang J., Huang Z., Chen S. and Li Q. 1996. *The Deep-Water Pelagic Fishes in the area from Nansha Islands to the Northeast part of South China Sea*, Science Publication Company, Beijing. 190 pp.

Zachariasse W.J., Hinsbergen D.J.J. and Fortuin A.R. 2011. Formation and fragmentation of a late Miocene supradetachment basin in central Crete: implications for exhumation mechanisms of high-pressure rocks in the Aegean forearc, *Basin Research*, 23, 678-701.

Δελτίο της Ελληνικής Γεωλογικής Εταιρίας, τομ. XLVII , 2013
Πρακτικά 13ου Διεθνούς Συνεδρίου, Χανιά, Σεπτ. 2013

Bulletin of the Geological Society of Greece, vol. XLVII 2013
Proceedings of the 13th International Congress, Chania, Sept. 2013

EARLY-MIDDLE MIOCENE FROM KOTAPHI HILL SECTION (NICOSIA, CYPRUS): PRELIMINARY BIOSTRATIGRAPHY AND PALEOCEANOGRAPHIC IMPLICATIONS

Athanasiou M.[1], Triantaphyllou M.[1], Dimiza M.[1], Gogou A.[2], Bouloubassi I.[3], Tsiolakis E.[4] and Theodorou G.[1]

[1] National and Kapodistrian University of Athens, Faculty of Geology and Geoenvironment, athanasioum@geol.uoa.gr

[2] Hellenic Centre for Marine Research, Institute of Oceanography, 190 13 Anavyssos, Attiki

[3] Laboratoire d'Océanographie et du Climat, Expérimentation et Approche Numérique, Université Pierre et Marie Curie, Paris Cedex 05, France

[4] Geological Survey Department of Cyprus, 1 Lefkonos Street, 2064 Strovolos Lefkosia Cyprus

Abstract

Calcareous nannofossil biostratigraphy from Kotaphi Hill section allowed not only the biostratigraphic zonation of the Miocene units but also provided evidence for a distinct warm phase known as the Middle Miocene Climate Optimum (MMCO). Kotaphi Hill section is located in Agrokipia village (Nicosia region, Cyprus) and consists of cyclic marine deposits of the Pakhna Formation. High resolution sampling has been conducted and 84 samples were collected. Preliminary results indicated that several important calcareous nannofossil events can be consistently recognized along the studied section. High abundances of Discoaster druggii and Highest occurrence (HO) of Sphenolithus procerus suggest the presence of NN2 biozone while, LO of Sphenolithus belemnos has been used to recognize the base of biozone NN3. Upwards, Lowest Common Occurrence (LCO) of Sphenolithus heteromorphus marked the NN3-4 boundary-level. Biozone NN4 in Kotaphi Hill section is featured by high abundance of S. heteromorphus whereas total absence of the species together with the LO of Helicosphaera walbedorfensis mark the Paracme Beginning (PB) of S. heteromorphus interval. High abundance of warm indicators such as Discoasterids, S. heteromorphus, S. moriformis and Helicosphaera carteri observed in our material may partly reflect the warm phase of MMCO.
Key words: *Agrokipia village, Pakhna Formation, Cyprus, Sphenolithus heteromorphus, Middle Miocene Climate Optimum.*

Περίληψη

Η βιοστρωματογραφική ανάλυση με βάση τα ασβεστολιθικά ναννοπολιθώματα που διεξήχθη στην τομή Κοτάφι επέτρεψε τον προσδιορισμό βιοζωνών του Μειόκαινου, καθώς και το συσχετισμό με τη θερμή φάση του Κλιματικού Βέλτιστου του Μέσου Μειόκαινου (Middle Miocene Climate Optimum, MMCO). Η τομή Κοτάφι βρίσκεται στον οικισμό Αγροκηπιά (Λευκωσία, Κύπρος) και αποτελείται από θαλάσσια ιζήματα με έντονη κυκλικότητα του Σχηματισμού της Πάχνας. Η υψηλής ανάλυσης

δειγματοληψία που πραγματοποιήθηκε, περιλαμβάνει συνολικά 84 δείγματα. Τα πρώτα αποτελέσματα επέτρεψαν την αναγνώριση διαδοχικών συμβάντων του ασβεστολιθικού νανnοπλαγκτού. Η υψηλή αφθονία του είδους Discoaster druggii και η ανώτερη παρουσία (HO) του είδους Sphenolithus procerus παραπέμπουν στη βιοζώνη NN2 ενώ, η βάση της βιοζώνης NN3 αναγνωρίστηκε με τη κατώτερη παρουσία (LO) του είδους Sphenolithus belemnos. Επιπλέον, το όριο των βιοζωνών NN3-NN4 προσδιορίστηκε με βάση τη κατώτερη συχνή παρουσία (LCO) του είδους Sphenolithus heteromorphus. Η βιοζώνη NN4 χαρακτηρίζεται από την υψηλή αφθονία του είδους S. heteromorphus ενώ στα ανώτερα στρώματα της τομής, η πλήρης απουσία αυτού σε συνδυασμό με τη κατώτερη παρουσία (LO) του είδους Helicosphaera walbedorfensis σηματοδοτούν το κατώτερο όριο του διαστήματος παρακμής (PB) του S. heteromorphus. Η αφθονία των θερμών αντιπροσώπων Discoasterids, S. heteromorphus, S. moriformis και Helicosphaera carteri που καταγράφεται, πιθανόν να αντανακλά τη θερμή φάση του MMCO.
Λέξεις κλειδιά: *Αγροκηπία, Σχηματιμός της Πάχνας, Κύπρος, Sphenolithus heteromorphus, Κλιματικό Βέλτιστο Μέσου Μειόκαινου.*

1. Introduction

The continuing collision of the European and African plates resulted to the final closure of the Tethys Ocean and the birth of the Mediterranean Sea. The last vestiges of the Mesozoic Tethys oceanic crust are today represented by the ophiolitic chain of the Troodos Massif, located on the hanging wall of the Cyprus subduction zone (Robinson & Malpas, 1990). Geologically, Cyprus can be generally divided into five main geological terranes (1) Troodos Ophiolite Complex, (2) Mamonia Terrane, (3) Keryneia Terrane, (4) Circum-Troodos Sedimentary Succession and (5) Quaternary units. Ophiolite genesis started at Late Cretaceous and formed the Troodos Ophiolite Complex (TOC) which was obducted much later in the Middle Miocene. The subsequent period of low tectonic activity was dominated by deposition of carbonate rich sediments, commencing with the deep marine Lefkara Formation. However, an abrupt change to more localised, tectonically controlled deposition took place in the Early Miocene, initiating deposition of the Pakhna Formation. This phase was then followed by the formation of numerous shallow depositional basins containing gypsiferous sub-units of the Messinian salinity crisis that occurred when the Mediterranean was closed and sea levels dropped (Rouchy et al., 2001). Salinity crisis was followed by an abrupt uplift of the area that occurred during the Pleistocene at ~2 Ma, resulting to the deposition of Pleistocene fanglomerates, mainly on the northern flanks of the Troodos Massif.

Middle Miocene is not only considered as crucial time interval for the evolution of the Earth climatic system, but also for the dynamic geologic evolution of the Mediterranean region. Such important geodynamic and paleoclimatic issues need a well-established biogeochronologic framework. Calcareous nannofossil have been proven extremely useful for the biostratigraphy of marine sediments, providing essential time-constrain for regional and worldwide biostratigraphic correlations. (e.g., Perch-Nielsen, 1985).

Aim of the present study is to test the reliability of Early to Middle Miocene calcareous nannofossil biohorizons at the Kotaphi Hill section (Cyprus Island), in order to improve the time resolution in the region and to provide paleoceanographic implications during the Middle Miocene Climate Optimum (MMCO) in south-eastern Mediterranean.

2. Materials and Methods

2.1. Study Area

Kotaphi Hill section (05° 13’ E, 38 °78’ N) is located in Agrokipia village (Nicosia region, Figure 1). It consists of well-preserved cyclic marine sediments of Pakhna Formation, which includes a

range of shallow-to deeper-water carbonates and subordinate terrigenous sediments that were mainly deposited by pelagic and gravity-controlled processes. Pakhna Formation is overlain by the evaporitic Kalavasos Formation (Follows & Robertson, 1990), which are similar to the Messinian evaporites elsewhere in the Mediterranean (e.g., Hsü, 1973), and is underlain by complete successions of Late Cretaceous-Oligocene deep-water pelagic limestones and calciturbidites of the Lefkara Formation (Robertson, 1976). Although the base of the Pakhna Formation appears to be of Aquitanian age in northern and southeastern Cyprus, (Robertson et al., 1991) limited data from southern Cyprus indicate ages ranging from Burdigalian to Langhian, implying the diachronous base of the formation. Two members are recognized within the Pakhna Formation: the Early Miocene Terra Member and the Late Miocene Koronia Member. The first phase, of Terra Member (Aquitanian-Burdigalian), is exposed only in SE and W of Cyprus while the latter, Koronia Member (Tortonian), is exposed, both fringing the Troodos Massif in north, south and west Cyprus, and on the Akamas Peninsula of NW Cyprus (Follows & Robertson, 1990). Both phases of Pakhna Formation witness progressive changes through the Miocene that resulted from a combination of local Cyprus tectono-stratigraphic effects, general Mediterranean features and global climatic control.

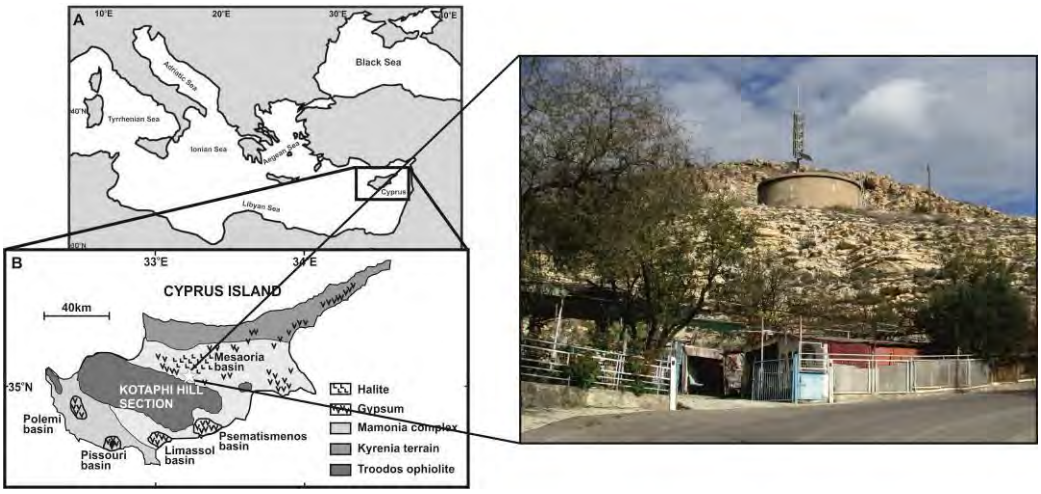

Figure 1 - Geologic sketch map of Cyprus Island. The location of Kotaphi Hill section is marked.

Our data cover mainly the Early Miocene deposits, outcropping in Kotaphi Hill section. Our first results refer to the lower part the section (Figure 2), with total height of 16.50 m. The lower 1.5 m consists of marly chalk layers, which are passing to 7 m of laminated chalky layers, alternating with chalky marl layers. The following 10.5-13.5 m of the section is characterized by chalky layers alternating with marls and marly chalks. Sediments of the uppermost 3 m (13.5 -16.50 m) are featured by laminated alternations between chalk and chalky marls. High resolution sampling of the section has been conducted with an average sampling resolution of 20-30 cm. A total number of 84 samples were collected and 25 samples from different levels of the section have been used for the purpose of this study.

2.2. Calcareous Nannofossil Analysis

For calcareous nannofossil analysis the preparation of samples followed the standard smear slide technique described by Perch Nielsen (1985). All sediment samples were routinely examined under a light microscope at a magnification of 1250 x, carried out using a Leica DMSP polarising light microscope (Dept. of Hist. Geology and Paleontology). In order to obtain accurate biostratigraphic estimations, up to 100 fields of view have been investigated per slide. Calcareous

Figure 2 - Detailed lithostratigraphy of Kotaphi Hill section and sample location.

nannofossil biostratigraphy, mainly based on the appearance/disappearance and relative abundance patterns of selected species, provided high time resolution and accurate correlation with regional and global stratigraphy and time scales for the Miocene marine successions (e.g., Fornaciari et al., 1996; Fornaciari & Rio, 1996; Lourens et al., 2004; Raffi et al., 2003; 2006, Hüsing et al., 2010). Lowest (LO) and highest (HO) occurrence of the index species, concern their first and last occurrence respectively, whereas LCO (Lowest Consistent Occurrence) and HCO (Highest Consistent Occurrence) indicate biohorizons which mark the beginning and end, respectively, of the consistent (continuous and/or common) distribution of index species. A LCO biohorizon thus represents an increase in abundance above the first appearance of the taxon, while an HCO biohorizon corresponds to a consistent drop in abundance prior to the extinction. Furthermore, PB (Paracme Beginning) and PE (Paracme End) indicate biohorizons which mark the beginning and end, respectively, of an interval in which the index taxon is temporarily absent, or present with scattered single specimens (Paracme interval).

Abundances of the taxa encountered in this paper were recorded as follows: A, abundant: more than one specimen every field of view; C, common: 1 specimen/10 fields of view; R, rare: 1 specimen/ 50 fields of view; P, present: 1 specimen/ >100 fields of view; RW, reworked specimens. The taxonomy of the determined calcareous nannofossil species has been based on

Aubry (1984-1999) and Perch-Nielsen (1985). The determination of the biostratigraphic events has followed Martini (1971), Fornaciari et al., (1996), Fornaciari & Rio (1996), Raffi et al. (2003, 2006). Numerical ages of biozone boundaries are given according to Lourens et al. (2004), Raffi et al. (2006).

3. Results and Discussion

Preliminary biostratigraphic results for the Kotaphi Hill section are plotted in Figure 3 LO of *Sphenolithus belemnos*, LCO of *Sphenolithus heteromorphus,* PB of *S. heteromorphus* and LO *Helicosphaera ampliaperta* are some of calcareous nannofossils biohorizons that have been recorded in the Kotaphi Hill section. Semiquantitative results of the major representatives of calcareous nannofossils evaluated in the studied samples of the Kotaphi Hill section are presented in Table 1.

Table 1 - Species frequencies of calcareous nannofossils per sample of the Kotaphi Hill section as follows: A: abundant, C: common, R: rare, P: present, RW: reworked.

Sample/ caclacreous Nannofossil species	*Discoaster druggii*	*Sphenolithus procerus*	*Sphenolithus dissimilis*	*Sphenolithus disbelemnos*	*Sphenolithus belemnos*	*Sphenolithus heteromorphus*	*Helicosphaera carteri*	*Helicosphaera euphratis*	*Helicosphaera ampliaperta*	*Helicosphaera walbersdorfensis*
KΔ 5	A	R	P				C	C		
KΔ10	A	R	P				C	C		
KΔ15	C	P	R				C	R		
KΔ19	C		R				A	R		
KΔ21	C		R	P	R		A	R	P	
KΔ25	C		P	P	R		A	R	C	
KΔ27	C			R	C	R	A	R	C	
KΔ31	R		P	R	C	R	A	R	R	
KΔ35	C			R	C	R	A	R	R	
KΔ40	C			R	R	R	A	R		
KΔ43	C			P	R	R	A	R		
KΔ45	C			P	R	C	A	R		
KΔ49	C				RW	C	A	R		
KΔ53	C				RW	C	A	R		
KΔ57	C			RW	RW	C	A	R	P	
KΔ60	R				RW	C	C	C		
KΔ62	C				RW	C	C	C		
KΔ65	C			RW	RW	C	C	C		P
KΔ68	C				RW	C	A	C	P	
KΔ70	C						A	C	P	
KΔ73	C					R	A	C	P	P
KΔ77	C						A	C		P
KΔ80	P						A	P	P	P
KΔ82	P						A	P		P

3.1. Biozone NN2 (MNN2)

High abundance of *D. druggii* and low percentages of *Discoaster deflandrei* along with the HO of *Sphenolithus procerus* and continuous presence of *Sphenolithus dissimilis* in the first 4.9 m of the section, enable the biostratigraphic correlation with biozone NN2 (Martini, 1971). Based on the calcareous nannofossil analysis, the rare presence of *S. procerus* in the investigated assemblage is strengthening our biozonal determination. In the Mediterranean region, the HCO of *Helicosphaera*

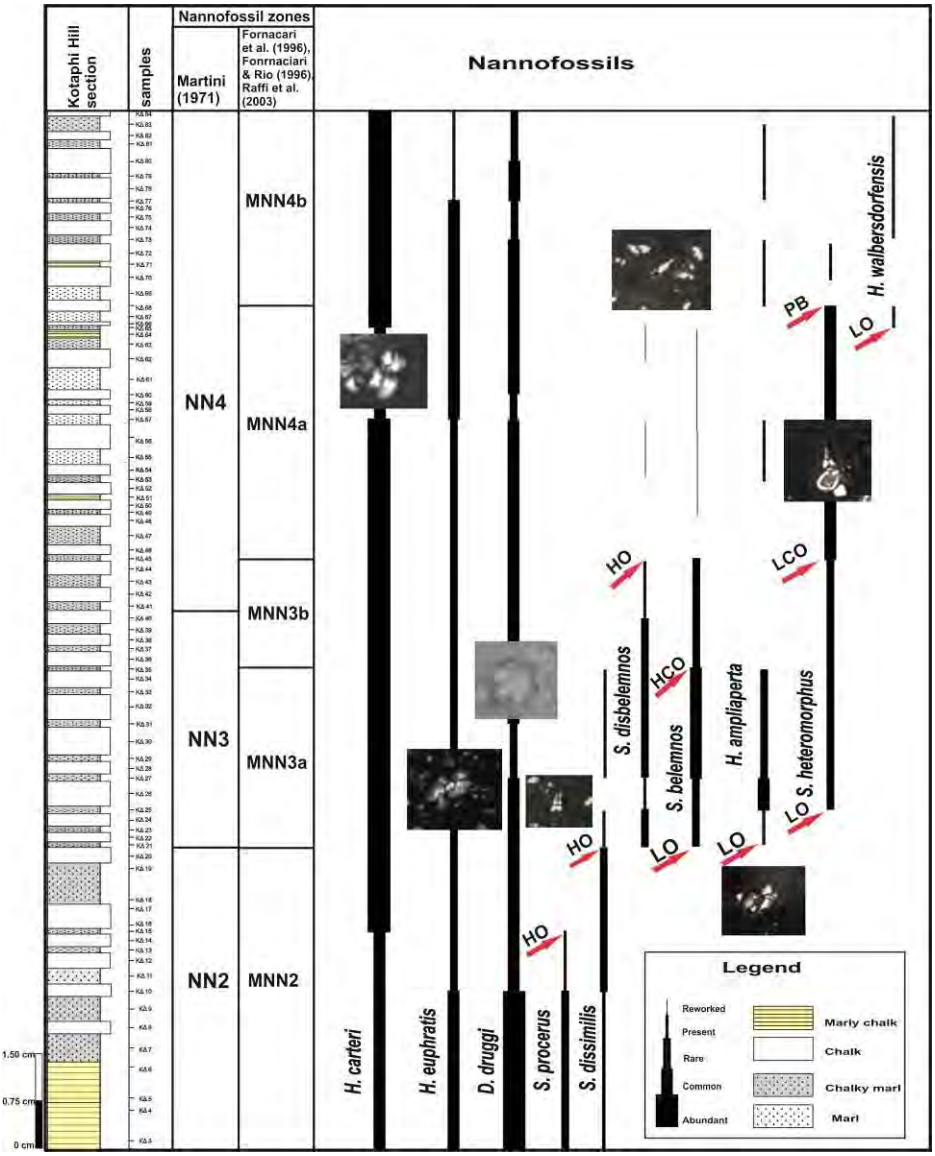

Figure 3 - Preliminary calcareous nannofossil biostratigraphy of Kotaphi Hill section.

euphratis has been correlated with the LCO of *Helicosphaera carteri* in the NN2 biozone (Coccioni et al., 1997). According to Fornaciari, & Rio (1996), the dominance of *H. carteri* over *H. euphratis* is very distinctive in this interval. Our data document the dominance of *H. carteri* over *H. euphratis,* thus supporting the biostratigraphic recognition of biozone NN2. Minor components in our assemblages are also *Sphenolithus compactus* and *Sphenolithus conicus,* while the abundant presence of *Sphenolithus moriformis* is also noted.

3.2. Biozone NN3 (MNN3)

Although there are some contradictions in the literature concerning the presence of *S. belemnos* in the Mediterranean stratigraphic record, LO and HCO of this species is very often used to define NN3 zone. First rare representatives of *S. belemnos* together with the presence of *Sphenolithus disbelemnos* above the first 4.9 m of Kotaphi Hill section are used in this study to define the boundary between NN2/NN3. Despite the fact that generally, LO of *S. disbelemnos* is recorded

slightly below the LO of *D. druggii* (Fornaciari, & Rio, 1996), *S. disbelemnos* is totally absent within NN2 range in our section. According to Fornaciari & Rio (1996) the absence of this species in NN2 biozone and its re-appearance at the lower part of NN3 seems to be a useful biostratigraphic evidence for this interval in the Mediterranean. In addition, Fornaciari & Rio (1996) and Raffi et al. (2003), also mentioned that HCO of *S. belemnos* is used to define the boundary level between MNN3a/MNN3b. The transition of common to rare presence of *S. belemnos* along with the increased in abundance of *S. heteromorphus* over the ~7.7m of the section may reflect this boundary level in our material. Discoasters are characterised by abundant presence of *D. deflandrei* and common presence of *D. druggii,* while among sphenoliths,

S. moriformis seems to be the dominant species. Among helicoliths, the presence of *H. ampliaperta* is common whereas the abundant presence of *H. carteri* is the dominant feature of the assemblage.

3.3. Biozone NN4 (MNN4)

Martini (1971) defines the HO of *S. belemnos* and LO of *S. heteromorphus* as the marker events for the NN3/NN4 boundary. Co-occurrence of both species is reported by some authors (e.g., Bukry, 1972; Takayama & Sato 1985) while others have indicated that the range of the two species cannot be considered to overlap (Olafsson 1989; Rio et al., 1990b). In the Mediterranean region, the intervals of high abundance of the two species do not overlap, but between the HCO of *S. belemnos* and the LCO of *S. heteromorphus*, the two forms may be present discontinuously and in low abundances (Olafsson, 1991; Fornaciari, & Rio, 1996). Based on Marini (1971) biozonation, rare presence of *S. belemnos* after 8.5 m of Kotaphi Hill section along with the common presence of *S. heteromorphus* is likely to mark the NN3/NN4 boundary. Furthermore, Fornaciari & Rio (1996) and Raffi et al. (2003), mentioned that in the Mediterranean region the boundary level of MNN3b/MNN4a is defined by the LCO of *S. heteromorphus.* The transition from rare to common presence of *S. heteromorphus* above 9.5m of the section is possibly marking the LCO of the species and therefore the boundary level MNN3b/MNN4a in the studied material. Scattered and discontinuous presence of *S. belemnos* above the 9.5m of the section may be due to enhanced reworking effect observed in our study material. Following Fornaciari et al. (1996), the lower boundary of the NN4 zone (MNN4a) is based on the LCO of *S. heteromorphus,* while the upper part of the zone (MNN4b) is characterized by the temporary absence (paracme beginning, PB) of the species. In our study material, at about 13.5 m of the section, *S. heteromorphus* seems to be intensively reduced and rapidly disappeared afterwards, a pattern that continues upwards covering the last 3m of the studied section. *H. ampliaperta* is common and continuously present at the lower part of NN4 (MNN4a) zone whereas at the upper part (MNN4b), its presence becomes discontinuous (Fornaciari et al., 1996). Such pattern of continuous presence of *H. ampliaperta* is not observed in the study area possibly due to regional and/or ecological criteria or other environmental factors that are still to be investigated. Similar distribution pattern with scattered and discontinuous presence or even absence of the species in the Mediterranean region within the NN4 zone was previously mentioned by other authors (Olafsson, 1991) and recently by Di Stefano (2011). Total assemblages from Kotaphi Hill contain abundant-common presence of *H. carteri* while *H. intermedia, H. mediterranea* and *H. euphratis* are also present. Among the sphenoliths, *S. heteromorphus* and *S. moriformis* are dominant mainly in the lower part of the interval. At the upper part of NN4 (MNN4b) the abundant presence of *S. moriformis* over *S. heteromorphus* and the total absence or very low abundance of the latter species represents a clear pattern. *D. deflandrei* is usually abundant dominating among discoasterids, while *Discoaster exilis* and *Discoaster variabilis* appear for the first time within this interval. The absence of *S. heteromorphus* together with the discontinuous presence of *H. walbersdorfensis* at the uppermost 3m of the studied section, are likely to mark the PB of *S. heteromorphus*. This interval of virtual absence or reduced abundance ("paracme") of *S. heteromorphus* distribution range is well documented in several Langhian Mediterranean sections (e.g., Fornaciari et al. 1996; Di Stefano et

al. 2008), representing a useful and reliable correlation tool within the Mediterranean Miocene sediments (Di Stefano, 2011).

3.4. Biochronologic Assignment and Paleoceanographic Implications

The calcareous nannofossil biostratigraphy applied at the studied samples recovered from the lower 16.50 m of Kotaphi Hill section, enabled biostratigraphic assignment of the studied deposits to NN2-NN4 (MNN2-MNN4) biozones. Therefore based on the astronomically calibrated data for the Neogene (Louerns et al., 2004: Raffi et al., 2006), the studied section possibly spans ca. 22.8-15.0 Ma, within the Aquitanian - Langhian time interval.

The Miocene Climate Optimum (MMCO) warm event occurred at about 15.0 Ma and represents one of the last warm periods of the Neogene. In general, Miocene is considered to be a time period of global climatic changes. More specifically, the Early and Middle Miocene were marked by a several million-year period of warm climate, which came to an end during the Middle Miocene global climate transition. The MMCO is traced by changes in the oxygen isotope values from the deep-sea sediment cores from ocean floor (e.g., Zachos et al., 2001), as well as by the marine and continental fossil record (e.g., Ivanov et al. 2002; Jiménez-Moreno, 2006). MMCO reached its maximum during 15.0-17.0 Ma (Zachos et al., 2001), within the standard nannoplankton zones NN4 and NN5.

The uppermost part of our study material (NN2-NN4) can be partly referred to the beginning of the MMCO, in particular the detected high abundances of discoasterids and sphenoliths support the prevalence of warm water conditions (e.g., Rio et al., 1990). In addition high abundance of helicoliths (particularly *H. carteri*) indicates warm surface waters with a medium to high content of nutrients (Negri & Villa, 2000; Melinte, 2005).

4. Conclusions

Preliminary biostratigraphic results from Kotaphi Hill section indicated that several important calcareous nannofossil events can be traced along the studied section, including HO of *S. procerus*, and increased presence of *H. carteri*, suggesting that the lower 4.9 m of the section is probably correlated with NN2 (MNN2) biozone (Martini, 1971; Fornaciari & Rio, 1996; Fornaciari et al., 1996, Raffi et al., 2003). The base of NN3 biozone is marked by the LOs of *S. belemnos* and *S. disbelemnos*, while the range of both species along with low abundances of *S. heteromorphus* are indicative of the NN3 (MNN3) biostratigraphic interval. Based on Fornaciari & Rio (1996) and Raffi et al. (2003), the HCO of *S. belemnos* is the marker event for the MNN3a/MNN3b that is placed at ~ 7.7m of the studied section.

Moving upwards, the LCO of *S. heteromorphus* is used to define the MNN3b/ MNN4 located at the 9.5m of the section. Biozone NN4 (MNN4) in Kotaphi Hill section is featured by abundant presence of well developed *S. heteromorphus* forms and increased presence of *D. deflandrei,* associated with the appearance of other forms of discoasterids such as *D. exilis* and *D. variabilis*. A pattern of almost total absence or low abundance of *S. heteromorphus* at 13.5m from the base of the section and the dominance of *S. moriformis* together with the discontinuous presence of *H. walbersdorfensis* observed at the last 3 m of the section are the events marking the *S. heteromorphus* (PB) interval.

The preliminary calcareous nannofossil biostratigraphic results derived from the semiquantitative analysis of the studied samples recovered from the lower 16.50 m of Kotaphi Hill section, enabled the biostratigraphic assignment of the studied deposits to NN2-NN4 (MNN2-MNN4) biozones, spanning ca. 22.8-15.0 Ma, within the Aquitanian-Langhian time interval. High abundance of warm indicators such as discoasterids, *S. heteromorphus*, *S. moriformis,*and *H. carteri* may partly reflect the onset of the warm phase of MMCO global climatic event. On-going detailed quantitative analysis of nannofossil assemblages from the whole Kotaphi Hill section will provide further improvements to the proposed biostratigraphic and paleoceanographic assignments.

5. Acknowledgments

Funding was provided by the European Research Project EraNet/MarinERA, MedEcos and Research Project KA 70/4/11078 of the University of Athens. Thoughtful discussions with Emma Sheldon are greatly appreciated. Special thanks to Cyprus Geological Survey for all the support provided during the sampling of the section and to the two anonymous reviewers for providing constructive criticism.

6. References

Aubry M.P. 1984, 1988, 1989, 1990, 1999. *Handbook of Cenozoic Calcareous Nannoplankton*, Vol. 1-5, Micropress, American Museum of Natural History, New York.

Bukry D., 1972. Coccolith stratigraphy Leg 1, Init. Rep. DSDP 14, 487–494.

Coccioni R., Montanari A., Fornaciari E., Rio D. and Zevenboom D. 1997. Potential integrated stratigraphy of the Aquitanian to Upper Burdigalian section at Santa Croce di Arcevia (NE Apennines, Italy), in: Montanari, A., Odin, G.S., Coccioni, R., (Eds), *Mioc. Stratigr.* An Integrated Approach, pp. 275–295.

Di Stefano A., Foresi L.M., Lirer F., Iaccarino S.M., Turco E., Amore F.O., Mazzei R., Morabito S., Salvatorini G. and Abdul Aziz H. 2008. Calcareous plankton high resolution bio–magnetostratigraphy for the Langhian of the Mediterranean area, Riv. Ital. *Paleontol. Stratigr.,* 114(1), 51–76.

Di Stefano A., Verducci M., Cascella A. and Iaccarino S.M. 2011. Calcareous plankton events at the Early/MiddleMiocene transition of DSDP Hole 608: comparison with Mediterranean successions for the definition of the Langhian GSSP, *Stratigr.*, 8, 89–110.

Follows E.J. and Robertson A.H.F., 1990. Sedimentology and structural setting of Miocene reefal limestones in Cyprus, in: Moores, E., et al., (Eds), *Ophiolites and Oceanic Lithosphere*, *Proc. Int, Symp*., Nicosia, Cyprus, Oct. 1987, pp. 207–215.

Fornaciari E. and Rio D. 1996. Latest Oligocene to early Middle Miocene quantitative Calcareous Nannofossil Biostratigraphy in the Mediterranean region, *Micropaleont*., 42 (1), 1–36.

Fornaciari E., Di Stefano A., Rio D. and Negri A., 1996. Middle Miocene quantitative calcareous nannofossil biostratigraphy in the Mediterranean region. *Micropaleont*., 42 (1), 37–63.

Hsü K.J., 1973. The desiccated deep basin model for the Messinian events, in: Drooger, C.W., (Ed.), *Messinian Events in the Mediterranean*, North-Holland, Amsterdam, pp. 60-70.

Hüsing S.K., Cascella A., Hilgen F.J., Krijgsman W., Kuiper K.F., Turco E. and Wilson D. 2010. Astrochronology of the Mediterranean Langhian between 15.29 and 14.17 Ma, *Earth Planet. Sci. Lett*., 290, 254–269.

Ivanov D., Ashraf A.R., Mosbrugger V. and Palamarev E. 2002. Palynological evidence for Miocene climate change in the Forecarpathian Basin (Central Paratethys, NW Bulgaria), *Palaeogeogr., Palaeoclimatol., Palaeoecol.*, 178, 19–37.

Jiménez-Moreno G. 2006. Progressive substitution of a subtropical forest for a temperate one during the middle Miocene climate cooling in Central Europe according to palynological data from cores Tengelic-2 and Hidas-53 (Pannonian Basin, Hungary), *Review of Palaeobot. and Palynol.*, 142, 1–14.

Lourens L., Hilgen F., Shackleton N.J., Laskar J. and Wilson J. 2004. The Neogene period, in: Gradstein, F.M., et al., (Eds), *A Geologic Time Scale* 2004, Cambridge University Press, pp. 409–440.

Martini E. 1971. Standard Tertiary and Quaternary calcareous nannoplankton zonation. In: Farinacci, A., (Ed.), *Proceedings of the Second International Conference on Planktonic Microfossils*, Roma, Rome, Ed. Tecnosci, vol. 2, pp. 739–785.

Melinte M.C. 2005. Oligocene palaeoenvironmental changes in the Romanian Carpathians, revealed by calcareous nannofossils, in: Tyszka, J., Oliwkiewicz-Miklasinska, M., Gedl, P., Kaminski, M.A., (Eds), *Methods and Applications in Micropalaeont.*. Studia Geologica Polonica, vol. 124, pp. 341–352.

Negri A. and Villa G., 2000. Calcareous nannofossil biostratigraphy, biochronology and paleoecology at the Tortonian/Messinian boundary of the Faneromeni section (Crete), *Palaeogeog. Palaeoclim., Palaeoecol.*, 156, 195–209.

Olafsson G. 1989. Quantitative calcareous nannofossil biostratigraphy of upper Oligocene to Middle Miocene sediment from ODP hole 667A and Middle Miocene sediments from DSDP Site 754, *Proc. ODP Sci. Results*, 108, 9–22.

Olafsson G. 1991. Quantitative calcareous nannofossil biostratigraphy and biochronology of early through late Miocene sediments from DSDP Hole 608, *Medd. Stockholm Univ. Inst. Geol. Geok.*, 203 (4), 28 pp.

Perch-Nielsen K. 1985. Cenozoic calcareous nannofossils, in: Bolli, H.M., Saunders, J.B., Perch-Nielsen, K., (Eds), *Plankt. Stratigr.*, Cambridge Earth Science Series, pp. 427–554.

Raffi I., Mozzato C.A., Fornaciari E., Hilgen F.J. and Rio D. 2003. Late Miocene calcareous nannofossil biostratigraphy and astrobiochronology for the Mediterranean region, Micropaleontol. 49, 1–26.

Raffi I., Backman J., Fornaciari E., Pälike H., Rio D., Lourens L. and Hilgen F. 2006. A review of calcareous nannofossil astrobiochronology encompassing the past 25 million years, *Quarter. Scien. Rev*., 25, 3113–3137

Rıo D., Fornacıarı E. and Raffi I. 1990a. Late Oligocene through Early Pleistocene calcareous nannofossils from western equatorial Indian Ocean (Leg 115), *Proceedings of the Ocean Drilling Program, Scientific Results*, 115, 175–235.

Rio D., Raffi I. and Villa G. 1990b. Pliocene–Pleistocene calcareous nannofossil distribution patterns in the Western Mediterranean, *Proc. ODP Sci. Results*, 107, 513–533.

Robertson A.H.F. 1976. Pelagic chalks and calciturbidites from the Lower Tertiary of the Troodos Massif, Cyprus, *J. Sediment. Petrol.,* 46, 1007–1016.

Robertson A.H.F., Eaton S., Follows E.J. and McCallum J.E. 1991. The role of local tectonics versus global sea-level change in the Neogene (Miocene-Pliocene) evolution of the Cyprus active margin. In: D.I.M. MacDonald (Editor), Sedimentation, Tectonics and Eustacy, *Int. Assoc. Sedimentol., Spec. Publ*., 12, 331–372.

Robinson P.T. and Malpas J. 1990. The Troodos ophiolite of Cyprus: new perspectives on its origin and emplacement, in: Malpas, J, (Ed.), *Ophiolites–oceanic crust analogues, Proceedings of the Troodos 1987*, Symposium, Nicosia, Cyprus Geological Survey, pp. 13–26

Rouchy J.M., Orszag-Sperber F., Blanc-Valleron M-M., Pierre C., Rivière M., Combourieu-Nebout N. and Panayides I. 2001. Paleoenvironmental changes at the Messinian– Pliocene boundary in the Eastern Mediterranean (Southern Cyprus basins): significance of the Messinian Lago–Mare, *Sedimentol. Geol*., 145, 93–117.

Takayama T. and Sato T. 1985. Coccolith biostratigraphy of the North Atlantic Ocean, Deep Sea Drilling Project Leg 94, in: Ruddiman, W.F., Kidd, R.B., Thomas, E., et al., (Eds), *Initial Reports of Deep Sea Drilling Project*, vol. 94, pp. 651-702.

Zachos J.C., Pagani M., Sloan L., Thomas E. and Billups K. 2001. Trends, rhythms, and aberrations in global climate 65 Ma to present, *Science*, 292, 686–693.

Δελτίο της Ελληνικής Γεωλογικής Εταιρίας, τομ. XLVII , 2013
Πρακτικά 13ου Διεθνούς Συνεδρίου, Χανιά, Σεπτ. 2013

Bulletin of the Geological Society of Greece, vol. XLVII 2013
Proceedings of the 13th International Congress, Chania, Sept. 2013

GEOLOGICAL STUDY FOR A WETLAND RESTORATION: THE CASE OF THE DRAINED MOURIA LAKE (W. PELOPONNESE)

Chatziapostolou A.[1], Siavalas G.[1], Kalaitzidis S.[1, 2] and Christanis K.[1]

[1] *University of Patras, Faculty of Science, Department of Geology, 265 04 Rio-Patras, Greece*
achatzia@gmail.com, christan@upatras.gr

[2] *Integral Resource Consulting Pty Ltd, 143 Charlotte Street, QLD 4000, Brisbane, Australia*

Abstract

The Mouria Lake was drained for cultivation during late 1960's. A 0.5-ha large pilot-scale wetland is now constructed in order to study the sedimentological lake-restoration aspects. The uppermost horizons (up to 3 m thick) consist of fine sediments (mud, silt, clay) of fluvial origin, deposited in a lacustrine environment and constituting the lagoonal bottom material, which extents all over the area ever covered by the original Mouria Lake. A sand layer (3 m beneath the current surface) constitutes the substrate of the lagoonal bottom revealing a higher energy deposition environment in comparison to the overlying fine sediments. High pH and electric conductivity values reveal strong alkaline environment and high content of dissolved solids, respectively. The sediments reveal high CEC, as a result of high clay minerals content. Other main mineral phases that occur include quartz, feldspars and calcite. The weathering of marginal rocks is the major factor controlling the mineralogical-geochemical composition of the sediments. The strong alkaline features of the sediments inhibit trace element mobilization. Continuous monitoring of the chemical composition is necessary in order to predict and prevent a possible mobilization of hazardous trace elements and the subsequent release to the environment.

Key words: *Re-flooding, depositional environment, mineralogical composition, geochemical composition.*

Περίληψη

Η Λίμνη Μουριά αποξηράνθηκε στα τέλη της δεκαετίας του 1960, λόγω των αυξημένων αναγκών για καλλιεργήσιμες εκτάσεις. Στην παρούσα μελέτη εξετάζονται τα ιζηματολογικά χαρακτηριστικά μίας μικρής έκτασης της πρώην λίμνης, στην οποία κατασκευάστηκε μία πιλοτική λίμνη. Οι ανώτεροι ορίζοντες (πάχους περίπου 3 m) αποτελούνται από λεπτόκοκκο υλικό ποτάμιας προέλευσης, που αποτέθηκε σε λιμναίο περιβάλλον, σχηματίζοντας το λιμνοθαλάσσιο πυθμένα που εκτείνεται σε όλη την περιοχή της αποξηραμένης λίμνης. Σε βάθος 3 m απαντάται στρώμα άμμου, το οποίο αποτέθηκε σε περιβάλλον υψηλής ενέργειας και αποτελεί το υπόβαθρο του λιμνοθαλάσσιου πυθμένα. Τα ιζήματα χαρακτηρίζονται πολύ έντονα αλκαλικά με υψηλή περιεκτικότητα σε διαλυμένα στερεά. Η υψηλή ικανότητα ιοντοανταλλαγής (CEC) οφείλεται αποκλειστικά στην παρουσία αργιλικών ορυκτών. Χαλαζίας, άστριοι, αργιλικά ορυκτά και ασβεστίτης είναι τα κύρια ορυκτολογικά συστατικά. Η ορυκτολογική και γεωχημική

σύσταση των ιζημάτων οφείλεται κυρίως στην αποσάθρωση των περιβαλλόντων σχηματισμών. Οι έντονα αλκαλικές συνθήκες (υψηλό pH), που επικρατούν στα ιζήματα της περιοχής, δρουν ανασταλτικά στην κινητικότητα των ιχνοστοιχείων. Απαιτείται συνεχής παρακολούθηση της χημικής σύστασης των ιζημάτων της πιλοτικής λίμνης, γιατί ενδεχόμενη μεταβολή των συνθηκών που επικρατούν σήμερα, θα διαταράξει την ισορροπία του συστήματος της πιλοτικής λίμνης προκαλώντας ενδεχόμενα αύξηση της κινητικότητας των ιχνοστοιχείων και αποδέσμευσή τους στο περιβάλλον.
Λέξεις κλειδιά: *Επαναπλημμυρισμός, περιβάλλον απόθεσης, ορυκτολογική σύσταση, γεωχημική σύσταση.*

1. Introduction

In the early 1920's, several wetlands were drained in Northern Greece, in order to provide agricultural land to refugees from Asia Minor, as well as to protect the health of local population against malaria (Psilovikos, 1992; Bouzinos et al., 1994; Christanis, 1996). This practice was applied in the next decades all over the country until late 1960's when the last lakes were drained, namely these of Mouria and Agoulinitsa in Western Peloponnese. The areas of both lakes were converted into urban and agricultural land (Manariotis and Yannopoulos, 2004; Sofikitis et al., 2007; Chatziapostolou et al., 2008) (Figure 1a).

The Mouria Lake was located approximately 5 km WSW from Pyrgos town (Prefecture of Ileia), at the northwest of Alfeios River delta (Figure 1a, b). Through two narrow openings to the sea side seawater entered the lake creating brackish water conditions, Today the c. 600-ha large area is used mainly for cultivation, grazing and waste dumping.

In the last decades two environmental projects were carried out, in order to assess all the necessary requirements for the ecological restoration of the drained lake. In the first project the environmental parameters and requirements for the re-flooding of the former Mouria Lake were studied (Georgiadis et al., 1998). In 2005, a multidisciplinary scientific team from the Departments of Geology and Biology of the University of Patras, as well as the Pyrgos Municipal Enterprise for Development was established in order to implement an integrated restoration and rehabilitation plan of the original lake, based on the knowledge and experience that were acquired during the construction and monitoring of a pilot-scale wetland (Chatziapostolou, 2009; Karagianni, 2009; Karapanos, 2009). A 0.5-ha large, pilot-scale wetland was constructed with the purpose to meet both the scientific and the social (aesthetic, recreational, educational, commercial etc.) needs; it is located in the SW part of the drained Mouria Lake (Figure 1b) (Chatziapostolou et al., 2008; Chatziapostolou, 2009; Karagianni, 2009; Karapanos, 2009).

The objective of the present study is to assess the geological and pedological features in the pilot-scale wetland, focusing on the physical properties of the sediments, as well as on their mineralogical and chemical composition. The aim is a better understanding of the factors that controlled the wetland's temporal and spatial evolution, as well as the assessment of the post-drainage anthropogenic impact, emphasizing on the degree of soil degradation.

2. Geological Setting

The Mouria Lake once covered the eastern part of the Neogene Pyrgos Basin, which formed during the post-alpidic extensional phase. The bedrock consists of Palaeocene limestone of the Ionian zone and evaporites (Kamberis, 1987). Neogene alternations of clay, sand and sandstone and conglomerate constitute the northern part of the surrounding area of the original lake (Hageman, 1977; Streif, 1980; Kamberis, 1987) (Figure 1a). According to Streif (1980), the sediments filling the drained Mouria Lake are Holocene alluvial deposits. The eastern, western and northern margins of the drained area consist of Holocene lagoonal sediments, while a sand barrier

system and marine deposits constitute the southern margins (Figure 1a). More specifically the drained area is covered by sandy mud and mud, whereas the coastal area consists of sand. Silty sand covers a small part at the southwest and west of the former lake (Chatziapostolou, 2009).

Geomorphologically, the entire area is characterized by a smooth relief. The region is flat at the Mouria Lake area (-2.2 to +2 m altitude) and semi-mountainous at the western, northern and northeastern margins (Figure 1a). The Mouria sub-basin evolution is controlled by the Pyrgos Fault striking W-E at the Mouria Lake area and NNW-SSE at the Agoulinitsa Lake area (Koukouvelas et al., 1996).

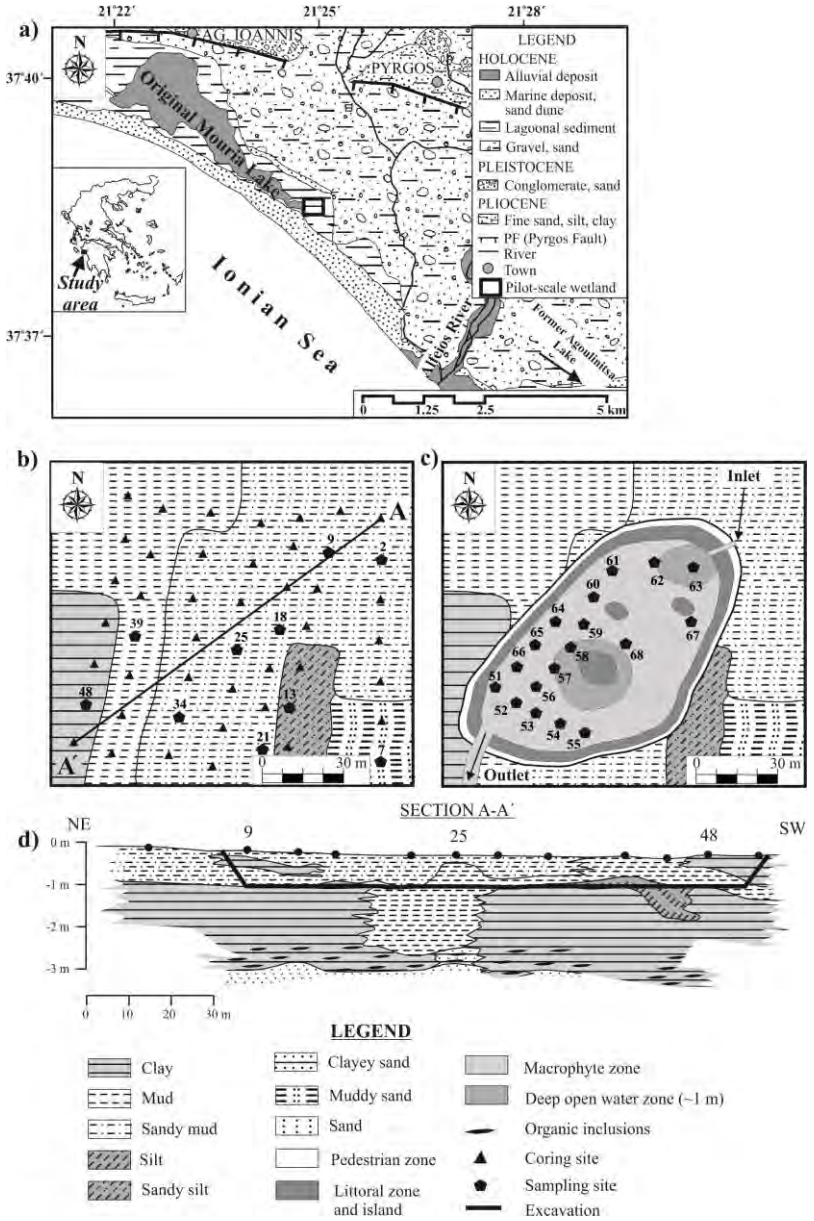

Figure 1 - a) Simplified geological map of the Pyrgos area (after Chatziapostolou et al., 2008), b) Geological map of the pilot-scale wetland before its construction, c) Sketch-map of the pilot-scale wetland and the sampling sites, after re-flooding with rainwater, d) Cross section AA'.

The study area has a typical temperate Mediterranean climate, with cold-wet winters and warm-dry summers. According to data from the Hellenic National Meteorological Service (Karapanos, 2009), during the last 25 years the mean annual precipitation is 828 mm. Mediterranean salt meadows and Thermo-Mediterranean riparian galleries dominate at the drained Mouria Lake, while reed beds (*Phragmites australis*, *Typha domingensis*) develop in the draining channels. Towards the coast an elongate zone with Mediterranean tall humid herb grasslands of the *Molinio-Holoschoenion* alliance occurs besides the embryonic shifting dunes. Sand dune vegetation is mainly composed of *Ammophiletea* species (Chatziapostolou et al., 2008; Karagianni, 2009).

3. Materials and Methods

Detailed geological mapping was conducted at the 0.5-ha large area, where the pilot-scale wetland was constructed (Figure 1b). Twenty-four sediment samples up to 3 m depth (Figure 1b) were collected prior to the construction of the wetland, from four freshly dug pits, using a hand-driven corer. After the construction of the pilot-scale wetland and the re-flooding with rainwater, sixteen sediment samples (Figure 1c) were picked up from the substrate of the lake using a hand-driven corer.

The pH and the electric conductivity values were measured in aqueous solution (1:10 sample/water ratio). Cation exchange capacity was determined according the US EPA 9081 method (Chapman, 1965). Particle size analysis was performed using the pipette method, while the sand fraction was determined after dry sieving (Gee and Bauder, 1986). The samples were classified according to Folk's (1954) classification, while the estimation of statistical grain-size parameters was accomplished using the mathematical formulas of Folk and Ward (1957) and Buller and McManus (1972).

The mineralogical analyses of the samples were carried out using a Bruker D8 Advance X-ray diffractometer equipped with a LynxEye® detector. The scanning area covered the 2θ interval 3-60°, with a scanning angle step of 0.015° and a time step of 0.3 s. Clay minerals were identified on the bulk samples (2θ=3-60°), as well as on the samples after treatment with ethylenoglycole (2θ=3-30°) and after heating at 490°C for 2 h (2θ=3-30°), with a scanning angle step of 0.015° and a time step of 0.1 s (Gee and Bauder, 1986; Moore and Reynolds, 1997). The mineral phases were identified with the use of EVA software and quantified using a Rietveld-based quantification routine with the TOPAS® software.

Total element concentrations were determined in solutions, which were prepared after microwave-assisted acid digestion (US EPA, 1996), applying Flame Atomic Absorption Spectrometry (for Ca, Fe, K, Mg, Na) and Inductively Coupled Plasma – Mass Spectrometry (for As, Co, Cr, Cu, Li, Mn, Ni, Pb and V).

4. Results and Discussion

4.1. Lithological data

Sandy mud and mud cover the greatest part of the study area, except the SW part where clay dominates, and the SE part which consists of sandy silt and muddy sand (Figure 1b). The uppermost horizons of the sediments (up to 1 m depth) overlie 2 m-thick clay. The sand layer (up to 3 m depth) constitutes the substrate of the lagoonal environment representing the dune system that was developed across the coastline (Figure 1d, Chatziapostolou, 2009). This layer hosts a brackish confined aquifer body.

The pilot-scale wetland was constructed (Figure 1c) according to the guidelines of Bendoricchio et al. (2000).

4.2. Laboratory Determinations

The high pH values of all the sediment samples reveal strong alkaline environment (Table 1). The electric conductivity (EC) values are high in surface samples from soil pits and cores revealing high content of dissolved solids (salt). In contrast EC values in samples from the re-flooded with rainwater wetland are lower than those before the construction, because of the dissolution effect of rainwater. The Cation Exchange Capacity (CEC) of the samples from soil pits and cores range from 9.7 to 25.4 meq/100 g and from the re-flooded with rainwater wetland from 17.7 to 23.4 meq/100 g (Table 1).

Table 1 – Physical properties of the sediments.

Physical properties		Sample Site					
		Soil pits				Cores	Re-flooded pilot-scale wetland
		7	13	25	34	2, 9, 18, 21, 39, 48	51-68
pH	Min	9.5	10.1	9.3	9.5	9.3	8.6
	Max	9.7	10.4	9.9	10.3	10.3	9.6
	Average	9.6	10.3	9.6	9.9	9.9	9.3
EC (μS/cm)	Min	568.0	222.0	82.0	601.0	754.0	592.0
	Max	1209.0	916.0	1067.0	836.0	850.0	758.0
	Average	889.0	606.0	472.0	723.0	802.0	675.0
CEC (meq/100 g)	Min	10.2	24.6	13.5	13.1	9.7	17.7
	Max	13.2	25.4	23.3	20.5	16.9	23.4
	Average	11.7	25.0	19.0	17.7	13.7	20.6

The results of particle size analysis of the samples from the soil pits and cores are presented in Figure 2. The statistical grain-size parameters, such as median (Md), mean size (Mz), sorting (σ_I), skewness (Sk_I), kurtosis (K_G) and quartile deviation (Qda), were estimated and plotted on scatter diagrams in order to determine the origin of the sediments and the depositional environments (Figs. 3a-d) (Stewart, 1958; Buller and McManus, 1972; Amaral and Pryor, 1977; Friedman, 1979). According to the scatter diagrams the fine sediments are of fluvial origin and were deposited in quiet water under low energy conditions (lacustrine environment). The sand is of coastal origin revealing high-energy depositional environment (wind and wave interaction) (Figs. 3a-d). According to Kraft et al. (2005) the sand layer belongs to the Agoulintsa barrier system, which was formed during the Early Mycenaean period (1600-1400 B.C.) and underlie the actual barrier system, which started forming during the Classical period (500 B.C.) and is still active.

4.3. Mineralogical Composition

The quantitative determinations of the mineral matter reveal that quartz (7.8-47.7 wt.%), K-feldspars (2.3-18.8 wt.%), plagioclases (2.3-30.0 wt.%), clay minerals such as illite (3.3-69.7 wt.%), chlorite (4.0-10.6 wt.%), vermiculite (0.4-10.0 wt.%) and kaolinite (1.4-10.9 wt.%), and calcite (5.7-58.0 wt.%) are the main mineral phases. Dolomite occurs only in 5 samples and its content ranges from 1.1 to 14.0 wt.%. Halite (0.2-10.1 wt.%) and sylvite (0.2-2.8 wt.%) constitute minor phases.

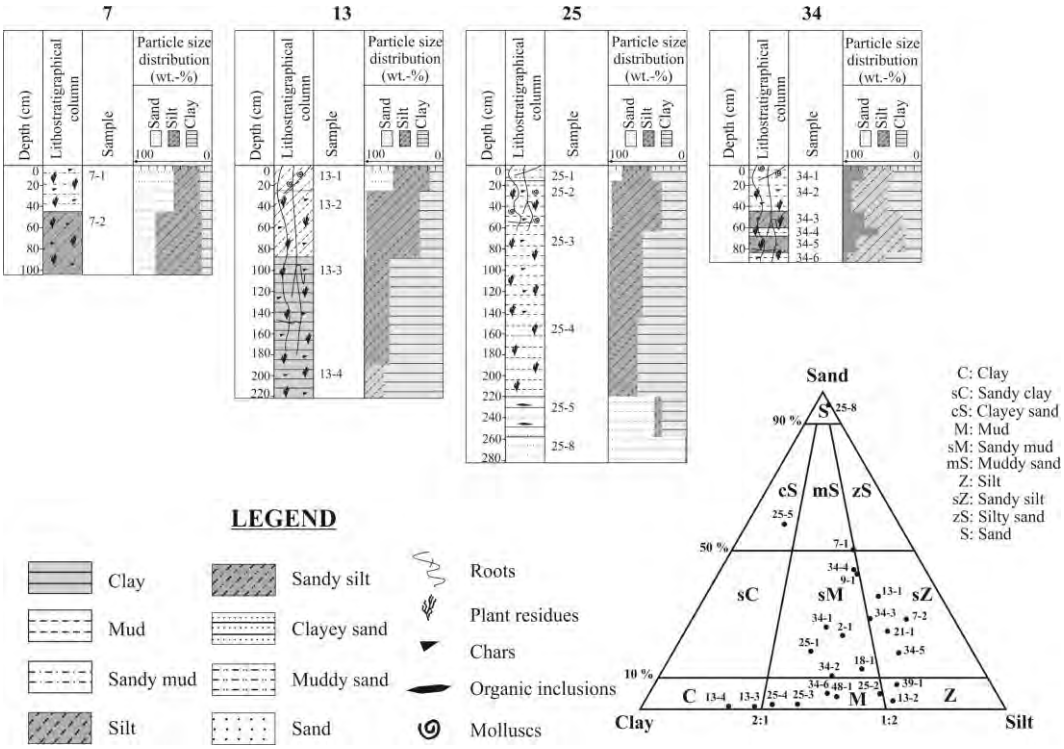

Figure 2 - Detailed lithostratigraphical columns showing the vertical particle size distribution (wt.%) of the soil pits and ternary diagram for the classification of all the samples according to Folk (1954).

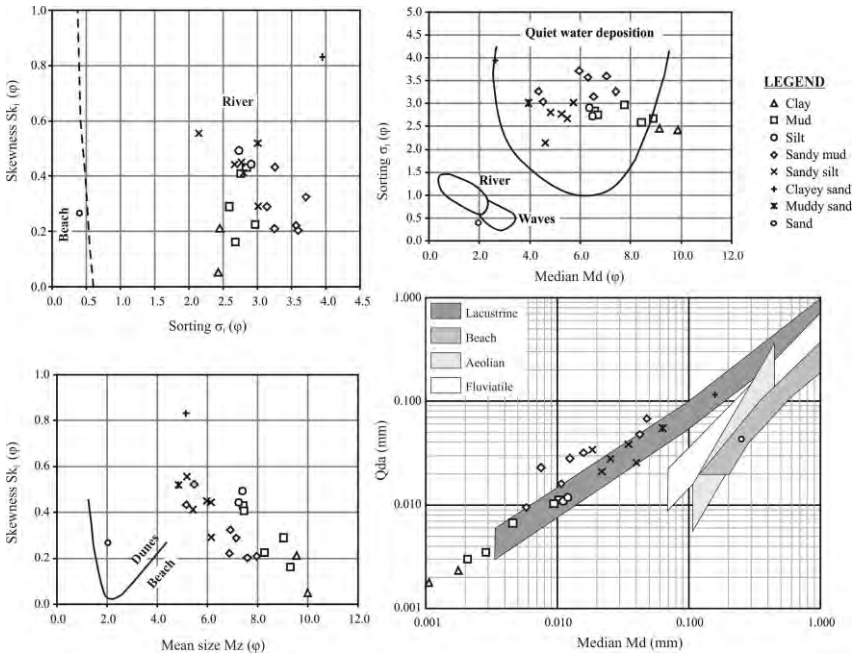

Figure 3 – Scatter diagrams of the statistical particle-size parameters (Stewart, 1958; Buller and McManus, 1972; Amaral and Pryor, 1977; Friedman, 1979) showing the origin of the sediments and the deposition environment.

In the study area, quartz, clay minerals (illite, chlorite) and feldspars are having a clastic origin (Drees et al., 1989; Huang, 1989), deriving from the weathering and erosion of the surrounding Neogene and Quaternary rocks. Vermiculite and kaolinite are formed from the weathering of mica and chlorite and rarely by feldspars alteration (Paquet and Clauer, 1997). Calcite has clastic or authigenic origin (Doner and Lynn, 1989; Paquet and Clauer, 1997) from Ca-rich waters originated from limestone and evaporite dissolution. Dolomite has clastic origin (Paquet and Clauer, 1997). Halite and sylvite may have clastic or authigenic origin (Doner and Lynn, 1989; Paquet and Clauer, 1997) and seems to derive from the sea spray.

4.4. Chemical Composition

The average values of the major element concentrations in the sediments from the soil pits and cores, as well as from the re-flooded with rainwater pilot wetland are presented in Table 2. The high content of the sediments in Ca, compared to the average content in upper crust (Wedepohl, 1995) and in soils and sediments worldwide (Reimann and Caritat, 1998), is due to the significant presence of clastic calcite and feldspars. Additionally, Ca may be contained in the samples as exchangeable cation in clay minerals or as a component in the skeletal remains of molluscs. The average Fe content of the sediments is 3.6 wt.%; iron in soils and sediments is mainly associated with clay minerals, such as vermiculite and chlorite (Dixon and Weed, 1989; Siegel, 2002). Amorphous phases (e.g. iron oxides and hydroxides) or sulphide minerals might be contained in the sediments in low amounts, since they were not detected on the X-ray diffractograms.

Table 2 – Chemical composition of the studied samples (in mg/kg, on dry basis, except otherwise cited.

	Average in soil pits and cores	Average in the re-flooded pilot-scale wetland	Upper crust[1]	Soils and sediments worldwide[2]
Ca (%)	6.8	NA	2.9	1.4
Fe (%)	3.6	NA	3.1	3.5
K (%)	1.5	1.9	2.9	1.4
Mg (%)	0.9	NA	1.4	0.9
Na (%)	1.1	NA	2.6	1.0
As	7	9	2	5
Co	20	28	12	10
Cr	150	178	35	80
Cu	34	51	14	25
Li	35	38	22	20
Mn	916	1044	527	530
Ni	117	164	19	20
Pb	18	21	17	17
V	83	NA	53	90

NA: not analysed, [1]: average concentration in the upper crust, according to Wedepohl, 1995, [2]: average concentration in soils and sediments worldwide, according to Reimann and Caritat, 1998)

The Fe-ions in groundwater of Western Peloponnese (Karapanos, 2009) and the presence of iron-rich minerals in the study area is due to the weathering and erosion of the Upper Jurassic – Low

Cretaceous cherts of the Pindos zone, which constitute the eastern margins of the broad surrounding area (Varnavas and Panagos, 1983; Lambrakis et al., 2004). The significant occurrence of kaolinite and feldspars explains the K content in all the samples. The comparison of the average K content in soil samples to that from the re-flooded pilot wetland shows that K concentration has not changed and is not influenced by the flooding. The Mg in the sediments from the study area is associated with the presence of aluminosilicate minerals and dolomite. The high Na content compared to the average content in the upper crust (Wedepohl, 1995) and in soils and sediments worldwide (Reimann and Caritat, 1998) is due to the presence of feldspars, clays and halite.

The studied samples display medium concentrations in As, Li, Pb and V and high concentrations in Co, Cr, Cu, Mn and Ni, compared to the average contents in soils and sediments worldwide (Reimann and Caritat, 1998). The weathering of the pre-Neogene and Neogene formations of the marginal areas is considered to be the major factor controlling the chemical composition of the sediments, although anthropogenic activities, such as pesticide application and waste dumping, seem to contribute as well. Background element concentrations are needed in order to assess possible contamination. The comparison among the average concentrations of As, Co, Cr, Cu, Li, Mn, Ni, Pb and V in the samples taken from the substrate of the re-flooded new lake, with those of the samples taken before the construction reveal similar variation without any significant differentiation.

5. Concluding Remarks

The fine sediments, which constitute the uppermost horizons (up to 3 m thickness) of the study area have fluvial origin and were deposited under low energy conditions (lacustrine deposition environment). These sediments constitute the lagoonal bottom material, which extents all over the area ever covered by Mouria Lake. The sand layer (up to 3 m depth) constitutes the substrate of the lagoonal environment revealing high energy depositional conditions.

The major factor controlling the chemical composition of the sediments is the weathering of the pre-Neogene and Neogene formations outcropping in the surrounding areas.. Anthropogenic activities, such as the application of pesticides and uncontrolled waste dumping, may contribute as well.

The strong alkaline conditions prevailing in soils and sediments of the study area inhibited trace element mobilization. Continuous monitoring of the variation in chemical composition and physical properties of the sediments in the pilot wetland, is necessary, in order to predict and prevent a possible mobilization of hazardous trace elements and the subsequent release to the environment.

6. Acknowledgments

The authors would like to thank G.S.R.T./Greek Ministry of Development for financial support in the frame of the PENED 2003 Programme, which was co-funded by the E.U. (80%), the Hellenic State (20%), as well as the Pyrgos Municipal Enterprise for Development (ADEP) and Pyrgos Municipality. Drs. E. Karapanos, P. Karagianni, K. Katsanou, S. Koulouris, A. Bouzinos, Mr. E. Sofikitis and Mr. G. Kerasias, as well as ADEP are here acknowledged for their assistance during field and laboratory work. Chatziapostolou thanks also the Greek State Scholarship's Foundation for financial support.

7. References

Amaral E.J. and Pryor W.A. 1977. Depositional environment of the St. Peter sandstone deduced by textural analysis, *J. Sediment. Petrol.*, 47, 32-52.

Bendoricchio G., Cin L.D. and Persson J. 2000. Guidelines for free water surface wetland design, *EcoSys Bd.*, 8, 51-91.

Bouzinos A., Broussoulis J. and Christanis K. 1994. Conservation and Management of Greek Fens: a "model" to avoid, *Proc. Int. Symposium Conservation and Management of Fens*, Warsaw-Biebrza, Poland, 6-10 June, 225-230.

Buller A.T. and McManus J. 1972. Simple metric sedimentary statistics used to recognize different environments, *Sedimentology*, 18, 1-20.

Chapman H.D. 1965. Cation Exchange Capacity. In Black, C.A., ed., *Methods of Soil Analysis (Part 2: Chemical and Microbiological Properties)*, Soil Science Society of America Inc., American Society of Agronomy Inc., Madison, Wisconsin, 891-900.

Chatziapostolou, A., 2009. *Geological-soil parameters of the drained Mouria Lake (Prefecture of Ileia), controlling the rehabilitation and sustainable management of wetlands*, Ph.D. Thesis, University of Patras, Patras, Greece, 365 pp. [in Greek with English abstract].

Chatziapostolou A., Karapanos E., Karagianni P., Siavalas G., Kalaitzidis S., Lamprakis N., Tiniakou A., Georgiadis T., Papastergiadou E. and Christanis K. 2008. Planning and implementation of a pilot-scale wetland rehabilitation at the Mouria area, SW Greece, *Proc. of the 13th International Peat Congress*, Tullamore, Ireland, 8-13 June, 147-150.

Christanis K. 1996. The peat resources in Greece. In Lappalainen, E., ed., *Global Peat resources*, Jyskä (International Peat Society), 87-90.

Dixon B.J. and Weed B.S. 1989. *Minerals in soil environments*, Soil Science Society of America, Madison, Wis., USA, 1244 pp.

Doner H.E. and Lynn W.C. 1989. Carbonate, Halide, Sulfate, and Sulfide minerals. In Dixon, B.J., Weed, B.S., eds., *Minerals in soil environments*, Soil Science Society of America, Madison, Wis., USA, 279-330.

Drees L.R., Wilding L.P., Smeck N.E. and Senkayi A.L. 1989. Silica in soils: Quartz and disordered silica polymorphs. In Dixon, B.J., Weed, B.S., eds., *Minerals in soil environments*, Soil Science Society of America, Madison, Wis., USA, 913-974.

Folk R.L. 1954. The distinction between grain size and mineral composition in sedimentary rock nomenclature, *J. Geol.*, 62, 334-359.

Folk R.L. and Ward W.C. 1957. Brazos river bar: a study of significant of grain size parameters, *J. Sediment. Petrol.*, 27, 3-26.

Friedman G. 1979. Differences in size distributions of populations of particles among sands of various origins: addendum to IAS Presidential Address, *Sedimentology*, 26, 859-862.

Gee G.W. and Bauder J.W. 1986. Particle-size analysis. In Klute, A. ed., *Methods of Soil Analysis (Part 1: Physical and Mineralogical Methods)*, Soil Science Society of America Inc., American Society of Agronomy Inc., Madison, Wisconsin, 383-411.

Georgiadis T., Giannopoulos P., Kaspiris P., Tiniakos L., Dimitrellos G., Theocharopoulos M. and Papandronopoulos D. 1998. *Investigation of environmental parameters and requirements for the re-flooding of the drained Mouria Lake (Prefecture of Ileia)*, University of Patras and Ileiaki S.A., Patras, Greece, 196 pp. [in Greek].

Hageman J. 1977. Stratigraphy and sedimentary history of the upper Cenozoic of the Pyrgos-area (Western-Peloponnesus), Greece, *Ann. Geol. Pays Hell.*, 28, 299-333.

Huang P.M. 1989. Feldspars, Olivines, Pyroxenes and Amphiboles, In Dixon, B.J., Weed, B.S., eds., *Minerals in soil environments*, Soil Science Society of America, Madison, Wis., USA, 975-1050.

Kamberis E. 1987. Geological and oil-geology study of NW Peloponnesus, *Ph.D. Thesis*, Athens Polytechnical School, Athens, Greece, 143 pp. [in Greek with English abstract].

Karagianni P. 2009. Habitat types ecology of the vegetation of the drained Mouria Lake ((Prefecture of Ileia), *Ph.D. Thesis*, University of Patras, Greece, 251 pp [in Greek with English abstract].

Karapanos E. 2009. Hydrogeological-hydrochemical parameters of the drained Mouria Lake (Prefecture of Ileia), controlling the rehabilitation and the sustainable management of wetlands, *Ph.D. Thesis*, University of Patras, Greece, 310 pp [in Greek with English abstract].

Koukouvelas I., Mpresiakas A., Sokos E. and Doutsos T., 1996. The tectonic setting and earthquake ground hazards of the 1993 Pyrgos earthquake, Peloponnese, Greece, *J. Geol. Soc. London*, 153, 39-49.

Kraft J.C., Rapp G., Gifford J.A. and Aschenbrenner S.E. 2005. Coastal change and archaeological settings in Elis, *Hesperia*, 74, 1-39.

Lambrakis N., Soren J., Panagopoulos G. and Pytikakis M. 2004. Hydrochemical conditions groundwater quality in the lowland zone of the Pineios River basin, Prefecture of Ileia. *Proc. of the 10th International Congress of the Geological Society of Greece*, Thessaloniki, 15-17 April, 2002-2011 [in Greek].

Manariotis I. and Yannopoulos P. 2004. Adverse effects on Alfeios River basin and an integrated management framework based on sustainability, *Environ. Management*, 34, 261-269.

Moore D.M. and Reynolds R.C. 1997. *X-Ray diffraction and the identification and analysis of clay minerals*, Oxford University Press Inc., New York, 378 pp.

Paquet H. and Clauer N. 1997. *Soils and sediments. Mineralogy and Geochemistry*, Springer Verlag, Berlin, Heidelberg, 369 pp.

Psilovikos A. 1992. Changes in Greek wetlands during the 20th century: the cases of the Macedonian inland waters and of the river deltas of the Aegean and Ionian coasts. The cases of the wetlands in Macedonia and the deltas of the Aegean and Ionian Sea, In Gerakis, P.A., ed., Conservation and management of the Greek wetlands, *Proc. of the Workshop Conservation and management of Greek wetlands*, Thessaloniki, 17-21 April, 179-208.

Reimann C. and Caritat P. 1998. *Chemical elements in the environment. Factsheets for the geochemist and environmental scientist*, Springer-Verlag, Berlin, Heidelberg, New York, 397 pp.

Siegel F.R. 2002. *Environmental geochemistry of potentially toxic metals*, Springer-Verlag, Berlin, Heidelberg, New York, 218 pp.

Sofikitis E., Siavalas G., Chatziapostolou A., Kalaitzidis S. and Christanis K. 2007. Greek coastal mires: A preliminary study of the Agoulinitsa peatland, Western Peloponnese, *Proc. of 11th International Congress of the Geological Society of Greece*, Athens, 24-26 May, 191-200.

Stewart H.B. 1958. Sedimentary reflections of depositional environments in San Miguel Lagoon, Baja California, Mexico, *Am. Assoc. Petr. Geol. Bull.*, 42, 2567-2618.

Streif H. 1980. *Geological map of Greece, Pyrgos Sheet, Scale 1: 50.000*, Institute of Geological and Mining Research, Athens.

US EPA 1996. *Microwave assisted acid digestion of siliceous and organically based matrices*, US EPA 3052 method, USA, 20 pp.

Varnavas S.P. and Panagos A.G. 1983. The use of trace metals in elucidating the genesis of some Greek and Cyprus manganese and ferromanganese deposits, In Augustithis, S.S., ed., *The significance of trace elements in solving petrogenetic problems and controversies*, Theophrastus publ., Athens, 819-857.

Wedepohl K.H., 1995. The composition of the continental crust, *Geochim. Cosmochim. Acta*, 59, 1217-1232.

Δελτίο της Ελληνικής Γεωλογικής Εταιρίας, τομ. XLVII , 2013
Πρακτικά 13ου Διεθνούς Συνεδρίου, Χανιά, Σεπτ. 2013

Bulletin of the Geological Society of Greece, vol. XLVII 2013
Proceedings of the 13th International Congress, Chania, Sept. 2013

ON SOMELOCAL RESTRICTED MAASTRICHTIAN ENVIRONMENTS OF THE "HAŢEG ISLAND" (TRANSYLVANIA, ROMANIA)

Codrea V.[1], Solomon Al.[1], Fărcaş C.[1] and Barbu O.[1]

[1] Babeş-Bolyai University, Faculty of Biology and Geology, Department of Geology,1 Kogălniceanu Str., 400074 Cluj-Napoca, Romania, codrea_vlad@yahoo.fr, alex_solomon88@yahoo.com , farcas2002@yahoo.com , ovidiu.barbu@ubbcluj.ro

Abstract

The continental Maastrichtian formations from Transylvania are notorious mainly for bearing peculiar fossils related to an island realm known as the "Haţeg Island". The thick piles of sedimentary rocks accumulated in fluvial environments. The "red beds" are in dominance. However, local peculiar environments are of interest for specific types of fossilization (plants, invertebrates or vertebrates), i.e. ox-bow lakes or fluvial temporary abandoned channels. In such deposits the fossil record can be different compared to the red beds, especially when the oxygen content was low. Case studies as the ones from Pui (Haţeg Basin) or Oarda de Jos (SW Transylvanian Basin) are exposed. The relationships of fossil taxa and these restricted environments are discussed.
Key words: *Latest Cretaceous, fluvial deposits, palaeontology.*

1. Introduction

TheMaastrichtian continental environments of Europe are of special interest for their peculiar plant, invertebrate, but mainly vertebrate fossils. A lot of them are documenting island evolutions during the late Cretaceous (Dalla Vecchia, 2002, 2006; Csiki et Benton, 2010). Among the areas of interest, Transylvania is notorious mainly for the respective dwarf dinosaur fauna. Although the first reported findings in southwestern Transylvanian Basin were discovered in 1866 (Téglas, 1886), the first who recognized their dinosaur origin was the Transylvanian palaeontologist baron Nopcsa (1897) based on some bones and teeth collected in the Haţeg Basin (South Carpathians). Afterwards, for over a century the research on the Maastrichtian continental deposits from Transylvania continued, more or less intensively. Hence, the knowledge on biodiversity, systematics, taphonomy, sedimentology, environment reconstructions etc. has progressed significantly.

This workis focused on some peculiar, although rare continental restricted environments preserving fossils that have been recorded in the southwestern Transylvanian and Haţeg sedimentary basins in specific manner.

2. Geological Setting

The studied Maastrichtian vertebrate localities (labelled 3 and 4 in Figure 1) are located in western Romania, in Transylvania, i.e. in the Transylvanian Depression and Southern Carpathians.

The last major overthrusts during the latest Cretaceous occurred both in the South Apuseni Mountains and the South Carpathians ("the second Getic phase"; Săndulescu, 1984). After the erection of the Transylvanian, Getic and Supragetic nappes, rather large areas became emerged and a long continental history began in Transylvania. The related continental deposits are parts of post-tectonic covers for Transylvanindes and Median Dacidic nappes.

The new born relief started to be eroded by rivers and large amounts of fluvial deposits accumulated since the Early Maastrichtian. Their impressive extent can only be understood if the thickness of these formations, exceeding 2 km, is take into consideration (Grigorescu, 1992). That means that the subtropical Maastricthtian climate (Van Itterbeek et al., 2004), with a mean temperature between 14 ^{0}C and 10 ^{0}C (Bojar et al., 2010)had at least a season rich in rainfalls, when the river debits considerably increased, even during short episodes.

Figure 1–Location of the Maastrichtian continental sedimentary exposures bearing vertebrate fossils in Romania: 1. Northwestern Transylvanian Basin (Jibou Formation; Jibou and Iara areas); 2. Southwestern Transylvanian Basin (Metaliferi sedimentary area, Șard Formation); 3. Haţeg Basin (Ciula-Densuș and Sânpetru formations); 4. Rusca Montană Basin.

This land was related to an island realm since Nopcsa's (1915) attempts to explain the dwarf-sized dinosaurs firstly described by him. This land is also known as the Haţeg Island. For instance, a clear, doubtless areal extension of this island could never be done, in spite of several geological surveys carried out in Transylvania. The island outline is difficult to be reconstructed because of several gaps in the existinggeological data. Parts or entireMaastrichtian continental sequences were probably erased by subsequent erosion, but also their original positions changed due to translation and rotations that occurred during the Cenozoic (Panaiotu, 2010). For instance, only a few Transylvanian areas are documenting such deposits and even fewer are bearing fossils: apart from Haţeg Basin (related references in Grigorescu, 2010), other evidence is coming from southwestern and northwestern Transylvanian basin (Codrea et al., 2010 a, b, c) and Rusca Montană Basin (Codrea et al., 2009, 2012a) (Figure 1).

Westwards, the continuity of these deposits can only be presumed, buthard evidence is still lacking. It would be possible that a large surface actually belonging to the Apuseni Mountains could once have bared the same sedimentary cover, but the long Cenozoic erosion episodes removed these rocks. One can even extend this supposition to some structures now forming the basement of

the Pannonian basin. However,such rocks were never recorded in the numerous boreholes drilled either in western Romania (Paraschiv et al., 1975) or in eastern Hungary (Haas et al., 2001).

The dominant Maastrichtian fluvial deposits are *red beds*. However, inside these red beds one can also distinguish on restricted vertical and lateral extensions some peculiar deposits, the sedimentation of which evolved in local environments like ox-bow lakes or abandoned channels. Such deposits worth special attention for their fossils, being far richer compared than the red beds. The following analysis concerns the study of two case-study localities.

The lithostratigraphy of the Maastrichtian localities of interest for this workconcernsthe following rock formations:

- in southwestern Transylvanian Basin the main formation bearing Maastrichtian land fossils is the fluvial Şard Formation (Codrea et Dica, 2005; Codrea et al., 2010 a, b, c) with Oarda de Jos as the most interesting locality;
- in Haţeg Basin, the fluvial Sânpetru Formation (Grigorescu et Anastasiu, in Grigorescu et al., 1990) with the exposures on the Bărbat River, at Pui (Codrea et Solomon, 2012) stands out.

3. Peculiar restricted Maastrichtian environments in Transylvania

3.1. Oarda de Jos

This locality belongs to the Metaliferi sedimentary area (Codrea and Dica, 2005). There, the continental Maastrichtian exposures can be observed mainly along the Mureş, Ampoi, Sebeş and Secaş valleys. Two main outcrops are located in this locality, on Sebeş River, Oarda A and B (Codrea et al., 2010a; a different separation of the Oarda outcrops in Vremir, 2010). Although both are exposing nearly similar deposits, for this study only Oarda A is of interest. Red mudstones are interfingering with extensive channels filled by microconglomerate and various sized sands.

All these deposits yielded various fossils like tree trunks (*Mastixia amygdalaeformis* was reported by Givulescu et al., 1995), but the vertebrates are prevailing. Dinosaur taxa include sauropods, the hadrosaur *Telmatosaurus transsylvanicus* and possibly, the euronithopod *Zalmoxes* (Codrea et al., 2010 a, b). Besides dinosaurs, other associated reptiles concern turtles (*Kallokibotion*, Dortokidae indet.), crocodiles (*Allodaposuchus precedens*; Delfino et al., 2008) and pterosaurs. Some bird remains (eggs, eggshells and bones) interpreted as an enantiornithine breeding colony have been also reported (Dyke et al., 2012). These fossils are not very numerous, but their preservation can be considered as fair or even exceptional. The bones are dark coloured, indicating a fast burial after the death of animals. However, for instance no partial or complete skeleton has been recorded. The vertebrate remains always are occurring isolated, indicating that the carcasses were decomposed and the bones were scattered before their final burial. All these taxa lived either inside the fluvial waters, or innerby related environments.

In contrast with this kind of deposits there is a lens-like channel filled by light coloured fine grained sediments, recorded at the top of the Oarda A succession.The lateral extension of the lens-like deposits is ranging close to four meters, while the maximum thickness is nearly one meter. Laterally, this deposit is gradually balking until its gets vanished completely passing into red mudstone.

Being different from the other deposits, this one is extremely rich in vertebrate remains, mainly microvertebrates, but also in medium and even large vertebrates, as well as in plants (charophytes) and some invertebrates. The vertebrate fossils are not uniformly ranged inside the sediment, their richness being high just at the base of the channel on near 15-20 cm. Above this level, such remains are very rare are even missing. Just above the channel bottom there is also a level of calcretions, removed from their original position and rolled by water flows, with diameters usually under a dozen of centimetres. Sometimes, these calcretions are bearing small fragments of bones.

The plant remains refer exclusively to charophyte gyrogonites (Pl. I, Figure 1) where*Microchara cristata*is clearly dominant. Apart frombeing a stratigraphic marker (*M. cristata* – zone), this species is indicative for the presence of Maastrichtian shallow freshwater lakes (*e.g.*Villalba-Breva et al., 2012) and ponds.

The invertebrates are documented by small-sized freshwater gastropods (Pl. I, Figure 2) and frequent crab chelae (Pl. I, Figure. 4). The largest collected crab claw has a dimension of 31 mm in length. It is notclear if these crabs were freshwater dwellers or if they are allochthonous representatives originating from further marine environments that arrived in this fluvial deposit as prey of some other animals.

The fish remains are numerous (several hundreds of scales and isolate teeth), but the systematic diversity is rather poor, restricted only the dominant gar-fish (Lepisosteidae) (Pl. I, Figure 5) and Characidae (Codrea et Jipa, 2011)(Pl. I, Figure 6), which have been documented only by a small sample. These freshwater fish were autochtonous dwellers of this environment.

A rich sample of amphibians was recovered by wet sieving nearly 2.5 tons of sediments.There are numerous for instance indeterminate frog remains, but also frequent Albanerpetontids (Pl. I, Figure 9), which lived at somewhat further distances from this channel.

Other documented small reptiles consist of lizards (their study, in progress) (Pl. I, Figure 10 a,b,c).

Two kinds of turtles have been recorded: the cryptodire *Kallokibotion bajazidi* (Pl. I, Figure 14) and a plurodire, dortokid representative (Pl. I, Figure 12). Their remains are represented always by isolate carapace or plastron plates. The preference of dortokids for lake and pond-like environments is obvious, if considering the frequency of finds in such environments either in Maastrichtian deposits (Codrea et Solomon, 2012) or thebasal Cenozoic ones(Gheerbrant et al., 1999; Lapparent de Broin et al., 2004).

A rich sample of osteoderms, cranial fragments and post-cranial bones document the crocodiles. Moreover, this environment seems to have been infested by crocodiles if considering the frequency of such remains as well as the signs of their presence, as numerous bite-marks (Codrea et al., 2010a).The crocodilian diversity was probably high. Apart fromthe obvious presence of *Allodaposuchus* (Pl. I, Figure 16), some other crocodile taxa have been also present in this environment, such as *Doratodon* and *Acynodon* (Pl. I, Figures 19 and 17).

The dinosaur remains are less frequent. However, several taxa have been recorded in these sediments: the euornithopod *Zalmoxes*(Pl. I, Figure 30), the hadrosaur *T. Transylvanicus* (Pl. I, Figure 26), sauropods (Pl. I, Figure 28) and various remains of indeterminate theropods (Pl. I, Figures 22 and 23), in majority small-sized. The dinosaur teeth and bones are always isolated, without signs of long weathering before their definitive burial. These preservations are in concordance with some of the taphonomic mode C21 (Csiki et al., 2010). These dinosaurs lived either close to the rivers, or to a certain distance, visiting the area just for drinking water.

Other reptiles represented in this accumulation are the pterosaurs (medium-sized). Their remains, although not very frequent, have been sometimes recovered. The pterosaurs were allochthonous representatives, their remains arriving in the channel fill by fortuitous processes.

Other remains belong to Enanthiornithinae birds and mammals. The mammals that have been recovered until now at Oarda belong exclusively to the multituberculate Kogaionidae, documented only by isolate teeth (Pl. I, Figure 31). Some of these teeth expose marks of at least medium distance water transport. After processing the sediment, 73 multituberculate teeth are available for study. All the cheek teeth from Oarda can be related rather to *Barbatodon*, based on their morphology.Several differences in cheek teeth morphology are now mentioned, probably reflecting intra-specific variations. Kogaionids are a European group, which crossed the K/T boundary and until now it has been recorded only in Romania, France, Spain and Belgium. Their origin remains

unclear, but it may be presumed that they have originate from ancestors probably living in early Cretaceous(Codrea et al., 2012b).

Besides bones and teeth, this level at Oarda yielded also numerous egg shells (Pl. I, Figure 3a,b). Several morphotypes are already recorded, with their study being in progress. The first investigations revealed ?*Pseudogeckoolithus* as well as Megaloolithidae (Codrea et al., 2010a).

3.2. Pui

This locality is a classical one for the Haţeg Basin, being the southeasternmost one in this basin. The fluvial deposits from Pui have been reported since the beginning of the 20th century by Nopcsa (1905).These Uppermost Cretaceous fluvial deposits have been related since a rather long time ago to the Sânpetru Formation (Nopcsa, 1905; Grigorescu et al., 1985; Grigorescu et Anastasiu, 1990; Grigorescu, 1992). However, Therrien et al. (2002) pointed out differences between the Sânpetru Formation deposits exposed on the Sibişel Valley and the ones at Pui. Later, Therrien (2005) called the exposures from Bărbat River as "Pui beds", but suggested also a distinct name for this continental sequence i.e. "Bărbat Formation", underlining the difficulties in correlating the terrestrial Uppermost Cretaceous sequences exposed in different areas of the basin.

The Lower Maastrichtian age of these deposits is documented either by pollen (Van Itterbeeck et al., 2005) or microvertebrates (e.g. Folie et Codrea, 2005), but also by palaeomagnetic studies (beginning of the Chron C32n.1n - end of the Chron 31n; Panaiotu et Panaiotu, 2010).

At Pui, the *red beds* dominate. Van Itterbeeck et al. (2004) considered the sub-horizontal red beds as a result of the evolution of an ancient fluvial system trended ENE-WSW. The Maastrichtian climate has been interpreted as semi-arid, with seasonal control of rainfall. The micaceous red silts (rich in smectite and illite, besides smaller amounts of chlorite and kaolinite) dominate the red beds, bearing calcrete horizons, with intercalations of green conglomerates and sandstones.

Inside these *red beds*there are three levels of black silt rich in white mica, bearing also pyrite concretions, sharply contrasting with the dominant red beds usually exposed in the riverbed. These three successive levels have been recently named from base to top, "Pui Gater", "Pui Depozit" and "Pui Islaz" (Codrea et Solomon, 2012). The lowermost level is rather rich in plant, invertebrate and vertebrate fossils (Codrea et Solomon, 2012; Vasile et Panaitescu, 2012), while the uppermost is very scarce in such remains. The richest silt levelin fossils is the middle one, yielding plant remains, invertebrates (large-sized ostracods, snails), but mainly vertebrates. Different from Oarda, is the colour of the teeth and bones. Commonly, the bones preserved in the red beds at Pui are white, with cracked surfaces filled by red clay, indicating a rather long weathering before their burial. With very few exceptions, such bones are always isolated, devoid of anatomical connections, but exceptionally, parts of associated skeletons can also be observed (the case of at least two *Zalmoxes* partial skeletons). These processes are related toa well-drained floodplain environment (Csiki et al., 2010). On the contrary, in these dark coloured mudstones, the bones are fossilized in a very different manner, being black or gray, sometimes covered by pyrite (i.e. *Telmatosaurus* tibia, Pl. I, Figure 25 c). The pyrite is in abundance as concretions into the sediment too. The teeth and bones are in their absolute majority, isolated. Only two ornithopod metacarpals could possibly be in connection. However, it is possible that this dominance of isolate skeleton parts could be just the result of the digging bias.

The systematic similarities and differences between Oarda and Pui Depozit will be further underlined. At Pui, the gar-fish is extremely rare, documented by only a single scale (Pl. I, Figure 6). The Characidae are missing.Among amphibians, the Albanerpetontids are frequent, documented mostly by a rich sample of skull (Pl. I, Figure 8) and limb fragments being comparable to Oarda. Among lizards, *Becklesius* cf. *nopcsai* is present at Pui (Pl. I, Figures 10 a, b, c), but the remains are not, too numerous. Like in Oarda, the Dortokidae turtle remains (Pl. I, Figure 13) are present, in larger numbers than *Kallokibotion*(Pl. I, Figure 11). Same environmental conditions like in Oarda have to be concluded for Pui too. The crocodiles are documented both by

numerous teeth, but also by bite-marks (Codrea and Solomon, 2012). The crocodiles (Pl. I, Figures 15 and 18) were seemingly numerous and are specific for these pond-like environments. Among dinosaurs, one can note theropods (Pl. I, Figures 20 and 21), sauropods (Pl. I, Figure 27 a, b), the same hadrosaur species (Pl. I, Figures 24, 25a, b, c) as well as the euornithopod *Zalmoxes* (Pl. I, Figure 29).

4. Maastrichtian Environments at Oarda de Jos and Pui

Fluvial Maastricthian deposits at Oarda de Jos should be considered as documenting a poorly drained floodplain. Inside this floodplain sometimes abandoned channels occurred, like the one already described. In such channels, the water flow was just episodic, probably related to the rainy season. The lateral and especially vertical extensions at Oarda are very restricted, not exceeding few meters reflecting ephemeral existence. The sediments are of light color. Large vegetal remains are missing, the only plants documented in this taphocoenosis being the charophytes. In spite of such an evolution, the water probably never had low oxygen tendencies. Some of the fossils were autochthonous (fish, frogs, crocodiles, turtles) or had been transported from minor distances (hadrosaur or sauropod remains). On the opposite, some others originated from a longer distance, like theropods or mammals. The majority of vertebrate fossils belong to micro- or medium-sized vertebrates, the large ones being almost rare. Some taxa, such as the multituberculate mammals are well represented in the faunal record at Oarda, while they are completely missing from Pui Depozit.

The Maastrichtian terrestrial deposits of Pui are related to a braided fluvial system (Therrien, 2005). The floodplain was well drained, its distal status being documented by the dominance of fine sediments*vs.* rough channel fills. The black mudstone here reported at Pui Depozit is sharply contrasting with the dominant red beds, but the restricted vertical and probably, lateral extensions are indicating that these rocks accumulated just for short episodes. They issued from closed abandoned channels that occurred randomly in the floodplain, which evolved in this case to true ox-bow lakes where fine sediments and organic matter accumulated (Collinson, 1996). The black color of this sediment, now rich in diagenetic pyrite indicates that the environment was poorly oxygenated, with clear tendency to anoxic stagnant pond-like waters.

5. Conclusions

In Transylvania, the Maastrichtian fluvial deposits that occurred after the last major tectonogenesis that erected nappes in the Apuseni Mountains or in the Southern Carpathians can now be observed only on small exposures. Apart from the notorious Haţeg Basin, interesting complementary data can be added in the Transylvanian and Rusca Montană basins. In these areas the dominance of red beds is obvious. However, a closer look to these deposits allowsdistinguishing local restricted environments, related to abandoned channels or to true ox-bow lakes. The first situation is illustrated by the case study at Oarda de Jos on Sebeş River, while the second one appears in a repetitive manner at Pui, on Bărbat River. The main difference between these two cases concern the highest tendency to low oxygen water at Pui compared to Oarda de Jos. As a consequence, the lithology is specific for each deposit. The sediments of Oarda de Jos are light colored, reflecting differences with Pui, where the sediments are dark. Same colors are recorded for the fossil teeth and bones collected in these localities.
Such local environments are of interest for their fossil record, notably for its richness and fair preservation of fossils. While the plants could be interpreted as originating from the channel waters or the river banks, the vertebrates had more diverse environmental origins, being either autochthonous, or allochthonous representatives.

6. Acknowledgments

This study is a contribution to the Romanian Ministry of Education and Research CNCS grant PN-II-ID-PCE-2011-3-0381.Authors thank all people involved in the diggings at Pui, especially to

Răzvan Andrei. Special thanks to Carles Martin-Closas (Universitat de Barcelona) for his kind help on the assignation of some Oarda charophytes and to Mihai Dumbravă (Babeş-Bolyai University Cluj-Napoca) for the data provided about Pui Gater. Last but not least, a lot of thanks to JulienCillis, Thierry Smith and Pascal Godefroit (Royal Institute of Natural Sciences Bruxelles) for the SEM photos.Authors acknowledge Dr. George Iliopulos and an anonymous reviewer for their comments and improvements of the manuscript.

7. References

Bojar A.V., Bojar H.P., Ottner F. and Grigorescu D. 2010. Heavy mineral distributions of Maastrichtian deposits from the Haţeg basin, South Carpathians: Tectonic and palaeogeographic implications, *Palaeogeogr., Palaeoclimat., Palaeoecol*.,293, 319-328.

Codrea A.V. and Dica P. 2005. Upper Cretaceous-lowermost Miocene lithostratigraphic units exposed in Alba Iulia-Sebeş-Vinţu de Jos area (SW Transylvanian Basin), *Studia Univ. Babeş-Bolyai, Geol*., 50, 19-26.

Codrea V., Godefroit P., Smith T. and Jipa-Murzea C. 2009. Maastrichtian land vertebrates in Rusca Montană Basin (Romania), in Godefroit, P., Lambert, O. (Eds.), *Tribute to Charles Darwin and Bernissart Iguanodons: New Perspectives on Vertebrate Evolution and Early Cretaceous Ecosystems*, IRSN Bruxelles, 29.

Codrea V., Vremir M., Jipa C., Godefroit P., Csiki Z., Smith T. and Fărcaș C. 2010a. More than just Nopcsa's Transylvanian dinosaurs: A look outside the Haţeg Basin, *Palaeogeogr., Palaeoclimat., Palaeoecol.*, 29, 391-405.

Codrea V., Barbu O. and Jipa-Murzea C. 2010b. Upper Cretaceous (Maastrichtian) landvertebrate diversity in Alba District (Romania), *Bull. Geol. Soc. Greece (Proc. 12th Int. Congr., Patras)*, XLIII, 2,594-601.

Codrea V., Jipa-Murzea C., Csiki Z. and Barbu O. 2010c. Maastrichtian dinosaurs in SW Transylvania (Romania), *Sci. Ann., School of Geol., Aristotle Univ. of Thessaloniki, Proc. XIX CBGA Congr*, Spec. Vol., 99, 69-74.

Codrea V. and Jipa C. 2011. New data on the Maastrichtian fishes (Lepisosteidae and Characiformes) from Transylvania, *9th Annual Meeting of the EAVP, Heraklion, Abstract Volume*,pp. 19.

Codrea V. and Solomon Al. 2012. Peculiar fossilization and taphonomy in Maastrichtian terrestrial deposits of Pui (Haţeg Basin, Romania), Bistriţa, *Stud. şi cercet. (Geol.-Geogr.)*, *17*, 51-69.

Codrea V., Godefroit P. and Smith T. 2012a, First Discovery of Maastrichtian (Latest Cretaceous) Terrestrial Vertebrates in Rusca Montană Basin (Romania), in Godefroit, P, (Ed.), *Bernissart Dinosaurs and Early Cretaceous Terrestrial Ecosystems*, Indiana University Press, 571-581.

Codrea V., Smith T., Venczel M., Solomon Al. and Fărcaş C. 2012b. Maastrichtian multituberculates from Oarda de Jos, Metaliferi sedimentary area (Transylvania, Romania), *4th International Geologica Belgica Meeting*, Abstract Volume, pp 153.

Collinson J. D. 1996. Alluvial sediments. In: Reading, H.G. (Ed.).*Sedimentary Environments: Processes, Facies and Stratigraphy*, Third Edition, Blackwell Science, 37-82.

Csiki Z., Benton, M.J. 2010. An island of dwarf – Reconstructing the Late Cretaceous Haţeg palaeoecosystem. . *Palaeogeogr., Palaeoclimat., Palaeoecol*., 293, 265-270.

Csiki Z., Grigorescu D., Codrea V. and Therrien F. 2010. Taphonomic modes in the Maastrichtian continental deposits of the Haţeg Basin, Romania—Palaeoecological and palaeobiological inferences. *Palaeogeogr., Palaeoclimat., Palaeoecol*., 293, 375-390.

Dalla Vecchia F.M. 2002. Cretaceous dinosaurs in the Adriatic-Dinaric carbonate platform (Italy and Croatia): paleoenvironmental implications and paleogeographical hypotheses. *Mem. Soc. Geol. Ital.*, 57, 89-100.

Dalla Vecchia F. M. 2006.*Telmatosaurus* and the other hadrosaurids of the Cretaceous European Archipelago. An overview. *Natura Nascosta*, 32, 1-55.

Delfino M., Codrea V., Folie A., Dica P., Godefroit P., Smith T. 2008. A complete skull of *Allodaposuchus precedens* NOPCSA, 1928 (Eusuchia) and a reassessement of the morphology of the taxon based on the Romanian remains, *Journ.Vertebr. Paleont.*, 28, 1, 111-122.

Dyke G., Vremir M., Kaiser G., Naish D. 2012. A drowned Mesozoic bird breeding colony from the Late Cretaceous of Transylvania. *Naturwiss,* 99, 6, 435-442.

Folie A. and Codrea V. 2005. New lissamphibians and squamates from the Maastrichtian of Haţeg Basin, Romania, *Acta Palaeont. Pol.,* 50, 1, 57-71.

Gheerbrant E., Codrea V., Hosu Al., Sen S., Guernet C., Lapparent de Broin F. and Riveline, J. 1999. Découverte de vertébrés dans les Calcaires de Rona (Thanétien ou Sparnacien), Transylvanie, Roumanie: les plus anciens mammiferes cénozoiques d'Europe Orientale. *Eclog. Geol. Helvet.,* 92, 517-535.

Givulescu R., Codrea V. and Vremir M. 1995. A New Contribution to the Kwnoledge of Romanian Fossil Flora, *Acta Paleobot*., 35 ,2, 233-236.

Grigorescu D., Hartenberger J.L., Rădulescu C, Samson P. M. and Sudre J. 1985. Découverte de mammiféres et Dinosaures dans le Crétacé supérieur de Pui (Roumanie), *C. R. Acad. Sc. Paris*, 301, II, 19, 1365-1368.

Grigorescu D. 1992. Nonmarine Cretaceous formations of Romania. In Matter, N.J, Chen, P.-j. (Eds.). *Aspects of Nonmarine Cretaceous Geology*, China Ocean Press, 142-164.

Grigorescu D. and Anastasiu N. 1990. Densuş-Ciula and Sînpetru formations (Late Maastrichtian-?Early Paleogene), in: Grigorescu, D., Avram., E., Pop., G., Lupu, M., Anastasiu, N., Rădan, S. (Eds.): *Guide to Excursions A + B, IGCP Project 245: Nonmarine Cretaceous Correlation Project 262: Tethyan Cretaceous Correlation*, 42-54.

Grigorescu D. 2010. The Latest Cretaceous fauna with dinosaurs and mammals from the Haţeg Basin - A historical overview. *Palaeogeogr., Palaeoclim., Palaeoecol*., 293, 271–282.

Haas J., Hámor G., Jámbor Á., Kovács S., Nagymarosy A. and Szederkényi T. 2001.In: Haas, J. (Ed.), *Geology of Hungary*, Eötvös University Press, 317pp.

Lapparent de Broin F., Murelaga Bereikua X. and Codrea V. 2004. Presence of Dortokidae (Chelonii, Pleurodira) in the Earliest Tertiary of the Jibou Formation, Romania: palaeobiogeoraphical implications, *Acta Palaeont. Rom*., 4, 203-215.

Nopcsa F. 1897. Vorläufiger Bericht über das Auftreten von oberer Kreide im Hátszeger Thale in Siebenbürgen, *Verhand. d. K.-K. Akad.Wiss.*,273-274.

Nopcsa F. 1905. A Gyulafehérvár, Déva, Ruszkabánya és a Romániai határ közé eső vidék geológiája. *A Mag. Kir. Földt. Int. Évk.* , 1, 82-254.

Nopcsa F., 1915. Die Dinosaurier der siebenbürgischen landesteile Ungarns. *Mitt. Jahr. K.-K. Ungar.Geol. Reich.*, 1–24.

Panaiotu C. and Panaiotu C. 2010. Palaeomagnetism of the Upper Cretaceous Sânpetru Formation (Haţeg Basin, South Carpathians). *Palaeogeogr., Palaeoclimat., Palaeoecol*., 293, 343-352.

Paraschiv D., Ghenea C., Vasilescu G., Opran C., Pricăjan A. and Goliţa N. 1975. The research stage of thermal waters in Romania andpossibilities to evidence new aquifers, *St. th.ec.*, E, 12, 111–37.

Săndulescu, M. 1984. Geotectonica României.*Ed. th.*, 336 pp.

Téglás G. 1886. Ujabb adatok az Erdély medencze ősemlőseihez. *Földt. Közl.*, 16, 39–44.

Therrien F. 2005. Paleoenvironments of the Late Cretaceous (Maastrichtian) dinosaurs of Romania: insights from fluvial deposits and paleosols of the Transylvanian and Haţeg basins.*Palaeogeogr., Palaeoclimat., Palaeoecol*., 218, 15-56.

Therrien F., Jianu, C.M., Bogdan S., Weishampel D.B. and King, J.W. 2002. Paleoenvironmental reconstruction of the Latest Cretaceous dinosaur-bearing formations of Romania: preliminary results, *Sargetia*, 1, 33-59.

Van Itterbeeck J., Săsăran E., Codrea V., Săsăran L. and Bultynck P. 2004. Sedimentology of the Upper Cretaceous mammal- and dinosaur-bearing sites along the Râul Mare and Bărbat rivers, Haţeg Basin, Romania, *Cret. Res.*, 25, 517-530.

Van Itterbeeck J., Markevich V.S. and Codrea V. 2005. Palynostratigraphy of the Maastrichtian dinosaur and mammal sites of the Râul Mare and Bărbat Valleys (Haţeg Basin, Romania), *Geol. Carpath*., 56, 137-147.

Vasile, Ş. and Panaitescu D. 2012. Primele resturi de vertebrate din "mlaştina" Cretacicului terminal de la Pui (Bazinul Haţeg, România), *Lucr. XI Simp. Naţ. Stud. "Geoecologia"*,59-62.

Villalba-Breva S., Martín-Closas C., Marmi J., Gomez B. and Fernández-Marrón T. 2012. Peat-forming plants in the Maastrichtian coals of the Eastern Pyrenees, *Geol. Acta*, 10,2, 189-207.

Vremir M.M. 2010. New faunal elements from the Late Cretaceous (Maastrichtian) continental deposits of Sebeş area (Transylvania), *Acta Mus. Sebesiensis*, 2, 635-684.

Plate I – Maastrichtian fossils from Oarda de Jos and Pui

1. Charophytegyrogonite (Oarda de Jos); 2. Gastropode (Oarda de Jos); 3. Egg shells (Oarda de Jos); 4. Crabe claw (Oarda de Jos); 5. Lepisosteidae indet., tooth (Oarda de Jos); 6. Idem, scale, external view (Pui); 7. Characidae indet., tooth (Oarda de Jos); 8. *Albanerpeton*sp., dentary in lingual view (Pui); 9. Idem, dentary in lingual view (Oarda de Jos); 10. *Becklesius* sp., fragment of dentary in labial(a) and lingual (b) views, and (c) a detail of the teeth in lingual view (Pui); 11. cf. *Kallokibotion bajazidi*,carapace fragment dorsal view (Pui); 12. Dortokid turtle, illium in lateral view (Oarda de Jos); 13. ?Dortokid, peripheral plate in dorsal view (Pui); 14. cf. *Kallokibotion bajazidi*, pleural plate in dorsal view (Oarda de Jos); 15. *Allodaposuchus precedens*,isolated tooth in lingual view (Pui); 16. Idem, isolated tooth in lingual view (Oarda de Jos); 17. *Acynodon*sp., posterior tooth in occlusal view (Oarda de Jos); 18. *Doratodon* sp., isolated tooth in lingual view (Pui); 19. Idem., isolated tooth in lingual view (Oarda de Jos); 20. Theropoda *incertae sedis*,ungual phalanx in lateral view (Pui); 21. Idem: *Richardoestesia* morphotype, isolated tooth in lateral view (Pui); 22. Velociraptorine dromeosaurid, isolated tooth in lateral view (Oarda de Jos); 23. Theropoda *incertae sedis*,ungulal phalanx in lateral view (Oarda de Jos). 24. *Telmatosaurus transsylvanicus*, left lower jaw, medial view (Pui); 25. Idem, left tibia in lateral(a) and proximal (b) views, with a detail (c) of a high pyrite concentration on bone surface (arrows indicate some pyrite crystals) (Pui); 26. Idem, isolated maxillary tooth, in lingual view (Oarda de Jos); 27. Titanosauria indet., incomplete left humerus in cranial(a) and caudal(b) views (Pui); 28. Idem, caudal vertebra in lateral view (Oarda de Jos); 29. *Zalmoxes* sp., isolated tooth fragment in lingual view (Pui); 30. Idem, isolated tooth fragment in lingual view (Oarda de Jos); Kogaionid multituberculate, right p4 in lingual view (Oarda de Jos).

Scale bars : 200 ɥm for 1; 400 ɥm for 7; 1 mm for 2, 5, 17; 2 mm for 3a, 3b, 6, 8, 9, 10a, 10 b, 18, 19, 31; 3 mm for 20, 21, 22; 5 mm for 15, 16; 1 cm for 4, 26, 29, 30; 2 cm for 12, 23; 3 cm for 13, 14; 5 cm for 24, 25a, 25b; 10 cm for 11, 27a, 27b, 28.

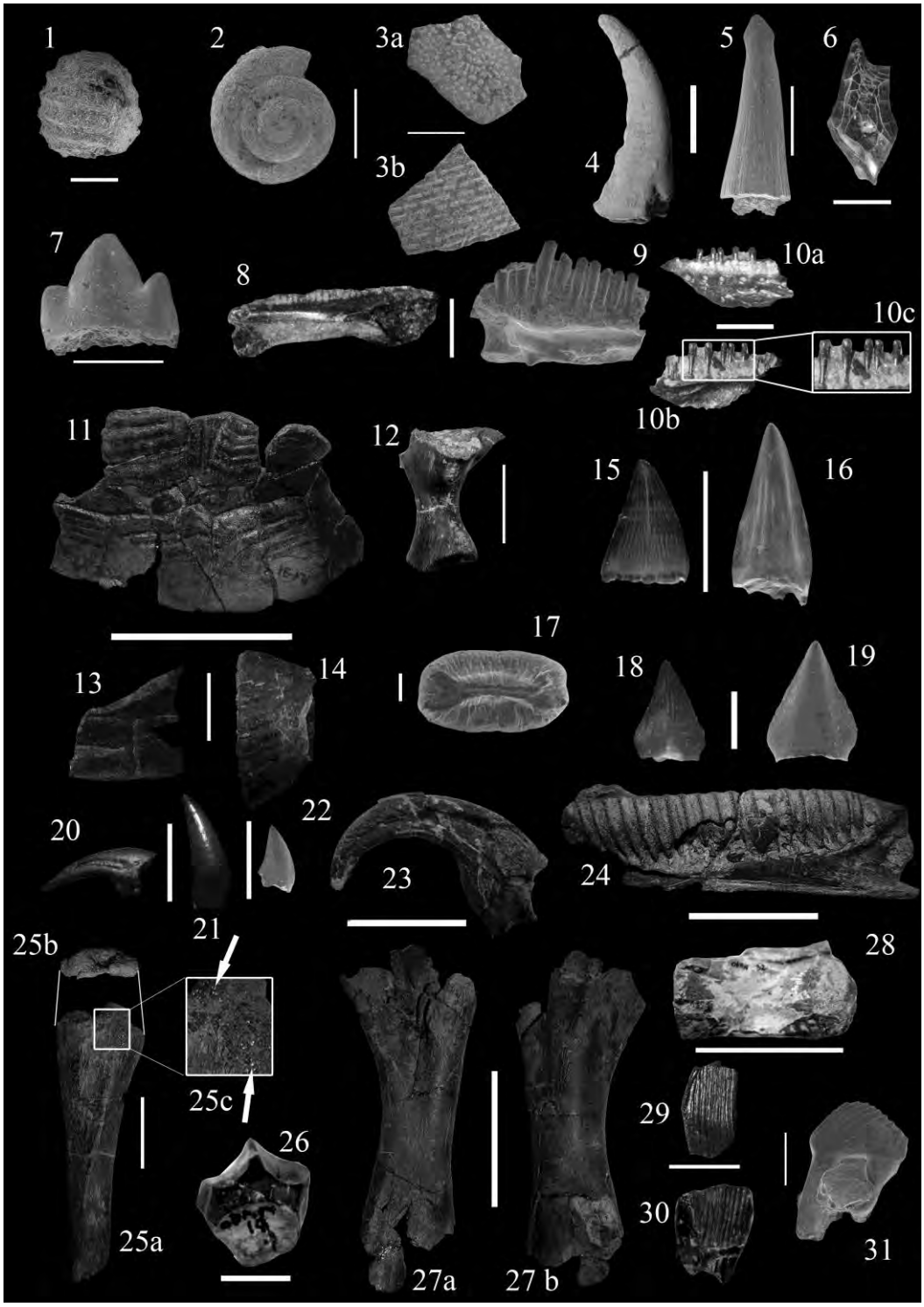
1
2
3a
3b
4
5
6
7
8
9
10a
10b
10c
11
12
13
14
15
16
17
18
19
20
21
22
23
24
25a
25b
25c
26
27a
27 b
28
29
30
31

Δελτίο της Ελληνικής Γεωλογικής Εταιρίας, τομ. XLVII , 2013
Πρακτικά 13ου Διεθνούς Συνεδρίου, Χανιά, Σεπτ. 2013

Bulletin of the Geological Society of Greece, vol. XLVII 2013
Proceedings of the 13th International Congress, Chania, Sept. 2013

CLIMATIC VS TECTONIC CONTROL ON THE EARLY LATE MIOCENE TECTONO-STRATIGRAPHIC DEPOSITS OF THE PRE-APULIAN ZONE, WESTERN GREECE

Drinia H.[1]

[1] *National and Kapodistrian University of Athens, Faculty of Geology and Geoenvironment, Department of Hist. Geology - Paleontology, cntrinia@geol.uoa.gr*

Abstract

Here, we elucidate the relationship between tectonics and climate and their influence on sedimentation. A number of marine sediment samples were collected from a section located in the northern margin of the Agios Petros Basin (Early Tortonian, Levkas Island, W. Greece) for micropalaeontological analysis, in order to establish and interpret of the palaeoenvironmental and palaeobathymetric changes. The distribution patterns of the dominant and associated benthic foraminiferal species (Siphonina reticulata and Cibicidoides kullenbergi), together with the decreased Benthic Foraminiferal Number (BFN) values, elevated diversities and higher planktonic-to-benthic ratios, suggest deposition at bathyal water depths with moderate organic matter fluxes and elevated oxygen contents of the bottom water, typical for this water depth interval. The early Late Miocene infilling of the Agios Petros basin is related to the westward advances of the Ionian zone which induced flexural loading and subsequent relative sea-level rise.
Key words: *Early Tortonian, foraminifera, palaeobathymetry, tectonics, climate.*

Περίληψη

Στην εργασία αυτή διευκρινίζεται η σχέση μεταξύ τεκτονικής και κλίματος και η επιρροή τους στην ιζηματογένεση. Για το σκοπό αυτό μελετήθηκε ένας αριθμός θαλάσσιων δειγμάτων από μία τομή που βρίσκεται στο βόρειο περιθώριο της λεκάνης του Αγίου Πέτρου (Κατ. Τορτόνιο, Λευκάδα, Δυτική Ελλάδα), προκειμένου να διαπιστωθούν και να ερμηνευθούν οι παλαιοπεριβαλλοντικές και παλαιοβαθυμετρικές αλλαγές. Τα πρότυπα κατανομής των κυρίαρχων και των συναφών βενθονικών τρηματοφόρων (Siphonina reticulata και Cibicidoides kullenbergi), σε συνδυασμό με τον μειωμένο αριθμό βενθονικών τρηματοφόρων (BFN), την αυξημένη ποικιλότητα και την υψηλή αναλογία πλαγκτονικών-βενθονικών τρηματοφόρων, δείχνουν εναπόθεση στη βαθύαλη ζώνη με μέτρια εισροή οργανικής ύλης και αυξημένη περιεκτικότητα σε οξυγόνο. Οι ιζηματογενείς αποθέσεις της λεκάνης του Αγίου Πέτρου, ηλικίας Κατώτερο Τορτόνιο σχετίζονται με την προς τα δυτικά προέλαση της Ιόνιας ζώνης η οποία προκάλεσε κάμψη λόγω φόρτισης και την επακόλουθη άνοδο της σχετικής στάθμης της θάλασσας.
Λέξεις κλειδιά: *Κατώτερο Τορτόνιο, Τρηματοφόρα, Παλαιοβαθυμετρία, τεκτονισμός, κλίμα.*

Δελτίο της Ελληνικής Γεωλογικής Εταιρίας, τομ. XLVII , 2013
Πρακτικά 13ου Διεθνούς Συνεδρίου, Χανιά, Σεπτ. 2013

Bulletin of the Geological Society of Greece, vol. XLVII 2013
Proceedings of the 13th International Congress, Chania, Sept. 2013

CLIMATIC VS TECTONIC CONTROL ON THE EARLY LATE MIOCENE TECTONO-STRATIGRAPHIC DEPOSITS OF THE PRE-APULIAN ZONE, WESTERN GREECE

Drinia H.[1]

[1] *National and Kapodistrian University of Athens, Faculty of Geology and Geoenvironment, Department of Hist. Geology - Paleontology, cntrinia@geol.uoa.gr*

Abstract

Here, we elucidate the relationship between tectonics and climate and their influence on sedimentation. A number of marine sediment samples were collected from a section located in the northern margin of the Agios Petros Basin (Early Tortonian, Levkas Island, W. Greece) for micropalaeontological analysis, in order to establish and interpret of the palaeoenvironmental and palaeobathymetric changes. The distribution patterns of the dominant and associated benthic foraminiferal species (Siphonina reticulata and Cibicidoides kullenbergi), together with the decreased Benthic Foraminiferal Number (BFN) values, elevated diversities and higher planktonic-to-benthic ratios, suggest deposition at bathyal water depths with moderate organic matter fluxes and elevated oxygen contents of the bottom water, typical for this water depth interval. The early Late Miocene infilling of the Agios Petros basin is related to the westward advances of the Ionian zone which induced flexural loading and subsequent relative sea-level rise.
Key words: *Early Tortonian, foraminifera, palaeobathymetry, tectonics, climate.*

Περίληψη

Στην εργασία αυτή διευκρινίζεται η σχέση μεταξύ τεκτονικής και κλίματος και η επιρροή τους στην ιζηματογένεση. Για το σκοπό αυτό μελετήθηκε ένας αριθμός θαλάσσιων δειγμάτων από μία τομή που βρίσκεται στο βόρειο περιθώριο της λεκάνης του Αγίου Πέτρου (Κατ. Τορτόνιο, Λευκάδα, Δυτική Ελλάδα), προκειμένου να διαπιστωθούν και να ερμηνευθούν οι παλαιοπεριβαλλοντικές και παλαιοβαθυμετρικές αλλαγές. Τα πρότυπα κατανομής των κυρίαρχων και των συναφών βενθονικών τρηματοφόρων (Siphonina reticulata και Cibicidoides kullenbergi), σε συνδυασμό με τον μειωμένο αριθμό βενθονικών τρηματοφόρων (BFN), την αυξημένη ποικιλότητα και την υψηλή αναλογία πλαγκτονικών-βενθονικών τρηματοφόρων, δείχνουν εναπόθεση στη βαθύαλη ζώνη με μέτρια εισροή οργανικής ύλης και αυξημένη περιεκτικότητα σε οξυγόνο. Οι ιζηματογενείς αποθέσεις της λεκάνης του Αγίου Πέτρου, ηλικίας Κατώτερο Τορτόνιο σχετίζονται με την προς τα δυτικά προέλαση της Ιόνιας ζώνης η οποία προκάλεσε κάμψη λόγω φόρτισης και την επακόλουθη άνοδο της σχετικής στάθμης της θάλασσας.
Λέξεις κλειδιά: *Κατώτερο Τορτόνιο, Τρηματοφόρα, Παλαιοβαθυμετρία, τεκτονισμός, κλίμα.*

1. Introduction

Ionian Islands in western Greece represent one of the most tectonically active regions of the Eastern Mediterranean. They constitute part of the para-autochthonous Apulian foreland of the Hellenide orogen and include rocks of the Pre-Apulian (or Paxos) and Ionian isopic zones (Aubouin, 1957; 1965; Underhill, 1989). The Pre-Apulian or Paxos zone corresponds to mixed neritic/pelagic sedimentation, reaching into the Aquitanian, overlain by Miocene marl sequence. This zone was previously regarded as the undeformed Hellenides foreland but more recent work revealed that it was dominated by shortening during Tertiary-Quaternary times (Underhill, 1989).

In Levkas Island, the Pre-Apulian zone is represented in Agios Petros area which covers the southwestern part of the island and is separated from the Ionian limestones by a major NE-SW oriented thrust fault, known as the Ionian or Kalamitsi Thrust (Figure 1).

In spite of some general studies carried out by Bornovas (1964) and de Mulder (1975), little attention has been directed to the Miocene infill of the Agios Petros Basin (Cushing, 1985; Rondoyanni-Tsiambaou, 1997) which is marked by a fundamental change in its palaeogeographic configuration: at about the transition Oligocene-Miocene, the pre-existing shallow platform with flourishing larger foraminiferal faunas subsided and marls and clays which point to quiet sedimentation conditions with only subordinate supply of displaced coarser material were deposited until the Late Miocene (Bornovas, 1964; de Mulder, 1975).

The purpose of this study is to establish the magnitude of palaeoenvironmental and palaeobathymetric changes and to explore the possible causes that led to these changes, throughout the Early Tortonian part of the pre-Apulian zone from Levkas Island, by means of benthic foraminiferal analysis. This study represents the prosecution of a more general stratigraphic/ palaeoecological work carried out on the same section (Drinia et al., 2007). In the previous paper, the microfossil content (benthic foraminifera) of the Manassi section has been described revealing that deposition took place in upper to middle bathyal depths, during a period of intense tectonic activity. However, this study does not give an adequate representation of the depositional history of the Early Tortonian sediments across the Agios Petros Basin and does not provide possible explanations for changes in sea level.

2. Study Location and Methods

The studied section, which is proximal to the Kalamitsi thrust fault, is located on the eastern slope of a N-S running valley, near the village of Manassi (Figure 1). The succession consists of blue grey marls and clays with some fine grained sandstone interbeds. The intercalations of these thin, clastic beds and especially of positively graded sandstones in the studied succession reflect the influence of density currents, which supplied coarser material from a distant hinterland (de Mulder, 1975). The Manassi section is the only section in the environs of the thrust fault that is entirely exposed in outcrop, where closely packed stratigraphic samples can be undertaken. Yet, at 17 m of the record, an erosional hiatus is implied (Figure 2). The detailed biostratigraphy is retained as reported in Drinia et al. (2007) and Antonarakou (2010). In accordance with these authors, the section covers the time interval between 11.54 and 11.2 Ma, having a lower Tortonian age, above the Serravallian/Tortonian boundary (Paragloborotalia siakensis planktonic foraminiferal zone).

A total of 26 samples (391-1 to 391-26) were re-examined from the micropalaeontological point of view. The data set was recovered from Drinia et al. (2007).

Based on the faunal counts, benthic foraminiferal numbers (BFN; number of specimens per gram dry sediment) were re-calculated with a view to cross – check with the already published values in Drinia et al. (2007). The reason for the revised values has been brought about by the fact that BFN number gives information on the taphonomy of the original living assemblage, the oxygen level (e.g. Ernst & van der Zwaan, 2004), the energy level in which the sediments were deposited (high

abundance in low energy), and to a minor extent the productivity or organic flux (Ernst & van der Zwaan, 2004). Species diversity of benthic foraminifera was estimated by the Fisher α index (α), using the program "PAST" of Hammer et al. (2001).

Moreover, the percentage of planktonic species in the total foraminiferal association (%P) calculated as 100*P/(P+B) and retained from Drinia et al. (2007) , was used in order to reconstruct palaeodepth and track sea-level changes.

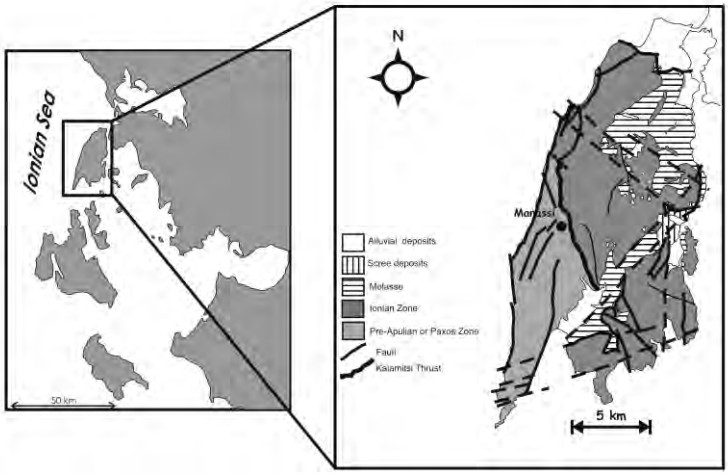

Figure 1 - Geological map of Levkas island, showing the location of the section studied.

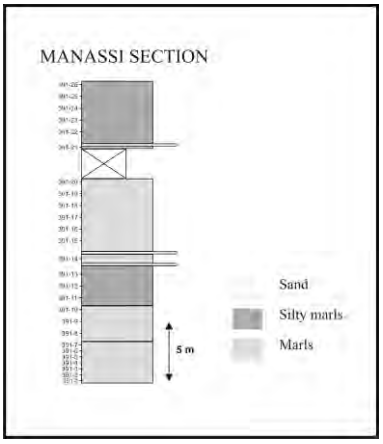

Figure 2 - Stratigraphic column of the measured section.

3. Results and Analysis

3.1. Benthic Foraminiferal Trends

Figure 3 shows the frequency of the dominant benthic species in the samples as this is reported in Drinia et al. (2007). The most abundant species recovered from the section were *Siphonina reticulata, Cibicidoides kullenbergi, Melonis barleeanum, Cibicidoides italicus*. These taxa abundantly and persistently occur from the base of the section up to the level of 14 m and from 20 to 22 m, along with *Globocassidulina subglobosa, Gyroidinoides neosoldanii and Uvigerina semiornata rutila*, representing a fairly diverse open marine association. These benthic taxa are

commonly found in open marine Mediterranean environments of late Miocene age (Kouwenhoven et al., 2006), and are characterized by their mutual preference for well – oxygenated environments with normal salinity (Lutze, 1977; van der Zwaan, 1982; Lutze & Thiel, 1989; Verhallen, 1991; Sjoerdsma & van der Zwaan, 1992; Kaiho, 1994; Sgarrella et al., 1999; Kouwenhoven & van der Zwaan, 2006). High abundances of *S. reticulata* seem to coincide with periods of relatively cooler and more dense surface waters and thus enhanced deep – water mixing and circulation (Sgarrella et al., 1999).

The marked occurrence of *Globocassidulina subglobosa* in the lower part of the record suggests an environment with low organic matter flux.

The upper part of the record marks an abrupt faunal change in the benthic foraminiferal assemblage. The benthic assemblage in this interval constitutes a new fauna with a subordinate component of *Cibicidoides* taxa. *Elphidium* spp., *Cibicides lobatulus*, *Cibicides refulgens* and *Asterigerinata planorbis* are highly abundant from 15 to 17 m, at 19.95 m and from 23.2 to 24.2 m where they exceed 50% of total abundance. These species are reported to live in shallow shelf areas generally above 200 m (Murray, 1991; Seidenkratz et al., 2000), but they are also found in greater depths to which they are often transported passively. These species are extremely tolerant and adaptable to large variations in temperature, salinity and food supply (Linke & Lutze, 1993). The abundance of these species is considered as an indication of erosional processes from shallow shelf seas and therefore not a part of the fossil community.

BFN (Figure 3) remains relatively stable exhibiting low values apart from the lower part of the record, at 1.2 m, where BFN shows an abrupt increase (from 2110 to 12800). The diversity of the benthic foraminiferal assemblage varies from 22 – 50 benthic foraminiferal taxa per ~200 counted specimens. The Fisher diversity index (alpha index) (Figure 3), representing the assemblage diversity, fluctuates between 9 and 21 over the sampled interval, fluctuating in between 10 and 15. In general, from the base of the section up to 6.2 m, diversity is relatively low with a mean value alpha=13. Two samples, i.e. at 7.2 and 12 m, show unusually high alpha index. The Fisher diversity index for the rest of the succession is distinctly lower compared (for the interval from 13 to 23.2 m: alpha values vary between 13.5 and 19, Figure 3). Higher up, the Fisher diversity index further decreases, reaching a value around 10.

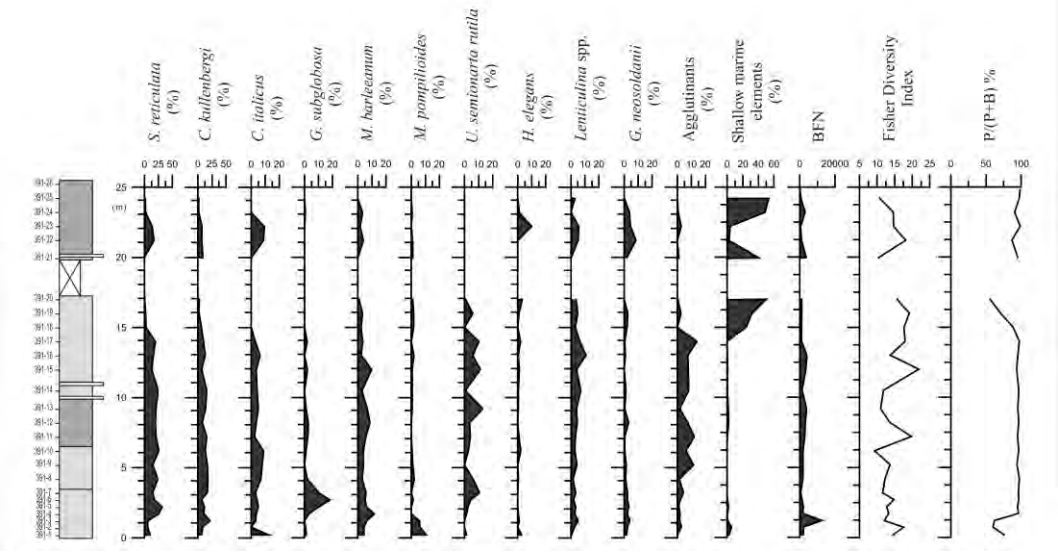

Figure 3 - Occurrence and relative abundance of the most characteristic benthic foraminiferal groups in the studied section together with faunal parameters (BFN, P/P+B%, Fisher-α diversity).

The result of planktonic percentage analyses performed in this study is shown graphically in Figure 3. Planktonic/benthic ratios vary between 55 and 98% of the benthic assemblage. The common occurrence of planktonic foraminifera, throughout the succession, suggests open marine connections to the oceanic realm. With the exception of samples 391-1 to 391-3 and 391-20, the planktonic percentage in all observed Manassi samples is greater than 90. According to data compiled by Murray (1991) and van der Zwaan et al. (1990) this relates to an average water depth of about 1000 m (lower bathyal zone).

4. Discussion

4.1. Palaeoenvironmental Significance of the Benthic Foraminiferal Parameters

In the early Tortonian Manassi section the distribution patterns of the dominant and associated species (*S. reticulata* and *C. kullenbergi*), together with the decreased BFN values, elevated diversities and higher planktonic-to-benthic ratios, suggest deposition at bathyal water depths with moderate organic matter fluxes and elevated oxygen contents of the bottom water, typical for this water depth interval (e.g. Schmiedl et al., 1997).

Relatively high diversity values, with Fisher-α more than 10 also support a bathyal environment of deposition. According to Murray (1991) and Hayward (1986), diversity in benthic foraminifera in modern foraminiferal assemblages reaches a maximum in upper bathyal assemblages with values of Fisher- α index typically in the range of 20-30.

However, at 1.2 m of the record, there is a horizon with higher benthic foraminiferal content (abrupt increase in BFN value, Figure 3). This horizon also contains other shallow-water debris, such as echinoid spines and gastropods and is interpreted as a turbidite sourced from a shallower water environment. Another reason for this abrupt increase in the abundance of benthic foraminifera could have a secondary, taphonomic origin, which would imply that the original benthic foraminiferal assemblage is best preserved in this level and that the remainder of the section does suffer from preferential dissolution. However, the actual assemblage quality (in situ fauna) is identical to other levels, and there is no evidence that dissolution-sensitive species are better preserved in this level.

4.2. Estimating Palaeobathymetry Using Benthic Foraminiferal Census Data

Palaeobathymetry curve presented for Manassi section in Figure 4 is based on quantitative benthic foraminiferal census data reported by Drinia et al. (2007). To estimate the depositional depth of the sediments, the general relationship between depth and the fraction of planktonic foraminifera with respect to the total foraminiferal population (%P) (van der Zwaan et al., 1990) was used, following sample selection and counting procedures described in van Hinsbergen et al. (2005). If samples with evidence for downslope transport and carbonate dissolution are discarded, the relationship between %P and depth of van der Zwaan et al. (1990) allows the estimation of the depositional depth of sediments with approximately 50 m of uncertainty at levels of a few hundreds of metres, to 150 m at depths around 1 km.

According to the palaeobathymetric curve and as reported by DRINIA et al. (2007), deposition began at ~530 m (deep upper bathyal) during the deposition of sample 391-1 and regressed to ~340 m (upper bathyal) in sample 391-3. The sea then transgressed to a palaeodepth of ~1130 m (deep lower middle bathyal) during the deposition of sample 391-17. An ensuing rapid regression saw sea-levels attain a palaeodepth ~270 m (upper bathyal) during the deposition of sample 391-20. At 17 m, just above sample 391-20, an erosional hiatus, associated with shoaling conditions that caused the change in foraminiferal assemblages, is implied. Indeed, declining Cibicidoides, Siphonina and Cassidulina abundances coupled with increasing Elphidium and A. planorbis abundances indicate a shallowing from the outer neritic to bathyal zone to the middle neritic zone,

with shallowing continuing to inner neritic depths. However, the high percentage of planktonics indicate download transport and mixing with the bathyal fauna.

Based on the constructed palaeobathymetric curve, the sea then transgresses abruptly to ~1100 m (deep middle bathyal) at the time of sample 391-21 and remained relatively constant with short-term fluctuations from sample 391-22 till 391-25.

4.3. Differentiating Glacio-eustasy and Tectonics

The palaeobathymetric evolution of the studied sediments together with the faunal pattern as this is presented in Figure 3 provide the key to unlocking the broader question as to whether the depositional pattern within this part of the Agios Petros Basin was driven by tectonic or eustatic change. It is frequently difficult to separate the contributory effects of eustatic and tectonic change as they usually act in concert.

4.3.1. Eustatic Control

Based on the biostratigraphy, the studied sequence has been deposited just above the global sequence boundary Ser4/Tor1, dated at 11.7 Ma, which represents a low sea-level event, corresponding to MSi-4 oxygen cooling event of Abreu & Anderson (1998) which is time equivalent to Mi5 cooling event of Miller et al. (1991), (Figure 5).

However, the tentative sea-level curve for the Manassi section generally corresponds to a transgressive event. This differentiation from the global sea level trend may suggest that some other controls have affected sedimentation prior to and during the Manassi sedimentation. Such controls may involve external/allocyclic or internal/autocyclic factors, such as relative sea-level changes, tectonics, basement topography (shape and size of the basin), character of the source area and sedimentary processes within the receiving basin, most of which are interactive.

To identify possible relationships between palaeodepth variation on the Manassi record, sea level changes and/or tectonic events, the palaeodepth curve is compared with the global δ18O record of Zachos et al. (2001). Oxygen isotopes provide a minimum estimate for absolute sea level changes, by interpreting the amplitude of δ18O variation and assuming a constant ice volume effect. Hence, an increase in δ18O suggests increased ice volume and hence the associated sea level fall and depletion in δ18O corresponds to high sea-level stands. Integration of all these different parameters leads to a robust palaeobathymetric reconstruction of the early Tortonian Manassi succession.

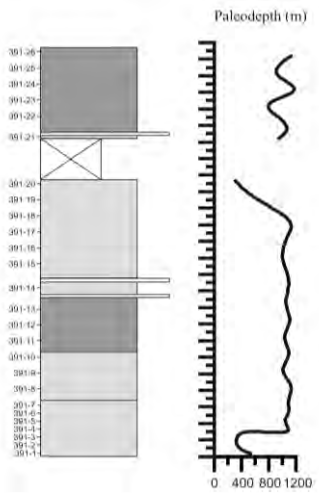

Figure 4 - Palaeobathymetric curve of the studied section, based on quantitative benthic foraminiferal census data (Drinia et al. 2007).

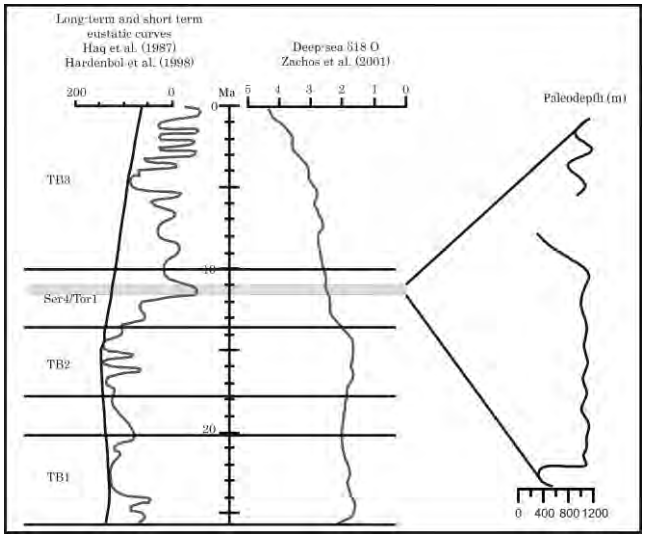

Figure 5 - Comparison of the reconstructed palaeodepth curve with the isotope record of Zachos et al. (2001) and the eustatic curves of Haq et al. (1987) and Hardenbol et al. (1998).

Comparison between the palaeodepth curve and the isotopic record shows opposite trend of the two curves throughout the investigated interval. The isotope record shows a positive excursion coinciding with the shallowing trend in the eustatic curve. This correspondence contradicts with the transgressive event which has taken place during that period, in Levkas Island. According to Flecker et al. (1995), during the Early Tortonian, the transgression and rapid relative sea-level rise that affected at least a large area of the Eastern Mediterranean are regional events rather than being the local effects of small scale tectonic activity within individual basins.

However, the presence of abrupt depth changes may reflect an increased tectonic activity during this interval. In addition, high amplitude fluctuation of the water depth at the upper part of the Manassi section was probably caused by fluxes of sediment from shallower parts of the basin with excess benthic foraminifera, which make the estimation shallower than the actual water depth.

4.3.2. Tectonic Control

The studied sediments at the northern part of the Agios Petros Basin represent part of the Pre-Apulian zone which has been deposited from 11.54 to 11.21 Ma, a time interval which corresponds to a phase of compression and flexural subsidence which affected the external Ionian Zone and the Pre-Apulian Zone in Levkas island (Meulenkamp, 1982; van Hinsbergen et al., 2006; Accordi et al., 1998; Karakitsios & Rigakis, 2007). According to Clews (1989), at the end of the Early Miocene the Kalamitsi Thrust became active and caused uplift and erosion across the basin. Although the Kalamitsi thrust was active in the early Miocene (Clews 1989), extensional growth faulting in the Pre-Apulian zone continued through to early Pliocene times (Sorel 1976) and acted as a major control on sedimentary patterns. Marine transgression was due to this extensional faulting, in response to load-induced flexure resulting from thrusting of the Ionian zone to the west. The rapid subsidence event is attributed to the formation of a deep, underfilled foreland basin caused by continued thrusting. During this period, the Pre-Apulian zone became increasingly dominated by clastic influences.

The detailed study of the Miocene sediments of the Manassi section reveals that at certain levels within the succession, events such as uplift had occurred in the hinterland. This is indicated by the generally higher influx of quartz in samples 391-21 to 391-26, and is further supported by the high percentages of inner neritic taxa indicating that marginal marine and continental influxes became overwhelmingly dominant.

The fraction of transported benthic foraminiferal species relative to the total amount of benthic foraminifera can be also used as an indication of relative sea level (Figure 4). The lower half part of the section is dominated by outer neritic and oceanic taxa, indented by small excursions of inner neritic ecological groups, reflecting relatively outer neritic to open marine conditions. From 15 to 17 m and at 19.95 m, an upward increase of inner neritic benthic foraminifera indicates increasing influence of marginal marine settings. Slightly higher in the record, the composition of the benthic foraminifera association changes again abruptly and becomes dominated by outer neritic – bathyal taxa.

4.4. Subsidence History

In this work it is not our intention to reconstruct the subsidence history and relative sea level for the studied area as this is not possible as we miss tie points of stratigraphy (primarily boundaries of nannozones and stages). However, some general implications can be made. Subsidence history based on the palaeobathymetric estimations shows that the development of depositional depth in the Manassi section was primarily determined by tectonics. That is the general sea level rise trend in the Agios Petros Basin has been caused by tectonically induced subsidence.

In the lower part of the record minor amplitude, short duration uplift may be due to local reorientation of stress field takes place followed by a rapid, high rate subsidence. The stratigraphic interval from 1.7 to 14 m is characterized by a relative long period of tectonic quiescence. From 14 to 17 m, significant uplift took place due to regional compression. This points to a radical change in early Tortonian basin evolution. However, the strange looking drop and jump of the basin and seafloor maybe an artefact, probably caused by an overestimation of palaeowater depth. This compressive event resulted in the formation of a sedimentary gap (from 17 to 20 m)

5. Conclusions

The main objective of this study was the interpretation and documentation of the factors that led to changes in relative sea level of the early Late Miocene tectono-stratigraphic deposits of the Pre-Apulian zone, in Levkas Island, Western Greece. Moreover, we attempted to integrate the estimated palaeobathymetric trend into a wider, global context of sea level changes.

Previous work of Drinia et al. (2007) revealed that the distribution patterns of the dominant and associated benthic foraminiferal species together with the estimated faunal parameters, suggest a bathyal depositional environment.

The palaeodepth history of this part of the Pre-Apulian Foreland Basin as revealed by the comparison of the tentative sea level curve with the global δ18O, is mainly dominated by tectonics and not by eustatic signal.

Flexural loading is inferred to have resulted in regional tectonic subsidence and consequently in relative sea- level rise.

6. Acknowledgments

Financial support for this research was provided by the Research Project 70/4/11078 of the University of Athens. The author wishes to thank Prof. V. Karakitsios and an anonymous reviewer for their constructive comments that helped improve the manuscript.

7. References

Abreu V.S. and Anderson J.B. 1998. Glacial eustasy during the Cenozoic: sequence stratigraphic implications, *American Association Petroleum Geologist Bulletin*, 82, 1385–1400.

Accordi G., Carbone F. and Pignatti J. 1998. Depositional history of a Palaeogene carbonate ramp (Western Cephalonia, Ionian Islands, Greece), *Geologica Romana*, 34, 131–205.

Antonarakou A. 2010. Plankton Biostratigraphy and palaeoclimatic implications of an early Late Miocene sequence of Levkas island, Ionian Sea, Greece, *Bulletin of the Geological Society of Greece*, XLIII, 568 – 578.

Aubouin J. 1957. Essai de corrélation stratigraphique de la Grèce occidentale, *Bulletin de la Société Géologique de France*, 7, 281–304.

Aubouin J. 1965. Geosynclines, *Developments in Geotectonics*, 1 – 335, Elsevier, Amsterdam,

Bornovas J. 1964. Géologie de l'île de Lefkade, *Geological and Geophysical Research (I.G.S.R)*, 10, 1 - 142.

Clews J.E. 1989. Structural controls on basin evolution: Neogene to Quaternary of the Ionian zone, Western Greece, *Journal of the Geological Society*, London, 146**,** 447-457.

Cushing M. 1985. Evolution structurale de la marge nord oust hellénique dans l'île de Levkas et ses environs (Grèce nord occidentale), *Unpublished Thèse 3me cycle*, Université de Paris-Sud, Centre d' Orsay.

De Mulder E.F.J. 1975. Microfauna and sedimentary-tectonic history of the Oligo-Miocene of the Ionian Islands and Western Epirus (Greece), *Utrecht Micropalaeontological Bulletins,* 13, 1–139.

Drinia H., Antonarakou A., Kontakiotis G., Tsaparas N., Segou M. and Karakitsios V. 2007. Palaeobathymetric Evolution of the Early Late Miocene Deposits of the Pre-Apulian Zone, Levkas Island, Ionian Sea, *Bulletin of the Geological Society of Greece*, 40, 39-52.

Ernst S. and Van der Zwaan B. 2004. Effects of experimentally induced raised levels of organic flux and oxygen depletion on a continental slope benthic foraminiferal community, *Deep-Sea Research I*, 51**,** 1709–1739.

Jorissen F.J., de Stigter H.C. and Widmark J.G.V. 1995. A conceptual model explaining benthic foraminiferal microhabitats*, Marine Micropalaeontology*, 26, 3-15.

Flecker R., Robertson A.H.F., Poisson A. and Müller C. 1995. Facies and tectonic significance of two contrasting Miocene basins in south coastal Turkey, *Terra Nova*, 7, 221-232**.**

Hammer Ø., Harper D.A.T. and Ryan P.D. 2001. PAST: palaeontological statistics software package for education and data analysis, *Palaeontologia Electronica*, 4, 9 p.

Hayward B.W. 1986. A guide to palaeoenvironmental assessment using New Zealand Cenozoic foraminiferal faunas, *New Zealand Geoogical Survey Report PAL*, 109, 73 p.

Kaiho K. 1994. Benthic foraminiferal dissolved – oxygen levels in the modern ocean, *Geology*, 22, 719 – 722.

Karakitsios V. and Rigakis N. 2007. Evolution and Petroleum Potential of Western Greece, *Journal of Petroleum Geology*, 30, 197-218.

Kouwenhoven T.J. and Van der Zwaan G.J. 2006. A reconstruction of late Miocene Mediterranean circulation patterns using benthic foraminifera, *Palaeogeography Palaeoclimatology Palaeoecology*, 238, 373-385.

Kouwenhoven T.J., Morigi C., Negri A., Giunta S., Krijgsman W. and Rouchy J.M. 2006. Paleoenvironmental evolution of the eastern Mediterranean during the Messinian: Constraints from integrated microfossil data of the Pissouri Basin (Cyprus), *Marine Micropaleontology*, 60, 17 – 44.

Linke P. and Lutze G.F. 1993. Microhabitat preferences of benthic foraminifera—a static concept or a dynamic adaptation to optimize food aquisition? *Marine Micropalaeontology*, 20, 215–234.

Lutze G.F. 1977. Neogene benthonic foraminifera from Site 369, Leg 41 DSDP, *Initial Reports of the Deep Sea Drilling Project*, 41, 659 – 666.

Lutze G.F. and Thiel H. 1989. Epibenthic foraminifera from elevated microhabitats: Cibicidoides wuellerstorfi and Planulina ariminensis, *Journal of Foraminiferal Research*, 19, 153 – 158.

Miller K.G., Wright J.D. and Fairbanks R.G. 1991. Unlocking the icehouse: Oligocene–Miocene oxygen isotope, eustacy, and margin erosion, *Journal of Geophysical Research*, 96, 6829–6848.

Meulenkamp J.E. 1982. On the pulsating evolution of the Mediterranean, *Episodes*, 1, 13–16.

Murray J.W. 1991. Ecology and Palaeoecology of Benthic Foraminifera. Harlow, Essex, UK, *Longman Scientific and Technical Publishers*, 1-451.

Rondoyanni-Tsiambaou Th. 1997. Les séismes et l'environnement géologique de l'île de Lefkade, Grèce: Passé et Future, in: Marinos G., Koukis G., Tsiambaos Th. and Stournaras G. (Eds), Engineering Geology and the Environment, Paper presented at the *International Symposium on Engineering Geology and the Environment*, A.A. Balkema, Rotterdam, 1469–1474.

Seidenkrantz M.S., Kouwenhoven T.J., Jorissen F.J., Shackleton N.J. and Van der Zwaan G.J. 2000. Benthic foraminifera as indicators of changing Mediterranean–Atlantic water exchange in the late Miocene, *Marine Geology*, 163, 387–407.

Schmiedl G., Mackensen A. and Müller P.J. 1997. Recent benthic foraminifera from the eastern South Atlantic Ocean: dependence on food supply and water masses, *Marine Micropalaeontology*, 32, 249–288.

Sgarrella F., Sprovieri R., Di Stefano E., Caruso A., Sprovieri M. and Bonaduce G. 1999. The Capo Rossello borehole (Agrigento, Sicily) cyclostratigraphic and paleoceanographic reconstructions from quantitative analysis of the Zanclean foraminiferal assemblages, *Rivista Italiana di Paleontologia e Stratigafia*, 105, 303 – 322.

Sjoerdsma P.G. and van der Zwaan G.J. 1992. Simulating the effect of changing oceanic flux and oxygen content on the distribution of benthic foraminifers, *Marine Micropaleontology*, 19, 163 – 180.

Sorel D. 1976. Etude néotectonique des iles ioniennes de Cephalonie et Zante et de l' Epire occidentale (Grèce*), Thèse du 3^{e} cycle*, Université de Paris-Sud, Centre d' Orsay.

Underhill J.R. 1989. Late Cenozoic deformation of the Hellenic foreland, Western Greece, *Geological Society of America Bulletin*, 101 613–634.

Van der Zwaan G.J. 1982. Paleoecology of late Miocene Mediterranean foraminiferam, *Utrecht Micropaleontological Bulletins*, 25. 201 pp.

Van der Zwaan G.J., Jorissen F.J. and De Stigter H.C. 1990. The depth dependency of planktonic/benthonic foraminiferal ratios: constraints and applications, *Marine Geology*, 95, 1–16.

Van der Zwaan G.J., Duijnstee I.A.P., Den Dulk M., Ernst S.R., Jannink N.T. and Kouwenhoven T.J. 1999. Benthic foraminifers: proxies or problems? A review of palaeocological concepts, *Earth Science Revues*, 46, 213-236.

Van Hinsbergen D.J.J., Kouwenhoven T.J. and Van der Zwaan G.J. 2005. Palaeobathymetry in the backstripping procedure: Correction for oxygenation effects on depth estimates, *Palaeogeography Palaeoclimatology Palaeoecology*, 221 245–265.

Van Hinsbergen D.J.J., Van der Meer D.G., Zachariasse W.J. and Meulenkamp J.E. 2006. Deformation of western Greece during Neogene clockwise rotation and collision with Apulia, *International Journal of Earth Science*, 95, 463-490.

Verhallen P.J.J.M. 1991. Late Pliocene to early Pleistocene Mediterranean mud – dwelling foraminifera; influence of changing environment on community structure and evolution, *Utrecht Micropaleontological Bulletins*, 40, 219 pp.

Zachos J., Pagani M., Sloan L., Thomas E. and Billups K. 2001. Trends, rhythms, and aberrations in global climate 65 Ma to present, *Science*, 292, 686-93.

Δελτίο της Ελληνικής Γεωλογικής Εταιρίας, τομ. XLVII , 2013
Πρακτικά 13ου Διεθνούς Συνεδρίου, Χανιά, Σεπτ. 2013

Bulletin of the Geological Society of Greece, vol. XLVII 2013
Proceedings of the 13th International Congress, Chania, Sept. 2013

FORAMINIFERAL BIOSTRATIGRAPHY AND PALAEOENVIRONMENTAL ANALYSIS OF THE BASAL PART OF KALAMAVKA FORMATION (LATE MIOCENE, IERAPETRA BASIN, EASTERN CRETE)

Drinia H.[1], Antonarakou A.[1] and Louvari M. A.[1]

[1] National and Kapodistrian University of Athens, Faculty of Geology and Geoenvironment, Department of Hist. Geology - Palaeontology, cntrinia@geol.uoa.gr, aantonar@geol.uoa.gr, melinaluvari@geol.uoa.gr

Abstract

This work involves a preliminary quantitative analysis of benthic foraminifera for the purpose of the determination of palaeoenvironmental parameters (oxygenation, palaeobathymetry) of the depositional environment of the lower part of the typical section of Kalamavka Formation, in Ierapetra Basin, eastern Crete. The sediments of the studied section contain a rich foraminiferal fauna, mainly dominated by planktonic species. High resolution planktonic foraminiferal record reveals the presence of N. atlantica praeatlantica, N. acostaensis, P. siakensis suggesting an early Tortonian chronostratigraphic age. The quantitative assessment of palaeodepth, suggests deposition at middle shelf to bathyal water depths with moderate organic matter fluxes and elevated oxygen contents of the bottom water, typical for this water depth interval.

Key words: *Early Tortonian, microfauna, palaeobathymetry, Eastern Mediterranean.*

Περίληψη

Η εργασία αυτή αφορά στην πρόδρομη ποσοτική ανάλυση των βενθονικών τρηματοφόρων για το σκοπό του καθορισμού των παλαιοπεριβαλλοντικών παραμέτρων (οξυγόνωση, παλαιοβάθος) του περιβάλλοντος απόθεσης του κατώτερου τμήματος της τυπικής τομής του σχηματισμού Καλαμαύκα, στην λεκάνη της Ιεράπετρας, ανατολική Κρήτη. Τα ιζήματα του μελετώμενου τμήματος περιέχουν μια πλούσια πανίδα τρηματοφόρων, όπου επικρατούν τα πλαγκτονικά είδη. Το υψηλής ευκρίνειας αρχείο των πλαγκτονικών τρηματοφόρων αποκαλύπτει την παρουσία των ειδών N. atlantica praeatlantica, N. acostaensis, P. siakensis υποδεικνύοντας χρονοστρωματογραφική ηλικία Κατώτερο Τορτόνιο. Η ποσοτική εκτίμηση του παλαιοβάθους, έδειξε εναπόθεση στη μέση κρηπίδα έως την ανώτερη βαθύαλη ζώνη με μέτρια εισροή οργανικού υλικού και σχετικά αυξημένη περιεκτικότητα σε οξυγόνο, χαρακτηριστικό για αυτό το περιβάλλον.

Λέξεις κλειδιά: *Κατώτερο Τορτόνιο, Μικροπανίδα, Παλαιοβαθυμετρία, Ανατολική Μεσόγειος.*

1. Introduction

The Eastern Mediterranean region, which defines the region lying between the Caspian Sea and the Adriatic Sea through Caucasus, Anatolia, Aegean Sea and Greece, is one of the most tectonically active regions and one of the key regions for the understanding of fundamental tectonic processes, including continental rifting, passive margins, ophiolites, subduction, accretion, collision and post-collisional exhumation.

The island of Crete is located in the south eastern Mediterranean region. Its Late Tertiary–Quaternary tectonic evolution has been investigated since several decades by many researchers (e.g. Aubouin et al., 1976; Angelier, 1979; Le Pichon & Angelier, 1979; Hall et al., 1984; van Hinsbergen et al., 2005; among others) because of its significance in the geodynamic evolution of the eastern Mediterranean.

The present study concerns an integrated study of an early late Miocene (early Tortonian) succession located in the Ierapetra Basin, eastern Crete (Kalamavka Formation of Fortuin, 1977, 1978). The Kalamavka section provides an ideal archive spanning the early Tortonian, a time period characterized by intense tectonic activity in this region. The time of deposition of the Kalamavka Formation (Late Serravallian - Early Tortonian) coincides with the beginning of the fragmentation stage of the Aegean microplate (break - up stage), during extensional movements and thus the beginning of the "modern history" of the Aegean region. During this period, many lithostratigraphic and palaeogeographic changes took place. The Kalamavka Formation is considered to represent one lithologic unit that reflects the prevailing sedimentary regime at the time.

In order to establish the magnitude of palaeoenvironmental an palaeobathymetric changes, during the deposition of Kalamavka Formation, a highly successful and diverse group of amoeboid protists which belong within the newly-established supergroup Rhizaria (Nikolaev et al., 2004), were used as a tool of analysis.

2. Geology and Sedimentology

The study area is located in the Ierapetra Basin, in the eastern part of Crete (Fig. 1). Crete is part of the Hellenides mountain range created by the same tectonic activity that was responsible for the orogenesis of the Alps and the formation of the Mediterranean Sea.

The Neogene in eastern Crete was studied by a number of researchers (Dermitzakis, 1969; Gradstein, 1973; Zachariasse, 1975; Fortuin, 1977, 1978; Meulenkamp et al., 1979a, b; Meulenkamp & Hilgen, 1986; Drinia, 1989; Postma & Drinia, 1993; Pipponzi et al., 2004; Drinia et al., 2008) in various details. According to them, in the Ierapetra Basin, sedimentation started with the deposition of Middle Miocene terrigenous clastics followed by the Upper Miocene fluviolacustrine and open marine shelf, slope and basin-floor sediments. The lowermost Pliocene sediments are generally found as slump components and debris flow deposits (“marl breccias” sensu Fortuin, 1977). These deposits overlie the lower Messinian carbonates (Meulenkamp, 1985). According to Peters (1985), the marl breccias resulted from the spasmodic subsidence along the pre-existing but still active E–W and N–S trending fault systems. Deep marine marls and clays continued in the sedimentary succession. Finally, Quaternary deposits consisting of bioclastic limestones and Tyrrhenian marine terraces are found mainly on the south coast of the Ierapetra Basin (Angelier, 1979; Pirazzoli et al., 1982).

The studied section is exposed in the road section just north of the village of Kalamavka and it comprises bluish, fossiliferous, calcareous mudstones with occasional lenses or layers of fine to very fine grained sandstone. The mudstone is generally massive but in places thin laminations are visible. The sandstone beds are very thin and increase in abundance and thickness in higher stratigraphic levels (Fig. 2). The marls are generally massive due to bioturbation. At non-

bioturbated intervals structures produced by traction and suspension fall-out are preserved (Drinia, 1989).

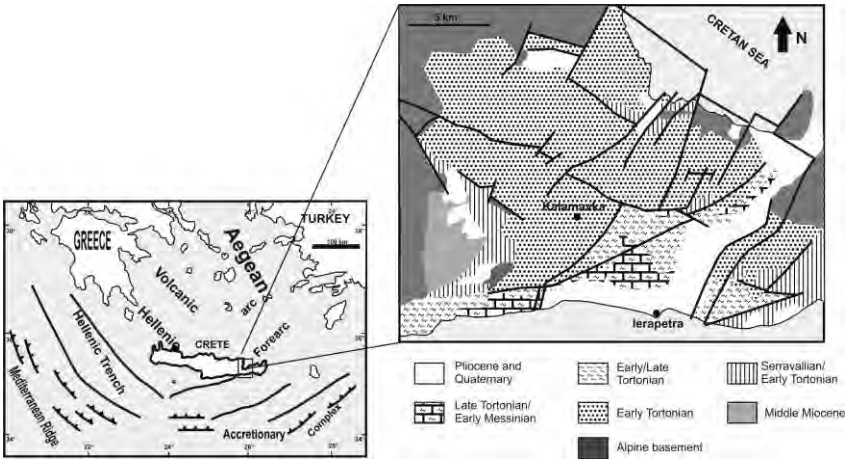

Figure 1 - Geological Sketch map of the Ierapetra Basin (modified from Fortuin 1977, 1978).

Figure 2 - General view of the studied section depicting intercalations of carbonate-rich marls with occasionally pure limestone layers.

3. Materials and Methods

A total of 20 samples were examined for the micropalaeontological analysis using standard laboratory procedures. Benthic foraminifera were picked from the 125-595 μm fractions after washing in water and wet-sieving, and splitting to the right size allowing picking the statistically significant number of 200-300 specimens of benthic foraminifera. The foraminifera were identified, sorted taxonomically, counted and the data compiled on to an Excel spreadsheet.

The number of planktonic foraminiferal tests was also recorded during picking.

The percentage of planktonic species in the total foraminiferal association (%P) was calculated as 100*P/ (P+B), in order to reconstruct palaeodepth and track sea-level changes. Interpretation of the obtained data was done according to Murray (1991), with divisions into inner shelf (<20% planktonic tests), middle shelf (20–50%), outer shelf (50–70%) and upper bathyal zones (>70% planktonic tests).

To estimate the depositional depth of the sediments, the general relationship between depth and the fraction of planktonic foraminifera with respect to the total foraminiferal population (%P) (Van der Zwaan et al., 1990) was used, following the equation: Depth (m) = $e^{3.58718 + (0.03534 * \%P)}$, where %P

is the percentage of the total planktonic foraminifera of the association, calculated according to 100*P/(P+B), where P is the number of planktonic foraminifera specimens and B the benthic specimens. The reliability of the calculated palaeodepth can be biased by observation that the plankton/benthos ratio (P/B – ratio) is not only influenced by depth, but also by changes in oxygenation of bottom waters (Sen-Gupta & Machain-Castillo, 1993; Jorissen et al., 1995). Moreover, discrepancy between calculated palaeodepth and sedimentology has been pointed out by Hohenegger (2005). For this reason, Van Hinsbergen et al. (2005) excluded from the calculations of %B the deep infaunal (%S), which is not directly related to the depth.

4. Results and Analysis

4.1. Biostratigraphy

The biostratigraphic analysis was based on the qualitative analysis of planktonic foraminifera species performed on the total of samples. The specific identifications were conducted according to reference publications (Dermitzakis, 1978; Iaccarino, 1985; Hilgen et al., 2000; Foresi et al., 2002). For the biostratigraphic range of the studied section we only considered the appearance/disappearance of marker species.

The planktonic foraminifera assemblages consist of 16 categories: *Globigerina bulloides* gr., *Turborotalita quinqueloba, Globigerinita glutinata, Globoturborotalita druryi/nepenthes* gr., *Globoturborotalita decoraperta, Globigerinoides obliquus, Globigerinoides quadrilobatus* gr., *Catapsydrax parvulus, Globorotalia scitula, Globorotalia praemenardii/menardii* gr., *Globorotalia miozea, Paragloborotalia siakensis, Paragloborotalia partimlabiata, Orbulina* spp., *Neogloboquadrina atlantica-praeatlantica* and *Neogloboquadrina acostaensis*.

Among the taxa more or less continuously present, *G. bulloides*, *G. quadrilobatus*, *Orbulina* spp. are the most abundant species, whereas *G. glutinata*, *G. scitula*, and *Turborotalita quinqueloba* are rare. Specimens of *G. druryi/nepenthes* occur mainly in the lower part. *G. praemenardi/menardii* shows two main intervals of significant occurrence: in the lower and upper part of the section. *C. parvulus* and *P.* cf. *partimlabiata* are also present. In our record, *P. siakensis* occurs almost in all samples being more abundant in the middle –upper part. *N. acostaensis* is discontinuously present and *N. atlantica praeatlantica* occurs from the base of the section.

Within the studied interval we recorded the absence of *G. subquadratus* while *G. obliquus* exists in all the samples. The last common occurrence of *G. subquadratus* has been dated at 11.54 Ma (Hilgen et al., 2003; Lirer et al., 2002) while the first regular occurrence of *G. obliquus* is recorded at the same time. In the Mediterranean, this event coincides with the end of the first influx of the neogloboquadriniids. A paracme interval in its distributional range in the Mediterranean recorded at 11.54 to 11.2 Ma. The biostratigraphic boundaries of this paracme interval are determined by the last occurrence of *G. subquadratus* and the last occurrence of *P. siakensis* at 11.2 Ma (Hilgen et al., 2000; Caruso et al., 2002; Di Stefano et al., 2002; Foresi et al., 2002; Lirer et al., 2004; Iaccarino et al., 2004).

According to the distributional pattern of the neogloboquadriniids, the occurrence of *P. siakensis*, the absence of *G. subquadratus* and the presence of *G. obliquus* in all the samples, the section spans the time interval between 11.54 -11.2 Ma, suggesting an early Tortonian chronostratigraphic age.

4.2. Characteristics of the Benthic Foraminiferal Assemblages

The section is characterized by (i) ecological groups of benthic foraminifera faunas dominating in circalittoral environments (*Cibicides dutemplei* and *C. kullenbergi*) and bathyal (*Bulimina costata, Pullenia bulloides* and *Uvigerina* spp.); (ii) high diversity; and (iii) abundant planktonic foraminifera. The common occurrence of planktonic foraminifera, throughout the succession, suggests open marine connections to the oceanic realm. Textularids as well as miliolids are rare.

Upper-neritic taxa occur at variable relative abundances, including epiphytic species that live on aquatic vegetation in the photic zone such as *Cibicides lobatulus* and *C. refulgens*.

The result of planktonic percentage analyses performed in this study is shown graphically in Fig. 3. Planktonic/benthic ratios vary between 25 and 75% of the benthic assemblage. Application of van der Zwaan et al. (1990) regression indicates that deposition (Fig. 3), began at ~450 m (deep upper bathyal) and remained relatively stable (upper bathyal) for the first 80 cm of the record. An ensuing rapid regression resulted the sea level to fall 350m, attaining a palaeodepth ~100 m (middle shelf).

Based on the constructed palaeobathymetric curve, the sea then gradually transgresses (upper bathyal) and remained relatively constant with short-term fluctuations.

5. Discussion

5.1. Estimating Palaeobathymetry Using Benthic Foraminiferal Census Data

It has long been known that the percentage of planktonic foraminifera in modern sediments increases with water depth e.g. (Van der Zwaan et al., 1990, 1999; Van Hinsbergen et al., 2005; Boltovskoy & Wright, 1976; Gibson, 1989). The percentage (%) of planktonic foraminifera (P/P+B*100) is one of the most consistent proxies to assess palaeo-water depths. According to Murray (1976), the inner shelf is characterized by up to 20% of planktonic specimens, the middle shelf between 10 and 60%, the outer shelf between 40 and 70%, and the upper bathyal zone > 70%. The highest values, roughly 90%, are observed in the lower bathyal zone (Valchev, 2003). Finally, based on data from the Gulf of Mexico, Pflum & Frerichs (1976) consider that a %P of < 50% corresponds to the neritic zone, from 50% to 90% to the upper bathyal zone (200-1000 m) and > 90% to the middle and lower bathyal zone (1000-4000 m). Vella (1962) determined two deep water biofacies, based on high populations of planktonic foraminifera: (1) the semi-pelagic biofacies (600-1200 m), with percentage of planktonic foraminifera from 40%-60% and (2) the eupelagic biofacies (1200-4000 m), with percentage of planktonic foraminifera from 70% - 100%. The same author, however, points out that high percentage of planktonic foraminifera values can also sometimes be present in shallow environments owing to the predominance of inshore winds.

In our record, the percentage of planktonic foraminifera (P/B ratio, Fig. 3) varies between 38% and 75%, indicating an outer shelf to upper bathyal, semi-pelagic to temporaly eupelagic biofacies. The abrupt decline to 26% in sample KLM 6, at 100 cm (Fig. 3) implies sedimentation in the middle shelf (75-100 m). Based on Speijer & Schmitz (1998), this drop likely resulted from the dissolution of calcareous planktonic foraminiferal shells during the formation of the fossilized assemblages. In exceptional cases this change may also represent a real palaeoenvironmental change. If so, it is necessary to analyze the composition of planktonic foraminiferal assemblages.

5.2. Environmental Setting Derived from Benthic Foraminiferal Ecological Groups

It is well documented that the main factors controlling the distribution of foraminifera are two inversely related parameters, the flux of organic matter to the sea floor and the oxygen concentration of the bottom–water and sediment pore-water (Lutze & Coulbourn, 1984; Van der Zwaan et al. 1999; Linke & Lutze, 1993; Jorissen et al., 1992, 1995; Jorissen, 1999). In particular, changes in oxygen concentrations at the sediment-water interface play a major role in controlling benthic foraminiferal assemblages with some species exhibiting a tolerance to hypoxia and opportunistic life histories, and developing high population densities in some low oxygen environments, particularly in areas associated with high organic enrichment (Phleger & Soutar, 1973; Bernhard, 1986). Generally, in low-oxygen environments, benthic foraminifera are of ecological significance as they dominate the eukaryotic biomass in the benthic ecosystem (Moodley et al. 1997; Gooday et al. 2000a).

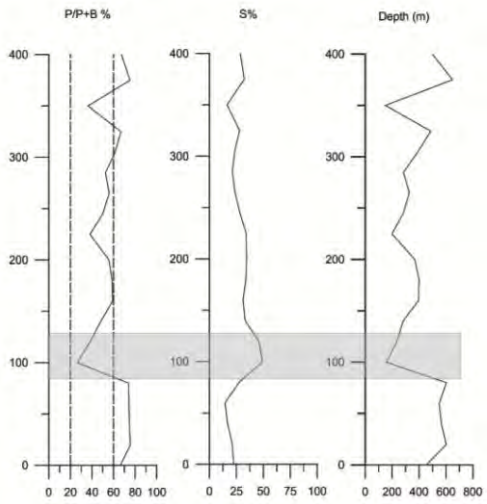

Figure 3 - Planktonic/Benthic ratio together with well-established redox front dwelling taxa and palaeobathymetric curve.

Many authors have noted the dominance in modern and anoxic low-oxygen environments of particular "opportunistic", r-selected species, (Bernhard, 1986; Mackensen & Douglas, 1989; Koutsoukos et al., 1990; Alve & Bernhard, 1995; Bernhard et al., 1997; Jorissen et al., 1998; Bernhard & Bowser, 1999; Fontanier et al., 2002). These taxa also occur in deep-infaunal microhabitats in well-oxygenated settings.

In general, there is a direct relationship between the level of oxygenation of the water and the mode of life of the benthic foraminifera, so that, in low oxygen conditions, deep infauna taxa, also known as environmental stress markers, predominate (van Hinsbergen et al., 2005). This group of taxa constitutes the "*well-established redox front dwelling taxa*" of Rogerson et al. (2006) and consists of *Bolivina* spp. except *B. plicatella* and *B. pseudoplicata*, *Bulimina* spp. (excluding the costate species); *Uvigerina* spp. (*U. semiornata* excluded); *Rectuvigerina* spp., *Valvulineria* spp., *Cancris* spp., *Fursenkoina* spp., *Stainforthia* spp., *Globobulimina* spp. and *Chilostomella* spp.

In this study, the percentage value of the "*well-established redox front dwelling taxa*" (Fig. 3) is used as an approximate measure of the degree of oligotrophy/eutrophy and related oxygen level in the studied record, based on data derived from modern oceans (Corliss & Chen, 1988; Rusoff & Corliss, 1992; Kaiho, 1994) and similarly used for interpreting trophic and oxygen conditions in ancient seas (Thomas, 1990; Widmark, 1995).

In the studied record, moderate values of stress markers (16 to 50%) with the co-occurrence of oxiphylic species suggest more or less oligotrophic, well oxygenated bottom waters, where a significant amount of food is consumed at the sediment surface and only a smaller portion enters the sediment, restricting deep infaunal life. The palaeoenvironment, with mixed sub-/dysoxic and oxiphylic species, was characterized by well-aerated bottom water with a redox boundary a few centimetres from the seafloor which was colonized by sub- and dysoxic foraminifers.

Based on our data and using the model proposed by Jorissen et al. (1995) to explain the microhabitats in terms of trophic conditions and oxygen concentrations, extreme oligotrophic and extreme eutrophic environments may be excluded. In the former, all metabolizable food would be consumed at the sediment surface and the underlying sediment would contain only small quantities of (refractory) organic material that would cause the absence of infaunal foraminifera. In the latter, epifaunal foraminifera are absent due to decreased oxygen content caused by the decomposition of organic matter. At the same time, opportunistic infaunal foraminifera shift to or near the sediment surface following the shift of the redox front towards the sediment surface.

6. Conclusions

The present study was undertaken to provide an indication of the palaeobathymetric range of deposition of the basal part of the Kalamavka Formation, located in the Ierapetra basin in eastern Crete. The biostratigraphic analysis based on planktonic foraminifera indicated a Lower Tortonian age (between 11.54 and 11.21 Ma). This time interval is considered very crucial for the studied area as it coincides with the beginning of the fragmentation stage of the Aegean microplate (break - up stage), during extensional movements and thus the beginning of the "modern history" of the Aegean region.

Based on the bathymetric/palaeobathymetric calculations, the Kalamavka section has been deposited at an estimated palaeodepth corresponding to the outer shelf to the middle bathyal zone (150- 600 m). Partly, a middle shelf depth of deposition was attained.

The fluctuations of the frequency values of stress-marker species indicated oligotrophic to mesotrophic conditions and well-oxygenated bottom waters..

7. Acknowledgments

Financial support for this research was provided by the Research Project 70/4/11078 of the University of Athens.

8. References

Alve E. and Bernhard J.M. 1995. Vertical migratory response of benthic foraminifera to controlled oxygen concentrations in an experimental mesocosm, *Marine Ecology Progress Series*, 116, 137-151.

Angelier J. 1979. Recent Quaternary tectonics in the Hellenic arc: Examples of geological observations on land, *Tectonophysics,* 52, 267–275.

Aubouin J., Bonneau M., Davidson J., Leboulanger J., Matesco P. and Zambetakis A. 1976. Esquisse structurale de l'arc egeen externe: des Dinarides aux Taurides, *Bulletin de la Societe Geologique de France*, Serie 7 (18), 327– 336.

Bernhard J.M. and Bowser S.S. 1999. Benthic foraminifera of dysoxic sediments: chloroplast sequestration and functional morphology, *Earth-Science Reviews*, 46 (Suppl.), 149-165.

Bernhard J.M. 1986. Characteristic assemblages and morphologies of benthic foraminifera from anoxic, organic-rich deposits - Jurassic through Holocene, *Journal of Foraminiferal Research*, 16, 207-215.

Bernhard J.M., Sen Gupta B.K. and Borne P.F. 1997. Benthic foraminiferal proxy to estimate dysoxic bottom-water oxygen concentrations: Santa Barbara basin, Us Pacific continental margin, *Journal of Foraminiferal Research*, 27, 301-310.

Boltovskoy E. and Wright R. 1976. *Recent Foraminifera*, The Hague, 532pp.

Caruso A., Sprovieri M., Bonnano A. and Sprovieri R. 2002. Astronomical calibration Serravallian-Tortonian Case Pelacani section (Sicily, Italy), in S.M. Iaccarino (ed.), Integrated Stratigraphy and Palaeoceanography of the Mediterranean Middle Miocene, *Rivista Italiana di Palaeontologia e Stratigrafia*, 108, 297-306.

Corliss B.H. and Chen C. 1988. Morphotype patterns of Norwegian Sea deep-sea benthic foraminifera and ecological implications, *Geology*, 16, 716-719.

Dermitzakis M.D. 1969. Geological researches of the Neogene Deposits of the Hierapetra Province in Crete, *Annales Geologiques des Pays Helleniques,* 21, 342–484.

Dermitzakis M.D., 1978. Stratigraphy and sedimentary history of the Miocene of Zakynthos (Ionian Islands, Greece), *Annales géologique des Pays helléniques,* 29, 47-186.

Di Stefano E., Bonomo S., Caruso A., Dinares-Turell J., Foresi L., Salvatorini G. and Sprovieri R. 2002. Calcareous-plankton bio-events in the Miocene Case Pelacani section (Southeastern

Sicily, Italy). In S.M. Iaccarino (ed.), Integrated Stratigraphy and Palaeoceanography of the Mediterranean Middle Miocene, *Riv. Ital. di Palaeontologia e Stratigr.*, 108, 307-324.

Drinia H. 1989. Shallow marine sandy carbonate clastic sedimentation in a forearc basin, (Kalamavka Formation, Late Serravallian-Early Tortonian, E. Crete), *Master thesis*, University of East Anglia, Norwich, U.K. 122 pp.

Drinia H., Antonarakou A. and Kontakiotis G. 2008. On the occurrence of Early Pliocene marine deposits in the Ierapetra Basin, Eastern Crete, Greece, *Bull. of Geosciences,* 83(1), 63–78.

Fontanier C., Jorissen F.J., Licari L., Alexandre A., Anschutz P.M. and Carbonel P. 2002. Live benthic foraminiferal faunas from the Bay of Biscay: faunal density, composition, and microhabitats, *Deep-Sea Research I*, 49, 751-785.

Foresi L.M., Bonomo S., Caruso A., Di Stefano A., Di Stefano E., Iaccarino S. M., Lirer F., Salvatorini G. and Sprovieri R. 2002. High resolution calcareous plankton biostratigraphy of the Serravallian succession of the Tremiti Islands (Adriatic Sea, Italy), in: S.M. Iaccarino (ed.), ntegrated Stratigraphy and Palaeoceanography of the Mediterranean Middle Miocene, *Rivista Italiana di Palaeontologia e Stratigrafia*, 108, 257–273.

Fortuin A.R. 1977. Stratigraphy and sedimentary history of the Neogene deposits in the Ierapetra region, Eastern Crete. *GUA Paper of Geology*, 1(8).

Fortuin AR. 1978. Late Cenozoic history of eastern Crete and implications for the geology and geodynamics of the southern Aegean Sea, *Geologie en Mijnbouw*, 57, 451–464.

Gibson T.G. 1989. Planktonic/benthonic foraminiferal ratios: modern patterns and Tertiary applicability, *Mar. Micropalaeontol*., 15, 29-52.

Gooday A.J., Bernhard J.M., Levin L.A. and Suhr S. 2000. Foraminifera in the Arabian Sea oxygen minimum zone and other oxygen deficient settings: taxonomic composition, diversity, and relation to metazoan faunas, *Deep-Sea Research II,* 47, 25-54.

Gradstein F.M. 1973. The Neogene and Quarternary deposits in the Sitia district of eastern Crete, *Annales Geologiques des Pays Helleniques,* 24, 527–572.

Hall R., Audley-Charles M.G. and Carter, D.J. 1984. The significance of Crete for the evolution of the Eastern Mediterranean, in: Dixon, J.E., Robertson, A.H.F. (Eds.), The Geological Evolution of the Eastern Mediterranean, *Special Publication-Geological Society of London*, 17, 499– 516.

Hilgen F.J., Abdul Aziz H., Krijgsman W., Raffi I. and Turco E. 2003. Integrated stratigraphy and astronomical tuning of the Serravallian and lower Tortonian at Monte dei Corvi (Middle–Upper Miocene, northern Italy), *Palaeogeography Palaeoclimatology Palaeoecology*, 199, 229–264

Hilgen F.J., Krijgsman W., Raffi I., Turco E. and Zachariasse W.J. 2000. Integrated stratigraphy and astronomical calibration of the Serravallian/Tortonian boundary Section at Monte Gibliscemi (Sicily, Italy), *Marine Micropalaeontology*, 38, 181–211.

Hohenegger J. 2005. Estimation of environmental palaeogradient values based on presence/absence data: a case study using benthic foraminifera for palaeodepth estimation, *Palaeogeography Palaeoclimatology Palaeoecology*, 217, 115-130.

Iaccarino S. 1985. Mediterranean Miocene and Pliocene planktic Foraminifera, in Bolli H.M., Saunders J.B. & Perch-Nielsen K. (eds), *Plankton Stratigraphy,* Cambridge University Press, London, 283-314.

Iaccarino S. M., Lirer F., Bonmo S., Caruso A., Di Stefano A., Di Stefano E., Foresi L. M., Mazzei R., Salvatorini G., Sprovieri R. and Turco E. 2004. Astrochronology of Late Middle Miocene Mediterranean sections. In B. D' Argenio, A.G. Fischer, I. Premoli-Silva, H. Weissert and V. Ferreri (eds), *Cyclostratigraphy: An Essay of Approaches and Case Histories, Society of Sedimentary Geology*, 81, 25-42.

Jorissen F.J. 1999. Benthic foraminiferal microhabitats below the sediment-water interface. In: Sen Gupta, B.K., ed., *Modern Foraminifera*, Kluwer Academic Press, London, 161-179

Jorissen F.J., Barmawidjaja D.M., Puskaric S. and Van der Zwaan G.J. 1992. Vertical distribution of benthic foraminifera in the northern Adriatic Sea: the relation with the organic flux, *Marine Micropalaeontology,* 19, 131-146.

Jorissen F.J., de Stigter H.C. and Widmark J.G.V. 1995. A conceptual model explaining benthic foraminiferal microhabitats, *Marine Micropalaeontology,* 26, 3-15.

Jorissen F.J., Wittling I., Peypouquet J.P., Rabouille C. and Relexans J.C. 1998. Live benthic foraminiferal faunas off Cap Blanc, NW-Africa: community structure and microhabitats, *Deep-Sea Research I*, 45, 2157-2188.

Kaiho K. 1994. Benthic foraminiferal dissolved-oxygen index and dissolved-oxygen distribution patterns, palaeocommunities levels in the modern ocean, *Geology*, 22, 719-722.

Koutsoukos E.A.M., Leary P.N. and Hart M.B. 1990. Latest Cenomanian – earliest Turonian low-oxygen tolerant benthonic foraminifera: a case-study from the Sergipe basin (N.E. Brazil) and the western Anglo-Paris basin, *Palaeogeography Palaeoclimatology Palaeoecology*, 77, 145-177.

Le Pichon X. and Angelier J. 1979. The Hellenic arc and trench system: a key to the neotectonic evolution of the Eastern Mediterranean area, *Tectonophysics*, 60, 1-42.

Linke P. and Lutze, G.F. 1993. Microhabitat preferences of benthic foraminifera – a static concept or a dynamic adaptation to optimize food acquisition, *Marine Micropalaeontology,* 20, 215-234.

Lirer F., Caruso A., Foresi L.M., Iaccarino S. and Iacumin P. 2004. Palaeoclimatic changes in the Serravallian record of the Mediterranean area. In R. Coccioni, S. Galeotti and F. Lirer (eds), Proceedings of the first Meeting of Environmental Micropalaeontology for Young Italian Researcher, *Grybowski Foundation Special Publication*, 9, 77-96.

Lirer F., Caruso A., Foresi L.M., Sprovieri M., Bonomo S., Di Stefano A., Di Stefano E., Iaccarino S. M., Salvatorini G., Sprovieri R. and Mazzola S. 2002. Astrochronological calibration of the Upper Serravallian/Lower Tortonian sedimentary sequence at Tremiti Islands (Adriatic Sea, Southern Italy), in: Iaccarino S. (ed.), Integrated Stratigraphy and Palaeoceanography of the Mediterranean Middle Miocene, *Rivista Italiana di Palaeontologia e Stratigrafia*, 108, 241-256.

Lutze G.F. and Coulbourn W.T. 1984. Recent benthic Foraminifera from the continental margin of northwest Africa: community structure and distribution, *Marine Micropalaeontology*, 8, 361-401.

Mackensen A. and Douglas R.G. 1989. Down-core distribution of live and deas deepwater benthic foraminifera in box cores from the Weddell Sea and the California continental borderland, *Deep-Sea Research I*, 36, 879-900.

Meulenkamp J.E. 1985. Aspects of the Late Cenozoic evolution of the Aegean region, 307–321. In Stanley, D.J. and Wezel, F.C. (eds) *Geological evolution of Mediterranean Basin*, Springer-Verlag, New York.

Meulenkamp J.E. and Hilgen, F. J. 1986. Event stratigraphy, basin evolution and tectonics of the Hellenic and Calabro-Sicilian arcs, In Wezel, F.C. (ed.) *The origin of arcs*, Elsevier Science Publishers B.V., 327–350.

Meulenkamp J.E., Jonkers H.A. and Spaak P. 1979a. Late Miocene to Early Pliocene development of Crete, *Proceedings of the 6th Colloquium of the Geology of the Aegean Region*, Athens 1, 137–149.

Meulenkamp J.E., Dermitzakis M., Georgiadou-Dikeoulia E., Jonkers H.A. and Boger H. 1979b. *Field Guide to the Neogene of Crete*. 32 pp. Publications of the Department of Geology and Palaeontology, University of Athens.

Moodley L., Van der Zwaan G.J., Herman P.M.J., Kempers L. and Van Breugel P. 1997. Differential response of benthic meiofauna to anoxia with special reference to Foraminifera (Protista: Sarcodina), *Marine Ecology Progress Series,* 158, 151-163.

Murray J.W. 1976. Comparative studies of living and dead benthic foraminiferal distributions. In: Hedley R.H., Adams C.G. (Eds.), Foraminifera, Academic Press.Valchev, B. 2003. On the potential of Small Benthic Foraminifera as Palaeoecological Indicators: Recent Advances, *Annual of University of Mining and Geology*, 46, Geology and Geophysics, 189-194.

Murray J.W. 1991. *Ecology and Palaeoecology of Benthic Foraminifera*. 397 pp. Longman Harlow, Harlow.

Nikolaev S.I, Berney C., Fahrni J.F., Bolivar I., Polet S., Mylnikov A.P., Aleshin V.V., Petrov N.B. and Pawlowski J. 2004. The twighlight of Heliozoa and rise of Rhizaria, an emerging supergroup of amoeboid eukaryotes, *Proceedings of the National Academy of Sciences of the United States of America,* 101, 8066-8071.

Peters J.M. 1985. Neogene and Quarternary vertical tectonics in the south Hellenic arc and their effect on concurrent sedimentation processes, GUA – *Papers of Geology,* 1, 1–247.

Pipponzi G., Cosentino D. and Gliozzi E. 2004. Upper Messinian Lago-Mare deposits in the stratigraphy of the Messara Basin (central Crete, Greece), *4th International Congress "Environment and Identity in the Mediterranean. Session The Messinian Salinity crisis revisited"*, Corte (Corsica), 19–25 Luglio 2004, 70.

Pirazzoli P.A., Thommeret J., Thommeret Y., Laborel J. and Montaggioni L.F. 1982. Crustal block movements from Holocene shorelines: Crete and Antikythira (Greece), *Tectonophysics,* 86, 27–43.

Pflum C.E. and Frerichs W.E. 1976. Gulf of Mexico Deep-Water Foraminifera, *Cushman Foundation for Foraminiferal Research*, Special Publication, 14, 1-124.

Phleger F.B. and Soutar A. 1973. Production of benthic foraminifera in three east Pacific oxygen minima, *Micropalaeontology,* 19, 110-115.

Postma G. and Drinia H. 1993. Architecture and sedimentary facies evolution of a marine expandinghalf-graben, (Crete, Late Miocene), *Basin Research,* 5, 103-124.

Rogerson M., Kouwenhoven T.J., Van Der Zwaan G.J., O'Neill B.J., Van Der Zwan C.J., Postma G., Kleverlaan K. and Tijbosch H. 2006. Benthic foraminifera of a Miocene canyon and fan, *Marine Micropalaeontology,* 60, 295–318.

Rosoff D.B. and Corliss B.H. 1992. An analysis of Recent deepsea benthic foraminiferal morphotypes from the Norwegian and Greenland seas, *Palaeogeography Palaeoclimatology Palaeoecology*, 91, 13-20.

Sen Gupta B.K. and Machain-Castillo M.L. 1993. Benthic foraminifera in oxygen-poor habitats, *Marine Micropalaeontology*, 20, 183–201.

Speijer R.P. and Schmitz B. 1998. A benthic foraminiferal record of Palaeocene sea level and trophic/redox conditions at Gebel Aweina, Egypt, *Palaeogeography Palaeoclimatology Palaeoecology*, 137, 79-101.

Thomas E. 1990. Late Cretaceous through Neogene deepsea benthic foraminifers (Maud Rise, Weddell Sea, Antarctica), *Proceedings of the Ocean Drilling Program, Scientific Results*, 113, 571-594.

Valchev B. 2003. On the potential of Small Benthic Foraminifera as Palaeoecological Indicators: Recent Advances.- Ann. UMG, 46, Part I – *Geol. and Geophys*., 51-56.

Van der Zwaan G.J., Duijnstee I.A.P., den Dulk M., Ernst S.R., Jannink N.T. and Kouwenhoven T.J. 1999. Benthic foraminifers: proxies or problems? A review of palaeoecological concept, *Earth-Science Reviews,* 46, 213-235.

Van der Zwaan G.J., Jorissen F.J. and De Stigter H.C. 1990. The depth dependency of planktonic/benthonic foraminiferal ratios: constraints and applications, *Marine Geology*, 95, 1-16.

Van Hinsbergen D.J.J., Kouwenhoven T.J. and Van der Zwaan G.J. 2005. Palaeobathymetry in the backstripping procedure: Correction for oxygenation effects on depth estimates, *Palaeogeography Palaeoclimatology Palaeoecology*, 221, 245-265.

Vella P. 1962. Determining Depths of New Zealand Tertiary Seas, *Tuatara*, 10, 19-39.Speijer, R.P. & Schmitz, B. 1998. A benthic foraminiferal record of Palaeocene sea level and trophic/redox conditions at Gebel Aweina, Egypt, *Palaeogeography, Palaeoclimatology, Palaeoecology*, 137, 79-101.

Widmark J.G.V. 1995. Multiple deep-water sources and trophic regimes in the latest Cretaceous deep sea: evidence from benthic foraminifera, *Mar. Micropalaeontol*., 26, 361-384.

Zachariasse W.J. 1975. Planktonic foraminiferal biostratigraphy of the Late Neogene of Crete (Greece), *Utrecht Micropalaeontological Bulletin,* 11, 1–171.

Δελτίο της Ελληνικής Γεωλογικής Εταιρίας, τομ. XLVII , 2013
Πρακτικά 13ου Διεθνούς Συνεδρίου, Χανιά, Σεπτ. 2013

Bulletin of the Geological Society of Greece, vol. XLVII 2013
Proceedings of the 13th International Congress, Chania, Sept. 2013

EASTERN MEDITERRANEAN FORAMINIFERAL PALAEOECOLOGICAL RESPONSE TO MID- LATE PLIOCENE CLIMATIC REGIME: A PRELIMINARY NOTE

Drinia H.[1], Antonarakou A.[1], Mihalakopoulos S.[1] and Tsiolakis E.[2]

[1] National and Kapodistrian University of Athens, Faculty of Geology and Geoenvironment, Department of Hist. Geology - Palaeontology, cntrinia@geol.uoa.gr, aantonar@geol.uoa.gr, archaeodiscus@gmail.com

[2]Geological Survey of Cyprus, etsiolakis@gmail.com

Abstract

The main objective of this work is to investigate the climatic influence on the sedimentation during mid to late Pliocene in Cyprus island. For this reason, a section located in Pissouri sub-basin, southern Cyprus, was chosen to be studied. The section comprises a nearly uninterrupted succession of marine sediments, dominated by grey marls, which are cyclically alternating with yellowish silty marls. The identification of age diagnostic planktonic foraminifera suggests a mid to upper Pliocene age. The calculated faunal parameters document cyclic fluctuations consistent with shifts in such climate belts. A good age resolution of the cycles and an indication of sedimentation rate would be required in order to connect cyclicity to orbital perturbations.

Key words: *mid to late Pliocene, foraminifera, biostratigraphy, palaeoecology, clim ate, Cyprus.*

Περίληψη

Ο κύριος στόχος της εργασίας αυτής είναι η διερεύνηση της κλιματικής επίδρασης στην ιζηματογένεση του Μέσου –Ανώτερου Πλειοκαίνου στη νήσο Κύπρο. Για το λόγο αυτό, επιλέχθηκε να μελετηθεί μια γεωλογική τομή της υπολεκάνης του Πισσουρίου στη νότια Κύπρο. Η τομή περιλαμβάνει μια σχεδόν αδιάκοπη εναλλαγή θαλάσσιων ιζημάτων, όπου επικρατούν γκρι μάργες, οι οποίες κυκλικά εναλλάσσονται με κιτρινωπές ιλυώδεις μάργες. Η βιοστρωματογραφική ανάλυση με βάση τα πλαγκτονικά τρηματοφόρα έδειξε ηλικία Μέσο-Ανώτερο Πλειόκαινο. Οι πανιδικές παράμετροι που υπολογίστηκαν επιδεικνύουν κυκλικές διακυμάνσεις που συνάδουν με τις αλλαγές στις ζώνες του κλίματος. Υψηλής ευκρίνειας βιοστρωματογραφική ανάλυση και υπολογισμός της ταχύτητας ιζηματογένεσης απαιτούνται προκειμένου να συνδεθούν οι κυκλικες διακυμάνσεις με τις τροχιακές παραμέτρους.

Λέξεις κλειδιά: *Μέσο-Ανώτερο Πλειόκαινο, Τρηματοφόρα, Βιοστρωματογραφία, Παλαιοοικολογία, κλίμα, Κύπρος.*

1. Introduction

The Mediterranean basin is one of the most appealing natural laboratories in the world to study geodynamic and palaeoclimatic processes on different scales (e.g. Pinardi & Masetti, 2000; Krijgsman, 2002). Sediments in the Mediterranean Sea form an important archive for understanding climate and environmental conditions during the geological past. This is mainly due to its palaeo – latitudinal position in combination with its semi – enclosed, land – locked configuration (Krijgsman, 2002).

At present, the Mediterranean Sea is characterized by geographical variations in oceanographic conditions: the eastern part of the basin is characterized by warm and oligotrophic surface waters whereas in the western part the surface waters are colder and richer in nutrients (Béthoux et al., 1999; Pinardi & Masetti, 2000). This modification in the hydrological condition is mirrored in the faunal distribution (Thunell, 1978; Pujol & Vergnaud-Grazzini, 1995).

Cyprus with an area of 9,251 km² is the third biggest island in the Mediterranean Sea, and the biggest island in Eastern Mediterranean region. The mid- to low- latitude positioning of Cyprus within the eastern Mediterranean places the island between high latitude obliquity and mid to low latitude precessional impact. Previous studies have shown that the critical location of Cyprus within the Mediterranean semi-enclosed basin and between two major oscillatory atmospheric cells makes the area integrally sensitive to the smallest of climatic perturbations (Casford et al., 2003; Marino et al., 2007; Rohling et al., 2009).

This study constitutes a preliminary note on the mid to late Pliocene foraminiferal paleoecology in Cyprus. Mid-Pliocene is the most recent interval of sustained global warmth, which can be used to examine conditions predicted for the near future. Foraminifera are sensitive indicators of seafloor and water column ecology and therefore provide important archives of climate and ocean state interactions.

2. Geological Setting and Sedimentology

The sedimentary succession of Cyprus is affected by a complex uplift history, which is attributed to its unstable position in a fore-arc setting of the convergence zone between Africa and Eurasia (e.g. Robertson, 1998; Orszag-Sperber et al., 1989).

Four sedimentary sub-basins developed in this area during Miocene time, the Polemi, Pissouri, Limassol and Psematismenos basins (Figure 1, Orszag-Sperber et al., 1989; Robertson et al., 1995; Stow et al., 1995; Krijgsman et al., 2002).

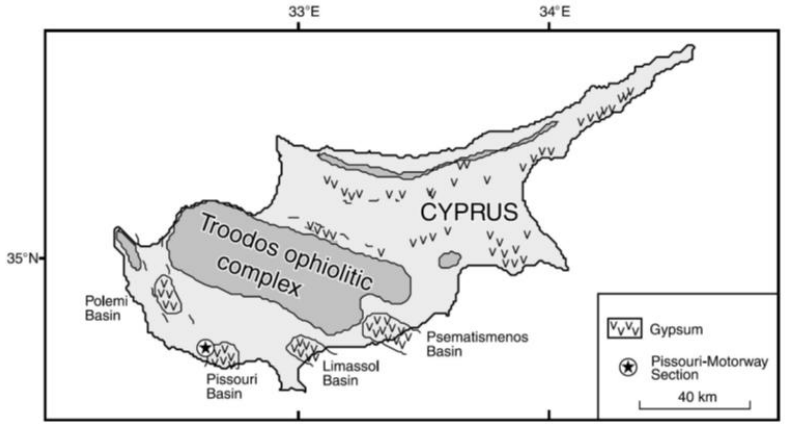

Figure 1 - Geological Sketch map of the Cyprus Island (modified after Robertson et al., 1991; Stow et al., 1995; Krijgsman et al., 2002; Kouwenhoven et al., 2006).

The Pissouri Basin contains one of the most suitable sedimentary sequences for studying the onset of the MSC in the Eastern Mediterranean (Krijgsman et al., 2002). It provides one of the most continuous sedimentary successions related to the MSC, comprising the pre-evaporitic, evaporitic and post-evaporitic deposits which cover the period from the late Tortonian up to the early Pliocene (Krijgsman et al., 2002; Orszag-Sperber et al., 2009). Palaeodepth estimations in the Pissouri Section are based on foraminifera, bivalves and gastropods (Rouchy et al. 2001; Krijgsman et al., 2002; Kouwenhoven et al. 2006). A progressive shallowing occurred from approximately 500 m in depth during the Tortonian and Early Messinian to very shallow water conditions during the late Messinian.

With the beginning of the Pliocene, deeper water conditions were re-established (Rouchy et al., 2001; Krijgsman et al., 2002). The subsequent tectonic opening of the Strait of Gibraltar in the early Pliocene (Rohling et al., 2009) and ensuing marine transgression (Rouchy et al., 2001; Soria et al., 2008) signifies the initiation of sedimentation (marine, grey clayey silts). Since this episode, a general pattern of regression is documented in the sedimentary succession of Cyprus manifested in the transition from marine clayey silts through to fan delta deposits, ultimately culminating in raised beaches and alluvial fans. The Pliocene-Pleistocene sedimentary fill of Pissouri basin is interpreted as representing a fan-delta complex with braid channels, which shows a broadly progradational sequence influenced by both sea-level fluctuation and tectonic activity (Stow et al., 1995).

The studied section (Figure 2) is located in the centre of the Pissouri sub-basin, in southern Cyprus (Pissouri basin) and contains a relatively thick succession (thickness of ~42 m) of rhythmically bedded marls, which constitute regularly bedded, fining upward packages. Each package typically has a sharp-based fine-grained, frequently laminated sandstone/siltstone bed fining upwards into claystone. It constitutes the stratigraphic continuation of the early Pliocene Pissouri South section studied by Triantaphyllou et al. (2008, 2010).

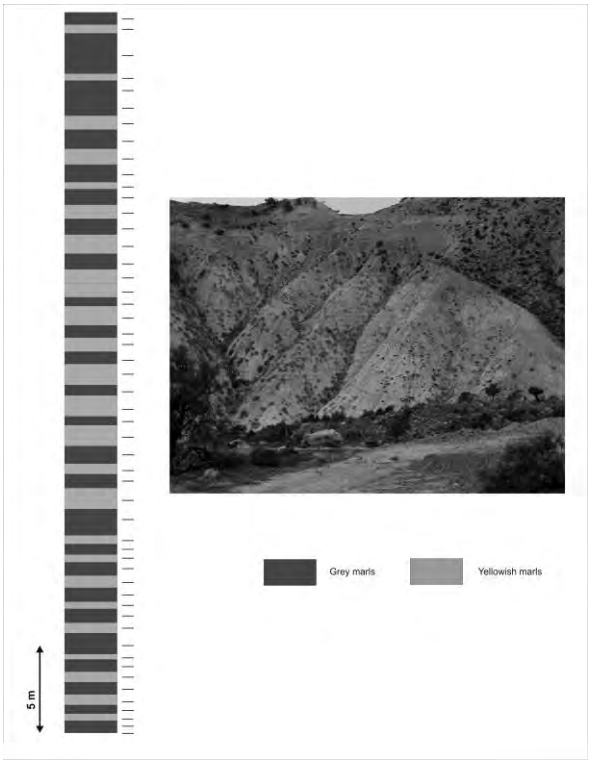

Figure 2 - Lithology and position of samples of the studied section.

3. Materials and Methods

A total of 52 samples collected at 0.5 m to 1 m intervals, were examined from the micropalaeontological point of view.

Samples were processed for foraminifera using standard separation techniques. Each sample was split into fractions, depending on sample size. A minimum of 300 complete specimens per sample were collected.

Based on the faunal counts, benthic foraminiferal numbers (BFN; number of specimens per gram dry sediment) were calculated. This number gives information on the taphonomy of the original living assemblage, the oxygen level (e.g. Ernst & Van der Zwaan, 2004), the energy level in which the sediments were deposited (high abundance in low energy), and to a minor extent the productivity or organic flux (Ernst & Van der Zwaan, 2004). The percentage of planktonic species in the total foraminiferal association (%P) was calculated as 100*P/(P+B), in order to reconstruct palaeodepth and track sea-level changes. To estimate the depositional depth of the sediments, the general relationship between depth and the fraction of planktonic foraminifera with respect to the total foraminiferal population (%P) (Van der Zwaan et al., 1990) was used, following sample selection and counting procedures described in Van Hinsbergen et al., (2005). If samples with evidence for downslope transport and carbonate dissolution are discarded, the relationship between %P and depth of Van der Zwaan et al. (1990) allows the estimation of the depositional depth of sediments with approximately 50 m of uncertainty at levels of a few hundreds of metres, to 150 m at depths around 1 km. Reconstruction of bottom water conditions concerning oxygen content was based on the presence of the dysoxic indicators in the assemblage. For this purpose, the percentage occurrence of the well established redox front dwelling taxa (*Bulimina exilis, Bulimina costata, Globobulimina* spp., *Bolivina spathulata/dilatata*) which according to Rogerson et al. (2006) is related to disturbance and/or environmental stress, was calculatet.

4. Results and Analysis

4.1. Age Determination

Biostratigraphic analysis was performed based on the qualitative analysis of planktonic foraminifera species recognized into the faunal assemblages of the entire material.

Planktonic foraminiferal assemblages are dominated by high abundances of *G. ruber, G. obliquus, G. extremus, G. apertura, G. trilobus-sacculifer* and *O. universa*. High abundances are also recorded for *Neogloboquadrina* sp. dextral coiled specimens, whereas presence and/or absence of the species *Sphaeroidinellopsis*, *G. puncticulata*, and *G. crassaformis* is used to detect the biostratigraphic framework of the section following the zonation of Cita (1973, 1975), emended by Sprovieri (1993).

Six planktonic foraminiferal bioevents were recognized: (1) appearance of *Globorotalia crassaformis*, (2) appearance of *Globorotalia bononiensis*, (3) LO of *Shaeroidinellopsis* s.l., (4) FO of *Neogloboquadrina atlantica*, (5) LO of *Neogloboquadrina atlantica* and (6) LO of *G. bononiensis*.

From the biostratigraphic point of view the studied interval lies above the Pissouri section of Triantaphyllou et al. (2008, 2010). The quantitative analysis of planktonic foraminiferal assemblages of the studied section revealed that up to 14.4 m *Sphaeroidinellopsis* s.l. is present in all the samples. *Globorotalia crassaformis* appears in our data at 10 m, corresponding to the *G. crassaformis* reappearance bioevent (3.35 Ma, Lourens et al., 1996; 2004). This event predates the appearance of *G. bononiensis* (at 10.5 m), dated at 3.31 Ma (Lourens et al., 1996; 2004). These bioevents constitute the typical association of MPL4b biozone. The last occurrence of *Sphaeroidinellopsis* is recorded some cm above this level, at 14.4 m, dated at 3.19Ma (Lourens et al., 2004) and notes the transition to MPL5a subzone. *Neogloboquadrina atlantica atlantica* first

occurs at 20.5 m and it is commonly present up to 37.4 m. The occurrence of this species in the Mediterranean Pliocene has been dated from 2.72 Ma to 2.41 Ma (Lourens et al., 2004). At the same level of the studied interval, the last occurrence of *G. bononiensis* is recorded, dating the top of the section at 2.41 Ma, (Lourens et al., 2004). Consequently, the section falls into the Piacenzian-early Gelasian Stages, ending in MPL5a subzone.

4.2. Faunal Parameters

Benthic and planktonic foraminifera are present in all samples and show highly variable temporal changes in assemblage composition, relative abundance and preservation. Moreover, the common occurrence of planktonic foraminifera, throughout the succession, suggests open marine connection to a rather oceanic realm. The taxonomic concept of each individual species is beyond the scope of this study but it will be discussed in detail in Drinia et al. (in prep.).

BFN remains relatively stable exhibiting low values apart from the stratigraphic level of 11 m, where BFN shows an abrupt increase (up to 80,000, Figure 3). This horizon also contains other shallow-water debris, such as echinoid spines and gastropods and is interpreted as a turbidite sourced from a shallower water environment. Another reason for this abrupt increase in the abundance of benthic foraminifera could have a secondary, taphonomic origin, which would imply that the original benthic foraminiferal assemblage is best preserved in this level and that the remainder of the section does suffer from preferential dissolution. However, the actual assemblage quality (in situ fauna) is identical to other levels, and there is no evidence that dissolution-sensitive species are better preserved in this level.

Well-established redox front dwelling taxa S% dominate throughout the succession, strongly fluctuating in the range of 0.94–96.54%. These taxa practice an opportunistic life strategy, and are able to tolerate periodic reductions in dissolved oxygen contents by modifying their microhabitat from infaunal to epifaunal (Jorissen et al., 1992; Kaiho, 1994). In particular and according to Van der Zwaan (1982), Verhallen (1991), Jorissen et al. (1992), Kaiho (1994) and Loubère (1996, 1997), this group of species tends to increase in abundance when the influx of terrigenous organic matter dominates the environment. It shows opportunistic behaviour and a tolerance to dysoxia, but also to elevated bottom water salinity. The highly shifting abundances of redox fauna species, observed in the lower part of the record (Figure 3) may reflect cyclic changes in sediment input and/or circulation.

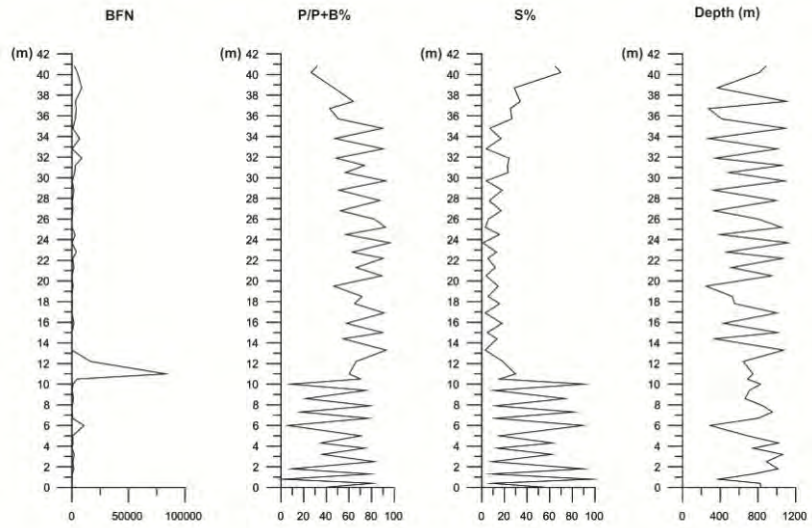

Figure 3 - Calculated benthic foraminiferal faunal parameters of the studied section together with palaeobathymetry.

The percentage (%) of planktonic foraminifera is one of the most consistent proxies to assess palaeo-water depths. It has been known for a long time that the percentage of planktonic foraminifera in modern sediments increases with water depth (e.g. Boltovskoy & Wright, 1976; Gibson, 1989; Van der Zwaan et al., 1990, 1999). Van der Zwaan et al. (1990, 1999) and Leckie et al. (1998) emphasized the significance of nutrients for the P/B ratio, in particular for benthic foraminifera. Because the density of planktonic and benthic foraminifera depends on the organic flux, and the amount of organic matter reaching the sea floor decreases with increasing water depth because of oxidation, the P/B ratio as anticipated has to increase with depth (Van der Zwaan et al., 1999). Other parameters such as temperature, salinity, substrate-type or circulation patterns may play a minor role.

In our record, the benthic and planktonic foraminifera relative abundance (P/B-ratio, Figure 3) ranges between 2.3 to 96.24%. A simple interpretation of this ratio using modern analogies (e.g. Gibson, 1989) points to very rapid changes in water-depth between middle shelf and lower bathyal, which is very unlikely and not supported by any other evidence. Hence, the ecologic reason for these enormous differences cannot be water-depth alone.

High fluctuations in the P/B ratio are interpreted as unstable conditions in the upper water layers. However, an increasing oceanic influence is implied by the increasing content of planktonic foraminifera. As bottom-water stress is developing, the P/B ratios are no longer reliable palaeodepth-indicators, since declining benthic faunas could erroneously suggest apparent deepening (Van der Zwaan et al., 1999).

Moreover, the high %P (>90%), observed in a number of samples does not seem realistic when compared with the benthic assemblages, which suggest that the palaeodepth of the succession studied was rather stable at around 300–500 m.

On the other hand, the abrupt declining of the P/B ratio in some intervals of the record may merely reflect periodic dilution of the autochthonous deep-water fauna with transported shallower faunas (e.g. Robertson, 1998). It is likely that, in these beds, some degree of faunal reworking has occurred, displacing shallow water taxa into deeper water faunas.

5. Discussion

As seen in Figure 3, the calculated foraminiferal parameters of mid-Pliocene Pissouri section document cyclic but irregular fluctuations. Numerous studies across the Mediterranean postulate a climatic control on cyclical alternations in marine and terrestrial successions, invoking a linkage with the changeable variations in the Earth's orbital parameters (e.g. Postma & Drinia,1993; Weltje & De Boer, 1993; Kroon et al., 1998; Van Vugt et al., 1998; Wehausen & Brumsack, 1999; Foucault & Mélières 2000; Lourens et al., 2001; Joannin et al., 2007; amongst others). Therefore, it is likely that the sediments of Cyprus should provide a relatively intact archive of past climatic variability, likely to be recognizable on orbital timescales.

Indeed, as seem in Figure 3, rhythmically recurrent deepening and shallowing is taking place, with a maximum palaeodepth recorded at 1119m and a minimum at 248m. Additionally, the geometry of the palaeobathymetric curve does not denote a stable trend of deepening or shallowing, but for the most part, particularly in the upper half of the section, has an approximately sinusoidal shape. Although the palaeobathymetric changes depicted in the palaeobathymetric curve, cannot be attributed solely to variations of the global sea level-as this cannot cause variations in bathymetry of more than 200m - however the almost constant periodicity and amplitude lead us to the conclusion that the alternating depth values recorded should rather be attributed to periodic climatic influences.

The dominance of infaunal benthic foraminifera and stress indicators (%S), suggests an ecologically stressed habitat (Nolet & Corliss, 1990; Jorissen et al., 1995; Kouwenhoven, 2000; Schmiedel et al., 2003; Drinia et al., 2005; Abu-Zied et al., 2008). Presumably the stressed

conditions are likely to be related to the influx of organic matter through freshwater input (e.g. analogous to periods of sapropel formation).

Palaeo-climatic changes enhanced palaeoproductivity and limited the availability of dissolved oxygen in bottom waters, temporarily establishing dysoxic conditions. Wetter and drier and/or cooler and warmer periods will be reflected on an orbital cyclicity within foraminiferal assemblages and facies changes. It is assumed that changes in foraminiferal ecology will reflect the orbital variations in atmospheric cells. An initial hypothesis, using the modern day climatic conditions as analogy, would predict that warm, dry conditions would be reflected through a dominantly oligotrophic foraminiferal assemblage, whilst cool, wet periods would favour the proliferation of eutrophic species.

A sapropel-like interval was deposited under these conditions. We maintain that the Pliocene sediments in the Pissouri Basin are probably linked to climate-driven changes in surface runoff (i.e. warmer temperatures and/or lower salinities), which influenced the levels of primary productivity. The implications of these hydrological changes would have had a profound influence on the local accumulation of sapropel-like sediments. According to Hilgen (1991), individual sapropels in the eastern Mediterranean can be correlated with minima of the precessional cycle. Other studies support the precessional cycle as the dominant factor influencing the lower to upper Pliocene climatic evolution (Tiedemann et al. 1994). In the absence of high resolution stratigraphic control, we can only speculate as to the precise nature of astronomical forcing behind the brown-white marl cycles studied herein. Apparently, this is a characteristic event of the Eastern Mediterranean Basin, which points to a major modification of the oceanographic conditions with the eutrophic situation becoming widely distributed.

It may be argued that the cyclicity documented in the depositional systems could be the product of mechanisms other than climate, such as tectonics and/or autocyclicity.

Episodic tectonic movements are known to induce rhythmic deposition of sediments. However, it would be expected that features typical of structurally unstable regimes would accompany such an interpretation, perhaps in the form of syn-depositional faulting, deformation structures, abrupt facies changes and/or angular unconformities between successive cycles. These features are rare to absent within the successions, only occurring between major changes in depositional regime

6. Conclusions

Cyprus constitutes an area inherently sensitive to the smallest of climatic perturbations. In this study it is concluded that changing foraminiferal ecology is consistent with shifts in the climate belts. However, a good age resolution of the cycles and an indication of sedimentation rate would be required.

7. Acknowledgments

Financial support for this research was provided by the Research Project 70/4/11078 of the University of Athens.

8. References

Abu-Zied R.H., Rohling E.J., Jorissen F.J., Fontanier C., Casford J.S.L. and Cooje S. 2008. Benthic foraminiferal response to changes in bottom-water oxygenation and organic carbon flux in the eastern Mediterranean during LGM to Recent times, *Marine Micropaleontology*, 67, 46–68.

Béthoux J.P., Gentili B., Morin P., Nicolas E., Pierre C. and Ruiz-Pino D. 1999. The Mediterranean Sea: a miniature ocean for climatic and environmental studies and a key for the climatic functioning of the North Atlantic, *Progress in Oceanography*, 44, 131–146.

Boltovskoy E., Wright R. (Eds.). 1976. *Recent Foraminifera*. Dr. W. Junk b.v., The Hague.

Casford J.S.L., Rohling E.J., Abu-Zied R. H., Fontanier C., Jorissen F. J., Leng M. J., Schmiedl G. and J. Thomson. 2003. A dynamic concept for eastern Mediterranean circulation and oxygenation during sapropel formation, *Palaeogeogr. Palaeoclimatol. Palaeoecol.,* 190, 103–119.

Cita M.B. 1973. Pliocene biostratigraphy and chronostratigraphy, in W.B.F. Ryan, K.J. Hsu et al, (eds), *Initial Reports of the Deep Sea Drilling Project*, v. 13. U.S. Government Printing Office, Washington, 1343-1379.

Cita M.B. 1975. Studi sul Pliocene e sugli strati di passaggio da1 Miocene al Pliocene VIII. Planktonic foraminiferal biozonation of the Mediterranean Pliocene deep sea record, revision, *Rivista Italiana di Paleontologia*, 81 (4), 527-544.

Drinia H., Koskeridou E. and Antonarakou A. 2005. Late Pliocene benthic foraminifera and mollusks from the Atsipades section, central Crete: paleoecological distribution and use in paleoenvironmental assessment, *Geobios*, 38(3), 315–324.

Ernst S.R. and Van Der Zwaan G.J. 2004. Effects of experimentally induced raised levels of organ-ic flux and oxygen depletion on a continental slope benthic foraminiferal community, *Deep –Sea Research,* 51, 1709-1739.

Foucault A. and Mélières F. 2000. Paleoclimatic cyclicity in central Mediterranean Pliocene sediments: The mineralogical signal, *Palaeogeog. Palaeoclimatol. Palaeoecol.,* 158, 311–323.

Gibson T.G. 1989. Planktonic/benthonic foraminiferal ratios: modern patterns and Tertiary applicability, *Marine Micropaleontology*, 15, 29–52.

Hilgen F.J. 1991. Astronomical calibration of Gauss to Matuyama sapropels in the Mediterranean and implication for the geomagnetic polarity time scale, *Earth Planet. Sci. Lett.,* 104, 226–244.

Joannin S., Quillévéré F., Suc J.P., Lécuyer C. and Martineau F. 2007. Early Pleistocene climate changes in the central Mediterranean region as inferred from integrated pollen and planktonic foraminiferal stable isotope analyses, *Quaternary Research*, 67, 264–274.

Jorissen F.J., Barmawidjaja D.M., Puskaric S. and Van der Zwaan G.J. 1992. Vertical distribution of benthic foraminifera in the northern Adriatic Sea: the relation with the organic flux, *Marine Micropalaeontology.,* 19, 131– 146.

Jorissen F.J., De Stigter H.C. and Vidmark J.V. 1995. A conceptual model explaining benthic foraminiferal microhabitats, *Marine Micropalaeontology*, 37, 67-76.

Kaiho K. 1994. Benthonic foraminiferal dissolved-oxygen index and dissolved levels in the modern ocean, *Geology,* 22, 719–722.

Kouwenhoven T.J. 2000. Survival under stress: benthic foraminiferal patterns and Cenozoic biotic crises, *Geologica Ultraiectina*, 186, 1–206.

Kouwenhoven, T.J. and van der Zwaan G.J. 2006. A reconstruction of late Miocene Mediterranean circulation patterns using benthic foraminifera, *Palaeogeogr. Palaeoclimatol. Palaeoecol.,* 238, 373–385.

Kouwenhoven T., Morigi C., Giunta S., Negri A., Krijgsman, W. and Rouchy J.M. 2006. Unravelling Messinian marine environments in the Eastern Mediterranean (Pissouri Basin, Cyprus): Constraints from integrated microfossil data, *Marine Micropaleontology,* 60, 17–44.

Krijgsman W., Blanc-Valleron M.M., Flecker R., Hilgen F.J., Kouwenhoven T.J., Merle D., Orszag-Sperber F. and Rouchy J.M. 2002. The onset of the Messinian salinity crisis in the Eastern Mediterranean Pissouri Basin, Cyprus, *Earth and Planetary Science Letters*, 194, 299–310.

Krijgsman W. 2002. The mediterranean mare nostrum of earth sciences, *Earth Planet Sci Lett.,* 205, 1–12

Kroon D., Alexander I., Little M., Lourens L.J., Matthewson A., Robertson A.H.F. and Sakamoto T. 1998. Oxygen isotope and sapropel stratigraphy in the eastern Mediterranean during the last 3.2 million years, in: Robertson, A.H.F., Emeis, K.-C., Richter, C., Camerlenghi, A.

(Eds.), Proceedings of the Ocean Drilling Program, *Scientific Results Ocean Drilling Program*, College Station, TX, 181–190.

Leckie R.M., Yuretich R.F., West O.L.O., Finkelstein D. and Schmidt M. 1998. Paleoceanography of the southwesternWestern Interior Sea during the time of the Cenomanian-Turonian boundary Late Cretaceous, *SEPM Concepts in Sedimentology and Paleontology*, 6, 101–126.

Loubère P. 1996. The surface ocean productivity and bottom water oxygen signals in deep water benthic foraminiferal assemblages, *Marine Micropaleontology*, 28, 247–261.

Loubère P. 1997. Benthic foraminiferal assemblage formation, organic carbon flux and oxygen concentrations on the outer continental shelf and slope, *Journal of Foraminiferal Research*, 27, 93–100.

Lourens L.J., Antonarakou A., Hilgen F.J., Van Hoof A.A.M., Vergnaud-Grazzini C. and Zachariasse W.J. 1996. Evaluation of the Plio–Pleistocene astronomical timescale, *Paleoceanography*, 11 (4), 391–413.

Lourens L.J., Wehausen R. and Brumsack H.J. 2001. Geological constraints on tidal dissipation and dynamical ellipticity of the Earth over the past three million years, *Nature*, 409, 1029–1032.

Lourens L.J., Hilgen F.J., Shackleton N.J., Laskar J. and Wilson D. 2004. The Neogene Period. In: Gradstein F., Ogg I., Smith A. (Eds.), *A Geologial Timescale 2004*. Cambridge University Press, UK.

Marino G., Rohling E.J., Rijpstra W.I., Sangiorgi F., Schouten S. and SinninghеDamste J.S. 2007. The Aegean Sea as driver of hydrographic and ecological changes in the eastern Mediterranean, *Geology,* 35 (8), 675–678.

Nolet G.J. and Corliss B.H. 1990. Benthic foraminiferal evidence for reduced deep-water circulation during sapropel deposition in the eastern Mediterranean, *Marine Geology*, 94, 109–130.

Orszag-Sperber F., Rouchy J.M. and Elion P. 1989. The sedimentary expression of regional tectonic events during the Miocene–Pliocene transition in the southern Cyprus basins, *Geol. Mag.*, 126, 291–299.

Orszag-Sperber F., Caruso A., Blanc-Valleron M.-M., Merle D. and Rouchy J.-M. 2009. The onset of the Messinian salinity crisis: Insights from Cyprus sections, *Sediment. Geol.,* 217, 52‑64.

Pinardi N. and Masetti E. 2000. Variability of the large scale general circulation of the Mediterranean Sea from observations and modelling: a review, *Palaeogeog. Palaeoclimatol. Palaeoecol.*, 158, 153–173.

Postma G. and Drinia H. 1993. Architecture and sedimentary facies evolution of a marine expanding half-graben (Crete, Late Miocene), *Basin Research*, 5, 103–124.

Pujol C. and Vergnaud-Grazzini C. 1995. Distribution of live planktic foraminifers as related to regional hydrography and productive systems of the Mediterranean Sea, *Marine Micropaleontology,* 25, 187–217.

Robertson A.H.F., Eaton S., Follows E.J. and McCallum J.E. 1991. The role of tectonics versus global sea-level change in the Neogene evolution of the Cyprus active margin, *International Association of Sedimentologists*, Special Publication, 12, 331-369.

Robertson A.H.F., Eaton S.E., Follows E.J. and Payne A.S. 1995. Sedimentology and depositional processes of Miocene evaporites from Cyprus, *Terra Nova*, 7, 233–254.

Robertson B.E. 1998. Systematics and paleoecology of the benthic Foraminiferida from the Buff Bay section, Miocene of Jamaica, *Micropaleontology*, 44, 1–266.

Rogerson M., Kouwenhoven T.J., Van der Zwaan G.J., O' Neill B.J., Postma G., Kleverlaan K. and Tijbosch H. 2006. Benthic foraminifera of a Miocene canyon and fan, *Marine Micropalaeontology,* 60, 295-318.

Rohling E.J., Abu-Zied R., Casford J.S.L., Hayes A. and Hoogakker B.A.A. 2009. The marine environment: present and past, in: Woodward, J.C. (Ed.), *The Physical Geography off the Mediterranean.* Oxford University Press, Oxford, pp. 33-67.

Rouchy J.M., Orszag-Sperber M., Blanc-Valleron F., Pierre M.-M., Rivière C., Combourieu-Nebout M. and Panayides N. 2001. Paleoenvironmental changes at the Messinian–Pliocene boundary in the eastern Mediterranean: southern Cyprus basins, *Sediment. Geol.,* 145, 93–117.

Schmiedl G., Mitschele A., Bec S., Emeis K.C., Hemleben C., Schulz H., Sperling M., Weldeab S. 2003. Benthic foraminiferal record of ecosystem variability in the eastern Mediterranean Sea during times of sapropel S5 and S6 deposition, *Palaeogeog. Palaeoclimatol. Palaeoecol.,* 190, 139– 164.

Soria J. M., Caracuel J. E., Corbí H., Dinarès-Turell J., Lancis C., Tent-Manclús J. E. and Yébenes A. 2008. The Bajo Segura Basin (SE Spain): implications for the Messinian salinity crisis in the Mediterranean margins, *Stratigraphy,* 5 (3-4), 257-263.

Sprovieri R. 1993. Pliocene Early Pleistocene astronomically forced planktonic foraminifera abundance fluctuations and chronology of Mediterranean calcareous plankton bioevents, *Rivista Italiana di Paleontologia e Stratigrafia*, 99 (3), 371-414.

Stow D.A.V., Braakenburg N.E. and Xenophontos C. 1995. The Pissouri Basin fan-delta complex, southwestern Cyprus, *Sedimentary Geology*, 98, 254-262.

Thunell R.C. 1978. Distribution of recent planktonic foraminifera in surface sediments of the Mediterranean Sea, *Marine Micropaleontology*, 3, 147– 173.

Tiedemann R., Sarnthein M. and Shackleton N.J. 1994. Astronomical timescale for the Pliocene Atlantic $d^{18}O$ and dust flux records of ODP Site 659, *Paleoceanography*, 9, 619– 638.

Triantaphyllou M. V., Antonarakou A., Drinia H., Dimiza M. D., Kontakiotis G., Tsiolakis E. and Theodorou G. 2010. High resolution biostratigraphy and paleoecology of the early Pliocene succession of Pissouri basin (Cyprus island), *Bulletin of the Geological Society of Greece,* Proceedings of the 12th International Congress, Patras, May, 2010.

Triantaphyllou M., Antonarakou A., Lourens L., Ziveri P., Tsolakis E., Tsaila-Monopolis S., Theodorou G., Dermitzakis M., Kontakiotis G., Konstantinidou E. and Athanasiou M. 2008. Calcareous plankton events and climate variability during late Zanclean in the eastern mediterranean (Pissouri basin, Cyprus), *33th International Geological Conference* (IGC), Oslo, Norway.

Van der Zwaan G.J. 1982. Paleoecology of Late Miocene foraminifera, *Utrecht Micropaleontological Bulletin*, 25, 1–201.

Van der Zwaan G.J., Duijnstee I.A.P., den Dulk M., Ernst S.R., Jannink N.T. and Kouwenhoven T.J. 1999. Benthic foraminifers: proxies or problems? A review of paleoecological concepts, *Earth-Science Reviews*, 46, 213–236.

Van der Zwaan G.J., Jorissen F.J. and de Stigter H.C. 1990. The depth dependency of planktonic/benthic foraminiferal ratios: constraints and applications, *Marine Geology*, 95, 1–16.

Van Hinsbergen D.J.J., Langereis C.G. and Meulenkamp J.E. 2005: Revision of the timing, magnitude and distribution of Neogene rotations in the western Aegean region, *Tectonophysics*, 396, 1-34.

Van Vugt N., Steenbrink J., Langereis C.G., Hilgen F.J. and Meulenkamp J.E. 1998. Magnetostratigraphy-based astronomical tuning of the early Pliocene lacustrine sediments of Ptolemais (NW Greece) and bed-to-bed correlation with the marine record, *Earth and Planetary Science Letters*, 164, 535-551.

Verhallen P.J.J.M. 1991. Late Pliocene to Early Pleistocene Mediterraneanmud-dwelling foraminifera: influence of a changing environment on community structure and evolution, *Utrecht Micropaleontol. Bull.*, 40, 220 pp.

Δελτίο της Ελληνικής Γεωλογικής Εταιρίας, τομ. XLVII , 2013
Πρακτικά 13ου Διεθνούς Συνεδρίου, Χανιά, Σεπτ. 2013

Bulletin of the Geological Society of Greece, vol. XLVII 2013
Proceedings of the 13th International Congress, Chania, Sept. 2013

TAPHONOMICAL OBSERVATIONS ON THE PYGMY HIPPOPOTAMUS SITE IN AGHIA NAPA, CYPRUS

Filippidi A.[1], Stathopoulou E.T.[1] and Theodorou G.[1]

[1] National and Kapodistrian University of Athens, Faculty of Geology and Geoenvironment, Department of Hist. Geology - Paleontology, afilip@geol.uoa.gr,estathop@geol.uoa.gr, gtheodor@geol.uoa.gr

Abstract

In this paper data concerning the taphonomy of the Upper Pleistocene site Aghia Napa in Cyprus is presented. The site is dominated by skeletal material belonging to the pygmy Hippopotamus species Phanourios minor, and consists a littoral rock-shelter. The fossiliferous assemblage is spread in a total area of about 72 m2 and a significantly large number of specimens were collected, indicating the presence of more than 160 individuals at the site. In this paper, we attempt to identify the causes or mechanisms that led to the accumulation of the endemic hippopotamus remains, focusing also on the palaeo-environmental parameters that might had affected the survivorship of the fossils. The taphonomical analysis is also based on parameters, which provide information concerning skeletal element representation and thus survivorship. The study of the skeletal material shows signs of abrasion, cracking and significant fragmentation which are related to the type, size and shape of the skeletal elements. The bone assemblage is interpreted as a result of transportation of the skeletal material from longer or shorter distances in the surrounding area while the impact of man concerning their accumulation is still under discussion.
Key words: *Phanourios minor, taphonomy, Upper Pleistocene.*

Περίληψη

Στην εργασία αυτή παρουσιάζονται τα αποτελέσματα ταφονομικής ανάλυσης της Άνω-πλειστοκαινικής θέσης της Αγίας Νάπας στην Κύπρο. Η πανίδα της απολιθωματοφόρου θέσης κυριαρχείται από σκελετικό υλικό νάνων ιπποπόταμων του είδους Phanourios minor, και εντοπίζεται κάτω από ένα φυσικό στέγαστρο εντός των ασβεστολιθικών σχηματισμών της περιοχής. Η εμφάνιση εκτείνεται σε μια περιοχή περίπου 72 τ.μ. από την οποία έχει συλλεχθεί ιδιαίτερα μεγάλος αριθμός ευρημάτων που υποδεικνύει την ύπαρξη περισσότερων από 160 ιπποπόταμων στη θέση. Στόχο της μελέτης αποτελεί και η απόδοση της αυξημένης συσσώρευσης του οστεολογικού υλικού σε συγκεκριμένους μηχανισμούς, εστιάζοντας στους παλαιοπεριβαλλοντικούς παράγοντες που πιθανά έχουν επηρεάσει και την επιβίωση του. Η ανάλυση στηρίζεται και σε παραμέτρους που μας πληροφορούν σχετικά με την αντιπροσώπευση και άρα την επιβίωση των διαφόρων σκελετικών στοιχείων. Η μελέτη του υλικού ανέδειξε την ύπαρξη λείανσης, κατακερματισμού και σημαντικής θραύσης, φαινόμενα που σχετίζονται με τον τύπο, το μέγεθος και το σχήμα των σκελετικών στοιχείων. Η συσσώρευση του υπό μελέτη υλικού ερμηνεύεται ως αποτέλεσμα φυσικής μεταφοράς τους στη θέση από την γύρω περιοχή, ενώ ο ρόλος του ανθρώπου σε αυτήν είναι ακόμη υπό διερεύνηση.
Λέξεις κλειδιά: *Phanourios minor, ταφονομία, Ανώτερο Πλειστόκαινο.*

1. Introduction

The increasing interest of Palaeontologists in taphonomical analysis rendered the latter a necessary and much promising aspect of palaeontological research in fossiliferous sites. It is obvious, that the accuracy and validity of the taphonomical results greatly depend on the appropriate collection of material and data during the excavation. The objective of this paper is to give a full presentation of the findings derived from the Upper Pleistocene fossiliferous site of Aghia Napa in Cyprus till the 2007 excavation and also to provide taphonomical analysis results based on the collected material.

The first excavation at the site of Aghia Napa was realized in 2000 by Ioannis Panayides, from the Geological Survey Department of Cyprus. Since then, six systematic palaeontological excavations have been conducted at the site, under the supervision of Professor G. Theodorou from Athens University and in collaboration with the Geological Survey Department of Cyprus.

Based on the large quantity of skeletal material derived from Aghia Napa, the fauna is dominated by pygmy hippopotami, which have also been described in numerous other sites on the island, e.g. Aetokremnos, Akanthou, Xylophagou, etc (Bate, 1906; Houtekamer and Sondaar, 1979; Held, 1992; Reese, 1995). Except for the material belonging to hippopotamuses, a number of samples have been attributed to other animal groups. With the exception of the carnivore species *Genetta plestictoides* (Theodorou et al., 2007), most of the latter material has not been thoroughly studied yet. Recently, material belonging to elephants (Stathopoulou et al., 2008) was recovered and is currently being studied. This is the first report of the presence of elephants in Aghia Napa. Work has also been done on the ear bones of the hippo material (Provatidis et al, 2011).

According to Bate (1906) and Houtekamer and Sondaar (1979), Hippopotami and Elephants colonized Cyprus during the Late Pleistocene, starting their journey from Asia Minor and swimming across the shallow Mediterranean waters of that time. The processes of insular dwarfism then began, gradually leading to the reduction of the animals' size in order for them to adapt to their new environment, characterized by hot and dry summers. Furthermore, morphological alterations, such as the development of a more-or-less pig-like foot and the lowering of the eyes and nostrils occurred, due to their adjustment to a more terrestrial mode of life (Houtekamer and Sondaar, 1979).

Through the taphonomical analysis of the Aghia Napa site, we speculate on the mechanisms that led to the accumulation of the hippopotamus remains. We also focus our study on the palaeo-environmental parameters that affect survivorship of the fossils. The important issue of the coexistence of hippopotamus and man on the island and whether the latter could be responsible for the hippopotamuses' extinction has preoccupied many scientists, including the authors. All data that could possibly lead us towards a theory, was thoroughly examined, in hope of shedding some light on this intriguing matter.

1.1. The Site of Aghia Napa

The site of Aghia Napa is located at the South-Eastern part of Cyprus, 500m east of the city of Aghia Napa at an altitude of 25m (Figure 1). The bedrock of this area consists of an Upper Cretaceous mélange, which includes bentonitic clays, siliceous – clastic sandstones, lavas, pelagic limestones and red radiolarites. The mélange is followed by the Late Cretaceous – Early Miocene Lefkara Formation consisting of gently dipping pelagic chalks containing irregular lenses and thin beds of porcelaneous chert. These are overlain by the patch reefs of the Aquitanian – Burdigalian Terra Member (Pakhna Formation). The sediment in the hollows between coral colonies is coarse bioclastic debris as well as aggregate grains and lime mud. Coral - dominated patch reefs passed outwards into algal dominated deposits, foraminiferal packstones, grainstones and pelagic carbonates. The fossiliferous beds are found within the remnants of the Miocene coral reefs (Follows et al, 1996).

The numerous fossils are embedded in red clays, deposited in a littoral rock – shelter comprised from limestones. The excavation site covers an area of more than 72m^2, while the fossiliferous

layers' thickness seems to range between 1 and 1.5 meters (Figure 2). Large limestone pieces from the shelter's roof, found in the sediment, indicate its partial collapse through time.

Despite the various references for the existence of pygmy hippopotamuses in Aghia Napa (Bate, 1906; Reese, 1995), the first palaeontological excavation was realized in the area in 2001. During this excavation, evidence suggesting a previous illicit dig were found. According to local people, it took place 70-80 years ago. The disturbance caused by this dig, led to the creation of relatively loose sediment, which can be distinguished from the cohesive sediment of the undisturbed bone-bed. In figures 2 and 3 (vertical sections of site), the richness of fossils in both layers, total range of the excavation site and total depth of the rock-shelter can be observed.

The collected skeletal material has been attributed to the pygmy hippopotamus *Phanourios minor* (Theodorou, et al., 2004); an endemic species that lived exclusively on Cyprus. Based on the Electron Spin Resonance (ESR) dating of dental material, carried out at the National Centre for Scientific Research "Demokritos" in Athens, by Dr. Y. Bassiakos, the site can be dated back to 11,000-13,500 years B.P. (Theodorou et al., 2007).

2. Material and Methods

2.1. Material

Until 2007, more than 14,000 specimens of biological origin have been collected at the site. The material belonging to *P. minor* represents the majority of the total specimens, while material from other animal groups, such as carnivores, reptiles and birds, micromammals and marine molluscs has been reported. In order to proceed with the taphonomical analysis of the site, the total amount of the findings has been studied, focusing on the pygmy hippopotamus skeletal material.

2.2. Field Work

A 9 x 8m grid, divided into $1m^2$ excavation squares, was used in order to document the exact position of the findings and all available information was recorded. Detailed drawings, corresponding photographs and sections were also prepared, combined with systematic macroscopic observations. The samples were then removed and the sediment was sieved, in order to collect possible fragments of small objects or bones of small animals.

2.3. Lab Work

Lab work included the conservation-preparation, documentation, and assignment, statistical and biometrical analysis of all skeletal material and the weighing of the fragments found throughout the excavation area. Due to the nature of the bone bearing sediments and the excellent state of preservation of the osteological material, the findings were only rinsed with tap water. In several cases, especially when preparing cranial material, acrylic resins such as Paraloid B72 and Polyfilla were used for the adhesion and fixation of the fragmented samples. All samples were macroscopically observed in order to detect any possible repetition of characteristic features.

All hippo material was separated according to element type, age and presence of erosion and then all identifiable bones were separated into three main categories per type (right, left, fragments) and per bone part (proximal, distal, diaphysis). Important taphonomical factors where then calculated. Specifically: The Number of Identifiable Specimens (NISP), the Minimum Number of Individuals (M.N.I.) and the Minimum Number of Elements (MNE) were estimated according to Lyman (1994). The MNI factor represents the total number of elements that can be attributed to whole samples. The Fragmentation Index was estimated for all skeletal elements, according to Lyman (1994); Lyman (2008) and Yeshurun et al. (2007), by comparing NISP to MNE (NISP/MNE). Various other important taphonomic indices (Behrensmeyer and Boaz, 1980; Matthews, 2002; Weissbrod et al., 2005; Broughton et al., 2006; Montalvo et al., 2008) were also calculated. As far as the differences between the bone type distributions are concerned, the Relative Abundance (Ri) was calculated (Andrews, 1990): Ri=Ni/MNI x Ei (Ni: number of elements i, Ei: number of

element i in the skeleton). The proportions of skeletal elements were evaluated, using the method proposed by Andrews (1990) and Lloveras et al. (2008). This includes the calculation of six indices. The PCRT/CR (Post-cranial / cranial (mandibles, maxilla and teeth), the PCAP/CR (appendicular skeleton elements / cranial material) and PCRLB/CR (long bones / mandibles and maxilla), that compare post-cranial to cranial material, the AUT/ZE (autopodium / zigopodium and stylopodium elements) and the Z/E (zigopodium / stylopodium elements) that compare autopodium to stylopodium and zigopodium elements and the AN/PO, that compares forelimb to hindlimb elements.

Figure 1 - The island of Cyprus and the location of Aghia Napa.

Figure 2 - View of a section of the undisturbed bone beds revealing their high density

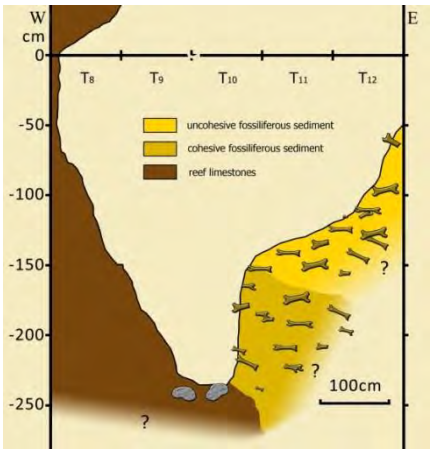

Figure 3 - W-E section of the excavation site.

All the above processing of the drawings and photographs taken during the excavations to define various aspects, such as anatomical relation of bones, despite the fact that during the macroscopic observations made at the excavation area, no such indications were found. Afterwards, a database containing the exact coordinates of all findings was created and used in G.I.S. software, for the projection of the specimens, allowing us to combine different types of information (for example, the distribution of juveniles in the site), in the most efficient way.

3. Results and Discussion

3.1. Skeletal Element Representation

To date (data from all excavations except for the last one held in 2008), the exact number of specimens derived from the site of Aghia Napa, is 14,299, of which 13,817 have been attributed to pygmy hippopotami (96.6%). According to the complementary biometrical analysis carried out

during this study, we were able to confirm the attribution of our material to one species, *Phanourios minor* (Theodorou et al., 2004). The remaining 3.4% has been attributed to other animal groups, such as carnivores, reptiles and birds, micromammals and marine molluscs.

In the context of the whole excavated beds, the calculated fossiliferous density (Montalvo et al., 2008) is 817 remains/m^3, a value that verifies an extremely high density assemblage of skeletal material. 8.3% of the collected hippopotamus specimens consists non-identifiable fragments (mentioned as FNU) and the total NISP per element type is presented in Figure 4 and Table 1. Interestingly, 10% of the skeletal elements belong to juveniles. The MNI and MNE values are presented in Figure 5 and Table 1, with the right humerus (medial epicondyle of the distal epiphyses) defining the presence of the remains of at least 169 animals at the site.

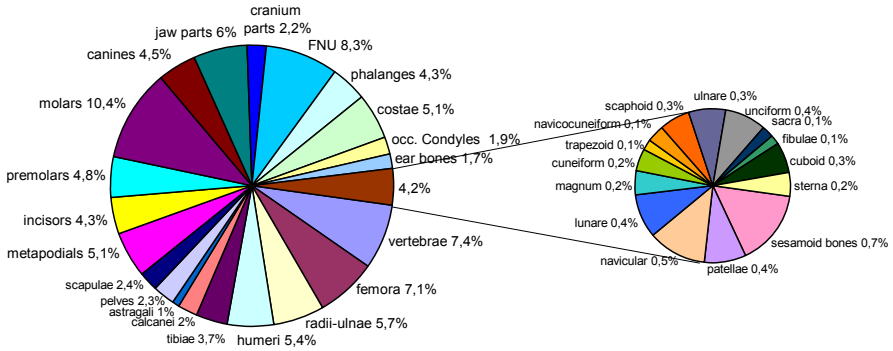

Figure 4 - NISP % per skeletal element type.

Table 1 - Descriptive data and key taphonomical variables.

bone type	NISP	MNI	MNE	Fragmentation index	Ri%
sacrum	15	15	15	1	8,90%
femur	985	129	250	3,9	76,30%
radius-ulna	782	168	328	2,4	99,40%
humerus	751	169	337	2,2	100%
tibia	505	106	207	2,4	62,70%
calcaneum	275	138	275	1	81,60%
astragalus	142	79	142	1	46,70%
pelvus	324	116	229	1,4	68,60%
scapula	329	126	248	1,3	74,60%
ulnare	46	27	46	1	16%
lunare	54	28	54	1	16,60%
navicular	72	39	72	1	23,00%
magnum	29	15	29	1	8,80%
unciform	49	29	49	1	17,20%
cuneiform	28	22	28	1	13%
scaphoid	38	20	33	1,2	11,90%
navicocuneiform	20	13	20	1	7,70%
trapezoid	13	8	13	1	4,70%
cuboid	37	20	37	1	11,80%
patella	50	27	50	1	16%
occipital	269	145	264	1,01	85,80%
petrus	239	57	106	2,3	33,70%
fibula	11	7	11	1	4,10%

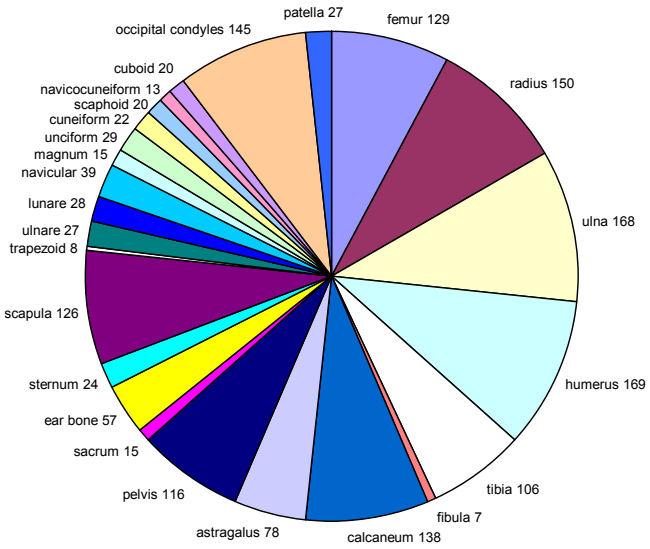

Figure 5 - MNI representation of the Hippo skeletal material.

The material was studied as two separate categories: cranial and post-cranial, which represents 36% and 64% of the total respectively (Figure 6). Despite the great amount of teeth that has been collected, the post-cranial material is significantly richer. The studied cranial material (4,951 elements), includes cranium parts (6%), jaw parts (17%), ear bones (5%), occipital condyles (5%) and teeth (incisors, canines, premolars and molars) (67%). Teeth are the most common cranial material (3,316 specimens). The detailed description of teeth is given in Figure 7, in which it is obvious that the proportion of the teeth present does not coincide with the expected if all teeth remained in situ. Molars seem to be the most enriched whole tooth type, a fact that can be explained by the low percentage of fragmentation. The same observation applies to the premolars, although the total amount of the specimens is much less than the expected. Their small size could be the explanation to their low representation, which combined with transportation led to their loss. Concerning the canines and the incisors, they present a high percentage of fragmented elements, probably due to their shape. The layer of enamel, which covers canines, might be the reason for their toughness, hence, their high degree of survivorship.

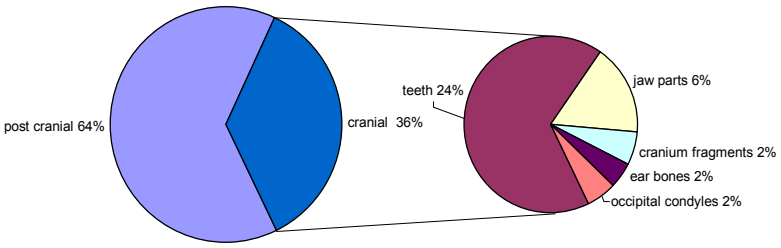

Figure 6 - Proportion of cranial and post-cranial hippo material and representation of cranial elements, at the Aghia Napa site.

In Figure 8 and 9, one may observe an analytical description of the forelimb and hindlimb, respectively. In both figures, elements belonging to the large sized bones appear in greater quantities than the small ones but on the other hand only a small percentage of those represent complete remains, contrary to autopodium elements.

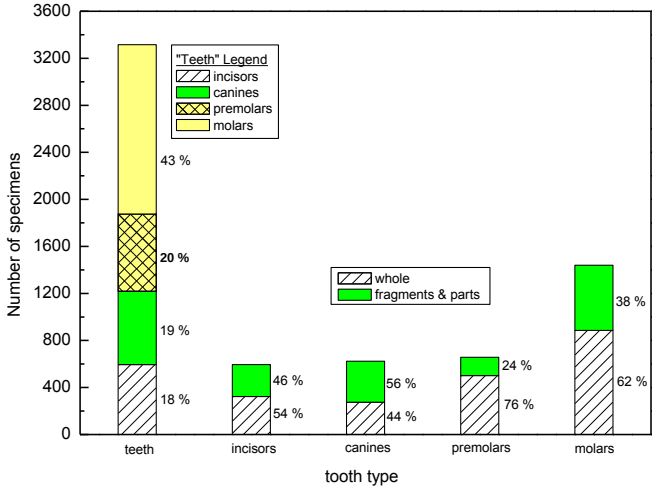

Figure 7 - Representation of whole and fragmented teeth in Aghia Napa. The amounts given in the first column from the left concern whole specimens.

Table 2 - Proportion of different parts of the skeleton.

Indices	Values
PCRT/CR	1,25
PCRAP/CR	1,22
PCRLB/CR	5,7
AUT/ZE	0,8
Z/E	0,9
AN/PO	1,27

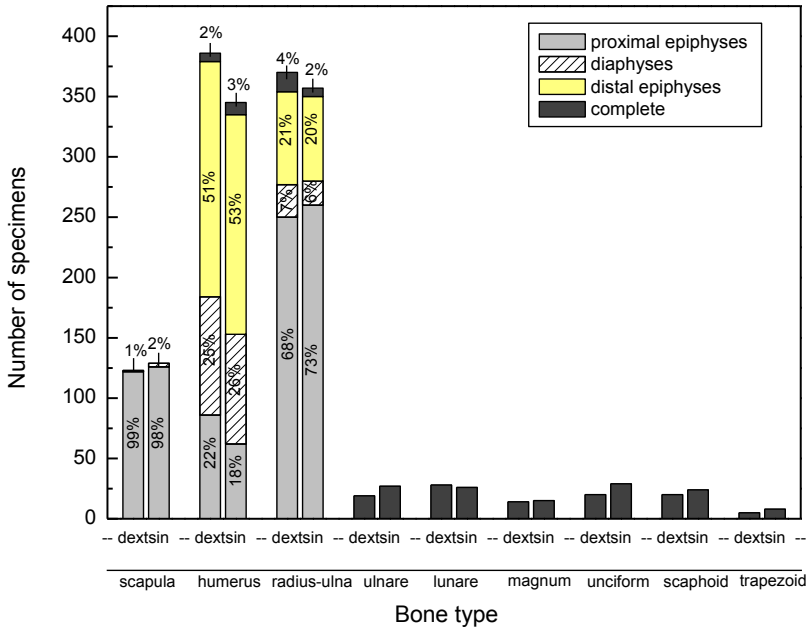

Figure 8 - Numeric representation of the skeletal material of the fore limb.

3.2. Element Fragmentation and Survivorship

According to the proportions of skeletal elements evaluated (Andrews, 1990; Lloveras et al., 2008) (Table 2), the PCRT/CR, the PCAP/CR and PCRLB/CR indicate a deficiency of cranial material, especially in the case of PCRLB/CR. Concerning the loss of distal limb elements, the AUT/ZE and the Z/E reveal the systematic loss of smaller (and lower) limb elements when compared to the larger (and upper) bones. The last index used, AN/PO shows the greater survival of the anterior skeletal elements. These results are consistent to the data, given in figures 8 and 9.

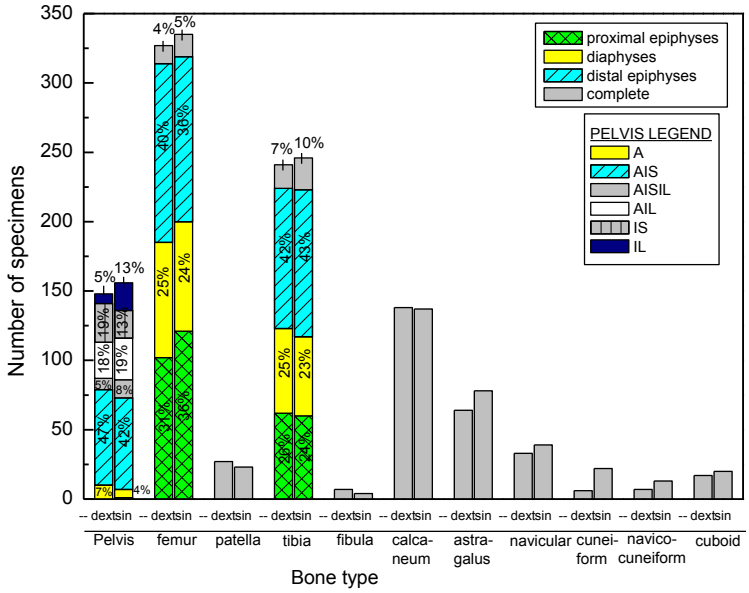

Figure 9 - Numeric representation of skeletal elements of the hind limb. Pelvis parts: A: acetabulum, AIS: acetabulum + ischium, AISIL: acetabulum + ischium + ilium, AIL: acetabulum + ilium, IS: ischium, IL: ilium (Lloveras et al., 2008).

The results and values concerning the Fragmentation Index, estimated for all skeletal elements, are presented in Figure 10 and Table 1. A fragmentation of one means that the NISP and MNE are equal, and thus no fragmentation has occurred. Increases in the index, suggest greater breakage.

Our own results prove once again that the bigger the skeletal element, the less resistant to fragmentation it appears to be. As seen in Figure 11, the Relative Abundance values indicate that the large/long bones appear more abundant than small/compact bones. At this point we would like to point out the effect of the previously mentioned illicit dig, on such indices. Fragmentation of material has been observed to be importantly increased by this disruption. Thus, we have two types of fragmentation, that of the disrupted material (by the illicit dig) and that of the undisrupted material. Unfortunately these could not be statistically differentiated.

3.3. Macroscopical Observation of Skeletal Elements

3.3.1. Abrasion

During the excavations, an important amount of samples with signs of abrasion were observed and collected. This feature was considered to be important, as it might help explain the accumulation mechanism that has occurred through time. Transportation of skeletal material by water and wind or even weathering due to exposure in situ and soil flow, is known to have caused such phenomena. Various degrees of abrasion where observed, but regardless of this, only total percentages of abraded remains per bone type were estimated. The total amount of skeletal elements exhibits 22.6% abrasion. In Figure 12, it becomes obvious that the more fragmented the

elements, and thus containing more broken and irregular surfaces, the less resistant to abrasion they become. Furthermore, a comparison between the abrasion of adults and juvenile individuals was made (Figure 13), and greater presence of abrasion in the latter group was observed. The distribution of the abrasion in juveniles, follows the general pattern presented in Figure 12, but appears at a larger extent, possibly due to the extra surfaces created by the unfused epiphyses. Juvenile bones, due to their small size were possibly exposed to similar conditions throughout their extent, thus presenting a more homogenous abrasion.

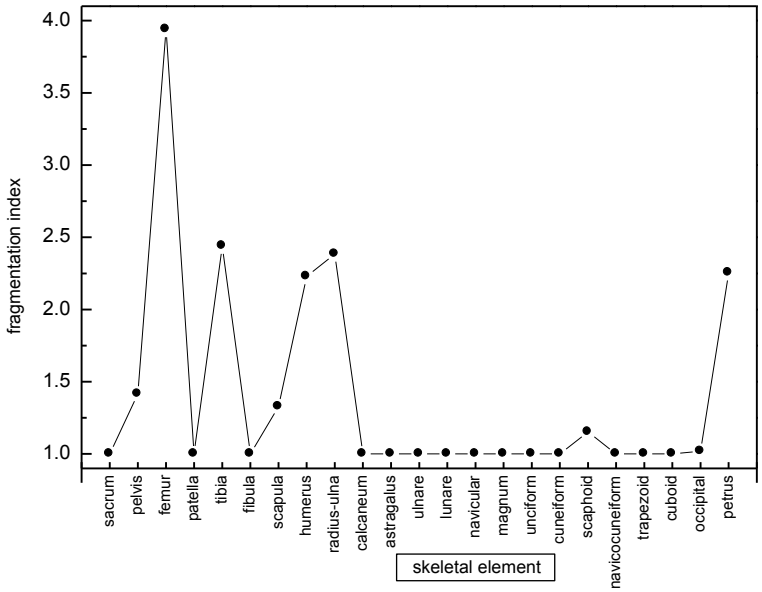

Figure 10 - Comparison of the fragmentation index for each bone type (NISP/MNE).

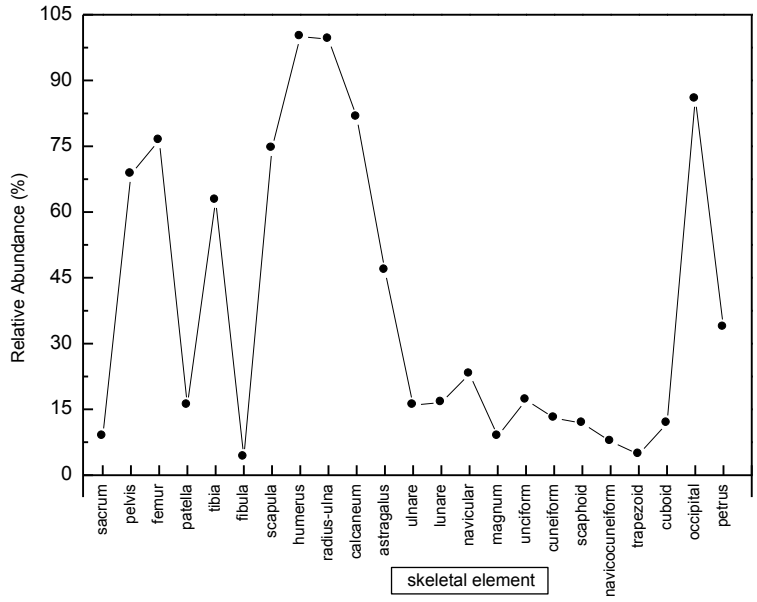

Figure 11 - The Relative Abundance for each bone type.

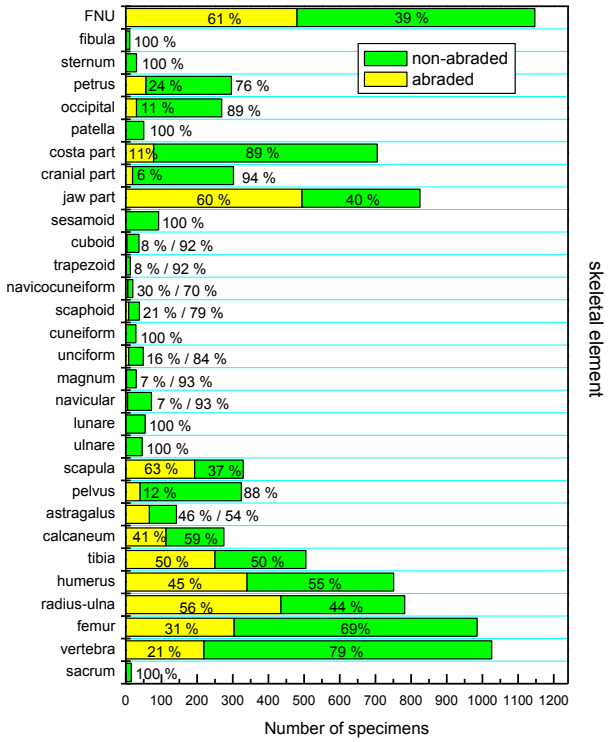

Figure 12 - Numeric representation of the skeletal elements' abrasion.

3.3.2. Surface Marks and Features

A preliminary study of the skeletal remains' surface has begun, concerning signs resulting from biological activity and post-depositional procedures, such as the dissolution and precipitation of calcium carbonate from the cave walls.

Biological marks, such us tooth marks and gnawing have not yet been verified, while signs of root development can be observed in certain cases. Further study on the above is already in progress, but the restricted appearance of these phenomena till now, does not allow the extraction of important conclusions. Post depositional precipitation of calcium carbonate was identified either as crust development on the surface of bones and teeth, or as the formation of extremely compact bone breccias with a calcareous matrix. This calcareous material was produced by the partial dissolution of the limestone cave walls, due to the climatic conditions of the area, probably following fluctuations of seasonal humidity. In a few cases, the above climatic variations have also led to the superficial erosion of the bones, which is limited to specific areas of the fossils, probably those exposed to the atmospheric conditions. This appears as a system of mesoscopic cracks, which are often responsible for the exfoliation of the bones.

3.3.3. Cracking

Cracking of the fossil long bones seems to occur in two types. The first can be described by multiple fractures, limited to the surface of the bone, indicating extensive pressure either from the overlaying sediments and fallen rocks or the weight of passing animals and men. The second type includes larger fractures that may some times lead to the separation of the bone into parts, often accompanied by their shifting. This type might have occurred following natural processes (which are described in the first case) including diagenetic procedures combined with regional movement of the non cohesive sediment, but also due to the significant disturbance of the site from recent human activity, including the mentioned illicit dig.

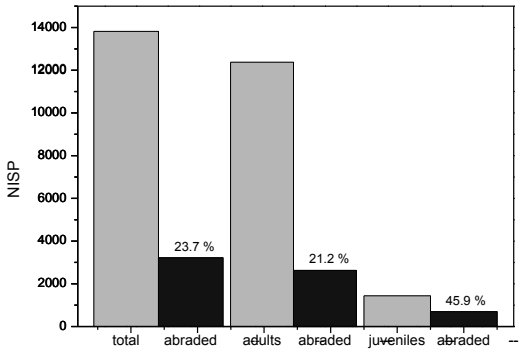

Figure 13 - Comparative presentation of the abraded adult and juvenile individuals.

Figure 14 –Fragmentation of bones in a non parallel maner.

3.4. Diagenesis of Skeletal Material

As part of our taphonomical analysis, previous results on the diagenesis of the skeletal material were also taken under consideration (Stathopoulou, 2005; 2008). According to these, the skeletal material of the fossiliferous site is characterized by numerous diagenetic changes in bone, especially in terms of histology. This is mainly expressed as a result of microbial activity, leading to the partial destruction of this microstructure. Dentine reacts similarly to bone, while enamel is the hardest and less vulnerable to diagenetic processes. Alterations of our material also concerns crystallinity, chemistry and structural parameters of the biomaterial as well as permineralization. All results suggest a wet and warm climate, capable of allowing phenomena such as microbial activity and the type of preservation observed in Aghia Napa.

These have also shed light on the important issue of black coloured bones and teeth found at the site (Stathopoulou, 2005; 2008; Stathopoulou, et al., 2004). Similar occurrences in other pygmy hippo sites in Cyprus have been reported as evidence of fire, based on macroscopic observations on the material, either caused by direct burning by man, or as a result of human activity above the fossiliferous horizons (hearths) (Simmons, 1999). The extensive study of the the black bones proved that the colouration of the currently studied material is a result of staining by Fe and Mn oxides and not of burning. No correlation to the presence and effect of man on the material can be implied by these findings till now (Stathopoulou et al., 2004).

3.5. Theories on the Taphonomical History of Aghia Napa

As described in detail above, the fossiliferous site in Aghia Napa is characterized by an extremely dense accumulation of hippo skeletal remains. The results of the taphonomical analysis reinforce the macroscopic observation, concerning the absence of any significant anatomical relation between the findings' distribution. Attempting to limit the effect of the illicit-dig on the results of our study, the unidentified bone and tooth fragments found throughout the excavation, were weighed. By doing this, we were able to observe the fragments' distribution in every excavation square and at different depths (distribution per 10 cm). The division chart, containing the data for the depth of 70-80 cm defined the upper limit of the undisturbed fossiliferous layer approximately at that depth (Filippidi and Mourkou, 2007).

Based on the calculated taphonomical parameters and indices, we are led to the following theories. Given the extremely high MNI, and the great density of fossils in relation to the small total excavating area, we can assume that this assemblage was the result of a gradual deposition of hippopotamus' skeletal material. The presence of various size groups of both adult and juvenile material, suggests that the living hippopotamuses were subjected to environmental stress, caused by either climatic changes and reduction of available food supplies or the possible impact of man, given the absence of other large predators, which eventually led to their death and accumulation at

the site. Reviewing the results of the fragmentation index (Lyman, 1994) and the indices concerning the proportion of skeletal elements (Andrews, 1990; Lloveras et al., 2008), one may conclude that there has been transportation of the material at some extent. Specifically, the relative abundance of the autopodium elements compared to that of the stylopodium and zygopodium elements, combined with the highly fragmented cranial material suggests that most of the fossils found at the site have been transported from the surroundings. On the other hand, the full representation of all skeletal elements implies that the distance covered must have been relatively limited and that in some way; the rock shelter represented the last obstacle during their journey.

According to Behrensmeyer and Boaz (1980), the ratio of isolated teeth to vertebra can provide us with the characterization of a fossil assemblage as being hydrodynamically biased before burial. In the case of Aghia Napa, this index (teeth/vertebra=3,4) suggests that isolated teeth are more frequent than vertebra, although they should appear in similar numbers if the association had a complete representation of the skeletal elements. This agrees with the results derived from relevant indices mentioned above. Furthermore, the complete absence of anatomical relation observed at the site in the undisturbed layers, proves the transportation of the material and can be explained as a result of the disarticulation of the hippopotamus skeletons before burial and before or/and during transportation. The extent of the transportation is also unknown to us, as the degree of abrasion and representation of the various skeletal elements differs greatly. The large quantity of fragments found throughout the bone beds, present different degrees of abrasion, indicating that fragmentation preceded the processes of transportation and burial. This allows their discrimination from the more recent fragments, produced during the illicit dig or even the excavation periods. The transportation mechanism might still be active, as the surficial erosion of the landscape is a continuous procedure.

The thorough observation at the excavation site, combined with the study of the drawings and photographs led us to the conclusion that findings' position in the extremely rich undisturbed fossiliferous layer do not follow a certain pattern. Having examined the direction of the long bones, they do not appear parallel even in the same layers. The random orientation of the bones cannot be attributed to a single factor, such as sediment flow or even the action of the drainage network. The same can be noted in the case of the cracking of the bones (Figure 14).

According to the results of the documentation of the materials position by GIS, we can also point out the absence of a specific accumulation of the skeletal remains based on their type, shape, size or weight. In Figure 15, this can be observed in the case of various adult bone types and in addition most of the findings seem to be gathered near the rock-shelters' walls.

Summarizing, the degree of the fragmentation, abrasion and representation of skeletal elements, throughout the site does not allow the attribution of the assemblage to a thanatocenosis. Our data lead to the conclusion that the present condition of the fossil assemblage has resulted from the transportation of the skeletal remains some time after their death, unknown to us, and their deposition. Due to its location, the roof-shelter might have acted as a natural trap for either transported skeletal material, or even for some of the actual animals themselves, in their seek for drinking water (Hadjisterkotis and Reese, 2008). In any case, this is not opposed to the theory that hippopotamuses might have lived in or nearby the cave at some time.

We must also point out the possibility of transportation of a certain amount of the material by scavenging animals or even by man. Despite the fact, that the recovery of material belonging to *Genetta plestictoides* from the hippopotamus fossiliferous beds, is considered to be indirect evidence of the coexistence of hippopotamuses and man on the island; no specific evidence of their coexistence has been reported in Aghia Napa. Also, some of the marine molluscs found at the site, cannot be attributed to transportation by birds. Still, although these are indications for the presence of man at the site, they are far from being proof of their co-existence and their interaction with the hippopotamuses. We have also not found any tool marks, tools or proof for the use of fire in the cave yet.

The site of Aghia Napa is indisputably a fossil assemblage of significantly controversial features and thus of taphonomical interest. We consider to have only attempted to reveal a part of the total picture and intend to continue our study in the future.

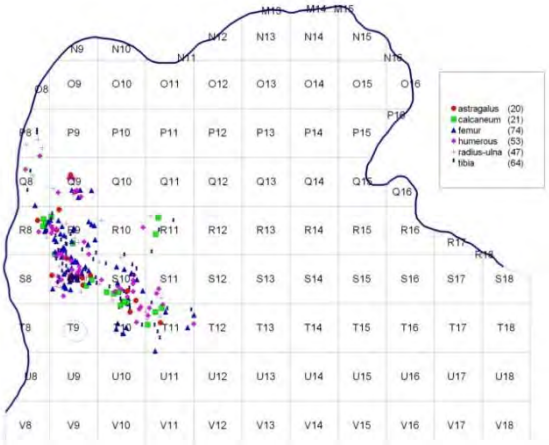

Figure 15 - Spatial projection of specific adult bone types (femur, tibia, astragalus, calcaneum, humerus, radius-ulna) from the undisturbed layer.

4. Acknowledgments

Acknowledgments are owed to the General Secretariat for Research and Technology (Greece), the Special Account for Research Grants of Athens University and the Geological Survey Department of Cyprus (UOA programs 70/3/6050, 70/3/6017, 70/3/7093, 70/4/3670) and the Municipality of Aghia Napa for funding this study. We would also like to thank I. Panayides for giving us the opportunity to study this material and Lecturer N. Evelpidou for the spatial and statistical analysis of the geographical data in a GIS environment.

5. References

Andrews P. 1990. *Owls, Caves and Fossils*, Chicago; IL: Natural History Museum and University of Chicago Press, 231 pp.

Bate D.M.A. 1906. The pygmy hippopotamus of Cyprus, *Geological Magazine*, 3(6), 241-245.

Behrensmeyer A.K. and Dechant B. 1980. The recent bones of Amboseli Park, Kenya, in relation to East African paleoecology, in Behrensmeyer, A.K. and Hill, A.P., (eds), *Fossils in the Making, Vertebrate Taphonomy and Paleoecology*. 72-92, Chicago: University of Chicago Press, 350 pp.

Broughton M.J., Cannon, I.V., Arnold S., Bogiatto J.R. and Dalton K. 2006. The Taphonomy of Owl-Deposited Fish Remains and the Origin of the Homestead Cave Ichthyofauna, *Journal of Taphonomy*, 4(2), 69-95.

Filippidi A. and Mourkou M. 2007. Taphonomical Observations on Pygmy Hippopotamuses at Aghia Napa, Cyprus, using G.I.S. software, *Unpublished undergraduate thesis*, University of Athens, pp.134.

Follows E.J., Robertson A.H.F. and Scoffin T.P. 1996. Tectonic controls of Miocene reefs and related carbonate facies in Cyprus, in Fransee, E.K., Esteban, M., Ward, C.W. and Rouchy, J.-M (eds), *Models for Carbonate Stratigraphy from Miocene Reef Complexes of Mediterranean Regions*, 5, 295-316.

Hadjisterkotis E. and Reese S.D. 2008. Considerations on the potential use of cliffs and caves by the extinct endemic late Pleistocene hippopotami and elephants of Cyprus, *European Journal of Wildlife Research*, 54: 122-133.

Held S. 1992. Pleistocene fauna and Holocene humans: A gazetteer of palaeontological and early archaeological sites on Cyprus, *Studies in Mediterranean Archaeology*, Monographs, No 95, Astrom Editions, 195 pp.

Houtekamer J.L. and Sondaar P.Y. 1979. Osteology of the forelimb of the Pleistocene dwarf Hippopotamus from Cyprus with special reference to phylogeny and function, *Proceedings Koninklijke Nederlande Akademie van Wefenschappen* (B), 82(4), 411-448.

Lloveras L., Moreno-Garcia M. and Nadal J. 2008. Taphonomic study of leporid remains accumulated by the Spanish Imperial Eagle (*Aquila adalberti*), *Geobios*, 41, 91-100.

Lyman L.R. 1994. Vertebrate Taphonomy, Cambridge, *Cambridge Unversity Press*, 524pp.

Lyman R. L. 2008. Quantitative Paleozoology, Cambridge, *Cambridge University Press*, 345 pp.

Matthews T. 2002. South African Micromammals and Predators: Some Comparative Results, *Archaeometry*, 44(3), 363-370.

Montalvo C.I., Melchor R.N., Visconti G. and Cerdeño E. 2008. Vertebrate taphonomy in loess-paleosol deposits: a case study from the Miocene of central Argentina, *Geobios*, 41, 133-143.

Provatidis C. G., Theodorou E.G. and Theodorou G. E., 2011. Computed Tomography and CAD/CAE methods for the study of the osseous inner ear bone of Greek Quaternary endemic mammals, *Mediterranean Archaeology and Archaeometry*, 11(2), 121-127.

Reese D.S. 1995. The Pleistocene vertebrate sites and fauna of Cyprus, *Geological Survey Department Bulletin*, 9, 230.

Simmons A.H. 1999. *Faunal extinction in an island society, Pygmy hippopotamus hunters of Cyprus,* New York, Kluwer Academic, 381 pp.

Stathopoulou E., 2008. Contribution to the Study of the Internal Micromorphology and Fossilization of Cenozoic Vertebrates by Radioanalytical Technique, *Phd thesis*, *GAIA*, No 19, University of Athens, 369 pp.

Stathopoulou E. T. 2005. First results on the fossilization of Dwarf Hippo skeletal remains from Aghia Napa, Cyprus, *Monografies de la Societat d'Historia Natural de les Balears*, 12, 319-324.

Stathopoulou E. T., Theodorou G., Panayides I., and Bassiakos Y. 2004. Diagenesis of bone and colouration: the example of Aghia Napa, Cyprus, *Proceedings of the 5th International Symposium on Eastern Mediterranean Geology*, Thessaloniki, 14-20 April, 1: 347-350

Stathopoulou E., Filippidi A., Theodorou G. and Panayides I. 2008. Preliminary study of the first possible elephant remain at Aghia Napa, Cyprus, *5th Symposium on Archaeometry of the Hellenic Society of Archaeometry*, Athens, 8-10 October, Book of Abstracts.

Theodorou G., Panayides I. 2003. First data on the fossil hippopotamus from Agia Napa Cyprus, *International Symposium* "*Insular Vertebrate evolution: The palaeontological approach*", Palma de Mallorca, Spain, 16-20 September, pp 65.

Theodorou G., Panayides I., Stathopoulou E., Papaspyropoulos C., Agiadi K. and Tsolakis E. 2004. Remarks on the endemic fossil Hippopotamus from Aghia Napa (Cyprus), *Proccedings of the 5th International Symposium on Eastern Mediterranean Geology*, Thessaloniki, 14-20 April, 1: 355-358.

Theodorou G., Roussiakis S.I., Athanassiou A., Giaourtsakis I. and Panayides I., 2007. A late Pleistocene endemic Genet (Carnivora, Viverridae) from Aghia Napa, Cyprus, *Bulletin of the Geological Society of Greece : Proceedings of the 11th International Congress*, vol. XXXX, p. 201-208.

Weissbrod L., Dayan T., Kaufman D. and Weinstein-Evron M., 2005. Micromammla taphonomy of el-Wad Terrace, Mount Carmel Israel: distinguising cultural from natural depositional agents in the Late Natufian, *Journal of Archaeological Science*, 32, 1-17.

Yeshurun R., Marom, N. and Bar-Oz G. 2007. Differential Fragmentation of Different Ungulate Body-Size: A Comparison of Gazelle and Fallow Deer Bone Fragmentation in Levantine Prehistoric Assemblages, *Journal of Taphonomy*, 5(3), 137-148.

Δελτίο της Ελληνικής Γεωλογικής Εταιρίας, τομ. XLVII , 2013
Πρακτικά 13ου Διεθνούς Συνεδρίου, Χανιά, Σεπτ. 2013

Bulletin of the Geological Society of Greece, vol. XLVII 2013
Proceedings of the 13th International Congress, Chania, Sept. 2013

BIOSTRATIGRAPHY AND SEDIMENTOLOGY OF THE IONIAN ZONE AMMONITICO ROSSO IN THE MAVRON OROS AREA (NW EPIRUS, GREECE) – PALEOGEOGRAPHIC IMPLICATIONS

Karakitsios V.[1] and Chatzicharalampous E.[2]

[1] National and Kapodistrian University of Athens, Faculty of Geology and Geoenvironment, Department of Hist. Geology - Paleontology, vkarak@geol.uoa.gr

[2] School of Civil Engineering, National Technical University of Athens, Zografou Campus, 15780 Athens, Greece, chatzieliza@central.ntua.gr

Abstract

New biostratigraphic and sedimentologic data on the Ammonitico Rosso (AR) formation in the Mavron Oros area (Ionian zone, NW Epirus) show that its thickness progressively reduces towards the N-NW (from 15 to 7m). Two sections were studied, in the thick (A) and thin succession (B) respectively. The ammonite fauna indicates a stratigraphic range for the AR from the early Toarcian to the Aalenian, in section A, and from the upper part of Middle Toarcian to the Aalenian, in section B. Thus, AR deposition was transgressive, confirming the stratigraphic pinching-out of the synrift formations, observed in the same area towards the N-NW. Sedimentologic observations showed that the AR in section B (where AR base is missing) consists of nodular mud-to wackestones with subsolved ammonite shells, and clear indices of early lithification and subsequent solution of fine carbonate material. These observations indicate low rates of sedimentation and repeated phases of non-deposition and submarine erosion, characteristic for seamount environment.
Key words: *Ionian zone, Ammonitico Rosso, half-graben, synrift formations.*

Περίληψη

Νέα βιοστρωματογραφικά και ιζηματολογικά στοιχεία για το Ammonitico Rosso (AR) στην περιοχή Μαύρον Όρος (Ιόνια ζώνη, ΒΔ Ήπειρος) δείχνουν ότι το πάχος του ελαττώνεται προοδευτικά προς τα Β-ΒΔ (από 15 σε 7 μέτρα). Μελετήθηκαν δυο τομές, η Α με AR μεγαλύτερου πάχους και η Β με AR μικρότερου πάχους. Η πανίδα των αμμωνιτών δίνει στρωματογραφικό εύρος για το AR της τομής Α, από το Κατώτερο Τοάρσιο ως το Ααλένιο, ενώ για την τομή Β, από το ανώτερο τμήμα του Μέσου Τοάρσιου μέχρι το Ααλένιο. Συνεπώς, η απόθεση του AR ήταν επικλυσιγενής, επιβεβαιώνοντας την στρωματογραφική αποσφήνωση των συνταφρογενών σχηματισμών, η οποία παρατηρείται στην ίδια περιοχή προς τα Β-ΒΔ. Οι ιζηματολογικές παρατηρήσεις έδειξαν ότι το AR της τομής Β (όπου λείπει η βάση του AR) αποτελείται από κονδυλώδεις ασβεστόλιθους (mud-ως wackestones) με υποδιαλυμένα αμμωνιτικά όστρακα και μεταγενέστερη διάλυση του λεπτομερούς ανθρακικού υλικού. Αυτές οι παρατηρήσεις δείχνουν χαμηλούς ρυθμούς ιζηματογένεσης και επαναλαμβανόμενες φάσεις μη απόθεσης και υποθαλάσσιας διάβρωσης που χαρακτηρίζουν υποθαλάσσιο ύβωμα.
Λέξεις κλειδιά: *Ιόνια ζώνη, Ammonitico Rosso, ημιτάφρος, συνταφρογενείς σχηματισμοί.*

1. Introduction

The Ionian zone of NW Greece (Epirus region) constitutes part of the most external zones of the Hellenides (Pre-Apulian zone, Ionian zone, Gavrovo zone; Figure 1). The evaporite base of the Ionian series, dated Scythian-Anisian (Pomoni-Papaioannou & Tsaila-Monopolis, 1983, Dragastan et al., 1985) is capped by the Foustapidima limestones, dated Ladinian-Rhaetian by Karakitsios & Tsaila-Monopolis (1990). These are overlain by the Pantokrator limestones, classically dated as Lower Jurassic (Aubouin, 1959; IGRS-IFP, 1966; Karakitsios & Tsaila-Monopolis; 1988). These neritic platform deposits give way to mainly carbonate, locally silicified, pelagic deposits of Pliensbachian age (Karakitsios, 1992, 1995). Pelagic deposits begin with either the Siniais limestones (with rare bands and lenses of replacement chert) or their lateral equivalent, the Louros limestones (no cherts). The facies and thickness variations of these deposits are indicative of active tectonic spreading related to the opening of the Pindos oceanic branch of Neo-Tethys Ocean (Karakitsios 1990, 1992, 1995; Karakitsios & Rigakis 2007). The period of Siniais and Louros limestones deposition is important in the history of Ionian zone in Greece and in Albania as it saw the onset of rifting. What until then had been extensive, monotonous carbonate platforms (e.g. Pantokrator neritic *Palaeodasycladus mediterraneus* limestones) broke up as a pelagic sedimentary basin formed.

The break-up of the carbonate platforms was followed by intense internal differentiation of the Ionian Basin. This differentiation separated the initial basin into smaller palaeogeographic units with half-graben geometry, as it is recorded in the abruptly changing thickness and facies of the synrift formations which take the form of synsedimentary wedges (Karakitsios 1995). In the deeper parts of the half-grabens, these include complete Toarcian-Tithonian successions with Ammonitico Rosso or Lower Posidonia beds at their base, while in the elevated parts of the half-grabens, the succession is interrupted by unconformities. The directions of synsedimentary structures (e.g. slumps, synsedimentary faults, and stratigraphic pinch-outs of the synrift formations) indicate that deposition was controlled by structures formed during extension related to the opening of the Pindos Ocean compounded by halokinesis involving the evaporites at the base of the Ionian carbonate sequence (Karakitsios, 1995). In the Early Cretaceous (Berriasian) the transgression is complete, as is it shown by the onset of the pelagic Vigla limestones deposition in the entire Ionian zone (Karakitsios 1992; Karakitsios & Koletti 1992). Thus, the base of the Vigla limestones represents the beginning of the Ionian basin postrift period. After Vigla limestones deposition, the pelagic conditions persisted (pelagic sedimentation accompanied by calciturbidites derived from the adjacent Gavrovo and Apulia platforms) until the Late Eocene, when flysch sedimentation began.

This work dates precisely the lower part of the complete synrift successions from the locally abundant macro-fauna (ammonites), and specifies the age distribution of the Ammonitico Rosso in a half-graben sub-basin of northwestern Greece (NW Epirus). Additionally, paleo-bathymetric and sedimentological observations related to the stratigraphic pinching out of the Ammoninico Rosso formation, attest the presence of a small sub-basin with half-graben geometry (due to the internal differentiation of the Ionian basin) and its transgressive synsedimetary filling.

2. Geological Observations

According IGRS-IFP (1966) and Karakitsios (1990, 1992), Mavron Oros hill allows to distinguish, from south to north (for a length of less than two kilometers), the passage from a palaeogeographic zone with complete Siniais limestones-Lower Posidonia beds-limestones with Filaments-Upper Posidonia beds succession, to a zone where the Lower Posidonia beds are replaced by the Ammonitico Rosso and then progressively pass to a hiatus zone where the Vigla limestones repose directly on the Pantokrator limestones. This facies passage was attributed to a synsedimentary fault, which could serve as barrier between Lower Posidonia beds and Ammonitico Rosso facies.

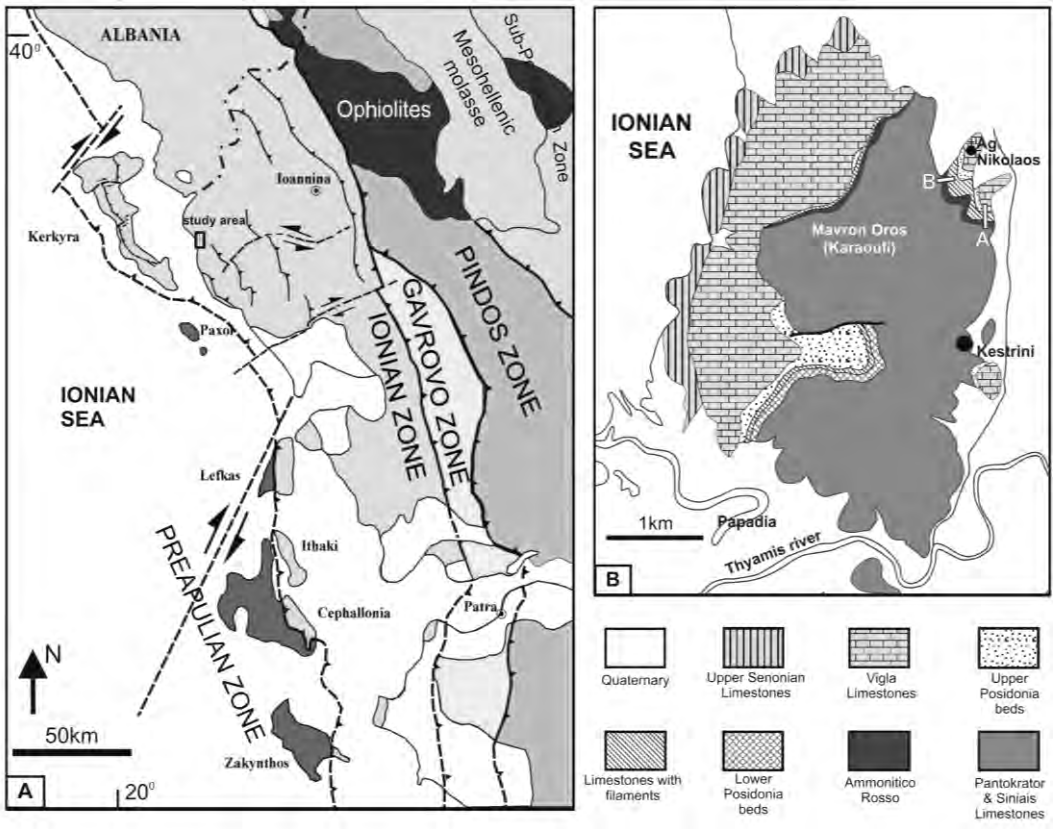

Figure 1 - A: Simplified geological map of Western Greece. B: Geological map of the study area (A and B location of the sections of Figure 2).

We undertook again the study of this area in order to conduct; firstly detailed field observations and secondly, by using detailed biostratigraphical and sedimentological data to verify the above hypothesis.

2.1 Field Observations

In the south part of the hill, which is tectonically lowered by at least 100 meters relative to the northern part, the stratigraphic succession, over the well developed Siniais limestones, is:

-30 m of Lower Posidonia beds: bleu frequently bituminous marls, being red at the upper part of the formation. In all stratigraphic levels the marls are rich in lamellibranches Bosistra buchi (Posidonia). It is very clear in the field (Figure 1B) that this formation abuts by fault against the Siniais limestones of the north compartment. It is clear too, that this fault does not affect the Vigla limestones; thus it corresponds to a synsedimentary fault separating two different sub-basins.

-5 m of Limestones with filaments: intraformational limestone breccias in a limonitic matrix;

-more than 50 m of Upper Posidonia beds: cherty beds with green siliceous argillite interbedding. Abundant radiolaria are present in all stratigraphic levels, while Posidonia fossils are restricted to the lower part of the formation.

In the northeastern part of the hill (north of the synsedimentary fault) over the moderately developed Siniais limestones, are observed:

-15 to 7 m Ammonitico Rosso (which will be studied in detail below),

-8 to 6 m Limestones with filament,

-6 to 3 m Upper Posidonia beds.

At the extreme north of the Mavron Oros hill, Vigla limestones repose uncomfortably directly on the Pantokrator limestones, by progressive disposition of Upper Lias-Malm formations, except for some levels of limestone breccias with filaments intercalated between Vigla and Pantokrator limestones. Thus, there is a hiatus of the total synrif succession (Upper Lias-Malm), which is found in the deeper part of the half-grabens where sedimentation is continuous during the internal differentiation of Ionian zone.

These observations clearly show that in Ionian basin, the sedimentary filling of the half-graben with the synrift formations toward the elevated part of the half-graben, is transgressive (Figure 4). This transgression is completed in the early Cretaceous (Berriasian), as it is deduced by the onset of the pelagic Vigla limestones deposition in this area, and generally in the entire Ionian zone (Karakitsios 1992; Karakitsios & Koletti 1992). Thus, the Vigla limestones blanket the earlier irregular Ionian basin bottom topography and their base represent the beginning of the Ionian postrift deposition.

In order to observe when the sedimentary filling of the half-grabens with the synrift formations started, and to verify whether they stratigraphically pinch-out (which should be recorded by a gap in the base of the Ammonitico Rosso toward the N-NW direction) we undertook two geologic sections in the thicker and less thick part of the Ammonitico Rosso outcrop (Figure 2).

2.2. Sections and Faunas

Mavron Oros hill in NW Epirus (NW Greece), emerge from Quaternary sediments of the Kalamas River Delta. This hill, allows the observation of the Early Jurassic to Middle Cretaceous Ionian sequence. Two sections were realized, the first (A) in the thick and the second (B) in the thin AR formation respectively. The zone attribution of the collected ammonites in the different stratigraphic levels of the sections is conformable to the Tethyan standard established by Elmi et al. (1994). The Ammonites of the present work are deposited in the Laboratory of Historical Geology & Paleontology (collection of Professor V. Karakitsios).

2.2.1. Mavron Oros Section A (Figure 2)

This section is located NE of the eastern side of Mavron Oros hill (1.5 km north of Kestrini village, two hundred meters south of Agios Nikolaos chapel). The Ammonitico Rosso overlies in stratigraphic continuity some 60 meters thick of white, well-bedded bioclastic lime wackestones with rare bands and lenses of black replacement chert, corresponding to the Siniais limestones formation (Karakitsios 1990, 1992). The overlying Ammonitico Rosso presents a total thickness of 15 meters. It commences by some 5 meters of green to reddish marls with some breccias intercalations, and marly nodular limestones as well. It follows 10 meters of nodular limestones alternating with red marls which are becoming scarce to the formation top, where Limestones with filaments formation is beginning. The Ammonitico Rosso formation has delivered in almost all levels a rich ammonite fauna, among which were determined (Karakitsios, 1990, 1992):

-1st level (upper part of marls and first meter of the base of nodular Amonitico Rosso): *Polyplectus pluricostatus* (HAAS), and *Hildaites* gr. *serpentinum* (REINECKE). This fauna attributes an Early Toarcian age to the corresponding stratigraphic level (*Serpentinum* zone).

-2nd level (the following two meters of nodular Amonitico Rosso): *Nodicoeloceras* sp., and *Nodicoeloceras* sp. close to *N. incrassatum* (SIMPSON). This fauna corresponds to the Early Toarcian or the base of the Middle Toarcian.

-3rd level (next two meters of nodular Amonitico Rosso): *Mercaticeras mercati* (HAUER), *Phymatoceras* ? *caroli* (MERLA), *Hildoceras lusitanicum* (MEISTER), *Hildoceras* sp. This fauna

attributes this stratigraphic level to the base of the Middle Toarcian (*H. graecum* zone of KOTTEK).

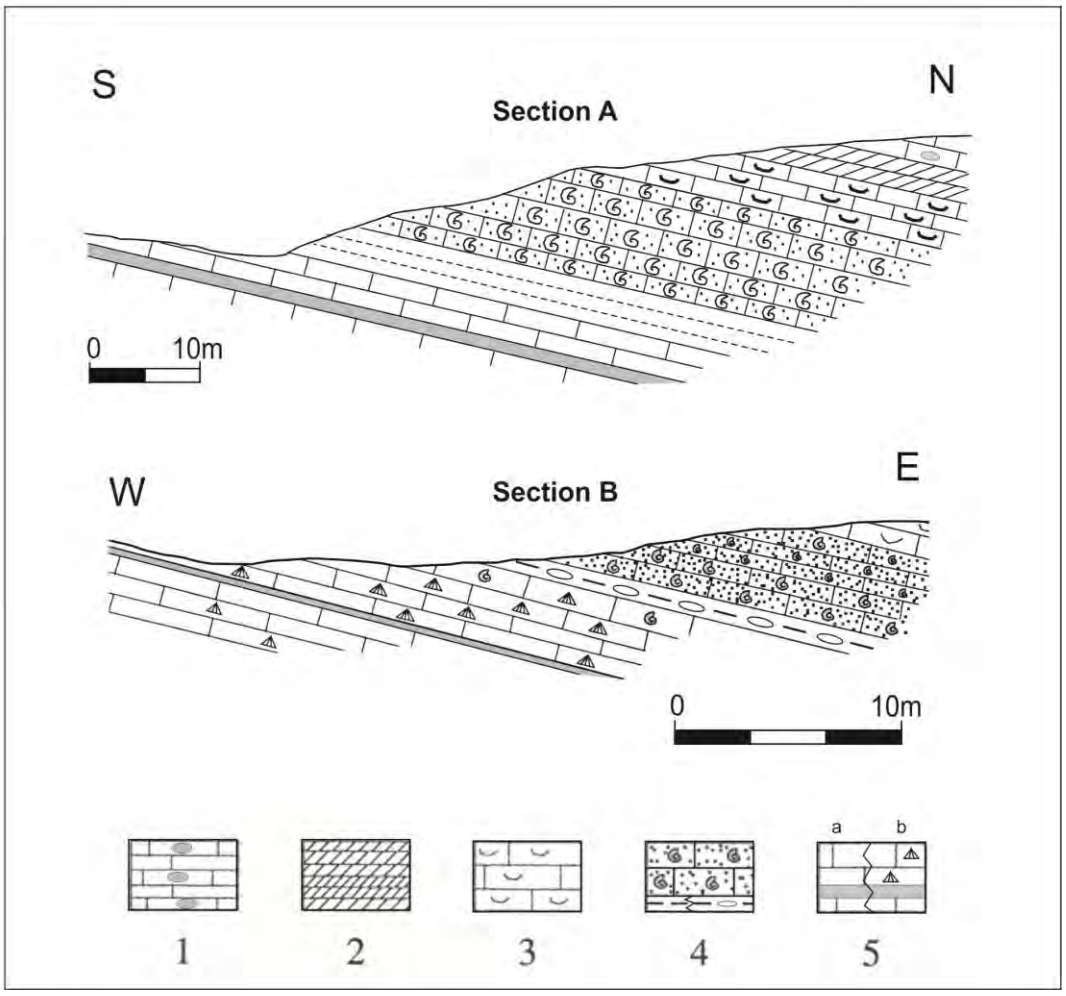

Figure 2 - Mavron Oros sections (locations are referred in Figure 1); 1: Vigla limestones; 2: Upper Posidonia beds; 3: limestone with filaments; 4: Ammonitico Rosso and base marls and/or breccias intercalations; 5: a. Siniais limestones, b. Siniais-Louros transitional limestones.

-4th level (next two meters of nodular Amonitico Rosso): *Brodieia* sp., *Phymatoceras* gr. *erbaense* (HAUER), *Polyplectus* sp., *Calliphylloceras* sp., *Phymatoceras fabale*? (SIMPSON), *Phylloceras* sp. This fauna indicates a Middle Toarcian age (*B. bayani* zone of KOTTEK).

-5th level (next meter of nodular Amonitico Rosso): *Harpoceras* sp., *Pseudogrammoceras* cf. *aratum* with very thin edges, *Peronoceras*? sp. fragment. This fauna corresponds to the upper part of Middle Toarcian.

-6th level (next meter of nodular Amonitico Rosso): *Phylloceras perplanatum* (PRINZ), *Catulloceras dumortieri* (THIOL). This association indicates the middle interval of Late Toarcian (Meneghinii zone).

-7th level (last meter of nodular Amonitico Rosso): *Erycites* sp., showing a time interval extended from the Toarcian top (?) to Aalenian.

This section, corresponding to continuous sedimentation during the syn-rift period of the Ionian basin, shows that the stratigraphic extension of the Ammonitico Rosso formation is Toarcian to Aalenian (p.p.), without any hiatus with the underlying Siniais limestones. It should be noted that at the same section, IGRS-IFP (1966) and Galbrun et al. (1994), attributed the Ammonitico Rosso to the Middle Toarcian (Bifrons and Gradata zones). The observed ammonite fauna in this work extends the age of the Ammonitico Rosso formation to the entire Toarcian which was also found in analogous complete synrift successions in other places of Epirus (Aubouin, 1959; IGRS-IFP, 1966. Karakitsios, 1990, 1992).

2.2.2. Mavron Oros Section B (Figure 2)

This section is located some 400 meters NW of the previous section (a hundred meters W-SW of Agios Nikolaos chapel). Below the Ammonitico Rosso, lies a predominantly packstone limestone formation (some 50 meters thick), whose facies is intermediate between the Louros and the Siniais limestones formations (Karakitsios & Tsaila-Monopolis 1988; Karakitsios 1990, 1992). From the final bed before the Ammonitico Rosso, which is rich in brachiopods and ammonites (particularly difficult to remove from), Dommergues et al. (2002) collected an Ammonite fauna indicative of Late Pliensbachian age (Middle Domerian; Bertrandi and Algovianum horizons). The overlying Ammonitico Rosso presents a total thickness of 7 meters. It commences by some decimeters of nodular marls, followed by mainly nodular limestones alternating with red marls until the end of the formation. The Ammonitico Rosso formation has delivered in almost all levels a rich ammonite fauna, among which were determined:

-1st level (lower two meters of the section): *Phymatoceras cornucopiae* (MERLA), *Phymatoceras caroli* (MERLA), *Phylloceras* sp., *Porpoceras* sp., *Crassiceras* sp. This fauna indicates the upper part of Middle Toarcian (Gradata zone).

-2nd level (next meters of the section): *Phylloceras perplanatum* (PRINZ), *Catulloceras dumortieri* (THIOL), *Phymatoceras* sp., *Pseudogrammoceras* sp., *Brodieia* sp., *Erycites* sp. This fauna attributes this stratigraphic level to Upper Toarcian-Aalenian.

Consequently, the total Ammonitico Rosso formation of section B is attributed to the upper part of Middle Toarcian to Aalenian (p.p.) time interval, with a clear hiatus of the lower part of the complete Toarcian-Aalenian formation observed in the previous section. This data confirms the stratigraphical pinching-out of the Ammonitico Rosso. A number of age significant ammonites are illustrated in Figure 3.

2.3 Sedimentological Analysis of the *Ammonitico Rosso* Facies

The sedimentological analysis of the nodular Ammonitico Rosso facies in section A shows that the hall facies corresponds to wackestone-packstone with peloids, radiolaria and planktonic foraminifera, pelagic bivalves, and gastropods. Additionally, the ammonite shells are not -or are moderately- subsolved, and the carbonate material presents low degree of early lithification and subsequent solution. This is in contrast with the corresponding observations in section B, as we will see below. The nodular Ammonitico Rosso facies in section B, allowed the distinction of the following sedimentological groups:

1st group. The lower part corresponds to wackestone-packstone with peloids, radiolaria and planktonic foraminifera and pelagic bivalves, and probably a gastropod.

Figure 3 - 1: *Polyplectus pluricostatus* HAAS, 2: *Hildaites* gr. *serpentinus* (REINECKE), 3: *Mercaticeras mercati* (HAUER), 4: *Brodieia* sp., 5: *Phymatoceras* gr. *erbaense* (HAUER), 6: *Phymatoceras*? *caroli* (MERLA), 7: *Catulloceras dumortieri* THIOL, 8: *Phylloceras perplanatum* PRINZ.

2nd group. This part of the formation is consisted mainly of wackestone with ammonite nuclei, small low-spiraled gastropods, planktonic foraminifera, and small radiolaria.

3rd group. The lower part of this unit corresponds to wackestone with planktonic and benthonic foraminifera, radiolaria, and filaments. Sponge spicules together with radiolaria dominate in the lowermost part of this stratigraphic level, while filaments presence increases in its upper part.

4th group. This part is mainly consisted of wackestone with radiolaria, small ammonites, filaments, planktonic foraminifera, crinoids, sponge spicules, and fragments of echinoderma.

In all stratigraphic levels of section B it is observed that ammonite shells are subsolved, and there are clear indices of early lithification and subsequent solution of fine carbonate material. These phenomena indicate low rates of sedimentation characteristic for seamount environments. Consequently, this section occupies an intermediate position of the sub-basin with half-graben geometry (closer to its elevated part), in which the first section occupies its deeper part. As far as the stratigraphic disposition at the extreme north of the Mavron Oros hill is concerned, after a progressive disposition of Upper Lias-Malm formations (s. supra), the Vigla limestones finally repose directly on the Pantokrator limestones (Figure 2A); thus it corresponds to the most elevated part of the same half-graben.

3. Discussion and Conclusions

Field observations together with biostratigraphical and sedimentological data clearly show that in the Ionian basin the sedimentary filling of the half-grabens with the synrift formations, started in the Lower Toarcian. This is confirmed by the ammonite fauna observed at the base of the complete succession of the Ammonitico Rosso (section A). Towards NW direction of the Mavron Oros hill, the progressive reduction of the Upper Lias-Malm formations thickness leads to the direct unconformity of the Vigla limestones over the Pantokrator limestones (except for some 2-3 m of filament limestone's breccias intercalated between Vigla and Pantokrator limestones).

The data of the present work would integrate to the palaeogeographic interpretation of Figure 4. According to this interpretation, during Toarcian-Tithonian times, the sections' area corresponded to a half-graben bounded by synsedimentary faults. The section A corresponds to the deeper part of this half-graben, the section B to an intermediate position, whereas the stratigraphic disposition at the extreme north of the Mavron Oros hill (with hiatus of the Upper Lias-Malm formations) corresponds to the elevated part of the half-graben. Following Westermann (1988) and Batt (1989) bathymetric interpretations of the observed ammonite morphotypes, both methods give

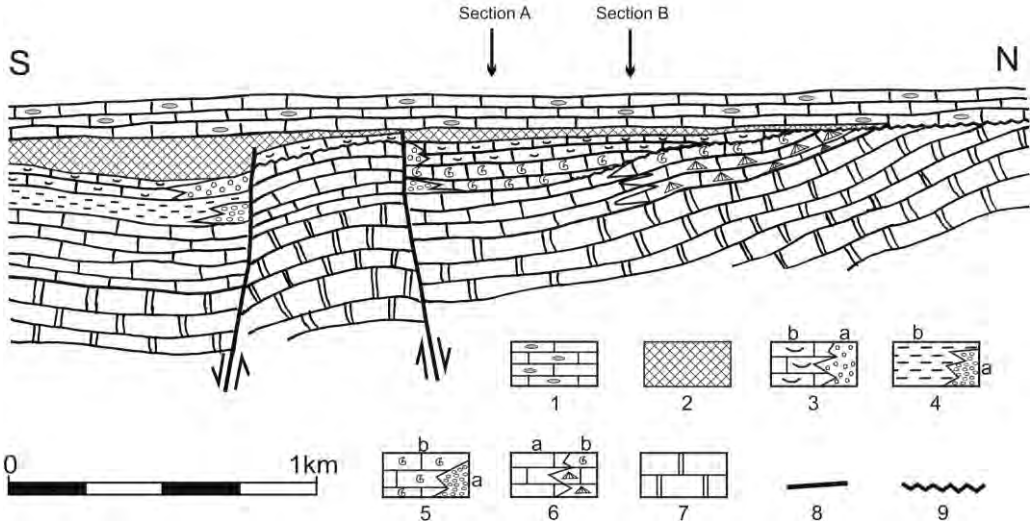

Figure 4 - Reconstruction of the deposit's architecture during Early Cretaceous; 1: Vigla limestones; 2: Upper Posidonia beds; 3: intraformational breccias (a), limestone with filaments (b); 4: intraformational breccias (a), LowerPosidonia beds (b); 5: debris flow (a), Ammonitico Rosso (b); 6: Siniais limestones (a), Louros limestones (b); 7: Pantokrator limestones; 8: fault; 9: uncomformity.

approximately the same water depth, ranging between 80 and 250 m at the upper part and more than 200 m at the lower part of both sections. Nevertheless, compared the section A and B faunas, there is a trend indicating a somewhat shallower depositional depth of the section B. Concerning the above methodologies, it seems that the composition of the faunas is only indirectly related to water depth as the relatively large forms (chiefly macroconchs) were most probably adapted to swimming in an deep marine environment (Guex, 1969) and might also have undergone post-mortal dispersal. Besides, as these methods are based on the composition of ammonite assemblage, the number of collected ammonites, due to the difficulty of their extraction from the nodular limestone, is not representative of the real number of genera present in the rock. Consequently, it is difficult to arrive at any well-reasoned bathymetric estimation from the faunal content. However, the relative depths estimated by these methods are not incompatible with the proposed palaeogeographic scheme of the present work and the palaeogeographic position of the two sections in the corresponding half-graben sub-basin (Figure 4).

Concerning the sedimentary filling, it coincides with the well-known regression/transgression passage at the Lower Toarcian observed in the epicontinental seas of NW Europe (Mouterde et al. 1980; Brandt 1986; Haq et al. 1988; de Graciansky et al. 1988; Wignall & Maynard 1993, Morard et al. 2003).

The sedimentary filling is transgressive as it is shown by the pinching-out of the Ammonitico Rosso (section B) and the rest of the synrift formations toward the elevated part of the half-graben. The transgression is completed in the Early Cretaceous (Berriasian), as it is deduced by the onset of the pelagic Vigla limestones deposition in this area (Figure 1B and 4) and generally in the entire Ionian zone (Karakitsios 1992; Karakitsios & koletti 1992). The base of the Vigla limestones which covers all the earlier sea bottom topography of the Ionian basin consequently represents the beginning of the Ionian basin postrift period.

5 Acknowledgments

This research has been funded by the University of Athens program “The petroleum systems of Western Greece (Epirus, Akarnania, Ionian Islands) and the Peloponnese” (Kapodistrias 70/4/11708).

6 References

Aubouin J. 1959. Contribution à l'étude géologique de la Grèce septentrionale: les confins de l'Epire et de la Thessalie, *Ann. géol. Pays Hell.*, IX(1), 1-483.

Batt R.J. 1989. Ammonite shell morphotype distribution in the western interior Greenhorn Sea and some paleoecological implications, *Palaios*, 4, 32-42.

Brandt K. 1986. Glacioeustatic cycles in the early Jurassic?, *N. Jb. Geol. Pal. Mhft*, 6, 257-274.

De Graciansky P.-C., Jacquin T. and Hesselbo S.P. 1988. The Ligurian cycle: an overview of Lower Jurassic 2nd-order transgressive/regressive facies cycles in Western Europe. In Graciansky, de P.-C., Hardenbol J., Jacquin T., Vail P.R., Mesozoic and Cenozoic sequence stratigraphy of European basins, *SEPM Spec. Publ.*, 60, 467-479.

Dragastan O., Papanikos D. and Papanikos P. 1985. Foraminifères, algues et microproblematica du Trias de Mesopotamos, Epire (Grèce continentale), *Revue de Micropaléontologie*, 27(4), 244-248.

Dommergues J.L., Karakitsios V., Meister C. and Bonneau M. 2002. New ammonite data about the earliest syn-rift deposits (Lower Jurassic) in the Ionian Zone of N-W Greece (Epirus), *N. Jb. Geol. Paläont. Abh.*, 233(3), 299-316.

Elmi S., Gabilly J., Mouterde R., Rulleau L. and Rocha R.B. 1994. L’étage Toarcien de l’Europe et de la Téthys: divisions et correlations, *Geobios*, Mém. Sp. 17, 149-159.

Galbrun B., Mouterde R., Baudin F. and Danelian T. 1994. L'Ammonitico-Rosso Toarcien de la zone ionienne (Epire, Grèce): Magnétostratigraphie et biostratigraphie, *Eclogae Geol. Helv.*, 87(1), 91-111.

Guex J. 1969. Sur le sex des ammonites, *Bul. Soc. vaud. Sci. nat.*, 70, 1-6.

Haq B.U., Hardenbol J., and Vail P.R. 1988. Mesozoic and Cenozoic chronostratigraphy and cycles of sea-level changes, Sea-level changes, an integrated approach, *SEPM Spec. Publ.*, 42, 71-108.

IGRS-IFP 1966. Étude Géologique de L' Épire (Grèce Nord-occidentale), *Technip (eds)*, 306 p.

Karakitsios V., 1990. Chronologie et géometrie de l'ouverture d'un bassin et de son inversion tectonique: le bassin ionien (Epire, Grèce), *PhD*, Univ. Paris 6, (Mémoire 411), 310 p.

Karakitsios V. 1992. Ouverture et inversion tectonique du bassin ionien (Epire, Grèce), *Ann. Geol. Pays Hell.*, 35, 185-318.

Karakitsios V. 1995. The Influence of Structure and Halokinesis on Organic Matter Preservation and Thrust System Evolution in Ionian Basin, NW Greece, *AAPG Bulletin*, 79(7), 960-980.

Karakitsios V. and Tsaila-Monopolis S. 1988. Données nouvelles sur les niveaux supérieurs (Lias inférieur-moyen) des Calcaires de Pantokrator (zone ionienne moyenne, Epire, Grèce continentale). Description des Calcaires de Louros, *Rev. Micropaleont*., Paris, 31(1), 49-55.

Karakitsios V. and Tsaila-Monopolis S. 1990. Données nouvelles sur les niveaux inférieurs (Trias supérieur) de la série calcaire ionienne en Epire (Grèce continentale). Conséquences stratigraphiques, *Rev. Paleobiologie*, 9(1), 139-147.

Karakitsios V. and Koletti L. 1992. Critical revision of the age of the basal Vigla Limestones (Ionian zone-Western Greece) based on Nannoplankton. Paleogeographic consequences. 4th International Nannoplankton Association Conference proceedings, Prague 8-14 September 1991. Nannoplankton Research. Hamrsmid B. & Young J.R. (eds). Issued by the Moravian Oil Company, *Hodonin. Knihovnicka ZPN*, 14a, 1992, 1, 165-177.

Karakitsios V. and Rigakis N. 2007. Evolution and petroleum potential of Western Greece, *Journal of Petroleum Geology*, 30(3), 197-218.

Karakitsios V., Danelian T., and De Wever P. 1988. Datations par les Radiolaires des Calcaires à Filaments, Schistes à Posidonies supérieurs et Calcaires de Vigla (zone ionienne, Epire, Grèce) du Callovien au Tithonique terminal, *C. R. Acad. Sc.*, Serie II, 367-372.

Morard A., Guex J., Bartolini A., Morettini E. and De Wever P, 2003. The new scenario for Domerian-Toarcian transition, *Bull. Soc. Géol. Fr.*, 174(4), 351-356.

Kottek A.V. 1966. Die Ammonitenabfolge des Griechischen Toarcium, *Ann. Geol. Pays Hell.*, 17, 1-157.

Mouterde R., Tintant H., Gabilly J., Hanzo M., Lefavrais A. and Rioult M. 1980. Lias, In Megnien, C., eds., Synthèse géologique du bassin de Paris, *Mém. BRGM*, 101, 75-123.

Pomoni-Papaioannou F. and Tsaila-Monopolis S. 1983. Petrological, Sedimentological and Micropaleontological studies of an evaporite outcrop, West of Ziros lake (Epirus-Greece), *Riv. Ital. Paleont. Strat.*, 88, 387-400.

Westermann G. 1988. New developments in Ecology of Jurassic-Cretaceous ammonoids. Proc. Atti II Int. "Jurassic-Cretaceous Ammonoids Ecology". F.E.A;, Pergola, 1987, 459-478.

Wignall P.B. and Maynard J.R. 1993. The sequence stratigraphy of transgressive black shales. In Katz, B., Pratt L.M., eds., Source rocks in a sequence stratigraphic frame work, *AAPG Studies in Geology*, 37, 35-47.

Δελτίο της Ελληνικής Γεωλογικής Εταιρίας, τομ. XLVII , 2013
Πρακτικά 13ου Διεθνούς Συνεδρίου, Χανιά, Σεπτ. 2013

Bulletin of the Geological Society of Greece, vol. XLVII 2013
Proceedings of the 13th International Congress, Chania, Sept. 2013

REMARKS ON THE MESSINIAN EVAPORITES OF ZAKYNTHOS ISLAND (IONIAN SEA, EASTERN MEDITERRANEAN)

Karakitsios V.[1], Roveri M.[2], Lugli S.[3], Manzi V.[2], Gennari R.[2], Antonarakou A.[1], Triantaphyllou M.[1], Agiadi K.[1] and Kontakiotis G.[1]

[1] National and Kapodistrian University of Athens, Faculty of Geology and Geoenvironment, Department of Hist. Geology - Paleontology, vkarak@geol.uoa.gr

[2] Dipartimento di Fisica e Scienze della Terra, Università degli Studi di Parma, Italy, marco.roveri@unipr.it, vinicio.manzi@unipr.it, rocco. gennari@unipr.it .

[3] Dipartimento di Scienze Chimiche e Geologiche, Università degli Studi di Modena e Reggio Emilia, Modena, Italy, stefano.lugli@unimore.it.

Abstract

Detailed mapping of the Neogene deposits on Zakynthos Island shows that the Messinian primary evaporite basins, formed over Ionian basement, are delimited by the westernmost outcrop of the Triassic evaporitic diapirs, located west of the Kalamaki-Argasi Messinian gypsum unit. The post-Miocene external Ionian thrust is emplaced west of the Triassic diapirs. Planktonic foraminifera biostratigraphy indicates that primary evaporite accumulation took place probably during the first stage of the Messinian salinity crisis (5.96-5.60 Ma), in shallower parts of a foreland basin, formed over the Pre-Apulian and the Ionian zone basement. Establishment of these depositional environments, before the Ionian thrust emplacement, was probably due to the particularities of the foreland basin, which extended from the external Ionian to the internal Pre-Apulian zone. Field observations, borehole data and an onshore seismic profile show that the Neogene sediments over the Pre-Apulian basement correspond to the foredeep through forebulge domain of the foreland basin, as it is documented from their spatial thickness distribution. In contrast, the Neogene sediments over the Ionian basement correspond to the wedge top of the foreland basin, which was less subsiding, as it is deduced by their reduced thickness. This lower subsidence rate was the result of the concurrent diapiric movements of the Ionian Triassic evaporites. In Agios Sostis area, located over Pre-Apulian basement, the Neogene sequence is intercalated by decametre-thick resedimented blocks consisting of shallow water selenite. To the southeast, this mass-wasting Messinian gypsum passes to mainly gypsum turbidite. In Kalamaki-Argasi area, located over Ionian basement, the shallow water environment led to the deposition of the observed primary gypsum. Erosion of the primary gypsum of both forebulge and wedge top supplied the foreland basin's depocenter with gypsum turbidites.
Key words: *gypsum, Messinian Salinity Crisis, Pre-Apulian zone, foreland basin.*

Περίληψη

Η λεπτομερής χαρτογράφηση των Νεογενών αποθέσεων της Ζακύνθου δείχνει ότι οι λεκάνες πρωτογενούς Μεσσήνιας εβαποριτικής απόθεσης, που σχηματίστηκαν πάνω

σε Ιόνιο υπόβαθρο, οριοθετούνται από τη δυτικότερη εμφάνιση των Τριαδικών εβαποριτικών διάπειρων (δυτικά της Μεσσήνιας ενότητας γύψου Καλαμάκι-Αργάσι). Η μετα-Μειοκαινική εξωτερική Ιόνια επώθηση τοποθετείται δυτικά αυτών των Τριαδικών διάπειρων. Βιοστρωματογραφική ανάλυση των συναθροίσεων πλαγκτονικών τρηματοφόρων στα Νεογενή ιζήματα δείχνει ότι η συσσώρευση πρωτογενούς εβαπορίτη έλαβε χώρα πιθανά κατά το πρώτο στάδιο της κρίσης αλμυρότητας του Μεσσηνίου (5.96-5.60 Εκατ.χρ.), στα αβαθέστερα τμήματα της λεκάνης προχώρας, η οποία σχηματίστηκε πάνω στο Προ-Απούλιο και Ιόνιο αλπικό υπόβαθρο. Ο σχηματισμός των περιβαλλόντων ιζηματογένεσης, πριν από την Ιόνια επώθηση, πιθανά οφείλεται στις ιδιαιτερότητες της λεκάνης προχώρας, η οποία εκείνο το διάστημα εκτείνονταν από την εξωτερική Ιόνια ως την εσωτερική Προ-Απούλια ζώνη. Νέα δεδομένα υπαίθρου, σε συνδυασμό με τη βιοστρωματογραφία, τα στοιχεία γεωτρήσεων και μία διαθέσιμη σεισμική τομή δείχνουν ότι τα Νεογενή ιζήματα πάνω στο Προ-Απούλιο υπόβαθρο αντιστοιχούν στον τμήμα της λεκάνης προχώρας, από το προβύθισμα (foredeep) ως την πρόσθια ανύψωση (forebulge), όπως αυτό διαπιστώνεται από την χωρική κατανομή του πάχους τους. Αντίθετα, τα Νεογενή ιζήματα πάνω στο Ιόνιο υπόβαθρο αντιστοιχούν στο τμήμα της λεκάνης προχώρας που βρίσκεται πάνω στο μετωπικό πρίσμα της ορογένεσης (wedge top), το οποίο βυθίζονταν λιγότερο όπως συνάγεται από το ελαττωμένο πάχος των ιζημάτων. Ο μικρότερος ρυθμός βύθισης οφείλεται στις διαπειρικές κινήσεις των Τριαδικών εβαποριτών. Στη Νεογενή ακολουθία, που βρίσκεται πάνω σε Προ-Απούλιο υπόβαθρο (περιοχή Άγιος Σώστης), παρεμβάλλονται επανιζηματοποιημένα μπλοκ δεκαμετρικού πάχους αποτελούμενα από σεληνίτη μικρού βάθους απόθεσης. Προς νότο, αυτή η βαρυτικά μεταφερόμενη μάζα της Μεσσήνιας γύψου μεταπίπτει κυρίως σε τουρβιδιτική γύψο. Στην περιοχή Καλαμάκι-Αργάσι που βρίσκεται πάνω σε Ιόνιο υπόβαθρο, το αβαθές περιβάλλον οδήγησε στην απόθεση της παρατηρούμενης πρωτογενούς γύψου. Η διάβρωση της πρωτογενούς γύψου τόσο της πρόσθιας ανύψωσης όσο και του μετωπικού πρίσματος επώθησης τροφοδότησαν το προβύθισμα της λεκάνης προχώρας με τουρβιδίτες γύψου.
Λέξεις κλειδιά: *γύψος, κρίση αλμυρότητας, Προ-Απούλια ζώνη, λεκάνη προχώρας.*

1. Introduction

Several analytical studies of the Messinian marine and evaporite deposits have been conducted across the Mediterranean realm over the past decades (Butler et al., 1995; Riding et al., 1998; Krijgsman et al., 1999**;** Iaccarino et al., 1999; Roveri et al., 2001; Krijgsman et al., 2002; Gargani et al., 2008; CIESM, 2008; El Euch-el Koundi et al., 2009; Mertz-Kraus et al., 2009; Lugli et al., 2010; Roveri et al., 2014). Few references and scarce analytical studies however exist on the Hellenic realm. This work presents the first results of a large study to investigate the Messinian salinity crisis in this area. In particular, the evaporite sequences in the Zakynthos Island are herein described. These consist of both primary shallow water gypsum, deposited into the shallower part of a basin, and gypsum turbidites deposited to its deeper part. It is determined that the tectonics of the foreland basins in front of the Ionian overthrust was the driving mechanism to the differentiation of the depositional environments.

2. Geological setting

The Island of Zakynthos is based on Alpine rocks belonging mainly to the Pre-Apulian (Paxos) and partly to the Ionian zone (Fig. 1). These two zones are separated by the Ionian thrust, whose emplacement took place in the Early Pliocene (BP, 1971; Sorel, 1976; Nikolaou, 1986; Underhill, 1989; Karakitsios, 2013). The Pre-Apulian zone of Zakynthos comprises upper Cretaceous to Pleistocene sediments, while the Ionian zone is represented by Triassic breccias and gypsum (corresponding to the lower stratigraphic unit of this zone); Cretaceous-Oligocene carbonates

outcrop only in the Marathonisi Islet (2.5 km east of Keri, Fig. 1) and probably represent a lateral transitional facies between Ionian and Pre-Apulian zone (Nikolaou, 1986). These sediments are followed by similar Neogene and Quaternary deposits as those of the Pre-Apulian zone, which are however less thick and characterized by unconformities.

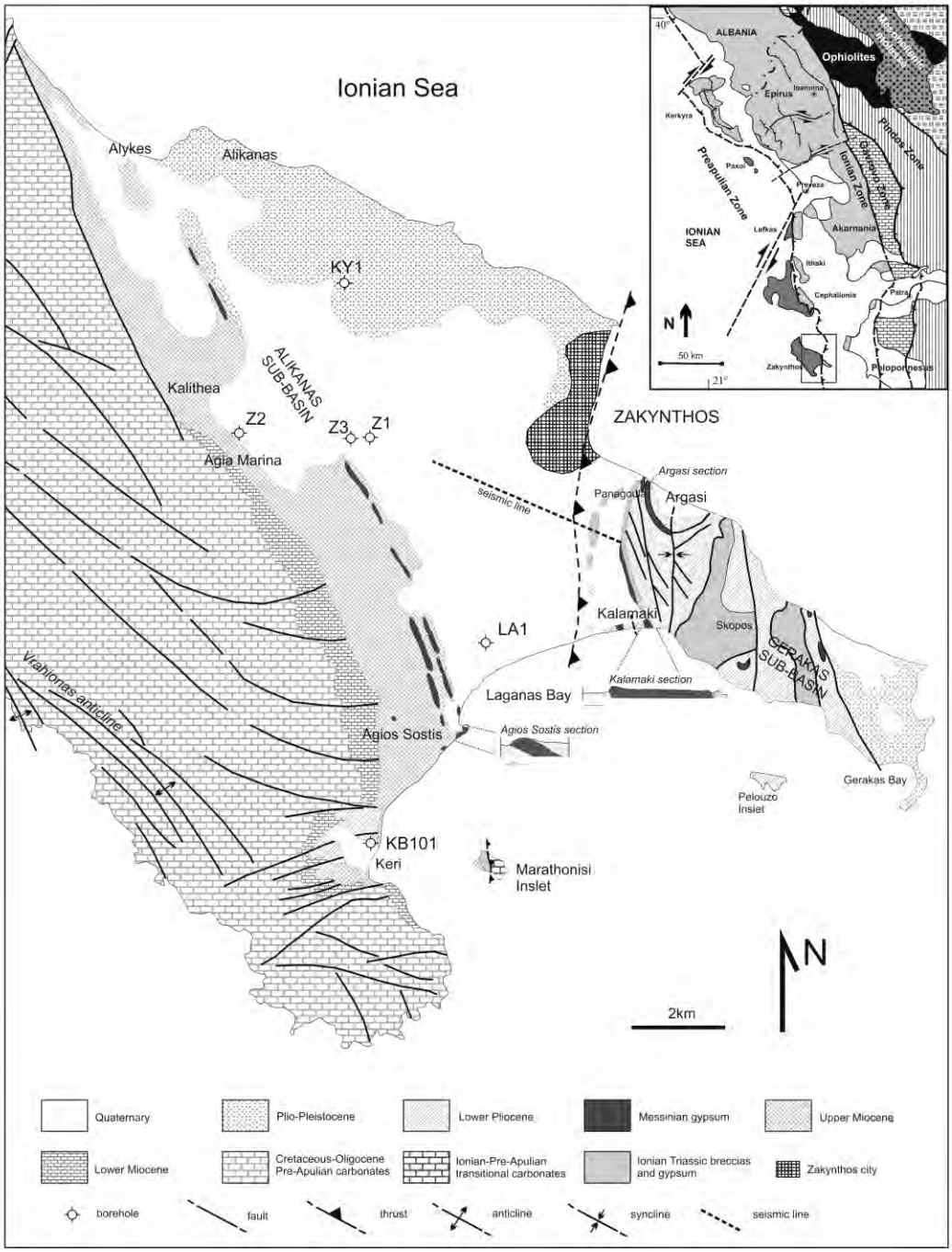

Figure 1 - Geological map of Zakynthos Island. The regional location is indicated in the inset map.

Significant shortening is seen in numerous NW-SE oriented reverse faults cutting through the Pre-Apulian Cretaceous-Oligocene sequence and within the late Miocene interbedded sandstone and marl sequences exposed in costal sections between Agios Sostis and Keri (Fig. 1). There, numerous post Miocene folds and reverse folds occur, indicating a post-Miocene age for the Ionian thrust emplacement (Underhill, 1989; Karakitsios, 2013). The Zakynthos Neogene and Quaternary deposits have been studied in several localities, mainly along the southeastern part of the island (Dermitzakis, 1977; Nikolaou, 1986; Triantaphyllou, 1996; Kontopoulos et al. 1997; Zelilidis et al. 1998; Duermeijer et al. 1999; Pierre et al., 2006; Agiadi et al. 2010). Based on these studies, the Lower Miocene Basin of Zakynthos Island was filled in the west by mainly clastic, flysch-type sediments, which eastward passed to shelf deposits. These deposits were followed by late Messinian marls and shales of 30-100 meters thickness, intercalated by Messinian gypsum beds. These evaporites have been interpreted as littoral to sabkha deposits (Dermitzakis, 1977; Nikolaou, 1986) or concentrated brines into shallow basins of less than 500m depth (Fabricius et al. 1978) or even as gypsum turbidites which were accumulated in water depths of less than a few hundred meters (Kontopoulos et al. 1997). The early Pliocene deposits on the Island comprise calcareous marls with pelagic fauna ("trubi" limestone) and sandstone intercalations. Middle Pliocene-Pleistocene corresponds to a transgressive sequence consisting of marls, clays, mudstones and sandstones in its lower part, while in the upper part it passes to an alternation of marls and marly limestones (Dermitzakis, 1977; Nikolaou, 1986).

3. Methodology

New field observations were made on the Argasi-Kalamaki and Agios Sostis areas, which were combined with detailed sampling. The field observations refer to the sedimentological and tectonic attributes of the Miocene to early Pliocene deposits in the study areas. In particular, field stratigraphic and sedimentological observations of the evaporite outcrops were carried out in order to distinguish the Triassic gypsum diapirs from the Messinian gypsum deposits in the southeastern part of Zakynthos Island (in the area between Kalamaki and Argasi), where both types crop out. Tectonic observations in conjunction with the available seismic profiles, allowed to precise the cartographic trace position of the Ionian thrust. Furthermore, the different types of evaporites were distinguished and cyclic deposition was also investigated in the evaporite sequence, as well as in the overlying "trubi" formation and the overlying lower Pliocene deposits. The work was focused in particular on the biostratigraphy and sedimentology of the lower and upper boundary transition of the Messinian evaporites. Overall, the palaeogeographic distribution of the Messinian gypsum deposits was determined by the integration of field and borehole data.

High-resolution sampling was carried out in order to perform integrated stratigraphy based on micro- and macropaleontological analyses (planktonic and benthic foraminifera, calcareous nannoplankton, ostracods, invertebrates and fish) and biogeochemical analyses (TOC content, stable isotope and organic biomarkers). Furthermore, core samples were obtained for magnetostratigraphic measurements, which are still under process.

The presented biostratigraphic analysis is based on the planktonic foraminifera assemblages. Planktonic foraminifera biostratigraphy of the Kalamaki section is based on the stratigraphic distribution of several late Miocene marker species supplemented by the coiling ratios of *Neogloboquadrina acostaensis*. The biostratigraphic analyses were carried out on 65 samples from the stratigraphic intervals below and above the gypsum *s.s.* deposits (samples Kal1-139 and Tr1-3).

4. Field observations

4.1 Kalamaki–Argasi Area

The Neogene sequence of the Kalamaki-Argasi area has been deposited over the Ionian zone basement. This section (Fig. 2) begins with a 15 meter-thick succession of alternating massive and

laminated marls with rare calcareous marls and calcarenite intercalations. In the middle part of the succession bivalves, *Discospirina*, pteropods and molluscs have been observed. This succession is followed by 10 meters of slumped and folded sediments of the same lithology, partially covered by Quaternary debris, in turn overlain by the 98 meter-thick evaporitic unit. Six cycles of depositional gypsum types are identified within the evaporite unit, corresponding to massive, massive stratified, banded and branching selenite facies (Lugli et al., 2010); in the upper third of the succession also thin gypsrudites and gypsarenites intercalations are present. These deposits can be ascribed to the Primary Lower Gypsum unit (PLG; Roveri et al., 2008) deposited during the 1st stage of the Messinian salinity crisis (5.971-5.60; CIESM, 2008; Manzi et al., 2013). The last 8 meters of the gypsum unit are clastic sediments, comprising laminated greenish marls, intercalated (after the first meter of the succession) by a decimetric gypsarenite bed. Overlying the gypsum unit, with a low-angle angular unconformity (Messinian Erosional Surface; MES; CIESM, 2008; Roveri et al., 2014), are approximately 4 meters of an irregular alternation of greenish marls and discontinuous calcareous marl beds belonging to the 'LagoMare' facies. In stratigraphic continuity over the latter, follows the "trubi" carbonate formation. The "trubi" formation begins with 3 meters of massive marly limestones which are overlain by an alternation of decimetric carbonate and laminated marl beds.

In Argasi area (Fig. 1) a gypsum unit is recorded, which is very similar to that of Kalamaki. Here, eight lithological gypsum beds have been recognized. However, in this area it is not possible to observe the stratigraphic transition of the gypsum unit to the overlying and the underlying formations, due to the tectonics and the Quaternary debris that cache them. To the south-easternmost Skopos area some minor outcrops of Messinian gypsum are present consisting of reworked gypsum and sporadic gypsum turbidites.

4.2 Agios Sostis Area

The Neogene sequence of Agios Sostis area has been deposited over the Pre-Apulian zone basement. In this section (Fig. 2), the first 10 meters consist of decimetre-thick shale-sandstone alternations showing an upward decrease of clastic input. They are followed by 3 meters of thin sandstone beds and marl alternations, which further pass to a 3 meters alternation of laminated green shales and marls. An erosional surface (MES) separates this lower unit from the overlying gypsum unit. The unit is about 15 meters thick, consisting of many alternations of primary (cumulate) and clastic (gypsrudite, gypsarenite and gypsiltite) gypsum. This evaporitic unit, largely characterized by clastic deposits and lacking the typical shallow-water bottom-grown evaporitic facies described in the Kalamaki–Argasi area, can be ascribed to the Resedimented Lower Gypsum unit (RLG, Roveri et al., 2008). This unit that derives from the dismantlement and resedimentation of the PLG deposits has been deposited during the 2nd stage of the Messinian salinity crisis (5.60-5.55; CIESM, 2008; Roveri et al., 2008). The whole sequence presents an upward increase of the siliclastic component and may be divided into four cycles, each topped by a centimetric marly bed. Some 2 meters of hybrid sandstone beds follow, which, after 1.5 meters of observation gap, pass to a 18-meters-thick succession comprising graded sandstone and marl alternations. This succession exhibits an upward decrease of clastic input. Two meters of whitish marls finish the section. North of the section's end, at a distance of 60 meters, the rocky elevation of the Agios Sostis port consists exclusively of "trubi" carbonates.

Following a NNW direction (Fig. 1), starting from a point about 800 meters WNW of the Agios Sostis section, the Neogene sequence is intercalated by decametre-thick resedimented blocks consisting of shallow water selenite. They linearly crop out for a distance of approximately 3 kilometres. To the southeast, this mass-wasting Messinian gypsum outcrops passes to mainly gypsum turbidites as the ones observed in Agios Sostis section. These gypsum turbidites also present a second linear and more extensive outcrop, which is parallel to the shallow water selenite outcrops (Fig, 1). It becomes clear that the second linear outcrops correspond to gypsum turbidites derived from the first one, and located basinward along the Messinian paleoslope.

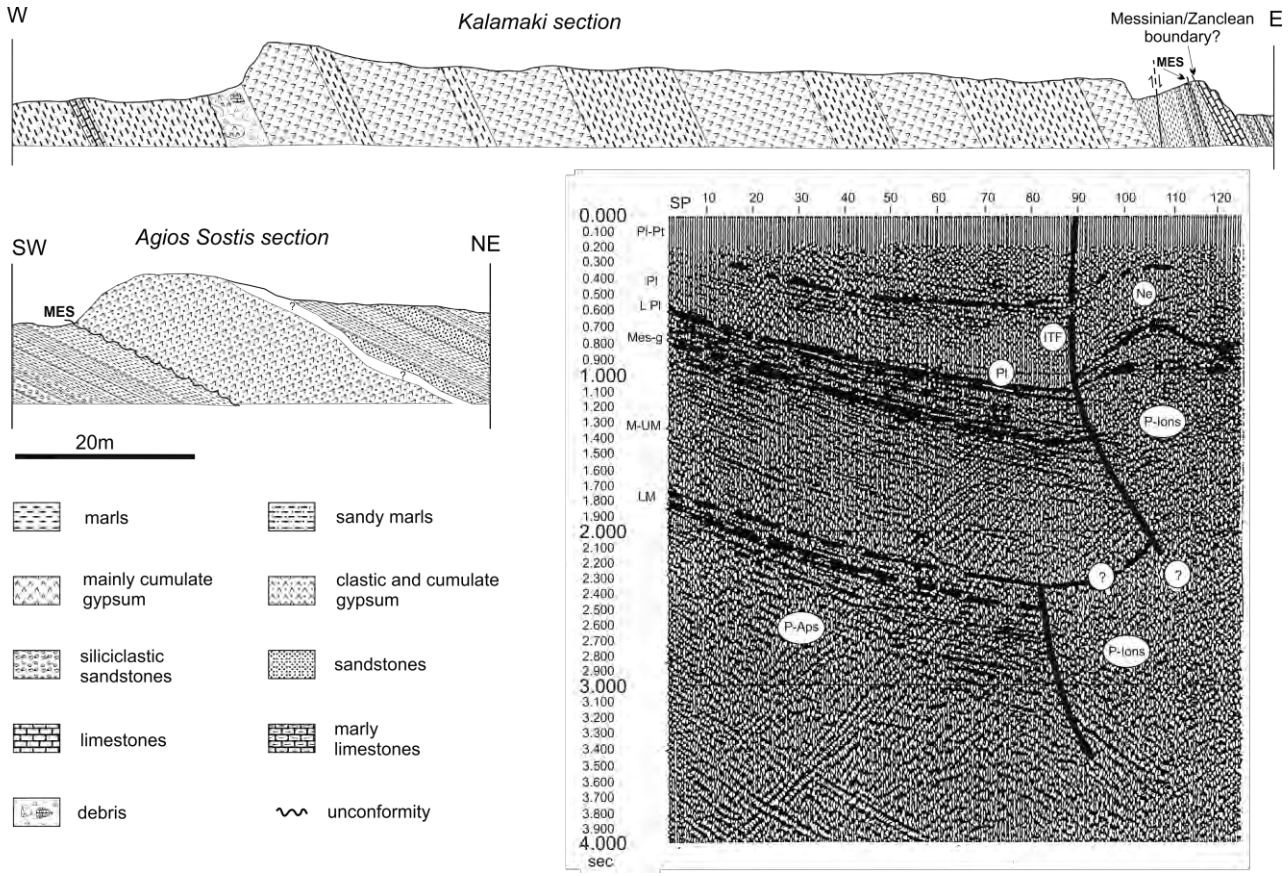

Figure 2 - Kalamaki and Agios Sostis sections. MES: Messinian Erosional Surface. Seismic profile of the Fig. 1 seismic line (modified from the initial interpretation by Marinescu; in Nikolaou 1986): Pl-Pt: Pliocene-Pleistocene, Pl: Pliocene, LPl: Lower Pliocene, Mes-g: Messinian Gypsum, M-UM: Middle-Upper Miocene, LM: Lower Miocene, P-Aps: Pre-Neogene sequence of Pre-Apulian zone, P-Ions: Pre-Neogene sequence of Ionian zone–Triassic evaporites, ITF: Ionian Thrust Front, Ne: Undifferentiated Neogene, SP: Shot point, sec: Time in seconds.

5. Biostratigraphy

In the Kalamaki section, the stratigraphic interval below gypsum unit *s.s.* (samples 1 to 91) is attributed to the Late Messinian based on the distribution range of *Turborotalita multiloba*. Planktonic foraminiferal assemblages are characterized mainly by *Turborotalita quinqueloba* and *Turborotalita multiloba*, whereas *Globigerinoides obliquus*, rare specimens of *Globigerinoides quadrilobatus*, *Globigerina bulloides*, *Orbulina* spp., *Globigerinita glutinata, Neoquoboquadrina acostaensis* and rare specimens of *Globoturborotalita decoraperta* are also present in several samples. *Turborotalita multiloba* as well as *N. acostaensis* dextral coiling specimens occur in the assemblages from the base of the studied section. According to Krijgsman et al (1999), Sierro et al. (2001), Blanc-Valleron et al. (2002) and Drinia et al. (2007, 2008), *T. multiloba* shows its first influx at 6.42 Ma, predating the *N. acostaensis* sinistral to dextral coiling change at 6.36 Ma. Sinistral coiled specimens of the latter species are very rare in our assemblages indicating that the studied interval may be placed within the MMi 13c *Turborotalita multiloba* interval Zone, dated above the age of 6.36 Ma.

The stratigraphic interval overlying the gypsum and below the 'trubi' carbonates records the presence of planktonic foraminifers in a few levels. In samples 113 to 117 rare planktonic and benthic foraminifers occurs in the scarce residues. The assemblage is characterized by the presence *N. acostaensis* dextral coiled specimens, *Globoturborotalita nepenthes*, *Sphaeroidinellopsis* spp. *G. obliquus*, *Orbulina* spp. *G. glutinata* and *G. bulloides.*

The base of 'trubi' carbonates (sample Tr 1) is characterized by rare specimens of *G. bulloides, G. obliquus, N. acostaensis* dextral coiling, very similar to the ones at the lowermost part of MPl 1 biozone. The acme zone of *Sphaeroidinellopsis* spp. is determined at the second meter of the "trubi" formation (sample Tr 2). The assemblage is well preserved and diversified and mainly consists of *Sphaeroidinellopsis* spp. Other species such as *O. universa, G. bulloides, N. acostaensis, G. obliquus extremus, G. apertura, T. quinqueloba, G. trilobus* are very abundant. *Globorotalia scitula* dextral coiled specimens exist in the fourth meter of the "trubi" formation (sample Tr 3). Specimens of *G. margaritae* were not recognized.

6. Discussion on the Neogene Basin's Palaeogeographic and Structural Evolution

Field observations indicate that the Neogene sediments, in the main part of Zakynthos Island, have been deposited over the Pre-Apulian zone formations, whereas those in the southeastern part have been deposited over the Ionian zone. The correlation of field data with the available boreholes and seismic sections (Fig. 2 and 3) demonstrates that the Neogene Pre-Apulian formations, east of the Vrahionas anticline (Fig. 1), form a monocline dipping approximately 30º ESE. Borehole stratigraphies (Fig. 1) show that Neogene deposits (Messinian gypsum included) increase their thickness toward the dipping monocline. Indeed, the Neogene sediments are 800 m thick in the west, and 1350 m thick in the east (Fig. 3). It is also noted that in the largest depocentral area (Agios Sostis area) the western-most gypsum outcrops consist of eradicated blocks of Primary Lower Gypsum whereas the eastern ones consist of gypsum turbidites and cumulates (e.g. Agios Sostis). This means that erosion of the PLG deposits accumulated in a shallow basin located in the western part of the Zakynthos Island (now completely eroded) provided the clastic material which was deposited toward the depocenter of the Neogene basin. On the other hand, Neogene formations over the Ionian zone, in the southeasternmost part of the Island, present a much lower thickness (between 200-300m). Gypsum deposits very close to the Ionian thrust correspond to primary gypsum (PLG unit), but going to the east (Skopos area) only some rare minor gypsum outcrops may be observed, mainly reworked gypsum and occasionally gypsum turbidites. These differences show that the Zakynthos Neogene basin was not uniform, but subsidence in the monocline area (over

Pre-Apulian basement) was more rapid, providing greater sea depths compared to the eastern area (over Ionian basement).
The above observations may be explained by a simple model of continental foreland-directed migration of the Hellenide (Alpine) thrusting, during the late Neogene and Pliocene. The foreland basin in front of the Ionian thrust was compared integrated to the foreland basin systems of De-Celles & Giles (1996), although it is necessary to take into consideration the particular role that the Ionian Triassic evaporites movements may have played. In this foreland basin system, the Neogene formations over the Pre-Apulian zone corresponded to the foredeep and the flank between foredeep and forebulge, whereas those overlying Ionian zone rocks corresponded to the wedge top. The intense subsidence characterizing the foredeep and flank to forebulge areas was reflected in the great thickness of the clastic Neogene formations over Pre-Apulian zone (between 800-1350m) which partially derived from the eroded Pre-Apulian forebulge. Simultaneously, the diapiric movement of the Ionian Triassic evaporites prevented substantial subsistence to occur. As a result, the eastern part of the Neogene basin, over the Ionian zone basement, corresponded to a land-subsiding wedge top. This is reflected in the observed thin clastic Neogene formations derived from the Ionian orogen erosion.

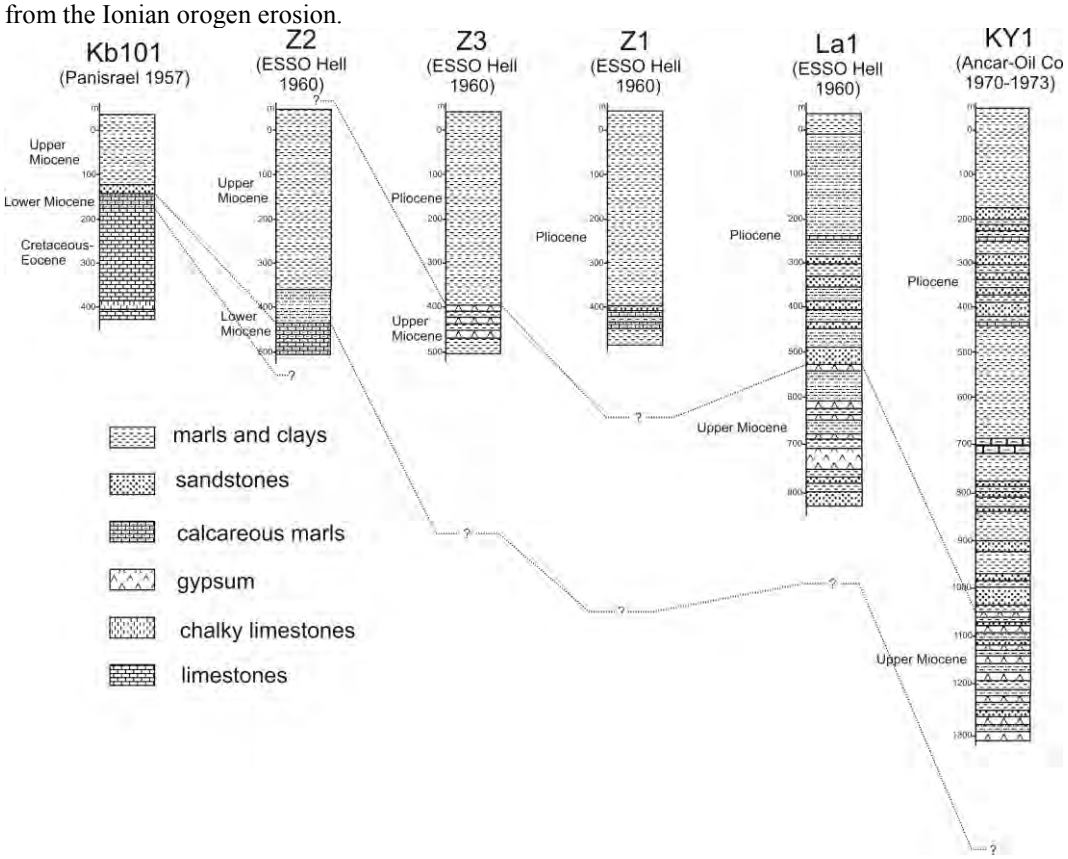

Figure 3 - Available borehole logs and correlations. Well operators are indicated.

The progressive filling of the foreland's basin Pre-Apulian part, during the Messinian, led the basin's area near to its forebulge to shallower depths. These depths together with the Upper Messinian overall negative hydrological balance (Mertz-Kraus et al., 2009) led to the deposition of the Primary Lower Gypsum unit. The subsequent erosion of PLG produced clastic gypsum that was deposited through gravity flows in the basin depocenter. At the same time, the wedge-top basin was characterized by shallower depths due mainly to the uplift of Triassic gypsum. Thus, the area close to the Ionian thrust received the observed primary gypsum deposits. Eroded gypsum material from these primary deposits supplied additional material to the foreland's basin foredeep

(to the west). In contrast, in the eastern areas (e.g. Skopos) the observed gypsum deposits are represented only by some relics of reworked gypsum and sporadic gypsum turbidites.

7. Conclusions

Detailed mapping of the Messinian deposits on Zakynthos Island shows that the primary evaporite basins, formed over Ionian basement, are delimited by the westernmost outcrop of the Triassic diapirs, located west of the Kalamaki-Argasi Messinian gypsum unit. The post-Miocene external Ionian thrust is emplaced west of the Triassic diapirs.

In Kalamaki-Argasi area, located over Ionian basement, the deposition of primary gypsum indicates a shallow water environment. Based on facies analysis these deposits have been ascribed to the Primary Lower Gypsum unit (PLG; Roveri et al., 2008; 2014; Lugli et al., 2010)

Planktonic foraminifera biostratigraphy of the Zakynthos Messinian outcrops indicates that primary evaporite accumulation took place, probably during the 1st stage of the Messinian salinity crisis (5.971-5.60 Ma), within shallower parts of a foreland basin, which was formed over the Pre-Apulian and the Ionian Alpine basement.

In Agios Sostis area, located over Pre-Apulian basement, the Neogene sequence is intercalated by decametre-thick resedimented blocks consisting of shallow water selenite. To the southeast, this mass-wasting Messinian gypsum passes to mainly gypsum turbidites, indicating a deeper environment. These deposits deriving from the dismantlement and resedimentation of the PLG unit can be ascribed at the 2nd stage of the MSC (5.60-5.55 Ma)

The development and distribution of the depositional environments before the activation of the Ionian thrust was probably due to the particularities of the foreland basin, which, at that time, extended from the external Ionian to the internal Pre-Apulian zone (Karakitsios & Rigakis, 2007). Field observations, borehole data and the available onshore seismic profile show that the Neogene sediments over the Pre-Apulian basement increase their thickness toward the E-SE direction, following the dipping of Alikanas monocline (the sediments thickness ranges between 800m in the west and 1350m in the east). In contrast, the Neogene sediments over the Ionian basement present reduced thickness (between 200-300m). Thus, subsidence rates were higher in the Pre-Apulian domain than in the Ionian domain. This is consistent with halokinetic movements of the Ionian Triassic evaporites (Karakitsios, 1995).

The above data may be integrated to the following foreland basin's scheme. In this basin, the Neogene formations over the Pre-Apulian zone corresponded to the foredeep and the flank between foredeep and forebulge, whereas those overlying Ionian zone rocks corresponded to the wedge top, which is consistent with the diapiric movements of the Ionian Triassic evaporites. Erosion of the primary gypsum of both forebulge and wedge top supplied the foreland basin's depocenter with gypsum turbidites.

8. Acknowledgments

This research has been co-financed by the European Union (European Social Fund – ESF) and Greek national funds through the Operational Program "Education and Lifelong Learning" of the National Strategic Reference Framework (NSRF) - Research Funding Program: THALIS –UOA- "Messinian Salinity Crisis: the greatest Mediterranean environmental perturbation and its repercussions to the biota".

9. References

Agiadi K., Triantaphyllou M., Girone A., Karakitsios V. and Dermitzakis M. 2010. Paleobathymetric interpretation of the fish otoliths from the lower - middle quaternary de-

posits of kephallonia and zakynthos islands (Ionian Sea, Western Greece), *Rivista Italiana di Paleontologia e Stratigrafia*,116(1), 63-78.

BP Co. Ltd .1971. *The Geological results of petroleum exploration in western Greece*, Institute for Geology and Subsurface Research (now I.G.M.E.), Special Report, 10, Athens.

Blanc-Valleron M.-M., Pierre C., Caulet J.P., Caruso A., Rouchy J.-M., Cespuglio G., Sprovieri R., Pestrea S. and Di Stefano E. 2002. Sedimentary, stable isotope and micropaleontological records of paleoceanographic change in the Messinian Tripoli Formation (Sicily, Italy), *Palaeogeogr. Palaeoclimatol. Palaeoecol*., 185, 255-286.

Butler R.W.H., Lickorish W.H., Grasso M., Pedley H.M. and Ramberti L. 1995. Tectonics and sequence stratigraphy in Messinian basins, Sicily: constraints on the initiation and termination of the Mediterranean salinity crisis, *Geolog. Soc. America Bull*., 107(4), 425-439.

CIESM 2008. *The Messinian salinity crisis from mega-deposits to microbiology. A consensus report*, In Briand, F., ed., CIESM Workshop Monographs, 33, 91-96.

Dermitzakis M.1977. Stratigraphy and sedimentary history of the Miocene of Zakynthos (Ionian Islands, Greece), *Ann. Geol. Pays Hell*., 29, 47-186.

DeCelles P.G. and Giles K.A. 1996. Foreland basin systems, *Basin Research*, 8(2), 105-123.

Drinia H., Antonarakou A., Tsaparas N. and Kontakiotis G. 2007. Palaeoenvironmental conditions preceding the MSC: a case study from Gavdros Island, *Geobios*, 40, 251-265.

Drinia H., Antonarakou A. and Kontakiotis G. 2008. On the occurrence of early Pliocene marine deposits in the Ierapetra Basin, eastern Crete, Greece, *Bull. Geosci*., 83(1), 63-78.

Duermeijer C.E., Krijgsman W., Langereis C.G., Meulenkamp J.E., Triantaphyllou M.V. and Zachariasse W.J. 1999. A late Pleistocene clockwise rotation phase of Zakynthos (Greece) and implications for the evolution of the western Aegean arc, *EPSL*, 173(3), 315-331.

El Euch-el Koundi N., Ferry S., Suc J.-P., Clauzon G., Melinte-Dobrinescu M.C., Gorini C., Safra A. and Zargouni F. 2009. Messinian deposits and erosion in northern Tunisia: Inferences on Strait of Sicily during the Messinian Salinity Crisis, *Terra Nova*, 21(1), 41-48.

Fabricius F.H., Heimann K.O. and Braune K. 1998. Comparison of site 274 with circum-Ionian land sections: implications for the Messinian "salinity crisis" on the basis of a dynamic model, *Initial reports DSDP*, 42, 927-942.

Gargani J., Moretti I. and Letouzey J. 2008. Evaporite accumulation during the Messinian Salinity Crisis: The Suez Rift case, *Geophysical Research Letters*, 35(2), L02401.

Iaccarino S., Castradori D., Cita M.B., Di Stefano E., Gaboardi S., McKenzie J.A., Spezzaferri S. and Sprovieri R.1999. The Miocene–Pliocene boundary and the significance of the earliest Pliocene flooding in the Mediterranean, *Mem. Soc. Geol. Ital*., 54, 109-131.

IGRS-IFP.1966. *Etude Geologique de l'Epire (Grece Nord-Occidentale)*, Ed. Technip., 306 pp.

Karakitsios V.1995. The influence of preexisting structure and halokinesis on organic matter preservation and thrust system evolution in the Ionian basin, northwestern Greece, *AAPG Bulletin*, 79, 960-980.

Karakitsios V. and Rigakis N. 2007. Evolution and petroleum potential of western Greece, *Journal of Petroleum Geology*, 30(3), 197-218.

Karakitsios V. 2013. Western Greece and Ionian Sea petroleum systems, *AAPG Bulletin*, DOI: 10.1306/02221312113.

Kontopoulos N., Zelilidis A., Piper D.J.W. and Mudie P.J.1997. Messinian evaporites in Zakynthos, Greece, *Palaeo3*, 129(3-4), 361-367.

Krijgsman W., Langereis C.G., Zachariasse W.J., Boccaletti M., Moratti G., Gelati R., Iaccarino S., Papani G. and Villa G.1999. Late Neogene evolution of the Taza-Guercif Basin (Riffian Corridor, Morocco) and implications for the Messinian salinity crisis, *Marine Geology*, 153(1-4), 147-160.

Krijgsman W., Blanc-Valleron M.-M., Flecker R., Hilgen F.J., Kouwenhoven T.J., Merle D., Orszag-Sperber F. and Rouchy J.M. 2002. The onset of the Messinian salinity crisis in the Eastern Mediterranean (Pissouri Basin, Cyprus), *EPSL*, 194(3-4), 299-310.

Lugli S., Manzi V., Roveri M. and Schreiber B.C. 2010. The Primary Lower Gypsum in the Mediterranean: A new facies interpretation for the first stage of the Messinian salinity crisis, *Palaeogeography Palaeoclimatology Palaeoecology*, 297, 83–99.

Manzi V., Gennari R., Hilgen F., Krijgsman W., Lugli S., Roveri M. and Sierro F.J. in press. Age refinement of the Messinian salinity crisis onset in the Mediterranean, *Terra Nova*.

Mertz-Kraus R., Brachert T.C., Reuter M., Galer S.J.G., Fassoulas C. and Iliopoulos G. 2009. Late Miocene sea surface salinity variability and paleoclimate conditions in the Eastern Mediterranean inferred from coral aragonite δ18O, *Chemical Geology*, 262(3-4), 202-216.

Nikolaou C.1986. Contribution to the knowledge of the Neogene, the geology and the Ionian and pre-Apulian limits in relation to the petroleum geology observations in Strophades, Zakynthos and Kephallinia islands*, PhD thesis* (*unpublished)*,University of Athens, 228 pp.

Pierre C., Caruso A., Blanc-Valleron M.M., Rouchy J.M. and Orzsag-Sperber F. 2006. Reconstruction of the paleoenvironmental changes around the Miocene-Pliocene boundary along a West-East transect across the Mediterranean, *Sed. Geol*., 188-189, 319-340.

Riding R., Braga J.C., Mart n .M. and Sánchez-Almazo I.M.1998. Mediterranean Messinian Salinity Crisis: constraints from a coeval marginal basin, Sorbas, southeastern Spain, *Marine Geology*, 140, (1-40), 1-20.

Roveri M., Bassetti M.A. and Ricci Lucchi F. 2001. The Mediterranean Messinian salinity crisis: an Apennine foredeep perspective, *Sedimentary Geology*, 140(3-4), 201–214.

Roveri M., Lugli S., Manzi V. and Schreiber B.C. 2008. The Messinian Sicilian stratigraphy revisited: new insights for the Messinian salinity crisis, *Terra Nova*, 20(6), 483-488.

Roveri M., Flecker R., Krijgsman W., Lofi J., Lugli S., Manzi V., Sierro F.J., Bertini A., Camerlenghi A., De Lange G.J., Govers R., Hilgen F.J., Hubscher C., Meijer P.Th., Stoica M., 2014. The Messinian Salinity Crisis: past and future of a great challenge for marine sciences, *Marine Geology*, 35: 25-58.

Sierro F.J., Hilgen F.J., Krijgsman W. and Flores J.A. 2001. The Abad composite (SE Spain): A Mediterranean reference section for the Mediterranean and the APTS, *Palaeo3*, 168,141-169.

Sorel D. 1976. Etude néotectonique dans l'arc égéen externe occidental, *Thèse 3^{e} c.*, Paris XI, 200 pp.

Triantaphyllou M.V. 1996. Biostratigraphical and ecostratigraphical observations based on calcareous nannofossils of the eastern Mediterranean Plio-Pleistocene deposits, *GAIA*, 1, Athens, 229 pp.

Underhill J.R. 1989. Late Cenozoic deformation of the Hellenide foreland, western Greece, *Geol. Society of America Bull*., 101: 513-634.

Zelilidis A., Kontopoulos N., Avramidis P. and Piper D.J.W. 1998. Tectonic and sedimentological evolution of the Pliocene-Quaternary basins of Zakynthos Island, Greece: Case study of the transition from compressional to extensional tectonics, *Basin Research*, 10(4), 393-408.

Δελτίο της Ελληνικής Γεωλογικής Εταιρίας, τομ. XLVII2013
Πρακτικά 13ου Διεθνούς Συνεδρίου, Χανιά, Σεπτ. 2013

Bulletin of the Geological Society of Greece, vol. XLVII 2013
Proceedings of the 13th International Congress, Chania, Sept. 2013

THE APPLICATION OF GRAIN SIZE TREND ANALYSIS IN THE FINE GRAINED SEABED SEDIMENT OF ALEXANDROUPOLIS GULF

Karditsa A.[1] and Poulos S.E.[1]

[1] *University of Athens, Faculty of Geology and Geoenvironment, Department of Geography & Climatology, Panepistimioupolis – Zografou, 15784, Attika, Greece kkarditsa@geol.uoa.gr, poulos@geol.uoa.gr*

Abstract

Grain size trend analysis is a method that determines sediment transport direction, based on the relationship of grain size parameters (mean size, sorting, skewness). The application of the method in the seabed sediments of Alexandroupolis Gulf showed that there are three different sub areas of distinctive sediment movement of bottom sediments (water depths <40 m):(i) the eastern part, which is mainly influenced by the Evros river water/sediment influxes; (ii) the central part that is primarily controlled by the wave activity; and, (iii) the western part that is mainly influenced by the wind driven and/or thermo-saline coastal circulation.
Key words: *sediment transport pathways, grain size, NE Aegean Sea.*

Περίληψη

Η ανάλυση της τάσης των κοκκομετρικών παραμέτρων είναι μία μέθοδος που καθορίζ ει την διεύθυνση μεταφοράς των ιζημάτων με βάση τη σχέση μεταξύ των κοκκομετρικ ών παραμέτρων (μέσο μέγεθος, διαβάθμιση, ασυμμετρία). Η εφαρμογή της μεθόδου στα επιφανειακά ιζήματα του Κόλπου της Αλεξανδρούπολης έδειξε ότι υπάρχουν τρεις διαφορετικές υποπεριοχές με διαφορετική μεταφορά των επιφανειακών ιζημάτων (βάθη <40m): (i) το ανατολικό τμήμα, το οποίο επηρεάζεται κυρίως από την παροχή νερού/ιζήματος από το ποτάμι του Έβρου, (ii) το κεντρικό τμήμα το οποίο ελέγχεται κυρίως από την κυματική δραστηριότητα και (iii) το δυτικό τμήμα το οποίο επηρεάζεται από την ανεμογενή και/ή θερμοαλατική παράκτια κυκλοφορία.
Λέξεις κλειδιά: *διάδρομοι μεταφοράς ιζημάτων, κοκκομετρία, ΒΑ Αιγαίο.*

1. Introduction

A variety of techniques have been developed to assess sediment mobility and transport pathways (e.g. McLaren, 1981; McLaren & Bowles, 1985; Gao & Collins, 1991, 1992, 1994; Le Roux, 1994). The application of these methods is based on the spatial relationship between grain size parameters (i.e., mean size, sorting, skewness) of seabed sediments. The primary assumption of grain size trend analysis models is that spatial variations in grain size parameters are the result of sediment transport processes, such as abrasion, selective transport and the mixing of sediments from varying sources. Relative variations in grain size parameters also indicate two dominant trends: (i) sediment are better sorted, finer and more negatively skewed in the direction of

transport; and (ii) sediment become better sorted, coarser and more positively skewed in the direction of transport.

These techniques have been applied in a variety of environments i.e. beaches, rivers, continental shelves. Among these applications of sediment trend analysis, the two dimensional and most widely used in open marine environments for the definition of trend vectors approach is the Grain Size Trend Analysis (GSTA)method, introduced by Gao and Collins (1991; 1992; 1994) and assessed positively by Poizot (2006).The technique can be applied to inner continental shelves and coastal environments and has been appliedin several cases with varying success (e.g. Rhone River coast by Masselink (1992), La Salie beach at Southwest French coast by Gao et al. (1994), the Belgian continental shelf by Pedreros et al. (1996) and Van Wesenbeeck & Lanckneus (2000).

One basic requirement of the technique is that its application should not extend beyond the boundaries of a particular sedimentary environment (Gao and Collins, 1992), being characterised by (at least) one major process response mechanism. However, most frequently there are several mechanisms acting either independently in different parts of the system or sequentially within the same area (Reineck & Singh, 1973).

The purpose of this contribution is to investigate sediment transport pathways in the Alexandroupolis Gulf (water depths from 5 up to 40 m) with the application of the Grain Size Trend Analysis (GSTA) method of Gao and Collins (1992).

2. Study Area

The Gulf of Alexandroupolis, which belongs to the inner continental shelf of the NE Aegean Sea (Samothraki Plateau), has a smooth subaqueous relief with very low gradients (<1%). Seabed has a zonal granulometric distribution with the nearshore sediments (<10m depth) consisting of sand, those extending in the middle area (10-30m depth) consisting of fine–grained (muddy) material, while sediments in the offshore area (water depths >30m) being characterized as muddy sandsrepresent a transitional zone to relict sand deposits (Karditsa & Poulos, 2013) that extent from water depths>40m) up to 60m (Perrisoratiset al., 1988; Pehlivanoglou, 1989; 2000).

The study area, as part of the North Aegean Sea, is a tideless environment with astronomical tidal range <10 cm (Tsimplis, 1994), although, meteorological forcing induced by southerly winds may occasionally increase sea level up to 0.80 m (HHS, 2005). In terms of wind-induced waves, the coast of the Gulf is predominately exposed to SW (4.8%), S (1.8%) and SE (0.8%) directed waves.The overall offshore water circulation in Alexandroupolis Gulf is mainly controlled by the fringes of the Samothraki anti-cyclone, which implies an eastward circulation in the offshore waters of the Gulf (Zervakis & Georgopoulos, 2002; Olson et al., 2007). However, wind driven currents formed under strong winds are able to change offshore current direction (Kourafalou & Tsiaras, 2007). In addition, a cyclonic circulation along the northern coast has founded to exist during summer period (Zervakis & Georgopoulos, 2002) and, in particular, under the influence of southerly winds (Androulidakis & Kourafalou, 2011).

The distribution pattern of Evros river plume is mainly directed either southwards under the influence of Samothraki anticyclonic circulation or westwards under the influence of Coriolis Effect and the prevailing NE winds. In addition, plume dispersion has also identified within the nearshore zone having also a westward direction and being associated with nearshore wave induced currents (Georgopoulos, 2002; Kanellopoulos et al., 2009; Karditsa, 2010).

3. Methodology

A total of fifty-three (53) bottom sediment samples were collected from the area under investigation, with the use of a VanVeen grab, during a sampling campaign in September 2008 (Figure 1). After the granulometric analysis of the sediment samples, the grain size parameters,

mean size (Mz), sorting (σ_I) and skewness (Sk_I) (according to Folk, 1980) were defined.Kurtosis is not considered a measurement that can provide any further information onthe grain-size distribution, for use in the interpretation of sediment transport (McLaren,1981).

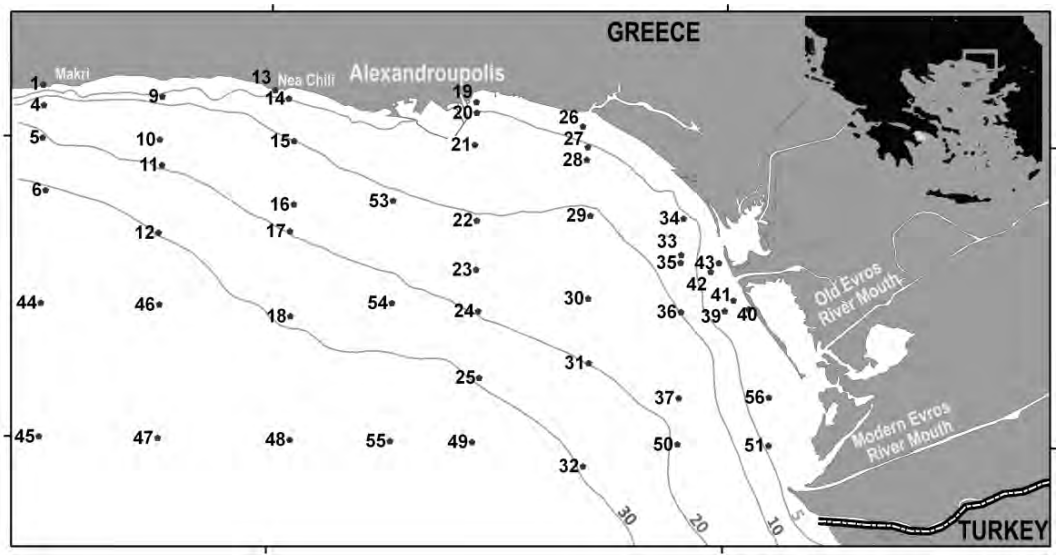

Figure 1- Sampling sites for the seabed sediments.

For the identification of sediment transport pathways, the GSTA method (Gao and Collins, 1992) was applied, which is based on the spatial relationship between grain size parameters (mean size, sorting, skewness) of seabed sediments. The major assumptions of the GSTAmethodare: (i) trend vectors are defined within a grid of sampling site by comparing sediment samples with all its neighbouring samples within a characteristic distance (D_{cr}) that is defined as the space-scale of sampling.; (ii) at each sampling site, vectors are summed to produce a single trend vector; (iii) An average of the sediment trend vectors is applied for the characteristic distance (D_{cr}) used; and (iv) a statistical test can be performed to validate the significance of the transport vectors. In addition, one principal consideration of the method is that Sediment trends can predict the direction of the transport but not the magnitude(Gao and Collins, 1994); this indicates that assigning a vector length, other thanunity, will create a bias towards one of the grain size parameters.

Taking into consideration that problems often arise during the comparison of samples collected on the basis of an irregular grid and in order to increase the spatial resolution of the method, transformation of the data sets can be made by applying an interpolation method. This acceptance is based on the principle that, in any sedimentary environment where the basic requirements of the trend analysis are fulfilled, the grain size parameters of the surficial sediments can be considered as regionalised (i.e. spatially continuous) variables (Davis, 1986).

One underlying requirement of the technique is that its application should not extend beyond the boundaries of a particular sedimentary environment (Gao and Collins, 1992). Therefore, the technique would not promise a successful application in the complex environment of Alexandroupolis Gulf. In order to overcome the limitations of the technique it is applied only to the fraction of the fine grained material (<0.0625 mm), whose origin is primarily associated to Evros terrestrial influx.

In order to describe transport patterns, the application of the GSTA method Gao and Collins (1992) is based on the spatial relationship of the granulometric parameters (M_z,σ_I, Sk_I)between two successive points A and B.Considering that the net sediment transport is from A to B,the derivation of the transport trendscould be identifiedon the basis of two cases:

- Case A:$\sigma_I B \leq \sigma_I A$, $M_z B \geq M_z A$ και $Sk_I B \leq Sk_I A$

- Case B: $\sigma_I B \leq \sigma_I A$, $M_z B \leq M_z A$ και $Sk_I B \geq Sk_I A$

Since the method requires a regular grid, 2 km cells were created after transformation with an interpolation (krigging) method. In addition, in order to avoid edge effects only the sites within the grid were used.

4. Results and Discussion

Following the application of GSTA method only to the fine grained (<0.625mm) fraction of the seabed sedimentthe distribution patterns of mean grain size, sorting and skewness coefficients are shown in Table 1 and in Figure 2. Mean grain size pattern shows that sediments become finer to seawards, while relatively finer sediment observed in front of the Evros mouth areas and along a N-S belt trending offshore from the west area of Alexandroupolis port. Sorting improves to seawards with the eastern area to present relatively poorer sorting than the western part, with respect to port location. The best sorted sediments are associated with Evros river delta front area (depths 5-10 m).High positive skewness values are located at water depthsbetween 10 and 20 m to the west of the port and secondarily at the Evros river mouth area; the former is related to the erosion of coastal Quaternary formations of Makri, while the latter to riverine sediment inputs. Generally, in water depths greater than 30m, fine-grained sediment are characterised by mean sizes >7.5 φ, are less poorly sorted (<1.9 φ) and almost symmetrical ($Sk_I \approx 0$).

Table 1 – Granulometric parameters results.

Station	x (Greek Grid)	y (Greek Grid)	Mz(φ)	σ_I(φ)	Sk_I(φ)
37	414214,33	4512932,24	7,42	1,93	0,02
36	414288,64	4515582,97	8,12	1,6	0,04
39	415643,37	4515613,66	7,81	1,73	0,02
38	416382,43	4515675,59	7,32	1,69	0,13
40	415908,74	4515945,56	7,28	1,82	0,06
41	415959,76	4516104,11	7,18	1,71	0,19
42	415208,59	4516823,23	7,13	1,73	0,18
43	415457,77	4517094,23	7,06	1,64	0,27
35	414279,55	4517104,09	7,35	1,88	0,04
34	414362,83	4518466,86	6,79	2,08	0,01
33	414296,40	4517344,44	6,95	1,7	0,21
1	394613,31	4522597,07	6,59	1,69	0,2
4	394632,49	4521971,31	7,35	1,88	0,05
5	394597,13	4520970,66	6,8	1,96	0,11
6	394683,67	4519350,21	7,3	1,78	0,06
12	398168,89	4518031,92	7,27	1,83	0,1
11	398276,39	4520121,51	5,91	1,99	0,52
10	398208,47	4520905,22	5,85	2,04	0,55

Station	x (Greek Grid)	y (Greek Grid)	Mz(φ)	$\sigma_I(\varphi)$	$Sk_I(\varphi)$
9	398284,36	4522230,99	6,54	1,73	0,09
13	401773,43	4522426,17	6,6	1,86	0,14
14	402194,35	4522165,21	7,09	1,84	0,11
15	402355,52	4520856,64	7,13	1,96	0,05
16	402338,11	4518900,91	6,87	2,04	0,08
17	402221,80	4518078,99	6,75	1,97	0,17
18	402236,41	4515460,37	7,8	1,7	0,08
25	408063,93	4513561,16	7,19	1,8	0,1
24	408031,78	4515615,53	6,85	1,94	0,15
23	407966,10	4516893,14	6,8	2,04	0,14
22	407991,98	4518408,32	6,38	2,12	0,23
21	407933,85	4520738,75	6,72	1,95	0,09
20	407988,32	4521726,21	6,89	1,92	0,14
19	407982,68	4522063,06	6,9	1,86	0,09
26	411261,88	4521312,36	7,02	1,75	0,17
27	411410,20	4520672,19	7,11	1,97	-0,01
28	411380,13	4520274,71	6,64	2,1	0,08
29	411488,89	4518558,07	7,71	1,98	0,01
30	411421,77	4516005,32	6,9	1,94	0,09
31	411441,49	4514010,35	7,12	1,85	0,09
32	411261,30	4510827,98	7,57	1,74	0,08
46	398190,50	4515822,12	7,44	1,79	0,02
44	394534,27	4515873,33	7,68	1,92	0,01
45	394475,62	4511756,75	7,8	1,83	-0,01
47	398133,88	4511705,54	7,92	1,85	-0,03
48	402214,24	4511650,57	7,8	1,87	-0,01
55	405309,67	4511610,36	7,84	1,85	-0,02
54	405364,08	4515865,67	7,82	1,86	-0,01
53	405404,32	4519010,92	7,85	1,86	-0,02
49	407842,30	4511578,42	7,84	1,86	-0,01
50	414173,85	4511502,37	7,85	1,86	-0,02
51	416987,86	4511470,31	7,84	1,86	-0,01
56	417004,45	4512950,41	7,84	1,86	-0,01
36	414288,64	4515582,97	7,84	1,86	-0,01

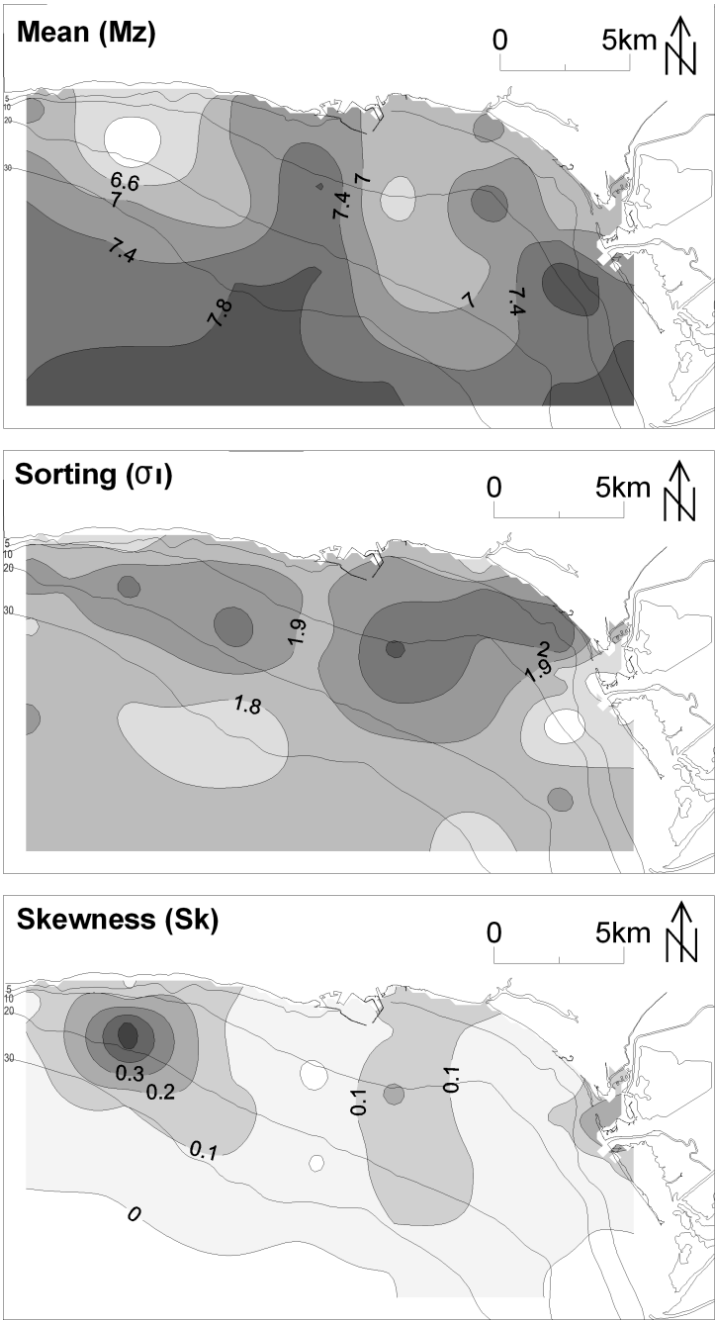

Figure 2- Distribution of grain size parameters (mean, sorting and skewness) (in φ units).

In Table 2 and Figure 3, sediment transport pathways of the surficial seabed sediments are presented schematically, after the application of the GSTA method. On the basis of these results and assuming that they are the product of the prevailing hydrodynamic conditions, three different sub areas of distinctive directions of sediment movements in the Alexandroupolis Gulf have been identified; these are: (i) the eastern part (A), where the dominant direction of sediment movement is towards the SW, indicating the influence of the river Evros plume and associating with offshore

dispersion of muddy sediment; (ii) the central and SE part (B), where fine grained seabed sediments are generally directed northwards, primarily, controlled by the hydrodynamic (wave) processes related to seabed sediment resuspension and transport (Karditsa & Poulos, 2013), which are modified by the NW dispersion of Evros plume from its current mouth; and (iii) the coastal north-western part (C), where the NW directed sediment transport, indicates that in addition to wave activity other factors are being participated, such as the advection of fine-grained products of coastal erosion (e.g., Makri Quaternary formations) and their offshore transport in suspension by the wind driven and/or thermo-saline coastal circulation.

Table 2 – Grain Size Trend Analysis results.

Number	x (Greek Grid)	y (Greek Grid)	Vector length	Vector Direction
1	394475,63	4510828,00	1,03	10,19
2	396978,81	4510828,00	1,29	0
3	399482,03	4510828,00	2,03	353,14
4	401985,22	4510828,00	1,41	355,06
5	404488,44	4510828,00	1,09	12,88
6	406991,63	4510828,00	0,43	58,97
7	409494,84	4510828,00	0,43	58,97
8	411998,03	4510828,00	0,63	11,18
9	414501,25	4510828,00	0,33	0
10	417004,44	4510828,00	0,94	348,82
11	394475,63	4513182,00	1,09	12,88
12	396978,81	4513182,00	1,13	8,2
13	399482,03	4513182,00	1,53	356,98
14	401985,22	4513182,00	1,16	4
15	404488,44	4513182,00	0,79	5,9
16	406991,63	4513182,00	0,26	66,61
17	409494,84	4513182,00	0,14	145,37
18	411998,03	4513182,00	0,38	12,39
19	414501,25	4513182,00	0,27	323,93
20	417004,44	4513182,00	1,06	360
21	394475,63	4515535,50	0,43	58,97
22	396978,81	4515535,50	0,44	47,94
23	399482,03	4515535,50	0,71	353,42
24	401985,22	4515535,50	0,07	359,99
25	404488,44	4515535,50	0,18	360
26	406991,63	4515535,50	0,59	146,96
27	409494,84	4515535,50	0,28	145,38

Number	x (Greek Grid)	y (Greek Grid)	Vector length	Vector Direction
28	411998,03	4515535,50	0,38	120,85
29	414501,25	4515535,50	0,11	133,25
30	417004,44	4515535,50	0	163,93
31	394475,63	4517889,50	0,7	44,16
32	396978,81	4517889,50	0,44	33,39
33	399482,03	4517889,50	0,97	4,79
34	401985,22	4517889,50	0,31	15,18
35	404488,44	4517889,50	0,89	0
36	406991,63	4517889,50	0,28	196,72
37	409494,84	4517889,50	0,1	308,28
38	411998,03	4517889,50	0,37	180
39	414501,25	4517889,50	0,31	195,18
40	417004,44	4517889,50	0,06	0,01
41	394475,63	4520243,00	0,26	66,62
42	396978,81	4520243,00	0,18	66,62
43	399482,03	4520243,00	0,75	12,39
44	401985,22	4520243,00	0,53	351,16
45	404488,44	4520243,00	1,11	0
46	406991,63	4520243,00	0,56	0
47	409494,84	4520243,00	0,36	0
48	411998,03	4520243,00	0,17	29
49	414501,25	4520243,00	0,31	164,82
50	417004,44	4520243,00	0,4	197,47
51	394475,63	4522597,00	0,7	15,18
52	396978,81	4522597,00	0,56	360
53	399482,03	4522597,00	1,4	0
54	401985,22	4522597,00	1,29	360
55	404488,44	4522597,00	1,23	0
56	406991,63	4522597,00	1,12	353,78
57	409494,84	4522597,00	0,4	342,53
58	411998,03	4522597,00	0,31	336,62
59	414501,25	4522597,00	0,13	246,62
60	417004,44	4522597,00	0,2	246,62

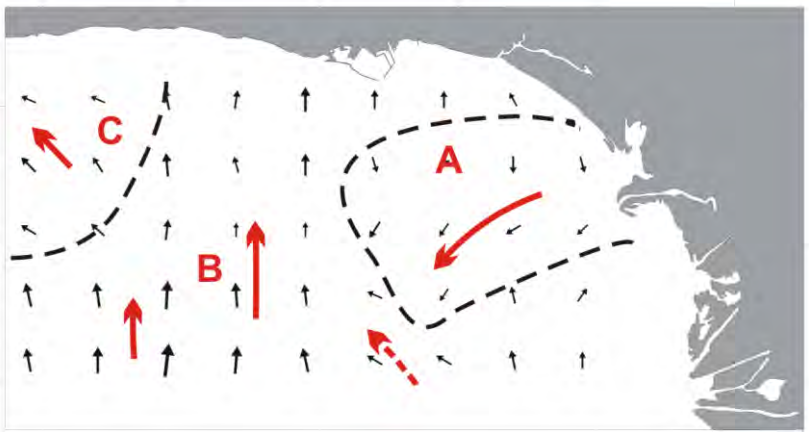

Figure 3- Sediment transport pathways over the fine grained seabed sediments of the Alexandroupolis Gulf.

5. Conclusion

The application of GSTA method in the fine grained material of the surficial sediments of Alexandroupolis Gulf describe three distinct trends of sediment transport: a SW movement at its eastern part, a general N movement at its central and southeastern part and a NW movement at its coastal north-western part. These sediment pathways are associated with the prevailing hydrological conditions, i.e. the westward Evros river plume dispersion, the wave induced hydrodynamic activity and coastal circulation pattern.

6. Acknowledgments

Dr A. Karditsa acknowledges the State Scholarship Foundation for the financial support during data collection and analyses. In addition, during the preparation of this manuscript the authors were supported by the co-financed by the European Union (European Social Fund – ESF) and Greek national funds through the Operational Program "Education and Lifelong Learning" of the National Strategic Reference Framework (NSRF)- Research Funding Program: THALES- MARE (MIS: 375655). Investing in knowledge society through the European Social Fund.

7. References

Androulidakis S.Y. and Kourafalou H.V. 2011. Evolution of a buoyant outflow in the presence of complex topography: The Dardanelles plume (North Aegean Sea), *J. Geophys. Res., 116*, doi:10.1029/2010JC006316.

Cheng P., Gao S. and Bokuniewicz H. 2004. Net Sediment Transport Patterns over the BohaiStrait Based on Grain Size Trend Analysis, *Estuar. CoastShelf S.*, 60(2), 203-212.

Davis J. C. 1986. *Statistics and Data Analysis in Geology* (2nd Edition). John Wiley & Sons, New York.

Gao S. and Collins M. 1991. A critique of the Mc Laren Method for defining sediment transport paths: discussion, *J. Sediment. Petrol*., 61 (1), 143–146.

Gao S. and Collins M. 1992. Sand sediment transport patterns inferred from grain-size trends based upon definition of transport vectors, *Sediment. Geol*., 80, 47–60.

Gao S. and Collins M. 1994. Analysis of grain size trends, for defining sediment transport pathways in marine environments, *J. Coast. Res*., 10 (1), 70–78.

Gao S., Collins M.B., Lanckneus J., De Moor G. and Van Lancker V. 1994. Grain size trends associated with net sediment transport patterns: an example from the Belgian Continental, *Shelf. Mar. Geol*., 121, 171-185.

Georgopoulos D. 2002. Water masses, dynamics and circulation in the Northern *Aegean Sea*. *Unpublished PhD Thesis*, University of Patras, Patra, Greece (in Greek), 324 p.

HHS (Hellenic Hydrographic Service), 2005. Tidal data from Greek Ports. *Hydrographic Service, Hellenic Army Navy, Athens*, 94 p.

Kanellopoulos T.D., Angelidis M.O., Kaberi H. and Assimakopoulou G., 2009. Suspended particulate matter geochemistry of the Alexandroupolis Gulf, northeastern Aegean, Sea, *Fresen. Environ. Bull*., 18, 429-437.

Karditsa A. 2010. Recent Sedimentation Processes in the Inner Continental Shelf of Alexandroupolis Gulf (North East Aegean Sea). *Unpublished PhD Thesis*, National and Kapodistrian University of Athens, Greece (in Greek), 245 pp.

Karditsa A. and Poulos S.E., 2013. Sedimentological investigations in a tideless river-influenced coastal embayment: The case of inner continental shelf of the NE Aegean Sea, *Cont. Shelf Res*., 55, 86-96, doi.org/10.1016/j.csr.2013.01.014.

Kourafalou V. and Tsiaras K. 2007. A nested circulation model for the North Aegean Sea, *Ocean Sci*., 3, 1-16.

Le Roux J.P., 1994. An alternative approach to the identification of sand sediment transport paths based on a grain-size trends, *Sediment. Geol*., 94, 97–107.

Masselink G. 1992. Longshore variation of grain size distributions along the coast of Rhone Delta, Southern France: a test of the McLaren model, *J. Coastal Res*., 8, 286-291.

Mc Laren P. 1981. An interpretation of trends in grain size measures, *J. Sediment. Petrol*., 51 (2), 611–624.

Mc Laren P. and Bowles D. 1985. The effects of sediment transport on grain-size distributions, *J. Sediment. Petrol*., 55 (4), 457–470.

Olson D.B., Kourafalou V.H., Johns W.E., Samuels G. and Veneziani M. 2007. Aegean surface circulation from a satellite-tracked drifter array*, J. Phys. Oceanogr*. ,37, 1898–1917.

Kourafalou V. and Tsiaras, K. 2007. A nested circulation model for the North Aegean Sea, *Ocean Sci*., 3, 1-16.

Pedreros R., Howa H.L. and Michel D. 1996. Application of Grain Size Trend Analysis for the Determination of Sediment Transport Pathways in Intertidal Areas, *Mar. Geol*., 135(1-4), 35-49.

Pehlivanoglou K. 1989. Evros delta, evolution of continental shelf sediments,*Mar.Geol*.,87,27- 29.

Pehlivanoglou K., Tsirambides A. and Trontsios G. 2000. Origin and Distribution of Clay Minerals in the Alexandroupolis Guf, Aegean Sea, Greece, *Estuar. Coast Shelf S*.,51, 61-73.

Perissoratis C., Moorby S.A, Papavasiliou C., Cronan D.S., Angelopoulos I., Sakellariadou F. and Mitropoulos D. 1988. Mineral concentrations in the recent sediments of Eastern Macedonia, Northern Greece, *Mar. Geol*., 7, 209-224.

Poizot E., Mear Y., Thomas M., and Garnaud S., 2006. The application of geostatistics in defining the characteristic distance for grain size trend analysis, *Comput. Geosci*., 32, 360–370.

Reineck H.E. and Singh I.B. 1973. Depositional Sedimentary Environments, *Springer Verlag*, Berlin.

Stevens R.L., Bengtsson H. and Lepland A. 1996. Textural provinces and transport interpretations with fine-grain sediments in the Skarerrak, *J. Sea Res*., 96, 1-3, 99-110.

Tsimplis M.N., 1994. Tidal oscillations in the Aegean and Ionian Seas. *Estuar. Coast, Shelf Sci*. 3, 201–208.

Vanwesenbeeck V. and Lanckneus J. 2000. Residual transport paths on a tidal sand bank: a comparison between the modified McLaren model and bedform analysis*, J. Sediment. Res*., 70, 470–477.

Vinther N., Christiansen C., Bartholdy J., Sorensen C. and Lund-Hansen L.C. 2004. Sediment transport across a tidal divide in the Danish Wadden Sea. Danish, *J. Geogr*. 104 (1), 71-86.

Zervakis V. and Georgopoulos D. 2002. Hydrology and Circulation in the North Aegean (eastern Mediterranean) throughout 1997-1998, *Mediterr. Mar. Sci*., 3(1), 7-21.

Δελτίο της Ελληνικής Γεωλογικής Εταιρίας, τομ. XLVII , 2013
Πρακτικά 13ου Διεθνούς Συνεδρίου, Χανιά, Σεπτ. 2013

Bulletin of the Geological Society of Greece, vol. XLVII 2013
Proceedings of the 13th International Congress, Chania, Sept. 2013

LATE QUATERNARY PALAEOENVIRONMENTAL CHANGES IN THE AEGEAN SEA: INTERRELATIONS AND INTERACTIONS BETWEEN NORTH AND SOUTH AEGEAN SEA

Kontakiotis G.[1], Antonarakou A.[1] and Zachariasse W.J.[2]

[1] National and Kapodistrian University of Athens, Faculty of Geology and Geoenvironment, Department of Hist. Geology - Paleontology, gkontak@geol.uoa.gr, aantonar@geol.uoa.gr

[2] Faculteit Aardwetenschappen, Universiteit Utrecht, wzachariasse@hetnet.nl

Abstract

The present study describes the Late Quaternary palaeoenvironmental evolution and the main palaeoceanographic changes of the Aegean Sea reconstructed using planktonic foraminifera. This approach, including Q-mode and R-mode cluster analyses, gives an insight into the relationships between sea surface environmental changes between north and south Aegean, and furthermore serves as a baseline data set for palaeoclimatic and palaeoceanographic reconstructions of the eastern Mediterranean Sea.

Key words: *planktonic foraminifera, last glacial cycle, palaeoceanography, palaeoecological reconstruction, eastern Mediterranean.*

Περίληψη

Η παρούσα μελέτη περιγράφει την παλαιοπεριβαλλοντική εξέλιξη και τις κύριες παλαιοωκεανογραφικές μεταβολές του Αιγαίου Πελάγους κατά τη διάρκεια του Ανωτέρου Τεταρτογενούς, με βάση τα πλαγκτονικά τρηματοφόρα. Η πολυπαραγοντική τους ανάλυση, που πραγματοποιήθηκε με βάση την ιεραρχική ανάλυση κατά συστάδες Q- και R-τύπου, αντανακλά τις περιβαλλοντικές αλλαγές μεταξύ βορείου και νοτίου Αιγαίου και επιπλέον χρησιμεύει ως βάση δεδομένων για τις παλαιοκλιματικές και παλαιοωκεανογραφικές αναπαραστάσεις της ανατολικής Μεσογείου.

Λέξεις κλειδιά: *Πλαγκτονικά τρηματοφόρα, τελευταίος παγετώδης κύκλος, παλαιοωκεανογραφία, παλαιοοικολογική αναπαράσταση, ανατολική Μεσόγειος.*

1. Introduction

The Aegean Sea has been the focus of intensive studies during the last half-century. The crucial importance of this small marginal basin is in its capability to register and amplify the smallest climatic variations occurring at the mid-latitude regions. The signals registered by changes in abundance and distribution of fossil micro-organisms, such as the planktonic foraminifera, represent one of the most powerful tools in many environmental reconstructions, and in the study area they provide a reliable and well-documented record at both global and local scales. They have proven to be reliable indicators in palaeoceanographic and palaeoclimatic studies, because they are seen as "fingerprints" of the water masses in which they live, behaving as indicators of temperature, salinity, and nutrient content and making it possible to identify past circulation

through the sedimentary record (Kennett, 1982). The uses of sediment cores have confirmed the importance of the information obtained from the study of these organisms. Evidence is mainly provided by high-sedimentation cores from open-ocean areas. In the eastern Mediterranean, accumulation rates are generally low, and as a result, only a few studies have focused on the last 30.000 years (e.g. Geraga et al., 2005; Triantaphyllou et al., 2010). An exception is the Aegean Sea, an area with unusually high sedimentation rates, where a large number of high quality gravity cores have been recovered. Therefore in the present study, we focus our attention on the Aegean Sea and especially on the planktonic foraminifera retrieved from this area, which contribute to palaeoenvironmental reconstruction of the last glacial cycle.

2. Materials and Methods

2.1. Study Sites

We have studied two gravity cores (NS-40 and SK-1) along the Aegean Sea. Core SK-1 recovered during the R/V Discovery cruise of 1982 in the north-central Aegean Basin (38° 80′ N and 23° 80′ E), at present day water depth of 1000 m. The core NS-40 recovered during the R/V Aegaio cruise of 1998, from a similarly deep site (1078 m depth), at the easternmost edge of the recent Aegean volcanic arc in south Aegean Sea (37° 01′ N and 26° 19′ E). Both cores consist of grey hemipelagic mud, intercalated with Santorini tephra layer Z2, the most recent sapropel S1 and turbidite layers (Zachariasse et al., 1997; Triantaphyllou et al. 2009; Kontakiotis, 2012). The established chronology of the cores NS-40 and SK-1 has led to an expanded palaeoecological reconstruction of the Late Glacial-Holocene archive in the Aegean Sea, spanning approximately the last 30 kyr_{nc} BP and 16 kyr_{nc} BP respectively (Kontakiotis, 2012).

2.2. Micropalaeontological Analyses

Detailed quantitative micropalaeontological analyses have been performed on 104 samples from the studied cores (55 from the core NS-40 and 49 from the core SK-1). After washing and drying at 60^{o}C, the samples were sieved through 150 and 63 μm mesh. The >150 μm size fraction was split into aliquots, from which 300 specimens of planktonic foraminifera were picked, identified and counted following the taxonomic concept of Hemleben et al. (1989). For palaeoenvironmental reconstructions, Q-mode and R-mode cluster analyses have been performed on the data set, after exclusion of rare species (< 2%) and grouping of species that have a discontinuous, scattered distribution at generic level. Q-mode cluster analysis was used to determine the overall statistical similarity between samples. R-mode cluster analysis was performed in order to obtain a more accurate differentiation of the planktonic foraminiferal assemblages extracted from the Q-mode cluster analysis, into environmentally significant groups.

2.3. Taxonomical Concept

The quantitative analysis of the planktonic foraminifera identified follows a stable taxonomical concept in both cores, in order to establish a planktonic foraminiferal biostratigraphic framework for the studied sections and examine the changes in sea-surface conditions and climate. Species with phylogenetic affinities and similar ecological characteristics were counted together and grouped to better interpret distribution patterns.

We identified 23 species lumped into 17 groups according to the following modifications. The *Globigerina bulloides* group includes the species *G. bulloides* and *G. falconensis,* because they present the same ecological requirements. All morphotypes of *G. ruber* (*G. ruber, G. elongatus, G. pyramidalis*, kummerform type) are plotted together, distinguishing only the “alba” and “rosea” varieties due to different ecological characteristics. The *Globigerinoides trilobus* group includes *G. trilobus* and *G. sacculifer* type, using the taxonomic concept of Hemleben et al. (1989), and the *Globigerinella siphonifera* group includes the species *Globigerinella aequilateralis, Globigerina calida* and *Globigerina digitata*. Moreover, the species *Globoturborotalita rubescens* and

Globoturborotalita tenella were counted and plotted together because of the similarity of their ecological characteristics (Capotondi et al., 1999). Furthermore, the species *Globigerinita glutinata* includes the morphotypes with and without bulla. Within the group of Neogloboquadriniids, two types have been discerned: *N. pachyderma* and *N. dutertrei*. Their different coiling directions have been counted and plotted separately, due to their different oceanographic requirements. Finally, the species *G. sacculifer, H. pelagica, G. rubescens, O. universa, G. digitata, G. tenella,* and *G. siphonifera* were grouped as SPRUDTS group (Rohling et al., 1993).

3. Results and Discussion

3.1. Planktonic Foraminiferal Trends

The faunal pattern of planktonic foraminiferal taxa for each core is plotted in Figures 1 and 2.

The *G. ruber alba* is abundant in north and south Aegean, being the main faunal constituent throughout the cores. Its maximum abundance occurs in the upper part of the cores and particularly during the deposition of sapropel S1. In the middle part of the cores, its distribution pattern is marked by a sharp increase in the abundance of *G. ruber alba*, corresponding to the last deglaciation. This is more pronounced in south Aegean (core NS-40). In the lower part of the cores, the distribution pattern of this species is limited, with the exception of the interval attributed to the Last Glacial Maximum. The distribution pattern of *G. ruber rosea* is characterized by high percentages in the upper part of both cores, with its maximum percentages to occur during the deposition of sapropel S1 and then decreasing gradually. This species is totally absent during the glacial period. *Globigerina bulloides* is continuously present, displaying almost the same distributional pattern in both cores. It reaches higher abundance values mostly in the upper part of the cores (Holocene) and in the lower part corresponding to the glacial period. It is worth noting the elevated percentages of *G. bulloides* in north Aegean during the deposition of the sapropel S1, which are attributed to a combination of increased river outflow and flushing of the Black Sea due to restored inflow of saline Mediterranean water at that time (Zachariasse et al., 1997). The *G. trilobus-sacculifer* group totally disappears within the glacial period, existing only in the upper part of the cores. More explicitly, its relative abundance curve displays a highly variable downcore pattern during the Holocene, occasionally reaching significant percentages during the deposition of S1. *O. universa* displays a sporadic distribution pattern being more abundant in the upper part of the cores. It shows several peaks in abundance during the deposition of S1, while it is almost absent in the lower part of the core, with its restricted occurrence in small percentages during the transition from the Late Glacial to the Holocene. The distributional pattern of *G. rubescens* is comparable with the relevant pattern of *G. siphonifera,* showing an overall upward increase. Moreover, the latter species shows a more sporadic distribution pattern than the former. On the contrary, *G. glutinata* displays a highly variable downcore pattern. It presents a continuous distribution in the core NS-40, with its maximum percentage values to occur in the middle and the lower part of the core, and a more sporadic distribution pattern in the core SK-1. *T. quinqueloba* is discontinuously present in both cores, occurring mostly in the lower part of the cores. During the Holocene, it displays a differential distributional pattern, since it mostly occurs below and above sapropel deposition and within the interruption in the core NS-40 and within the sapropel S1 in the core SK-1. In core NS-40, *G. inflata* reaches maximum abundance immediately above and below the deposition of, within the interruption of sapropel, as well as within the middle part of the core. In core SK-1 its occurrence is restricted at the end of S1, where it displays pronounced high values. *G. scitula* displays the same distribution pattern, existing in small percentages in the lower part of the cores, with only slight influxes to be recorded during the Younger Dryas (core SK-1) and the Holocene (upper part of S1a –core NS-40). *Groborotalia truncatulinoides* is present only in core NS-40, where it mainly restricted at the lower part of the core. Neogloboquadriniids, represented by *N. pachyderma* and *N. dutertrei*, are absent in the sapropel intervals. During the Holocene, they mainly occur within the interruption and above the sapropel interval. On the contrary, these

species are abundant during the glacial period, being the main faunal constituent (Geraga et al., 2005). However, *N. pachyderma* and *N. dutertrei* sinistrally coiled specimens, show significant influxes in the lower part of the core NS-40, which can be attributed to Heinrich events.

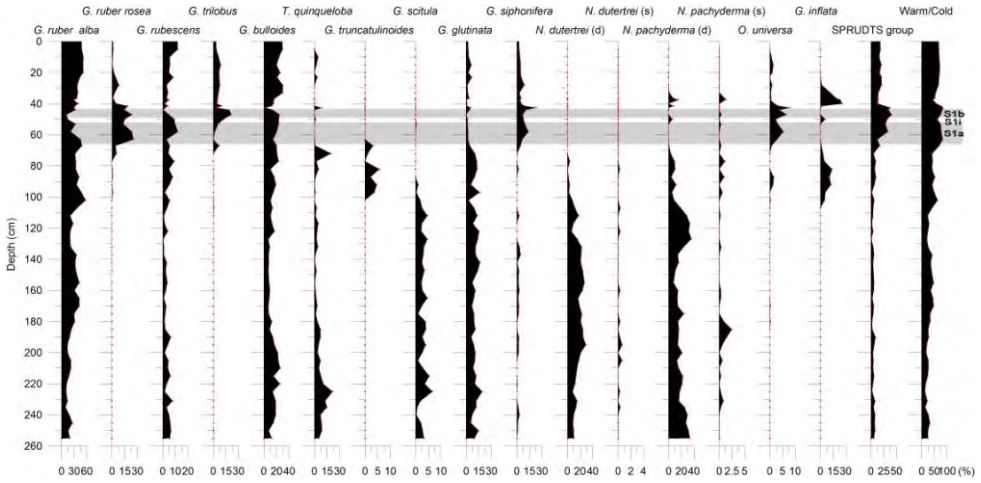

Figure 1 - Frequency curves of the most indicative planktonic species in core NS-40.

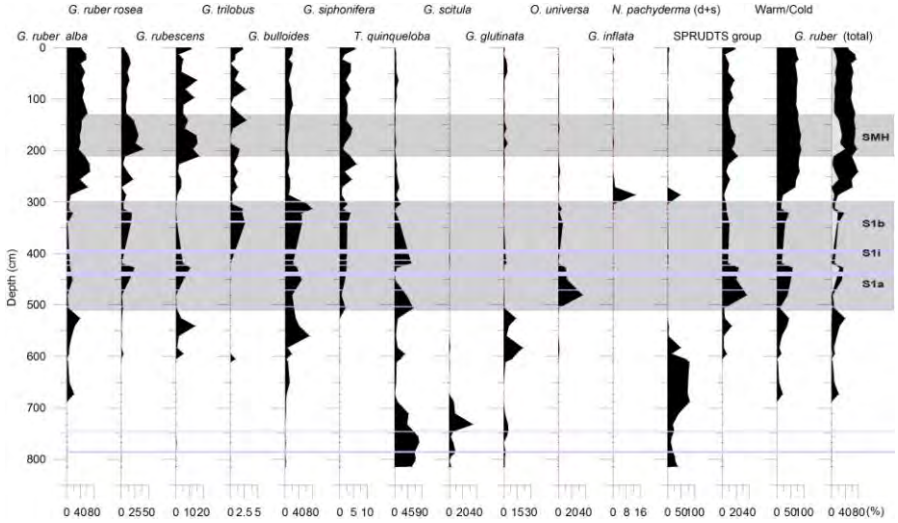

Figure 2 - Frequency curves of the most indicative planktonic species in core SK-1.

3.2. Planktonic Foraminiferal Assemblages

3.2.1. Q-mode Cluster Analysis

In order to describe the faunal succession, the samples of each core were treated with Q-mode cluster analysis to discriminate critic patterns in planktonic foraminiferal assemblages. Four and three distinct assemblages of planktonic foraminifera were identified by Q-mode cluster analysis in north and south Aegean respectively, reflecting different biotopes during the Late Quaternary (Figure 3 and 4). Each assemblage is characterized by dominant species as follows:

- **South Aegean (Figure 3):**
  - Biotope I (Assemblage Neogloboquadriniids): It contains 29 samples (OS27-OS56) and represents the lower part (107-255 cm) of the core NS-40 corresponding to the glacial period. This assemblage is dominated by individuals of neogloboquadriniids (N.

pachyderma and N. dutertrei) (26.33-51.08%, average 38.71%) and separated into two sub-assemblages depending on the principal representative species N. dutertrei (assemblage IA) or the species N. pachyderma (assemblage IB). The next abundant species is G. ruber (9.73-42.24%, average 25.98%), with its high abundance to be representative of the interglacial intervals. The third most abundant species is G. glutinata (5.37-18.88%, average 12.13%), while the species T. quinqueloba also has a significant presence in this assemblage (1.00 to 21.28%, average 11.14%). The species G. scitula (0.34-6.65%, average 3.45%) and G. rubescens (0.62-6.48%, average 3.55%) are also involved in lower percentages. It is also noteworthy the variability of the species G. bulloides, with its percentages to range from 7.16 to 25.59% (average 16.37%). This biotope is characterized by the seasonal thermal stratification of surface waters (glacial-interglacial periods) (Kontakiotis, 2012). The latter consists of the development of a warm mixed layer, which is accompanied by expansion of the thermocline during interglacial periods, as opposed to the abrupt reversal of the water column in cooler glacial intervals.

- Biotope II (Assemblage G. ruber alba-G. inflata-G. bulloides): It contains 26 samples (OS1-OS10, OS16, OS19-OS26) and represents sporadic parts of the core, at different periods, reflecting transitional assemblages. The first and the third branch (samples OS1-OS10, OS16, OS19) correspond to sub-assemblage IIA and IIΓ reflecting the modern water column of the southern Aegean, while the second branch (samples OS21-OS25) corresponds to the sub-assemblage IIB which is indicative of the deglaciation. This assemblage is dominated by the species G. ruber alba (11.60-57.19%, mean 34.4%) and G. bulloides (10.40-29.86%, average 20.13%), and contains both cold and warm water indicators. Its subdivision on each one of the three sub-assemblages depends on the presence or absence of temperate species (G. inflata, N. pachyderma, G. truncatulinoides). The sub-assemblage IIA is dominated by the species G. ruber alba and G. inflata. The abundance of the species G. bulloides and N. pachyderma is also significant. The relative abundance primarily in G. ruber alba and additionally in N. pachyderma implies strongly stratified surface and subsurface waters in the south Aegean Sea. In contrast, the high relative abundance of G. inflata and the significant presence of G. bulloides exhibit an isothermal and homogeneous water column (Coulbourn et al., 1980), as a result of the strong vertical mixing. However, their coexistence highlights the strong seasonal contrasts governing this sub-assemblage. The sub-assemblage IIB is characterized by the prevalence of the species G. ruber alba (33.80-47.11%, average 40.46%) and the simultaneous significant presence of species such as G. bulloides (10.40-23.10%, average 16.75%), G. inflata (4.51-13.60%, average 9.05%), N. pachyderma (5.06-11.59%, average 8.32%), G. glutinata (5.54-15.81%, average 10.68%), G. truncatulinoides (0-5.60%, average 2.80%), indicating a mesotrophic environment. This transitional fauna corresponds to the transition from cold and eutrophic water column of the glacial period in warm oligotrophic water column of the Holocene. The sub-assemblage IIΓ is characterized by the prevalence of G. bulloides (19.87-29.86%, average 24.67%) versus G. inflata (almost absent), and by the maintenance of the species G. ruber alba at the same high levels (33.12-51.94%, average 42.53%), indicating an oligotrophic-mesotrophic environment with strong seasonal fluctuations.
- Biotope III (Assemblage G. ruber alba-Sprudts group-G. bulloides): It contains 7 samples (OS11-OS15 and OS17-OS18) representing the deposition of the most recent sapropel S1. This assemblage is mainly dominated by species representative of warm and oligotrophic waters (G. ruber alba, G. ruber rosea, G. trilobus, G. siphonifera, O. universa), and furthermore shows a significant reduction in the relative percentages of G. bulloides, compared to previous biotopes.

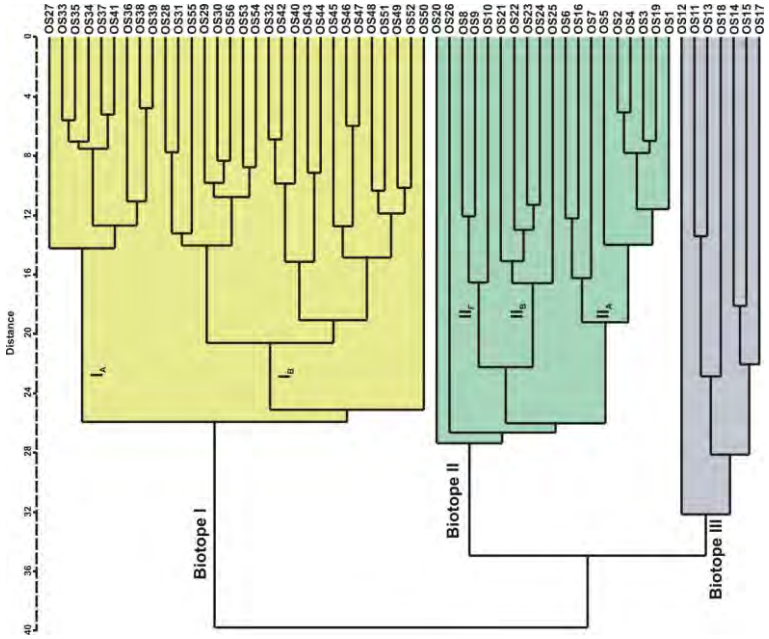

Figure 3 - Dendrogram resulting from Q-mode cluster analysis and the biotopes identified in core NS-40 (south Aegean).

- **North Aegean (Figure 4):**
  - Biotope I (Assemblage G. bulloides): It contains 9 samples (SK22-SK25, SK27-SK28 and SK32-SK33) representing the deposition of the most recent sapropel S1. The species G. bulloides plays dominant role in it, with its percentages reaching up to 80% of the total fauna. This species is living at the surface or subsurface waters and withstands large fluctuations in temperature, salinity and density (stratification) of the water column, without being limited from these physical parameters (Rohling et al., 1993, 1997). Particularly, the elevated percentages during the deposition of sapropel highlight the activity of neighboring rivers and therefore reflect a stratified water column. This finding is supported by the significant presence of the species T. quinqueloba, and O. universa, which have been associated with the reduced surface salinity conditions during the deposition of sapropel S1 (Zachariasse et al., 1997). However, the faunal composition of this assemblage indicates that the stratification of the water column is not limited to the surface, but it is continuous throughout the water column. G. ruber rosea is an indicator of maximum stratification of the water column and furthermore, the species G. siphonifera and Orbulina universa have the ability to live at greater depths during the summer, when the euphotic zone is strongly stratified. Thus, an increase in the abundance of all these species can be interpreted as an indication of the increase of the depth and the extent of the thermocline.
  - Biotope II (Assemblage G. ruber alba-SPRUDTS group-G. bulloides): It contains 20 samples (SK1-SK20) and represents the upper part of the core (0-271cm). This assemblage is mainly characterized by the prevalence of both varieties of the species G. ruber. Also abundant are the species belonging to the SPRUDTS group, with G. rubescens to be their main component (3.70-22.59%, average 13.15%). Next in abundance species is G. bulloides (6.42-22.02%, average 14.22%), but significantly lower compared to the previous assemblage. This assemblage is divided into three individual sub-assemblages, which show remarkable seasonal contrasts in temperature (sub-assemblage IIA), productivity (sub-assemblage IIB) and stratification of the water

column (sub-assemblage IIΓ), depending on the relative abundances of species involved. In sub-assemblage IIA the high percentages (> 60%) of G. ruber alba combined with the maximum concentrations of the species T. quinqueloba reveal the seasonal, in terms of temperature, development of the stratified water column. In sub-assemblage IIB, the simultaneous presence of oligotrophic (G. ruber alba, G. ruber rosea, G. rubescens, G. trilobus/sacculifer group, O. universa and G. siphonifera) and eutrophic (G. bulloides, N. pachyderma, T. quinqueloba and G. glutinata) species certifies the seasonal contrast according to the available food supply, which characterizes this sub-assemblage. The factor of seasonality is also reinforced by the continuous presence (even in small amounts; 0.20-3.90%, average 2.05%) of G. glutinata, since this species can survive both in oligotrophic surface, and in more eutrophic waters by changing its diet from diatoms to crysophytes (Hemleben et al., 1989). Finally, in sub-assemblage IIC the significantly high percentages of the species belonging to the SPRUDTS group, and the presence of the species G. inflata and N. pachyderma (Hemleben et al., 1989; Rohling et al., 1993, 1997) allow us to assess the role of water column stratification.

- Biotope III (Assemblage Neogloboquadriniids): It contains 7 samples (SK21, SK34 and SK36-SK40) and represents the middle part of the core, which corresponds mostly to the transition from glacial to Holocene period. This assemblage is characterized by the predominance of neoglobo-quadriniids (47.24-81.28%, average 64.26%). The fauna complement the species T. quinqueloba (0.96-19.47%, average 10.21%), G. bulloides (1.70-12.61%, average 7.16%), G. glutinata (0-20.70%, average 10.35%), G. inflata (0-13.20%, average 6.60%) and G. ruber alba (0-21.22%, average 10.61%). All these species present strong variations in their distribution pattern. Overall, this assemblage implies the existence of a mesotrophic to eutrophic, low-salinity environment. Furthermore, it should be noted that the relatively low percentages of G. ruber alba (compared to the same period covered by the same assemblage in the southern Aegean) are indicative of a cooler water column, which means that the transition from the glacial period to the Holocene was more abrupt in the north than in the south Aegean Sea.

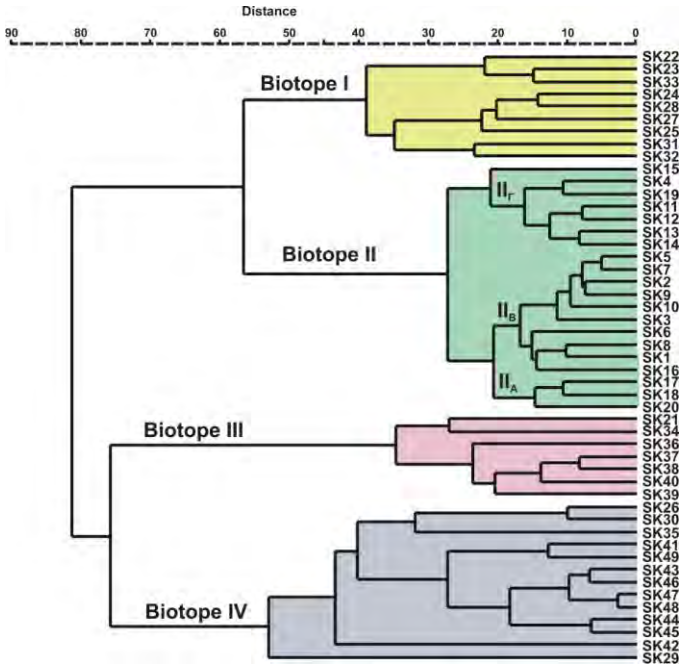

Figure 4 - Dendrogram resulting from Q-mode cluster analysis and the biotopes identified in core SK-1 (north Aegean).

- Biotope IV (Assemblage T. quinqueloba-Neogloboquadriniids): It contains 13 samples (SK26, SK29-SK30, SK35 and SK41-SK49), the majority of which represent the lower part of the core corresponding to the glacial period. It also includes the parts indicative of increased productivity and low salinity within the sapropel S1. The principal denominator in both cases of the north Ae-gean Sea is the dominance of the species T. quinqueloba (33.50-80.76%, average 57.13%). How-ever, within the glacial period, it is remarkable the high percentages of the Neogloboquadriniids (11.16-40.61%, mean 25.89%). Their high abundance in combination with the lower percentages of other cold-water species (e.g. G. scitula; 0.50-35.00%) reflect the presence of particularly cold and eutrophic water masses in the north Aegean Sea. Moreover, the lower response of neoglobo-quadriniids in northern compared to the southern Aegean Sea indicates the weakening of the Deep Chlorophyll Maximum that can be locally linked to the deepening of the pycnocline/noutrocline below the euphotic zone.

3.2.2. R-mode Cluster Analysis

R-mode cluster analysis was also performed in order to obtain a more accurate differentiation of the planktonic foraminiferal assemblages extracted from the Q-mode cluster analysis, into environmentally significant groups. Inspection of the R-mode cluster analysis dendrograms (Figure 5 and 6) allows the identification of 3 planktonic foraminiferal groupings for south Aegean and 2 for the north Aegean Sea.

- **South Aegean (Figure 5):**
  - Group A consists of the species G. trilobus, G. ruber rosea, G. siphonifera and O. universa indi-cating a warm and strongly stratified water column, which characterizes most of the Holocene, and especially the period of sapropel S1 deposition. Their abundance is mainly controlled (beyond temperature) by the stratification of the water column (Rohling et al., 1997), which varies depend-ing on the degree of development and the extent of the thermocline. This layer is essentially sepa-rating the species typical of warm and oligotrophic waters from those of cool and eutrophic waters. During the deposition of sapropel, as well as before and after this, the species G. ruber rosea and G. trilobus play the dominant role in fauna. They occur close to the surface, where there are the maximum levels of solar radiation and specifically into the low fertility mixed layer, which charac-terizes a strong vertical stratification of surface waters during the summer months (Hemleben et al., 1989). Similarly, the other species of this group live above the thermocline in a warm and well stratified water column (Rohling et al., 1993). Therefore, we interpret this group as indicative of the total area occupied by the layer of the thermocline.
  - Group B consists of the species T. quinqueloba, G. scitula, G. glutinata, N. pachyderma, N. duter-trei, G. bulloides, G. ruber alba and G. rubescens, which can be considered typical of the condi-tions prevailing during the glacial period. However, the ecological correlations between them al-low the additional separation of the last three species from the remaining species of this group, resulting in the sub-division of group B into two distinct sub-groups. Specifically, the first five species characterize very cold waters and increased productivity, while the last three species char-acterize less cold and mesotrophic-eutrophic waters. Therefore, we interpret the first sub-group as indicative of glacial intervals (stadials) and the second sub-group as indicative of interglacial periods (interstadials) during the glacial period.
  - Group C consists of the species G. inflata and G. truncatulinoides, indicating a homothermal water column throughout the euphotic zone, as a consequence of the strong convective mixing. Particularly, G. inflata prefers isothermal water masses (Coulbourn et al., 1980) during the winter or mesotrophic environments (Pujol & Vergnaud-Grazzini, 1995). In these nutrient-rich mixed waters, it prefers to live in the

deeper levels of the water column (50-150 m), whereas in mesotrophic environments they live in the upper 50 m of the water column. Specifically, during early summer where the stratification begins and DCM is absent, it lives below the seasonal thermocline, while in periods where the DCM is developed it lives in it. Moreover, it is indicative of horizontal exchange of water masses across the Mediterranean basin, with its high percentages in the western Mediterranean to reflect the influx of Atlantic waters and its low percentages in the eastern Mediterranean, to demonstrate the minor water exchange between the above sub-basins (Pujol & Vergnaud-Grazzini, 1995). Moreover, the coexistence of the temperate species G. truncatulinoides indicates the presence of intermediate to the previous two groups water masses, with the intense action of Levantine Intermediate Waters (LIW) in the basin of the south Aegean and Eastern Mediterranean in general (Rohling et al., 1997).

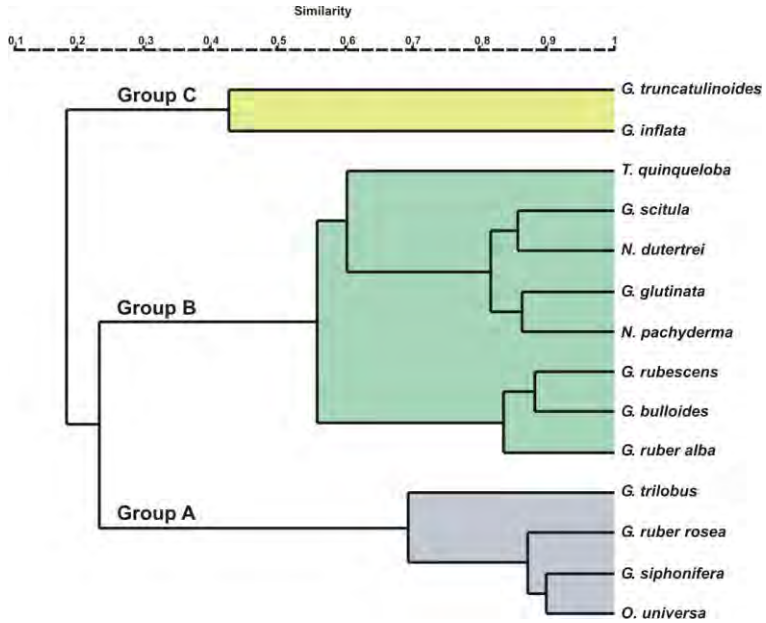

Figure 5 - Dendrogram resulting from R-mode cluster analysis and the assemblages identifie d in core NS-40 (south Aegean).

- **North Aegean (Figure 6):**
  - Group A is characterized by warm and oligotrophic water indicators, including the species G. ruber alba, G. ruber rosea, G. trilobus, O. universa, G. siphonifera, G. rubescens and G. bulloides. These species (with the exception of G. bulloides) often referred to the literature as «SPRUDTS group» (Jorissen et al., 1993; Rohling et al., 1993); this group is indicative of the deposition conditions of the most recent sapropel S1 and have been recorded in various Mediterranean regions (including the Aegean Sea). However, this group seems to characterize the water column of the north Aegean throughout the Holocene, culminating in the post-sapropel period where they reach their maximum percentages. The difference with the corresponding group (group A) of the core NS-40 is due to the incorporation of G. bulloides, which has the ability to live in various environments, by extracting its favor trophic elements from the water column (Rohling et al., 1997). Its capacity, to move vertically and migrate to different water depths, depending on the available food supply every season, offers it the opportunity to live all year round, justifying thus the strong seasonal contrasts governing modern water column of the north Aegean Sea.

– Group B is characterized by eutrophic, cold water indicators and includes the species N. pachyderma, N. dutertrei, T. quinqueloba, G. scitula and G. glutinata. This group also includes the temperate, mesotrophic species G. inflata and G. truncatulinoides, which reflect transitional conditions prevailing in north Aegean after the termination of the glacial period. Their co-existence in the same group shows that the conditions prevailing at the end of the glacial period in the northern Aegean, although improved, did not change significantly. This means that the transition from the glacial period to the Holocene period was not as gradual as in south Aegean.

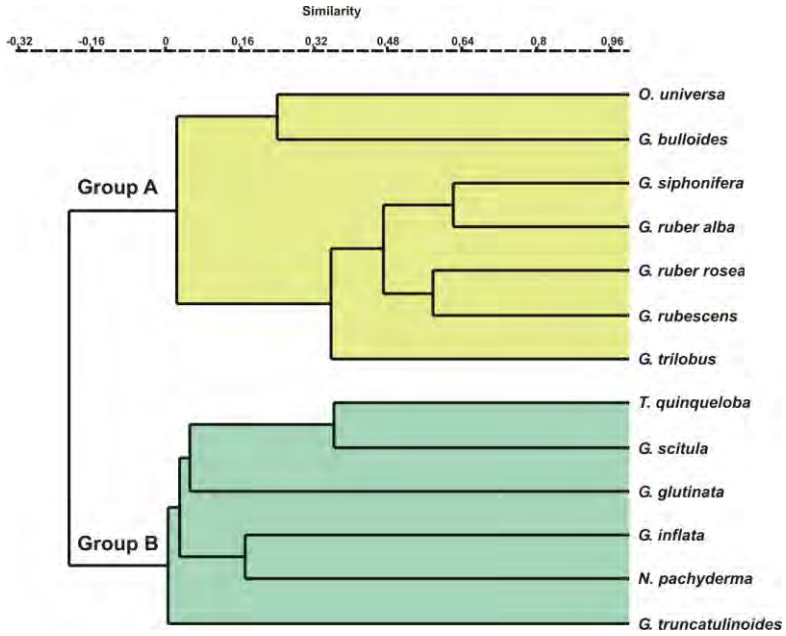

Figure 6 - Dendrogram resulting from R-mode cluster analysis and the assemblages identified in core SK-1 (north Aegean).

4. Conclusions

This study highlights the planktonic foraminiferal abundance variations during the last glacial cycle from two gravity cores (SK-1 and NS-40) along a north–south transect in the Aegean Sea. Q-mode multivariate cluster analysis describes four and three distinct assemblages of planktonic foraminifera in north and south Aegean respectively. The succession of assemblages allows dividing Late Quaternary sediments into four palaeoceanographic stages: 1) a warm-oligotrophic stage (typical of Holocene) characterized by the prevalence of *Globigerinoides ruber alba*-SPRUDTS group-*Globigerina bulloides*, 2) upwelling and runoff-low salinity conditions dominated by *Globigerina bulloides*, 3) a relatively warm to temperate with seasonal contrasts on temperature, productivity and stratification of the water column stage characterized by the *Globigerinoides ruber alba, Globorotalia inflata* and *Globigerina bulloides*, 4) a cool-eutrophic stage characterized by Neogloboquadriniids and *Turborotalita quinqueloba*. According to their stratigraphic distribution, the first and the second assemblages are typical for the deposition of sapropel S1 in south and north Aegean respectively, while the third is referring as a transitional assemblage of the last glacial-interglacial transition and the fourth one is corresponding to the last glacial period.

5. Acknowledgments

The authors are grateful to Associate Professor M. Triantaphyllou for providing part of the study material (core NS-40). Dr. Theodora Tsourou is also warmly thanked for her constructive suggestions during the processing of the images.

6. References

Capotondi L., Borsetti A.M. and Morigi C. 1999. Foraminiferal ecozones, a high resolution proxy for the Late Quaternary biochronology in the central Mediterranean Sea, *Mar. Geol*., 153, 253-274.

Coulbourn W.T., Parker G.L. and Berger W.H. 1980. Faunal and solution patterns of planktonic foraminifera in surface sediments of the North Pacific, *Mar. Micropaleontol.,* 5, 329-399.

Geraga M., Tsaila-Monopolis St., Ioakim Chr., Papatheodorou G. and Ferentinos G. 2005. Short-term climate changes in the southern Aegean Sea over the last 48000 years, *Palaeogeogr. Palaeoclimatol. Palaeoecol.*, 220, 311-332.

Hemleben C., Spindler M. and Erson O.R. 1989. *Modern Planktonic Foraminifera*, Springer, Berlin, 363 pp.

Jorissen F.J., Asioli A., Borsetti A.M., Capotondi L., de Visser J.P., Hilgen F.J., Rohling E.J., van der Borg K., Vergnaud Grazzini C. and Zachariasse W. 1993. Late Quaternary central Mediterranean biochronology*, Mar. Micropal*., 21, 169-189.

Kennett J. 1982. *Marine Geology*, Prentice-Hall Inc, Englewood Cliffs, 538-559.

Kontakiotis G. 2012. Palaeoceanographic and palaeoclimatic study of Eastern Mediterranean during Late Quaternary, based on planktonic foraminiferal assemblages, *PhD Thesis*, National & Kapodistrian University of Athens, Greece, pp. 1-247.

Pujol C. and Vergnaud-Grazzini C. 1995. Distribution patterns of live planktic foraminifers as related to regional hydrography and productive systems of the Mediterranean Sea, *Mar. Micropal*. 25, 187-217.

Rohling E.J., Jorissen F.J. and De Stigter H.C. 1997. 200 year interruption of Holocene sapropel formation in the Adriatic Sea, *J. Micropal*., 16, 97-108.

Rohling E.J., Jorissen F.J., Vergnaud-Grazzini C. and Zachariasse W.J. 1993. Northern Levantine and Adriatic Quaternary planktic foraminifera: Reconstruction of paleoenvironmental gradients, *Mar. Micropaleontol*., 21, 191-218.

Triantaphyllou M.V., Antonarakou A., Dimiza M. and Anagnostou Ch. 2010. Calcareous nannofossil and planktonic foraminiferal distributional patterns during deposition of sapropels S6, S5 and S1 in the Libyan Sea (Eastern Mediterranean), *Geo-Mar. Lett.*, 30(1), 1-13.

Triantaphyllou M.V., Antonarakou A., Kouli K., Dimiza M., Kontakiotis G., Papanikolaou M.D., Ziveri P., Mortyn P.G., Lianou V., Lykousis V. and Dermitzakis M.D. 2009. Late Glacial-Holocene ecostratigraphy of the south-eastern Aegean Sea, based on plankton and pollen assemblages, *Geo. Mar. Lett.*, 29(4), 249-267.

Zachariasse W.J., Jorissen F.J., Perissoratis C., Rohling E.J. and Tsapralis V. 1997. Late Quanternary foramineteral changes and the nature of sapropel S1 in Skopelos Basin, *5th Hell. Symp. Oceanogr. Fish*, NCMR Athens, Procceedings, 1, 391-394.

Δελτίο της Ελληνικής Γεωλογικής Εταιρίας, τομ. XLVII , 2013
Πρακτικά 13ου Διεθνούς Συνεδρίου, Χανιά, Σεπτ. 2013

Bulletin of the Geological Society of Greece, vol. XLVII 2013
Proceedings of the 13th International Congress, Chania, Sept. 2013

MOLLUSCAN ASSEMBLAGES IN A HIGHLY VARIABLE SETTING IN LITTORAL BOTTOMS OF THE LOWER PLEISTOCENE OF RHODES (GREECE)

Koskeridou E.[1], Thivaiou D.[1] and Giamali Ch.[1]

[1] National and Kapodistrian University of Athens, Faculty of Geology and Geoenvironment, Department of Hist. Geology - Paleontology, ekosker@geol.uoa.gr, dthivaiou@geol.uoa.gr, gchristi@geol.uoa.gr

Abstract

Highly diverse and well preserved marine mollusc associations from a sandy horizon of the Lower Pleistocene shallow water deposits of Rhodes island are here presented. Four significantly different molluscan assemblages characterize neighboring environments and document a variety of niches provided by the lateral change of bottom type. Molluscs of hard substrate to sandy seabed of the Infralittoral Zone were documented. A total of 55 molluscan species were identified. Gastropods dominate with 29 species. For the first time, the Ervilia castanea assemblage is described for the Lower Pleistocene of Greece.
Keywords: *Molluscs, Lower Pleistocene, Rhodes, Greece.*

Περίληψη

Στην εργασία αυτή μελετήθηκε η πλούσια και καλά διατηρημένη πανίδα μαλακίων που περιέχεται σε αμμώδες στρώμα ρηχών θαλάσσιων αποθέσεων του Κατωτέρου Πλειστοκαίνου της νήσου Ρόδου. Πιστοποιήθηκαν 4 διαφορετικές συγκεντρώσεις μαλακίων γειτονικών περιβαλλόντων καθώς και οι οικολογικές τους φωλεές οι οποίες καθορίζονται από την πλευρική μεταβολή του τύπου του υποστρώματος. Αναγνωρίστηκαν αντιπρόσωποι μαλακίων σκληρού υποστρώματος έως και αμμώδους βυθού της παράκτιας ζώνης. Προσδιορίστηκαν 55 είδη μαλακίων εκ των οποίων 29 είδη γαστερόποδων. Πιστοποιήθηκε η παρουσία της Ervilia castanea και της αντιπροσωπευτικής φάσης της στο Κατώτερο Πλειστόκαινο της Ελλάδας για πρώτη φορά.
Λέξεις κλειδιά: *Μαλάκια, Κατώτερο Πειστόκαινο, Ρόδος, Ελλάδα.*

1. Introduction

Rocky bottoms often neighbor soft-bottom sandy areas in the sea. These two habitat types support very different communities of plants and animals. Fossil organisms of high-energy shallow water marine environments characterized by siliciclastic sedimentation are usually uncommon because of the transportation by bottom currents, the fragmentation and dissolution of their skeletons. On the contrary, fossil shallow marine hard bottoms provide an exception as they constitute stable substrates where rich fauna is developed. A good example of this are the Gelasian drowned beachrock beds of northeastern part of Rhodes island which have been studied by Moissette et al.

(2013). These beds served as a zone of carbonate production and accumulation within a siliciclastic-dominated otherwise poor populated environment.

The Ervilia castanea (Montagu, 1803) facies characterizes wave exposed beaches from the Atlantic and the Mediterranean Sea has been studied and/or referred to by many authors (e.g. Morton et al. 1998, Zenetos et al. 2005). This facies is also one of the most representative siliciclastic facies in the deposits of Kritika member of Rhodes island.

In this study, highly diverse and well preserved marine mollusc associations accumulated in these deposits of the Lower Pleistocene have been recovered.

The main objectives of this paper are to compare the results obtained from the molluscs of the sandy bed from the Lower Pleistocene of Rhodes with those reported from the present-day Mediterranean and use this information to reconstruct the paleoenvironment and depositional conditions

2. Geology

The island of Rhodes is located at the easternmost part of the Hellenic sedimentary fore-arc, which resulted from the Cenozoic subduction of the African Plate under the Aegean-Anatolian Block (Fig.1).The Pliocene-Pleistocene sediments encountered at the northeastern part of the island provide basinal to littoral fossiliferous deposits that are well exposed in steep palaeovalleys cutting through the Hellenic Mesozoic basement (Meulenkamp et al. 1972, Pirazzoli et al. 1989, Hanken et al. 1996). This basement is mainly carbonated calcareous and it was faulted in different directions. Thus occur the numerous steep horsts and grabens that later defined the deposits of this age as far as their nature and geographical distribution is concerned (Mutti et al. 1970). The embayments of the Lower Pleistocene (Gelacian) formed the depositional environment of the Kritika Member of Rhodes Formation (Cornée et al., 2006). This age is given according to the recent redefinition of the Pleistocene (now inclunding the Gelasian Stage/Age as its lowermost unit, (Gibbard & Head, 2010)). It is composed of pebbles, gravels, sands and clays of estuarine to marine terrigenous origin. These beds are fossiliferous thus preserving a diverse range of taxa that correspond to fossil assemblages belonging to precise environments (paralic, nearshore).

The present study focuses on sandy beds of one outcrop of the Kritika Member (Rhodes Formation) which is composed predominantly of siliciclastic deposits intercalated with hard bottom levels formed by the drowning of former beachrock beds (Cornée et al., 2006; Moissette et al., 2013).

3. Materials and Methods

Molluscan faunas were examined in one representative sample recovered from the studied succession (Fig. 1). The field observations included considerations of shell orientation, disarticulation, fragmentation and encrustations to distinguish whether or not the shells had been transported before final deposition. The benthic fauna was separated from the terrigenous fraction using a 0.5 mm sieve for molluscs and a 0.062 mm sieve for foraminifera. The molluscs, encountered within the >0.5 μm size fraction were classified to species level, using the descriptions based on numerous works by molluscan researchers. Then, they were semi qualitatively analyzed and an estimation of the number of specimens of each species was made.

Palaeoecological and palaeoenvironmental interpretation of species was based on a series of researches on modern analogue communities especially from the Mediterranean.

4. Results

The sediments have been assigned to shallow marine sandy shell bed where the shell debris accumulated due to wave action and storm events.

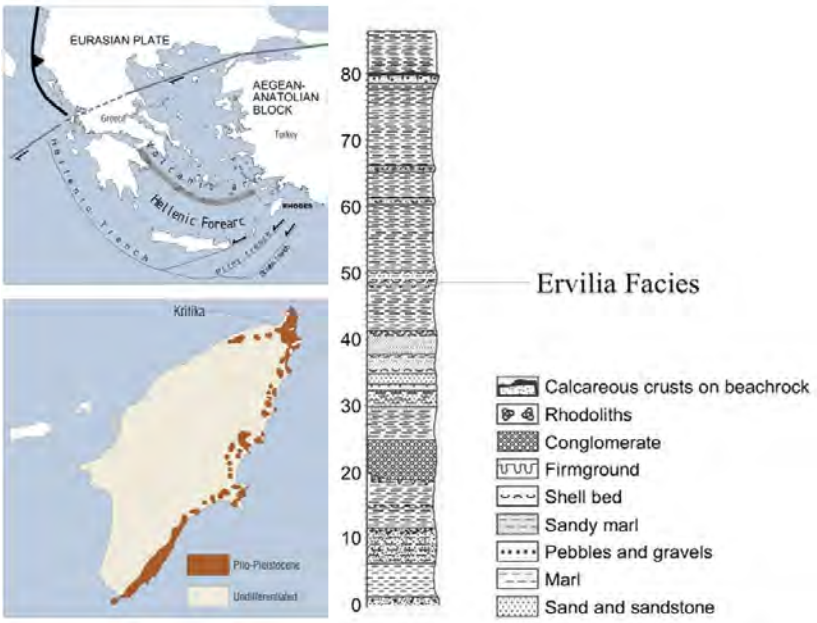

Figure 1 - Geographical location of the Island of Rhodes, location and lithological column of the Kritika Member section, Rhodes Formation.

The bivalves are represented by 26 species. The most abundant is the burrowing bivalve *Ervilia castanea* which is highly numerical dominated and is recorded for the first time in the Lower Pleistocene of Greece. The next most dominant species is the transported *Anomia ephippium.*

The benthic gastropod assemblage of 29 species is dominated by small climbing herbivorous forms, most of them grazing on epiphytes.

Many epibyssate forms have been identified: *Talochlamys multastriata, Lima inflata, Mytilus galloprovincialis* and *Mytilaster lineatus, Acar clathrata, Barbatia barbata, Arca noae, Arca tetragona*.

Nestling species as *Cardita calyculata* and *Striarca lacteal* also occur.

The infaunal elements that have been recognized are: *Tellina distorta, Tellina donacina, Callista chione, Lucinella divaricata, Dosinia exoleta*, *Dosinia lupinus, Diplodonta rotundata, Cardites antiquatus, Acanthocardia tuberculata, Donacilla cornea, Callista chione*, *Venus verrucosa*, *Timoclea ovata, Euspira catena, Natica* sp., *Neverita josephinia.*

The encrusting forms are: *Anomia ephippium,Chama gryphoides, Vermetus* sp., *Dedropoma* sp.

The crawling herbivores are: *Haliotis tuberculata, Bolma rugosa, Jujubinus striatus*, *Jujubinus exasperates, Gibbula magus*, *Gibbula ardens, Clelandella miliaris, Danilia tinei, Alvania cancellata, Alvania lineata, Rissoa* sp., *Tricolia pullus, Bittium reticulatum*, *Bittium latreillei.*

The carnivores *Naticarius stercusmuscarum*, *Nassarius* spp., *Euspira catena, Natica* sp., *Neverita josephinia, Ringicula ventricosa, Diodora graeca, Diodora gibberula*, *Buccinulum corneum, Bolinus brandaris*, have been also recovered.

The less dominant species are *Ringicula* sp., *Nassarius* sp., *Callista chione, Mytilaster lineatus* and Naticidae and rare species (1 specimen/species) are *Striarca lactea, Acar clathrata, Mytilus galloprovincialis, Acanthocardia tuberculata, Lucinella divaricata, Lucinella divaricata, Talochlamys multistriata, Tellina distorta, Danilia tinei*, *Bolinus brandaris.*

Except for the vermetids, all the other gastropods are well preserved. Among the bivalves the only articulated is *Ervilia castanea* while the while the remaining species are preserved unarticulated or fragmented.

5. Discussion – Conclusions

Most of the taxa collected in this work, exist in the present Mediterranean Sea (e.g. Pérès & Molinier, 1957, Pérès & Picard, 1964, Pérès, 1967, Logan, 1979, Zibrowius, 1980, Riedl, 1983, Barash & Danin, 1988, 1992; Zenetos et al. 2005), which enables a comparison between the palaeofauna and recent assemblages.

The studied malacofauna is the result of heterogeneous mixing of shells with different rates of abrasion, fragmentation and disarticulation, belonging to species typical of normal marine conditions and rocky, sandy or algal substrates from the littoral marine environments. Two different types of concentrations can be defined:

Autochthonous concentrations of bivalves found articulated in sandy substrates and parautochthonous concentrations of gastropods and bivalves, including some mixed allochthonous elements represented by abraded and fragmented shells of relatively deeper sublittoral species. These concentrations can be interpreted as the result of accumulation during storm events.

Four assemblages are found living on different substrates:

1. A vermetid assemblage. The upper mediolittoral zone biota of exposed rocky substrates is represented by *Dedropoma* and *Vermetus* fragments.
2. *Ervilia castanea* assemblage. Coarse sand habitat occurs in sand-wave formations in shallow water where the infauna is characterized by the small bivalve Ervilia castanea (Morton et al. 1998). The dense populations of this species in the studied material indicate that it is a very successful coloniser of such energetic environment. A comparison between the fossils from the studied deposits and the present day analogue communities suggest that some of the elements belonging to the original biocoenosis are absent. Thus the other main associated species of this habitat as small opportunistic capitellid and spionid polychaetes and isopods that are adapted to living in a highly perturbed environment, have not been fossilized. *Dosinia lupinus* and *Donacilla cornea* are also present in the otherwise impoverished fauna of this environment and confirm shallow water sandy environment (Koukouras & Russo, 1991). This is the only articulated in situ preserved assemblage.
3. Hard bottom biota assemblage. It consists of a wide variety of skeletal organisms and characterizes a habitat that has been formed by the drowning of former beachrock beds (Cornée et al., 2006; Moissette et al., 2013). The most representative taxa of those living on rocky substrates are: *Cardita calyculata, striarca lactel, Bolma rugosa, Haliotis tuberculata, Diodora graeca, Diodora gibberula.* Among those associated with seaweeds are: rissoids, *Jujubinus exasperatus, J. striatus, Tricolia pullus, Alvania cancellata, Bittium reticulatum, B. latreillei, Euspira catena, Neverita josephinia* and *Clelandella milliaris.* The latter may be enclaves within the following assemblage of *Posidonia oceanica* meadows. The hard rock substrates are very important since they provide both biological and geological information. They provide a stable environment for living organisms and they present a relatively high biodiversity.
4. *Posidonia oceanica* biota assemblage. The most representative species of sea grasses highlighted by this study, are: *Gibbula ardens, Alvania lineata, Tricolia pullus, Bittium reticulatum, Jujubinus striatus*, and the bivalves *Arca noae*, *Barbatia barbata, Lima inflata, Talochlamys multistriata, Venus verrucosa.*

Such fossilized species in hard bottom and *Posidonia oceanica* environments have been studied before in Rhodes (Moissette et al. 2007, Moissette et al. 2013), but in that case they are not in situ and they are represented with the other assemblages of the littoral bottom.

The "*Ervilia castanea*'' deposits acted as a "refuge" for the parautochthonous elements of hard bottom and relatively deeper water assemblages, due to storm events and probably quick sedimentation.

The analysis of these four assemblages led to the reconstruction of the littoral palaeoenvironment represented in Figure 2.

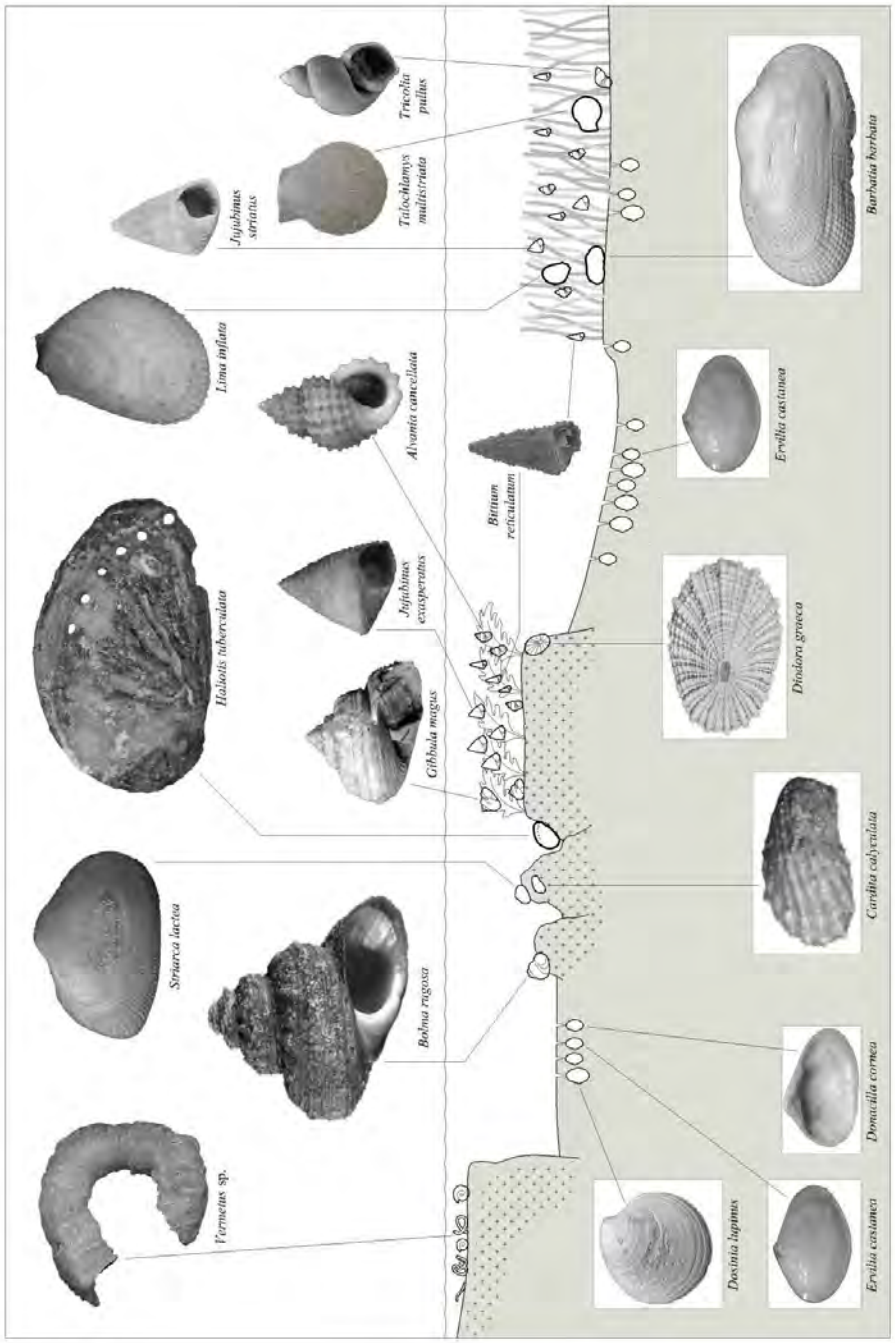

Figure 2 - Reconstruction of the sea bottom environment.

6. Acknowledgments

The study was carried out with the support of Pierre Moissette and Jean-Jacques Cornée and financially supported by the National and Kapodistrian University of Athens (Research Project 70/4/5849). During the preparation of drawings, Petros Patrianakkos provided great help.

7. References

Barash A. and Danin Z. 1988. Marine Mollusca at Rhodes, *Israel Journal of Zoology*, 35, 1–74.

Barash A. and Danin, Z. 1992. *Fauna Palaestina. Mollusca I. Annotated list of Mediterranean molluscs of Israel and Sinai*, The Israel Academy of Sciences and Humanities, Keterpress Enterprises, Jerusalem, 405 pp.

Cornée J.J., Moissette P., Joannin S., Suc J.P., Quillévéré F., Krijgsman W., Hilgen F., Koskeridou E., Mónch P., Lécuyer C. and Desvignes P. 2006, Tectonic and climatic controls on coastal sedimentation: the Late Pliocene-Middle Pleistocene of northeastern Rhodes, Greece, *Sedimentary Geology*, 187 pp.

Gibbard P.L. and Head M.J. 2010. The newly-ratified definition of the Quaternary System/Period and redefinition of the Pleistocene Series/Epoch, and comparison of proposals advanced prior to formal ratification, *Episodes*, 33(3), 152–156.

Hanken N.-M., Bromley R.G. and Miller J. 1996. Plio-Pleistocene sedimentation in coastal grabens, north-east Rhodes, Greece, *Geological Journal*, 31, 271– 296.

Koukouras A. and Russo A. 1991. Midlittoral soft substratum macrofaunal assemblages in the north Aegean Sea. Pubblicazioni della Stazione Zoologica di Napoli, *Marine Ecology*, 12, 293-316.

Logan A. 1979. The Recent Brachiopoda of the Mediterranean Sea, *Bulletin de l'Institut Océanographique*, 72 (1434), 1-112.

Meulenkamp J.E., De Mulder E.F.J. and Van De Weerd A. 1972, Sedimentary history and paleogeography of the Late Cenozoic of the Island of Rhodos, *Zeitschrift der Deutschen Geologischen Gesellschaft*, v. 123, 541–553.

Moissette P., Koskeridou E., Cornée J-J., Guillocheau F., Lécuyer C. 2007. Spectacular preservation of seagrasses and seagrass-associated communities from the pliocene of rhodes, Greece. *Palaios*, 22, 200–211.

Moissette P., Koskeridou E., Cornée J-J. and André J.J. 2013. Fossil assemblages associated with submerged beachrock beds as indicators of environmental changes in terrigenous sediments: Examples from the Gelasian (Early Pleistocene) of Rhodes, Greece, *Palaeogeography Palaeoclimatology and Palaeoecology*, 369, 14-27.

Mutti E., Orombelli G. and Pozzi R. 1970. Geological map of Rhodes Island (Greece), *Annales Géologiques des Pays Hélléniques*.

Morton B. 1990. The biology and functional morphology of *Ervilia castanea* (Bivalvia: Tellinacea) from the Azores, *Acoreana, Supplement,* 75-96.

Morton B., Britton J., Martins A. 1998. *Ecologia Costeira dos Acores,* Sociedade Afonso Chaves, Ponta Delgada, 249 pp.

Pérès J.M. and Molinier R. 1957. Compte rendu du colloque tenu à Gênes par le comité du benthos de la Commission Internationale pour l'Exploration Scientifique de la Mer Méditerranée, *Recueil des travaux de la Station marine d'Endoume,Marseille*, 22(13), 5-15.

Pérès J.M. and Picard J. 1964. Nouveau manuel de bionomie benthique de la mer Méditerranée, *Recueil des travaux de la Station marine d'Endoume, Marseille,* 47(31), 3–137.

Pérès J.M. 1967. The Mediterranean benthos, *Oceanography and Marine Biology, An Annual Review*, 5, 449–533.

Pirazzoli P.A., Montaggioni L.F., Saliege J.F., Segonzac G., Thommeret Y. and Vergnaud-Grazzini C. 1989. Crustal block movements from Holocene shorelines: Rhodes Island (Greece), *Tectonophysics*, 170, 89–114.

Riedl R. 1983. Fauna und Flora des Mittelmeeres. Ein systematischer Meeresfóhrer fór Biologen und Naturfreunde*, 3rd edition, Verlag Paul Parey*, Hamburg. 836 pp.

Zenetos A., Vardala-Theodorou E. and Alexandrakis C. 2005. Update of the marine Bivalvia Mollusca checklist in Greek waters, *Journal of Marine Biological Association U.K.,* 85, 993– 998.

Zibrowius H. 1980. Les scléractiniaires de la Méditerranée et de l'Atlantique nord-oriental, *Mémoires de l'Institut océanographique*, 11, 1–284.

Δελτίο της Ελληνικής Γεωλογικής Εταιρίας, τομ. XLVII , 2013
Πρακτικά 13ου Διεθνούς Συνεδρίου, Χανιά, Σεπτ. 2013

Bulletin of the Geological Society of Greece, vol. XLVII 2013
Proceedings of the 13th International Congress, Chania, Sept. 2013

?KIMMERIDGIAN-TITHONIAN SHALLOW-WATER PLATFORM CLASTS FROM MASS FLOWS ON TOP OF THE VARDAR/AXIOS OPHIOLITES

Kostaki G.[1], Kilias A.[1], Gawlick H. J.[2] and Schlagintweit F.[3]

[1] *Aristotle University of Thessaloniki, School of Geology, Department of Geology, gkostaki@geo.auth.gr, kilias@geo.auth.gr*

[2] *University of Leoben, Department Applied Geosciences and Geophysics, Chair of Petroleum Geology, Hans-Juergen.Gawlick@unileoben.ac.at*

[3]*Lerchenauer Str. 167, 80935 München, Germany, Felix.Schlagintweit@gmx.de*

Abstract

The Late Jurassic to Early Cretaceous sedimentary succession of the Neochorouda Unit lies unconformably on top of the Oreokastro ophiolites of the Vardar/Axios "suture zone" in northern Greece. This succession consists of turbidites and mass flows and provides an upper limit for ophiolite emplacement. New biostratigraphic and microfacies analysis from the clasts in the mass flows were carried out for a better understanding of the Late Jurassic to Early Cretaceous geodynamic history. Microfacies and organism content prove the onset of Late Jurassic carbonate platforms on top of a Middle to Late Jurassic nappe stack striking from the Eastern Alps to the Hellenides.

Middle to Late Jurassic nappe stacking towards WNW to NW followed late Early to Middle Jurassic intra-oceanic thrusting in the Western Vardar/Axios (= Neotethys) Ocean and subsequent ophiolite obduction onto the Pelagonian Units forming a thin-skinned orogen on the lower plate. After ophiolite emplacement Kimmeridgian-Tithonian carbonate platforms sealed widespread this tectonic event. Tithonian extension due to mountain uplift resulted in partial erosion of these platforms and new extensional basins were formed. Late Tithonian to earliest Cretaceous erosion of the uplifted nappe stack including the obducted ophiolites resulted in sediment supply into the newly formed basins also east of the Pelagonian Units.

Key words: *Neotethys, Tectonics, Stratigraphy.*

Περίληψη

Η Άνω Ιουρασική-Κάτω Κρητιδική ιζηματογενής ακολουθία της ενότητας Νεοχωρούδας βρίσκεται ασύμφωνα πάνω στους οφιολίθους του Ωραιοκάστρου, που ανήκουν στη ζώνη συρραφή του Άξιου στη Βόρεια Ελλάδα. Αυτή η ακολουθία αποτελείται από ροές μαζών και τουρβιδίτες και δίνει το ανώτατο όριο για την τοποθέτηση των οφιολίθων. Νέα βιοστρωματογραφική ανάλυση και ανάλυση μικροφάσεων έγινε για την καλύτερη κατανόηση της γεωδυναμικής ιστορίας του Άνω Ιουρασικού-Κάτω Κρητιδικού. Οι μικροφάσεις και οι μικροοργανισμοί που εμπεριέχονται αποδεικνύουν την ύπαρξη ανθρακικών πλατφόρμων του Άνω

Ιουρασικού, που δημιουργήθηκαν πάνω από τη συσσώρευση καλυμμάτων του Μέσου-Άνω Ιουρασικού από τις ανατολικές Άλπεις έως τις Ελληνίδες.
Η συσσώρευση καλυμμάτων ηλικίας Μέσο-Άνω Ιουρασικού με φόρα προς τα ΔΒΔ και η τοποθέτηση των οφιολίθων πάνω στις ενότητες της Πελαγονικής ακολουθήσαν την ενδοωκεάνια λεπίωση στο δυτικό τμήμα της Νεοτηθύος που έλαβε χώρα κατά τη διάρκεια του Ανωτέρου Κατωτέρου-Μέσου Ιουρασικού. Μετά την τοποθέτηση των οφιολίθων ανθρακικές πλατφόρμες Κιμμεριδίου-Τιθωνίου σφράγισαν αυτό το τεκτονικό γεγονός. Στο Τιθώνιο εκτατική τεκτονική συνδεδεμένη με φλοϊκή ανύψωση προκάλεσε μερική διάβρωση των ιζημάτων πλατφόρμας και νέες λεκάνες δημιουργήθηκαν. Η διάβρωση των ανυψωμένων καλυμμάτων και των επωθημένων οφιολίθων που έλαβε χώρα κατά το τέλος του Τιθώνιου έως της αρχές του Κρητιδικού συνεισέφερε υλικό που αποτέθηκε στις πρόσφατα δημιουργημένες λεκάνες και ανατολικά των ενοτήτων της Πελαγονικής.
Λέξεις κλειδιά: *Νεοτηθύς, Τεκτονική, Στρωματογραφία.*

1. Introduction and Geological Overview

The Vardar/Axios zone is located parallel to the Hellenide-Dinaride chain in Northern Greece, FYROM, and Serbia. Kossmat (1924) was the first who described the Vardar/Axios zone as a 30 to 70 km wide NNW-SSE trending belt between the Serbomacedonian massif to the east and the Pelagonian Zone (and equivalents) to the west, e.g. in Northern Greece.

The Greek part of Vardar/Axios zone has been subdivided by Mercier (1968) into three subzones according to their palaeogeographic characteristics: from west to east the Almopias, Paikon and Peonias zones. Neochorouda area, which is a material area for this study, belongs to Peonias subzone. The dominant rocks of the Peonias subzone are Mesozoic sedimentary and igneous rocks, various types of metamorphic rocks and ophiolites with associated mélanges, including the Oreokastro ophiolites. The latter together with the ophiolites of Guevguely, Thessaloniki and Chalkidiki form the Innermost Hellenic Ophiolite Belt (Bebien et al., 1986). The presence of ophiolites is of great interest for the geotectonic evolution and crucial for the still controversially discussed palaeogeographic setting of them and therefore a key for the geodynamic interpretation of the whole Hellenides.

These ophiolites represent the remnants of the Mesozoic oceanic lithosphere (Neotethys domain) within the Hellenide-Dinaride segment of the Alpine orogenic system in a north-south trending belt (Smith & Spray, 1984; Channell & Kozur, 1997). The formation of these ophiolites should have happened between 170-155 Ma in the back-arc region of the intra-oceanic subduction of the Meliata-Maliac (= Neotethys) Ocean that took place on the eastern border of the Vardar/Axios Ocean (e.g., Stampfli et al., 2000; Zachariadis et al., 2006). About the palaeogeographic position of the Peonias oceanic basin see also Brown & Robertson (2003). These authors proposed that the Vardar/Axios ocean was a back arc basin (SSZ ophiolites) behind the Paikon volcanic arc (for a different view: Ricou et al., 1998; Vergely & Mercier, 2000), which should have remained open at least until the Late Cretaceous (Robertson et al., 2012), but earlier the westward thrusting in this independent ocean basin was considered as Late Jurassic.

According to other authors the Vardar/Axios ophiolites were thrusted on top of the Pelagonian units (e.g., Roddick et al., 1979; Brown & Robertson, 2004) around the Middle/Late Jurassic boundary caused by intra-oceanic thrusting and westward ophiolite obduction. They should therefore represent the easternmost part of a huge ophiolite nappe which derived from the Neotethys Ocean (e.g., Schmid et al., 2008; Gawlick et al., 2008; Kilias et al., 2010). According to the last two author groups the western part of the Neotethys Ocean was closed in early Late Jurassic times whereas the eastern part remained open as SSZ Vardar Ocean.

In the study area Oreokastro ophiolites to the east are in tectonic contact with a Late Triassic-Early Late Jurassic (Dimitriadis & Asvesta, 1993) turbiditic succession (Melissochori formation). To the west the ophiolites are overlain by a fossiliferous ?latest Jurassic to Early Cretaceous sedimentary succession (Neochorouda Unit) (Kockel et al., 1977; Meinhold et al., 2009) (Figure 1). This succession consists of mass flows which contain components of different reefal limestones of Late Jurassic age (Figures 2 and 3). These Late Jurassic shallow-water limestone clasts are of different microfacies and were detected near the village of Neochorouda.

The present paper describes the mass-flow components in the Neochorouda Unit (Figure 2) together with new biostratigraphic and microfacies data. Our results allow to reconstruct the formation of a Late Jurassic carbonate platform on top of the nappe stack of Vardar/Axios ophiolites sealing their emplacement. The results are important for the reconstruction and the timing of the thrusting processes of the Vardar/Axios ophiolites. Their emplacement can be dated as older then the creation of the shallow-water carbonates on top and therefore at least as late Middle to early Late Jurassic. The sequence of the Neochorouda Unit in the Vardar/Axios zone with the incorporated eroded components resemble identical successions known west of the Pelagonian units, e.g. in Albania or Serbia.

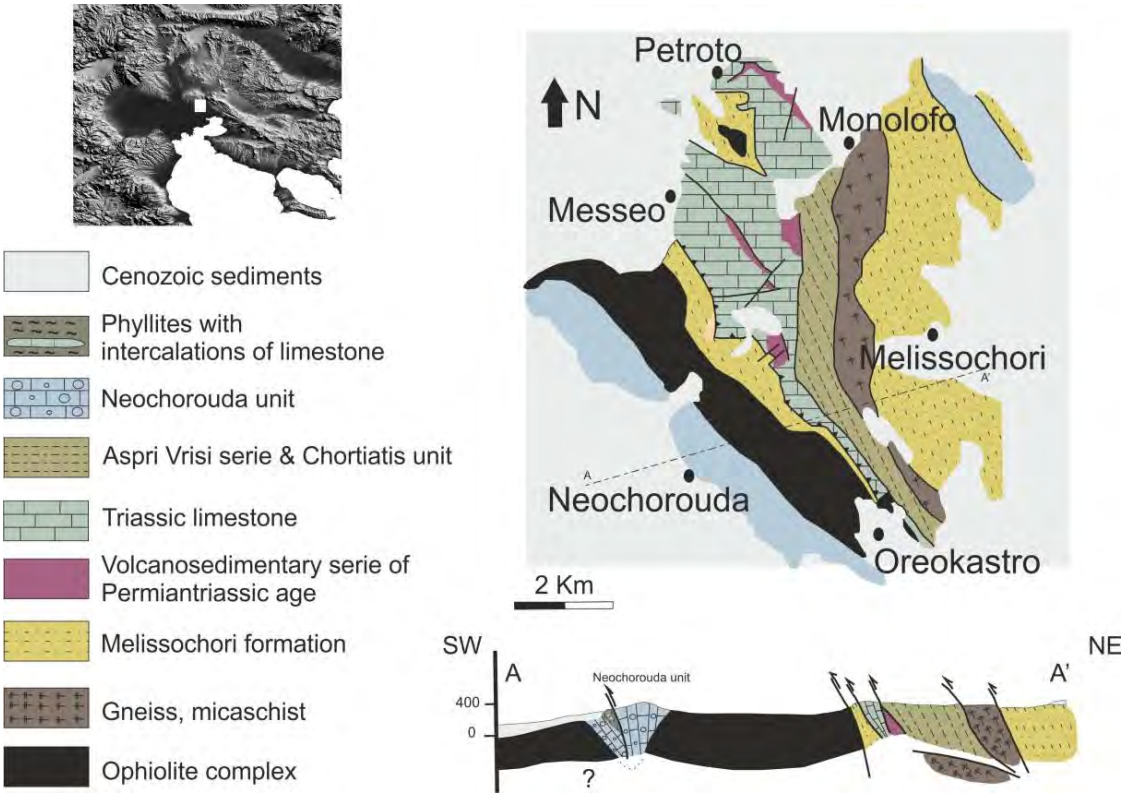

Figure 1 - Geological map of Neochorouda area modified after Kockel & Mollat (1977).

2. Stratigraphy and Platform Reconstruction

2.1 Neochorouda Unit

This succession of mass flows has a thickness of about 320 m and the components size ranges from a few centimetres up to half a meter (Figure 2). According to the biostratigraphic and microfacies analysis of the clasts in the mass flows we distinguish from bottom to top:

a) A breccia of approximately 10 m thickness with gabbroic and few shallow-water carbonate clasts with *Labyrinthina mirabilis* Weynschenk and *Griphoporella jurassica* (Endo) (Figure 4).

b) A coarse-grained breccia of about 6 m thickness with mixed ophiolite material and shallow-water carbonate clasts containing besides corals and other reef builders also *Neoteutloporella socialis* (Praturlon), *Crescentiella morronensis* (Crescenti), *Perturbatacrusta leini* Schlagintweit & Gawlick, *Labes atramentosa* Eliasova (Figure 5).

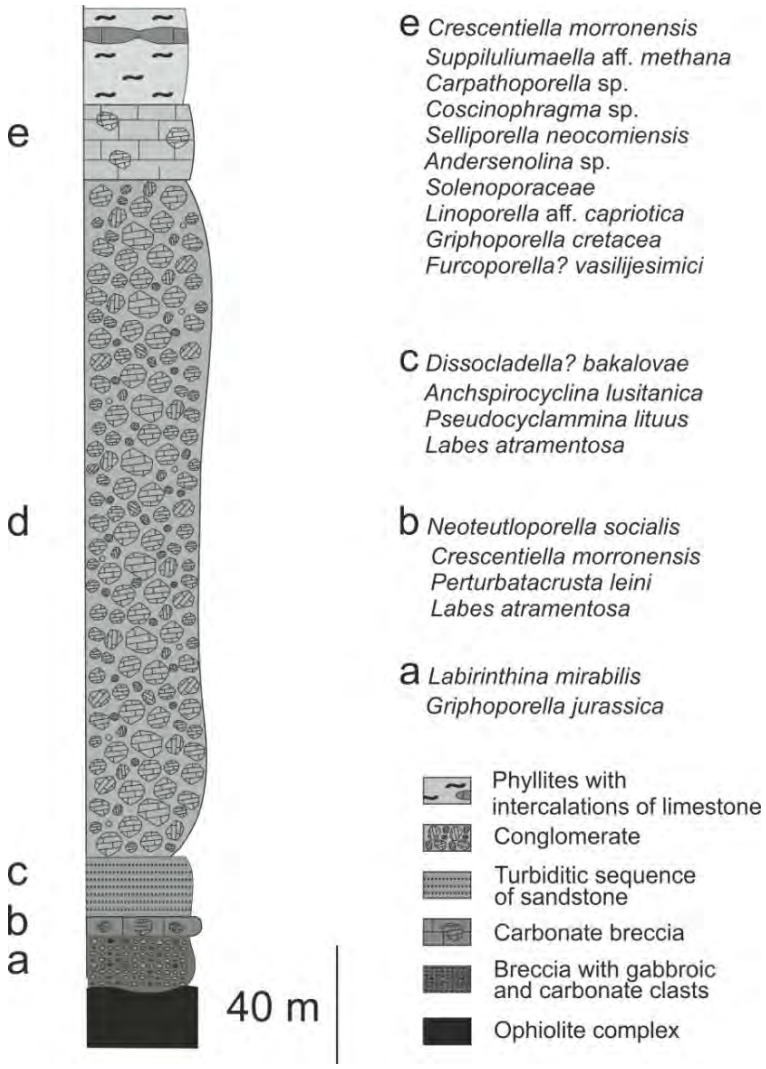

Figure 2 - Stratigraphic column of the Neochorouda Unit.

c) A 20 meters turbiditic sequence of sandstones, with some intercalated coarse-grained mass flows. This sequence contains ammonites of Berriasian age (Mussallam & Jung, 1986). The carbonate clasts contain *Dissocladella*? *bakalovae*, *Anchispirocyclina lusitanica* (Egger), *Pseudocyclammina lituus* (Yokoyama), *L. atramentosa* Eliasova (Figure 6).

d) A polymictic conglomerate of approximately 250 m thickness with e.g. quartzite's resp. metamorphic radiolarites, different metamorphosed shallow-water clasts of most probably Middle Triassic age but without ophiolite components (Figure 7) and

e) again shallow-water carbonates with a thickness of 30 m with *C. morronensis* (Crescenti), *Suppiluliumaella* aff. *methana* Dragastan & Richter, *Carpathoporella* sp., *Coscinophragma* sp., *Selliporella neocomiensis* (Radoicic), *Andersenolina* sp., *Solenoporaceae*, *Linoporella* aff. *capriotica* (Oppenheim), *Griphoporella cretacea* (Dragastan), *Furcoporella*? *vasilijesimici* Radoicic (Figure 8). This part of the series is Berriasian to Valanginian in age.

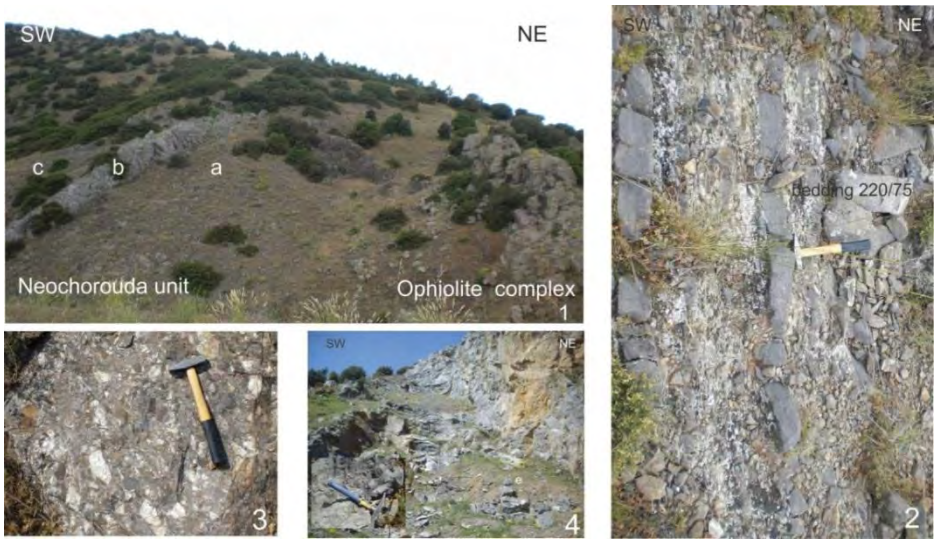

Figures 3 - 1 Neochorouda Unit overlying the Oreokastro ophiolite complex of the Vardar/Axios zone. The letters a, b, c indicates the samples locations for the biostratigraphic analysis. 2 The turbiditic sandstone sequence and sampling point c. 3 Conglomerate with different clasts. Sampling point d. 4 Shallow-water carbonates. Sampling point e.

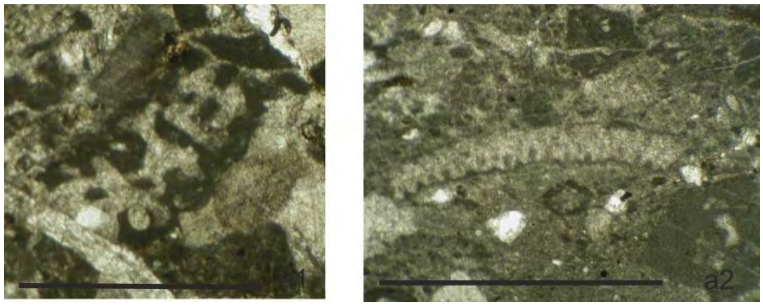

Figure 4 - Microfossils from shallow-water carbonate clasts inside the breccia from Neochorouda Unit. a1. *Labyrinthina mirabilis*, a2. *Griphoporella jurassica*.

2.2 Reconstruction of the Jurassic to Early Cretaceous tectonic evolution

Specifically interesting are the coarse-grained breccias with mixed ophiolite material and shallow-water carbonate clasts below the early Berriasian turbidites. The clasts derive from fore-reef, reef, back-reef and open lagoonal areas containing different microencruster associations, stromatoporoids, sponges, corals and also *Neoteutloporella socialis* (Praturlon)*, Perturbatacrusta leini* Schlagintweit & Gawlick. Common microencrusters include *Radiomura cautica* Senowbari-Daryan & Schäfer, *Crescentiella morronensis* (Crescenti) and *Labes atramentosa* Eliasova (Figure 5). We interpret these clasts as erosional products of a ?Kimmeridgian-Tithonian carbonate platform which was formed on top of the ophiolites.

Age dating of the whole sequence including component analysis and detection of an eroded Late Jurassic platform led to following reconstruction of the geodynamic evolution:

The closure of the western part of the Neotethys Ocean in late Early to Middle Jurassic was triggered by intra-oceanic subduction. This convergence east of the "Pelagonia continent" resulted in west-directed late Middle to early Late Jurassic ophiolite obduction and WNW to NW directed nappe stacking of the sediment cover units of "Pelagonia" in the western Vardar/Axios (= Neotethys) Ocean (Kilias et al., 2010). Ophiolite obduction onto the Pelagonian Units and imbrication of the Pelagonian sedimentary sequence are related to the same thrusting process. This process was followed by the onset of a shallow-water platform on top of the nappe stack. This Late Jurassic carbonate platform evolution on top of the Middle to Late Jurassic nappe stack can be traced from the Eastern Alps to the Hellenides (Gawlick et al., 2008; Schlagintweit et al., 2008; Missoni et al., 2011). The new biostratigraphic and microfacies analysis of the clasts in the mass flows at Neochorouda Unit provides us new information about this platform pattern, which was eroded in the study area around the Jurassic/Cretaceous boundary.

Late Tithonian to Early Cretaceous extension and updoming of the nappe stack including the obducted ophiolites due to mountain uplift resulted in a reconfiguration of the nappe stack and newly formed basins west and east of the Pelagonian Units. Late Tithonian to earliest Cretaceous erosion of the uplifted nappe stack including the obducted ophiolites resulted in sediment supply into these basins. Erosion of the Late Jurassic carbonate platform together with ophiolite material and later the occurrence of metamorphic Triassic clasts clearly prove updoming of the nappe pile, crustal extension and gravitational sliding of the nappe pile to the west and to the east, as it can be demonstrated by identical successions on both sides of the Pelagonian Units in Greece (this paper, Dragastan & Richter, 2003), Albania (Schlagintweit & Gawlick, 2007, Schlagintweit et al., 2008) and Serbia (Radoicic, 1982). First the topmost nappes including their sedimentary cover (ophiolites and Late Jurassic platform sediments) became eroded (around the Jurassic/Cretaceous boundary - Berriasian). Later, but still in the earliest Cretaceous (Berriasian) the metamorphosed Triassic-Jurassic Pelagonian sedimentary rocks started to erode: The thick conglomerates with the metamorphic carbonate clasts of Pelagonian derivation were deposited, maybe in the course of a sea-level drop.

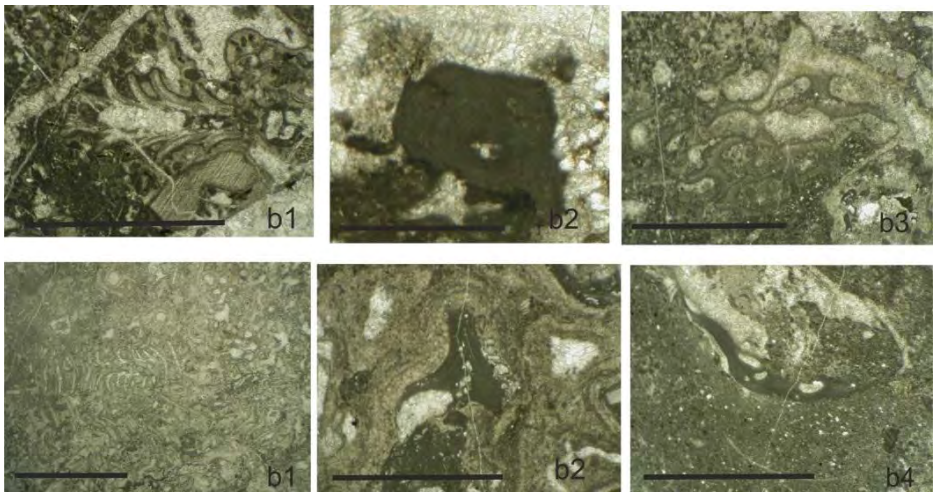

Figure 5 - Microfossils from shallow-water clasts inside the coarse-grained breccia from Neochorouda Unit. b1. *Neoteutloporella socialis*, b2. *Crescentiella morronensis*, b3. *Pertu-batacrusta leini*, b4. *Labes atramentosa*.

In the study area the first erosional stages can be proven by the existence of the Berriasian turbiditic sequence of immature sandstones with coarse-grained mass flows below and intercalated (Figure 3.2). The carbonate clasts contain *Dissocladella*? *bakalovae*, *Anchispirocyclina lusitanica* (Egger), *Pseudocyclammina lituus* (Yokoyama), *L. atramentosa* Eliasova (Figure 6). In the next stage due to the exhumation of the metamorphic dome (Berriasian) deep erosion led to the

formation of the polymictic conglomerate of the Neochorouda succession (Figure 3.3) with e.g. quartzite, metamorphic radiolarites, and different metamorphosed shallow-water clasts of most probably late Middle Triassic age (Figure 7).

This earliest Cretaceous succession was again sealed by a newly formed ?Late Berriasian-Valanginian shallow-water platform most probably in the course of the next sea-level rise resp. highstand. The latter is represented in Neochorouda area by the shallow-water carbonates (Figure 3.4) with *C. morronensis* (Crescenti), *Suppiluliumaella* aff. *methana* Dragastan & Richter, *Carpathoporella* sp., *Coscinophragma* sp., *Selliporella neocomiensis* (Radoicic), *Andersenolina* sp., *Solenoporaceae*, *Linoporella* aff. *capriotica* (Oppenheim), *Griphoporella cretacea* (Dragastan), *Furcoporella? vasilijesimici* Radoicic (Figure 8).

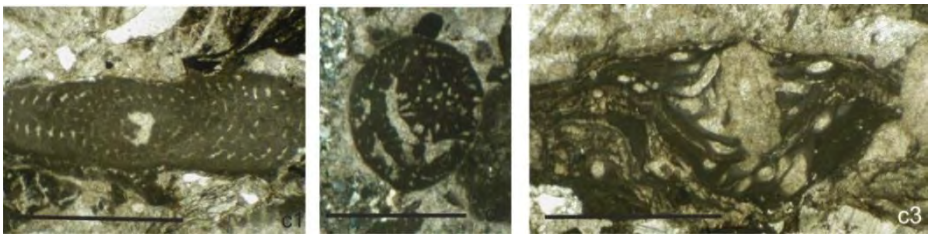

Figure 6 - Microfossils from the carbonate clasts inside the turbiditic sequence from Neochorouda Unit. c1. *Anchispirocyclina lusitanica*, c2. *Pseudocyclammina lituus*, c3. *Labes atramentosa*.

Plate convergence and westwards thrusting continued during Aptian to Albian times. N-S trending overturned isoclinal folds with vergence towards west and an impressive eastwards dipping S2 foliation parallel to the folds axis plane was developed during that time (Figure 9). Upper Cretaceous limestones and Palaeocene flysch sediments overlay unconformably these tectonics structures and the Late Jurassic to Early Cretaceous sedimentary succession. After that the Neochorouda Unit has been affected by the younger Tertiary tectonics including compression and nappe stacking, followed by extension and again an orogenic collapse.

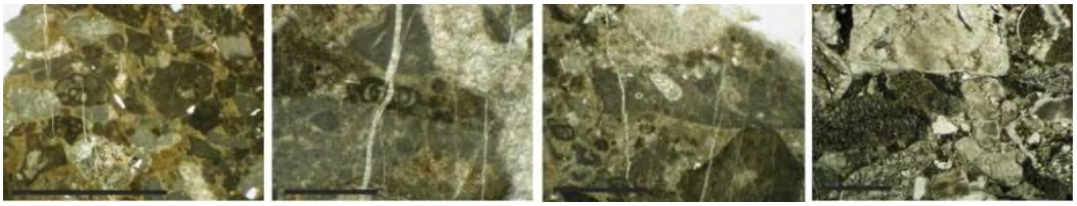

Figure 7 - Conglomerate with different clasts from the Neochorouda Unit, e.g. quartzite's resp. metamorphic radiolarites, different metamorphosed shallow-water clasts of most probably Middle Triassic age and carbonate clasts containing foraminifera.

Microfacies and organism content at Neochorouda Unit resembles the Late Jurassic carbonate platforms formed on top of the Middle to Late Jurassic nappe stack striking from the Eastern Alps to the Hellenides. In detail, an equivalent sequence of shallow-water limestones and clastic sediments is recognized further to the west in Albania, where it seals the Mirdita ophiolitic nappe stack (Gawlick et al., 2008). The same scenario with ophiolite obduction in Middle-Late Jurassic followed by formation of shallow-water platforms, extensional collapse due to tectonic thickening and mountain uplift before the Jurassic/Cretaceous boundary, and infilling of the foreland basins with the erosional products of the orogeny in Early Cretaceous has also been described in the Eastern Alps (Missoni & Gawlick, 2011). Additionally, west of the Pelagonian Units occurs the carbonate sequence of Acrocorinth and of the Perachora peninsula, which has been interpreted as lagoonal facies areas of a Late Jurassic to Early Cretaceous carbonate platform (Dragastan & Richter, 2003).

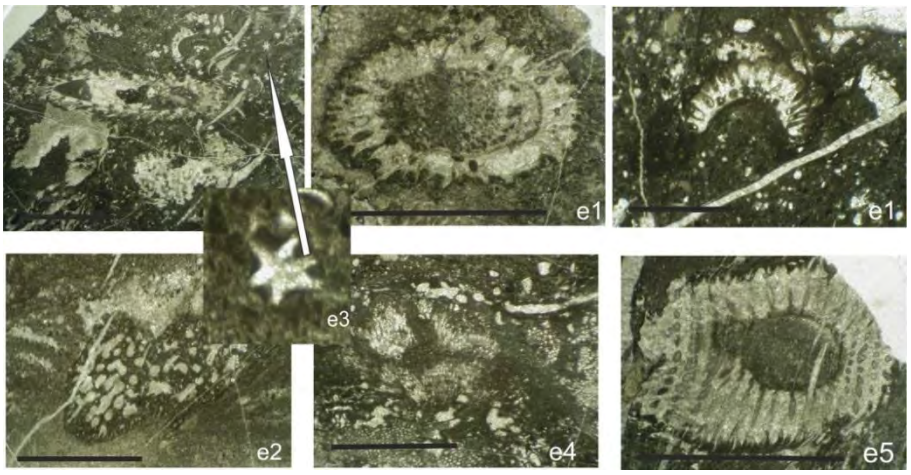

Figure 8 - Microfossils from shallow-water carbonates from the Neochorouda Unit. e1. *Suppiluliumaella* aff. *methana*, e2. *Coscinophragma* sp., e3 debris of tufts of secondary laterals of *Selliporella neocomiensis*, e4. *Solenoporaceae*, e5. *Linoporella* aff. *capriotica*.

Figure 9 - Isoclinals folds of Early Cretaceous with S2 foliation. Schmidt diagram of the geometrical data of the fold (Lower hemisphere).

3. Discussion and Conclusions

The Late Jurassic to Early Cretaceous sedimentary succession of the Neochorouda Unit lies unconformably on top of the Oreokastro ophiolites of the Vardar-Axios "suture zone" in Northern Greece. This succession consists of mass flows and provides an upper limit for ophiolite emplacement. New biostratigraphic and microfacies analysis of the clasts in the mass flows were carried out for a better understanding of the Late Jurassic to Early Cretaceous evolution and provide new information about the derivation of the ophiolite complex.

- Middle to Late Jurassic nappe stacking towards WNW to NW was related to intra-oceanic thrusting in the western Vardar/Axios (=Neotethys) Ocean and subsequent ophiolite obduction onto the Pelagonian Units. After ophiolite emplacement Kimmeridgian-Tithonian carbonate platforms sealed widespread this tectonic event.
- Tithonian extension due to mountain uplift resulted in partial erosion of these platforms including the ophiolites and new basins were formed. Later the metamorphosed Triassic carbonates became eroded and re-deposited. The erosional products of the Neochorouda Unit in the Vardar/Axios zone resemble the erosional products known west of the Pelagonian units, e.g. in Albania or Serbia and should derive therefore from the same palaeogeographic provenance area.

- Late Tithonian to earliest Cretaceous erosion of the uplifted nappe stack including the obducted ophiolites resulted in sediment supply into the newly formed basins east and west of the Pelagonian Units. The coarse-grained succession was sealed by a newly formed ?Late Berriasian-Valanginian shallow-water platform, also known west of the Pelagonian units.

This paper contributes to previous works at least since Kober (1914) proposing that in Triassic to Early Cretaceous times the area from the Eastern Alps in the north to the Hellenides in the south underwent the same geodynamic history (see also Kossmat, 1924). Formation of the Neotethys oceanic crust since Late Anisian, onset of intra-oceanic thrusting in the Jurassic, westward ophiolite obduction and formation of the nappe pile on the lower plate from late Middle Jurassic times onward followed by the formation of Kimmeridgian-Tithonian shallow-water platforms, a latest Jurassic extensional collapse due to tectonic thickening and mountain uplift around the Jurassic/Cretaceous boundary, and infilling of the foreland basins with the erosional products of this orogeny in Early Cretaceous as known from the Eastern Alps/West Carpathians, the Southern Alps, Dinarides, and Albanides (e.g., Gawlick et al., 2008; Schlagintweit et al., 2008; Missoni et al., 2011).

4. Acknowledgments

This study comes as a sequence of work that took place at Leoben University through the European Community Action Scheme for the Mobility of University Students program. Use of the laboratory facilities of the Department of Applied Geosciences and Geophysics, Chair of Petroleum Geology at the University of Leoben are gratefully acknowledged. Special thanks go to Sigrid Missoni for her helpful assistance during the laboratory work.

5. References

Bebien J., Dubois R. and Gauthier A. 1986. Example of ensialic ophiolites emplaced in wrench zone: innermost Hellenic ophiolite belt (Greek Macedonia), *Geology*, 14, 1016-1019.

Brown S.A.M. and Robertson A.H.F., 2004. Evidence for the Neotethys ocean rooted in the Vardar zone: evidence from the Voras Mountains, NW Greece, *Tectonophysics*, 381, 143-173.

Channell J.E.T. and Kozur H.W. 1997. How many oceans? Meliata, Vardar and Pindos oceans in the Mesozoic Alpine paleogeography, *Geology*, 25, 183-186.

Dimitriadis S. and Asvesta A. 1993. Sedimentation and magmatism related to the Triassic rifting and later events in the Vardar-Axios Zone, *Bull. Geol. Soc. Greece*, 28, 149-168.

Dragastan O. and Richter D.K. 2003. Late Jurassic oolites from the Acrocorinth (NE-Peloponnesus): Calcareous-micro-algae as an exceptional paleoecologic indicator, *Bochumer geologische und geotechnische Arbeiten*, 53, 149-172.

Gawlick H.J., Frisch W., Hoxha L., Dumitrica P., Krystyn L., Lein R., Missoni S. and Schlagintweit F. 2008. Mirdita zone ophiolites and associated sediments in Albania reveal Neotethys Ocean origin, *Int. J. Earth Sci*., 94, 865-881.

Kilias A., Frisch W., Avgerinas A., Dunkl I., Falalakis G. and Gawlick H.J. 2010. Alpine architecture and kinematics of deformation of the northern pelagonian nappe pile in the Hellenides, *Austrian Journal of Earth Sciences*, 103/1, 4-28.

Kober L. 1914. Die Bewegungsrichtung der alpinen Deckengebirge des Mittelmeeres, *Geographische Mitteilungen*, 60, 250-256, Petermanns.

Kockel F. and Mollat, H. 1977. Geological map of the Chalkidiki peninsula and adjacent areas (Greece), Scale 1:100000, *Bundesanstalt fur Geowissenschaften und Rohstoffe,* Hannover.

Kossmat F. 1924. Die Kriegsschauplatze 1914-1918 geologisch dargestellt. Heft 12: Geologie der zentralen Balkanhalbinsel. Mit einer Übersicht des dinarischen Gebirgsbaus, *(Borntraeger)* 198 pp.

Meinhold G., Kostopoulos D., Reischmann T., Frei D. and BouDagher-Fadel M.K. 2009. Geochemistry, provenance and stratigraphic age of metasedimentary rocks from the eastern Vardar suture zone, northern Greece, *Palaeogeography Palaeoclimatology Palaeoecology*, 277, 199-225.

Mercier J. 1968. Etude geologique des zones internes hellenides en Macedoine centrale (Grece). Contribution a l etude du metamorphisme et de l evolution magmatique des zones internes des Hellenides, *Annales geologiques des pays helleniques*, 20, 1-792.

Missoni S. and Gawlick H.J. 2011. Evidence for Jurassic subduction from the Northern Calcareous Alps (Berchtesgaden; Austroalpine, Germany), *Int. J. Earth Sci.,* 100, 1605-1631.

Mussallam K. and Jung D. 1986. Geology und Bau des Sithonia-Ophioliths (Chalkidiki, NE Griechenland: Anmerkungen zur Bildung ozeanischer Krusten), *Geologische Rundschau*, 75, 383-409.

Radoicic R. 1982. Carbonate platforms of the Dinarides: The example of Montenegro-West Serbia Sector, *Bulletin de l'Académie Serbe des sciences et des arts, Classe des sciences naturelles et mathematiques*, 22, 35-46.

Ricou L.E., Burg J.P., Godfriaux I. and Ivanov Z. 1998. Rhodope and Vardar: the metamorphic and the olitostromic paired belts related to the Cretaceous subduction under Europe, *Geodinamica Acta*, 11, 285-309.

Robertson A.H.F. 2012. Late Palaeozoic-Cenozoic tectonic development of Greece and Albania in context of alternative reconstructions of Tethys in the Eastern Mediterranean region, *International Geology Review*, 54, 373-454.

Robertson A.H.F., Trivic B., Djeric N. and Bucur I.I. 2012. Tectonic development of the Vardar ocean and its margins: Evidence from the Republic of Macedonia and Greek Macedonia, *Tectonophysics,* Available online at: http://dx.doi.org/10.1016/j.tecto.2012.07.022

Roddick J., Cameron W. and Smith A.G. 1979. Permotriassic and Jurassic Ar/Ar ages from Greek ophiolites and associated rocks, *Nature*, 279, 788-790.

Schlagintweit F. and Gawlick H.J. 2007. Analysis of the Late to Early Cretaceous algal debris-facies of the Plassen carbonate platform in the Northern Calcareous Alps (Germany, Austria) and in the Kurbnesh area of the Mirdita zone (Albania) – a tool to reconstruct tectonics and paleogeography of eroded platforms, *Facies*, 53, 209-227.

Schlagintweit F., Gawlick H.J., Missoni S., Hoxha L., Lein R. and Frisch W. 2008. The eroded Late Jurassic Kurbnesh carbonate platform in the Mirdita ophiolite Zone of Albania and its bearing on the Jurassic orogeny of the Neotethys realm, *Swiss Journal of Geosciences*, 101, 125-138.

Schmid S.M., Bernoulli D., Fugenschuh B., Matenco L., Scheffer S., Schuster R., Tischler M. and Ustaszewski k. 2008. The Alps-Carpathians-Dinarides connection: a correlation of tectonic units, *Swiss Journal of Geosciences*, 101 (1), 139-183.

Smith A.G. and Spray J.G., 1984. A half-ridge transform model for the Hellenic-Dinaric ophiolites. in: Dixon, J.E. & Robertson, A.H.F. (eds), The Geological evolution of the Eastern Mediterranean, *Geological Society of London,*Special Publications, 17, 629-644.

Stampfli G.M., 2000. Tethyan oceans. In: Tectonics and magmatism in Turkey and the Surrounding Area, *Geological Society of London*, Special Publications, 173, 1-23.

Vergely P. and Mercier, J. 2000. Données nouvelles sur les chevauchements d'âge post-Crétacé supérieur dans le massif du Païkon (zone de l'Axios-Vardar, Macédoine, Grèce): un nouveau modèle structural, *Comptes Rendus de l'Académie des Sciences de Paris*, 330, 555-561.

Zachariadis P. 2007. Ophiolites of the eastern Vardar Zone, N. Greece, *PhD Thesis*, University of Mainz, Germany.

Δελτίο της Ελληνικής Γεωλογικής Εταιρίας, τομ. XLVII , 2013
Πρακτικά 13ου Διεθνούς Συνεδρίου, Χανιά, Σεπτ. 2013

Bulletin of the Geological Society of Greece, vol. XLVII 2013
Proceedings of the 13th International Congress, Chania, Sept. 2013

PRELIMINARY RESULTS OF HIGH RESOLUTION PALEOCEANOGRAPHY AND PALEOCLIMATOLOGY DURING SAPROPEL S1 DEPOSITION (SOUTH LIMNOS BASIN, NORTH AEGEAN SEA)

Kostopoulou S.[1], Triantaphyllou M.B.[1], Dimiza M.D.[1], Gogou A.[2], Boulou-bassi I.[3], Rousakis G.[2], Parinos C.[2], Diamantopoulou An.[4], Geraga M.[4] and Lykousis V.[2]

[1]*Faculty of Geology and Geoenvironment, National and Kapodistrian University of Athens, Panepistimiopolis 15784, Athens, kost.sofia@hotmail.com*

[2] *Hellenic Centre for Marine Research, Institute of Oceanography, 190 13 Anavyssos, Attiki*

[3]*Laboratoire d'Océanographie et du Climat, Expérimentation et Approche Numérique, Université Pierre et Marie Curie, Paris Cedex 05, France*

[4]*Faculty of Geology, University of Patras, 26100 Rio–Patra*

Abstract

The paleoenviromental conditions during the depositional interval of sapropel S1 in the northeastern Aegean (gravity core M-4, length 2.53 m; south Limnos basin) are studied based on quantitative micropaleontological (benthic and planktonic foraminifera) and geochemical (OC, $\delta^{13}C_{org}$) analyses. Special feature of core M-4 is the thickness of S1 layer (96 cm). Our study points that sapropelic layer S1a has been deposited in more dysoxic and warmer conditions in respect to S1b. Both primary productivity and preservation of organic material are more intense during the lower part of S1. An interruption of the sapropelic conditions at 8.0 Ka BP which is mainly characterized by the increase of agglutinated foraminiferal forms confirms both higher oxygen bottom conditions and freshwater input.
Key words: *sapropel S1, foraminifera, geochemical indices, Aegean Sea.*

Περίληψη

Οι παλαιοπεριβαλλοντικές συνθήκες κατά τη διάρκεια απόθεσης του σαπροπηλού S1 στο Βόρειο Αιγαίο (πυρήνας βαρύτητας M-4, μήκους 2,53 m, λεκάνης νότιας Λήμνου) προσδιορίζονται με βάση την ποσοτική ανάλυση μικροπαλαιοντολογικών (βενθονικά και πλαγκτονικά τρηματοφόρα) και γεωχημικών (OC, $\delta^{13}C_{org}$) δεικτών. Χαρακτηριστικό του πυρήνα M-4 είναι η μεγάλη εμφάνιση του S1 που φτάνει το πάχος των 96 cm. Η μελέτη κατέδειξε ότι, το κατώτερο σαπροπηλικό στρώμα S1a αποτέθηκε σε θερμότερες συνθήκες, εντονότερης δυσοξίας, σε σχέση με το ανώτερο σαπροπηλικό στρώμα S1b.. Αύξηση της παραγωγικότητας και καλύτερη διατήρηση του οργανικού υλικού πιστοποιήθηκαν στο κατώτερο τμήμα του S1. Η διακοπή των σαπροπηλικών συνθηκών στα 8,0 Ka BP που χαρακτηρίζεται κυρίως από την αύξηση της σχετικής συχνότητας των συμφυρματοπαγών μορφών των βενθονικών τρηματοφόρων υποστηρίζει συνθήκες υψηλής οξυγόνωσης του πυθμένα και εισροή γλυκών υδάτων.
Λέξεις κλειδιά: *σαπροπηλός S1, τρηματοφόρα, γεωχημικοί δείκτες, Αιγαίο.*

1. Introduction

The Aegean Sea is located at the northern part of NE Mediterranean region, linked to the Black Sea through the Dardanelles and the Bosporus Straits and to the eastern Mediterranean through the Cretan Straits, being recognized as a particularly important area for both regional and global climate changes. Numerous major rivers from the surrounding areas of the Balkans and Turkey flow into the Aegean Sea, providing the 75% of the North Aegean sediment influx (Lykousis et al., 2002; Roussakis et al., 2004; Ehrmann et al., 2007; Poulos, 2009), and they collectively constitute an important source of land-derived organic matter to the study area (e.g., Gogou et al., 2007). The Aegean receives low saline and cool BSW (Black Sea Water) through the Bosporus Strait (between Black Sea and Marmara Sea) and the Dardanelles (between Marmara Sea and Aegean Sea). The cold (9 - 22 °C) and low saline (24 - 28‰) BSW flows along the eastern coast of Greece until it reaches the southwestern Aegean, and enhances the productivity in the northern Aegean Sea (Lykousis et al., 2002). The warm (16 - 25 °C) and saline (from 39.2 to 39.5‰) Levantine surface waters flow northward along the eastern Aegean Sea to the Dardanelles Straits (e.g., Zervakis et al., 2004). Especially for the basin of north Aegean Sea, it can be described as a «continental margin» ecosystem, and is characterized by generally cyclonic circulation (Lykousis et al., 2002).

The positive shift of the Aegean Sea's freshwater budget during sapropel deposition – possibly supplemented by enhanced freshwater inputs from the Southern European margin (Kotthoff et al., 2008) – weakened the basin's deepwater circulation and resulted in oxygen starved conditions at the seafloor. Recent paleoceanographic findings (e.g., Gogou et al., 2007; Triantaphyllou et al., 2009 a,b; Katsouras et al., 2010; Kouli et al., 2012) suggest that during the Holocene, a rather mild climatic period, between 10 and 6 kyr BP, appeared in the sediments through the deposition of the most recent sapropel layer S1. Besides the monsoonal system, precipitation and inflow of Black Sea waters may have also contributed in modifying the freshwater budget during times of S1 formation (e.g., Kuhnt et al., 2007). A centennial-scale cold event centered on 8.2 ka (Alley et al., 1997) coincides with the S1 interruption, and has been ascribed to a deepwater overturning reinforcement and reventilation.

In this study, we have performed micropaleontological (benthic and planktonic foraminifera) and geochemical (Organic Carbon; OC, $\delta^{13}C_{org}$) analyses in sediments of core M-4 collected in the south Limnos basin, aiming to determine the paleoenvironmental changes during sapropel S1 deposition in north eastern Aegean Sea.

2. Materials and Methods

2.1. Core Description

Gravity core M-4 (length 2.53 m) has been recovered in south Limnos basin (Figure 1a) from water depth 216 m, at 39° 38.662´N 25° 35.165´E. Sapropel S1 is very well exposed in between 128-32 cm, with overall thickness reaching 96 cm. The uppermost 32 cm mainly consist of gray mud with shells (e.g., *Ostrea*) and shell debris. Based on sediment color and the concentration of OM, the S1 layer is divided into two sub-units (hereafter termed S1a and S1b, respectively), which are separated by an 8 cm thick (from 58 to 51 cm) lighter gray interval interpreted as the S1 interruption (Figure 1b). In this paper only the interval relative to sapropel S1 will be examined.

2.2. Chronology

Three accelerator mass spectrometry (AMS) radiocarbon ^{14}C datings were performed at the laboratories of the oceanographic institute LOCEAN/Universite P.-M. Curie, on cleaned hand-picked planktonic foraminifera from core M-4. Conventional ^{14}C ages have been calibrated by using Calib vs. 6.1.0 software (Stuiver et al., 1993) and the MARINE04 calibration dataset with a regional reservoir age correction (ΔR) of 139 ± 40 (Facorellis et al., 1998). The age model of the core M-4

resulted from the linear interpolation between three calibrated datings. According to this model, S1a is deposited between 9.7-8.0 ka BP, whereas S1b spans 7.6-6.5 Ka BP. The age resolution between the samples is 38-163 years for S1b, 38-39 years for the interruption and 24-73 years for S1a.

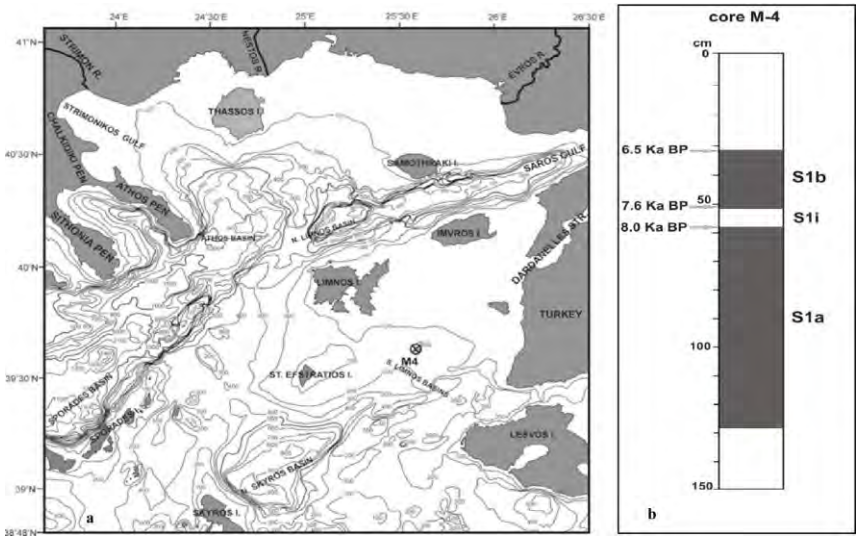

Figure 1 - (a) Location map of the study area in the north-eastern Aegean Sea, (b) Gravity core M-4 (the upper 150 cm).

3. Methods

Two hundred and thirty samples were collected at 0.5 cm resolution for organic carbon (OC) content, $\delta^{13}C_{org}$. Analyses were performed using an automatic analyzer type "NA-1500 Nitrogen Analyzer". Stable carbon isotope ratios were expressed in terms of $\delta^{13}C_{org}$ values against V-PDB for carbon, with overall analytical error based on duplicate measurements at ±0.2‰.

For benthic foraminiferal analyses, sixty four sediment samples of approximately 2 g dry weight each were wet sieved over 63 μm sieve at resolution 0.5-3 cm. For each sample, a subset containing at least 300 benthic foraminifera were separated from the >125 μm fraction using a Leica APO S8 stereoscope. A scanning electron microscope analysis (SEM Jeol JSM 6360, Dept. of Hist. Geology-Paleontology) has been used for taxonomical purposes. Relative abundances of benthic foraminifera are presented and discussed in this study. Benthic foraminifera have been used as tracers for the nutrient content and oxygen concentration of the bottom water (e.g., Jorissen et al., 1995).

Forty six samples were used for planktonic foraminifera analysis. The mean sampling interval for the faunal analyses was 2 cm. The samples were disintegrated by hydrogen peroxide and then sieved through a 125-μm mesh. The dry and weighed samples were split into separate aliquots. At least 200 planktonic specimens were identified and counted in each sample. Planktonic foraminifera have been proven useful in the reconstruction of palaeoceanographic and palaeoclimatic conditions (Bé &Tolderlund, 1971; Pujol & Vergnaud Grazzini, 1995). The sum of the percentages of species considered as indicative of warm waters versus the sum of those indicative of cool waters obtained as an index for the examination of the of the sea surface palaeotemperature and will be referred as PSST (Planktonic Sea Surface Temperature). *Globigerinoides ruber*, *Globigerinoides sacculifer*, *Orbulina univera* and *Globigerinella* spp. are considered warm-water indicators and *Turborotalita quinqueloba*, *Globigerinita glutinata* and *Globorotalia scitula* cold-water indicators (Thunell, 1978; Pujol & Vergnaud Grazzini, 1995).

4. Results

4.1. OC and $\delta^{13}C_{org}$

Higher OC values correspond to sapropel layers S1a and S1b (Figure 2). The maximum value of 1.94% is observed at 8.9 Ka BP during the deposition of S1a, whereas 1.67% is identified at 7.1 Ka BP. The interval of 8.0-7.6 Ka BP (S1 interruption) is characterized by a reduction of OC, however an increase to 1.26% exists at 7.7 Ka BP, just before the onset of S1b. $\delta^{13}C_{org}$ values of range from -26.1 ‰ to -22.9 ‰ (Figure 2). The minimum values of $\delta^{13}C_{org}$ were found during the interruption of sapropel S1 (7.7 Ka BP).

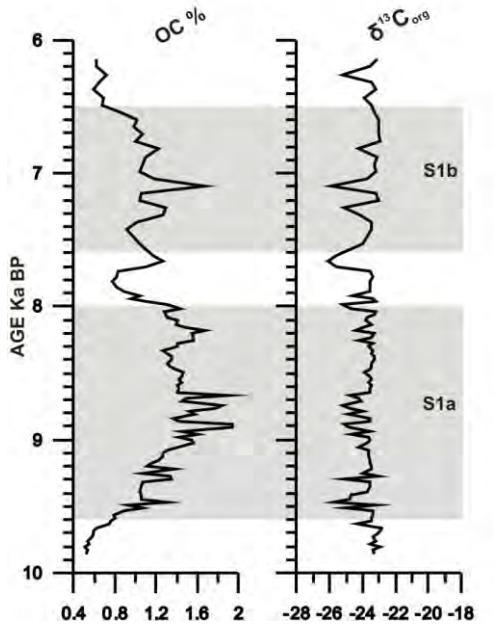

Figure 2 – Percentage concentration of organic carbon and vertical distribution of $\delta^{13}C_{org}$ values of gravity core M-4.

4.2. Benthic Foraminifera

The presence of benthic foraminifera is continuous throughout the core M-4 (Figure 3). *Chilostomella mediterranensis* is found in S1 lobes reaching almost 30% at 8.6 Ka BP during S1a and 25.4% at 6.8 Ka BP. *Bolivina striatula* peaks at 8.1 Ka BP (12.9%), decreases during the interruption of S1, but culminates again during the deposition of S1b. *Bolivina spathulata* displays low values during S1a; the highest abundance (29.9%) is observed at 7.8 Ka BP, followed by a gradual reduction during S1b. *Brizalina alata* is strongly fluctuating during S1 deposition, with abundances more pronounced within S1a. *Bulimina* spp. represents a significant component of sapropel microfauna, with an increasing trend in between 9-8.3 ka BP. The species *Globobulimina affinis* dominates the benthic assemblages of S1a, reaching 71.8% at 9 Ka BP. After 8 Ka BP, it is practically absent, with sporadic appearances, not exceeding 1 - 2%. *Cassidulinoides bradyi* is featured by a similar pattern, but with much lower abundance (max. 4.9% at 9.2 Ka BP). *Uvigerina mediterranea* reaches up to 24.2% at the beginning of layer S1a (9.6 Ka BP). Upwards it presents a gradual decrease, with another peak of 16.9% at the top of S1a (7.9 Ka BP); values are also increasing during S1b but to lesser degree. *Hyalinea balthica* increases significantly within S1b, showing a maximum of 16.7%, at 7 Ka BP whereas *Melonis barleeanum,* agglutinants and miliolids occur in very low rates inside S1, but increase significantly outside the sapropel depositional interval.

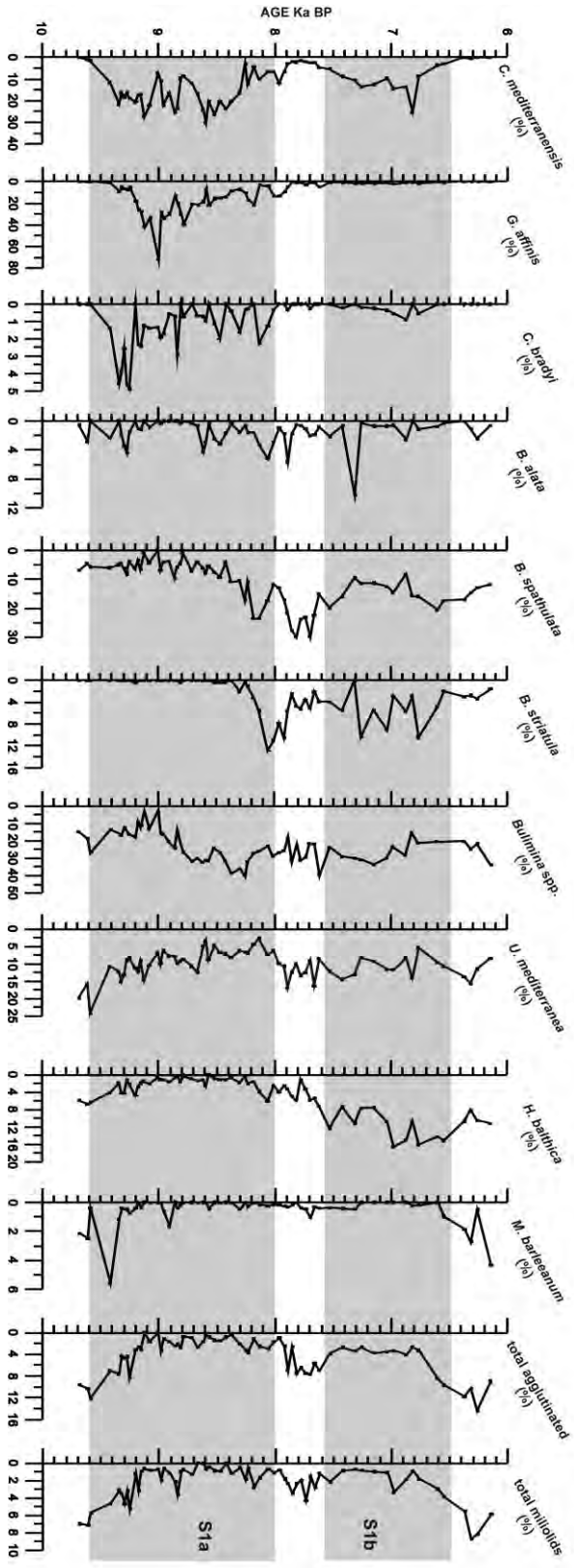

Figure 3 - Relative abundances of the main benthic foraminiferal species of core M-4.

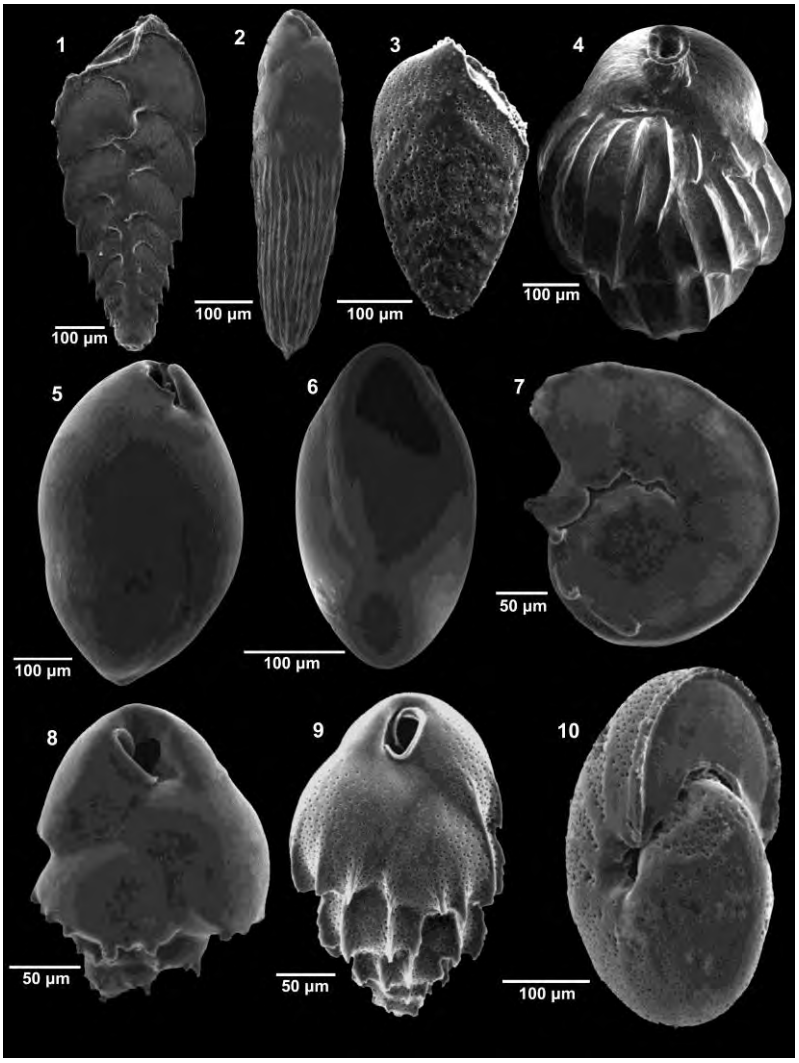

Plate I – 1. *Bolivina alata* (Seguenza), M-4, 88-88.5 cm 2. *Brizalina striatula* (Cushman), M-4, 38-38.5 cm 3. *Bolivina spathulata* (Williamson), M-4, 38-38.5 cm 4. *Uvigerina mediterranea* (Hofker), M-4, 33-33.5 cm 5. *Globobulimina affinis* (d'Orbigny), M-4, 63-63.5 cm 6. *Chilostomella mediterranensis* (Cushman & Todd), M-4, 90-90.5 cm 7. *Hyalinea balthica* (Schröeter), M-4, 63-63.5 cm 8. *Bulimina marginata* (d'Orbigny), M-4, 38-38.5 cm 9. *Bulimina costata* (d'Orbigny), M-4, 88-88.5 cm 10. *Melonis barleeanum* (Williamson), M-4, 110-110.5 cm.

4.3. Planktonic Foraminifera

Along the core sediments planktonic foramifera assemblages are abundant and consist mainly of *Gs. ruber* (0–30%), *Gs. sacculifer* (0–13%), *Or. universa* (0-7%), *Globigerina bulloides* (5-45%), *T. quinqueloba* (5–75%), *G. glutinata* (0–5%), *Neogloboquadrina* spp. (0-13%) and *Globorotalia inflata* (0-12%). Similar is also the modern foraminiferal assemblages in the studied area (Thunell, 1978). The downcore variations of the PSST index presents an increasing trend upwards (Figure 4). The eutrophicated species have always high participation in the planktonic assemblages ranging about 60 to 90% of the total association, suggesting high eutrophicated levels throughout the deposition of S1. However the largest percentages occur during the deposition of S1a.

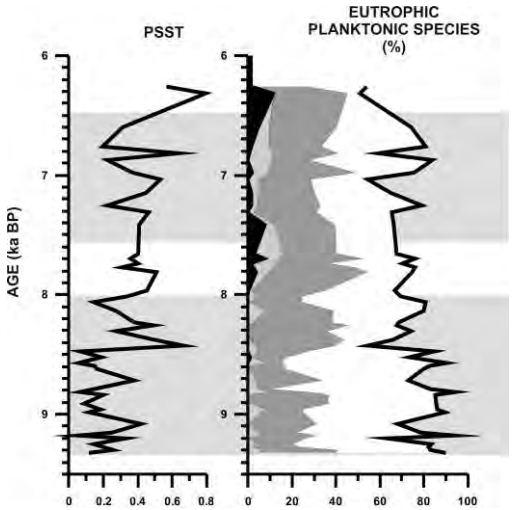

Figure 4 – a. Downcore variation of the Planktonic Sea Surface Temperature (PSST) curve, b. Relative abundances of the eutrophic planktonic foraminifera species of core M-4 (colours: black: *Gr. inflata*; light gray: Neogloboquadrinds; dark gray: *G. bulloides*; white: *T. quinqueloba*).

5. Discussion and Conclusions

Sapropel S1a interval in south Limnos basin is characterized by the intense presence of anoxic/dysoxic benthic species (Figure 3), such as *C. mediterranensis, G. affinis* and *C. bradyi* (e.g., Bernard & Sen Gupta, 1999; Fontanier et al., 2002; Kuhnt et al., 2007; Abu-Zied et al., 2008). In addition, *Bulimina* spp. (*B. aculeata*, *B. marginata* and *B. costata*), which are indices of extreme eutrophic and dysoxic conditions (e.g., Bernhard & Alve, 1996), along with the presence of *B. spathulata, B. striatula* and *B. alata* which are also living in low oxygen environments, and are relatively tolerant to non-oxic conditions (e.g., Jorissen et al., 1995) support dysoxic conditions within sapropelic layer S1a. However, S1a depositional interval is also featured by the presence of *U. mediterranea*, which has low tolerance to dysoxic conditions and prefers mesotrophic to eutrophic environments (e.g., Jorissen et al., 1995; Schmiedl et al., 2000). *H. balthica*, although in low abundances, indicates well oxygenated waters (e.g., Aksu et al., 1995; Morigi et al., 2001; Abu-Zied et al., 2008), while *Gyroidinoides* spp. also support higher oxygen conditions (e.g., Edelmann-Furstenberg et al., 2001). Therefore, there is ample evidence that less severe dysoxia has been developed in south Limnos basin during the deposition of layer S1a, in respect to what has been documented before for other Aegean basins (e.g., Kuhnt et al., 2007; Abu-Zied et al., 2008; Triantaphyllou et al., 2009a, b; Geraga et al., 2005, 2010).

Higher values of OC during the deposition of S1a than those of S1b indicate highest organic matter production and preservation in S1a, supporting previous results in the Aegean area (e.g., Gogou et al., 2007; Triantaphyllou et al., 2009b; Katsouras et al., 2010). The almost constant values of $\delta^{13}C_{org}$ during S1a, confirm the hypothesis that the deposition of sapropel S1 depends on primary productivity and preservation of organic matter (Katsouras et al., 2010). During the depositions of S1a and S1b the dominant planktonic species are *T. quinqueloba* and *G. bulloides* (Figure 4). *T. quinqueloba* is indicative of cool waters, but is also tolerant to fairly low salinity and/or enhanced fertility in surficial waters (Rohling et al., 1997). High percentages of this taxon have been reported in the sediments of S1 in Aegean Sea. However, this pattern seems to be stronger in N. Aegean basins (Geraga et al., 2010) rather than in S. Aegean basins (e.g., Geraga et al., 2000; Triantaphyllou et al., 2009a). *G. bulloides* is indicative of sub-polar water masses highly dependent on enhanced food levels (upwelling, strong seasonal mixing or freshwater inputs, Lourens et al., 1994). The abundant presence of *G. bulloides* and *T. quinqueloba* suggests the development of a

low salinity surficial layer rich in nutrients over south Limnos basin during the deposition of S1a and S1b.

The interruption of sapropel S1 at 8.0 Ka BP can be associated with the north hemisphere cold event at 8.2 Ka BP. During the sapropel interruption interval, the increase of agglutinated forms confirms both higher oxygen bottom conditions and freshwater input (e.g., Alve, 1995). This is accompanied by decrease in OC and the presence of planktonic foraminifera assemblages which suggest stronger mixing of the water column at least during winter. The more negative values of $\delta^{13}C_{org}$ identified at 7.7 Ka BP (-26.1 ‰) are indicative of terrigenous organic matter (e.g., Meyers & Arnaboldi, 2008; Katsouras et al., 2010) that may caused high value (1.26%) of OC, during the interruption interval.

Within the sapropelic layer S1b dysoxic foraminiferal species abundances are once more increased but to a lesser degree when comparing with S1a; in accordance with OC values and the relatively lower participation of the eutrophic planktonic assemblages. *U. mediterranea*, *H. balthica*, miliolids and agglutinants are increased, supporting even less dysoxia for S1b interval in respect to S1a, in south Limnos basin. Furthermore, the gradual increase of *H. balthica,* an indicator of cold environments (e.g., Aksu et al., 1995), during S1b confirms that this interval is featured by lower temperature conditions (e.g., Gogou et al., 2007; Triantaphyllou et al., 2009b). This fact is also supported by the increase of *U. mediterranea* (Figure 4)*,* a species that occurs at the final stage or subsequently after cold events (Kuhnt et al., 2007).

Minimum values of the PSST have been obtained during the S1a deposition. Low PSST values are also recorded during the deposition of S1b. Both these intervals are associated with the high abundance of *T. quinqueloba*. This taxon is indicative of high fertility and cool waters but is also tolerant to fairly low salinity (Rohling et al., 1997). Therefore the low PSST values may have been partly misled from the prevalence of low salinity surface waters occurred in that time. However the establishment of cool surface waters during the deposition of S1 is in agreement with other relative studies (i.e. Aksu et al., 1995). Low PSST values occur also at the late stages of S1a in accordance to the prevalence of the cold event at 8.2 Ka (Alley et al., 1997).

An increase in the abundances of *Gr. inflata* and Neogloboquadrinds is obtained during the interruption of S1 and the late stages of the deposition of S1b. *Gr. inflata* is associated with cool and deep mixed waters (Thunell, 1978; Pujol & Vergnaud Grazzini, 1995; Casford et al., 2002) and Neogloboquadrinids of eutrophicated waters associated with the formation of a Deep Chlorophyll Maximum (DCM) layer (Fairbanks & Wiebe, 1980). Therefore their strong presence in these two intervals indicates less stratified waters in relation to those prevailed during the deposition of S1a and S1b.

All acquired data records present rapid simultaneous fluctuations, suggesting short term paleoceanographic and palaeoclimatic changes in the studied area. Rapid palaeoclimatic changes during the discussed interval have been also reported in pollen records from N. Aegean Sea (Kotthoff et al., 2008).

6. Acknowledgments

This work has been made possible thanks to the financial support provided by the European Research Project MarinERA/ MedEcos and Research Project KA 70/4/11078 of the University of Athens. Thoughtful discussions with T. Kuhnt are greatly appreciated. Thanks are due to two anonymous reviewers for providing constructive comments on the manuscript.

7. References

Abu-Zied R.H., Rohling E., Jorissen F.J., Fontanie C., Casford, J.S.L. and Cooke S. 2008. Benthic foraminiferal response to changes in bottom-water oxygenation and organic carbon flux in the eastern Mediterranean during LGM to Recent times, *Mar. Micropal.*, 67, 46–68.

Aksu A.E., Yasar D., Mudie P.J. and Gillespie H. 1995. Late glacial-Holocene paleoclimatic and paleoceanographic evolution of the Aegean Sea: micropaleontological and stable isotopic evidence, *Mar. Micropal.*, 25, 1–28.

Alley R.B., Mayewski P.A., Sowers T., Stuiver M., Taylor K.C. and Clark P.U. 1997. Holocene c limatic instability: a prominent, widespread event 8200 yr ago, *Geology*, 25, 483– 486.

Alve E. 1995. Benthic foraminifera response to estuarine pollution: a review, *J. Foraminiferal Res.,* 25, 190–203.

Bé A.W.H. and Tolderlund D.S., 1971, Distribution and ecology of living planktonic foraminifera in surface waters of the Atlantic and Indian Oceans, In: Funnell, B.M., Riedel, W.R., (Eds), *The Micropalaeontology of Oceans*, Cambridge University Press, 105–149

Bernhard J.M. and Alve E. 1996. Survival, ATP pool, and ultrastructural characterization of benthic foraminifera from Drammensfjord (Norway): response to anoxia, *Mar. Micropal.*, 28, 5–17.

Bernard J.M. and Sen Gupta B.K. 1999. Foraminifera of oxygen-depleted environments, In: Sen Gupta, B.K. (Ed.), *Modern Foraminifera*, Kluwer Academic Publishers, 201–216.

Edelmann-Furstenberg Y., Scherbacher M., Hemleben C. and Almogi- Labin A. 2001. Deep-sea benthic foraminifera from the central Red Sea, *J. Foraminiferal Res.,* 31, 48–9.

Casford J.S.L., Rohling E.J., Abu-Zied R., Cooke S., Fontanier C., Leng M. and Lykousis V., 2002. Circulation changes and nutrient concentrations in the late Quaternary Aegean Sea: a nonsteady state concept for sapropel formation, *Paleoceanography*, 17, 1024–1034.

Ehrmann W., Schmiedl G., Hamann Y., Kuhnt T., Hemleben C. and Siebel W. 2007. Clay minerals in late glacial and Holocene sediments of the northern and southern Aegean Sea, *Palaeogeogr. Palaeoclimatol. Palaeoecol.*, 249, 36–57.

Facorellis Y., Maniatis Y. and Kromer B. 1998. Apparent 14C ages of marine mollusk shells from a Greek island: calculation of the marine reservoir effect in the Aegean Sea, *Radiocarbon*, 40, 963–973.

Fairbanks R.G. and Wiebe P.H., 1980. Foraminifera and Chlorophyll Maximum: vertical distribution, seasonal succession, and paleoceanographic significance, *Science*, 209, 1524–1526.

Fontanier C., Jorissen F.J., Licari L., Alexandre P., Anschutz P. and Carbonel P. 2002. Live benthic foraminiferal faunas from the Bay of Biscay: faunal density, composition, and microhabitats, *Deep-Sea Res. Oceanogr., A*, 49, 751–785.

Geraga M., Tsaila-Monopolis S., Ioakim C., Papatheodorou G. and Ferentinos G. 2000. Evaluation of palaeoenvironmental changes during the last 18,000 years in the Myrtoon basin, SW Aegean Sea, *Palaeogeogr. Palaeoclimatol. Palaeoecol.*, 156, 1–17.

Geraga M., Tsaila-Monopolis S., Ioakim C., Papatheodorou G. and Ferentinos G. 2005. Short-term climate changes in the southern Aegean Sea over the last 48,000 years, *Palaeogeogr. Palaeoclimatol. Palaeoecol.*, 220, 311–332.

Geraga M., Ioakim C., Lykousis V., Tsaila-Monopolis S. and Mylona G. 2010. The high resolution palaeoclimatic and palaeoceanographic history of the last 24,000 years in the central Aegean Sea, Greece, *Palaeogeogr. Palaeoclimatol. Palaeoecol.*, 287, 101–115.

Gogou A., Bouloubassi I., Lykousis V., Arnaboldi M., Gaitani P. and Meyers P.A. 2007. Organic geochemical evidence of abrupt late glacial-Holocene climate changes in the North Aegean Sea, *Palaeogeogr. Palaeoclimatol. Palaeoecol.*, 256, 1–20.

Jorissen F.J., De Stigter H.C. and Widmark J.G.V. 1995. A conceptual model explaining benthic foraminiferal microhabitats, *Mar. Micropal.*, 26, 3–15.

Katsouras G., Gogou A., Bouloubassi I., Emeis K.C., Triantaphyllou M., Roussakis G. and Lykousis V. 2010. Organic carbon distribution and isotopic composition in three records from the eastern Mediterranean Sea during the Holocene, *Org. Geochem.*, 41, 935-939.

Kotthoff U., Pross J., Muller U.C., Peyron O., Schmiedl G., Schulz H. and Bordon A. 2008. Climate dynamics in the borderlands of the Aegean Sea during formation of sapropel S1 deduced from a marine pollen record, *Quat. Sci. Rev.*, 27, 832–845.

Kouli K., Gogou A., Bouloubassi I., Triantaphyllou M.V., Ioakim Chr., Katsouras G., Roussakis G. and Lykousis V. 2012. Late postglacial paleoenvironmental change in the 129 northeast-

ern Mediterranean region: Combined palynological and molecular biomarker evidence, *Quat. Int.*, 261, 118–127.

Kuhnt T., Schmiedl G., Ehrmann W., Hamann Y. and Hemleben C. 2007. Deep-sea ecosystem variability of the Aegean Sea during the past 22kyr as revealed by Benthic Foraminifera, *Mar. Micropal.*, 64, 141–162.

Lourens L.J., Hilgen F.J., Gudjonsson L. and Zachariasse W.J. 1994. Late Pliocene to Early Pleistocene astronomically forced sea surface productivity and temperature variations in the Mediterranean, in: Lourens, L.J., (Ed.), *Astronomical Forcing of Mediterranean Climate During the Last 5.3 Million Years*, Universiteit Utrecht, 37–58.

Lykousis V., Chronis G., Tselepides A., Price N.B., Theocharis A., Siokou-Fragou I., van Wambeke F., Danovaro R., Stavrakakis S., Duineveld G., Georgopoulos D., Ignatiades L., Souvermezoglou A. and Voutsinou-Taliadouri F. 2002. Major outputs of the recent multidisciplinary biogeochemical researches undertaken in the Aegean Sea, *J. Mar. Syst.*, 33–34, 313–334.

Meyers P.A. and Arnaboldi M. 2008. Paleoceanographic implications of nitrogen and organic carbon isotopic excursions in mid-Pleistocene sapropels from the Tyrrhenian and Levantine Basins, Mediterranean Sea, *Palaeogeogr. Palaeoclimatol. Palaeoecol.*, 266, 112–118.

Morigi C., Jorissen F.J., Gervais A., Guichard S. and Borsetti A.M. 2001. Benthic foraminiferal faunas in surface sediments off NW Africa: Relationship with the organic flux to the ocean floor, *J. Foraminiferal Res.,* 31, 350–361.

Poulos S.E. 2009. Origin and distribution of the terrigenous component of the unconsolidated surface sediment of the Aegean floor: A synthesis, *Cont. Shelf Res.*, 29, 2045–2060.

Pujol C. and Vergnaud Grazzini C. 1995. Distribution patterns of live planktic foraminifers as related to regional hydrography and productive systems of the Mediterranean Sea, *Mar. Micropal.*, 25, 187–217.

Rohling E.J., Jorissen F.J. and De Stigter H.C. 1997. 200 year interruption of Holocene sapropel formation in the Adriatic Sea, *J. Micropaleontol.*, 16, 97–108.

Roussakis G., Karageorgis A.P., Conispoliatis N. and Lykousis V. 2004. Last glacial-Holocene sediment sequences in N. Aegean basins: structure, accumulation rates and clay mineral distribution, *Geo-Mar. Lett.*, 24, 97–111.

Schmiedl G., de Bovée F., Buscail R., Charrière B., Hemleben C., Medernach L. and Picon P. 2000. Trophic control of benthic foraminiferal abundance and microhabitat in the bathyal Gulf of Lions, western Mediterranean Sea, *Mar. Micropal.*, 40, 167–188.

Stuiver M. and Reimer P.J. 1993. Extended C-14 data-base and revised Calib 3.0 C-14 age calibration program, *Radiocarbon*, 35, 215–230.

Thunell R.C. 1978. Distribution of recent planktonic foraminifera in surface sediments of the Mediterranean Sea, *Mar. Micropal.*, 3, 147–173.

Triantaphyllou M.V., Antonarakou A., Kouli K., Dimiza M., Kontakiotis G., Papanikolaou M., Ziveri P., Mortyn G., Lianou V., Lykousis V. and Dermitzakis M.D. 2009a. Comparing Late Glacial - Holocene Plankton ecozones and Pollen Assemblage Zones: Basis for a multi-proxy ecostratigraphy in the south-eastern Aegean Sea (E. Mediterranean), *Geo-Mar. Lett.*, 29, 249–267.

Triantaphyllou M.V., Ziveri P., Gogou A., Marino G., Lykousis V., Bouloubassi I., Emeis K.C., Kouli K., Dimiza M., Rosell-Mele A., Papanikolaou M., Katsouras G. and Nunez N. 2009b. Late Glacial-Holocene climate variability at the south-eastern margin of the Aegean Sea, *Mar. Geology*, 266, 182–197.

Zervakis V., Georgopoulos D., Karageorgis A.P. and Theocharis A. 2004. On the response of the Aegean Sea to climatic variability: a review, *Int. J. Climatol.*, 24, 1845–1858.

Δελτίο της Ελληνικής Γεωλογικής Εταιρίας, τομ. XLVII , 2013
Πρακτικά 13ου Διεθνούς Συνεδρίου, Χανιά, Σεπτ. 2013

Bulletin of the Geological Society of Greece, vol. XLVII 2013
Proceedings of the 13th International Congress, Chania, Sept. 2013

PALAEOBOTANICAL STUDY OF POLICHNITOS REGION, SOUTHERN PART OF LESBOS ISLAND, GREECE (PRELIMINARY RESULTS ON ANGIOSPERM WOOD)

Mantzouka D.[1], Sakala J.[2], Kvaček Z.[2] and Karakitsios V.[1]

[1] National and Kapodistrian University of Athens, Faculty of Geology and Geoenvironment, Department of Hist. Geology - Paleontology, dmantzouka@geol.uoa.gr , vkarak@geol.uoa.gr

[2] Charles University of Prague, Czech Republic, Institute of Geology and Palaeontology, Albertov 6, 12843, Prague 2, rade@natur.cuni.cz, kvacek@natur.cuni.cz

Abstract

The present contribution brings new scientific data for the palaeoflora of Lesbos based on new collections of plant fossils which were discovered in 2011 at six new localities from the southern part of Lesbos Island. This study resumes the published data both on the palaeovegetation of the Petrified Forest and the palaeogeography of Lesbos Island during the Neogene.

The new palaeobotanical study with more than seventy new samples of fossilized wood from the broader area of Polichnitos region gives new information about the palaeobotanical and palaeontological content of this area.

It is reported for the first time here the existence of a diversified fossil wood assemblage from the southern part of the Island as long as the identification of three types of lauraceous wood according to their idioblasts characteristics.

Key words: *plant fossil anatomy, Lauraceae, idioblasts, Petrified Forest of Lesbos.*

Περίληψη

Η εν λόγω εργασία φέρνει στο φως νέα επιστημονικά δεδομένα για την παλαιοχλωρίδα της Λέσβου που βασίζονται σε νεοσυλλεχθέντα φυτικά απολιθώματα τα οποία ήρθαν στο φως το 2011και προέρχονται από έξι νέες θέσεις από το νότιο τμήμα της νήσου Λέσβου. Η συγκεκριμένη μελέτη ανακεφαλαιώνει τα ήδη δημοσιευμένα δεδομένα αναφορικά με την σύνθεση της παλαιοβλάστησης του Απολιθωμένου Δάσους καθώς και με την παλαιογεωγραφία της νήσου Λέσβου κατά το Νεογενές.

Η νέα παλαιοβοτανική μελέτη με περισσότερα από εβδομήντα νέα δείγματα απολιθωμένων δέντρων από την ευρύτερη περιοχή του Πολυχνίτου δίνει νέες πληροφορίες σχετικά με το παλαιοβοτανικό και παλαιοντολογικό περιεχόμενο της συγκεκριμένης περιοχής.

Στην εν λόγω εργασία γίνεται για πρώτη φορά αναφορά στην ύπαρξη ποικίλων συγκεντρώσεων απολιθωμένου ξύλου από το νότιο τμήμα του νησιού, καθώς και ο προσδιορισμός τριών τύπων της οικογένειας των Δαφνίδων σύμφωνα με τα χαρακτηριστικά των ιδιόβλαστων κυττάρων τους.

Λέξεις κλειδιά: *Ανατομία απολιθωμένου ξύλου, Οικογένεια Δαφνίδων, ιδιόβλαστα κύτταρα, Απολιθωμένο Δάσος Λέσβου.*

1. Introduction

The importance of the plant fossils of Lesbos Island has been underlined having also the privilege to be the first place of the world where the palaeobotanical research took place by Theophrastus from Eressos, Lesbos Island (372-287 B.C.) at the 3rd century B.C. Theophrastus wrote down all his observations for the fossil trees of Lesbos in his book 'On Petrifactions' ('Περί Λιθουμένων'), which, unfortunately is not saved, although there are some references about the fossil trees inside his book 'On Stones' ('Περί Λίθων') (Theophrastus, *Complete Works* 8. 1. 4; 8. 2. 12; 8. 2. 16; 8. 2. 17; 8. 6. 38). The main occurrences of the plant fossils have been found at the western peninsula of the Island (Petrified Forest park; Nissiopi park; Sigri park; Plaka park; Skamiouda park) which has been declared as a Protected Natural Monument since 1985 with a special Presidential Decree (No 443/1985, in Velitzelos et al., 1999). Up to now the great majority of the studied woods were attributed to "gymnosperms" (especially conifers), while the described leaves belong rather to angiosperms (Velitzelos & Zouros, 2008).

This study focuses on the new findings – of both conifers and angiosperms – from new plant fossiliferous localities from Polichnitos region (which is rather distant from the protected area of the Petrified Forest-Western Peninsula).

2. Geological Setting

Lesbos Island is located at the NE part of Aegean and it belongs to the Pelagonian geotectonic zone of Greece which represents a fragment of the Cimmerian Continent (Mountrakis, 1983; 1986).

According to previously published data (Hecht, 1972b; 1974, Katsikatsos et al. 1982; 1986, Fytikas et al., 1984, Mountrakis et al., 1983; 2001, Thomaidou, 2009) the geology of Lesbos is documented in Figure 1 and it consists of an autochnthonous and two allochthonous units.

Polichnitos – Vatera area is located at the southern part of the Lesbos Island (Figure 1). In this area there are six different localities from where samples of fossil wood were obtained. The stratigraphic sequence is presented in Figure 2.

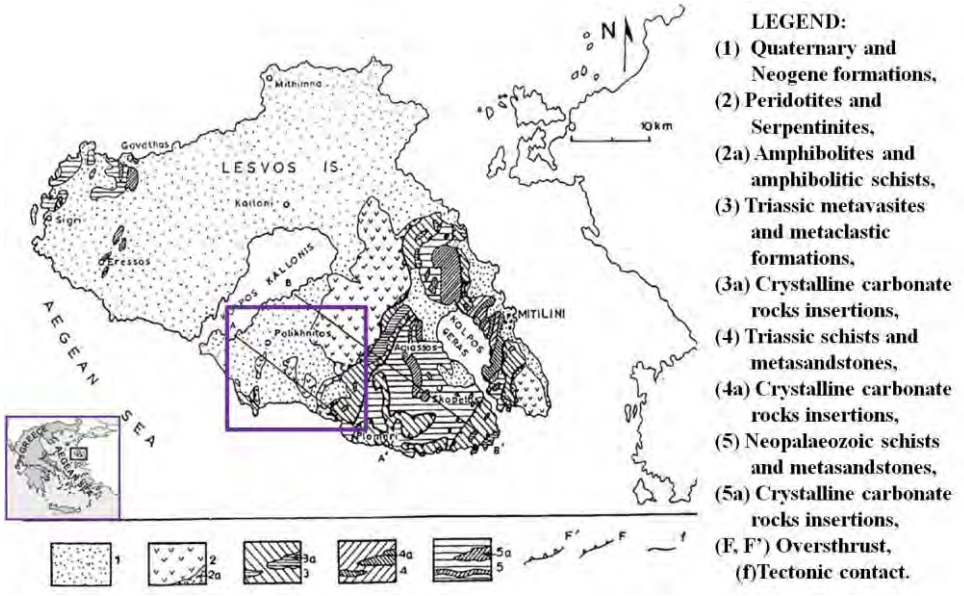

Figure 1 - Geological map by Katsikatsos et al. (1986), modified. Polichnitos-Vatera study area is included in the rectangular.

The stratigraphic sequence of our section fits almost perfectly with the one presented by Katsikatsos et al. (1982) for Polichnitos area, with the difference of a tephra horizon (formation 'e.i' in Fig.2) – which can be attributed to the 'volcanic rocks (+) formation' – under Polichnitos ignimbrite (formation 'c' in Fig.2) as it is shown in Figure 2.

Our outcrops (from the bottom to the top layer) consist of:

- Miocene Terra rossa with a thickness of approximately 12 m (formation 'b' in Fig.2). This is the layer which has the same stratigraphic position with the thick deposits of conglomerates and pyroclastic materials of the area of Sigri - Antisa, which are also lying under the ignimbrites and have at their lower part (and mainly at their basis) marly layers which host small lignitic deposits (Katsikatsos et al., 1986). According to Lamera (2004) it might represent a 'lahar' formation. The basement / underlying layer is not seen at the outcrop but the general view of the area shows that the basement consists of ultrabasic rocks.

- Over the Terra rossa there is a tephra horizon of 1,5 m thickness (formation 'e. i' in Fig.2, left column) and over this there are volcanics of beige color – consisting of 2 horizons, one of 0,4 m ('e. ii' formation in Fig.2, left column) and one of 2 m thickness ('e. iii' formation in Fig.2, left column) – with a total thickness of 2.4 m which are underlying the

- Ignimbrite of Polichnitos with a thickness of 4 m (formation 'c' in Fig.2). According to Pe-Piper & Piper, 1993 the only radiometric date of Polichnitos ignimbrite in 17.2 ± 0.5 Ma 'was made by Borsi et al. (1972) corrected to the Steiger & Jäger, (1977) decay constant'. Polichnitos ignimbrite formation belongs to the magnetic epoch 17 with an age of ~ 18.4 – 17.2 Ma (Pe-Piper, 1980; Pe-Piper & Piper, 1993 while, according to the proposed categorization of Lesbos ignimbrites by Lamera (2004), it represents the PU unit. The fossil plants of our study come from the layers which are underlying Polichnitos ignimbrite and especially from the upper and lower part of the tephra horizon (ei, eii, b in Fig. 2, left column).

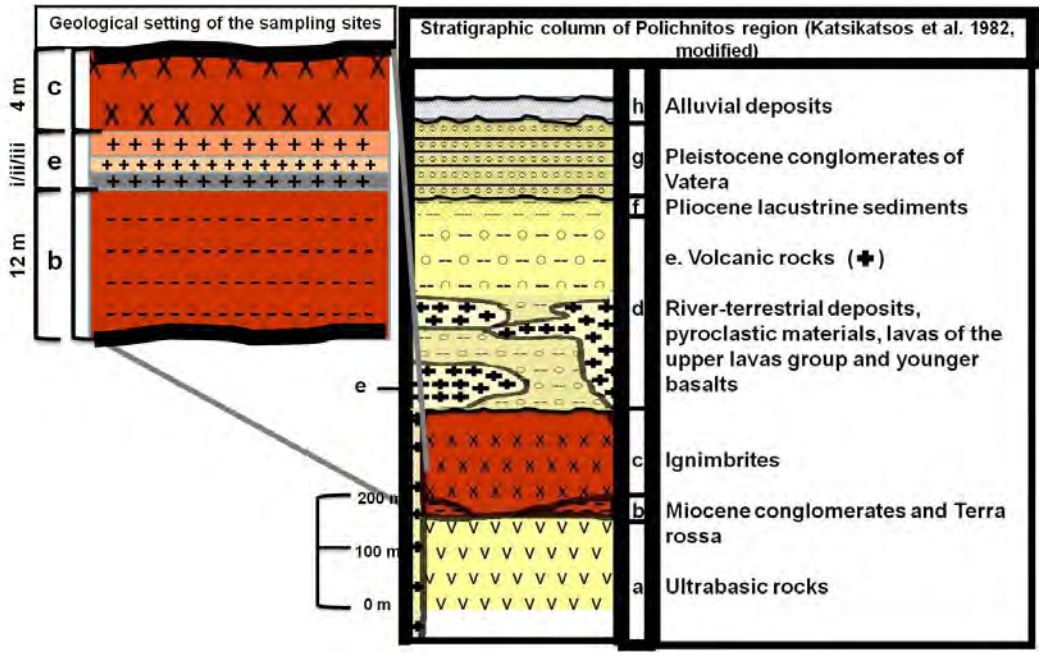

Figure 2 - "Polichnitos – Vatera" area stratigraphic column (from the bottom to the top layer) according to Katsikatsos et al. (1982), modified and the geological setting of the new fossiliferous sites.

Figure 3 - An example of the outcrops of the localities in Polichnitos region (Locality: DMAL, date: 21/08/11).

3. Materials and Methods

During 2011 and 2012 almost 400 specimens were collected by one of us (DM) from six new localities in Polichnitos region. The fossil plants were photographed, their dimensions were measured and they were catalogued. Thin slides for more than 70 samples were prepared (three for each sample: transversal, radial and tangential) in order to study their anatomical features under the microscope.

The thin sections were observed under an Olympus BX51 microscope, in the facilities of Charles University, Prague. Data tables were subsequently created using the Microsoft Office Excel. The anatomical description is in accordance with the IAWA Hardwood List (IAWA Committee 1989) and Wheeler (1986) for angiosperms and the IAWA Softwood List (IAWA Committee 2004) for conifers. In several steps of the study the ArcMap - ArcGIS Program was used, in order to have the already existing knowledge and the new data of the palaeogeographical history of Lesbos Island portrayed.

In Polichnitos region two fossiliferous sites are known (Figure 4):

1. Rougada from which one fossil trunk had been found [*Taxaceoxylon biseriatum* SÜSS & VELITZELOS]. The tree trunk is ash-gray color, is 12.5 m long with a diameter ranging from 80 to 95 cm and was embedded in an ignimbrite layer (Süss & Velitzelos, 1994a).
2. Vatera where the Pliocene vertebrate fauna was discovered and studied by the University of Athens (Dermitzakis, 2002).

Among the material that was collected there were also carbonized fossils (Fig. 5a), or permineralised (Fig. 5b) with the great majority of them having the wood, the bark and the extraxylary tissues preserved in a detailed way.

4. Systematical Part

4.1 Historical Research of the Fossil Plants of Lesbos Island

From 1845 till 2012, 25 species of gymnosperm wood and only 5 species of angiosperm wood have been identified in the Neogene palaeoflora of Lesbos Island, while in some of them there is also information about their preservation. This information is of great value for the taphonomic processes (Appendix). Moreover the references concerning the angiosperm wood species come from the 19th century. The opposite phenomenon – with 5 gymnosperms and 29 angiosperms – occurs at leaves' findings.

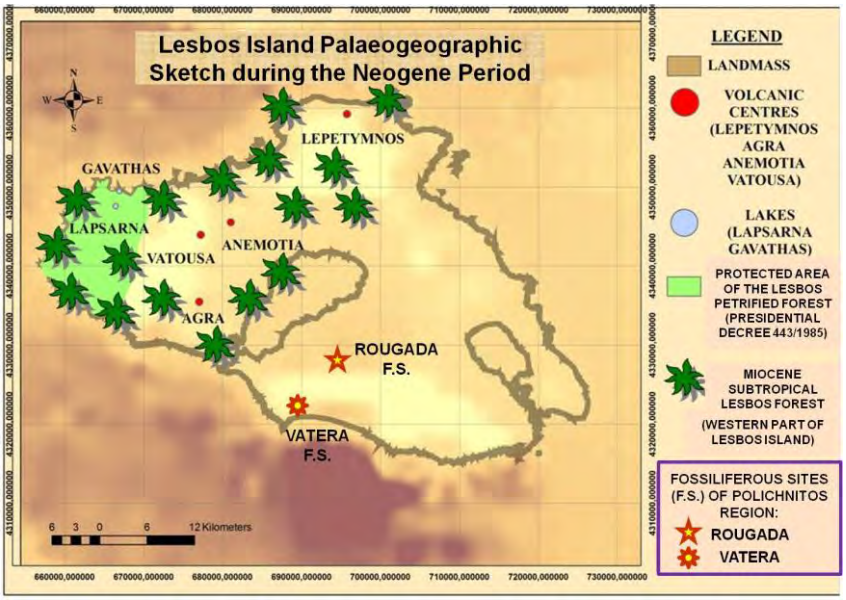

Figure 4 - Palaeogeographic sketch of Lesbos Island during the Neogene Period (Mantzouka 2009a, b, modified).

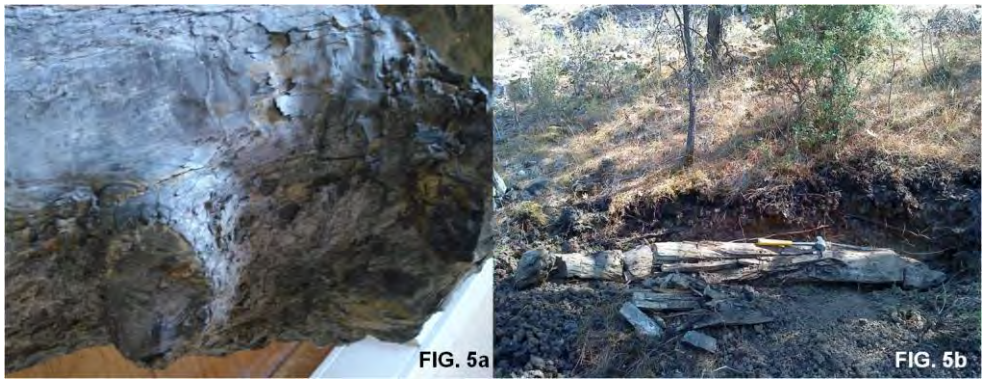

Figure 5 - a. Detail of the external structure of a fossil trunk: the knots and even the bark are preserved (Sample: DMAL 6, date: 21/8/11); b. Among the specimens there is also a lying trunk 2 meters long (Locality: DMRO, date: 17/09/11).

4.2 Preliminary Results

Both conifers and angiosperms have been identified in the samples collected from Polichnitos area. Some of the sampling localities contain only one of these two groups; the others have both of them. However, in this paper only the results from the angiosperms are reported.

Among the newly discovered angiosperm woods we were able to identify anatomical characteristics resembling *Quercus*, *Rhamnus* and Lauraceae family. So far, we recognize seven wood specimens which are similar to the later family according to their typical features as described by Richter in Metcalfe (1987): wood with frequently diffuse porous, vessel solitary or in radial multiples (never exclusively solitary), alternate intervessel pits and tyloses, paratracheal parenchyma, rays 1–3–(5)-seriate, and heterocellular fibers with pitting on radial walls only. Such a fossil wood can be attributed to the morphogenus *Laurinoxylon* FELIX.

Concerning lauraceous woods, they were categorized in different groups, based on their oil cells characteristics. According to Richter (1981) the oil and/or mucilage cells can be of potential

diagnostic value, since the difference in their shape and distribution can lead to different taxonomic groups. There are three different groups of idioblasts connected to: a. the ray parenchyma, and b. the vertical strand parenchyma or c. isolated from parenchyma tissues, embedded among the fibers). Three types of lauraceous woods were observed: 1) three samples (Fig. 6b, 7) with oil and/or mucilage cells (idioblasts) connected only to the ray cells, 2) three samples with idioblasts connected to the ray cells and among the fibers and 3) one sample with oil and/or mucilage cells in rays, axial parenchyma and among the fibers. However, a more detailed study is required to obtain solid conclusion.

The samples that have been attributed to the Lauraceae, have some macroscopic characteristics in common: they belong to small stems, which are enclosed to volcanic material (Fig. 6a, b), they are silicified, light, porous, whitish red-brown with distinct growth ring boundaries that can be seen with naked eye, while, most of the times, there is a strange coloration type of circles (possible because of inclusions, of an insect impact or due to mineralization).

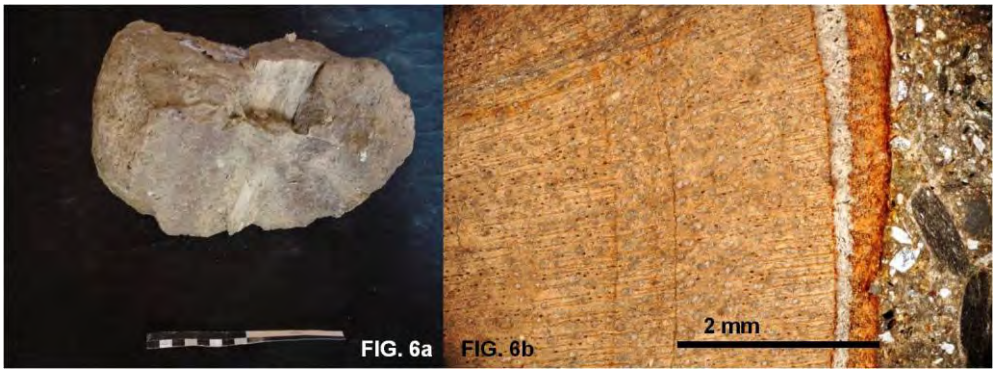

Figure 6 - a. The stem of *Laurinoxylon* type enclosed in volcanic material (sample DMDA 2, dimensions in cm: 18x9x4); b. A stem/branch of type 1 of *Laurinoxylon* (sample DM 17) enclosed in volcanic material (transversal section No. DM17a). The occurrence of the growth ring boundaries is also shown.

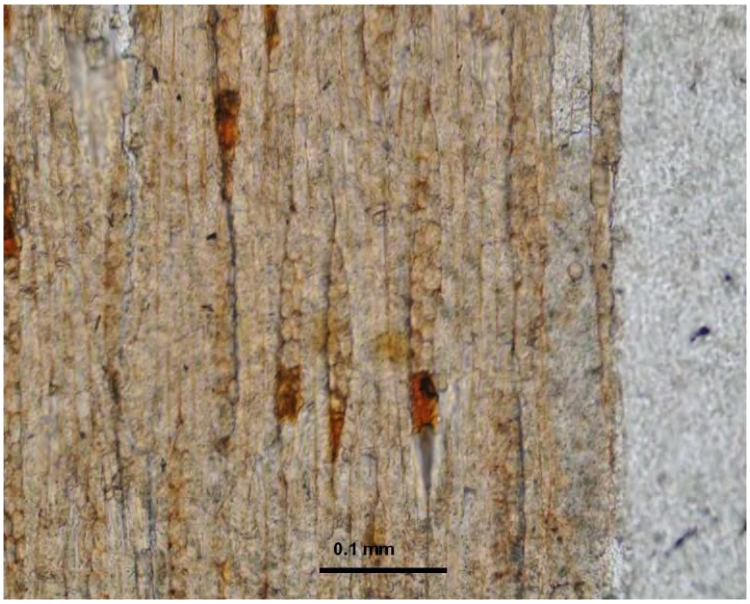

Figure 7 - The oil and/or mucilage cells associated only with the ray parenchyma cells from the same sample DM17 (tangential section No. DM17c).

5. Conclusions

This paper presents preliminary results of a study during which new localities of palaeobotanical interest were discovered in the region of Polichnitos (Vatera) in Lesbos Island; an area that was already well known for its palaeofauna findings. The microscopical study of the collected samples brings new data to the Neogene palaeobotanical record of the Island. Through the study of the new samples there is going to be an effort for collecting as much data as possible in order to follow the 'whole – plant' concept (Sakala 2004) and put together the pieces of the puzzle of reconstructing Lesbos palaeoflora species. Since September of 2012, the whole Island of Lesbos belongs to the Global Geoparks Network of Unesco, which is a recognition of the diversified and many geosites of the Island. By conducting this study we would like to contribute by showing that the occurrences of the petrified trees in other parts of the Island (i.e. apart from the Western peninsula) are not just sporadic but with the right support, protection and scientific study can become geomorphosites/geosites of great importance for the palaeontological heritage of Greece (Zouros & Valiakos 2007).

As far as the stratigraphy is concerned further studies could be conducted by volcanologists and petrologists, since there are localities among the plant fossiliferous ones where the fossils are enclosed inside the volcanic material and others where it seems that the fossiliferous horizon is hosted within the ignimbrite or within lahar deposits. This kind of differentiation of the lithological setting could have a different reflection to the process of silicification, to the palaeoenvirmonment (e.g. the silicification is faster in volcanic lahars) and also could provide more information about the preservation of fossils (Ballhaus et al. 2012). Furthermore, future radiometric dating of specific volcanic layers in the sampling areas will enable the characterization of a biozone and of an exact age.

5. Acknowledgments

Special thanks to Prof. EvangelosVelitzelos, also to the Natural History Museum of the Lesbos Petrified Forest and to the Natural History Collection of Vrisa – part of the Museum of Palaeontology and Geology of University of Athens for providing a part of the needed literature, to Prof. Georgia Pe-Piper for the important advices for the geology of the new fossiliferous localities, to Prof. Nikolaos Christodoulakis, to Prof. George Theodorou for their collaboration and help concerning the new findings and to Dr Elizabeth Stathopoulou and PhD Candidate Mrs Olga Koumoutsakou for their great help for the preparation of the thin slides. Special thanks also to the Institute of Geology and Paleontology, Faculty of Science, Charles University in Prague, to the Department of Historical Geology & Paleontology, Faculty of Geology & Geoenvironment, National and Kapodistrian University of Athens and to the Faculty of Botany, Department of Biology, for the permission of using their facilities for the achievement of the scientific anatomic description and consequently taxonomic identification of the new material. This research was partly supported by the grant MSM0021620855 and PRVOUK P44 project, Faculty of Science, Charles University.

6. References

Ballhaus C., Gee C.T., Bockrath C., Greef K., Mansfeldt T. and Rhede D. 2012. The silicification of trees in volcanic ash-An experimental study, *Geochimica et Cosmochimica Acta* 84, p. 62-74.

Dermitzakis M. (ed) 2002. "On Late Plio/Pleistocene extinction and evolution in the Paleartic. The Vatera site". *Annales Géologiques des Pays Helleniques.* Vol. 1/39. Athenes, Department de Geologie, Panepistimioupolis. Sponsored: Ministery of Aegean, Prefecture of Lesbos G.S.R.T. & Municipality of Polichnitos.

Fliche P. 1898. Note sur les bois fossiles de Metelin, Appendice in De Launay, L. 1898, *Etudes geologiques sur la Mer Egee. La geologie des iles de Metelin (Lesbos), Lemnos et Thasos.* Paris, p. 141-151.

Fytikas M., Innocenti F., Manetti P., Mazzuoli R., Peccerillo A. and Villari L. 1984. Tertiary to Quaternary evolution of volcanism in the Aegean region, in: *The Geological Evolution of the Eastern Mediterranean*, eds: Dixon J.E. and Robertson A.H.F., *Spec. Publ. Geol. Soc. London*, No17, p.687-699.

Gregory M., Poole I. and Wheeler, E.A. 2009. Fossil dicot wood names. An annotated list with full bibliography, *IAWA Journal*, Supplement 6, 2009.

Hecht J. 1972. *Geological map of Greece*, 1:50.000, Lesbos Island — Plomari/Mytilene.

Hecht J. 1974. *Geological map of Greece*, 1:50.000, Lesbos Island — Polichnitos.

IAWA Committee 2004. Richter, H. G.; Grosser, D.; Heinz, I. & Gasson, P. E. (eds.), IAWA List of microscopic feature for softwood identification, *IAWA Journal* 25: 1–70.

IAWA Committee. 1989. Wheeler, E. A.; Baas, P. & Gasson, P.E. (eds.), IAWA list of microscopic features for hardwood identification, *IAWA Bulletin* n.s. 10 (3): 219-332. Leiden, The Netherlands.

Katsikatsos G., Mataragas D., Migiros G. and Triantaphyllis E. 1982. Geological study of Lesbos Island. *I.G.M.E. (Internal report in greek)* Athens. p.p.92.

Katsikatsos G., Migiros G., Triantaphyllis M. and Mettos A. 1986. Geological structure of internal Hellenides (E. Thessaly – SW Macedonia – Euboea – Attica – northern Cyclades Islands and Lesbos), *Geol. & Geoph. Res. Sp.* Vol. 191-212.

Lamera S. 2004. The Polichnitos Ignimbrite of Lesbos island*, PhD Thesis*. University of Patras, Department of Geology, p.p.272

Mantzouka D. 2009a. Palaeogeographical study of Lapsarna area (Lesbos Island) based on the new palaeontological findings of the lower Miocene period*, Master thesis,* Department of Geography. University of Aegean. p.p. 143 (in greek).

Mantzouka D. 2009b. Palaeogeographical study of Lapsarna area according to palaeontological findings of the lower Miocene period (fish otoliths) "Earth heritage and nature conservation: Geopark's management and action plans on sustainable tourism", *Proceedings of the International Conference & Intensive course on Geoparks*, Lesbos, Greece.

Metcalfe C.R. 1987. Anatomy of the dicotyledons: Vol. III Magnoliales, Illiciales and Laurales. 2nd Ed. Clarendon Press, Oxford.

Mountrakis D. 1983. Structural geology of the North Pelagonian zone s.l. and geotectonic evolution of the internal Hellenides. *Unpubl. Habilitation*, Univ. Thessaloniki, 283.

Mountrakis D. 1986. The Pelagonian zone in Greece: a polyphase deformed fragment of the Cimmerian continent and its role in the geotectonic evolution of East Mediterranean, *Journal of Geology* 94, p.p. 335 – 347.

Pe-Piper G. 1980. The Cenozoic volcanic sequence of Lesbos, Greece. *Z. Dt. Geol. Ges.*, 131, 889-901.

Pe-Piper G. and Piper D.J.W. 1993. Revised stratigraphy of the Miocene volcanic rocks of Lesbos Greece. *Neues Jahrbuch für Geologie und Palaontologie*, Mh., H.2, 97-110.

Richter H.G. 1981. *Anatomie des sekundären Xylems und der Rinde der Lauraceae.* Sonderbände des Naturwissenschaftlichen Vereins in Hamburg. p.p 148.

Sakala J. 2004. The 'Whole-Plant' concept in palaeobotany with examples from the Tertiary of northwestern Bohemia, Czech Republic with particular reference to fossil wood, *PhD Thesis*, Université Pierre-et-Marie, Paris & Charles University, Prague. p. 1-94.

Selmeier A. and Velitzelos E. 2000. Neue Aufsammlungen von verkieselten Holzresten aus tertiären Schichten Griechenlands (Lesbos, Kastoria, Thrakien), *Mitt. Bayer. Staatsslg. Palaeont. Hist. Geol.* 40, 213-227.

Süss H. 1997. *Tetraclinoxylon velitzelosi sp. nova.* ein neues fossiles Holz aus tertiären Schichten des Versteinerten Waldes von Lesbos, *Feddes Repertorium,* 108, 289-298.

Süss H. 2003. Zwei neue fossile Hölzer der Morphogattung *Ginkgoxylon* SAPORTA emend. SÜSS aus tertiären Schichten der Insel Lesbos, Griechenland, mit einer Übersicht über Fossilien mit ginkgoaler Holzstruktur, *Feddes Repertorium,* 114, 5–6, 301–319.

Süss H. and Velitzelos E. 1994a. Ein neues fossiles Koniferenholz, *Taxaceoxylon biseriatum sp. nova*, aus tertiären Schichten der Insel Lesbos, Griechenland, *Feddes Repertorium,*105, 257-269.

Süss H. and Velitzelos E. 1994b. Zwei neue tertiäre Hölzer der Gattung *Pinoxylon* KNOWLTON emend, READ aus dem Versteinerten Wald von Lesbos, Griechenland, *Feddes Repertorium,*105, 403–423.

Süss H. and Velitzelos E. 1997. Fossile Hölzer der Familie Taxodiaceae aus tertiären Schichten des Versteinerten Waldes von Lesbos, Griechenland, *Feddes Repertorium,* 108, 1-30, 5 Abb., 7 Taf.

Süss H. and Velitzelos E. 1998. *Thujoxylon antissurn sp. nov.*. ein fossiles Wurzelholz aus tertiären Schichten des Versteinerten Waldes von Lesbos, Griechenland, *Feddes Repertorium,* 109, 341-350.

Süss H. and Velitzelos E. 1999. *Chimairoidoxylon gen. nov. sp. nova*, ein endemisches Holzfossil aus dem Tertiar von Lesbos, Griechenland, *Feddes Repertorium,* 110, 329-339.

Süss H. and Velitzelos E. 2000. Zwei neue fossile Hölzer der Formgattung Podocarpoxylon GOTHAN aus tertiären Schichten der Insel Lesbos, Griechenland, *Feddes Repertorium,* 111, 135-149.

Süss H. and Velitzelos E. 2001. *Chimairoidoxylon conspicuum sp. nova*, ein neues fossiles Holz der Formgattung Chimairoidoxylon SÜSS & VELITZELOS emend. SÜSS, mit einer Übersicht über das Vorkommen fossiler Hölzer auf der Insel Lesbos, Griechenland, *Feddes Repertortium,* 112, 149–157.

Süss H. and Velitzelos E. 2009. Zwei neue fossile Hölzer der Morphogattung *Pinoxylon* KNOWLTON emend. READ aus dem Tertiär der Insel Lesbos, Griechenland, *Feddes Repertorium,* 120, 3–14.

Süss H. and Velitzelos E. 2010. *Lesboxylon gen. nov.,* eine neue Morphogattung mit dem Typus Lesbosoxylon ventricosuradiatum sp.nova aus dem Tertiar der Insel Lesbos, Griechenland, *Feddes Repertorium,* 121, 1–2, 18–26.

Theophrastus. *Complete Works: On Plants History, On Stones* (Athens: Kaktos Editions, 1998)

Thomaidou, E., 2009. The geological structure of Lesbos Island *PhD thesis,* AUTH, p. 39.

Unger F. 1845. *Synopsis plantarum fossilium.* Lipsiae apud Leopoldum Voss, Bibliopolam.

Unger F. 1847. *Chloris protogaea.* Beitrage zur Flora der Vorwelt. Leipzig.

Unger F. 1850. *Genera et species plantarum fossilium,* Wien.

Velitzelos, E., Petrescu, I. and Symeonidis N. 1981a. Tertiary Plant Reminants from Aegiis. Macro – Palaeo – Flora of Lesbos Island (Τριτογενή Φυτικά Λείψανα εκ της Αιγηΐδος. Μακρο-Παλαιο-Χλωρίδα της Νήσου Λέσβου), *Annales Géologiques des Pays Helléniques* XXX/ 2-1981, 500-514, Athens.

Velitzelos E., Petrescu I. and Symeonidis N. 1981b. Tertiäre Pflanzenreste von der Ägäischen Insel Lesbos (Griechenland) [Tertiary Plant Fossils from Lesbos Island (Aegean, Greece)], *Cour. Forsch. Inst. Senckenberg,* 50, 49-50, Frankfurt.

Velitzelos E. and Zouros N. 2008. *The Petrified Forest of Lesbos*, Natural History Museum of the Lesbos Petrified Forest, Topio Publications, Athens, p.p. 155.

Velitzelos E., Zouros N. and Velitzelos D. 1999. Contribution to the study of the palaeoflora of the Lesbos Petrified Forest. *Proceedings of the International Symposium 'Protected natural areas and environmental education'*. Sigri, Lesbos Island.

Wheeler E.A. 1986. Vessels per square millimetre or vessel groups per square millimetre? *IAWA Bull.* n.s. 7, 73-74.

Zouros N. and Valiakos H. 2007. Geosite assessment and management, *Proceedings of 8th Pan-Hellenic Geographical Conference of the Hellenic Geographic Society*, Athens, Vol. 1, 612-620.

APPENDIX:

GYMNOSPERM WOOD

Thujoxylum peucinum UNGER emend. SÜSS & VELITZELOS [Lesbos unknown locality: ?Sigri described by Unger (1847, p.31, 32). The genus has been emended by Süss & Velitzelos (1998)].

Taxoxylum priscum UNGER [Lesbos unknown locality: ?Sigri described by Unger (1847, p.33, 34). Revised as *Taxoxylon priseum* by Unger (1850, p.390, 391)].

Peuce lesbia UNGER (= *Cedroxylon lesbium* KRAUS) [Lesbos unknown locality: ?Sigri described by Unger (1844, p. 34, 37, Tab. X)].

Cedroxylon sp. [Lesbos – western part: Ordymnos seashore and NE part of Ordymnos described by Fliche (1898, p. 143, 148) (lignitic and permineralized samples)].

Pityoxylon sp. [Lesbos – western part: NE part of Ordymnos described by Fliche (1898, p. 149) (permineralized sample)].

Taxaceoxylon biseriatum SÜSS & VELITZELOS [Lesbos: Rougada - Polichnitos region, described by Süss & Velitzelos (1994, p. 259, Taf. I, II)].

Pinoxylon paradoxum (SÜSS & VELITZELOS) SÜSS & VELITZELOS [Lesbos – western part: Bali Alonia, described by Süss & Velitzelos (1994, p. 407, Taf. I, II, III, IV). In 2010 it was revised as *Lesbosoxylon paradoxum* by SÜSS & VELITZELOS].

Pinoxylon pseudoparadoxum (SÜSS & VELITZELOS) SÜSS & VELITZELOS [Lesbos – western part: Bali Alonia, described by Süss & Velitzelos (1994, p. 409, Taf. V). In 2010 it was revised as *Lesbosoxylon pseudoparadoxum* by SÜSS & VELITZELOS].

Taxodioxylon gypsaceum (GOEPPERT) KRÄUSEL [Lesbos – western part: Sarakina, Molyvos, Bali Alonia and Lapsarna-Gavathas (Antissa) described by Süss & Velitzelos (1997, p. 5, Taf. I)].

Taxodioxylon albertense (PENHALLOW) SHIM*A*KURA [Lesbos – western part: Bali Alonia and Sarakina, described by Süss & Velitzelos (1997, p. 7, Taf. II, III)].

Taxodioxylon pseudoalbertense M. NISHIDA & H. NISHIDA [Lesbos – western part: Sarakina, described by Süss & Velitzelos (1997, p. 11, Taf. IV)].

Taxodioxylon megalonissum SÜSS & VELITZELOS [Lesbos – western part: Nisiopi (Megalonissi) described by Süss & Velitzelos (1997, p. 12, Taf. V)].

Taxodioxylon sp. [Lesbos – western part described by Süss & Velitzelos (1997, p. 14)].

Glyptostroboxylon microtracheidae SÜSS & VELITZELOS [Lesbos – western part described by Süss & Velitzelos (1997, p. 16, 18, 19, Taf. VI, VII)].

Tetraclinoxylon velitzelosi SÜSS [Lesbos – western part: Bali Alonia, Sarakina, Sigri, Gavathas described by SÜSS (1997, p. 290, 294, 295, Taf. I, II)].

Thujoxylon antissum SÜSS & VELITZELOS [Lesbos – western part: Lapsarna (Antissa) described by Süss & Velitzelos (1998)].

Chimairoidoxylon lesboense SÜSS & VELITZELOS [Lesbos – western part: Nissiopi (Megalonissi) and Gavathas described by Süss & Velitzelos (1999, p. 330-334, Taf. I, II, III)].

Podocarpoxylon articulatum SÜSS & VELITZELOS [Lesbos – western part: Bali Alonia (main Petrified Forest Park) described by Süss & Velitzelos (2000, p. 138, Taf. I, II)].

Podocarpoxylon graciliradiatum SÜSS & VELITZ*E*LOS [Lesbos – western part: Bali Alonia (main Petrified Forest Park), found lying next to *Taxodioxylon* sp. SÜSS & VELITZELOS (1994) described by Süss & Velitzelos (2000, p. 140, Taf. III, IV)].

Chimairoidoxylon conspicum SÜSS & VELITZELOS [Lesbos – western part: Gavathas, Bali Alonia and Eressos described by Süss & Velitzelos (2001, p. 151, Taf. I, II)].

Ginkgoxylon lesboense SÜSS [Lesbos – western part described by Süss (2003, p. 304-307, Taf. I, II)].

Ginkgoxylon diversicellulatum SÜSS [Lesbos – western part described by Süss (2003, p. 307-310, Taf. III, IV)].

Pinoxylon diversiradiatum SÜSS & VELITZELOS [Lesbos – western part: Eressos, described by Süss & Velitzelos (2009, p. 4, Taf. I, II). In 2010 it was revised as *Lesbosoxylon diversiradiatum* by SÜSS & VELITZELOS].

Pinoxylon graciliradiatum SÜSS & VELITZELOS [Lesbos – western part: Eressos, described by Süss & Velitzelos (2009, p. 6, Taf. III, IV). In 2010 it was revised as *Lesbosoxylon graciliradiatum* by SÜSS & VELITZELOS].

Lesbosoxylon diversiradiatum (SÜSS & VELITZELOS) SÜSS & VELITZELOS [Lesbos – western part: Eressos. Revision of the originally described *Pinoxylon diversiradiatum* by Süss & Velitzelos (2009, 2010, p. 22)].

Lesbosoxylon graciliradiatum (SÜSS & VELITZELOS) SÜSS & VELITZELOS [Lesbos – western part: Eressos Revision of the originally described *Pinoxylon graciliradiatum* by Süss & Velitzelos (2009, 2010, p. 22)].
Lesbosoxylon ventricosuradiatum SÜSS & VELITZELOS [Lesbos – western part: Eressos, described by Süss & Velitzelos (2010, p. 19, Taf I, II)].
Lesbosoxylon paradoxum (SÜSS & VELITZELOS) SÜSS & VELITZELOS [Lesbos – western part: Bali Alonia main Petrified Forest Park. Revision of the originally described *Pinoxylon paradoxum* by Süss & Velitzelos (1994, 2010 p. 22)].
Lesbosoxylon pseudoparadoxum (SÜSS & VELITZELOS) SÜSS & VELITZELOS [Lesbos – western part: Chamandroula. Revision of the originally described *Pinoxylon pseudoparadoxum* by Süss & Velitzelos (1994, 2010, p. 22)].
ANGIOSPERM WOOD
Juglandinium mediterraneum (UNGER) [Lesbos unknown locality: ?Sigri described by Unger (1845, p. 241). Syn: *Juglandoxylon mediterraneum* (UNGER) (KRAUS 1882 a,b)].
Mirbellites lesbius (UNGER) [Lesbos unknown locality: ?Sigri described by Unger (1845, p.. 241, 242). Syn: *Juglandinium mediterraneum* (Unger 1850; Fliche 1898; Duperon 1988) Syn: *Juglandoxylon mediterraneum* (UNGER) (KRAUS 1882 a,b)].
Brongniartites graecus UNGER [Lesbos unknown locality: ?Sigri described by Unger (1845, p. 264)].
Palmoxylon sp. [Lesbos – western part: Ordymnos seashore described by Fliche (1898, p. 144) (lignitic sample, it looked also like *Sabal* or *Chamaerops*)].
Ebenoxylon sp. [Lesbos – western part: Ordymnos seashore described by Fliche (1898, p. 146) and related to modern *Diospyros* (lignitic sample). Note: Süss 1987 said ?Eben.].
Betulaceae (? *Alnus*), Euphorbiaceae (?), Fagaceae (? *Fagus*, ? *Quercus*), Lauraceae (? *Laurus*, ? *Cinnamomum*, ?), Leguminosae (? *Robinia*), Monimiaceae (?), Myrtaceae (?), Platanaceae (? *Platanus*) [Lesbos – western part: Eressos, Mesotopos. Tab. 1, p. 218 in Selmeier & Velitzelos 2000]

LEAVES
PTERYDOPHYTES
Pronefrium stiriacum (UNGER) KNOBLOCH & KVACEK [Lesbos – western part: Eressos described by Velitzelos (1993)]
GYMNOSPERMS
Tetraclinis sp. [Lesbos – western part described by Velitzelos (1993)]
Pinus sp. [Lesbos – western part. Referred by Velitzelos & Zouros (2008)]
Cunninghamia miocenica ETTINGS HAUSEN [Lesbos – western part. Referred by Velitzelos & Zouros (2008)]
Sequoia abietina (BRONG.) KNOBLOCH [Lesbos – western part. Referred by Velitzelos & Zouros (2008)]
Tetraclinis salicornoides (UNGER) KVAČEK [Lesbos – western part. Referred by Velitzelos & Zouros (2008)]

ANGIOSPERMS
Cinnamomum polymorphum HEER sensu GRANGEON [Lesbos – western part: at the outcrop of the road Antissa-Sigri described by Velitzelos et al. (1981)]
Laurus sp. [Lesbos – western part: at the outcrop of the road Antissa-Sigri described by Velitzelos et al. (1981)]
Laurus primigenia UNGER [Lesbos – western part. Referred by Velitzelos et al. (1999)]
Litsea primigenia (UNGER) TAKHT. [Lesbos – western part: at the outcrop of the road Antissa-Sigri described by Velitzelos et al. (1981)]
Lindera ovata KOLAK. [Lesbos – western part: at the outcrop of the road Antissa-Sigri described by Velitzelos et al. (1981)]
Oreodaphne heeri GAUDIN [Lesbos – western part: at the outcrop of the road Antissa-Sigri described by Velitzelos et al. (1981)]
Lauraceae [Lesbos – western part: at the outcrop of the road Antissa-Sigri described by Velitzelos et al. (1981)]
Daphnogene polymorpha AL.BRAUN ETT. [Lesbos – western part. Referred by Velitzelos et al. (1999)]
Quercus sp. [Lesbos – western part. Referred by Velitzelos et al. (1999)]
Quercus apocynophyllum ETT. [Lesbos – western part: at the outcrop of the road Antissa-Sigri described by Velitzelos et al. (1981)]

Pungiphyllum crutiatum (AL. BRAUN) FRANKENHÄUSER et WILDE (= *Quercus cruciata* AL. BRAUN) [Lesbos – western part described by Velitzelos (1993) as *Quercus cruciata*]
Pungiphyllum crutiatum (AL. BR.) FRANKENHÄUSER et WILDE [Lesbos – western part. Referred by Velitzelos et al. (1999)]
Carpinus pliofaurei RATIANI forma *helladae* VELITZELOS et al.n. f. [Lesbos – western part: at the outcrop of the road Antissa-Sigri described by Velitzelos et al. (1981)]
Carpinus uniserrata (KOLAKOVSKI) RATIANI (?) [Lesbos – western part: at the outcrop of the road Antissa-Sigri described by Velitzelos et al. (1981)]
Alnus cycladum UNGER forma *parvifolia* VELITZELOS et al. n. f. [Lesbos – western part: at the outcrop of the road Antissa-Sigri described by Velitzelos et al. (1981)]
Alnus cycladum UNGER [Lesbos – western part. Referred by Velitzelos et al. (1999)]
Populus balsamoides GOEPP. [Lesbos – western part: at the outcrop of the road Antissa-Sigri described by Velitzelos et al. (1981)]
Populus sp. [Lesbos – western part: at the outcrop of the road Antissa-Sigri described by Velitzelos et al. (1981)]
Tilia sp. [Lesbos – western part: at the outcrop of the road Antissa-Sigri described by Velitzelos et al. (1981)]
Diospyros brachysepala AL. BRAUN. [Lesbos – western part: at the outcrop of the road Antissa-Sigri described by Velitzelos et al. (1981)]
Myrsinites sp. [Lesbos – western part: at the outcrop of the road Antissa-Sigri described by Velitzelos et al. (1981)]
Rhus sp. [Lesbos – western part: at the outcrop of the road Antissa-Sigri described by Velitzelos et al. (1981)]
Sapotaceae (?) [Lesbos – western part: at the outcrop of the road Antissa-Sigri described by Velitzelos et al. (1981)]
Rubus sp. [Lesbos – western part. Referred by Velitzelos & Zouros (2008)]
Engelhardia sp. [Lesbos – western part. Referred by Velitzelos et al. (1999)]
Engelhardia orsbergensis (WESSEL et WEBER) JÄHNICHEN et al. [Lesbos – western part. Referred by Velitzelos & Zouros (2008)]
Phoenix sp. [Lesbos – western part described by Velitzelos (1993)]
Platanus sp. [Lesbos – western part described by Velitzelos (1993)]
Acer sp. [Lesbos – western part described by Velitzelos (1993)]

Δελτίο της Ελληνικής Γεωλογικής Εταιρίας, τομ. XLVII , 2013
Πρακτικά 13ου Διεθνούς Συνεδρίου, Χανιά, Σεπτ. 2013

Bulletin of the Geological Society of Greece, vol. XLVII 2013
Proceedings of the 13th International Congress, Chania, Sept. 2013

SEDIMENTATION PROCESSES AND PALAEOGRAPHIC EVOLUTION OF MAKRILIA PLIOCENE DEPOSITS, SE CRETE

Moforis L.[1], Kostopoulou S.[2], Panagopoulos G.[3], Pyliotis I.[3], Triantaphylou M.[2], Manoutsoglou E.[3] and Zelilidis A.[1]

[1] University of Patras, Department of Geology, Laboratory of Sedimentology, Patra, 26110, Greece, a.zelilidis@upatras.gr

[2] National & Kapodistrian University of Athens, Faculty of Geology & Geo-Environment, Department of Historical Geology – Paleontology, Athens, 15784, Greece, mtriant@geol.uoa.gr

[3] Technical University of Crete, Department of Mineral Resources Engineering, Research Unit of Geology, Chania, 73100, Greece, emanout@mred.tuc.gr

Abstract

Detailed sedimentological analysis in Makrylia cross-section deposits showed at least five coarsening-upward cycles that were developed in a shelf environment. The main lithology is sandy silt and the sediments were transported as homogenous suspension in a low energy environment that deposited in a shallow water basin. The content of calcium carbonate ($CaCO_3$) is low and tends to increase to the coarse-grained clasts. Organic carbon (TOC) measurements showed the presence of many samples with high content in TOC suggesting potential hydrocarbon source rocks. There is mostly a negative correlation between $CaCO_3$ and TOC introducing generally anoxic conditions. Biostratigraphic analysis showed that the studied deposits are of Pliocene age that were precipitated in alternating conditions of oxic- anoxic events. According to the above results and taking into account previous results from the surrounding sediments it seems that the studied deposits accumulated in a shallow, low energy, intra-mountain basin at the margins of the main Ierapetra basin.
Key words: *Makrylia, TOC, $CaCO_3$, grain-size analysis, biostratigraphy.*

Περίληψη

Η λεπτομερής ιζηματολογική ανάλυση των αποθέσεων της τομής Μακρυλιά, έδειξε την ύπαρξη τουλάχιστον 5 κύκλων ιζηματογένεσης με αυξανόμενο προς τα πάνω κοκκομετρικό μέγεθος που αναπτύχτηκαν σε ένα περιβάλλον υφαλοκρηπίδας. Η κύρια λιθολογία είναι αμμούχος πηλός και τα ιζήματα μεταφέρθηκαν ως ομογενές αιώρημα. Το ποσοστό του ανθρακικού ασβεστίου είναι χαμηλό και τείνει αυξανόμενο προς τα πιο αδρομερή κλάσματα. Οι μετρήσεις του οργανικού υλικού έδειξε την παρουσία αρκετών δειγμάτων με αυξημένο οργανικό υλικό προτείνοντας την ύπαρξη εν δυνάμει μητρικών πετρωμάτων για την γένεση υδρογονανθράκων. Η σχέση μεταξύ του ανθρακικού ασβεστίου και οργανικού υλικού είναι κύρια αρνητική προτείνοντας ανοξικές συνθήκες. Η βιοστρωματογραφική ανάλυση έδειξε Πλειοκαινική ηλικία των ιζημάτων που αποτέθηκαν σε εναλλασσόμενες οξικές – ανοξικές συνθήκες. Από τα παραπάνω αποτελέσματα και περνώντας υπόψη τα υπάρχοντα αποτελέσματα των

ιζημάτων που περιβάλλουν την περιοχή μελέτης φαίνεται πως οι μελετηθείσες αποθέσεις συγκεντρώθηκαν σε μια ρηχή με ήσυχα νερά ενδο-ορεινή λεκάνη στα περιθώρια της κύριας λεκάνης της Ιεράπετρας.
Λέξεις κλειδιά: *Μακρυλιά, TOC, $CaCO_3$, κοκκομετρικό μέγεθος, βιοστρωματογραφία.*

1. Introduction

The grain size analysis, aims to determine the lithology and grain size parameters in order to understand the depositional conditions. Continental shelves constitute one of the preferential zones for the productivity of biomass (Biju-Duval, 2002) which is converted into hydrocarbons. Source rock prediction requires an understanding of the structural and stratigraphic evolution of the sedimentary succession within a basin. Characterizing the organic matter from sedimentary rocks is now widely recognized as a critical step in the evaluation of the hydrocarbon potential (Lafargue et. al., 1998). According to Hauck et al., (2012), $CaCO_3$ distribution and contribution to the marine carbon cycle is connected to environmental parameters as water depth, width of the shelf and primary production. Under conditions of intense sedimentation the amount of calcium carbonate increases towards the finer fractions (delta-rivers) and in marine sediments with low sedimentary rate, where carbonate material increases to the coarse fractions (Saadellah and Kukal, 1969).

In this paper a cross-section in Makrylia area was studied in detail, where 36 samples were analysed in order to determine grain-size, TOC and $CaCO_3$ content, and the age of the sediments.

2. Geological Setting

The Ierapetra graben has an asymmetric architecture with the oldest deposits generally outcropping in the south (Figure 1). The pre-Neogene rocks surrounding the western Ierapetra graben are, from younger to older, the Upper unit, the Pindos unit, the Tripolitza unit, Phyllite-Quartzite Series and the Plattenkalk Group (see Creutzburg et al., 1977, for description of units). According to Fortuin and Peters (1984), the pebbles in the Mithi Formation were almost exclusively derived from the Upper unit, whereas the pebbles in the overlying Males Formation are dominantly from the Pindos unit. The overlying Early Tortonian Breccia Series contains debris from the Tripolitza unit. The above indicate progressive exhumation of footwall units during graben development.

Neither thickness and grain size, nor the spatial arrangements of the cobbles of Mithi Formation sediments have a distinct relationship to graben-related faults (ten Veen and Postma, 1999). The sediments of the Males Formation are deposited in alluvial fans, which had their apex against the Kritsa fault zone (Postma et al., 1993), indicating that faulting and deposition of the alluvial fans were related to each other. Therefore, the age of the Males Formation suggests that activity on the Kritsa fault zone commenced in latest Serravallian time (14-12Ma). Fluvial conglomerates of the Males Formation have directed westerly, axial-parallel palaeocurrent directions, whereas breccia deposits close to the larger faults were shed from the north (Postma et al., 1993).

Cross-cutting relationships show that the Kritsa and also the Kroustas fault zones, in the northern Ierapetra graben, are offset by NNE-striking normal faults. In the central and southern Ierapetra graben, the Makrilla and Parathiri fault zones are two major WNW-striking normal faults (Figure 2). The Makrilla fault zone is either cut or cross-cuts these NNE-striking faults, whereas the Parathiri fault zone, further south, mainly cuts the NNE-striking faults. These relationships provide robust evidence that the Kritsa fault zone belongs to the oldest generation of graben-related faults. Along the southern coast, a series of east–west oriented Late Pleistocene marine terraces exist, demonstrating the significant coastal uplift of this area (Gaki-Papanastassiou et al., 2009).

Figure 1 - A) Crete island where the area under study is shown. B) Geological map of Ierapetra graben according to Fortuin & Peters (1984) and Postma et. al. (1993).

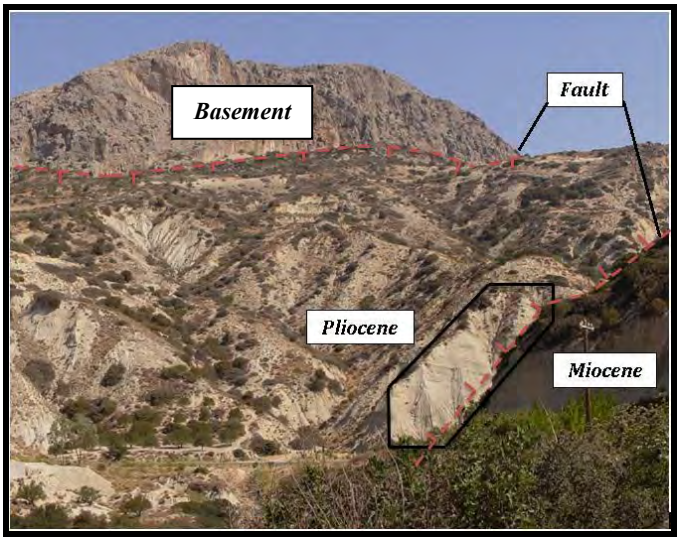

Figure 2 - Makrilia Pliocene deposits accumulated in a fault controlled basin. Box shows the studied cross-section of Figure 3.

3. Stratigraphy

3.1. Lithostratigraphy

A cross-section up to 48m thick was studied, of a total more than 110 m thick sequence, where five (5) cycles with an upward coarsening trend were observed (Figures 3 and 4). More specifically, each cycle, from the lower to the upper, consists of:

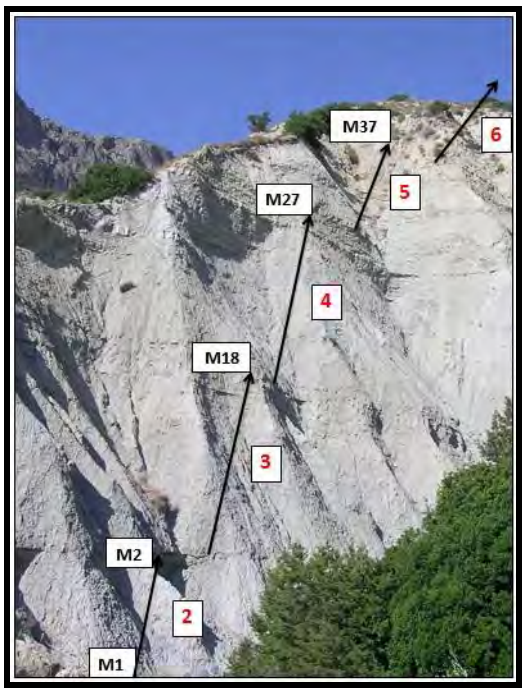

Figure 3 - Panoramic view of the studied cross-section where the upper 5 cycles with coarsening upward trend is shown.

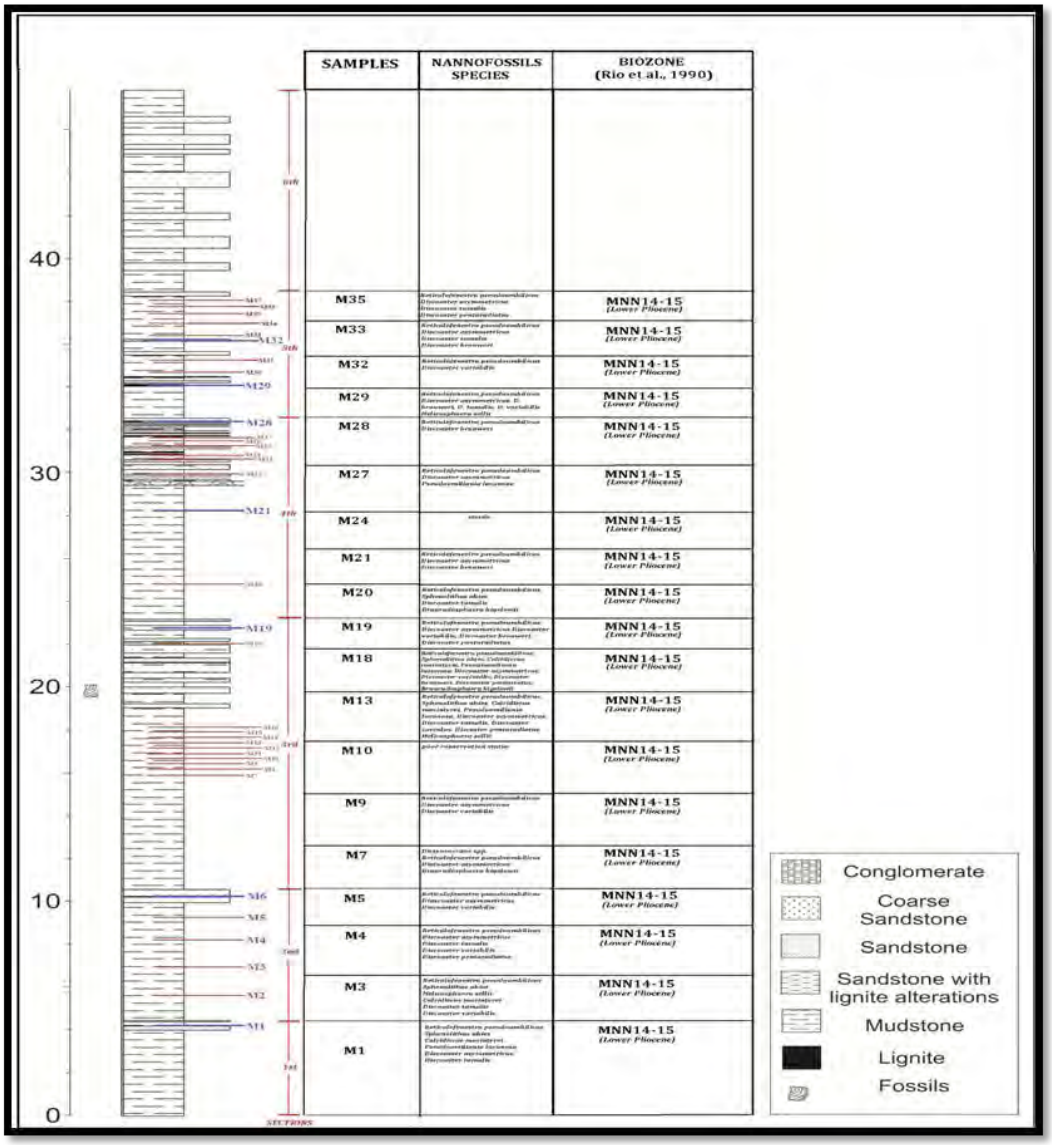

Figure 4 - Stratigraphic description of the studied cross-section.

The first cycle has a total thickness of 4.5m. The lower part consists of massive grey clay. Within clayey spheroid structures were formed as a result of the rapid water escape through the sediment, indicating rapid sedimentation conditions. The upper part, of a total thickness 40cm, is composed of two sand beds (15cm and 5cm respectively), with a massive white-grey in color clay, up to 20cm thick.

The second cycle has a total thickness of 6m. The lower part consists of massive white to grey siltstone, up to 5.5m thick. The cycle ends with sandy deposits, up to 60cm thick. These sandy deposits are composed upwards of: 5cm coarse sand with a brown-yellow color, next 25cm exhibit a fining trend with a brown color, 5cm with the presence of four coal horizons of about 1cm each in thickness, a 4 cm thick fossiliferous horizon, and finally 26 cm of light to dark sand with sparce pebbles.

The third cycle has a total thickness of 12m. The lower part, up to 8m thick, consists of siltstones, with white, dark blue, grey and red colors. The upper part, up to 4m thick consists of interbedded

sand, mud and coal beds. Coal beds thickness ranging from 1 to 2 cm, whereas the thickness of sand deposits is ranging from 2 to 10 cm.

The fourth cycle, up to 10m thick, is composed of massive gray siltstone at the lower 6m and thin interbedded sand – mud and coal beds in the upper 4m. Within this upper part a conglomeratic bed up to 20cm was formed. Coal interbeds, up to 13 horizons, have an average thickness 1cm, whereas sand/mud ratio range from 1:1 to 1:2.

The fifth cycle has a total thickness of about 6m. The lower part consists of massive mud and the upper part of sand and coal beds, with 5-10cm thick.

The uppermost studied cycle (sixth cycle) has a total thickness up to 10m, and consists of massive sand-mud beds. Over the sixth cycle and for the next 15m, although it was difficult to analyze or to select samples, it seems that there is a continuity of sand-mud interbeds.

Finally, as a general conclution, it seems that there is an upward increase both in the thickness of sandy beds and in grain size.

3.2. Biostratigraphy

The analysis of the samples (total samples: 36), showed the following species of nannofossils (Figure 4): *Reticulofenestra pseudoumbilicus* (in abundance over 10%), *Discoaster asymmetricus*, *Discoaster tamalis*, *Discoaster pentaradiatus*, *Discoaster brouweri*, *Discoaster variablis*, *Helicosphaera sellii*, *Pseudoemiliana lacunosa*, *Sphenolithus abies*, *Braarudospaera bigelowii*, *Calcidiscus macintyrei*, *Discoaster surculus*, *Dictyococcites spp*. According to the above and in relation with the biochronological data for the calcareous data of the Mediterranean (Lourens et al., 2004), the age of Makrilia's section placed between 4.12Ma-3.84Ma (biozone MNN14-15, Rio et al., 1990), which corresponds to the age of Lower Pliocene.

4. Laboratory Analysis and Results

4.1. Grain Size Analysis

The grain size analysis (sieve and pipette method) aims to determine the lithology, whereas grain size parameters, according to Folk and Ward (1957) methodology, were used in order to determine depositional conditions.

The grain size analysis showed that the main lithology is sandy clay. The diagram of Passega (1969), showed that sediment transportation was mostly as a uniform suspension. According to Stewart's diagram (1958), samples are close to the stagnant waters, whereas according to Valia & Cameron (1977) and Moiola & Visher (1968), sedimentation took place in low basin depths (Figures 5, 6 and 7).

4.2. $CaCO_3$ Method and Results

For the determination of the % content of calcium carbonate ($CaCO_3$), the method for the calcium carbonate ($CaCO_3$) decomposition with acetic acid (CH_3COOH) was used, as described by Varnavas (1979).

Calcium carbonate content of the Makrilia studied sediments exhibits variable contents ranging from 11,26% to 37,26%, with an average value of 20,17% (Figure 8). At the first sedimentary cycle (sample M1), is only one sample with a 31,01% percentage of calcium carbonate. At the second sedimentary cycle (samples M2-M6), max value of $CaCO_3$ occurs at M5 (30,25%), while minimum value occurs at sample M3 (20,40%). At the third sedimentary cycle (samples M7-M19), a major peak occurs at M7 (31,50%), while minimum value occurs at M12 (11,26%). A the fourth sedimentary cycle (samples M20-M28), max value occurs at M25 (37,26%), while minimum value occurs at M26 (12,8%). At the fifth sedimentary cycle (samples M29-M37), the maximum value occurs at M34 (23,63%), while minimum value was observed in the sample M35 (13,62%).

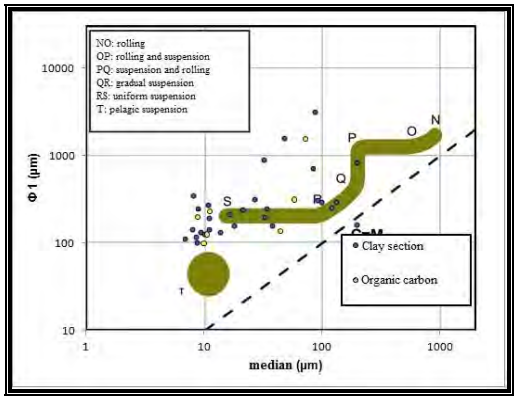

Figure 5 - Diagram of Passega (1957, 1969).

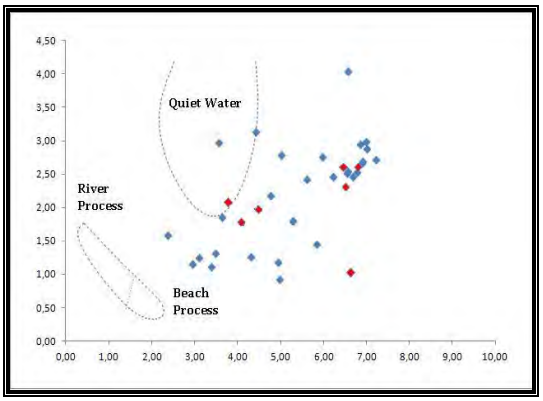

Figure 6 - Diagram of Stewart (1958).

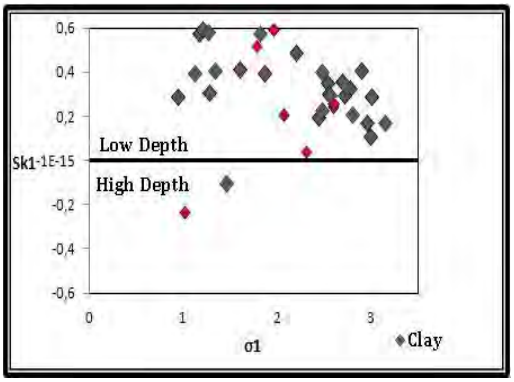

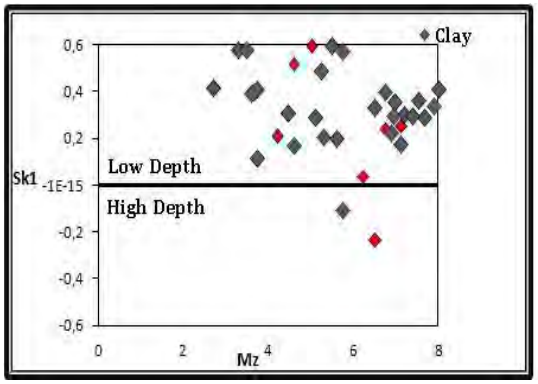

Figure 7 - Diagrams of Valia & Cameron (1979).

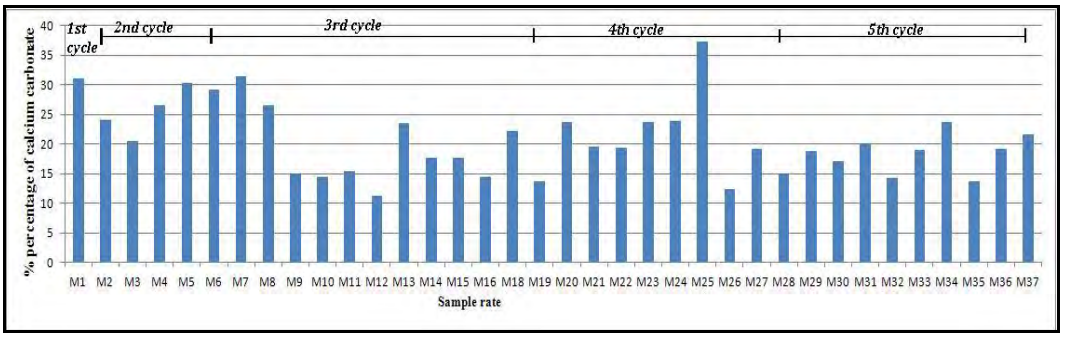

Figure 8 - Calcium carbonate percentages (%) in sediments of study area.

The analysis of the calcium carbonate showed that the samples are not very rich in calcium carbonate. The increase or decrease of calcium carbonate in sediments shows a sequence of sedimentary conditions. In marine sediments with low sedimentary rate, carbonate material increases to the coarse fractions (Saadellah and Kukal, 1969). In the study area the calcium carbonate ratio is moderate and the percentage of calcium carbonate tends to increase to the coarse clasts.

4.3. TOC Method and Results

The measurement of organic carbon content was based on the method of titration (Gaudette et al., 1974). The analysis showed that the percentage of the contribution of organic carbon in the samples ranged from 0% to 2.26% with an average value of 0,41% (Figure 9). At the first sedimentary cycle (sample M1), we have only one sample with a value at 1,15%. At the second sedimentary cycle (samples M2-M6), max value occurs at M6 (1,71%), while minimum value occurs at M2 (0,02%). At the third cycle (samples M7-M19), maximum value occurs at M19 (2,27%), while minimum value correspond to M8 (0%). At the fourth sedimentary cycle (samples M20-M28), max value occurs at M28 (1,13%), while minimum value occurs at M24 (0%). At the fifth sedimentary cycle (sample M29-M37), max value occurs at M35 (2,06%), while minimum value occur at M37 (0,1%).

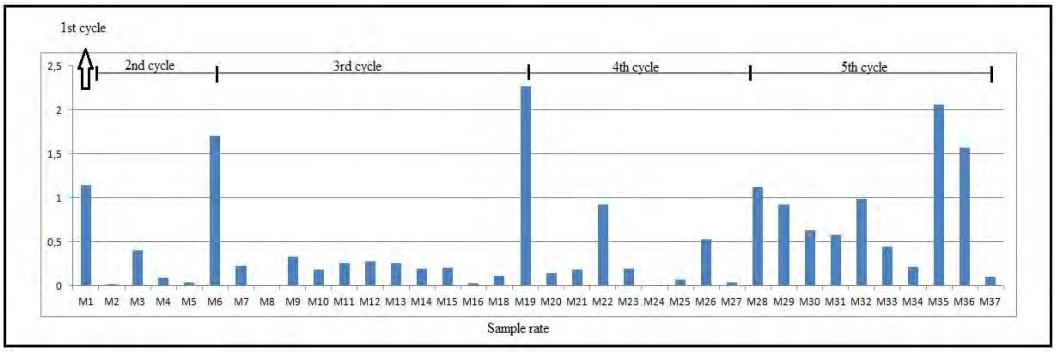

Figure 9 - Organic carbon percentages (%) in sediments of study area

The analysis of organic carbon showed that several samples are of particular interest in organic carbon. The organic carbon content shows depositional conditions (Folk, 1968). In the open shelf environment the content of the organic carbon is less than 1%, while at a lagoon is more than 1% (Kukal 1971). In marine sediments TOC ranged from 0.5-1%, while in coastal sediments content ranges from 1-5% (Trask 1939). In study samples many samples showed high TOC content indicating possible source rocks.

4.4. Correlation Between TOC-$CaCO_3$

A synthetic diagram of organic carbon and calcium carbonate contents was constructed in order to compare results. From the correlation diagram (Figure 10) we can observe that generally there is an inverse correlation between those two parameters. Either an increase of organic carbon and reduce of calcium carbonate, or a decrease of organic carbon and an increase of calcium carbonate. The first case is related with anoxic conditions whereas the second case is related to oxic conditions due to which organic carbon is oxidised, while the oxidizing environment favours the precipitation of carbonates resulting in increased CaCO3 contents.

4.5. Correlation Between (TOC-$CaCO_3$)- Benthic Foraminifera

The detailed analysis of benthic foraminifera in samples M6 and M28, where the organic carbon increases and the calcium carbonate reduces indicating a low oxygen environment, showed that the benthic foraminifera of M6 consists of markers of oxygenated water, whereas the benthic foraminifera of sample M28 are characteristic for environments with low oxygen conditions.

The above correlation depicts the necessity of a more detailed investigation for the sedimentation's conditions and a more detailed sedimentary interpretation of the relationship between TOC-CaCO3 and the environmental conditions, as is recommended by the benthic foraminifera.

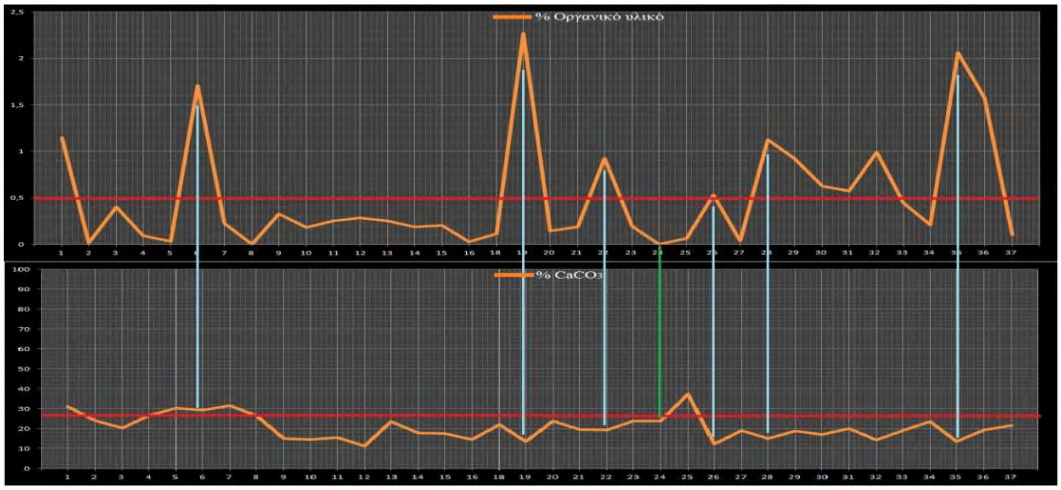

Figure 10 - Correlation diagram between TOC and $CaCO_3$.

5. Conclusion

Detailed sedimentological analysis showed low sedimentation rates in a low energy environment. Depositional environment was an intra-mountain basin formed during early Pliocene as a trench due to the WNW trending normal faults activity. The main lithology is sandy clay and the sediments transported mostly as a uniform suspension.

Organic carbon analysis showed that many samples have a high TOC content and could be act as source rocks for hydrocarbon generation.

The inverse correlation between TOC - $CaCO_3$ is owed to different depositional conditions (sometimes oxic and some others anoxic).

The detailed study of benthic foraminifera in two samples showed that the results of the above inverse correlation between TOC - $CaCO_3$ must be reexamined and the use of benthic foraminifera must support the above correlation.

Finally, and taking into account the above results and the presence of at least 6 cycles with coal beds in the top of each cycle, we could suggest the existence of a protected intra-mountain basin that it's connection with the major basin was at least six times disturbed, producing semi closed shallow marine conditions.

Since Pliocene basins south of Crete are potential hydrocarbon fields a detailed analysis of Pliocene deposits in outcrops of south Crete is necessary.

6. Acknowledgments

This research has been co-financed by the European Union (European Social Fund – ESF) and Greek national funds through the Operational Program "Education and Lifelong Learning" of the National Strategic Reference Framework (NSRF) - Research Funding Program: THALIS –UOA- "Messinian Salinity Crisis: the greatest Mediterranean environmental perturbation and its repercussions to the biota" (70/3/11605, MIS: 375405).

7. References

Biju-Duval B. 2002. Sedimentary Geology. *Sedimentary Basins, Depositional Environments, Petroleum Formation: xiii + 642 pp*. Paris: Editions Technip.

Gaki-Papanastassiou K., Karymbalis E., Papanastassiou D. and Maroukia H. 2009. Quaternary marine terraces as indicators of neotectonic activity of the Ierapetra normal fault SE Crete (Greece), *Geomorphology*, 104, 38-46.

Gaudette H.E., Flight W. R., Toner L. and Folger D.W. 1974. An inexpensive titration method for the determination of organic carbon in recent sediments, *Jour. Sed. Petr.,* 44, 249-253.

Creutzburg N., Drooger C.W. and Meulenkamp J.E. 1977. *Geological map of Crete* (scale 1: 200.000), Institute of Geology and Mineral Exploration (IGME), Athens.

Fortuin A.R. and Peters J.M. 1984. The Prina complex in Eastern Crete and its relationship to possible Miocene strike-slip tectonics, *J. Struct. Geol.,* 6, 459-476.

Folk R. L. 1968. *Petrology of Sedimentary Rocks*, Hemphill Publishing Co, Austin, Texas, 170 pp.

Folk R. L. and Ward, W.S. 1957. Brazos river bar: a study in the significance of grain size parameters, *Jour. Sed. Petr.,* 27, 3-26.

Hauck J., Gerdes D., Hillenbrand C.D., Hoppema M., Kuhn G., Nehrke G., Völker Ch. and Wolf-Gladrow D. 2012. Calcium carbonate content in surface sediments and benthic fauna on Antarctic shelves, supplement to: Hauck J., Gerdes D., Hillenbrand C. D., Hoppema M., Kuhn G., Nehrke G., Völker Ch. and Wolf-Gladrow D. 2012: Distribution and mineralogy of carbonate sediments on Antarctic shelves, *Journal of Marine Systems,* 90 (1), 77-87; PANGAEA - Data Publisher for Earth & Environmental Science. http://dx.doi.org/10.1594/PANGAEA.757933

Kukal Z. 1971. *Geology of recent sediments,* Academic Press London and New York, 490 pp.

Lafargue E., Marquis, F. and Pillot D. 1998. Rock-Eval 6 applications in hydrocarbon exploration, production and soil contamination studies, *Rev. Inst. Fr. Pét.* 53/4, 421– 437.

Lourens L. J., Hilgen F. J., Laskar J., Shackleton N. J. and Wilson D. 2004. *The Neogene Period*. In: Gradstein, F. M., Ogg, J. G., Smith, A. G. (Eds.), A Geologic Time Scale 2004. Cambridge University Press, Cambridge, 409-440 pp.

Moiola R.J. and Visher D. 1968. Textural parameters: an evaluation, *Jour. Sed. Petr.,* 260, 45-63.

Passega R. 1957. Texture as characteristic of clastics deposition, *Am. Soc. Asoc. Petrol. Geol. Bull.,* 41, 1952-1984.

Passega R. and Byramjee R. 1969. Grain size image of Clastic deposits, *Sedimentology,* 13, 233-253.

Postma G., Fortuin A. R. and van Wamel W.A. 1993. Basin-fill patterns controlled by tectonics and climate: the Neogene "fore-arc" graben of eastern Crete as a case history, *Spec. Publs Int. Ass. Sediment.,* 20, 335-362.

Ring U., Layer P. W. and Reischmann T. 2001. Miocene high-pressure metamorphismin the Cyclades and Crete, Aegean Sea, Greece: Evidence for large magnitude displacement on the Cretan detachment, *Geology,* 29, 395-398.

Saadellah A. and Kukal Z. 1969. Grain size and carbonate content in costal sediment of Iraq, *Jour. Iraq G. Soc*, 2, 3-10.

Stewart H. B. and Jr 1958. Sedimentary reflections of depositional environments in San Miguel Lagoon, Baja California, Mexico, *Am. Assoc. Petr. Geol. Bull.,* 42, 2567-2618.

ten Veen J. H. and Postma G. 1999. Neogene tectonics and basin fill patterns in the Hellenic outer-arc (Crete, Greece), *Basin Res.,* 11, 223-241.

Trask P. D. 1939. Organic content of recent marine sediments, *Recent marine sediments,* 428- 453.

Valia H S., and Cameron B. 1977. Skewness as a Paleoenvironmental indicator, *Jour. Sed. Petr.,* 47, 2, 784-793.

Varnavas S. P. 1979. Geochemistry of sediments from the eastern Pacific, *Ph.D. Thesis,* University London, 431 pp.

Δελτίο της Ελληνικής Γεωλογικής Εταιρίας, τομ. XLVII , 2013
Πρακτικά 13ου Διεθνούς Συνεδρίου, Χανιά, Σεπτ. 2013

Bulletin of the Geological Society of Greece, vol. XLVII 2013
Proceedings of the 13th International Congress, Chania, Sept. 2013

BIOSTRATIGRAPHICAL AND SEDIMENTOLOGICAL STUDY OF AN UPPER CRETACEOUS SUCCESSION IN THE SAMI AREA (CENTRAL AREA OF KEFALLINIA, W. GREECE)

Zoumpouli E.[1], Pomoni-Papaioannou F.[2], Zelilidis A. [1] and Iliopoulos G.[1]

[1]University of Patras, Department of Geology, Laboratory of Sedimentology, 26500, Patras, Greece, elzoumpouli@upatras.gr, a.zelilidis@upatras.gr, iliopoulosg@upatras.gr

[2] Department of Geology and Geoenvironment, Section of Historical Geology and Palaeontology, National University of Athens, Panepistimiopolis, 157 84 Athens, Greece, fpomoni@geol.uoa.gr

Abstract

On the island of Kefallinia, which lies at the external edge of the Hellenides fold and thrust system, appear the Paxi and the Ionian Zones. In this study, an Upper Cretaceous carbonate succession, which is a part of the Paxi Zone, cropping out near the area of Sami (central area of Kefallinia), is discussed in detail with regard to its depositional facies, microfacies, biostratigraphy and palaeoenviroments. Detailed sedimentological and palaeontological investigations have been carried out on seven sections and petrographic analysis of thin-sections that led to the recognition of a number of microfacies types grouped into four facies zones. There was recorded a supratidal- intertidal (restricted)-intertidal (open lagoon)- subtidal (or shallow subtidal) vertical transition. Supratidal facies are characterized by fenestral and peloidal wackestone / packstone, intertidal (restricted) facies are represented by bioclastic wackestone and bindstone, whereas intertidal (open lagoon) facies are indicated by bioclastic packstone. Finally subtidal facies are dominated by bioclastic floatstone and grainstone. Benthic foraminifera are especially abundant and along with calcareous algae are the most important fossils used for age determination. The benthic foraminiferal genera that were identified (Cuneolina sp., Quinqueloculina sp., Nezzazata sp., Pseudonummoloculina sp., Dicyclina sp.), in addition with the observed calcareous algae, rudist and gastropods provide significant data for the depositional environments and the paleoecology of the Paxi Zone during the Upper Cretaceous.

Key words: *Upper Cretaceous microfacies, Paxi Zone, Benthic foraminifera.*

Περίληψη

Η περιοχή μελέτης καλύπτει ένα μέρος των ανθρακικών αποθέσεων της ζώνης Παξών, που αποτέθηκαν κατά τη διάρκεια του Μεσοζωικού, στο νησί της Κεφαλονιάς. Η Κεφαλονιά ανήκει στις Εξωτερικές Ελληνίδες και δομείται από δύο διαφορετικές γεωτεκτονικές ζώνες, με γενική διεύθυνση ΒΒΔ-ΝΝΑ, την Προαπούλια ή ζώνη Παξών στα δυτικά και την Ιόνια ζώνη στα ανατολικά η οποία και επωθείται στην προηγούμενη. Πιο συγκεκριμένα η περιοχή μελέτης βρίσκεται κατά μήκος του τοπικού οδικού δικτύου Σάμης - Αργοστολίου, που ανήκει στη ζώνη Παξών. Σκοπός

της παρούσας εργασίας είναι η λεπτομερής απεικόνιση των αποθετικών περιβαλλόντων με βάση την μικροφασική και βιοστρωματογραφική ανάλυση. Πραγματοποιήθηκε λεπτομερής μικροφασική ανάλυση λεπτών τομών η οποία μας οδήγησε στην αναγνώριση μικροφασικών τύπων που αντικατοπτρίζουν τέσσερις φασικές ζώνες. Παρατηρήσαμε μία κατακόρυφη μετάβαση από την επιπαλιρροιακή - μεσοπαλιρροιακή ζώνη(περιορισμένη λιμνοθάλασσα) σε μεσοπαλιρροιακή (ανοιχτή λιμνοθάλασσα)- υποπαλιρροιακή ζώνη. Οι φάσεις που ανήκουν στην επιπαλιρροιακή ζώνη χαρακτηρίζονται από κοκκοστηριζόμενους/ιλυοστηριζόμενους ασβεστόλιθους με πελοειδή, οι μεσοπαλιρροιακές φάσεις αντίστοιχα χαρακτηρίζονται από ασβεστόλιθους με βιοκλάστες στους οποίους συχνά υποκρύπτεται η ύπαρξη φυκών και στην υποπαλιρροιακή ζώνη επικρατούν κοκκοστηριζόμενοι ασβεστόλιθοι βιοκλαστών. Τα βενθονικά τρηματοφόρα, τα οποία βρίσκονται σε αφθονία, μαζί με τα ασβεστολιθικά φύκη αποτελούν σημαντικούς βιοδείκτες. Τα γένη των βενθονικών τρηματοφόρων που έχουν προσδιοριστεί (Cuneolina sp., Quinqueloculina sp. Nezzazata sp., Pseudonummoloculina sp., Dicyclina sp.) σε συνδυασμό με την ύπαρξη ασβεστολιθικών φυκών, ρουδιστών, και γαστερόποδων μας δίνουν σημαντικά στοιχεία για τα περιβάλλοντα απόθεσης καθώς επίσης και για την παλαιοοικολογία στην ζώνη Παξών κατά τη διάρκεια του Ανώτερου Κρητιδικού.
Λέξεις κλειδιά: *Μικροφάσεις, Ζώνη Παξών, Βενθονικά Τρηματοφόρα*.

1. Introduction

Sedimentological and paleontological studies have carried out on an Upper Cretaceous shallow-water carbonate succession near the area of Sami (central Kefallinia Figure 1), which is a part of the of the Paxi zone. The Apulian platform is one of the Bahama-type platforms created on the Tethys passive southern continental margin. Paxi zone is the transitional zone (slope) between the Apulian platform and the Ionian basin (Nikolaou, 1986; Accordi et al., 1998; Karakitsios and Rigakis, 2007). By studying the carbonate unit of the Sami stratigraphic section we attempted to understand the depositional setting and to distinguish between subtidal, intertidal and supratidal carbonates, by focusing on diagnostic criteria using microfacies and micropaleontological analysis (Flügel, 2004).

The high-resolution stratigraphic analysis has shown a number of lithofacies organized in groups (lithofacies associations), suggesting, on the whole, sedimentary environments ranging from lagoonal to peritidal context. The peritidal deposits are easy to be recognized in outcrops and in thin sections. They are important paleo-bathymetric indicators, reflecting sea-level fluctuations (Flugel, 2004; Brescia et al., 1996; D'Argenio et al., 1997, 1999).

In many cases, the sedimentary structures and the great abundance of bioclasts are indicative of depositional environments. Especially benthic foraminifera have been taken into consideration in order to enhance the environmental interpretation provided by lithofacies. It is well known that, as the fossil accumulations are important sources of paleontological and paleoenvironmental data, the taphonomic and sedimentological characteristics of the fossils assemblages reflect the dynamic environmental conditions. Furthermore, the study of fossil concentrations is critical for the reconstruction of the long- term, as well as of the short-term, environmental variation and, as a consequence, for the interpretation of depositional sequences and sea-level changes.

The objective of this paper is to establish a detailed analysis of the vertical variations of the microfossils associations in relation with the distribution of the lithofacies. The study is based on seven stratigraphic sections extending along 4km, with thickness averaging 400 m. In total, 150 samples have been collected for centimetre scale microfacies analysis.

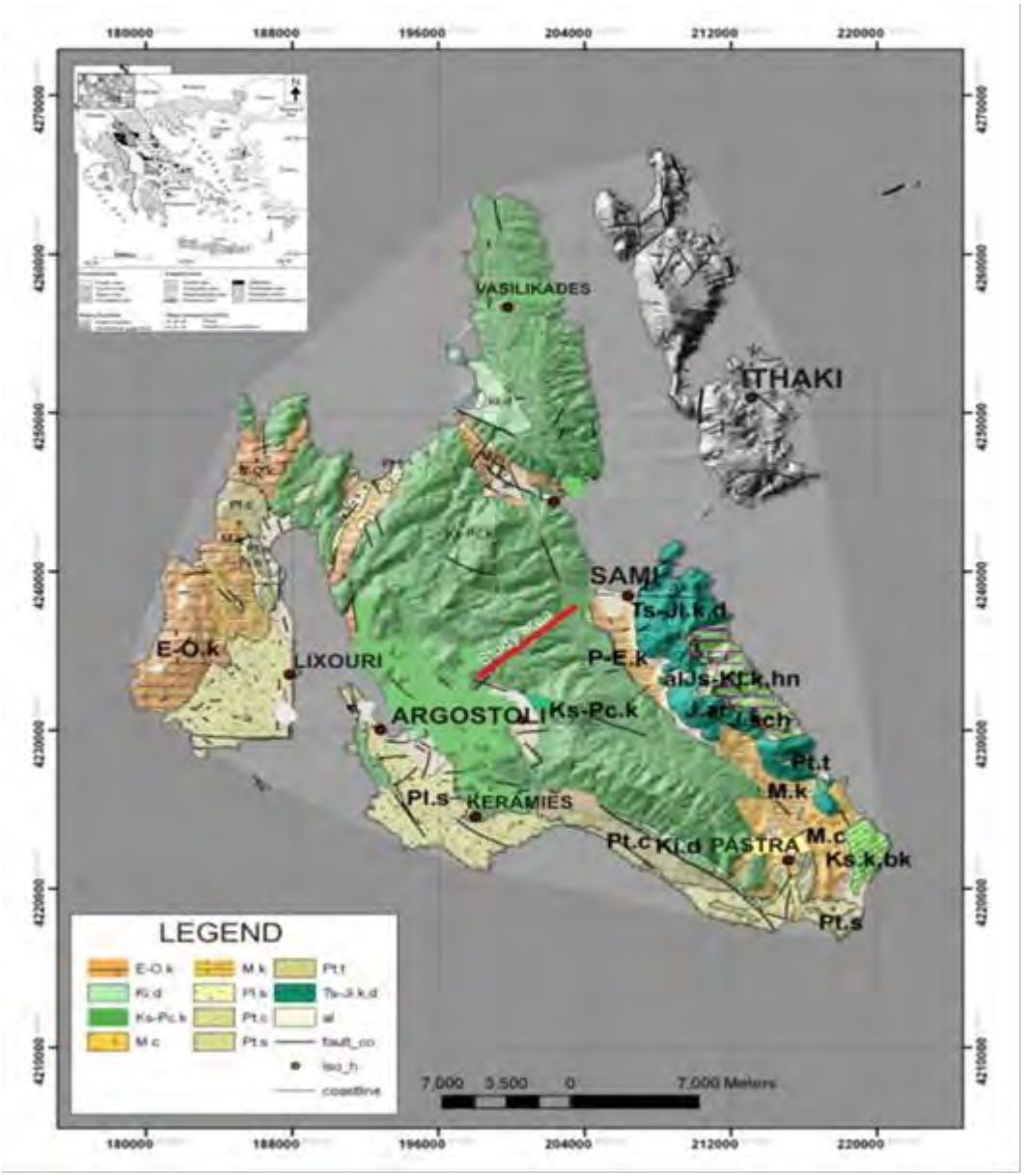

Figure 1 -Kefallinia Island. Geological map of Kefallinia showing the studied cross section.

2. Geological Setting

Kefallinia lies at the external (foreland) edge of the Hellenides fold-and-thrust system created in response to Cenozoic continental collision following closure of the Tethyan Ocean. The external Hellenides lie to the west of the Pindos thrust and are subdivided into three isopic zone: Gavrovo-Tripolitza, Ionian, and Paxi zones. The Gavrovo-Tripolitza and the Ionian zones have been considered to represent the external large Hellenide thrust sheets emplaced onto the relatively stable Paxi autochthon, as a part of the latest Hellenide events (Aubouin and Dercourt, 1962; Jenkyns, 1968; Smith and Moores, 1974; Underhill, 1989).

During the Early Mesozoic times, an extensive rifting had been developed in the western Greek territory, which in Early–Middle Jurassic times, was subdivided into ridges and basins, that corresponded to the Gavrovo and Apulian platforms and the Ionian basin respectively. Paxi zone is the slope between the Apulian platform and the Ionian basin. Post-rift sedimentation persisted throughout the Cretaceous leading to shallow marine carbonates on the ridges, mixed pelagic/neritic sedimentation on the slope (Paxi zone) and deep-water carbonates in the basin (Karakitsios, 1992; 1995; Getsos, 2005; Getsos et al., 2007).

From the Triassic to the Upper Cretaceous, Western Greece was part of the Apulian continental block on the southern passive margin of Tethys. The island of Kefallinia is characterized by widely exposed Cretaceous limestones of the Paxi and Ionian zones, which were deposited at the margin of the Apulian carbonate platform. The Paxi zone consists of Triassic to Miocene deposits, mainly neritic carbonates. The Ionian zone comprises sedimentary formations ranging from Triassic evaporites to Jurassic- Upper Eocene carbonates, including minor cherts and shales, overlain by Oligocene flysh (Karakitsios and Rigakis, 2007).

The Paxi zone forms the major part of the island of Kefallinia. It has been regarded as being the autochthonous foreland of the Hellenide fold-thrust belt, which is generally believed to have been unaffected by major shortening (Aubouin, 1965; Jones, 1968; British Petroleum Co. Ltd., 1971; Smith and Moores, 1974; Underhill, 1989).

Sami lies immediately to the west of the Ionian thrust and is composed entirely of thick Upper Cretaceous limestones that have been folded into a broad, open, northwest-southeast – trending pericline. The studied sections belong to the Paxi zone and lie across the main road of Sami-Argostoli where well exposed outcrops occur (Figure 1).

3. Materials and Methods

The Upper Cretaceous carbonate succession in Sami is characterised by excellent outcrops, which are commonly characterised by wide lateral extents of several hundreds of metres. This outcrop situation allowed detailed field studies concentrating on lithology, sedimentary structures, and sequence-stratigraphic patterns. Five sections were analysed with regard to microfacies, biostratigraphy, and sequence stratigraphy and were correlated in detail. The sections were sampled very closely, the distance between two samples being less than 10 cm in important intervals, but reaching a few metres in more uniform intervals. Microfacies analyses of samples were performed on about 300 thin sections representing various shallow water microfacies types. Determination of stratigraphic position of the investigated succession is based on the identification of microfossils assemblages (benthic foraminifera and calcareous algae Dasycladales) and on using their taxa as index fossils.

Shallow-marine bedded carbonate sequences need a detailed sampling program, because they exhibit high microfacies variability due to changing subtidal and tidal depositional sites and common occurrence of cyclic sedimentation patterns.

In the studied succession, the high-resolution stratigraphic analysis has shown a number of lithofacies organized in groups. The vertical arrangement of these lithofacies allows the identification of a cyclic recurrence of the depositional and early diagenetic features, including a meteoric overprint that may be observed on top of the elementary cycles.

4. Biostratigraphical Observations

Biostratigraphic interpretation of the mainly shallow-marine Upper Coniacian to Lower Campanian deposits is based on benthic organisms. Benthic foraminifera assemblages are the signal biostratigraphical tool for subdivision of the Cretaceous platform carbonate succession. Ranges of the foraminiferal taxa recognized in the Sami Cretaceous sections are shown in Figure

2. Benthic foraminiferal taxa are represented by *Quinqueloculina* sp. D'Orbigny, *Cuneolina* sp. D'Orbigny, *Dicyclina* sp. Munier-Chalmas, *Pseudonummoloculina* sp. *Spiroloculina* sp. D'Orbigny, *Moncharmontia* sp. De Castro and *Nezzazata* sp. Omara The determined assemblage include, except for the benthic foraminifera, Thaumatoporella, Dasyclad green algae, Rudist in shell debris and Ostracods. Gastropods occur locally and sporadically. Generic attributions of the benthic foraminifers' taxa are based on Loeblich& Tappan, 1988 classification. A compilation of the most important taxa and their biostratigraphic ranges for the studied area is given below, in Figure 2.

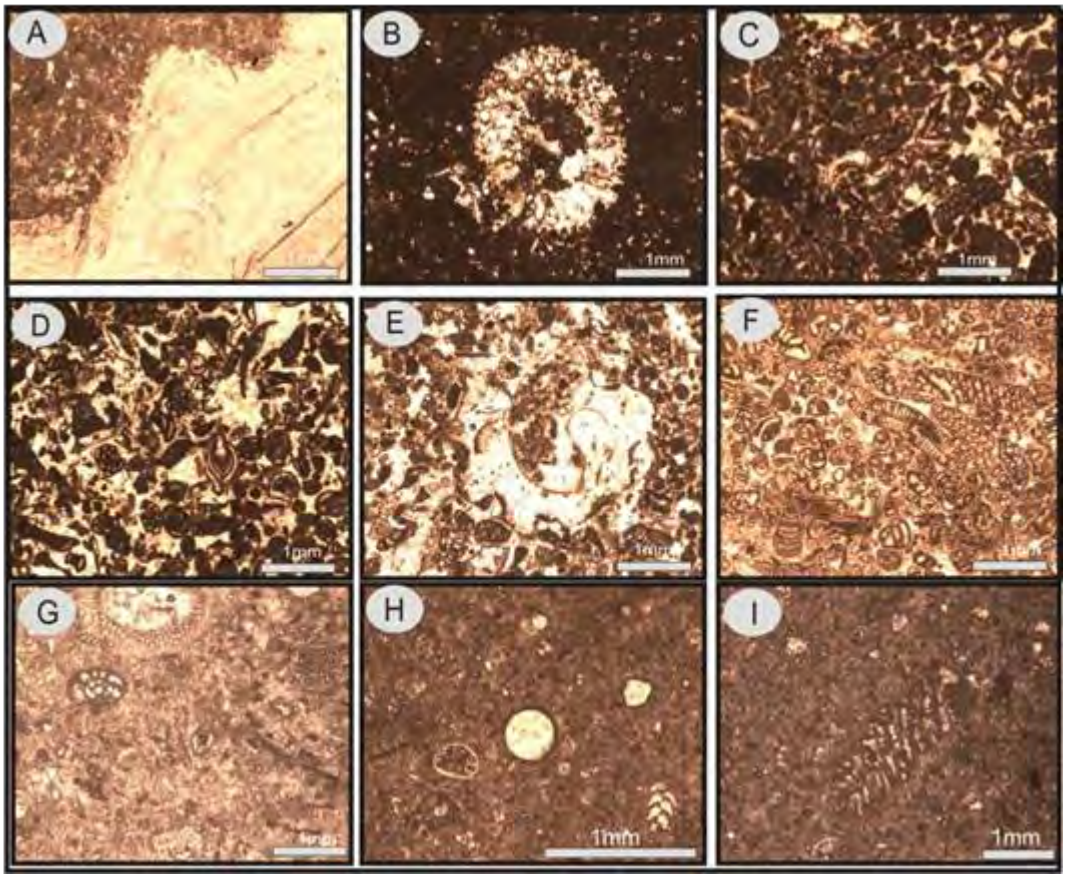

Figure 2 - A)Rudist, B)Dasyclad green algae, C)*Quinqueloculina* sp. , *Dicyclina* sp., D) *Spiroloculina* sp. *Pseudonummoloculina* sp., *Quinqueloculina* sp. E) Gastropods & Miliolidae, F) *Cuneolina* sp., *Pseudonummoloculina* sp., *Dicyclina* sp., *Nezzazata* sp., *Quinqueloculina* sp., G) *Thaumatoporella* sp., *Moncharmontia* sp., H) *Thaumatoporella* sp., Ostracods, I) *Dicyclina* sp.

5. Lithofacies and Paleoenviromental Interpretation

This carbonate platform is represented by a monotonous succession of cream coloured, medium to thick-bedded (10-40 cm) limestones (Figure 3). The most common lithofacies are wackestone/mudstone with thin shelled ostracods and *Thaumatoporella*, laminated packstone with contribution of benthic foraminifera, grainstone with benthic foraminifera and finally floatstone with Rudist debris occur sporadically.

Five Standard Microfacies Types can be distinguished (Pomoni-Papaioannou et al., 2012):

- SMF 9 represented by bioclastic wackestone/floatstone with various shells.
- SMF 18 represented by packstone/grainstone benthic foraminifera with abundant miliolids and calcareous green algae. Miliolid foraminifera are very common in lagoonal environments, restricted inner platforms and inner ramps.
- SMF 18b represented by bioclastic packstone/floatstone. Fossils are fragments of benthic foraminifera, Rudist, Gastropods or Dasycladacea. Bedded limestones with larger foraminifera and molluscs represent the shallow part of the lagoon. The composition of the gastropod fauna reflects changes from open marine to more restricted conditions.
- SMF 19 represented by bindstone with laminated fabric consisting of millimetre thick laminae. SMF type 19 is often used as indicator for intertidal and supratidal environments. The main criteria are lamination textures caused by microbial/ algal mats and fenestral fabrics.
- SMF 20 and SMF 21 are also used as indicators for intertidal and supratidal environments. The main criteria are lamination textures caused by microbial/algal mats and fenestral fabrics.

Figure 3 –Sami section: A typical peritidal carbonate unit.

The diagnostic criteria of the Standard Microfacies indicate two different Facies zones of the Wilsons' model, FZ 7 which represents a shallow open-marine platform and FZ 8 which represents a restricted marine platform (Table 1). Particularly, Facies zone FZ 7 includes SMF 9 and sporadically SMF 18. Respectively, FZ 8 includes SMF 18, SMF 18b, SMF 20 and SMF 21.

The specific biostratigraphical and sedimentological characteristics of the recognized Facies zones are the following:

FZ 7 Open- marine platform

Setting: Flat platform top within euphotic zone, normally above fair-weather wave base.

Lithofacies/Biota: **SMF 9** mudstone/wackestone with Thaumatoporella, Ostracods, Rudist, Benthic foraminifera as *Quinqueloculina* sp., *Moncharmontia* sp. and **SMF 18** packstone/grainstone with peloids and benthic foraminifera (Mililolidae (*Quinqueloculina* sp.))

FZ 8 Restricted-marine platform

Setting: Platform less well connected with the open ocean which is within the ephotic zone and represents shallow, cut-off ponds and lagoons with restricted circulation and hypersaline water.

Lithofacies/Biota: **SMF 18** Packstone/grainstone with peloids and benthic foraminifera (*Quinqueloculina* sp., *Dicyclina sp., Cuneolina sp., Spiroloculina sp. Pseudonummoloculina sp*.), **SMF 18b** floatstone with large intraclast as Gastropods, Dasycladacea or Rudists and benthic foraminifera ((*Quinqueloculina* sp., *Dicyclina sp., Cuneolina sp., Spiroloculina sp.),* **SMF 19** densely laminated bindstone, **SMF 20** Laminated stromatolitic bindstone and finally **SMF 21** fenestral packstone and bindstone.

The predominance of mud-rich lithologies with oligotypic fauna (ostracods, algae and miliolidae) and the presence of a low diversity foraminiferal association indicate a restricted platform (Pomoni-Papaioannou, 2008, Pomoni-Papaioannou & Kostopoulou, 2008), very shallow lagoon with low to moderate hydraulic energy, subjected to periodic emersions (fenestrae). Upwards, the succession consists of limestones enriched in benthic foraminiferal but still characterized by a low diversity. The dominance of miliolidae and the presence of algal laminations indicate a very shallow lagoon with moderate to high hydraulic energy (restricted platform, intertidal to shallow subtidal). Occasionally, open-marine influence is confirmed by the presence of floatstone with Rudist shell fragments associated with a comparatively diverse benthic foraminiferal assemblage.

Small-scale cycles, formed in a low-energy peritidal environments are characterized by the repetitive stacking of the facies types which are presented in Figure 4.

Table 1 – Sami Section: lithofacies associations.

Facies Zone	Microfacies	Discription
FZ 7 Open-marine platform	SMF 9	Mudstone/wackestone with Thaumatoporella, Ostracods, Rudist, Benthic foraminifera (*Quinqueloculina* sp., *Moncharmontia* sp.)
	SMF 18	Packstone/grainstone with peloids and benthic foraminifera (Mililolidae (*Quinqueloculina* sp.))
FZ 8 Restricted-marine platform	SMF 18	Packstone/grainstone with peloids and benthic foraminifera (*Quinqueloculina* sp., *Dicyclina sp., Cuneolina sp., Spiroloculina sp. Pseudonummoloculina sp*.)
	SMF 18b	Floatstone with large intraclast as Gastropods, Dasycladacea or Rudists and benthic foraminifera ((*Quinqueloculina* sp., *Dicyclina sp., Cuneolina sp., Spiroloculina sp.)*
	SMF 19	Densely laminated bindstone
	SMF 20	Laminated stromatolitic bindstone
	SMF 21	Fenestral packstone and bindstone

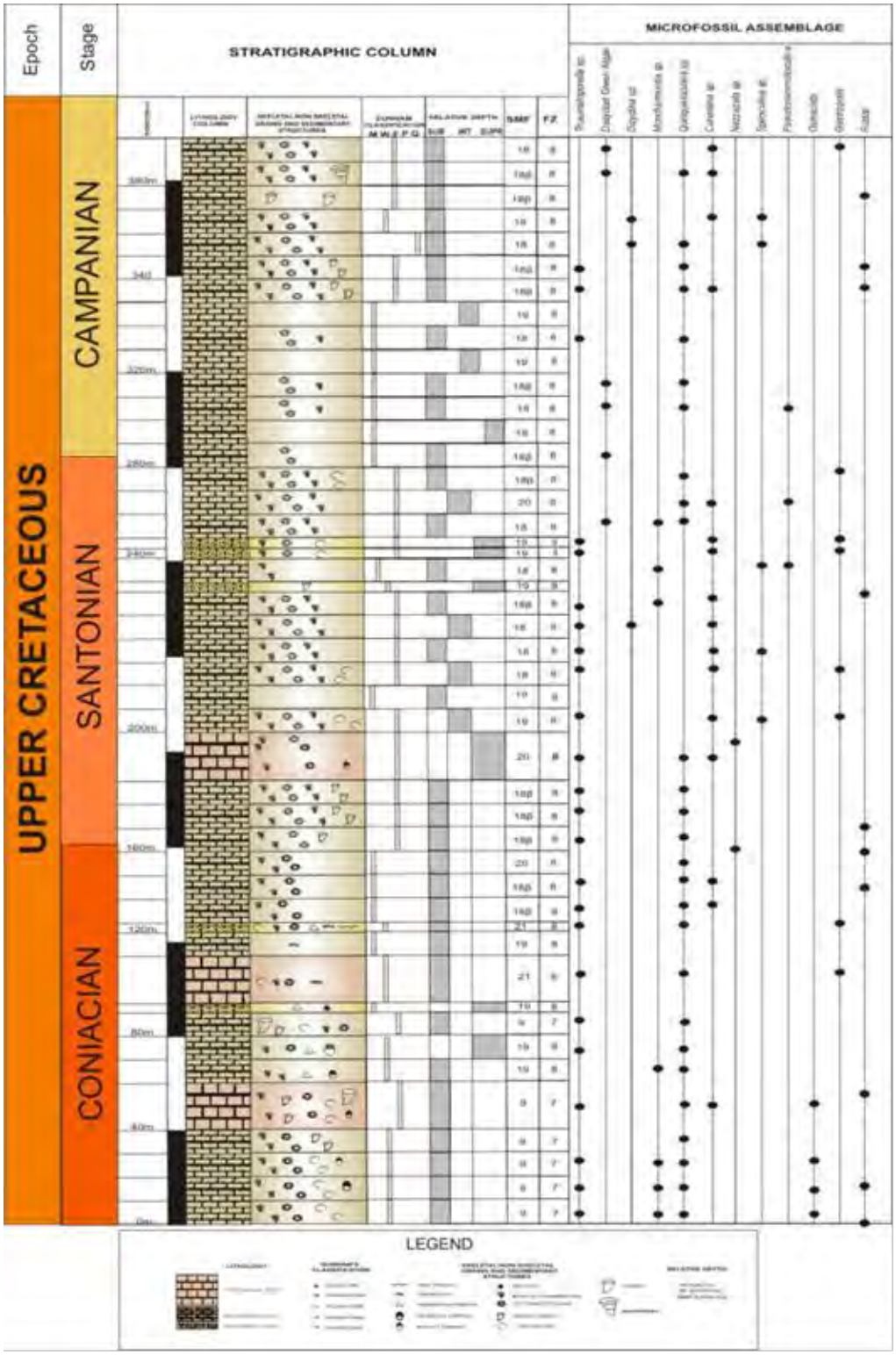

Figure 4 - Stratigraphic column of the Upper Cretaceous carbonate sequence of the Sami area.

6. Conclusions

The combination of biostratigraphic and stratigraphic correlation of the studied Upper Coniacian to Lower Campanian succession allows us to interpret the depositional environments of the carbonate succession of the Paxi zone in the Sami area. The data presented in this paper illustrates that Paxi zone, during the Upper Cretaceous, was tectonically controlled. Sami area represents an uplifted part of this slope, exhibiting shallow water deposits, while others are characterized by mixed pelagic/neritic sedimentation. The high-resolution stratigraphic analysis has shown a number of lithofacies organized in groups (lithofacies associations), suggesting, on the whole, sedimentary environments ranging from lagoonal to peritidal context.

7. References

Aubouin J. 1962. Zone preapulienne et zone du Gavrovo en Peloponnese occidental, *Bulletin de Société Geologique de la France*, v.4, 785-794.

Accordi G., Carbone, F. and Pignatti J. 1998. Depositional history of a Paleogene carbonate ramp (Western Cephalonia, Ionian Islands, Greece), *Geologica Romana* 34: 131-205.

Brescia M., D'Argenio B., Ferreri V., Pelosi N., Rampone S. and Tagliaferri R. Neural net aided detection of astronomical periodicities in geologic records, *Earth Planet. Sci. Lett*., v.139, 33–45.

Buonocunto F.P., D'Argenio B., Ferreri V. and Raspini A. 1994. Microstratigraphy of highly organized carbonate platform deposits of Cretaceous age, The case of Serra Sbregavitelli (Matese, central Apennines), *Giorn. Geol*., 56, 179–192.

Flügel E. 2004. *Microfacies Analysis of Carbonate Rocks*, Springer Verlag, Berlin, 745pp.

Getsos K., 2005. Ionian basin analysis and its evolution,during the Triassic-Paleogene time interval and the relation with hydrocarbon plays, *PhD Thesis,* University of Patras.

Getsos K., Pomoni-Papaioannou F. and Zelilidis A. 2007. A carbonate ramp evolution in the transition from the Apulia platform to the Ionian basin during Early to Late Cretaceous (NW Greece), *Proceedings of the 11th Intern. Congress of the Geological society of Greece, Bull of the Geol.Soc.Greece*, v. XXVII, 53-63.

Jenkyns D.A.L. 1972. Structural development of western Greece, *American Association of Petroleum Geologists Bulletin,* v. 56, 128-149.

Jones W.D.V. 1968. Results of recent geological surveys in central-western Greece, *Geological Society of London*. Proccedings, v. 1645, 306-310.

Karakitsios V. and Rigakis N. 2007. Evolution and petroleum potential of western Greece, *Journal of Petroleum Geology*, v. 30(3), 197-218.

Loblich A. and Tappan H. 1988. *Foraminiferal Genera and their classification*, Copyright @ Van Nostrand Reinhold.

Pomoni-Papaioannou F. 2008. Facies analysis of the Lofer cycles (Upper Triassic), in Argolis Peninsula (Greece), *Sedimentary Geology*, v. 208, 79-87.

Pomoni-Papaioannou F. and Kostopoulou V. 2008. Microfacies and cycle stacking pattern in Liassic peritidal carbonate platform strata, Tripolitza-Gavrovo platform, Greece, *Facies*, 54, 417-431.

Pomoni-Papaioannou F., Zoumpouli E., Zelilidis A. and Iliopoulos G. 2012. Microfacies and benthic foraminiferal assemblages of the carbonate succession of the Cretaceous platform in the Sami area (NW of Kefallinia, W Greece): Biostratigraphy and palaeoenvironments, *29th IAS Meeting of Sedimentology*. Schladming, Austria on 10th-13th September 2012, Abstract (Poster).

Smith A.G., and Moores E.M. 1974. Hellenides, in Spencer-Verlag. Mesozoic and Cenozoic orogenic belts, *Geological Society of London Special Publication*, v. 4, 159-185.

Underhill J. 1989. Late Cenozoic deformation of the Hellenide foreland western Greece, *Geological Society of America Bulletin*, v. 101, 613-634.

Δελτίο της Ελληνικής Γεωλογικής Εταιρίας, τομ. XLVII, 2013
Πρακτικά 13ου Διεθνούς Συνεδρίου, Χανιά, Σεπτ. 2013

Bulletin of the Geological Society of Greece, vol. XLVII 2013
Proceedings of the 13th International Congress, Chania, Sept. 2013

MAGNETIC SUSCEPTIBILITY AS A TOOL FOR THE DISCRIMINATION OF ANTHROPOGENIC AND LITHOGENIC HISTORY OF TOPSOILS: PRELIMINARY RESULTS FROM THE BROADER AREA OF THESSALONIKI CITY

Aidona E.[1], Kazakis N.[2], Mavroidaki K.[1] and Voudouris K.[2]

[1] *Department of Geophysics, School of Geology, Aristotle University of Thessaloniki, 54124 Thessaloniki - Greece, aidona@geo.auth.gr*

[2] *Laboratory of Engineering Geology & Hydrogeology, School of Geology, Aristotle University of Thessaloniki, 54124 Thessaloniki - Greece, kazakis@geo.auth.gr*, *kvoudour@geo.auth.gr*

Abstract

In the recent years the measure of the magnetic susceptibility has been proved to be a reliable tool for the monitoring of pollution in topsoils. However the increase of magnetic susceptibility is not always correlated with polluted sources but it is possible to reflect the geological background of the area. In the present study a broad area in the southeast part of Thessaloniki city has been investigated by means of magnetic susceptibility measurements. In total 77 profiles up to 70 cm depth have been sampled. Magnetic susceptibility was measured in two different frequencies (0.47 and 4.7 KHz) and the percentage of frequency dependence was calculated. The spatial distribution of the magnetic susceptibility values was performed using GIS techniques. The results revealed the presence of two areas with high susceptibility values. These areas are investigated in details in order to distinguish the anthropogenic or the lithogenic influence.

Key words: *Environmental magnetism, soil pollution, GIS, Anthemountas river basin.*

Περίληψη

Τις τελευταίες δεκαετίες η μέτρηση της μαγνητικής επιδεκτικότητας έχει αποδειχθεί ως ένα χρήσιμο εργαλείο για τον εντοπισμό και την παρακολούθηση της επιφανειακής ρύπανσης των εδαφών. Παρόλα αυτά η αύξηση της μαγνητικής επιδεκτικότητας δεν συνδέεται πάντα με πηγές ρύπανσης αλλά είναι δυνατόν να αντανακλά το γεωλογικό υπόβαθρό της περιοχής. Στην παρούσα μελέτη έχει ερευνηθεί η ευρύτερη περιοχή νοτιοανατολικά της πόλης της Θεσσαλονίκης με τη χρήση δεδομένων μαγνητικής επιδεκτικότητας. Συνολικά έχουν συλλεχθεί δείγματα εδάφους από 77 θέσεις μέχρι το βάθος των 70 cm. Η μαγνητική επιδεκτικότητα μετρήθηκε σε δύο συχνότητες (0.47 και 4.7 KHz) και υπολογίστηκε το ποσοστό της εξαρτώμενης από τη συχνότητα επιδεκτικότητας. Η χωρική κατανομή των τιμών της μαγνητικής επιδεκτικότητας πραγματοποιήθηκε με τη χρήση τεχνικών GIS. Τα αποτελέσματα υποδεικνύουν την ύπαρξη δύο περιοχών με αυξημένες τιμές επιδεκτικότητας. Οι περιοχές αυτές μελετώνται λεπτομερειακά για να διαπιστωθεί αν η αύξηση αυτή οφείλεται σε ανθρωπογενείς ή γεωλογικές επιδράσεις.

Λέξεις κλειδιά: *Περιβαλλοντικός μαγνητισμός, ρύπανση εδάφους, GIS, Λεκάνη Ανθεμούντα.*

1. Introduction

Magnetic susceptibility indicates the degree of magnetization of a studied material when it is placed in a uniform magnetic field. Therefore, it is a very sensitive parameter to the presence of ferromagnetic minerals. Dearing (1994) reported that 0.01% of magnetite, in typical soil magnetic population, contributes about 85% to the total magnetic susceptibility. Magnetic minerals present in soils could be derived from the parent rocks (lithogenic origin) or could be originated from anthropogenic activities. When the parent rock has a weak magnetization and therefore has a negligible contribution to the magnetic properties of the soil, the measure of magnetic susceptibility can play an important role for monitoring the pollution since several toxic compounds such as heavy metals are highly increased in urban airborne materials.

The measurement of magnetic susceptibility is widely used during the last decades for the detection of environmental pollution of soils, sediments and dusts. Several studies have been performed indicating the enhancement of magnetic susceptibility in industrial areas, highways and urban areas. Thompson and Oldfield (1986) reported that soils near urban and industrial areas have an increased magnetic susceptibility, representative of the deposition of magnetic particles, such as, dusts of industries and fly ashes of the coal combustion. Moreover, magnetic susceptibility mapping was successfully applied in different countries for the estimation of anthropogenic pollution (Strzyszcz, 1993; Dearing et al., 1996; Scholger, 1998; Petrovsky et al., 1998, 2000; Kapicka et al., 2001; Lecoanet et al., 2001; Boyko et al., 2004; Jordanova et al., 2004; Lu and Bai, 2006; Magiera et al., 2006). Despite this big development especially in Europe, in Greece only few studies have been performed during the last decades (Scoullos et al., 1979, Sarris et al., 2009, Zananiri et al., 2010).

In this study, the preliminary results of magnetic susceptibility data obtained from the broader area of Thessaloniki City in the Anthemountas basin are presented. The main target of this work is folded: a) to investigate the spatial distribution of the results of the magnetic susceptibility of the topsoil using GIS techniques and determine the highly magnetic areas, and b) to investigate if this enhancement is due to anthropogenic or lithogenic origin.

2. Geomorphological and Geological Settings

The study area of the present work is located in the Anthemountas basin, in northern Greece at the eastern part of the Thermaikos gulf. It covers an area of 374 km^2 with high hills of semi-mountainous relief, according to Dikau's (1989) classification. The mean altitude and slope of the study area are 259 m and 20%, respectively.

From a geological point of view, Anthemountas basin is a part of the Servo-Macedonian, Circum-Rhodope and Paeonian geotectonic zone (Mountrakis, 1985). The mountainous part of the basin consists of Mesozoic ophiolithic, crystalline and carbonate rocks whereas in the lowlands Neogene and Quaternary sediments represent 65% of the formations. The Neogene sediments are mainly located at the southern part of the area and consist of sandstone-marl (sandstones, marls, sands and gravels), red-clay (clay with lenses of sands) and conglomerate series (conglomerates, gravels, sands). The Quaternary sediments are alluvial deposits (sands, gravels and clays) in the western part of the basin and terrace systems (sands, pebbles) in the east (Figure 1). Carbonate rocks outcrop in the south-central part of the basin near Agia Paraskevi and Tagarades and consist of Triassic limestones.

3. Sampling and Methodology

Soil samples have been collected from 77 different sites within the studied area. The exact positions of sampling points are shown in Figure 2. In every sampling site, a hand core drilling was used in order to obtain the soil sample. The sampling was performed in vertical profiles of

maximum depth of 70cm. The collecting material of every 10 cm was homogenised and considered as one sample representative for this depth (e.g. 0-10 cm).

In total 503 samples were collected. The soil samples were dried and sieved (in order to remove all the impurities) and placed in cylindrical plastic boxes (2x2x2 cm).

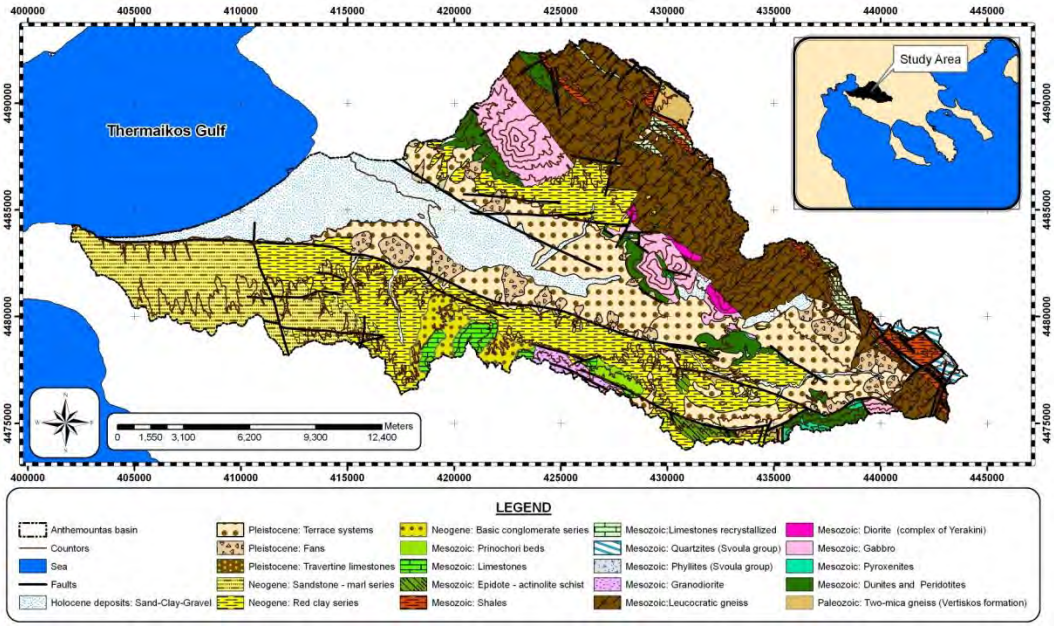

Figure 1 - Geological Map of the Anthemountas river basin.

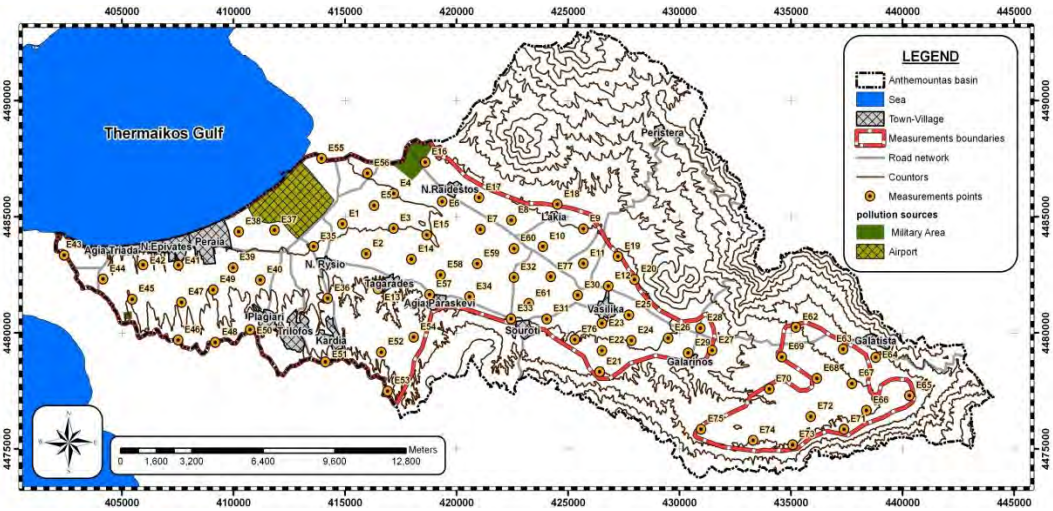

Figure 2 - Schematic map indicating the sampling locations (orange dots) and the possible pollution sources (green areas).

Magnetic susceptibility is a measure of the ease which a material can be magnetised. The volume susceptibility is defined by the relation $\kappa=M/H$, where M is the acquired magnetisation when a uniform magnetic field (H) is applied. In SI units both M and H are expressed in A/m, consequently k is dimensionless. Mass specific susceptibility χ is defined as: $\chi=\kappa/\rho$, where ρ is the density and has units m^3/kg in SI.

In the present study the measurements of the magnetic susceptibility have been performed using the Bartington MS2B sensor. As our samples were weighted before the measurements all the results are expressed as mass specific susceptibility (χ). The magnetic susceptibility was measured in low (0.47 kHz) and high (4.7 kHz) frequency, allowing the calculation of the percentage of the frequency –dependent susceptibility (χ_{fd} %) using the simple formula: χ_{fd} (%)=[(χ_{lf} - χ_{hf})/χ_{lf}]x100, where χ_{lf} and χ_{hf} is the susceptibility in low and high frequency respectively. This parameter is sensitive to magnetic grain size as it indicates the presence of superparamagnetic (SP) grain (Dearing, 1994).

4. Results

The spatial distribution of magnetic susceptibility values from the topsoil (0-10 cm) is shown in Figure 3. The χ values exhibit a wide variation ranging from 6.4 up to 423x10^{-8} m^3/kg. The most enhanced values are observed in two areas: along a zone northwest - southeast of the studied area, and in west part indicating medium to high values (50-200 x10^{-8} m^3/kg). The lower values are found in the central part of the studied area. As it is shown in Figure 3, the high values of the topsoil in the west side revealed in an area close to the airport and in the intense urban network, an area which can be considered as a pollution source. Along the zone in the northwest-southeast edges and especially in the southeast part where the biggest anomaly is observed, no visible pollution source in the vicinity seems to be associated with this anomaly. On reverse, this zone appears to correlate with the big ophiolite outcrops following the same direction of the enhanced magnetic susceptibility values.

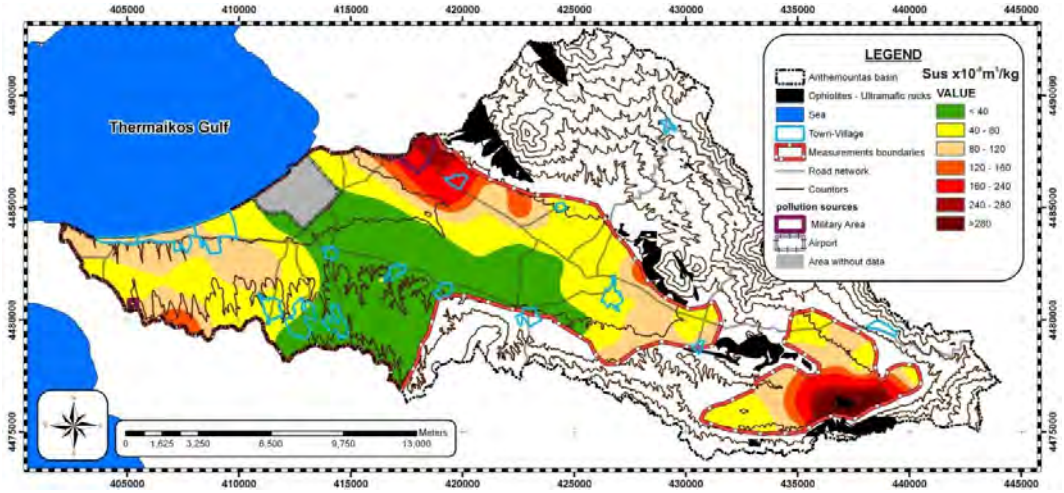

Figure 3 - Spatial distribution of the magnetic susceptibility of the topsoil (0-10cm depth).

The distribution of the χ_{fd}% for the same depth (0-10cm) shows that in the magnetically enhanced areas the percentage of the frequency dependent susceptibility is lower ranging from 0-3%, while in the central part of the area the same parameter obtains much higher values reaching even 21% (Figure 4).

The vertical distribution through the studied profiles can divided in 4 groups. The highly magnetic area in the west part present, in the majority of the samples, decreased magnetic susceptibility values with depth (Figure 5a). This is another indicator for the influence of the topsoil from different pollution sources in the area. In the other zone northwest-southeast, the vertical profiles shows more complex trends. There are samples that show increased values with depth as shown in Figure 5b and samples showing high values along the whole profile with no variation with depth. The first behavior is characteristic of soils that are influenced by the highly magnetic geological background as it is in this case the presence of the ophiolite belt. In the central part of the studied area

where the lower susceptibilities are observed their vertical distribution show no significant change (Figure 5c). Finally there are only few cases throughout the whole area where the vertical profiles does not shown any reasonable change with depth which is most probable due to erroneous sampling (Figure 5d).

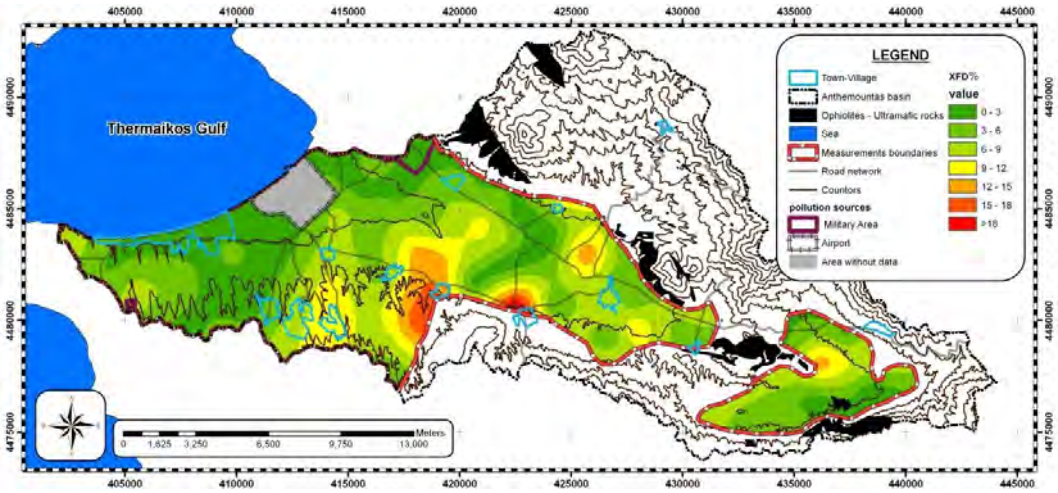

Figure 4 - Spatial distribution of the frequency dependent susceptibility (χ_{fd}).

5. Discussion

The studied area is a complex area since it compiles urban areas and pollution sources with a rich geological background. The spatial distribution of our results revealed the presence of enhanced magnetic areas. As it is shown from the vertical profiles in some cases the χ values are decreased with depth while there are cases where the opposite phenomenon is observed.

These different trends with depth are characteristics in soils influenced by near surface pollution and by strong geological background respectively. Several authors have studied and compared there two types of vertical distribution leading to the same conclusions. Maher (1986) investigated several types of soils in order to characterize them by the mineral magnetic measurements. Examples of soils developed on doleritic parent rock showed a steady increase in χ with depth accompanied with a correspondent decrease in χ_{fd}.

Furthermore, soils that have been affected from atmospheric pollution showed the reverse behavior; decreased values of χ with depth followed with increased χ_{fd}. Similar results concerning the variation of χ and χ_{fd} in vertical soils profiles from China have been reported by Lu and Bai, (2006). Magiera et al., (2006) tried to discriminate the lithogenic and anthropogenic influence on topsoil using magnetic susceptibility measurements. The study of the vertical profiles showed again increased χ values with depth in the forest soils and decreased in the polluted areas. They conclude that the anthropogenic origin of enhanced topsoils can be confirmed by the following observations: anomalies in χ close to industrial and urban areas, strongest enhancement of the topsoil located in the topsoil (uppermost 8 cm), topsoil enhancement in forest is higher than in arable field of the same area, χ enhancement is accompanied by increased heavy metal content.

Following the observations of Magiera et al., (2006) and compare them with the available data in the present study we can conclude that the west part of our studied area can be considered as polluted from local pollution sources originated either from the intense human activities or the airport. In order to reinforce this observation the difference between the χ values of the topsoil and the bottom χ values is calculated. The spatial distribution of this difference is presented in Figure 6. High positive values are observed in the west part of the plot, confirming the anthropogenic

influence by the presence of highly magnetic horizons in the upper most part of the soil close to urban areas.

The second enhanced area (northwest-southeast zone) is more complex since both urban zones and the ophiolite belt zone are present. As Magiera et al., (2006) reported the lithogenic origin of enhanced topsoil can be confirmed by: a) localization of observed anomaly in areas remote from urban sources of pollution, b) the χ values increase gradually with depth, c) topsoil χ values are significantly lower than the measured in an arable field and d) heavy metal content is low and no correlated with χ.

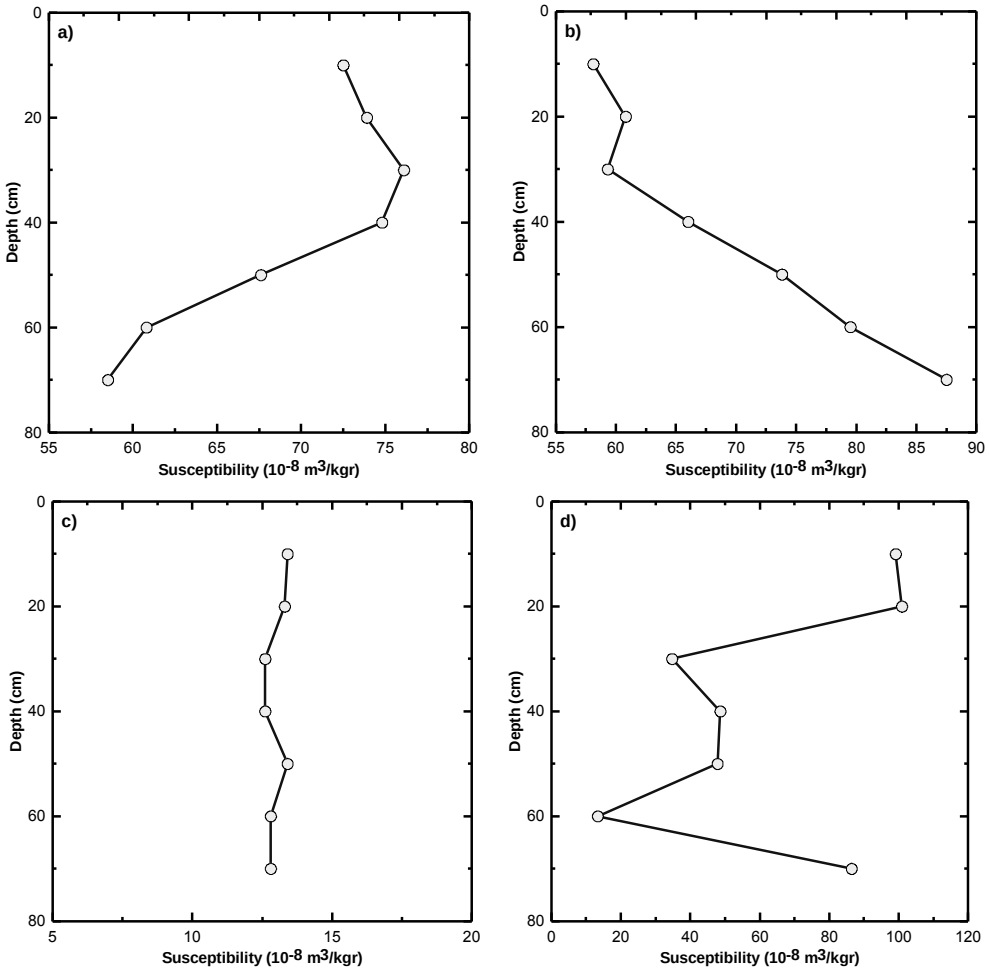

Figure 5 - Vertical profiles of magnetic susceptibility. Typical examples of the enhanced magnetically area in the west part (a), along the northwest-south east part (b), from the central part with the lower values of susceptibility (c) and wrong sampling (d).

From the above observations only the first two are available in the present study and only the first one is fulfilled. As it is already mentioned above, the vertical distribution of χ values is not uniform in this zone. Some of the samples display similar trend as Magiera et al., (2006) reported (that is increase with depth) but also no big changes in the vertical profiles are observed. This dual behavior is recorded in Figure 6 where no clear indication on the lithogenic influence of the soils is observed. If the geological influence was dominant, this zone should be characterized by high negative values (green color in Figure 6). The mixture that is observed reflects the complexity of

the area. A possible plausible explanation for the big positive anomaly in the northern part of the zone can be the vicinity of the sampling point to an urban area and also close to the highway.

The most interesting part is the south edge of the zone where both high positive and high negative values are observed. This area is remote from any industrial or urban area, so the ophiolithic influence in the χ values should be expected. This is confirmed only in the north and south ends where high negative values are displayed. In contract in the middle of this area two (2) high positive values are recorded, indicating the enhancement of χ in the upper most part of the soil. This area consists of arable soils. The main cultures in those areas are corn, cotton and vegetables and characterized by high demands in fertilizers, whereas the excessive use of the fertilizers reflected in the nitrates concentration in the groundwater exceeding 50 mg/L (Kazakis, 2013). The use of the fertilizers possible affects the χ_{lf} values (Figure 3) in the agricultural area, as well as the difference between the top and bottom soil (Figure 6) creating these high values, which are recorded in the southeast part of the study area.

On the other hand, Magiera et al., (2006) showed that in arable soils the observed topsoil χ is higher that the nearby forest soil. During the ploughing of arable soil, ferromagnetic minerals from the parent rock are transported upward, while in the forest soil they are concentrated in the bottom of the studied soil cores. So, it seems that ploughing plays an important role in the distribution of the magnetic minerals and consequently can be an alternative explanation for this 'unexpected' behavior of the soils in the present study.

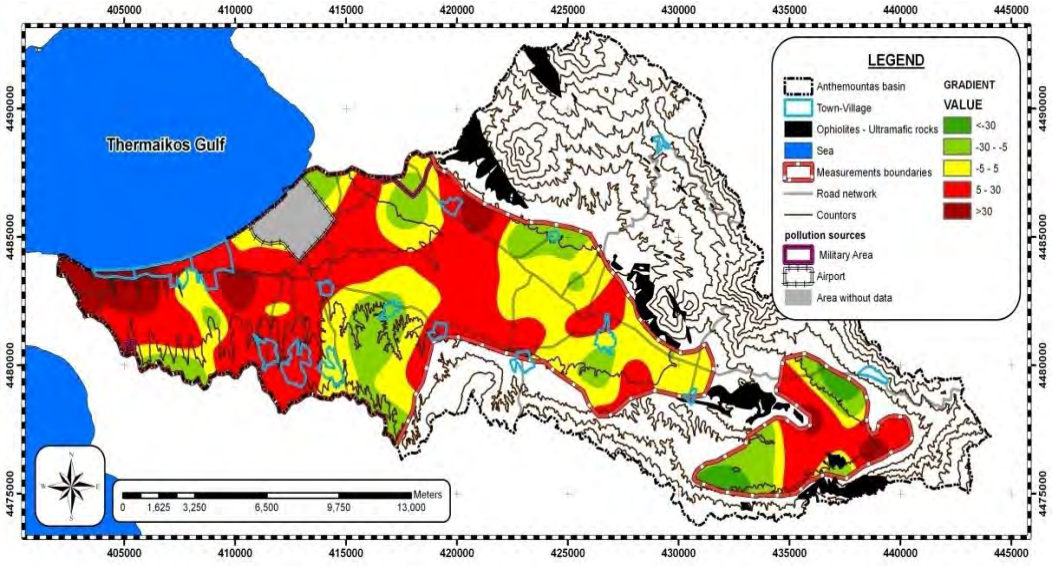

Figure 6 - Distribution of the difference between the topsoil and the bottom soil from all studied locations.

6. Conclusions

Magnetic susceptibility measurements of soils have been performed in the Anthemountas river basin close to Thessaloniki City. The spatial distribution of χ (mass specific susceptibility) indicates areas with big magnetic anomalies. The first one is located west of the studied area and characterised by high values of χ in the topsoil samples, indicative for their anthropogenic origin. The second enhanced area is a zone northwest–southeast of the studied area which appears more problematic. This area is remote from any industrial or urban area, so the magnetic anomalies should be attributed to the presence of ophiolithic rocks, which are rich in ferromagnetic minerals.

In order to confirm the above results a more detailed sampling should be performed especially in the more problematic areas. Moreover heavy metal analysis will validate our assumptions and will certain enlighten the research regarding the possible sources of pollution.

The mapping of magnetic properties of soils can be very helpful for outlining areas affected by different pollution sources. However, as our preliminary results shows, the enhancement of the magnetic properties is not always lead to the pollution sources, hence, the geology of the area has to be seriously considered when interpreting the data. This is essential for the discrimination of anthropogenic contribution from the natural magnetic effects.

7. Acknowledgments

Nerantzis Kazakis is grateful to STATE SCHOLARSHIPS FOUNDATION OF GREECE (IKY) for the financial support of a part of this scientific work.

8. References

Boyko T., Scholger R. and Stanjek H. 2004. Topsoil magnetic susceptibility mapping as a tool for pollution monitoring: repeatability of in situ measurements, *J. Appl. Geophys.* 55, 249-259.

Dearing J.A. 1994. Environmental magnetic susceptibility: Using the Bartington MS2 System. Chi Publishing, Kenilworth, UK.

Dearing J.A., Hay K.L., Bahan S.M.J., Huddleston A.S., Wellington E.M.H. and Loveland P.J. 1996. Magnetic susceptibility of soil: an evaluation of conflicting theories using a national data set, *Geophysical Journal International*, 127, 728-734.

Dikau R. 1989. The application of a digital relief model to landform analysis, in: Raper, J. F. (Ed.) 1989: *Three dimensional applications in Geographical Information Systems*. Taylor and Francis, London, pp. 51-77.

Jordanova D., Hoffmann V. and Fehr K.T. 2004. Mineral magnetic characterization of anthropogenic magnetic phases in the Danube river sediments (Bulgarian part), *Earth Planet Sci. Lett.* 221, 71-89.

Kazakis N. 2013. Groundwater pollution risk assessment in Anthemountas basin. *PhD Thesis*, Department of Geology, Aristotle University of Thessaloniki (in Greek).

Kapicka A., Petrovksy E., Jordanova N. and Podrazsky V. 2001. Magnetic parameters of forest top soils in Krkonose Mountains, Czech Republic, *Phys. Chem. Earth A Solid Earth Geod.,* 26, 917-922.

Lecoanet H., Leveque F. and Ambrosi J-P. 2001. Magnetic properties of salt-marsh soils contaminated by iron industry emissions (southeast France), *J. Appl. Geophys.* 48, 67-81.

Lu S.G. and Bai S.Q. 2006. Study on the correlation of magnetic properties and heavy metals content in urban soils of Hangzhou City, China, *J. Appl. Geophys.* 60 , 1-12.

Magiera T., Strzyszcz Z., Kapicka A. and Petrovsky E. 2006. Discrimination of lithogenic and antropogenic influences on topsoil magnetic susceptibility in Central Europe, *Geoderma* 130, 299-311.

Maher B. 1986. Characterisation of soils by mineral magnetic measurements, *Physics of the Earth and Planetary Interior,* 42, 76-92.

Mountrakis D. 1985. Geology of Greece, Thessaloniki, University Studio Press, 257 pp.

Petrovsky E., Kapicka A., Zapletal K., Sebestova E., Spanila T., Dekkers M.J. and Rochette P. 1998. Correlation between magnetic parameters and chemical composition of lake sediments from Northern Bohemia – preliminary study, *Phys. Chem. Earth,* 23, 1123-1126.

Petrovsky E., Kapicka A., Jordanova N., Knab M. and Hoffmann V. 2000. Low-field magnetic susceptibility: a proxy method of estimating increased pollution of different environmental systems, *Environ. Geol.* 39, 312-318.

Sarris A., Kokkinou E., Aidona E., Kallithrakas-Kontos N., Koulouridakis P., Kakoulaki G., Droulia K. and Damianovits O. 2009. Environmental study for pollution in the area of Megalopolis Power Plant (Peloponnesus, Greece), *Environmental Geology,* 58, 1769-1783.

Scholger R. 1998. Heavy metal pollution monitoring by magnetic measurements applied to sediments of the river Mur (Styria, Austria), *Eur. J. Environ. Eng. Geophys.* 3, 25-37.

Scoullos M., Oldfield F. and Thompson R. 1979. Magnetic monitoring of marine particulate pollution in the Elefsis Gulf, Greece, *Mar. Pollut. Bull.*, 10, 287-291.

Strzyszcz Z. 1993. Magnetic susceptibility of soils in the areas influenced by industrial emissions, in Schullin, R. (eds), *Soils Monitoring: Early Detection and Surveying of Soils Contamination and Degradation*, Birkhauser, Basel, Switzerland, pp. 225-269.

Thompson R. and Oldfield F. 1986. Environmental Magnetism, Allen and Unwin, London.

Zananiri I., Kondopoulou D. and Spassov S. 2010. The application of environmental magnetism techniques for pollution assessment in urban and suburban areas in Greece: State of the art and case studies, *Bull. Geol. Soc. Greece,* XLIII/4, 1972-1982.

Δελτίο της Ελληνικής Γεωλογικής Εταιρίας, τομ. XLVII , 2013
Πρακτικά 13ου Διεθνούς Συνεδρίου, Χανιά, Σεπτ. 2013

Bulletin of the Geological Society of Greece, vol. XLVII 2013
Proceedings of the 13th International Congress, Chania, Sept. 2013

MAPPING EROSION AND DEPOSITION CHANGES IN THE PROTECTED WETLANDS OF THE AXIOS RIVER DELTA, N. GREECE USING REMOTE SENSING AND GIS

Griffiths H.M.[1], Kalivas D.P.[2], Petropoulos G.P.[1] and Dimou P.[2]

[1] Institute of Geography and Earth Sciences, Llandinam Building, Penglais Campus, Aberystwyth University, Aberystwyth, Wales, UK, SY23 3DB, hmg@aber.ac.uk, gep9@aber.ac.uk,

[2] Geographical Information Systems Research Unit, Department of Natural Resources Management & Agricultural Engineering, Agricultural University of Athens, 75 Iera Odos, Athens, GR-118 55, kalivas@aua.gr, e_vi_dim@hotmail.com

Abstract

Our study explores the use of a range of image processing methods combined with Landsat TM imagery for mapping the morphodynamics of the delta of the Axios River, one of the largest rivers of Greece, between 1984 and 2009. The techniques evaluated ranged from the traditional spectral bands arithmetic operations to unsupervised and supervised classification method. Changes in coastline morphology and erosion and deposition magnitudes were also estimated from direct photo-interpretation of the TM images, forming our reference dataset. Our analysis, conducted in a GIS environment, showed noticeable changes in the coastline of the study area, with erosion occurring mostly in the early periods followed by deposition later on. In addition, relatively similar patterns of coastline change were obtained from the different approaches, albeit of different magnitude. The differences observed were largely attributed to the varying ability of the different approaches to utilise the spectral information content of the TM data, strongly linked to the relative strengths and weaknesses underlying the implementation of the different techniques. Notably, supervised classifiers based on machine learning showed the closest results to the photo interpretation of TM, evidencing a promising potential for monitoring shoreline changes over long timescales in a cost-effective and rapid manner.
Keywords: *coastal, Landsat, estuary, fluvial, sediment.*

Περίληψη

Στην παρούσα εργασία γίνεται χρήση διαφορετικών μεθόδων επεξεργασίας δορυφορικών εικόνων Landstat TM για την χαρτογράφηση των αλλαγών, μεταξύ 1984 και 2009, του Δέλτα του Αξιού ποταμού, ενός από τους μεγαλύτερους ελληνικούς ποταμούς. Οι χρησιμοποιηθείσες τεχνικές περιλαμβάνουν από τις παραδοσιακές αριθμητικές επεξεργασίες των φασματικών δεδομένων των διαφορετικών καναλιών, έως τις μη επιβλεπόμενες και επιβλεπόμενες μεθόδους ταξινόμησης. Αλλαγές στην μορφολογία της ακτογραμμής καθώς και στη διάβρωση και στην απόθεση υλικών εκτιμήθηκαν επίσης από άμεσες φωτοερμηνευτικές παρατηρήσεις στις TM εικόνες που χρησιμοποιήθηκαν. Η ανάλυση των δεδομένων, που έγινε σε περιβάλλον GIS, έδειξε σημαντικές αλλαγές στην ακτογραμμή της περιοχής μελέτης, με την διάβρωση να κυριαρχεί στα πρώτα χρόνια και στη συνέχεια να ακολουθεί η απόθεση υλικών. Επιπροσθέτως σχετικά ίδιες τάσεις αλλα-

γής της ακτογραμμής παρατηρήθηκαν σε όλες τις μεθόδους επεξεργασίας των εικόνων, διαφορετικού όμως μεγέθους. Οι διαφορές που παρατηρήθηκαν οφείλονταν κυρίως στην διαφορετική ικανότητα των μεθόδων να χρησιμοποιούν τις φασματικές πληροφορίες των TM δεδομένων, γεγονός στενά συνδεδεμένο με τα πλεονεκτήματα και μειονεκτήματα κάθε μιας μεθόδου. Σημαντικό είναι ότι επιβλεπόμενες ταξινομήσεις, βασισμένες σε αλγορίθμους εκπαίδευσης έδειξαν πιο παραπλήσια προς την φωτοερμηνεία αποτελέσματα, γεγονός που αναδεικνύει μια σημαντική δυνατότητα για την παρακολούθηση των αλλαγών των ακτογραμμών κατά τη διάρκεια μεγάλων χρονικών διαστημάτων με οικονομικό και γρήγορο τρόπο.
Λέξεις κλειδιά: *ακτή, Landsat, εκβολές, ποτάμιες, ίζημα.*

1. Introduction

Characterizing and measuring land and water resources in coastal regions is dependent on an accurate knowledge of the position of the coastline (Liu and Jezek, 2004). River deltas or estuaries are areas of transition between the riverine zone, dominated by fluvial processes and the estuarine zone where coastal processes driven by tidal and oceanic processes are dominant. They are complex, dynamic environments which can often be characterized as wetlands and as such, are significant ecological resources. The management and protection of these recourses, safe navigation and sustainable coastal development and planning require accurate mapping of the coastline and change detection (Di et al., 2004).

To this end, Earth Observation (EO) data and image processing methods applied to such types of data have become increasingly important because they can provide digital imagery in infrared spectral bands where the land–water interface is well defined (Alemayehu et al., 2006, Alesheikhet al., 2007, Ekercin, 2007, Durduran, 2010). Furthermore, EO data can be integrated with Geographic Information Systems (GIS) as an effective tool for analyzing and extracting reliable and consistent information based on satellite imagery (Bausmith and Leinhardth, 1997, Goodchild, 2001, Jaiswal et al., 2002, Durduran, 2010). With reference to coastline changes mapping, EO data have been exploited to study coastline dynamics in the Yellow River delta (Yang, et al., 1999, Li et al., 2004, Chang et al., 2004, Chu et al., 2006, Cui and Li., 2011), the Bohai sea (Jiang, et al., 2003, Huang and Fan, 2004), Fujian coast (Sun and Zhang, 2004) the Pearl River delta (Li and Damen, 2010), Santa Barbara, USA (Komar 1998), Hualien, Taiwan (Hsu et al. 2000), Fortaleza, Brazil (Maia et al. 1998), the Northeastern Nile Delta, Egypt (Frihy et al. 1998, White et al. 1999), Nouakchott, Mauritania (Wu, 2007) and in Greece in particular on the Thermaikos Gulf (Zalidis et al., 2007) the Nestos delta (Mallinis et al., 2011) and the Kotychi Lagoon (Kalivas et al., 2003).

In Mediterranean countries such wetland areas face numerous problems: agricultural development, over-grazing of livestock, over-fishing, decreases in water discharge, drainage works, urbanization and pollution (Maragou and Montziou, 2000). In Greece in particular, the Axios River, one of the longest in Greece, as well as neighbouring rivers have been extensively modified during recent years and have been impacted by dam-building upstream. Despite these problems, the Axios River delta in particular is still of outstanding importance mainly because it perform functions such as trapping of river-borne sediment, nutrient removal, shoreline anchoring and food chain support. As well as being hugely important for wildlife it is economically important – agricultural activity in the Axios delta area is intensive. Rice production in the Axios and Alkiamnonas deltas together account for approximately 60% of total Greek production and shellfish farming activity in the area comprises 85% of the total Greek shellfish output (Karageorgis et al., 2005). Morphological changes caused by erosion and deposition of sediment directly impact the flora and fauna of these wetlands. These processes may be influenced by changes in anthropogenic activities upstream, but they may also reflect changes in climate. There is, therefore, a need to develop a greater understanding of the spatial and temporal dynamics of these areas over a range of temporal timescales in order to inform

the development of integrated catchment and coastal management plans to protect, improve and maintain the environment and improve the quality of group decision processes.

The aim of this paper is to characterize and quantify the changes in coastline position that have occurred at the delta of the Axios River on a decadal timescale. This has been achieved by analysis of four sets of Landsat TM data acquired in the area over a period spanning of ~25 years, using five different image processing techniques. Not only will this provide information on the nature, rates and patterns of change in the delta, but it will also provide valuable information on the suitability of these different image processing methodologies (supervised and unsupervised, machine learning etc) for the detection of geomorphological changes.

2. Materials and methods

2.1. Study Region

The delta of the Axios River is located in the prefecture of Macedonia, Greece (Figure 1). The river rises near Vrutok in the Scardos Mountains (Smardon, 2007) and is the longest river in the Former Yugoslav Republic of Macedonia (FYROM). It passes through Gostivar, Skopje and into Veles, crosses the Greek border near Gevgelija, Polykastro and Axioupoli, before emptying into the northwestern part of the Aegean Sea in Central Macedonia west of Thessaloniki, northern Greece. In total it is 388 km long, with the final 80 km in Greece. Its catchment area is 23747 km^2, 90 % of which is in the FYROM and has a mean annual discharge of 85 m^{3}s^{-1} but displays significant interannual variability (Albanis et al., 1994). The Axios River delta is part of a larger complex of wetlands on the Thermaikos Gulf coast which also includes the mouths of the Alkiamnonas, Gallikos and Loudias rivers protected by the Ramsar Convention (1971).

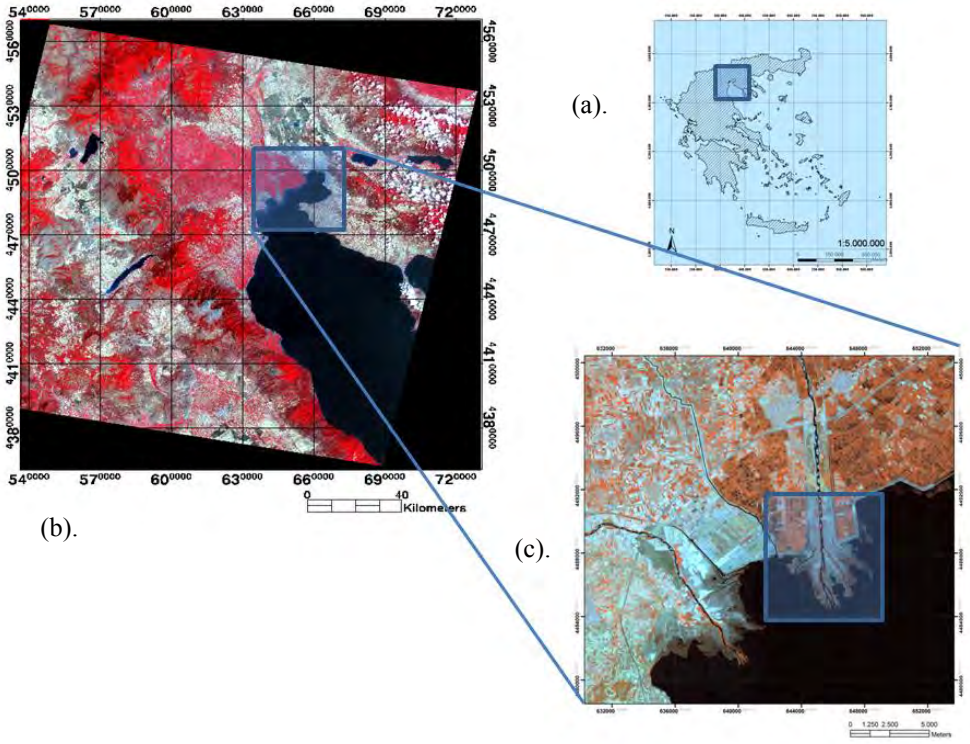

Figure 1 - (a): Location of the study area (B4G3R2); (b): an example of one of the Landsat TM images acquired over studied region shown in the square box (acquired on July 26th, 1984; B7G5R4); (c): the Landsat TM subset on which we focused our analysis in the present study.

2.2. Datasets

Landsat TM images (path: 182, row: 34) were exploited to map coastline changes in the study region over a period of 25 years (1984-2009). The TM images were acquired on the 26th July 1984, 11th July 1990, 16th August 2003 and 31st July 2009. An example of one of the acquired TM images is shown in Figure 1b. All images were obtained from the United Stated Geological Survey (USGS) archive (http://glovis.usgs.gov/) at no cost. Images were provided geometrically corrected, geometrically resampled, and registered to a geographic map projection with elevation correction applied (Level-1T processing). Selection of the specific images was based on the fulfilment of criteria that included clear atmospheric conditions, high sun conditions, low water vapour, near-nadir viewing and acquisition seasonal temporal proximity in order to minimize effects of atmosphere and vegetation phenology. In addition, the global digital elevation model (GDEM) derived from the Advanced Spaceborne Thermal Emission and Reflection Radiometer (ASTER) sensor was acquired. The ASTER GDEM product was released in 2009 and it was acquired as a "geotiff" image at geographic lat/long projection and WGS84/EGM96 datum from the NASA's Land Warehouse Inventory Search Tool (WIST, https://wist.echo.nasa.gov/~wist/api/imswelcome/).

2.3. Methodology

TM images were imported to ENVI platform and were converted to radiance values as described in the Landsat 7 Science data users' handbook for ETM+ (Irons, 2011). Subsequently, all the bands apart from thermal band 6 from each image were layer stacked to form a single image file corresponding to the various acquisition dates. Empirical line normalization was then applied to all three TM images to relatively match the atmospheric effects using the 1984 image as a base. No further correction for topographic effects was necessary since images were already terrain-corrected. Finally, image to image co-registration between the TM images as well as the DEM was performed. Approximately 20 ground control points (GCPs) commonly identified on both the reference and target images were manually selected at random. Positional root mean square (RMS) error was kept below one pixel (i.e. 30 m) in both x and y directions while georeferencing. Image warping was performed by applying the nearest neighbour method, allowing a co-registration of all the images into a common UTM 34N projection under a WGS84 ellipsoid. Finally, an area of approximately 46 km^2 was subset around Axios River delta (Fig. 1c).

This step also increased computational efficiency of the different image processing techniques employed in our study for delineating the coastline and analysing the changes occurred. The resulting dataset for each image subset for each image acquired was subsequently used to extract the coastline each time via direct photo-interpretation and subsequently by performing different image classification. In particular, a coastline from each TM image was extracted based on the following semi-automatic techniques:

- Direct digitisation (photo-interpretation –bands 4,5,7 – e.g. Li and Damen, 2010)
- Band Ratio (TM2/TM5 – e.g Cui & Li, 2011)
- ISODATA unsupervised classification (Richards, 1999)
- Support vector machines (SVMs, Vapnik, 1998) and maximum Likelihood (ML) supervised classification (Richards, 1999).

Subsequently, coastline estimates from the different techniques applied were compared and erosion and deposition rates were estimated based on the coastline surface area (km^2) changes during the years of analysis.

3. Results

Figure 2 shows the areas of erosion (i.e. those areas classified as land in the earlier image and as water in the later image) in red and the areas of deposition in green in the Axios river delta for all three time intervals for all five image processing methods used. Figure 3 presents the total areas (in

m^2) of land being characterised as having been lost to erosion (red) and gained through deposition (green). As expected the erosion and deposition processes are proven to be more intense along the outfalls of the main river channels. Our reference data set obtained through photo-interpretation of the Landsat TM imagery indicates that the Axios delta has experienced net erosion between 1984 and 2009. Within this period, net deposition has taken place between 1984 and 1990; net erosion took place between 1990 and 2003, with a reversion to erosion between 2003 and 2009. Between 1984 and 1990, the magnitude of deposition was 474.59 km^2, between 1990 and 2003 erosion reached a magnitude of 1603.35 km^2 and deposition between 2003 and 2009 was 373.55 km^2. Between 1984 and 2009 the total erosion reached a magnitude of 1487.91 km^2.

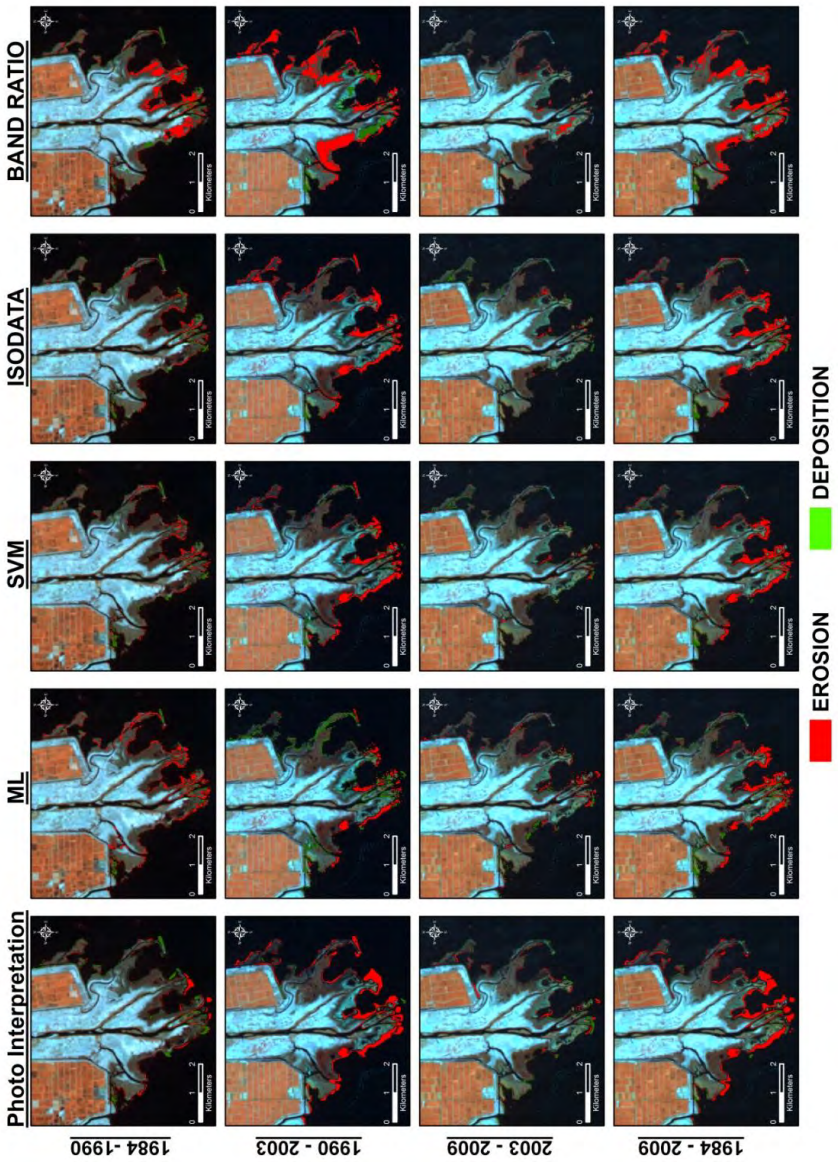

Figure 2 - Maps showing areas of erosion (red) and deposition (green) in the Axios River delta in 1984-1990, 1990-2003, 2003-2009 and 1984-2009 using five methods of analysis (photo interpretation, ML, SVM, ISODATA and Band Ratio). The background image is a false colour composite of the Landsat TM image (B7G5R4), with orange areas representing vegetated areas and blue representing bare earth.

The ISODATA method is in agreement with the photo interpretation method, but in contrast, ML, SVM and Band Ratio methods indicate that delta was experiencing net erosion between 1984 and 1990. Band Ratio recorded the largest area of land eroded (1232.71 km^2) compared to the other methods. This area represented 5.41 % of the area classified as land in 1984. Although the photo-interpretation and ISODATA methods indicated that net deposition occurred during this period, there is generally good agreement between these methods and the SVM in terms of the surface area eroded. Between 1990 and 2003, erosion seems to be the dominant process in the delta, with SVM, Band Ratio and ISODATA methods all in agreement with photo interpretation indicating that the delta experienced net erosion. Indeed, the area of land eroded according to Band Ratio was 2273.59 km^2 (10.36 %) and all five methods indicated that the surface eroded during this period was higher than that which was eroded in 1984-1990. Of course, this could be due to the fact that 1990-2003 is a longer time period than 1984-1990 rather than that the rate of erosion has increased or that the rate of deposition has decreased. In contrast to 1984-1990, there is no agreement between ML and the other methods, with the former indicating that deposition was the dominant process.

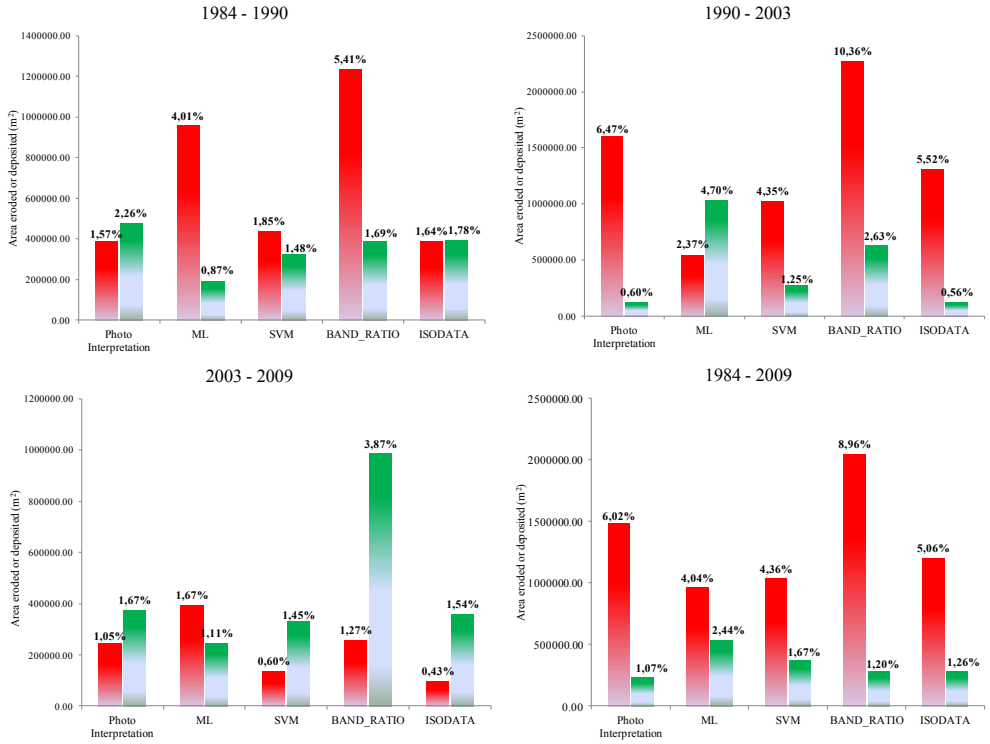

Figure 3 - Erosion (red) and deposition (green) in the Axios River delta for all time periods and for all methods.

Between 2003 and 2009 the surface areas of erosion and deposition calculated by the five methods are, in general, lower than for 1984-1990 and 1990-2009. Overall, the methodologies characterised this period as one in which net deposition occurred in the delta, with SVM, Band Ratio and ISODATA all in agreement with photo interpretation in this respect, whereas ML indicated net erosion. Once again, the Band Ratio method indicates the greatest magnitudes of deposition (984.86 km^2 or 3.87 %) compared to the other methods, which are markedly lower. Finally, analysis of the figures for the period 1984-2009 clearly shows that all methods are in agreement that the delta has eroded, although there are differences between methods regarding the magnitude of this process. There is good agreement between the ML and SVM methods in terms of the magnitude of erosion that has occurred (961.32 km^2 and 1032.42 km^2, respectively) while photo interpretation, Band Ratio

and ISODATA seem to correspond in terms of the magnitude of deposition (225.56 km^2, 275.46 km^2 and 278.46 km^2, respectively). Once again, Band Ratio has indicated the greatest magnitude of erosion during this period at 2042.52 km^2, indicating that 8.96 % of the surface characterized as land in 1984 had been eroded by 2009. A crude calculation would give an annual rate of 81.70 km^2, however it is clear from the results presented that the rate of erosion is not constant, with some periods displaying faster rates of erosion than others, and some periods displaying overall net deposition (2003-2009). This complexity is confirmed by Figure 4, which shows that, overall, the surface area characterized as land has decreased between 1984 and 2009, and that the surface are characterized as water has increased, there are fluctuations between each time period, with some methodologies showing an increase in land area followed by a decrease and vise versa.

4. Discussion

Analysis of the results of the photo interpretation method, which we may regard as the reference method, indicates that although the coastline of the Axios River Delta has eroded between 1984 and 2009, net deposition was evident between 1984 and 1990 and between 2003 and 2009, with the majority of erosion occurring in the period 1990-2003. Many previous studies have noted that the Axios River delta has been subject to anthropogenically-driven degradation over the second half of the twentieth century. For example, Kapsimalis et al., (2005) noted that in contrast to the period 1916-1956 during which increased sediment load and delta progradation occurred as a result of channelisation, land reclamation, the coastline experienced significant retreat between 1956 and 2000. This was primarily due to a reduction in the delivery of sediment to the delta because extensive dam-building in the upper reaches of the Axios had trapped significant proportions of the river's load. In addition Athanasiou (1990) showed that approximately 525 ha of the coastal wetland were lost between 1945 and 1970 due to erosion and subsidence (Smardon, 2009). The findings of the present study also confirms those of a similar study by Zalidis et al., (2007) who showed, using EO data, that the surface area of the delta characterized as water had increased by 13.6 % between 1994 and 2004. The authors also attribute this pattern to the influence of dams and of decreasing river discharge at the delta, possibly as a result of increased water abstraction upstream. This trend of eroding coastline is in common with many deltaic regions across the world, many of which are also responding to increased anthropogenic activities in their catchments (e.g. the Nile delta – White and El Asmar, 1999, and the Yellow River – Chu et al., 2006; Cui and Li, 2011).

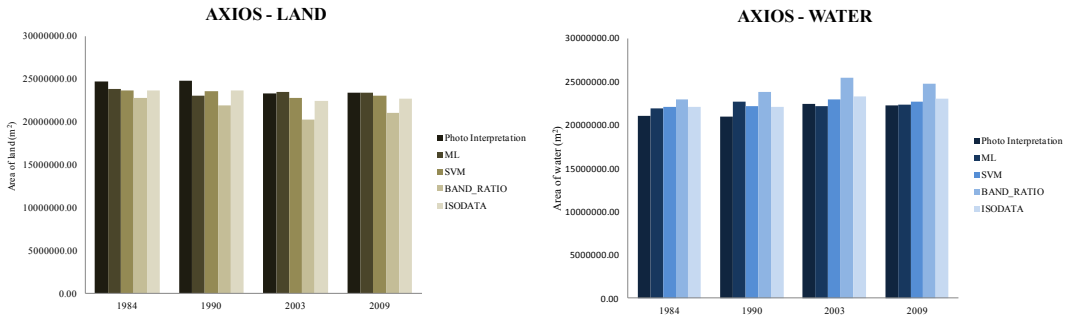

Figure 4 - Graphs showing the changes in the areas characterized as land and water between 1984 and 2009 for all methods used.

The evidence of net deposition during some periods is interesting in the context of the longer term trend of coastline erosion. Whether this deposition (e.g. in 2003-2009) indicates a decrease in the longer term trend of erosion, and whether or not these changes are due to changes in anthropogenic (e.g. agricultural intensification on floodplains causing an increase in sediment load) or climatic (e.g. changes in flood frequency and magnitude) remains to be seen, and will be explored elsewhere. What is evident from these data is that, overall, the surface area available for utilisation by human

activity has decreased. Concurrently, the surface area required by humans for settlement expansion and agricultural activity as a result of an increase in population has increased. Zalidis et al., (2007) showed that settlements had expanded by 27 % since 1994 and an expansion of 8 % in road area. Thus the pressure on land use, and thus on the ecological and geomorphological sustainability of this region has increased not just as a result of an expansion of human activity but as a result of the reduction in the available land surface. Dealing with the tensions which this conflict may cause will be a significant challenge for catchment managers in the future. Whether this level of urbanisation in the delta region has impacted on hydrological and sedimentological pathways and processes is a matter for further research. Interestingly, Zalidis et al., (2007) also found that the irrigated area was relatively stable between 1994 and 2004 and suggested that this showed that irrigation had reached capacity before 1994. However, 22 % of the irrigation had to change location. As well as being due to salinisation, drainage or EU policy reasons, this could indicate an increasing pressure on land caused by coastal erosion.

A preliminary analysis of the similarities and differences between the different image analysis techniques shows that for the most part, the SVM, Band Ratio and ISODATA methods correspond reasonably well to the photo interpretation method. However, different quantitative results were obtained between the methods in estimating the total erosion and deposition rates in the area. This can be attributed largely to the different operation and assumptions each technique. For example, ML as a parametric classifier requires the assumption of normally distributed classes over the area to be classifier, which might not always be the case in nature. Evidently, between all methods included in our study herein, SVMs provided the closest results to photo-interpretation (our reference dataset). This can be due to a number of reasons. SVMs offer additional benefits in contrast to alternative classification models, for example artificial neural networks (ANNs) or ML. SVMs have been designed to be able to identify an optimal separating hyperplane for classes' separation, which makes those classifiers resilient to getting trapped in local minima, as for example with ANNs. Also, their implementation does not require the assumption of statistical distribution of the data to be classified, as for example ML classifier. On the other, a key disadvantage of all classifiers applied herein is that those do not operate on a sub-pixel level. The latter can theoretically significantly reduce the accuracy of those classifiers especially when applied with coarse spatial resolution data, due to possible mixture problems occurred that result to misclassification errors.

Although the magnitude of erosion and deposition vary between methods, in general, these methods are in agreement as to whether the delta is experiencing net erosion or net deposition. The exception to this is in the period 1984-1990 where only the ISODATA method agreed with the photo interpretation in showing that net deposition was taking place, whereas the other three methods indicated erosion was taking place. With the exception of the period 1984-2009, the ML method disagreed with the photo interpretation method.

5. Conclusions

This study has utilised freely distributed high resolution remotely sensed data and GIS and different image processing techniques to demonstrate that the Axios River delta has experienced extensive erosion between 1984 and 2009. Although there are differences between each method for different time periods, all are in agreement that this hugely significant coastal region has degraded during the past ~ 25 years. This study has also shown that it is possible to use a wide variety of different methods of analysing remotely sensed data in order to obtain measurements of geomorphic processes at long decadal timescales and at large spatial scales. The differences in each method demonstrate, however, that more work is needed to validate estimates from such methods and that efforts should be made to integrate remotely sensed data with ground-based observations and topographic surveys where possible. These results may be used to inform future catchment management schemes in order to ensure the geomorphological, ecological and economical sustainability of the region.

6. Acknowledgments

Authors wish to thank USGS for the free distribution of the LandsatTM data, which allowed materialising the present study.

7. References

Albanis T. A., Danis T. G., and Kourgia M. K. 1994. Transportation of pesticides in estuaries of the Axios, Loudias and Aliakmon rivers (Thermaikos Gulf), Greece. *Science of the total environment*, 156(1), 11-22.

Alemayehu T., Ayenew T. and Kebede S. 2006. Hydrogeochemical and lake level changes in the Ethiopian Rift, *Journal of Hydrology*, 316 (1–4), 290-300.

Alesheikh A.A., Ghorbanali A. and Nouri N. 2007. Coastline change detection using remote sensing, *International Journal of Environmental Science and Technology*, 4 (1), 61-66.

Athanasiou H. 1990. Wetland Habitat Loss in Thessaloniki Plain, Greece. *M.Sc. Dissertation*, London: University College, 45 pp., plus appendices.

Bausmith J.M. and Leinhardth G. 1997. Middle school students' map construction: understanding complex spatial displays, *Journal of Geography,* 97, 93-107.

Chang J., Liu G.H. and Liu Q. S. 2004. Analysis on spatio-temporal feature of coastline change in the yellow river estuary and its relation with runoff and sand-transportation, *Geographical Research*, 23(5), 339-346.

Chu Z.X., Sun X.G., Zhai S.K. and Xu K.H. 2006. Changing pattern of accretion/erosion of the modern Yellow River (Huanghe) subaerial delta, China: Based on remote sensing images, *Marine Geology,* 227, 13-30.

Cui B. and Li X. 2011. Coastline change of the Yellow River estuary and its response to the sediment and runoff (1976–2005), *Geomorphology*, 127, 32-40.

Di K., Ma R., Wang J. and Li. R. 2003. Coastal Mapping and Change Detection Using High-Resolution IKONOS Satellite Imagery. *National Conference for Digital Government Research "dg.o 2003"*, Boston, MA, May 18-21, pp. 343-346.

Durduran S.S. 2010. Coastline change assessment on water reservoirs located in the Konya Basin Area, Turkey, using multitemporal landsat imagery, *Environmental Monitoring and Assessment*, 164, 453-461.

Ekercin S. 2007. Coastline change assessment at the Aegean Sea coasts in Turkey using multitemporal Landsat imagery, *Journal of Coastal Research*, 23 (3), 691-698.

Frihy O.E., Dewindar K.M. and Banna L.M. 1998. Natural and human impact on the northeastern Nile delta coast of Egypt, *Journal of Coastal Research*, 14, pp. 1109-1118.

Goodchild M.F. 2001. Metrics of scale in remote sensing and GIS, *International Journal of Applied Earth Observation and Geoinformation*, 3, 114-120.

Hsu T., Ou S. and Tzang S. 2000. Evaluations on coastal topographical changes at Hualien Coast, Taiwan, *Journal of Coastal Research*, 16, 790-799.

Irons J. 2011. Landsat 7 science data user's handbook, *Report 430-15-01-003-0*. National Aeronautics and Space Administration, http://landsathandbook.gsfc.nasa.gov/

Jaiswal R.K., Mukherjee S., Raju K.D. and Saxena R. 2002. Forest fire risk zone mapping from satellite imagery and GIS, *International Journal of Applied Earth Observation and Geoinformation*, 4, 1-10.

Kalivas D.P., Kollias V.J. and Karantounias G. 2003. A GIS for the assessment of the spatio-temporal changes of the Kotychi Lagoon, Western Peloponnese, Greece. *Water Resources Management*, 17, 19-36.

Kapsimalis V., Poulos S.E., Karageorgis A.P., Pavlakis P., and Collins, M. 2005. Recent evolution of a Mediterranean deltaic coastal zone: human impacts on the Inner Thermaikos Gulf, NW Aegean Sea, *Journal of the Geological Society*, 162(6), 897-908.

Karageorgis A.P., Skourtos M.S., Kapsimalis V., Kontogianni A.D., Skoulikidis N.Th., Pagou K., Nikolaidis N.P., Drakopoulou P., Zanou B., Karamanos H., Levkov Z. and Anagnostou Ch.

2005. An integrated approach to watershed management within the DPSIR framework: Axios River catchment and Thermaikos Gulf. *Regional environmental change* 5 (2-3) 138-160.

Komar P.D. 1998. Beach Processes and Sedimentation, Upper Saddle River, NJ: Prentice- Hall, Inc., 429pp.

Li A.I., Li G., Cao L., Zhang Q. and Deng S. 2004. The coast erosion and evolution of the abandoned lobe of the Yellow River Delta, *ACTA GEOGRAPHICA SINICA-CHINESE EDITION*, 59(5), 737-743.

Li X., and Damen M.C.J. 2010. Coastline change detection with satellite remote sensing for environmental management of the Pearl river Estuary, China, *Journal of Marine systems*, 82, 54-61

Liu H. and Jezek K.C. 2004. Automated extraction of coastline from satellite imagery by integrating Canny edge detection and locally adaptive thresholding methods, *International Journal of Remote Sensing*, *25*(5), 937-958.

Maia L.P., Jimenez J.A., Serra J., Morais J. and Sanchez-arcilla A. 1998. The Fortaleza (NE Brazil) Waterfront: port versus coastal management, *Journal of Coastal Research*, 14, 1284-1292.

Mallinis G., Emmanoloudis D., Giannakopoulos V., Maris F. and Koutsias N. 2011. Mapping and interpreting historical land cover/land use changes in a Natura 2000 site using earth observational data: the case of Nestos delta, Greece, *Applied Geography*, *31*(1), 312-320.

Maragou P., Montziou D. 2000. *Assessment of the Greek Ramsar Wetlands*, Athens: WWF-Greece, 59 pp.

Richards J.A., 1999. Remote Sensing Digital Image Analysis, Berlin, *Springer-Verlag*, p. 240.

Smardon R. 2009. The Axios River Delta – Mediterranean Wetland Under Siege, in Smardon R. (Ed) *Sustaining the World's Wetlands, Setting Policy and Resolving Conflicts*, Springer, New York, p. 57-92.

Sun M., Zhang W. 2004. Study on coastline remote sensing survey and application in Fujian Province, *Journal of Oceanography in Taiwan Strait*, 23 (2), 213-219.

Vapnik V. 1998. Statistical Learning Theory, New York, Wiley.

White K. and El Asmar. H.M. 1999. Monitoring changing position of coastlines using Thematic Mapper imagery, an example from the Nile Delta, *Geomorphology*, 29, 93-105.

Wu W. 2007. Coastline evolution monitoring and estimation-a case study in the region of Nouakchott, Mauritania, *International Journal of Remote Sensing*, 28(24), 5461-5484.

Yang X., Damen M.C.J. and Van Zuidam R.A. 1999. Use of Thematic Mapper imagery with a geographic information system for geomorphologic mapping in a large deltaic lowland environment, *International Journal of Remote Sensing*, 20 (4), 659-681.

Zalidis C.G., Silleos N.G., Alexandridis T.K., Lazaridou E., Chantzaridou A. and Nikolaou 2007. Deriving indicators for monitoring European Ramsar wetlands using Earth Observation: The case study of delta Axios-Loudias-Aliakmonas, Greece, *Proceedings of the 10th International Conference of Environmental Science and Technology*, B903-B910.

Δελτίο της Ελληνικής Γεωλογικής Εταιρίας, τομ. XLVII , 2013
Πρακτικά 13ου Διεθνούς Συνεδρίου, Χανιά, Σεπτ. 2013

Bulletin of the Geological Society of Greece, vol. XLVII 2013
Proceedings of the 13th International Congress, Chania, Sept. 2013

CONTRIBUTION TO THE EVOLUTION OF THE PERAMA CAVE (IOANNINA, NW GREECE)

Ifandi E.[1], Tsikouras B.[1,2] and Hatzipanagiotou K.[1]

[1]*University of Patras, Department of Geology, Section of Earth Materials, 265 00, Patras, Greece*
selena.21@windowslive.com, v.tsikouras@upatras.gr, k.hatzipanagiotou@upatras.gr,

[2]*University of Brunei Darussalam, Department of Petroleum Geoscience, Jalan Tungku Link, Gadong BE1410, Bandar Seri Begawan, Brunei Darussalam*

Abstract

This study includes the description of thirty three speleothem types, which were found in the Perama cave, Ioannina, NW Greece, according to the international literature, along with the interpretation of their formation, for the first time in Greece. The detailed study of these speleothems coupled with observations of the way of their formation and their spatial distribution enabled us to suggest that the Perama cave evolved through a sequence of episodes that include dissolution of the host Senonian limestone, collapse of its roof formations, as well as alternating events of formation of stalactitic- and stalagmitic-type speleothems with excess water flow and/or flooding, which resulted in the development of stream formations
Key words: *speleothem classification, carbonate minerals, cave formation.*

Περίληψη

Με την έρευνα αυτή δίδεται η συστηματική ταξινόμηση τριάντα τριών τύπων σπηλαιοθεμάτων από το σπήλαιο Περάματος Ιωαννίνων, μαζί με την ερμηνεία σχηματισμού τους, σύμφωνα με τη διεθνή βιβλιογραφία, για πρώτη φορά στην Ελλάδα. Η λεπτομερής μελέτη των σπηλαιοθεμάτων σε συνδυασμό με παρατηρήσεις αναφορικά με τον τρόπο και τη θέση σχηματισμού συγκεκριμένων ομάδων σπηλαιοθεμάτων μας οδήγησαν να προτείνουμε την εξέλιξη του σπηλαίου Περάματος μέσω μιας σειράς διαδοχικών επεισοδίων, τα οποία συμπεριλαμβάνουν τη διάλυση των Σενώνιων ασβεστόλιθων, την κατάρρευση της οροφής του σπηλαίου, καθώς και εναλλασσόμενα επεισόδια σχηματισμού σπηλαιοθεμάτων σταλακτιτικού και σταλαγμιτικού τύπου με εκτεταμένες ροές νερού ή/και πλημμύρες, οι οποίες οδήγησαν στην ανάπτυξη μορφών ροής.
Λέξεις κλειδιά: *ονοματολογία σπηλαιοθεμάτων, ανθρακικά ορυκτά, σχηματισμός σπηλαίων.*

1. Introduction

Although caves represent popular and attractive geological formations, the exact mechanism for the development of speleothems in most cases, is not fully known. Greece has some of the prettiest caves of the world but a systematic classification, according to international standard descriptions (e.g. Hicks, 1950; Cabrol, 1974; Renault, 1976; Hill and Forti, 1997; Charles and Hill, 2003; Fairchild and Baker, 2012) is lacking. Eight types of caves are recognized according to their

mechanism of formation. The most common type includes the solutional caves, which are typically formed from karstic weathering of limestones (Galdenzi, 2012). In this case, atmospheric CO_2 reacts with rainwater producing the weak carbonic acid, which subsequently reacts with limestones leading to their karst weathering (Moore, 1962). During the water-filled stage, variable void spaces appear whereas speleothems form subsequently, when $CaCO_3$ precipitates from the supersaturated fluid, due to decrease of P_{CO2}, in the air-filled stage (Fairchild and Baker, 2012). The Perama cave is a solutional cave that has been accidentally discovered during the Second World War and first described thoroughly by Petrocheilou (1952). The scope of this study is to describe, classify and explain the formation of the speleothems from Perama Cave, according to international standards for the first time in Greece, pointing towards the interpretation of its development.

2. Geological Setting

The Perama Cave occurring in the interior of the Goritsa hill, Ioannina, is hosted in brecciated, Senonian limestones that overlie the Vigla Limestone, of the Ionian Zone (Figure 1). The Ionian Zone in western Greece is characterized by evaporitic formations at its base and a subsequent, continuous, carbonate sedimentation from Triassic to Cretaceous (Aubouin and Dercourt, 1962; Thiebault, 1982; Mountrakis, 1987). The Perama cave is located close to the north shores of the Pamvotis Lake, whose water surface apparently controls the aquifer of the broad area.

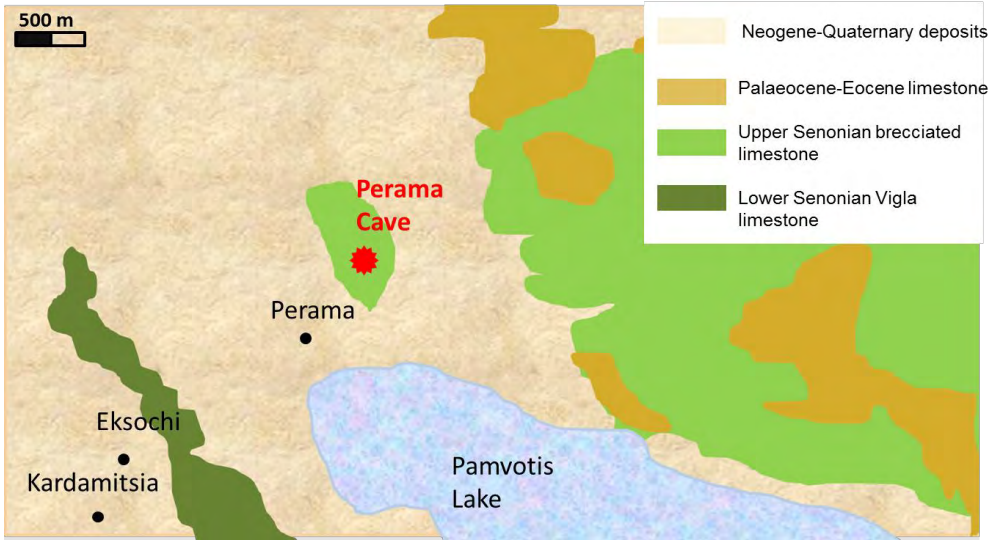

Figure 1 – Simplified geological map of the area around the Perama Cave (modified after IGME 1967).

3. Description of the Speleothems

Thirty three different speleothem types were recognized during this investigation and have been described and classified according to Hill and Forti (1997) and Fairchild and Baker (2012) and references therein; their description below is given in order of decreasing appearance in the Perama cave while photographs of representative types are illustrated:

Flowstones are laminar deposits covering the walls and the floor of the cave (Figure 2A). They arise through deposition of calcite over these surfaces and may adopt a wide variety of shapes, from thin layers to thicker ones. Flowstone masses are often fluted with draperies at their lower end. *Shelfstones* comprise ledges grown from speleothems dipped in pools, at the air/water interface, thus comprising a great indicator of past pool levels (Figure 2B). Calcite commonly

precipitates on top of cave pools, hence its deposition continues to add growth laterally and underneath the dipped speleothem. *Soda straws* comprise deposition of calcite on the roof of the cave and are characterized by their cylindrical shape (Figure 2C). They grow downwards until a detrital grain blocks or a calcite grain develops in such a way that obstructs the water drip. *Soda straws with coralloids*, have a soda straw core covered with coralloids (for a description see below) due to the fact that the initial soda straws were sunk in water for a long period (Figure 2D). These types are frequently formed on pre-existing speleothems like columns with shelfstones. *Stalagmites* are observed as floor formations that built up by water dripping, derived either from roof speleothems or directly from roof joints, above it. Unlike stalactites, they grow upwards forming massive calcite mounds (Figure 2E); they lack soda straw interiors. *Stalactites*, one of the most well-known speleothems, are recognized due to their conical form evolving downwards, ranging in size from few centimeters to several meters (Figure 2F). They are developed after water dripping in a soda straw is prevented, as described above. Then, water overflows from the base of the cone resulting in a nearly conical thickening, due calcite deposition sideways the soda straw; typically their interiors contain soda straw reminiscents. In some stalactites, black stained soda straw interiors are most likely due to the presence of organic material, perhaps related to microbial activity (Jones, 2010). *Coralloids* comprise calcite nodules with concentric, botryoidal structure, concentrating in small aggregates (Figure 2G). Some of them show tiny branch-shape terminations. They have no central duct and their colors vary from yellowish white to dark brown, due to the presence of impurities. Coralloids of subaqueous origin display smooth, rounded surface, unlike corraloids that have been formed in a subaerial environment; their underwater formation is also implied from coexisting formations that form in a subaqueous environment. Subaqueous coralloids predominate in the Perama cave whereas fewer subaerial coralloids are observed. *Bottlebrushes* comprise composite speleothems which are composed of a stalactite interior covered by coralloid formations (Figure 2H). They are formed when stalactites are immersed for a long period in cave pools, as it is also implied from coexisting subaqueous speleothems like coralloids. As a consequence of supersaturation of the pool water in $CaCO_3$, stalactite is firstly coated with spar calcite while after a long period it is covered by coralloids. *Microgours* are tiny rimstone dams usually found on flowstone and resemble wrinkles or ripple marks (Figure 2I). Commonly, coralloids have been formed in their inner parts. *Rimstone dams* are floor barriers that prevent flow of streams, hence forming shallow pools in the Perama cave (Figure 2J). They are normally composed of calcite, which grows under running water and its height is more increased in steeper areas. *Lotus rimstones* refer to a subtype of rimstone dams with a circular to convoluted shape resembling that of water lilies/lotus (Figure 3A). They usually coexist with the previous type and are grown locally or in a larger scale. *Columns* are formed by the coalescence of stalagmites and stalactites (Figure 3B). In places, large collapsed blocks of rocks are covered by flowstones, which have reached the cave roof, may be considered as another subtype of columns. *Draperies* are deposited from calcite-laden solutions flowing along an inclined ($\approx 45^{o}$), overhung surface leaving calcite trails. These initial trails become the preferential routes for continued flow giving rise to the delicate sheets (Figure 3C). *Volcano cones* are found in pools with stagnant water. Their shape resembles truncated cone with a concave, crater-like top (Figure 3D). They grow up vertically like stalagmites from a submerged floor, by water dripping into the pools. *Punched speleothems (also known as bottles)* are very similar to the volcano cones, however their crater-like top is assigned either to drops of low pH water that dissolves their top or to high mechanical energy of the water drops that impact on a stalagmite's surface (Figure 3E). Measurements of pH of the water in the Perama cave revealed that it is neutral to mildly alkaline, therefore the possibility that the punched speleothems formed due to acid water is less likely. *Splattermites* are platy, upright protrusions growing around a central axis fed by rings of drip splash that rebound from the formation's growing tip (Figure 3F). Splattermites tend to form within tall cave chambers, from very rapid calcite deposition, where ceiling drops build up lots of speed and "bounce potential". Their final form resembles that of a cactus. *Boxwork* consists of a mesh network of thin blades of crystalline material protruding along joints of the roof bedrock. It is particularly present in brecciated zones, where the joints act as conduits of the water (Figure

3G). *Coral pipes* are thin pipe-like structures, which form in a shallow pool environment. Their height is less than 10cm and form clusters spaced a few cm apart. *Paraschute shields or Jelly-fishes (Meduses)* comprise a subtype of flowstone, which are exclusively present in the biggest hall of the Perama cave. They form voluminous formations occurring as isolated hangings from the cave roof. An initial shield forms on the roof of the cave, from water running through cracks, which subsequently is covered by flowstone giving its characteristic shape (Figure 3H). *Helictites and Heligmite*s are delicate and fragile speleothems whose growth seems to defy gravity, formed exclusively inside cave passages that are protected from air-currents, temperature fluctuations, animal activities etc. and away from the touristic route. They can be filiform, rosary, vermiform or branching. In analogy to stalactites and stalagmatites, helictites and heligmites are formed on the roof (and wall) and on the floor (and over other speleothems), respectively (Figure 3I). *Deflected stalactites* are unusual types that show downwards growth, which however, decline from the vertical position (Figure 3J). Although their growth mechanism is not well understood yet, it is proposed that their curved shapes are due to air currents. *Speleogens* comprise erosional structures due to dissolution of bedrock, forming typical voids on it. Usually, it is reported that they occur on the bedrock of speleothem-free caves. However, this type has been rarely seen on the bedrock of the Perama cave whilst more commonly is observed on older speleothems forming typical cavities (Figure 4A). *Moonmilk* is a white paste-like deposit on older speleothems or on the wall and floor of the cave (Figure 4B). It is typically located near the entrance of the Perama cave, in the twilight zone, and it is composed of a variety of carbonate minerals, mainly hydromagnesite, nesquehonite and huntite. Their genesis is probably related to the action of micro-organisms living in the cave, which are thought to be involved in the breakdown of calcite of the older speleothem. *Crusts* comprise encrustations covering locally the walls, the ceilings and sediments within the Perama Cave (Figure 4C). They are composed primarily of a variety of carbonate minerals where calcite predominates. *Pearls* are concentric, ooid concretions, resembling oolites observed in shallow cave pools (Figure 4D). They usually form from deposition of calcite layers around a nucleus of whatever origin. Their typical round shape is due to the uniform growth of the pearl and not to any sort of rotation due to dripping. This can be explained as the sphere allows the greatest amount of deposition for the smallest surface area and is thus most likely, even if the nucleus is highly irregular. *Turnips*, are stalactite-type speleothems having a bulbous (welt-like) shape and an additional soda straw end beneath. *Orange sticks* include helictites or aragonite flowers of which the free extremities are wrapped in little white tufts of a porous consistency. Their formation is probably attributed to the deposition of magnesium salts on moonmilk type formations. *Rafts* are thin, sheet-like deposits that have been rarely observed on the surface of water of the cave pools. Their formation is assigned to spreading of a calcite crust on the surface of water, when $CaCO_3$-rich water-drops fall on pool surfaces. The periodic change of water level does not allow the extensive growth of these delicate formations. *Soda straw columns with welt* are composite speleothems that have formed from planar excrescences growth along fractures of soda straw columns; their formation is likely only if cracks open very slowly. *Christmas tree* is a composite frostwork stalagmite, constituting mainly of aragonite outlying a form which has spiny limbs like a fir tree. *Rootsicles* are found near the entrance of the cave, along with moonmilk, where the cave roof is rather thin, therefore plant roots extending downwards in a quest for water, appear in the cave interior (Figure 4E). In most cases, they have been coated with calcite, and essentially have been fossilized. The *Cross stalagmite*, is an extremely rare speleothem type, which has been first reported in Perama cave by Petrocheilou (1952) and comprises one of the most attractive shows of the cave. To our knowledge, a similar speleothem has also been reported only in the Grand Roc cave, Dordogne, France (http://www.geolocation.ws/v/W/File%3AGrotte%20du%20Grand%20Roc%20%20Stalagmite%_20en%20croix%20-%2020090923.jpg/-/en). Obviously, it has a cross shape and despite the fact that it is referred only one individual of this type, during our investigation we have discovered other two similar formations outside the touristic route (Figure 4F). Its formation is interpreted to be the result of a broken piece of stalactite that remained on a vertical position on a stalagmite rough top, perhaps with the assistance of mud. As stalagmite growth persisted, calcite deposition covered the fallen fragment.

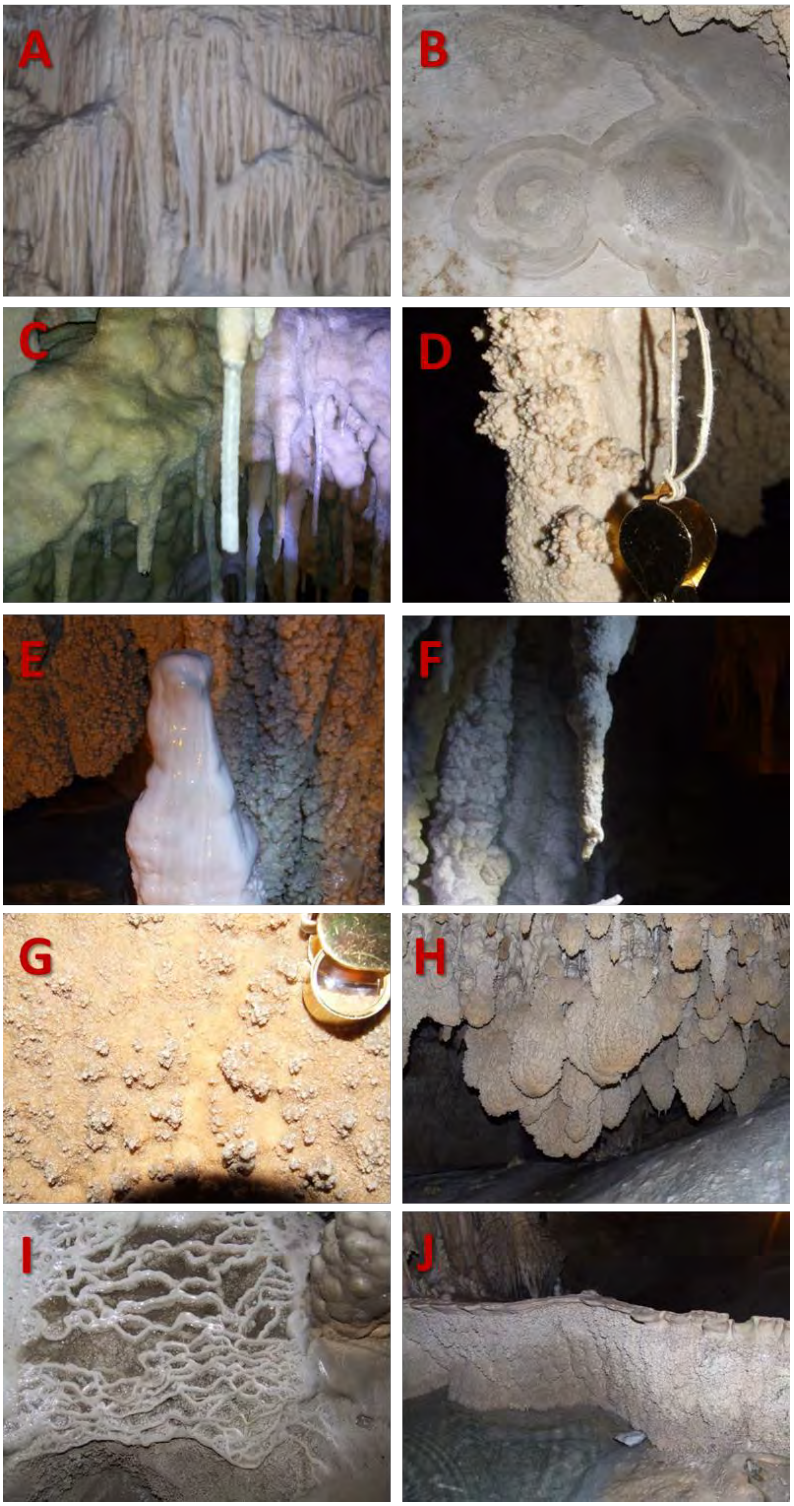

Figure 2 - Speleothem types observed in the Perama cave: A) Flowstone, B) Shelfstones, C) Soda straws, D) Soda straw with coralloids, E) Stalagmite, F) Stalactite, G) Coralloids, H) Bottlebrushes, I) Microgours, J) Rimstone dam.

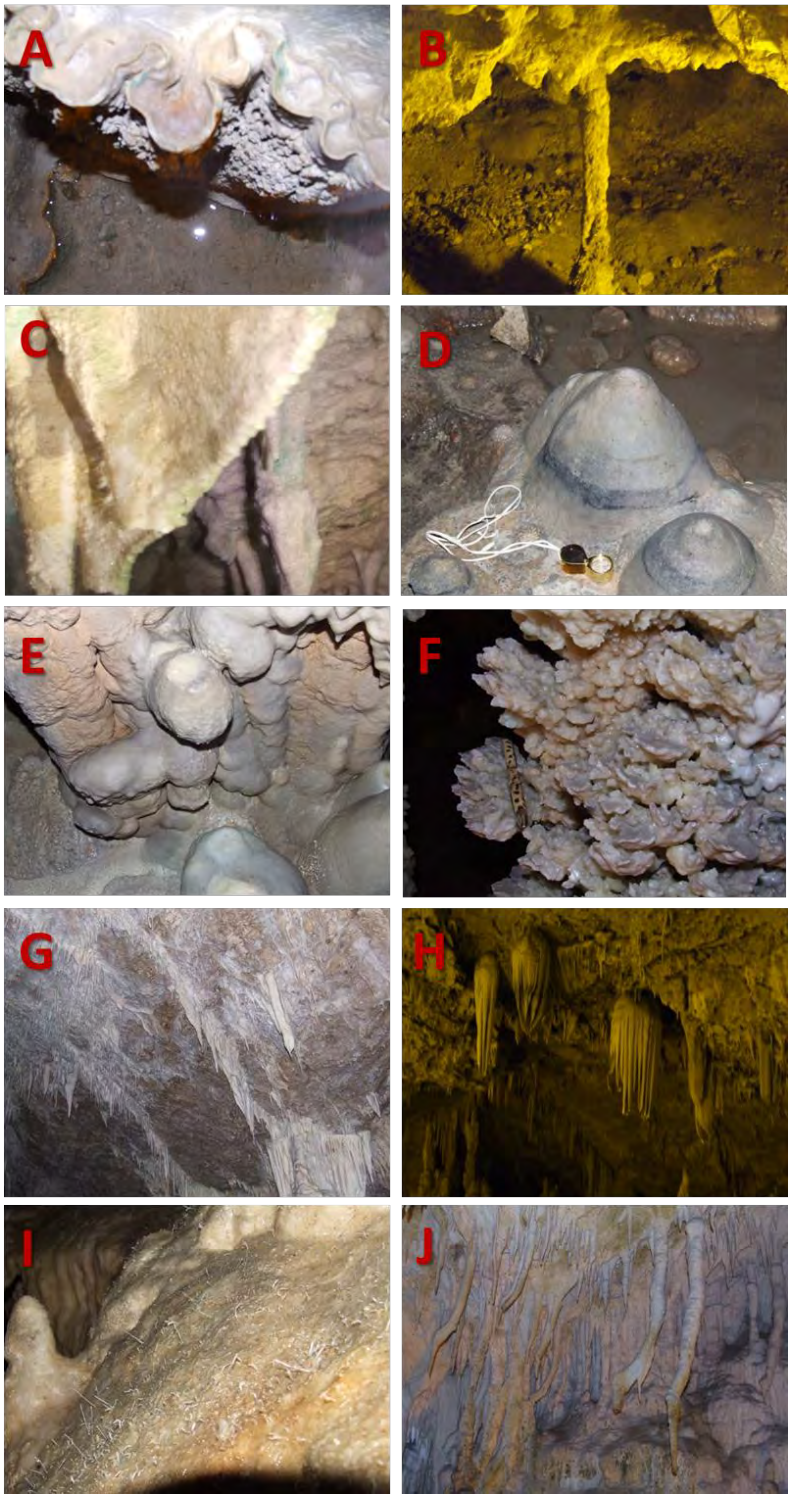

Figure 3 - Speleothem types observed in the Perama cave: A) Lotus rimstones, B) Columns, C) Draperies, D) Volcano cones, E) Punched speleothems, F) Splattermite, G) Boxwork, H) Paraschute shields, I) Heligmites, J) Deflected stalactites.

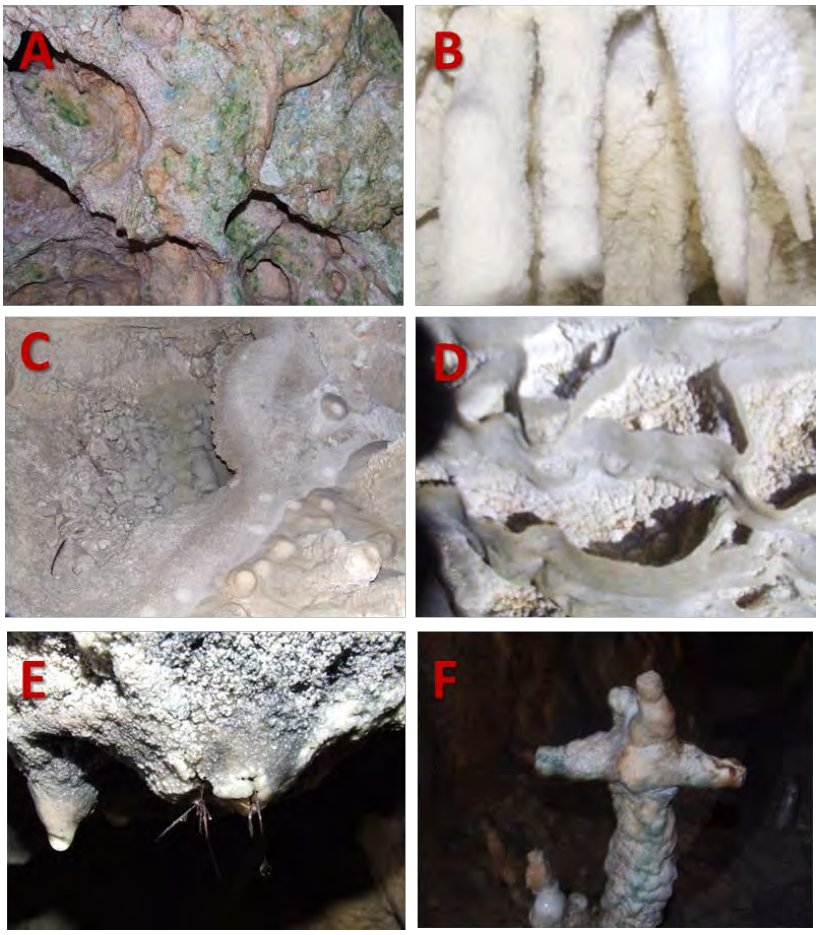

Figure 4 – Speleothem types observed in the Perama cave: A) Speleogens, B) Moonmilk, C) Crusts, D) Pearls, E) Rootsicles, F) Cross stalagmite.

4. Discussion

4.1 Evolution of Speleothems

In this work, the speleothems from the Perama cave are classified into five main categories, on the basis of their main mechanism of formation. Stalactitic-type speleothems are found on cave roofs and formed by dripping water. As the water drop falls down, the dissolved in water CO_2 escapes in the atmosphere of the cave, hence P_{CO2} in the fluid along with the solubility of $CaCO_3$ content decrease, leading to its precipitation. Continuous calcite precipitation is always preceded by the formation of a soda straw, which is the core of all stalactitic-type speleothems, such as soda straws with corals, soda straws with welts, stalactites and turnips. Air currents may affect calcite deposition, forming the deflected stalactites. Another composite variety of the stalactitic-type speleothems are the bottlebrushes, which initially formed subaerially, like typical stalactites, and subsequently their surface covered by subaqueous poolspar or corralloids, when the cave flooded again. Stalagmitic-type speleothems are products of calcite deposition on a surface, ordinarily on the cave floor. The distance of the dripping spot, various flooding and tectonic episodes led to the formation of a large variety of stalagmitic-type speleothems, such as common stalagmites, coral pipes, splattermites, volcano cones, punched stalagmites and cross stalagmites. The Christmas tree is stalagmitic-type speleothem, which has an aragonitic core formed in a first stage, while in a

second stage calcite covered the surface of the aragonitic frostwork, giving the speleothem its final shape. Stream formations are very common in the Perama cave including flowstones, draperies and crusts that developed through calcite precipitation on layers, when water run on an uneven surface. Rimstone dams formed when calcite deposited on inclined surfaces, where the water locally acquired a zero mechanical energy. If this process happens on an existing flowstone, microgours appear. On the contrary, when calcite deposition occurs due to the combined action of water flow and dripping, then the speleothem shape is more circular creating lotus rimstones. Pool speleothems were generated into cave pools, leading to the formation of more botryoidal speleothems with smooth surfaces like coralloids, and pearls. Rafts and flowstone developed on the water/air interface due to CO_2 escape during light rippling. Shelfstones created a thin crust that covered the pools planes. The last category, unclassified speleothems includes all other speleothems that do not fit in the previous categories, such as columns, helictites, heligmites, boxwork, moonmilk, rootsicles and speleogens, which usually involve very complex growth mechanisms, perhaps except columns.

4.2 Evolution of the Perama Cave

Several speleogenetic episodes have been implicated in the evolution of the Perama cave. Superposition of younger speleothems over older ones, referred as coras (Charles and Hill, 2003), is frequent and must not be misinterpreted as a single formation. Careful observations of the complex speleothem layers that occur in the Perama cave enabled us to unravel the sequence of the processes that took place during its development. Firstly, some stalactitic- and stalagmitic-types speleothems had an extended growth, in places leading to formations of columns. A tectonic event of unknown age most likely affected the cave by causing significant collapse of its roof and rupturing of the existing speleothems. This is particularly evident in the central part of the cave, which is poor of speleothems. A period with vast quantities of flowing water led mainly to the development of stream formations, so that flowstones covered the collapsed rock blocks along with the largest part of the cave. A new episode of stalactitic- and stalagmitic-types formation is implied by the superposition of new speleothems of these types over older ones. A later major flooding episode has affected the western part of cave as it is implicated by the growth of subaqueous formations over older speleothems. Such This event is followed by a stage of large water flow, which covers all the previous speleothems. Nowdays, the Perama cave is still very active with several growth mechanisms in operation, but water dripping and flowing are mostly dominant.

5. Conclusions

The Perama cave has a large variety of speleothems, which have been recognized, classified and categorized in certain types. It contains at least thirty three different speleothem types, which reveal the sequential episodes that involved in its development. The Perama cave developed through multiple events whose initial formation from the dissolution of Senonian limestone (water-filled stage) was followed by various air-filled (or semi air-filled) stages that formed the marvelous and complex decoration in its interior. This new entry to the Greek bibliography is intended to act as a guide for further study of the evolution of Greek caves and their speleothems, as well as to provide complementary information for geotouristic purposes. Due to the fact that limestone outcrops are very extensive in Greece, and so are the caves, the geologists, the speleologists, the cave-funs and the speleological societies can be offered a database of speleothem types and formations.

6. Acknowledgments

The senior author expresses her gratitude to the Onassis Foundation for financial support through a scholarship for postgraduate studies. The authors are grateful to Konstantinos Gogos, President of the Organization of Perama Cave for his kind assistance during our investigation. We greatly

appreciate the support of Ephoreia of Palaeoanthropology – Speleology of North Greece for providing the license to investigate the cave. Thoughtful reviews by Dr. E. Dotsika and Dr. D. Moraetis are gratefully acknowledged.

7. References

Aubouin J. and Dercourt J. 1962. Zone Preapulliene zone Ionienne et zone du Gavrovo en Peloponnese occidentale, *Bulletin de Société Géologique de la France*, 4, 785 – 794.

Cabrol P. 1974. Complement d'information sur le presence et le fonctionnement de disques de calcite dans un reseau karstique, *Bulletin Fédération Tamaise de Spéléo-Archéologie, "Travaux de Recherches"*, 11, 1-7.

Charles A.S. and Hill C.A. 2003. How speleothems grow: An introduction to the ontogeny of cave minerals, *Journal of Cave and Karst Studies*, 65, 130-151.

Fairchild I.J. and Baker A. 2012. *Speleothem Science. From Process to Past Environment*, Wiley-Blackwell, 416 pp.

Galdenzi S. 2012. Corrosion of limestone tablets in sulfidic ground-water: measurements and speleogenetic implications, *International Journal of Speleology*, 41, 149-159.

Hicks F.L. 1950. Formation and mineralogy of stalactites and stalagmites, *National Speleological Society Bulletin*, 12, 63-72.

Hill C.A. and Forti P. 1997. *Cave minerals of the world*, Second edition, National Speleological Society, 463 pp.

IGME 1967. *Geological map of Greece, Ioannina sheet*, IGME, Athens.

Jones B. 2010. Microbes in caves: agents of calcite corrosion and precipitation. In Pedley, H.M., Rogerson, M., eds., *Tufas and Speleothems: Unravelling the Microbial and Physical Controls*, Geological Society of London, Special Publications 336, 7-30, doi: 10.1144/SP336.2.

Moore G.W. 1962. The growth of stalactites, *National Speleological Society Bulletin*, 24, 95-106.

Mountrakis D.1987. *Geology of Greece*, Thessaloniki, University Publications, 257 pp. (in Greek).

Petrocheilou A. 1952. Caves in Epirus, *Bulletin of the Speleological Society of Greece*, 1, 262-316 (in Greek).

Renault P. 1976. Les concretions en disque, *Spelunca*, 16, 55-60.

Thiebault F. 1982. Evolution geodynamique des Hellenides externs en Peloponnese meridional (Grece), *Société Géologique du Nord*, 6, 1–574.

Δελτίο της Ελληνικής Γεωλογικής Εταιρίας, τομ. XLVII , 2013
Πρακτικά 13ου Διεθνούς Συνεδρίου, Χανιά, Σεπτ. 2013

Bulletin of the Geological Society of Greece, vol. XLVII 2013
Proceedings of the 13th International Congress, Chania, Sept. 2013

LANDFORM CLASSIFICATION USING GIS TECHNIQUES. THE CASE OF KIMI MUNICIPALITY AREA, EUBOEA ISLAND, GREECE

Ilia I.[1], Rozos D.[1] and Koumantakis I.[1]

[1] National University of Athens, School of Mining and Metallurgical Engineering, Department of Geological Studies, Laboratory of Engineering Geology and Hydrogeology, Iroon Polytechneiou, 15780, Zografou, Greece, gilia@metal.ntua.gr, rozos@metal.ntua.gr, koumantakisioannis@gmail.com.

Abstract

The main objective of this paper is to classify landforms in Kimi municipality area of Euboea Island, Greece using advanced spatial techniques. Landform categories were determined by conducting morphometric analysis through the use of advanced GIS functions. In particular, the process of classifying the landscape into landform categories was based on Topographic Position Index (TPI).

The main topographic elements such as slope inclination, aspect, slope shape (curvature), topographic wetness index and stream power index were obtained from the DEM file of the study area. Landform classification was obtained using TPI grids and the classes were related with the geological pattern and the land cover by sophisticated spatial analysis function.

The knowledge obtained from the present study could be useful in identifying areas prone to land degradation and instability problems in which landforms are identified as an essential parameter.

Key words: *Landforms, morphometric analysis, TPI, DEM, Kimi Euboea.*

Περίληψη

Ο κύριος στόχος της παρούσας εργασίας είναι η ταξινόμηση των γεωμορφών στην περιοχή της Κύμης Εύβοιας, με τη χρήση προηγμένων τεχνικών χωρικής ανάλυσης. Οι γεωμορφές προσδιορίστηκαν με την μορφομετρική ανάλυση χρησιμοποιώντας τις προηγμένες λειτουργίες των Γεωγραφικών Πληροφοριακών Συστημάτων. Ειδικότερα, η διαδικασία ταξινόμησης των γεωμορφών σε κατηγορίες βασίστηκε στον υπολογισμό του Τοπογραφικού Δείκτη εντοπισμού (Topographic Position Index, TPI). Τα κύρια τοπογραφικά στοιχεία, όπως οι κλίσεις, η διεύθυνση μορφολογικών κλίσεων, η καμπυλότητα καθώς και οι Τοπογραφικοί Δείκτες ύγρανσης (Topographic Wetness Index, TWI) και Ορμητικότητας ρεμάτων (Stream Power Index, SPI), προέκυψαν χρησιμοποιώντας το Ψηφιακό Υπόβαθρο Εδάφους (DEM) της περιοχής μελέτης. Οι κατηγορίες των γεωμορφών που προέκυψαν συσχετίστηκαν με τις κατηγορίες των χρήσεων γης και τις λιθολογικές ενότητες της περιοχής έρευνας.

Η γνώση που προκύπτει από την παρούσα μελέτη μπορεί να αποτελέσει χρήσιμο εργαλείο στον εντοπισμό περιοχών επιρρεπών σε προβλήματα αστοχιών, στα οποία η κατηγοριοποίηση των γεωμορφών διαδραματίζει ουσιαστικό ρόλο.

Λέξεις κλειδιά: *Γεωμορφές, μορφομετρική ανάλυση, Τοπογραφικός Δείκτης Θέσης, Ψηφιακό Μοντέλο Εδάφους, Κύμη Εύβοια.*

1. Introduction

The knowledge of the extension and distribution of the landforms, either complex such as ridges, hills and mountains or simple such as highly productive plains and valleys, is very important (Lindenmayer et al, 2006). Currently, there are several researches available which are aimed to the determination and classification of the landforms by using automatic or semiautomatic algorithms (Dehn et al., 2001; Shary et al., 2002; Schmidt et al., 2004; Bolongaro-Crevenna et al, 2005; Jordan et al., 2005; Dragut et al., 2006; Prima et al., 2006; Minár and Evans, 2008, Batuk et al., 2008, Tagil & Jennesse, 2008, Gercek, 2010).

From a geological and engineering geological point of view, landforms are of specific interest as they were created by geological processes (Karsten et al., 2009). Landforms that develop upon a particular kind of bedrock are related to its structural features such as bedding planes, joints, folds and faults and to its mineralogical composition. In terrain developed upon faulted and eroded sedimentary rocks, there is a strong relationship between rock type, structure, and the ensuing topography. Rock structure determines both major landforms and details of the landscape. Therefore, it is of great significance to determine landform categories and to relate them with geological aspects, land cover and landform classes in a landscape developed or affected by human activities. The existing landforms play a significant role in identifying areas prone to land degradation and instability. Geomorphometry provides a quantitative description of the shapes of landforms and is derived using a combination of mathematics, engineering and computer science (Tagil & Jennesse, 2008). The possibility of recognizing basic geomorphological features using Digital Elevation Models and Geographic Information Systems Techniques is examined by Gioti (2010) in the area of Antiparos Island, Aegean Sea. Adediran et al. (2004) also demonstrated the ability of the delineated landform elements to be overlaid on any digital map and imagery for further applied research using the application of GIS and multivariate statistical analysis in the area of Crete Island, Greece. In the past, geomorhometric properties were measured calculating the geometry of the relative position with a landform (Blaszczynski, 1997). The field was revolutionized by the computer manipulation of spatial arrays of terrain heights, or digital elevation models (DEMs), which can quantify and depict ground-surface form over large areas (Maune, 2001). Morphometric procedures are routinely implemented by commercial geographic information systems (GIS) and specialized software (Harvey and Eash, 1996; ESRI, 1997; Dikau and Saurer, 1999; Wilson and Gallant, 2000; Guth, 2001).

In this paper, landform categories were determined by conducting geomorphometric analysis through the use of advanced GIS functions, obtaining several topographic gradients from the DEM file of the Kimi area in, Euboea, Greece. These gradients were related with the geological pattern, the land cover and the landform classes by sophisticated spatial analysis function.

2. Materials and Methods

2.1. Geological Settings

Euboea is the second largest island of Greece and the third largest island of the Eastern Mediterranean sea. It is located eastern of Attica, along the eastern coast of continental Greece (Figure 1). Geologically speaking, in Euboea Island outcrop three tectonic units, the 'Pelagonian Unit', the 'South Euboea Blueschist Belt' and under these units, the 'Almyropotamos Unit' (Aubuin, 1957, Katsikatsos et al. 1986, Katsikatsos, 1991, Shaked et al. 2000). As presented in previous studies (Koumantakis et al, 2008, Ilia et al, 2008, Rozos et al., 2009, Ilia et al., 2010, Tsangaratos et al., 2011), the lithological formations that consist the wide research area are listed as follows (Figure 2):

- Quaternary deposits, which include bed river deposits, debris, fluviatile terraces and dilluvial depositions.

- Neogene sediments that consist of, calcareous and clayey marls with conglomerate intercalations, as well as base conglomerate.
- Volcanic rocks presented in the south - eastern part of Kimi with dacides - andesites.
- Flysch formation consists of clayey sales, sandstones, conglomerates and limestones.
- Ultrabasic rocks consist of peridotites, dounites and at places serpentinites.
- Carbonate formations usually Mesozoic limestones, and at some places, Palaiozoic ones.
- Granites are outcrop in the Western part of Kimi basin, and they are Carboniferous in age.

Figure 1 - Study area of Kimi, Euboea Greece.

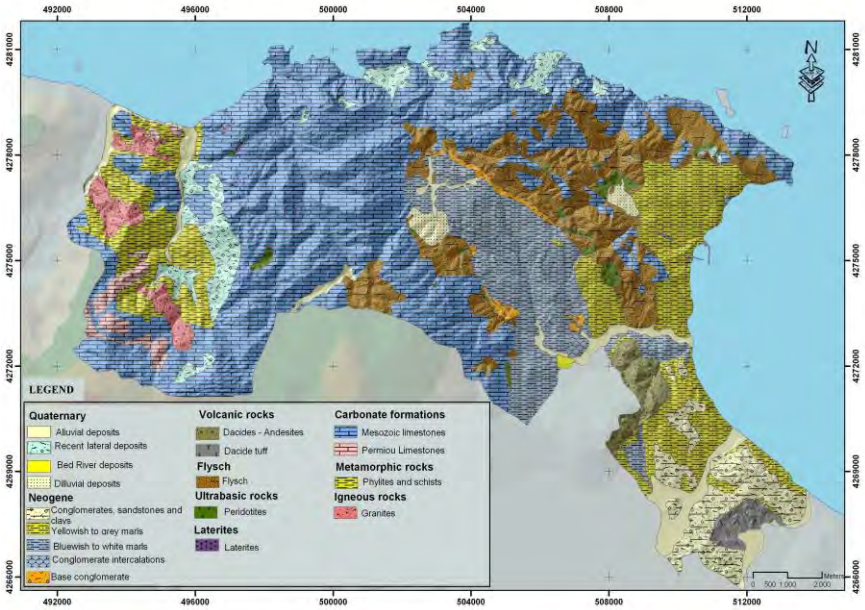

Figure 2 - Geological Map of Kimi Municipality.

2.2. Calculating Topographic Attributes

The methodology applied in the research area of Kimi, Euboea, Greece and uses the GIS techniques of the software programs ArcView 3.1 and ArcGIS 9.3. The analyzed data included the Digital Elevation Model (DEM) of the Ktimatologio S. A. with 5m resolution, a Geological map of the research area at a scale of 1:25000 (Ilia et al., 2008, Ilia et al., 2010) and the Corine Land cover of 2006 (European Environmental Agency, 2006) (Figure 2, 3). The DEM was used in order to compute the topographic parameters of elevation, slope inclination, aspect, curvature, topographic wetness index and stream power index (Figure 4). Slope inclination and aspect maps show the magnitude and direction of the vector tangent to the topographic surface pointing downhill at a point (Tagil and Jennesse, 2008). ESRI functions were used in order to calculate curvature based on the algorithms of Zevenbergen and Thorne (1987). A 3x3 cell neighbourhood represented the curvature of a 5x5 m area. Topographic Wetness and Stream Power Indices were used in order to quantify flow intensity and accumulation potential. Topographic Wetness Index (TWI) is also known as Compound Topographic Index (CTI) or Topographic Moisture Index (TMI). TWI at a particular point of the landscape is the ratio between the catchment area contributing to that point and the slope at that point (Wilson and Gallant, 2000):

Equation 1 – Topographic Wetness Index

$$TWI=ln\ (catchment\ area/tan\beta),$$

where β=slope in radiants. Higher positive values are wetter and lower negative values are drier.

The Stream Power Index (SPI) was calculated as:

Equation 2 – Stream Power Index

$$SPI=catchment\ area x tan\beta,$$

where β=slope in radiants (Moore et al., 1993).

The SPI is closely related to the Topographic Wetness Index and is used in order to estimate the erosive power of the terrain.

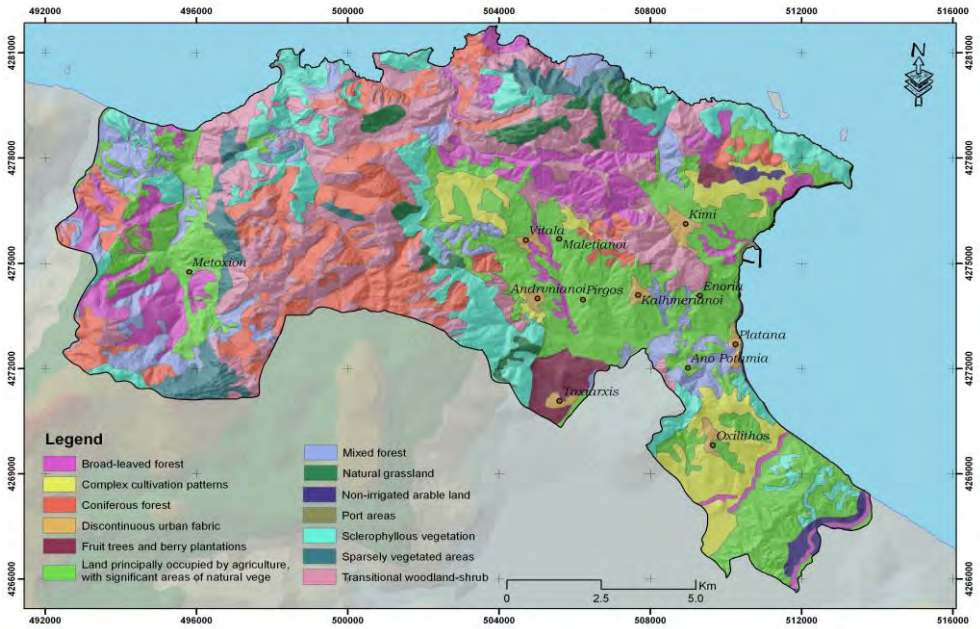

Figure 3 – Land cover classes classified from Corine 2006.

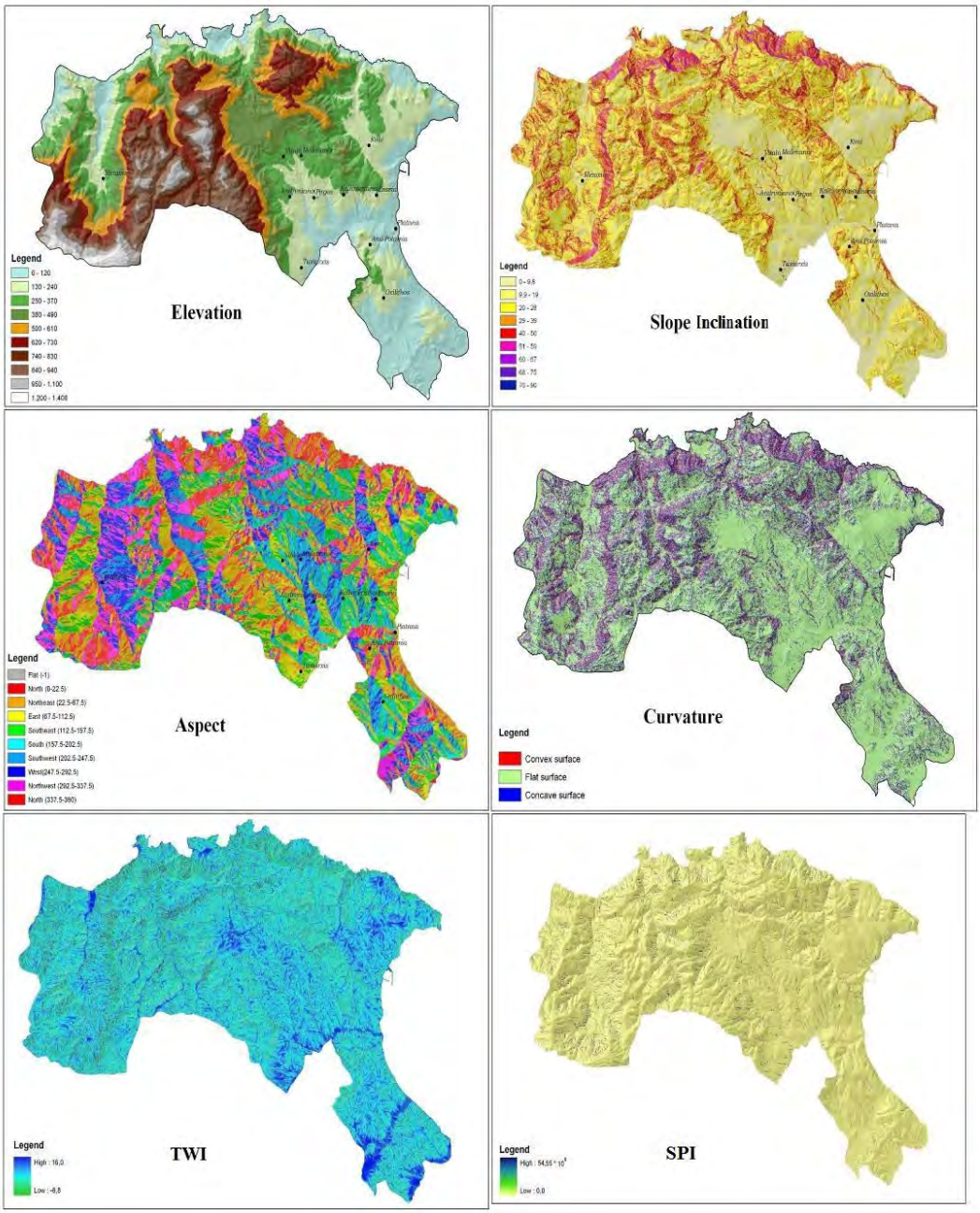

Figure 4 - Topographic attributes: elevation, slope inclination, aspect, curvature, topographic wetness index and stream power index.

2.3. Calculating TPI

Topographic Position Index (TPI) is the difference between the elevation at a cell and the average elevation in a cell surrounding that cell. Local mean elevation is subtracted from the elevation value at centre of the local window. An algorithm is provided as an ESRI script by Jenness Enterprises (Jenness, 2006) and it has local window options, which are rectangular, circular and annulus in shape. Positive TPI values represent locations that are higher than the average of the

local window e.g. ridges. Negative TPI values represent locations that are lower e.g. valleys. TPI values near zero are either flat areas (where the slope is near zero) or areas of constant slope (where the slope of the point is significantly greater than zero), high positive values relate to peaks and ridges (Gercek, 2010).

The neighbourhood size and shape is critical to that analysis and is based on the scale of landscape feature being analyzed. To classify very small features, small neighbourhood is used. To identify large canyons or mountains, we use large neighbourhood (Figure 5).

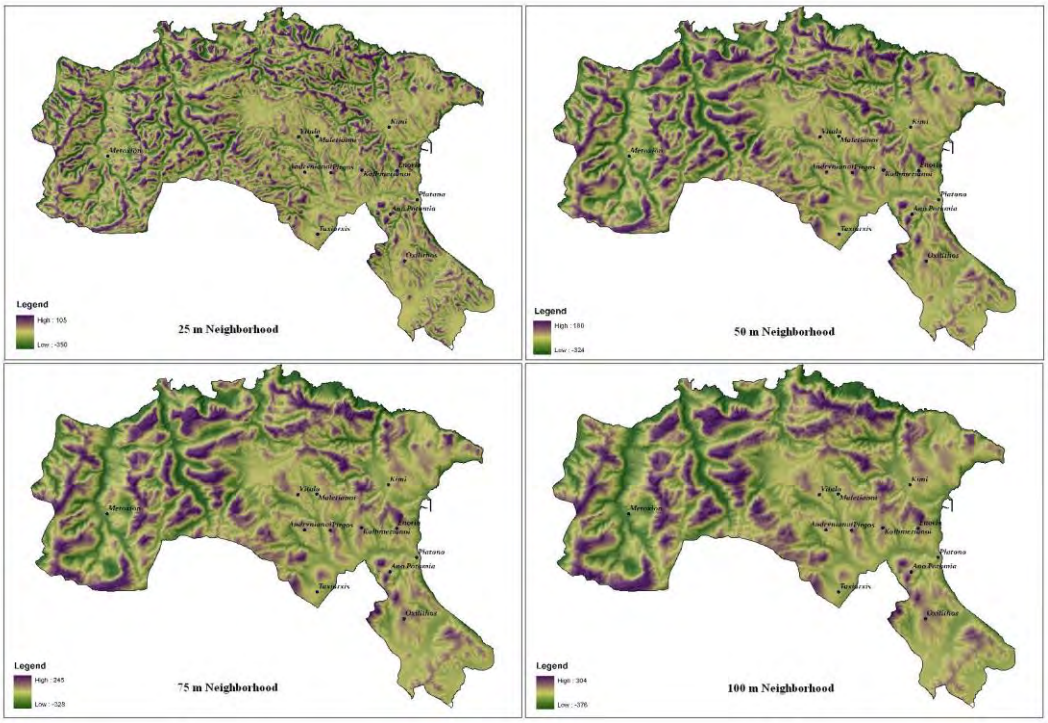

Figure 5 - TPI grids using 4 different neighbourhoods.

2.4. Landforms Classification

TPI values calculated from two neighbourhood sizes provide more information about the general shape of the landscape than the TPI values from a single neighbourhood and therefore, more complex landscape features can be identified by combining TPI grids generated at different scales (Tagil and Jenness, 2008). Combining TPI at a small and large scale allows a variety of nested landforms to be distinguished (Figure 6).

As a general rule, since elevation tends to be spatially auto correlated, the range of TPI values increases with scale. One method to address this problem is to standardize the TPI grids to mean = 0 and stdev = 1. This lets the same basic equations to be used to classify any scale combinations of TPI grids (Weiss, 2001).

In our case, 25 and 100 m grid in combination with slope were used and classified landforms using criteria described by Weiss (2001). The high and low TPI values were distinguished by setting a threshold of ±1 SD, (SD, standard deviation). A full description of each morphological classification is described by Weiss (2001) and Jenness (2006).

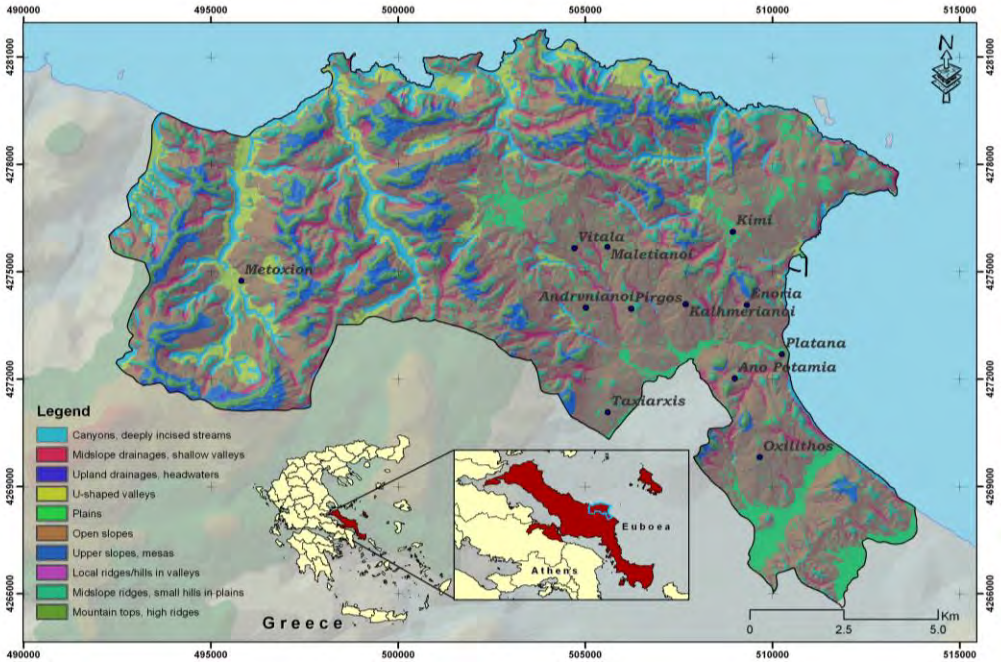

Figure 6 - Landforms using Weiss (2001) classes based on 25 m neighbourhood.

3. Results and Discussion

In Figure 7, the percentage of each landform class that covers the research area is provided. Furthermore, the ground truthing was verified by field surveys. The figure shows that the ~54% of the study area is classified as Open slopes, followed by Upper slopes (~7.3%), Mountain tops, high ridges (~7.2%), Canyons and deeply incised streams (~6.9%) and the other landform classes in smaller percentages. This is attributed to the fact that the area is intersected by several rivers.

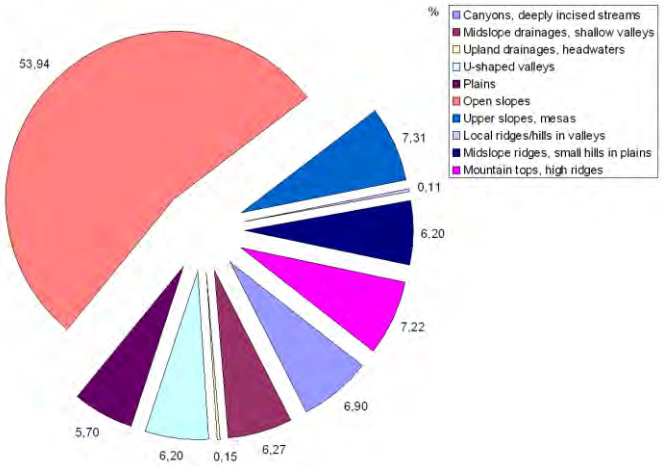

Figure 7 - Landforms using Weiss (2001) classes based on 25 m neighbourhood.

In Tables 1 and 2, the land cover and the lithological units were related with the landform classes, while in Table 3 it is presented the proportion of the lithological units in each landform class.

More specifically, as seen in Table 1, canyons and deeply incised streams (L1) appear to be covered by forest and Transitional woodland-shrub (69.86%), plains and open slopes (L5 and L6)

are covered by land principally occupied by agriculture, with significant areas of natural vegetation (37.28 % and 31.72 % respectively) while upper slopes, mesas (L7), local ridges/hills in valleys (L8), midslope ridges, small hills in plains (L9) and mountain tops, high ridges (L10) appear mostly in transitional woodland-shrub (30.82 %, 36.82 %, 27.62 %, 35.28 % respectively).

Concerning the correlation between the lithological units and the landform classes (Tables 2, 3), it seems that the Quaternary deposits (alluvial deposits, dilluvial deposits, bed river deposits) appear mostly in plains, the marly formations (conglomerates, sandstones and clays, yellowish to gray and bluish to white marls), flysch formations, philites - schists and peridotites appear mostly in open slopes. These areas are prone to slope instability problems and comprise structurally controlled topography, depending on the resistance to weathering and erosion, factors that are interrelated to the mineralogical composition, the cementation, the bedding planes and joints. The recent lateral deposits appear mostly in U-shaped valleys, since they are broken down relatively rapidly by weathering and produce strongly linear or stepped topography.

Table 1 – Landform classes in relation with land cover units (%).

LandForm classes	C1	C2	C3	C4	C5	C6	C7	C8	C9	C10	C11	C12	C13
Canyons, deeply incised streams (L1)	0.03	0.13	0.00	0.02	0.21	10.29	14.67	18.94	11.89	0.64	14.78	24.36	4.05
Midslope drainages, shallow valleys (L2)	0.30	0.14	0.01	0.44	0.41	9.79	13.76	24.01	12.16	1.13	13.57	19.40	4.89
Upland drainages, headwaters (L3)	0.00	0.00	0.00	0.00	0.00	0.12	8.15	17.55	3.66	0.00	21.41	8.54	40.57
U-shaped valleys (L4)	0.00	0.26	0.00	0.00	0.19	24.28	11.72	12.03	14.05	1.04	11.21	21.54	3.68
Plains (L5)	3.71	0.12	7.98	2.08	25.09	37.28	10.19	2.21	3.18	0.37	3.45	4.00	0.32
Open slopes (L6)	1.93	0.03	0.71	2.77	7.71	31.72	9.85	11.02	7.02	1.53	10.05	13.68	1.99
Upper slopes, mesas (L7)	0.01	0.00	0.00	0.00	0.47	5.44	6.59	17.83	4.52	7.14	17.18	30.82	10.00
Local ridges/hills in valleys (L8)	0.00	0.00	0.00	0.00	0.00	0.11	0.60	11.23	1.42	6.47	23.95	36.82	19.40
Midslope ridges, small hills in plains (L9)	0.40	0.00	0.07	0.32	2.95	16.02	10.53	12.74	7.69	1.82	17.95	27.62	1.90
Mountain tops, high ridges (L10)	0.00	0.00	0.00	0.03	0.26	5.55	5.18	11.88	4.31	8.12	21.21	35.28	8.19

C1: Discontinuous urban fabric, C2: Port areas, C3: Non-irrigated arable land, C4: Fruit trees and berry plantations, C5: Complex cultivation patterns, C6: Land principally occupied by agriculture, with significant areas of natural vege, C7: Broad-leaved forest, C8: Coniferous forest, C9: Mixed forest, C10: Natural grassland, C11: Sclerophyllous vegetation, C12: Transitional woodland-shrub, C13: Sparsely vegetated areas.

Table 2 – Landform classes in relation with lithological units (%).

Landform classes	G1	G2	G3	G4	G5	G6	G7	G8	G9	G10	G11	G12	G13	G14	G15	G16	G17	G18
L1	5.90	4.21	0.00	0.17	0.00	4.3	1.57	0.00	0.40	0.03	0.00	8.41	0.72	0.00	61.93	2.15	6.78	3.42
L2	0.86	0.23	0.00	0.24	1.66	5.3	6.79	0.00	0.27	3.26	0.41	14.97	1.74	0.12	56.07	1.35	4.72	2.02
L3	0.00	0.00	0.00	0.00	0.00	0.00	0.00	0.00	0.00	0.47	0.00	4.29	0.00	0.00	88.10	0.00	2.93	4.22
L4	7.94	8.60	0.00	0.58	0.00	1.48	1.09	0.00	0.50	0.00	0.00	4.50	0.93	0.07	60.27	1.59	8.79	3.67
L5	26.54	0.22	0.97	3.50	6.86	13.5	25.70	0.16	0.83	0.32	2.43	7.78	0.95	0.02	8.82	0.13	0.76	0.48
L6	0.88	0.65	0.06	0.97	6.31	14.3	15.69	0.33	1.03	1.77	1.30	13.62	1.23	0.07	34.29	0.86	5.10	1.49

L7	0.00	0.00	0.00	0.00	2.05	0.27	0.08	0.00	0.00	1.89	0.00	7.11	0.29	0.14	79.53	1.76	5.29	1.60
L8	0.00	0.05	0.00	0.00	0.00	0.00	0.00	0.00	0.00	0.00	0.00	0.27	0.00	0.00	98.74	0.00	0.27	0.66
L9	0.26	0.35	0.00	0.19	5.67	4.25	4.11	0.00	0.28	1.09	0.78	13.87	0.53	0.02	54.87	2.89	7.42	3.42
L10	0.00	0.00	0.00	0.00	0.88	0.13	0.36	0.00	0.00	3.61	0.00	6.90	0.26	0.40	79.51	2.09	4.09	1.76

G1: Alluvial deposits, G2: Recent lateral deposits, G3: Bed River deposits, G4: Dilluvial deposits, G5: Conglomerates, G6: Yellowish to gray to white marls, sandstones and clays, G7: Bluewish to white marls, G8: Conglomerate intercalations, G9: Base conglomerate, G10: Dacides - Andesites, G11: Dacide tuff, G12: Flysch, G13: Peridotites, G14: Laterites , G15: Limestones, G16: Limestones Permiou, G17: Phyllites and Schists, G18: Granites.

Table 3 – Lithological units in relation with landform classes (%).

Lithological units	**L1**	**L2**	**L3**	**L4**	**L5**	**L6**	**L7**	**L8**	**L9**	**L10**
Alluvial deposits (G1)	13.79	1.82	0.00	16.69	51.08	16.07	0.00	0.00	0.54	0.00
Recent lateral deposits (G2)	23.73	1.20	0.00	43.60	1.02	28.68	0.00	0.00	1.76	0.00
Bed River deposits (G3)	0.00	0.00	0.00	0.00	63.91	36.09	0.00	0.00	0.00	0.00
G8: Dilluvial deposits (G4)	1.46	1.86	0.00	4.51	25.04	65.62	0.00	0.00	1.51	0.00
Conglomerates, sandstones and clays (G5)	0.00	2.34	0.00	0.00	8.73	76.28	3.36	0.00	7.87	1.42
Yellowish gray to white marls (G6)	3.12	3.49	0.00	0.96	8.08	81.27	0.21	0.00	2.77	0.10
Bluish to white marls (G7)	1.00	3.93	0.00	0.62	13.51	78.28	0.05	0.00	2.36	0.24
Conglomerate intercalations (G8)	0.00	0.00	0.00	0.00	4.72	95.25	0.00	0.00	0.03	0.00
Base conglomerate (G9)	0.11	12.40	0.04	0.00	1.09	57.99	8.39	0.00	4.11	15.86
Dacides – Andesites (G10)	3.98	2.40	0.00	4.47	6.74	79.88	0.00	0.00	2.53	0.00
Dacide tuff (G11)	0.00	2.81	0.00	0.00	15.18	76.73	0.00	0.00	5.28	0.00
Flysch (G12)	5.06	8.18	0.06	2.43	3.85	64.05	4.54	0.00	7.50	4.34
Peridotites (G13)	4.93	10.79	0.00	5.70	5.37	65.93	2.13	0.00	3.28	1.89
Laterites (G14)	0.32	8.07	0.00	4.76	1.14	43.01	10.55	0.00	1.21	30.94
Limestones (G15)	9.34	7.68	0.29	8.18	1.10	40.46	12.72	0.24	7.44	12.55
Limestones Permiou (G16)	11.77	6.72	0.00	7.84	0.57	36.72	10.20	0.00	14.19	11.98
Phyllites and Schists (G17)	8.91	5.63	0.09	10.38	0.83	52.42	7.37	0.01	8.75	5.62
Granites (G18)	12.53	6.71	0.34	12.07	1.46	42.65	6.20	0.04	11.25	6.75

4. Conclusions

GIS techniques were used in order to classify landscape into landform categories, based on Topographic Position Index (TPI). By this method, morphological types were generated for a semi-automated derivation of landform elements according to Weiss (2001). Digital elevation model (DEM) of the research area was a helpful tool in the effort of recognizing landscape morphological characteristics. This study also shows that DEMs offer many more potential habitat descriptors than simply a set of elevation values. Since landforms were created by geological processes and influenced by the land cover, it is of great significance to classify landforms in terms of understanding the potential and constraints within the landscape associated with them. The classification results can be used in applications related to precision agriculture, land degradation studies and spatial modelling applications, where landform is identified as an influential factor in the processes under study.

5. Acknowledgments

This paper is part of the PhD in progress entitled "Engineering geological features of marls in the wide area of Kimi, Euboea, their impact on construction problems and their treatment". The Authors would like to thank KTIMATOLOGIO S.A. for the supply of the Geospatial Data as well as the ELE of NTUA for the financial supporting of this work.

6. References

Adediran A.O., Parcharidis I., Poscolieric M. and Pavlopoulos K. 2004. Computer-assisted discrimination of morphological units on north-central Crete (Greece) by applying multivariate statistics to local relief gradients, *Geomorphology*, 58, 357–370.

Aubouin J. 1957. Sur la Géologie de la bordure Méridionale de la plaine de Trikkala, *Ann. Geol.des P. Hellen*., 8, Athènes.

Batuk F., Emem O., Gorum T. and Gokasan E. 2008. Implementation of GIS for Landforms of Southern Marmara. TS 7I - GIS Applications in Turkey, *Integrating Generations FIG Working Week 2008*, Stockholm, 14-19 June Sweden.

Blaszczynski J.S. 1997. Landform characterization with geographic information systems. *Photogrammetric Eng. Remote Sens.*, 63 (2), 183-191.

Bolongaro-Crevenna A., Torres-Rodrıguez V., Sorani V., Frame D. and Ortiz M.A. 2005. Geomorphometric analysis for characterizing landforms in Morelos State, Mexico. *Geomorphology*, 67, 407–422.

Dehn M., Gartner H., Dikau R. 2001. Principles of semantic modeling of landform structures. *Computers & Geosciences*, 27, 1005–1010.

Dikau R. and Saurer H. (eds). 1999. GIS for Earth Surface Systems Analysis and Modelling of the Natural Environment, Stuttgart, *Borntraeger*, 197 p.

Dragut L., Blaschke T., 2006. Automated classification of landform elements using objectbased image analysis. *Geomorphology*, 81, 330–344.

Environmental Systems Research Institute (ESRI), Inc., 1997. *Watershed Delineator Application - User's Manual*: Redlands, CA, ESRI, paging unknown.

European Environmental Agency, 2006. CORINE Land Cover, European Environmental Agency, Luxembourg.

Gercek D. 2010. Object - based classification of landforms based on their local geometry and geomorphometric context. *PhD Thesis*. Department of Geodetic and Geographic Information Technologies. Middle East Technical University.

Gioti E. 2010. Detecting basic geomorphological features using Remote Sensed Data and Geographic Information Systems, *Proceedings of the 9th Panhellenic Geographical Conference*, Athens, Greece, 633-641.

Guth P.L. 2001. Quantifying terrain fabric in digital elevation models, in Ehlen, Judy, and Harmon, R.S., eds, The environmental legacy of military operations, *Geological Society of America*. Reviews in Engineering Geology, v. 14, 13-25.

Harvey C.A. and Eash D.A. 1996. Description, instructions, and verification for BASINSOFT, a computer program to quantify drainage-basin characteristics. *U.S. Geological Survey*, Water-Resources Investigations Report, 95-4287, 25 p.

Ilia I., Koumantakis I., Rozos D., Markantonis K. and Tsagaratos P. 2008. Landslide Phenomena in Kimi area, Evia Island, Central Greece, *Geophysical Research Abstracts*, Vol. 10, EGU2008-A-06831, 2008 SRef-ID: 1607-7962/gra/EGU2008-A-06831 EGU General Assembly 2008.

Ilia I., Tsangaratos P., Koumantakis I. and Rozos D. 2010. Application of a Bayesian approach in GIS based model for evaluating landslide susceptibility. Case study Kimi area, Euboea, Greece. Proc. *12nd International Congress of the Geological Sosciety of Greece*.

Jenness J. 2006. Topographic Position Index (TPI) v 1.2. Extension for ArcView 3x. Jenness Enterprices. Available online at web site: http://www.jennessent.com

Jordan G. and Meijninger B.M.L., Van Hinsbergen D.J.J., Meulenkamp J.E. and Van Dijk P.M. 2005. Extraction of morphotectonic features from DEMs: Development and applications for study areas in Hungary and NW Greece, *International Journal of Applied Earth Observation and Geoinformation*, 7, 163–182.

Karsten D., Terralogix Consulting and Willem de Frey 2009. Landform classification using GIS. Ekoinfo, PositionIT, GIS Technical, 30-34.

Katsikatsos G., Mettos A., Vidakis M. and Dounas A. 1986. Geological Map of Greece in scale 1:50.000, "Athina-Elefsis" sheet, I.G.M.E. Publ., Athens.

Katsikatsos G. 1991. Geological map of Greece, Aliveri sheet. I.G.M.E. (Institute of Geology and Mineral Exploration, gen. di. V. Andronopoulos).

Koumantakis I., Rozos D., Markantonis K., Ilia I., Tsagaratos P., 2008. Landslide Phenomena of Kimi Municipality. Research Program founded by the Prefecture of Euboea Island.

Lindenmayer D.B. and Fischer J. 2006. Habitat Fragmentation and Landscape Change An Ecological And Conservation Synthesis. Island Press, USA, 2006.

Maune D.F., (eds), 2001. Digital Elevation Model Technologies and Applications, the DEM Users Manual. Bethesda, MD, American Society for Photogrammetry & Remote Sensing, 540 p.

Minár J., Evans I. S. 2008. Elementary forms for land surface segmentation: The theoretical basis of terrain analysis and geomorphological mapping. *Geomorphology* 95, 236-259.

Moore I.D., Gessler P.E., Nielsen G. A. and Peterson G. A., 1993. Soil attribute prediction using terrain analysis. *Soil Sci. Soc. Am. J*., 57 (2): 443-452.

Prima O., Echigo A., Yokoyama R. and Yoshida T. 2006. Supervised landform classification of Northeast Honshu from DEM-derived thematic maps. Geomorphology 78, 373–385.

Rozos D., Koumantakis I., Ilia I., Markantonis K. and Tsangaratos P. 2009. Urban suitability assessment in the area of Vitala Kimi. Research Program founded by the Prefecture of Euboea Island.

Schmidt J. and Hewitt A. 2004. Fuzzy land element classification from DTMs based on geometry and terrain position. *Geoderma*, 121, 243–256.

Shaked Y., Avigad D., and Garfunkel Z. 2000. Alpine high-pressure metamorphism at the Almyropotamos window (southern Evia, Greece). *Geol. Mag*., 137, 367-380.

Shary P. A., Sharaya L. S., Mitusov A. V., 2002. Fundamental quantitative methods of land surface analysis, *Geoderma*, 107, 1 –32.

Tagil S. and Jenness J., 2008. GIS-Based Automated Landform Classification and Topographic, Landcover and Geologic Attributes of Landforms around the Yazoren Polje, Turkey, *Journal of Applied Sciences* 8 (6): 910-921, ISSN 1812-5654, Asian Network for Scientific Information.

Tsangaratos P., Ilia I., Rozos D. 2011. Case Event System for landslide susceptibility analysis. *Proc. Second World Landslide Forum*, 3-7 October 2011, Rome (in press), 10 pp.

Weiss A. 2001. Topographic position and landforms analysis. Poster presentation, ESRI User Conference. San Diego, CA.

Wilson J.P., and Gallant, J.C., eds. 2000. Terrain analysis-Principles and Applications. Chichester UK & NY, Wiley, 479 p.

Zevenbergen L. W. and Thorne C. R., 1987. Quantitative analysis of land surface topography. Earth Surface Process and Landforms, 12, 47-56.

Δελτίο της Ελληνικής Γεωλογικής Εταιρίας, τομ. XLVII , 2013
Πρακτικά 13ου Διεθνούς Συνεδρίου, Χανιά, Σεπτ. 2013

Bulletin of the Geological Society of Greece, vol. XLVII 2013
Proceedings of the 13th International Congress, Chania, Sept. 2013

RETRIEVAL OF SIMILAR TOPOGRAPHIC AREAS

Kokinou E.[1], Panagiotakis C.[2] and Kinigopoulos Th.[3]

[1] *Technological Educational Institute Crete, Department of Natural Resources & Environment, Chania, Crete, Greece, ekokinou@chania.teicrete.gr*

[2] *Technological Educational Institute Crete, Department of Commerce and Marketing, Ierapetra, Crete, Greece; cpanag@staff.teicrete.gr*

[3] *University of Crete, Department of Computer Science, Heraklion, Crete, Greece; kynigop@csd.uoc.gr*

Abstract

Image processing and understanding and further pattern recognition comprises a precious tool for the automatic extraction of information using digital topography. The aim of this work is the retrieval of areas with similar topography using digital elevation data. It can be applied to geomorphology, forestry, regional and urban planning, and many other applications for analyzing and managing natural resources. In specifics, the user selects the area of interest, navigating overhead a high resolution elevation image and determines two (3) parameters (step, number of local minima and display scale). Furthermore the regions with similar relief to the initial model are determined. Experimental results show high efficiency of the proposed scheme.

Key words: *Digital topography, pattern matching, content based image retrieval.*

Περίληψη

Η επεξεργασία και ερμηνεία της εικόνας και στην συνέχεια η αναγνώρισή της αποτελούν ένα πολύτιμο εργαλείο για την αυτόματη εξαγωγή πληροφορίας με χρήση τοπογραφικών δεδομένων. Στόχος της παρούσας εργασίας είναι η ανάπτυξη αλγόριθμου σε πλατφόρμα Matlab, ο οποίος χρησιμοποιεί ως είσοδο ψηφιακά τοπογραφικά δεδομένα και εξάγει τις περιοχές με παρόμοια τοπογραφία. Μπορεί να εφαρμοστεί στην γεωμορφολογία, στην δασονομία, στον περιφερειακό και αστικό σχεδιασμό, και σε πολλές άλλες εφαρμογές που σχετίζονται με την ανάλυση και διαχείριση των φυσικών πόρων.

Ο χρήστης έχει την ευχέρεια να επιλέξει την περιοχή που τον ενδιαφέρει, με πλοήγηση σε υψηλής ανάλυσης τοπογραφική εικόνα και να προσδιορίσει τρεις παραμέτρους (βήμα, αριθμό των τοπικών ελαχίστων και κλίμακα απεικόνισης). Στην συνέχεια εντοπίζονται αυτόματα οι περιοχές με παρόμοια τοπογραφικά χαρακτηριστικά. Τα πειραματικά δεδομένα δείχνουν υψηλή απόδοση του προτεινόμενου αλγόριθμου.

Λέξεις κλειδιά: *Ψηφιακή τοπογραφία, σύγκλιση προτύπων, ανάκτηση εικόνας βάσει περιεχομένου.*

1. Introduction

Elevation data are widely accepted as one of the most important tools in many scientific branches. Topographic maps contain various spatial and thematic information, providing an ideal data source for Geographic Information Systems (GIS). Simultaneously, GIS comprises a domain experiencin g a rapid growth of both computational power and quantity of information, making large spatial da ta archives available over the Internet (Ruiz et al., 2011). The interest to share this information bet ween different users is also increased. Automatic interpretation of digital topography was firstly ap plied in cadastral maps and/or raster-to-vector conversion (Ablameyko, 1993; Mayer, 1994) and fu rther in data fusion and remote sensing fields (Csathó and Schenk 1998, Lee and Shan 2003, Bartel s et al. 2006, Chen et al. 2008, Elaksher 2008), and mainly for urban areas (Cornet et al. 2001, Fan elli et al. 2001, Wald and Ranchin 2001).

The automatic enhancement and detection of structures on real and complex 2-D images are important tasks on various applications of computer vision, medical analysis, and geosciences (Panagiotakis et al. 2011). The present work aims to automatically detect areas that look alike, based on elevations of all points. Newsam et al. (2010) describe and demonstrate a web-based system for performing content-based image retrieval in large sets of high-resolution overhead images. The system provides a familiar Google Maps interface to navigate the images and select regions of interest. Xia et al., (2010) suggest a satellite image indexing method relying on topographic maps and a shape based image indexing scheme. The proposed approach contains both the textural and structural information of satellite images. Sırmaçek and Ünsalan (2011) propose a novel building detection method using local feature vectors and a probabilistic framework in order to detect buildings from very high resolution (VHR) aerial and satellite images. The following methodology was implemented using commercial and free software such as Matlab[1], Global Mapper[2] and ArcGIS 9.3[3].

2. Methodology

Elevation Data

Global Mapper free software was used to download the elevation data, elaborated in Matlab in the context of the present work. The pre-mentioned software offers access in a variety of spatial datasets and supports a wide range of formats. The onshore Crete area (Fig. 1) was selected as the comparison area and an area located in the western part of Heraklion as the initial testing area. That is, the algorithm developed in this work, will search the entire Crete in order to find areas of similar topographic relief with the region, located west of Heraklion. Elevation data of the above areas is exported from Global Mapper in .xyz format corresponding to longitude, latitude and elevation.

Geographic Information System (GIS)

GIS techniques were used for mapping and estimate the topographic features of the initial testing area, located west of Heraklion. Scope of this approximation, using GIS techniques, was to have a detailed view of the topography corresponding to the initial for testing area and better control of the expected results.

Topographic visualisation (Goldfinger, 1994; Goldfinger et al., 1997) presents several basic forms: shaded relief plots, contour plots, and wire-frame plots. Deformation patterns are better revealed using shaded relief plots (Oguchi et al., 2003). The basic parameter of the hillshade tool is the illumination angle (Kennely, 2008), important to make plots with several angles and combine

[1] http://www.mathworks.com/products/matlab/
[2] http://www.globalmapper.com/
[3] http://www.esri.com/software/arcgis

interpretations. Additionally, GIS systems can generate many useful derivative datasets from topography. Two useful products for studying the topography are slope and aspect maps (Brewer and Marlow, 1993). A slope map assigns colours to the slope angle of each pixel of the elevation grid. This type of image can be used to isolate ranges of topographic slope angles for statistical treatment, predictive capabilities of slope stability, or outcrop exposure. Similarly, an aspect map assigns colours to the azimuth of the slope direction.

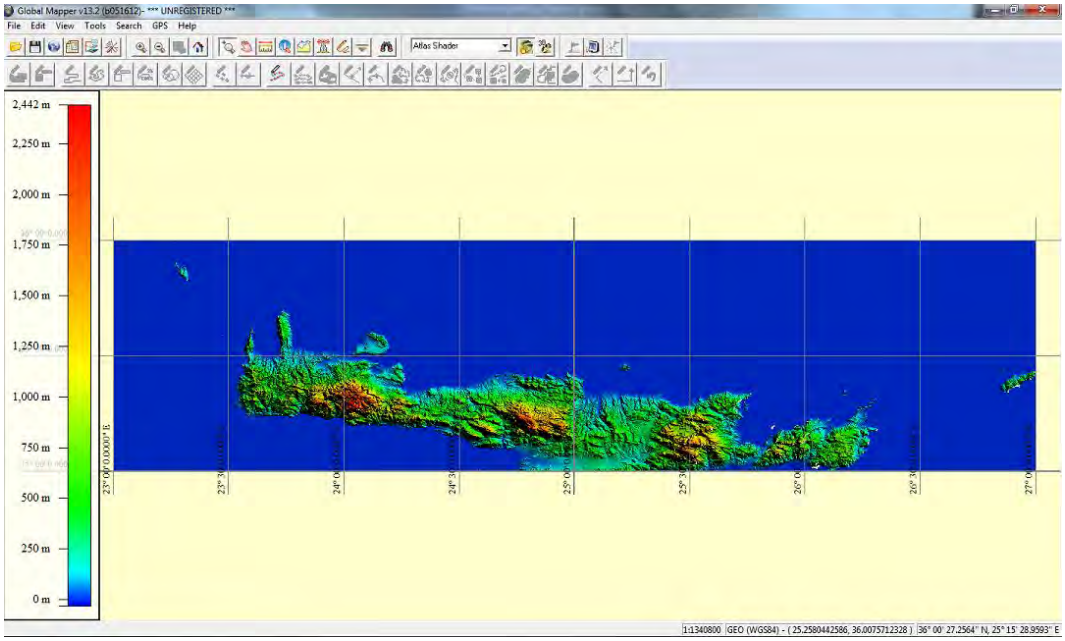

Figure 1 - Onshore Crete (from Global Mapper) was selected to be the comparison area.

Proposed Algorithm

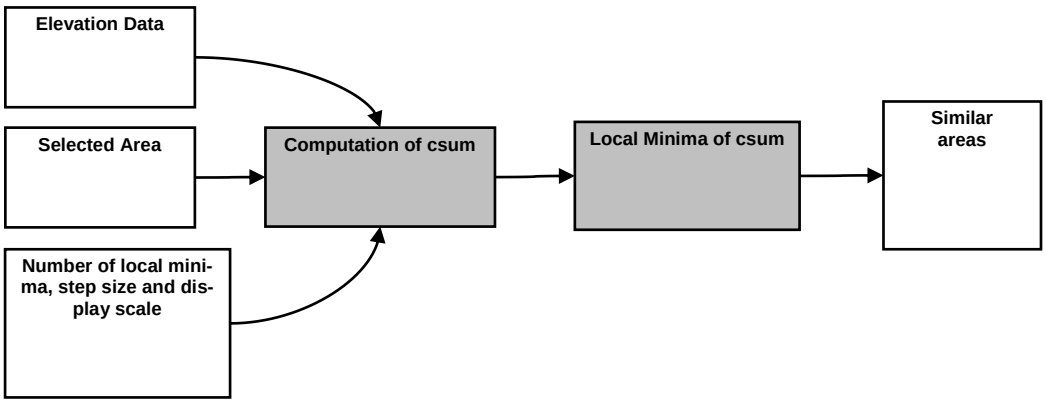

Figure 2 - The scheme of the proposed algorithm.

Figure 2 illustrates the scheme of the proposed algorithm. The input of the method is the given elevation data, the selected area, the step size, the number of local minima (N) that the algorithm will compute and the display scale. The output of the method is the N most similar areas with the initial selected area. Hereafter, we present the proposed method with details.

The present algorithm is executed in three steps as follows:

- Load files, initial variables, create arrays in the format used in the procedure. Input files are loaded in MATLAB in .xyz format that is in the form of tables with 3 columns corresponding to the longitude, the latitude and the altitude of each point. Then by using the command input the user is prompted to give three parameters as inputs and is checked so that when the user gives a non-positive value is requested to login again. These parameters are:

1. The step size, defining the neighborhoods that will be searched for local minimal. This parameter is used at the last part of the method (in local minima computation).

2. The number of local minimal (N) and therefore the number of related (similar) areas.

3. Scaling used to divide the map for better result in displaying.

- Create array (csum) for sum for each sub-region (z1) of the initial image (c) matched in the dimensions of the selected for comparison area (h). The sum of the absolute differences of all sub- regions (z1) in comparison with the original selected region (h) and placement in a new array (csum) of dimensions (s-s1) x (dd-dd1).

```
for i=1:s-s1
   for j=1:dd-dd1+1
          z1= c(i:i+s1-1,j:j+dd1-1)
          d= abs(z1-h)
          sd= abs(sum(sum(d)))
          csum(i,j)=sd
     end
end
```

- Finally, according to the step size we find the local minima of csum array and we print the retrieval results. The local minima are computed in ascending order (starting with the global minimum). The step size defines the minimum distance between two local minima. So, when a local minimum is computed we ignore all possible local minima in a squared region of size equal to step size.

The step size is the only parameter that affects the results of the algorithm. If this parameter is zero then it is possible that the algorithm will yield local minima in the same region. A default value of this parameter is the size of the initial selected area.

3. Experimental Results

In this work, Matlab and ArcGIS 9.3 were combined to ensure the reliability of the algorithm developed. Figure 3(a), (b) present the elevation of the initial testing area, located west of Heraklion, using the display tools of the pre-mentioned software programs. In the majority of this area, the elevation is ranging between 0-200 m and only in the south-western part increases up to 300 m. Figure 3 (c)-(e) show the hillshade, aspect and slope maps, respectively. Generally, prevailing aspects are east, southeast, west and northwest. The relief of the study area is mainly hilly. Steep slopes (>45%) prevail in the south-western part of this area.

Figure 4 (a) and (b) show the initial selected area that is located west of Heraklion and the most similar area with the initial selected area according to the proposed method. Figure (5) shows the result of the proposed method, depicting the most similar area with the initial selected area using as similarity measure the elevation and comparing the morphology of both areas mainly based on the slope and the aspect. The most similar area is located in the northwestern part of the Chania prefecture (Relevant Area No1). Other less similar to the Relevant Area No1 were respectively

detected in the Rethymno prefecture and in the Lasithi prefecture. It holds that both initial selected area and Relevant Area No1 present not only similar elevations but also similar morphological characteristics.

The above methodology is important for data fusion or map conflation concerning the extraction of the best-fit geometry data applied in geospatial databases as well as the most suitable data from existing datasets (Stankute and Asche (2009)). The problem of feature type matching comprises a n aspect of data fusion, a process that requires specific rules for automating the matching and fusio n step. In the present case the elevation was used as attribute for matching areas of similar topogra phy. Furthermore the morphological attributes of both areas were included in order to check the re sults of the applied algorithm.

4. Conclusions

In the context of the present work an algorithm was developed aiming to automatically detect topo graphically similar area(s) to an initial selected area. The similarity search is performed against a target dataset using as similarity measure the elevation. The morphology of both initial and relevan t areas was included to check the results.

The proposed method is simple and it can be easily applied under different metrics and type of input data. Experimental results show high efficiency of the proposed scheme. An extension of this work may include the retrieval of places that have similar topographic maps in the sense of shape, invariant rotation, translation and scaling transforms.

As demonstrated by this approach, the above methodology aids the automation of feature conflatio n and contributes towards developing other applications of pattern recognition and data analysis.

5. Acknowledgements

This work is partially co-funded by the EU Humanitarian Aid and Civil Protection under Grant Agreement No. 638494/2012/ECHO/A5/SUB - Project "Embracing Innovation for Preparedness in Civil Protection & Marine Pollution". We would like to thank two anonymous reviewer for their critical reviews, which help improved the manuscript.

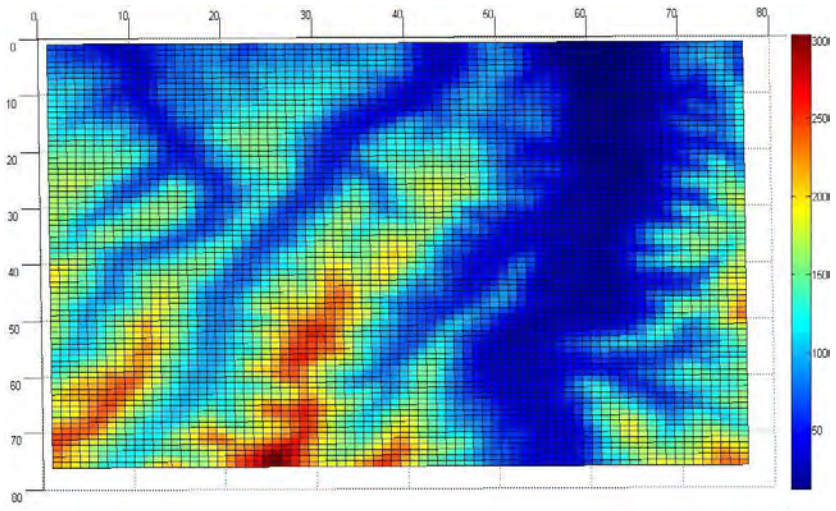

(a)

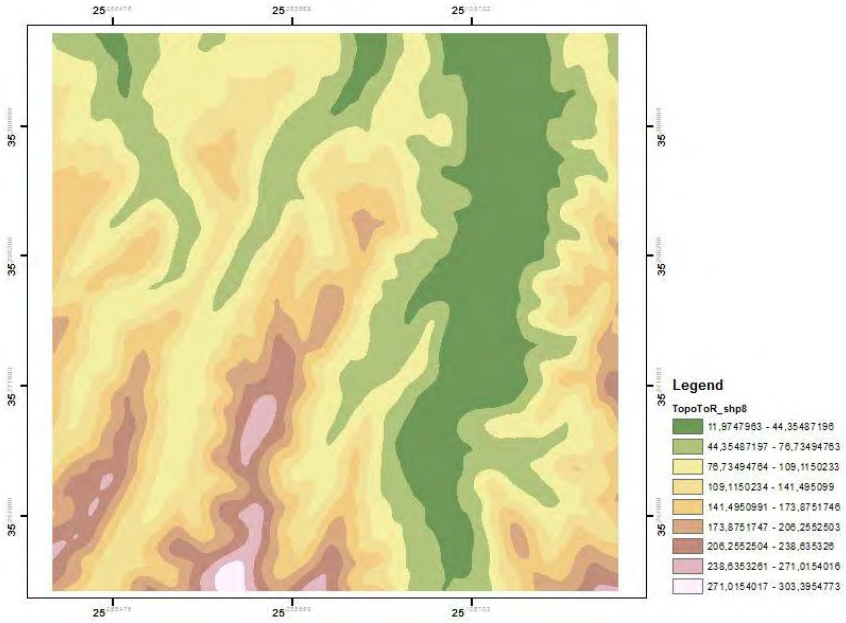
Legend
TopoToR_shp8
11,9747983 - 44,35487196
44,35487197 - 76,73494763
76,73494764 - 109,1150233
109,1150234 - 141,495099
141,4950991 - 173,8751746
173,8751747 - 206,2552503
206,2552504 - 238,635326
238,6353261 - 271,0154016
271,0154017 - 303,3954773

(b)

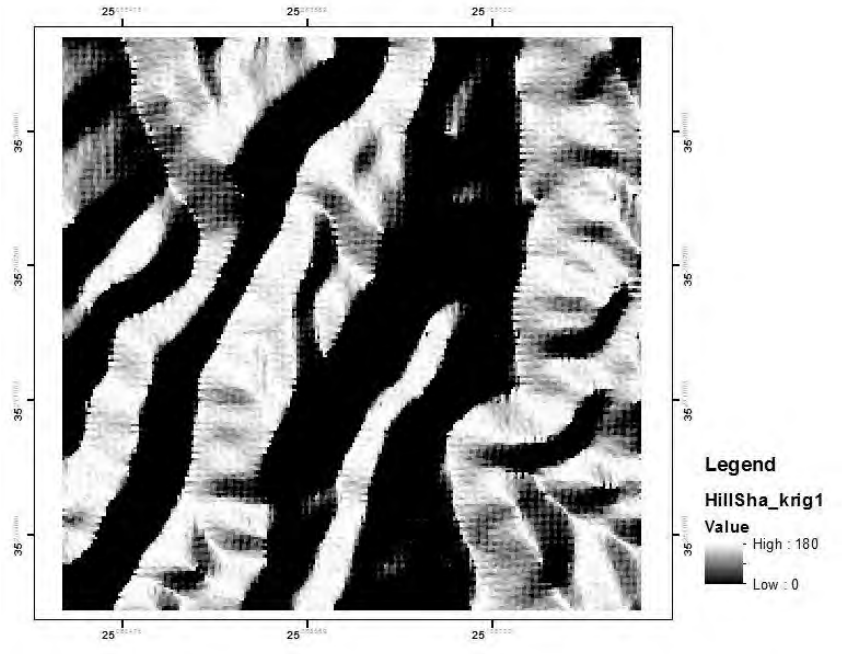
Legend
HillSha_krig1
Value
High : 180
Low : 0

(c)

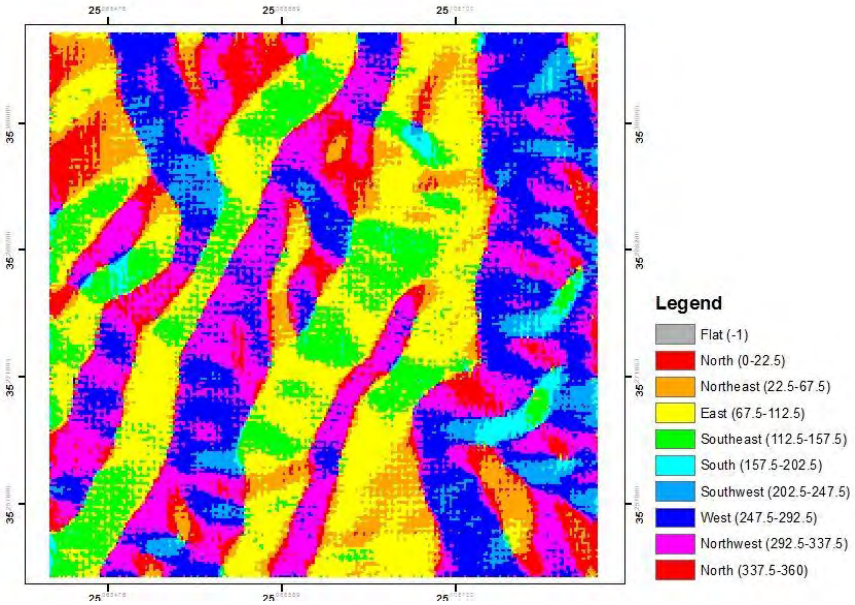

(d)

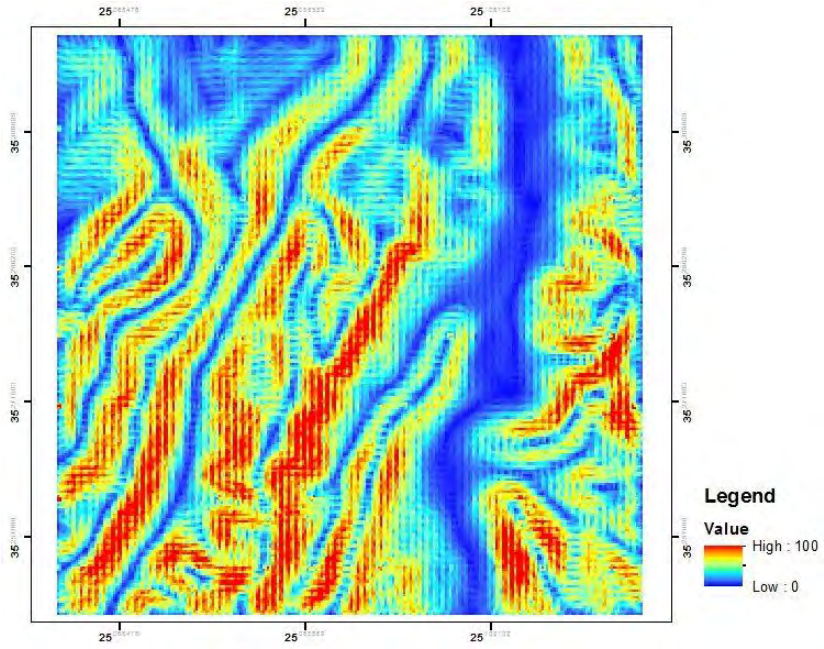

(e)

Figure 3 - (a): Selected area plotted using Matlab (scale represents the elevation in m), (b): the same area plotted using ARCGIS), (c): hillshade map of the same area, (d): aspect map, (e): slope map (%).

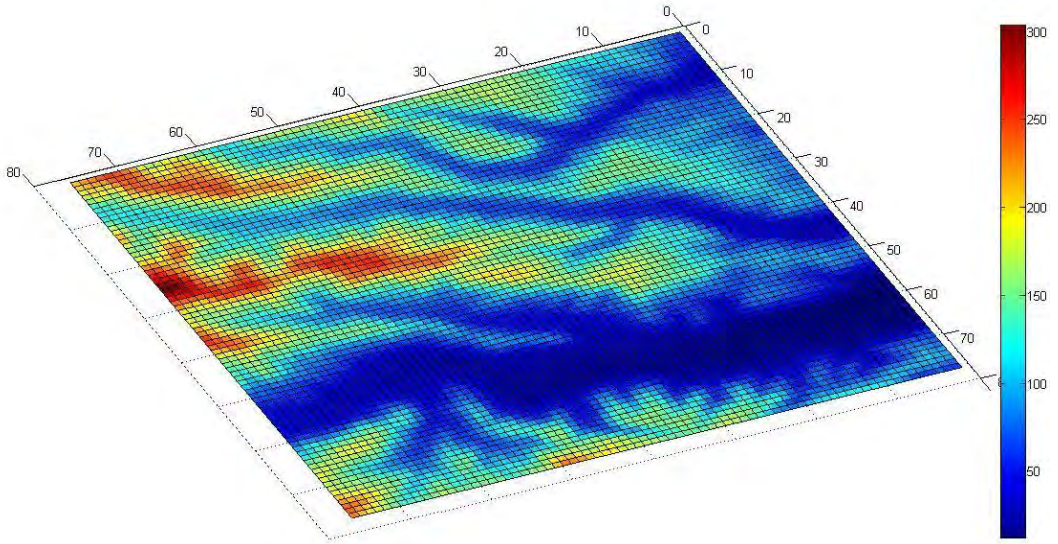

(a)

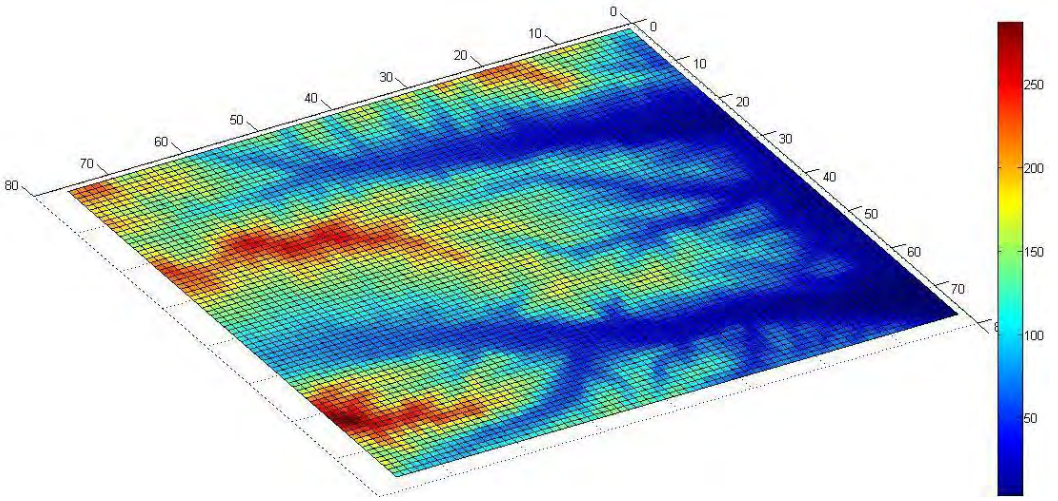

(b)

Figure 4 - (a) Initial selected area, (b): area with similar topographic characteristics detected using the algorithm developed in this work, (scale represents the elevation in m).

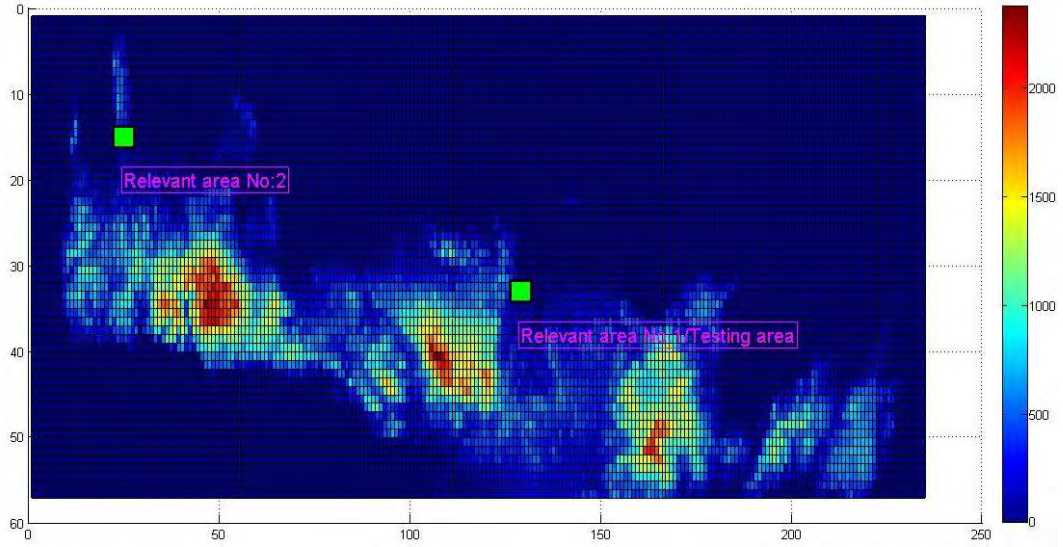

Figure 5 - Map of Crete showing two areas with similar topography, (scale represents the elevation in m).

6. References

Ablameyko S.V., Beregov B.S. and Kryuchkov A.N. 1993. Computer-Aided Cartographical System for Map Digitizing, *Proc. of the 2nd International Conference on Document Analysis and Recognition*, Tsukuba Science City, Japan, 115-118.

Bartels M., Wei H. and Ferryman J. 2006. Analysis of LIDAR data fused with co-registered bands. *Proc. of IEEE international conference on advanced video and signal-based surveillance*, Sydney, Australia, 22–24 November.

Brewer C.A. and Marlow K.A. 1993. Computer representation of aspect and slope simultaneously, *Proc. of the 11th International Symposium on Computer- Assisted Cartography (Auto-Carto-11)*, Minneapolis, Minnesota, 328–337.

Chen L. 2008. Shaping polyhedral Buildings by the fusion of vector maps and lidar point clouds, *Photogrammetric Engineering & Remote Sensing*, 74 (9), 1147–1157.

Cornet Y. 2001. RS Data fusion using local mean and variance matching algorithms: their respective efficiency in different urban context, *Proc. of IEEE/ISPRS Joint workshop on remote sensing and data fusion over urban areas*, Rome, Italy, 8–9 November.

Csathó B. and Schenk T. 1998. A multisensor data fusion for automatic scene interpretation, *The international archives of photogrammetry, remote sensing, and spatial information sciences*, Columbus, OH, US, 6–10 July, XXXII, 3(1), 429–434.

Elaksher A. 2008. Fusion of hyperspectral images and lidar-based dems for coastal mapping, *Optics and Lasers in Engineering*, 46 (7), 493–498.

Fanelli A., Leo A. and Ferri M. 2001. Remote sensing images data fusion: a wavelet transform approach for urban analysis, *Proc. of IEEE/ISPRS joint workshop on remote sensing and data fusion over urban areas*, Rome, Italy, 8–9 November.

Goldfinger C. 1994. Active Deformation of the Cascadia Forearc: Implications for Great Earthquake Potential in Oregon and Washington, Corvallis, Oregon State University, *PhD Thesis*, 202 pp.

Goldfinger C., Kulm L.D.,Yeats R.S., McNeill, L.C. and Hummon C. 1997. Oblique strike-slip faulting of the central Cascadia submarine forearc, *Journal of Geophysical Research*, 102, 8217-8243.

Kennely P.J. 2008. Terrain maps displaying hill-shading with curvature, *Geomorphology*, 102(5), 67–577.

Lee S. and Shan J. 2003. Combining LIDAR elevation data and IKONOS multispectral imagery for coastal classification mapping*, Marine Geodesy*, 26 (1–2), 117–127.

Mayer H. 1994. Automatic knowledge based extraction of objects of the real world from scanned maps. Internat. Arch. Photogrammet, *Remote Sensing,* (30) 3/2, 547–554.

Newsam S., Leung D., Caballero O., Floreza J. and Pulido J. 2010. *Proc. of the ACM GIS '10,* San Jose, CA, USA, November 2-5.

Oguchi T., Aoki T. and Matsuta N. 2003. Identification of an active fault in the Japanese Alps from DEM-based hill shading, *Computers and Geosciences*, 29, 885–891.

Panagiotakis C., Kokinou E. and Sarris A. 2011, Curvilinear Structure Enhancement and Detection in Geophysical Images, *IEEE Transactions on Geoscience and Remote Sensing*, 49 (6), 2040-2048.

Ruiz J.J., Ariza F.J., Ureña M.A. and Blázquez, E.B. 2011. Digital map conflation: a review of the process and a proposal for classification, *International Journal of Geographical Information Science*, 25, 9, 1439–1466.

Sırmaçek B. and Ünsalan C. 2011. A Probabilistic Framework to Detect Buildings in Aerial and Satellite Images, *IEEE Transactions on Geoscience and Remote Sensing*, 49, 1, 211-221.

Stankute S. and Asche H. 2009. An integrative approach to geospatial data fusion. In Gervasi, O., et al., eds, *Lecture in Computer Science*, 5592, Berlin, Springer, 490–504.

Wald L.and Ranchin T. 2001. Data fusion for a better knowledge of urban areas, *Proc. of IEEE/ISPRS joint workshop on remote sensing and data fusion over urban areas*, Rome, Italy, 1–14 June.

Xia G., Yang W., Delon J., Gousseau Y., Hong S.and Maitre H. 2010. Structural High-Resoloution Satellite Image Indexing, in Wagner W., Székely, B., eds., *ISPRS TC VII Symposium – 100 Years ISPRS*, Vienna, Austria, July 5–7, IAPRS, XXXVIII, 7A.

Δελτίο της Ελληνικής Γεωλογικής Εταιρίας, τομ. XLVII , 2013
Πρακτικά 13ου Διεθνούς Συνεδρίου, Χανιά, Σεπτ. 2013

Bulletin of the Geological Society of Greece, vol. XLVII 2013
Proceedings of the 13th International Congress, Chania, Sept. 2013

MORPHOTECTONIC ANALYSIS OF HERAKLION BASIN (CRETE, GREECE)

Kokinou E.[1], Skilodimou H. D.[2] and Bathrellos G.D.[2]

[1] *Technological Educational Institute Crete, Department of Natural Resources & Environment, Chania, Crete, Greece, ekokinou@chania.teicrete.gr*

[2] *National & Kapodistrian University of Athens, Faculty of Geology & Geoenvironment, Department of Geography & Climatology, University Campus, Zografou, ZC 15784, Athens, Greece, hskilodimou@geol.uoa.gr, gbathrellos@geol.uoa.gr*

Abstract

In the present study, geomorphological, geological data and morphotectonic analysis were combined in order to investigate the relation between the tectonic activity and the geomorphology in the Heraklion basin (Crete). GIS techniques were used for mapping the various topographic, geological and tectonic features of the study area. The digital elevation model (DEM) of the study area was created. The slope angle and aspect maps were derived from DEM and combined with fault system orientation. The influence of tectonism on the development of drainage system was examined by the comparison of fault and stream directions. Moreover, geomorphic indices are useful tools in evaluating tectonic activity, relating the sensitivity to rock resistance, climatic change and tectonic processes with the production of a certain landscape. The applied geomorphic indices, in the present study, are the mountain front sinuosity index (S_{mf}) and the valley floor width to valley height ratio (V_f). The fault zones of the study area are generally oriented N-S, NE-SW, NW-SE and E-W. According to the morphological analysis, steep slopes and sudden changes corresponding to the azimuth of the slope direction, are mainly related to N-S, NNE-SSW and NNW-SSE oriented faulting. The main channel directions of the drainage system are mainly controlled by faults striking N-S. The E-W, NE-SW and NW-SE general trending fault systems affect the low order streams. The S_{mf} and V_f values are low, implying that the tectonic activity influences the morphology of the study area. The above methodology was proved successful to examine the impact of the tectonic activity in the study area.

Key words: *Geomorphic indices, GIS, fault.*

Περίληψη

Στόχος της παρούσας εργασίας είναι να συνδυάσει τα γεωλογικά δεδομένα με την μορφολογική και μορφοτεκτονική ανάλυση με στόχο να καθοριστεί η επίδραση της τεκτονικής στην διαμόρφωση του επιφανειακού αναγλύφου για τμήμα της λεκάνης του Ηρακλείου στην Κρήτη. Τα Γεωγραφικά Συστήματα Πληροφοριών χρησιμοποιήθηκαν για να απεικονιστούν τα τοπογραφικά, γεωλογικά και τεκτονικά δεδομένα της περιοχής. Αρχικά δημιουργήθηκε το ψηφιακό μοντέλο υψομέτρων και στην συνέχεια προέκυψαν από αυτό ο χάρτης κλίσεων και ο χάρτης προσανατολισμού και συνδυάστηκαν με το τεκτονικό σύστημα της περιοχής. Η επίδραση του τεκτονισμού στην ανάπτυξη

του υδρογραφικού δικτύου εκτιμήθηκε, λαμβάνοντας υπόψιν τον προσανατολισμό των ρηγμάτων και των ρεμάτων. Επιπρόσθετα στα πλαίσια της παρούσας εργασίας προσδιορίστηκαν δύο μορφοτεκτονικοί δείκτες με στόχο να αξιολογηθεί η τεκτονική δραστηριότητα της περιοχής. Αυτοί αντιστοιχούν στον δείκτη ευθυγράμμισης του ορεογραφικού μετώπου (S_{mf}) και στον δείκτη λόγου πλάτους κοιλάδας προς ύψος κοιλάδας (V_f). Τα ρήγματα της περιοχής παρουσιάζουν γενικά προσανατολισμό Β-Ν, ΒΑ-ΝΔ, ΒΔ-ΝΑ και Α-Δ. Από την μορφολογική ανάλυση προκύπτει ότι οι απότομες κλίσεις καθώς και οι απότομες μεταβολές προσανατολισμού σχετίζονται με τα ρήγματα διεύθυνσης Β-Ν, ΒΒΑ-ΝΝΔ και ΒΒΔ-ΝΝΑ. Οι κύριοι κλάδοι του υδρογραφικού δικτύου πιθανόν ελέγχονται από τα ρήγματα γενικής διεύθυνσης Β-Ν. Οι δείκτες S_{mf} και V_f παρουσιάζουν χαμηλές τιμές, γεγονός που δείχνει ότι η μορφολογία της περιοχής έχει επηρεαστεί σε μεγάλο βαθμό από την τεκτονική δραστηριότητα. Η παραπάνω μεθοδολογία ανάλυσης αποδείχθηκε επιτυχής στους στόχους που έθεσε η παρούσα εργασία.
Λέξεις κλειδιά: *Μορφοτεκτονικοί δείκτες, Γ.Σ.Π., ρήγμα.*

1. Introduction

The wide area of Heraklion city is located in the Heraklion basin (Figure 1A), comprising a large Neogene basin (900 km^2) in central Crete. The Neogene deposits of Heraklion basin overlie basement rocks of the Upper Nappes (Gavrovo-Tripolis, Pindos and the heterogeneous Uppermost Unit). The Upper Nappes are separated from the HP-LT metamorphic rocks of the Lower Nappes (parautochtone Plattenkalk and Phyllite-Quarzite units) by the Cretan detachment (Zachariasse et al., 2011; Kokinou et al., 2012). This fault (or faults) is in many places exposed with a sense of shear either to both S and N (Kilias et al., 1994; Fassoulas, 1999), or dominantly top-to the north (Jolivet et al., 1996).

The evolution of a complex landscape is the result of the interactions involving climate, tectonic and surface progress. Therefore the study of the geomorphological features such as the drainage may assist in understanding the landscape evolution and recognize active tectonic movements (Riquelmea et al., 2003; Malik and Mohanty, 2007; Bathrellos et. al., 2009, Kamberis et al., 2012).

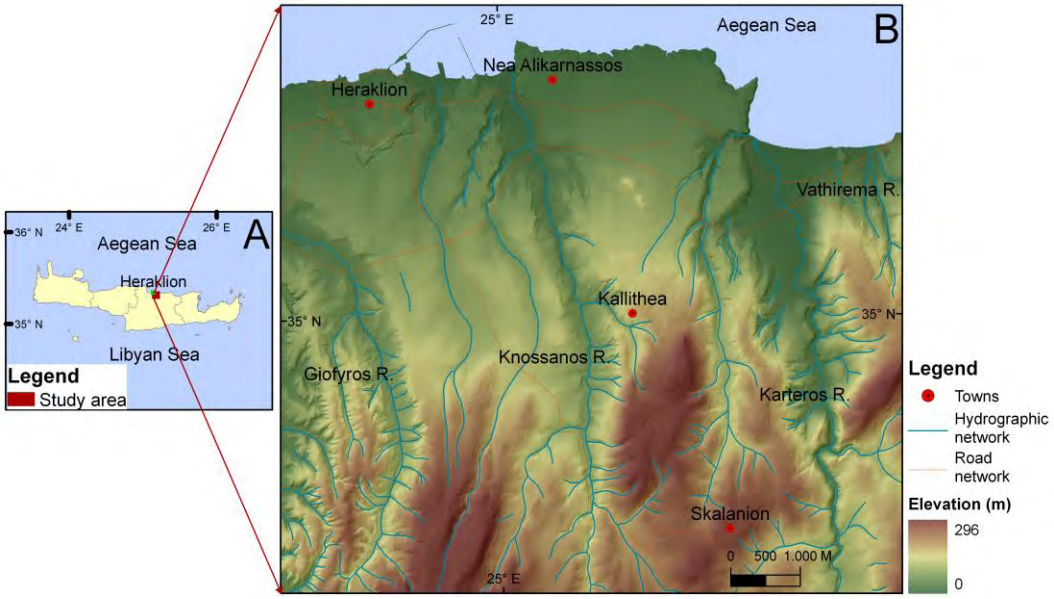

Figure 1 - A: **Map of Crete showing the study area, B: Elevation map of the study area.**

Several studies have proposed that the investigation of geomorphological features and geomorphic indices such as the mountain front sinuosity (S_{mf} index) and the valley floor width to valley height ratio (V_f index) provide useful information regarding the influence of tectonics on landscape evolution (e.g. Bull and McFadden, 1977; Rockwell et al., 1984; Keller, 1986; Burbank and Anderson, 2001; Theocharis and Fountoulis, 2002; Silva et al., 2003; Tsodoulos et al., 2008).

The main scope of the present study is to combine geomorphological, geological data and morphotectonic analysis in order to investigate the relation between the tectonic activity and the geomorphology in the Heraklion basin (Crete).

2. Geology of the Study Area

The Heraklion's basin comprises an almost flat area (maximum elevation at 296m) with the exception of some hilly areas, showing an extended development of the drainage. The rivers of the basin flow from South to North into Aegean Sea (Figure 1B).

The geological map (Figure 2) of the study area was created, based on the existing geological map (IGME, 1:50,000) and field observations.

The Heraklion's basin is mainly filled by fluvial and marine sediments of Holocene, Pleistocene, Lower-Middle Pliocene, Upper Miocene, Cretaceous – Middle Eocene and Upper Triassic-Upper Jurassic (Figure 2). The Holocene sediments (al) mainly comprise fluvial and closed basin deposits, situated in the western part of the city, on either site of the drainage network. Pleistocene–Holocene sediments (Qs) are generally located across the coastline, comprising of undivided marine terraces and coastal sands. The Pleistocene Heraklion formation (Pt) consists of marine bioclastic limestones, sandstones with cross-bedded conglomerates and marls. The majority of the basin's interior consists of Lower-Middle Pliocene sediments (Pl.m), comprising of white marls or marly limestones, grayish clays with brown, often thin bedded intercalations, white beige fossiliferous marls, laminated marls or diatomites and bioclastic limestones. The base of this formation consists in general of an unsorted "marly breccia". It overlies unconformably the Upper Miocene formation (M.k), consisting of bioclastic, reef limestones, marls or marly limestones (M.m) and gypsum (g). In the eastern part of Heraklion are situated Cretaceous–Middle Eocene (Ks-Ek) limestones, grey to black, medium-thick bedded to massive bituminous locally microbreciatted and dolomitic in the upper members. Finally the oldest formation of this area is the Triassic–Upper Jurassic (Ts-Js.Kd) limestones, dolomitic limestones and dolomites. They constitute the base of the external zones tectonic nappe resulting in a local mylonitization at their base due tectonism. They are karstic, mainly in the upper members.

The map and the rosediagram of Figure 2 show that the fault zones of the study area are oriented NE-SW to NNE-SSW, NW-SE to NNW-SSE and E-W.

3. Methodology

3.1. Geographic Information System (GIS)

According to Goldfinger et al. (1994), shaded relief plots, contour plots, and wire-frame plots comprise the main tools to render the topography of an area. Detailed faulting tectonics and pattern deformation is better determined based on shaded relief plots (Oguchi et al., 2003). According to Kennely (2008), the illumination angle is also important for combined interpretation. Tectonic geomorphological interpretation is also supported by 3D view (Figure 3, Smith and Clark, 2005).

Digitization techniques and GIS were applied for mapping representation of the data. The digital elevation model (McGullagh, 1998; El-Sheimy et al., 2005) was created by the digitization of the topographic map contours (1:5,000 scale maps), while the cell size of the digital elevation model was 4 m. A spatial database was created and ArcGIS 9.3 software was used to process the collected data. This study was carried out using topographic maps of a scale of 1:5,000, published

by the Hellenic Army Geographical Service (H.A.G.S.). A Digital Elevation Model (DEM) was created by digitizing the contours with 2 m intervals and triangulation points of the above mentioned topographic maps.

GIS systems can generate many useful derivative datasets from topography. Two useful products for tectonics are slope and aspect maps. A slope map (Figure 4) assigns colours to the slope angle of each pixel of the elevation grid. This type of image may illuminate tectonic activity not apparent otherwise, and can be used to isolate ranges of topographic slope angles for statistical treatment, predictive capabilities of slope stability, or outcrop exposure. Similarly, an aspect map assigns colours to the azimuth of the slope direction (Figure 5). Both of these plots can be used for either topography or subsurface horizons to illuminate trends associated with deformation (Evans, 1972; Moellering and Kimerling, 1990; Brewer and Marlow, 1993). For the production of the slope angle layer, the DEM of the study area was used. The slopes were grouped in six classes: (i) < 5o (very gentle slopes), (ii) 5 – 10o (gentle slopes) (iii) 11 – 20o (intermediate slopes), (iv) 21 – 30o (moderately steep slopes), (v) 31 – 40o (steep slopes), and (vi) > 40o (very steep slopes) (Figure 4). As the aspect is the slope direction for a terrain, the aspect map was created from the DEM. The azimuth of the slope direction was grouped in nine classes: (i) -1o flat, (ii) 337.5 – 22.5o north, (iii) 22.5 – 67.5o northeast, (iv) 67.5 – 112.5oeast, (v) 112.5 – 157.5o southeast, (vi) 157.5 – 202.5o south, (vii) 202.5 – 247.5o southwest, (viii) 247.5 – 292.5o west, (ix) 292.5 - 337.5o northwest .

3.2. Geomorphic Indices

Geomorphic indices are useful tools in evaluating tectonic activity, relating the sensitivity to rock resistance, climatic change and tectonic processes with the production of a certain landscape. The most useful indices are the mountain front sinuosity (S_{mf} index; Bull and McFadden, 1977) and the valley floor width to valley height ratio (V_f index; Bull, 1977, 1978).

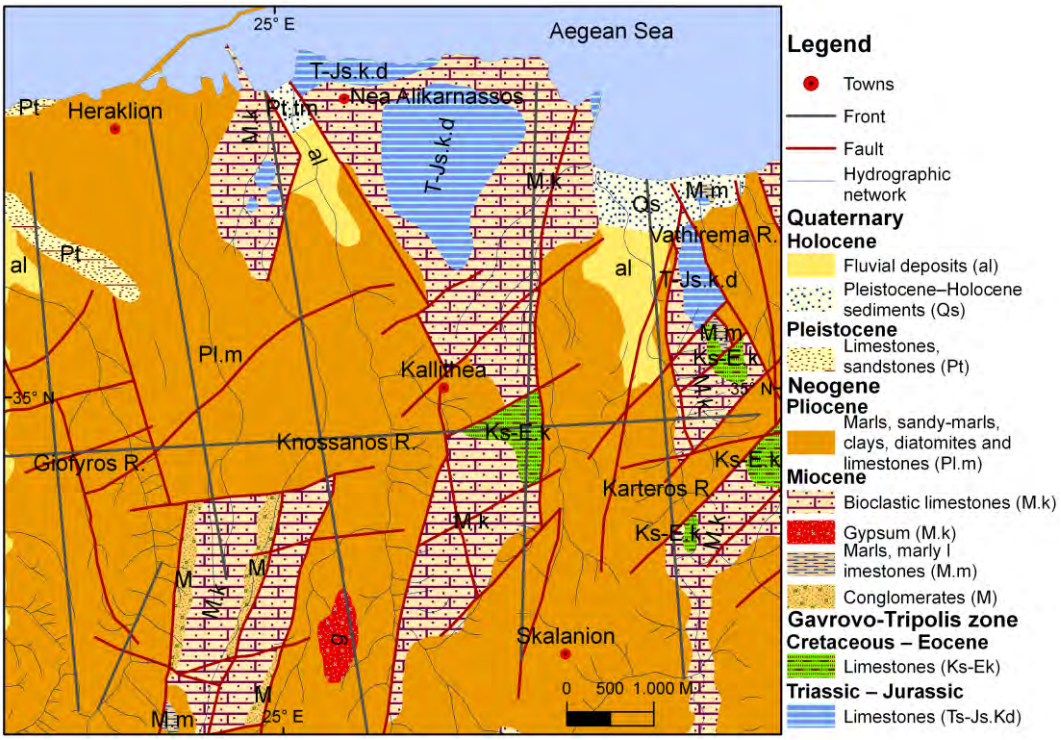

Figure 2 - Geological map of Heraklion (according to the geological map of IGME, Vidakis et al., 1996). The rose diagram (upper right) presents the orientation of the main faults.

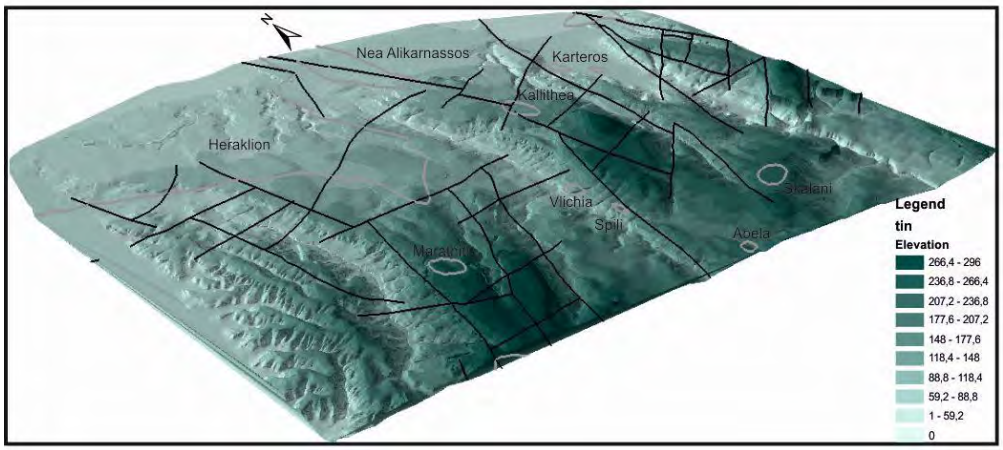

Figure 3 - 3D Topographic visualisation of the study area. Black lines correspond to faults.

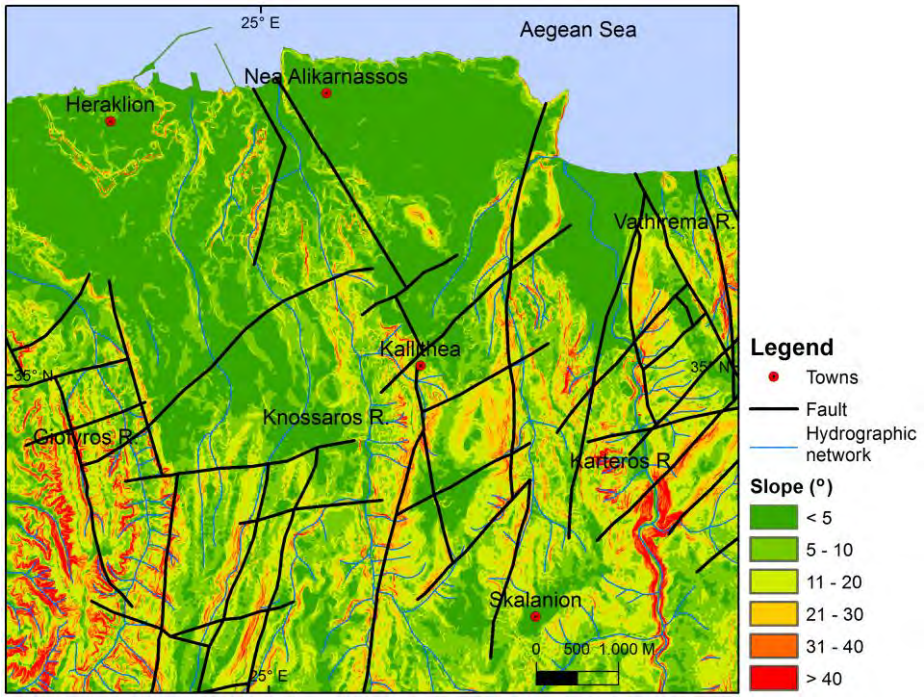

Figure 4 - Slope map of the study area.

Mountain front sinuosity is determined by measuring the length of the mountain front along the foot of the mountain Lmf and the straight line length of the mountain Ls. So, the mountain front sinuosity Smf = Lmf/Ls is achieved (Bull and McFadden, 1977). The balance between erosion that tends to produce asymmetrical or sinuous fronts and tectonic forces that tend to create a straight mountain front coincident with an active range–bounding fault is presented by the above mentioned index. On the most tectonically active fronts, values of Smf approach 1.0, whereas Smf increases if the rate of uplift is reduced and erosional processes begin to form a front that becomes more irregular with time. Smf values lower than 1.4 indicate tectonically active fronts (Rockwell et al., 1984; Keller, 1986; Burbank and Anderson, 2001) while higher Smf values (>3) are normally associated with inactive fronts in which the initial range–front fault may be more than 1Km away from the present erosional front (Bull and McFadden, 1977).

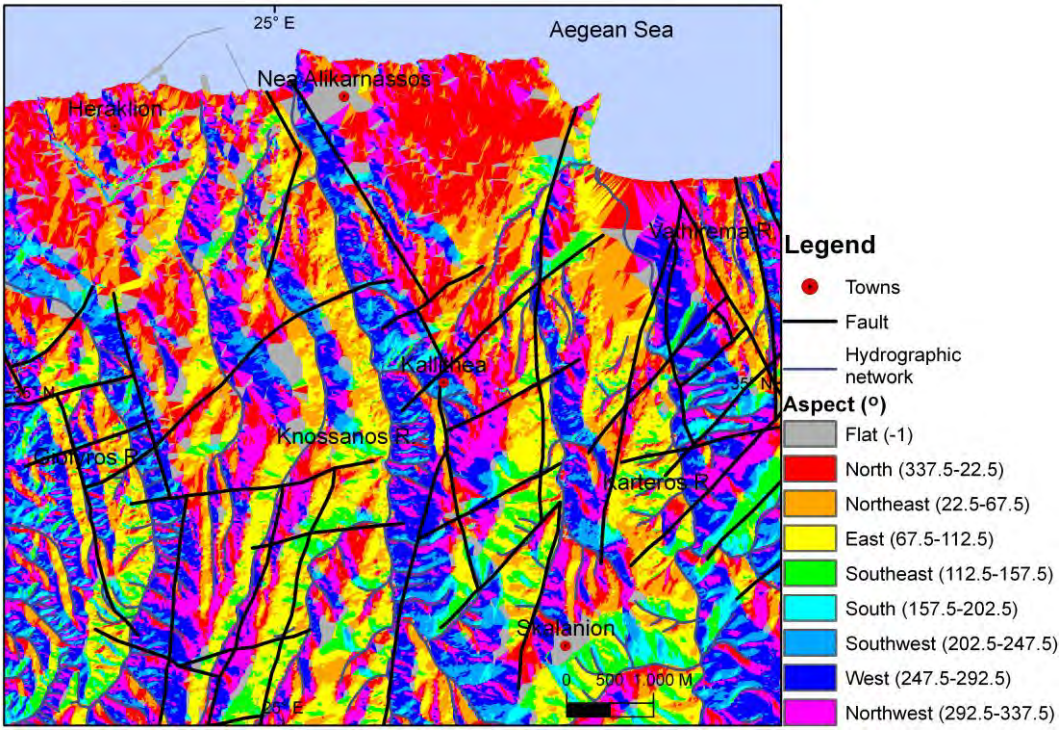

Figure 5 - Aspect map of the study area.

In this study, fronts are defined by a major fault bounded topographic range fronts with measurable relief exceeding two contour intervals (4m) in 1:5000 maps, which is the working scale used. The application of the Smf index was utilized in seven discrete segments (Figure 2), corresponding to major fault zones in the study area and taking into account similar geological and morphological characteristics especially concerning the drainage network. For the separation the following criteria were applied (Wells et al., 1988): a) intersection with large in scale cross–cutting drainage, relative to the front, b) abrupt changes in lithology (as it occurs in the western and eastern segments), c) changes in hill front orientation.

The Vf index reflects the difference between V-shaped valleys that are down cut in response to active uplift (low values of Vf) and broad-floored valleys that are eroding laterally into adjacent hill slopes in response to base level stability (high values of Vf) (Bull, 1978). The ratio of valley floor width to valley height (Vf) may be expressed as:

Equation 1 - Ratio of Valley Floor Width to Valley Height

$$Vf = \frac{2 \times Vf_w}{(E_{ld} - E_{sc}) + (E_{rd} - E_{sc})}$$

Where V_{fw} is the width of valley floor, E_{ld} and E_{rd} are elevations of the left and right valley divides, respectively, and Esc is the elevation of the valley floor (Bull & McFadden, 1977). Comparison of the width of the floor of a valley with its mean height provides an index that indicates whether the stream is actively down cutting or is primarily eroding laterally into the adjacent hillslopes. The index reflects in this way differences between broad –floored canyons (U–shaped) with relatively high values of V_f and V–shaped canyons with relatively lower values (Keller, 1986).

4. Results and Discussion

Morphological analysis of topographic features is often used for tectonic and structural studies. Digital elevation models (DEMs) and DEM analysis methods are used for fault recognition as about 90% of fault geomorphic indices can be defined quantitatively. At this point we have to mention that lithological contacts and intersection of bedding and topography, glacial features and wind erosion may also appear as lineaments in the derivative maps extracted from DEMs. So the use of indicated methods of DEMs analysis without geological data does not permit us to determine the fault morphology.

Slope and aspects superimposed by the faults and the drainage system are shown in Figures 4 and 5 respectively. The relief of the study area is mainly smooth with slopes ranging between 0 and 20^o, while prevailing aspects are east, west, north and northwest. It is obvious that steep slopes ($>30^o$) are mainly related to N-S, NNE-SSW and NNW-SSE oriented faulting. Additionally sudden changes corresponding to the azimuth of the slope direction are generally in agreement with the presence of steep slopes in the vicinity of the pre-mentioned faulting.

The influence of tectonism on the development of drainage system was examined by the comparison of fault and stream directions. As it is presented in Figures 4 and 5 the main channels of the drainage system of the study are parallel and generally oriented N-S. This direction is probably related to N-S, NNE-SSW and NNW-SSE oriented faulting. Regarding the low order streams of the drainage system, they develop directions mainly E-W, NE-SW and NW-SE. These stream directions have affected from E-W, NE-SW and NW-SE trending fault systems.

The values of the S_{mf} and V_f index were calculated for each front of the study area along with their trend and length (Table 1). Fronts were generally selected to be near or in the vicinity of major faults and/or near to rivers or streams. Fronts (1) and (2) are located in the western part of the study area in the vicinity of Giofyros river, while their lengths are 6.186 and 1.838Km respectively. Front (1) is partially parallel to faults trending mainly N-S to NNW-SSE while front (2) is sub-parallel to a fault trending NNE-SSW. Both fronts are mainly located in the Lower-Middle Pliocene (Pl.m) and Pleistocene sediments. The value of the S_{mf} corresponding to fronts (1) and (2) is 1.17 and 1.36 respectively, while the average value for V_f is 0.32 and 0.076.

Front (3) is located between Giofyros and Knossanos rivers being partially parallel to faults trending N-S to NNW-SSE and crosses the Upper Miocene formation (M.k) and the Lower-Middle Pliocene sediments (Pl.m). It is 5.513Km long. The value of the S_{mf} is 1.26 while the average value for V_f is 0.45.

Front (4) is almost parallel to Knossanos river trending N-S to NNW-SSE and it is 7.6Km long. It crosses the Triassic–Upper Jurassic (Ts-Js.Kd) limestones, the Upper Miocene formation (M.k) and the Lower-Middle Pliocene sediments (Pl.m) and finally the Pleistocene sediments (Pt.m). The value of the S_{mf} is 1.13 while the average value for V_f is 0.56.

Front (5) is located between Knossanos and Karteros rivers trending N-S to NNE-SSW and crosses the Cretaceous–Middle Eocene (Ks-Ek) limestones, the Upper Miocene formation (M.k) and the Lower-Middle Pliocene sediments (Pl.m). It is 6.64Km long. The value of the S_{mf} is 1.1 while the average value for V_f is 0.34.

Front (6) is almost parallel to Karteros river trending almost N-S and it is 5.75Km long. It crosses the Upper Miocene formation (M.k), the Lower-Middle Pliocene sediments (Pl.m), the Pleistocene – Holocene sediments (Qs) and the Holocene sediments (al) . The value of the S_{mf} is 1.04 while the average value for V_f is 0.42.

Finally, front (7) is parallel to faults trending mainly E-W and it is 9.372Km long. It crosses the Cretaceous–Middle Eocene (Ks-Ek) limestones, the Upper Miocene formation (M.k), the Lower-Middle Pliocene sediments (Pl.m) and the Holocene sediments (al). The value of the Smf is 1.26 while the average value for Vf is 0.44.

Table 1Values of geomorphological indices for the fronts (1-7) shown in Figure 2.

Front Num.	Location	Bounding rocks	Front trend	Front length (km)	S_{Mf}	Average V_f
1	Giofyros	Pl.m, Pt, al	N-S	6.186	1.17	0.32
2	Giofyros	Pl.m	NNE-SSW	1.838	1.36	0.076
3	Between Giofyros and Knossanos	M.k, Pl.m	N-S	5.513	1.26	0.45
4	Knossanos	T-Js.kd, Mk, Pl.m, Pt.m	N-S	7.6	1.13	0.56
5	Between Knosanos and Karteros	Ks-E.k, M.k, Pl.m	NNE-SSW	6.64	1.1	0.34
6	Karteros	M.k, Pl.m, al, Qs	N-S	5.75	1.07	0.42
7	Giofyros-Karteros	Ks-E.k, M.k, Pl.m, al	E-W	9.372	1.26	0.44

The Smf values along the different fronts in the study area are generally varying between 1.07 and 1.36. As already mentioned, Smf values lower than 1.4 near or in the vicinity of faults, indicate tectonically active fronts (Rockwell et al., 1984; Keller, 1986; Burbank and Anderson, 2001). The fronts generally cross Miocene - Pliocene sediments, showing approximately the same resistance to the erosion. The low Smf values (close to 1) indicate that the area is affected by tectonic activity rather than erosion processes.

Similarly, Vf index values are low ranging between 0.076 and 0.56. According to Silva et al (2003) values of Vf < 1.0 express the develop of V-shaped valleys indicating tectonic activity. Both index values suggest that the involved fault systems fall under the category of Class-I, representing high tectonic activity.

5. Conclusions

In the present study morphological and geomorphotectonic analysis are combined in order to determine the impact of the tectonic activity in the Heraklion area.

DEM analysis methods are used for fault recognition but the use of these methods without geological data does not permit to determine the fault morphology. The analysis of the morphological features indicated that steep slopes (>30º) and sudden changes corresponding to the azimuth of the slope direction are mainly related to N-S, NNE-SSW and NNW-SSE oriented faulting.

The comparison of the fault and stream directions suggests the influence of the tectonic activity on the drainage system. The main channel directions of the drainage system are mainly related to faults striking N-S, NNE-SSW and NNW-SSE. The E-W, NE-SW and NW-SE trending fault systems controls the low order streams. Geomorphic indices, used in the present study, are the mountain front sinuosity index (S_{mf}) and the valley floor/width ratio index (V_f). The S_{mf} and V_f values are low, indicating that the active tectonism influences the geomorhological evolution of the study area.

6. Acknowledgements

We would like to thank Assoc. Professor Rondoyanni Th. and Dr. Chatzipetros A. for their critical reviews, which help improved the manuscript.

7. References

Bathrellos G.D., Antoniou V.E. and Skilodimou H.D. 2009. Morphotectonic characteristics of Lefkas Island during the Quaternary (Ionian Sea, Greece), *Geologica Balcanica*, 38(1-3), 23-33.

Brewer C.A. and Marlow K.A., 1993. Computer representation of aspect and slope simultaneously, *Proc. of the 11th International Symposium on Computer- Assisted Cartography (Auto-Carto-11*), Minneapolis, Minnesota, 328–337.

Bull W. 1977. Tectonic geomorphology of the Mojave Desert, *U.S. Geol. Surv. Contact Rep*. 14–08–001–G–394, Office of Earthquakes, Volcanoes and Engineering, Menlo Park, Calif., 188.

Bull W. 1978. Geomorphic tectonic activity classes of the south front of the San Gabriel Mountains, California, *U.S. Geol. Surv*. *Contact Rep.* 14–08–001–G–394, Office of Earthquakes, Volcanoes and Engineering, Menlo Park, Calif., 59.

Bull W. and McFadden L. 1977. Tectonic geomorphology north and south of the Garlock Fault, California, Geomorphology in Arid regions, in Doehring, D.O., ed*., Publications in Geomorphology*, State University of New York at Bingamton, 115–138.

Burbank D.W. and Anderson R.S. 2001. Tectonic geomorphology, Blackwell Science, Inc. *USA*.

El-Sheimy, N., Valeo, C., Habib, A., 2005. *Digital Terrain Modeling: Acquisition, Manipulation and Applications*, Artech House Publishers, Boston. 270 pp.

Evans I. 1972. General geomorphometry, derivatives of altitude and descriptive statistics. In Chorley, R.J., ed., Spatial Analysis in Geomorphology*: Harper and Row*, New York, 17–90.

Fassoulas C. 1999. The structural evolution of Central Crete: insight into the tectonic evolution of the South Aegean (Greece), *J. Geodynam*., 27, 23-43.

Goldfinger C., Kulm L.D., Yeats R.S., McNeill L.C. and Hummon C. 1997. Oblique strike-slip faulting of the central Cascadia submarine forearc*, Journal of Geophysical Research*, 102, 8217-8243.

Jolivet L., Goffé B., Monie P., Truffert-Luxey C., Patriat M. and Bonneau M. 1996. Miocene detachment on Crete and exhumation P-T-t paths of high-pressure metamorphic rocks. *Tectonics*, 15, 1129-1153.

Kamberis E., Bathrellos G., Kokinou E. and Skilodimou H. 2012. Correlation between the structural pattern and the development of the drainage network in the area of Western Thessaly basin (Greece), *Central European Journal of Geosciences*, 4(3), 416-424, doi: 10.2478/s13533-011-0074-7.

Keller E. 1986. Investigation of active tectonics: use of surficial earth processes. In Wallace, R. E., eds, *Active Tectonics studies in Geophysics*, Nat. Acad. Press, Washington, DC, 136–147.

Kennely P.J. 2008. Terrain maps displaying hill-shading with curvature, *Geomorphology*, 102, 567–577.

Kilias A., Fassoulas C. and Mountrakis D., 1994. Tertiary extension of continental crust and uplift of Psiloritis metamorphic core complex in the central part of the Hellenic Arc (Crete,Greece), *Geol. Rundsch*., 83, 417-430.

Kokinou E., Alves T. and Kamberis E. 2012. Structural decoupling on a convergent forearc setting (Southern Crete, Eastern Mediterranean), *Geol. Soc. Am. Bulletin*, 124(7/8), 1352–1364, doi:10.1130/B30492.1.

McCullagh M.J. 1998. Quality, use and visualisation in terrain modeling. In: Lane, S.N., Richards, K.S., Chandler, J.H. (Eds.), *Landform Monitoring, Modeling and Analysis*, John Wiley & Sons, Chichester, 95–117.

Moellering H., Kimerling and A.J. 1990. A new digital slope-aspect display process, *Cartography and Geographic Information Systems*, 17, 151–159.

Oguchi T., Aoki T. and Matsuta N. 2003. Identification of an active fault in the Japanese Alps from DEM-based hill shading, *Computers and Geosciences*, 29, 885–891.

Riquelmea R., Martinod J., Herail G., Darrozesa J. and Charrierb R. 2003. A geomorphological approach to determining the Neogene to Recent tectonic deformation in the Coastal Cordillera of northernChile (Atacama), *Tectonophysics*, 361, 255–275.

Rockwell T., Keller E. and Johnson D. 1984. Tectonic geomorphology of alluvial fans and mountain fronts near Ventura, California, in Morisawa, M., Hack T. J., eds., *Tectonic Geomorphology,* Publ. In *Geomorphology*, State University of New York, Binghamton, 183–207.

Silva P.G., Goy J.L., Zazo C. and Bardají T. 2003. Fault-generated mountain fronts in southeast Spain: geomorphologic assessment of tectonic and seismic activity, *Geomorphology*, 50, 203–225.

Smith M.J. and Clark C.D. 2005. Methods for the visualization of digital elevation models for landform mapping, *Earth Surface Processes and Landforms,* 30, 885–900.

Theocharis D. and Fountoulis I. 2002. Morphometric indices and tectonically active structures: the case of Salamis island, *Proc. of the 6th Panhellenic Geographical Congress, Geogr. Soc. Greece*, I, 97-106, (in Greek with English abstract).

Tsodoulos I., M. Koukouvelas I. K. and Pavlides S. 2008. Tectonic geomorphology of the easternmost extension of the Gulf of Corinth (Beotia, Central Greece), *Tectonophysics*, 453, 211–232.

Wells S.G., Bullard T. F., Menges C. M., Drake P. G., Karas P. A., Kelson, K. I., Ritter, J. B. and Wesling J. R. 1988. Regional variations in tectonic geomorphology along a segmented convergent plate boundary, Pacific coast of Costa Rica, *Geomorphology*, 1, 239–265..

Vidakis M., Meulenkamp J.E., Koutsouveli A., Ioakim Ch., Papazeti E. and Skourtsi-Koronaiou V. 1996. *Geological Map of Greece* in 1:50,000 scale – Heraklion Sheet. IGME, Athens.

Zachariasse W.J., van Hinsbergen, D.J.J. and Fortuin, A.R. 2011. Formation and fragmentation of a lateMiocene supradetachment basin in central Crete: implications for exhumationmechanisms of high-pressure rocks in the Aegean forearc, *Basin Res.*, 23, 678–701, doi: 10.1111/j.1365-2117.2011.00507.x.

Δελτίο της Ελληνικής Γεωλογικής Εταιρίας, τομ. XLVII , 2013
Πρακτικά 13ου Διεθνούς Συνεδρίου, Χανιά, Σεπτ. 2013

Bulletin of the Geological Society of Greece, vol. XLVII 2013
Proceedings of the 13th International Congress, Chania, Sept. 2013

MORPHOTECTONIC ANALYSIS OF FAULTS IN SPERCHIOS BASIN (FTHIOTIS, CENTRAL GREECE)

Michail M.[1] and Chatzipetros A.[1]

[1] Aristotle University, Department of Geology, 54124, Thessaloniki, Greece
mariamichail@geo.auth.gr, ac@geo.auth.gr

Abstract

This paper aims to study one of the major neotectonic, fault-controlled, features of the Hellenides, Sperchios basin, with the application of specific morphotectonic indices. The study area includes well exposed fault-bounded mountain fronts with dominant footwall relief. The most prominent structures of this WNW-ESE trending neotectonic basin are WNW-ESE to NW-SE trending faults, the most prominent of which is the Sperchios Fault System (SFS) causing mainly subsidence toward the NNE. The antithetic Coastal Fault System (CFS) also forms a distinct, yet gentler relief at the NE basin boundary. The segmentation of these neotectonic faults allowed detailed measurements, based on morphotectonic characteristics, of each segment separately. Mountain-front sinuosity (S_{mf}) as well as the ratio of valley floor width to valley height (V_f) were among the indices used in this study and contributed to the identification of the potential fault activity. The results show that there is a strong correlation between uplift rates and the morphotectonic signature of faulting, as well as a clear morphotectonic differentiation of fault segments.
Key words: *segmentation, morphotectonic indices, Sperchios basin, central Greece, active tectonics*

Περίληψη

Η παρούσα εργασία έχει ως στόχο τη μελέτη μίας από τις σημαντικότερες νεοτεκτονικές δομές των Ελληνίδων, τη λεκάνη του Σπερχειού, με την εφαρμογή συγκεκριμένων μορφοτεκτονικών δεικτών. Το εντυπωσιακό ανάγλυφο της περιοχής, με τις απότομες αλλαγές στη μορφολογική κλίση, διαμορφώνεται κυρίως λόγω της τεκτονικής. Οι πιο σημαντικές δομές αυτής της νεοτεκτονικής λεκάνης, με διάταξη ΔΒΔ-ΑΝΑ είναι τα ρήγματα ΔΒΔ-ΑΝΑ και ΒΔ-ΝΑ παράταξης, τα σημαντικότερα εκ των οποίων συνιστούν το Σύστημα Ρηγμάτων του Σπερχειού (SFS) με διεύθυνση βύθισης κυρίως προς τα ΒΒΑ. Το παράκτιο σύστημα ρηγμάτων (CFS), ορίζει επίσης τη λιγότερη έντονη μορφολογία στα ΒΑ όρια της λεκάνης. Η τμηματοποίηση των νεοτεκτονικών ρηγμάτων συντέλεσε στη λεπτομερή μελέτη του κάθε τμήματος χωριστά και στη πραγματοποίηση μετρήσεων, με βάση τα μορφοτεκτονικά τους χαρακτηριστικά. Η δαντέλωση στους πρόποδες των βουνών (Smf) καθώς και ο λόγος πλάτους κοιλάδας προς ύψος (V_f) ήταν μεταξύ των δεικτών που υπολογίστηκαν στην εργασία αυτή και συνέβαλαν στην αναγνώριση του δυναμικού δραστηριότητας των ρηγμάτων. Τα αποτελέσματα της εργασίας δείχνουν ότι υπάρχει ισχυρή συσχέτιση μεταξύ του ρυθμού ανύψωσης και των μορφοτεκτονικών χαρακτηριστικών των

ρηγμάτων, καθώς και μια σαφή διαφοροποίηση των δεικτών μεταξύ των τμημάτων της ρηξιγενούς ζώνης.
Λέξεις κλειδιά: *τμηματοποίηση, μορφοτεκτονικοί δείκτες, λεκάνη Σπερχειού, κεντρική Ελλάδα, ενεργός τεκτονική.*

1. Introduction - Geological Setting

The quantitative measurement of an active tectonic landscape, as well as landform evaluation, could provide us with basic information necessary for estimating long-term deformation. Sperchios Basin is one of the most important neotectonic features of Greece, within an area where active tectonics have drastically controlled and formed the landscape. Sperchios basin is located in the Fthiotis area, East Central Greece. It has a mean WNW-ESE axis, and it extends from Mt. Tymfristos to the west, to Maliakos Gulf to the east (Kranis, 1999). The basin is defined by the mountainous areas of Timfristos to the west, Othris to the east and Kallidromo to the south. Extension has dominated the deformation of the region in the Quaternary period, starting at Late Pliocene - Early Pleistocene, continuing until today. The most important structures are the WNW-ESE to NW-SE trending, NNE-dipping faults that control the margins of this neotectonic basin. However, faults with ENE-WSW and/or NE-SW strike are also present. In this paper we focus on the tectonically young southern margin of Sperchios Basin, which is dominated by large normal faults of E-W to WNW-ESE strike, like most of the neotectonic structures of central Greece (Psomiadis, 2010; Tzanis et al., 2010).

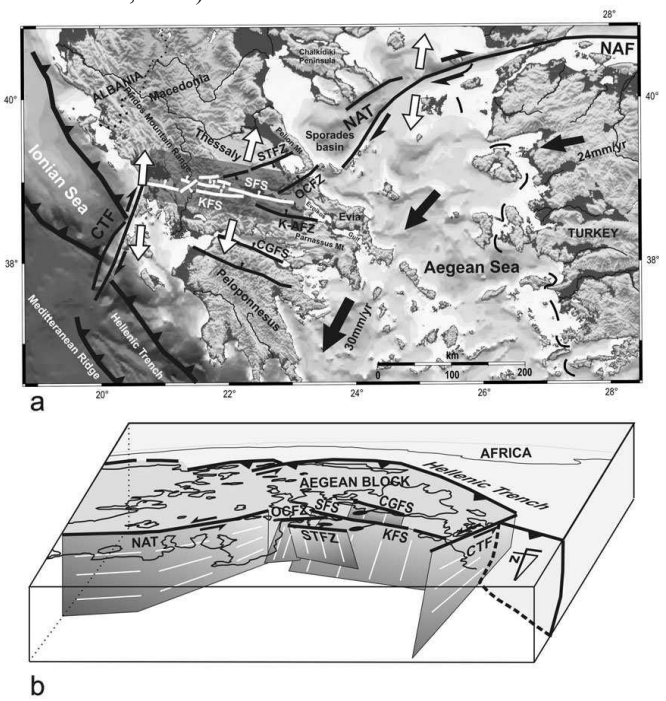

Figure 1 - (a) Generalized shaded relief map, showing the major structures that control Sperchios basin and the suggested relationship between the Sperchios Fault System (SFS) with the right-lateral North Aegean Trough (NAT), the Kefallonia Transform Fault (CTF), Kallidromo Fault System (KFS), Corinthos Golf Fault System (CGFS). The arrows indicate the different kinematics (contractional, extensional, strike-slip) and (b) 3D-tectonic sketch indicating the relationship of the KFS and SFS in Central Greece with the right lateral strike-slip CTF and NAT. The relative motion of the faults is indicated with white lines. (after Kilias et al. 2008).

The southern part of Sperchios basin is comprised by the Sperchios Fault System (SFS) (Figure 1, 2), which consists of two major fault segments, Sperchiada and Kompotades faults, at its western and eastern part, respectively, and the Coastal Fault System (CFS), the western part of the south coast of the North Gulf of Evia, comprising three main faults, the Arkitsa-Longos fault to the east, the Agios Konstantinos fault in the middle and the Kamena Vourla fault to the west (Ganas, 1997; Kranis, 1999) (Figure 2). In addition, it is suggested that the Sperchios Fault System (SFS), together with the Coastal Fault System (CFS), interact through an underlapping crustal relay zone, which accommodates the differential movement between the North Aegean Fault to the east and the Kefallonia Transform Fault to the west, on the western termination of the Hellenic Arc (Kilias et al., 2008). The basin includes pre-rift formations such as limestones, flysch, radiolarites, ophiolites and a volcaniclastic sequence, Neogene deposits and synrift formations of Tertiary and Quaternary age (alluvial fans) (Figure 2). Eliet & Gawthorpe (1995) studied the sedimentary supply of Sperchios basin in relation to active tectonics and footwall uplift, as recorded mainly in the Quaternary sedimentary sequences.

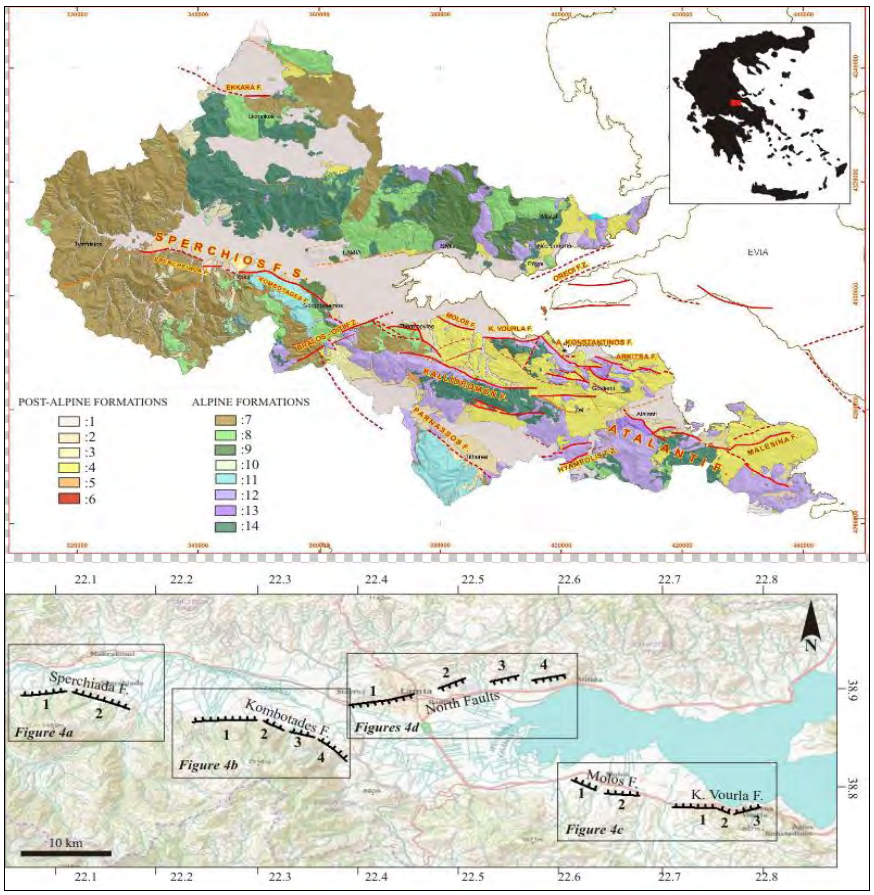

Figure 2 - Top: Geological – Neotectonic map of Fthtiotis (from Kranis, 1999). Post-Alpine formations: 1 - alluvial deposits, 2 - lateral scree, 3 - Pleistocene sediments, 4 - Neogene sediments, 5 - Molassic sediments, 6 - Quaternary volcanics (Lichades & Ag. Konstantinos areas) Alpine formations, 7 - Flysch, 8 - Upper Cretaceous carbonates, 9 - Schist-chert formation, 10 - Pindos and Vardousia carbonates, 11 - Parnassos carbonates, 12 - sub-Pelagonian carbonates, 13 - Volcanosedimentary complex, 14 - Ophiolites. Bottom: Topographic map indicating the faults and their segments of the current study (Sperchiada, Kompotades, Molos, Kamena Vourla and North Faults).

Geomorphic indices have been applied to mountain ranges worldwide in order to determine the relative tectonic activity (e.g. Bull & McFadden, 1977; Keller & Pinter, 1996; Gawthorpe & Leeder, 2000; Bull 2007, 2009). In this paper the faults that have been studied are the Sperchiada fault that bounds the southern part of the basin, Kompotades fault, which controls the central part of the basin, Molos and Kamena Vourla faults on the east-southern part and the North Faults, which are smaller scale faults at the northern part of the basin (Figure 2). The selection of those faults was based on the idea of collecting information from several parts of the basin (north, south, south-east, south-west), with the aim to make a general estimation of the current morphogenetic processes acting on the study area, thus to compare the tectonic activity between the different fault segments, in both southern and northern margins of the basin. The first stage was to separate the fault zones into smaller segments, based on published studies and field data (e.g. changes in the mountain front orientation, overstepping of fault strands, etc.). The second stage included the application of geomorphic indices along the segments of those neotectonic faults. The fault segmentation contributed to the general morphometric analysis of the area and the estimation of the degree of activity for each segment.

2. Methodology

The methodology used in this paper was based on the calculation of specific geomorphic indices, using a detailed Digital Elevation Model for the area and the characterization of fault segments in terms of activity, based on the results.

2.1. Geomorphic Indices

In this paper we have applied certain well-established and useful geomorphic indices associated with fluvial systems:

- **Transverse Topographic Symmetry (T)**

The Transverse Topographic Symmetry Factor is defined as:

$$T = \frac{D_a}{D_d} \tag{1}$$

where D_a is the distance from the midline of the active meander belt and D_d is the distance from the basin midline to the basin divide. For an absolutely symmetrical basin, T=0. As long as T increases and approaches the 1, the asymmetry increases. T is a vector, with direction and magnitude that varies from 0 to 1. The direction of a regional migration of the main stream channel could be an indication of the ground tilting in this direction. Values of T are calculated for different segments of a valley and indicate preferred migration of streams perpendicular to the drainage basin axis (Keller & Pinter, 1996). This method does not provide us with direct evidence of ground tilting, but it is an important fault activity indicator.

- **Mountain front sinuosity (Smf)**

Mountain front sinuosity (**S_{mf}**) is defined as:

$$S_{mf} = \frac{L_{mf}}{L_s} \tag{2}$$

where L_{mf} is the length of the mountain front along the foot of the mountain and L_s is the straight line length of the mountain front (Bull & McFadden, 1977; Keller & Pinter, 1996). This indicator reflects the balance between uplift, that tends to maintain a relatively straight front, and erosion, that tends to produce irregular fronts. Mountain fronts connected with active uplift are quite straight, but if the rate of uplift is reduced, erosional processes will begin to form a sinuous front that becomes more asymmetrical with time. S_{mf} values ranging between 1.0 and 1.6 values indicate

tectonically active fronts. Higher S_{mf} values (>3) are normally associated with inactive fronts in which the initial range front fault may be more than 1km away from the present erosional front (Bull & McFadden, 1977).

- **Ratio of Valley-Floor Width to Valley Height (Vf)**

The ratio of the width of valley floor to valley height (V_f) may be expressed by:

$$V_f = \frac{2 \cdot V_{fw}}{(E_{ld} - E_{sc}) + (E_{rd} - E_{sc})} \tag{3}$$

where V_{fw} is the width of valley floor, E_{ld} and E_{rd} are the elevations of the left and right valley divides respectively looking downstream and E_{sc} is the elevation of the valley floor (Bull & McFadden, 1977). This index reflects in this way differences between broad –floored canyons (U– shaped) with relatively high values of V_f (V_f values >1) and V–shaped canyons with relatively lower values of V_f (V_f values < 1) (Keller, 1986). Comparison of V_f values provide us with the information whether the streams are actively down cutting in response to active tectonics, forming V-shaped valleys, or are being eroded laterally, forming broad valleys, because of front stability and drainage.

- **Drainage Basin Asymmetry (AF)**

The asymmetry factor is expressed by:

$$AF = 100 \cdot \frac{A_r}{A_f} \tag{4}$$

where A_r is the area of the basin to the right (facing downstream) of the main stream and A_t is the total area of the drainage basin (Cox, 1994). In the area where drainage develops together with active tectonic deformation, the network tends to have a specific geometry. If the stream network continues to flow in a stable setting, AF should be almost equal to value 50. Values of AF greater or less than 50 infer "Tilting" to the left or to the right respectively.

2.2. Fault Segmentation

Fault segmentation is applied to different long faults around the world. The theories imply that faults initiate as separate faults, propagate, and ultimately link to form a long fault (e.g. Ganas & Papoulia, 2000). In order to achieve a better result in our study, we segmented the following faults into smaller sections, taking into consideration the changes in the mountain front orientation and the morphology along the faults.

- **Sperchiada Fault (Figure 3a) and Kompotades Fault (Figure 3b)**

Sperchiada fault to the west and Kompotades fault to the east are the two major segments of Sperchios Fault System, which control the southern margin of the Sperchios basin and have a total length of almost 80 km. We have distinguished two segments for the Sperchiada fault and four segments for the Kompotades Fault. The strike of those faults is E-W to WNW-ESE, while they dip to the NNE. The main criterion for distinguishing smaller segments is the small change in their orientation. This does not necessarily reflect their actual structural segmentation, but there is definitely a geomorphic segmentation that corresponds to different geomorphic quantification.

- **Molos Fault (Figure 3c) and Kamena Vourla Fault (Figure 3c)**

Molos and Kamena Vourla Faults are dipping to the NNW. Molos is a probable westward extension of the Coastal Fault System which controls the western part of southern coast of the North Gulf of Evia (Ganas, 1997). It is characterised by NW-SE strike and we have segmented it into two parts. Kamena Vourla fault, at the west part of the Coastal Fault System, is a high angle structure with an E-W strike.

- **North Fault zone (Figure 3d)**

The last fault zone tested in this paper is the North Fault zone. In contrast with the previously mentioned faults, North Fault zone controls the northern margin of Sperchios basin. It is approximately 10 km long with fault striking NE-SW and dipping to the SE. Four segments are proposed for the North Fault zone.

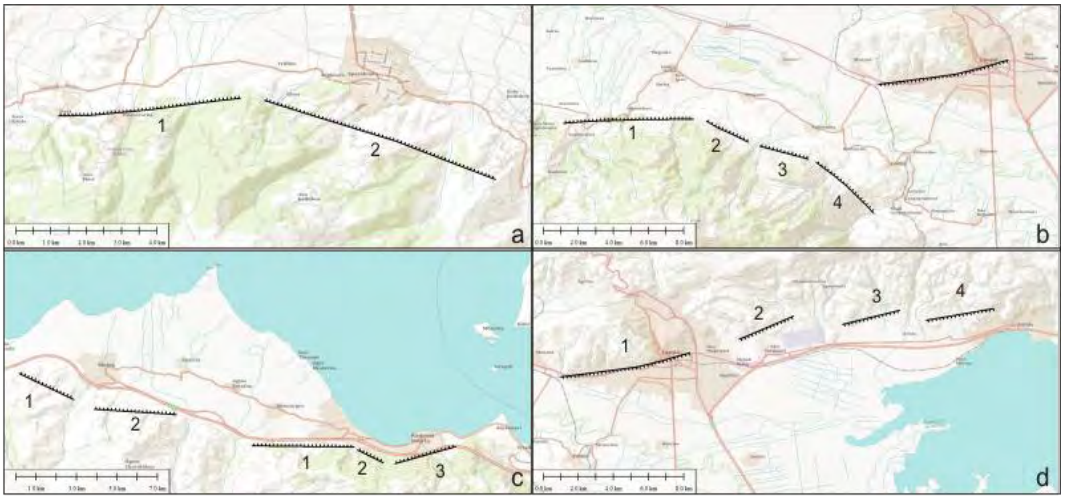

Figure 3 - Segmentation of the studied faults. (a) Sperchiada F. divided into two segments (b) Kompotades F. divided into four segments (c) Molos (two segments) and Kamena Vourla F. (three segments), (d) North Fault (four segments).

3. Data

The morphometric analysis in this paper is based on the application of geomorphic indices derived from a Digital Elevation Model (DEM) of the broader area. The work comprised of collection of published geological maps (IGME 1967, 1970), information based on publications, processing and evaluation of data and finally implementing the principal morphotectonic indicators on the fault segments by using Global Mapper 12 software. The data source was Aster GDEM, Worldwide Elevation Data (1.5 arc-second resolution) and the projection used was Greek Grid (GGRS87).

3.1. Tilting of Sperchios Basin

Two indices have been applied in order evaluate the Sperchios Basin asymmetry: Transverse Topographic Symmetry, T (Figure 4), and Drainage Basin Asymmetry, AF (Figure 5). In order to calculate the T index, the basin midline of Sperchios River was determined in the middle with a red line (Figure 4). Along this midline we have separated 13 equal 4-km long segments. Based on the results shown in the table of Figure 4, it is evident that T factor at the first segment as well as between sites p8 and p10, has the highest values, ranging from 0,35 to 0,45, suggesting that the asymmetry at the beginning and in the centre of the basin increases, in comparison to the other segments. Figure 4 shows the drainage basin asymmetry of Sperchios Basin. The area enclosed within the yellow line, along the watershed, is the total area of the basin. The red shaded area is the area to the right (facing downstream) of the main stream of Sperchios (blue). The asymmetry factor in Sperchios Basin has a value of 55, showing that the basin has a tectonic rotation (tilting) to the North. One would expect that the basin would show tilt towards the South, where the main fault zone is. However this is not the case for this basin. Our interpretation is that Sperchios fault zone produced a great footwall uplift, causing extensive erosion and hence formation of very big alluvial fans, e.g. the huge Vamvakia alluvial fan at the central part of the basin. These fans have

shifted the position of Sperchios River towards the North, overprinting the tectonic signature of Sperchios fault.

Transverse Topographic Symmetry factor of Sperchios Basin (T)				
Distance	Spot	Da	Dd	T
4 km	p1	6,8	14,5	0,47
8 km	p2	3,1	15,1	0,21
12 km	p3	1,6	16,1	0,10
16 km	p4	1,6	15	0,11
20 km	p5	3,5	15,7	0,22
24 km	p6	0,33	11,2	0,03
28 km	p7	1,9	11,3	0,17
32 km	p8	4,7	13,6	0,35
36 km	p9	7,2	15,9	0,45
40 km	p10	6,8	17,5	0,39
44 km	p11	3,8	14,8	0,26
48 km	p12	3,1	12,8	0,24
52 km	p13	1,5	11,1	0,14

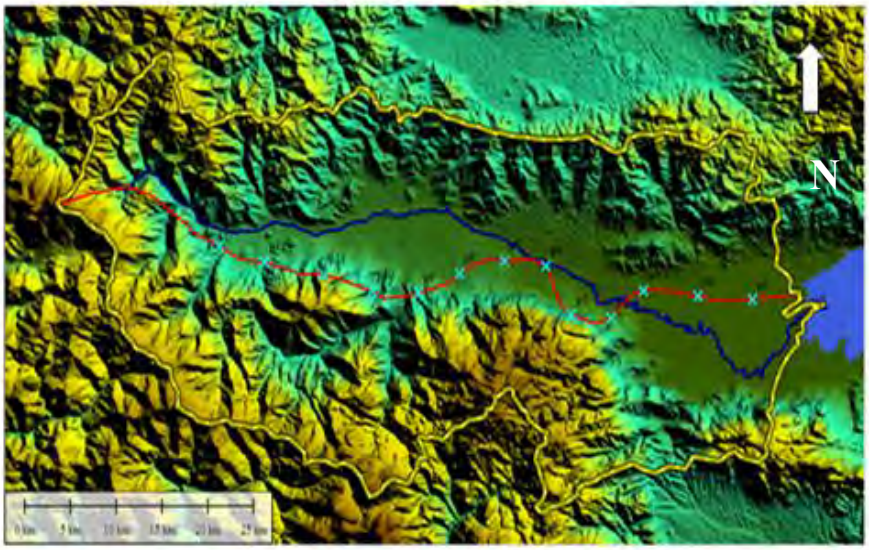

Figure 4 - (a) Table with the results of Transverse Topographic Symmetry (T) along the whole Sperchios Basin. (b)View from Global mapper, showing the 4-km long segments (p1, p2, …, p13) separated by a light blue x symbol, along basin midline, blue line: main river, red line: basin midline, yellow line: Sperchios basin watershed.

3.2. S_{mf} and V_f values for Sperchios, Kompotades, Molos, Kamena Vourla and North Faults

The application of S_{mf} and V_f geomorphic indices along the segments of the these faults can contribute towards a comprehensive overview of the neotectonic activity. The V_f values are plotted with the S_{mf} values on a same diagram. This combination provides quantitative information of the relative degree of tectonic activity classes of the segmented faults and allows individual mountain fronts to be assigned in different tectonic activity classes (Bull & McFadden, 1977; Keller & Pinter, 1996). The S_{mf} and the mean V_f values of all the segmented faults in our study, are shown in the S_{mf} vs. V_f diagrams (Figure 6 a, b, c).

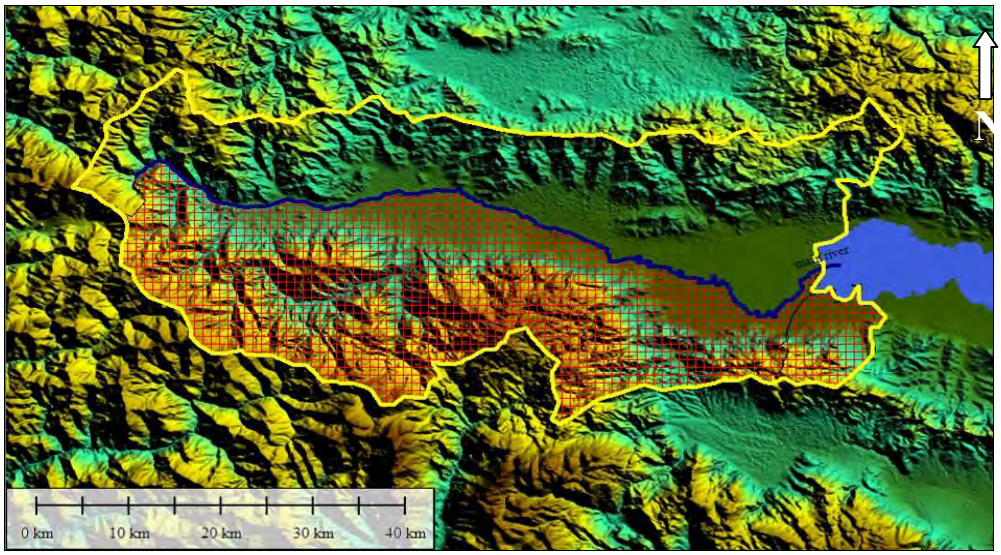

Figure 5 - Drainage Basin Asymmetry (AF). Red area: A_r, the area of the basin to the right (facing downstream) of the main stream, area within yellow line: A_t, the total area of the drainage basin. A_t: 1,830 km^2, A_r : 1,015 km^2.

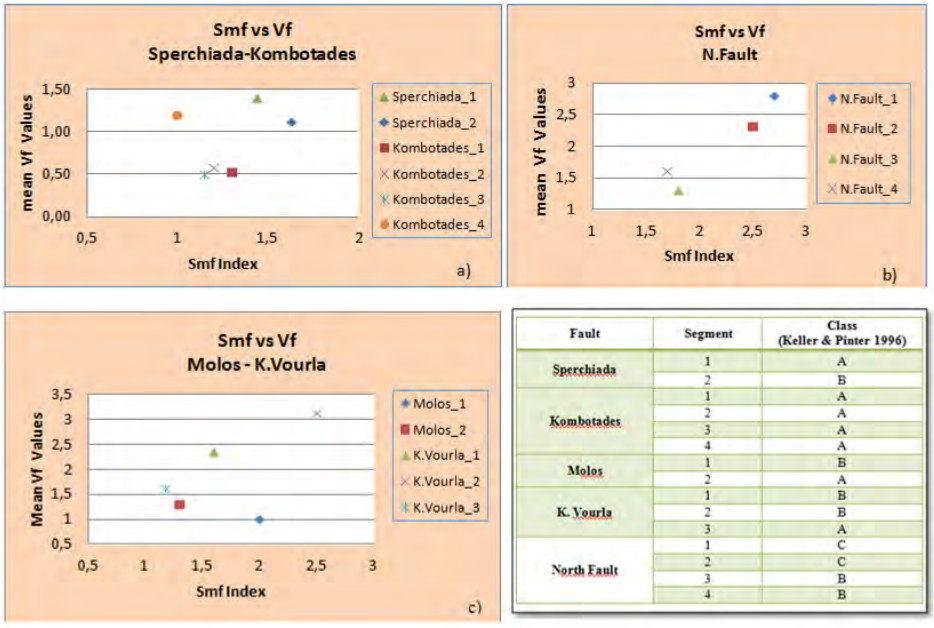

Fault	Segment	Class (Keller & Pinter 1996)
Sperchiada	1	A
	2	B
Kombotades	1	A
	2	A
	3	A
	4	A
Molos	1	B
	2	A
K. Vourla	1	B
	2	B
	3	A
North Fault	1	C
	2	C
	3	B
	4	B

Figure 6 - Plot of mean S_{mf} and V_f values of all the segmented faults of this study (a) Sperchiada and Kompotades faults, (b) North faults, (c) Molos and Kamena Vourla faults. Table: Classification of segments of each fault separately, according to the tectonic class division by Keller & Pinter (1996).

According to the active tectonic classification suggested by Keller & Pinter (1996), each fault segment appears to have a different activity, regardless their position or the fact that some of them even belong to the same Fault. The first (A) tectonic class comprises values of S_{mf} lower than 1.5

and V_f values lower than 1.2. The second class consists of S_{mf} lower than 2.5 and V_f lower than 1.5 and the third class is characterized by S_{mf} higher than 2.6.

The two segments of Sperchiada Fault are of tectonic class A and B, for the western and eastern part respectively. In addition, for the Kompotades fault case its eastern part has lower S_{mf} values related to its western part, however all of the segments belong to the A class, which characterizes the more active faults. The results are in good agreement with Zovoili et al. (2004). Moreover, Molos fault, is separated into two different segments which show a different activity, with the western part (Molos_1) less active than the eastern. Three segments have been distinguished for Kamena Vourla fault. All of them reveal an active behaviour with the eastern segment (K.Vourla_3) showing higher activity (class A). Finally, North faults seem to have a lower activity in comparison with the southern marginal large faults.

4. Conclusions

The aim of this paper was to make a general estimation of the neotectonic signature of faulting to the relief in Sperchios basin and to compare the tectonic activity between the different fault segments, in both southern and northern margins of the basin. The application of the geomorphic indices associated with fluvial systems (T, AF, S_{mf}, V_f) on Sperchios basin and Sperchiada, Kompotades, Molos, Kamena Vourla and North faults, helped in correlating the current landscape form with the neotectonic evolution of the area. Based on the combination of the derived geomorphic indices, Sperchios Basin appears to have a tectonic tilting (high T values in the centre of the basin) to the North (AF=55). After having all the above faults classified based on their S_{mf} and V_F values, we suggest that North Faults appear to be less active (B to C class) in comparison with all the others (A to B class). In addition we observed that even along the same fault the segments seem to have a different tectonic activity.

In respect to segmentation, quantitative morphotectonic analysis can provide valuable information, complementary to structural criteria in order to segment a fault zone. In Sperchios basin the morphotectonic segmentation is in good agreement with the segmentation derived from mapping and structural analysis. It has to be noted however that quantitative morphotectonic analysis can only provide indications, not evidence of recent tectonic activity. It is therefore important to extend the deformation record of Sperchios fault zone by geological methods (i.e. paleoseismology), in order to enhance the morphotectonic observations.

5. Acknowledgements

The authors would like to thank reviewers Drs. A. Ganas and S. Kokkalas, for their critical and helpful comments, which led to substantial improvement of this paper. The second author has been partly supported by the project “Characterization of site conditions in Greece for realistic seismic ground motion simulations: pilot application in urban areas”, a THALES programme project, funded by the General Secretariat for Research and Technology of Greece.

6. References

Bull W. and McFadden L. 1977. Tectonic geomorphology north and south of the Garlock Fault, California, Geomorphology in Arid regions, D.O., Doehring, ed., *Publications in Geomorphology*, State University of New York at Bingamton, 115–138.

Bull W. 2007. *Tectonic geomorphology of mountains: a new approach to paleoseismology.* Wiley-Blackwell; 1 edition.

Bull W. 2009. *Tectonically Active Landscapes.* Wiley-Blackwell; 1 edition.

Cox R.T. 1994. Analysis of drainage basin symmetry as a rapid technique to identify areas of possible quaternary tilt block tectonics: an example from the Mississippi embayment, *Geol. Soc. Am. Bull.*, 106, 571 – 581.

Eliet P.P.and Gawthorpe R.L. 1995. Drainage development and sediment supply within rifts, examples from the Sperchios Basin, central Greece, *Journal of the Geological Society of London*, 152, Part 5, 883-893.

Ganas A. 1997. Fault segmentation and seismic hazard assessment in the Gulf of Evia Rift, central Greece. *Unpublished PhD thesis,* University of Reading*,* 369 pp.

Ganas A. and Papoulia I., 2000. High-resolution, digital mapping of the seismic hazard within the Gulf of Evia Rift, Central Greece using normal fault segments as line sources, *Nat. Hazards,* 22(3), 203-223.

Gawthorpe R.L. and Leeder M.R. 2000. Tectono-sedimentary evolution of active extensional basins, *Basin Research,* 12, 195–218

IGME 1967. Geological map of Greece, scale 1:50,000, Lamia sheet. *Institute of Geology and Mineral Exploration,* Athens*.*

IGME, 1970. Geological map of Greece, 1:50,000, Sperchias sheet, *Institute of Geology and Mineral Exploration,* Athens*.*

Keller A.E.and Pinter N. 1996. *Active Tectonics: Earthquakes, Uplift and Landscape,* Prentice Hall, 338 p.

Keller E. 1986. Investigation of active tectonics: use of surficial earth processes. In: Wallace, R.E. (Ed.), *Active Tectonics*. *Studies in Geophysics*. Nat. Acad. Press, Washington, DC, p136-147.

Kilias A., Tranos M., Papadimitriou E., Karakostas V., 2008. The recent crustal deformation of the Hellenic orogen in Central Greece; the Kremasta and Sperchios Fault Systems and their relationship with the adjacent large structural features, *Z. dt. Ges. Geowiss*., 159/3, 533-547.

Kranis H.D. 1999. Neotectonic activity of fault zones in central-eastern mainland Greece (Lokris). *Ph.D. Thesis.*

Psomiadis E. 2010. Research of geomorphological and environmental changes in the Sperchios River Basin utilizing new technologies, *Ph.D. Thesis.*

Tzanis E., Kranis H. and Chailas S. 2010. An investigation of the active tectonics in central Greece with imaging and decomposition of topographic data, *Journal of Geodynamics,* 49, 55-67.

Zovoili E., Konstantinidi E. and Koukouvelas I.K. 2004. Tectonic geomorphology of escarpments: the cases of Kompotades and Nea Anchialos faults, *Bulletin of the Geological Society of Greece*, 36, 1716-1725.

Δελτίο της Ελληνικής Γεωλογικής Εταιρίας, τομ. XLVII , 2013
Πρακτικά 13ου Διεθνούς Συνεδρίου, Χανιά, Σεπτ. 2013

Bulletin of the Geological Society of Greece, vol. XLVII 2013
Proceedings of the 13th International Congress, Chania, Sept. 2013

ASSESSMENT OF THE SUSCEPTIBILITY OF THE COAST OF ASTYPALAEA ISLAND (S.E. AEGEAN SEA) TO SEA-LEVEL RISE

Papoulia M.[1], Karymbalis E.[2], Gaki-Papanastassiou K.[1] and Maroukian H.[1]

[1] Department of Geography-Climatology, Faculty of Geology and Geoenvironment, National and Kapodistrian University of Athens, Greece, papoulia.m@gmail.com, gaki@geol.uoa.gr, maroukian@geol.uoa.gr

[2] Department of Geography, Harokopio University, Athens, Greece, karymbalis@hua.gr

Abstract

The aim of this paper is the classification of the coast of Astypalaea Island (S.E. Aegean Sea) according to its susceptibility to an anticipated future sea-level rise, using the Coastal Sensitivity Index (CSI), and utilizing GIS technology. This index allows the following six physical variables: geomorphology, coastal slope, relative sea-level rise rate, shoreline erosion or accretion rate, mean tidal range and mean wave height, to be related in a semi-quantitative manner. Each variable is ranked on the basis of its potential contribution to physical changes on the coast as sea-level rises. Following the CSI calculation, a map is produced for the coastline of the island. This map showed that an extensive length of the coast (121.5 km, corresponding to 84.6% of the island's coastline) is characterized as very low and low sensitive. Only 12.1 km of the coast, corresponding to 8.5% of the entire coastline, is characterized as very highly and highly sensitive to sea- level rise, primarily due to the low topography and the presence of highly erodible geological formations and landforms. Areas of high and very high CSI values host socio-economically important land uses and activities as well as environmentally protected areas.

Key words: *Coastal Sensitivity Index (CSI), coastal geomorphology.*

Περίληψη

Σκοπός της εργασίας είναι η κατηγοριοποίηση των ακτών της νήσου Αστυπάλαιας (Ν.Α. Αιγαίο) ως προς την επιδεκτικότητά τους στην αναμενόμενη (μελλοντική) άνοδο της θαλάσσιας στάθμης, εφαρμόζοντας το Δείκτη Επιδεκτικότητας Ακτών με τη χρήση της τεχνολογίας των Συστημάτων Γεωγραφικών Πληροφοριών. Ο δείκτης αυτός επιτρέπει τη συνεκτίμηση με ημι-ποσοτικό τρόπο έξι μεταβλητών: γεωμορφολογία, παράκτια κλίση, ρυθμός μεταβολής της σχετικής ανόδου της θαλάσσιας στάθμης, ρυθμός προέλασης/υποχώρησης της ακτογραμμής, μέσο εύρος παλίρροιας και μέσο σημαντικό ύψος κύματος. Η κάθε παράμετρος κατηγοριοποιήθηκε με βάση τις φυσικές μεταβολές που ενδέχεται να υποστεί η ακτή από την άνοδο της θαλάσσιας στάθμης. Η εφαρμογή του δείκτη οδήγησε στη σχεδίαση ενός χάρτη επιδεκτικότητας του νησιού στην άνοδο της θαλάσσιας στάθμης. Σημαντικό μήκος της ακτογραμμής (121.5km που

αντιστοιχεί στο 84.6% του συνόλου των ακτών του νησιού), εμφανίζει χαμηλή ως πολύ χαμηλή επιδεκτικότητα. Υψηλή και πολύ υψηλή επιδεκτικότητα στην άνοδο της στάθμης της θάλασσας, κυρίως λόγω της χαμηλής τοπογραφίας και της παρουσίας ιδιαίτερα επιρρεπών στη διάβρωση γεωλογικών σχηματισμών και γεωμορφών, εμφανίζουν μόλις 12.1 km των ακτών, που αντιστοιχούν στο 8.5% του συνόλου της ακτογραμμής . Οι περιοχές υψηλής και πολύ υψηλής επιδεκτικότητας συγκεντρώνουν σημαντικές κοινωνικοοικονομικά χρήσεις γης και τουριστικές δραστηριότητες, ενώ περιλαμβάνουν και περιβαλλοντικά προστατευόμενες περιοχές.
Λέξεις κλειδιά: *Δείκτης Επιδεκτικότητας Ακτών, παράκτια γεωμορφολογία.*

1. Introduction

The global average temperature has increased over the past century. Although the global warming in the previous century was estimated to be 0.8^{o}C, the rise in temperature in the last 30 years alone was 0.6^{o}C at a rate of 0.2^{o}C per decade as greenhouse gases became the dominant climate forcing (Rosenzweig et al., 2008). Perhaps the most commonly recognized impact of global warming is the eustatic rise in sea- level due to the thermal expansion of seawater and the addition of ice- melt water (Allen et al., 2006). The IPCC report of 2007 predicted that global sea- level will rise at least 59cm by 2100.

Recent projections of global sea- level rise due to climate change have generated an interest in coastal science to determine the response of coastlines to sea- level change. Various approaches have been proposed to predict the evolution of the coastal zone under the influence of anticipated sea-level rise. Each approach has its shortcomings or can be invalid for certain applications. The most important among these methods include the extrapolation of historical data (predominantly concerning the shifting of the shoreline), the application of static inundation models or simple geometric models like the Bruun Rule application of sediment dynamics models and probabilistic simulation based on parameterized physical forcing variables (Thieler and Hammar- Klose, 1999). Although a viable totally quantitative prediction of the coastal response to the sea-level rise is not available, the relative susceptibility of different coastal environments to sea-level rise may be quantified taking into account information on coastal geomorphology, rate of sea-level rise and other related factors.

The aim of this paper is to classify the coastal zone of Astypalaea Island with respect to its sensitivity to the anticipated future sea- level rise, through the calculation of the Coastal Sensitivity Index (CSI), similar to the formula proposed by Thieler and Hammar- Klose (1999). Identifying sections of shoreline susceptible to long- term sea-level rise is necessary for more effective coastal zone management, to increase resilience, and to help reduce the impacts of climate change on both infrastructure and human beings. Similar CSI calculation approaches have already been applied in Greece for the Aegean Sea Coast (Alexandrakis et al., 2009) as well as in a more detailed scale for the coasts of northeast Attica (Chatsieleftheriou et al., 2010), Argolikos Gulf (Gaki-Papanastassiou et al., 2011) and the Gulf of Corinth (Nasopoulou et al., 2012; Karymbalis et al., 2012).

In this study, the term sensitivity (which means susceptibility) is used rather than vulnerability because the latter term generally refers to human vulnerability to particular hazards and therefore requests a consideration of socioeconomic factors such as population, infrastructure, etc.

2. Study Area

Astypalaea Island, the westernmost island of the Dodecanese group, 300km SE of mainland Greece, has an area of 96km^2 and a coastline of 143.5 km (Figure 1).

The island has 1,310 inhabitants, (2011 Census). Along with numerous smaller uninhabited offshore islets (the largest of which are Syrna and Ofidoussa), it forms the municipality of Astypalaea which belongs to the Kalymnos regional unit. Astypalaea is an island that has suffered from coastal natural hazards in the past with most severe the 1956 AD southern Aegean Tsunami (Dominey-Howes et al., 2000; Okal et al., 2009).

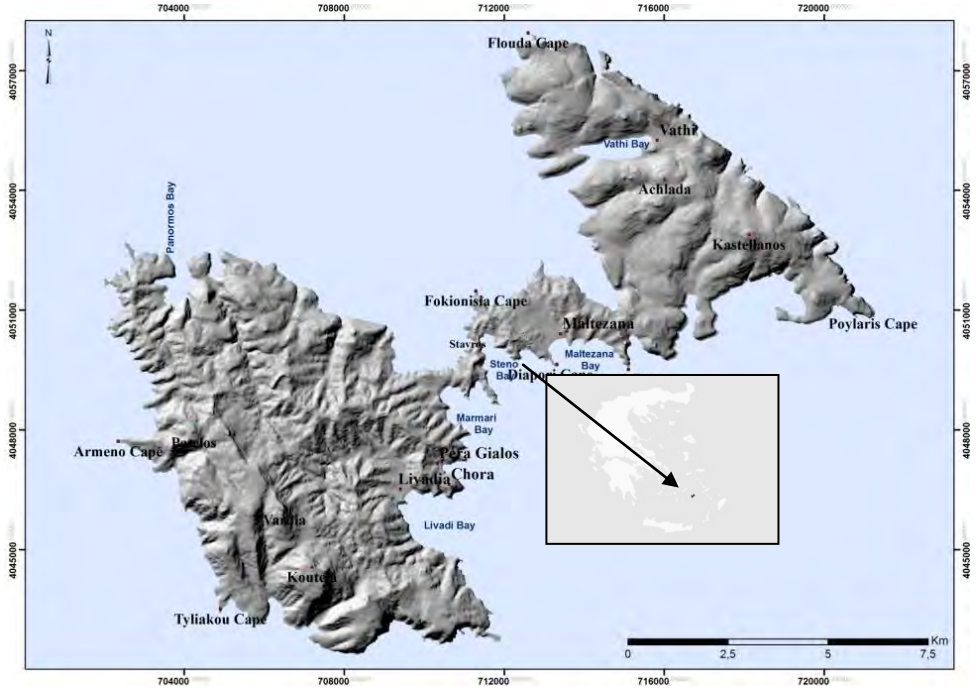

Figure 1 - Location and morphology of study area.

A small band of land of roughly 10km, almost separates the island into two sections: the inner and the outer island (hence the name butterfly island). The low-land of the island is centered on this band of land. The highest mountain top has an altitude of 481m and is located in the western part of the island. Morphologically, the central part of the island is characterized by a gentle topography in whereas the western and eastern parts have a rough relief.

Astypalaea Island is situated between the Late Cretaceous - Eocene high-pressure metamorphic belt of the Cyclades and the Miocene high-pressure metamorphic belt of the External Hellenides. It is made up of weakly metamorphosed limestones and marls of the Tripolis geotectonic unit, which are overlain by Eocene to Oligocene flysch formations (IGME, 1986). The post Alpine formations include Quaternary deposits such as coastal sediments and calcarenites.

The 93.6% of the coastline of Astypalaea consists of coastal cliffs. Nearly 14.22% is occupied by rocky cliffs with slope greater than 30 degrees, 46.8% of the coastline is made of medium cliffs (slope values between10 and 30 degrees) and the rest is occupied by rocky cliffs with slope less than 10 degrees. Apart from cliffs, there are also other rocky coastal landforms on the island such as sea caves and coastal benches. Almost all the beaches of the island are characterized as pocket beaches and consist of cobble, pebbles and rarely sands. Pocket beaches are located mainly in Maltezana, Livadia and Panormos Bays.

Astypalaea has been selected s a case study for the application of the Coastal Sensitivity Index mainly due to the geomorphic variation in coastal environments in addition to the prevailing socioeconomically important land uses and activities of the island such as agriculture and tourism.

3. Methodology and Data Collection

The CSI estimated in this study is a modification of the Coastal Vulnerability Index proposed by Thieler and Hammar- Klose (1999), which modified the original index produced by Gornitz et al. (1994). This index allows six variables to be related in a quantifiable manner to express the relative sensitivity of the coast to physical changes due to future sea- level rise. The CSI is calculated as the square root of the product of six variables divided by their total number (six) (equation 1). The variables are ranked from 1 to 5 according to table 1, with a rank of 1, indicating very low sensitivity and a rank of 5 indicating very high sensitivity. For some of the variables, the ranges of sensitivity ranking proposed by Karymbalis et al. (2012) specifically for the coastal environment of Greece are taken into consideration. The six variables are: geomorphology, coastal slope, historic shoreline change, relative sea level rise rate, mean tidal range and mean significant wave height.

Equation 1- Formula for CSI calculation

$$CSI=\sqrt{(a*b*c*d*e*f)/6}$$

Data concerning the geomorphology variable were derived from detailed (at the scale of 1:5,000) field coastal geomorphological mapping. Since this variable also represents the bedrock outcropping along the shoreline, data for the rock types were interpreted from the geological map of the island at a scale of 1:50,000 published by the Greek Institute of Geology and Mineral Exploration (IGME, 1986). In order to estimate the coastal slope (in percentage), a slope map of the coastal zone was created with the use of the detailed 1:5,000 topographic maps of the area. By using this map as the main elevation source, the digital elevation model (DEM), of the coastal zone was created. Next for the zone, the slope map was implemented within ArcGis spatial analysis extension environment, and the map of slope zones (according to table 1) was produced. Finally, for the assignment of the proper slope categorization to each coastline segment, the intersection of slope zones with the coastline was performed. Mean shoreline erosion or accretion rates were obtained from interpretation of aerial photos of the island taken in 1986 and 2009 respectively.

Table 1- Ranges for sensitivity ranking of the six variables.

VARIABLES	Categories				
	1	2	3	4	5
Geomorphology	rocky cliffed coasts (limestone cliffs)	medium cliffs (flysch cliffs)	low cliffs (calcarenite cliffs)	cobble beaches	sandy beaches
Shoreline erosion (-)/accretion (+) rate m/year	>(+2.0)	(+2.0)-(+1.0)	(+1.0)-(-1.0)	(-2.0)-(-1.0)	<(-2.0)
Coastal slope (%)	>12%	9-12%	6-9%	3-6%	<3%
Relative sea-level rise (mm/year)	<1,8	1,8-2,5	2,5-3,0	3,0-3,4	>3,4
Mean wave height (m)	<0,3	0,3-0,6	0,6-0,9	0,9-1,2	>1,2
Mean tide range (m)	>6,0	4,0-6,0	2,0-4,0	1,0-2,0	<1,0
Sensitivity	Very low	Low	Moderate	High	Very high

Although relative sea- level change is the combination of both the global eustatic sea-level rise as well as local isostatic and/or tectonic land movements, for this study this variable includes only the

eustatism component. This is because no recent local tide gauge measurements of the relative sea-level change or published information concerning the slip rates of the faults of the broader area of the island were available. Mean tidal range was deduced from published information (Tsimplis, 1994). The mean annual values of significant wave height have been abstracted from the Wave and Wind Atlas of the Hellenic Seas (Soukisian et al, 2007) which is based on offshore measurements for the time period between 1999 and 2007 (POSEIDON program).

To obtain a preliminary assessment of the impacts of the anticipated sea-level rise on socio-economic activities, land cover of the coastal zone was identified utilizing the relevant map of the Corine 2000 Land Cover Program (table 2). Seven land cover categories were recognized, including urban areas, natural vegetation, cultivations etc. Land cover classes were compared with areas of higher CSI values, which represent the highly and very highly sensitive segments of the shoreline.

GIS software ArcGis (ver. 10.0), provided the platform for the coastal mapping and calculation of the index. For each variable the entire coastline of the island is segmented into five sensitivity classes, and a sensitivity rank number is assigned to each segment of the coast indicating the sensitivity level in terms of the given variable. The method of computing CSI in this study is similar to that applied by Pendelton et al (2005) and Thieler and Hammar- Klose (1999). In order to display the results of the index derived from integration of the variables, a template of segments has been derived for the coast. The segment-based template has been used to store and portray data for each of the variables in an attribute table (in vector format using shapefiles in ArcGis), for adjacent segments along the coast. For each of the six variables, a ranking on a scale of 1-5 was assigned to each segment (with rank 1 representing very low sensitivity and rank 5 indicating very high sensitivity) following the classification scheme outlined in table 1. The final CSI map generated combining all the variables, showed 503 segments of the coast each having a unique identity in its corresponding attribute table. Another field is added to this attribute table for the CSI formula so that the system generated the CSI values for all the coastline segments of the island. The resulting output of CSI values were categorized into five classes by applying the natural breaks classification method such that the discrete index values of coastline segments are ranked in terms of their magnitude for the construction of the final CSI zonation map.

Table 2 - Shoreline segments' length and corresponding percentage of the seven land cover categories that occupy the five sensitivity classes along the coast of Astypalaea Island (land cover data obtained from Corine, 2000).

LAND USE TYPES	**Sensitivity**									
	Very low		**Low**		**Moderate**		**High**		**Very high**	
	%	*Km*	*%*	*Km*	*%*	*Km*	*%*	*Km*	*%*	*Km*
Natural grassland	78,40	87,35	69,43	6,94	74,25	7,39	79,82	8,51	19,96	0,31
Airport	0,23	0,25	-	-	-	-	-	-	-	-
Discontinuous urban fabric	0,72	0,80	-	-	-	-	0,84	0,09	-	-
Sclerophyllous vegetations	19,74	22,00	28,84	2,88	23,55	2,34	13,36	1,42	15,29	0,24
Complex cultivation patterns	0,75	0,83	0,48	0,05	2,20	0,22	4,68	0,50	53,92	0,83
Agricultural land, with areas of natural vegetation	0,16	0,18	1,25	0,13	-	-	1,03	0,11	-	-

Non-irrigated arable land	-	-	-	-	-	-	0,26	0,03	10,82	0,17
Total	100	111,43	100	10,0	100	9,95	100	10,66	100	1,54

4. Results

4.1. CVI Variables

The geomorphology variable is a non numerical one and expresses the relative response of different types of coastal landforms to sea- level rise (Gaki-Papanastassiou et al., 2011). It considers also the relative resistance of various geological formations occurring along the shoreline to marine erosion processes. Thus, it is ranked qualitatively according to the relative strength of the coastal landforms and rocks. The main coastal landforms of the study area identified during the field coastal geomorphological mapping were marine cliffs composed of various rock types such as limestones and flysch, as well as gravelly beaches. Marine cliffs represent the main landform of the island occupying a total length of 134.4 km, which corresponds to 93.66% of the coastline. Cobble beaches occupy 5.4km or 3.74% of the coastline while sandy beaches occupy 3.7km or 2.6% of the total coastline (Figure 2). Most of the beaches on the island are recognized as pocket beaches. The different landforms recognized were classified as shown in the table of Figure 2.

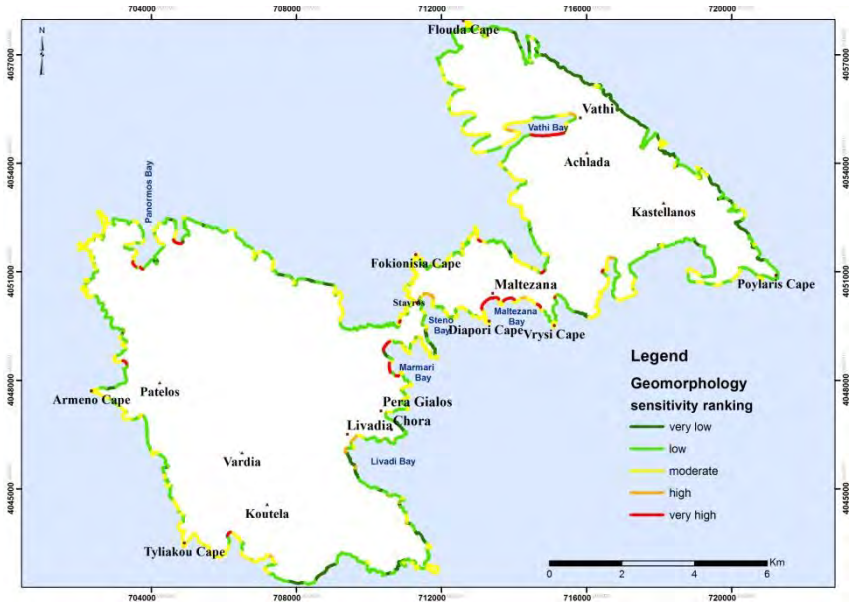

Geomorphology	rocky, cliffed coasts	medium cliffs	low cliffs	cobble beaches	sandy beaches	total
length (%)	14,22	46,81	32,63	3,74	2,6	100
length (km)	20,4	67,2	46,8	5,4	3,7	143,5
Sensitivity	very low	low	moderate	high	very high	

Figure 2 - Table and map of sensitivity classification of the Astypalaea Island coastline according to the variable of geomorphology.

Among the considered variables, coastal slope is the main indicator of inundation risk. Determination of the regional coastal slope identifies the relative sensitivity of inundation and the

potential rapidity of shoreline retreat as low-sloping coastal regions should retreat faster than steeper ones (Dwarakish et al., 2009). Regions with coastal slope less than 3% were characterized as very highly sensitive, while cliffs with slope higher than 12% were of very low sensitivity. The 5.25% of the coastal zone, mainly in Maltezana and Livadi Bays, is low-lying and is characterized as highly susceptible to inundation. More than 79% of the coastline, which corresponds to more than 114km of the total coastline, is characterized as very low sensitive. That's due to the presence of steep rocky cliffs (Figure 3).

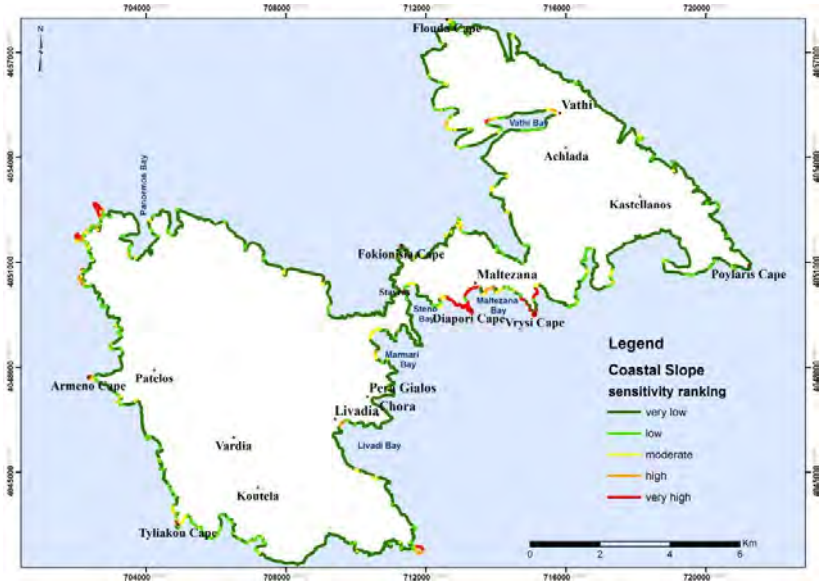

Coastal Slope (%)	>12%	12-9%	9-6%	6-3%	<3%	total
length (%)	79,5	5,6	5,34	4,31	5,25	100
length (km)	114,2	8,01	7,6	6,2	7,5	143,5
Sensitivity	very low	low	moderate	high	very high	

Figure 3- Table and map of sensitivity classification of the Astypalaea Island coastline according to the variable of coastal slope.

Coastline change rates in Astypalaea Island incorporate change rates from +1m/year of accretion (moderate sensitivity) to -2m/year of erosion (very high sensitivity) between 1986 and 2009. A shoreline length of 138.6km (or 96.5% of the entire coastline) is relative stable (mean shoreline shifting rate within ± 1 m/year), while only 0.7km (or 0.5% of the coastline) belongs to the class 5 – very high sensitivity (Table 1). Field coastal geomorphological mapping has verified that erosion is the main process along Maltezana beach in Maltezana Bay.

Relative sea- level change is considered to have the same value along the island's coastline. During the field survey submerged archaeological ruins of Late Roman- Early Byzantine age were found in Maltezana at about 50cm below the present sea-level. Considering Lambeck's (1996) sea-level curve for the Aegean Sea it is obvious that submergence is the result of glacio-eustatic rise of sea-level. This indicates that eustatism is the main sea-level rise cause for the island since that period. Hence, this variable took the value 1.8mm/year (low sensitive- class 2 in table 1), which is the mean eustatic global sea- level rise rate for the time period 1850-1950 (Solomon et al., 2007).

The variable of tidal range is linked to both inundation and erosion hazards (Gornitz, 1991). Micro-tidal coasts (tidal range< 2m), are at high risk and macro-tidal (tidal range > 4m) coasts are at low risk (Abuodha et al., 2010). The reason for this ranking is the potential influence of storms

on coastal evolution and their impact relative to the tide range. A micro–tidal coast is essentially near high tide and therefore always at the greatest risk of inundation from storms. Astypalaea Island is a micro-tidal region with astronomical tide range < 0.15m (Tsimplis, 1994). As such, the tidal range variable is ranked according to Thieler and Hammar- Klose (1999) with the value 5 (highly sensitive).

Wave height is proportional to the square root of wave energy, which is a measure of the capacity for erosion. The wave climate of the island is dominated by offshore significant wave heights of 0.6-1.2m, according to the output of the wave model (Poseidon program), which have been calibrated with the use of offshore field measurements (Soukisian et al., 2007). Hence, 30.78% of the coastline along the southern part of the island (which corresponds to 44.2km of the entire coastline) is considered to have moderate sensitivity and the rest of the coastline is considered to have high sensitivity.

4.2. The CSI Values

The calculated CSI values along the coastline of Astypalaea Island range between 3.87 and 25.81. The median value of the index for the study area is 10.0, and the standard deviation is 4.36. CSI values above 17.89 are classified as indicative of very high sensitivity. Only 12.1 km of the coastline corresponding to 8.5% of the entire coastline, is characterized as very highly and highly sensitive to sea- level rise, primarily due to low topography and the presence of highly erodible geological formations and landforms. Nearly 111.5 km of the shoreline (or 77.60% of the total coastline) is characterized as very low sensitive with CSI values between 3.87 and 7.74 (Figure 4). Very highly sensitive areas are located in Maltezana Bay (Maltezana village), Vathi Bay and Livadia Bay (Livadia village). Highly sensitive areas are found in Marmari Bay, west of Diapori Cape and on the northwest part of the island.

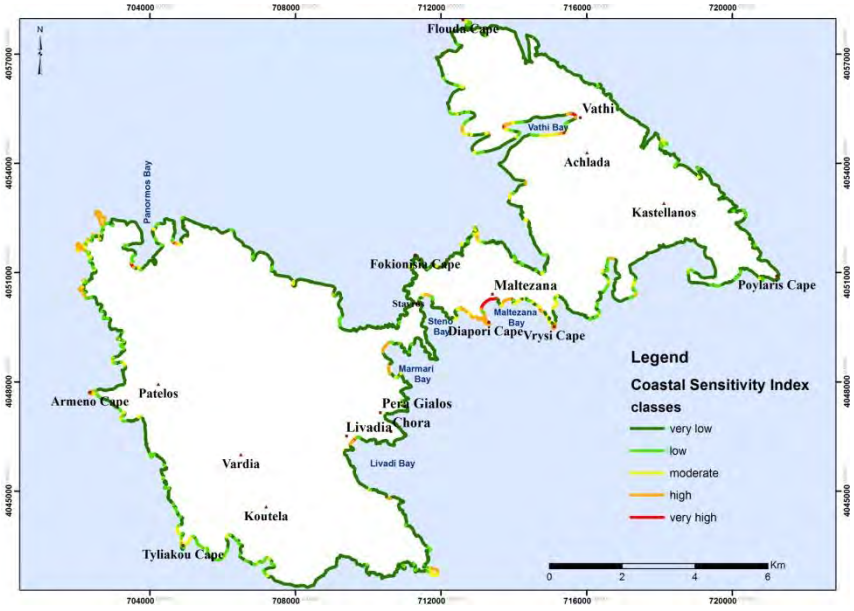

CSI	3,87-7,74	7,75-11,18	11,19-14,14	14,15-17,88	17,89-25,81	total
length (%)	77,6	6,97	6,93	7,43	1,07	100
length (km)	111,5	10	9,9	10,6	1,5	143,5
Sensitivity	very low	low	moderate	high	very high	

Figure 4- CSI Table and map of the Astypalaea Island coastline.

In terms of the socio-economic impacts of the anticipated sea-level rise, most of the coastal villages as well as tourism activities and facilities are concentrated along very highly and highly sensitive coastal segments. Furthermore, areas of high and very high CSI values are environmentally protected by International Conventions.

5. Conclusions

In this study the relative sensitivity of Astypalaea Island to environmental changes due to future rise in sea-level is assessed with the calculation of the Coastal Sensitivity Index. Calculated CSI values along the studied coastline vary between 3.87 and 25.81. All variables incorporated into the CSI assessment can be considered factors contributing to coastal change. However, some variables make a larger contribution to index variability than others. Of the six variables, coastal slope and coastal geomorphology introduce the greatest variability to the CSI values. Among the other variables, shoreline change rate and mean significant wave height shows a small variation, while mean tidal range and relative sea level change have the same value along the coastline.

According to the criteria of coastal sensitivity, as defined in this study, an extensive segment of the island's coastline is of very low (111.5km) and low (10.0km) sensitivity. Only 12.1km, corresponding to 8.5% of the entire coastline, is characterized as very highly and highly sensitive to sea- level rise. These sections of the coast include low gradient coasts such as pocket beaches composed of unconsolidated sediments. These areas will be more susceptible to both erosion and inundation. Highly sensitive regions (CSI values>14.15), are Maltezana, Livadia and Vathi. The shoreline of Maltezana village is the most rapidly eroding part of the island with obvious results of erosion along the beach zone of the settlement.

A small length of the highly and very highly sensitive coastal zone is occupied by agricultural land while hosts the most important settlements of the island as well as tourism activities. It is estimated that during the summer period the population of the island is almost 13 times higher than the resident population.

This study provides a detailed spatial GIS database of topographic, geological and physio-geogrpahical characteristics, as well as land cover information for 143.5 km of shoreline, which could be renewed and expanded further in order to incorporate newly available data (e.g. storm surge), including new variables (e.g sediment budget), in the future for better results of a modified CSI. Besides the integration of CSI physical variables with further social cultural and economic factors may enable a broader assessment of the vulnerability of sections of the coast and the communities that live there.

6. References

Abuodha PAO. and Woodroffe C.D. 2010. Assessing vulnerability to sea-level rise using a coastal sensitivity index: a case study from southeast Australia, *J Coast Conserv.*, 14, 189-205.

Alexandrakis G., Karditsa A., Poulos S., Gionis G. and Kampanis N. 2009. Assessment of the Aegean coasts vulnerability to sea-level rise, *Proceedings of the 9th Pan-Hellenic Symposium on Oceanography and Fisheries*, Patras, 13-16 May, vol. I, 327-332.

Allen J.C. and Komar P.D. 2006. Climate controls on US west coast erosion processes, *J Coast Res.*, 22, 511-529.

Chatzieleftheriou M., Alexandrakis G., Poulos S., Gaki-Papanastassiou K. and Maroukian H. 2007. Assessment of vulnerability to a future sea-level rise of the E and NE coast of Attica, *Proccedings of the 8th Pan-Hellenic Geographical Conference*, vol 1, 298-305.

Dominey-Howes D., Cundy A. and Croudace I. 2000. High energy marine flood deposits on Astypalaea Island, Greece: possible evidence for the AD 1956 southern Aegean tsunami, *Marine Geology*, 163, 303-315.

Dwarakish G.S., Vinay S.A., Natesan U., Asano T., Kakinuma T., Ventakaramana K., Jagedeesha B. and Badita M.K. 2009. Coastal vulnerability assessment of the future sea-level rise in Udupi coastal zone of Karnataka state, west coast of India, *Ocean and Coastal Management*, 52, 467-478.

Gaki-Papanastassiou K., Karymbalis E., Poulos S., Seni A. and Zouva C. 2001.Coastal Vulnerability assessment to sea-level rise based on geomorphological and oceanographical parameters: the case of Argolikos Gulf, Peloponnese, Greece, *Hellenic Journal of Geosciences*, 45, 109-121.

Gornitz V., Daniels R.C., White T.W. and Birdwell K.R. 1994. The development of a coastal vulnerability assessment database: vulnerability to sea-level rise in the U.S. Southeast, *J Coast Res*, Special Issue 12, 327-338.

Gornitz V. 1991. Global coastal hazards from future sea-level rise, *Palaeogeography, Palaeoclimatology, Palaeoecology (Global and Planetary Change Section)*, 89, 379-398.

IGME 1986. Geological map of Greece, Astypalaea sheet, *IGME*, Athens.

Intergovernmental Panel on Climate Change, 2007. Climate Change 2007: The Physical Science Basis, Contribution of Working Group I to the fourth assessment report of the Intergovernmental Panel on Climate Change, Cambridge, United Kingdom and New York, N.Y., U.S.A., Cambridge University Press.

Karymbalis E., Chalkias Ch., Chalkias G., Grigoropoulou E., Manthos G. and Ferentinou M. 2012. Assessment of the sensitivity of the Gulf of Corinth (Peloponnese, Greece) to sea- level rise,*Cent. Eur. J. Geosci.*, doi: 10.2478/s13533-012-0101-3.

Lambeck K. 1996. Sea-level change and shoreline evolution in Aegean Greece since upper Palaeolithic Time, Antiquity, 70, 588-611.

Nasopoulou I., Poulos S., Karymbalis E. and Gaki-Papanastassiou K. 2012. Coastal vulnerability assessment of the northern coast (Antirio-Eratini) of the western Corinth Gulf to the anticipated sea-level rise, *Proceedings of the 10th Panhellenic Symposium of Oceanography and Fishery* (CD Rom).

Okal E.A., Synolakis C.E., Uslu B., Kalligeris N. and Voukouvalas E. 2009. The 1956 earthquake and tsunami in Amorgos, Greece, *Geophys. J. Int.*, 178, 1533-1554.

Pendleton E.A., Thieler E.R. and Jefress S.W. 2005. Coastal vulnerability assessment of Golden Gate National Recretion Area to sea-level rise, *USGS Open File Report*, 2005-1058.

Rosenzweig C., Koroly D., Vicarelli M., Neofotis P., Wu Q., Casassa G., Menzel A., Root R.L., Estrella N., Sequin B., Tryjanowski P., Liu C., Rawlins S. and Imeson A. 2008. Attributing physical and biological impacts to anthropogenic climate change, *Nature*, 453, 353-357.

Soukisian T., Hatzinaki M., Korres G., Papadopoulos A., Kallos G. and Anadranistakis E. 2007. Wave and Wind Atlas of the Hellenic Seas, *Hellenic Centre for Marine Research Publ.*, 300pp.

Thieler E.R. and Hammar-Klose E.S. 1999. National assessment of coastal vulnerability to sea-level rise, U.S. Atlantic Coast, *USGS Open File Report*, 99-593.

Tsimplis M.N. 1994. Tidal oscillations in the Aegean and Ionian Seas, *Estuarine, Coastal and Shelf Science*, 39, 201-208.

Δελτίο της Ελληνικής Γεωλογικής Εταιρίας, τομ. XLVII , 2013
Πρακτικά 13ου Διεθνούς Συνεδρίου, Χανιά, Σεπτ. 2013

Bulletin of the Geological Society of Greece, vol. XLVII 2013
Proceedings of the 13th International Congress, Chania, Sept. 2013

RECENT COASTLINE CHANGES OF FAN-DELTAS IN THE WESTERN GULF OF CORINTH, CENTRAL GREECE

Perrou Th.[1], Kaza I.[1], Efthymiadis V.[1], Karymbalis E.[1] and Chalkias C.[1]

[1] *Department of Geography, Harokopio University of Athens, 70 El. Venizelou Str., 17671 Athens, Greece, dperrou@central.ntua.gr, Ioanna.Kaza.1988@gmail.com, bilefth@hotmail.com, karymbalis@hua.gr, xalkias@hua.gr*

Abstract

This study deals with the assessment of recent shoreline change rates along the fan-deltas of Finix, Tholopotamo, Lagadi, Meganitas, Selinous, Kerinitis, and Vouraikos streams by using GIS and Remote Sensing techniques. These Late Holocene fan-deltas have been formed by high gradient braided streams that deposit their coarse sediment load along the southern coast (North Peloponnese) of the western Gulf of Corinth. For the purposes of the study a spatial database was constructed, organized and implemented consisting of analogue detailed (at the scale of 1:5000) topographic diagrams, and orthorectified aerial photos taken in 1945, 1996 and 2008. Comparisons of fan-deltas shoreline positions for the periods 1945 vs. 1996 and 1945 vs. 2008 were made and the segments of the coastline along the aprons of the fan-deltas which are subject to erosion accretion were defined. Coastal erosion is the main dominant geomorphic process along a significant part of the fan deltas coastline. The highest retreat rate value (2.44 m/yr for the period 1945-1996) was estimated for the Finix stream fan delta, about 150 m west of the river mouth, while the highest accretion rates since 1945 (3.10 and 3.00 m/yr) occurred at the mouths of Vouraikos and Selinous rivers respectively.

Key words: *Geographic Information System (GIS), shoreline change rates, fan-deltas, Gulf of Corinth, Greece.*

Περίληψη

Στην παρούσα εργασία επιχειρείται η εκτίμηση των πρόσφατων μεταβολών της ακτογραμμής των δελταϊκών ριπιδίων των ποταμών Φοίνικα, Θολοπόταμο, Λαγκάδι, Μεγανίτα, Σελινούντα, Κερυνίτη και Βουραϊκού, με τη χρήση μεθόδων τηλεπισκόπησης και ΣΓΠ. Τα δελταϊκά αυτά ριπίδια ηλικίας Ανώτερου Ολόκαινου έχουν σχηματισθεί από ποτάμια μεγάλης μορφολογικής κλίσης που αποθέτουν το αδρομερές φορτίο ιζημάτων τους κατά μήκος των νότιων ακτών του δυτικού Κορινθιακού κόλπου (Β. Πελοπόννησος). Για τους σκοπούς της εργασίας δημιουργήθηκε και οργανώθηκε μια ψηφιακή βάση δεδομένων για την περιοχή αποτελούμενη από λεπτομερή (κλίμακας 1:5.000) τοπογραφικά διαγράμματα και γεωμετρικά διορθωμένες και γεωαναφερμένες αεροφωτογραφίες λήψης 1945, 1996 και 2008. Η σύγκριση των ακτογραμμών των δελταϊκών ριπιδίων κατά τα έτη 1945, 1996 και 2008 οδήγησε στον προσδιορισμό των τμημάτων της ακτογραμμής που υπόκεινται σε διάβρωση καθώς και εκείνων που προελαύνουν. Η κύρια διεργασία κατά μήκος του μεγαλύτερου μήκους της ακτογραμμής είναι η διάβρωση. Ο

μεγαλύτερος ρυθμός διάβρωσης ήταν 2,44 m/έτος (μεταξύ των ετών 1945 και 1996) και σημειώθηκε περίπου 150 m δυτικά των εκβολών του ποταμού Φοίνικα. Αντίθετα οι υψηλότεροι ρυθμοί προέλασης μετά το 1945 ήταν 3,10 και 3,00 m/έτος και σημειώθηκαν στις περιοχές των ενεργών εκβολών των ποταμών Βουραϊκού και Σελινούντα αντίστοιχα.
Λέξεις κλειδιά: *Γεωγραφικά Συστήματα Πληροφοριών (ΣΓΠ), ρυθμοί μεταβολής ακτογραμμής, δελταϊκά ριπίδια, Κορινθιακός Κόλπος, Ελλάδα.*

1. Introduction

Coastal monitoring and research-informed decision-making have a crucial role in assisting local authorities to develop their shoreline management plans. Quantitative assessment of recent shoreline change rates is a part of the coastal monitoring that helps significantly in long-term predictions of shoreline positions (Esteves et al., 2009). Such predictions are a useful tool for coastal managers who need to propose future shoreline management and development strategies.

In Greece the most distinctive coastline changes concern beach zones of low lying coastal plains (mainly river deltas) and are associated with the progradation of active river mouths or the retreat of abandoned channels (Maroukian & Karymbalis, 2004). Extremely high mean erosion rates up to more than 20 m/yr are very rare and characterize certain deltaic locations such as the Acheloos river delta. These extreme retreat rates are associated with human interference including dam constructions, stream flow diversion etc. Usually erosion rates in deltaic and low-lying coastal plains are less than 2 m/yr. By contrast, active river mouths appear to be areas of rapid accretion with progradation rates up to more than 4m/yr (Papadopoulos, 2009). In beaches that are not near large river deltas retreat rates range from 0.5 to 1 m/yr (Foteinis et al., 2010).

This paper aims at assessing mean shoreline change rates along the fan deltas of Finix, Tholopotamos, Lagadi, Meganitas, Selinous, Kerinitis, and Vouraikos streams using remote sensing data and GIS techniques. The fan deltas of the study area are located along the southern coast of the western Gulf of Corinth and have been prograding in deep waters since the deceleration of Holocene sea-level rise.

2. Study Area

The study area shoreline lies on the southern coast of the Gulf of Corinth, extending for 31.4 km, from the village Lampiri in the west to the city Diakopto in the east, and is oriented along the WNW-ESE direction (Figure 1). The coastal zone comprises a series of seven coastal alluvial fans of Late Holocene age, formed by seven torrential streams that drain the mountainous northern Peloponnese (Figure 1a). The drainage basins of these streams range in area from 7.8 km^2 (Lagadi stream catchment) to 330.5 km^2 (Selinous River catchment) (Rozos et al., 2011). The coast along the fans' aprons consists of unconsolidated alluvial deposits (mainly pebbles, cobbles, gravels and coarse sand).

The Gulf of Corinth (or the Corinth Rift) is one of the most active neotectonic features of the Eastern Mediterranean. It is a 'back arc' elongated graben, formed by normal faulting associated with an approximately N-S crustal extension (Armijo et al., 1996). The southern side of the Gulf, where the coast of the study area is located, is affected by the North dipping active normal faults of Aigion, and Eliki (Figure 1). The fan deltas' coastline lies on the hanging walls of the faults. The Gulf is a bathymetrically restricted marine embayment, with a nearly 105 km longitudinal axis lying in the E-W direction (Figure 1b). The embayment has an average width of approximately 320 km, whilst water depths are in excess of 900 m in the central section. To the west, the gulf is linked with the Gulf of Patras through the narrow and shallow silled Rion Straits (2 km wide and 65 m deep), which, in turn, is connected to the open Ionian Sea. The Corinth Canal (an artificially

dredged channel, 8 m deep and 21 m wide) links the Gulf of Corinth with the Saronikos Gulf and the western Aegean Sea, to the east.

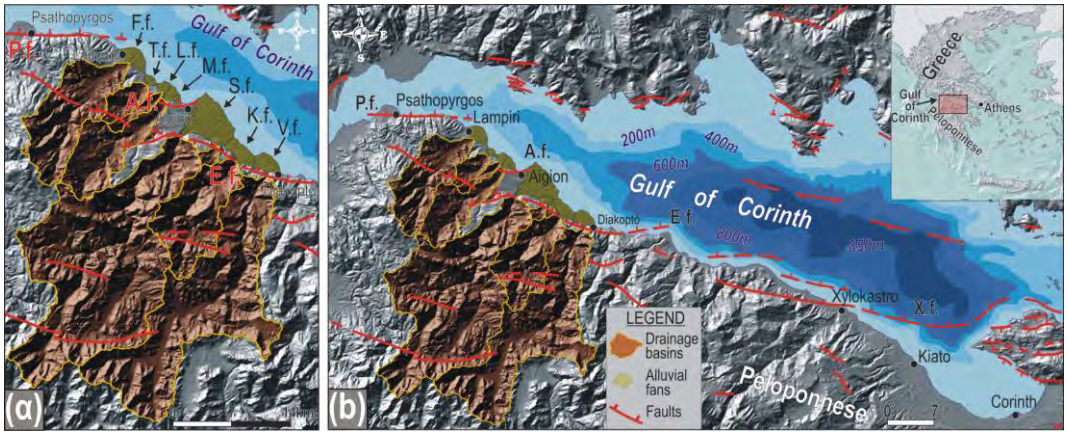

Figure 1 - (a) Location of the study area coastline. The map shows the fan deltas and their co rresponding catchments. The main active normal faults that affect the coastline of the study area are also depicted. (F.f.: Finix fan, T.f.: Tholopotamo fan, L.f.: Lagadi fan, M.f.: Meganit as fan, S.f.: Selinous fan, K.f.: Kerinitis fan, V.f. Vouraikos fan, P.f.: Psathopyrgos fault, A.f.: Aigion fault, E.f.: Eliki fault, X.f.: Xylokastro fault). (b) Subaqueous morphology of the Gulf of Corinth.

The submarine bathymetry of the Gulf of Corinth consists of the continental shelf, the continental slope, the continental rise, and the abyssal plain (Heezen et al., 1966). The southern continental shelf is narrow (<1 km) and relatively steep (4-8°), with the shelf break occurring at a water depth of approximately 100 m. In contrast, the northern continental shelf slopes gently (1-2°) and extends into the central part of the gulf into water depths of approximately 200 m. The southern slope is narrow (1.5-2.5 km) and steep (14-18°), whereas the northern slope varies at between 3 and 7 km in width with a gradient of 5-7° (Poulos et al., 1996)]. In the north, the continental rise is narrower (1-2.5 km) and steeper (2-5°) than in the south, where the width ranges between 1 and 5.5 km and the slope gradients are 1-3°. The southern characteristics are the result of coalescing submarine fans, which extend offshore from the steep southern continental slope to the abyssal plain. Finally, the abyssal plain occupies the middle section of the central basin at water depths >800 m. The plain is essentially a flat area with gradients of <0.5°.

The Gulf can be characterized as a microtidal environment with an average mean tidal range of 0.15 m (Bariagin, 1972; Tsimplis, 1994). The surface water circulation is dominated by the funneling of both wind and water through the narrow Rion Straights and the adjacent western Gulf, where mean surface current velocities can exceed 100 cm/s (Piper et al., 1990). The funneling also results in a highly bi-modal distribution of predominant wind directions either from the E or the WSW. Data for the University of Patras (Piper et al., 1982) suggest the easterly winds are both stronger and more persistent. The fetch from the E is much greater than from the SSW, since the Rion Straits minimize the passage of waves from the Gulf of Patras. Wave climate is primarily wind driven with offshore mean significant wave heights average heights < 0.3 m according to the output of the wave model (POSEIDON program) (Soukisian et al., 2007; Tsimplis, 1994), which have been calibrated with the use of offshore field measurements (Figure 2).

The general climatic conditions of the study area are typical of the temperate Mediterranean. The mean annual precipitation ranges from 800 mm near the coastline to more than 1,200 mm in the southernmost highlands. Rain is unevenly distributed between the cold and the hot period of the year, with most falling during the winter months. The mean annual temperature fluctuates between 15 and 17 °C.

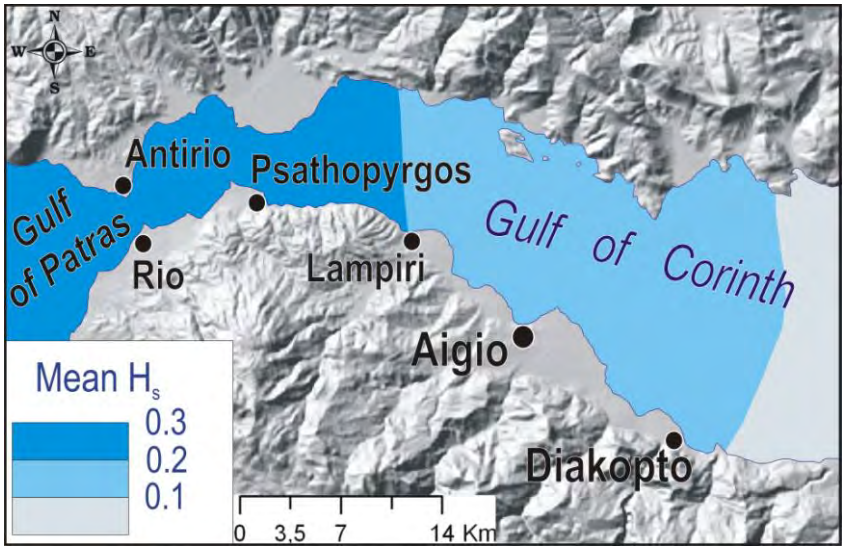

Figure 2 - Map of the mean significant wave height for the Gulf of Corinth. The map is modified from the Wave and Wind Atlas of the Hellenic Seas (Soukisian et al., 2007), which is based on offshore measurements taken between 1999 and 2007 (POSEIDON program). The entire coast of the study area is affected by waves with mean significant heights lower than 0.2m.

3. Materials and Methods

Shoreline erosion or accretion rates were derived using remote sensing data and utilizing Geographic Information System (GIS) techniques. Recent shoreline changes along the aprons of the seven fan deltas have been calculated from three series of orthorectified aerial photographs taken in 1945, 1996, and 2009. Detailed aerial photos of 1945 and 2008, at the scale of 1:1,000, were obtained from the Hellenic Cadastre (Ktimatologio S.A.) whereas 1996 aerial photos, at the scale of 1:33,000, were provided by the Greek Ministry of Rural Development and Food. For the purposes of this study a GIS spatial data base derived from detailed (at the scale of 1:5,000) topographic diagrams of the Hellenic Millitary Geographical Service, and the afore mentioned geometrically corrected aerial photographs was designed, organized and implemented using ESRI's ArcGIS9.3 software aiming at the creation of a number of thematic and synthetic layers and maps in a common projection system (Hellenic Geodetic Reference System 1987 – HGRS'87). The digitizing of the shoreline as well as all measurements and calculations of coastal displacement rates for the two time periods were processed using GIS functions.

Aerial photographs were matched and a mosaic image of the study area was created for each date. The photomosaics of these aerial photos were manipulated within the GIS environment to digitize the shorelines of 1945, 1996, and 2008. The shoreline was defined as the observable land-sea interface at the time of photography. The thematic layers (in vector format) of the 1945, 1996, and 2008 shorelines were overlaid, and with the use of GIS-based distance analysis functions, the final shoreline change maps for the time periods of 1945-1996 and 1996-2009 were obtained with estimated accretion and erosion rates. For all analyses the coast of the study area was sectioned into seven analysis regions (Figures 3, 4) each of which corresponds to an individual fan delta. Using the 1945 digitized shoreline, 628 measurement sites were created every 50m using an automated procedure. Coastal retreat or progradation was calculated for the interval between the dates of the imagery by measuring the distance separating the two shorelines (in vector format) perpendicular to the older shoreline. These distances were then divided by the number of years to provide average annual coastal retreat or accretion rates.

4. Results and Discussion

For the presentation of the recent shoreline changes the study area is divided into seven sections. Each section corresponds to a fan delta. Coastline shifting rates were compiled for two periods: 1945-1996 and 1945-2008. Table 1 includes the regional results of the shoreline change analyses as well as the maximum accretion and erosion rates for each fan delta respectively. Horizontal shoreline changes of the study area for the 1945-1996 period varied from -124 m to +158 m (negative changes are erosional) and for the 1945-2008 period from -130m to +195m.

Table 1 - Maximum coastline change (retreat or accretion) rates estimated along the fan deltas' aprons for the periods 1945-1996 and 1945-2008. The table includes also the length of the eroded and prograted coastline for each fan delta.

1945-2008							
Fan delta	**Shoreline Length (km)**	**Retreat**			**Accretion**		
		km	**%**	**Maximum rate**	**km**	**%**	**Maximum rate**
Finix	5.75	5.50	95.7	-2.06	0.15	2.6	+0.10
Tholopotamos	1.95	1.70	87.2	-0.53	0.20	10.3	+0.43
Lagadi	1.90	1.70	89.5	-0.41	0.20	10.5	+0.20
Meganitas	3.65	2.15	58.9	-0.49	1.45	39.7	+3.09
Selinous	9.75	4.95	50.8	-1.00	4.50	46.2	+2.32
Kerinitis	3.30	2.50	75.8	-0.96	0.80	24.2	+1.60
Vouraikos	5.10	2.75	53.9	-0.40	2.20	43.1	+2.29
1945-1996							
Fan delta	**Shoreline Length [m]**	**Retreat**			**Accretion**		
		km	**%**	**Maximum rate**	**km**	**%**	**Maximum rate**
Finix	5.75	4.90	85.2	-2.44	0.65	11.3	+0.22
Tholopotamos	1.95	1.55	79.5	-0.59	0.35	17.9	+0.49
Lagadi	1.90	1.00	52.6	-0.49	0.85	44.7	+0.53
Meganitas	3.65	2.20	60.3	-0.36	1.40	38.4	+1.18
Selinous	9.75	3.95	40.5	-1.19	4.80	49.2	+3.00
Kerinitis	3.30	2.15	65.2	-1.22	0.95	28.8	+2.08
Vouraikos	5.10	2.40	47.1	-0.41	2.35	46.1	+3.10

A total length of 21.25 km which corresponds to the 67.7 % of the total shoreline length of the seven fan deltas is being eroded with mean retreat rates varying between -0.10 and -2.06 m/yr. Almost the entire Finix fan delta coastline (95.7% of its total length) is retreating with mean long-term erosion rates reaching -2.06 m/yr for the period between 1945 and 2008. Additionally, 89.5% and 87.2% of the Tholopotamos and Lagadi fan deltas shoreline is erosional, retreating at a maximum mean rate of -0.53 and -0.43 m/yr between 1945 and 2008. The results indicate that erosion is the main process for fan deltas with small areas whereas an extensive segment of the large deltas such as those of Selinous and Vouraikos is prograding at rates reaching up to +2.32 m/yr and +2.29. The most extensive fan deltas have resulted from drainage networks which drain

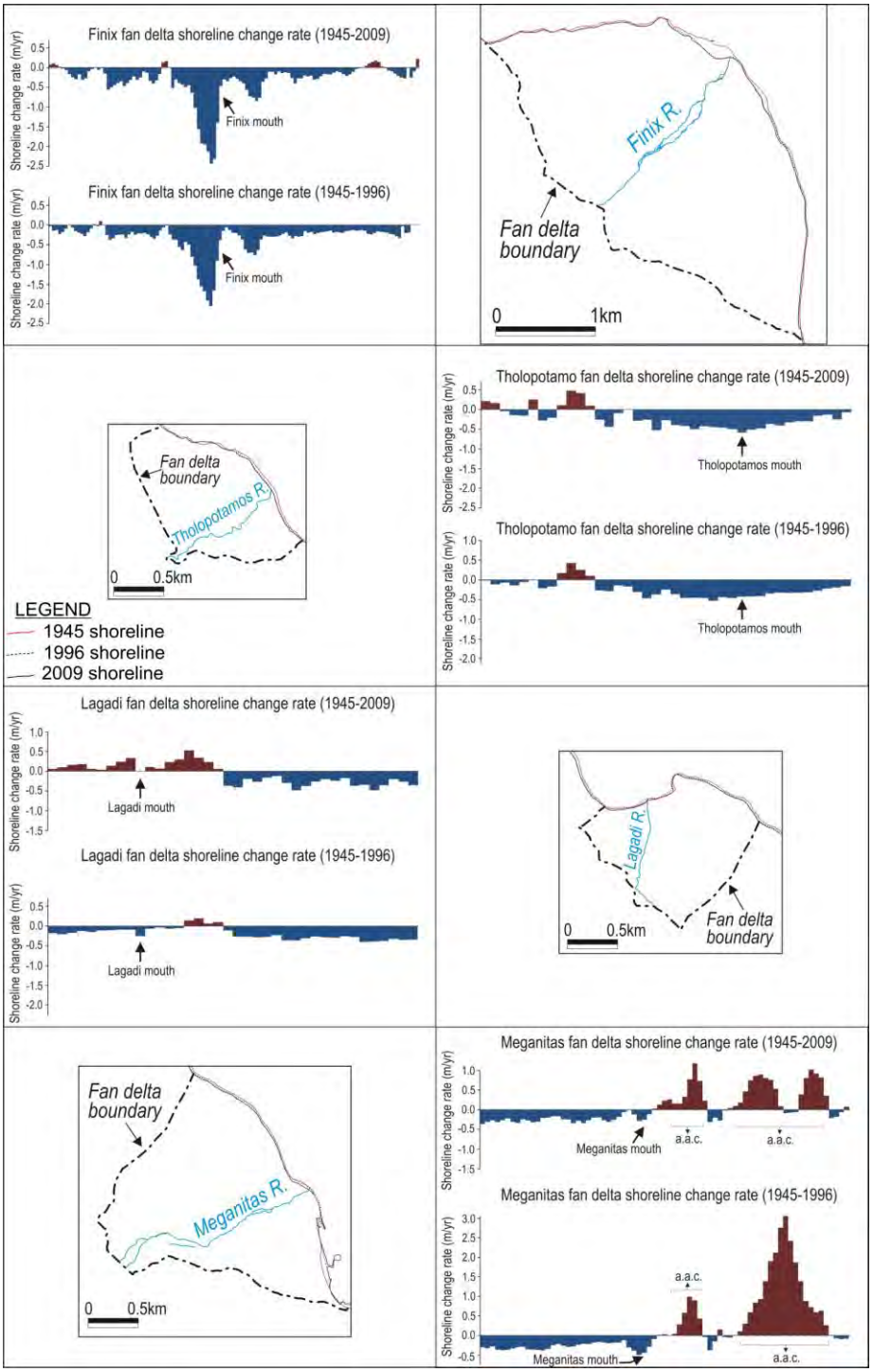

Figure 3 - Shoreline change rates for the fan deltas of Finix, Tholopotamo, Lagadi and Meganitas. Bar diagrams show mean shoreline change (retreat or progradation) rates for each 50 m segment along the fan delta coastline. Maps show the relative positions of the coastline along the apron of each one of the four fan deltas in 1945, 1996 and 2008 respectively (a.a.c.: artificially armored coast).

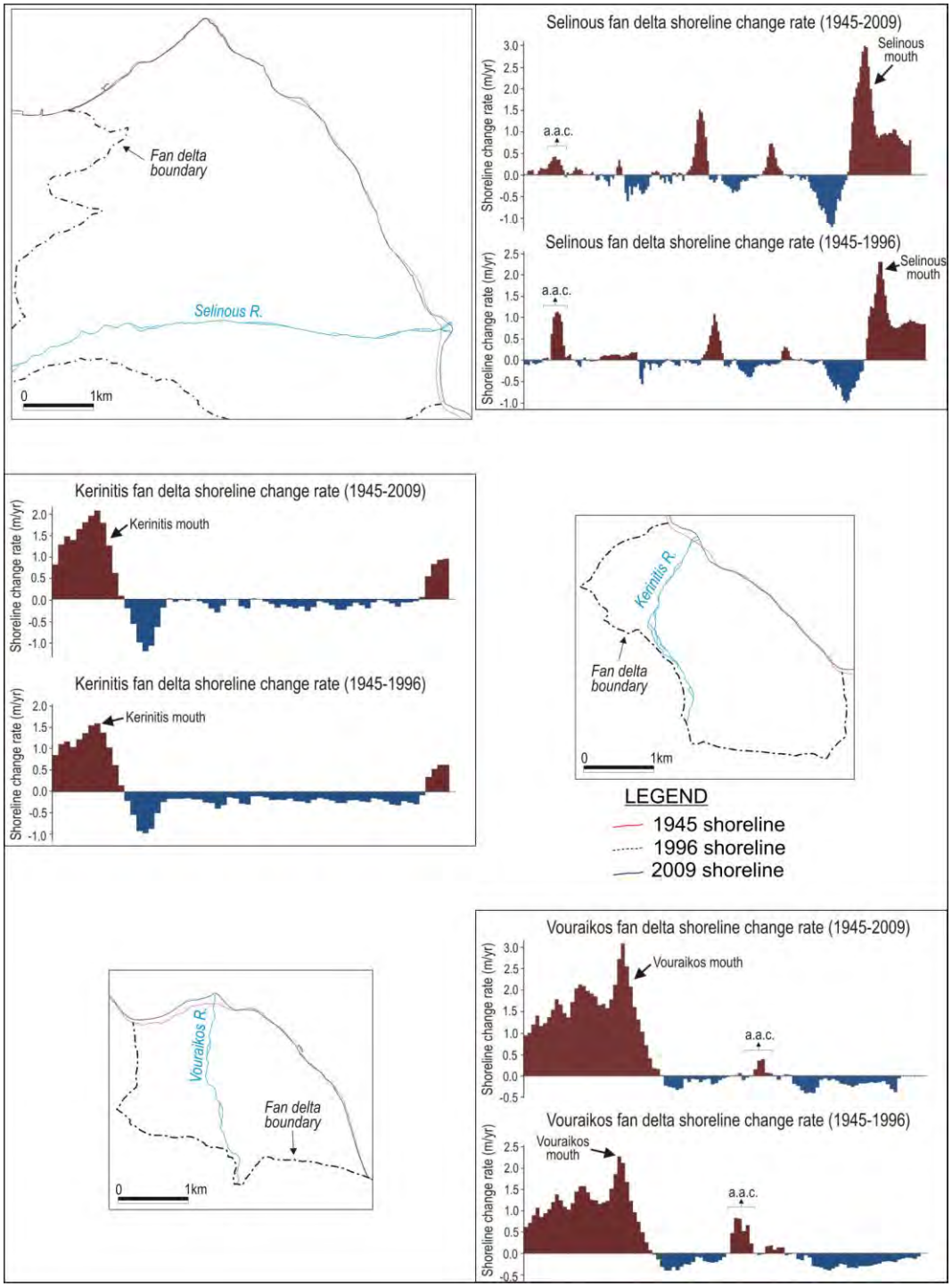

Figure 4 - Shoreline change rates for the fan deltas of Selinous, Kerinitis and Vouraikos. Bar diagrams show mean shoreline change (retreat or progradation) rates for each 50 m segment along the fan delta coastline. Maps show the relative positions of the coastline along the apron of each one of the three fan deltas in 1945, 1996 and 2008 respectively(a.a.c.: artificially armored coast).

extensive mountainous areas composed mainly of highly erodible geological formations. For instance 57.8% of Vouraikos River drainage basin and 52,0% of Selinous River catchment consist of easily erodible geological formations (Karymbalis & Gaki-Papanastassiou, 2011). Seaward progradation occurred mainly at the locations around the active mouths of these major rivers due to increased fluvial supply. Thus high rates of accretion can be attributed to high influxes of sediment from river systems of perennial flow especially during the rainy period of the year.

High mean progradation rates reaching 3.09 m/yr are also observed along artificially armored segments of the shorelines at the fans of Meganitas, Selinous and Vouraikos streams. consequently the long term accretional signal is likely related not only to large fluxes of sediment from the larger river systems but also to artificially armored segments of the coastline.

The spatial distribution of coastal retreat rates is presented in Figures 3 and 4. The maps of the Figures show that the greatest erosion rates correspond to shorelines with NW-SE orientation that are exposed to easterly winds which according to Piper et al., (1990) are both stronger and more persistent. The fetch from the E is much greater than from the SSW. Given the fact that wave climate of the Gulf is primarily wind driven (Poulos et al., 1996) wave action must be the main cause of erosion.

The coastline of some of the fans of the study area has suffered earthquake induced instability events. The main mechanism responsible for the observed mass movements include the frequent seismic activity in the region, the high sedimentation rates of the numerous river mouths, heavy rainfall and high seas, and the steep slopes (Hassiotis et al., 2002). Historical observations that give evidence of earthquake induced nearshore sediment failures are: the destruction of Eliki (Helice) and the surrounding area in 373 BC after a severe seismic shock of an estimated magnitude 7.3 R (Papazachos and Papazachou, 1989) and the submergence of coastal strips between Meganitas and Vouraikos rivers in the southern Corinth Gulf in 1817 and 1861 due to the 6.5 R and 6.7 R earthquakes, respectively (Hassiotis et al., 2002). It is estimated that the entire alluvial plain of the fan deltas of Kerinitis and Vouraikos Rivers, which lay at the hanging wall of the eastern segment of the Eliki fault, has subsided at a rate of 1.4 mm/yr resulting in the burial of the Late Hellenistic-Roman occupation horizons under 3 m of fluvial sediments (Koukouvelas et al., 2001; Pavlides et al., 2004). Coastal failures, slumping, liquefaction, ground cracking and tectonic ground ruptures have also been certified during the last 40 years along the coast of the study area (Palyvos et al., 2005). The most affected by these secondary processes fans are those of Finix, Selinous and Meganitas. On June 15 1995, a locally destructive earthquake of Ms=6.2 R with a hypocenter of a depth of about 10 km occurred in the western Gulf of Corinth (Bernard et al., 1997), causing coastal sediment failures in the broader area of Aegion (Papatheodorou and Ferentinos, 1997). From the above mentioned it is obvious that erosion along segments of the Finix, Selinous, Meganitas and Vouraikos fan deltas coastline can be also attributed to both long-term subsidence and earthquake induced instability events.

5. Conclusions

In this analysis the assessment of shoreline changes for a part of the coast of the north Peloponnese using orthorectified aerial photos from 1945, 1996 and 2008 and utilizing GIS techniques is attempted. Data procedure in the analytical context of GIS provided data integration which includes a common geographical reference system (which was HGRS'87), common spatial and temporal coverage, and similar scale and quality of the data.

Today coastal erosion is the main dominant geomorphic process along a significant part (about 68%) of the fan deltas coastline. Maximum mean coastal retreat rates for the period 1945-1996 range from -0.36 m/yr (Meganitas fan delta) to -2.44 m/yr (Finix fan delta) whereas for the 1945-2008 period calculated maximum erosion rates range between -0.40 m/yr (Vouraikos fan delta) and -2.06 m/yr (Finix fan delta).

The spatial distribution of coastal erosion shows that retreat correspond to shoreline segments with the ENE exposures which is consistent with the fact that waves, which are driven by the easterly winds are both stronger and more persistent.

One additional reason for the coastal erosion of the fans of Finix, Meganitas, Selinous and Vouraikos seems to be instability events triggered by earthquakes. Coastal failures, slumping, liquefaction and ground cracking have been certified during the last 40 years for fans of the north Peloponnese while the coastline of some of these fan deltas has suffered severe earthquake induced submarine instability events.

Estimated maximum mean coastal accretion rates for the periods 1945-1996 range from +0.22 m/yr (Finix fan delta) to +3.00 m/yr (Selinous fan delta) whereas for the 1945-2008 period maximum progradation rates range between +0.10 m/yr (Finix fan delta) and +3.09 m/yr (Selinous fan delta). Overall rates of shoreline accretion are higher in extensive fan deltas like those of Vouraikos and Selinous Rivers as compared with smaller fans. Seaward progradation occurred mainly in the locations of the active mouth of these streams. This can be attributed mainly to the higher sediment supply since these rivers drain extensive mountainous areas of relatively easily erodible lithology. Additionally, high mean accretion rates were associated with sites of artificially armored coastlines. Thus high accretion rates are likely related to influxes of sediment from large river systems as well as to artificially armored segments of the shoreline.

6. References

Armijo R., Meyer B., King G., Rigo A. and Papanastassiou D. 1996. Quaternary evolution of the Corinth Rift and its implications for the Late Cenozoic evolution of the Aegean, *Geophys J Int*, 126, 11-53.

Bariagin M.A. 1972. *Tides and tidal data for Greek harbours*, Hydrographic Service, Athens (in Greek).

Bernard P., Briole P., Meyer B., Lyon-Caen H., Gomez J.M., Tiberi C., Berge C., Cattin R., Hatzfeld D., Lachet C., Lebrun B., Deschamps A., Courboulex F., Larroque C., Rigo A., Massonnet D., Papadimitriou P., Kassaras J., Diagourtas D., Makropoulos K., Veis G., Papazisi E., Mitsakaki C., Karakostas V., Papadimitriou E., Papanastassiou D., Chouliaras G. and Stavrakakis G. 1997. The Ms=6.2R June 15 1995 Aegion Earthquake (Greece): Evidence for low angle normal faulting in the Corinth rift, *J. Seismol.,* 1, 131-150.

Esteves L.S., Williams A., Nock A. and Lympery G. 2009. Quantifying shoreline changes along the Sefton coast (UK) and the implications for research-informed coastal management, *Journal of Coastal Research*, Special Issue 56, 602-606.

Foteinis S., Papadopoulos C., Koutsogiannaki I. and Synolakis C. 2010. Coastal erosion and accret ion rates in Greece, *Geophysical Research Abstracts*, 12, EGU2010-7499.

Hassiotis T., Papatheodorou G., Bouckovalas G., Corbau C. and Ferentinos G. 2002. Earthquake-induced coastal sediment instabilities in the western Gulf of Corinth, Greece, *Marine Geology*, 182, 319-335.

Heezen B.C., Ewing M. and Johnson G.L. 1966. The Gulf of Corinth floor, *Deep Sea Research* 13, 381-411.

Karymbalis E. and Gaki-Papanastassiou K. 2011. Investigation of relationships between fan delta and drainage basin morphometric variables along the southwestern coast of Gulf of Corinth, Northern Peloponnesus, Greece, in: Efe, R., Cravins, G., Ozturk, M., and Atalay, I., eds., *Natural Environment and Culture in the Mediterranean Region II*, 87-106, Cambridge Scholars Publishing UK.

Koukouvelas I., Stamatopoulos L., Katsonopoulou D. and Pavlidis S. 2001. A palaeoseismological and geoarchaeological investigation of the Eliki fault, Gulf of Corinth, Greece, *Journal of Structural Geology*, 23, 531-543.

Maroukian H. and Karymbalis E. 2004. Geomorphic evolution of the fan delta of the Evinos river in western Greece and human impacts during the last 150 years, *Z Geomorphol* 48,201-217.

Palyvos N., Pantosti D., De Martini P.M., Lemeille F., Sorel D. and Pavlopoulos K. 2005. The Aigion-Neos Erineos coastal normal fault system (western Corinth Rift, Greece): Geomorphological signature, recent earthquake history, and evolution, *Journal of Geophysical Research*, 110, B09302.

Papadopoulos C. 2009. Comprehensive assessment of coastal erosion in the regions of north A mvrakikos Gulf, Acheloos delta, Nestos delta, Kos, Limnos, and Kitros, *Diploma Thesis*, T echnical University of Crete, Chanea, Greece.

Papatheodorou G. and Ferentinos G. 1997. Submarine and coastal sediment failure triggered by the 1995, Ms=6.1R Aegion earthquake, Gulf of Corinth, Greece, *Marine Geology*, 137, 287-304.

Papazachos B. and Papazachou K. 1989. *The seismicity of Greece*, Ziti Publ., Thessaloniki.

Pavlides S.B., Koukouvelas I.K., Kokkalas S., Stamatopoulos L., Keramydas D. and Tsodoulos I. 2004. Late Holocene evolution of the East Eliki fault, Gulf of Corinth (Central Greece), *Quaternary International,* 115-116, 139-154.

Piper D.J.W., Kontopoulos N., Anagnostou C., Chronis G. and Panagos A.G. 1990. Modern fan-deltas in the western Gulf of Corinth, Greece, *Geo-Marine Letters*, 10, 5-12.

Piper D.J.W., Panagos A.G., Kontopoulos N. and Spiliotopoulou M. 1982. Coastal Processes and morphology, Gulfs of Patras, Greece, *Z Geomorphol*, 26, 365-374.

Piper D.J.W., Stamatopoulos L., Poulimenos G., Doutsos T. and Kontopoulos N. 1990. Quaternary history of the Gulfs of Patras and Corinth, Greece, *Z Geomorphol*, 34, 451-458.

Poulos S.E., Collins M.B., Pattiaratchi A., Cramp A., Gull W., Tsimplis M. and Papatheodorou G. 1996, Oceanography and sedimentation in the semi-enclosed, deep-water Gulf of Corinth (Greece), *Marine Geology*, 134, 213-235.

Rozos D., Bathrellos G.D. and Skillodimou H.D. 2011. Comparison of the implementation of rock engineering system and analytic hierarchy process methods, upon landslide susceptibility mapping, using GIS: a case study from the Eastern Achaia Country of Peloponnesus, Greec e, *Environ Earth Sci*, 63, 49-63.

Soukisian T., Hatzinaki M., Korres G., Papadopoulos A., Kallos G. and Anadranistakis E. 2007, *Wave and wind Atlas of the Hellenic Seas*, Hellenic Centre for Marine Research Publ.

Tsimplis M.N. 1994. Tidal oscillations in the Aegean and Ionian Seas, *Estuarine, Coastal and Shel f Science*, 39, 201-208.

Δελτίο της Ελληνικής Γεωλογικής Εταιρίας, τομ. XLVII , 2013
Πρακτικά 13ου Διεθνούς Συνεδρίου, Χανιά, Σεπτ. 2013

Bulletin of the Geological Society of Greece, vol. XLVII 2013
Proceedings of the 13th International Congress, Chania, Sept. 2013

GEOMORPHOLOGICAL QUANTITATIVE ANALYSIS OF SPERCHIOS RIVER BASIN AREA (CENTRAL GREECE) UTILIZING GEOGRAPHICAL INFORMATION SYSTEMS

Psomiadis E.[1], Migiros G.[1] and Antoniou V.[1]

[1] *Agricultural University of Athens, Laboratory of Mineralogy & Geology, Iera Odos 75, 118 55, Athens, mpsomiadis@gmail.com, bagm@aua.gr, vantoniou@gmail.com*

Abstract

In the present study the analysis of the morphometric quantitative parameters of Sperchios river basin, and specifically of the 8 main sub-basins of the northern and southern part, have been made. The integrated use of a Geographic Information System (GIS) allows a thorough spatial analysis of the data derived from digital terrain spatial models that reveal the geomorphological characteristics of an area.
The thorough analysis of the results shows the significant difference of the morphological characteristics of the northern and southern part of the catchment area, due to the impact of the neotectonic activity of the area, which creates this asymmetrical topography.
Key words: *Drainage network, morphometry, tectonics, spatial models.*

Περίληψη

Στην παρούσα μελέτη πραγματοποιήθηκε η ανάλυση των μορφομετρικών ποσοτικών παραμέτρων της λεκάνης του ποταμού Σπερχειού, και συγκεκριμένα των 8 κύριων υπολεκανών του βόρειου και νότιου τμήματος. Η ολοκληρωμένη χρήση ενός Γεωγραφικού Συστήματος Πληροφοριών (GIS) επιτρέπει μια λεπτομερή χωρική ανάλυση των δεδομένων που προκύπτουν από τα ψηφιακή μοντέλα εδάφους, που αναδεικνύουν τα γεωμορφολογικά χαρακτηριστικά μιας περιοχής. Η διεξοδική ανάλυση των αποτελεσμάτων δείχνει τη σημαντική διαφορά των μορφολογικών χαρακτηριστικών του βόρειου και νότιου τμήματος της λεκάνης απορροής, λόγω της επίδρασης της νεοτεκτονικής, όπου δημιουργεί αυτή την ασύμμετρη τοπογραφία.
Λέξεις κλειδιά: *Υδρογραφικό δίκτυο, μορφομετρία, τεκτονική, χωρικά μοντέλα.*

1. Introduction

The development of the drainage network and the morphological features within a river basin affected and dependent on many, complex and interacting parameters (Deffontaines & Chorowicz, 1991). These factors can be classified as internal, external and complex. Essentially, the complex factors are the combination of internal and external factors. Internal factors derived from the behavior of the bedrock and controlled mainly by lithology and structure. The lithology affect through physical (permeability, increased susceptibility to erosion, hardness, etc.) and chemical properties (diagenesis, dissolution, chemistry of groundwater, etc.) of rocks. The factor of structure arises in various ways, such as the geometry, composition and thickness of rocks, and the switch in tectonic regime of rocks, which can create faults and folds (Schumm 1986). The external factors incorporate climate, vegetation and human activity.

The study area is the basin of river Sperchios in Central Greece, which lies between 38° 44' and 39° 05' N, and 21° 50' and 22° 45' N (Figure 1). In the following sections the statistics and quantitatively characteristics of the 8 main sub-basins, 4 at the south part [Roustianiti (Ro), Inachou (In), Gorgopotamou (Go) and Assopou (As)] and 4 at the north part [Vitioliotis (Vi), Archanorema (Ar), Drimarorema (Dr) and Xerias-Lamias (Xe)] of Sperchios river catchment area, are elaborated (Figure 2). Quantitative measurements of the landscape shape and drainage network characteristics allowed us to compare different landforms and to calculate the geomorphic indices that are useful to identify the landscape evolution of the basin. Geographic Information Systems (GIS) technology, focus on efficiently collecting, maintaining, manipulating and analyzing geomorphic information and a variety of spatial data (Minár et al., 2006). In particular, the core of geomophological analysis using a GIS is based on the fundamental concept of geomorphology which says that activities of geomorphological processes are explicitly represented in the shape of the georelief. This means that analysis of georelief provides correct information about the origin and development of a landscape as well as relevant data about activities of recent and present-day processes. (Psomiadis et al. 2005 ; Psomiadis, 2010).

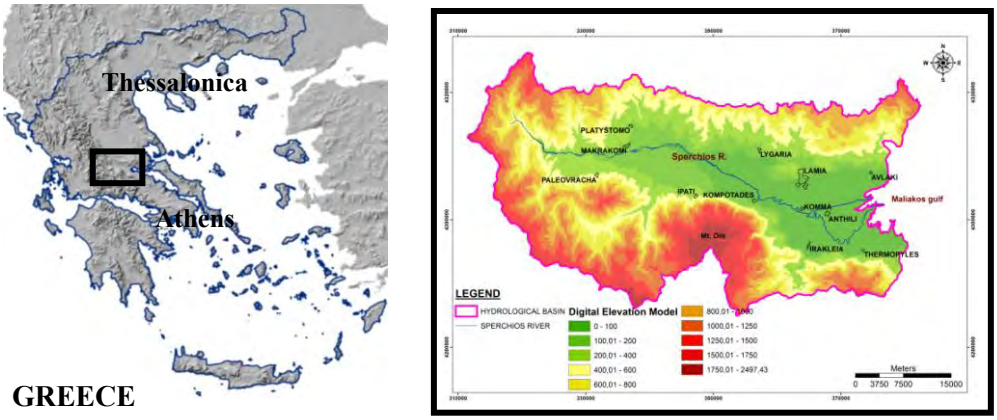

Figure 1 - Location of the study area [Digital Elevation Model (DEM) of Sperchios river basin].

2. Data - Methodology

For the present study, digital elevation model (DEM), derived spatial data (such as slope, aspect etc), drainage network and structural geology have been used, originated from 12 topographic and geological maps of 1:50.000 scale. Consequently, all the geospatial data were processed and analyzed through ArcGIS software suite v.9.2). The classification of the drainage network was accomplished using Strachler's classification system Strahler (1957). Using the spatial analysis of the Geographic Information System, morphometric parameters for all sub-basins and their characteristics have been calculated and analyzed. In order to investigate the relation between tectonic and drainage network development, the imprint of both high angle normal faults and small-angle reverse faults (overthrust, thrust) was made. Subsequently, a statistical analysis of the linear elements using Georient software v.8.0 and the creation of frequency (rf) and density (rd) rose diagrams, have been accomplished, both for normal and reverse faults (Figure 4) and additionally for each separately stream order of the drainage network, so as to explore the relation between drainage system and tectonic activity.

3. Study area

3.1. Physical Geographical and Morphological Settings

River Sperchios runs through a valley, which is a graben-like asymmetrical depression. Drainage network throughout the basin is dendritic and drains mountains Tymphristos, Oiti and Othrys.

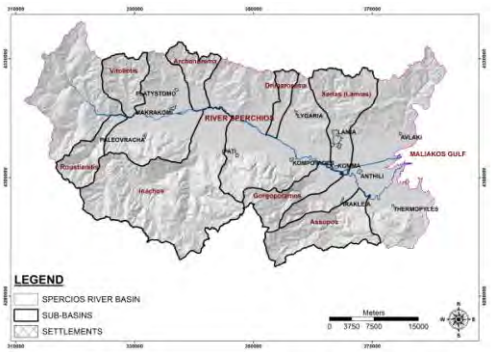

Figure 2 - The distribution of the 8 sub-basins, 4 in the north and 4 in the south par t of Sperchios' river catchment area.

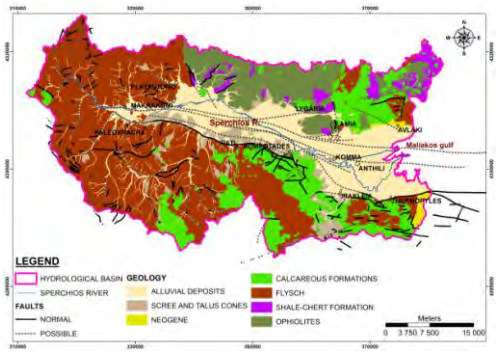

Figure 3 Simplified lithological map of Sper chios river basin, including faults and prob able faults of the area.

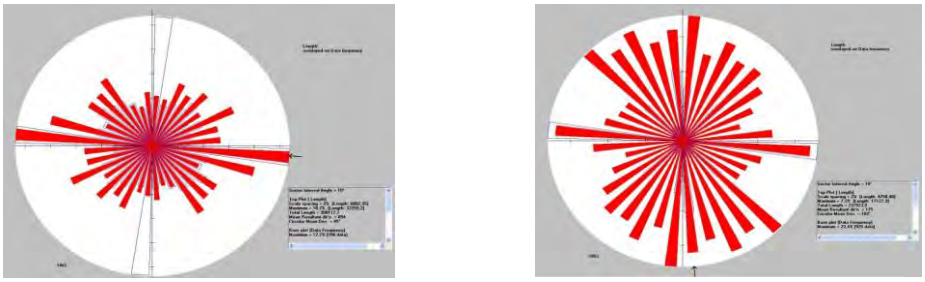

(α) Normal faults (β) Reverse faults

Figure 4 - Rose diagrams of frequency (rf) and density (rd) for (a) high angle normal faults [(rf=88^o & rd=94^o (E-W)]; and (b) small-angle reverse faults (overthrust, thrust) [rf=174^o & rd=175^o (SSE-NNW)].

In the case of Sperchios basin, separating the basin in two parts based on river's flow direction, in north and south part, significant differences between them can be distinguished. According to the diagram of elevation and elevation areas aggregation curves (Figure 5), the southern part exhibits higher relief than the northern part, while presenting more convex curve from 200 to 1.000m, compared with the north in which the corresponding curve are more concave. This curvature of the curve means that from 200 to 1.000m, the area is increasing, as the elevation increases, while it was expected that should decrease. The cause of this anomaly is mainly due to intense tectonism and particularly at the southern part. Moreover, a large area with elevation less than 100m, due to the elongation of Sperchios river central bed and the spread of alluvial deposits can be depicted. Also, significant differences in terms of relief between the southern and the northern part can be distinguished, using a diagram representing the percentage of each elevation zone (Figure 6).

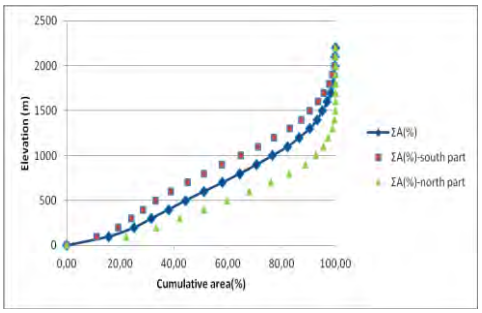

Figure 5- The relation of elevation and elev ation areas aggregation (%).

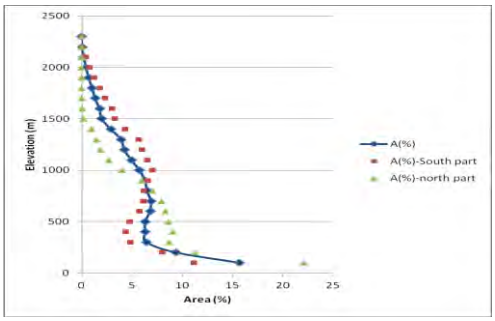

Figure 6 - The percentage of each elevation zone (%).

In the northern part the percentages show highest values in elevations ranging from 400 to 700m, and then decrease rapidly. In contrast in the southern part the percentages normally increase normally up to approximately 1.000m and then decrease smoothly at higher altitudes. The difference in elevation curve for the two parts (south and north) is due to the fact that the main river bed of Sperchios, is a graben-like asymmetrical depression with a WNW-ESE direction, parallel to the active fault of Atalanti, where the southern part is lifted and the northern is sinking (Mariolakos, 1976).

3.2. Geological Setting

The valley of river Sperchios is a part of a tectonic trough, which is controlled by major NW-SE and E-W trending faults parallel to Atalanti normal fault zone. More specifically, from the fault rose diagrams that have been created, it can be observed that high angle normal faults have a direction E-W, while low angle reverse faults (thrust faults) have a NW-SE direction (Figure 4). The high angle normal faults in the south and central part of the basin have a W-E and NW-SE direction, while in the north part have mainly a NE-SW direction. The fault tectonism took place at the end of the Pliocene and beginning of the Pleistocene periods. The area experienced strong earthquakes, like those which occurred in 426 B.C. and 1894 A.D. and induced big disasters in the broader study area (Mouyiaris, 1988; Pirazzoli et al. 1999).

In the drainage basin of River Sperchios, there are three distinct lithological regions according to Ferrière (1977); these are: (i) the western part that is composed of Paleocene-Eocene flysch of the East Pindus and Parnassos geotectonic zones; it is composed of alternating beds of argillite-siltstone-fine conglomerate and intercalations of shale. There is also a limited occurrence of pelagic and marly limestones of the Vardoussia zone in this area, (ii) the south-eastern portion of the basin is composed of Middle Triassic-Jurassic massive dolomites and limestones of the Pelagonian zone; Upper Cretaceous flysch consisting of coarse sandstone alternating with shale and sandy marl belonging to the zone of Beotia; and Upper Cretaceous thickl-bedded limestones and Eocene flysch, composed of sandstone, clay and marl of the Parnassos geotectonic zone, and (iii) in the north and north-eastern part, which is formed by an ophiolithic complex in a shale-chert formation composed of shales, cherts and limestones with ultra-basic and basic igneous rocks-peridotite, dunite, pyroxenite, gabbro, serpentine, diabase, dolerite and metamorphosed green phyllites and schists; belonging to Maliakos (Subpelagonian) zone. In addition, Neogene and Quaternary unconsolidated deposits occupy the central and lower (elevations <500 m) part of the elongated drainage basin of the Sperchios river (Maroukian & Lagios, 1987).

4. Analysis and Results of the selected basins

4.1. Northern Part

4.1.1. Vitoliotis

The Vitoliotis stream sub-basin is located in the northwestern part of Sperhios river basin and has a NW-SE direction (Figure 7a). The basin according to its morphometric characteristics (Table 1) is quite mountainous, susceptible according to its shape to flash flood phenomena. The frequency and density of the drainage network show high values, 3.73 and 9.74 respectively. These values indicate a basin which is formed mostly by impermeable rocks (flysch) and a relatively high relief favoring surface runoff and the creation of a dense drainage network. Finally, the sinuosity index is low while instead, in the main stream branch there is a tendency of elongation. The rose diagrams of faults direction indicate that stream of low Strahler's order have been affected by neotectonic activity. The streams of the 4th, 5th and 6th order streams are influenced mainly by low angle reverse faults or older faults of the area (Table 3).

4.1.2. Archanorema

The Archanorema sub-basin is located in the north and central part of Sperchios river basin and has a NW-SE direction (Figure 7b). This basin according to its morphometric characteristics (Table 1) is a small basin (47.4 km^2), semi-mountainous, with low relief. The frequency and density of the drainage network show very high values, 3.81 and 10.21 respectively. These values indicate a basin which is characterized by the presence of semi-permeable and impermeable formations (flysch and ophiolites) leading to a dense drainage network. Finally, the sinuosity index is very low indicating the absence of meander. The rose diagrams of faults direction indicate that the streams of 1st, 2nd and of 4th up to 6th order present a SE-NW direction, following the low angle reverse faults. Oppositely, the 3rd order streams, present a SW-NE direction, following the high angle normal faults, affected by neotectonic activity (Table 3)

4.1.3. Drimarorema

The Drimarorema sub-basin is situated in the north-central part of Sperchios river basin and has a NE-SW direction (Figure 7c). This basin according to its morphometric characteristics (Table 1) is a small basin (26.6 km^2), with a very low total relief and mean slope value. The elongation ratio shows a tendency of elongation. The frequency and density of the drainage network represent high values, 3.7 and 8.75 respectively. These values indicate a basin which is characterized by the presence of semi-permeable formations (ophiolites) leading to the creation of a dense drainage network. Finally, the sinuosity index is very low indicating the absence of meander. The rose diagrams of faults direction indicate that the streams of 3rd up to 5th order (main branch) present a SE-NW direction, following the low angle reverse faults. Oppositely, the 1st and 2nd order streams, present a W-E and NE-SW direction, following the high angle normal faults, affected by neotectonic activity of the area (Table 3).

4.1.4. Xerias (Lamias)

The Xerias (Lamias) sub-basin is situated in the northeastern part of Sperchios river basin at the west part of Othrys Mountain and has a N-NW to S-SE direction (Figure 7d). This basin according to its morphometric characteristics (Table 1) is a medium to large basin (109.7 km^2), the largest of the northern part. It has a high total relief and the elongation ratio shows a tendency of elongation. The frequency and density of the drainage network represent low values, 2.08 and 4.12 respectively. These values indicate a basin which is characterized by the presence of permeable formations (calcareous) leading to the creation of a sparse drainage network. The low values of frequency, is also due to the low relief and slopes of the basin. Finally, the sinuosity index is low indicating the absence of meander. The rose diagrams of faults direction indicate that the streams of 1st up to 4th order present a E-W direction, following the high angle normal faults affected by neotectonic activity of the area, while the main branch of the stream (5th order) present a NE-SW direction following the low angle reverse faults or older faults of the area (Table 3)

4.2. Southern Part

4.2.1. Roustianitis

The Roustianitis sub-basin is situated in the southwestern part of Sperchios river basin and has a SW to NE direction (Figure 8a). The 85% of this sub-basin lies in elevations higher than 600m, while the 75% belongs to the very mountainous area. This basin according to its characteristics (Table 2) is a medium size basin (53.11 km^2). It has high values of mean elevation, total relief and steep slopes. Similar high values of relief ratio and slope index is observed. The length-width ratio appears high, presenting an elongated basin, affected probably also by the neotectonic activity of the area. Regarding the frequency and density of the drainage network, this present low values, 2.33 and 3.86 respectively. Oddly, these values are mismatched with the fact that the basin is formed mainly with flysch which gives usually a dense drainage network. Instead of that the drainage network is sparse, due apparently to the presence of the very high relief and the steep

slopes of the basin. The rose diagrams of faults direction indicate that the streams of 1st and 2nd order present a SE-NW and E-W direction, respectively, following the high angle normal faults. On the contrary, the branches of 3rd, 4th and 5th order present a NE-SW direction following the structure of low angle reverse faults (upthrusts, overthrusts) (Table 3).

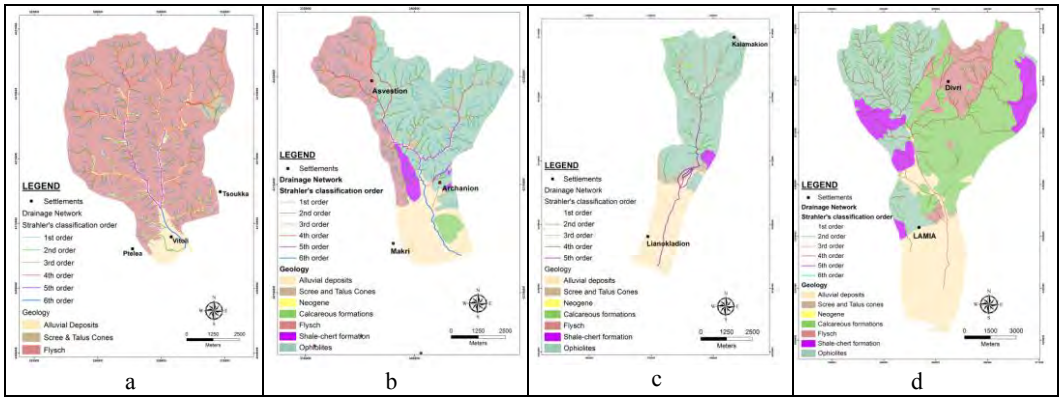

Figure 7 - The 4 sub-basins of the northern part (a)Vitoliotis, (b)Archanorema, (c) Drima-rorema and (d) Xerias (Lamias). It is presented the geology and the drainage network.

Table 1 - The morphometric characteristics of the northern part sub-basins.

Parameter	Symbol/ Equation	Vito-liotis	Archano-rema	Drima-rorema	Xerias (Lamias)
Area (km^2)	(A)	58.85	47.40	26.62	109.74
Basin Length (km)	(Lb)	10.47	12.22	11.84	17.63
Basin width (km)	(Br=A/Lb)	5.62	3.88	2.18	6.22
Perimeter (km)	(P)	36.28	38.54	30.84	57.63
Maximum Elevation hmax (m)	-	1,281.31	826.45	820.5	1,085.51
Minimum Elevation - hmin (m)	-	215.00	100.00	30.8	12.00
Total relief (m)	H= hmax-hmin	1,066.31	726.45	789.70	1,073.51
Median elevation - hmedian (m)	-	670.00	420.00	285.00	593.14
Mean Elevation - hmean (m)	-	747.41	452.64	456.14	540.00
Basin mean slope (%)	BS = ΣLi d/A	44.00	32.00	28.00	30.00
Relief ratio (RH) (m/km)	RH=H/(Lb)	101.84	59.45	66.70	60.89
Length-Width index (S)	S=(Lb)/(Br)	1.86	3.15	5.43	2.83
Basin shape index	$Rf = A/ Lb^2$	0.54	0.32	0.19	0.35
Basin circularity ratio	$Rc = 4\pi A/P^2$	0.56	0.40	0.35	0.42
Basin elongation ratio	$Re = 1.129(A)^{0,5}/Lb$	1.54	0.64	0.49	0.67
Dr. network density index	$Co=0.282P/(A)^{0,5}$	1.33	1.58	1.69	1.55
Number of streams	(Nu)	573.00	484.00	233.00	452.00
Total stream length (km)	(L)	219.77	180.78	98.48	228.48
Main stream length (km)	Lm	11.56	14.46	12.49	19.30
Density (km/km^2)	D=(L)/(A)	3.73	3.81	3.70	2.08
Frequency ($1/km^2$)	F=(N)/(A)	9.74	10.21	8.75	4.12
Sinuosity index	C= Lm/Lb	1.10	1.18	1.06	1.10
Slope index (m/km)	Sr=H/Lm	92.24	50.23	63.23	55.62

4.2.2. Inachos

The Inachos sub-basin is situated in the southwestern part of Sperchios river basin, covering a very big part of it and has a SW to NE direction (Figure 8b). The main branch of the river, according to the Strahler's classification, is of the 7th order, which intersects with Sperchios, giving the final 8th order that flows into Maliakos gulf. The 89% of this basin lies in elevations higher than 600m, while the 78.5% belongs to mountainous area. This basin according to its morphometric characteristics (Table 2) is the biggest sub-basin of Sperchios (341.86 km^2). It has a very high value of mean elevation and total relief. As far as it concerns the frequency and density of the drainage network present very high values, 3.49 and 8.45 respectively. These values are due to the domination of flysch formation in the basin. The high value of frequency indicates also that the basin is influenced by the tectonic activity of local fault zones. The sinuosity is relatively low indicating the absence of meander. The rose diagrams of faults direction indicate that the streams of 1^{st} order show an E-W following the high angle normal faults. The branches of 3^{rd} and 4^{th} order present a S/SE-N/NW direction following the structure of the low angle reverse faults. The branches of 2^{nd}, 3^{rd}, 6^{th} and 7^{th} order present a NE-SW direction, following the normal faults, but they are mainly affected from the existing geological structure (Table 3).

4.2.3. Gorgopotamos

The Gorgopotamos sub-basin is situated in the southeastern part of Sperchios river basin, originates from the eastern part of mountain Oiti and has a W-SW to E-NE direction (Figure 8c). The 76.3% of this basin lies in elevations higher than 600m, while the 74.6% belongs to the mountainous area. A special feature of this basin is the well known from historical events canyon of Gorgopotamos. The creation of the canyon is due to the steep slopes of the basin and the transition of the geological formations from flysch to carbonate rocks. The presence of the impermeable flysch formation at the upper part of the basin causes a very high surface runoff of rainfall water, while the steep slopes of the basin lead to a very fast water flow. At the transition point that embarks on the existence of the carbonate rocks, which are much more erodible than the flysch formation, the creation of the canyon is started up. The whole process is further enhanced by the Sperchios southern part lifting processes, which along with the existing steep slopes favor the retrogressive erosion creation. This basin according to its morphometric characteristics (Table 2), is a medium size basin (67.62 km^2) and it has high total relief and steep slopes. The elongation ratio is rather high, presenting an elongated basin, affected probably and by the neotectonic activity of the area. As regards the frequency and density of the drainage network they have medium to high values, 2.75 and 5.87 respectively. These values indicate a basin which is characterized by the presence of permeable calcareous formations, leading to the creation of a sparse drainage network, except from the north part of the basin that flysch formation is appeared. Finally, the sinuosity index is low indicating the absence of meander. The rose diagrams of faults direction indicate that the streams of 1^{st} up to 4^{th} order present mainly a E-W direction, following the high angle normal faults, as well as the main branch of the river (5^{th} order) presenting a NE-SW direction and seems to be affected either from high angle normal faults and other older faults of the area (Table 3).

4.2.4. Assopos

The Assopos sub-basin is situated in the southeastern part of Sperchios river basin, originates from southeastern part of mountain Oiti and has a W-SW to E-NE direction (Figure 8d). In nowadays, subsequently to the infrastructure and drainage constructions that occurred the last decades in the coastal area of Sperchios basin, Assopos is the only river that supply at the downstream part of Sperchios river. The 73.6% of this basin lies in elevations higher than 600m, while the 58.8% belongs to the very mountainous area. The values of the elongation ratio and the length-width index, present an elongated basin, affected by the neotectonic activity of the area. As far as it concerns, the frequency and density of the drainage network have medium values, 2.35 and 4.64 respectively. These values indicate a basin which is characterized by the presence of permeable

calcareous formations that lead to the creation of a sparse drainage network. The high value of the frequency indicates also the basin is influenced by the tectonic activity of the local fault zones. The sinuosity is relatively low and indicates the absence of meander. The rose diagrams of faults direction indicate that the streams of 1st up to 4th order exhibit an E-W and SE-NW direction, following the high angle normal faults, as well as the main branch of the river (5th order) which presents a NE-SW direction and seems to be affected either from high angle normal faults and other older faults of the area (Table 3).

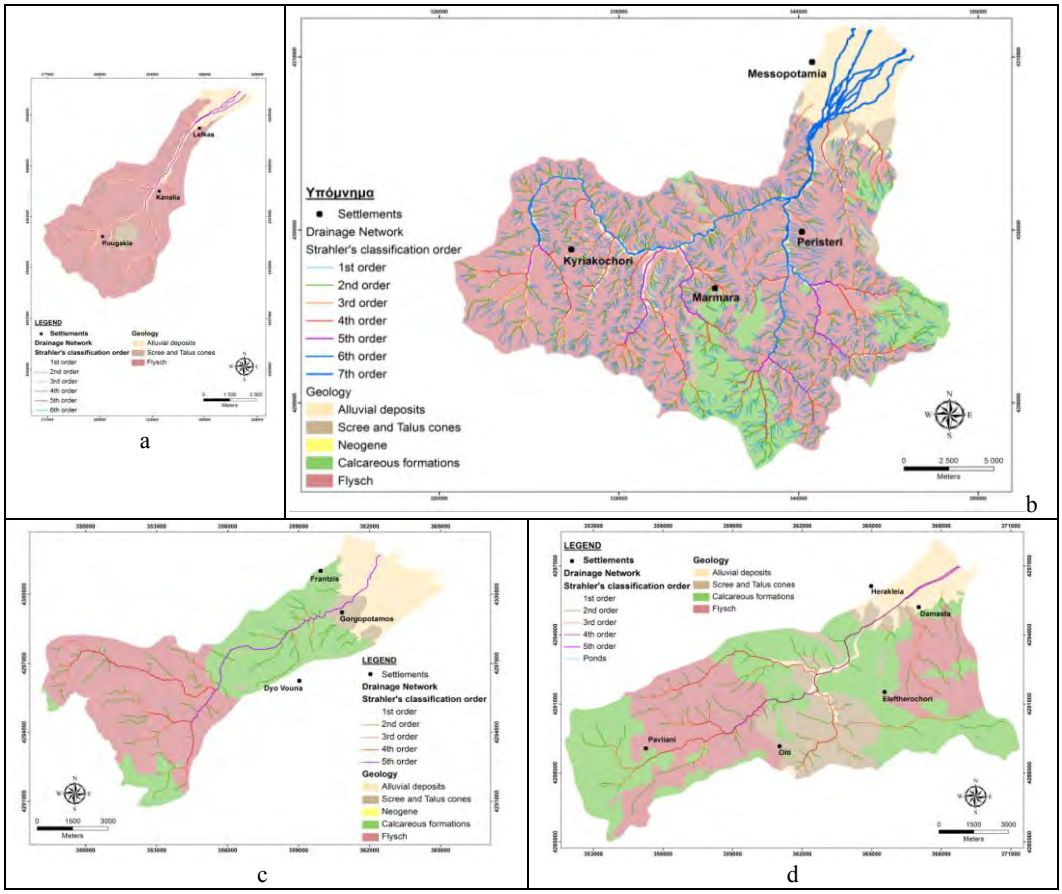

Figure 8 - The 4 sub-basins of the southern part (a) Roustianitis (b)Inachos, (c) Gorgopotamos and (d)Assopos. It is demonstrated the geology and the drainage network.

Table 2 - The morphometric characteristics of the southern part sub-basins.

Parameter	Sym-bol/Equation	Roustiani-tis	Ina-chos	Gor-gopota-mos	As-sopos
Area (km^2)	(A)	53.11	341.86	67.62	112.97
Basin Length (km)	(Lb)	14.61	29.21	15.06	19.45
Basin width (km)	(Br=A/Lb)	3.64	11.70	4.50	5.81
Perimeter (km)	(P)	39.67	104.58	52.90	58.95
Maximum Elevation hmax (m)	-	1,724.61	2,293.64	2,150.61	1,804.25
Minimum Elevation hmin (m)	-	240.50	90	14.00	8.00
Total relief (m)	H= hmax-hmin	1,484.11	2,203.64	2,136.61	1,796.25
Median elevation - hmedian (m)	-	940.00	962.00	1.320.00	680.00

Mean Elevation - hmean (m)	-	998.70	1,155.36	1.089.70	946.94
Basin mean slope (%)	BS = ΣLi d/A	0.40	0.42	0.41	0.46
Relief ratio (RH) (m/km)	RH=H/(Lb)	101.58	75.44	141.87	92.35
Length-Width index (S)	S=(Lb)/(Br)	4.01	2.50	3.35	3.35
Basin shape index	$Rf = A/ Lb^2$	0.25	0.40	0.30	0.30
Basin circularity ratio	$Rc = 4\pi A/P^2$	0.42	0.39	0.30	0.41
Basin elongation ratio	$Re = 1.129(A)^{0,5}/ Lb$	0.21	0.72	0.62	0.62
Dr. network density index	$Co=0.282P/(A)^{0,5}$	1.53	1.60	1.82	1.56
Number of streams	(Nu)	205.00	2,887.00	397.00	524.00
Total stream length (km)	(L)	123.64	1,193.69	185.74	259.91
Main stream length (km)	Lm	15.50	30.40	15.88	21.60
Density (km/km2)	D=(L)/(A)	2.33	3.49	2.75	2.30
Frequency (1/km2)	F=(N)/(A)	3.86	8.45	5.87	4.64
Sinuosity index	C= Lm/Lb	1.06	1.04	1.05	1.11
Slope index (m/km)	Sr=H/Lm	95.75	72.49	134.54	83.16

Table 3 – Drainage network orientation of frequency (rf) and density (rd) according to the relevant rose diagrams

Parameter		**Vi**	**Ar**	**Dr**	**Xe**	**Ro**	**In**	**Go**	**As**
		North part				**South part**			
	Order	**rf, rd**	**rf, rd**	**rf, rd**	**rf, rd**	**rf, rd**	**rf, rd**	**rf, rd**	**rf, rd**
Frequency and Density drainage orientation	1	E-W	S/SE-N/NW	E-W	E-W	SE-NW	E-W	E-W	SE-NW
	2	E-W	S/SE-N/NW	W/NW-E/SE	E-W	E-W	N/NE-S/SW	E-W	SE-NW
	3	E-W	E/NE-W/SW	N/NE-S/SW	W/NW-E/SE	N/NE-S/SW	N/NE-S/SW	W/NW-E/SE	E-W
	4	N/NE-S/SW	SE-NW	N/NE-S/SW	W/NW-E/SE	W/SW-E/NE	S/SE-N/NW	E-W	E-W
	5	S/SE-N/NW	N/NE-S/SW	N/NE-S/SW	NE-SW	NE-SW	S/SE-N/NW	NE-SW	NE-SW
	6	S/SE-N/NW	SE-NW	-	-	-	N/NE-S/SW	-	-
	7	-	-	-	-	-	N/NE-S/SW	-	-

5. Conclusions

Based on a thorough geospatial analysis of the features in the 8 main sub-basins of Sperchios catchment area, a wealth of useful information on the morphology was extracted. In particular it is clear that the sub-basins at the southern part are clearly longer and have relatively smaller width according to their size, while the basins at the northern part, present higher circularity. Additionally, the relief at the south is steeper, with steeper slopes, higher total relief and mean elevation. These characteristics are due probably to the influence of neotectonic activity of the area and the effects of EW faults, which conduce to the lift process of the southern part and the sinking and widening process of the northern part. The drainage network follows these movements and as

a consequence the branches of the streams in the south are longer and sparse, while in the north are shorter, and dense. Moreover, at the evolution processes of the drainage network, the geological background of the area constitutes a fundamental parameter. In Sperchios basin, the western and southwestern part of the basin are dominated by impermeable rocks (flysch), which form a dense drainage network, while in the south-southeastern part of the basin dominated the permeable calcareous rocks, which form a sparse network.

The frequency and density of the drainage network have mostly moderate to high values, mainly due to geological bedrock and the recent ongoing neotectonic activity of the area. Moreover, the highest values of density are noted at the impermeable and semi-permeable geological formations. According to the frequency and density rose diagrams of the drainage network, can be detected that in the sub-basins of the southern part the main orientation is E-W and less E/SE-W/NW and E/NE-W/SW following the high angle normal faults, which affect and form the whole basin of Sperchios. A small exception can be noticed in the sub-basin of Inachos river, where is affected also from older local faults and shows a NE rotation around of a NE-SW axis. This phenomenon influences the drainage network development. Oppositely, at the northern part the drainage network presents a S/SE-N/NW and less NE-SW orientation, following the low angle reverse faults (upthrust, overthrusts). An exception of that is occurred in the western part, which is affected mainly by the normal faults or from older local faults with an E-W orientation.

6. Acknowledgments

During preparation of the manuscript the State Scholarships Foundation of Greece supported one of the authors (E. Psomiadis).

7. References

Deffontaines B., Chorowicz J., 1991. Principles of drainage basin analysis from multisource data: Application to the structural analysis ofthe Zaire basin. In: J. Fourniguet & G. Pierre (Eds), Neotectonics. Tectonophysics, 194, pp. 237-263.

Mariolakos H., 1976. Thoughts and views on certain issues of Geology and Tectonics of the Peloponnese. Ann.Geol.Pays Hellen.,27, 215-313.

Maroukian H., Lagios E., 1987. Neotectonic movements in the Sperkhios River basin, Central Greece. Z.Geomorph.N.F., Suppl.-Bd. 63, 133-140.

Mentlík P., Jedlička K., Minár J., Barka I., 2006. Geomorphological information system: physical model and options of geomorphological analysis. Geografie, Sborník České Geografické Společnosti, p. 15-31.

Mouyiaris N.K., 1988. Destructive historical earthquakes in N. Euboicos and Maliacos Gulfs-Their significance to the evolution of the area. Proceedings of the Engineering geology of ancient works, monuments and historical sites-Preservation and Protection, Vol. 3, pp. 1249-1256, Balkema, Rotterdam.

Pirazzoli P.A., Stiros S.C., Arnold M., Laborel J., Laborel-Deguen F., 1999. Late Holocene coeseismic vertical displacements and tsunami deposits near Kynos, gulf of Euboea, central Greece. Phys. Chem. Earth (A), Vol.24, No 4, 361-367.

Psomiadis E., Parcharidis I., Stamatis G., Foumelis M., 2005. Remotely sensing data and thematic mapping for sustainable developing in Sperchios river basin (Central Greece). Proc. of SPIE 5983, Remote Sensing for Environmental Monitoring, GIS Apps and Geology.

Psomiadis E., 2010. Geomorphologic and environmental changes research in the Sperchios river basin utilizing new technologies (Remote Sensing & GIS). Doctorate Thesis elaborated at the Agricultural University of Athens, Lab. of Mineralogy & Geology, p. 394.

Schumm S.A., 1986. Alluvial river response to active tectonics. In: R.E. Wallace (Eds), Active Tectonics. Natl. Acad. Press, Washington, D.C., pp. 80-94.

Strahler N.A., 1957. Quantitative analysis of watershed geomorphology. Amer. Geophys. Union, Trans., 38 (6), 1117-1142.

Δελτίο της Ελληνικής Γεωλογικής Εταιρίας, τομ. XLVII , 2013
Πρακτικά 13ου Διεθνούς Συνεδρίου, Χανιά, Σεπτ. 2013

Bulletin of the Geological Society of Greece, vol. XLVII 2013
Proceedings of the 13th International Congress, Chania, Sept. 2013

GEOMORPHOLOGICAL MAPPING OF MESSOGIA PLAIN (EAST ATTICA, GREECE)

Skentos A.[1], Liosis N.[1] and Pavlopoulos K.[1]

[1] Harokopio University of Athens, Department of Geography, thanskentos@hua.gr, nikos.liosis@gmail.com, kpavlop@hua.gr

Abstract

This study concerns the geomorphological mapping of the area included in the map sheets Koropi and Plaka of the Hellenic Military Geographical Service map distribution in scale 1:50.000. This is an extensive area of East Attica which presents a complex terrain and a wide variety of landforms, due to its intense tectonism and the natural processes that shaped its morphology. The primary data that were used in the creation of the map mainly included geological and topographic maps, from which thematic layers of the topography, hydrography and geology were constructed through GIS processes. A Digital Elevation Model was also constructed, from which the slope and aspect maps were created. The thematic maps of slope and lithology were classified into categories, which were combined to constitute detection criteria of landforms. Decisive contribution in mapping was provided by the available orthophotomaps and aerial photographs, as well as the field work. Finally, with the appropriate combination of colors and symbols the geomorphological map of the study area was produced.
Key words: *GIS, multi-component analysis, semi automated, Geomorphological mapping.*

Περίληψη

Η παρούσα μελέτη αφορά τη γεωμορφολογική χαρτογράφηση της περιοχής που περιλαμβάνεται στα φύλλα χάρτη Κορωπί και Πλάκα της διανομής της Γ.Υ.Σ. σε κλίμακα 1:50.000 . Πρόκειται για μια εκτεταμένη περιοχή της Ανατολικής Αττικής η οποία παρουσιάζει σύνθετο ανάγλυφο και μεγάλη ποικιλία γεωμορφών, λόγω του έντονου τεκτονισμού της και των φυσικών διεργασιών που διαμόρφωσαν τη μορφολογία της. Για τη δημιουργία του χάρτη χρησιμοποιήθηκαν κυρίως γεωλογικοί και τοπογραφικοί χάρτες, από τους οποίους κατασκευάστηκαν μέσω Γεωγραφικών Συστημάτων Πληροφοριών τα θεματικά επίπεδα της τοπογραφίας, της υδρογραφίας και της γεωλογίας, ενώ κατασκευάστηκε επίσης και το Ψηφιακό Μοντέλο Εδάφους, από το οποίο προέκυψαν οι χάρτες κλίσεων και έκθεσης. Οι θεματικοί χάρτες των κλίσεων και της λιθολογίας ταξινομήθηκαν σε κατηγορίες οι οποίες συνδυάστηκαν αποτελώντας κριτήρια εντοπισμού γεωμορφών. Στη χαρτογράφηση συνέβαλλαν καθοριστικά οι διαθέσιμοι ορθοφωτοχάρτες και αεροφωτογραφίες, όπως επίσης η εργασία πεδίου. Στη συνέχεια, με τον κατάλληλο συνδυασμό χρωμάτων και συμβολισμών δημιουργήθηκε ο γεωμορφολογικός χάρτης της περιοχής μελέτης, η οποία αποτελείται από τμήματα διαφοροποιημένων μορφολογικών χαρακτηριστικών του αναγλύφου.
Λέξεις κλειδιά: *ΓΣΠ, πολυ-κριτηριακή ανάλυση, Ημι-αυτοματοποιημένες μέθοδοι γεωμορφολογικής χαρτογράφησης.*

1. Introduction

The study area is located at the central part of eastern Attica (Figure 1). Specifically, the area includes the northern part of Lavrion, Messogia plain, the mountains of Hymettus, Paneion and Merenda, the central part of the eastern coast of Attica and part of the coast of the Saronic Gulf. At the East the area is bordering to the South Evian Gulf while at the southwest it ends to the Saronic Gulf.

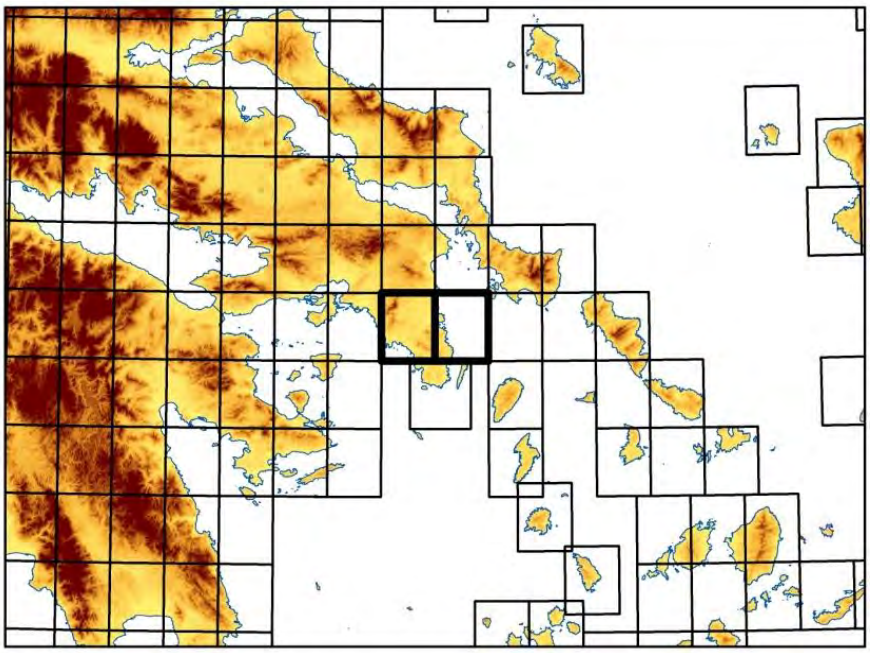

Figure 1 - Map location of the study area.

The study area consists of alpine and post alpine geological formations. The alpine rocks occur mainly in the mountains and hills and they are consisted of limestones, marbles, schists, phyllites, dolomites and ophiolites (Latsoudas, 2003; Papanikolaou et al., 2004). The post alpine geological formations include Neogene and Quaternary deposits.
The intense tectonic activity of the area defines the configuration of the folds of the relief, settles the mountains and the plains bordering basins, such as the main Messogia basin.
The climate of the region of Attica belongs to the dry Mediterranean type. During the winter season it appears characteristics of the temperate climate zone, with mild, wet winters, and during the summer season characteristics of subtropical climate zones of high pressure, with hot and dry summers.

2. Methodology

2.1. Data Used

The first stage of the research was the collection of analogue maps and remote sensing data of the study area. The analogue maps include large scale (1/5.000) and medium scale (1/50.000) topographic sheets that were gathered by the Hellenic Military Geographical Service as well as the geological map of the region from the Institute of Geology and Mineral Exploration. Remote sensing data include large scale aerial photos that were taken by the National Cadastre and the Ministry of Agriculture. Furthermore, specific aerial photographs were acquired in analogue format for stereoscopic analysis.

2.2. Dem and Slope Map

The Digital Terrain Model (DTM) was created from all the digitized contours and the elevation points. The original format was a Triangular Irregular Network (TIN) that was transformed into a reticular layer (raster), with cell size 25m.

The slope map is considered as one of the most important data generated by the DTM concerning geomorphological mapping (Gustavsson et al., 2009). Slope is one of the main features of geomorphological analysis, as different landforms occur in different inclinations. The cell values were grouped into 6 categories (Figure 2) in accordance with the uniform system of symbolism («Unified Key») which was established by the IGU Commission on Geomorphological Survey and Mapping during the 1960s – 1970s (Gustavsson et al., 2006).

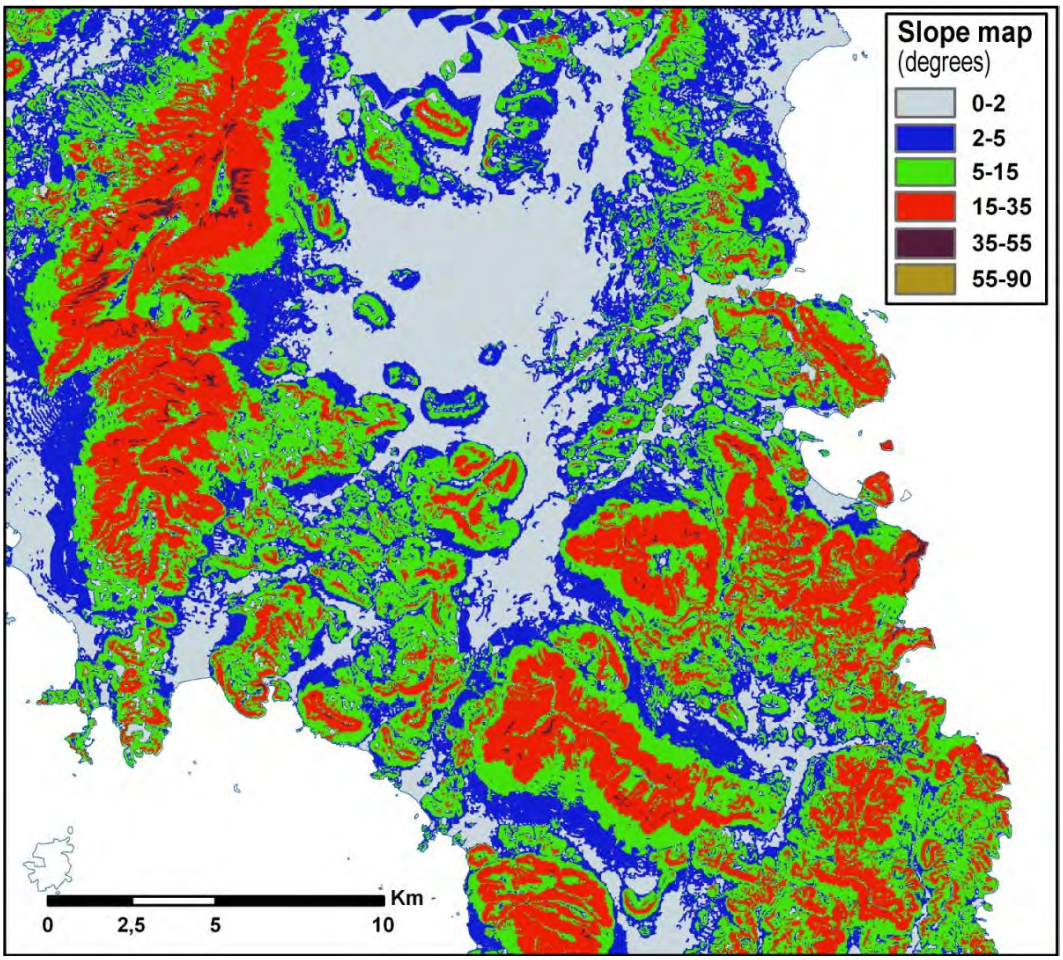

Figure 2 - Slope map of the study area.

2.3. Semi - Automated Geomorphological Mapping

Basic criteria for the identification of the landforms were slope and lithology. Various combinations of the specific criteria were used as shown in Table 1 (Van Asselen et al., 2006).

For the identification of the cliffs of the region were used as primary criteria high ground slope (> 35^{o}) in combination with the presence of alpine formations. The areas that were marked by the automated process were verified by aerial photos and fieldwork (Pavlopoulos et al., 2009).

Table 1 - Criteria for multi-variable analysis

Landforms	Criteria	Success
Cliffs	• Slopes > 35º • Alpine formations	Great
Planation surfaces	• Slopes < 5º • Alpine formations	Great
Alluvial cones and side debris	• 35º > slopes > 5º • Pleistocene deposits	Medium
Terraces	• Slopes < 5º • Post alpine formations • Buffer 100 m. from streams	Medium
Deep erosion	• Slopes > 35º • Buffer 50 m. from streams	Low

To determine the planation surfaces were used as criteria smooth relief slopes (<5º) combined with the presence of alpine formations. The application of this combination was very successful as it revealed most of the planation surfaces. Furthermore, classes of elevation of DTM were used to classify surfaces levelling depending on the altitude, as also the layer of the aspect map, generated by the DTM to determine the direction in which they creep.

The multivariable analysis to identify alluvial cones and side debris had less successful but still satisfactory results. Further classification of Quaternary deposits depending on the grade of coherence of the sediment may give better results. In this paper, for the identification of specific landforms, analogue methods were used which include qualitative interpretation of aerial photos and field work.

Regarding the detection of Inselbergs were used as primary criteria alpine formations that are surrounded by post alpine sediments. After identifying these regions, the elevation criterion was used to determine whether they are hills or not.

The coastal landforms were determined by the combined study of topography, geological structure and remote sensing data. The steep slopes of the shores were already recognized during the multivariable analysis for the identification of the cliffs.

The automated methods for the identification of the shape of the valleys and the terraces had low degree of successful determination.

All the multi-criteria determinations of landforms, verified by field work and remote sensing methods.

2.4. Map Compilation

The geographical entities were classified according their characteristics following the rules of cartographic generalization, abstraction and simplification (Gustavsson, 2005). Specifically, discrete levels of information were generated concerning topographic, hydrographic, geological, geomorphological and anthropogenic elements (Figure 3). For each geographical entity were used appropriate cartographic symbols. In individual cases were created new symbols for the accurate interpretation of the information (Figure 3).

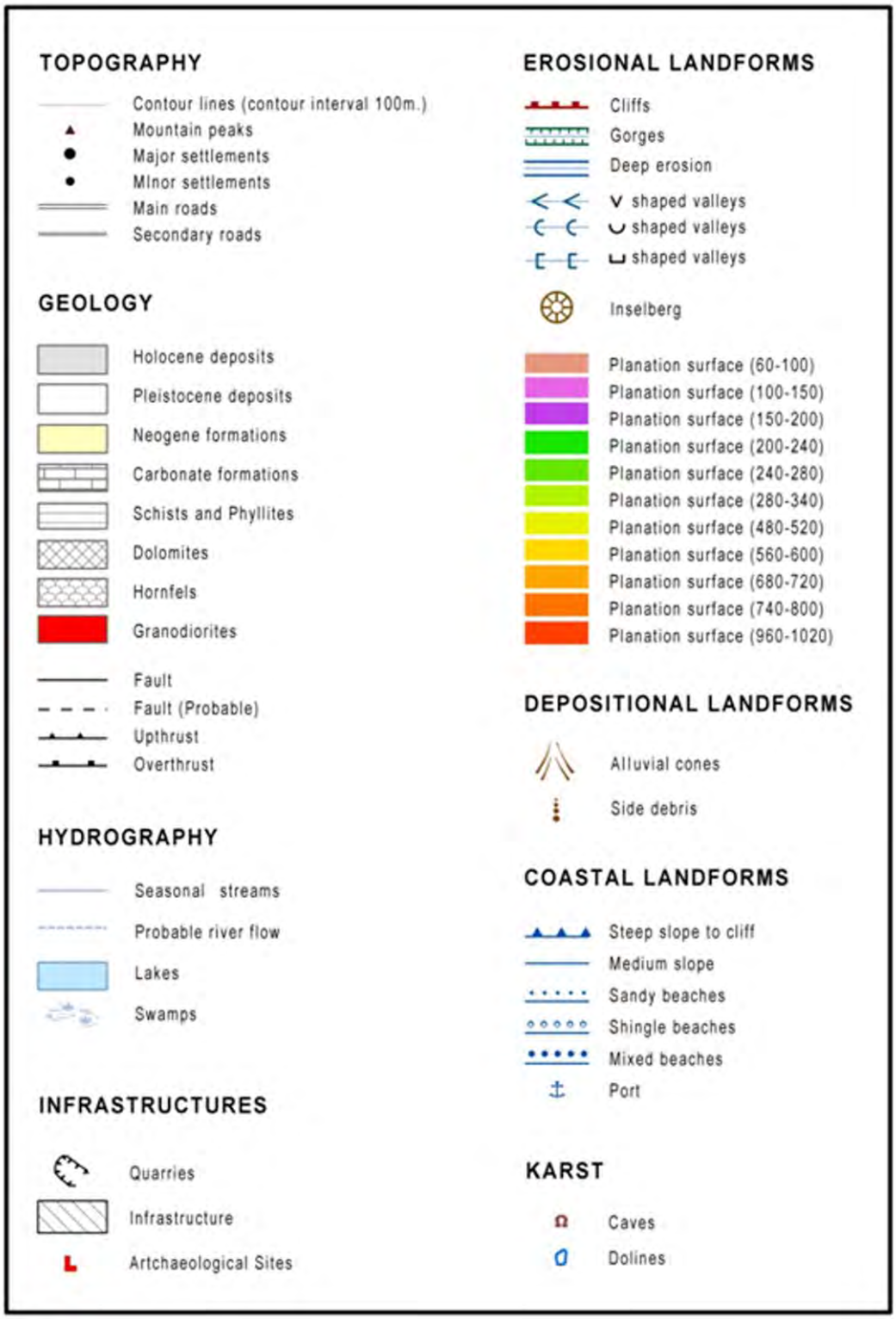

Figure 3 - Map Legend.

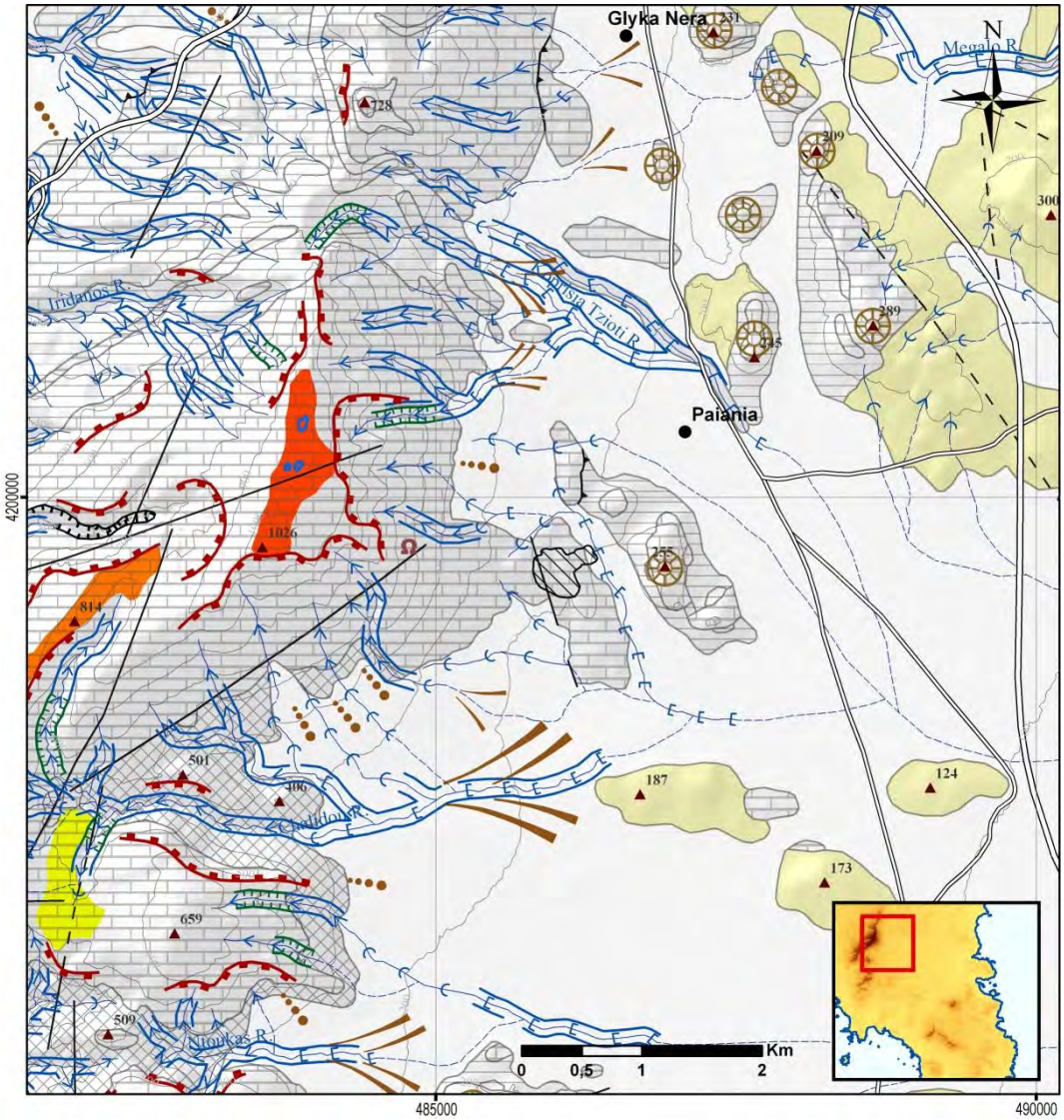

Figure 4 - Hymettus and the western plain of Mesogia - Part of the geomorphological map of Messogia plain, scale 1/50.000.

3. Results

Messogia plain outlines the characteristics of a mild terrain traversed by stage of maturity and characterized by smooth slopes, extensive alluvial areas and inselbergs (Figure 4). Messogia basin owes its genesis to the intensive tectonic movements that took place during the Alpine orogenesis and completed during the Upper Pliocene - Lower Pleistocene with the lifting of the surrounding mountains (Boskos, 2008).

During the Upper Miocene, seasonal lakes were located in the northern part of the main basins as documented by the lacustrine deposits of the specific period. Those lakes were either covered by sediment deposits from the neighboring mountains or dried after periods of intense drought. Moreover, marine transgression did not cover the entire area of Messogia (Papachatzis, 1953).

The Pleistocene deposits of the plain indicate the active tectonism and the intense processes of erosion and deposition of that period where the uplift of the surrounding mountains was still going on. The Holocene deposits are less extensive, due to limited runoff. The intense, deep erosion of Megalo Rema and Erasinos River that appear during the Upper Pleistocene is probably due to tectonic causes or to sea level changes (Figure 5).

The asymmetric morphology of Hymettus, where the eastern slopes appear steeper than the west is due to the intense tectonic activity of the region after the Lower Pliocene (Figure 4) (Krohe et al., 2010). From this period onwards was intensified the deep erosion of the valleys and gorges were created as their relative uplift was accompanied by the lowering of the hydrographic network. The erosional landforms took their present shape as the processes that created them continued along the tectonic and climatic changes of the Pleistocene (Pavlopoulos et al., 2005).

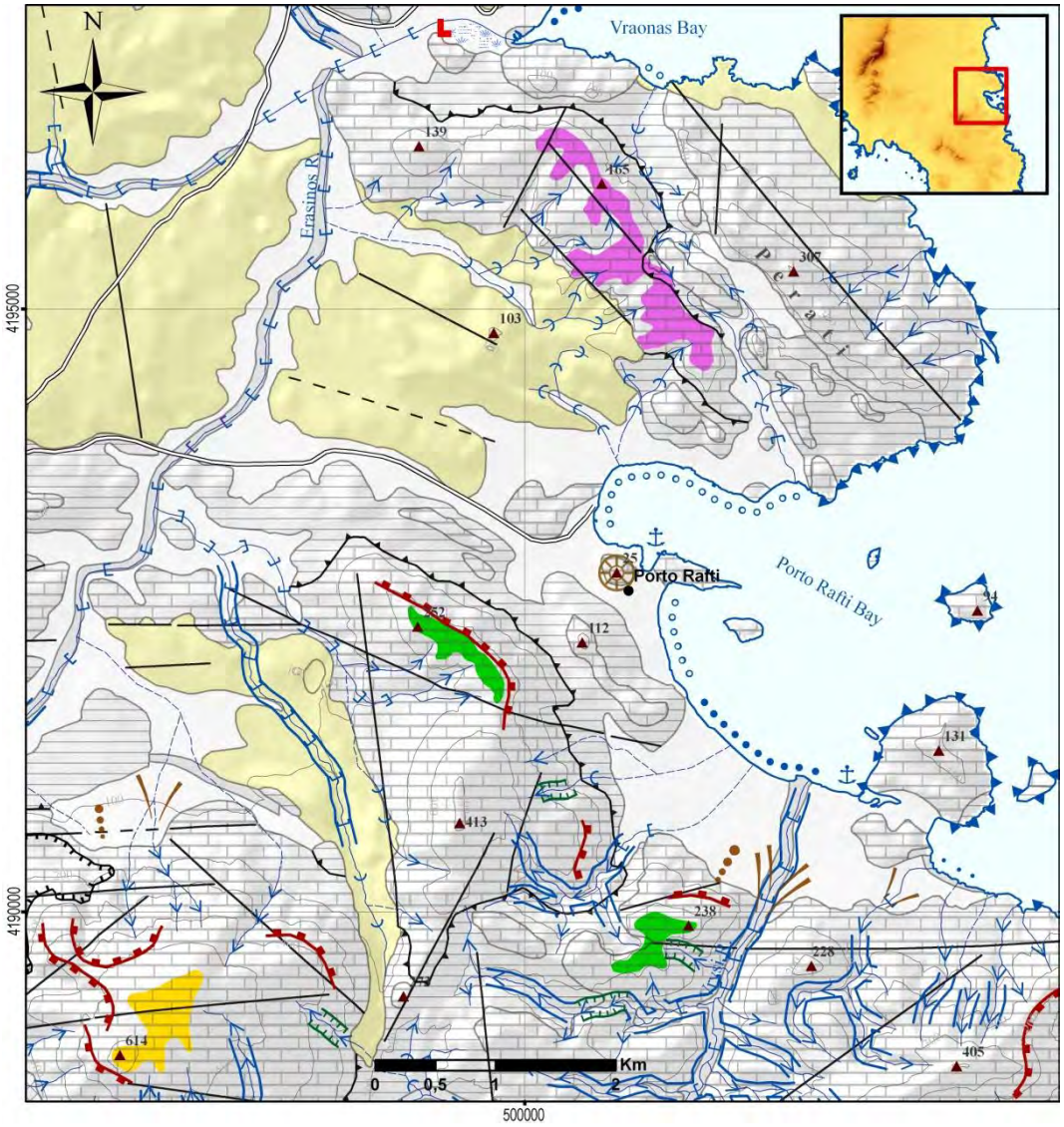

Figure 5 - Porto Rafti region - Part of the geomorphological map of Messogia plain, scale 1/50.000.

The planation surfaces of Hymettus at altitudes from 500 to 800 meters were formed probably during Miocene while the planation surfaces from 940 to 1000 meters can be considered older, and are correlated by lithology and altitude with the planation surfaces of Penteli Mountain (Pavlopoulos et al, 2005).

The planation surfaces of the lower elevations of Hymettus present south and west exposure and represent subsequent evolutions of the landscape (Figure 4). The planation surfaces from 200 to 240 m. and 240 to 280 m. are likely to be associated with the inselbergs of the basin, whose creation is associated with different susceptibility to corrosion of the lithological formations of the pre-Neogene relief.

Similar aspect present the planation surfaces of the central eastern coastal region at altitudes greater than 150 m. The planation surfaces identified in the southeast present aspect and morphological slope to the northeast, which means that this part behaves differently as documented by the differentiated morphology of the river networks (Figure 5) (Pavlopoulos, 1992).

The geomorphological evolution of the area is mainly controlled by the tectonic evolution and the climate change of the Pleistocene, while the upper part of the Holocene is also influenced by human interventions. The alluvial deposits show slow progress or stagnation, as the artificial arrangement of the streams and the anthropogenic formation of the surrounding areas impedes the natural deposition processes.

4. Discussion

The geomorphological map of Messogia plain presents the main landforms of the study area, showing clearly the characteristics of the relief to the extent permitted by the scale study. Recognition of landforms through modern methods of mapping provided by GIS was performed primarily by analyzing the morphological characteristics of the relief. The semi-automated identification techniques of the major landforms through multi-component analysis provided very satisfactory results which were verified by the study of cartographic data, remote sensing data and field work. For the attribution of geomorphology at larger scales the range of values of the criteria should be broaden. These values include quantitative parameters, such as distances and slopes, or qualitative parameters such as classification of the geological formations. In conclusion, automated analysis methods in geomorphological mapping are an important tool where output data should be verified in any case.

The analysis of the geomorphological map shows that Messogia plain is a basin which owes its genesis to the intensive tectonic movements that took place during the Alpine orogenesis and completed during the Upper Pliocene - Lower Pleistocene with the uplift of the surrounding mountains. The Quaternary climate changes have resulted to the accumulation of sediment within the basin and the creation of side debris and alluvial fans on the slopes of the surrounding mountains. Finally, the current status of the morphology of the area is due to the human factor.

5. References

Boskos E. 2008. Neogene and Quartenery Sediments of the North Part of Athens Basin and the Broad Area of Kapandriti. Contribution to the Palaiogeographical Evolution of the Athens Basin from the Upper Neocene till Nowadays, *Mineral Wealth 149/2008,* 1 - 18.

Gustavsson M. 2005. Development of a Detailed Geomorphological Mapping System and GIS Geodatabase in Sweden, Licentiate Thesis.

Gustavsson M., Kolstrup E. and Seijmonsbergen A.C. 2006. A new symbol-and-GIS based detailed geomorphological mapping system: Renewal of a scientific discipline for understanding landscape development, *Geomorphology 77*, 90 – 111.

Gustavsson M., Seijmonsbergen A. C. and Kolstrup E. 2009. Combining digital elevation data (SRTM/ASTER), high resolution satellite imagery (Quickbird) and GIS for geomorphological mapping: A multi-component case study on Mediterranean karst in Central Crete, *Geomorphology 112*, 106 – 121.

Krohe A., Mposkos E., Diamantopoulos A. and Kaouras G. 2010. Formation of basins and mountain ranges in Attica (Greece): The role of Miocene to Recent low-angle normal detachment faults, *Earth-Science Reviews 98*, 81 – 104.

Latsoudas Ch.(2003), Geological map of Greece, scale 1:50.000, "Koropi-Plaka" sheet, IGME, Athens.

Papachatzis N. 1953. Morphogenetical Researches about the Mesogia Basin of Attica, *Bull. Geol. Soc. Greece*, V, 236-258.

Papanikolaou D., Bassi E.-K., Kranis Ch. and Danamos G. 2004. Paleogeographic evolution of the Athens basin from Late Miocene up to present. Bulletin of the Geological Society of Greece XXXVI, 816–825.

Pavlopoulos K. 1992. Geomorphological Evolution of Southern Attica, *Gaia No2*, University of Athens, *PhD Thesis*.

Pavlopoulos K., Kotampasi X. and Skentos A., 2005. Geomorphological Evolution of the Athens Basin, *Bull. Geol. Soc. Greece*, XXXVIII, 1 - 13.

Pavlopoulos K, Evelpidou and N. Vassilopoulos A. 2009. Mapping Geomorphological Environments, Springer, 1-230.

Van Asselen S. and Seijmonsbergen A.C. 2006. Expert-driven semi-automated geomorphological mapping for a mountainous area using a laser DTM, *Geomorphology 78*. 309 – 320.

Δελτίο της Ελληνικής Γεωλογικής Εταιρίας, τομ. XLVII , 2013
Πρακτικά 13ου Διεθνούς Συνεδρίου, Χανιά, Σεπτ. 2013

Bulletin of the Geological Society of Greece, vol. XLVII 2013
Proceedings of the 13th International Congress, Chania, Sept. 2013

ANALYSIS OF RELATIONSHIPS AMONG COASTAL ALLUVIAL FANS AND THEIR CONTRIBUTING CATCHMENTS IN NORTH EVOIKOS GULF (CENTRAL GREECE)

Valkanou K.[1], Karymbalis E.[1], Papanastassiou D.[2], Gaki-Papanastassiou K.[3] and Giles P.[4]

[1]Department of Geography, Harokopio University, Athens, Greece (kvalkanou@hua.gr; karymbalis@hua.gr)

[2]Institute of Geodynamics, National Observatory of Athens, Greece (d.papan@noa.gr)

[3]Department of Geography-Climatology, Faculty of Geology & Geoenvironment, National Kapodistrian University of Athens, Greece (gaki@geol.uoa.gr)

[4]Department of Geography, Saint Mary's University, Halifax, Nova Scotia, Canada

Abstract

This paper deals with the morphometric analysis of 42, late Holocene, coastal alluvial fans located along the coasts of the tectonically active North Evoikos Gulf in central Greece. Thirty six of the fans have been formed by streams that discharge along the east coast of the Gulf (Evia Island) while the rest are located on the opposite side (Continental Greece). Selected morphometric parameters of the drainage basins were measured using topographic maps at the scale of 1:50,000 while those of the fans were derived from detailed topographic diagrams at the scale of 1:5,000 utilizing ESRI's ArcGIS9.3 software. Fans were classified into four groups according to the primary depositional processes (fluvial and/or debris flow). Another classification criterion was the relationship between the location of the fan-catchment system and the local tectonic patterns (active faults). Fan-basin morphometric relationships for each fan group were also investigated. A strong positive relation was found between the size of the fan and the drainage basin area while the correlation between drainage area and fan slope was negative. Large catchments located near fault terminations have formed gently sloping fans dominated by fluvial processes, whereas torrents with small rough drainage basins, developed on the footwall, have formed steep fans likely dominated by debris-flow along the east coast of the Gulf.
Key words: *Coastal alluvial fans, Quantitative Geomorphology, North Evoikos Gulf, Greece.*

Περίληψη

Στην παρούσα εργασία αναλύονται μορφομετρικά 42 παράκτια αλλουβιακά ριπίδια ηλικίας Ανώτερου Ολόκαινου, που βρίσκονται κατά μήκος των ακτών του τεκτονικά ενεργού Βόρειου Ευβοϊκού Κόλπου στην κεντρική Ελλάδα. Τριάντα έξι από τα αυτά ριπίδια έχουν σχηματισθεί από χείμαρρους που εκβάλλουν κατά μήκος της ανατολικής ακτής του Κόλπου (Εύβοια), ενώ τα υπόλοιπα βρίσκονται στην απέναντι ακτή (Στερεά Ελλάδα). Εκτιμήθηκαν επιλεγμένες μορφομετρικές παράμετροι των λεκανών από το-

πογραφικούς χάρτες κλίμακας 1:50,000, ενώ οι παράμετροι των ριπιδίων μετρήθηκαν από λεπτομερή τοπογραφικά διαγράμματα κλίμακας 1:5,000 με χρήση του λογισμικού ArcGIS9.3 της ESRI. Τα αλλουβιακά ριπίδια ταξινομήθηκαν σε τέσσερις ομάδες λαμβάνοντας υπόψη τις πρωτογενείς διεργασίες απόθεσης (ποτάμια τροφοδοσία με ίζημα και/ή διεργασίες που σχετίζονται με ροή υλικών λόγω βαρύτητας). Άλλο ένα κριτήριο για την ταξινόμηση ήταν η θέση του συστήματος ριπίδιο-λεκάνη σε σχέση με τα κύρια ενεργά ρήγματα της περιοχής. Επιπλέον μελετήθηκαν οι σχέσεις μεταξύ μορφομετρικών παραμέτρων ριπιδίου-λεκάνης για κάθε ομάδα ριπιδίων. Η σχέση μεταξύ της έκτασης του ριπιδίου και του εμβαδού της λεκάνης απορροής ήταν θετική και ισχυρή ενώ η συσχέτιση μεταξύ έκτασης λεκάνης και μορφολογικής κλίσης ριπιδίου ήταν αρνητική. Μεγάλης έκτασης λεκάνες που έχουν αναπτυχθεί κοντά στις απολήξεις ρηγμάτων έχουν διαμορφώσει μικρής κλίσης ριπίδια όπου κυριαρχούν οι ποτάμιες διεργασίες, ενώ χείμαρροι με μικρές τραχείς λεκάνες απορροής, που βρίσκονται στα ανυψούμενα τεμάχη ρηγμάτων, έχουν δημιουργήσει απότομα ριπίδια όπου πιθανά κυριαρχεί η κίνηση υλικών λόγω βαρύτητας στην ανατολική ακτή του Κόλπου.
Λέξεις κλειδιά: *Παράκτια αλλουβιακά ριπίδια, Ποσοτική Γεωμορφολογία, Βόρειος Ευβοϊκός Κόλπος, Ελλάδα.*

1. Introduction

Alluvial fans are sedimentary deposits with a form resembling the segment of a cone radiating downslope from a point where a channel emerges from an upland (Blair and McPherson, 1994). Fans are subaerial features; however, if they extend into water, they are called fan deltas.

According to Blair and McPherson (1994), there are three necessary conditions for optimal alluvial fan development: (a) a topographic setting where a channel becomes unconfined by emerging from an upland drainage basin to a relatively flat lowland, (b) sufficient sediment production in the drainage basin for fan construction, and (c) infrequent intense precipitation to create high water discharge needed to transport the sediment from the drainage basin to the fan site.

The aim of this study is to classify the fans according to the primary depositional processes (fluvial and/or debris flow) controlling their formation and recent evolution, through quantitative morphometry. Among the principal objectives of this paper is to present fan-basin morphometric relationships for the fans, and to investigate the possible relationship between the geographic distribution of fans and basins and the local tectonic patterns.

In Greece, similar attempts have been made to classify fan-deltas along the coast of the Gulf of Corinth (Karymbalis, 2007; Karymbalis et al., 2010; Karymbalis et al., 2012).

2. Study Area

The studied fans are located on the east and west coasts of the North Evoikos Gulf, a NW-SE trending graben, 100km long, which separates north Evia Island to the east from continental Greece to the west (Figure 1). The Gulf of Evia rift system is a significant geomorphological feature, a Quaternary structure accommodating N-S crustal extension in Central Greece (Roberts & Jackson, 1991). The amount of extension (from geodetic estimates for the whole of Central Greece) is about 1cm/yr, implying a fast mean extension rate (Ganas & Papoulia, 2000). Recent research using local seismological networks has demonstrated that in this area seismic stress may not necessarily be released with strong earthquakes, but instead with intense microearthquake activity, usually in seismic swarms (Papanastassiou et al., 2001; Papoulia et al., 2006). Several major normal fault zones, in a step-like arrangement striking WNW-ESE and dipping to the north bound the high relief along both coasts. According to Goldsworthy and Jackson (2001) the coastal fault system (Atalanti and Kandili fault zones) is probably the most active and recent (Figure 1). Apart

from these major coastal faults, there are also NE-SW minor fault zones with motions during the Quaternary (Palyvos, et al., 2006).

The coastal landscape of the west coast of the Gulf has undergone significant changes during the Quaternary which can be recognized in the form of raised terraces, raised or submerged beachrocks and marine notches while on the lowlands tsunami deposits are found (Cundy et al. 2000; Gaki-Papanastassiou et al. 1999). The central-eastern mainland of Greece is a tectonically active region which hosts well-known WNW-ESE tectonic structures, such as the Atalanti, Arkitsa-Agios Konstantinos-Kamena Vourla and Kallidromon Fault zones (Ganas & White, 1996)

Some historical earthquakes are known in the region from historical sources and archaeological findings, but most cannot be associated with a particular fault. Only one, in 1894, is known to have ruptured the surface and this occurred on the coastal fault system east of Atalanti (Goldsworthy and Jackson, 2001; Goldsworthy et al., 2002; Pantosti et al., 2004; Pavlides et al., 2004). According to Goldsworthy and Jackson, (2001), hanging wall migration of the faulting has occurred, while they maintain that the basins in the Gulf of Evia (Evoikos Gulf) can change from substantial subsidence to substantial uplift, erosion and re-deposition all within 1 million years.

The west coastal zone of North Evoikos Gulf, along the hanging wall of the Arkitsa fault, is dominantly erosional (probably due to sediment starvation), with deposition confined to moderate to large fan deltas (Cundy et al., 2010), while on the other hand the footwall sourced fan deltas of the east side are generally smaller (Leeder and Jackson, 1993).

At the east coastal zone of North Evoikos Gulf the attitude of the normal faults switches from dominantly N-dipping near Kamena Vourla in the west, to S-dipping and then finally to N-dipping along the coastline of NE Evia (Goldsworthy et al., 2002). Normal faults along the east coast of Evoikos Gulf are responsible for uplifted marine notches containing lithophaga (also along the coastline of NE coastline of Evia) (Stiros et al., 1992). No modern earthquakes have occured in this region but several historic events are noted.

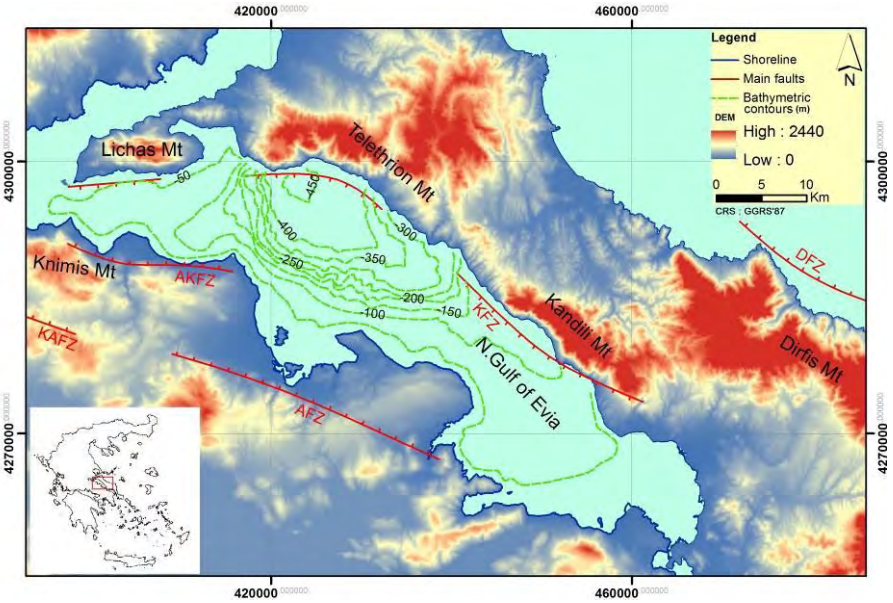

Figure 1 - DEM of the broader area of North Evoikos Gulf. The main normal faults and the subaqueous morphology are also depicted (DFZ: Dirfys fault zone, KFZ: Kandili f.z, AFZ : Atalanti f.z, KAFZ: Kallidromon f.z, AKFZ: Arkitsa-Kammena Vourla f.z) (insert map of Greece shows the location of the study area).

3. Data Used and Methodology

The identification and delineation of the fans was based on field observations, aerial photo interpretation (at 1:33,000 scale, taken in 1996, obtained from the Greek Ministry of Rural Development and Food), and the use of detailed topographic maps (at 1:5,000 scale with 2 m contour lines) obtained from the Hellenic Geographical Military Survey and geological maps of the sub-aerial geology obtained from the Institute of Geology and Mineral Exploration of Greece (IGME). These detailed topographic maps were also the source for the measurement of fan morphometric variables. Measurement of fan morphometric parameters was restricted to the portion of fan sediments above sea-level since the subaqueous portions could not be measured due to the lack of detailed hydrographic data.

Drainage networks and source catchments were delineated from topographic maps at 1:50,000 scale, with 20 m contour intervals, and aerial photo interpretation (at 1:33,000 scale, taken in 1996). The same maps were used for the measurement of the morphometric parameters of the catchments. Measurements, calculations and visualization of the results were performed using ESRI's ArcGIS9.3 software.

The morphometric parameters for the fans and their catchments, which provided the most interesting results, are given below:

- Drainage basin area (A_b), the total planimetric area of each basin, measured in km^2.
- Drainage basin slope (S_b), obtained using the equation $e\Sigma Lc/Ab$, where e=equidistance, L = total length of contour lines and A_b=basin area.
- Drainage basin crest (C_b), the maximum elevation of the drainage basin, measured in m.
- Drainage Basin Perimeter (P_b), the length of the basin border, measured in km.
- Length of channels (L_c), the total length of the channels within the drainage basin, measured in km.
- Drainage basin Relief (R_b), the vertical difference between the basin crest and fan apex, given in m.
- Melton's ruggedness number (M), obtained using the formula $R_b*A_b^{-0.5}$.
- Drainage basin circularity (Cir_b), obtained using the formula $4\pi A_b/Pb^2$.
- Drainage basin density (D_b), the ratio of the total length of the channels to the total area of the basin, L_c/A_b.
- Total length of 20m contour lines within the drainage basin (ΣL_c), measured in km.
- Fan area (A_f), the total planimetric area of each fan, measured in km^2.
- Fan apex (Ap_f), the elevation of the apex of the fan, in m.
- Fan length (L_f), the distance between the toe (in our case coastline) and apex of the fan, measured in m.
- Fan slope (S_f), the mean gradient measured among the axial part of the fan.
- Fan concavity (C_f), obtained using the formula a/b, where a=the elevation difference between the fan axis profile and the midpoint of the straight line joining the fan apex and toe and b=the elevation difference between the fan toe and the midpoint.

The relationships between selected basin and fan parameters were investigated by plotting log-log graphs and determining the power functions that describe these relations.

4. Geological Background

The Alpine basement of the catchments consists of the geological formations of the Pelagonian geotectonic zone. According to the geological mapping of the Institute of Geology and Mineral Exploration of Greece - IGME - the formations of the Alpine basement of the study area is composed of igneous rocks (intrusives such as diabases, peridotites, dunites, pyroxenites and ophiolites), Upper Paleozoic greenschists, schists, phyllites, and greywackes with conglomerates and limestone or dolomite intercalations, Permo-Triassic limestones, greywackes, schists, prasinites and volcanites. Trias and Jurassic are primarily represented by limestones and dolomites while schist-chert formation (including radiolarites, sandstones, pelites with limestone lenses and enclosed ophiolitic bodies) of Jurrassic age also occur in the study area. The younger Alpine rocks are limestones (mainly biosparudites), crystalline limestones and marbles of Upper Cretaceous age.

Post-Alpine formations consist of lacustrine and terrestrial deposits (conglomerates, sands, clayey material, marls and marly limestones) of Upper Miocene-Pliocene age and Plio-Pleistocene fluvio-lacustrine deposits such as sands, conglomerates, clays, and peat or lignite beds. Valley bottoms along of the major streams are covered by alluvial deposits of Holocene age. The mountainous relief, the numerous torrents and the occurrence of extensive areas covered by erodible formations (e.g., loose Quaternary deposits, Neocene sediments, flysch formation) can amplify the action of the erosion process. As a consequence Evia Island exhibits a high frequency of landslides and represents one of the sites in Greece with the highest landslide susceptibility (Rozos et al., 2013).

In order to investigate the influence of the drainage basin lithology on the evolution of the fans the lithological units cropping out in the catchments were grouped into four classes based on their permeability (IGME, 2010). The first group includes marls and clays, schists, ophiolites, volcanic formations and FeNi deposits. The second group includes limestones, limestone conglomerates, dolomites, sipolines. The third group consists of alluvial sediments, sandstones and travertine; and the fourth group contains clastic sediments and molassic deposits. The relative distribution of each one of the four main lithological types in the area of each basin was estimated and the dominant catchment lithology group has been correlated to the fan area and the fan gradient. This correlation showed that the role of the bedrock control on fan formation processes is not clear, probably because of the complexity of the system.

5. Classification of the Coastal Fans

Table 1 includes the values of the morphometric variables estimated for the coastal alluvial fans and their drainage basins. The total number of fans is 42. By far the largest among the fans is Dipotamon having an area of 10.62 km^2 (Figure 3). It has developed at the hanging wall of Arkitsa-Kammena Vourla fault zone and can be characterized as a delta, dominated by fluvial supply and wave activity, formed by a relatively large river with perennial flow. The area of the other fans range between 0.01 and 3.78 km^2. An important factor for the discrimination between the alluvial fan processes is the size of the drainage basin (represented by the area and the total length of the drainage network channels) (Crosta & Frattini, 2004). Morphometric parameters of the fans and corresponding basins along with the tectonic setting of the fan-catchment systems were the main criteria for the classification of the fans into the following four groups (Figure 2).

Group 1 includes five fans, four located on Evia Island (7-18-25-35) and fan 41 fan which lies on the opposite side of the Gulf (Figure 2 & Figure 3). These have been developed laterally and partially cover larger fluvial-dominated fans of the other groups. Their shape is conical and they do not have well-developed channels. These fans are small (mean fan area is 0.09km^2) with small catchments (mean basin area is 1.05km^2). Fan gradients for this group are high (mean fan slope equals 0.09). Their morphology, as well as the morphometric characteristics of their catchments, indicates that they are likely debris flow-dominated fans.

Group 2 contains 22 fans (1-2-3-4-5-6-8-15-16-17-19-20-21-22-23-24-26-30-31-32) on Evia Island, and fans 37 and 38 on the west side of the Gulf (Figure 2 & Figure 3). The main characteristic of this group's fans is their tectonic setting. Both fans and drainage basins are situated on the footwall of the main active normal faults which tend to be parallel to the east and west coast of the Gulf. Both fans and catchments of this group are more extensive than those of the previous group (mean area values are 0.33km^2 and 4.09km^2 respectively) whereas fans are less steep (mean fan slope equals 0.07). Most of them have a triangular shape and are characterized as fluvial-dominated.

Group 3 is comprised of ten fans (9-10-11-12-13-14-27-28-29-36) (Figure 2 & Figure 3), which have developed along the coastline of the Evia Island. Fan-catchment systems of this group are not directly affected by major faults as they lie between fault segments or near their terminations. This type of tectonic setting provides enhanced opportunities for drainage growth (Leeder and Jackson 1993). These fans have a more semicircular morphology and are generally aggrading fans with an active prograding area near the river mouth. They are more extensive than the previous group (mean fan area is 0.68km^2) and have more extensive catchments (mean basin area is 9.95km^2). They are characterized as fluvial-dominated.

Group 4 includes five fans (33-34 on Evia Island and 39-40-42 on the west side of the Gulf) (Figure 2 & Figure 3). In this category, basins lie on the footwall of active faults while their corresponding fans are on the hanging wall. In this group the fans have the greater mean area (2.87km^2) and the lower mean slope (0.03) and are typical fluvial-dominated fans formed by extensive drainage basins which are located on the uplifting block of active faults.

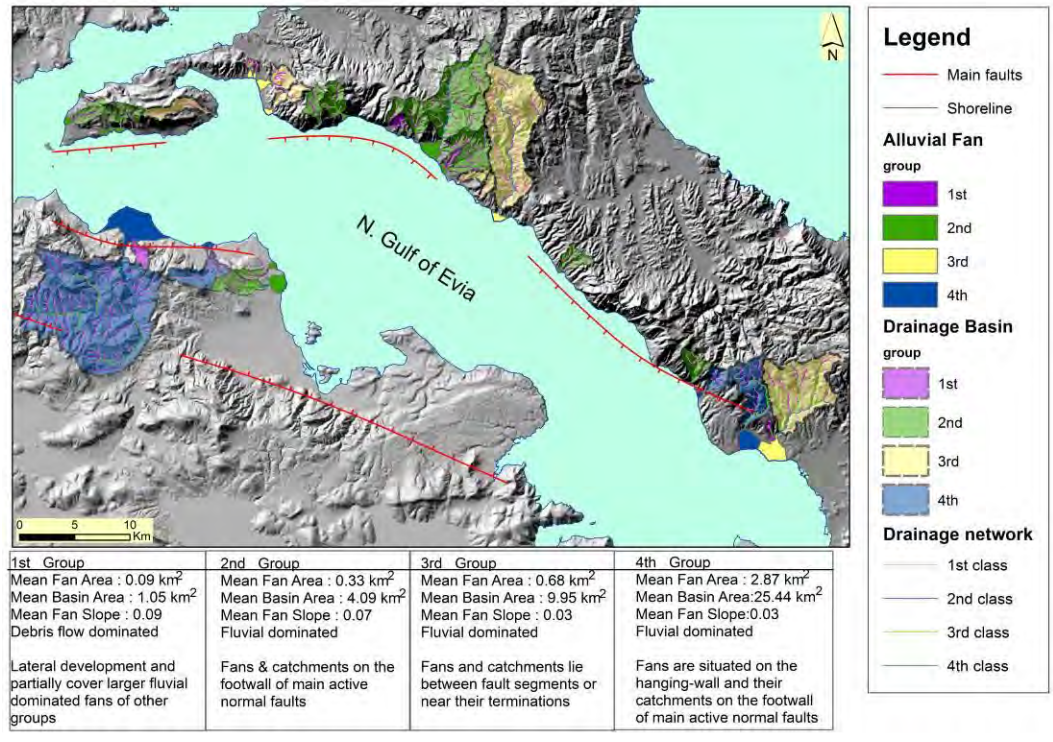

1st Group	2nd Group	3rd Group	4th Group
Mean Fan Area : 0.09 km^2 Mean Basin Area : 1.05 km^2 Mean Fan Slope : 0.09 Debris flow dominated Lateral development and partially cover larger fluvial dominated fans of other groups	Mean Fan Area : 0.33 km^2 Mean Basin Area : 4.09 km^2 Mean Fan Slope : 0.07 Fluvial dominated Fans & catchments on the footwall of main active normal faults	Mean Fan Area : 0.68 km^2 Mean Basin Area : 9.95 km^2 Mean Fan Slope : 0.03 Fluvial dominated Fans and catchments lie between fault segments or near their terminations	Mean Fan Area : 2.87 km^2 Mean Basin Area:25.44 km^2 Mean Fan Slope:0.03 Fluvial dominated Fans are situated on the hanging-wall and their catchments on the footwall of main active normal faults

Figure 2 – Hillshade map of the North Evoikos Gulf with the classification of fans and their corresponding catchments into four (4) groups according to the primary depositional processes and their position with respect to the local tectonic pattern. Comments on fan and basin characteristics as well as on their formation and their location are also shown.

Table 1 - Values of the morphometric parameters for the coastal fans and their drainage basins

	Name	A_b	P_b	L_c	ΣL_c	D_b	S_b	Cir_b	C_b	M	Ap_f	R_b	A_f	L_f	S_f	C_r
Group 1 (n=5)	7	0.2	2.2	0.70	4.6	3.68	0.49	0.52	380	0.28	20	360	0.01	108.5	0.129	2.50
	18	1.1	4.6	1.56	35.0	1.39	0.62	0.68	810	0.69	80	730	0.05	409.1	0.132	1.45
	25	0.8	4.2	1.50	8.3	2.00	0.22	0.53	280	0.28	40	240	0.12	508.8	0.055	1.33
	35	0.7	4.2	2.37	10.0	3.20	0.27	0.52	290	0.40	48	242	0.16	587.0	0.041	1.18
	41	2.5	7.1	4.29	50.9	1.75	0.42	0.61	630	0.36	60	570	0.10	313.0	0.077	0.71
Group 2 (n=22)	1	1.2	5.8	2.69	24.1	2.32	0.42	0.43	670	0.38	20	650	0.21	707.5	0.028	2.33
	2	3.1	8.6	6.56	39.3	2.13	0.25	0.52	670	0.15	19	651	0.39	709.2	0.027	0.73
	3	1.1	5.4	1.93	18.9	1.77	0.35	0.47	670	0.21	36	634	0.31	772.1	0.047	2.00
	4	1.0	4.7	1.52	19.4	1.49	0.38	0.58	580	0.31	41	539	0.14	472.4	0.087	1.28
	5	2.3	8.2	3.56	43.5	1.58	0.39	0.43	690	0.41	40	650	0.28	529.0	0.076	1.50
	6	0.3	2.6	0.93	6.6	3.10	0.44	0.55	410	0.14	24	386	0.03	233.6	0.103	1.18
	8	1.6	6.2	3.46	37.5	2.11	0.46	0.54	710	0.19	40	670	0.10	417.7	0.096	1.67
	15	4.1	10.5	6.99	75.4	1.69	0.36	0.48	890	0.32	60	830	0.06	469.3	0.128	1.61
	16	5.5	10.3	7.76	154.3	1.42	0.56	0.65	870	0.13	40	830	0.16	533.9	0.075	1.11
	17	2.2	7.1	3.24	61.5	1.50	0.57	0.54	970	0.92	36	934	0.11	423.2	0.085	1.00
	19	0.3	2.6	2.25	10.0	7.03	0.63	0.59	650	0.89	144	506	0.08	731.3	0.197	1.12
	20	0.3	2.7	1.97	9.9	5.97	0.60	0.56	630	0.30	100	530	0.05	551.3	0.181	0.92
	21	5.3	9.5	7.61	145.8	1.45	0.56	0.74	970	0.32	100	870	0.15	790.0	0.127	0.92
	22	32.3	27.9	58.55	664.0	1.81	0.41	0.52	930	0.35	56	874	1.77	2107.7	0.027	0.70
	23	3.3	8.8	7.77	70.8	2.35	0.43	0.54	850	0.43	62	788	0.39	1132.8	0.055	1.58
	24	0.4	2.8	0.84	3.8	2.40	0.22	0.58	210	0.64	26	184	0.15	603.6	0.043	1.17
	26	9.2	14.5	16.86	136.3	1.84	0.30	0.55	930	0.30	20	910	0.22	586.9	0.034	0.67
	30	2.0	6.8	3.98	44.4	1.96	0.44	0.55	350	0.60	20	330	0.09	533.1	0.038	1.86
	31	2.0	7.0	3.25	45.9	1.67	0.47	0.50	430	0.37	16	414	0.03	395.6	0.040	1.29
	32	4.3	9.5	7.01	116.3	1.63	0.54	0.59	1090	0.83	24	1066	0.02	272.9	0.088	2.00
	38	2.1	7.7	5.14	24.4	2.47	0.23	0.45	350	0.23	20	330	0.41	840.1	0.024	1.00
	37	6.2	13.3	11.02	70.4	1.79	0.23	0.44	440	0.16	39	401	2.03	1683.1	0.023	1.44
Group 3 (n=10)	9	5.7	15.4	8.39	88.2	1.46	0.31	0.31	740	0.53	20	720	0.08	547.8	0.037	0.67
	10	0.2	2.3	0.22	4.0	1.00	0.37	0.51	200	0.30	24	176	0.12	556.0	0.043	0.71
	11	0.7	3.5	4.99	12.7	7.13	0.36	0.70	230	0.24	28	202	0.33	1039.4	0.027	1.00
	12	0.2	1.7	1.23	2.8	7.69	0.35	0.66	110	0.22	22	88	0.17	839.8	0.026	1.75
	13	4.0	9.2	13.48	63.1	3.37	0.32	0.59	420	0.38	36	384	0.94	1538.7	0.023	1.77
	14	3.9	10.6	8.21	87.1	2.13	0.45	0.44	670	0.70	44	626	0.41	973.5	0.045	0.76
	27	2.2	7.6	2.54	35.9	1.16	0.33	0.47	470	0.43	24	446	0.13	463.3	0.052	1.40
	28	2.0	7.2	2.45	30.3	1.26	0.31	0.48	470	0.61	24	446	0.08	384.3	0.062	1.18
	29	48.5	36.9	81.13	888.2	1.67	0.37	0.45	930	0.52	16	914	0.79	1235.5	0.013	0.78
	36	32.2	30.4	55.04	450.0	1.71	0.28	0.44	830	0.30	36	794	3.78	2863.9	0.013	1.25
Group 4 (n=5)	33	4.0	8.8	7.91	108.5	1.96	0.54	0.66	850	0.23	40	810	0.28	639.1	0.063	2.33
	34	14.5	20.9	25.44	259.3	1.75	0.36	0.42	850	0.51	44	806	2.94	1881.1	0.023	1.20
	42	100.1	49.9	170.52	1661.4	1.70	0.33	0.51	930	0.09	64	866	10.62	4538.0	0.014	1.29
	40	7.4	14.0	6.88	116.6	0.47	0.32	0.47	650	0.22	40	610	0.38	1409.8	0.028	0.82
	39	1.2	6.4	2.77	14.9	2.27	0.24	0.37	390	0.33	28	362	0.14	675.7	0.041	0.56

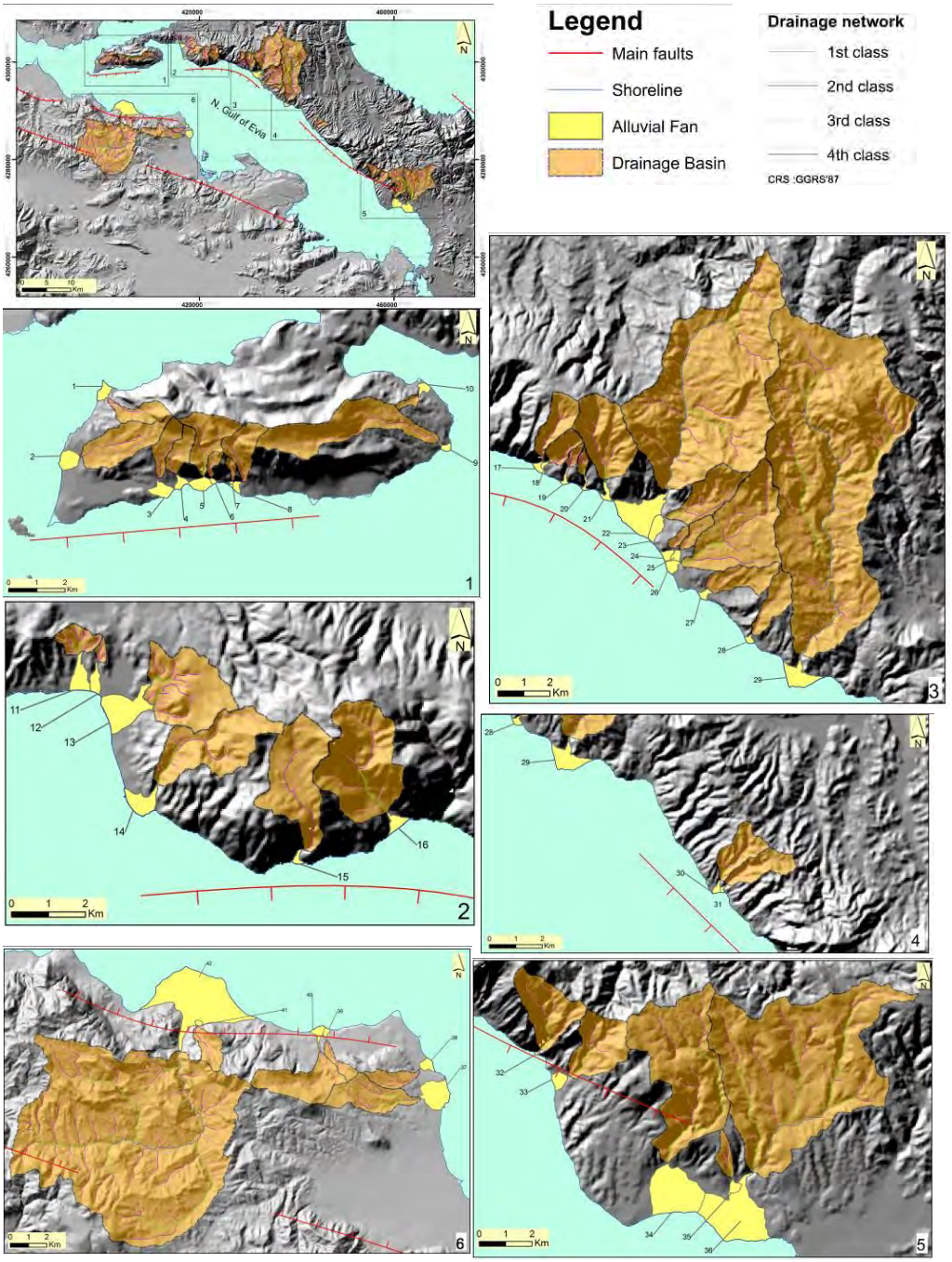

Figure 3– Hillshade map of the North Evoikos Gulf (Gulf of Evia) showing the main faults and the location of the studied fans and their catchments.

6. Alluvial Fan - Drainage Basin Morphometric Relationships

The study of the morphomerty of alluvial fans and drainage basins reveals information regarding fan evolution and the dynamics of hydrological processes responsible for fan formation (Harvey,

1997). The correlation between the geomorphic features of the studied fans and their drainage basins include the investigation of the relationship between basin area and fan delta area, as well as between basin area and fan delta slope.

6.1. Drainage Area (Ab) versus Fan Area (Af)

The most commonly compared feature of the alluvial fan and its drainage basin have been their respective areas. Bull (1962) was the first to recognize that as drainage basin area increases, the size of the alluvial fan increases. He quantified the relationship with a simple power function:

$$A_f = cA_b^k \qquad (1)$$

where A_f is alluvial fan area, A_d is drainage basin area and c is an empirical derived coefficient representing the area of an alluvial fan with a drainage basin area of 1.0. The exponent k is the slope of the regression line and measures the rate of change in fan area with increasing drainage basin area. Comparison of these two parameters offers the most interesting correlation for the total of the coastal fans of the study area. As drainage basin area is the most effective factor for the fan area, the comparison of coarse sediment supply is carried out by use of regression lines between drainage basin areas and fan areas. By representing this relation on a log–log plot (Figure 4a) it becomes clear that the data fit the following single exponential function:

$$A_f = 0.12A_b^{0.7} \qquad (1.1)$$

with a positive correlation coefficient of 0.89. The reason for this strong positive relation is that sediment discharge out of the catchment increases as drainage area increases. This shows that the size of the contributing basin is an important control on the availability of sediment for transport to the fan.

The coefficient c, which according to Harvey (1997) typically ranges from 0.1 to 2.2, has the value of 0.12 for the study area. The exponent k attains the value 0.7 and is in agreement with the aspect that the exponent varies from 0.7 to 1.1 (Harvey, 1997) and that it is generally less than 1.0 (Hooke and Rohrer, 1977). In the literature different values of the exponent k and the coefficient c for humid and sub-humid region fans have been reported (Crosta and Frattini, 2004). This variability has been attributed to different factors, such as climate conditions, tectonic setting, and relative erodibility of source area rock types. The variability of the exponent value for the four groups of fans reflects variations in tectonic setting.

The graph of basin area vs. fan area (Figure 4a) shows that while there is a general trend of increasing fan area with increasing basin area, as expected, there is wide variation in fan areas for given basin areas. The variation in fan area attributed to different tectonic setting is hypothesized to be one of the reasons why basin area alone is not a strong predictor of fan area. Another suggested reason is that the morphology of the fans is strongly affected locally by secondary processes (such as coastal erosion) which mobilize and modify sediments previously transported by primary processes.

6.2. Drainage Area (Ab) versus Fan Slope (Sf)

Another relationship that has been investigated in the literature is the one between the drainage basin area and the fan gradient (Hooke, 1968; Harvey et al., 1999).

$$S_f = cA_b^k \qquad (2)$$

The relation between these two parameters for the total number of the fans (Figure 4b) can also fit a potential type function of the following form:

$$S_f = 0.06A_b^{-0.23} \qquad (2.1)$$

The value of the exponent (-0.23) falls within the range of values determined for the majority of examples described by other authors (-0.35 to -0.15) (Harvey, 1997) while the coefficient (0.06) is

in the range of typically reported values (0.03-0.17). The reason for this correlation is that water discharge increases with drainage area resulting in higher flow velocities and bed shear stress. Thus the flow is capable of transporting on a lower slope the same material transported by smaller discharges on a higher slope. Variability among the values of exponent and coefficient for the fans of the four groups can be attributed to different tectonic settings of the fan-catchment systems.

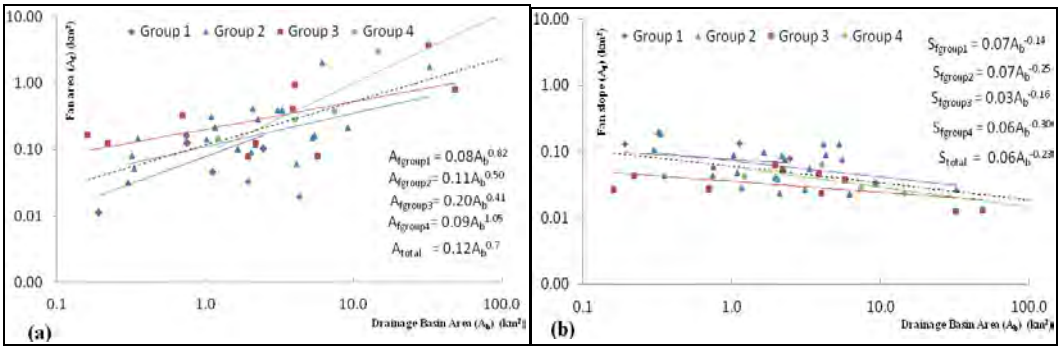

Figure 4 - (a) Drainage basin area vs. Fan area and (b) Drainage basin area vs. Fan slope log – log plots (dashed lines refer to total of the fans).

All the above mentioned relationships, for each group and for the total of fans, can be summarized in Table 2. Group 4 shows the best correlation coefficient for both functions (Drainage Basin area (A_b) vs Fan area (A_f) and Drainage Basin area (A_b) vs Fan slope (S_f)).

Table 2 - Summary of relationships' functions for each of the four fan groups

	Drainage Basin area vs Fan area (Af)	Drainage Basin area vs Fan slope (Sf)
Group 1	$A_f = 0.08A_b^{0.82}$	$S_f = 0.07A_b^{-0.14}$
Group 2	$A_f = 0.11A_b^{0.50}$	$S_f = 0.07A_b^{-0.25}$
Group 3	$A_f = 0.20A_b^{0.41}$	$S_f = 0.03A_b^{-0.16}$
Group 4	$A_f = 0.09A_b^{1.05}$	$S_f = 0.06A_b^{-0.30}$
Total	$A_f = 0.12A_b^{0.7}$	$S_f = 0.06A_b^{-0.23}$

7. Conclusions

This study deals with the identification and morphometric analysis of alluvial fans and their contributing catchments along the coast of North Evoikos Gulf. Qualitative and quantitative geomorphological observations led to an initial classification of the fans.

Four main fan types with distinct different morphological features, formed in different tectonic settings, were recognized. The first group includes small relatively steep fans likely affected by debris-flow processes. Fan-catchment systems of the second group are located on the footwalls of the main active normal faults and have generally small, short and steep feeder channels due to tectonic uplift. The fans of the third group are "open" with low gradient, and are fluvial-dominated with larger feeder channels. Both fans and corresponding catchments of this group lie between fault segments or near their terminations. Finally, the fourth group includes the more extensive,

gently sloping fluvial fans that have developed on the hanging walls of major faults formed by extensive basins which are located on the uplifting blocks.

A strong positive relationship between fan area and drainage basin area was identified for the combined group of fans of the study area. The exponential function for the fan area – basin area relationship showed that larger basins supply proportionally less sediment to coastal fans than the smaller ones. Although there is a general trend of increasing fan area with increasing basin area, there is wide variation in fan areas for given basin areas. One of the reasons why basin area alone is not a strong predictor of fan area is hypothesized to be the variations in fan area attributed to different tectonic settings.

8. Acknowledgments

We would like to thank Dr. A. Ganas and an anonymous reviewer for their comments and corrections that significantly improved the paper.

9. References

Blair T.C. and McPherson J.G. 1994. Alluvial fan processes and forms, in: Abrahams A. D. and Parsons A.J., eds., *Geomorphology of Desert Environments*. London: Chapman & Hall, 354-402.

Bull W.B. 1962. Relations of alluvial fan size and slope to drainage basin size and lithology in western Fresno County,CA., *U.S. Geological Survey Professional Paper*.

Clarke P.J., Davies R.R., England P.C., Parsons B., Billiris H., Paradissis D., Veis G., Cross P.A., Denys P.H., Ashkenazi V., Bingley R., Kahle H.G., Muller M.V. and Briole P. 1998. Crustal strain in central Greece from repeated GPS measurements in the interval 1989-1997, *Geophysical Journal International*, 135, 195-214.

Crosta G. and Frattini P. 2004. Controls on modern alluvial fan processes in the central Alps, Northern Italy, *Earth Surface Processes and Landforms*, 29, 267-293.

Cundy A. B., Gaki-Papanastassiou K., Papanastassiou D., Maroukian H., Frogley M. R., and Cane T. 2010. Geological and geomorphological evidence of recent coastal uplift along a major Hellenic normal fault system (the Kamena Vourla fault zone, NW Evoikos Gulf, Greece), *Marine Geology*, 271, 156-164.

Cundy A.B., Kortekkas S., Dewez T., Stewart I., Crousace W., Maroukian H., Papanastassiou D., Gaki-Papanastassiou P., Pavlopoulos K. and Dawson A. 2000. Coastal impacts of the 1894 Gulf of Atalanti earthquakes, Cental Greece, *Marine Geology*, 170, 3-26.

Gaki-Papanastassiou K., Maroukian H., Papanastassiou D. and Palyvos N. 1999. Archaeogeology and morphotectonics of the area of Livanates-Kynos-Arkitsa during the Holocene. *5th Greek Geographical Congress*, Athens 11-13 November, 1999, 101-111.

Ganas A. and White K. 1996. Neotectonic fault segments and footwall geomorphology in the Eastern Central Greece from Landsat TM data. *Geological Society Greece Sp. Pub.*, 6, 169-175.

Ganas A. and Papoulia I. 2000. High-resolution, Digital Mapping of the Seismic Hazard within the Gulf of Evia Rift, Central Greece Using Normal Fault Segments as Line Sources, *Natural Hazards,* 22 (3), 203-223.

Goldsworthy M., Jackson J. and Haines J. 2002. The continuity of active fault systems in Greece, *Geophysical Journal International*, 148(3), 596-618.

Goldsworthy M. and Jackson J. 2001. Migration of activity within normal fault systems: examples from the Quaternary of mainland Greece, *Journal of Structural Geology*, 23, 489-506.

Harvey A. M., Silva P.G., Mather A. E., Goy J. L., Stokes M. and Zazo C. 1999. The impact of Quaternary sea-level and climate change on coastal alluvial fans in the Cabo de Gata ranges, southeast Spain, *Geomorphology*, 28, 1-22.

Harvey A. M. 1997. The role of alluvial fans in arid zone fluvial systems. In: Thomas D.S.G. (eds.), *Arid Zone Geomorphology: Process, Form and Change in Dry lands*, John Wiley and Sons Limited, Chichester, 231-259

Hooke R. L. and Rohrer W. L.1977. Relative erodibility of source area rock types from second order variation in alluvial fan size. *Geological Society of America Bulletin*, 88, 1177-1182.

Hooke R. L. B. 1968. Steady-state relationships on arid region alluvial fans in closed basins, *American Journal of Science*, 266, 609-629.

IGME, 2010. *Hydrolithological map, scale 1:200,000*, Project "Definition and assessment of hydrogeological characteristics of aquifer systems of Greece, Water district of E. Central Greece", IGME, Division of water resources and environment, Department of Hydrogeology, Compilation by Dandolos, E., Zorapas, V.

Karymbalis E., Giles P., Ferentinou M. and Gaki-Papanastassiou K.. 2012. Analysis of relationships among morphometric parameters of coastal alluvial fans and source basins in North Peloponnese, Greece. *Proceedings of the 16th Joint Geomorphological Meeting (Rome)*, 91-94.

Karymbalis E.,Gaki-Papanastassiou,K. and Ferentinou M. 2010. Fan deltas classification coupling morphometric analysis and artificial neural networks : The case of NW coast of Gulf of Corinth, Greece, *Hellenic Journal of Geosciences*, 45, 133-146.

Karymbalis E. 2007. Fan Deltas Geomorphology in the Northern Coast of Gulf of Corinth, Greece, *Proceeding of the Eighth International Conference on the Mediterranean Coastal Environment, MEDCOAST 07*, Alexandria, Egypt, 13-17 November 2007, 1321-1332

Leeder M. and Jackson J. 1993. The interaction between normal faulting and drainage in active extensional basins, with examples from the western United States and central Greece, *Basin Research*, 5, 79-102.

Palyvos N., Bantekas I. and Kranis H. 2006. Transverse fault zones of subtle geomorphic signature in northern Evia island (central Greece extensional province) : An introduction to the Quaternary Nileas graben. *Geomorphology*, 76, 363-374.

Pantosti, D.,De Martini P.M.,Papanastassiou D.,Lemeille F.,Palyvos N., and Stavrakakis G. 2004. Paleoseismological trenching across the Atalanti fault (Central Greece): Evidence for the ancestors of the 1894 earthquake during the middle ages and Roman times, *Bull. Seism. Soc. Am.,* 94, 531-549.

Papanastassiou D. Stavrakakis G. and Makaris D. 2001. Recent micro-earthquake activity at Northern Evoikos Gulf, Central Greece. *Bulletin of the Geological Society of Greece, Proceedings of the 9th Inernational Congress,* Athens, XXXIV/4, 1567-2572.

Papoulia J.,Makris J. and Drakopoulou V.2006. Local seismic array observations at north Evoikos, central Greece, delineate crustal deformation between the North Aegean Trough and Corinthiakos Rift, *Tectonophys*. 423, 97-106.

Pavlides S.B., Valkaniotis S., Ganas A., Keramydas D. and Sboras S. 2004. The Atalanti active fault: Re-evaluation using new geological data, *Bulletin of the Geological Society of Greece, Proceedings of the 10th Inernational Congress,* Thessaloniki, XXXVI/4, 1560-1567.

Roberts S. and Jackson J. 1991. Active normal faulting in central Greece: an overview. In: A. M. Roberts, G. Yielding and B. Freeman (eds.). *The Geometry of Normal Faults*. London: *Geological Society* Spec. Pub.56.

Rozos D., Skilodimou H. D., Loupasakis C. and Bathrellos G. D. 2013. Application of the revised universal soil loss equation model on landslide prevention. An example from N. Euboea (Evia) Island, Greece, *Environmental Earth Sciences*.

Stiros S. C., Arnold M., Pirazzoli P. A., Laborel F. and Papageorgiou S., 1992. Historical coseismic uplift on Euboea island, Greece, *Earth and Planetary Science Letters,* 108, 109-117.

Δελτίο της Ελληνικής Γεωλογικής Εταιρίας, τομ. XLVII , 2013
Πρακτικά 13ου Διεθνούς Συνεδρίου, Χανιά, Σεπτ. 2013

Bulletin of the Geological Society of Greece, vol. XLVII 2013
Proceedings of the 13th International Congress, Chania, Sept. 2013

MULTI-STAGE HISTORY OF COMPOUND MANTLE XENOLITHS FROM WESTERN USA: IMPLICATIONS FOR METASOMATIC PROCESSES IN THE DEEP MANTLE

Baziotis I.[1,2], Asimow P.D.[3], Koroneos A.[1], Poli G.[2] and Ntaflos T.[4]

[1] Department of Mineralogy, Petrology and Economic Geology, Aristotle University of Thessaloniki, 54124, Thessaloniki, Greece, ibaziotis@geo.auth.gr

[2] Department of Earth Sciences, University of Perugia, 06100, Perugia, Italy

[3] California Institute of Technology, Division of Geological and Planetary Sciences, Pasadena, California, USA

[4] Department of Lithospheric Research, University of Vienna, 1090, Vienna, Austria

Abstract

The compound mantle xenoliths from Cima Volcanic Field and Chino Valley (Western U.S.A.) represent outstanding candidates to illustrate the processes that occur prior to their delivery to the surface by alkali-basaltic volcanism. The xenoliths share characteristics like pyroxene zonation, amphibole breakdown and formation of glass and armalcolite. Their petrogenetic evolution involved partial melting of the silicate minerals, infiltration of reactive melts and dissociation of minerals en route to the surface, suggesting that these rocks followed multi-stage histories that initiated deep in the mantle (>1.0 GPa) and proceeded during a very short period of time.
Key words: *lherzolite; partial melting; mantle metasomatism.*

Περίληψη

Στην παρούσα εργασία μελετήθηκαν σύνθετοι μανδυακοί ξενόλιθοι από τις περιοχές Cima Volcanic Field και Chino Valley, (Δυτικές Η.Π.Α.). Αποτελούν τα ιδανικά πετρώματα που μπορούν να εκφράσουν τις διεργασίες πριν την επιστροφή στην επιφάνεια κατά τη διάρκεια της αλκαλο-βασαλτικής ηφαιστειότητας. Αυτοί οι μανδυακοί ξενόλιθοι περιλαμβάνουν χαρακτηριστικά όπως η ζώνωση των πυροξένων, η διάσπαση της αμφιβόλου και ο σχηματισμός γυαλιού και αρμαλκολίτη. Η πετρογενετική εξέλιξη των ξενολίθων περιλαμβανει τη μερική τήξη των πυριτικών ορυκτών, φιλτράρισμα τηγμάτων και διάσπαση της αμφιβόλου κατά την επιστροφή τους προς την επιφάνεια. Τα προηγούμενα δείχνουν ότι οι μανδυακοί ξενόλιθοι ακολούθησαν πολύπλοκη ιστορία η οποία ξεκίνησε σε μεγάλο βάθος κι έλαβε χώρα σε πολύ σύντομο χρονικό διάστημα.
Λέξεις κλειδιά: *λερζόλιθος, μερική τήξη, μετασωμάτωση μανδύα.*

1. Introduction

The mantle is the major geochemical reservoir of most rock-forming elements in the Earth. Convection and plate-tectonic driven processes act to generate local and regional heterogeneity

within the mantle, which in turn through thermal and chemical interactions modulates ongoing geophysical processes; this feedback shapes the dynamics of the deep interior. Consequently, these processes contribute to the evolution of the Earth throughout its geological history.

Up to now, the heterogeneity of the mantle has been extensively studied in terms of conventional methods using basalt chemistry, bulk rock analysis of isolated xenolith specimens of varying lithology, and massif exposures. In the current study we focus on multi-layered xenoliths. In particular we choose lherzolites with amphibole-rich veins and lherzolites with websterite/clinopyroxenite contacts. The mineral assemblages of such layers carry information about partial melting and mantle metasomatism. Our major goal is to identify the signatures that were recorded during the ascent of these mantle xenoliths toward the surface in their alkali basalt host liquids. After that, we hope be able to unravel the principal processes that, earlier in the evolution of these samples, controlled the formation of the different layers of the mantle xenoliths.

2. Sampling Areas - Description

2.1. Geological Setting

For the purpose of the current study we used selected compound xenoliths from Cima Volcanic Field and Chino Valley (Fig. 1). The Cima Volcanic Field represents an isolated late Cenozoic basaltic field, part of the southern Basin and Range province, and is located in the Mojave Desert, southeastern California, USA. Chino Valley is in central Arizona, just off the southwestern edge of the Colorado Plateau occur within the Transition Zone which has a variable width (60 to 100 km). The tectonic framework of the area is characterized by extension of the Basin and Range crust related with Cordilleran metamorphic core complexes and synchronous felsic volcanism. The volcanic fields in Arizona share five petrologic types: a) lamprophyres, b) latites, c) basalt-dominated fields, d) basalt-rhyolite fields and andesite-rhyolite-dominated fields (Nealey and Sheridan, 1989).

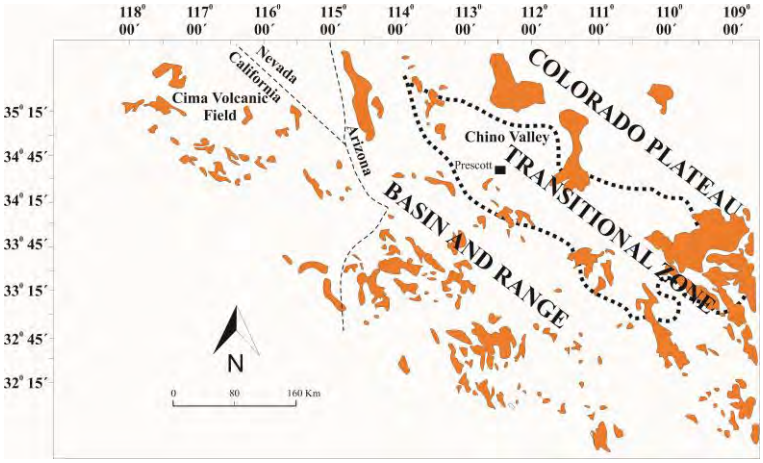

Figure 1 – Simplified map showing the locations of Cenozoic volcanics (in orange) that host the mantle xenoliths used in this study (Cima Volcanic Field and Chino Valley). (Map modified after Reynolds, 1988 and Farmer *et al.*, 1995).

2.2. Mantle Xenoliths

The composite xenoliths occur within Cenozoic volcanics rocks. The Cima Volcanic Field, provides samples with contacts among different lithologies. Such diverse lithologies represented by Cr-diopside spinel peridotite, websterite, gabbro, clinopyroxenite and wehrlite, commonly occur in alkali basaltic lavas (Irving, 1980; Wilshire *et al.*, 1991). The Chino Valley xenoliths include lithologies like garnet websterites, phlogopite-bearing websterite and garnet-amphibole

rocks but the predominant type is garnet clinopyroxenite (Schulze *et al*., 1978; Wilshire *et al*., 1991). All the samples are from the Howard Wilshire collection archived at the Smithsonian Institution, Washington DC, USA. The criteria for the selection of these compound xenoliths were freshness and integrity of specimens, maximum distance on both sides of lithologic contacts, and rock types thought most likely to represent subsolidus juxtaposition of different lithologies that later partially melted in contact.

3. Analytical Methods

Major element compositions of minerals were determined in polished thin sections using a CAMECA SX 100 electron microprobe equipped with four wavelength-dispersive spectrometers (WDS) and one energy-dispersive spectrometer (EDS) at the University of Vienna, Department of Lithospheric Research (Austria). Operating conditions were accelerating voltage 15 kV. For minerals, a 20 nA beam current and 20 s counting time on peak position were used. For glass analyses, a slightly defocused beam with 5 μm diameter and 10 s counting time were used. Natural mineral used as standards as follows: albite (Na, Si, Al), wollastonite (Ca), olivine (Mg), almandine (Fe), spessartine (Mn), orthoclase (K), rutile (Ti), chromite (Cr) and Ni-oxide (Ni). Representative mineral compositions are given in Table 1.

Table 1- Representative mineral compositions from the studied mantle xenoliths.

Sample	**Ci-1-254**									**Ci-1-546**		
Mineral	**Ol^c**	**Ol^r**	**Cpx-1**	**Cpx-2**	**Opx**	**Amp**	**Spl-1**	**Spl-2**	**Pl**	**Gl-1**	**Gl-2**	**Arm**
SiO_2	40.5	40.7	52.0	47.0	55.3	42.1	0.06	0.06	56.3	59.1	56.7	0.14
TiO_2	-	-	0.31	2.21	0.09	2.12	0.11	0.73	0.29	3.09	2.73	72.3
Al_2O_3	0.04	0.73	5.05	8.87	3.75	14.8	55.1	49.1	26.7	17.3	18.5	1.84
Cr_2O_3	-	0.05	0.67	1.23	0.35	1.29	12.4	16.8	-	0.01	0.02	2.68
NiO	0.43	0.31	0.08	0.07	0.13	-	0.41	0.39	-	-	-	-
FeO	10.1	9.57	3.02	2.75	6.59	4.20	11.5	12.7	0.42	2.70	3.72	9.71
MnO	0.14	0.15	0.08	0.04	0.15	0.06	0.08	0.12	0.01	0.04	0.04	0.04
MgO	48.6	47.9	16.2	14.2	33.0	16.9	20.6	19.9	0.17	2.68	4.00	12.1
CaO	0.08	0.25	21.9	22.9	0.84	11.5	0.03	0.04	9.61	3.92	7.94	0.16
Na_2O	-	-	0.76	0.46	0.04	2.81	-	-	5.50	3.64	3.84	-
K_2O	-	-	-	-	0.01	1.17	-	-	0.53	4.43	1.31	0.11
ZnO	-	-	-	-	-	-	0.12	0.09	-	-	-	-
Total	99.9	99.7	100.1	99.7	100.3	96.9	100.3	99.9	99.5	97.0	98.9	99.1

c: core; r: rim. Mineral abbreviations: Ol: olivine, Cpx: clinopyroxene, Opx: orthopyroxene, Amp: amphibole, Spl: spinel, Pl: plagioclase, Gl: glass, Arm: armalcolite.

4. Petrography

4.1. Cima Volcanic Field

4.1.1. Sample Ci-1-254

Mantle xenolith is in contact with the host basalt. The compound xenolith consists of two predominant layers: websterite and lherzolite, characterized as coarse-grained and porphyroclastic, respectively (Mercier and Nicolas, 1975). Discrete veins penetrate the lherzolite layer, probably originated from the host basalt. On the other hand, the websterite shows recrystallization features

at the contact with the host basalt (Fig. 2a). The lherzolite is amphibole-bearing; infiltrated melts crystallized Ti-rich pargasite (Table 1) showing no reaction relation with peridotite minerals (see Wilshire *et al*., 1991). However, the amphibole is decomposed, probably due to rapid decompression melting en route to the surface. Olivine grain size in the lherzolites is smaller than orthopyroxene grain size in the websterite layer.

4.1.2. Sample Ci-1-546:

Mantle xenolith is in contact with the host basalt (Fig. 2b). The compound xenolith consists of alternating layers of porphyroclastic clinopyroxenite (2 layers), coarse-grained lherzolite (4 layers) and orthopyroxenite (1 layer). The majority of the amphiboles are located within lherzolite (near the host basalt) and the adjacent clinopyroxenite layer. Lherzolites host large olivine crystals whereas the clinopyroxenite contains small crystals with a well-developed preferred orientation.

4.2. Chino Valley

4.2.1. Sample PN-1-14:

Mantle xenolith with a distinct crude central cumulate-like layer characterized by coarse dark clinopyroxene (>85 vol. %) with a size >0.5 mm (Fig. 2c). Clinopyroxene exhibits a spongy texture, enclosing and surrounded by tiny Fe-Ti oxides. Fe-Ca-Ti oxides (mainly ilmenite and titanite) were observed as discrete grains in the matrix as well. The clinopyroxene-ilmenite assemblage shows a moderately-developed preferred orientation. The contact is clear, although gradational (decreasing grain size), on both sides of the clinopyroxene-rich layer.

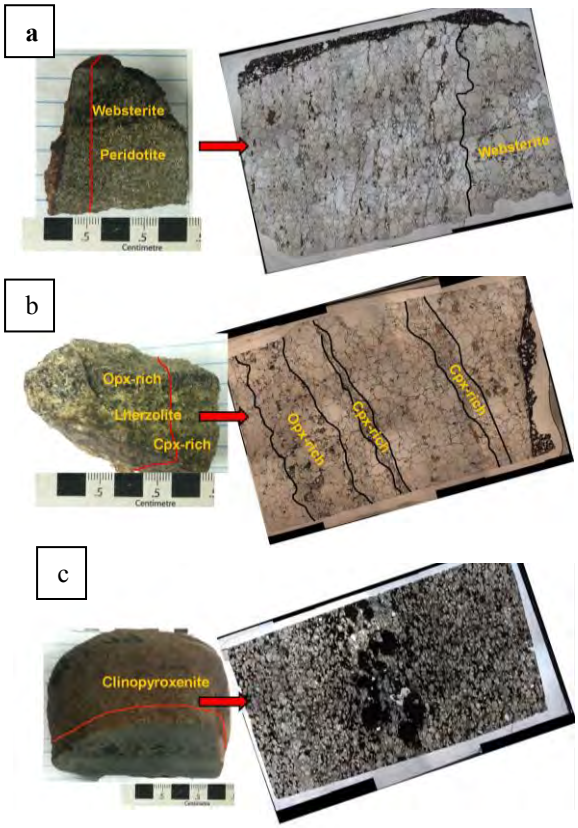

Figure 2 – Images of samples a) Ci-1-254, b) Ci-1-546 from Cima Volcanic Field and c) Pn-1-14 from Chino Valley. a,b) xenoliths with a multi-layered structure and c) cumulate rock with abundant clinopyroxene and widespread ilmenite-rutile grains.

5. Results and Discussion

In a websterite layer from the composite xenolith Ci-1-254 of Cima Volcanic Field, primary clinopyroxene is overgrown by secondary one. Secondary clinopyroxene is enriched in Al_2O_3, CaO, Cr_2O_3 and TiO_2, and depleted in SiO_2, Na_2O, FeO and MgO compared to the primary clinopyroxene (Table 1). The adjacent amphibole corresponds to a Ti-rich pargasite (Table 1). Between secondary clinopyroxene and amphibole, a 30 µm wide zone occurs with neo-formation of orthopyroxene, spinel (Spl-2), olivine (Ol-2), glass and armalcolite (Fig. 3). The presence of secondary clinopyroxene along with the reaction zone probably signifies two contemporaneous events. The first event is characterized by penetration of Ca and Ti-rich melt (inferred from glass-1 composition; see Table 1) and the second is associated with the decomposition of the amphibole. During the same event, the primary clinopyroxene (Cpx-1) reacts with the infiltrated melt forming the secondary clinopyroxene (Cpx-2). Alternatively, the second clinopyroxene elemental inhomogeneity could be related with rapid crystallization. This process displaces the system toward more calcic-aluminous-titaniferous compositions. At the same time, the amphibole breakdown is facilitated by the presence of the remnant melt (Fig. 3a). The breakdown zone occurs nearly at the same time with the clinopyroxene suggested by the inclusions of spinel (Spl-2) and glass at the rim of the Cpx-2 (Fig. 3c). These phenomena occur during decompression, and at relative fast rates, otherwise crystallization at depth would prefer the formation of larger crystals and absence of glass.

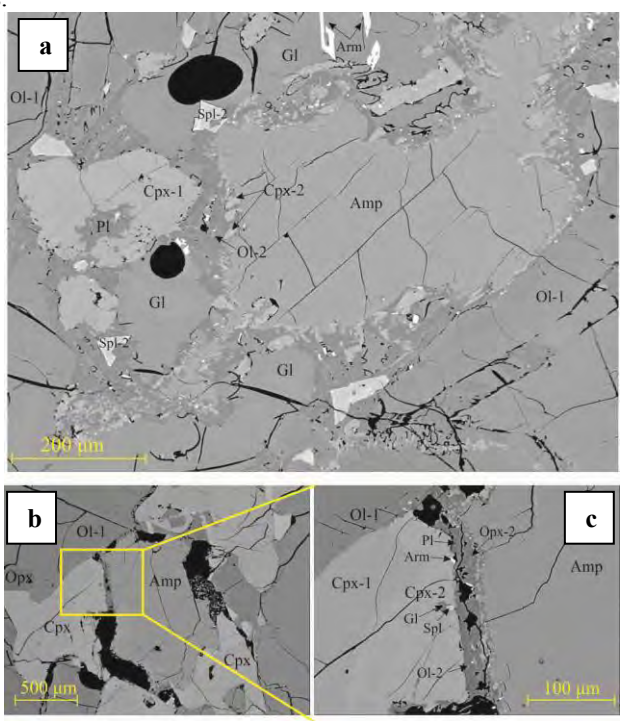

Figure 3 – a) Amphibole surrounded by small idiomorphic clinopyroxene (Cpx-2), olivine (Ol-2) and spinel (Spl-2) crystals and plagioclase in a matrix composed by olivine (Ol-1) and clinopyroxene (Cpx-1). Glass occurs as interstitial patches developed at the expense of amphibole. It is characterized by the presence of armalcolite as well, b, c) amphibole (Amp), clinopyroxene and olivine (Ol-1) in contact within a websterite layer. Ca-Tschermak rich clinopyroxene (Cpx-2) overgrown on diopside-rich (Cpx-1), c) decomposition of amphibole showing a 30 µm wide zone composed by clinopyroxene (Cpx-2), olivine (Ol-2), orthopyroxene (Opx-2) and plagioclase (Pl). Glass and small quench spinel (Spl) crystal are enclosed at the Cpx-2, probably during the simultaneous processes of amphibole breakdown and infiltration of a melt. a-c: backscatter electron (BSE) images.

In another composite xenolith (sample Ci-1-546) from the Cima Volcanic Field, the amphibole-bearing lherzolite has Ti-rich pargasite that is surrounded by glass-1, spinel, plagioclase, clinopyroxene, olivine and armalcolite (Fig. 3a, 4a). The latter is entrained within the glass pocket and has a skeletal crystal shape suggesting rapid growth at high pressures (>1.0 GPa but most probably at ~1.3 GPa due to Cr-Al content; see Friel *et al*., 1977 and Grègoire *et al*., 2000) and low oxygen fugacity at mantle depths (e.g., Medvedev, 1996). The presence of glass-1 is associated with rapid melting (e.g., Francis, 1991) and breakdown of pargasite to Ol+Cpx+Spl+Gl-1) en route to the surface. Isolated glass-2 is observed, interstitially along grain boundaries of pyroxenes and olivine; it is depleted in Si, Ti, K and enriched in Ca, Mg, Al compared to glass-1 (Fig. 4; Table 1).

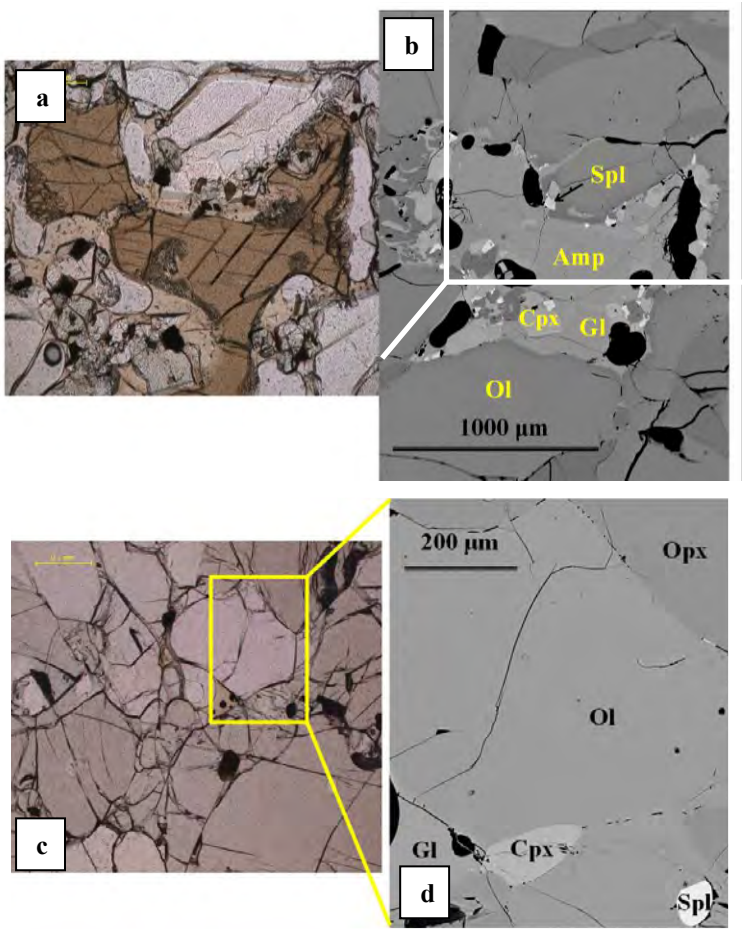

Figure 4 – a, b) Amphibole (Amp) surrounded by small idiomorphic spinels (Spl), clinopyroxene (Cpx) and glass (Gl). Note empty cavities associated with volatile escape. The presence of glass surrounding amphibole suggests rapid decompression melting of the amphibole en route to the surface and c, d) formation of glass interstitial between olivine Ol), clinopyroxene (Cpx) and orthopyroxene (Opx). Orthopyroxene contain brown idiomorphic spinel inclusions. a, c: photomicrographs PPL; b, d: BSE images.

Fe-Ti minerals identified in the selected xenoliths include armalcolite and ilmenite (Fig. 5). In the Chino Valley clinopyroxenite (Pn-1-14), Nb-rich and Nb-free rutile both occur as inclusions in titanite (Fig. 5a, b). Commonly rutile is replaced by ilmenite and less commonly by armalcolite (Fig. 5a, b, d). Thus textural relationships suggest that rutile may represent a primary mineral in

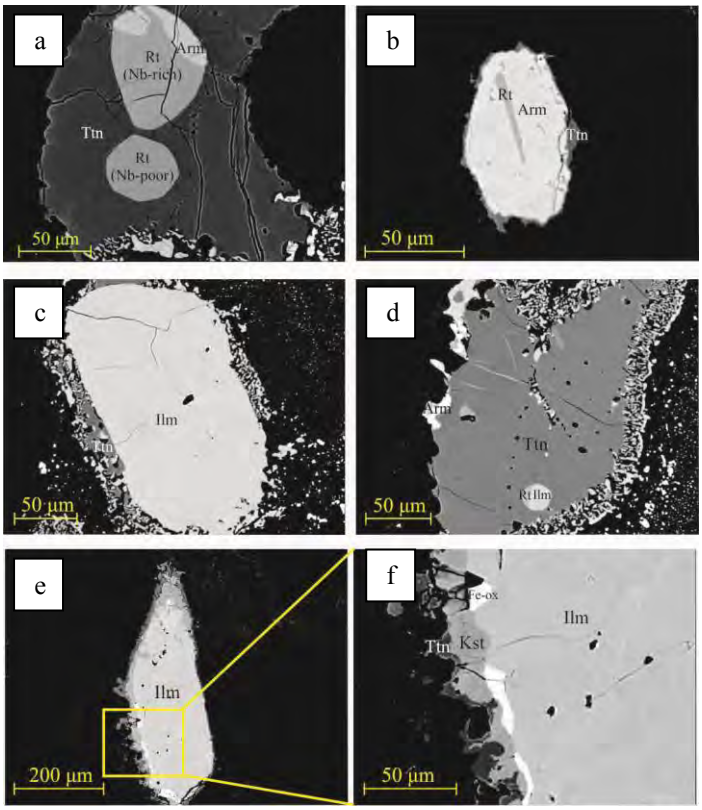

Figure 5 – a) Two rutile (Rt) grains (Nb-rich and Nb-free) occur as inclusions in titanite (Ttn). Nb-rich rutile is partly replaced by armalcolite (Arm), b) rutile lamellae within armalcolite; the latter is being replaced by titanite, c, d, e) sieved-texture around ilmenite (Ilm; c, e) and titanite (d). Titanite has rounded inclusion composed by rutile and ilmenite with straight contact, f) ilmenite mantled by kassite (Kst; a very rare Ca-Ti hydrous oxide) and Fe-oxide (Fe-Ox) and then by titanite. a-f: BSE images.

the Chino Valley clinopyroxenite. Alternatively, rutile could be the product after armalcolite breakdown as previously suggested by Lindsley *et al*. (1974). Moreover, ilmenite is mantled by Fe-oxide + kassite (a rare hydrous Ca-Ti oxide) and then by titanite (Fig. 5f). These mineral assemblages imply a change from Fe-Ti to Ca-rich silicate metasomatic agents percolating through the host rock. Further, such Ti-enriched mineral assemblages, indicated by the specific enrichment in high-field strength elements (HFSE; e.g., Nb) have been extensively studied in harzburgitic xenoliths from Kerguelen Islands by Grègoire *et al*. (2000). The authors suggest that exchange reactions of a parental melt with the peridotite wall-rock are essential steps in the formation of armalcolite.

There has been an increasing scientific interest on the origin and transport of the volatiles in the upper mantle. Though, several amphibole-bearing xenoliths found in alkali-basaltic rocks from worldwide occurrences have been extensively studied (Hawaii, USA, Mason, 1968; Massif central, France, Brown *et al*., 1980; Engaruka, Tanzania, Dawson and Smith, 1982). On these studies, pargasites and titaniferous pargasites occurring in Cr-diopside represent upper mantle products. Also, study of interstitial glass in amphibole-bearing spinel-wehrlite xenoliths from Foster Crater in Antarctica suggested that it originated elsewhere in the upper mantle and not by in-situ melting (Gamble and Kyle, 1987). Gamble and Kyle (1987) based this conclusion on textural similarities of glass in association with olivine and clinopyroxene micro-phenocrysts and on the liquidus phases of the glasses enclosed by amphibole crystals. Recently, Harvey *et al*.

(2012) using major and trace element analyses suggest that interstitial glass from Kilbourne Hole peridotite xenoliths provide clues for a single metasomatic event. Moreover, the presence of sub-micron grain boundary phases like ilmenite, rutile, armalcolite from the same rocks, suggest another metasomatic event operated at HP conditions. In our study, glasses occur in different textural associations (isolated intergranular to clinopyroxene and olivine or as surrounding products of amphibole) and have large variance in their chemistry, supporting an origin through in-situ melting. External fluids/melts play an important role in enrichment of alkalis (e.g., K_2O; as observed in glass-1) in these mantle rocks. Metasomatic agents that can flux in-situ partial melting include carbonatites, Na-alkali and K-alkali silicate (Coltorti *et al*., 1999, 2000). Using the Ti, K, Ca and Na content of our glasses we infer from the TiO_2+K_2O vs. CaO+Na_2O diagram of Coltorti *et al*. (2000) that the metasomatizing agents had carbonatitic and Na-alkalic affinities. Finally, our samples suggest extended multi-stage histories involving partial melting to form primary minerals, a period of metasomatic alteration, and a short timescale of decompression upon eruption.

6. Conclusions

Mineralogical, textural and compositional characteristics of the assemblages observed within the mantle xenoliths from Cima Volcanic Field and Chino Valley reveal a continuous frame of metasomatic processes. In particular, a switch in metasomatism from Fe-Ti to Ca-rich silicate melt is evidenced by the presence of Fe-Ti oxides (ilmenite, armalcolite) overgrown by Ca-silicate mineral (titanite, kassite) rims. Further, rapidly quenched crystals (e.g., spinel), glass and armalcolite formation indicate a very short-timescale of reactions en route to the surface. The mantle xenoliths infiltrated by alkali-basaltic melts interacted with the peridotite-wall rock increasing the HFSE budget of the minerals (presence of Nb-rich and Nb-poor rutile).

7. Acknowledgments

We gratefully acknowledge our sincere thanks to Prof. E.Manoutsoglou for his outstanding efforts on editorial handling and two anonymous reviewers for their suggestions. The research project was funded for I.B. and is implemented within the framework of the Action «Supporting Postdoctoral Researchers» of the Operational Program "Education and Lifelong Learning" (Action's Beneficiary: General Secretariat for Research and Technology), and is co-financed by the European Social Fund (ESF) and the Greek State.

8. References

Brown G.M., Pinsent R.H. and Coisy P. 1980. The petrology of spinel-peridotite xenoliths from the Massif Central, France, *Am. J. Sci.*, 280-A, 471-498.

Coltorti M., Bonadiman C., Hinton R.W., Siena F. and Upton B.G.J. 1999. Carbonatite metasomatism of the oceanic upper mantle: evidence from clinopyroxenes and glasses in ultramafic xenoliths of Grande Comore, Indian Ocean, *J. Petrol.*, 40, 133-165.

Coltorti M., Beccaluva L., Bonadiman C., Salvini L. and Siena F. 2000. Glasses in mantle xenoliths as geochemical indicators of metasomatic agents, *EPSL*, 183, 303-320.

Dawson J.B.and Smith J.V. 1982. Upper-mantle amphiboles: a review, *Min. Mag.*, 45, 35-46.

Farmer G.L., Glazner A.F., Wilshire H.G., Wooden J.L., Pickthom W.J .and Katz M. 1995. Origin of late Cenozoic basalts at the Cima volcanic field, Mojave Desert, California, *J. Geophys. Res.*, 100, 8399-8415.

Francis D. 1991. Some implications of xenolith glasses for the mantle sources of alkaline mafic magmas, *Con. Min. Pet.*, 108, 175-180.

Friel J.J., Harker R.I. and Ulmer G. 1977. Armalcolite stability as a function of pressure and oxygen fugacity, *Geochim. Cosm. Acta*, 41, 403-410.

Gamble J.A. and Kyle P.R. 1987. The origins of glass and amphibole in spinel-wehrlite xenoliths from Foster Crater, McMurdo Volcanic Group, Antarctica, *J. Petrol.*, 28, 755-779.

Grègoire M., Lorand J.P., O`Reilly S.Y. and Cottin J.Y. 2000. Armalcolite-bearing, Ti-rich metasomatic assemblages in harzburgitic xenoliths from the Kerguelen Islands: Implications for the oceanic mantle budget of high-field strength elements, *Geochim. Cosm. Acta*, 64, 673-694.

Harvey J., Yoshikawa M., Hammond S.J. and Burton K.W. 2012. Deciphering the trace element characteristics in Kilbourne Hole peridotite xenoliths: Melt-rock interaction and metasomatism beneath the Rio Grande Rift, SW USA, *J. Petrol.*, doi: 10.1093/petrology/egs030.

Irving A.J. 1980. Petrology and Geochemistry of Composite Ultramafic Xenoliths in Alkalic Basalts and Implications for Magmatic Processes within the Mantle, *Am. J. Sci.*, 280, 389-426.

Lindsley D.H., Kesson S.E., Hartzman M.J.and Cushman M.K. 1974. The stability of armalcolite: Experimental studies in the system MgO-Fe-Ti-O, *Proc. 5th Lunar Conf.* (supplement 5, *Geochim. Cosm. Acta*), 1, 521-534.

Mason B. 1968. Kaersutite from San Carlos, Arizona, with comments on the paragenesis of this mineral, *Min. Mag.*, 36, 997-1002.

Medvedev A.Ya. 1996. Synthetic armalcolite and pseudobrookite, *Min. Mag.*, 60, 347-353.

Mercier J-C.C. and Nicolas A. 1975. Textures and fabrics of upper-mantle peridotites as illustrated by xenoliths from basalts, *J. Petrol.*, 16, 454-487.

Nealey L.D. and Sheridan M.F. 1989. Post-Laramide volcanic rocks of Arizona and northern Sonora, Mexico, and their inclusions, in Jenney, J.P., Reynolds, S.J., (eds). Geologic Evolution of Arizona: Tuscon, *Arizona Geological Society Digest*, 17, 609-647.

Reynolds S.J. 1988. *Geologic map of Arizona*: Arizona Geological Survey Map 26, scale 1:1.000.000.

Schulze D.J., Helmstaedt H. and Cassie R.M. 1978. Pyroxene-ilmenite intergrowths in garnet pyroxenite xenoliths from a New York kimberlite and Arizona latites, *Am. Min.*, 63, 258-265.

Wilshire H.G., Nielson Pike J.E., Meyer C.E.and Schwarzman E.C. 1980. Amphibole-rich veins in Lherzolite xenoliths, Dish Hill and Deadman Lake, California, *Am. J. Sci.*, 280-A, 576-593.

Wilshire H.G., McGuire A.V., Noller J.S.and Turrin B.D. 1991. Petrology of Lower Crustal and Upper Mantle Xenoliths from the Cima Volcanic Field, California, *J. Petrol.*, 32(1), 169-200.

Δελτίο της Ελληνικής Γεωλογικής Εταιρίας, τομ. XLVII , 2013
Πρακτικά 13ου Διεθνούς Συνεδρίου, Χανιά, Σεπτ. 2013

Bulletin of the Geological Society of Greece, vol. XLVII 2013
Proceedings of the 13th International Congress, Chania, Sept. 2013

THERMAL BEHAVIOUR OF STEVENSITE AT TEMPERATURES UP TO 800°C

Christidis G.E[1] and Koutsopoulou E.[2]

[1] *Technical University of Crete, Department Mineral Resources Engineering, 73100 Chania, Greece. christid@mred.tuc.gr*

[2] *University of Patras, Department Geology, 26500 Patras, Greece ekoutsop@upatras.gr*

Abstract

Stevensite is a Mg-trioctahedral smectite with layer charge stemming from vacancies in the octahedral sheet. In the present work we studied the thermal behavior of Jbel Ghassoul stevensite from Morocco, known as Ghassoulite or Rhassoulite, free of talc layers. The clay fraction of the material was separated by sedimentation, it was subsequently heated from 250° to 800° C and the end products were examined with X-ray diffraction (XRD) and Fourier Transform Infrared (FTIR) spectroscopy. The influence of heating on the stevensite structure begins at 400°C and is completed at 500°C. It involves irreversible collapse of the layers at ~10Å, which do not re-expand in ethylene glycol (EG) vapors. In contrast, heating at lower temperatures does not affect the stevensite layers, which expand completely in EG. The FTIR spectra indicate the formation of talc-like (kerolite) layers after heating at temperatures exceeding 400°C. Within the current experimental setup, the transition to kerolite layers takes place without the formation of an intermediate mixed-layer stevensite/talc phase. Heating at higher temperatures does not change the transformation pattern, until 800°C where complete dehydroxylation of the 2:1 layer takes place, which is associated with the formation of enstatite. The results of this study clearly demonstrate that opposite to common trioctahedral and dioctahedral smectites, stevensite converts to another layer silicate prior to dehydroxylation.

Key words: *trioctahedral smectite, kerolite, XRD, Thermal treatment, transformation.*

Περίληψη

Ο στιβενσίτης είναι μαγνησιούχος τριοκταεδρικός σμεκτίτης με φορτίο κρυσταλλικής δομής που προέρχεται από κενές οκταεδρικές θέσεις. Στην παρούσα εργασία μελετήθηκε η θερμική συμπεριφορά ενός καθαρού στιβενσίτη (χωρίς φύλλα τάλκη) από το Μαρόκο, γνωστού ως Ghassoulite ή Rhassoulite. Το αργιλικό κλάσμα του υλικού αποχωρίστηκε με καθίζηση, θερμάνθηκε σε θερμοκρασίες 250-600°C και εξετάστηκε με περιθλασιμετρία ακτίνων Χ (XRD) και φασματοσκοπία υπερύθρου (FTIR). Επίδραση της θέρμανσης στη δομή του στιβενσίτη ξεκινά στους 400°C και ολοκληρώνεται στους 500°C. Λαμβάνει χώρα μη αντιστρεπτή συρρίκνωση των φύλλων στα ~10Å, τα οποία δε διογκώνονται μετά από έκθεση σε αιθυλαινογλυκόλη. Αντίθετα έκθεση σε χαμηλότερες θερμοκρασίες δεν επηρεάζει τη συμπεριφορά των

στιβενσιτικών φύλλων, τα οποία διογκώνονται πλήρως σε περιβάλλον ατμών αιθυλαινογλυκόλης. Τα φάσματα FTIR δείχνουν τη δημιουργία φύλλων τάλκη (κερολίτη) όταν οι θερμοκρασίες υπερβαίνουν τους 400°C. Με τις παρούσες πειραματικές συνθήκες η μετάβαση σε φύλλα τάλκη δεν έλαβε χώρα μέσω μικτής δομής στιβενσίτη/τάλκη. Έκθεση σε υψηλότερες θερμοκρασίες δε μεταβάλλει την πορεία του μετασχηματισμού μέχρι τους 800 °C, όπου λαμβάνει χώρα αφυδροξυλίωση, η οποία συνδέεται με δημιουργία ενστατίτη. Η παρούσα μελέτη δείχνει σαφώς, ότι ο στιβενσίτης παρουσιάζει διαφορετική συμπεριφορά από τους υπόλοιπους διοκταεδρικούς και τριοκταεδρικούς σμεκτίτες, αφού μετατρέπεται σε άλλο φυλλοπυριτικό ορυκτό πριν την αφυδροξυλίωση.
Λέξεις κλειδιά: *Τριοκταεδρικός σμεκτίτης, κερολίτης, XRD, θερμική επίδραση, μετατροπή.*

1. Introduction

The structural and crystal chemical characteristics of smectites have been studied extensively in the past by several independent analytical methods including X-ray diffraction (XRD), various spectroscopic methods including FTIR, Mössbauer and EPR spectroscopy, thermal analysis, chemical analysis (e.g. Lagaly & Weiss 1975; Talibudeen & Goulding 1983; Lim & Jackson 1986; Decarreau et al., 1987; Goodman et al., 1988; Iwasaki & Watanabe 1988; Lagaly 1994; Christidis & Dunham 1993; 1997; Christidis & Eberl, 2003; Christidis, 2006). Identification of smectite compositional characteristics is important for most industrial applications (Christidis, 2011). Hence several classification schemes of smectites have been proposed, based on their crystal chemical and thermal properties (Grim & Kulbicki, 1961; Schultz; 1969; Brigatti & Poppi, 1981; Newman & Brown, 1987; Alberti & Brigatti; 1985; Güven, 1988; Drits et al., 1998; Wolters et al., 2009).

X-ray diffraction (XRD) and Fourier Transform Infrared (FTIR) Spectroscopy are powerful techniques used for the characterization of structural characteristics of smectites. Special tests have been proposed for fast distinction of the different smectite species such as the Hoffman-Klemmen effect, which provides a fast tool for distinction of beidellite from montmorillonite (Greene-Kelly, 1953). However, most previous work on the identification and characterization of smectites focus on the dioctahedral smectites. In contrast, characterization of the trioctahedral smectites by XRD methods is very basic and includes merely identification of the trioctahedral character, based on the position of the 060 diffraction maximum (e.g. Moore and Reynolds, 1997).

The main trioctahedral smectite species are saponite with predominantly tetrahedral charge and stevensite and hectorite mainly with octahedral charge. Stevensite is different from its counterparts because the layer charge stems from octahedral vacancies rather than substitutions in the structure (Brindley, 1984). The layer charge of stevensites is low and typically does not exceed 0.25 electrons per half unit cell (e/huc). Studies on the stevensite thermal properties are rather rare (Shimoda, 1971; Brindley, et al. 1977; Benhammou et al., 2009). Moreover, in several occurrences, stevensite occurs in the form of mixed layer stevensite/kerolite (e.g. Eberl, et al. 1982; Dekov et al. 2008). In contrast pure stevensites are rather rare. Recently Christidis & Mitsis (2006) described a new Ni-stevensite in Othrys mountain, Central Greece. The aim of this study was to describe the thermal characteristics of the Jbel Ghassoul stevensite from Morocco, and to display possible differences compared to the remaining trioctahedral smectites and a well characterized talc from Egypt. The particular stevensite was selected, because it is well characterized and it is well known that it does not contain traceable kerolite layers (Benhammou et al., 2009)

2. Materials and Methods

The stevensite sample from Jbel Ghassoul was supplied by Prof. K. El Ass, University of Rabat, Morocco. It is a gray-pink soft clay with a low grit content and soapy texture. The Egyptian talc was provided by IONIAN KALK SA (Kefalonia, Greece). Bulk mineralogy was determined by X-ray diffraction (XRD) with a Bruker D8 Advance XRD, equipped with a Lynx Eye strip silicon detector, using Ni filtered CuKα radiation (35kV, 35mA), 0.298° divergence and antiscatter slits, and a step size of 0.019 °2θ, with 47.7 s count time per step. XRD analysis was performed from 4 to 70 °2θ. The collected data were evaluated with the EVA® software provided by SOCABIM. 3 g of the bulk sample were heated at 800°C for 2 h and examined with the same diffractometer. Clay mineralogy was determined by dispersion of the sample in distilled water using an ultrasonic probe (20 seconds) and repeated washing until practically free of salts (electric conductivity < 25 μS/cm). The <2 μm fraction was separated by settling and dried on glass slides at room temperature. The glass slides with the calibration samples were heated at 250, 300, 400, 500, 550 and 600 °C for 90 min and were subsequently solvated with ethylene-glycol (EG) vapour at 60 °C overnight (min. 16 h) to ensure maximum saturation. XRD analysis was performed from 2 to 35°2θ with the same diffractometer.

The clay fractions of the stevensite in the raw state and after heating at 500°C were examined with infrared (IR) spectroscopy using a Perkin Elmer 1000 Fourier Transform Infrared (FTIR) spectrometer in the range 400-4000cm^{-1}. Each spectrum was the average of 50 scans collected at 4 cm^{-1} resolution. 1.5 mg of the clay fractions was diluted in 200 mg KBr and pressed in 13mm KBr disks, which were subsequently dried at 150°C for 15 hours, prior to FTIR analysis (Russell 1987).

3. Results

3.1 X-Ray Diffraction

The XRD trace of the bulk stevensite sample is shown in (Fig. 1a). The material consists of stevensite, with minor illite, chlorite, quartz, dolomite, K-feldspar and albite. The hump at 10-18 ° 2θ is due to instrumental artifact. The stevensite content exceeds 90%. The clay fraction contains >95% stevensite and traces of chlorite illite and quartz (Fig. 1b). The existence of a low angle shoulder in the 001 diffraction maximum of the EG solvated XRD trace might be indicative of random interstatification, possibly with kerolite layers. However the higher order diffraction maxima are rational suggesting that if kerolite layers are present, they should not exceed 5%. Therefore the smectite is considered to be pure stevensite. After heating at 800°C for 2 h a diffraction maximum at ~9° 2θ (9.8 Å) is present, which corresponds to the collapsed stevensite layer (see below), and enstatite forms (Fig. 1a). These results are in full accordance with Benhammou et al. (2009). The coexistence of 9.8 Å (kerolite-like) layers and enstatite indicates that the onset of dehydroxylation occurs at lower temperatures. A small amount of kerolite-like layers still persists after heating at 950°C for 2 h, and simultaneously enstatite becomes more abundant (data not shown). As expected, chlorite, mica and dolomite also decomposed after heating. Therefore the first recrystallization product of Morocco stevensite *after* dehydroxylation is enstatite. The Ni-stevensite from Othrys mountain also collapsed at below 500°C, dehydroxylated at temperatures higher than 750°C and yielded enstatite at 800°C (Christidis & Mitsis 2006). Such behaviour is comparable to pure talc, which also recrystallizes to enstatite after dehydroxylation at higher temperature i.e. 900-1000°C (Brindley & Lemaitre, 1987).

Heating of the clay fractions of stevensite up to 300°C and subsequent EG solvation did not affect the position of the 001 diffraction maximum. Only a progressive decrease of the diffraction intensity was observed instead (Fig. 2). At higher temperatures the 001 diffraction maximum collapsed to ~ 9.8 Å and did not re-expand after EG solvation. Moreover, the intensity of the new diffraction maximum increased with increasing heating temperature. The appearance of the new diffraction maximum strongly indicates the formation of a kerolite-like phase. The onset of

formation of this phase is observed at ~400°C, and it is fully developed at temperatures higher than 500 °C. The rational order of the higher order basal reflections attests to the lack of intermediate stevensite/kerolite mixed layer phase during progressive heating.

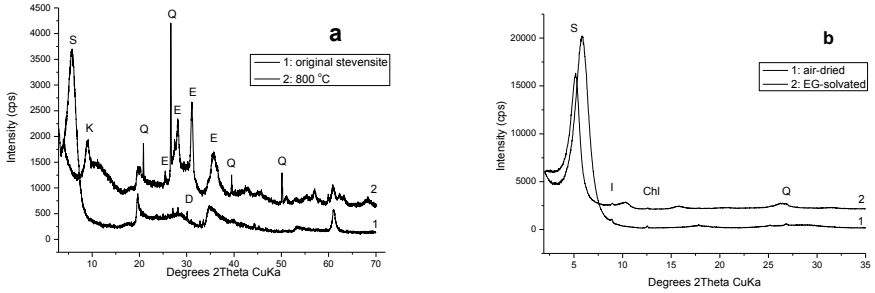

Figure 1 – a) XRD traces of the Jbel Ghassoul stevensite (bulk sample) in raw state and after heating at 800°C. b) XRD traces of the oriented clay fractions of the original stevensite sample. Key to the symbols: S= stevensite, K= kerolite, Q= quartz, E= enstatite, D= dolomite, Chl= chlorite, I= illite. See text for discussion.

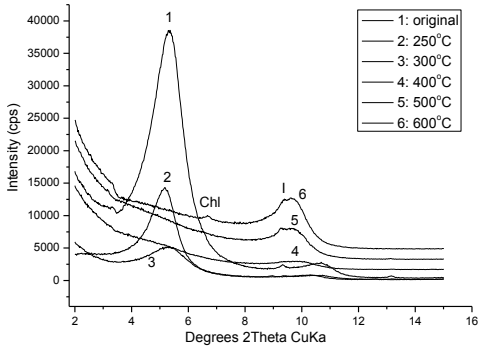

Figure 2– Oriented XRD traces of Jbel Ghassoul stevensite heated at 250-600°C and ethylene glycol solvated. Chl = chlorite, I = illite.

3.2 FTIR Spectra

The FTIR spectra of the original and heated stevensite (500°C) are shown in Fig. 3. For terms of comparison the FTIR spectrum of a talc is also included. In the OH-streching region all spectra display the characteristic band at 3677 cm^{-1} attributed to Mg_3OH (Petit, 2005). The location of the band is identical in all three spectra, but the intensity in stevensite heated at 500°C is clearly higher compared the original stevensite and certainly lower than that of talc. In the region of lattice vibrations, the FTIR spectra of the original clay fractions are broader, while the bands of the heated sample seem to be more symmetric. The bands at 451 cm^{-1}, 471 cm^{-1} and 533 cm^{-1} are attributed to Si-O-Mg vibration, Mg-O and/or translational OH-vibration and Mg-O vibration respectively. In the Mg_3OH bending region the stevensite and the heated stevensite display a doublet (668 and 690 cm^{-1}) but the intensity of the two bands is reversed after heating. Talc displays is single band (668 cm^{-1}). In conclusion, although heating caused structural differences in the structure of stevensite, the heated sample has clearly distinct structural features compared to well crystallized talc, being more typical to kerolite (Christidis & Mitsis, 2006).

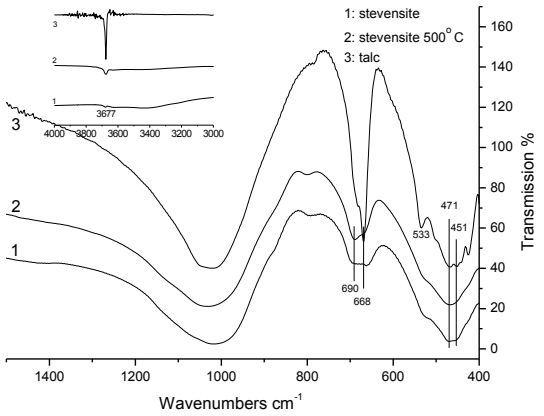

Figure 3 – Mid FTIR spectra of the Jbel Ghassoul stevensite in raw state and after heating at 500°C. The IR spectrum of talc is shown for comparison. See text for discussion.

4 Discussion

This work has clearly shown that stevensite is different than the remaining trioctahedral smectites not only due to the origin of layer charge (octahedral vacancies *vs* ionic substitution in the structure) but also because although it has comparable dehydroxylation temperature with saponite and hectorite (Paterson and Swaffield, 1987), the swelling properties are lost after heating well below the dehydroxylation temperature. This difference in thermal behaviour has been used recently as part of a new approach to identify the trioctahedral smectites (Christidis and Koutsopoulou, 2013). The loss of swelling is associated with the solid state transformation of stevensite to kerolite-like layers. Kerolite is disordered talc with similar XRD characteristics as smectites, which does not swell in EG vapours (Brindley 1984). It often forms random mixed layer phases with stevensite in nature (Eberl et al., 1982; Dekov et al., 2008). The lack of intermediate mixed layer stevensite/kerolite indicates the presence of homogeneous stevensite domains in the original clay. If minor kerolite domains were present in the original clay, then they should form distinct areas and should not be mixed with stevensite domains (Christidis and Mitsis, 2006). Such a hypothesis explains the XRD traces after EG solvation, which are not compatible with the existence of mixed layer phases. In this scenario, any trace distinct kerolite domains would possibly be masked by the 002 diffraction maximum of stevensite, due to their low abundance.

Heating at 800°C shed additional light on the structural characteristics of stevensite. The coexistence of abundant kerolite-like layers and neoformed enstatite crystals is in accordance with the widely accepted influence of kinetics on the transformation of kerolite to enstatite (Brindley & Lemaitre, 1987). What is not known with certainty is if this kinetic influence on the transformation, is due to existence of energy barriers, or due to structural heterogeneity of the original stevensite. This study has shown that the stevensite layers are relatively homogeneous, due to the apparent lack of kerolite domains. However, the Jbel Ghassoul stevensite contains 1.31% Al_2O_3 (Benhammou et al., 2009), suggesting the presence of saponite layers, although part of this Al_2O_3 is due to the presence of traces of chlorite and illite. It is thus suggested that the presence of saponite layers, which also yield enstatite at temperatures higher than 800°C (Brindley and Lemaitre, 1987), may also affect the kinetics of transformation of stevensite.

Due to their high dehydroxylation temperatures trioctahedral smectites in general have good potential for application in the foundry industry (iron ore pelletization and foundry sand binders) and as fire retardants (Christidis, 2011). However it is clear that stevensite does not follow this trend, because it converts to a kerolite-like phase at least 400°C lower than the dehydroxylation temperature. Therefore, the swelling properties which are of vital importance for foundry applications deteriorate at temperatures lower than the *trans*-vacant smectites, which

dehydroxylate at 500-550°C (Drits et al. 1998; Guggenheim & Koster van Groos, 2001). It is well known that *trans*-vacant smectites are not suitable for foundry applications (Christidis, 2011). This underlines the significance of identification of stevensite layers during assessment of bentonite deposits, in areas where it occurs in close association with saponite, such as the Vicalvaro Basin, Spain (Cuevas et al. 2003). In contrast, due to its fine grain size and swelling properties, coupled with the chemical composition, stevensite is used as a gelling agent, especially after modification with organic compounds, and in the formulation of cordierite ceramics (Benhammou et al. 2009).

5. Conclusions

The Jbel Ghassoul stevensite was heated in the temperature range 250-800°C. Heating above 400°C resulted to collapse of the stevensite layers and to formation of non-swelling kerolite-type layers. This transformation occurs well below the dehydroxylation temperature of stevensite. At 800°C enstatite forms but the transformation of the kerolite layers is not complete. Identification of stevensite layers is a vital importance during assessment of bentonites containing trioctahedral smectites, especially for high temperature applications such as the foundry industry.

6. References

Alberti A. and Brigatti M.F. 1985. Crystal chemical differences in Al-rich smectites as shown by multivariate analysis of variance and discriminant analysis, *Clays and Clay Minerals,* 33, 546-558

Benhammou A., Tanouti B., Nibou L., Yaacoubi A. and Bonnet J.-P. 2009. Mineralogical and physicochemical investigation of Mg-smectite from Jbel Ghassoul, Morocco. *Clays and Clay Minerals*, 57, 264-270.

Brigatti M.F. and Poppi L. 1981. A mathematical model to distinguish the members of the dioctahedral smectite series. *Clay Minerals,* 16, 81-89.

Brindley G.W. 1984. Order-disorder in clay mineral structures, in Brindley G.W., and Brown G. (eds) *Crystal Structures of Clay Minerals and their X-ray Identification*, 319-370, London, Mineralogical Society, Monograph 5.

Brindley G.W., Bish D.L. and Wan H-M. 1977. The nature of kerolite, its relation to talc and stevensite, *Mineralogical Magazine*, 41, 443-452.

Brindley G. and Lemaitxe, J. 1987. Thermal, oxidation and reduction reactions of clay minerals. In Newman, A.C.D. and Brown, G. (eds), *Chemistry of Clays and Clay Minerals,* 319-370, London, Mineralogical Society.

Christidis G.E. 2006. Genesis and compositional heterogeneity of smectites, Part III, Alteration of basic pyroclastic rocks, A case study from the Troodos Ophiolite Complex, Cyprus, *American Mineralogist*, 91, 685-701

Christidis G.E. 2011. Industrial clays, in Christidis, G.E. (ed) *Advances in the Characterization of Industrial Minerals*, 341-414, London, EMU Notes in Mineralogy, vol. 9, Mineralogical Society, 485 pp.

Christidis G. and Dunham A.C. 1993. Compositional variations in smectites derived from intermediate volcanic rocks. A case study from Milos Island, Greece, *Clay Minerals,* 28, 255-273.

Christidis G. and Dunham A.C. 1997. Compositional variations in smectites, Part II: Alteration of acidic precursors. A case study from Milos Island, Greece. *Clay Minerals,* 32, 255-273.

Christidis G.E. and Eberl D.D. 2003. Determination of layer charge of smectites, *Clays and Clay Minerals*, 51, 644-655.

Christidis G.E. and Mitsis I. 2006. A new Ni-rich stevensite from the ophiolite complex of Othrys, central Greece, *Clays and Clay Minerals*, 54, 653-666.

Christidis G.E. and Koutsopoulou E. 2013. A novel approach to identify trioctahedral smectites by X-ray Diffraction. *International Conference*, "*Minerals for Life: Overcoming Resource Constraints*" 17-20 June, 2013, Edinburgh, UK, Book of Abstracts.

Cuevas J., de la Villa, R.V., Ramirez S, Petit S., Meunier A. and Leguey S. 2003. Chemistry of Mg smectites in lacustrine sediments from the Vicalvaro sepiolite deposit, Madrid, Neogene Basin (Spain), *Clays and Clay Minerals*, 51, 457-472

Decarreau A., Colin F., Herbillon A., Manceau A., Nahon D., Paquet H., Trauth-Badeaud D. and Trescases, J.J., 1987. Domain segregation in Ni-Fe-Mg-smectites, *Clays and Clay Miner*als, 35, 1-10.

Dekov V.M., Cuadros J., Shanks, W.C. and Koski R.A. 2008 Deposition of talc-kerolite-smectite - smectite at seafloor hydrothermal vent fields: Evidence from mineralogical, geochemical and oxygen isotope studies**,** *Chemical Geology*, 247, 171-194.

Drits V.A., Lindgreen H., Salyn A.L., Ylagan R. and McCarty D.K., 1998. Semi quantitative detrmination of trans-vacant and cis-vacant 2:1 layers in illites and illite-smectites by thermal analysis and X-ray diffraction. *American Mineralogist,* 83, 1188-1198.

Eberl D.D., Jones B.F. and Khoury, H.N., 1982. Mixed-layer kerolite/stevensite form the Amargosa Desert, Nevada. *Clays and Clay Minerals*, 30, 321-326.

Goodman B.A., Nadeau P.H., and Chadwick, J. 1988. Evidence for the multiphase nature of bentonites from Mossbauer and EPR spectroscopy, *Clay Miner*als, 23, 147-159.

Greene-Kelly R. 1953. Irreversible dehydration in montmorillonite, Part II, *Clay Miner*als *Bulletin,* 2, 52-56.

Grim R.E. and Kulbicki G. 1961. Montmorillonite: High temperature reactions and classification. *American Mineralogist,* 46, 1329-1369.

Guggenheim S. and Koster van Groos A.F. 2001. Baseline studies of the Clay Minerals Society Source YS: Thermal Analysis, *Clays and Clay Minerals*¸ 49, 433-443.

Güven N. 1988. Smectite, In Bailey, S.W., ed., *Hydrous Phyllosilicates* 497-559, Reviews in mineralogy, 19, Mineralogical Society of America.

Iwazaki T., and Watanabe T. 1988. Distribution of Ca and Na ions in dioctahedral smectites and interstratified dioctahedral mica/smectites. *Clays and Clay Minerals.* 36, 73-82.

Lagaly G. and Weiss A. 1975. The layer charge of smectitic layer silicates, *Proceedings International Clay Conference Mexico*, 157-172.

Lagaly G., 1994. Layer charge determination by alkylammonium ions, in Mermut, A.R., ed., *Layer charge characteristics of 2:1 silicate clay minerals,* 2-46, Boulder Colorado, CMS Workshop lectures, 6. The Clay Minerals Society.

Lim C.H. and Jackson M.L. 1986. Expandable phyllosilicate reactions with lithium on heating, *Clays and Clay Minerals,* 34, 346-352.

Moore D.M. and Reynolds, R.C., Jr., 1997. *X-ray diffraction and the identification and analysis of clay minerals*. 2nd edition, Oxford University Press, New York.

Newman A.C.D. and Brown, G., 1987. The chemical constitution of clays. In Newman, A.C.D., ed., *Chemistry of Clays and Clay Minerals*, 1-128, London, Mineralogical Society.

Paterson E. and Swaffield R. 1987. Thermal Analysis. In Wilson M.J., ed. *A Handbook of Determinative Methods in Clay Mineralogy,* 99-132, Glasgow, UK, Blackie & Son Limited.

Petit S. 2005. Crystal-chemistry of talcs: A NIR and MIR spectroscopic approach. In J.T. Kloprogge. (ed), *The Application of Vibrational Spectroscopy to Clay Minerals and Layered Double Hydroxides*, 41-64, Aurora CO 80046-0130, The Clay Minerals Society, 285 pp.

Russell J.D. 1987. Infrared Methods. In: M.J. Wilson (ed.) *A handbook of determinative methods in clay mineralogy,* 133-173, Glasgow & London, Blackie.

Schultz L.G. 1969. Lithium and potassium adsorption, dehydroxylation temperature and structural water content of aluminous smectites, *Clays and Clay Minerals,* 17, 115-149.

Shimoda S. 1971. Mineralogical studies of a species of stevensite from the Obori Mine, Yamagata prefecture, Japan, *Clay Minerals,* 9, 185-192.

Talibudeen O. and Goulding, K.W.T. 1983. Charge heterogeneity in smectites. *Clays and Clay Minerals,* 31, 37-42.

Wolters F., Lagaly G., Kahr G., Nüesch R. and Emmerich, K. 2009. A comprehensive characterization of dioctahedral smectites, *Clays and Clay Minerals*, 57, 115-133.

Δελτίο της Ελληνικής Γεωλογικής Εταιρίας, τομ. XLVII , 2013
Πρακτικά 13ου Διεθνούς Συνεδρίου, Χανιά, Σεπτ. 2013

Bulletin of the Geological Society of Greece, vol. XLVII 2013
Proceedings of the 13th International Congress, Chania, Sept. 2013

MINERALOGY AND CHEMISTRY OF AMPHIBOLES AND THERMOBAROMETRY OF PAPIKION MT PLUTON, RHODOPE, NORTHERN GREECE

Drakoulis A.[1], Koroneos A.[1], Soldatos T.[1] and Papadopoulou L.[1]

[1]Aristotle University of Thessaloniki, Faculty of Science, School of Geology, Dept of Mineralogy-Petrology-Economic Geology.

Abstract

Papikion Mt pluton which intrudes Kardamos Dome, consists of biotite (Bi), hornblende (Hbl) and biotite-hornblende (Bi-Hbl) bearing rock types. In this work the relationship among the amphiboles of each Hbl-bearing rock type is studied. Moreover, their minimum crystallization pressure and temperature are estimated. The amphiboles of the Hbl granodiorite (GRD), the Bi-Hbl diorite (DR) and the Hbl diorite (DR) are classified mainly as magnesiohornblende and ferrohornblende and the amphiboles of the Bi-Hbl GRD as ferroedenite and hanstingsite. It is to note that some samples contain amphibole crystals showing a sieved texture with quartz. These sieved amphiboles have no chemical differences from the rest amphibole crystals. This texture can probably derive from the breakdown of mafic minerals of an assimilated xenolith such as pyroxenes and hornblende itself, leaving quartz. Using the Al-in-hornblende geobarometer and the plagioclase-hornblende geothermometer), minimum crystallization pressures from 4.6 to 5.2 kbar and temperatures from 700 to 740 °C were estimated for the Bi-Hbl GRD. The DR shows crystallization pressures ranging from 6.4 to 7.4 kbar and temperatures ranging from 620 to 700 °C. The Hbl GRD shows the lowest P-T values, thus an average crystallization pressure about 3 kbar and an average temperature about 600 °C were estimated.
Key words: *sieved hornblende, crystallization pressure and temperature, subsolidus cooling.*

Περίληψη

Ο πλουτωνίτης του Παπικίου Όρους που διεισδύει στο Δόμο του Κάρδαμου, αποτελείται από Bi, Hbl και Bi-Hbl τύπους πετρωμάτων. Σε αυτή την εργασία μελετάται η σχέση μεταξύ των αμφιβόλων του κάθε πετρογραφικού τύπου που τις περιέχει. Οι αμφίβολοι του κεροστιλβικού γρανοδιορίτη (Hbl GRD), του βιοτιτικού-κεροστιλβικού διορίτη (Bi-Hbl DR)και του κεροστιλβικού διορίτη (Hbl DR) ταξινομούνται κυρίως ως μαγνησιοκεροστίλβες και σιδηροκεροστίλβες και οι αμφίβολοι του βιοτιτικού-κεροστιλβικού γρανοδιορίτη (Bi-Hbl GRD) ως σιδηροεδενίτες και χαστινγκσίτες. Πρέπει να σημειωθεί ότι ορισμένα δείγματα περιέχουν κρυστάλλους αμφιβόλου που παρουσιάζουν κοσκινινοειδή υφή με χαλαζία. Αυτές οι κοσκινοειδείς αμφίβολοι δεν διαφέρουν χημικά από τις υπόλοιπες. Η υφή αυτή μπορεί να προέρχεται από την αποδόμηση των φεμικών ορυκτών ενός αφομοιωμένου ξενόλιθου όπως οι πυρόξενοι αλλά και η ίδια η κεροστίλβη, αφήνοντας πίσω χαλαζία. Χρησιμοποιώντας το γεωβαρόμετρο Al στην κεροστίλβη και το γεωθερμόμετρο κεροστίλβης-πλαγιοκλάστου, υπολογί-

στηκαν ελάχιστη πίεση κρυστάλλωσης 4,6 - 5,2 kbar και θερμοκρασίες 700 - 740 °C για το Bi-Hbl DR και 6,4 έως 7,4 kbar και θερμοκρασίες από 620 έως 700 °C στην ομάδα DR.. Ο Hbl GRD δείχνει τις χαμηλότερες τιμές P-T, με μέση πίεση κρυστάλλωσης περίπου 3 kbar και με μέση θερμοκρασία περίπου 600 °C.
Λέξεις κλειδιά: *Κοσκινοειδής κεροστίλβη, πίεση και θερμοκρασία κρυστάλλωσης, ψύξη σε συνθήκες υπο-αγχιτηκτικής κατάστασης.*

1. Introduction

In the eastern Rhodope two large tectonic windows appear, called Kesebir-Kardamos Dome and Biela Reka–Kechros Dome. The greek part of Kesebir-Kardamos Dome is known as Kardamos Complex. The Papikion Mt. Pluton, intruding Kardamos Dome, consists of biotite (Bi), hornblende (Hbl) and biotite-hornblende (Bi-Hbl) bearing rock types. A noteworthy observation concerns the morphology of some Hbl crystals in some samples. In detail, these crystals are sieved, mainly subhedral in shape and enclose randomly anhedral quartz. This work aims at studying the mineralogy and chemistry of the amphiboles of Hbl-bearing rock types and contributes to the estimation of the crystallization conditions. Efforts are made in order to explain the origin of the above mentioned sieved hornblendes.

2. Geological Setting

The evolution of the Rhodope massif has been extensively studied through the past years. The Greek Rhodope massif has been divided into two tectonic units: the Lower Tectonic Unit (LTU), also known as Pangaion and the Upper Tectonic Unit (UTU) also known as Sidironero (Papanikolaou and Panagopoulos, 1981, Mposkos, 1989, Mposkos and Liati, 1993). The LTU extends towards the NW, into Bulgaria, where it is called Pirin Unit. This terrain represents a microcontinent with a carbonate platform that cores the large antiform from the Rila Mountains to the Thassos island through the Pirin and Pangaion mountains (e.g. Kronberg et al., 1970, Kronberg and Raith, 1977). The LTU is mainly composed of a succession of orthogneiss and migmatitic gneiss with a few paragneiss occurrences in Bulgaria (Ivanov, 1988) and a succession of alternating pelitic gneisses, amphibolites and marbles in Greece (Mposkos, 1998, Krohe and Mposkos, 2002). The UTU is of higher metamorphic grade (upper amphibolite-facies and, at least partly, granulite-facies) and is separated from the LTU (upper greenschist-facies to lower amphibolite-facies) by a major WNW trending thrust plane, known as the Nestos Thrust Zone (Papanikolaou and Panagopoulos, 1981, Zachos and Dimadis, 1983, Mposkos, 1989, Gerdjikov and Milev, 2005). The UTU comprises interlayered amphibolites, marbles, metapelitic schists and various gneisses enclosing eclogite and metaophiolite lenses (Ivanov, 1988, Burg et al., 1996).

According to Burg (2012) LTU is exposed also in eastern Rhodope as a string of four separated domes. These are, from northwest to southeast, the Chepinska, Arda, Kesebir and Biela Reka "units" in Bulgaria; the last two are called Kardamos (Mposkos and Krohe, 2000) and Kechros (Mposkos and Krohe, 2000) in Greece. These domes expose monotonous, quartz-feldspathic, strongly deformed gneisses of dioritic composition intruded by metagranitoids, some of which are presumably syntectonic. The Kesebir (Bulgaria)-Kardamos (Greece) is a subelliptical extensional gneiss dome that trends NE–SW (Bonev et al., 2006, Krenn et al., 2010) (Fig. 1a).

The Papikion Mt. pluton intrudes Kardamos Dome (Fig. 1a&b). It spreads from Iasmos in the east, to Komotini to the west and from the Xanthi-Komotini fault in the south to the Greek-Bulgarian borders to the north. This pluton, with characteristic gneissic texture, covers about 100 km^2 in the SW part of Kardamos Dome in Greece. It is bordered by marbles to the SW, where typical skarn minerals appear, epidote and garnet, and by gneiss to the NE, intruding the Kardamos Dome (Bonev et al., 2006 and references therein). The thickness of the skarn zone ranges from 0.5 m to 1.5 m. The gneisses represent the lower unit of Kardamos Dome and the marbles represent the

intermediate unit, therefore the Papikion Mt. pluton intrudes both the lower and intermediate units of the Kardamos Dome.

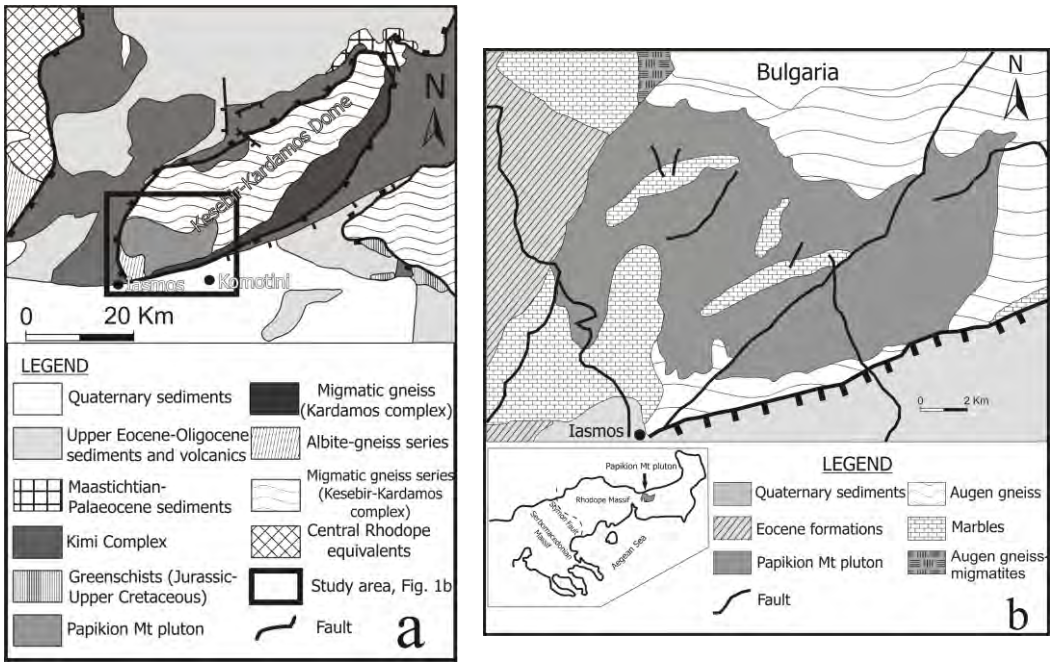

Figure 1 – a) Geological map of Kesebir-Kardamos Dome (Modified after Bonev et al., 2006). b) Geological map of Papikion Mt pluton (Modified after Dimades and Zachos, 1985).

3. Petrology

Papikion Mt pluton consists mainly of six rock types which have been classified on the basis of field observations, mineralogical composition and the Q'-ANOR diagram (Streckeisen & Le Maitre, 1979, not shown). These types are biotite granite (Bi GR), biotite granodiorite (Bi GRD), biotite hornblende granodiorite (Bi-Hbl GRD), hornblende granodiorite (Hbl GRD), biotite hornblende diorite (Bi-Hbl DR) and hornblende diorite (Hbl DR). Aplitic dykes intrude the above rock types. The Bi GRD contains fine to medium grained, ellipsoidal, mafic microgranular enclaves (MME) with length ranging from 5 to 30 cm. Xenoliths, mainly of amphibolitic composition, also exist mostly in Bi & Bi-Hbl GRD. About 200 samples were collected from the plutonic and the basement rocks and a group of 65 samples have been analyzed by X-Ray Fluorescence (XRF) for major and trace elements (as part of the PhD thesis of the first author). In general, all the rocks are evidently foliated. The relationship among the rock types is rather obscure. There is no field evidence of one rock type intruding the other. In addition, there are some locations where mingling phenomena are characteristic.

In all Hbl-bearing rocks, the hornblende is the main mafic mineral. The Hbl DR contains in average 60% Hbl, the Bi-Hbl DR contains 42% Hbl, while the Hbl GRD contains 30% Hbl and Bi-Hbl GRD contains 18% Hbl.

4. Petrography and Mineral Chemistry

In general, hornblende has colours ranging from light green to brown and shows no zoning. In some cases, it is enclosed by biotite although elsewhere biotite encloses hornblende. Many samples, mostly those collected at the margins of the pluton, have gneissic texture, however, hornblende crystals do not display any preferred orientation. Hbl forms euhedral to subhedral

(from now on will be called “normal”) crystals and in some samples sieved crystals (Fig. 2 a&b). Sieved crystals are mainly subhedral in shape and enclose randomly anhedral quartz. However, samples with both Hbl textures, normal and sieved, were observed.

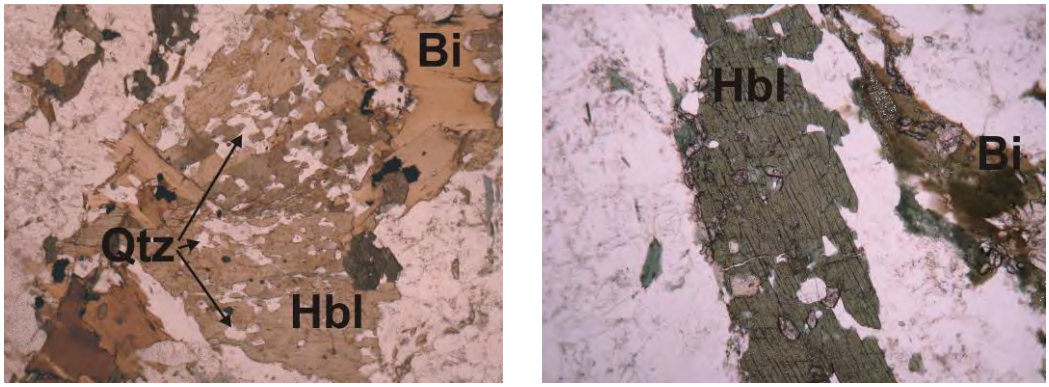

Figure 2 - Photos of hornblende a) with a quartz sieved texture and b) with normal texture. The long dimension of each photo corresponds to 4mm, parallel Nicols.

Representative samples of the Hbl-bearing rock types were selected for microanalyses. Mineral chemical analyses were carried out at the Scanning Microscope Laboratory, A.U.Th., using a JEOL JSM-840A Scanning Electron Microscope (SEM) equipped with an Energy Dispersive Spectrometer (EDS) with 20kV accelerating voltage and 0.4 mA probe current. Pure Co was used as an optimization element. For SEM observations, the samples were coated with carbon – average thickness of 200 Å – using a vacuum evaporator JEOL-4X.

The results of representative amphibole analyses from each Hbl-bearing rock type are given in Table 1. Ferric iron was estimated according to Schumacher (1997). The Si content varies between from 6.29 to 7.47 atoms per formula unit (apfu). According to the classification diagram of Leake (1997), all the amphiboles belong to the calcic group. Amphiboles of the Bi-Hbl GRD plot in the area of ferroedenite and hastingsite (Fig. 3a). On the other hand, the amphiboles of Bi-Hbl DR and Hbl DR, plot mainly in the magnesiohornblende field and the ferrohornblende field (Fig. 3b). Finally, the amphiboles of Hbl GRD are displayed only in the magnesiohornblende field (Fig. 3c). From Figures 3b and 3c, it is obvious that sieved hornblendes are not chemically different from the normal ones. Plagioclases appear to be homogeneous and no zoning was observed. Plagioclase compositions range from An_{23} to An_{40} in all Hbl-bearing rock types.

5. Thermobarometry

The average, minimum and maximum crystallization pressures for each rock type as resulted from the application of amphibole barometry are given in Fig. 6a. In all cases chemical analyses were chosen from the rim of the amphibole crystals and constraints of each barometer were taken into account.

The higher mean pressure values were found in the group of DR, while the lower in Hbl GRD. The highest crystallization pressure was found in the DR with the Schmidt geobarometer (6.9 ±0.6 kbar). To calculate the pressure by the geobarometer of Anderson and Smith (1995) a mean temperature of 740 °C was accepted for Bi-Hbl GRD, 700 °C for the DR group and 600 °C for Hbl GRD. Mean temperatures were estimated by the amphibole-plagioclase geothermometer (Holland and Blundy, 1994).

The application of the amphibole-plagioclase geothermometer gave values, in average, from 600 (± 40)°C (Hbl GRD) to 725 (± 40)°C (Bi Hbl GRD) (Fig. 6b). Plagioclase compositions were in the range of An_{25}-An_{35}.

6. Discussion

Amphiboles are present both with sieved texture enclosing randomly anhedral quartz and with normal texture. No chemical difference was observed among the two.

According to Collins (2003) and Collins and Collins (2002 and references therein) sieved hornblende texture has been ascribed to K- and Si-metasomatism after solidification of the plutonic rock. In this case, an initial mafic igneous rock, uniform in composition and fabric, crystallized from magma. If this rock is deformed so that fluids can enter and cause metasomatism at temperatures below melting conditions, a granite with a uniform appearance can be the final product. During this process, plagioclase in the original mafic rock could be partially replaced by K-feldspar while the rest recrystallizes as sodic plagioclase. Si-metasomatism causes replacement of hornblende and/or biotite by quartz resulting in sieve texture. This could explain the occurrence of a low-temperature mineral, such as quartz, enclosed in the high-temperature hornblende crystals. Because most of the ferromagnesian silicates are replaced by quartz, the final product is a granite whose composition lies on or near the eutectic minimum. In magmatic or metasomatic granites, the mineral assemblages are the same and stable at the same P-T conditions.

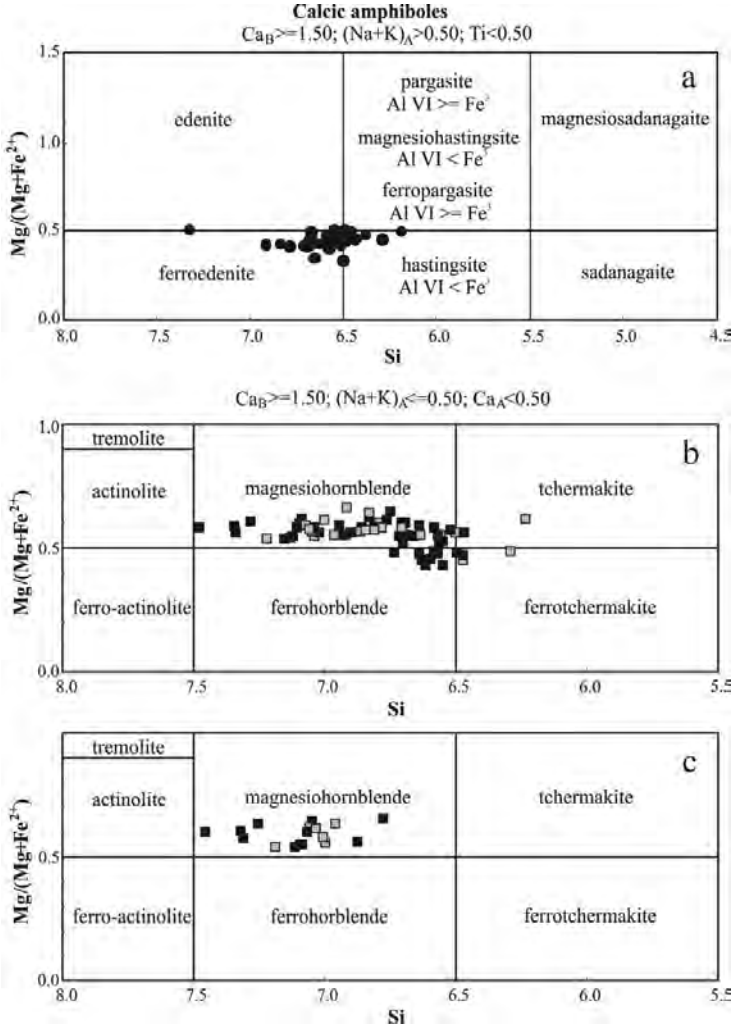

Figure 3 - Classification diagrams after Leake et al. (1997, 2003) a) Bi Hbl GRD, b) Bi-Hbl DR and Hbl DR, c) Hbl GRD; grey squares: sieved crystals, black squares: normal crystals.

According to Beard et al. (2005) sieved hornblende may be the result of bulk assimilation of xenoliths from the magma during crust-mantle mixing. In this case, xenoliths containing mica or amphibole are incorporated into host magma and are subjected to dehydration melting producing plagioclase, pyroxene, Fe-Ti oxides, and hydrous melt. Due to partial melting, the xenolith begins to disintegrate and "xenolithic melt" and crystals are mixed into the host magma. At this stage, pyroxenes and oxides undergo hydration crystallization reactions that lead to the formation of feldspars, amphiboles and micas. Replacement of pyroxene by amphibole results in the formation of quartz at amphibole-pyroxene contact. Eventually, when pyroxene is consumed, a quartz-sieved hornblende texture remains.

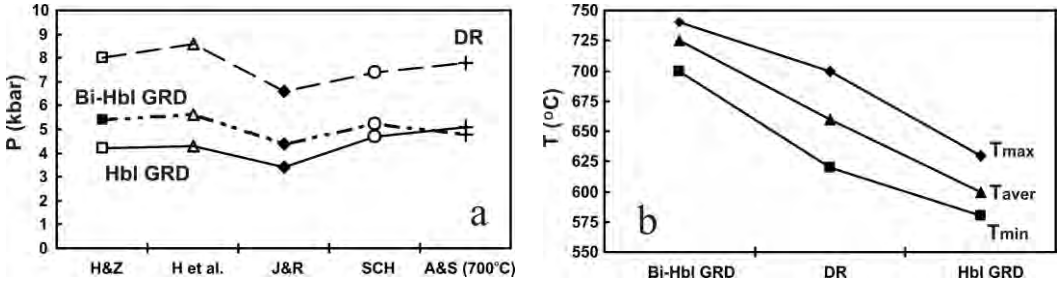

Figure 6 a & b – a) Maximum, minimum and average values of crystallization pressures of Hbl-bearing rock types of Papikion Mt pluton, based on amphibole barometry. H&Z: Hammarstrom and Zen (1986), H et al.: Hollister et al. (1987), J&R: Johnson & Rutherford (1989), SCH: Schmidt (1992) and A&S: Anderson and Smith (1995).b) Maximum, minimum and average values of crystallization temperatures of Hbl-bearing rock types of Papikion Mt pluton, based on the amphibole-plagioclase geothermometer.

There are many geothermometers used in metamorphic rocks and many of them are applied to plutonic rocks. The specificity of plutonic rocks is that mineral phases can crystallize in a wide range of pressures and temperatures and it is uncertain whether they have reached equilibrium conditions during magma crystallization. Many minerals continue to equilibrate and change composition after magma crystallization, during cooling in the solid state (subsolidus cooling), indicating continuous reaction with the melt. Ion exchange between minerals can continue well below the solidus temperature. The use of many different thermometers can lead to reliable conclusions concerning the conditions of magma crystallization. The amphibole-plagioclase geothermometer of Holland and Blundy (1994) used in the Hbl-bearing rocks of Papikion Mt. yields average temperatures, with an error of ± 40 °C, of 600 °C (Hbl GRD), 660 °C (DR) and 725 °C (Bi Hbl GRD) that are considered low for dioritic and granodioritic magmas. These temperatures possibly represent the equilibrium temperatures of amphibole and plagioclase, i.e. the time that ion diffusion ceased rather than crystallization temperatures.

7. Conclusions

The hornblende occurs as the basic mafic component in Bi-Hbl GRD and Bi-Hbl DR and is the only mafic mineral of Hbl GRD and Hbl DR. According to the nomenclature diagrams, the amphiboles of the Hb GRD, the Bi-Hbl DR and the Hbl DR are classified mainly as magnesiohornblende and ferrohornblende and the amphiboles of the Bi-Hbl GRD are ferroedenite and hanstingsite. The sieved crystals of hornblende differ from the normal ones only morphologically and not chemically. This texture can probably derive from the destruction of mafic minerals such as pyroxenes and hornblende itself, leaving quartz. Some samples present particular gneiss texture, but the crystals of hornblende in these samples are not oriented. The low temperatures estimated for the Papikion Mt pluton could be ascribed to high oxygen fugacity partial pressure (fO2), as been noted for other granitoids, particularly for I-type granitic rocks

Table 1 - Representative analyses of amphiboles from each Hbl-bearing rock type of Papikion Mt pluton based on 23 O.

Sample	15			925			602			603			911			14			220		
	core	int	Rim	core	int	rim	core	int	rim	core	int	rim	core	int	rim	core	int	rim	core	rim	rim
SiO_2	44.91	45.06	45.87	47.28	46.39	46.36	43.94	45.94	42.27	44.97	42.92	43.49	48.34	51.21	47.85	44.09	43.25	43.37	42.62	41.30	41.52
TiO_2	0.42	0.50	0.54	0.77	0.65	0.53	0.54	0.39	0.50	0.39	0.79	0.66	0.44	0.00	0.22	0.60	0.51	0.48	0.64	0.84	0.77
Al_2O_3	11.02	11.88	11.70	10.90	12.16	11.23	12.30	8.68	15.01	10.66	11.83	12.71	7.29	4.91	7.82	9.50	9.71	9.68	10.26	8.09	9.95
FeO	17.21	15.26	16.46	14.43	14.65	14.19	17.84	16.78	17.30	18.40	18.46	18.87	15.25	15.95	15.81	20.44	20.66	20.71	20.36	26.20	20.83
MnO	0.20	0.57	0.36	0.39	0.41	0.49	0.54	0.60	0.68	0.67	0.47	0.52	0.58	0.56	0.53	0.73	0.92	0.58	0.34	0.40	0.46
MgO	9.95	10.48	10.06	10.16	10.37	10.60	9.59	11.35	8.20	8.83	8.43	7.56	12.01	12.26	12.05	8.50	8.69	8.14	8.62	6.09	8.68
CaO	12.56	12.44	12.02	11.74	11.40	11.98	11.33	12.55	11.96	12.13	12.31	12.10	12.49	12.48	12.71	11.63	12.20	12.16	12.12	11.65	12.12
Na_2O	0.89	0.66	1.01	0.69	0.87	1.14	1.01	0.82	1.54	0.88	0.76	0.95	1.05	0.54	0.83	1.36	1.05	1.38	1.29	0.98	1.36
K_2O	0.43	0.36	0.34	0.52	0.54	0.53	0.58	0.67	0.43	0.74	0.89	0.69	0.82	0.48	0.60	1.45	1.59	1.54	1.75	1.88	1.67
Total	97.73	97.31	98.37	96.89	97.49	97.05	97.65	97.78	97.89	97.67	97.03	97.57	98.28	98.37	98.42	98.30	98.58	98.06	98.02	97.43	97.37
Si	6.664	6.642	6.716	6.965	6.781	6.845	6.501	6.795	6.294	6.737	6.498	6.550	7.110	7.479	7.001	6.682	6.537	6.628	6.496	6.501	6.383
Al IV	1.336	1.358	1.284	1.035	1.219	1.155	1.499	1.205	1.706	1.263	1.502	1.450	0.890	0.521	0.999	1.318	1.463	1.372	1.504	1.499	1.617
T	*8.000*	*8.000*	*8.000*	*8.000*	*8.000*	*8.000*	*8.000*	*8.000*	*8.000*	*8.000*	*8.000*	*8.000*	*8.000*	*8.000*	*8.000*	*8.000*	*8.000*	*8.000*	*8.000*	*8.000*	*8.000*
Al VI	0.592	0.705	0.737	0.857	0.876	0.799	0.646	0.308	0.927	0.619	0.610	0.807	0.374	0.323	0.350	0.379	0.267	0.372	0.339	0.002	0.187
Ti	0.047	0.055	0.060	0.085	0.072	0.059	0.060	0.044	0.056	0.044	0.090	0.074	0.049	0.000	0.024	0.068	0.058	0.055	0.073	0.099	0.089
Fe^{3+}	0.314	0.324	0.198	0.004	0.181	0.014	0.553	0.459	0.240	0.215	0.321	0.135	0.018	0.033	0.261	0.241	0.492	0.191	0.318	0.628	0.521
Cr	0.000	0.000	0.000	0.000	0.000	0.000	0.000	0.000	0.000	0.000	0.000	0.000	0.000	0.000	0.000	0.000	0.000	0.000	0.000	0.000	0.000
Mg	2.202	2.303	2.197	2.231	2.260	2.332	2.115	2.503	1.821	1.972	1.903	1.697	2.634	2.670	2.630	1.920	1.957	1.855	1.959	1.429	1.988
Fe^{2+}	1.822	1.558	1.810	1.774	1.610	1.739	1.626	1.617	1.914	2.090	2.017	2.243	1.858	1.915	1.673	2.350	2.119	2.456	2.276	2.821	2.157
Mn	0.023	0.055	0.000	0.048	0.002	0.057	0.000	0.070	0.042	0.060	0.059	0.044	0.067	0.059	0.062	0.042	0.106	0.071	0.035	0.021	0.058
C	*5.000*	*5.000*	*5.000*	*5.000*	*5.000*	*5.000*	*5.000*	*5.000*	*5.000*	*5.000*	*5.000*	*5.000*	*5.000*	*5.000*	*5.000*	*5.000*	*5.000*	*5.000*	*5.000*	*5.000*	*5.000*
Mg	0.000	0.000	0.000	0.000	0.000	0.000	0.000	0.000	0.000	0.000	0.000	0.000	0.000	0.000	0.000	0.000	0.000	0.000	0.000	0.000	0.000
Fe^{2+}	0.000	0.000	0.008	0.000	0.000	0.000	0.028	0.000	0.000	0.000	0.000	0.000	0.000	0.000	0.000	0.000	0.000	0.000	0.000	0.000	0.000
Mn	0.002	0.016	0.045	0.001	0.049	0.004	0.067	0.005	0.043	0.025	0.002	0.022	0.005	0.009	0.004	0.052	0.011	0.004	0.010	0.032	0.001
Ca	1.996	1.965	1.886	1.853	1.786	1.895	1.796	1.989	1.908	1.947	1.996	1.952	1.969	1.953	1.992	1.889	1.976	1.991	1.979	1.965	1.997
Na	0.002	0.019	0.061	0.147	0.166	0.101	0.109	0.006	0.049	0.029	0.002	0.026	0.026	0.038	0.004	0.059	0.013	0.005	0.011	0.003	0.002
B	*2.000*	*2.000*	*2.000*	*2.000*	*2.000*	*2.000*	*2.000*	*2.000*	*2.000*	*2.000*	*2.000*	*2.000*	*2.000*	*2.000*	*2.000*	*2.000*	*2.000*	*2.000*	*2.000*	*2.000*	*2.000*
Na	0.255	0.170	0.227	0.052	0.082	0.224	0.180	0.230	0.395	0.227	0.220	0.251	0.274	0.114	0.231	0.339	0.294	0.402	0.371	0.297	0.405
K	0.082	0.068	0.064	0.097	0.102	0.101	0.109	0.126	0.082	0.142	0.172	0.133	0.153	0.089	0.112	0.281	0.306	0.301	0.341	0.377	0.328
A	*0.337*	*0.238*	*0.291*	*0.149*	*0.184*	*0.325*	*0.288*	*0.356*	*0.477*	*0.370*	*0.392*	*0.385*	*0.427*	*0.202*	*0.344*	*0.620*	*0.600*	*0.703*	*0.712*	*0.674*	*0.733*

Table 1 (continue) - Representative analyses of amphiboles from each Hbl-bearing rock type of Papikion Mt pluton based on 23 O.

Sample	15			925			602			603			911			14			220		
	core	int	Rim	core	int	rim	core	int	rim	core	int	rim	core	int	rim	core	int	rim	core	rim	rim
SiO_2	44.91	45.06	45.87	47.28	46.39	46.36	43.94	45.94	42.27	44.97	42.92	43.49	48.34	51.21	47.85	44.09	43.25	43.37	42.62	41.30	41.52
TiO_2	0.42	0.50	0.54	0.77	0.65	0.53	0.54	0.39	0.50	0.39	0.79	0.66	0.44	0.00	0.22	0.60	0.51	0.48	0.64	0.84	0.77
Al_2O_3	11.02	11.88	11.70	10.90	12.16	11.23	12.30	8.68	15.01	10.66	11.83	12.71	7.29	4.91	7.82	9.50	9.71	9.68	10.26	8.09	9.95
FeO	17.21	15.26	16.46	14.43	14.65	14.19	17.84	16.78	17.30	18.40	18.46	18.87	15.25	15.95	15.81	20.44	20.66	20.71	20.36	26.20	20.83
MnO	0.20	0.57	0.36	0.39	0.41	0.49	0.54	0.60	0.68	0.67	0.47	0.52	0.58	0.56	0.53	0.73	0.92	0.58	0.34	0.40	0.46
MgO	9.95	10.48	10.06	10.16	10.37	10.60	9.59	11.35	8.20	8.83	8.43	7.56	12.01	12.26	12.05	8.50	8.69	8.14	8.62	6.09	8.68
CaO	12.56	12.44	12.02	11.74	11.40	11.98	11.33	12.55	11.96	12.13	12.31	12.10	12.49	12.48	12.71	11.63	12.20	12.16	12.12	11.65	12.12
Na_2O	0.89	0.66	1.01	0.69	0.87	1.14	1.01	0.82	1.54	0.88	0.76	0.95	1.05	0.54	0.83	1.36	1.05	1.38	1.29	0.98	1.36
K_2O	0.43	0.36	0.34	0.52	0.54	0.53	0.58	0.67	0.43	0.74	0.89	0.69	0.82	0.48	0.60	1.45	1.59	1.54	1.75	1.88	1.67
Total	97.73	97.31	98.37	96.89	97.49	97.05	97.65	97.78	97.89	97.67	97.03	97.57	98.28	98.37	98.42	98.30	98.58	98.06	98.02	97.43	97.37
Si	6.664	6.642	6.716	6.965	6.781	6.845	6.501	6.795	6.294	6.737	6.498	6.550	7.110	7.479	7.001	6.682	6.537	6.628	6.496	6.501	6.383
Al IV	1.336	1.358	1.284	1.035	1.219	1.155	1.499	1.205	1.706	1.263	1.502	1.450	0.890	0.521	0.999	1.318	1.463	1.372	1.504	1.499	1.617
T	*8.000*	*8.000*	*8.000*	*8.000*	*8.000*	*8.000*	*8.000*	*8.000*	*8.000*	*8.000*	*8.000*	*8.000*	*8.000*	*8.000*	*8.000*	*8.000*	*8.000*	*8.000*	*8.000*	*8.000*	*8.000*
Al VI	0.592	0.705	0.737	0.857	0.876	0.799	0.646	0.308	0.927	0.619	0.610	0.807	0.374	0.323	0.350	0.379	0.267	0.372	0.339	0.002	0.187
Ti	0.047	0.055	0.060	0.085	0.072	0.059	0.060	0.044	0.056	0.044	0.090	0.074	0.049	0.000	0.024	0.068	0.058	0.055	0.073	0.099	0.089
Fe^{3+}	0.314	0.324	0.198	0.004	0.181	0.014	0.553	0.459	0.240	0.215	0.321	0.135	0.018	0.033	0.261	0.241	0.492	0.191	0.318	0.628	0.521
Cr	0.000	0.000	0.000	0.000	0.000	0.000	0.000	0.000	0.000	0.000	0.000	0.000	0.000	0.000	0.000	0.000	0.000	0.000	0.000	0.000	0.000
Mg	2.202	2.303	2.197	2.231	2.260	2.332	2.115	2.503	1.821	1.972	1.903	1.697	2.634	2.670	2.630	1.920	1.957	1.855	1.959	1.429	1.988
Fe^{2+}	1.822	1.558	1.810	1.774	1.610	1.739	1.626	1.617	1.914	2.090	2.017	2.243	1.858	1.915	1.673	2.350	2.119	2.456	2.276	2.821	2.157
Mn	0.023	0.055	0.000	0.048	0.002	0.057	0.000	0.070	0.042	0.060	0.059	0.044	0.067	0.059	0.062	0.042	0.106	0.071	0.035	0.021	0.058
C	*5.000*	*5.000*	*5.000*	*5.000*	*5.000*	*5.000*	*5.000*	*5.000*	*5.000*	*5.000*	*5.000*	*5.000*	*5.000*	*5.000*	*5.000*	*5.000*	*5.000*	*5.000*	*5.000*	*5.000*	*5.000*
Mg	0.000	0.000	0.000	0.000	0.000	0.000	0.000	0.000	0.000	0.000	0.000	0.000	0.000	0.000	0.000	0.000	0.000	0.000	0.000	0.000	0.000
Fe^{2+}	0.000	0.000	0.008	0.000	0.000	0.000	0.028	0.000	0.000	0.000	0.000	0.000	0.000	0.000	0.000	0.000	0.000	0.000	0.000	0.000	0.000
Mn	0.002	0.016	0.045	0.001	0.049	0.004	0.067	0.005	0.043	0.025	0.002	0.022	0.005	0.009	0.004	0.052	0.011	0.004	0.010	0.032	0.001
Ca	1.996	1.965	1.886	1.853	1.786	1.895	1.796	1.989	1.908	1.947	1.996	1.952	1.969	1.953	1.992	1.889	1.976	1.991	1.979	1.965	1.997
Na	0.002	0.019	0.061	0.147	0.166	0.101	0.109	0.006	0.049	0.029	0.002	0.026	0.026	0.038	0.004	0.059	0.013	0.005	0.011	0.003	0.002
B	*2.000*	*2.000*	*2.000*	*2.000*	*2.000*	*2.000*	*2.000*	*2.000*	*2.000*	*2.000*	*2.000*	*2.000*	*2.000*	*2.000*	*2.000*	*2.000*	*2.000*	*2.000*	*2.000*	*2.000*	*2.000*
Na	0.255	0.170	0.227	0.052	0.082	0.224	0.180	0.230	0.395	0.227	0.220	0.251	0.274	0.114	0.231	0.339	0.294	0.402	0.371	0.297	0.405
K	0.082	0.068	0.064	0.097	0.102	0.101	0.109	0.126	0.082	0.142	0.172	0.133	0.153	0.089	0.112	0.281	0.306	0.301	0.341	0.377	0.328
A	*0.337*	*0.238*	*0.291*	*0.149*	*0.184*	*0.325*	*0.288*	*0.356*	*0.477*	*0.370*	*0.392*	*0.385*	*0.427*	*0.202*	*0.344*	*0.620*	*0.600*	*0.703*	*0.712*	*0.674*	*0.733*

(Soltani and Carr, 2007, Toummite et al., 2012). Conclusion about the conditions of the crystallization of Papikion Mt pluton is that the pluton penetrated in deep and in relatively high pressures, about 5 kbar, considering the thin skarn zone (0,5-1,5 m approx.) of the pluton with the marbles (Bucher and Frey, 2002). Also the use of amphibole-plagioclase thermometer shows that the system has prevailed ion diffusion in the solid state to succeed a balance.

8. Acknowledgments

The first author wants to thank SCF (State Scholarship Foundation) for the financial support in the early years of his graduate studies.

9. References

Anderson J.L. and Smith D.R. 1995. The effect of temperature and oxygen fugacity on Al-in-hornblende barometry, *Amer. Mineral.*, 80, 549-559.

Beard J.S., Ragland P.C. and Crawford M.L. 2005. Reactive bulkassimilation: A model for crust-mantle mixing insilicic magmas, *Geological Society of America*, 33(8), 681–684.

Bonev N., Burg J.-P. and Ivanov Z. 2006. Mesozoic-Tertiary structural evolution of an extensional gneiss dome–the Kesebir-Kardamos dome, eastern Rhodope (Bulgaria-Greece), *Int. J. Earth. Sci.*, 95(2), 318-340.

Bucher K. and Frey M. 2002. *Petrogenesis of metamorphic rocks*, 7th edition, Springer-Verlag Berlin, Heidelberg, Germany, 341pp.

Burg J-P, Ricou L-E, Ivanov Z, Godfriaux I, Dimov D and Klain L. 1996. Syn-metamorphic nappe complex in the Rhodope Massif. Structure and kinematics, *Terra Nova*, 8, 6–15.

Burg J.P. 2012. Rhodope: From Mesozoic convergence to Cenozoic extension. In: Emmanuel Skourtsos and Gordon S. Lister (eds), *The Geology of Greece. Review of petro-structural data in the geochronological frame Journal of the Virtual Explorer*, Electronic Edition, ISSN 1441-8142, volume 42, paper 1.

Collins L.G. 2003. Transition from magmatic to K-metasomatic processes in granodiorites and Pyramid Peak granite, Fallen Leaf Lake 15-Minute Quadrangle, California. ISSN 1526-5757, no. 48, available online at: http://www.csun.edu/~vcgeo005/Nr48Fallen.pdf

Collins L.G. and Collins J.B. 2002. Myrmekite formation at Temecula, California, revisited: A photomicrographic essay illustrating replacement textures. ISSN 1526-5757, no. 43, available online at: http://www.csun.edu/~vcgeo005/Nr43Temecula.pdf

Dimades E. and Zachos S. 1985.Geological map of Rhodope 1:200.000. *IGME*.

Gerdjikov I. and Milev P. 2005. Nestos Shear Zone and structure of the metamorphic basement in the area south of Mesta graben, SW Bulgaria, *C.R. Acad. bulg. Sci.*, 58(2), 197-204.

Hammarstrom J.M. and Zen E.-A. 1986. Aluminium in hornblende: an empirical igneous geo-barometer, *American Mineralogist*, 71, 1297-1313.

Holland T. and Blundy J. 1994. Non-ideal interactions in calcic amphiboles and their bearing on amphibole-plagioclase thermometry, *Contrib. Mineral. Petrol.*, 116, 433-447.

Hollister L.S., Grisom G.C., Peters E.K., Stowell H.H. and Sisson V.B. 1987. Confirmation of the empirical correletion of Al in hornblende with pressure of solidification of calc-alkaline plutons, *American Mineralogist*, 72, 231-239.

Ivanov Ž. 1988. Aperçu général sur l'évolution géologique et structurale du massif des Rhodopes dans le cadre des Balkanides, *Bull. Soc. géol. Fr.*, 8, 227-240.

Johnson M.C. and Rutherford M.J. 1989. Experimental calibration of the aluminium-in-hornblende geobarometer with application to Long Valley caldera (California) volcanic rocks, *Geology*, 17, 837-841.

Krenn K., Bauer C., Proyer A., Klötzli U. and Hoinkes G. 2010. Tectonometamorphic evolution of the Rhodope orogen, *Tectonics*, 29.

Krohe A. and Mposkos E. 2002. Multiple generations of extensional detachments in the Rhodope Mountains (northern Greece): evidence of episodic exhumation of high-pressure rocks, in:

Blundell D. J., Neubauer F. and Von Quadt A. (eds). *The timing and location of major ore deposits in an evolving orogen*. Geological Society, Special Publication 204, London, 151-178.

Kronberg B., Meyer W. and Pilger A. 1970. Geologie der Rila-Rhodope-Masse zwischen Strimon und Nestos (Nord-Griechenland), *Beih. geol. Jb.*, 88, 133-180.

Kronberg B. and Raith M. 1977. Tectonic and metamorhism of the Rhodope crystalline complex in the Eastern Greek Macedonia and parts of the Western Thrace, *N. Jb. Geol. Paleont. Mh.*, 11, 697-704.

Leake B.E., Wooley A.R., Arps C.E.S., Birch W.D., Gilbert M.C., Grice J.D., Hawthorne F.C., Kato A., Kisch H.J., Krivovichev V.G., Linthout K., Laird J., Mandarino J.A., Maresh W.V., Nickel E.H., Rock N.M.S., Schumacher J.C., Smith D.C., Stephenson N.C.N., Ungaretti L., Whittaker E.J.W. and Youzhi G. 1997. Nomenclature of Amphiboles: Report of the Subcommittee on Amphiboles of the International Mineralogical Association, Commission on New Minerals and Mineral Names, *Can. Mineral.*, 35, 219-246.

Mposkos E. 1989. High-pressure metamorphism in gneisses and schists in the East Rhodope zone (N. Greece), *Mineral. Petrol.*, 41, 25-39.

Mposkos E. 1998. Cretaceous and tertiary tectonometamorphic events in Rhodope zone (Greece). Petrological and geochronological evidences, *Bull Geol Soc Greece*, 32(3):59–67.

Mposkos E. and Liati A. 1993. Metamorphic evolution of metapelites in the high-pressure terrane of the Rhodope zone, Northern Greece, *Can. Mineral.*, 31(2), 401-424.

Mposkos E.and Krohe A. 2000. Petrological and structural evolution of continental high-pressure (HP) metamorphic rocks in the Alpine Rhodope domain. In: Panaydes, I., Xenophontos, C., Malpas, J. (eds), *Proceedings of the 3rd international conference geology East Mediterranean*. Geol Surv Nicosia, Cyprus 1, 221–232.

Papanikolaou D. and Panagopoulos A. 1981. On the structural style of the Southern Rhodope, Greece, *Geol. Balc.*, Sofia, 11 (3), 13-22.

Schmidt M.W. 1992. Amphibole composition in tonalite as a function of pressure: an experimental calibration of the Al-in-hornblende barometer, *Contrib. Mineral. Petrol.*, 110, 304-310.

Schumacher J.C. 1997. The estimation of the proportion of ferric iron in the electron-microprobe analysis of amphiboles, *Can. Mineral.* 35, 238-246.

Soltani A. and Carr P.F. 2007. Thermobarometry of Ca-amphibole in a Typical Low–temperature I-type Granite from Kashmar, Iran, *Journal of Technology & Education*, 1(3), 47-54.

Streckeisen A. and Le Maitre R.W. 1979. A chemical approximation to the modal QAPF classification of the igneous rocks, *N. Jb. Min. Abh*., 136, 169-206.

Toummite A., Ikenne M. and Beraaouz E.H. 2012. Geothermobarometry of Askaoun Pluton in Ouzellarh-Sirwa Promontory (Central Anti-Atlas; Morocco), *Open Journal of Geology*, 2, 136-147.

Zachos S. and Demades E. 1983. The geotectonic position of the Scaloti-Echinos granite and its relationship to the metamorphic formation of Greek Westarn and Central Rhodope, *Geol. Balc.*, 13(5), 17-24.

Δελτίο της Ελληνικής Γεωλογικής Εταιρίας, τομ. XLVII , 2013
Πρακτικά 13ου Διεθνούς Συνεδρίου, Χανιά, Σεπτ. 2013

Bulletin of the Geological Society of Greece, vol. XLVII 2013
Proceedings of the 13th International Congress, Chania, Sept. 2013

MINEROLOGICAL AND PHYSICO-CHEMICAL PROPERTIES OF THE BUILDING MATERIALS OF KOULE CASTLE, HERAKLION, CRETE

Karampatsou G.[1], Markopoulos Th.[1], Repouskou E.[1] and Triantafyllou G.[1]

[1] Technical University of Crete, Dept. of Mineral Resourses Engineering, GR-73100 Chania, Greece gkarampatsou@isc.tuc.gr, markopou@mred.tuc.gr, repusku@mred.tuc.gr, gtriant@mred.tuc.gr

Abstract

This study was designed to determine the physical and technical characteristics of the building stones and mortars of the Koule Castle Heraklion, in order to use compatible materials in future restoration works. Five core samples of rocks and masonry mortars have been extracted from different parts of the monument. Both mortar and rock samples have been studied by optical microscopy and X-ray diffraction (XRD). Their morphological characteristics, granulometry and mineralogical composition have been determined. In the old mortars a thermogravimetric analysis was carried out, while mortar samples have also been studied by scanning electron microscopy. The building stones of Koule Castle are in their majority biomicritic breccia limestones and bioclastic limestones. The binder of the studied mortars consists of calcite, as a result of the lime carbonation. The inert material of the mortars consists mainly of calcite and secondarily of quartz. The inert to binder material ratio was determined by volume from 1/0,96 to 2,6 /1. In conclusion, the mortars to be used in future restoration works, should consist of compatible materials to the old mortars. The inert materials of the mortars should consist of quartz (70%) and secondarily of calcite (30%) and the binder of hydraulic lime NHL 3.5, in an inert material/ binder ratio of 2,5 /1, in order to protect the mortars against marine corrosion.

Key words: *Monuments, Building stones, Mortars, Conservation, Crete.*

Περίληψη

Η παρούσα εργασία στοχεύει στη διερεύνηση των φυσικοχημικών και ορυκτολογικών ιδιοτήτων των δομικών λίθων και κονιαμάτων του φρουρίου Κούλε Ηρακλείου, με σκοπό να επιτευχθεί συμβατότητα μεταξύ των αρχικών υλικών του φρουρίου και των υλικών που θα χρησιμοποιηθούν σε εργασίες μελλοντικών επεμβάσεων συντήρησης – συμπλήρωσης κονιαμάτων. Πέντε δείγματα πυρήνων διατρημάτων δομικών λίθων και τρία δείγματα κονιαμάτων τα οποία έχουν εξαχθεί από διάφορα σημεία του ενετικού φρουρίου, εξετάστηκαν ορυκτολογικά με περιθλασιμετρία ακτίνων Χ και οπτική μικροσκοπία και προσδιορίστηκαν τα μορφολογικά τους χαρακτηριστικά. Επιπλέον, στα δείγματα των κονιαμάτων έγινε κοκκομετρική ανάλυση, θερμική ανάλυση υψηλών θερμοκρασιών (TGA) και παρατηρήθηκαν στο ηλεκτρονικό μικροσκόπιο σάρωσης. Οι δομικοί λίθοι του ενετικού φρουρίου είναι κυρίως βιοκλαστικοί και μικριτικοί λατυποπαγείς ασβεστόλιθοι. Η κονία των κονιαμάτων χαρακτηρίζεται ως ασβεστιτική

ενώ τα αδρανή είναι κυρίως χαλαζιακής και δευτερευόντως ασβεστιτικής σύστασης με αναλογία κονία/αδρανές από 1/0.96 έως 1/2.6 κατ'όγκο. Σε κάθε εργασία μελλοντικών επεμβάσεων συντήρησης – συμπλήρωσης κονιαμάτων πρέπει να αξιολογούνται οι προς σύνδεση δομικοί λίθοι και τα κονιάματα να είναι συγγενούς κοκκομετρικής διαβάθμισης. Τα αδρανή πρέπει να είναι χαλαζιακής σύστασης (~70%) και δευτερευόντως ασβεστιτικής σύστασης (~30%) και στη σύσταση των κονιών που πρόκειται να εφαρμοσθούν για εργασίες συμπλήρωσης, απαιτείται προσθήκη υδραυλικής ασβέστου NHL 3.5 σε αναλογίες αδρανών προς κονία 2.5/1, προκειμένου τα κονιάματα να είναι ανθεκτικά στη θαλάσσια διάβρωση.
Λέξεις κλειδιά: *Μνημεία, Δομικοί λίθοι, Κονιάματα, Συντήρηση, Κρήτη.*

1. Introduction

The Koule Castle is an impressive fortress that surrounds the harbor of Heraklion, Crete (Fig.1). The Castle was erected by the Venetians in the early 13th century, when they conquered the town. The Venetians, who were undoubtedly the dominant force of the Mediterranean Sea from the 12th to the 15th century, remained in Crete for about 450 years (1204-1669). During that period of time, Crete becomes the highlight of their conquests and the harbor of Heraklion plays the most significant role for the Venetian trade to the East.

The earliest description of the Koule Venetian Castle exists in the designs of the Florentine monk Christoforo Buondelmonti in 1429. The architecture of the Castle is the typical Venetian architectural style. The construction was such that the walls of the Castle could protect the breakwater of the harbor.

In the early 16th serious damages have been repeatedly presented to the masonry of the fortress due to the force of the waves. The Venetians decided to demolish the Castle and construct a new one, stronger and better fortified against the new war techniques.

According to the floor plan, the new Koule Castle has an extension of about 3600 m^2 and an unusual shape compared with other fortification constructions. The Castle consists of two distinct parts: the southwest part featuring a rectangular shape and the southeast part an oval shape. However, the Venetian mechanics had underestimated the force of the Cretan Sea and the Castle remained with broken walls and weak foundations. Hence, the Turks managed to conquer the fortress in 1669 and to obtain the control of the harbor of Heraklion until the late 19th century.

During the Turkish domination time, the Koule Castle maintained its original shape but the Turks constructed a smaller fortress opposite of the Venetian Castle which called it "little Koule Castle". Unfortunately, this monument was demolished in 1936 due to the development of the town.

The aim of the present study is to determine the physical and technical characteristics of the building stones and mortars of the Koule Castle, in order to use compatible materials in future restoration works.

Figure 1 - Koule Castle, Heraklion, Crete.

2. Materials and Methods

2.1 Sampling

Five core samples of rocks and masonry mortars have been extracted by the 13th Municipality of Byzantine Antiquities from different parts of the monument (Table 1).The core samples consist of three rock + mortar specimens and two rock specimens. Various analyses were carried out, in order to determine their physical and technical characteristics as well as well as their deterioration state. The rock specimens present in their majority salt efflorescence (Fig.2) due to the sea water that enters the Castle.

Table 1 - Samples of the building materials of Koule Castle.

Location		Building Stones	Sedimentary Rock Types	Masonry Mortars
Ground floor	Internal wall	**1**	bioclastic limestone	**B**
	External wall	**2**	micritic breccia limestone	**A**
Upper floor	Internal wall	**3**	bioclastic limestone	**C**
		4	micritic conglomerate limestone	
Pavement		**5**	dolomitic limestone	

Figure 2 - Salt efflorescence on the external wall of Koule Castle, Heraklion, Crete.

Figure 3 - Sampling position of a building stone from the internal wall of Koule Castle. The drill hole was covered with a non compatible mortar.

2.2 Mineralogical Analyses

The mineralogical phases of both mortar and rock samples were identified by X-ray diffraction (XRD) using a BruckerAXS D-8 Advance powder diffractometer with a tube Cu anode (35Kv, 35mA). Calcium carbonate was determined by the Dietrich Fruhling gas volumetric method. Loss of ignition was determined by heating to 1050^{O}C.

2.3 Electron Microscopy and EDS Analyses

The mineralogical phases identified by X-ray diffraction were confirmed by means of a Scanning Electron Microscope. Selected mortar prisms were cut into cubes of approximately $10mm^3$ size, one side of which was polished flat. The microstructure and mineralogy of the specimens were studied in a Jeol 5400 scanning electron microscope equipped with an energy dispersion spectrometer (EDS) detector.

2.4 Thermal Analysis

The mortars' binder material was examined by thermogravimetric analysis in order to confirm the mineralogical phases identified by the previous analytical techniques and methods. Because of the dynamic character of thermogravimetry, one can distinguish from slope variations the release of CO_2 resulting from carbonation, in contrast to that emerging from the natural calcite. TGA analysis was performed at a 10^o C/min heating rate from 40^o C to 910^oC.

2.5 Grain Size Distribution

The mortars particle size analysis was carried out by wet sieving, in order to determine the nature of the constituents and evaluate the inert to binder material ratio. The sum of the 2mm – 0.125mm fractions is regarded as inert material, whereas the material finer than 0.125mm is regarded as the binder (Markopoulos et al., 1994).

2.6 Optical Microscopy

The rock specimens were investigated in thin sections using optical microscope. Most of the thin sections were cut vertically to the surface of the samples, in order to study the external corrosion and the morphological and mineral properties of the building rocks.

3. Results and Discussion

3.1 Mineralogical Analyses

3.1.1 Rock Samples

The mineralogical phases identified by means of XRD of the rock samples are summarized in Table 2. The building stones of Koule Castle consist mainly of calcite and quartz and the sample 5 mainly of dolomite. The majority of the specimens contain mica and plagioclase while sample 2 contains clinoclhore and sample 1 and 5 contain talc in low quantities.

Table 2 - XRD identification of samples 1,2,3,4 and 5.

Sample	Calcite	Quartz	Dolomite	Plagioclase	Mica	Talc	Clinochlore
1	+++	++	-	+	+	+	-
2	+++	++	-	+	+	-	+
3	+++	++	-	+	+	-	-
4	+++	++	-	+	-	-	-
5	++	++	+++	-	-	+	-

+++: dominantly present, ++: present, +: present in low quantities, -: not present

The high proportions of $CaCO_3$ and $CaMg(CO_3)_2$ explain the high loss of ignition values determined of the rock samples (Table 3). Furthermore, the measured content of $CaMg(CO_3)_2$ in sample 5 confirms the XRD analysis, which indicated the presence of dolomite in the same sample.

Table 3 - Calcium carbonate (%), Calcium Magnesium carbonate (%) and loss of ignition (%) of the rock samples.

Sample	$CaCO_3$ (%)	$CaMg(CO_3)_2$ (%)	L.O.I. (%)
1	77.91	0	34.54
2	71.79	0	32.33
3	92.45	0	39.77
4	94.31	0	38.62
5	9.73	73.45	38.02

The building stones of Koule Castle are sedimentary rocks, excavated nearby the harbor of Heraklion, where the monument was constructed. In their majority, they are bioclastic limestones with various marine fossils (Fig.4),micritic breccias(Fig.5) and micritic conglomerate limestones. Dolomitic limestones exist only in the pavement of the Castle.

Figure 4 - Thin section photograph of bioclastic limestone. ⊥ pollars (specimen 1).

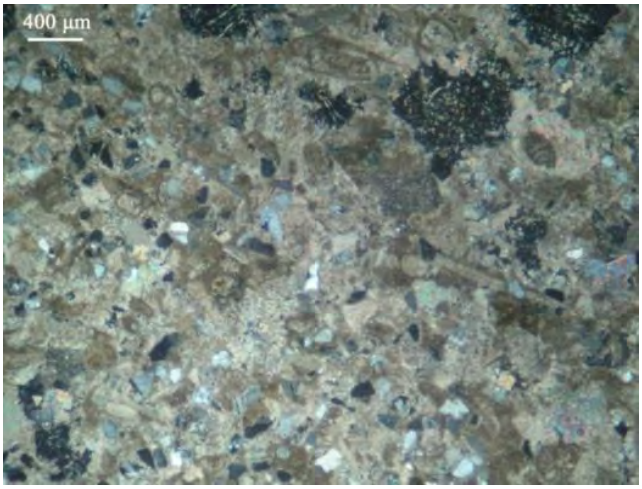

Figure 5 - Thin section photograph of micritic breccia limestone. ⊥ pollars (specimen 2).

3.1.2 Mortar Samples

The mineralogical phases identified by means of XRD of the mortar samples are presented in the XRD patterns below (Figs. 6, 7 and 8).

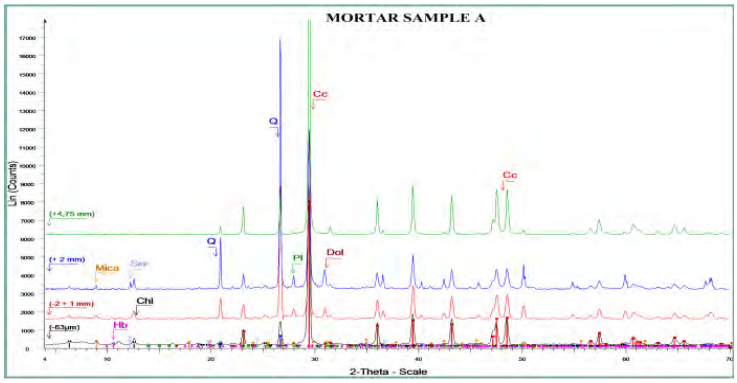

Cc: Calcite, Q: Quartz, Dol: Dolomite, Ser: Serpentine, Chl: Chlorite, Pl: Plagioclase, Hb: Hornblende

Figure 6 - XRD pattern of the binder and inert material of mortar sample A.

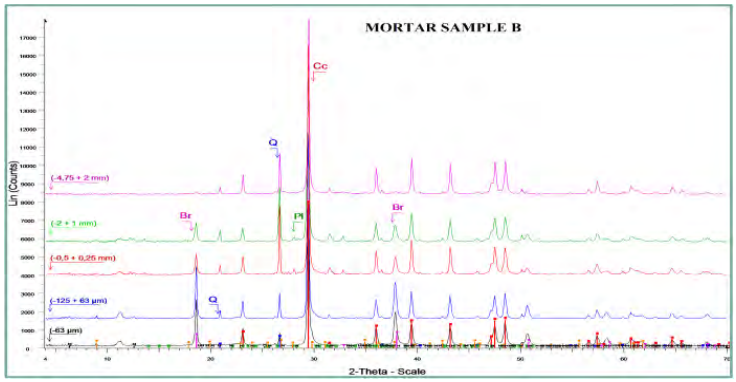

Br: Brucite

Figure 7 - XRD pattern of the binder and inert material of mortar sample B.

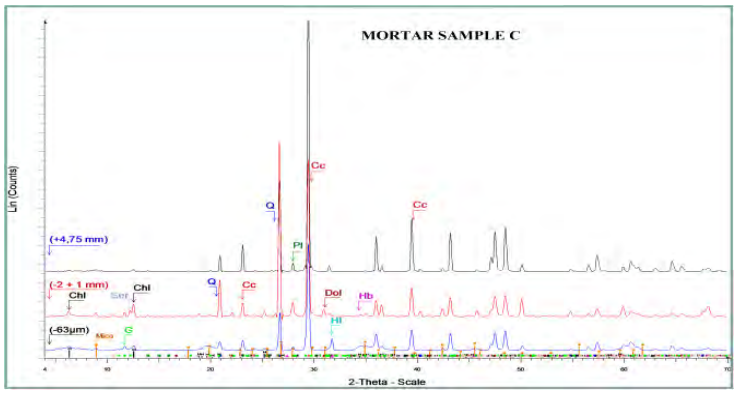

G: Gypsum Hl: Halite

Figure 8 - XRD pattern of the binder and inert material of mortar sample C.

Calcite and quartz were detected in the binder and in the inert material of the mortars. The quartz peaks in the XRD spectra are greater for the inert material while the calcite peaks are greater for the binder material of the mortars. Plagioclase, mica, chlorite and hornblende were detected in the binder and in the inert material of mortar samples A and C (Fig. 6, Fig. 8), while dolomite and serpentine exists only in the inert material of these mortars. Plagioclase, brucite and traces of mica and chlorite; were detected in the binder and in the inert material of mortar sample B. Consequently, the binder of the studied mortars consists mainly of calcite as a result of the lime carbonation. The inert material of the mortars consists mainly of quartz and secondarily of calcite. The presence of brucite in sample B (Fig. 7) is probably associated with the absence of adequate carbon dioxide in the interior parts of the castle. Furthermore, the presence of gypsum in sample C (Fig.8) is attributed to the process of mortar deterioration by sulfating. The sulfates, coming from the marine environment, were deposited on the surface and reacted with $CaCO_3$, present in the mortar, according to Eqs. 1a and 1b. The mechanism of sulfating has not resulted in the formation of ettringite because of the absence of "calcium aluminate hydrate"($3CaO\ Al_2O_36H_2O$) (Sabbioni et al., 2001).

$$\mathbf{CaCO_3 + SO_2 + 0.5\ H_2O \rightarrow CaSO_3 \cdot 0.5H_2O + CO_2} \quad (1a)$$

$$\mathbf{2CaCO_3 \cdot 0.5\ H_2O + O_2 + 3H_2O \rightarrow 2CaSO_4 \cdot 2H_2O} \quad (1b)$$

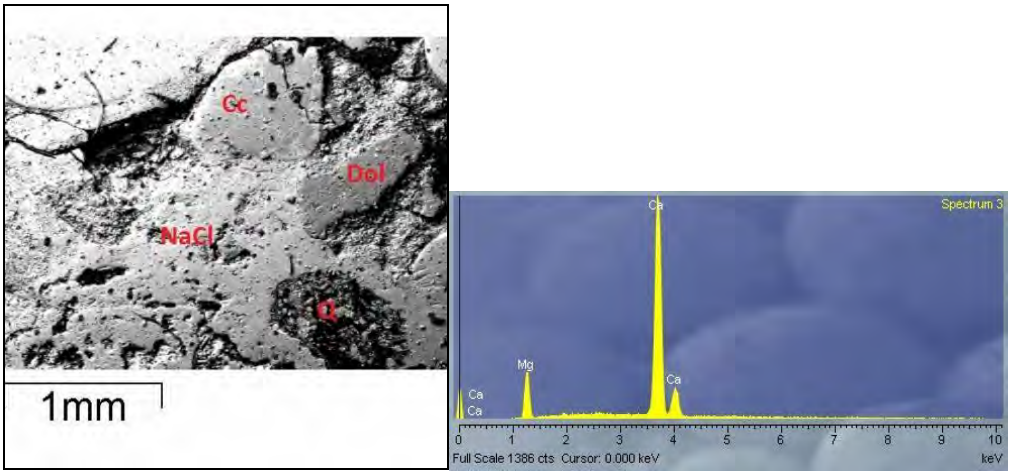

Figure 9 - Backscattering image of the mortar A and EDS analysis of dolomite.

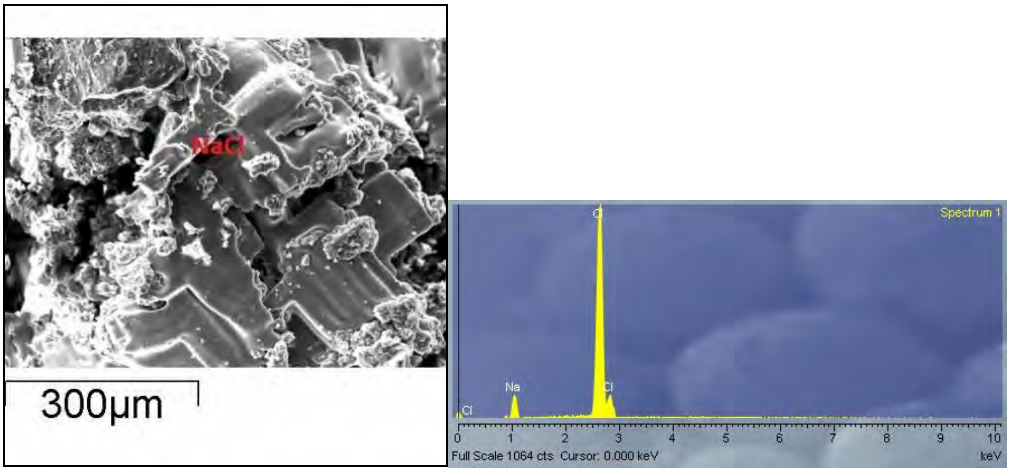

Figure 10 - SEM micrographic of the mortar C and EDS analysis of halite.

3.2 Thermal analysis

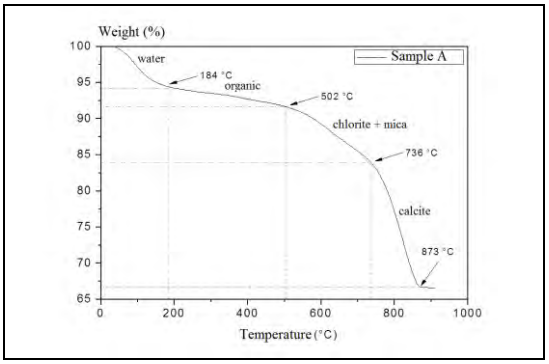

Figure 11 - Thermal curve of sample A.

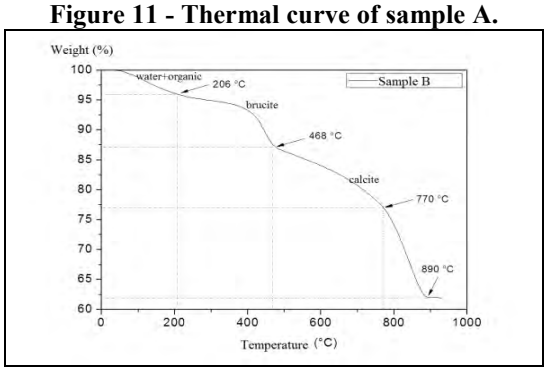

Figure 12 - Thermal curve of sample B.

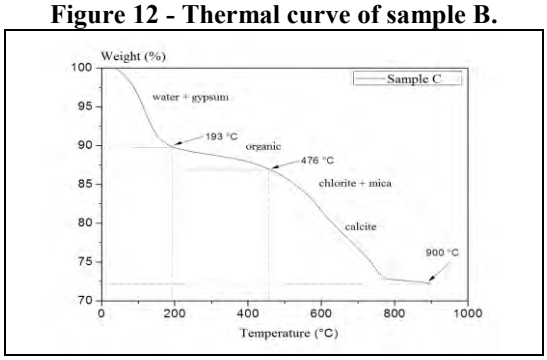

Figure 13 - Thermal curve of sample C.

Thermogravimetric (TG) analysis is necessary to establish the characteristics of the ancient mortars. TG analysis indicated a notable effect of calcite decomposition at about 900^{o}C, as a result of the carbonation of the original lime binder (Figs. 11, 12 and 13). Chlorite and mica decomposition took place at 500 ^{o}C – 600 ^{o}C in the samples A and C (Figs. 11 and 13).The losses of mass for the three mortars between 20 ^{o}C and 200 ^{o}C corresponded to the loss of water and to the loss of organic elements later. A greater loss of mass occurred between 20 ^{o}C and 200 ^{o}C in the sample C; which indicates the decomposition of the content gypsum. For the TG curve obtained of sample B, an endothermic peak was observed at about 400 ^{o}C which corresponds to the dissociation of brucite.

3.3 Grain Size Distribution

According to the histogram (Fig. 14) sample B presents a normal granulometric distribution. The inert to binder material ratio was determined 1.4/1, by volume. Sample A is the finest of the three studied mortars, due to the fact that more than 50% of this material is concentrated in the base

sieve. The inert to binder material ratio for the sample A was determined 0.96/1 by volume. Sample C contains much more aggregates than the other mortar samples. The inert to binder material ratio for the sample C was determined 2.6/1 by volume.

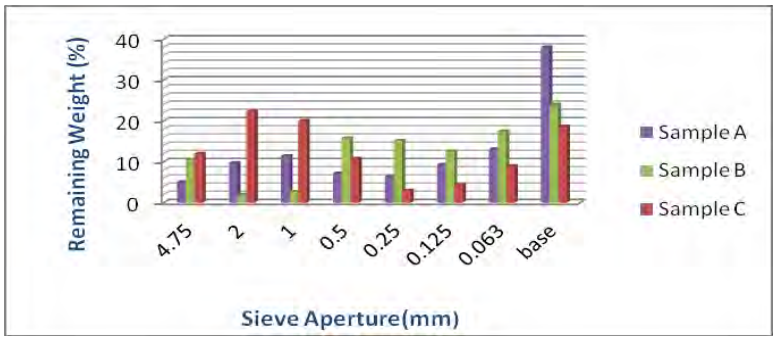

Figure 14 - Weight (%) of the samples which remains in every sieve aperture.

3. Conclusions

The following conclusions can be drawn from the study:

- The building stones of Kule Castle are bioclastic limestones, micritic breccia limestones, micritic conglomerate limestones and dolomitic limestones, excavated nearby the harbor of Heraklion.
- The mineralogical components of the building stones are mainly calcite and quartz and secondarily plagioclase, mica, talc and clinochlore. The dolomitic limestone contains dolomite as the main mineral phase.
- The inert material of the mortars consists mainly of quartz and secondarily of calcite. The inert to binder material was determined by volume from 0.96/1 to 2.6/1. Their examination revealed that beach sand has been used as inert material.
- The presence of brucite in the inert material of mortar B, as well as the presence of dolomite in the inert material of mortar A and mortar C, indicates the use of dolomites or Mg-rich limestones as aggregates. Due to the absence of adequate carbon dioxide, brucite was never converted to magnesium carbonate.
- The binder of the studied mortars consists mainly of calcite as a result of the lime carbonation. The lime used as binder of mortar A and mortar C came from bioclastic limestones, while the presence of brucite in the inert material of mortar B indicates that the lime used as binder of this mortar came from dolomites or Mg-rich limestones.
- The mortars to be used in future restoration works, should consist of compatible materials to the old mortars. The inert materials of the mortars should consist of quartz (70%) and secondarily of calcite (30%) and the binder of hydraulic lime NHL 3.5, in an inert material/ binder ratio of 2,5 /1, in order to protect the mortars against marine corrosion.

4. References

Markopoulos Th., Maravelaki P. and Repouskou E. 1994. The materials of the Venetian fortifications in Chania: properties, weathering forms and mechanisms. *III Inter. Symp. on the conservation of Monuments in the Mediterranean Basin,* Ed. By V. Fassina, H. Ott, F.Zezza. Venice, 22-25 june 1994, 687-692.

Sabbioni C., Zappia G., Riontino C., Blanco –Varela M.T., Aguilera J., Puertas F., Van Balend K. and Toumbakarid E.E. 2001. Atmospheric deterioration of ancient and modern hydraulic mortars, *Atm Envon.*, 539-548.

Δελτίο της Ελληνικής Γεωλογικής Εταιρίας, τομ. XLVII , 2013
Πρακτικά 13ου Διεθνούς Συνεδρίου, Χανιά, Σεπτ. 2013

Bulletin of the Geological Society of Greece, vol. XLVII 2013
Proceedings of the 13th International Congress, Chania, Sept. 2013

A MINERALOGICAL STUDY OF PIGMENTS USED IN TWO IAKOVIDIS PAINTINGS: VERIFICATION OF ARTWORK AUTHENTICITY USING RAMAN MICRO-SPECTROSCOPY METHOD

Kougemitrou I.[1], Economou G.[2], Giovanopoulos J.[3], Baziotis I.[4, 5], Leontakianakos G.[6] and Stathopoulos V.[6]

[1]Harokopio University, Department of Geography, 70 El. Venizelou, 17671 Kallithea, Athens, Greece, ekougemitrou@hua.gr

[2]Institute of Geology and Mineral Exploration (IGME), Department of Mineralogy and Petrography, c. entrance, Olympic village, 13677 Acharnai, Greece, dop@igme.gr

[3]Nikias Research Centre of Certification, Maintenance and Restoration of art works, Cyprou 57, Athens, Greece, info@nikias.gr

[4]Department of Mineralogy, Petrology and Economic Geology, School of Geology, Aristotle University of Thessaloniki, 54124, Thessaloniki, Greece, ibaziotis@geo.auth.gr, baziotis@metal.ntua.gr

[5]Department of Earth Sciences, University of Perugia, 06100 Perugia, Italy

[6]Technological Educational Institution of Halkida, 34400 Psachna, Evia Island, Greece, gleontakianakos@yahoo.gr, vasta@teihal.gr

Abstract

For the purpose of the current study, we examined two paintings, an original and a fake one, entitled "Still life with grapes", and claimed both to be created from the Greek Painter G. Iakovidis. The current Research Project has been carried out at the Centre Nikias, an innovative Research Centre specialised on certification, maintenance and restoration of art works.

Raman spectroscopic analysis has been carried to verify the authenticity of the used pigments and also the originality of the two paintings. The Raman spectra acquired confirmed four different colours in both painting`s pigments: red, blue, white and yellow. For the first painting Cinnabar for the red pigment, Ultramarine for the blue pigment, White earths for the white pigment and Yellow ochre for the yellow pigment. In the second painting the colours used verified as synthetic pigments. We identified the presence of Cadmium red for the red colour, Cobalt blue for the blue pigment, Zinc white for the white and Cadmium yellow for the yellow one.

Key words: *Raman spectroscopy, painting authenticity, archaeometry.*

Περίληψη

Για τον σκοπό της παρούσας μελέτης, εξετάσαμε δύο πίνακες, ένα πρωτότυπο και ένα πλαστό, με τίτλο «Νεκρή φύση με σταφύλια". Και οι δυο πίνακες θεωρητικά είχαν φιλοτεχνηθεί από τον Έλληνα ζωγράφο Γ. Ιακωβίδη. Η παρούσα ερευνητική εργασία πραγματοποιήθηκε στο Ερευνητικό Κέντρο Νικίας, ένα καινοτόμο Κέντρο που

εξειδικεύεται στην πιστοποίηση, συντήρηση και αποκατάσταση έργων τέχνης. Η ανάλυση των χρωστικών ουσιών πραγματοποιήθηκε με την χρήση της φασματοσκοπίας Raman προκειμένου να επαληθευτεί η γνησιότητα των χρησιμοποιούμενων χρωστικών και ως εκ τούτου η αυθεντικότητα των δύο πινάκων. Τα φάσματα Raman που αποκτήθηκαν επιβεβαιώνουν τέσσερα διαφορετικά χρώματα για τις χρωστικές που χρησιμοποιήθηκαν για τη ζωγραφική των δυο πινάκων: κόκκινο, μπλε, λευκό και κίτρινο. Για τον πρώτο πίνακα, η κιννάβαρι χρησιμοποιήθηκε για την κόκκινη χρωστική ουσία, το Ultramarine για τη μπλε χρωστική, οι Λευκές γαίες για την λευκή χρωστική και η κίτρινη ώχρα για την κίτρινη χρωστική ουσία. Στον δεύτερο πίνακα, τα χρώματα που χρησιμοποιήθηκαν είναι συνθετικές χρωστικές. Εντοπίσαμε την παρουσία κόκκινου του καδμίου για το κόκκινο χρώμα, το μπλε του κοβαλτίου για τη μπλε χρωστική ουσία, το λευκό του ψευδαργύρου για το λευκό χρώμα και το κίτρινο του καδμίου για το κίτρινο χρώμα αντίστοιχα.
Λέξεις κλειδιά:*Φασματοσκοπία Ραμαν, αυθεντικότητα πίνακα, αρχαιομετρία*.

1. Introduction

Art works have, for many centuries, constituted a point of high interest, and even worship. The quality and the spirituality the works have expressed, their creator's fame and their purchase value offered an elevation to their owners' status. Nowadays their acquisition, other than the aforementioned aesthetic and cultural education, it constitutes an alternative form of investment globally.

While this market began to extend, the value of many works of art soared to extraordinary amounts. At the same time the systematic copy and sale of counterfeit work was developed and extended. This fact created the need for a certification of the art work's authenticity. The long and insisting investigation and experimentation in materials along with different methods have helped individuals obtain the ability to distinguish the fakes from the originals. However, the development of technology and the ease of access in information, provide creators of counterfeit work with an arsenal of techniques and methods of reproduction that make it almost impossible to distinguish the authentic works by traditional means and methodology.

Raman spectroscopy has become an important technique in Art studies and Art History since about 1996, Ravindran et al. (2011), due principally to its non-destructive capacities, small amount of sample required, "no sample treatment", and high spatial resolution.

Textbook explanations of Raman Spectroscopy for Geologists, Gemmologists and Archaeologists are provided in Smith and Carabatos-Nedelec (2001) and Nasdala et al. (2004), and reviews on MRM applications are available in Smith (2002, 2005, 2006). Furthermore, various databases for art work, depicting minerals, media, pigments as well as synthetic pigments can be found in Bell et al. (1997), Burgio and Clark (2001), Bouchard (2001), Bouchard and Smith (2003).

Other commercially available databases are: S.T. Japan Europe GmbH (http://www.stjapan-europe.de) with 8.694 searchable Raman spectra of hydrocarbons, dyes, pigments, minerals and inorganics, Fiveash Data Management Inc. (http:// fdmspectra.com) with 6051 mineral spectra and 600 Raman spectra of organics, Thermo Fisher scientific Inc. (http://ramansearch.com) over 16000 Raman spectra and RASMIN Raman spectra database of minerals and inorganic materials.

An in situ analytical operation was carried out at the premises of Nikias Centre in two art works both to be claimed as G. Iakovidis's paintings. Extended, non-destructive analysis of the pigments was carried out in an attempt to identify the pigments and thus reveal the originality of the art works. One can simply edit the document you are now viewing.

2. Materials and Methods

Two painting were studied by means of Raman spectroscopy. The paintings studied are depicted in Figure 1.They are both of same dimensions 50.5×33 cm, made of oil in canvas.

A Delta Nu Inspector Raman was used at Nikias Research Centre of Athens, Greece. The analyses were carried out using a near infrared 785nm laser. A calibration of the instrument was obtained with a standard of Si yielding a characteristic peak at the 520.5 cm-1. Preparation of the samples was not at all necessary and the paintings were simply placed in front of the focused 785nm laser beam in their normal form. The video camera of the Raman system was employed in order to be able to observe magnified images on different areas of the paintings. The power of the laser was 120mW at the source. The Raman spectra were acquired using accumulation time of 10s for a frequency range 200-1800 cm-1. The Raman spectra were processed with the Nuspec software.

Figure 1 - Still life with grapes, oil in canvas. Both paintings claimed to be painted by G. Iakovidis.

3. Results and Discussion

The Raman spectra acquired during the analysis of the paintings, confirmed the authenticity of one of the paintings.

The examination has shown that different pigments were used in the two paintings. As regards the first painting the pigments detected were: Cinnabar for the red pigment used in red grapes, the signature of the artist, the patterns on the table cover and the inner part of the bowl. Cinnabar has its main characteristic Raman band at about 244cm-1 (Figure 2a). Ultramarine for the blue pigment used in blue grapes and the patterns on the table cloth. Ultramarine has its main characteristic Raman band at about 545cm-1 (Figure 2b). The white pigment used in light shading of the grapes, patterns, platter and bowl gave a Raman spectra with characteristic band at 385 and 1085 cm-1 attributable to white earths (Figure 2c). Yellow ochre which have characteristic peak at 368 cm-1(Figure 2d) has been used for the background, table cloth, bowl and platter.

The identification of the prementioned mineral pigments indicates that this painting represents the authentic one.

In the second painting, denoted as “fake”, the colours used verified as synthetic pigments. In particular, we identify the presence of Cadmium red (main Raman peaks at 1390, 1549 and 1592 cm-1) for the red pigment used to paint the red grapes, the red patterns on the table cloth and the signature of the artist (Figure 3a). Cadmium yellow (Raman peaks at 222, 317, 1301 and 1446 cm-1) for the yellow pigments used for the platter, bowl, table cloth and background (Figure 3b). Zinc white (Raman peaks at 438, 1299 and 1443 cm-1) for the white pigment used in lighting shades (Figure 3c) and Cobalt blue (Raman peaks at 1336 and 1524 cm-1) for the blue pigment used for blue grapes and pattern on the table cloth (Figure 3d).

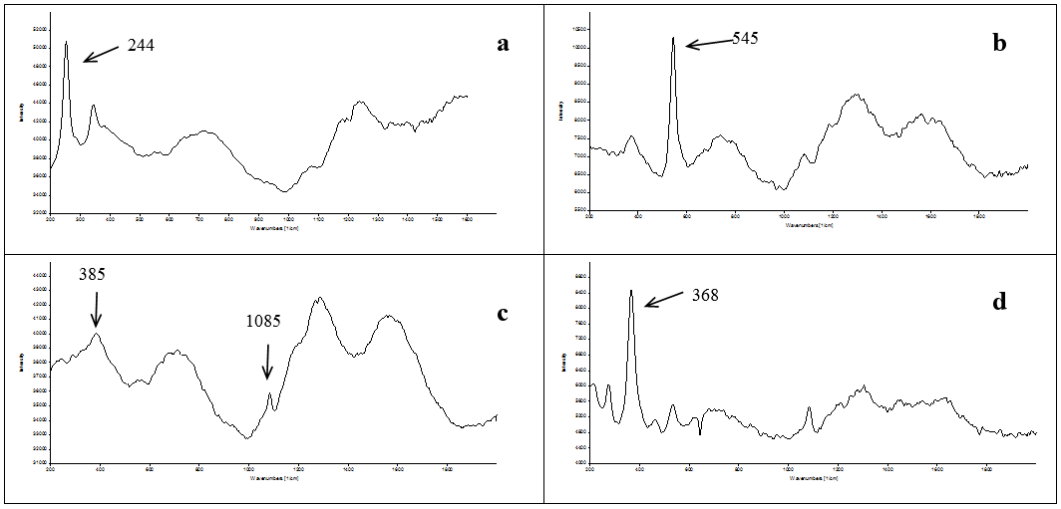

Figure 2 - Raman spectra of pigments used in the original Iakovidis's painting: a. Cinnabar, b. Ultramarine, c. White earths, d. Yellow ochre.

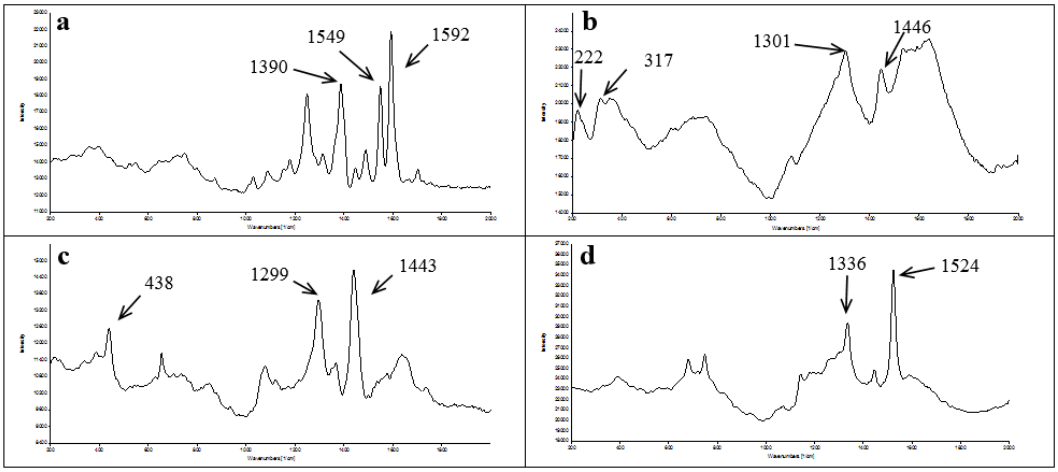

Figure 3 - Raman spectra used in the "fake" Iakovidis's painting: a. Cadmium red, b. Cadmium yellow, c. Zinc white, d. Cobalt blue.

The pigments used in the second painting were modern synthetic pigments which weren't in use during the active period of the mentioned painter (1853-1932 A.C.). A further comparison of the results with Centre Nikias's extended database demonstrates the release of the current synthetic pigments after Iakovidis death. During Iakovidis era, painters used mainly minerals as colorants due to their physical structure and reaction with binding agents (oil, gum Arabic, glue, gelatine etc.) which gave a superbly flexible and permanent paint film Willard et al. (1981), Arvin (1991).

4. Conclusions

The comparison of each spectrum with the extended database of Nikia's Centre revealed the presence of the pigments used in one of the paintings as following: Cinnabar for the red pigment, Ultramarine for the blue pigment, White earths for the white pigment and Yellow ochre for the yellow pigment. The identification of the mineral pigments indicates that this painting represents the authentic one. In the second painting, denoted as "fake", the colours used verified as synthetic

pigments. In particular, we identify the presence of Cadmium red for the red, Cadmium yellow for the yellow, Zinc white for the white and Cobalt blue for the blue pigment.

5. Acknowledgments

The authors would like to acknowledge Mr J. Giouvanopoulos owner of the Research Centre Nikias for the data provided.

6. References

Arvin L. 1991. Scribes, Scripts and Books: *The Book of Art from Antiquity to the Renaissance*, Chicago, IL: American Library Association.

Bell M., Clark R.J.H. and Gibbs P.J. 1997. Raman spectroscopic library of natural and synthetic pigments (pre w1850 AD), *Spectrochimica Acta,* A 53, 2159–2179.

Bouchard M. 2001. Evaluation des Capacités de la Microscopie Raman dans la Caractérisation Minéralogique et physicochimique de Matériaux Archéologiques: Métaux, Vitraux & Pigment, PhD dissertation, Museum national d'histoire naturelle, *Spectrochimica Acta,* Part A, 57, 1491–1521.

Bouchard M. and Smith D.C. 2003. Catalogue of 45 reference Raman spectra of minerals concerning research in art history or archaeology, especially on corroded metals and coloured glass, *Spectrochimica Acta,* Part A, 59, 227–266.

Burgio L. and Clark R.J.H. 2001. Library of FT-Raman spectra of pigments, minerals, pigment media and varnishes, and supplement to existing library of Raman spectra of pigments with visible excitation, *Spectrochimica Acta,* Part A, 57, 1491-1521.

Nasdala L., Smith D.C., Kaindl R., Gaft M. and Ziemann M.A. 2004. Raman spectroscopy: Analytical perspectives in mineralogical research, in: *Spectroscopic Methods in Mineralogy* (A. Beran & E. Libowitzky, editors). EMU Notes in Mineralogy 6, Eotvos University Press, Budapest, 281-343.

Ravindran T.R., Arora A.K., Ramya S., Subba Rao R.V. and Baldev Raj J. 2011. Raman spectroscopic study of medieval Indian art of 17th Century, *Raman Spectroscopy*, 42, 803.

Smith D.C. and Carabatos-Nedelec C. 2001. Raman Spectroscopy Applied to Crystals: Phenomena and Principles, Concepts and Conventions, in: LEWIS, I. and EDWARDS, H.G.M. (Eds), *A Handbook on Raman Spectroscopy*, 9, 349-422, Marcel Dekker Inc.

Smith D.C. 2002. Archaeoraman and Mobile Raman Microscopy (MRM): from pigments in aerial wall-paintings to gemstones in submarine archaeometry, *Congress Georaman, Acta Universitatis Carolinae, Geologica*, Praha, 46/1, 84-86.

Smith D.C. 2005. Jewellery and precious stones, Raman Spectrometry in Archaeology and Art History, *The Royal Society of Chemistry*, 21, 335-378.

Smith D.C. 2006. A review of the non-destructive identification of diverse geomaterials in the Cultural Heritage using different configurations of Raman Spectroscopy, in: Maggetti, M., Messiga, B. (Eds). Invited paper, ch. 2, 9-32. Proceedings, 32nd International Geological Congress, Florence, August 2004, "Geomaterials in Cultural Heritage", Geol. Soc. London, Spec. Pub., 257. .

Willard H.H., Meritt L.L., Dean J.A. and Settle F.A. 1981. *Instrumental Methods of Analysis*, 6th ed., Van Nostrand: New York, ch. 2.

Δελτίο της Ελληνικής Γεωλογικής Εταιρίας, τομ. XLVII , 2013
Πρακτικά 13ου Διεθνούς Συνεδρίου, Χανιά, Σεπτ. 2013

Bulletin of the Geological Society of Greece, vol. XLVII 2013
Proceedings of the 13th International Congress, Chania, Sept. 2013

METAMORPHIC RECORD IN METALHERZOLITE POCKETS WITHIN THE VIRSINI METAHARZBURGITE FROM THE KECHROS HP METAMORPHIC COMPLEX IN EASTERN RHODOPE, GREECE

Mposkos E.[1] and Perraki M.[1]

[1]*National Technical University of Athens, School of Mining and Metallurgical Engineering, 9 Heroon Politechniou St., 15773, Athens, mposkos@metal.ntua.gr, maria@metal.ntua.gr*

Abstract

The Virsini antigorite serpentinite from the Kechros HP metamorphic complex in eastern Rhodope is a serpentinized harzburgite with pockets of lherzolitic composition. In the metalherzolites the mantle assemblage is Ol-1+Opx+Cpx-1+Cr-Spl. The metamorphic assemblage is Atg+Ol-2+Cpx-2+Ol-3+Chl+Tr+Cr-Mag. Antigorite and Cr-magnetite formed in an early stage of the metamorphic event. With increase in metamorphic grade olivine (Ol-2) was formed at the expense of antigorite and with further increase tremolite, olivine (Ol-3) and chlorite were formed at the expense of clinopyroxene and antigorite. P-T conditions of ≈1.7 GPa/≈570 °C are recorded in neighbouring eclogites. For the temperature of 570 °C the reaction Di+Atg→Ol+Tr+H_2O occurs at pressure of ~1.2 GPa suggesting that the stability field of the mineral assemblage Atg+Ol+Tr in the metalherzolite is crossed during decompression.

Key words: *Antigorite serpentinite, high pressure, Kechros complex, Rhodope.*

Περίληψη

Ο αντιγοριτικός σερπεντινίτης της Βυρσίνης (Α. Ροδόπη) ανήκει στην υψηλών πιέσεων μεταμορφική ενότητα του Κέχρου. Πρόκειται για έναν σερπεντινιωμένο χαρτσβουργίτη με θύλακες λερζολιθικής σύστασης. Οι μεταλερζόλιθοι χαρακτηρίζονται από τη μανδυακή παραγένεση Ol-1+Opx+Cpx-1+Cr-Spl. Κατά τη μεταμόρφωση έχει σχηματιστεί το ορυκτολογικό άθροισμα Atg+Ol-2+Cpx-2+Ol-3+Chl+Tr+Cr-Mag. Ο αντιγορίτης και ο χρωμιούχος μαγνητίτης αναπτύσσονται κατά τα πρώτα στάδια της μεταμόρφωσης. Με αύξηση του βαθμού μεταμόρφωσης αναπτύσσεται αρχικά ολιβίνης (Ol-2) αντικαθιστώντας αντιγορίτη και στη συνέχεια τρεμολίτης, ολιβίνης (Ol-3) και χλωρίτης αντικαθιστώντας κλινοπυρόξενο και αντιγορίτη. Οι συνθήκες P-T στους γειτονικούς εκλογίτες είναι ≈1.7 GPa/≈570 °C . Για θερμοκρασία 570 °C η αντίδραση Di+Atg→Ol+Tr+H_2O λαμβάνει χώρα κατά την αποσυμπίεση σε πίεση ~1.2 GPa.

Λέξεις κλειδιά: *αντιγοριτικός σερπεντινίτης, μεταμόρφωση υψηλών πιέσεων, ενότητα Κέχρου.*

1. Introduction

Peridotite bodies occur in numerous high-pressure (HP) metamorphic terrains within orogens involving major continental collisions. They usually form lens-shaped masses, normally within metamorphosed continental crustal rocks, but also within rocks of oceanic affinity. The lenses range in size from small (ca. 1 m across) to enormous (>100 Km^2 in outcrop area). In general, peridotites in gneiss terrains record the emplacement of mantle material into the continental crust and reveal the composition of the upper mantle and the nature of mantle/crust interaction processes (Brueckner and Medaris, 2000). Peridotites in metamorphic terrains potentially provide excellent information about temperature regimes. Phase relations for peridotites of harzburgitic and lherzolitic bulk compositions have been used to decipher details of the metamorphic evolution of a terrain (i.e.Trommsdorff and Evans, 1974; Mposkos et al., 2010; Padron-Navarta et al., 2011).

The Rhodope Domain extends over large areas of northern Greece and southern Bulgaria. It incorporates several tectonic slivers of reprocessed pre-Alpine crust, including Variscan granitoids, post-Variscan oceanic and continental margin sediments as well as igneous rocks subsequently subjected to HP metamorphism(s) (for protolith- and metamorphic ages see references in Burg, 2011; and Liati et al., 2011).

Mposkos and Krohe (2000) and Krohe and Mposkos (2002) subdivided the Greek part of the Rhodope domain into several tectonometamorphic units. These segments differ in P-T conditions during their Alpine HP metamorphism, and timing of exhumation. In the eastern Greek Rhodope the upper tectonic unit (Kimi complex; Mposkos and Krohe, 2000; 2006, Figure 1), shows a late Jurassic high-temperature eclogite facies, followed by Cretaceous granulite and upper amphibolite facies metamorphisms. The lower tectonic unit (Kechros complex; Mposkos and Krohe, 2000) experienced a low temperature eclogite facies followed by albite-epidote amphibolite- to lower amphibolite facies metamorphism (Mposkos, 1989; Mposkos et al., 2012). Ultramafic rocks occur in both tectonic units.

In the Kimi complex a garnet-spinel bearing lherzolitic meta-peridotite which contains layers of spinel-garnet clinopyroxenites, indicates an early high temperature and (U)HP metamorphism followed by cooling at substantial depth associated with relatively little decompression (Mposkos and Krohe, 2006). P-T conditions of >3 GPa and 1235 ^{o}C were estimated from the assemblage Ol-Opx-Cpx-Spl-Grt (abbreviations after Whitney and Evans, 2010). In the clinopyroxenites, garnet- and spinel exsolution lamellae in clinopyroxenes, indicate that cooling started already in the garnet pyroxenite stability field. Hydration reactions like Grt+Opx+W→Ol+Hbl and Opx+Cpx+Spl+W→Hbl+Ol indicate decompression and cooling to below 1.2-1.3 GPa at 650-750 ^{o}C (Mposkos and Krohe, 2006).

In the Kechros complex large bodies of antigorite serpentinites like those from Dadia and Virsini areas (Figure1) represent the mantle assemblage. However, mineral assemblages, textures and mineral chemistry data which record the metamorphic evolution of these ultramafic rocks have yet to be reported.

In this paper we provide textural relationships and mineral compositions of the primary and the metamorphic mineral phases from metalherzolite pockets occurring within the Virsini antigorite serpentinite (metaharzburgite) and compare the metamorphic P-T path of the metaperidotite with that of the surrounding crustal rocks.

2. Geological Setting

The Kechros Complex consists of orthogneisses, reworked migmatites (containing muscovite metapegmatite lenses), pelitic gneisses, high-alumina metapelites and scarce marbles. Large serpentinized peridotites are tectonically intercalated. Within orthogneisses, serpentinites and between serpentinites and underlying metapelites, boudins of eclogites, eclogite amphibolites and

amphibolites occur. HP metamorphism at P-T conditions of 1.7-2.2 GPa and 570-620 ^{0}C were reported from the eclogites (Mposkos et al., 2012). In the orthogneisses and metapelites the HP event is indicated by the presence of high-Si phengites (Mposkos, 1989). In metapelites staurolite formed by the reactions Cld + Ph → St + Chl + Ms + Qz + H_2O and Cld + Ms + Qtz → St + Bt + H_2O suggests nearly isothermal decompression from maximum pressures of 2.2 GPa to 0.4 GPa (Mposkos 1989; Mposkos and Liati, 1993), implying rapid uplift. Orthogneisses and metapegmatites have Variscan protolith ages, as is indicated by Rb-Sr age of 334 Ma of magmatic muscovite from metapegmatite; (Mposkos and Wawrzenitz, 1995) and U-Pb ages between 326-299 Ma of magmatic zircons from orthogneisses (Peytcheva and von Quadt, 1995; Cornelius 2008; Liati et al., 2011). An U-Pb SHRIMP age of magmatic zircons from a kyanite-eclogite yielding 255 Ma is interpreted as the age of the gabbroic protolith (Liati et al., 2011) indicating that the subsequent HP metamorphism is Alpine in age. The minimum age of HP metamorphism is limited by Rb-Sr and Ar/Ar white mica ages of 36-42 Ma from mylonitic orthogneisses (Wawrzenitz and Mposkos, 1997; Lips et al., 2000). Emplacement of the Kechros complex to shallow crustal levels and juxtaposition against the Kimi complex by extensional deformation between 36 and 32 Ma is constrained by Rb-Sr biotite ages of granodiorites and subvolcanic rocks that intruded the Kechros complex and the overlying Kimi complex (Del Moro et al. 1988).

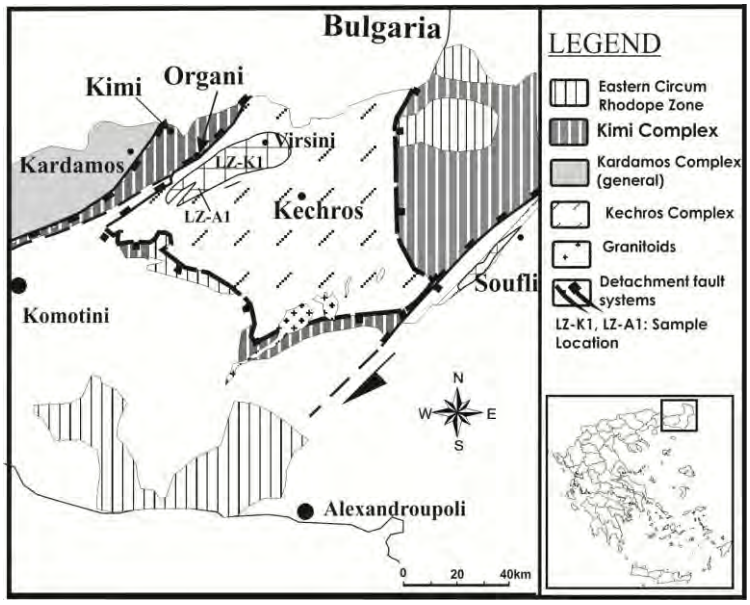

Figure 1 - Tectonic subdivision of eastern Greek Rhodope in northern Greece modified after Mposkos (1989) and Krohe and Mposkos (2002).

3. Ultramafic Rocks from the Kechros Complex

In the Kechros complex, metaperidotites occur as lens-shaped bodies (2 to 20 km in length and 0.5 to 5 km in width) intercalated between orthogneisses and metapelites. They are commonly associated with amphibolites and amphibolitized eclogites.The antigorite serpentinites from Dadia and Virsini areas (Figure 1) are the largest metaperidotite bodies in the Greek Rhodope. These ultramafic bodies contain dunitic boudins with chromitite pods, boudins of gabbroic pegmatites, diabase dykes, rodingitic gabbros and trondhjemites subsequently affected by HP metamorphism (Iliadis, 2006: Mposkos et al., 2012).

The Virsini antigorite serpentinite occupies an area of approximately 5×23 km and has a maximum thickness of about 300 m. It is a serpentinized and foliated clinopyroxene-bearing harzburgite with pockets of lherzolitic composition. Foliation is the result of penetrative deformation at albite-

epidote amphibolite/amphibolite facies conditions. The foliation strikes NE-SW and is similar to that of the surrounded phengite orthogneisses and metapelites.

Table 1: Bulk rock chemical- and norm composition of two metalherzolite samples (LZ- A1 and LZ-K1) from the Virsini metaperidotite.

	SiO_2	TiO_2	Al_2O_3	Cr_2O_3	Fe_2O_3	MnO	MgO	NiO	CaO	Na_2O	K_2O
LZ-A1	40.35	0.01	1.35	0.42	8.45	0.13	39.57	0.31	1.54	<0.01	<0.01
LZ-K1	42.80	0.02	1.70	0.29	8.34	0.11	37.35	0.26	1.54	0.05	0.01

LOI	Norm	Ol	En	Di	CaTs	MgTs	Chr
7.0	LZ-A1	72.51	18.96	5.02	1.58	1.47	0.67
7.16	LZ-K1	63.51	28.03	3.95	1.98	1.84	0.47

4. Petrography

The studied metalherzolites crop out as poorly foliated to massive lenses within the antigorite serpentinite. They are composed of Ol±Opx+Cpx+Atg+Chl+Tr±Cr-Spl+Mag. Relicts of the mantle assemblage olivine (Ol-1), orthopyroxene, clinopyroxene (Cpx-1), and Cr-spinel are still preserved within an antigorite matrix. Primary olivine (Ol-1) up to 3 mm in size shows undulatory extinction and deformation bands. It is replaced by antigorite at the grain boundaries and along deformation bands and fractures. Aggregates consisting of isometric olivine grains (Ol-2, 25-100 μm in size) overgrow Ol-1 and are in textural equilibrium with matrix antigorite and Cr-magnetite (Figure 2a). Orthopyroxene (up to 6 mm in size) contains inclusions of olivine and exsolution lamellae of clinopyroxene. Orthopyroxene is preserved only in lherzolite pockets which were affected by low degree of serpentinization. In lherzolite pockets affected by high degree of serpentinization orthopyroxene is completely replaced by antigorite forming bastite pseudomorphs. Primary clinopyroxene (Cpx-1, up to 4 mm in size) is marginally replaced by thin prismatic tremolite and olivine (Ol-3). Olivine-3 forms aggregates of isometric to longitudinal grains. Scanning electron microscope (SEM) images show that the primary clinopyroxene is replaced by olivine lamellae (Ol-3), diopside (Cpx-2), tremolite, antigorite, chlorite and magnetite (Figures 2b,c). The alternating diopside, olivine, antigorite and chlorite lamellae shown in Figures 2b, 2c suggest that the primary clinopyroxene contained exsolution lamellae of orthopyroxene which are completely replaced by antigorite; with increasing grade of metamorphism antigorite lamellae were partly replaced by lamellar olivine and chlorite (see metamorphic conditions). Clinopyroxene lamellae contain vermicular exsolutions of Cr-magnetite (Figure 2c). Antigorite participates with > 60 % in volume in the rock. It forms up to 0.5 mm large and 0.05 mm thick flakes replacing olivine and pyroxenes. In clinopyroxene porphyroclasts, the antigorite and chlorite flakes grow parallel to the prismatic crystal faces of the clinopyroxene, probably replacing former orthopyroxene exsolutions (Figures 2b,d). Tremolite (up to 0.8 mm, commonly 0.3-0.6 mm in size) is prismatic and occurs in textural equilibrium with Ol-3 and chlorite replacing clinopyroxene and antigorite (Figure 2e). Large tremolite crystals contain inclusions of diopside, antigorite and magnetite (Figure 2f). Primary Cr-spinel is still preserved in the lherzolite pockets affected by a low degree of serpentinization. In lherzolite pockets affected by a larger degree of serpentinization Cr-spinel is completely replaced by chlorite and Cr-magnetite. This Cr-magnetite contains inclusions of diopside and antigorite.

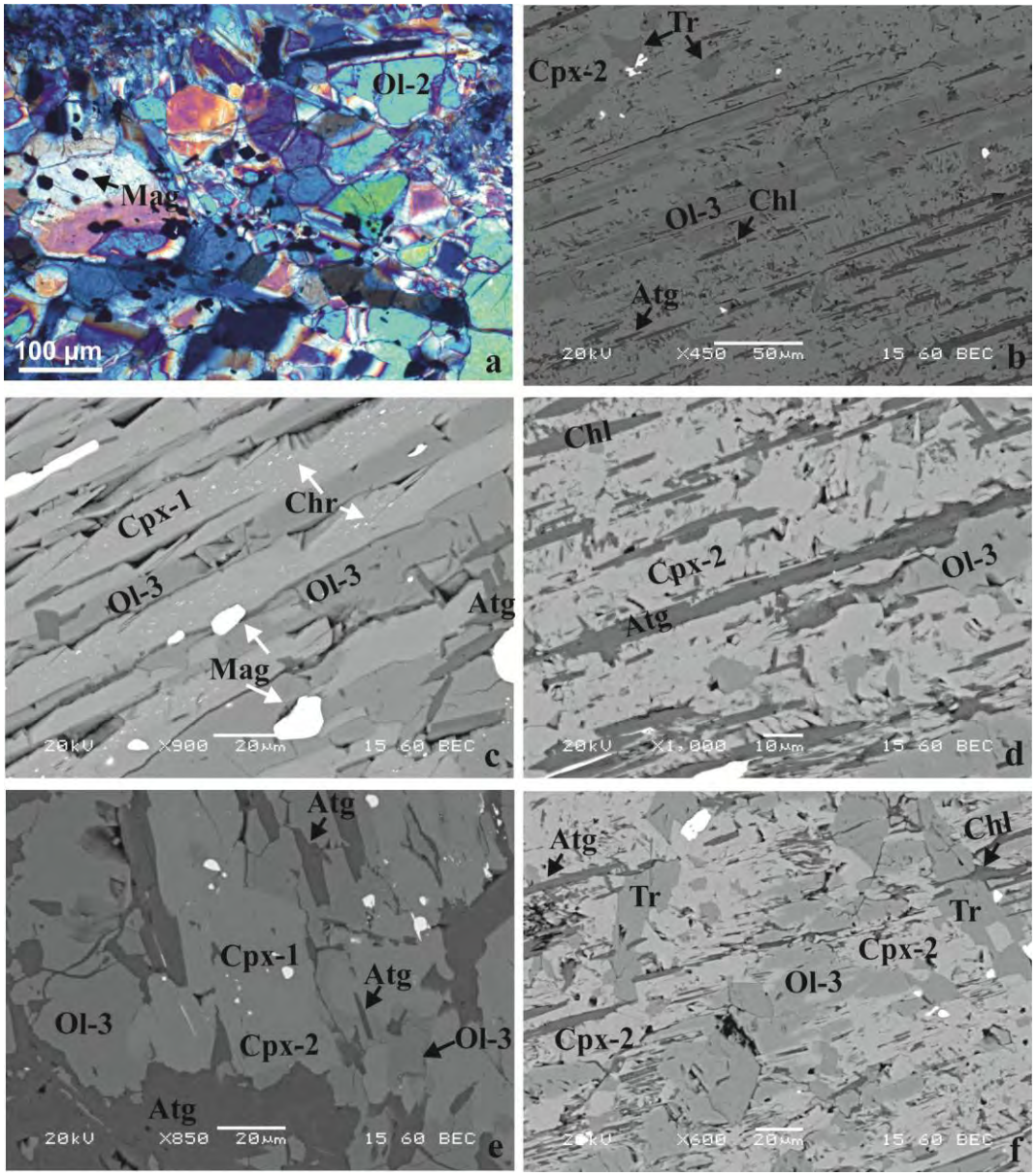

Figure 2 - Metalherzolite LZ-A1: a) Photomicrograph of isometric olivive grains (Ol-2) with inclusions of Cr-magnetite (black inclusions) b) Back-Scattered Electron (BSE) image of primary clinopyroxene replaced by diopside (Cpx-2), olivine (Ol-3), tremolite (Tr), antigorite (Atg) and chlorite (Chl). c) BSE image of lamellar clinopyroxene (Cpx-1) containing tiny chromite exsolutions. (Ol-3)=lamellar olivine, white grains Cr-magnetite, Atg=antigorite. d) BSE image pf alternating diopside (Cpx-2), antigorite and chlorite lamellae. The chlorite lamellae are in contact with lamellar olivine (Ol-3). e) BSE image of a zoned clinopyroxene (Al_2O_3= 1.16 wt % core, Al_2O_3=0 rim) with Cr-magnetite inclusions. Diopside (Cpx) contains antigorite inclusions and is marginally replaced by olivine (Ol-3). An antigorite flake is enclosed in diopside and in the overgrown olivine. f) BSE image of diopside (Cpx-2) and antigorite replaced by olivine (Ol-3), chlorite and tremolite. Tremolite contains inclusion of diopside (right edge of the picture). Antigorite, olivine and chlorite are lamellar in shape and oriented in diopside.

5. Mineral Chemistry

Two samples from the metalherzolites, LZ-K1 and LZ-A1, (major and minor element- and norm compositions are given in Table 1), were selected for analyses of the mineral compositions. In sample LZ-K1, which shows a low degree of the metamorphic overprint, the mantle assemblage Ol-1+Opx+Cpx-1+Cr-Spl dominates, whereas in sample LZ-A1, the metamorphic assemblage Atg+Ol-2+Tr+Chl+Ol-3+Cr-Mag dominates. Relicts of Ol-1 and Cpx-1 are preserved in both samples.

Table 2: Metalherzolite: Representative microprobe analyses of orthopyroxene, clinopyroxene, olivine, antigorite, chlorite, tremolite, Cr-spinel and Cr-magnetite.

	Opx	Opx	Cpx-1	Cpx-1	Cpx-2	Cpx-2	Ol-1	Ol-2/3	Tr	Atg	Atg
SiO_2	55.59	55.50	52.00	52.22	55.13	55.02	40.90	40.95	58.52	41.07	42.11
Al_2O_3	3.13	2.36	4.15	4.04	-	-	-	-	-	2.84	1.23
Cr_2O_3	0.86	0.73	1.04	0.95	-	0.19	-	-	-	0.64	-
FeO_t	5.65	6.15	3.13	3.03	1.17	0.91	8.58	9.15	1.49	3.35	4.66
MnO	-	-	-	-	-	-	-	-	-	-	-
MgO	33.27	33.40	19.28	18.92	17.72	17.79	50.11	49.51	23.77	40.12	39.95
NiO	-	-	-	-	-	-	0.37	0.41	-	0.16	0.28
CaO	1.48	1.40	20.36	20.80	25.83	25.76	-	-	13.63	-	-
Total	99.97	99.54	99.97	99.96	99.85	99.68	99.96	100.02	97.42	88.18	88.23
Si	1.921	1.931	1.882	1.890	2.001	1.999	0.998	1.001	7.996	7.638	7.857
Al	0.127	0.097	0.177	0.173	-	-	-	-	-	0.622	0.270
Cr	0.025	0.020	0.030	0.027	-	0.005	-	-	-	0.094	-
Fe	0.163	0.180	0.095	0.092	0.036	0.028	0.175	0.183	0.170	0.521	0.722
Mn	-	-	-	-	-	-	-	-	-	-	-
Mg	1.714	1.732	1.040	1.021	0.959	0.963	1.822	1.803	4.842	11.115	11.111
Ni	-	-	-	-	-	-	0.007	0.008	-	0.024	0.042
Ca	0.050	0.052	0.790	0.807	1.004	1.003	-	-	1.996	-	-
	Atg	Atg	Chl	Chl	Chl		Spl-c	Spl-r	Mag	Mag	Mag
SiO_2	40.78	41.77	30.64	34.81	33.52	Al_2O_3	43.73	40.58	-	1.17	-
Al_2O_3	3.80	1.37	18.37	11.46	12.13	Cr_2O_3	25.97	28.68	9.66	15.59	10.30
Cr_2O_3	-	0.67	2.49	2.36	3.78	Fe_2O_3	0.11	0.19	59.67	53.57	59.85
FeO_t	3.38	5.82	3.17	3.42	3.68	FeO	13.34	15.21	28.52	25.74	26.93
MnO	-	-	-	-	-	MnO	0.36	0.36	-	0.33	0.68
MgO	39.83	38.28	33.34	35.61	34.57	MgO	16.57	14.96	1.16	3.13	2.13
NiO	0.22	0.12	-	-	-	NiO	-	-	1.01	0.66	0.40
CaO	-	-	-	-	-						
Total	88.01	88.06	88.02	87.69	87.69		99.98	99.97	99.87	100.20	100.3
Si	7.579	7.864	5.755	6.558	6.359	Al	1.428	1.354	-	0.051	-
Al	0.832	o.308	4.064	2.545	2.712	Cr	0.569	0.642	0.291	0.456	0.306
Cr	-	0.100	0.369	0.352	0.568	Fe^{3+}	0.002	0.004	1.709	1.492	1.694
Fe	3.380	0.917	0.498	0.538	0.584	Fe^{2+}	0.309	0.360	0.903	0.797	0.847
Mn	-	-	-	-	-	Mn	0.008	0.009	-	0.010	0.022
Mg	39.830	10.742	9.355	10.000	9.777	Mg	0.685	0.631	0.066	0.173	0.119
Ni	0.220	0.020	-	-	-	Ni	-	-	0.031	0.020	0.012
Ca	-	-	-	-	-						

c=core, r=rim. Analyses were performed using a JEOL 6380 LV SEM equipped with energy dispersive system (EDS) at the School of Mining and Metallurgical Engineering, National Technical University of Athens. Representative mineral compositions are given in Table 2.

5.1. Mantle Assemblage:

The forsterite component in olivine (Ol-1) ranges between $Fo_{0.89}$ and $Fo_{0.91}$.In orthopyroxene the Al_2O_3 content ranges from 2.27 to 3.13 wt %, the Cr_2O_3 from 0.46 to 0.86 wt %, the CaO content

from 1.27 to 1.48 wt % and the Mg/(Mg+Fe) ratio from 0.9 to 0.91. Mantle clinopyroxene (Cpx-1) is Cr-diopside. The Al_2O_3 content ranges from 1.73 to 4.15 wt %, the Cr_2O_3 from 0.48 to 1.92 wt % and the Mg/(Mg+Fe) ratio from 0.92 to 0.94. Lower Al_2O_3 contents show rim compositions in zoned ortho- and clinopyroxene grains. Chromite is Cr-spinel with $Cr/(Cr+Al+Fe^{3+})$ ratio 0.28 in the core and 0.32 at the rim and $Mg/(Mg+Fe^{2+})$ ratio 0.68 and 0.63 respectively. The decrease in Al and Mg content from the core to the rim is attributed to alteration and partial replacement of the Cr-spinel by chlorite during the metamorphic processes.

5.2. Metamorphic assemblage:

The forsterite component in Ol-2 and Ol-3 ranges between $Fo_{0.90}$ and $Fo_{0.91}$. No remarkable differences are observed in the forsterite component between mantle Ol-1 and metamorphic Ol-2 and Ol-3. Cpx-2 shows a higher Mg/(Mg+Fe) ratio (0.96-0.97) compared to that of Cpx-1 (0.92-0.94). In Cpx-2 the Al_2O_3 content is below the detection limit and the Cr_2O_3 content from 0 to 0.19 wt%. Antigorite contains appreciable amounts of aluminium. The Al_2O_3 content ranges from 0.5 to 4.28 wt %. Higher Al_2O_3 values are measured in antigorite flakes replacing Cpx-1. The Cr_2O_3 content ranges from 0 to 1.52 wt %. Chlorite is clinochlore with 5.75 to 6.70 Si atoms per formula unit (a.p.f.u.), 2.21 to 4.06 Al a.p.f.u. and a Mg/(Mg+Fe) ratio ranging from 0.93 to 0.95. The Cr_2O_3 content in chlorite ranges from 2.36 to 3.78 wt % and total iron, expressed as FeO, from 3.17 to 4.49 wt %. The Mg/(Mg+Fe) ratio in tremolite ranges between 0.95 to 0.98; the Al_2O_3 content is below the detection limit. Cr-magnetite is formed at the expense of primary spinel, olivine (Ol-1), and clinopyroxene within the stability field of antigorite during the serpentinization. The Cr-magnetite inclusions in Ol-2 (Figure 2b) indicate that it is formed at an early stage of the prograde path of metamorphism. The Cr_2O_3 content ranges from 9.21 to 14.95 wt %, the MgO from 0 to 1.9 wt %, the NiO from 0.23 to 1.45 wt % and the Al_2O_3 content from 0 to 1.17 wt %.

6. Discussion

Textural relationships, mineral assemblages and mineral compositions in the metalherzolite pockets indicate that the Kechros metaperidotite is affected by the HP metamorphic event recorded in the neighboring crustal rocks (Mposkos, 1989; Mposkos et al., 2011). The mantle assemblage was Ol-1+Opx+Cpx-1+Cr-Spl and the metamorphic assemblage is Atg+Ol-2+Cpx-2+Ol-3+Chl+Tr+Cr-Mag. Mantle olivine (Ol-1) and orthopyroxene are replaced by antigorite. Antigorite and Cr-magnetite are formed in an early stage of the metamorphic event as indicate antigorite and Cr-magnetite inclusions in olivine (Ol-2 and Ol-3, Figure 2a). Antigorite occurs also as inclusion in Cr-magnetite. In most metalherzolite pockets orthopyroxene is absent. It is completely consumed by the antigorite forming reaction:

$$Ol+Opx+W \rightarrow Atg \qquad (1)$$

With increasing metamorphic grade and by crossing the olivine plus antigorite stability field, Ol-2 is formed at the expense of antigorite. With further increase of the metamorphic grade, or during decompression, tremolite, olivine (Ol-3) and chlorite are formed at the expense of clinopyroxene (Cpx-1) and antigorite as suggested by the textural relationships (Figures 2b,e,f). Tremolite and olivine are formed according to the reaction:

$$Atg+Di \rightarrow Ol+Tr+H_2O \qquad (2)$$

Antigorite lamellae in clinopyroxene are probably formed replacing lamellae of enstatite exsolutions in the primary clinopyroxene (Figures 2b,d) according to reaction 1. Olivine lamellae in clinopyroxene (Figures. 2b,c) are formed replacing antigorite lamellae according to reaction 2.

Chlorite is also formed by the replacement of the clinopyroxene, in addition to tremolite and olivine-3 (Figure 2f). The Tschermak component of the primary clinopyroxene (Cpx-1) was consumed according to the reaction:

$$Atg+Cts \rightarrow Tr+Fo+Chl+W \qquad (3)$$

The Al_2O_3 content in antigorite (it ranges from 0.5 to 4.28 wt %) was also an aluminum source for the chlorite formation.

The maximum P-T conditions were lower than those constrained by the reaction:

$$Atg \rightarrow Ol+Tlc+H_2O \qquad (4)$$

since antigorite is still stable and the assemblage olivine+talc was not formed.

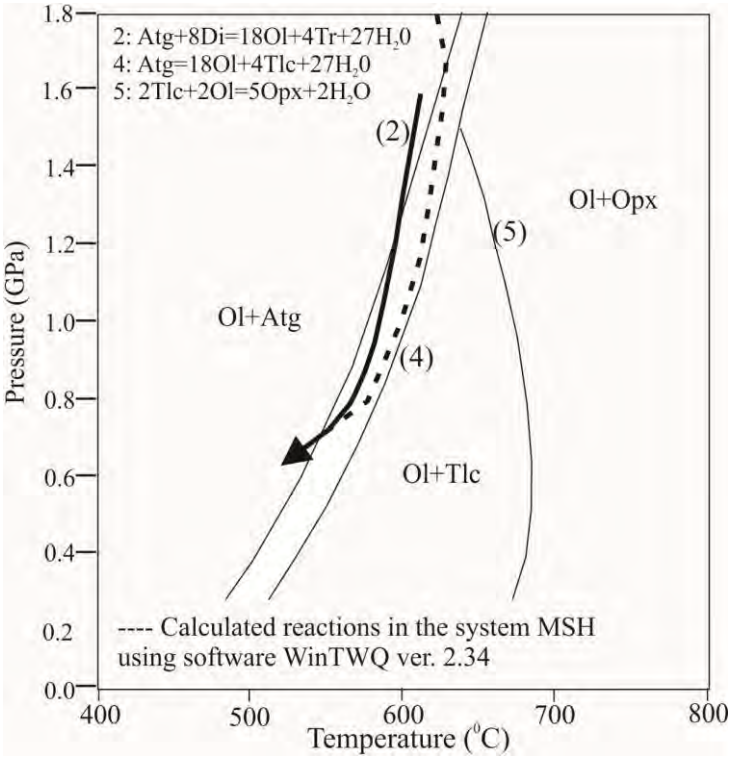

Figure 3 - Peak metamorphic PT conditions (adopted from neighboring eclogites, Mposkos et al., 2012, dotted line) and exhumation path of the Virsini metaperidotite from the Kechros complex in eastern Rhodope.

The metamorphic temperatures are constrained within the narrow field confined by the curves of the reactions 2 and 4 (Figure 3). This is also in accordance with the low Al-spinel component in the Cr-magnetite (up to ≈2 %) which suggests that Cr-magnetite is formed below the talc + olivine stability field (Evans and Frost, 1975). In talc-olivine rocks ferrit-chromites accommodate Al-spinel component up to 5 % and in chlorite-enstatite-olivine rocks up to 35 % (Evans and Frost, 1975; Mposkos et al., 2010). Boudins of amphibolitized eclogites and of omphacite-bearing meta-trondhjemites within the Virsini metaperidotite (Mposkos et al., 2012; Mposkos et al., 2013) indicate that the Kechros ultramafic rocks are metamorphosed at high pressures. For pressure of about 1.7 GPa (recorded in neighbouring eclogites) and assuming that the reaction 2 occurred at the prograde stage of metamorphism, the maximum temperature in the metaperidotite is constrained between 610 and 630 ^{o}C which is slightly higher than that obtained from the associated eclogites (≈570 ^{o}C at 1.7 GPa; Mposkos et al., 2012). At peak temperature of approximately 570 ^{o}C the curve of the reaction 2 is crossed during decompression. Assuming isothermal decompression as was recorded in the associated eclogites and metapelites the reaction curve was crossed at a pressure of ~ 1.2 GPa (Figure 3).

7. Conclusions

The Virsini metaperidotite from the Kechros HP metamorphic complex in eastern Rhodope is a sepentinized clinopyroxene-bearing harzburgite with pockets of lherzolitic composition. Dykes of amphibolitized eclogites and omphacite bearing metatrondjemites within the metaperidotite indicate that the metaperidotite underwent HP metamorphism similar to that recorded in the associated rocks of the continental crust assemblage.

In the metalherzolite pockets the mantle assemblage is Ol-1+Opx+Cpx-1+Cr-Spl. The metamorphic assemblage is Atg+Ol-2+Cpx-2+Ol-3+Chl+Tr+Cr-Mag. Antigorite and Cr-magnetite are formed in an early stage of the metamorphic event. Antigorite lamellae in clinopyroxene are probably formed replacing lamellae of "enstatite exsolutions" in the primary clinopyroxene. With increasing metamorphic grade and by crossing the olivine plus antigorite stability field olivine (Ol-2) is formed at the expense of antigorite. With further increase of metamorphic grade (or more probably during decompression), tremolite, olivine (Ol-3) and chlorite are formed at the expense of clinopyroxene and antigorite. Olivine lamellae in clinopyroxene replace antigorite- or former orthopyroxene lamellae in clinopyroxene. The aluminum source for the chlorite formation was the Al_2O_3 content in antigorite (up to 4.28 wt %) and the Tschermak component of the primary pyroxenes. The metamorphic temperatures are constrained within the stability field of the mineral assemblage Atg+Ol+Tr (Figure 3). At peak PT conditions ($\approx$ 1.7 GPa/570 ^{o}C recorded in neighbouring eclogites) the curve of the reaction $Di+Atg \rightarrow Ol+Tr+H_2O$ is crossed during decompression.

8. References

Burg J.P. 2011. Rhodope: From Mesozoic convergence to Cenozoic extension. Review of petro-structural data in the geochronological frame, *Journal of the Virtual Explorer,* 39, 1-44.

Brueckner H.K. and Medaris L.G. 2000. A general model for the intrusion and evolution of "mantle" garnet peridotites in high-pressure and ultra-high-pressure metamorphic terranes. *Journal of Metamorphic Geology,* 18, 123-133.

Cornelius N.K. 2008: UHP metamorphic rocks of the Eastern Rhodope Massif, NE Greece: new constraints from petrology, geochemistry and zircon ages, *PhD Thesis*, Johannes-Gutenberg Universität, Mainz.

Del Moro A., Innocenti F., Kyriakopoulos C., Manetti P. and Papadopoulos P. 1988. Tertiary granitoids from Thrace (Northern Greece): Sr isotopic and petrochemical data. *Neues Jahrbuch fuer Mineralogie Abhandlungen,* 159, 113–135.

Evans B.W. and Frost B.R. 1975. Chrome-spinel in progressive metamorphism-a preliminary analysis. *Geochimica et Cosmochimica Acta,* 39, 959-972.

Iliadis A 2006. Study of the ultrabasic rocks of Ano Virsini (Geology-Petrology-Metallogeny), *PhD Thesis*, National Technical University of Athens, pp. 236 (In Greek with English abstract).

Krohe A. and Mposkos E. 2002. Multiple generations of extensional detachments in the Rhodope Mountains (N.Greece): evidence of episodic exhumation of high-P rocks. In: Blundell, D.J., Neubauer, G. and Von Quant, A. (eds.): The timing and location of major ore deposits in an evolving orogen, *Geological Society of London,* Special Publication 204, 151-178.

Liati A., Gebauer D. and Fanning M. 2011. Geochronology of the Alpine UHP Rhodope zone: A review of isotopic ages and constraints on the geodynamic evolution. In Dobrzhinetskaya et al (ed), *Ultrahigh-Pressure Metamorphism. 25 years after the discovery of coesite and diamond* (ed) Dobrzhinetskaya et al. Elsevier, 295-324.

Lips A.L.W., White S.H. and Wijbrans J.R. 2000. Middle–Late Alpine thermotectonic evolution of the southern Rhodope Massif, Greece, *Geodinamica Acta,* 13*,* 281–292.

Mposkos E. 1989. High-pressure metamorphism in gneisses and pelitic schist in the East Rhodope zone (N Greece), *Mineralogy and Petrology,* 41, 25-39.

Mposkos E. and Krohe A. 2000. Petrological and structural evolution of continental high pressure (HP) metamorphic rocks in the Alpine Rhodope domain (N.Greece), *Proceedings of the 3rd International Conference on the Geology of the Eastern Mediterranean*, 221-232.

Mposkos E. and Liati A. 1993. Metamorphic evolution of metapelites in the high-pressure terrane of the Rhodope zone, northern Greece, *Canadian Mineralogist,* 31, 401-424.

Mposkos E. and Wawrzenitz N. 1995. Metapegmatites and pegmatites bracketing the time of HP-metamorphism in polymetamorphic rocks of the E Rhodope, N Greece: petrological and geochronological constraints, *Geological Society of Greece Special Publication,* 4, 602-608

Mposkos E. and Krohe A. 2006. *P-T*-deformation paths of closely associated UHP (diamond-bearing) crustal and mantle rocks of the Kimi Complex: Implications for the tectonic history of the Rhodope Mountains, northern Greece, *Canadian Journal of Earth Sciences,* 43, 1755-1776.

Mposkos E., Baziotis I. and Proyer A. 2010. Metamorphic reprocessing of a serpentinized carbonate-bearing peridotite after detachment from the mantle wedge: A P-T path constrained from textures and phase diagrams in the system CaO-MgO-Al_2O_3-SiO_2-CO_2-H_2O, *Lithos,* 118, 349-364.

Mposkos E., Baziotis I. and Proyer A. 2011. Pressure-temperature evolution of eclogites from the Kechros complex in the Eastern Rhodope (NE Greece), *International Journal of Earth Sciences (Geologische Rundschau)* DOI 10.1007/s00531-011-0699-2.

Mposkos E., Baziotis I. Leontakianakos G. and Barry P.H. 1012. The metamorphic evolution of the high-pressure Kechros complex in East Rhodope (NE Greece): implications from Na-Al-rich leucocratic rocks within antigorite serpentinites, *Lithos,* submitted.

Padron-Navarta J.A., Sanchez-Vincaino V.L., Garrido C. and Gomez-Pugnaire M.T. 2011. Metamorphic record of high-pressure dehydration of antigorite serpentinite to chlorite harzburgite in a subduction setting (Cerro del Almirez, Nevado-Filabride complex, southern Spain, *Journal of Petrology,* 52, 2047-2078.

Peytcheva I. and von Quadt A. 1995. U-Pb zircon dating of metagranites from Byala Reka region in the east Rhodopes, Bulgaria, *Proceedings XV Congress of the Carpathian-Balkan Geological Association, Special Publication,* 4, 637–642, Geological Society of Greece, Athens.

Trommsdorff V. and Evans B.W. 1974. Alpine metamorphism of peridotitic rocks, *Schweizerische Mineralogische Petrologische Mitteilungen,* 54, 333-52.

Wawrzenitz N. and Mposkos E. 1997. First evidence for Lower Cretaceous HP/HT-metamorphism in the eastern Rhodope, North Aegean region, North-East Greece. *European Journal of Mineralogy,* 9, 659-664.

Whitney D. and Evans B.W. 2010. Abbreviations for names of rock-forming minerals, *American Mineralogist,* 95, 185-187.

Δελτίο της Ελληνικής Γεωλογικής Εταιρίας, τομ. XLVII , 2013
Πρακτικά 13ου Διεθνούς Συνεδρίου, Χανιά, Σεπτ. 2013

Bulletin of the Geological Society of Greece, vol. XLVII 2013
Proceedings of the 13th International Congress, Chania, Sept. 2013

SYNTHESIS AND CHARACTERIZATION OF FOUR NEW HALLOYSITE–TIO_2 NANOCOMPOSITES

Papoulis D.[1], Komarneni S.[2], Toli D.[1], Panagiotaras D.[3] and Bakalis S.[1]

[1] *University of Patras, Department Geology, Papoulis@upatras.gr*

[2] *The Pennsylvania State University, Department of Ecosystem Science and Management and Materials Research Institute, Materials Research Laboratory, University Park, PA 16802, USA*

[3] *Technological Educational Institute of Patras, Department of Mechanical Engineering, 26334, Patras, Greece*

Abstract

The synthesis as well as the characterization of small-sized TiO_2 particles supported on Halloysite are presented. Hallloysite from Utah, USA as well as from Limnos, island Greece, were used to synthesize two nanocomposites for each halloysite with TiO_2 to halloysite weight ratios of 80: 20 and 60:40 and compare with published data of well formed nanocomposites of intermediate proportion (70-30) that were previously studied. All nanocomposites were prepared by deposition of anatase (TiO2) on the halloysite tubes using a sol–gel method under hydrothermal treatment at 180 °C. Phase composition, particle morphology and physical properties of these samples were characterized using X-Ray Diffraction (XRD), Scanning Electron Microscopy (SEM), Attenuated Total Reflection using Fourier Transform Infrared spectroscopy (ATR-FTIR) and N_2 surface area analysis by BET. Preparation of all halloysite–TiO2 nanocomposites led to the anticipated good dispersion of anatase particles on halloysite surfaces. ATR-FTIR results revealed the formation of hydrogen bonding between anatase and the outer surfaces of halloysite tubes. All halloysite-TiO2 nanocomposites largely showed interparticle mesopores of about 5.7nm and high SSAs.

Key words: *Anatase, clay minerals, Photocatalytic activity.*

Περίληψη

Η σύνθεση και ο χαρακτηρισμός των νανοσύνθετων TiO_2 αποτεθειμένων σε αλλοϋσίτη παρουσιάζονται σε αυτήν την εργασία. Χρησιμοποιήθηκε αλλοϋσίτης από τη Γιούτα (Η.Π.Α.) και από τη νήσο Λήμνο για τη σύνθεση δύο νανοσύνθετων για κάθε αλλοϋσίτη με αναλογίες μάζας TiO_2 προς αλλοϋσίτη 80:20 και 60:40 και να συγκριθούν με δεδομένα από καλοσχηματισμένα νανοσύνθετα με ενδιάμεσες αναλογίες (70:30) που έχουν παρασκευαστεί, χαρακτηριστεί και δημοσιευθεί στο παρελθόν. Όλα τα νανοσύνθετα παρασκευάστηκαν με απόθεση ανατάση στους επιμήκεις κρυστάλλους αλλοϋσίτη χρησιμοποιώντας μία μέθοδο διαλύματος-πυκτώματος σε υδροθερμική επεξεργασία στους 180 °C. Η ορυκτολογική ανάλυση, η μορφολογία των κρυστάλλων και οι φυσικές ιδιότητες προσδιορίστηκαν με τη χρήση περιθλασιμετρίας ακτίνων Χ, ηλεκτρονικού μικροσκοπίου σάρωσης, υπέρυθρης φασματοσκοπίας μετασχηματισμού κατά Fourier και προσδιορισμός της ειδικής επιφάνειας με τη μέθοδο BET. Η προετοιμασία όλων των νανοσύνθετων οδήγησε στη

επιθυμητή καλή διασπορά των κρυστάλλων ανατάση πάνω στις επιφάνειες των κρυστάλλων του αλλοϋσίτη. Από την υπέρυθρη φασματοσκοπία μετασχηματισμού κατά Fourier προσδιορίστηκε ο σχηματισμός δεσμών υδρογόνου μεταξύ του ανατάση και των εξωτερικών επιφανειών του αλλοϋσίτη. Μετά την επεξεργασία όλα τα νανοσύνθετα εμφάνισαν κυρίων μεσοπόρους μεγέθους περίπου 5.7nm και υψηλή ειδική επιφάνεια.
Λέξεις κλειδιά: *Ανατάσης, αργιλικά ορυκτά, φωτοκατάλυση.*

1. Introduction

It is well known that TiO_2 nanoparticles have good catalytic activities because of their large specific surface areas where reactions take place (Zhao et al., 2006). Titanium dioxide, especially in the form of anatase, has proven to be the most suitable semiconductor for widespread environmental applications such as the degradation of oil spills and the decomposition of many organic molecules as well as other air pollutants (Hoffmann et al., 1995; Michael et al., 1995; Fujishima et al., 2000; Martínez-Ortiz et al., 2003). TiO_2 powders, however, easily agglomerate into larger particles, reducing their photocatalytic activities (Zhao et al., 2006).

Clay minerals are attractive materials for adsorption and catalysis (Chmielarz et al., 2011) and when composited with TiO_2, they have been used in aqueous dispersions to enhance the removal of organic pollutants by photocatalytic degradation (Mogyorósi et al., 2002; Kibanova et al., 2009), as well as to increase the photocatalytic activities in decomposing air pollutants (e.g. Nikolopoulou et al., 2009; Papoulis et al., 2010; Papoulis et al., 2013a; Papoulis et al., 2013b). Previous investigations revealed that using clay minerals with microfibrous (Aranda et al., 2008; Karamanis et al., 2011) or tubular morphology (Papoulis et al., 2010; Papoulis et al., 2013a; Papoulis et al., 2013b) as a template and TiO_2 as the photocatalyst led to significantly increased TiO_2 photocatalytic activity in decomposing many pollutants. The dispersion of anatase nanoparticles onto halloysite surfaces under mild conditions is a promising method to resolve the agglomeration problem of TiO_2 (Papoulis et al., 2010; Papoulis et al., 2012). Recent studies showed that halloysite-TiO_2 nanoparticles have excellent photocatalytic activities in decomposing both inorganic and organic air pollutants (Papoulis et al., 2010; Papoulis et al., 2013b).

In present work, we describe the synthesis and characterization of nano-sized TiO_2 particles supported on two different halloysites (weight ratios of TiO_2 to Halloysite were 80:20 and 60:40) by using a novel method under mild conditions, which does not involve calcinations or stabilizing agents. The results are compared with recently published data for well prepared nanocomposites of different TiO_2-Halloysite proportions (70-30) that show very high photocatalytic activities in decomposing air and organic pollutants (Papoulis et al., 2013b). The aim of this study was to prepare well formed clay-based nanocomposites that could have increased photocatalytic efficiency in decomposing inorganic and organic air pollutants.

2. Materials and Methods

2.1. Sample Preparation

A halloysite sample from Utah, USA and a halloysite sample from Limnos island were used in this study. Both the samples were size fractionated to obtain <2 μm by gravity sedimentation followed by centrifugation to separate solid from liquid.

2.2. TiO_2 Stock Sol Dispersion

A stock TiO_2 sol dispersion was prepared by mixing titanium tetraisopropoxide, $Ti(OC_3H_7)_4$, with hydrochloric acid, nanopure water (3D) and absolute ethanol (Langlet et al., 2003). The TiO_2 stock dispersion was diluted in absolute ethanol to give a 0.05 M concentration of $Ti(OC_3H_7)_4$.

2.3. Halloysite-supported TiO_2

An aliquot of TiO_2 sol was stirred for 2 h and then the (1% w/w) halloysite-water dispersion was added to the TiO_2 dispersion in order to obtain the desirable TiO_2 content. The slurry was stirred for 24 h and the resulting dispersion was centrifuged for 10 min (3800 rpm) followed by three times centrifuge washing (with 3D water). The halloysite–TiO_2 composites were then dispersed in a 1:1 water:ethanol solution, prior to hydrothermal treatment in an autoclave for 5 h at 180 °C. The products were centrifuged for 15 min (at 3800 rpm) and oven-dried for 3 h (at 60 °C).

2.4. Characterization

The phase compositions of untreated and TiO_2 treated halloysite samples were determined by X-ray diffraction (using a Bruker D8 advance diffractometer, with Ni-filtered CuKα radiation). XRD patterns were obtained from oriented or random powder samples in a 2θ range of 2° to 60° at a scanning rate of 2 °/min. Random powder mounts for selected samples were prepared by gently pressing the powder into the cavity holder. Oriented clay powder samples were prepared by the dropper method. Halloysite-TiO_2 morphology was examined with a SEM LEO SUPRA 35VP. Attenuated total reflection infrared (ATR/FTIR) measurements were made with the ATR Miracle accessory of PIKE technologies (diamond crystal) attached to the EQUINOX 55 FT-IR spectrometer (BRUKER). Nitrogen adsorption-desorption isotherms for each sample degassed at 100 ^{o}C for 3 hours were obtained at 77K using Autosorb^{-1} (Quantachrome corporation). Brunauner-Emmet-Teller (BET) surface areas and pore size distribution were determined from the isotherms. Pore size distribution of each sample was obtained using density functional theory (DFT) method in which a N_2 adsorption branch model was selected.

3. Results and Discussion

3.1. X-Ray Diffraction

Both halloysite samples (from Utah and Limnos island), as it has been reported in previous studies, are pure with no detectable impurities, if any (not detected by XRD) (Papoulis et al., 2013b). Figure 1 shows the XRD patterns of the four nanocomposites prepared in this study from both halloysites compared with nanocomposites 70-30. All patterns show the presence of dehydrated halloysite and anatase, confirming their phase purity (Figure 1). The XRD patterns of all nanocomposites showed all the characteristic reflections of anatase (γ-TiO_2) at 25.3°, 37.9°, 47.6°, 54.8° 2θ, which intensity decreasing by decreasing TiO_2 amount. Additionally the intensity of the 001 reflection of dehydrated halloysite is increasing with increasing amount of dehydrated halloysite. The XRD patterns also indicated that the temperature of 180 °C involved in the synthesis of halloysite-TiO_2 nanocomposites did not modify the native mineral structure of dehydrated halloysite. It is well known that heating halloysite at 100-350 ^{o}C sharpens the basal reflection (001) and reduces the spacing but never to as low as the characteristic reflection of kaolinite (7.14 Å) (Brindley and Robinson, 1946; Joussein et al., 2005). In this study, the basal reflections of both halloysites after treatment were detected at 7.29 Å (Figure 1).

3.2. ATR-FTIR Spectra

The ATR-FTIR spectra of all four TiO_2-treated halloysites compared with nanocomposites 70-30 from both areas are generally similar (Figure 2), while the intensities of halloysite reflections are lower in the nanocomposites and especially in the nanocomposites with the lower amounts of halloysite (20%) in them. The reflections of the spectra confirm that the structures of both dehydrated halloysites were not changed after treating with TiO_2. None of the characteristic bands of dehydrated halloysite (Joussein et al., 2005; Bobos et al., 2001) were affected except the Si–O broad stretching band which shifted from about 997 cm^{-1} (Papoulis et al., 2010) to more than 1000 cm^{-1} (Figure 2) in all nanocomposites. The shifting of the Si–O broad stretching band increased with increasing amount of anatase (Figure 2). This shift is an indication of the formation of

hydrogen bonding between TiO_2 and the outer surfaces of halloysite tubes (tetrahedral sheet) which becomes stronger in the more anatase rich nanocomposites. The ATR-FTIR spectra of all nanocomposites confirmed that the treatment temperature of 180°C during the synthesis of halloysite-TiO_2 nanocomposites did neither destroy halloysites nor modified their native dehydrated halloysite mineral structure.

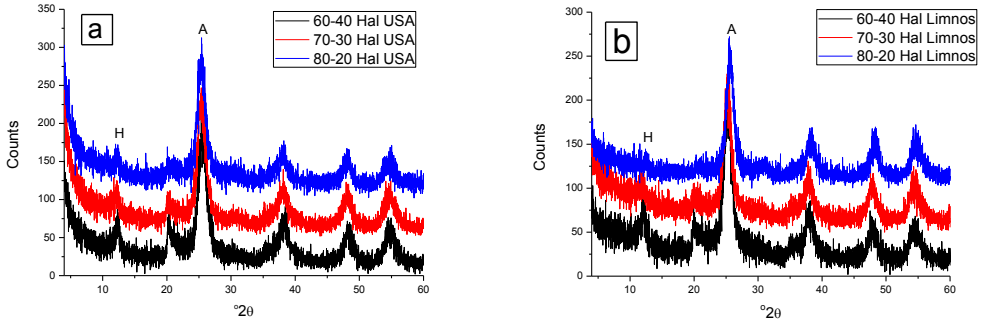

Figure 1 – XRD patterns of the four new Halloysite-TiO_2 nanocomposites (60-40, 80-20) from both areas compared with the two previously studied nanocomposites (70-30) a) nanocomposites using halloysite from Utah and b) nanocomposites using halloysite from Limnos (H: halloysite, A: anatase).

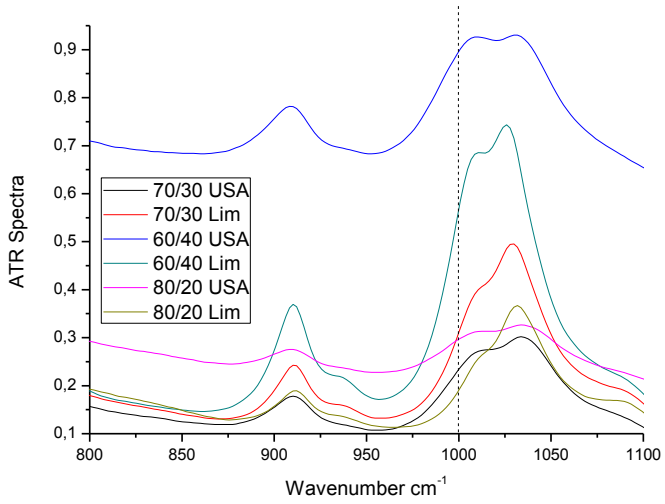

Figure 2 – ATR-FTIR Spectra of Halloysite-TiO_2 nanocomposites compared with the two previously studied nanocomposites (70-30) (Lim:Limnos).

3.3. Scanning Electron Microscopy (SEM) and Transmission Electron Microscopy (TEM)

In this investigation we present SEM micrographs of the four nanocomposites compared with nanocomposites 70-30 (Figure 3), while the morphologies of both halloysites have already been previously reported by us (Papoulis et al., 2010; Papoulis et al., 2013b). It should be noted that the halloysite tubes from Limnos island appear to be well formed (Papoulis et al., 2010), while those from Utah are not curved and rolled up that perfectly. The latter morphology, therefore, suggests

that more halloysite surfaces are available for TiO_2 nanoparticles to be dispersed in the sample from Utah (Papoulis et al., 2013b).

SEM observations of all nanocomposites showed that many uniform TiO_2 grains of about 10-30 nm were deposited on the external surfaces of halloysite tubes of all nanocomposites (Figure 3). The TiO_2 nanoparticles were found to be distributed very well on both halloysite external surfaces but not homogeneously (Figure 3) although homogeneous distribution of TiO_2 grains on halloysite tubes was anticipated (Papoulis et al., 2013b). TiO_2 nanoparticles seem to cover, at least partially, the lumen of most halloysite tubes (Figure 3). By increasing the amount of TiO_2 content, the deposited TiO_2 particles were found to be aggregated on the surfaces of the halloysite tubes (Figure 3) while decreasing the amount of TiO_2 led to aggregation of halloysite tubes from both sources.

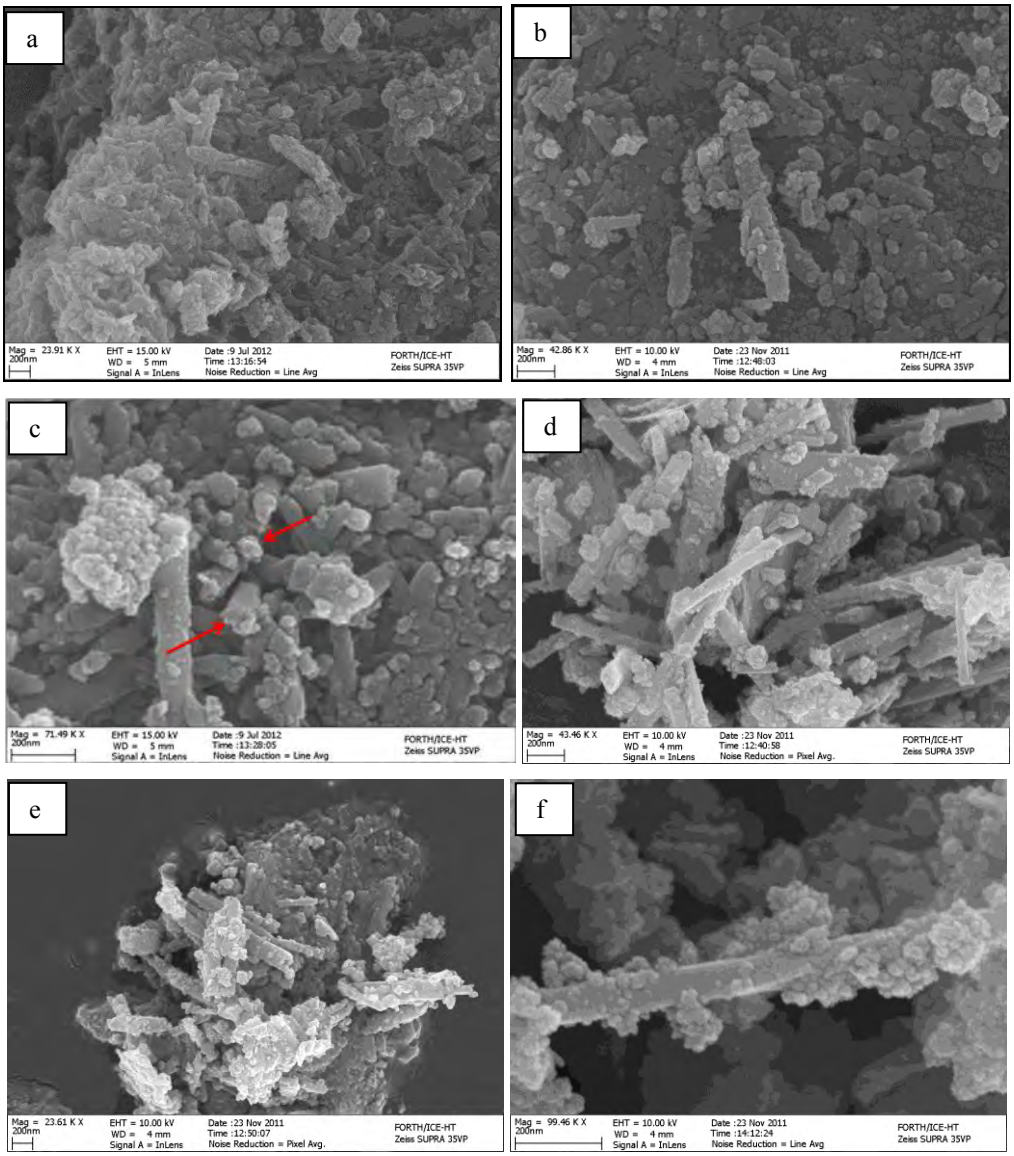

Figure 3 – SEM micrographs of Halloysite-TiO_2 nanocomposites from Utah (a: 60-40, b: 70-30, c: 80-20) and Limnos island (d: 60-40, e: 70-30, f: 80-20) (arrows: anatase nanoparticles partially covering halloysite lumen).

3.4. Determination of Specific Surface Areas (SSAs) and Porosity

Adsorption–desorption isotherms of nitrogen and pore size distributions for all four halloysites–TiO_2 nanocomposites compared with nanocomposites 70-30 are presented in Figures 4 and 5 and Figures 6 and 7, respectively. The isotherm shapes for all nanocomposites are of the same type (type IV) indicating both meso and micropores (IUPAC classification, 1994) (Sing et al., 1985; Sing et al., 2004). The different size of the hysteresis observed is due to the different proportions of halloysite and anatase, two minerals with major differences in size, shape and SSA. Additionally the two different halloysites are characterized by differences in size and SSA. The total pore volumes of the nanocomposites with halloysite from Utah were found to be significantly higher while the SSAs were found to be slightly smaller than those of the nanocomposites with halloysite from Limnos (Figures 6, 7). This could be attributed to the presence of more interparticle pores (macroporous) of the first samples while the second type of samples show more mesopopores at about 5.7 nm (Figures 6, 7) and retained the higher SSA (of halloysite from Utah) due to a better TiO_2 distribution on halloysite external surfaces. All nanocomposites largely showed mesopores of about 5.7 nm, while the macropores found in starting halloysite material (Papoulis et al., 2010) were considerably reduced apparently due to partial covering of the lumen of halloysite tubes by TiO_2 nanoparticles.

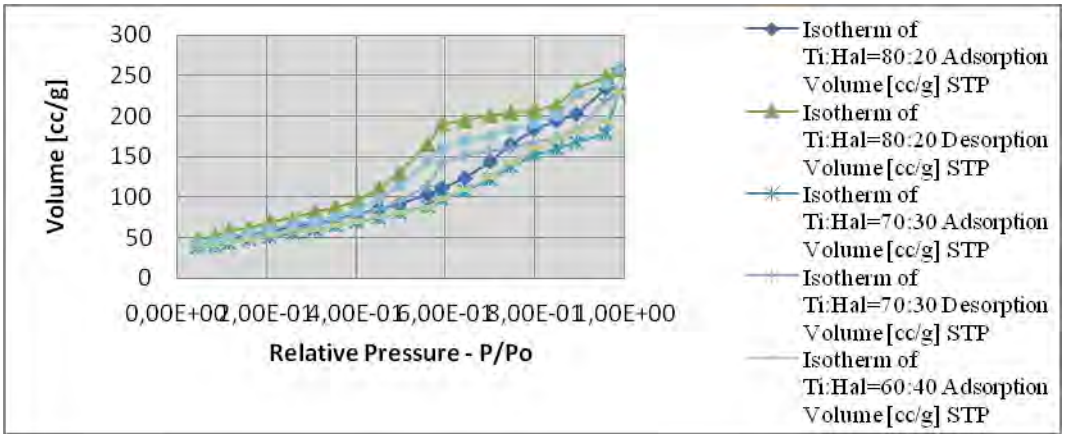

Figure 4 - Adsorption-desorption isotherms of nitrogen for nanocomposites using halloysite from Utah compared with the two previously studied nanocomposite (70-30).

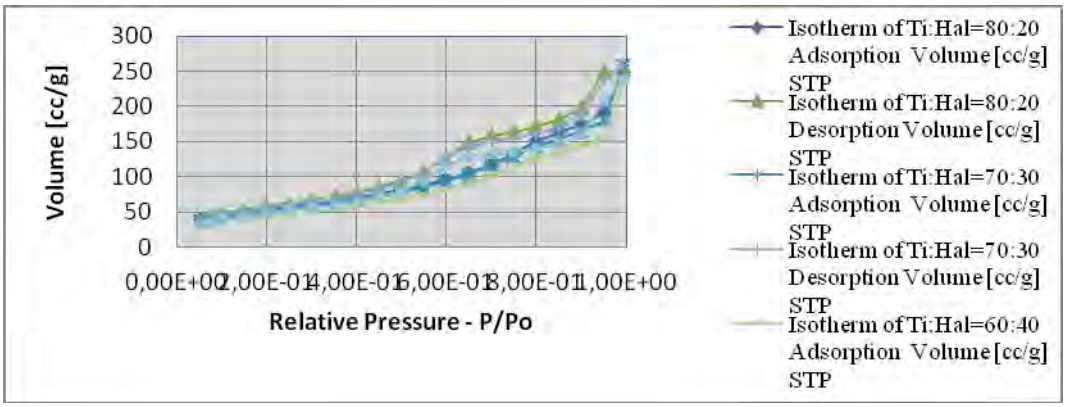

Figure 5 - Adsorption-desorption isotherms of nitrogen for nanocomposites using halloysite from Limnos compared with the previously studied nanocomposite (70-30).

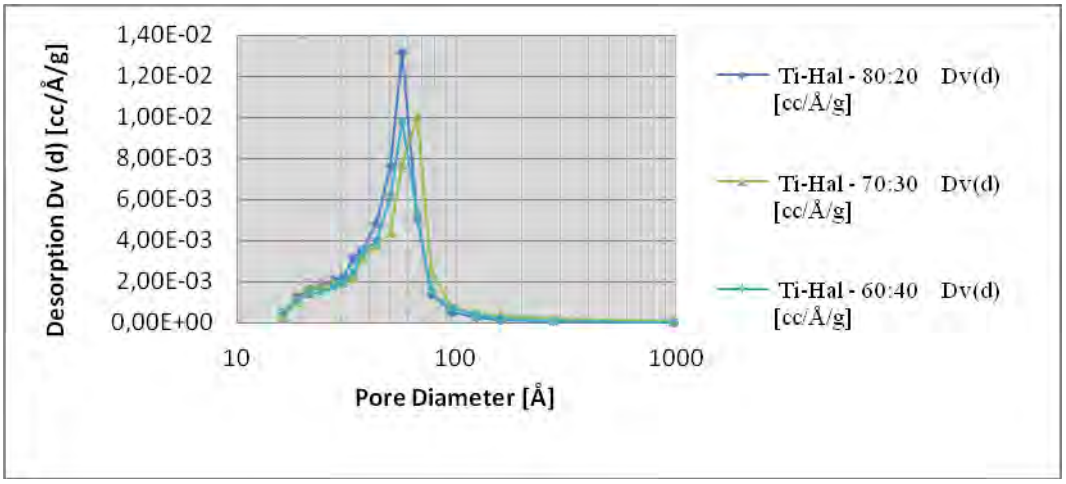

Figure 6 - Pore size distribution for nanocomposites using halloysite from Utah compared with the previously studied nanocomposite (70-30).

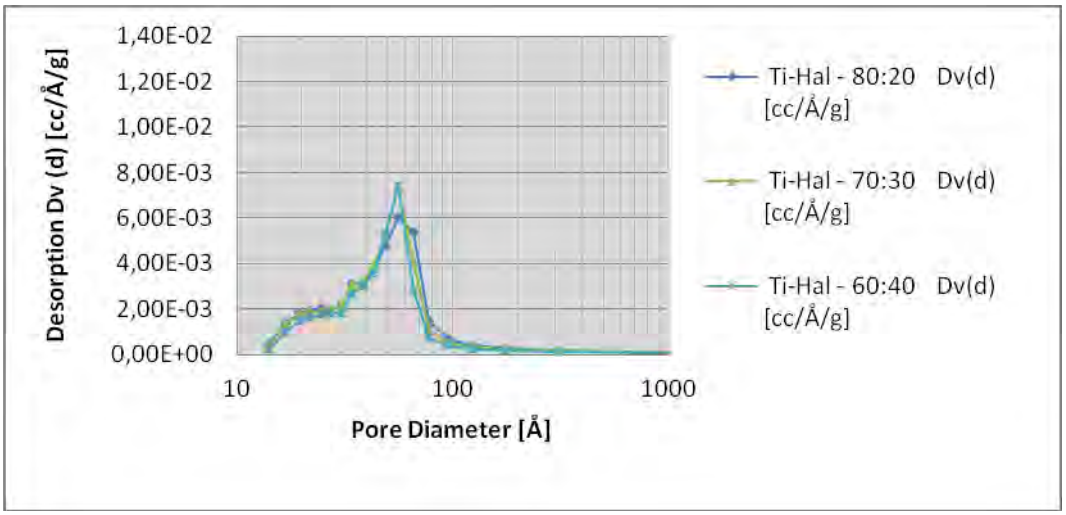

Figure 7 - Pore size distribution for nanocomposites using halloysite from Limnos compared with the previously studied nanocomposite (70-30).

4. Conclusions

Preparation of four new halloysite–TiO_2 nanocomposites using two different halloysites led to good dispersion of anatase on the external surfaces of halloysite tubes. Both halloysites were not destroyed by the treatment temperature, while the formation of hydrogen bonding between the outer surfaces of halloysite tubes and TiO_2 was detected. All nanocomposites largely showed interparticle mesopores of about 5.7nm. The characteristics of the nanocomposites presented here compared with the characteristics of already tested samples in different TiO_2-Halloysite proportion (70-30) that were presented in our recently published paper (Papoulis et al., 2013b) suggest promising photocatalytic activities in decomposing organic as well as inorganic air pollutants.

5. Acknowledgments

The authors would like to acknowledge financial support from the European Union (Lead Market European Research Area Network - LEAD ERA) and the Regional Authority of Western Greece

under the project ″Development and manufacturing of a new innovative nanotechnology-based decontaminant construction material for indoor building - INDOOR ECOPAVING″. The project is implemented under the Operational Programme "DEPIN 2007-2013" Priority Axis (PA) 'Digital convergence and entrepreneurship in Western Greece', action "Transnational Business Collaboration Western Greece" and is co-funded by the European Union –European Regional Development Fund and National Resources (NSRF 2007-2013).

The authors would like to thank Dr. Drakopoulos of the Foundation for Research and Technology-Hellas (FORTH) Institute of Chemical Engineering and High Temperature Chemical Processes (ICE/HT) Rio-Patras, Greece, for his help with SEM micrographs.

6. References

Aranda P., Kun R., Martín-Luengo M. A., Letaïef S., Dékány I., and Ruiz-Hitzky E. 2008. Tiatania-sepiolite nanocomposites prepared by a surfactant templating colloidal route, *Chem. Mater*., 20, 84-91.

Brindley G.W. and Robinson K., 1946. Randomness in the structures of kaolinitic clay minerals, *Tran. of the Far. Soc.,* 42B, 198-205.

Bobos I., Duplay J., Rocha J. and Gomes C. 2001. Kaolinite to halloysite-7 Å transformation in the kaolin deposit of Sao Vicente de Pereira. Portugal, *Clays and Clay Miner*., 49, 596-607.

Chmielarz L., Piwowarska Z., Kustrowski P., Węgrzyn A., Gil B., Kowalczyk A., Dudek B., Dziembaj R. and Michalik M. 2011. Comparison study of titania pillared interlayered clays and porous clay heterostructures modified with copper and iron as catalysts of the DeNOx process, *Appl. Clay Sci*., 53, 164-173.

Fujishima A., Tata N.R.and Donald A.T. 2000. Titanium dioxide photocatalysis, *J. Photochem. Photobio. C*., 1, 1–21.

Hoffmann M.R., Martin S.T., Choi W. and Bahnemann D.W. 1995. Environmental application of semiconductor photocatalysis, *Chem. Rev*., 95, 69–96.

Joussein E., Petit S. Churchman J., Theng B., Righi D.and Delvaux B. 2005. Halloysite clay minerals – A review, *Clay Miner.,* 40, 383-426.

Rouquerol J., Avnir D., Fairbridge C.W., Everett D.H., Haynes J.H., Pernicone N., Ramsay J.D.F.,
Sing K.S.W. and Unger K.K. 1994. Recommendations for the characterization of porous solids, IUPAC Recommendations, Technical Report, *Pure and Appl. Chem.,* 66, 1739-1758

Karamanis D., Ökte A.N., Vardoulakis E.and Vaimakis T. 2011. Water vapor adsorption and photocatalytic pollutant degradation with TiO_2-Sepiolite nanocomposites, *Appl. Clay Sci.,* 53, 181-187.

Kibanova D., Trejo M., Destaillats H. and Cervini-Silva J. 2009. Synthesis of hectorite–TiO_2 and kaolinite–TiO_2 nanocomposites with photocatalytic activity for the degradation of model air pollutants, *Appl. Clay Sci*., 42, 563-568.

Langlet M., Jenouvrier P., Kim A., Manso M. and Trejo-Valdez M. 2003. Functionality of aerosol-gel deposited TiO_2 thin films processed at low temperature, *J. Sol–Gel Sci. Technol*., 26, 759–763.

Martínez-Ortiz M.J., Fetter G. and Domínguez J.M. 2003. Catalytic hydrotreating of heavy vacuum gas oil on Al- and Ti-pillared clays prepared by conventional and microwave irradiation methods, *Mesopor. Mater*., 58, 73–80.

Michael R.H., Scot T.M., Wonyong C. and Detlef W.B. 1995. Environmental applications of semiconductor photocatalysis, *Chem. Rev*., 95, 69–96.

Mogyorósi K., Farkas A., Dékány I., Ilisz I. and Dombi A. 2002. TiO2 based photocatalytic degradation of 2-chlorophenol adsorbed on hydrophobic clay, *Environ. Sci. Technol*. 36, 3618–3624.

Nikolopoulou A., Papoulis D., Komarneni S., Tsolis-Katagas P., Panagiotaras D., Kacandes G.H., Zhang P., Yin S. and Sato T. 2009. Solvothermal Preparation of TiO_2/Saponite Nanocomposites and Photocatalytic Activity, *Appl. Clay Sci,*. 46, 363-368.

Papoulis D., Komarneni S., Panagiotaras D.and Katsuki H. 2012. Halloysite-TiO_2 nanocomposites: Synthesis and Characterization, *Modern Management of Mine Producing, Geology and Environmental Protection*, SGEM, Bulgary, 3, 459-466.

Papoulis D., Komarneni S., Panagiotaras D., Nikolopoulou A., Christoforidis K.C., Fernández-Garcia, HuiHui Li, Yin S. and Sato T. 2013a. Palygorskite-TiO_2 nanocomposites: Part 2. Photocatalytic Activities in decomposing air and organic pollutants, *Appl. Clay Sci.* (in press).

Papoulis D., Komarneni S., Panagiotaras D., Stathatos E., Toli D., Christoforidis K.C., Fernández-Garcia, HuiHui Li, Yin S., Sato T. and Katsuki H. 2013b. Halloysite-TiO_2 nanocomposites: Synthesis, characterization and photocatalytic Activity, *Appl. Catal. B. Env.,* 132-133, 416-422.

Papoulis D., Komarneni S., Nikolopoulou A., Tsolis-Katagas P., Panagiotaras D., Kacandes G.H., Zhang P., Yin S., Sato T. and Katsuki H. 2010. Palygorskite- and Halloysite-TiO_2 nanocomposites: Synthesis and Photocatalytic Activity, *Appl. Clay Sci.,* 50, 118-124.

Sing K.S.W., Everett D.H., Haul R.A.W., Moscou L., Pierotti R.A., Rouquerol N. and Siemieniewska T. 1985. Reporting physisorption data for gas/solid systems with special reference to the determination of surface area and porosity, *Pure Appl. Chem*., 57, 603–619.

Sing K.S.W. and Williams R.T. 2004. The use of molecular probes for the characterization of nanoporous adsorbents, *Part. Part. Syst. Charact*., 71–79.

Zhao D., Zhou J. and Liu N. 2006. Characterization of the structure and catalytic activity of copper modified palygorskite/TiO_2 (Cu_2+-PG/TiO_2) catalysts, *Mater. Sci. Eng*., A 431, 256–262.

Δελτίο της Ελληνικής Γεωλογικής Εταιρίας, τομ. XLVII , 2013
Πρακτικά 13ου Διεθνούς Συνεδρίου, Χανιά, Σεπτ. 2013

Bulletin of the Geological Society of Greece, vol. XLVII 2013
Proceedings of the 13th International Congress, Chania, Sept. 2013

ORIGIN OF THE HIGH-K TERTIARY MAGMATISM IN NORTHERN GREECE: IMPLICATIONS FOR MANTLE GEOCHEMISTRY AND GEOTECTONIC SETTING

Pipera K.[1], Koroneos A.[1], Soldatos T.[1], Poli G.[2] and Christofides G.[1]

[1]School of Geology, Aristotle University of Thessaloniki, 54124, Thessaloniki, Greece, piperakyr@gmail.com, koroneos@geo.auth.gr, soldatos@geo.auth.gr, christof@geo.auth.gr

[2]Department of Earth Sciences, University of Perugia, Piazza Università, 06100 Perugia, Italy, polig@unipg.it

Abstract

Tertiary plutonic and volcanic rocks cropping out in the Rhodope Massif (N. Greece) are studied using existing and new geochemical and isotopic data. Most of these rocks belong to the post-collisional magmatism formed as part of the prolonged extensional tectonics of the Rhodope region in Late Cretaceous–Paleogene time. This magmatism is considered to be of mantle origin; however, the character of the mantle source is controversial. Rock bulk chemistry and compositional variations show magmas with calc-alkaline to high-K calc-alkaline and shoshonitic features associated with magmatism at convergent margins. Initial $^{87}Sr/^{86}Sr$, $^{143}Nd/^{144}Nd$ ratios, Pb isotopes and REE composition of the mafic rocks indicate mainly an enriched mantle source, even if some rocks indicate a depleted mantle source. Low- and High-K mafic members of these rocks coexist indicating a strongly heterogeneous mantle source. The High-K character of some of the mafic rocks is primarily strongly related to mantle enrichment by subduction-related components, rather than crustal contamination. The geochemical characteristics of the studied rocks (e.g Ba/Th,Th/Yb,Ba/La, U/Th, Ce/Pb) indicate that primarily sediments and/or sediment melts, rather than fluid released by the subducted oceanic crust controlled the source enrichment under the Rhodope Massif.

Keywords: *Rhodope Massif, Mantle geochemistry, Geotectonic Setting, K-rich Magmatism.*

Περίληψη

Τριτογενή πλουτωνικά και ηφαιστειακά πετρώματα που απαντώνται στη Μάζα της Ροδόπης (Β. Ελλάδα) μελετώνται χρησιμοποιώντας υπάρχοντα και νέα γεωχημικά και ισοτοπικά δεδομένα. Τα περισσότερα από τα πετρώματα αυτά ανήκουν στο μετά τη σύγκρουση μαγματισμό ο οποίος συνδέεται με την παρατεταμένη εφελκυστική τεκτονική στην περιοχή της Ροδόπης που χρονολογείται από το Κρητιδικό έως το Παλαιογενές. Ο μαγματισμός αυτός θεωρείται μανδυακής προελεύσεως όμως, ο χαρακτήρας της μανδυακής πηγής είναι αμφιλεγόμενος. Η χημική σύσταση των πετρωμάτων και οι συστασιακές μεταβολές δείχνουν μαγματισμό ασβεσταλκαλικού έως υψηλού-Καλίου και σωσσονιτικό χαρακτήρα που συνδέεται με συγκλίνοντα

περιθώρια. Οι αρχικοί λόγοι $^{87}Sr/^{86}Sr$, $^{143}Nd/^{144}Nd$ καθώς και τα ισότοπα Pb και η σύσταση σε Σπάνιες Γαίες των βασικών πετρωμάτων δείχνουν κυρίως εμπλουτισμένη μανδυακή πηγή αν και κάποια πετρώματα δείχνουν εκπτωχευμένη. Χαμηλού- και Υψηλού-Καλίου βασικά πετρώματα συνυπάρχουν, δείχνοντας μια έντονα ετερογενή μανδυακή πηγή. Ο υψηλού-Καλίου χαρακτήρας ορισμένων από τα βασικά πετρώματα είναι έντονα συνδεδεμένος με το μανδυακό εμπλουτισμό παρά με τη φλοιική μόλυνση. Τα γεωχημικά χαρακτηριστικά των πετρωμάτων αυτών (π.χ Ba/Th,Th/Yb, Ba/La, U/Th, Ce/Pb) δείχνουν ότι κυρίως ιζήματα και/ή τήγματα ιζημάτων παρά ρευστών που απελευθερώνονται από την υποβύθιση της ωκεάνιας πλάκας έλεγχαν τον εμπλουτισμό της πηγής κάτω από τη μάζα της Ροδόπης.
Λέξεις κλειδιά: *Μάζα Ροδόπης, Γεωχημεία Μανδύα, Γεωτεκτονικό Περιβάλλον, Υψηλού-Καλίου μαγματιμός.*

1. Introduction

The Rhodope Massif (N. Greece) is defined as a key area for understanding the evolution of the Tethyan systems. Due to the complexity of the area many researchers have focused on its tectonic and magmatic evolution separately and some efforts have been made to combine petrology and tectonics. Various Tertiary plutonic and volcanic rocks crop out in the Rhodope Massif with most important occurrences those of Vrontou, Xanthi, Elatia, Maronia, Leptokarya-Treis Vryses-Chalasmata, Evros, Samothraki and Dipotama-Kalotyho (Figure 1). Different hypotheses have been suggested on the nature of the source and the crustal contamination controlling their composition. A great deal of research has been made regarding their geochemistry and evolution as well as their origin, and many geochemical data have been published (Del Moro et al., 1988; Eleftheriadis et al., 1989; Mavroudchiev et al., 1992; Jones et al., 1992; Pe-Piper et al., 1998; Christofides et al., 1998, 2002, 2011; Soldatos et al., 1998, 2008; Papadopoulou et al., 2004; Vlahou et al., 2006). The Tertiary magmatism of Rhodopes is considered as the result of crust-mantle interaction; however the nature of the mantle component is controversial. In order to address the nature of the mantle source, the role of crustal contamination and the process of their formation during the Tertiary tectonic events in Rhodope Massif the basic members of the magmatic rocks, which are considered crucial for the nature of their source, are studied. In detail, the trace element geochemistry and their isotopic characteristics are examined.

2. Geological Setting

2.1 The Rhodope Massif

The Rhodope Massif (RM) is a polymetamorphic terrain extending along the Greek-Bulgarian border and covers part of the north-eastern Macedonia and western Thrace in Greece and south-eastern Bulgaria (Figure 1) as well as a small part of north-western Turkey. It is located in the frontal part of the Eurasian continental margin. It was assumed to have been formed from the closure of one subduction-exhumation cycle, the closure of the Paleo-Tethys ocean. It comprises mostly continental rocks with intercalations of oceanic material and represents the northernmost part of a southwest vergent Alpine nappe stack that developed during convergence between Africa and Europe from Jurassic to Neogene times (Papanikolaou and Panagopoulos, 1981; Burg et al., 1996; Ricou et al., 1998; Barr et al. 1999).

The northern border of the RM is defined by the west-northwestern-striking Maritsa fault in Bulgaria, which is composed of a series of subparallel, mainly dextral strike-slip faults (Burg et al. 1996, Georgiev et al., 2009). To the west the top-to-the-SW Tertiary Strymon detachment (Dinter and Royden, 1993; Sokoutis et al. 1993; Dinter et al. 1995; Lips et al. 2000) separates the RM from the Serbomacedonian Massif. To the east, the RM is structurally overlain by the Circum

Rhodope Belt (Kaufmann et al., 1976; Kockel et al., 1977; Meinhold et al., 2010), comprising greenschist-facies rocks and ophiolites.

The subdivision of RM into different units is a subject of debates by many workers (e.g., Papanikolaou and Panagopoulos 1981; Mposkos 1989; Kilias and Mountrakis, 1990; Dinter et al., 1995; Burg et al. 1996; Krohe and Mposkos, 2002; Bonev et al., 2006; Georgiev et al., 2010; Turpaud, 2006; Bonev and Stampfli, 2008; Liati et al., 2011). Some schemes are based on structural criteria (e.g. Burg et al., 1996) other on metamorphic facies distinction (e.g. Krohe and Mposkos, 2002) and lately on geochronological data (Turpaud, 2006; Turpaud and Reischmann, 2010). A commonly used division for the Greek part of RM (central and western), based both on geological and petrological criteria, is the one proposed by Papanikolaou and Panagopoulos (1981), with an upper tectonic unit (UTU, also known as Sidironero unit) and a lower tectonic unit (LTU, also known as Pangaeo unit), separated by a SSE–NNW striking, northeast-dipping, thrust fault zone (Nestos thrust).

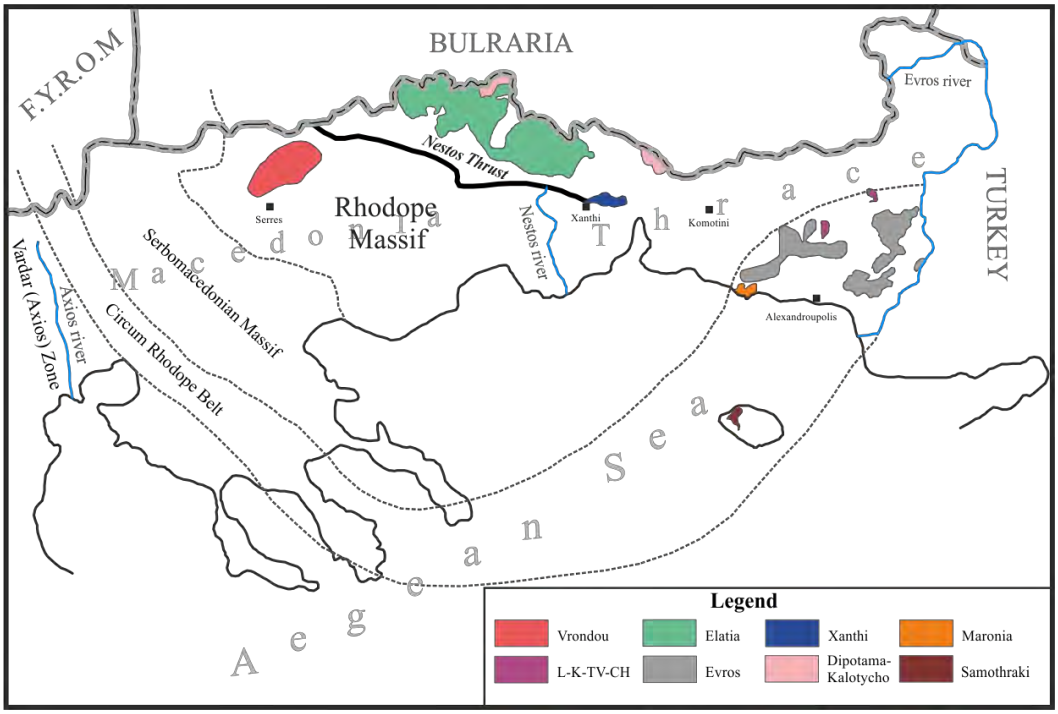

Figure 1 – Schematic map of Northern Greece with the locations of the studied rocks.

2.2 Tertiary Magmatic Activity

The extensional deformation of RM resulted in strong crustal thinning which started in Eocene (Kilias et al, 1999; Burchfiel et al., 2003; Brun and Sokutis, 2007) or earlier in Early Paleocene (Bonev et al, 2006). A strong crustal thinning in back-arc areas is usually associated with magmatism. Post – collisional magmatism of Paleogene to Neogene age (plutonic and volcanic, Figure 1) variable in composition, space, and time dominates the RM (Koukouvelas & Pe-Piper, 1991; Dinter et al., 1995; Burg et al., 1996; Kilias & Mountrakis, 1998; Christophides et al., 2001, 2004; Marchev et al., 2005; Bonev et al., 2006). Similar magmatic activity exists also in the continuation of RM in north-western Turkey (Bonev et al., 2007 and references therein). This magmatism is associated probably with the subduction of Pindos ocean; however, the remnant of the subducted slab of the Eastern margin of the opened, until the Tertiary time, Vardar-Axios ocean could also be the driving mechanism for the Tertiary magmatic activity in the Rhodope province or Vardar oceanic lithospheres (see Perugini et al., 2004; Kilias et al., 2011).

The presence of fault-controlled extensional basins with intrusive and extrusive magmatism dominated the RM. Volcanic rocks are found north of Xanthi in the Dipotama-Kalotycho are, in western Thrace in the extensive area of Alexandroupolis the Evros volcanic rocks (EVR) and in the island of Samothraki (Figure 1). The **Dipotama-Kalotycho** Oligocene volcanic rocks cut across the crystalline basement of the RM and are structurally associated with the formation of sedimentary (extensional) basins and consist mainly of intermediate to basic rocks apart from the Dipotama area where only felsic rocks occur (Eleftheriadis, 1995). The **EVR** are in close association with fault-controlled sedimentary basins. Three volcanic areas, namely Loutros-Feres-Dadia, Kirki-Esimi and Mesti-Petrota, after the corresponding basins, are distinguished. Their composition ranges from basaltic andesite to rhyolite through andesite, trachyandesite, trachydacite and dacite (Christofides et al, 2002). It is to note that, since so far isotopic data are not available for the EVR, these rocks are not included in the present study. The **Samothraki volcanic rocks** are overlying an Eocene clastic neritic sequence. They are distinguished in three main groups based on their field occurrence and geochronology: the "old" group comprising basalts to latites, the "intermediate" group of andesites to latites and the "young" group of latites and rhyolites (Vlahou et al., 2006).

Many plutonic rocks of post-collisional origin are also found in the RM, apart from the **Elatia pluton** that is considered to be of subduction tectonic environment (Soldatos et al., 2008). It constitutes the main part of the Elatia-Skaloti-Paranesti granitic complex. Its main lithology is a (hornblende)-biotite granodiorite with a marginal porphyritic phase. The eastern part of the pluton is occupied by a two-mica granite which intrudes the granodiorite. The **Maronia pluton** northwards and westwards intrudes marbles of the metasedimentary series of the Makri unit causing a rather wide zone of contact metamorphism (skarn) (Doryphoros, 1990). Eastwards it intrudes a metamorphic sequence of phyllites, greenschists and gneisses of the overlying metavolcanosedimentary series of the same unit causing intense thermal metamorphism to the surrounding rocks (hornfelses), while southwards the pluton itself is intruded by a small body of porphyritic micro-granite. Three main rock types have been distinguished: a) the basic group, with gabbros b) the intermediate group, with monzogranite to quartz-monzogranite and c) the felsic group, with granite in the form of dykes (Papadopoulou et al., 2004). The **Xanthi** pluton is in magmatic contact with Pangaion marbles to the west and gneisses and marbles of Sidironeron Unit. There is a contact metamorphic aureole typically a few hundred meters wide (Christofides, 1977; Liati, 1986). To the east the pluton cuts Eocene-Oligocene sedimentary rocks (dominantly flysch) which are intruded by andesitic dykes.

3. Analytical Methods

Some major elements used in the present study were taken from previous authors (Eleftheriadis, 1995; Christofides et al, 2002; Papadopoulou et al., 2004; Vlahou et al., 2006; Soldatos et al., 2008; Christofides et al. 2011) as well as the isotopic composition of Sr and Nd apart from the Xanthi and Vrontou plutons. The rest of the samples were analysed for major elements by X-ray fluorescence (XRF) in Saint Mary's Univeristy, Halifax, Nova Scotia, Canada, and the Acme Analytical Laboratories (Vancouver) Ltd, Canada. All trace elements and REE analyses were performed on a laser ablation quadrupole inductively coupled plasma mass spectrometry (LA ICP-MS) in the Department of Earth Sciences, University of Perugia, Italy and on an quadrupole inductively coupled plasma mass spectrometry (ICP-MS) in the Acme Analytical Laboratories (Vancouver) Ltd, Canada. Additional analyses of some transitional elements already analyzed by ICP-MS, were determined by X-ray fluorescence (XRF) at Saint Mary's Univeristy, Halifax, Nova Scotia, Canada. The isotopic Sr and Nd content from Xanthi and Vrontou samples were determined in the Department of Lithospheric Research, University of Vienna, Austria.

4. Geochemical Characteristics

4.1 Major Elements

Most samples both plutonic (Figure 2a) and volcanic (Figure 2b) belong to the calk-alkaline, high-K and shoshonitic series. All rocks demonstrate a wide range on SiO_2 content. The Elatia pluton consists mainly from felsic rocks and so far was considered to be of crustal origin. During the present work several mafic microgranular enclaves of basic composition were found on the northern part and analysed. This redefines the aspect of a crustal origin for the Elatia pluton and in the present paper is considered as a mantle derived rock.

4.2 Trace Elements

Geochemical characteristics for representative mafic rocks are illustrated for each area in primitive mantle normalized multi-element diagrams (Figure 3). Most of the rocks, show similar patterns with LILE enricjment and HFSE depletion. Few basic rocks indicate LILE depletion which is not accompanied by HFSE enrichment. One sample from Samothraki and one from Vrondou show relative Nb and Ta enrichment. In Figure 4 trace elements diagrams are used as indicators of fluid or sediment component enrichment (a and b) of the mantle wedge and the degree of the source enrichment (c).

4.3 Rare Earth Elements (REE)

The REE chondrite normalized patterns of the rocks are illustrated in the Figure 5. All rocks are enriched in LREE and slightly depleted in HREE. One sample of Samothraki exhibits parallel to Chondrite pattern showing a strongly depleted mantle source. Most samples exhibit negative Eu anomaly and some samples no Eu anomaly. Eu anomaly can be produced by plagioclase fractionation, residual plagioclase in the source or source contamination by slab-derived fluids and sediments (Ellam & Hawkesworth, 1988). Since most samples have high Al content it means that they have not undergone significant plagioclase fractionation but contamination from the Rhodope metamorphic lithologies or source contamination from the subducted crust.

4.4 Isotopic Data

In Figure 6 the $^{143}Nd/^{144}Nd$ vs $^{87}Sr/^{86}Sr$ available data are illustrated. There is a wide range on both Nd and Sr isotopes for each area which implies the different degrees of contamination. Most samples are plotted between EM-I (Enriched Mantle I) and EM-II (Enriched Mantle II) mantle reservoirs supporting the enriched mantle source of these rocks. There are samples that demonstrate a more depleted component both for Nd and Sr isotopes especially samples from Xanthi, Samothraki and Elatia and the trend of most samples is towards DMM reservoir rather than continental crust.

5. Discussion and Conclusions

The Rhodope magmatic rocks are undoubtedly of orogenic origin as already stated by many previous workers (see 2.2). A subduction mechanism proposed for the Tertiary magmatism of Rhodope which persisted for many million years. Due to the variations on the Rhodope magmatism many more complicated subduction models have been proposed (see Marchev et al., 2004). Morover asthenospheric contribution is confirmed in the Bulgarian part of Rhodope. Rollback and slab break off is one of them and was suggested for the magmatism in the Aegean region. It leads to the heating of the lithospheric mantle by upwelling of the asthenosphere and melting of its enriched layers. Different degrees of partial melting produce magmas ranging from alkaline to ultrapotassic, whereas slightly higher degrees of melting produce calk-alkaline melts. Another model is delamination of the thickened crust after the continental collision proposed by

Yanef et al. (1998). It differs from the slab break off model cause it predicts rapid intrusion of the asthenosphere in the place of the delaminated mantle and eclogitized lower crust resulting in uplift

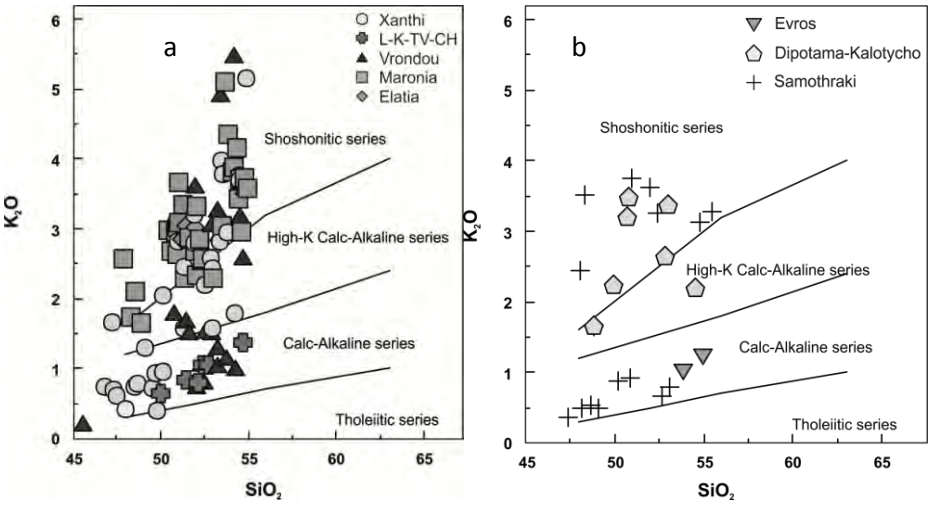

Figure 2 - SiO_2 vs K_2O of the plutonic rocks (a) and volcanic rocks (b) after Peccerillo & Taylor 1976.

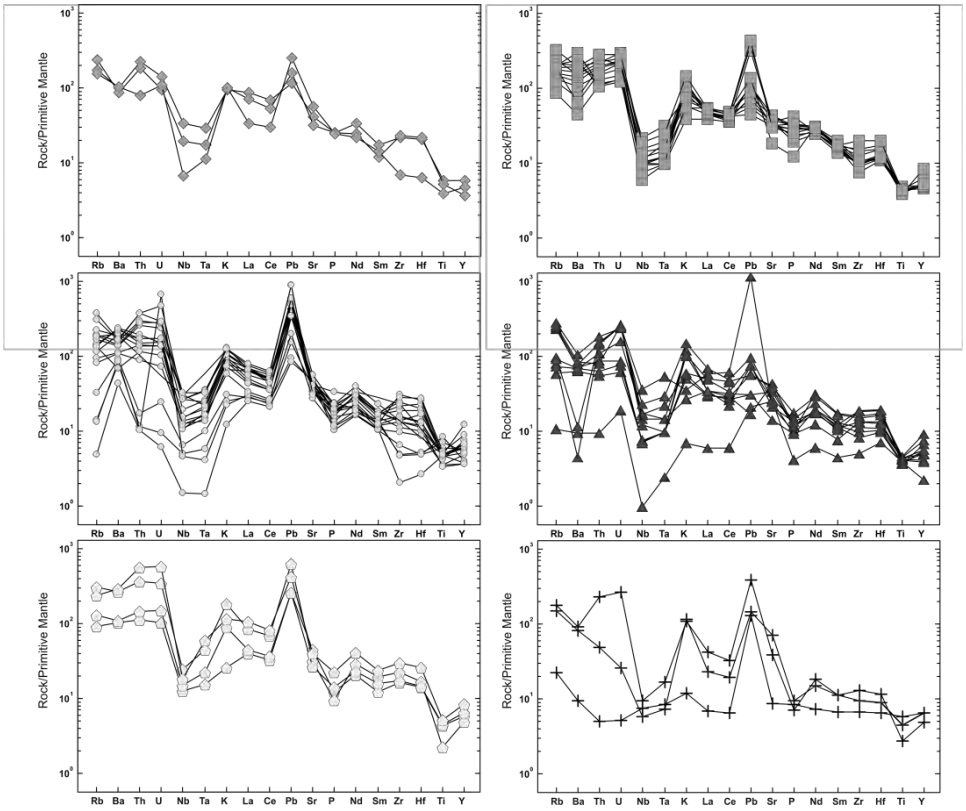

Figure 3 - Primitive mantle normalized multi-element diagrams. Normalization values after Sun & McDonough (1989). Symbols as in Figure 2.

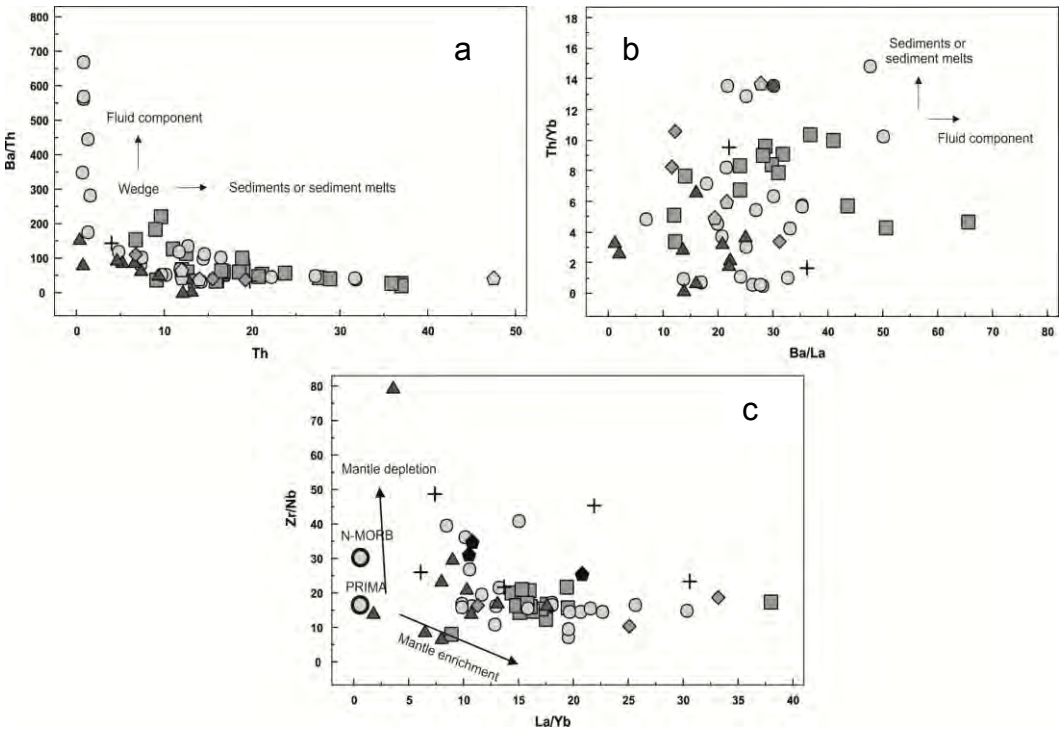

Figure 4 - a) Ba/Th vs Th as indicator of fluid or sediment component (Elliot et al., 1997) b) Th/Yb vs Ba/La as indicator of fluid or sediment component (Hawkesworth et al., 1997) c) Zr/Nb vs La/Yb for source enrichment (Münker, 2000). Symbols as in Figure 2.

and extensional collapse. Convective removal is another subduction model which predicts convective thinning of the unstable thickened lithospheric mantle and may result in removal of the whole mantle lithosphere and its replacement by hot asthenosphere. This will cause fast uplift of the overlying crust. According to Marchev et al. (2004) the above models have many shortcomings and are not able to describe the Rhodope magmatism. The same authors propose a form of convectional thinning of the lithosphere and of mantle diapirism due to asthenospheric origin of basalts they analyzed. So far, due to the lack of asthenospheric derived rocks in the Greek part of the Rhodope Massif, the above theory seems to interpret the Tertiary Rhodopian magmatism better than the previous. A more satisfactory explanation needs to be proposed and is under study for the Greek part of Rhodope.

Regarding the available geochemical data, an enriched and depleted mantle source existed simultaneously and generated the magmatic rocks of Rhodope. A 'leopard skin' mantle wedge during the Tertiary, which was able to produce a wide range of mafic magmas has been proposed from Perugini et al. (2004) to explain the heterogeneous mantle under RM. The same authors proposed the influence of the uprising asthenospheric mantle since the high K_2O and the high LILE abundances are not in agreement with the relatively low Sr and high Nd isotopic values. Nevertheless, satisfactory data to support the above proposal are missing.

The enrichment of the mantle wedge above the subducted oceanic crust was caused from sediments or sediment melts derived from the subducted ocean. The MORB-like patterns of some dykes from Samothraki reflects strong mantle depletion. The no-negative Nb-Ta anomaly of one sample from Samothraki may imply asthenospheric contribution. The present study is in progress and more geochemical and isotopic data are to be presented in order to give satisfactory explanations on the nature of the Rhodopian magmatism and the processes that took place.

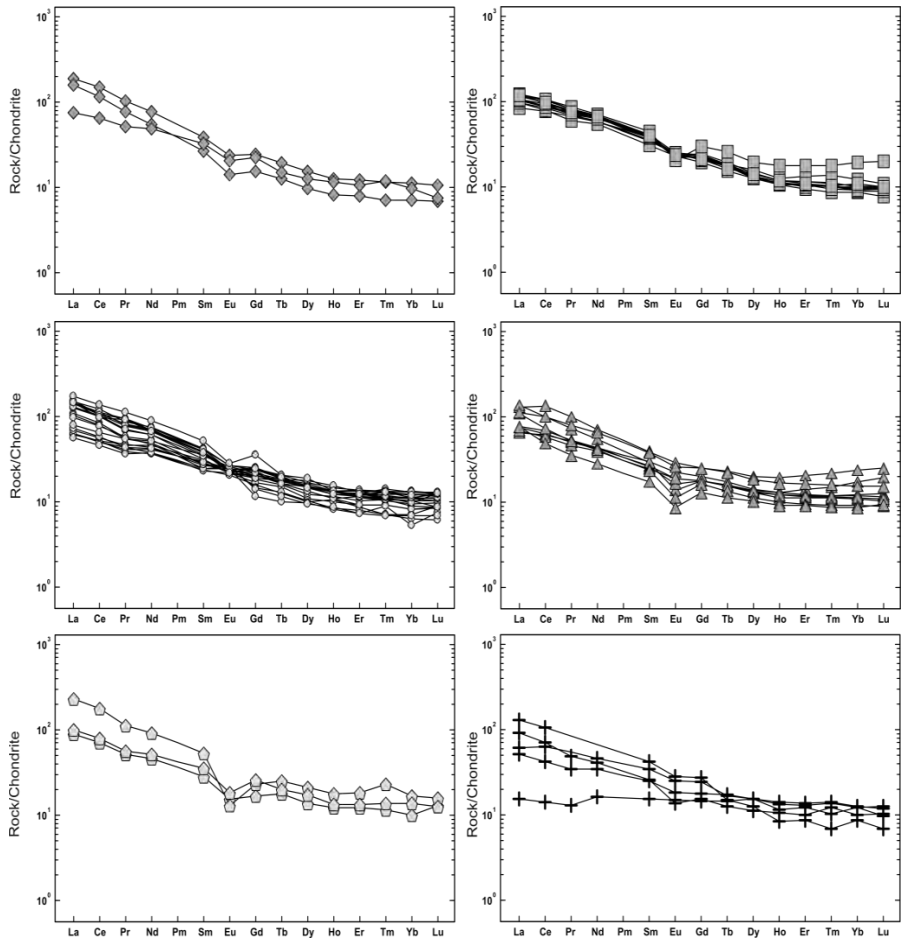

Figure 5 - Chondrite normalized multi-element diagrams. Normalization values after Boynton (1984). Symbols as in Figure 2.

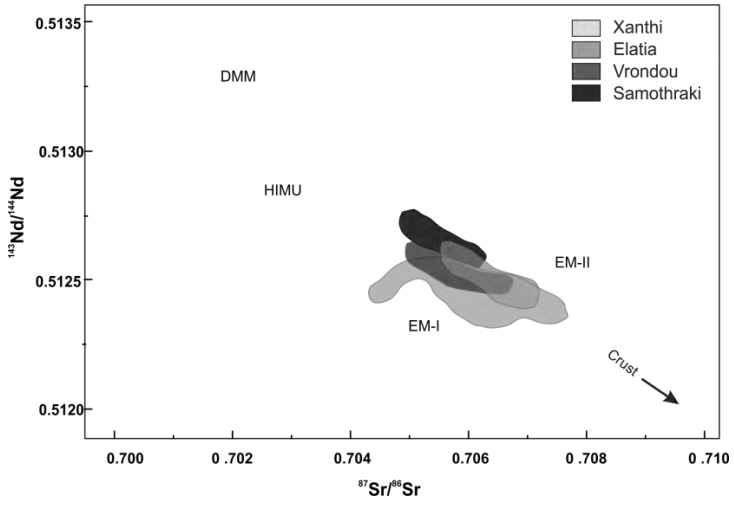

Figure 6 - $^{143}Nd/^{144}Nd$ vs $^{87}Sr/^{86}Sr$ with some mantle reservoirs illustrated. Symbols as in Figure 2.

6. Acknowledgments

This research has been co-financed by the European Union (European Social Fund – ESF) and Greek national funds through the Operational Program "Education and Lifelong Learning" of the National Strategic Reference Framework (NSRF) - Research Funding Program: Heracleitus II. Investing in knowledge society through the European Social Fund.

Authors would deeply like to thank Prof. Georgia Pe-Piper for the XRF analyses of some rocks. Critical reviews by Georgia Pe-Piper and two anonymous reviewers helped us improve the article.

7. References

Barr S.R., Temperley S. and Tarney J. 1999. Lateral growth of the continental crust through deep level subduction–accretion: a re-evaluation of central Greek Rhodope, *Lithos*, 46(1), 69-94.

Bonev N., Burg J. P. and Ivanov Z. 2006. Mesozoic–Tertiary structural evolution of an extensional gneiss dome-the Kesebir–Kardamos dome, eastern Rhodope (Bulgaria–Greece*), International Journal of Earth Sciences*, 95(2), 318-340.

Bonev N. and Beccaletto L. 2007. From syn-to post-orogenic Tertiary extension in the north Aegean region: constraints on the kinematics in the eastern Rhodope–Thrace, Bulgaria–Greece and the Biga Peninsula, NW Turkey, *Geological Society, London, Special Publications*, 291(1), 113-142.

Bonev N. and Stampfli G. 2008. Petrology, geochemistry and geodynamic implications of Jurassic island arc magmatism as revealed by mafic volcanic rocks in the Mesozoic low-grade sequence, eastern Rhodope, Bulgaria, *Lithos*, 100(1), 210-233.

Burg, J. P., Ricou, L. E., Ivano, Z., Godfriaux, I., Dimov, D., & Klain, L., 1996. Syn-metamorphic nappe complex in the Rhodope Massif. Structure and kinematics, *Terra Nova*, 8(1), 6-15.

Christofides G. 1977. Contribution to the study of plutonic rocks in the area of Xanthi, *Ph.D. thesis*, Univeristy of Thessaloniki, 249 pp.

Christofides G., Pecskay G., Eleftheriadis Z., Soldatos G. and Koroneos T. 2002. Tertiary Evros volcanic rocks, Thrace, Northeastern Greece: Petrology, K/Ar geochronology and volcanism evolution, *Extended Abstract CBGA*, Bratislava.

Christofides G., Soldatos T., Eleftheriadis G. and Koroneos A. 1998. Chemical and isotopic evidence for source contamination and crustal assimilation in the Hellenic Rhodope plutonic rocks, *Acta Vulcanologica*, 10, 305-318.

Christofides G., Koroneos A., Pipera K., Poli G. and Soldatos T. 2011. The Oligocene Xanthi Plutonic Complex (N. Greece): Petrogenetic implications inferred from major and trace element and Sr, Nd and Pb isotope geochemistry, *Abstract, VII Hutton Symposium on Granites and Related Rocks*, Avila, Spain.

Del Moro A., Innocenti F., Kyriakopoulos C., Manetti P. and Papadopoulos, P. 1988. Tertiary granitoids from Thrace (Northern Greece): Sr isotopic and petrochemical data, *Neues Jahrbuch für Mineralogie Abhandlungen*, 159, 113-135.

Dinter D.A., Macfarlane A., Hames W., Isachsen C., Bowering S. and Royden L. 1995.V-Pb and $^{40}Ar/^{39}Ar$ geochronology of the Symvolon granodiorite: Implications for the thermal and structural evolution of the Rhodope metamorphic core complex, northeastern Greece, *Tectonics*, 14(4), 886-908.

Dinter D. A., and Royden L. 1993. Late Cenozoic extension in northeastern Greece: Strymon Valley detachment system and Rhodope metamorphic core complex, *Geology*, 21(1), 45-48.

Doryphoros K. 1990. The Maronia pluton and its metamorphic effects on the surrounding rocks of the Makri series, *Ph.D. Thesis*, National Technical University of Athens, 166 pp.

Eleftheriadis G. 1995. Petrogenesis of the Oligocene volcanics from the Central Rhodope massif (N. Greece), *European Journal of Mineralogy*, 7(5), 1169-1182.

Ellam R.M and Hawkesworth, C. J. 1988. Elemental and isotopic variations in subduction related basalts: evidence for a three component model, *Contributions to Mineralogy and Petrology*, 98(1), 72-80.

Elliott T., Plank T., Zindler A., White W., and Bourdon B. 1997. Element transport from slab to volcanic front at the Mariana arc, *Journal of Geophysical Research*, 102(B7), 14991-15.

Georgiev N., Pleuger J., Froitzheim N., Sarov S., Jahn-Awe S. and Nagel T. J. 2010. Separate Eocene–Early Oligocene and Miocene stages of extension and core complex formation in the Western Rhodopes, Mesta Basin, and Pirin Mountains (Bulgaria), *Tectonophysics*, 487(1), 59-84.

Hawkesworth C., Turner S., Peate D., McDermott F. and van Calsteren, P. 1997. Elemental U and Th variations in island arc rocks: implications for U-series isotopes, *Chemical Geology*, 139(1), 207-221.

Jones C.E. Tarney J., Baker J. H., and Gerouki F. 1992. Tertiary granitoids of Rhodope, northern Greece: Magmatism related to extensional collapse of the Hellenic Orogen?, *Tectonophysics*, 210(3), 295-314.

Kauffmann G., Kockel F., Mollat H. 1976. Notes on the stratigraphic and paleogeographic position of the Svoula Formation in the Innermost Zone of the Hellenides (Northern Greece), *Bulletin de la Societe géologique de France* (7), 28, 2, 225-230.

Kilias A. and Mountrakis D. 1990. Kinematics of the crystalline sequences in the western Rhodope massif, *Geologica Rhodopica*, 2, 100-116.

Kilias A. and Mountrakis D. 1998. Tertiary extension of the Rhodope massif associated with granite emplacement (Northern Greece), *Acta Vulcanologica*, 10, 331-338.

Kilias A., Falalakis G., Sfeikos A., Papadimitriou E., Vamvaka A., and Gkarlaouni Ch. 2011. Architecture of Kinematics and Deformation History of the Tertiary Supradetachment Thrace Basin: Rhodope Province (NE Greece), New Frontiers in Tectonic Research - *At the Midst of Plate Convergence*, Uri Schattner (Ed.)

Kockel F., Mollat H. and Walther H.W. 1977. *Erläuterungen zur geologischen Karte der Chalkidhiki und angrenzender Gebiete 1:100,000 (Nord-Griechenland)*, Bundesanstalt für Geowissenschaften und Rohstoffe, Hannover, 119 pp.

KoukouveIas L., Pe-Piper G. 1991. The Oligocene Xanthi pluton, northern Greece: a granodiorite emplaced during regional extension, *J Geol Soc Lond*, 148, 749-758.

Krohe A. and Mposkos E. 2002. Multiple generations of extensional detachments in the Rhodope Mountains (northern Greece): evidence of episodic exhumation of high-pressure rocks, *Special Publication-Geological Society of London*, 204, 151-178.

Liati A. 1986. Regional metamorphism and overprinting contact metamosprhism of the Rhodope zone near Xanthi (N.Greece), *Ph.D. Thesis,* Techn. Univ. Braunschweig, 186 pp.

Liati A., Gebauer D. and Fanning, C.M. 2011. Geochronology of the Alpine UHP Rhodope zone: a review of isotopic ages and constraints on the geodynamic evolution. In: L.F. Dobrzhinetskaya, S.W. Faryad, S. Wallis, S. Cuthbert (Eds.), *Ultrahigh-Pressure Metamorphism: 25 Years After The Discovery of Coesite and Diamond*, Elsevier, London (2011), 295–316.

Lips A.L., White S. H. and Wijbrans J. R. 2000. Middle-late Alpine thermotectonic evolution of the southern Rhodope Massif, Greece, *Geodinamica Acta*, 13(5), 281-292.

Marchev P., Raicheva R., Downes H., Vaselli O., Chiaradia M., and Moritz R. 2004. Compositional diversity of Eocene–Oligocene basaltic magmatism in the Eastern Rhodopes, SE Bulgaria: implications for genesis and tectonic setting, *Tectonophysics*, 393(1), 301-328.

Marchev P., Kaiser-Rohrmeier, M., Heinrich C., Ovtcharova M., von Quadt A. and Raicheva R. 2005. Hydrothermal ore deposits related to post-orogenic extensional magmatism and core complex formation: The Rhodope Massif of Bulgaria and Greece, *Ore Geology Reviews*, 27(1), 53-89.

Mavroudchiev B., Nedyalkov R., Eleftheriadis G., Soldatos T. and Christofides G. 1993. Tertiary plutonic rocks from east Rhodope in Bulgaria and Greece, *Bull. Geol Soc. Greece*, XXVIII/2, 643-660.

Meinhold G., Kostopoulos D., Frei D., Himmerkus F. and Reischmann T. 2010. U–Pb LA-SF-ICP-MS zircon geochronology of the Serbo-Macedonian Massif, Greece: palaeotectonic constraints for Gondwana-derived terranes in the Eastern Mediterranean, *International Journal of Earth Sciences*, 99(4), 813-832.

Mposkos E. 1989. High-pressure metamorphism in gneisses and pelitic schists in the east Rhodope zone (N. Greece), *Mineralogy and Petrology*, 41(1), 25-39.

Münker C. 2000. The isotope and trace element budget of the Cambrian Devil River arc system, New Zealand: identification of four source components, *Journal of Petrology*, 41(6), 759-788.

Papadopoulou L., Christofides G., Koroneos A., Bröcker M., Soldatos T. and Eleftheriadis G. 2004. Evolution and origin of the Maronia pluton, Thrace, Greece, *Bulletin of the Geological Society of Greece*, 36.

Papanikolaou D. and Panagopoulos A. 1981. On the structural style of southern Rhodope, Greece, *Geologica Balcanica*, 11(3), 13-22.

Perugini D., Poli G., Christofides G., Eleftheriadis G., Koroneos A. and Soldatos T. 2004. Mantle-derived and crustal melts dichotomy in northern Greece: spatiotemporal and geodynamic implications, *Geological Journal*, 39(1), 63-80.

Pe-Piper G., Christofides G. and Eleftheriadis G. 1998. Lead and neodymium isotopic composition of Tertiary igneous rocks of northern Greece and their regional significance, *Acta Vulcanologica*, 10, 255-264.

Ricou L.-E., Burg J-P., Godfriaux I. and Ivanov Z. 1998. Rhodope and Vardar: the metamorphic and the olistostromic paired belts related to the cretaceous subduction under Europe, *Geodin Acta* 11, 285–309.

Sokoutis D., Brun J. P., Van Den Driessche J. and Pavlides, S. 1993. A major Oligo-Miocene detachment in southern Rhodope controlling north Aegean extension, *Journal of the Geological Society*, 150(2), 243-246.

Soldatos T., Koroneos A., Kamenov B. K., Peytcheva I., von Quadt A., Christofides G. and Sang H. 2008. New U-Pb and Ar-Ar mineral ages for the Barutin-Buynovo-Elatia-Skaloti-Paranesti batholith (Bulgaria and Greece): Refinement of its debatable age, *Geochem Mineral Petrol*, 46, 85-102.

Soldatos T., Poli G., Christofides G., Eleftheriadis G., Koroneos A. and Tommasini S. 1998. Petrology and evolution of transitional alkaline-subalkaline granitoids from Vrondou (NE Greece): evidence for fractional crystallization and magma mixing, *Acta Vulcanologica*, 10, 319-330.

Turpaud P. 2006. Characterization of igneous terranes by zircon dating: implications for the UHP relicts occurrences and suture identification in the Central Rhodope, Northern Greece, Northern Greece, *PhD thesis*, Johannes Gutenberg University, Mainz, 107 pp.

Turpaud P. and Reischmann, T. 2010. Characterisation of igneous terranes by zircon dating: implications for UHP occurrences and suture identification in the Central Rhodope, northern Greece, *International Journal of Earth Sciences*, 99(3), 567-591.

Vlahou M., Christofides G., Eleftheriadis G., Pinarelli L. and Koroneos A. 2006. Tertiary volcanic rocks from Samothraki island (north Aegean, Greece): Sr and Nd isotope constraints on their evolution. Postcollisional Tectonics and Magmatism in the Mediterranean Region and Asia, 409, 283.

Yanev Y., Innocenti F., Manetti P. and Serri, G. 1998. Upper Eocene-Oligocene collision-related volcanism in Eastern Rhodopes (Bulgaria)-Western Thrace (Greece): petrogenetic affinity and geodynamic significance, *Acta Vulcanologica*, 10, 279-292.

Δελτίο της Ελληνικής Γεωλογικής Εταιρίας, τομ. XLVII , 2013
Πρακτικά 13ου Διεθνούς Συνεδρίου, Χανιά, Σεπτ. 2013

Bulletin of the Geological Society of Greece, vol. XLVII 2013
Proceedings of the 13th International Congress, Chania, Sept. 2013

THE OCCURRENCES OF MG-HYDROXYCARBONATES IN SERPENTINITES OF THE WESTERN SECTION OF THE SOUTH AEGEAN VOLCANIC ARC (WEST ATTICA PENINSULA-NORTHEASTERN ARGOLIS PENINSULA), GREECE

Stamatakis M.G.[1] and Mitsis I.[1]

[1] National and Kapodistrian University of Athens, Faculty of Geology and Geoenvironment, Department of Economic Geology and Geochemistry, stamatakis@geol.uoa.gr mitsis@geol.uoa.gr

Abstract

In the area of West Attica Peninsula, Greece, ophiolitic rocks which outcrop mainly at the Geraneia Mountains, overlie Triassic-Jurassic limestone and covered by Plio - Pleistocene sedimentary rocks. The relatively widespread ophiolite occurrences are mainly serpentinized peridotites, considered as spinel lherzolites and dunites. In the Northeastern Argolis Peninsula several small remnants of an ophiolitic nappe outcrop which consists from serpentinized and tectonically deformed peridotites, overthrusted on the Eocene flysch. Both regions are characterized by manifestations of volcanic activity. Recently, white mineral aggregates have been discovered in several places in highly altered and serpentinized ultrabasic rocks of the above regions, with the form of irregular accumulations. The identified minerals are hydromagnesite, which predominates, and also magnesite, huntite, and minerals of pyroaurite group. For the study of the Mg-hydroxycarbonate minerals assemblages and the hosting material, PXRD mineralogical analysis, SEM investigations and SEM-EDS microprobe and chemical analyses has been performed. It is suggested that the origin of the secondary Mg-rich hydroxycarbonates was controlled by the alteration of the ophiolites due to a combining actions of intense hydrothermal activity with CO_2 -rich fluids, tectonism, as well as the groundwater chemistry that is characterized by high Mg/Ca ratio and alkaline pH values.
Key words: *Hydromagnesite, huntite, ultramafic, alteration, Geraneia.*

Περίληψη

Στα Γεράνεια όρη (Δυτική Αττική, Ελλάδα) απαντούν οφιολιθικά πετρώματα, υπερκείμενα Τριαδικών – Ιουρασκών ασβεστολίθων και υποκείμενα Πλειοπλειστοκαινικών ιζημάτων. Οι σχετικά εκτεταμένες οφιολιθικές εμφανίσεις συνίστανται κυρίως από σερπεντινιωμένους περιδοτίτες, θεωρούμενοι ως λερζόλιθοι με σπινέλιους, καθώς και δουνίτες. Στην Βορειοανατολική Αργολίδα απαντούν αρκετές μικρές εμφανίσεις σερπεντινιτών ως υπολείμματα ενός οφιολιθικού καλύμματος, συνιστάμενες από σερπεντινιωμένους και τεκτονικά παραμορφωμένους περιδοτίτες, επωθημένους στον Ηωκαινικό φλύσχη. Και οι δυο περιοχές

χαρακτηρίζονται από εκδηλώσεις ηφαιστειακής δραστηριότητας. Πρόσφατα ανακαλύφθηκαν αρκετές ακανόνιστες συγκεντρώσεις από λευκόχρωμα ορυκτά συσσωματώματα μέσα σε έντονα εξαλλοιωμένα και σερπεντινιωμένα υπερβασικά πετρώματα των περιοχών αυτών. Προσδιορίστηκαν τα ορυκτά υδρομαγνησίτης, το οποίο επικρατεί, μαγνησίτης, χουντίτης καθώς και ορυκτά της ομάδας των πυροαυριτών. Για την μελέτη των ορυκτών αυτών, καθώς και των ξενιστών τους, χρησιμοποιήθηκαν μέθοδοι όπως, PXRD ορυκτολογικές αναλύσεις, SEM και SEM-EDS παρατηρήσεις και μικροαναλύσεις, καθώς και χημικές αναλύσεις. Υποδεικνύεται ότι ο σχηματισμός των δευτερογενών αυτών ορυκτών ελέγχεται από την εξαλλοίωση των οφιολίθων, ως συνδιασμένη δράση της έντονης υδροθερμικής δραστηριότητας πλούσιων σε CO_2 διαλυμάτων, του τεκτονισμού, καθώς και του χημισμού του εδαφικού νερού που χαρακτηρίζεται από μεγάλες τιμές του λόγου Mg/Ca και του pH.
Λέξεις κλειδιά: *Υδρομαγνησίτης, χουντίτης, υπερβασικά, εξαλλοίωση, Γεράνεια.*

1. Introduction

There are several references for hydromagnesite (and similar minerals, as huntite, pyroaurite group minerals, as well as magnesite, hereinafter referred as Mg-hydroxycarbonates) related with ultramafic rocks (Hostetler et al., 1966, Barnes and O'Neil, 1969, Okamoto et al., 2006, Teir et al., 2009, Wilson et al., 2009). However, these reports, as well as the related occurrences and their extent are very limited on the spread of the ultramafic rocks. The occurrence of Mg-hydroxycarbonates (such as hydromagnesite and huntite etc) is mainly referred from sedimentary deposits in lacustrine basins of Tertiary to recent age (Calvo et al., 1995, Stamatakis, 1995, Russell et al., 1999, Zedef et al., 2000). However, many of the large magnesite deposits of commercial grade are hosted in ultrabasic rocks in the form of vein and stockwork (Dabitzias, 1980, Pohl, 1990, Zachmann and Johannes, 1989). Sometimes, concretionary magnesites occur in soil weathered ultramafics (Schroll, 2002).

The aim of this paper is the presentation for first time some occurrences of Mg-hydroxycarbonates in ultramafic rocks of Greece, mostly in Geraneia Mountain, as well their description and the mineralogical and geochemical constrains; their relationship with specific geotectonic environment such as the South Aegean Active Volcanic Arc also investigated.

2. Geologic-Tectonic and Geothermal Features

In areas in West Attica Peninsula, Greece (S in Figure 1), ophiolitic rocks which occur on the surface mainly at the Geraneia Mountains, are overlying Triassic-Jurassic limestone and covered by Plio-Pleistocene sedimentary rocks (Mettos et al., 1982, Vakondios, 1996). The ophiolites are consisting mainly from peridotites were considered as spinel lerzolites -Western Mediterranean type, which include dunite bodies (Vakondios, 1996). The wide South section (Crommyonia) is characterized by the presence of manifestations of volcanic/geothermal activity, which has finally resulted in the alteration of ultramafic rocks mainly in the Soussaki and Agia Marina regions. The alteration observed is represented by extensive silicification of the ultramafic rocks (opal and chalcedony formation), as well as by clays formation (smectite and halloysite), which are often Cr-bearing (Mitsis et al., 2009). The Crommyonia region constituted the NW end of the Aegean volcanic arc, characterized by the existence of geothermal field, as well as intense tectonic and seismic activity. The sparse outcrops of dacitic rocks are the remnants of the volcanic activity 4.0-2.3 Ma, late-Pliocene (Fytikas et al., 1986, Pe-Piper and Hatzipanagiotou, 1997). In places, a weak mineralization of vein-type magnesite was located and also some mineralization of authigenic minerals (mainly sulphates) formed from volcanic emanations has been studied (Kyriakopoulos et al., 1990, D'Alessandro et al., 2009). The peninsula of Methana, located in the Northeastern Argolis (M in fiure 1), is mostly formed of volcanic product consisting mainly from basaltic andesites

to dacites of Pleistocene age (0.9 Ma to historical time]). In the Northeastern Argolis Peninsula several small remnants of an ophiolitic nappe outcrop which consists from serpentinized and tectonically deformed peridotites, as well as ophiolitic mélange (Gaitanakis and Photiades, 1989, Hatzipanagiotou et al., 1988). The nappe is overthrusted on the Eocene flysch. These ophiolite rocks are generally serpentinized, altered, tectonized and mylonitized. The volcanic system of Soussaki is a recent but, extinct volcano, with the post volcanic activity manifestations restricted now to argillification processes, hydrothermal alteration-mineralization, acid leaching, fumaroles and thermal waters (Dotsika et al., 2009). Gas escape displays typical geothermal gas composition, with CO_2 as the main component (>950 mmol/mol), and CH_4 and H_2S as minor components (D'Alessandro et al., 2006). However, the volcanic/geothermal system of Methana shows much lower activity, which confirmed by the very low CO_2 output (D'Alessandro et al., 2008).

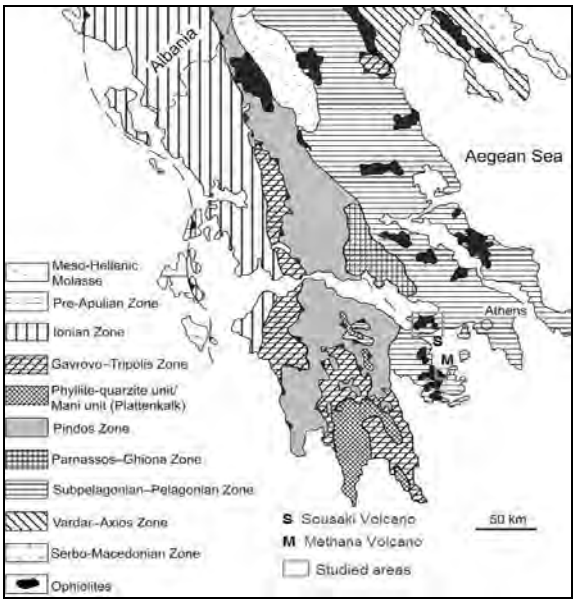

Figure 1 - Simplified geological map with the main tectonostratigraphic zones of the Hellenides and ophiolites also. The studied areas are: S (Sousaki-Geraneia) and M (Kaloni-Methana).

3. Materials and Methods

3.1. Studied Areas and Sampling

Recently, in highly altered, often earthy, serpentinite masses, white nodules and cotton-balls, fissure fillings and crusts, as well as veins (Figure 2) composed of Mg-rich hydroxycarbonates were identified mostly in Geraneia Mountain. The main development of the Mg-hydroxycarbonates was found to occur in the highly altered ultrabasic rocks; these rocks occur close to tectonic contact with limestones and close to regions with apparent signs of volcanic/geothermal activity. Away from such areas, the ultramafics are not intensely altered do not contain hydromagnesite, pyroaurite or huntite, but only locally vein-stockwork magnesite. In the South Geraneia Mt (Sousaki area) the ultrabasic rocks are very intensely altered due to volcanic and hydrothermal activity as well as tectonic activity. The Mg-hydroxycarbonate minerals (with the hydromagesite prevails) are well developed and include a variety of forms. Hydromagnesite with the form of cotton balls up to 4cm in diameter and as fissure fillings are located in several places within the highly altered serpentinite masses. Magnesite occurs mainly as small layers of white nodular accumulations, crusts or cauliflower forms with colloform texture. Also, boudinaged layers of huntite up to 2cm thick as well as nodules up to 2cm in diameter occur,

scattered near surface in totally weathered/altered ultrabasic rocks. The mineralogical analysis has shown that hydromagnesite systematically coexists with pyroaurite (Table 1). In the northern part of Geraneia Mt. (near Schinos area) hydromagnesite cotton balls occur also in totally altered ultrabasic rocks that appears as an earthy, clayey matrix of greenish or yellowish-brown color. The maximum visible thickness of the hydromagnesite horizon development exceeds 10 meters. The hydromagnesite cotton-balls range in size from few mm up to 5-7cm in diameter (Figure 2); the content of irregularly developed hydromagnesite in the host earthy-serpentinite can be close to 30%. In addition, rarely hard magnesite in the form of cauliflower or lettuce-leave assemblages is developed near the present-day surfaces, above hydromagnesite accumulations. In the east-southern Geraneia Mt at Ag Theodoroi area white nodular, botryoidal to nephroid and cauliflower accumulations of hard magnesite and rarely disseminated soft huntite nodules have been located in the intensely altered ultrabasic rocks.

In the Northeastern Argolis, at the Kaloni area, near Methana, white nodules, crusts and fissure fillings of hydromagnesite with pyroaurite (Table 1) occurred also in highly altered serpentinite masses. However, these occurrences are clearly quite limited (both in extent and frequency of occurrences) compared with those of Geraneia Mt.

Figure 2 - Hydromagnesite white nodules, fissure fillings and crusts, as well as veins in altered serpentinite in Geraneia Mt.

3.2. Analytical Methods and Techniques

All analytical procedures were performed at the laboratories of Faculty of Geology and Geoenvironment, UoA, with the following facilities:

X-ray diffraction measurements were carried out on a Bruker Model 5005 X-ray diffractometer in combination with the DIFFRACplus software package. The diffractometer was operated using Cu Ka radiation at 40 kV and 40 mA, with graphite monochromator, and employing the following scanning parameters: 0.020° step size and 1.0 sec. step time. The raw files were evaluated for mineralogical identifications by use of the EVA 10.0 program of the Bruker DIFFRACplus- software package. Electron probe microanalyses and SEM studies were carried out on a Scanning Electron Microscopy (SEM) JEOL JSM-5600, combined with microanalyzer energy dispersive system OXFORD LINK ISIS 300, with software ZAF correction quantitative analysis. The system was operating at 20KV, 0.5nA and 50sec dead time. Wet chemical analyses were performed with AAS spectrophotometer Perkin Elmer, model 1100b and with colorimetric method, using a HACH DR/4000 spectrophotometer.

4. Results

4.1. XRD Mineralogical Analyses

As it was resulted from the Powder XRD analyses (Table 1) the major Mg-hydroxycarbonates are: hydromagnesite, pyroaurite, magnesite and huntite. However, several cotton-balls, nodular or crust/fissure filling aggregates revealed that an Mg-Fe-(Ni-rich) hydroxyl-carbonate mineral of the pyroaurite group (Table 1, 2) occur, along with hydromagnesite and serpentine mineral.

Table 1 – PXRD Mineralogical analyses.

SAMPLE	SERP	HUN	HYM	MG	PAU
AT1	TR	MD		MJ	
AT2				MJ	
AD2	TR		MJ		MD
S7a	TR	MJ			
S7b	TR			MJ	
S7c	TR		MD	MJ	TR
S7nd	TR		MJ		MD
S7v	TR			MJ	
AT4	TR		MJ		MIN
AT11	TR		MJ		MIN
AM1	MJ		MIN		MD
AMcb	TR		MJ		MD
AMg	TR		MJ		MIN
AL2	TR		MJ		MIN
AL7	MD		MJ		TR
MPa2	MD		TR		MJ
MPb1	TR		MJ		TR
BPb	TR		MD		MJ
MPb2	TR		TR		MJ
MPb	TR				MJ
BPf	MD		TR		MJ
BPf1	MD		MJ		MD
F2b	TR		MJ		TR
F2f	MJ		MJ		MD
PNc	TR		MJ		TR
PN5	TR		MJ		MD
K2a			MJ		MIN
K2	MIN		MJ		MD
K3	TR		MJ		MD
K20	TR		MJ		MIN

Explanatory notes - SERP=serpentine, HUN =huntite, HYM=hydromagnesite, MG=magnesite, PAU=pyroaurite group. MJ=major constituent, MD=medium constituent, MIN= minor constituent, TR= trace constituent. (AD, S)=Sousaki area, (AM, AL)=Ag. Marina area, (PN,F)=Moni Panagia area, (AT)=Ag. Theodoroi area, (BP,MP)=Sxinos area, (K)=Kaloni area.

4.2. EPMA Analyses - SEM Micrographs and Study

SEM study on Mg-hydroxycarbonate phases and varieties of occurrences, shown that all these minerals are authigenic, as forms well developed microcrystals. Hydromagnesite forms euhedral crystals, as well large aggregations with pyroaurite and serpentine (Figure 3).

EPMA analyses, as well SEM semi qualitative analyses on free surface of Mg-carbonate phases and varieties of occurrences shown that: hydromagmesite is a pure phase, pyroaurite contains about 2.0 % NiO and Magnesite contains about 2.5 % CaO (Table 2).

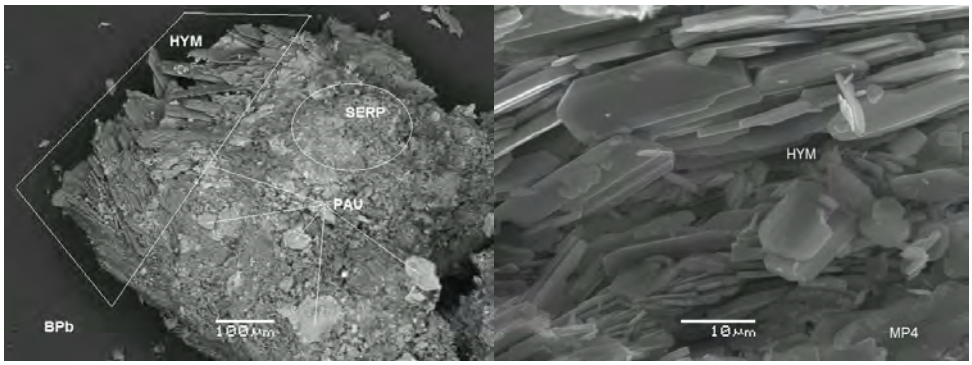

Figure 3 – SEM micrographs of Hydromagnesite (HYM) crystals (euhedral blades), in an aggregation with pyroaurite (PAU) and serpentine (SERP).

Table 2 – EPMA analyses (%).

Sample	PN5	F2f		BPb					AT2	
Mineral	PAU	HY	HY	PAU	HY	HY	PAU	SER	MG	MG
SiO_2	0.1	0.3	0.2	0.1	0.1	0.1	0.2	42.2	0.1	0.2
TiO_2	bdl	bdl	bdl	bdl	bdl	bdl	bdl	bdl	bdl	bdl
Al_2O_3	0.0	0.3	0.2	0.2	0.1	0.1	0.2	0.2	bdl	bdl
Fe_2O_3	24.8	0.1	0.1	24.2	0.1	0.1	23.9	3.7	0.1	0.1
MnO	bdl	bdl	bdl	bdl	bdl	bdl	bdl	bdl	0.1	0.2
MgO	34.3	41.6	42.5	33.7	41.6	42.2	33.4	41.8	43.2	42.7
CaO	bdl	bdl	bdl	0.2	0.1	0.1	0.2	0.1	2.6	2.8
Na_2O	bdl	bdl	bdl	bdl	bdl	bdl	bdl	bdl	bdl	bdl
K_2O	bdl	bdl	bdl	bdl	bdl	bdl	bdl	bdl	bdl	bdl
Cr_2O_3	bdl	bdl	bdl	bdl	bdl	bdl	bdl	0.2	bdl	bdl
NiO	1.9	bdl	bdl	2.2	bdl	bdl	2.3	0.3	bdl	bdl
Total	61.1	42.3	43.0	60.6	42.0	42.6	60.2	88.5	46.1	46.0

Explanatory notes - PAU: Pyroaurite, HYM: Hydromagnesite, SERP: Serpentine, bdl: below detection limits

4.3. Water Analyses

The water chemical analyses of all samples analyzed indicate waters of Mg-OH type (Table 3). Moreover, the high pH values, high magnesium and bicarbonates content, low calcium content and therefore high Mg/Ca ratio are characteristic of waters emanated from ultrabasic rocks (Papastamataki, 1977).

5. Discussion – Conclusions

It has been emphasized the presence of brucite in partially serpentinized dunites or in olivine rich peridotites (Hostetler et al., 1966, Mposkos and Perdikatsis, 1986). It is generally regarded that hydromagnesite and/or pyroaurite formed at the expense of brucite during weathering of ultrabasic rocks. In New Idria serpentinites the content of brucite in the partial serpentinized averages 7-8 per cent and its origin took place during the initial serpentinization of the olivine rich parent. However, it is almost absent from the surface weathering zone (Mumpton and Thompson, 1966). Instead in this zone pyroaurite and hydromagnesite are presented. The latter is localized above the water table often as pea-size concretions. These minerals are considered as alteration products of the brucite: the former in situ, while the hydromagnesite precipitated from ground waters if they

are in excess (Hostetler et al., 1966, Mumpton and Tompson, 1966). Also, been studied thoroughly the formation of pyroaurite at the expense of brucite during weahtering in dunitic serpentenite in Vourinos, Greece (Mposkos and Perdikatsis, 1986).

Table 3 - Spring waters chemical analyses.

	units	**AL Wf**	**MA Wf**	**BP Sp**	**SN Fn**
Conductivity	$\mu S\ cm^{-1}$	1098	1020	680	680
TDS	$mg\ L^{-1}$	605	520	340	341
pH		8.6	8.6	9.3	9
Eh	mV	-109.8	-103.3	-142.1	-124.1
T	^oC	21.4	20.2	19.4	20.0
NO_3^-	$mg\ L^{-1}$	3.5	3.5	3	4.4
HCO_3^-	$mg\ L^{-1}$	558	578	354	371
Ca	$mg\ L^{-1}$	3	2.8	0.8	1.2
Mg	$mg\ L^{-1}$	120	154	89	87
SO_4^{2-}	$mg\ L^{-1}$	15	15.6	2.1	0.3
Mg/Ca ratio		40	55	100	80

Explanatory notes : (MA, AL)=Ag. Marina area, (BP,SN)=Sxinos area

The typical occurrences of hydromagnesite, situated in the areas under investigation, are localized in highly weathered serpentinites. Typical also is the systematic involvement of the pyroaurite group minerals (Table 1, Figure 3); the intimately growth of the hydromagnesite with pyroaurite and serpentine in cotton balls is obvious. The coexistence of the two former minerals in almost all occurrences is remarkable (Table 1, 2). Has been suggested that brucite is converted to hydromagnesite if the partial pressure of CO_2 (P_{CO2}) is at least 10-6 atm., whereas probably even smaller P_{CO2} values are required for conversion of brucite to pyroaurite group (Hostetler, 1960, Hostetler et al., 1966). The coexistence of hydromagnesite with pyroaurite may indicate intermediate P_{CO2} values. However, the predominance of hydromagnesite is also related with the arrangement of the relevant supply of Mg and Fe (and Ni also). Note that the studied hydromagmesite is pure, while pyroaurite contains about 2.0% NiO (Table 2). If the concentration of Mg and the P_{CO2} are both high, magnesite forms, whereas low P_{CO2} favors the formation of hydromagnesite for a constant Mg/Ca ratio (Carpenter, 1962, Stamatakis, 1995). As the P_{H2O} approaches the vapor pressure of liquid water brucite or hydromagnesite are stable phases (White, 1997). Besides Mg^{2+} release from the original Mg-silicate minerals during serpentinization, some Fe^{2+}, as well some Ni^{2+} is also liberated, and it may be incorporated in precipitated brucite. Fe-bearing brucite, under small P_{CO2} values, is converted to pyroaurite (Hostetler, 1960, Hostetler et al., 1966). In addition, a partial oxidation of the soluble Fe^{2+} when exposed to mixing zone Eh-pH conditions to Fe^{3+} in the Mg^{2+} rich environment at pH around 8.5 leads to the precipitation of pyroaurite (Hansen and Taylor, 1990, Taylor et al., 1991). Pyroaurite has been formed in a zone beneath the water table and its formation appeared to be restricted to depths near and below the presumed zone of mixing of two different water layers of different composition (Taylor et al., 1991). These are in consistence with two main features of almost all studied occurrences: the weathering and hydrological regimes. The earthy (highly weathered) serpentinite outcrops in the studied areas containing several cotton-balls and veinlets hydromagnesite - pyroaurite occurrences (e.g. near Schinos, Ag. Dimitrios, Kaloni etc) are often wet, due to the present day circulation of surface and ground-water. Obviously, here do not expected to have retained brucite.The secondary Mg-hydroxycarbonates are constantly associated with these “foliated- friable -earthy” serpentinites, usually in areas of tectonic discontinuities and contacts, indicating that the fluid flow was controlled by reactions occurred in these easily accessible masses. Chemical analysis of spring water derived from the altered serpentinite, close to the contact with the limestone has high pH values, high magnesium and bicarbonates content, low calcium content and therefore high Mg/Ca

ratio (Table 3). The extremely low Eh values also revealed that the spring waters are derived from deep levels and environments isolated from the atmosphere (Garrels and Christ, 1965, Appelo and Postma, 2007). The Mg/Ca ratio is ranging between 40 and 100 and it is high enough to start the precipitation of metastable magnesium carbonate minerals such as hydromagnesite and huntite (Stamatakis, 1995, Konigsberger et al., 1999). Brucite formed during initial serpentinization must be regarded as a prime candidate for reaction with CO_2 solutions to form magnesite either hydromagnesite either pyroaurite (or coalingite or artinite). In natural environments at surface temperatures hydromagnesite (and/or nesquehonite) can precipitate directly from solutions (Hostleter, 1964); also hydromagnesite (and dipyngite) can precipitate at subsurface directly from solution (Wilson et al., 2009). Magnesite may form by dehydration of hydromagnesite, which forms more rapidly under aqueous conditions (Möller, 1989, Guthrie et al., 2001). The vein type magnesite deposit at Malentrata (Tuscany, Italy) considered as a result of interaction of fluids derived from the active Larderello-Travale high enthalpy geothermal field and the Ligurian serpentinites (Boschi et al., 2009). The serpentinite host rock were hydrothermally completely altered by Si- and CO_2 –rich geothermal fluids to a friable rock consisting mainly of opal, chalcedony, Al-Mg-Cr phyllosilicates and accompanied by the formation of a network of magnesite and dolomite veinlets. These researchers regard that the formation of magnesite may be the result of dehydration of a hydrated precursor (e.g. hydromagnesite). The presence of cauliflower or botryoidal-nodular magnesite with colloform texture at or near surface outcrops above hydromagnesite – pyroaurite occurrences, favoured for such an origin (dehydration of hydromagnesite) of these specific type magnesite aggregates in the studied areas of Geraneia ophiolites. In situ test for CO_2 fixation in serpentinite rock mass in the Iwanaidake ultramafic rocks, northern Japan, showed that the groundwater acidified by injected CO_2 dissolves brucite and serpentine minerals in the host serpentinite to increase its Mg content. It is possible that Mg- hydroxycarbonates precipitate from the highly alkaline groundwater by reaction between CO_2 and excess Mg component; hydromagnesite precipitate in the case of the dunitic serpentinite and pyroaurite or coalingite also formed (Okamoto et al., 2006). Also, serpentinite material from Finland has been acid leaching and then the products magnesium-rich solutions were carbonated by bubbling CO_2 and with raising the alkalinity to pH 9, hydromagnesite precipitated (Teir et al., 2009). Most of the required CO_2 for the formation of Mg-hydroxycarbonates of the studied areas is more likely to derive from the relevant geothermal system. The CO_2 needed for the Mg-hydroxycarbonates formation may derive from meteoric water, but especially in areas of the volcanic manifestations (e.g. gas emanations, fumes and vents in Soussaki area) the geothermal system should virtually be the only source of CO_2. Indeed the large amount of CO_2 discharged as diffuse and focused in Sousaki area, which estimated for an area of 0.015 Km^2 and for two small caves to be more than 50 tons/day (D'Alessandro et al., 2006). Obviously it is not necessary volcanic activity for the formation of Mg-hydroxycarbonates, but the high output CO_2 in Sousaki volcanic/geothermal area should be correlated with the relatively large and frequent their occurrences. The study of the carbon and oxygen isotopic compositions of the Mg-hydroxycarbonates would help to clarify the source of CO_2 as well the conditions of their deposition. The research on this topic is in progress and will be the subject of a forthcoming paper. However, the isotopic composition of carbon and helium of geothermal fluids at Sousaki suggest a prevalent origin from decarbonation reaction of subducted carbonates with only a minor contribution of mantle degassing (D'Alessandro et al., 2005, Dotsika et al., 2009). Obviously the limited occurrences of Mg-hydroxycarbonates at Kaloni area could be correlated with the very low activity of the volcanic/geothermal system of Methana and the very low CO_2 output (D'Alessandro et al., 2008).

Therefore, we attribute the relatively widespread Mg-hydroxycarbonate occurrences in Geraneia ophiolites, compared with other regions, in the combination of the following factors:

- The ultrabasic character of Geraneia ophiolites: spinel peridotites whith dunite bodies.
- The active and intense tectonic regime of this region.

- The great activity of the geothermal fluids and the high CO_2 output of Sousaki volcanic/geothermal system.

We conclude that there existed several phases of the evolution of the weathering and the hydrothermal alteration due to geothermal system and tectonic regime of the ultrabasic rocks. Hence, at early periods vein-type magnesite may formed, suggesting that P_{CO2} would be was quite high. At later stages, when the P_{CO2} and the temperature were lower, as well as the P_{H2O} approaches the vapor pressure of liquid water, as represents a geothermal system in their waning stage, hydromagnesite and pyroaurite are formed in highly altered, serpentinized masses irregularly developed in the ultrabasic rocks of the studied area. Part of the hydromagnesite then can be dehydrated to the cauliflower or botryoidal-nodular type magnesite with colloform texture, occurred at near surface outcrops, especially near to areas with volcanic/geothermal manifestations. Also, indicated that the Mg-hydroxycarbonate in Argolida may have limited extent due to the very low CO_2 output of the Methana volcanic system, in contrast to the case of the region of Sousaki volcano.

6. Acknowledgments

Thanks are expressed to the SPECIAL ACCOUNT FOR RESEARCH GRANTS, UoA for funding the fieldwork program under the Project No 70/4/11078. Also, the constructive reviews of two anonymous reviewers improved the text.

7. References

Appelo C.A.J. and Postma D. 2007. *Geochemistry, groundwater and pollution*, A.A. Balkema Publishers, London, 649pp.

Barnes I. and O'Neil J.R. 1969. The relationship between fluids in some fresh Alpine-type ultramafics and possible modern serpentinization, Western U.S., *Bull. Geol. Soc. America* 80, 1947-1960.

Boschi C., Dini A., Dallai L., Ruggieri G. and Gianelli G. 2009. Enhanced CO_2-mineral sequestration by cyclic hydraulic fracturing and Si-rich fluid infiltration into serpentinites at Malentrata (Tuscany, Italy), *Chemical Geology* 265, 209-226.

Calvo J.P., Stamatakis M.G. and Magganas A. 1995. Clastic huntite in Upper Neogene formations of the Kozani basin, Macedonia, northern Greece, *Journal of Sed. Research*, A65, 627-632.

Carpenter A.B. 1962. Solutions, minerals and equilibria. Combination diagrams, in Schmitt (ed) *Equilibrium diagrams for minerals*, Cambridge Mass. Geol. Club of Harvard 1962, 162pp.

D'Alessandro W., Kyriakopoulos K., Rotolo S., Bagnato M., Bruno C., Casa G., Minio M. and Plicanti F. 2005. Natural degassing activity of the geothermal system of Sousaki (Greece): Environmental impact and gas hazard issues, *ICGG8, 8th Intern. Conf. Gas Geochemistry*, Oct. 2-8, Palermo and Milazzo, Italy, 2005.

D'Alessandro W., Brusca L., Kyriakopoulos K., Rotolo S., Michas G., Minio M. and Papadakis G. 2006. Diffuse and focused carbon dioxide and methane emissions from the Sousaki geothermal system, Greece, *Geophysical Research Letters*, 33(5) L05307, doi:10.1029/2006GL025777, 5pp.

D'Alessandro W., Rotolo S., Kyriakopoulos K., Bellomo S., Brusca L., Calabrese S., Liotta M., Bruno C. and Plicanti F. 2009. Fumarolic alteration products at Sousaki (Greece): occurrence and environmental impact, *Proceed. 2nd Int. Conf. CEMEPE&SECOTOX*, Mykonos, June, 21-26 2009.

D'Alessandro W., Brusca L., Kyriakopoulos K., Michas G. and Papadakis G. 2008. Methana, the westernmost active volcanic system of the south Aegean arc (Greece): Insight from fluids geochemistry, *Journal of Volcanology and Geothermal Research* 178, 818–828.

Dabitzias S.G. 1980. Petrology and genesis of the Vavods cryptocrystalline magnesite deposits, Chalkidiki Peninsula, Northern Greece, *Economic Geology,* 75, 1138–1151.

Dotsika E., Poutoukis D., Michelot J.L. and Raco B. 2009. Natural tracers for identifying the origin of the thermal fluids emerging along the Aegean Volcanic arc (Greece): Evidence of Arc-Type Magmatic Water (ATMW) participation, *Journ. Volcan. Geotherm. Research* 179, 19-32.

Fytikas M., Innocenti F., Kolios N., Manetti P. and Mazzuoli R. 1986. The Plio-Quaternary Volcanism of Saronikos area (Western part of the Active Aegean Volcanic Arc), *Ann. Geol. Pays Hell*. 33, 23-45.

Gaitanakis P. and Photiades A.D. 1989. The ophiolitic units of Argolis (Peloponnese, Greece), *Bull. Geol.Soc. Greece,* (in Greece) 23-1, 363-380.

Garels R.M. and Christ C.L. 1965. *Solutions, Minerals and Equilibria,* Harper and Row (eds), New York, 450pp.

Guthrie G.D., Carey W.J., Bergfeld D., Byler D., Chpera S. and Ziock H.J., 2001. Geochemical aspects of the carbonation of magnesium silicates in aqueous medium, *Proceedings of the 1st National Conference on Carbon sequestration* p. 14. Washington DC, May 14-17, 2001.

Hansen H.C.B. and Taylor R.M. 1990. Formation of synthetic analogues of double metal-hydroxy carbonate minerals under controlled pH conditions: I. The synthesis of pyroaurite and reevesite, *Clay Miner*. 25, 161-179.

Hatzipanagiotou K., Tsikouras V. and Gaitanakis P. 1988. Study of ophiolitic outcrops in Central Argolis: Ophiolitic Melange and residual ophiolitic nappe, *Bull. Geol.Soc. Greece,* 33, 475-492 (in Greece).

Hostetler P. B. 1960. Low temperature relations in the system: MgO-SiO_2-CO_2 H_2O. *Ph.D. diss.,* Harvard Univ., Cambridge, Mass.168 pp.

Hostetler P.B. 1964. The degree of saturation of magnesium and calcium carbonate minerals in natural waters. General Assembly of Berkeley, *Commission of subterranean Waters, Publication* No 64, 34-49.

Hostetler P.B., Coleman R.G., Mumpton F.A. and Evans B.W. 1966. Brucite in Alpine serpentinites*, The American Mineralogist* 51, 75-98.

Konigsberger E., Konigsberger L. and Gamsjager H. 1999. Low temperature thermodynamic model for the system $Na_2CO_32MgCO_32CaCO_32H_2O$, *Geochimica et Cosmochimica Acta* 63 (19/20), 3105–3119.

Kyriakopoulos K.G., Kanaris-Sotiriou R. and Stamatakis M.G. 1990. The authigenic minerals formed from volcanic emanations at Soussaki, west Attica peninsula, Greece, *Canadian Mineralogist* 28, 363-368.

Mettos A., Gaitanakis P., Rontogianni Th., Bavay Ph., Ioakim Chr., Mitsaki V. and Koutsouveli A. 1982. Geological Study of "Loutraki-Sousaki" Region, *Geothermal Researches, IGME*, (in Greek) Greece, 65 (+Apx) pp.

Mitsis I., Godelitsas A., Gottlicher J., Steininger R., Gamaletsos P., Perraki M. and Stamatakis M., 2009. Chromium-bearing Clays from Crommyonia Volcanic Area, Greece, ICC 2009- *VIV International Clay Conference*, Castellaneta Marina, Italy, June 14-20 2009.

Möller P. 1989. Nucleation processes of magnesite, *Monograph series on mineral deposits*, 28, 287-292.

Mposkos E. and Perdikatsis V. 1986. Weahtering of Brucite and the formation of Pyroaurite in dunitic serpentenite in the region Xerolivado in the southern Vourjno, (in Greek) *IGME Special Issue*, 279-287.

Mumpton F.A. and Tompson C.S. 1966. The stability of brucite in the weathering zone of the New Idria serpentinite, *Clays and clay Minerals, Proc. Nat. Con* No .l4, 249-257.

Okamoto I., Yajima T., Mizuochi Y., Katoh T., Ninomiya A. and Ohsumi T., 2006. In-situ test for CO_2 fixation in serpentinite rock mass, *8th Int. Conf. on Greenhouse Gas Control Technologies (GHGT-8)*, Trondheim, Norway June 19-22 2006.

Papastamataki A. 1977. The alkalinity and the chemical composition of springs issuing from peridotites, *Anall. Geol des Pays Hellen*., 27, 551-566.

Pe-Piper G. and Hatzipanagiotou K. 1997. The Pliocene volcanic volcanic rocks of Crommyonia, western Greece and their implications for the early evolution of the South Aegean arc, *Geol. Mag.,* 134 (I), 55-66.

Pohl W. 1990. Genesis of magnesite deposits-models and trends, *Geologische Rundschau* 79-2, 291–299.

Russell M.J., Ingham J.K., Zedef V., Maktav D., Sunar F., Hall A. J. and Fallick A.E. 1999. Search for signs of ancient life on Mars: expectations from hydromagnesite microbialites, Salda Lake, Turkey, *Journal of the Geological Society* 156, 869-888.

Schroll E. 2002. Genesis of magnesite deposits in the view of isotope geochemistry, *Boletim Paranaense de Geociencias, Editora* UFPR, IGCP 443, 50, 59-68.

Stamatakis M.G. 1995. Occurrences and genesis of huntite-hydromagnesite assemblages, Kozani, Greece-important new white fillers and extenders, *IMM, Transactions-B*, 104, 179-186.

Taylor R.M., Hansen H.C.B., Stanger G. and Bender Koch C. 1991. On the genesis and composition of natural pyroaurite, *Clay Minerals* 26, 297-309.

Teir S., Eloneva S., Fogelholm CJ. and Zevenhoven R. 2009. Fixation of carbon dioxide by producing hydromagnesite from serpentinite, *Applied Energy* 86, 214-218.

Vakondios J. 1996. Study of the chromite metallogenesis associated with Mediterranean type ophiolites. An example from Tinos Island and Gerania Mt., Attica, Greece, *Unpublished Ph.D Thesis*, University of patras, Patras, 120pp.

White W. B. 1997. Thermodynamic equilibrium, kinetics, activation barriers and reaction mechanisms for chemical reactions in Karst Terrains, *Environmental Geology,* 30, 46-58.

Wilson S., Dipple G., Power I., Thom J. anderson R., Raudsepp M., Gabites J. and Southam G. 2009. Carbon Dioxide Fixation within Mine Wastes of Ultramafic-Hosted Ore Deposits: Examples from the Clinton Creek and Cassiar Chrysotile Deposits, Canada, *Economic Geology* 104, 95–112.

Zachmann D.W. and Johannes W. 1989. Cryptocrystalline magnesite, in Möller (ed), *On the formation of magnesite*, Monograph Ser. Mineral Deposits, Gebruder Borntraeger, Berlin, 28, 15-28.

Zedef V., Russel M., Fallik A. and Hall A.J. 2000. Genesis of vein stockwork and sedimentary magnesite and hydromagnesite deposits in the ultramafic terranes of southwestern Turkey: A stable isotope study, *Economic Geology* 95, 429-446.

Δελτίο της Ελληνικής Γεωλογικής Εταιρίας, τομ. XLVII , 2013
Πρακτικά 13ου Διεθνούς Συνεδρίου, Χανιά, Σεπτ. 2013

Bulletin of the Geological Society of Greece, vol. XLVII 2013
Proceedings of the 13th International Congress, Chania, Sept. 2013

PETROGRAPHY AND ZIRCON MORPHOLOGY OF SYN-TECTONIC GRANITOIDS ROCKS OF HAFAFIT AREA, SOUTH EASTERN DESERT (EGYPT)

Thabet I.[1& 2], Kilias A.[2], Koroneos A.[3] and Kamh S.[1]

[1] Geology Department, Faculty of Science, Tanta University, Tanta, Egypt.
eslam642004@yahoo.com., kilias@geo.auth.gr, koroneos@geo.auth.gr, kamh2002@yahoo.com.

[2]Geology and Palaeontology Department, School of Geology, Aristotle University of Thessaloniki, Greece.

[3]Department of Mineralogy, Petrology and Economic Geology, School of Geology, Aristotle University of Thessaloniki, Greece.

Abstract

The study deals with the petrography of the granitoid rocks intruding the five (A to E) domes of Hafafit Culmination. The morphological characteristics of zircon crystals are also examined, in order to elucidate the genesis of zircon and their host Hafafit granitoids. The granitoid rocks are tonalites, granodiorites and quartz diorites, all exhibiting gneissic texture. The zircon crystals from all the rock types intruding each one of the domes are examined in detail for colour, inclusions, crystal length, crystal width, elongation ratio, crystal form and habit, degree of roundness and corrosion, and are distinguished in groups on the basis of the previous characteristics. Two generations of zircons have been recognized; the first generation with magmatic features and the second one with post magmatic features. The first generation of zircon is attributed to the subduction, magmatic and deformation events while the second generation of zircon is attributed to metamorphism.

Key words: *Wadi Hafafit Culmination, Morphological parameters, evolution events.*

1. Introduction

The Hafafit domal structure (Wadi Hafafit Culmination, WHC) represents the largest antiformal structure in the Nubian Shield. It is considered to be of the most spectacular structures in the Eastern Desert, but its structural history has not been entirely clarified. The WHC has been subdivided into the eastern unit (Nugrus unit) which is composed mainly of low grade mica-schists and metavolcanics. This unit is associated with remnants of ophiolitic altered ultramafic rocks and metagabbros.

The western unit (Hafafit unit) has been subdivided into five separated gneissic domes (labeled A-E core gneisses; of various extends (El Ramly and Greiling, 1988) (Figure 1). The cores of all domes are intruded by tonalities and granodiorites which were considered to be the youngest rocks within the Hafafit succession (Greiling *et al*., 1988b; Rashwan, 1991). El Bahariya and Abd El Wahed (2003) considered the granitoid-diorite cores together with the genetically related foliated

metagabbro to represent the oldest intrusive rocks in the Hafafit area. The tectonic evolution of Hafafit culmination has been interpreted as a result of fold interference patterns involving multiply deformed sheath folds (Fowler and El Kalioubi, 2002) or as a consequence of tectono-magmatic and tectono-metamorphic processes in an active continental margin tectonic setting (El Bahariya and Abd El Wahed, 2003). The structural characteristics of the northern dome (dome A) of WHC, field descriptions of the dome and the surrounding rocks are discussed by Shalaby (2009) emphasizing to their relations with the overlying Pan-African cover nappes and the bounding ductile shear zones. He suggested that the emplacement of gneissic core occurred during accretion of the Pan–African nappes; later strike-slip shear zones of Najd Fault System and the associated Subsidiary shear arrays postdate the emplacement of the dome. In order to put some constraints on the petrogenesis of the migmatitic rock association, of the domes B and C, as well as the tectonic processes which accompanied metamorphism and orogenesis, El Bahariya (2008) studied the P-T conditions of the different mineral assemblages and he estimated P= 5 kb and T= 750 ^{o}C. It is to note that there are no tectonic or petrological data for domes D and E.

Four tectonic models were proposed to explain the exhumation of WHC and to decipher their origin: (1) development of fault-bend fold "antiformal stacks" (e.g. Hafafit domal structure; Greiling et al.,1988a), (2) orogen-parallel crustal extension (e.g. HaFafit, Sibai and Meatiq domal structures; Wallbrecher et al., 1993; Fritz et al., 1996,2002; Bregar et al.,2002; Loizenbauer et al., 2001; Abdel Wahed, 2008; Khudeir et al., 2008), (3) emplacement within regional domal structures (Ibrahim and Cosgrove, 2001) followed by extension parallel to their fold axes (e.g. Sibai dome, Fowler et al., 2007), and (4) interpreted the Hafafit Complex as a result of fold interference patterns involving multiply deformed sheath folds (Fowler and El Kalioubi, 2002). The aim of this study is to examine the zircon morphology of the gneissic granitoids intruding the five domes of Hafafit Culmination and relate them with the different evolution events of Hafafit Culmination.

2. Geological Setting

The rock assemblages in the Wadi Hafafit Culmination (WHC) (latitudes 24° 35′ 00′′ N and 24° 51′ 00′′ N and longitudes 34° 30′ 00′′ E and 34° 45′ 00′′ E) could be grouped into two main units which are separated by Nugrus Thrust which is associated with Nugrus shear zone.

The overlying unit (Nugrus unit) is mainly mode up of low grade mica-schists and metavolcanics that outcrop in eastern and northern part of the WHC. This unit is associated with remnants of serpentines altered ultramafic rocks and metagabbros. The underlying unit (Hafafit unit) is composed of tonalities, granodiorites and quartz diorite, it has been subdivided into five separated gneissic domes (labeled A-E core gneisses; of various areal extend (El Ramly and Greiling, 1988) (Figure 1). The basement rocks of the domes consist of banded amphibolites, overthrusted by ultramafic rocks, alternating bands of biotite- and hornblende-gneisses and psammitic gneiss at the rim of the domal structure. In some parts, the amphibolites are associated with metagabbro (Abd El-Naby and Frisch, 2006). Granitoids (tonalites granodiorites and quartz diorites) with gneissic texture intrude the cores of the domes. Tonalite prevails in the core of the northernmost dome (dome A), where the peripheral zone is strongly foliated and encloses conformable bands of foliated metagabbro. In places, the tonalite is intruded by numerous, thin pegmatite veins giving the erroneous impression of migmatites. Stern and Hedge (1985) gave an age of 680 Ma for the tonalite. In the outer rim of the core, tonalite is also intruded by pegmatite veins; it acquires a conspicuous white colour which is accentuated by the weathering and kaolinization of oligoclase. At the northern part of the dome, highly altered, irregularly-shaped, small masses of rusty brown serpentinite are enclosed in metavolcanic rocks. They are transformed along the peripheries of the intruding pegmatite veins into fibrous anthophyllite (Rasmy, 1974). The domes B and C, occupy the central eastern part of Hafafit unit. These outcrops include migmatitic rocks intruded by gneissic granitoid of tonalite and granodiorite composition with diffuse and irregular gradual

contacts. Migmatites and gneissic granite are surrounded by amphibolitic metagabbro and intruded later by leucogranite. Dome D occupying the central western part of Hafafit unit is a more elongated dome relative to the other domes. The core of this dome consists of gneissic tonalite and granodiorite while in the rim gneissic quartz diorite surrounded by foliated metagabbro is present. The contact between gneissic granite and foliated metagabbro is gradational. Dome E occupies the southern part of Hafafit unit. The core of this dome consists of gneissic tonalite surrounded by foliated metagabbro. The contact between gneissic tonalite and foliated metagabbro is a clear sharp contact; tonalite intrudes the metagabbro. Both units (Nugrus and Hafafit unit) have been intruded by undeformed leucogranites, especially along thrust zones.

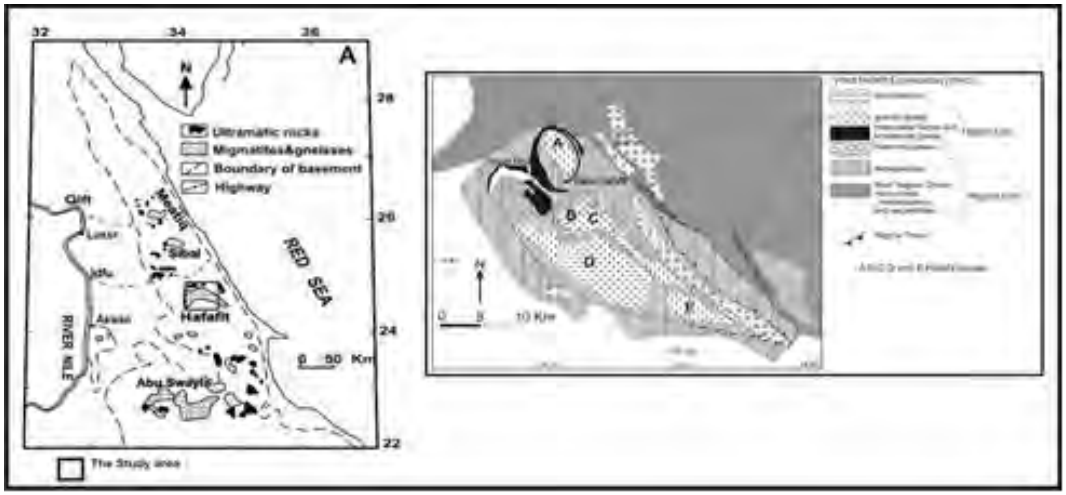

Figure 1 - Simplified geological map of the Wadi Hafafit area showing the main rock types, and structures. (Modified after El Ramly etal., 1993).

3. Petrography of the Hafafit Unit Granitoid Rocks

A brief petrographic description of the different granitoid rocks intruding the cores of Hafafit unit domes is given bellow:

3.1. Tonalites

Tonalites occupy the cores of all the Hafafit domes. They are composed of quartz, plagioclase, hornblende, and biotite as the main minerals and sphene, zircon and opaques are the accessories. Chlorite and epidote are secondary constituents. The tonalites are medium to coarse grained weakly to moderately deformed and show a gneissic texture marked by the parallel alignment of hornblende and biotite. Plagioclase shows lamellar twinning. It is weakly to moderately deformed with the twin lamellae sometimes curved. It is sometimes zoned except tonalite of dome E that is strongly deformed and altered to epidote. The single crystal of plagioclase shows deformation band and deformation twin. Quartz occurs as anhedral aggregates interstitial to the plagioclase and it is sometimes slightly elongated. It exhibits moderate deformation as indicated by the undulose extinction. This deformation is more abundant in the samples occurring near the faults planes. Biotite is dark brown in color forming tabular crystals and flakes marking the foliation planes. It is often altered to chlorite. Hornblende forming prismatic crystals is green to dark green in color. It is often associated with biotite, chlorite, opaque minerals and sphene. Rarely, large crystals of magnetite mineral exist in the tonalites, which may be inherited from the source rock. Zircon occurs as euhedral and subhedral prismatic crystals ranging in length from 0.03 to 0.25 mm and width from 0.010 to 0.1 mm. They are always included in biotite, plagioclase, hornblende and quartz. Apatite occurs mainly in dome D as long prism ranging in length from 0.03 to 0.14 mm

and in width from 0.02 to 0.06 mm. It appears as inclusions in hornblende and plagioclase. Magnetite occurs along hornblende cleavage planes in tonalites of dome D. Tonalites are characterized by high content of quartz which increases towards the rim of the domes. Biotite is more abundant close to the core and decreases towards the periphery whereas hornblende exhibits reverse relation. The deformation is more intense at the rims of domes compared to the cores.

3.2. Granodiorites

Granodiorites occupy the cores of the domes B, C and D where they intrude tonalites. They are composed mainly by quartz, plagioclase, K-feldspar, biotite and hornblende. Garnet, opaques, apatite and zircon are accessories whereas chlorite and epidote are secondary constituents. They are coarse-grained, foliated rocks showing hypidomorphic texture. The subparallel arrangement of biotite and hornblende forms a gneissic texture. Plagioclase is the dominating mineral. It occurs as subhedral to euhedral tabular crystals ranging from 1.4 to 7 mm in length and from 1.5 to 3.7 mm in width. Plagioclase crystals are corroded by quartz. They generally show lamellar twinning. Sometimes, plagioclase crystals are partially or completely altered to epidote. Quartz is found as subhedral to anhedral crystals of various shapes ranging in size from 1.5 to 5.8 mm in length and from 0.6 to 3.1 mm in width while quartz of granodiorites of domes B and C are characterized by undulose extinction. K-feldspar is mainly represented by microcline and microcline microperthite occuring as subhedral coarse crystals up to 5 mm across. It shows cross-hatch twinning with fine streaks of albite giving the perthitic texture. Biotite occurs as fine to medium, slightly curved to highly kinked, irregular flakes foliated between plagioclase and quartz. They are rarely altered to chlorite and iron oxides. Hornblende occurs as subhedral prisms. It ranges from 0.8 to 4.8 mm in length and from 1 to 2.3 mm in width. Hornblende crystals are pleochroic from pale to dark green. Zircon occurs as euhedral prismatic crystals; its length ranges from 0.030 to 0.1 mm and width ranges from 0.010 to 0.070 mm. It occurs as inclusions in biotite, plagioclase and quartz. Sometimes it occurs as bipyramidal crystals with smaller size. Apatite is rare as inclusion in biotite but occurs as long prismatic crystals. Magnetite fill the cracks of quartz as well as the cleavage planes of biotite and often surround biotite crystals.

3.3. Quartz Diorite

Quartz diorite occupies the outer part of tonalites of dome D. They are well foliated; they are sometimes strongly deformed showing gneissic texture. They are composed of plagioclase, quartz, biotite and hornblende. Accessory minerals are opaque, sphene and zircon. Plagioclase occurs as subhedral to anhedral crystals moderately to strongly sericitized or kaolinized. Some plagioclase crystals are corroded by quartz and show lamellar twining with the twin lamellae inclined to the foliation planes, moreover it has intense deformation and this is clear in deformation band and deformation twin. Quartz forms anhedral intercalated aggregates interstitial to the plagioclase. It is strongly deformed and shows partial recrystallization. Biotite is present in small amounts associated with hornblende. Biotite occurs as fine to medium, slightly curved to highly kinked, irregular flakes with brown to dark brown colour. Sometimes is partially altered to chlorite and contains inclusions of apatite, zircon and magnetite. Hornblende is green in colour, forming xenomorphic crystals often replaced by biotite. Sphene exists as irregular and sphenoid subhedral crystals corroded by quartz and biotite. The majority of sphene crystals appear to surround opaques. Zircon forms euhedral and subhedral normally prismatic and long prismatic crystals enclosed mainly in hornblende, plagioclase and quartz.

4. Zircon Morphology

Zircons from a particular rock type at different domes have distinctive characteristics (e.g. habit, elongation, colour and inclusions). For example, the very wide range of shapes, sizes, colours and other features shown by their zircon crystals characterize the host granitoid rocks. Alper and

Poldervaart (1957), Larsen and Poldervaart (1961), Spotts (1962), Zav'yalova *et al*. (1966), Forbes (1969) and Thabet (2008) show that the zircon features can be used as supporting evidence for establishing genetic relationships among geographically separated but chemically related igneous rocks. The systematic morphological study of each zircon crystal can be achieved through detailed investigation and determination of the following features (Figures 2 and 3 and tables 1 to 3):

4.1. Colour and Inclusions

The groups of the zircon crystals, of the studied Hafafit granitoids domes, distinguished on the basis of their colour are given in table 1and Figure 3A. Taking into account the proportion of crystals in each group it must be noted that the group of coloured zircons is more common in tonalite of dome E (Figure 2F) while colorless zircons are common in all domes A, B, C and D. Quartz diorite of dome D contains mainly colourless zircons.

Opaque minerals are found as inclusions in zircon crystals. They are present as irregular, regular and parallel to *c*-axis. They are characterized by dark brown to black colour. The grouping of the zircon crystals, distinguished on the basis of their inclusions is presented in Table 1and Figure 3B.

Some zircon crystals contain smaller zircon crystals as inclusions. This phenomenon being more common in domes A and D, implies that the granitoids of domes A and D have two zircon generations; the first generation has magmatic features while the second generation has post magmatic features. The orientation of C-axis of zircon crystals of the two generations is SE-NW being parallel to the main dominated lineation of hosting minerals (plagioclase, hornblende and biotite).

4.2. Crystal Length, Crystal Breadth and Elongation Ratio

The length of zircon crystals is usually measured along the *c*-axis. According to the length they have been distinguished in four groups (Table 1and Figure 3C). The short and the normally zircon crystal groups are the most frequent in all the studied domes. In all domes the majority of the zircon crystals (over 80%) are short while less than 20% are normally long. Long zircons are rare, only in tonalite of dome A and tonalite and granodiorite of dome D while very long zircons are absent.

Crystal breadth is measured along the *a*-axis of the crystal. The Hafafit zircons granitoids domes, have been distinguished in four groups (Table 2 and Figure 3D). Normally thick zircons are more abundant in domes A, D and E, very thick zircons are recorded only in tonalite of dome A and in all rock types of dome D.

The elongation ratio of a zircon crystal is the ratio of the length (L) over the breadth (B), L/B. According to the values determined, the zircon can be distinguished in four groups (Larsen and Poldervaart 1961) presented in table 2 and Figure 3E. It is clear that in tonalite of dome A, 38.55% of the zircons are normally elongated, 33.73% stout, 19.27% elongated and 8.43% highly elongated. Tonalite and granodiorite of domes B&C have 53.65% normally elongated zircons, 43.90% stout, 2.43% elongated while highly elongated zircons are absent. Tonalite of dome E has 38.46% normally elongated zircons, 57.69% stout, 3.84% elongated; highly elongated zircons are absent as well. Tonalite and granodiorite of dome D have 33.63% normally elongated zircons, 42.72% stout, 19.7% elongated, and 4.54% highly elongated. Quartz diorite of dome D has 23.07% normally elongated zircons, 63.46% stout, 13.46% elongated and no highly elongated. The above observations can be summarized as following:

1. The normally elongated zircon crystals are the most common in the Hafafit granitoid domes A and B&C rocks.
2. The highly elongated zircon crystals are recorded only in tonalite of dome A and in tonalite, and granodiorite of dome D.
3. The stout zircon crystals are frequent in tonalite of dome E and in quartz diorite of dome D.

Granitic rocks contain mostly normally elongated zircons (elongation ratio 2.0-3.0, Larsen and Poldervaart, 1961; Forbes, 1969); unusual in that respect are granites with relatively high proportions of stubby crystals (L/B <2.0) or of highly elongated crystals (L/B >4.0). Tonalites in general have mostly elongated zircons (L/B 3.0-4.0) and especially with L/B from 3.2.

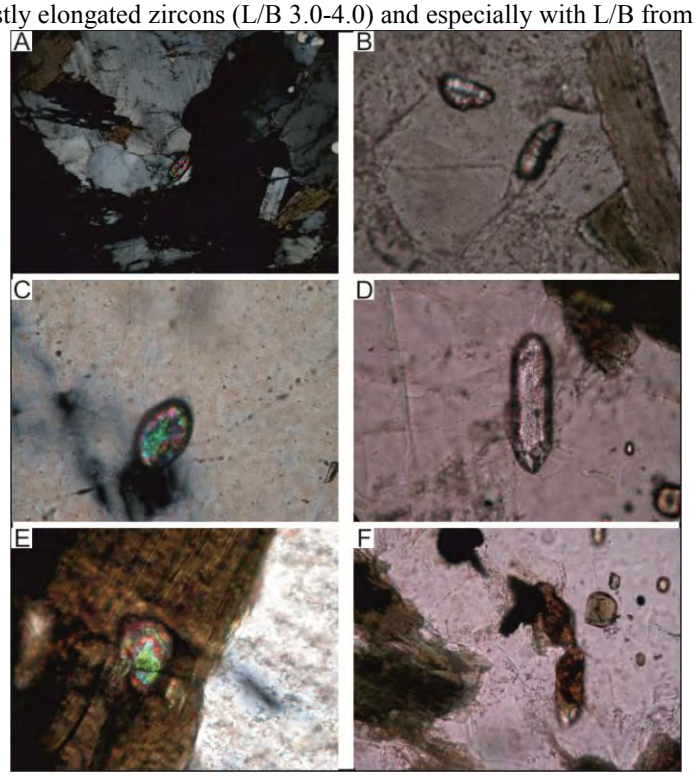

Figure 2 - Photomicrographs shows a) euhedral zircon combining prism with bipyramids found as inclusions in quartz (dome A), B) quartz hosting sub-rounded zircon long prism with primary evolution bipyramid has inclusion of opaques (dome A), C) euhedral zircon combining short prism with bipyramid found as inclusions in quartz (Dome B), D) plagioclase hosting euhedral zircon show combination of long prism and bipyramid, this zircon have inclusions of zircon and opaques (dome D), e) euhedral zoned core zircon combining short, thick prism with bipyramid found as inclusions in sheared biotite flakes (dome D), f) quartz hosting brown euhedral zircon show combination prism with bipyramid and also hosting of short prism colorless zircon (dome E).

4.3. Crystal Forms and Habits

The individual simple forms in which frequently the zircon crystals occur are:
i) Tetragonal prism {110}, ii) Tetragonal bipyramid "ordinary bipyramid" {111}, iii) Steep bipyramid {331}, iv) Basal pinacoid {001} and v) Single basal plane (pedion).
In any rock, zircons are generally characterized by different forms and habits, depending upon the relative development of prism with respect to the bipyramid. These habits can be described as:

1. Short stubby zircons: where the crystals are short prismatic and mostly with bipyramidal development.
2. Normally prismatic zircons: where the crystals are prismatic bipyramidal but the prism is moderately developed.
3. Long prismatic zircons: where the crystals are prismatic with bipyramidal but the prism is high developed.

4. Bipyramidal prismatic zircons: where the bipyramid is dominated and constitute about two-third of the crystal length. The crystal is consequently spindle-shaped.

The percentages of the zircon crystals, of the studied Hafafit granitoids domes, distinguished on the basis of their habit are given in table 2 and Figure 3F. The short stubby zircons are more common in tonalite and granodiorite of domes B&C rather than other domes (Figure 2C). The normally prismatic zircons dominate in all domes but they are more common in tonalite of dome E. The long prismatic zircons are more common in tonalite of dome A (Figure 2A) and in tonalite and granodiorite of dome D (Figure 2D). Bipyramidal prismatic zircons are recorded only in tonalite and granodiorite of dome D (Figure 2E). The alkali-granites can be distinguished from all other granites by the long-prismatic habit of their zircons. It is noteworthy that long-prismatic zircons are equally unusual in both alkaline and calc-alkaline rocks. Moreover, the prismatic habit is supplanted by a bipyramidal habit in many peralkaline rocks (Wyatt, 1954).

4.4. Degree of Roundness and Corrosion

The zircon crystals are distinguished in three groups on the basis of their edges and corners as follows:

1. Angular (or Euhedral) zircons, where the corners and edges of the crystals are sharp.
2. Subrounded zircons, where the crystals show considerable wear and the bipyramidal terminations show pronounced rounding, but the prism and most of the pyramidal faces still persist.
3. Rounded zircons, where the prism faces are smoothly curved and the pyramid terminations are rounded. The degree of roundness is a natural feature, most probably due to magmatic resorptions or might be produced during cooling of magma (Spotts, 1962). The percentages of the zircon crystals, of the studied Hafafit granitoids domes, distinguished on the basis of their degree of roundness are given in table 3 and Figure 3G. Tonalite of dome A has 83.13% euhedral zircon crystals, 14.45% subrounded crystals and 2.40% rounded crystals. Tonalite and granodiorite of domes B&C have 53.65% euhedral crystals 46.34% subrounded crystals while rounded crystals are absent. Tonalite of dome E has 46.15% euhedral zircon cystals, 53.84% subrounded crystals and rounded zircon crystals are absent as well. Tonalite and granodiorite of dome D have 63.63% euhedral zircon crystals, 31.81% subrounded crystals and 4.54% rounded crystals. Quartz diorite of dome D has 78.84% euhedral crystals, 19.23% subrounded crystals and 1.92% rounded crystals.

5. Discussion and Conclusions

Empirical studies by Pupin (1980) infer that the morphology of zircon reflects the source characteristics of host granitoids. Vavra (1990, 1993), Benisek and Finger (1993) and (Thabet, 2008) conclude that the morphologies of zircon crystals could only reflect the latest stages of granitoids evolution. The study of morphological characteristics of zircon crystals from different Hafafit domes concluded that coloured zircons is more common in tonalite of dome E, while colorless zircons are common in all domes A, B, C and D. Quartz diorite of dome D contains mainly colourless zircons. Mostly zircon of all domes is angular and sub-rounded crystal, the distribution of length and habit of zircon crystal show that domes A and D have long zircons and long prismatic zircons but domes B, C and E have high common short long zircon and short stubby habit. The long prismatic crystals are prismatic with bipyramidal but the prism is high developed. Bipyramidal prismatic zircons have the bipyramid, which dominates and constitutes about two-thirds of the crystal length. The crystal is consequently spindle-shaped. This means that domes A and D exposed to late regional extension and zircons are oriented SE-NW according to the general late orogenic extension. Some zircon crystals contain smaller zircon crystals as inclusions. This phenomenon being more common in domes A and D, implies that the granitoids of domes A and D have two zircon generations; the first generation has magmatic features while

Table 1- Distribution (%) of colour, inclusions and length of zircon form Hafafit granitoids.

Hafafit domes	Rock types	Colour			Inclusions			Length			
		Colour-less	Pale Coloured	Coloured	Zircon	Opaques	Free of inclusions	Short (<0.10)	Normally long (0.10-0.2)	Long (0.20-0.30)	Very Long (>0.30)
Dome A	Tonalite	42.16	21.68	36.14	3.61	51.80	44.57	79.51	19.27	1.20	0
Dome B&C	Tonalite & Granodiorite	39.02	26.82	34.14	0.00	46.34	53.65	95.12	4.87	0.00	0
Dome D	Tonalite & Granodiorite	44.55	18.18	37.27	6.36	60.00	33.63	80.00	17.27	2.72	0
	Quartz diorite	61.53	13.46	25.00	3.84	67.30	28.84	86.53	13.46	0.00	0
Dome E	Tonalite	11.53	11.53	76.92	0.00	61.53	38.46	92.30	7.69	0.00	0

Table 2- Distribution (%) of breadth, elongation ratio and habit of zircon form Hafafit granitoids.

Hafafit domes	Rock types	Breadth				Elongation ratio (L/B)				Habit			
		Slim (<0.025)	Normally thick (0.025-0.050)	Thick (0.025-0.050)	Very thick (>0.075)	Stout (1-2)	Normally elongated (2-3)	Elongated (3-4mm)	Highly elongated (>4mm)	Short stubby	Normally prismatic	Long prismatic	Bipyramidal prismatic
Dome A	Tonalite	33.73	43.37	20.48	2.40	33.37	38.55	19.27	8.43	9.63	38.55	51.80	0.00
Dome B&C	Tonalite & Granodiorite	48.78	39.02	12.19	0.00	43.90	53.65	2.43	0.00	53.65	39.02	7.31	0.00
Dome D	Tonalite & Granodiorite	28.18	41.81	22.72	7.27	42.72	33.63	19.09	4.54	17.27	22.72	43.63	16.36
	Quartz diorite	30.76	53.84	11.53	3.84	63.46	23.07	13.46	0.00	32.69	38.46	28.84	0.00
Dome E	Tonalite	30.76	65.38	3.84	0.00	57.69	38.46	3.84	0.00	34.61	53.84	11.53	0.00

Table 3- Distribution (%) of different roundness of zircon form Hafafit granitoids.

Hafafit domes	Rock types	Angular	Subrounded	Rounded
Dome A	**Tonalite**	83.13	14.45	2.40
Domes B&C	**Tonalite&Granodiorite**	53.65	46.34	0.00
Dome D	**Tonalite&Granodiorite**	78.84	31.18	4.54
	Quartz diorite	63.63	19.23	1.92
Dome E	**Tonalite**	46.15	53.84	0.00

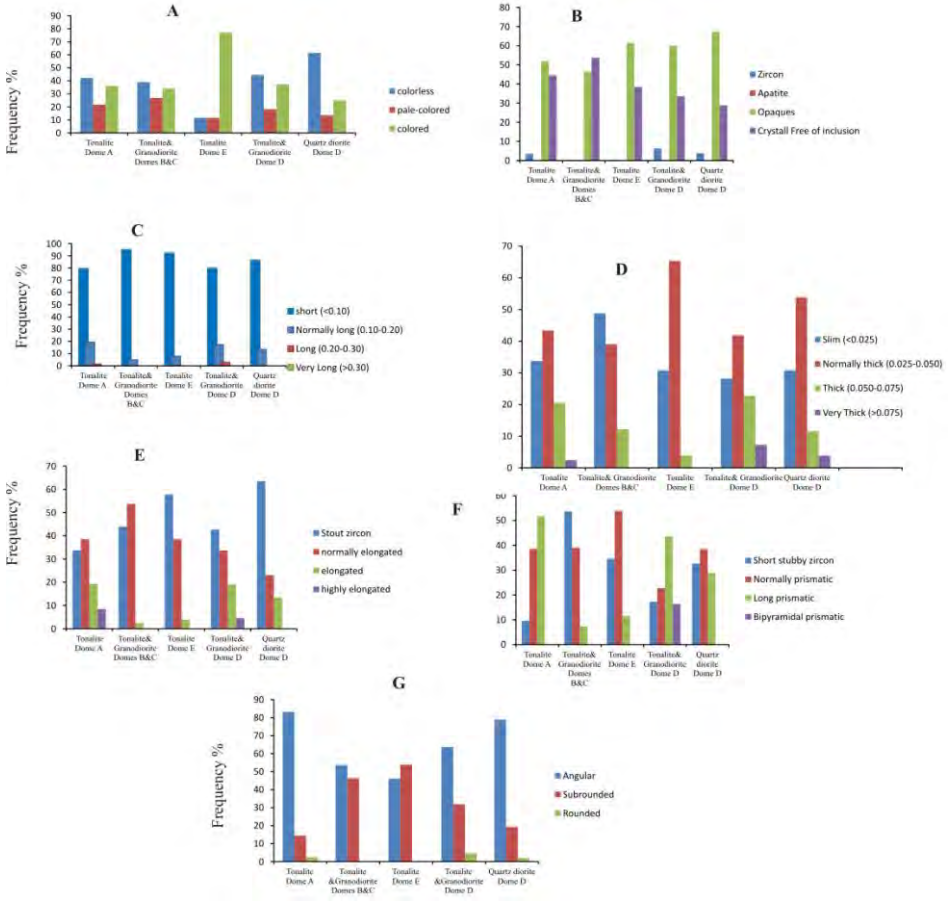

Figure 3 - Histograms showing the distribution (%) of different morphological characters of zircon crystals from Hafafit granitoids as A) color, B) inclusion, C) length, D) breadth, E) elongation ratio, F) habit G) degree of roundness.

the second generation has post magmatic features. The orientation of C-axis of zircon crystals of the two generations is SE-NW being parallel to the main dominated lineation of hosting minerals (plagioclase, hornblende and biotite). The first generation of zircon is attributed to the subduction, magmatic and deformation events while the second generation of zircon is attributed to metamorphism. However, C-axes of zircon crystals of the two generations are parallel to the main dominated lineation of hosting minerals (plagioclase, hornblende and biotite) and oriented SE-NW. The Wadi Hafafit culmination can be described by three events (Abd El Naby et al., 2008):

1. Subduction, magmatism and deformation event.

2. Metamorphism.
3. Orogenic extension oriented SE-NW.

According to Kroner et al. (1994) the zircon ages of granite samples from dome D yielded two Pb^{207}/ Pb^{206} ages 698±14 Ma and 677±9 Ma which are in agreement with the two zircon generations distinguished in the present study. Taking into account the zircon morphological characteristics, we attribute the first generation (magmatic zircon) with the age of magmatism, (698 Ma) and the second one (post magmatic zircon) with the age of 677 Ma representing the metamorphic event. Finally, the SE-NW orogenic extension oriented both generations parallel to the trend of the left-lateral shear zone of Najd fault system.

6. Acknowledgments

Our thanks are due to Greece Scholarships Foundation (IKY) for supporting the doctoral studies in Aristotle University Thessaloniki (Greece) our thanks are also Professor Mohamed Abdel Wahed for helping in field work.

7. References

Abd El Naby H., Frisch W. and Siebel W. 2008. Tectono-metamorphic evolution of the Wadi Hafafit Culmination (Central Eastern Desert, Egypt), Implication for Neoproterzoic core complex exhumation in NE Africa*, Geologica Acta,* 6, 4, 293-312.

Abd El-Naby H. and Frisch W. 2006. Geochemical constraints from the Hafafit Metamorphic Complex (HMC): evidence of Neoproterozoic back-arc basin development in the central Eastern Desert of Egypt, *Journal of African Earth Science,* 45, 173-186.

Abdel Wahed M. 2008. Thrusting and transpressional shearing in the Pan-African nappe southwest El-Sibai core complex, Central Eastern Desert, Egypt, *Journal of African Earth Science,* 50, 16-36.

Alper A.M. and Poldervaart A. 1957. Zircons from the Animas stock and associated rocks, New Mexico, *Economic Geology,* 52, 952-971.

Benisek A. and Finger F. 1993. Factors controlling the development of prism faces in granite zircons: a microprobe study, *Contribution Mineralogy and Petrology*, 114, 441-445.

Bregar M., Bauernhofer A., Pelz K., Kloetzli U., Fritz H. and Neumayr P. 2002. A late neoproterozoic magmatic core complex in the Eastern Desert of Egypt; emplacement of granitoids in a wrenchtectonic setting, *Precambrian Research,* 118, 59–82.

El Bahariya G. A. and Abd El-Wahed M. A. 2003. Petrology, mineral chemistry and tectonic evolution of the northern part of Wadi Hafafit Area, Eastern Desert, Egypt, *The 3rd international Conference on the Geology of Africa, Assiut, Egypt,* 2, 201-231**.**

El Bahariya G.A. 2008. Geology and petrology of neoproterozoic syntectonic anatectic migmatites around Wadi Abu Higlig, Hafafit region, Eastern Desert, Egypt, *Egyptian Journal of Geology,* 52, 25-54.

El Ramly M.F. and Greiling R. 1988. Wadi Hafafit Area-1:100,000 Geology map, *Technische Fachhoochschule,* Berlin.

El Ramly M.F., Greiling R.O., Rashwan A.A. and Rasmy A.H. 1993. Explanatory note to accompany the geological and structural maps of Wadi Hafafit area, Eastern Desert of Egypt, *Geological Survey of Egypt,* Paper No. 68.

Forbes W.C. 1969. Zircons of the White Mountain magma series: Belknai mountain complex, *American Mineralology*, 54, 787-795.

Fowler A. and El Kalioubi B. 2002. The Migif-Hafafit gneissic complex of the Egyptian Eastern Desert: fold interference patterns involving multiply deformed sheath folds, *Tectonophysics,* 346, 247-275.

Fowler A.R., Khamees H. and Dowidar H. 2007. El Sibai gneissic complex, Central Eastern Desert, Egypt: Folded nappes and syn-kinematic gneissic granitoid sheets-not a core complex, *Journal of African Earth Science,* 49(4), 119–135.

Fritz H., Dalmeyer D. R., Wallbrecher E., Loizenbauer J., Hoinkes G., Neumayr P. and Khudeir A.A. 2002. Neoproterozoic tectonothermal evolution of the Central Eastern Desert, Egypt: a

slow velocity tectonic process of core complex exhumation, *Journal of African Earth Science,* 34, 543–576.

Fritz H., Wallbrecher E., Khudier A.A., Abu El Ela F. and Dallmeyer R.D. 1996. Formation of Neoproterozoic metamorphic core complexes during oblique convegence, Eastern Desert, Egypt, *Journal of African Earth Science,* 23, 311–329.

Greiling R.O., El Ramly M., El akhal H. and Stern R. J. 1988a. Tectonic evolution of the northwestern Red Sea margin as related to basement structure, in: The Gulf of Suez and Red Sea Rifting, X. Le Pichon and J.R. Cochran (eds.), *Tectonophysics*, 153, 179-191.

Greiling R.O., Kröner A., El-Ramly M. F. and Rashwan A. A.1988b. Structural relationships between the southern and central parts of the Eastern Desert of Egypt: details of a fold and thrust belt, in: El-Gaby S, Greiling RO (eds) The Pan-African belt of NE Africa and Adjacent Areas, *Earth Evolution Science, Vieweg*, 121–145.

Ibrahim S. and Cosgrove J. 2001. Structural and tectonic evolution of the Umm Gheig/El-Shush region, central Eastern Desert of Egypt, *Journal of African Earth Sciences*, 33, 199–209.

Khudeir A., Abu El-Rus M., El-Gaby, S., El-Nady O. and Bishara, W. 2008. Sr–Nd isotopes and geochemistry of the infrastructural rocks in the Meatiq and Hafafit core complexes, Eastern Desert, Egypt: evidence for involvement of pre-Neoproterozoic crust in the growth of Arabian–Nubian Shield Island Arc, 17, 90–108.

Kröner A., Kruger J. and Rashwan A.A. 1994. Age and tectonic setting of granitoid gneisses in the Eastern Desert of Egypt and southwest Sinai, *Geologische Rundschau,* 83,502–513.

Larsen L.H. and Poldervaart A. 1961. Petrologic study of Bald Rock Batholith, near Bidwell Bar, California, *Geological Society American Bulletin*, 72, 69-92.

Loizenbauer J., Wallbrecher E., Fritz H., Neumayr P., Khudeir A.A. and Kloetzil U. 2001. Structural geology, single zircon ages and fluid inclusion studies of the Meatiq metamorphic core complex implications for Neoproterozoic tectonics in the Eastern Desert of Egypt, *Precambrian Research*, 110, 357–383.

Pupin J.P. 1980. Zircon and granite petrology, *Contributions Mineralogy and Petrology,* 73, 207-220.

Rashwan A.A. 1991. Petrography, geochemistry and petrogenesis of the Migif-Hafafit gneisses at Hafafit mine area, South Eastern Desert, Egypt, *Science. Series. Internnational. Bureau*, Volume 5, Forschangszentran Julich GmbH, pp. 359.

Rasmy A.H. 1974. Petrological, mineralogical and genetic studies of the Hafafit pegmatites and related mineralization, *Ph.D thesis,* Faculty of Science Ain Shams Univ., Cairo.

Shalaby A. 2009. The northern dome of Wadi Hafafit culmination,Eastern Desert, Egypt. Structural setting in tectonic framework of a scissor-like wrench corridor, *Journal of African Earth Science.*

Spotts J.H. 1962. Zircon and other accessories minerals, Coast Range Batholith, California, *Geological Society American Bulletin*, 73, 1221-1239.

Stern R.J. and Hedge C.E. 1985. Geochronologic and isotopic constraints on Late Precambrian crustal evolution in the Eastern Desert of Egypt, *Geology Society American Bulletin* 28, 97–127.

Thabet I.A. 2008. Petrogenetic implication of zircon as guide to physicochemical conditions of emplacement and crystallization of hosting rocks*, M.Sc. thesis,* Faculty of Science Tanta Univ., Tanta, Egypt.

Vavra G. 1990. On the kinematics of zircon growth and its petrogenetic significance: a cathode luminescence study, *Contributions Mineralogy and Petrology,* 106, 90-99.

Vavra G. 1993. A guide to quantitative morphology of accessory zircon, *Chemical Geology,* 110, 15-28.

Wallbrecher E., Fritz H., Khudeir A. A. and Farahat F. 1993. Kinematics of Pan-African thrusting and extension in Egypt. In: Thorweihe U, Schandehneier H (eds) *Geoscientific Research in Northeast Africa*, Balkema, Rotterdam, 27–30.

Wyatt M.1954. Zircon as provenance indicators, *American Journal of Mineralogy*, 39, (No. 11-12), 983-990.

Zav'yalova I.V., Vasilenko V.B. and Dorosh V.M. 1966. Correlation of habits of accessory zircon from the Eastern Transbaikal granitic rocks, *Geology geofiz,* 10, 112-115.

Δελτίο της Ελληνικής Γεωλογικής Εταιρίας, τομ. XLVII , 2013
Πρακτικά 13ου Διεθνούς Συνεδρίου, Χανιά, Σεπτ. 2013

Bulletin of the Geological Society of Greece, vol. XLVII 2013
Proceedings of the 13th International Congress, Chania, Sept. 2013

PETROLOGICAL IMPLICATIONS FOR THE PRODUCTION OF METHANE AND HYDROGEN IN HYPERALKALINE SPRINGS FROM THE OTHRYS OPHIOLITE, GREECE

Tsikouras B.[1,2], Etiope G.[3,4], Ifandi E.[1], Kordella S.[5], Papatheodorou G.[5] and Hatzipanagiotou K.[1]

[1]*University of Patras, Department of Geology, Section of Earth Materials, 265 00 Patras, Greece v.tsikouras@upatras.gr, selena.21@windowslive.com, k.hatzipanagiotou@upatras.gr,*

[2]*University of Brunei Darussalam, Department of Petroleum Geoscience, Jalan Tungku Link, Gadong BE1410, Bandar Seri Begawan, Brunei Darussalam*

[3]*Istituto Nazionale di Geofisica e Vulcanologia, Sezione Roma 2, Italy, Giuseppe.etiope@ingv.it*

[4]*Faculty of Environmental Science and Engineering, Babes-Bolyai University Cluj-Napoca, Romania*

[5]*University of Patras, Department of Geology, Laboratory of Marine Geology and Physical Oceanography, 265 00 Patras, Greece, stacato77@hotmail.com, gpapathe@upatras.gr*

Abstract

Altered mafic and ultramafic rocks were studied in correspondence with hyperalkaline, CH_4-bearing and very low-hydrogen spring waters in the Othrys ophiolite, whose chemical features are typical of present day serpentinisation. The H_2 paucity is interpreted as the result of the incorporation of high-silica, aqueous fluids, probably derived from mafic rocks. The vein assemblage of serpentine + magnetite is related to circulation of low-silica fluids whereas serpentine + talc, tremolite after garnet and Fe-rich serpentine in the interior of serpentine veins reflect a late circulation of low-temperature (likely below 120 °C), high silica activity fluids. The high-silica conditions might have limited or interrupted the production of H_2, which was subsequently consumed by CO_2 hydrogenation to produce CH_4. The lack of H_2 could also be due to peridotite alteration by CO_2-rich fluids. This would imply that the Othrys peridotites, among similar methane-bearing peridotites, may be considered as terrestrial analogues of Martian ultramafic rocks, which are thought to contribute to methane emission in the atmosphere of Mars. Understanding the mechanism of methane abiotic production will likely shed light to the details of some crucial aspects as the greenhouse-gas budget, the production of hydrocarbons and the origin of life on Earth.

Key words: *Abiotic methane, Othrys ophiolite, serpentinisation, methane seepage.*

Περίληψη

Μελετήθηκαν εξαλλοιωμένα βασικά και υπερβασικά πετρώματα, από το οφιολιθικό σύμπλεγμα της Όθρυος, σχετιζόμενα με υπεραλκαλικές πηγές, πολύ χαμηλής περιεκτικότητας σε υδρογόνο, από τις οποίες ανακαλύφθηκε ότι εκπέμπεται CH_4, ο χημισμός των οποίων υποδεικνύει ότι προέρχονται από τρέχουσα σερπεντινίωση. Η απουσία H_2 οφείλεται πιθανά στη συμμετοχή υδατικών διαλυμάτων υψηλής

ενεργότητας SiO_2, προερχόμενα από βασικά πετρώματα. Η παραγένεση σερπεντίνης + μαγνητίτης σε φλεβίδια, σχετίζεται με κυκλοφορία ρευστών χαμηλής ενεργότητας SiO_2 ενώ η παραγένεση σερπεντίνης + τάλκης, ο σχηματισμός τρεμολίτη σε βάρος γρανάτη και η παρουσία σερπεντίνη πλούσιου σε Fe, στο εσωτερικό φλεβιδίων σερπεντίνη, αντανακλούν μεταγενέστερη κυκλοφορία ρευστών χαμηλής θερμοκρασίας (πιθανά < 120°C) με υψηλή ενεργότητα SiO_2. Αυτά, πιθανά περιόρισαν ή διέκοψαν την παραγωγή H_2, που εξαντλήθηκε λόγω αντίδρασης με το CO_2 για να παράγουν CH_4. Η απουσία H_2 πιθανά οφείλεται ακόμα στην εξαλλοίωση των περιδοτιτών από ρευστά πλούσια σε CO_2. Οι περιδοτίτες της Όθρυος, μεταξύ άλλων περιδοτιτών που περιέχουν μεθάνιο, μπορούν να θεωρηθούν ως τα γήινα ανάλογα υπερβασικών πετρωμάτων του πλανήτη Άρη, τα οποία θεωρούνται ότι συμβάλλουν στην εκπομπή μεθανίου στην ατμόσφαιρα του. Η κατανόηση του μηχανισμού παραγωγής αβιοτικού μεθανίου είναι πιθανό να διαφωτίσει τις λεπτομέρειες κρίσιμων θεμάτων, όπως το ισοζύγιο των αερίων του φαινομένου του θερμοκηπίου, το σχηματισμό ανώτερων υδρογονανθράκων καθώς και το μυστήριο της προέλευσης της ζωής στη Γη.
Λέξεις κλειδιά: *Αβιοτικό μεθάνιο, οφιόλιθοι Όθρυος, σερπεντινίωση, διαφυγές μεθανίου.*

1. Introduction

Present-day serpentinisation (i.e. hydration by meteoric water) of ultramafic rocks on continents is a widespread process documented in many countries (Barnes *et al.*, 1978; Marques *et al.*, 2008 and references therein). It is typically revealed by the occurrence of hyperalkaline waters (pH>10) of Ca-OH type, depleted in magnesium and CO_2, but with abundant methane (CH_4) and hydrogen (H_2). Hydrogen is produced by the olivine hydration, and methane is assumed to derive by subsequent Fischer-Tropsch Type (FTT) reactions, like the Sabatier reaction, $CO_2 + 4H_2 = CH_4 + 2H_2O$, which may be catalysed by metallic minerals typically occurring in ultramafic lithologies, such as magnetite, chromite and awaruite (see review by Etiope and Sherwood Lollar, 2013). Present-day serpentinisation typically occurs at temperatures below 100 °C, which would imply that also abiotic methane synthesis takes place at such low temperatures (Etiope *et al.*, 2011, 2013). Accordingly, origin and exhalation of methane in serpentinised ultramafic rocks have attracted the interest of many scientists for its implication in planetary geology, astrobiology and energy resource exploration. In particular, serpentinites are considered as terrestrial analogues of hydrated olivine-bearing rocks on Mars, thus representing a possible source of methane observed in the Martian atmosphere (e.g., Oze and Sharma, 2005; Etiope *et al*., 2011, 2012). Moreover, understanding the exact mechanism for abiotic methane production will have significant implications to our knowledge on the origin of life (e.g., Holm *et al*., 2006; Russell *et al*., 2010), as well as on hydrocarbon formation (Etiope and Sherwood Lollar, 2013).

While complete molecular and isotopic analyses of the gases represent the first fundamental step to understand their origin and, indirectly, the links with the serpentinisation process, petrological analyses of the serpentinised ultramafic rocks is an essential task to directly show the low temperature mineralogical changes which drive gas production, and in some cases, gas consumption. With this aim, we present a preliminary petrological study on serpentinised ultramafic rocks in association with altered mafic sequences of the Othrys ophiolite, in central Greece. At this site hyperalkaline springs, characteristic of present-day serpentinisation, show significant amounts of methane, with isotopic composition similar to that observed in other serpentinisation sites and crystalline environment (Etiope *et al*., 2013). Unlike the gas in the Philippines, Turkey, New Zealand, Canada, Oman and Japan but similar to that found in peridotite inclusions in India and Oman, and in hyperalkaline springs in Italy and Portugal (Sachan *et al.*, 2007; Miura *et al*., 2011; Boschetti *et al*., 2013; Etiope *et al*., 2013 and references therein), the Othrys springs release extremely low amounts of H_2. Our petrological analysis was specifically

aimed at investigating mineralogical processes and features that may explain this H_2 depletion and the low temperature serpentinisation.

2. Geological Setting of the Othrys Ophiolite

The Othrys ophiolite comprises part of the eastern ophiolite belt in Greece, which is obducted to the west on the Pelagonian carbonate platform (e.g., Robertson, 2002; Papanikolaou, 2009; Robertson *et al*., 2009). It is a dismembered and inverted suite composing of three structural units: The lowermost Sipetorrema Pillow Lava unit (after Smith *et al*., 1975) includes pillow lavas, rare lava flows and interbedded siltstone and chert. The intermediate Kournovon Dolerite unit consists of minor cumulate gabbro cut by vertical sheeted dolerite dykes and local rhyolitic outcrops. The uppermost Mirna Group includes a series of inverted thrust sheets revealing lateral transition from continental material (clastic sediments and shallow water carbonates) to pelagic carbonates of the Mesozoic Pelagonian Zone (Smith *et al*., 1975; Smith, 1993). The higher structural members comprise dismembered oceanic mantle rocks dominated by serpentinised harzburgite with minor lherzolite, plagioclase lherzolite and dunite (e.g., Dijkstra *et al*., 2001; Barth *et al*., 2003; Barth and Gluhak, 2009; Tsikouras *et al*., 2009). In several places, massive chromitites predominate as podiform, lenticular or irregular ore bodies in serpentinised dunites within harzburgites, hosting platinum group elements and sulfides (Garuti *et al*., 1999). The peridotites are in tectonic contact with an ophiolitic, tectonic mélange consisting of fragments of dolerite, basalt, red chert and serpentinised peridotite incorporated in a tectonised, multi-coloured, pelitic matrix (Dijkstra *et al*., 2001; Tsikouras *et al*., 2009).

The area of interest extends between Archani and Ekkara, at the southwestern part of the Othrys ophiolite and includes mantle exposures of medium- to coarse-grained serpentinised harzburgite with lesser plagioclase-bearing lherzolite, as well as dunite forming thin layers few cm to few meters thick, intercalated in the harzburgite (Figure 1). A remnant doleritic sheeted-dyke complex is overthrust by the peridotites. Locally, whitish rodingite dykes are found in serpentinised harzburgites very close to the Archani spring (Tsikouras *et al*., 2009). The peridotites are in tectonic contact with an ophiolitic mélange, which in turn tectonically overlies a Late Cretaceous-Tertiary flysch. An active fault zone, the Leontari-Anavra line, extends immediately north of Ekkara, at the south border of the Thessaly Plain (Papathanassiou *et al*., 2007).

3. Petrography

3.1. Serpentinised Peridotites

The ultramafic samples collected from the study area include variably serpentinised (20 – 80%) harzburgites and lesser dunites and lherzolites. The most intensely serpentinised harzburgites display mainly mesh and lesser ribbon and bastitic textures; local interlocking, interpenetrating and hourglass textures occur as replacements on older serpentines. The less altered harzburgite contains relics of orthopyroxene porphyroclasts, clinopyroxene, olivine and Cr-spinel. Rare plagioclase occupies interstices of the porphyroclastic grains and along with neoblastic clinopyroxene and olivine are typical indicators for melt impregnation in the peridotite. The serpentinised dunite shows porphyroclastic to cataclastic textures with the predominance of fragmented olivine; fewer, disseminated Cr-spinel and traces of clinopyroxene participate in its primary assemblage, too. The serpentinised lherzolite samples have protogranular, porphyroclastic and cataclastic textures. Primary phases include strained olivine, orthopyroxene, clinopyroxene and Al-spinel.

Besides serpentine, the secondary assemblage includes variable percentages of actinolite, magnetite and scarce talc, brucite, chlorite and calcite. The presence of the low temperature lizardite and chrysotile polytypes of serpentine is suggested from X-ray diffraction patterns (not given). Magnetite is regularly found in mesh cores, formed typically after olivine breakdown or in veins associated with serpentine (Figure 2a); it frequently rims spinel grains, too. Local garnet ± tremolite

pseudomorphically replaces orthopyroxene (Figure 2b), while talc appears along cleavage planes or at the rims of orthopyroxene occasionally with magnetite (Figure 2c). Actinolite in the altered lherzolites is associated to diopside. Calcite is also present either within mesh cores or filling veins traversing the samples (Figure 2d).

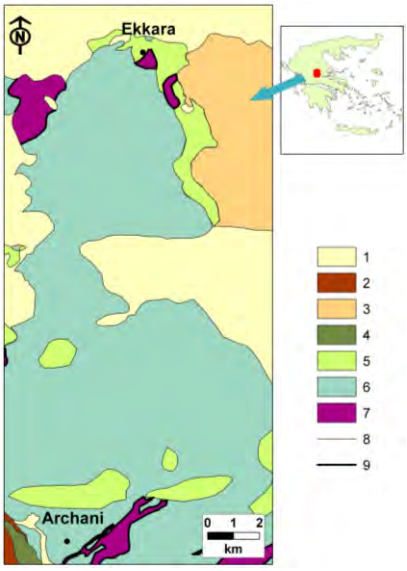

Figure 1 – Simplified geological map of the investigated area (modified after IGME, 1962, 1970; 1: Neogene – Quaternary deposits, 2: Eocene East Pindos flysch, 3: Upper Cretaceous transgressive limestone, 4: Lower Cetaceous sandstone, 5: Dolerite, 6: Serpentinised peridotite, 7: Ophiolite mélange, 8: normal contact, 9: tectonic contact).

Three vein assemblages were also observed: i) serpentine (mainly chrysotile), ii) serpentine + magnetite (Figure 2a; occasionally magnetite is altered to Fe-oxides and hydroxides), and iii) serpentine + talc ± Al-spinel (Figure 2e). Frequently a younger generation of serpentine richer in Fe is observed in the inner parts of veins rimmed by older serpentine richer in Mg (Figure 2f). Rarely, veins containing subsequent layers (from the outer to the inner parts) of chlorite, serpentine and magnetite were detected.

3.2. Dolerites

The collected dolerite samples show subophitic, porphyry and locally intergranular textures. They are composed mainly of plagioclase whereas relics of primary diopside occur, too. Accessory phases include titanite, magnetite, pyrite and chalcopyrite. Secondary products include actinolite, chlorite, Fe-Ti oxides, albite and quartz dispersed within the dolerite. Further petrographic details can be found in Tsikouras *et al.* (2009).

4. Discussion

Distinguishing present-day (meteoric water driven) from ancient (seawater driven) serpentinisation is not an easy task, as both events yield similar mineralogical products. The highly alkaline waters (pH = 10.7 – 11.3) of Ca-OH type from the Archani and Ekkara springs (Etiope *et al*. 2013) are very similar to brines that pass through present-day serpentinising peridotites (Barnes and O'Neil, 1969; Neal and Stanger, 1985). Indisputably, serpentinisation has also occurred as an ocean-floor metamorphic event in the ophiolite. Serpentinisation is a process that favours the production of fluids with low silica activity, normally of the order of $10^{-2.5}$ to 10^{-5}, depending on temperature.

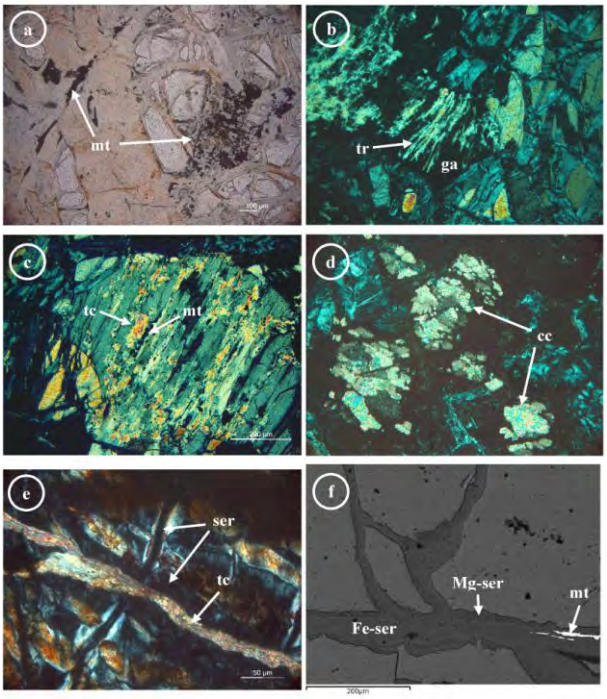

Figure 2 – Petrographic characteristics of ultramafic rocks from the Archani – Ekkara area: (a) Photomicrograph of magnetite filling veins with serpentine and occupies a mesh core (right); Nicols -, sample AR2; (b) Photomicrograph of garnet in a serpentinised harzburgite, which is replaced by tremolite; Nicols +, sample AR6; (c) Photomicrograph of talc and magnetite formation after orthopyroxene; Nicols +, sample AR6; (d) Photomicrograph of calcite precipitation in serpentinised harzburgite; Nicols +, sample AR6; (e) Photomicrograph of vein filled with talc crosscutting older serpentine vein; Nicols +, sample AR5; (f) Backscattered electron image of Fe-rich serpentine rimmed by older Mg-rich serpentine. Relic magnetite associated with Fe-rich serpentine is shown, too; sample AR2 (abbreviations: mt: magnetite, tr: tremolite, ga: garnet, tc: talc, cc: calcite, ser: serpentine).

This condition destabilises the fayalite and greenalite components of olivine and serpentine, respectively (Frost and Beard, 2007) and their hydration reactions produce magnetite (Katayama *et al*., 2010) and hydrogen (see reactions 1 and 2):

$$3Fe_2SiO_4 + 2H_2O \rightarrow 2Fe_3O_4 + 3SiO_{2(aq)} + 2H_2 \quad (1)$$

in olivine (fayalite) *magnetite*

$$Fe_3Si_2O_5(OH)_4 + H_2O \rightarrow Fe_3O_4 + 2SiO_{2(aq)} + H_2 \quad (2)$$

in serpentine (greenalite) *magnetite*

However, several authors argue that these reactions comprise probably oversimplifications for natural systems and overestimate the amount of the actually generated H_2 (Bach *et al*., 2006; McCollom and Bach, 2009). Magnetite may also form after olivine by a reaction similar to 3, which produces methane, independently of H_2 (Oze and Sharma, 2005):

$$24(Mg,Fe)_2SiO_4 + 26H_2O + CO_2 \rightarrow 12(Mg,Fe)_3Si_2O_5(OH)_4 + 4Fe_3O_4 + CH_4 \quad (3)$$

olivine *serpentine* *magnetite*

On the other hand, talc formation after orthopyroxene is promoted by rather high silica activity ($>10^{-2}$; Frost and Beard, 2007; Evans, 2008) and may appear by a reaction similar to 4, which produces directly methane, too:

$$48Mg_{0.75}Fe_{0.25}SiO_3 + 3H_2O + CO_2 \rightarrow 12Mg_3Si_4O_{10}(OH)_4 + 4Fe_3O_4 + CH_4 \qquad (4)$$

orthopyroxene *talc* *magnetite*

The lack of hydrogen in the Othrys springs can be explained either by: (i) its normal production (with the incorporation of low silica activity fluids alone, reactions 1 and 2) and subsequent consumption by CO_2 hydrogenation (Sabatier reaction) and/or expulsion to the surface by water degassing (H_2 solubility is one order of magnitude lower than that of CH_4); (ii) direct methanation (reactions 3 and 4) with the implication of low and high silica activity fluids. Although the first hypothesis cannot be excluded, there is enough petrological evidence that supports direct methanation in the case of the Othrys peridotite. The coexistence of magnetite and serpentine in mesh cores and bastitic textures, as well as in veins (Figure 2a) is compatible with the reaction 3 and the implication of low silica activity. Formation of garnet in the Othrys serpentinites provides further evidence for the establishment of low silica activity, which may have consequently partitioned ferrous iron in the andradite molecule (Beard and Hopkinson, 2000; Frost and Beard, 2007; Evans, 2008). Carbonate minerals (Figure 2d) are more stable phases relative to serpentine + brucite and their formation is favoured in CH_4-rich fluids and low pressures (Früh-Green *et al*., 2004), explaining the inferred brucite deficiency. However, often brucite forms cryptically in interlayers or is even misinterpreted as talc, serpentine, micas or clay minerals; hence its presence at higher percentages cannot be definitely precluded. Reaction 4 explains well the association of talc with orthopyroxene and magnetite (Figure 2c), as well its occurrence in veins with serpentine, denoting conditions of high silica activity. The CO_2, which is required for the above reactions 3 and 4 can be provided by meteoric water and/or deep fluids related to the Jurassic carbonate basement of the Pelagonian Zone underlying the ophiolitic block (e.g. Karipi *et al*., 2006).

The distribution of serpentine + magnetite veins indicates the flow directions of a fluid with low silica activity whereas the talc-bearing veins show the directions of a high silica activity fluid. Talc formation around orthopyroxene suggests large variations of silica activity even on the scale of a thin section. Notably, some talc-bearing veins crosscut some serpentine + magnetite veins (Figure 2e) and along with the formation of tremolite (a typical high-silica product) after garnet (Figure 2b) indicate a late stage entrance of the high silica activity fluids in the serpentinising system. Further evidence for a late high silica event is indicated by the presence of listwaenite after serpentinised peridotites, at the Iti Mountain, to the south part of the Othrys ophiolite (Tsikouras *et al*., 2006). Such an increase in the potential of SiO_2 can lead to reaction of magnetite towards growth of Fe-rich serpentine (Evans, 2008), similar to that observed in some vein centers in the Othrys serpentinised peridotites (Figure 2f). Formation of Fe-rich serpentine is favoured at low temperatures and high silica activity, being stable even at ambient conditions (Streit *et al*., 2012). Hence this younger Fe-rich serpentine most likely traces the present-day serpentinising episode. It is likely that the high silica activity fluid was sourced in the mafic sequence (e.g., dolerite or gabbro), lying tectonically below the ultramafic rocks in the Othrys ophiolite, being in equilibrium with their secondary assemblage (chlorite, actinolite, quartz). This rather hot fluid moves upwards and upon cooling, at near surface conditions, it is involved, concurrently with the existing low silica fluid, to reactions of serpentinisation, contributing to methane formation.

Methane and hydrogen emanations associated with high temperature (>100-200 ^{o}C) hydrothermal fluids in the mid-Atlantic Ridge have been widely studied (Charlou *et al*., 2002; Proskurowski *et al*., 2008; Lang *et al*., 2010). The occurrence of abiotic methane in low temperature (generally <100 °C) continental serpentinisation sites (Etiope *et al*., 2011; Etiope *et al.*, 2013) implies that high enthalpy hydrothermal conditions are not necessary for the hydrocarbon synthesis, which can then occur in a broad range of environments, either on Earth or other planets. Lizardite and chrysotile that occur in the assemblage of the Othrys peridotites are stable up to 300 – 350 ^{o}C, unlike an-

tigorite that is the high-temperature polytype of serpentine. Talc and tremolite are usually considered as high-temperature products, since they are predicted to form above 370 ^{o}C (Bucher and Frey, 2002; McCollom and Bach, 2009). However, talc is known to be stable at much lower temperatures, even at around 25 ^{o}C (Klein and Garrido, 2011), which is in line with the circulation of a low-temperature-high-silica fluid that also imposed the late Fe-rich serpentine in veins.

5. Conclusions

Petrographic observations on mafic and ultramafic rocks collected in the Othrys ophiolite, around methane-bearing hyperalkaline springs (Etiope *et al*, 2013) show some mineralogical features that may explain the paucity of H_2 in the brines. The serpentinised peridotites contain the secondary assemblage: serpentine (lizardite + chrysotile), magnetite, garnet, and minor brucite, indicating alteration under low silica activity conditions. Formation of talc after orthopyroxene and tremolite after garnet, as well as the occurrence of Fe-rich serpentine in vein centers are compatible with a late-stage involvement of a fluid of high silica activity. Two reactions of direct methanation of olivine and orthopyroxene are proposed as a possible explanation for the paucity of hydrogen in the Archani and Ekkara spring-waters, during present-day serpentinisation. Another explanation is that the implication of the high silica activity fluid that probably ascends upwards from the tectonically underlying mafic rocks may have prohibited further production of H_2, which then was consumed by hydrogenation and degassing. The occurrence of late-stage Fe-rich serpentine advocates to a low-temperature present-day serpentinising event while the occurrence of talc does not contradict low temperature serpentinisation, as documented in other similar sites. Future work must include petrographic observations in other present-day serpentinisation sites for comparison, as well as additional analyses, including Raman spectroscopy and geothermometric calculations, to better understand the production of methane and hydrogen in relation to the formation of certain mineral phases. Microbiological analyses are then planned to evaluate possible microbial contribution to gas production and consumption, providing further elements to understand the role of serpentinisation in the origin of life on Earth.

6. Acknowledgements

The authors gratefully acknowledge funding from the project “Low temperature methanation in geologic environments” by Petrobras. Critical reviews from Dr. I. Baziotis and two anonymous reviewers are gratefully acknowledged.

7. References

Bach W., Paulick H., Garrido C.J., Ildefonse B., Meurer W.P. and Humphris S.E. 2006. Unraveling the sequence of serpentinization reactions: Petrography, mineral chemistry, and petrophysics of serpentinites from MAR 15°N (ODP Leg 209, Site 1274), *Geoph. Res. Lett.,* 33, 13.

Barnes I. and O’Neil J.R. 1969. The relationship between fluids in some fresh Alpine-type ultramafics and possible modern serpentinization, Western United States, *Geol. Soc. Am. Bull.*, 80, 1947-1960.

Barnes I., O’Neil J.R. and Trescases J.J. 1978. Present day serpentinization in New Caledonia, Oman, and Yugoslavia, *Geochim. Cosmochim. Acta*, 42, 144–145.

Barth M.G. and Gluhak T.M. 2009. Geochemistry and tectonic setting of mafic rocks from the Othris Ophiolite, Greece, *Contrib. Mineral. Petrol.*, 157, 23–40.

Barth M.G., Mason P.R.D., Davies G.R., Dijkstra A.H. and Drury M.R. 2003. Geochemistry of the Othris Ophiolite, Greece: Evidence for Refertilization?, *J. Petrol.*, 44, 1759-1785.

Beard J.S., and Hopkinson L. 2000. A fossil, serpentinization-related hydrothermal vent, Ocean Drilling Program Leg 173, Site 1068 (Iberia Abyssal Plain): Some aspects of mineral and fluid chemistry, *J. Geoph. Res.*, 105, 16.527-16.539.

Boschetti T., Etiope G., Guerrot C., Pennini M., Romani M. and Toscani L.2013. Boron, lithium and methane isotope composition of hyperalkaline waters (Northern Apennines, Italy): terrestrial serpentinization or mixing with brine?, *Appl. Geochem.*, 32, 17-25.

Bucher K., Frey M. 2002. *Petrogenesis of metamorphic rocks*, 7th ed. Springer-Verlag, Berlin, Heidelberg, New York, 341 pp.

Charlou J.L., Donval J.P., Fouquet Y., Jean-Baptiste P. and Holm N. 2002. Geochemistry of high H_2 and CH_4 vent fluids issuing from ultramafic rocks at the Rainbow hydrothermal field (36°14'N, MAR), *Chem. Geol.*, 191, 345–359.

Dijkstra A.H., Drury M.R. and Vissers R.L.M. 2001. Structural petrology of plagioclase peridotites in the West Othris mountains (Greece): melt impregnation in mantle lithosphere, *J. Petrol.*, 42, 5-24.

Etiope G. 2012. Methane uncovered, *Nature Geosci.*, 5, 373-374.

Etiope G., Schoell M. and Hosgormez H. 2011. Abiotic methane flux from the Chimaera seep and Tekirova ophiolites (Turkey): understanding gas exhalation from low temperature serpentinization and implications for Mars, *Earth Planet. Sci. Lett.*, 310, 96-104.

Etiope G., Ehlmann B.and Schoell M. 2012. Low temperature production and exhalation of methane from serpentinized rocks on Earth: a potential analog for methane production on Mars, *Icarus*, http://dx.doi.org/10.1016/j.icarus.2012.05.009.

Etiope G. and Sherwood Lollar B.2013. Abiotic methane on Earth, *Rev. Geoph*., 51, doi:10.1002/rog.20011.

Etiope G., Tsikouras B., Kordella S., Idandi E., Christodoulou D.and Papatheodorou G. 2013. Methane flux and origin in the Othrys ophiolite hyperalkaline springs, Greece, *Chem. Geol.*, 347, 161-174.

Evans B.W. 2008. Control of the products of serpentinization by the $Fe^{2+}Mg^{-1}$ exchange potential of olivine and orthopyroxene, *J. Petrol.*, 49, 1873-1887.

Frost B.R. and Beard J.S. 2007. On silica activity and serpentinization, *J. Petrol.*, 48, 1351-1368.

Früh-Green G.L., Connolly J.A.D., Plas A., Kelley D.S.and Grobéty B. 2004. Serpentinization of oceanic peridotites: implications for geochemical cycles and biological activity, In Wilcock, W.S.D., Delong, E.F., Kelley, D.S., Baross, J.A., Craig Cary, S. eds., The subseafloor biosphere at Mid-Ocean-Ridges: *American Geophysical Union*, Washington, D.C., doi: 10.1029/144GM08.

Garuti G., Zaccarini F. and Economou-Eliopoulos M. 1999. Paragenesis and composition of laurite from chromitites of Othrys (Greece): Implications for Os-Ru fractionation in ophiolitic upper mantle of the Balkan peninsula, *Miner. Deposita*, 34, 312-319

Holm N.G, Dumont M., Ivarsson M. and Konn C. 2006. Alkaline fluid circulation in ultramafic rocks and formation of nucleotide constituents: a hypothesis, *Geochem. Trans.*, 7, 7 doi:10.1186/ 1467-4866-7-7.

IGME 1962. Geological Map of Greece, Leontarion Sheet, Institute of Geology and Mineral Exploration, Athens, Greece.

IGME 1970. Geological Map of Greece, *Sperkhias Sheet*, Institute of Geology and Mineral Exploration, Athens, Greece.

Karipi S., Tsikouras B. and Hatzipanagiotou K. 2006. The petrogenesis and tectonic setting of ultramafic rocks from Iti and Kallidromon Mountains, continental Central Greece: vestiges of the Pindos ocean, *Can. Mineral.*, 44, 267–287.

Katayama I., Kurosaki I. and Hirauchi K-I. 2010. Low silica activity for hydrogen generation during serpentinization: An example of natural serpentinites in the Mineoka ophiolite complex, central Japan, *Earth Plan. Sci. Lett.*, 298, 199-204.

Klein F. and Garrido C.J.2011. Thermodynamic constraints on mineral carbonation of serpentinized peridotite, *Lithos*, 126, 147-160

Lang S.Q., Butterfield D.A., Schulte M., Kelley D.S. and Lilley M.D. 2010. Elevated concentrations of formate, acetate and dissolved organic carbon found at the Lost City hydrothermal field, *Geochim. Cosm. Acta*, 74, 941–952.

Marques J.M., Carreira P.M., Carvalho M.R., Matias M.J., Goff F.E., Basto M.J., Graça R.C., Aires-Barros L. and Rocha L. 2008. Origins of high pH mineral waters from ultramafic rocks, Central Portugal, *Appl. Geochem.*, 23, 3278–3289

McCollom T.M. and Bach W. 2009. Thermodynamic constraints on hydrogen generation during serpentinization of ultramafic rocks, *Geochim. Cosmochim. Acta*, 73, 856-879.

Miura M., Arai S. and Mizukami T. 2011. Raman spectroscopy of hydrous inclusions in olivine and orthopyroxene in ophiolitic harzburgite: implications for elementary processes of serpentinization, *J. Miner. Petrol. Sci.*, 106, 91-96.

Neal C. and Stanger G. 1985. Past and present serpentinisation of ultramafic rocks from the Semail nappe of northern Oman. In Drever, J.I., ed., The Chemistry of Weathering, *Reidel. NATO ASI Series C*, *149*, 249-275.

Oze C. and Sharma M. 2005. Have olivine, will gas: serpentinization and the abiogenic production of methane on Mars, *Geoph. Res. Lett.*, 32. L10203.

Papanikolaou D. 2009. Timing of tectonic emplacement of the ophiolites and terrane paleogeography in the Hellenides, *Lithos*, 108, 262-280

Papathanassiou G., Valkaniotis S. and Pavlides S. 2007. Applying the INQUA scale to the Sofades 1954, Central Greece, earthquake, *Bull. Geol. Soc. Greece*, 40, 1226–1233.

Proskurowski G., Lilley M.D., Seewald J.S., Früh-Green G.L., Olson E.J., Lupton J.E., Sylva S.P. and Kelley D.S. 2008. Abiogenic hydrocarbon production at Lost City hydrothermal field, *Science*, 319, 604-607.

Robertson A.H.F. 2002. Overview of the genesis and emplacement of Mesozoic ophiolites in the Eastern Mediterranean Tethyan region, *Lithos*, 65, 1-67

Robertson A., Karamata S.and Šarić K. 2009. Overview of ophiolites and related units in the Late Palaeozoic–Early Cenozoic magmatic and tectonic development of Tethys in the northern part of the Balkan region, *Lithos*, 108. 1-36.

Russell M.J., Hall A.J. and Martin W.2010. Serpentinization as a source of energy at the origin of life, *Geobiology*, 8, 355-371.

Sachan H.K., Mukherjee B.K. and Bodnar R.J. 2007. Preservation of methane generated during serpentinization of upper mantle rocks: Evidence from fluid inclusions in the Nidar ophiolite, Indus Suture Zone, Ladakh (India), *Earth Planet. Sci. Lett.*, 257, 47-59.

Smith A.G. 1993. Tectonic significance of the Hellenic-Dinaric ophiolites, In Prichard, H.M., Alabaster, T., Harris, N.B.W., Neary, C.R., eds., Magmatic Processes and Plate Tectonics, *Geol. Soc. Sp. Publ.*, 76, 213-243.

Smith A.G., Hynes A.J., Menzies M., Nisbet E.G., Price I., Welland M.J.and Ferriere J. 1975. The stratigraphy of the Othris Mountains, eastern central Greece: a deformed Mesozoic continental margin sequence, *Eclog. Geol. Helv.*, 68, 463-481.

Streit E., Kelemen P. and Eiler J. 2012. Coexisting serpentine and quartz from carbonate-bearing serpentinized peridotite in the Samail Ophiolite, Oman, *Contrib. Mineral. Petrol.*, 164, 821-837.

Tsikouras B., Karipi S., Grammatikopoulos T.A.and Hatzipanagiotou K. 2006. Listwaenite evolution in the ophiolite melange of Iti Mountain (continental Central Greece), Eur. J. Mineral., 18, 243–255.

Tsikouras B., Karipi S., Rigopoulos I., Perraki M., Pomonis P. and Hatzipanagiotou K. 2009. Geochemical processes and petrogenetic evolution of rodingite dykes in the ophiolite complex of Othrys (Central Greece), *Lithos*, 113, 540–554.

Δελτίο της Ελληνικής Γεωλογικής Εταιρίας, τομ. XLVII , 2013
Πρακτικά 13ου Διεθνούς Συνεδρίου, Χανιά, Σεπτ. 2013

Bulletin of the Geological Society of Greece, vol. XLVII 2013
Proceedings of the 13th International Congress, Chania, Sept. 2013

A NON-EXTENSIVE STATISTICAL PHYSICS APPROACH TO THE CHARACTERIZATION OF THE PYROCLASTIC DEPOSITS OF THE KOS VOLCANIC CENTER

Vallianatos F.[1,2], Michas G.[2], Papadakis G.[2], Kyriakopoulos K.[3] and VasilakopoulosV.[3]

[1] *Laboratory of Geophysics and Seismology, Technological Educational Institute of Crete, Chania, GR 73133, Crete, Greece, (fvallian@chania.teicrete.gr)*

[2]*Institute for Risk and Disaster Reduction, University College London, Gower Street, London, WC1E 6BT, UK*

[3]*Department of Geology and Geoenvironment, National and Kapodistrian University of Athens, Panepistimiopolis, 157 84 AnoIlissia, Greece*

Abstract

*In this paper we present a Non-Extensive Statistical Physics (NESP) approach in order to investigate the grain size distribution of pyroclastic deposits from the Kos volcanic center that cover parts of the main Kos island as well as the surrounding areas. The Kos Plateau Tuff (KPT) of 161 K*a *represents the largest Quaternary volcanic explosion of eastern Mediterranean. Pyroclastic deposits are formed by the fragmentation of magma and rocks, the driving mechanism of explosive volcanic activity. Rocks fragmentation can be considered in general as a non-linear process, where long-range interactions and scaling are important. It is exactly these processes that NESP was formed for to describe. The results of the analysis indicate that NESP is an appropriate framework for the statistical physics interpretation of volcanic rock fragmentation processes phenomena.*
Key words: *Tsallis Entropy, south Aegean volcanism, volcanic rocks.*

Περίληψη

Στην εργασία αυτή χρησιμοποιούμε την γενικευμένη θεωρία της μη-εκτατικής στατιστικής φυσικής για την διερεύνυνση της κατανομής του μεγέθους των κόκκων των πυροκλαστικών αποθέσεων, προερχομένων από το ηφαιστειακό κέντρο της νήσου Κω. Οι αποθέσεις αυτές καλύπτουν κυρίως τμήματα της νήσου Κω και παρακείμενων περιοχών. Οι πυροκλαστικές αποθέσεις σχηματίζονται από τον κατακερματισμό του μάγματος και των πετρωμάτων κατά την διάρκεια της εκρηκτικής φάσης της ηφαιστειακής δραστηριότητας. Η διεργασία του κατακερματισμού των πετρωμάτων είναι μη γραμμική διαδικασία και ανήκει ακριβώς σε αυτές τις διαδικασίες που αναφέρεται η γενικευμένη θεωρία της μη-εκτατικής στατιστικής φυσικής. Τα αποτελέσματα της ανάλυσης δείχνουν ότι η μη-εκτατική στατιστική φυσική είναι ένα κατάλληλο εργαλείο για την ερμηνεία της διαδικασίας θρυμματοποίησης των ηφαιστειακών σχηματισμών.
Λέξεις κλειδιά: *Εντροπία Tsallis, ηφαιστειότητα νοτίου Αιγαίου, ηφαιστειακά πετρώματα.*

1. Introduction

Pyroclastic deposits are those formed by the fragmentation of magma melt and rocks, which is the main mechanism regarding the explosive volcanic activity. Mechanical and granulometric analyses are used extensively in volcanology and volcanic hazard assessment, as they can provide valuable information for the eruption dynamics (Walker, 1971; Pyle, 1989). Moreover, the mass, internal stratigraphy, textural and lithofacies characteristics and componentry of the pyroclastic deposits are useful qualitative indicators of temporal variations in eruption intensity (Allen, 2001).

Since the Sparks's (1978) pivotal work, magmatic fragmentation has been regarded as a consequence of magma vesiculation, i.e., with decreasing external pressure a gas-saturated magma body evolves through a bubbly–foamy stage to erupting gas–pyroclast dispersion due to the collapse of bubble walls. An alternative mechanism for magma fragmentation is by conduit shear stress, as has been proposed for the pyroclastic deposits of Kos volcanic center (Palladino et al., 2008).

Fragmentation process can be defined as the structural failure of the earth's brittle material by the propagation of multiple fractures at different length scales (Perfect, 1997). Recently, the statistical properties of the fracturing process have attracted a wide interest in the scientific community (Herrmann and Roux, 1990; Chakrabarti and Benguigui, 1997). In this context, fracture can be seen as the outcome of the irreversible dynamics of a long-range interacting, disordered system (Krajcinovic and Van Mier, 2000). Several experimental observations have revealed that fracture is a complex phenomenon, described by scale invariant laws and fractality (Turcotte, 1986; Sornette et al., 1990).

The main motivation of our work is to investigate the statistical physics properties of the fracturing process that takes place during explosive volcanism. Non-extensivity represents one of the most intriguing characteristics of systems that experience long-range spatial correlations or long-range memory effects. Since disorder and fractality are two of the key components of the fracturing process, we use a current generalization of Boltzmann-Gibbs (BG) statistical physics due to Tsallis, referred as Non-Extensive Statistical Physics (NESP) (Tsallis, 1988; 2009), to explore the grain size distribution of pyroclastic deposits from the Kos volcanic center. NESP is a suitable framework for studying complex dynamic systems where fractality and long-range interactions are important and has been successfully applied in geophysics (see Vallianatos and Telesca, 2012 and references therein).

The applicability of this approach in earth sciences has been demonstrated in a series of recent publications on seismicity (Abe and Suzuki, 2003; 2005; Silva et al., 2006; Telesca, 2010; 2012; Vilar et al., 2007), natural hazards (Vallianatos, 2009; 2013), plate tectonics (Vallianatos and Sammonds, 2010), geomagnetic reversals (Vallianatos, 2011) and rock physics (Vallianatos et al., 2011; 2012; Vallianatos and Triantis, 2012).

2. The KPT Eruption

The volcanic Kos-Nisyros area forms the easternmost end of the Hellenic active volcanic arc (Figure 1). The volcanic activity in this area initiated in Pliocene time (3.4 – 1.0 Ma) and continued during Pleistocene and Quaternary time (Bellon and Jarrige, 1979; Dalabakis and Vougioukalakis, 1993). The Kos Plateau Tuff (KPT) eruption took place at 161 ka (Smith et al., 1996) and was probably the largest eruption in the Pliocene–Quaternary South Aegean arc (Allen, 2001). The source is placed between Kos and Nisyros and resulted into a caldera collapse (Allen, 2001; Pe-Piper et al., 2005).

Pyroclastic deposits from this eruption are spread in the island of Kos, the surrounding islands of Kalymnos, Pserimos, Tilos and Pachia, as well as on the Turkish peninsula of Bodrum and Datça region (Allen and Cas, 1998). The eruption of KPT produced a sequence of a well preserved,

rhyolitic fallout, stratified pyroclastic-density-current deposits and massive ignimbrites (Allen, 2001). Six major stratigraphic units can be identified that represent a change in the eruptive conditions from initial and final phreatomagmatic activity depositing fallout and internally stratified pyroclastic density current deposits to dry explosive, during the more intense phases of the eruption that produced the formation of ignimbrites (Allen et al., 1999).

In the present work 12 samples of pyroclastic deposits have been collected, 9 samples from the island of Kos and 3 samples from the island of Kalymnos. The grain size distribution for each of the samples has been obtained through granulometric analysis and is being used further on in their analysis.

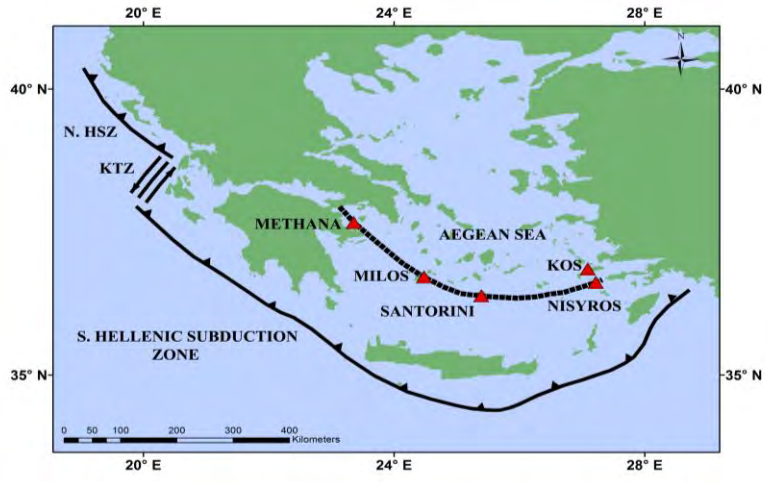

Figure 1- The location of the volcanic Kos-Nisyros area along the Hellenic volcanic arc. The modern active trenches (thick dark lines with solid barbs) for the Hellenic Subduction Zone (HSZ) are also presented, as Royden and Papanikolaou (2011) indicate them. The junction of the north and the south part of the HSZ, coincides with the Kephalonia Transform Zone (KTZ).

3. Non Extensive Statistical Physics Analysis

Non-Extensive Statistical Physics (NESP) refers to the non-additive entropy S_q (Tsallis, 1988; 2009), which is a generalization of Boltzmann–Gibbs entropy S_{BG} and has been frequently used to characterize complex dynamical systems that exhibit scale-invariance, (multi)fractality and long-range interactions (e.g. Gell-Mann and Tsallis, 2004; Tsallis, 2009). Tsallis entropy S_q is non-additive in the sense that is not proportional to the number of the system's elements as S_{BG} does. The Tsallis entropy S_q reads as:

Equation 1- Tsallis entropy

$$S_q = k_B \frac{1-\sum_{i=1}^{W} p_i^q}{q-1}, \quad q \in R$$

and in integral formulation as:

Equation 2- Integral formulation of Tsallis entropy

$$S_q = k \frac{1 - \int p^q(X) dX}{q - 1}$$

where k_B is Boltzmann's constant, p_i is a set of probabilities, W is the total number of microscopic configurations and q the entropic index. The latter index is a measure of the non-extensivity of the system and for the particular case q=1, the Boltzmann-Gibbs entropy S_{BG} is obtained:

Equation 3 -The Boltzmann-Gibbs entropy

$$S_{BG} = -k_B \sum_{i=1}^{W} p_i \ln p_i$$

The cases q>1 and q<1 correspond to subadditivity and superadditivity respectively. Although Tsallis entropy shares a lot of common properties with the Boltzmann- Gibbs entropy, S_{BG} is additive, whereas S_q ($q \neq 1$) is nonadditive (Tsallis, 2009). According to this property S_{BG} exhibits only short-range correlations and the total entropy depends on the size of the systems' elements. On the other hand, S_q allows all-length scale correlations and seems more adequate for complex dynamical systems when long-range correlations between the elements of the system are present.

The process of rock fragmentation, especially when high energies are involved, leads to the existence of long-range interactions between all parts of the object being fragmented. This type of entropy is nonadditive and depends on the object as a whole. Thus, the use of the non-extensive approach seems adequate to analyze the complex mechanism of fragments frequency-size distribution. Sotolongo-Costa and Posadas (2004), proposed a model for fragmentation considering the interaction of two rough profiles and the fragments filling the gaps between them, where the fragments are produced by the local breakage due to externally applied stress. In addition, Silva et al. (2006) have revisited the fragment asperity model for earthquakes, as it is introduced by Sotolongo-Costa and Posadas (2004), leading to a modified expression of frequency – magnitude distribution of earthquakes.

Following their approach, in order to estimate the probability distribution $p(\sigma)$ of a parameter σ, the surface of a fragment in our case, we maximized the non-extensive entropy under appropriate constraints, using the Lagrange multipliers method. The first constraint used refers to the normalization condition that reads as:

Equation 4 - Normalized condition

$$\int_0^\infty p(\sigma) d\sigma = 1$$

Introducing a generalized expectation value (q-expectation value), σ_q is defined as:

Equation 5- Definition of q-expectation value

$$\sigma_q = (\sigma)_q = \int_0^\infty \sigma P_q(\sigma) d\sigma$$

where the escort probability is given by (Tsallis, 2009) as follows:

Equation 6 – The escort probability

$$P_q(\sigma) = \frac{p_q(\sigma)}{\int_0^\infty p_q(\sigma) d\sigma}$$

The extremization of S_q with constraints (4) and (5) yields

Equation 7- Probability distribution of fragments' surface

$$p(\sigma) = \left[1 - \frac{1-q}{2-q}(\sigma - \sigma_q)\right]^{\frac{1}{1-q}}$$

where the q-exponential function is defined as:

Equation 8- Definition of q-exponential function

$$exp_q(X) = \begin{cases} \left[1+\left(1-q\right)X\right]1/(1-q) & (1+(1-q)\,X \geq 0) \\ 0 & (1+\left(1-q\right)X < 0) \end{cases},$$

whose inverse is the *q*-logarithmic function:

Equation 9 – The q-logarithmic function

$$ln_q(X) = \frac{1}{1-q}\left(X^{1-q}-1\right).$$

Following Sotolongo-Costa and Posadas (2004) and Silva et al. (2006), the proportionality between the fracture surface σ and grain size r becomes:

Equation 10

$$\sigma - \sigma_q = \left(\frac{r}{r_0}\right)^2,$$

where r_o is a geometric scaling factor.

Thus, the size distribution of fragments is obtained in the following manner: using equations (7) and (10) we lead to:

Equation 11 – The fragment size distribution function

$$p(r) = \frac{\frac{2r}{r_0^2}dr}{\left[1-\frac{1-q}{2-q}\left(\frac{r}{r_0}\right)^2\right]^{\frac{1}{1-q}}}.$$

The normalized cumulative number of fragments can be obtained by integrating equation (11) as:

Equation 12 – The normalized cumulative number of fragments

$$\frac{N(>r)}{N_0} = \int_r^{\infty} \frac{\frac{2r}{r_0^2}dr}{\left[1-\frac{1-q}{2-q}\left(\frac{r}{r_0}\right)^2\right]^{\frac{1}{1-q}}},$$

where $N(>r)$ is the number of fragments with size larger than r, and thus :

Equation 13

$$\frac{N(>r)}{N_0} = \left[1+\left(\frac{q-1}{2-q}\right)\left(\frac{r}{r_0}\right)\right]^{\frac{q-2}{q-1}}.$$

The latter expression has the form $P(>r) = \left[1+\left(\frac{q-1}{2-q}\right)\left(\frac{r}{r_0}\right)\right]^{\frac{q-2}{q-1}}$ which if we define $q = 2-\frac{1}{Q}$ leads to:

Equation 14

$$P(>r) = exp_Q\left(-r/r_0\right) = \left[1 + (Q-1)\left(\frac{r}{r_0}\right)\right]^{-\frac{1}{Q-1}}$$,

having a Q-exponential form. The inverse of Eq. (14) is the Q-logarithmic distribution $\ln_Q(P(>r))$. After the estimation of the appropriate Q that describes the observed distribution $P(>r)$, the Q-logarithmic distribution $\ln_Q(P(>r))$, where $\ln Q(x) = \frac{1}{1-Q}\left(x1\text{-}Q - 1\right)$, is linear with r (Abe and Suzuki, 2005). In the limit $Q \rightarrow 1$, the ordinary exponential and logarithmic functions are obtained from the $e_Q(x)$ and $ln_Q(x)$ functions, respectively.

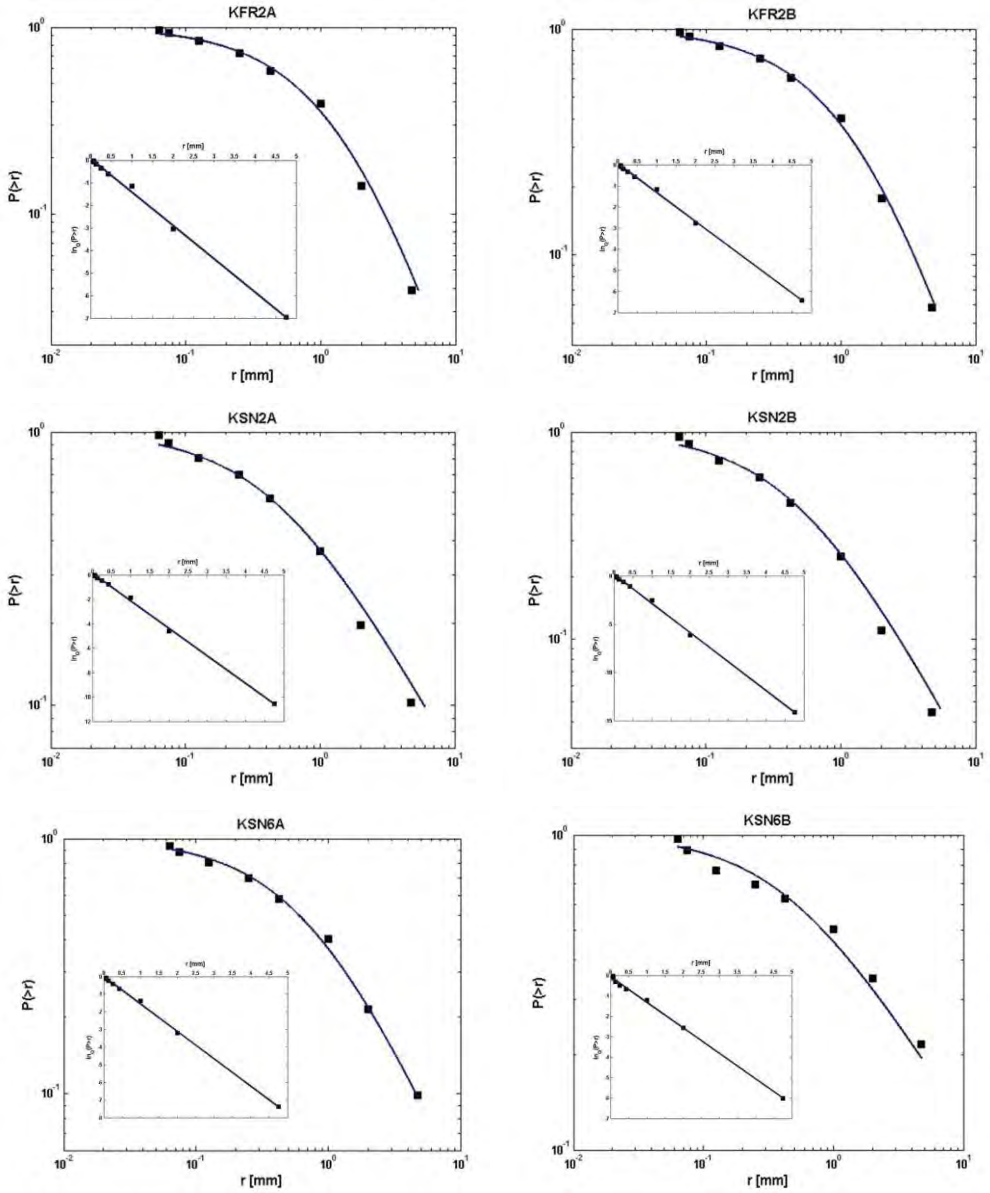

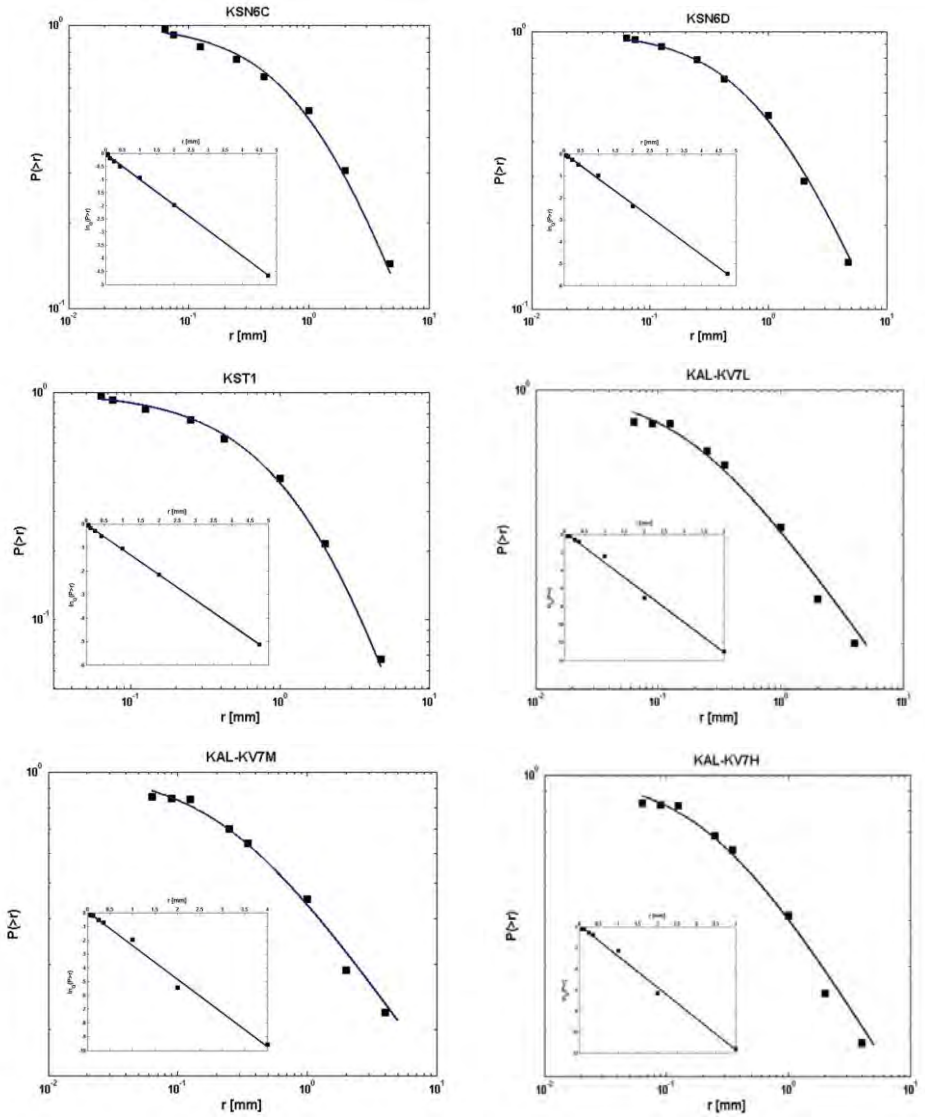

Figure 2 - Cumulative grain size distribution (squares) and the equivalent *Q*-exponential distribution according to Eq.(14) for each sample from the pyroclastic deposits collected from the islands of Kos and Kalymnos. In the inset of each figure the *Q*-logarithmic distribution is also plotted.

We have applied this approach to the cumulative grain size distributions $P(>r)$ of the pyroclastic deposits collected from the islands of Kos and Kalymnos. In Figure 2 the Q-exponential distribution according to Eq.(14) is plotted for each sample. We can see that for the appropriate values of q and r_0, the Q-exponential distribution can describe quit well the observed grain size distributions $P(>r)$. In the insets of each figure (Figure 2), the Q-logarithmic distribution is also plotted for each sample that approaches linearity with high correlation coefficients. The q and r_0 that resulted from the analysis, as well as the equivalent correlation coefficients are referred in Table 1.

Table 1 - The q and r_0 values that resulted from the regression analysis according to Eq.(14) and the equivalent correlation coefficients (ρ).

Sample	q-value	r_0 (mm)	ρ
KFR2 (A)	1.3	0.762	-0.9988
KFR2 (B)	1.34	0.786	-0.9995
KST1	1.302	0.885	-0.9998
KSN2 (A)	1.528	0.548	-0.9993
KSN2 (B)	1.448	0.405	-0.9994
KSN6 (A)	1.463	0.636	-0.9995
KSN6 (B)	1.6	0.671	-0.9991
KSN6 (C)	1.444	0.948	-0.9996
KSN6 (D)	1.489	0.925	-0.9994
KAL-KV7H	1.648	0.423	-0.9972
KAL-KV7M	1.677	0.469	-0.9963
KAL-KV7L	1.674	0.378	-0.9968

4. Conclusions

In the present work the statistical physics of one of the largest volcanic eruptions in the Pliocene–Quaternary age in South Aegean volcanic arc is being investigated (KPT eruption), by analyzing the grain size distribution of the pyroclasts that deposited in the islands of Kos and Kalymnos during the different stages of the eruption. For this purpose we used Non-Extensive Statistical Physics (NESP), a recent generalization of Boltzmann-Gibbs statistical physics that has been frequently used to describe complex dynamical systems. The analysis that was performed to the cumulative grain size distribution for each of the 12 samples according to the non-extensive model of Eq.(14) indicated that these distributions can be successfully described using NESP. These results imply that non-linear dynamics control the fragmentation process during explosive volcanism and that NESP is an appropriate framework for the statistical physics interpretation of complex Earth dynamic systems.

5. Acknowledgments

G. Michas and G. Papadakis wish to acknowledge the financial support of the Greek State Scholarships Foundation (IKY). The completion of this work has been accomplished in the framework of the postgraduate program and co-funded through the action “Program for scholarships provision I.K.Y. through the procedure of personal evaluation for the 2011-2012 academic year” from resources of the educational program “Education and Life Learning” of the European Social Register and NSRF 2007-2013.

6. References

Abe S. and Suzuki N. 2003. Law for the distance between successive earthquakes, *J. Geophys. Res.,* 108, B2, 2113, doi:10.1029/2002JB002220 .

Abe S. and Suzuki N. 2005. Scale-free statistics of time interval between successive earthquakes, *Phys. A*, 350, 588-596, doi:10.1016/j.physa.2004.10.040.

Allen S.R. 2001. Reconstruction of a major caldera-forming eruption from pyroclastic deposit characteristics: Kos Plateau Tuff, eastern Aegean Sea, *J. Volcanol. Geotherm. Res.*, 105, 141-162.

Allen S.R. and Cas R.A.F. 1998. Rhyolitic fallout and pyroclastic density current deposits from a phreatoplinian eruption in the eastern Aegean Sea, Greece, *J. Volcanol. Geotherm. Res*., 86, 219-251.

Allen S.R., Stadlbauer E. and Keller J. 1999. Stratigraphy of the Kos plateau tuff: Product of a major quaternary explosive rhyolitic eruption in the eastern Aegean, Greece, *Int. J. Earth Sci.,* 88(1), 132-156.

Bellon H. and Jarrige J.J. 1979. L'activité magmatique néogene et quaternaire dansl'ile de Kos, Greece: Données radio chronologiques, *C.R. Acad. Sci. Paris*, 288, 1359-1362.

Chakrabarti B.K. and Benguigui L.G. 1997. *Statistical Physics of Fracture and Breakdown in Disordered Systems*, Oxford, Oxford Science Publications.

Dalabakis P. and Vougioukalakis G. 1993. The Kefalos Tuff Ring (W. Kos): depositional mechanisms, vent position, and model of the evolution of the eruptive activity, *Bull. Geol. Soc. Greece*, 28 (2), 259-273.

Gell-Mann M. and Tsallis C. 2004. Nonextensive Entropy - Interdisciplinary Applications, New York, Oxford University Press.

Herrmann H.J. and Roux S. 1990. *Statistical Models for the Fracture of Disordered Media*, Amsterdam, North-Holland.

Krajcinovic D. and Van Mier J.G.M. 2000. *Damage and Fracture of Disordered Materials*, New York, Springer-Verlag.

Palladino D.M., Simei S. and Kyriakopoulos K. 2008. On magma fragmentation by conduit shear stress: Evidence from the Kos Plateau Tuff, Aegean Volcanic Arc, *J. Volcanol. Geotherm. Res.*, 178, 807–817.

Pe-Piper G., Piper D.J.W. and Perissoratis C. 2005. Neotectonics and the Kos plateau tuff eruption of 161 ka, south Aegean arc, *J. Volcanol. Geotherm. Res.*, 139, 315-338.

Perfect E. 1997. Fractal models for the fragmentation of rocks and soils: A review, *Eng. Geol.*, 48, 185-198.

Pyle D.M. 1989. The thickness, volume and grain size of tephra fall deposits, *Bull. Volcanol*., 51, 1-15.

Royden L.H. and Papanikolaou D.J. 2011. Slab segmentation and late Cenozoic disruption of the Hellenic arc, *Geochem. Geophys. Geosyst*., 12(3), Q03010, doi: 10.1029/2010GC003280.

Smith P.E., York D., Chen Y. and Evensen N.M. 1996. Single crystal ^{40}Ar-^{39}Ar dating of a Late Quaternary paroxysm on Kos, Greece: concordance of terrestrial and marine ages, *Geophys. Res. Lett.*, 23, 3047-3050.

Silva R., Franca G.S., Vilar C.S. and Alcaniz J.S. 2006. Nonextensive models for earthquakes, *Phys. Rev. E*, 73, 026102.

Sornette A., Davy P. and Sornette D. 1990. Growth of fractal fault patterns, *Phys. Rev. Lett.*, 65, 2266–2269.

Sotolongo-Costa O. and Posadas A. 2004. Fragment-asperity interaction model for earthquakes, *Phys. Rev. Lett.*, 92(4), 048501.

Sparks R.S.J. 1978. The dynamics of bubble formation and growth in magmas: a review and analysis, *J. Volcanol. Geotherm. Res.,* 3, 1–37.

Sparks R.S.J. and Walker G.P.L. 1973. The ground surge deposit: a third type of pyroclastic rock, *Nature Phys. Sci.*, 241, 62-64.

Telesca L. 2010. A non-extensive approach in investigating the seismicity of L' Aquila area (central Italy), struck by the 6 April 2009 earthquake (ML=5.8), *Terra Nova,* 22**,** 87-93, doi: 10.1111/j.1365-3121.2009.00920.x.

Telesca L. 2012. Maximum likelihood estimation of the nonextensive parameters of the earthquake cumulative magnitude distribution, *Bull. Seismol. Soc. Am.,*102(2), 886-891, doi: 10.1785/0120110093.

Tsallis C. 1988. Possible generalization of Boltzmann–Gibbs statistics, *J. Stat. Phys*., 52, 479-487, doi: 10.1007/BF01016429.

Tsallis C. 2009. *Introduction to Nonextensive Statistical Mechanics: Approaching a Complex World*, New York, Springer, doi: 10.1007/978-0-387-85359-8.

Turcotte D.L. 1986. Fractals and fragmentation, *J. Geophys.Res.*, 91, 1921–1926.

Vallianatos F. 2009. A non-extensive approach to risk assessment, *Nat. Hazards Earth Syst. Sci.* 9, 211-216.

Vallianatos F. 2011. A non-extensive approach to the polarity reversals of the geomagnetic field, *Phys. A,* 390, 1773-1778, doi:10.1016/j.physa.2010.12.040.

Vallianatos F. 2013. On the statistical physics of rockfalls: A non-extensive view, *Europhys. Let*., 101, 10007, doi: 10.1209/0295-5075/101/10007.

Vallianatos F. and Sammonds P. 2010. Is plate tectonics a case of non-extensive thermodynamics?, *Phys. A,* 389, 4989-4993, doi: 10.1016/j.physa.2010.06.056.

Vallianatos F. and Telesca L. 2012. Statistical mechanics in earth physics and natural hazards, *Acta Geophys.*, 60, 499-501.

Vallianatos F. and Triantis D. 2012. Is pressure stimulated current relaxation in amphibolite a case of non-extensivity?, *Europhys. Lett.,* 99, 18006, doi: 10.1209/0295-5075/99/18006.

Vallianatos F., Triantis D. and Sammonds P. 2011. Non-extensivity of the isothermal depolarization relaxation currents in uniaxial compressed rocks, *Europhys. Lett.,* 94, 68008, doi: 10.1209/0295-5075/94/68008.

Vallianatos F., Benson P., Meredith P. and Sammonds P. 2012. Experimental evidence of a non-extensive statistical physics behavior of fracture in triaxially deformed Etna basalt using acoustic emissions, *Europhys. Lett.*, 97, 58002, doi: 10.1209/0295-5075/97/58002.

Vilar C.S., Franca G.S., Silva R. and Alcaniz J.S. 2007. Nonextensivity in geological faults?, *Phys. A,* 377, 285-290, doi: 10.1016/j.physa.2006.11.017

Walker G.P.L. 1971. Grain-Size Characteristics of Pyroclastic Deposits, *J. Geol.*, 79(6), 696-714.

Δελτίο της Ελληνικής Γεωλογικής Εταιρίας, τομ. XLVII , 2013
Πρακτικά 13ου Διεθνούς Συνεδρίου, Χανιά, Σεπτ. 2013

Bulletin of the Geological Society of Greece, vol. XLVII 2013
Proceedings of the 13th International Congress, Chania, Sept. 2013

GENESIS OF ALPINOTYPE FISSURE MINERALS FROM THASOS ISLAND, NORTHERN GREECE - MINERALOGY, MINERAL CHEMISTRY AND CRYSTALLIZING ENVIRONMENT

Voudouris P.[1], Constantinidou S.[1], Kati M.[1], Mavrogonatos C.[1], Kanellopoulos C.[1] and Volioti E[1].

[1] National and Kapodistrian University of Athens, Faculty of Geology and Geoenvironment, Department of Mineralogy and Petrology, voudouris@geol.uoa.gr, geokonstantinidou@gmail.com, kati@geol.uoa.gr, kmavrogon@geol.uoa.gr, ckanellopoulos@gmail.com.

Abstract

Alpinotype fissure-minerals in Thasos Island are hosted in gneisses, amphibolites, Mn-rich schists and calc-silicate layers, and marbles of the Carboniferous-Permian Pangeon Unit, which represents the lower tectonostratigraphic unit of the southern Rhodope metamorphic core complex. Alpinotype fissures crosscut metamorphic fabrics and are closely related to the exhumation processes of the core complex during the Oligocene-Miocene. Most mineralized fissures occur close to a major detachment fault, which separates gneisses from marbles and amphibolites. The mineralogy of the alpinotype fissures is closely related to the host rocks: amphibolite-hosted fissures include adularia, albite, quartz, titanite, apatite, actinolite, chlorite, calcite, hematite and rutile. Fissures in para- and orthogneisses- and in metapegmatites are characterized by smoky and clear quartz, adularia, muscovite and hematite. Fissures within spessartite-piemontite schists contain quartz, chlorite, spessartite, hematite, rutile, albite, epidote and traces of zircon. Finally fissures in calc-silicate layers include Mn-grossular, quartz and Mn-clinozoisite. Hydrothermal alteration halos surrounding the fissures may suggest leaching of the wall rocks as a potential mechanism for mineral deposition. Scepter quartz crystals consist of a lower Tessin-habit crystal and several generations of upper prismatic quartz crystals, suggesting several stages of crystallization and changing P-T-x conditions with time. Chlorite geothermometry indicates temperatures of formation in the range between 286 and 366 °C. Tessin habit quartz was deposited from CO_2-bearing fluids, probably at the transition from a compressional to an extensional tectonic regime and was later dissolved by meteoric water dominated fluids resulting in the formation of quartz scepters. Oxidizing conditions are indicated by the widespread occurrence of hematite in the mineralization. The studied area represents a unique mineralogical geotope. Its geological-mineralogical heritage should be protected through establishment of a mineralogical-petrological geopark that will also promote sustainable development of the area.

Key words: *Alpinotype fissure-minerals, Thasos island, Rhodope.*

Περίληψη

Στην περιοχή της Θάσου, αλπινότυπα ορυκτά φιλοξενούνται εντός διακλάσεων γνευσίων, αμφιβολιτών, Mn-ούχων ασβεστοπυριτικών στρώσεων και σχιστολίθων

καθώς και μάρμαρων της κατώτερης ενότητας του μεταμορφικού πυρήνα της Ροδόπης. Οι αλπινότυπες διακλάσεις τέμνουν τις μεταμορφικές δομές και συνδέονται στενά με τις διαδικασίες εκταφιασμού του Ροδοπικού συμπλέγματος κατά το Ολιγόκαινο-Μειόκαινο. Οι περισσότερες αλπινότυπες διακλάσεις αναπτύσσονται κατά μήκος μίας μεγάλης ζώνης αποκόλλησης, που διαχωρίζει τους ανώτερους στρωματογραφικά γνεύσιους από τους κατώτερους αμφιβολίτες και μάρμαρα. Το ορυκτολογικό περιεχόμενο των διακλάσεων είναι στενά συνδεδεμένο με την ορυκτολογία των περιβαλλόντων πετρωμάτων. Σε διακλάσεις εντός αμφιβολιτών εμφανίζεται αδουλάριος, αλβίτης, χαλαζίας, τιτανίτης, απατίτης, ακτινόλιθος, χλωρίτης, ασβεστίτης, αιματίτης και ρουτίλιο. Σε διακλάσεις παρα-, ορθογνευσίων και μεταπηγματιτών κρυσταλλώνονται χαλαζίας, αδουλάριος, μοσχοβίτης και αιματίτης, ενώ σε διακλάσεις που αναπτύσσονται εντός σπεσσαρτινικών-πιεμοντιτικών σχιστόλιθων κρυσταλλώνονται χαλαζίας, χλωρίτης, σπεσσαρτίνης, αιματίτης, ρουτήλιο, αλβίτης, επίδοτο και ζιρκόνιο. Τέλος διακλάσεις εντός ασβεστοπυριτικών στρώσεων περιέχουν Mn-ούχο γροσσουλάριο, χαλαζία και Mn-ούχο κλινοζωισίτη. Οι εξαλλοιώσεις που παρατηρούνται στα τοιχώματα των διακλάσεων υποδηλώνουν διαδικασίες έκπλυσης των περιβαλλόντων πετρωμάτων από υδροθερμικά ρευστά. Οι κρύσταλλοι χαλαζία εμφανίζονται με μορφές σκήπτρου, σε πρισματικούς κρυστάλλους διάφορων γενεών να αναπτύσσονται πάνω σε χαλαζίες τύπου Tessin, υποδηλώνοντας πολλαπλά στάδια κρυστάλλωσης και αλλαγή των συνθηκών P-T-t. Η εφαρμογή γεωθερμόμετρου χλωρίτη υποδεικνύει αρχικές θερμοκρασίες σχηματισμού των παραγενέσεων τους 286 έως 366 °C. Οι χαλαζίες τύπου Tessin πιθανότατα δημιουργήθηκαν από ρευστά πλούσια σε CO_2 και πιθανόν στη μετάβαση από ένα συμπιεστικό σε εφελκυστικό τεκτονικό καθεστώς. Αντίθετα οι μεταγενέστερες γενεές σκήπτρων υποδεικνύουν συμμετοχή κατερχόμενων μετεωρικών νερών. Η περιοχή μελέτης αντιπροσωπεύει μοναδικό ορυκτολογικό Γεώτοπο. Η γεωλογική-ορυκτολογική αυτή κληρονομιά μπορεί να προστατευθεί μέσω της ίδρυσης ενός Γεωπάρκου που θα συμβάλει επιπλέον και στην προώθηση φιλικής προς το περιβάλλον ανάπτυξης της Θάσου.
Λέξεις κλειδιά: *αλπινότυπα ορυκτά, Θάσος, Ροδόπη.*

1. Introduction

Alpinotype fissure minerals occur in several regions in the world with alpine-type, late-stage collisional tectonics such as the Alps, Himalaya, as well as in older orogens like the polar Urals, Norway, USA, and Brazil (Stalder, 1964; Stalder and Touray, 1970; Mullis, 1988, 1996; Niedermayer, 1993). These minerals, usually in large euhedral crystals, occur in fissure veins, crosscutting the metamorphic fabric of the host rocks. Their formation took place after the peak metamorphic conditions and continued during the retrograde paths of orogenic evolution under transpressional, transtensional and finally to post-kinematic extensional conditions, during the late neo-Alpine tectonometamorphic phase of the Alpine evolution (Stalder and Touray, 1970; Mullis, 1988, 1996). Over the last two decades, Greece became a well-established alpinotype mineral province (Niedermayer, 1993; Wendel and Kapelas, 1996; Voudouris et al., 2004), where large, euhedral crystals of alpine-type quartz, are reported from Crete Island, Attica, Evia and Thasos Islands (Voudouris et al., 2004; Voudouris, 2005; Tsolakos et al., 2008; Maneta and Voudouris, 2010). Usually alpinotype fissures are characterized by mineralogical-geochemical zonation, with an external zone consisting of fresh host rock, grading inward to altered rocks, then to a monomineralic massive quartz zone and finaly to so-called alpine fissure that is characterized by very well crystallized minerals (Kandutsch and Wachtler, 2000). The above outward zonation is the result of gradually cooling hydrothermal solutions. The crystals are deposited on the quartz layer and grow with their greatest dimension perpendicular to the empty space of the fissure. The aim of the present study is to describe the mode of occurrence of alpinotype fissure minerals at Thasos Island and to present a

possible genetic model, based predominantly on the mineralogy, mineral chemistry and paragenetic relations.

2. Geology

Thasos Island consists mainly of low to medium grade metamorphic rocks of the Pangeon Unit, which is the lower tectonic unit of the Rhodope metamorphic complex (Brun and Sokoutis, 2007). The main lithological units of Thasos, from base to top, are (Brun and Sokoutis, 2007): (1) a lower unit consisting of marbles with intercalations of paragneisses and micaschists, (2) an intermediate unit consisting of orthogneisses, marbles with some intercalations of paragneisses, mica-schists and numerous amphibolite bodies, (3) an upper unit consisting of migmatites and gneisses. In places, the alpine sequence is unconformably covered by unmetamorphosed Neogene conglomerates. At least three major tectonic phases have affected these lithologies (Brun and Sokoutis, 2007): (a) a compressional phase (pre mid-Eocene), resulted to the thrusting of the gneisses/migmatites and the overlying marbles on top of the lower marble unit; (b) extensional ductile to brittle deformation (from mid-Eocene to mid-Miocene times) resulted to NE– trending st retching lineation, foliated fabric, and widespread boudinage formation; (c) Late Miocene normal faulting is responsible for the development of km-scale tilted blocks of rocks in the SW part of the island.

Alpinotype fissures on Thasos Island are developed in both the lower and intermediate units, and mainly controlled by a major thrust/detachment fault that separates these lithological units. The fissure veins at Thasos are elongate or sigmoidal, usually corresponding to systems of en echelon tensional gashes, and are developed as lens-like bodies perpendicular to the metamorphic rock fabric (Figure 1a to g). Their thickness varies between a few cm and about 2m. Their length ranges between 1 and 5m. An alteration halo surrounds the fissure veins including leached rock, which is then rimmed by the unaltered, fresh rock (Figure 1a). The mineralogy of fissure veins at Thasos is related to the composition of the host rocks: Alpinotype minerals in amphibolite-hosted fissures (Figure 1a to d) include amphibole, albite, adularia, titanite, chlorite, tourmaline, epidote, quartz, biotite, hematite, rutile and zircon. Fissures within spessartine-piemontite schists (Figure 1e) contain quartz, chlorite, spessartine, hematite, rutile, adularia, epidote and traces of zircon. Fissures hosted within Mn-rich calc-silicate layers contain Mn-clinozoisite, Mn-grossular and smoky quartz (Figure 1f). Finally ortho-, paragneiss- and metapegmatite-hosted fissures contain smoky quartz, muscovite, hematite, adularia, ilmenite and rutile (Figure 1g to i).

3. Materials and Methods

Fourty thin sections were studied by optical microscopy. A total of fifteen thin-and-polished sections were studied by scanning slectron microscopy (SEM-EDS) using a Jeol JSM 5600 SEM instrument, equipped with an Oxford ISIS 300 OXFORD system, with the following operating conditions: accelerating voltage 20 kV, beam current 0.5 nA, time of measurement 50 sec and beam diameter 1–2 μm. The spectra were processed using the ZAF program (3interactions). In addition, XRD analyses were carried out using a Siemens (Brooker) 5005 X-ray Diffractometer. Operating conditions were as follows: Cu Ka radiation at 40 kV, 40 nA, 0.020^{o} step size and 1.0 s step time. The XRD patterns were evaluated using the EVA v.10.0 program of the Siemens DIFFRACplus and the D5005 software package. All samples were studied at the laboratories of the Department of Geology and Geoenvironment, University of Athens.

4. Mineralogy and Mineral Chemistry

Quartz is the most abundant mineral in Thasos occuring in a variety of crystal forms and combinations (rock crystal, smoky quartz, prase). The green colour of prase (Figure 1b) is due to chlorite and actinolite inclusions. The color of smoky quartz varies from pale brown, brown-black to dark black. The majority of the quartz crystals show a Tessin habit (Figure 1c). Scepter crystals (several

scepter generations with prismatic habit, Figure 1i) occur as overgrowth on a basal Tessin habit crystal.

Garnet group minerals are found in fissures hosted by spessartite-piemontite schists (Figures 1e and 2a) and by clinozoisite-grossular-rich calc-silicate layers (Figure 1f) Electron microprobe analyses demonstrate that garnets from fissures within the spessartite-piemontite schists are spessartite, with 26.55 to 32.57 wt. % MnO (Table 1, Figure 3a). Pale yellow transparent Mn-rich grossular up to 0.3 cm, were also identified in clinozoisite-grossular fissures crosscutting Mn-rich calc-silicate layers (Figure 1f). They contain up to 3.6 wt. % MnO.

Chlorite is a common constituent in fissures of piemontite-spessartite schists and in amphibolites, where it is associated with quartz, spessartite, albite, adularia, muscovite, rutile, zircon, titanite, epidote, hematite and calcite (Figures 1b, c, e and 2a to e). It forms dark green pseudo-hexagonal crystals up to 3cm. Green quartz from amphibolite-hosted fissures includes wormy chlorite and sylvine crystals (Figure 2d). Chlorite from the spessartite-piemontite schists (rhipidolite and clinochlore) contain more MgO (up to 30.2 wt. %) and MnO (up to 1.4 wt. %) and less FeO (up to 5.4 wt. %) compared to chlorites from the amphibolitic host rocks (clinochlore and pycnochlorite) (Table 1; Figure 3b). Using the chlorite geothermometer of Cathelineau (1988), it is suggested that the chlorites in amphibolite-hosted fissures were formed at temperatures between 315 and 366 °C. The Mn-rich chlorites from the spessartite-piemontite schists were formed at temperatures ranging from 286 to 305 ºC.

Feldspar group minerals are abundant in the alpinotype fissures from Thasos Island Sodium-rich members (e.g. albite and oligoclase) occur in both piemontite-spessartite schists and amphibolites and are absent from the gneisses (Figures 2b, e and 3c). Albite crystals are translucent or milky colored and often twinned. Adularia (hydrothermal variety of K-feldspar), in translucent milky (up to 1 cm) crystals, occurs in all studied fissures. Adularia coexists with hematite, titanite, quartz, chlorite and spessartite, in the fissures of amphibolites and piemontite-spessartite schists (Figures 1d, e and 2 b, d, e). Paragneiss-, orthogneiss- and metapegmatite-hosted fissures contain adularia in association with smoky quartz, sometimes twinned after the Manebach and Baveno laws. Adularia contains up to 0.5 wt. % BaO in the structure (Table 1).

Epidote group minerals occur (a) in fissures hosted in piemontite-spessartite schists (Figure 2a), (b) in amphibolite-hosted fissures together with chlorite forming radial aggregates of idiomorphic green crystals up to 4 cm in size, and (c) pink-red coloured epidote-clinozoisite in fissures hosted by clinozoisite-grossular calc-silicate layers (Figure 1f). Electron microprobe analyses are presented in Table 1 and the results are plotted in Figure 3(d, e). Some epidotes-clinozoisites from the amphibolite-hosted fissures are characterized by relatively high Ce_2O_3, Sc_2O_3 and Cr_2O_3 contents (up to 4.4 wt. %, 1.2 wt. %, and 3.6 wt. % respectively). The fissures in the piemontite-spessartite schists contain epidote with up to 2.3 wt. % Mn_2O_3. The Ce-, Cr- and Sc-rich epidotes have lower percentage of Al (1.8 to 2.0 apfu) compared to all other epidotes (2.2-2.4 Al apfu), due to the substitution of trivalent Al by Ce, Cr and Sc (Table 1; Figure 3d). The pink-red colored epidotes from the clinozoisite-grossular calc-silicate layers have low Mn_2O_3 content (up to 0.56 wt. %; Table 1).

Muscovite is present in minor amounts in amphibolite-hosted fissures (Figure 2b, c). It mainly occurs in gneiss- and metapegmatite-hosted fissures, where it is intergrown with smoky and clear quartz forming pseudohexagonal crystals, up to 2 cm (Figure 1h).

Phlogopite occurs in minor amounts in the amphibolite-hosted fissures. Electron microprobe analyses (Table 1), indicate low TiO_2 probably in accordance to its hydrothermal origin.

Titanite forms olive-green-to yellow transparent crystals up to 0.3 cm. It accompanies adularia, quartz and chlorite in amphibolite-hosted fissures (Figures 1d and 2a, e).

Tourmaline is present in amphibolite-hosted fissures and forms black crystals up to 4 cm length. It is intergrown with chlorite, titanite and quartz.

Hematite iron roses, up to 5 cm in size, occur in amphibolite-hosted fissures (Figure 2c). Hematite is also abundant in piemontite-spessartite schists (Figures 1e and 2b). In gneiss- and metapegmatite-hosted fissures, hematite is intergrown with smoky quartz and adularia.

Rutile needles up to 1 cm in length occur in amphibolite-hosted fissures together with hematite, chlorite and quartz. They are usually enclosed, and/or intergrown with hematite (Figure 2c) considered to be the products of TiO_2 exsolution from previous ilmenite.

Calcite is present as euhedral crystals up to 4 cm in amphibolite-hosted fissures. They are often hydrothermally corroded and accompany chlorite and quartz (Figure 1c).

Amphibole, apatite, zircon, sylvine and **barite** are observed only under the microscope (Figure 2) and are minor fissure minerals at Thasos. Electron microprobe analyses of amphibole are given in Table 1 and the data are plotted in the magnesio-hornblende field of Figure 3f.

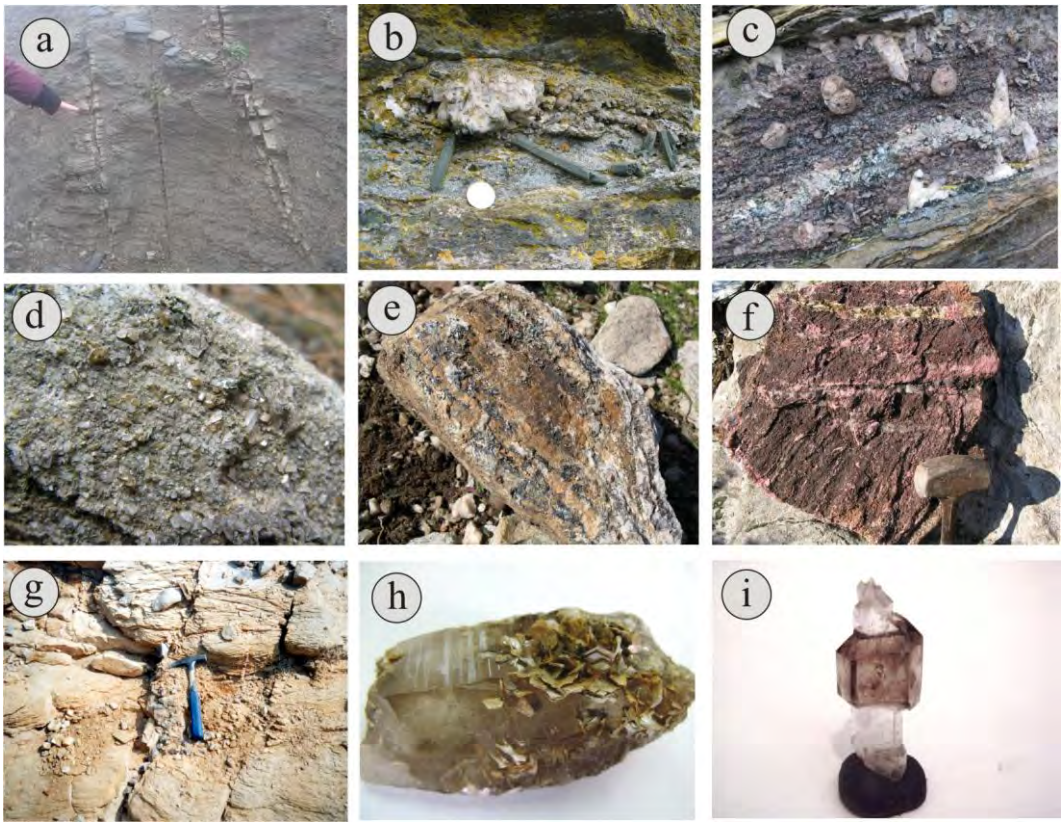

Figure 1 - (a) Amphibolite-hosted fissures with well-formed bleached alteration halo (white area). (b, c) Amphibolite-hosted fissures with euhedral crystals of Tessin habit chloritized quartz, clear quartz, hematite, calcite and chlorite. (d) Titanite and adularia coating the walls of an amphibolite-hosted fissure. (e) Hematite, spessartite, adularia and chlorite coating the wall of fissure of piemontite-spessartite schist. (f) fissures with manganese clinozoisite, quartz and grossular within a Mn-rich calc-silicate layer. (g) Orthogneiss-hosted fissures with smoky quartz. (h) smoky quartz associated with muscovite. (i) Three generations of prismatic quartz scepter.

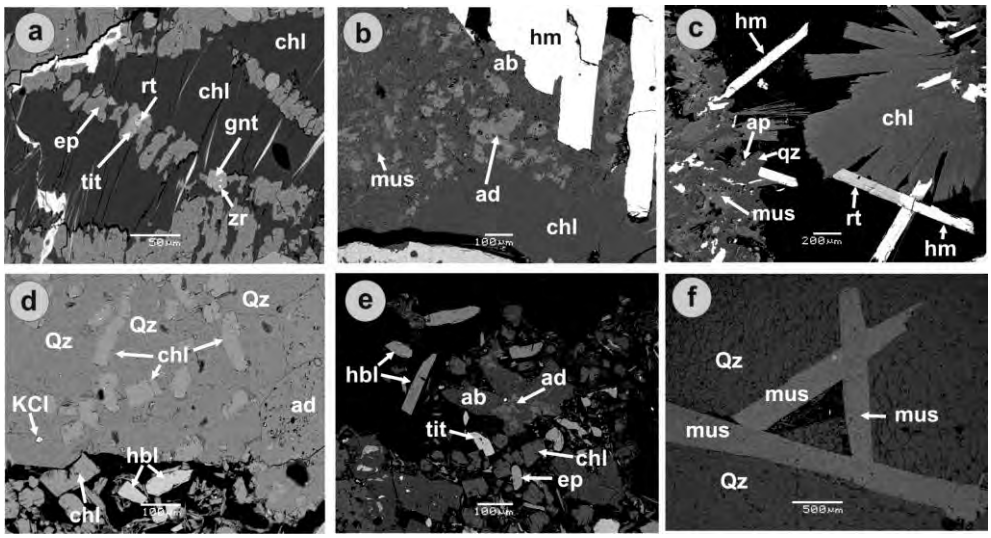

Figure 2 - Photomicrographs demonstrating mineralogical assemblages of alpine fissure content at Thasos (SEM-BSE images). (a,b) Piemontite-spessartite schist-hosted fissures containing chlorite (chl), garnet (gnt), hematite (hm), rutile (rt), albite (ab), adularia (ad), muscovite (mus), epidote (ep). The garnet and epidote crystals contain tiny zircon (zr) inclusions. (c to e) Amphibolite-hosted fissures with chlorite (chl), hematite (hm), epidote (ep), muscovite (mus), albite (ab), titanite (tit), albite (ab), adularia (ad), rutile (rt), quartz (qz), apatite (ap), amphibole (hbl) and sylvine (KCl). (f) Muscovite (mus) included in smoky quartz (qz) from a gneiss-hosted fissure.

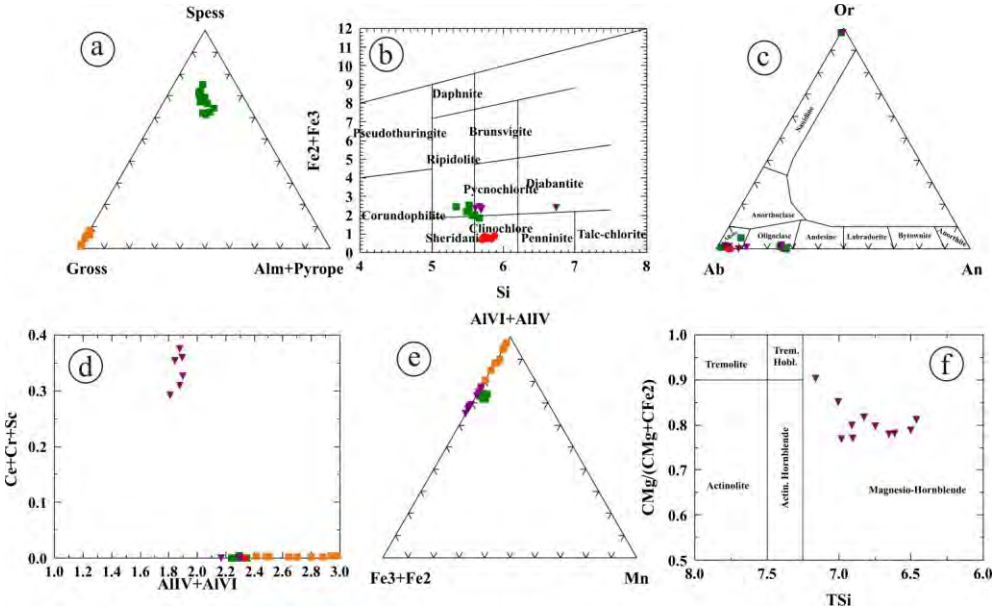

Figure 3 - (a) Compositions of garnet group minerals plotted in the Spess-Gross-(Alm+Pyrope) ternary diagram. (b) Compositions of chlorite plotted in the Si - (Fe^{2+}+Fe^{3+}) discrimination diagram. (c) Analysed feldspars plotted in the Or-Ab-An discrimination diagram. (d,e) Compositions of epidote plotted in the Al - (Ce+Cr+Sc) and Al – (Fe^{3+}+Fe^{2+}) - Mn and (f) Composition of hornblende. (Green squares = piemontite-spessartite quartzite, red bullets and purple triangles = metabasite, orange squares = Mn-rich calc-silicate layers).

Table 1 - Representative electron microprobe data of Chlorite (1-3), Muscovite (4), Phlogopite (5), Piemontite (6,7), Mn-clinozoisite, REE-rich Epidote (10,11), Albite (12), Adularia (13,14), Oligoclase (15), Hornblende (16,17), Spessartite (18,19), Mn-grossular (20,21) (*: iron as Fe_2O_3), (*manganese as Mn_2O_3).

Wt%	1	2	3	4	5	6	7	8	9	10	11	12	13	14	15	16	17	18	19	20	21
SiO_2	26.61	29.66	30.05	42.57	38.12	38.66	37.43	38.73	39.31	38.29	36.72	67.69	63.51	64.56	62.57	45.06	47.54	36.47	37.79	39.70	40.77
Al_2O_3	22.88	20.78	20.89	29.6	16.14	24.35	24.15	26.37	27.21	18.85	18.29	20.51	18.77	17.95	23.03	10.61	9.65	21.73	20.69	22.46	23.72
MgO	22.4	28.65	28.43	1.61	15.24	bd	bd	bd	bD	0.13	0.32	bd	bd	bd	bd	14.19	14.72	2.42	1.51	bd	0.01
FeO	14.68	5.07	4.49	2.59	12.04	*11.21	*11.27	*9.37	8.57	*12.32	*12.72	bd	bd	0.18	0.24	14.18	12.8	5.71	2.35	0.97	0.67
MnO	0.18	1.01	1.29	0.16	0.17	*1.41	*2.34	*0.56	0.34	bd	bd	bd	bd	bd	0.19	0.15	0.3	26.75	32.57	3.60	1.88
CaO	bd	0.04	0.04	bd	0.78	22.09	21.56	23.19	23.00	19.13	19.29	0.31	0.01	0.19	4.97	11.79	11.75	5.87	4.51	33.08	34.08
K_2O	bd	bd	bd	8.35	5.37	bd	0.20	bd	bd	0.05	0.01	0.1	15.57	16.25	0.27	0.4	0.34	bd	bd	bd	bd
Na_2O	bd	bd	bd	0.73	bd	bd	Bd	bd	bd	bd	0.01	10.61	0.19	0.11	8.04	1.3	1.03	bd	bd	0.31	0.13
TiO_2	0.04	0.02	bd	0.6	1.9	0.15	0.28	0.01	0.11	bd	bd	bd	bd	bd	bd	0.4	0.57	bd	0.4	bd	bd
Cr_2O_3	bd	0.07	bd	bd	bd	0.03	Bd	bd	bd	3.31	3.61	bd	bd	bd	bd	0.27	0.06	0.18	bd	bd	bd
V_2O_5	bd	0.08	bd	bd	bd	bd	bd	bd	bd	bd	bd	bd	bd	bd	bd	bd	bd	0.05	0.11	bd	bd
BaO	bd	bd	bd	bd	bd	bd	bd	bd	bd	bd	bd	0.14	0.53	bd	bd	bd	bd	bd	bd	bd	bd
Sc_2O_3	bd	bd	bd	bd	bd	bd	bd	bd	bd	1.1	0.79	bd	bd	bd	bd	bd	bd	bd	bd	bd	bd
Ce_2O_3	bd	bd	bd	bd	bd	bd	bd	bd	bd	2.96	4.41	bd	bd	bd	bd	bd	bd	bd	bd	bd	bd
Total	86.79	85.38	85.19	86.21	89.76	97.90	97.23	98.32	98.63	96.14	96.18	99.37	98.58	99.24	99.32	98.35	98.76	99.18	99.93	100.12	100.89
	28(O)	28(O)	28(O)	22(O)	22(O)	12.5(O)	12.5(O)	12.5(O)	12.5(O)	12.5(O)	12.5(O)	8(O)	8(O)	8(O)	8(O)	23(O)	23(O)	24(O)	24(O)	24(O)	24(O)
Si	5.34	5.76	5.84	6.23	5.61	3.12	3.08	3.07	3.10	3.15	3.06	2.97	2.98	3.01	2.8	6.44	6.67	5.88	6.07	5.98	6.05
Al	5.42	4.76	4.78	5.1	2.79	2.31	2.34	2.26	2.53	1.83	1.79	1.06	1.04	0.99	1.21	1.8	1.61	4.13	3.91	3.98	4.07
Mg	6.7	8.3	8.22	0.37	3.34	0.00	0.00	0.00	0.00	0.00	0.04	0.00	0.00	0.00	0.00	3.03	3.11	0.58	0.36	0.00	0.000
Fe	2.46	0.82	0.72	0.33	1.47	0.76	0.78	0.63	0.56	0.81	0.85	0.00	0.00	0.00	0.00	1.53	1.34	0.77	0.31	0.12	0.09
Mn	0.00	0.16	0.22	0.00	0.00	0.09	0.14	0.04	0.02	0.00	0.00	0.00	0.00	0.00	0.00	0.00	0.00	3.65	4.42	0.46	0.24
Ca	0.00	0.00	0.00	0.00	0.11	1.91	1.90	1.97	1.94	1.69	1.73	0.01	0.00	0.00	0.24	1.8	1.76	1.01	0.77	5.35	5.42
Na	0.00	0.00	0.00	0.22	0.00	0.00	0.00	0.00	0.00	0.00	0.00	0.9	0.02	0.00	0.69	0.35	0.27	0.00	0.00	0.09	0.03
K	0.00	0.00	0.00	1.54	0.99	0.00	0.00	0.00	0.00	0.00	0.00	0.00	0.93	0.97	-	0.08	0.08	0.00	0.00	0.00	0.00
Ti	0.00	0.00	0.00	0.07	0.22	0.00	0.00	0.00	0.00	0.00	0.00	0.00	0.00	0.00	0.00	0.00	0.08	0.00	0.05	0.00	0.00
Cr	0.00	0.00	0.00	0.00	0.00	0.00	0.00	0.00	0.00	0.21	0.23	0.00	0.00	0.00	0.00	0.00	0.00	0.00	0.00	0.00	0.00
Sc	0.00	0.00	0.00	0.00	0.00	0.00	0.00	0.00	0.00	0.08	0.06	0.00	0.00	0.00	0.00	0.00	0.00	0.00	0.00	0.00	0.00
Ce	0.00	0.00	0.00	0.00	0.00	0.00	0.00	0.00	0.00	0.08	0.13	0.00	0.00	0.00	0.00	0.00	0.00	0.00	0.00	0.00	0.00

5. Discussion

Previous work on alpinotype fissure vein mineralization suggest that their formation started after the peak metamorphic conditions and is mainly related to retrograde evolution from fluid circulation during the final stages of continental collision (Mullis et al., 1994). In Thasos Island, the formation of alpinotype fissures is closely related to the exhumation of the Southern Rhodope Metamorphic Core Complex during the Oligocene-Miocene (Brun and Sokoutis, 2007). At Thasos the mineralized extensional fissures occur close to the thrust fault separating the lower from the intermediate units and are probably related to a reactivation of this fault as a low-angle detachment during the exhumation stage (Brun and Sokoutis, 2007).

The presence of various forms of quartz, even in the same fissure, indicates several stages of deposition under fluctuating hydrothermal conditions. Changes in pressure, temperature and fluid composition, may have caused the variation in the observed mineralogical assemblages. Following initial deposition of Tessin-habit quartz crystals, later inputs of hydrothermal fluids in the fissures, resulted in partial dissolution of Tessin-habit crystals (under formation of skeletal quartz), overgrowths of scepter crystals, and/or intergrowth with several minerals as for example chlorite, muscovite, etc. The wallrock alteration halo surrounding the alpinotype fissures, suggest hydothermal leaching of chemical components from the host rocks and their contribution within the fissures, as already proposed by Niedermayer (1993).

The minerals within the alpinotype fissures of Thasos were probably started to form at temperatures between about 370 ° and 290 °C, as indicated by the geothermometry of chlorite associated with Tessin-habit quartz. Fluid inclusion data are not yet available for Thasos quartz, but the above temperatures are quite close to those obtained from fluid inclusion data of similar Tessin-habit smoky quartz at the neighboring Dassoto, Drama area (T_h between 300 and 380 ºC; Melfos and Voudouris, 2006). This temperarute range also fits very well to crystallization temperatures from Tessin-habit quartz from the Kavala, intrusion-related Bi-Te-Au deposit (Fornadel et al., 2011).

It has been suggested by Stalder and Touray (1970), Mullis (1975) and Mullis et al. (1994, 2001) that Tessin-habit quartz in the Alps can only be formed under high fCO_2 values of the hyodrothermal solutions. This is in accordance with available data from Dassoto and Kavala, where CO_2 bearing fluid inclusions occur in the Tessin-habit crystals (Melfos and Voudouris, 2006; Melfos et al., 2008; Fornadel et al., 2011). CO_2-bearing fluid must have prevailed during crystallization of Tessin-habit quartz in Thasos island and this should have taken place in the transition from a compressional to an extensional tectonic regime, as is the case in the central Alps (Heijboer, 2006; Heijboer et al., 2003). Late incursion of meteoric and/or seawater at depth may have caused the crystallization of the prismatic-habit quartz scepters at lower temperatures from NaCl- and KCl-bearing hydrothermal fluids (as suggested by Mullis et al., 1994).

Thasos Island (and Dassoto area of Drama) is to our knowledge a unique case among the Alpine fissure occurrences in Europe, where two types of quartz crystals (with both prismatic and Tessin-habit) coexist in the same fissure. Usually in the Alps these two types of quartz crystals occur in different fissures, as a result of deposition under different stress fields (Heijboer, 2006; Heijboer et al., 2003). The common characteristics of Alpinotype fissure quartz in Northern Greece (Dasoto, Thasos and Kavala) suggest common tectonometamorphic evolution during the exhumation of Southern Rhodope Core Complex. Future fluid inclusion, isotopic and geochronological studies will help better understand the genetic implications of alpinotype fissure minerals in Thasos Island and the broad Rhodope complex. Some fissure minerals on Thasos can be considered as gemstones. Alternatively the areas hosting alpinotype fissures should be considered as a Geotope and protected by integrating in a mineralogical Geopark under promotion of sustainable development in the area.

6. References

Brun J.P. and Sokoutis D. 2007. Kinematics of the Southern Rhodope Core Compex (North Greece), *Int. J. Earth Sci*., 96, 1079-1099.

Cathlelineau M. 1988. Cation size occupancy in chlorites and illites as a function of temperature, *Clay Minerals*, 23, 471-485.

Fornadel A.P., Spry P.G., Melfos V., Vavelidis M. and Voudouris P. 2011. The Palea Kavala Bi-Te-Sb±Au district: a reduced intrusion-related system, northeastern Greece, *Ore Geology Reviews*, 39, 119-133.

Heijboer T.C. 2006. Origin and pathways of pro- and retrograde fluids, PTt paths and fluid-mineral equilibria from Alpine veins of the Central Alps: Case studies of the Fibbia and Amsteg area, *Unpubl. PhD thesis*, University Basel, 173 pp.

Heijboer T.C., Mullis J. and de Capitani C. 2003. Prograde and retrograde fluid evolution and vein mineralization from tha southern Gotthard Massif, Switzerland, *EGS-AGU-EUG*, 6-11 April 2003, Abstract 4946.

Kandutsch G. and Wachtler M. 2000. Die Kristallsucher-Ein Gang durch die Jahrmillionen, Band 2, Christian Weise Verlag Munchen, 160 pp.

Koenigsberger J.G. 1972. *Die zentralalpinen Minerallagerstaetten*, Basel, 351 pp.

Maneta V. and Voudouris P. 2010 Quartz megacrysts in Greece: Mineralogy and environment of formation, *Bull. Geol. Soc. Greece*, XLIII, 685-696

Melfos V. and Voudouris P. 2006. Fluid inclusions and O-isotopes of an amethyst and smoky quartz occurrence in Kato Nevrokopi, Rhodope massif, Northern Greece, *11th Int. Conf. Experimental Mineralogy, Petrology and Geochemistry*, Abstract 50.

Melfos V., Voudouris P., Vavelidis M. and Spry P. 2008. Microthermometricresults and formation conditions of a new intrusion-related Bi-Te-Pb-Sb±Au deposit in the Kavala pluton, Greece, *Proc. XIII Inter. Con. Thermobarogeochemistry*, 2, 165-168.

Mullis J. 1975. Growth conditions of quartz crystals from Val d'Illiez (Valais, Switzerland), *Schweiz. Miner. Petr. Mitt.*, 55/3, 419-430.

Mullis J. 1988. Rapid subsidence and upthrusting in the northern Apennines deduced by fluid inclusion studies in the quartz crystals from Porreta Terme, *Schweiz. Miner. Petr. Mitt.*, 68, 157-170.

Mullis J. 1996. P-T-t path of quartz formation in extensional veins of the central Alps, *Schweiz. Miner. Petr. Mitt.*, 76, 159-164.

Mullis J., Dubessy J., Poty B. and O'Neil J. 1994. Fluid regimes during late stages of a continental collision: physical, chemical and stable isotope measurements of fluid inclusions in fissure quartz from a geotraverse through the Central Alps, Switzerland, *Geochim. Cosmochim. Acta*, 58, 2239-2267.

Mullis J., Vennemann T. and O'Neil J. 2001. Deep percolating meteoric waters in the central Alps, *EUG XI*, Strasbourg, Abstract, 6(1), 279.

Niedermayer G. 1993. Alpine Kluefte, *Mineralien Welt*, 6, 57-59.

Stalder H.A. 1964. Petrographische und mineralogische Untersuchungen im Grimselgebiet (Mittleres Aarmassiv), *Schweiz. Miner. Petr. Mitt*., 44/1, 187-398.

Stalder H.A. and Touray J.C. 1970. Fensterquarze mit Methan-Einschlüssen aus dem westlichen Teil der schweizerischen Kalkalpen, *Schweiz. Miner. Petr. Mitt*., 50/1, 109-130.

Tsolakos A., Voudouris P. and Papanikitas A. 2008. Kristallklüfte in Attika und auf Euböa. Bergkristall, Amethyst und Rauchquarz aus Griechenland, *Lapis*, 5, 36-39.

Voudouris P. 2005. Minerals of Eastern Macedonia and Western Thrace: Geological framework and environment of formation, *Bull. Geol. Soc. Greece*, 37, 62-77.

Voudouris P., Katerinopoulos A. and Melfos V. 2004. Alpine-type fissure minerals in Greece, *Documenta Naturae*, 151, 23-45.

Wendel W. and Kapelas Ch. 1997. Alpine smoky quartz from Attica, *Lapis*, 22/3, 35-37.

Δελτίο της Ελληνικής Γεωλογικής Εταιρίας, τομ. XLVII , 2013
Πρακτικά 13ου Διεθνούς Συνεδρίου, Χανιά, Σεπτ. 2013

Bulletin of the Geological Society of Greece, vol. XLVII 2013
Proceedings of the 13th International Congress, Chania, Sept. 2013

AMETHYST OCCURRENCES IN TERTIARY VOLCANIC ROCKS OF GREECE: MINERALOGICAL AND GENETIC IMPLICATIONS

Voudouris P.[1], Psimis I.[2], Mavrogonatos C.[1], Kanellopoulos C.[1], Kati M.[1] and Chlekou E.

[1]National and Kapodistrian University of Athens, Faculty of Geology and Geoenvironment, Department of Mineralogy and Petrology, voudouris@geol.uoa.gr, kmavrogon@geol.uoa.gr, ckanellopoulos@gmail.com, *kati@geol.uoa.gr,*

[2] Maccaferri Hellas Ltd, Athens, giannis.psimis@gmail.com

Abstract

Epithermal-altered volcanic rocks in Greece host gem-quality amethyst veins in association with various silicates, carbonates, oxides, sulfides and halides. Host rocks are Oligocene to recent calc-alkaline to shoshonitic lavas and pyroclastics of intermediate- to acid composition. The amethyst-bearing veins occur in the periphery of porphyry-type and/or high-sulfidation epithermal mineralized centers in northern Greece (e.g. Sapes, Kirki, Kornofolia/Soufli, Lesvos island) and on Milos island in the active Aegean Volcanic Arc. Hydrothermal alteration around the quartz veins includes sericitic, K-feldspar (adularia), argillic, propylitic and zeolitic types. Precipitation of amethyst in the northern Greece occurrences, took place during the final stages of the magmatic-hydrothermal activity from near-neutral to alkaline fluids, as indicated by the presence of gangue adularia, calcite, smectite, chlorite, sericite, pyrite, zeolites (laumontite, heulandite, clinoptilolite), analcime and minor amounts of barite, halite, epidote and fluorite in the quartz veins. Amethyst at Milos Island (Chondro Vouno and Kalogries-Vani areas), is accompanied by barite, smectite and lepidocrocite. Colloform-crustiform banding with alternations of amethyst, chalcedony and/or carbonates is a common characteristic of the studied amethyst-bearing veins. Fluid inclusion- and mineralogical data suggest that the studied amethyst were formed at: 174-246 °C (Sapes area), 100-175 °C (Kirki and Kornofolia areas) and 223-234°C (Lesvos island). The amethyst formation requires oxidizing conditions and is probably the result of mixing between meteoric or seawater with upwelling hydrothermal fluids. The involvement of seawater in the studied mineralization is supported by the presence of halite and abundant barite in the veins. Finally, the studied amethyst deposits should be evaluated as potential gemstone sources in Greece.
Key words: *amethyst, volcanic rock, hydrothermal alterations, gemstones.*

Περίληψη

Ηφαιστειακά πετρώματα της Ελλάδας, που καλύπτουν ένα εύρος ηλικιών από το Ολιγόκαινο έως σήμερα, φιλοξενούν εμφανίσεις αμέθυστου. Τα ηφαιστειακά αυτά πετρώματα αποτελούνται από ασβεσταλκαλικές-σοσονιτικές λάβες και πυροκλαστίτες όξινης έως ενδιάμεσης σύστασης. Οι αμέθυστοι, εμφανίζονται σε φλέβες που

αναπτύσσονται στην περιφέρεια μεταλλοφοριών πορφυρικού ή/και υψηλής-θείωσης επιθερμικού τύπου, όπως στις περιοχές Κίρκη, Σάπες, Κορνοφωλιά/Σουφλί και Λέσβο. Επίσης, αμέθυστοι έχουν εντοπιστεί και στη Μήλο, που ανήκει στο σύγχρονο ηφαιστειακό τόξο του Αιγαίου. Οι αμεθυστούχες φλέβες συνοδεύονται από υδροθερμικές εξαλλοιώσεις διαφόρων τύπων όπως σερικιτική, Κ-ούχος, αργιλλική, προπυλιτική και ζεολιθική. Η κρυστάλλωση των αμέθυστων πραγματοποιήθηκε κατά τα τελευταία στάδια της μαγματικής-υδροθερμικής δραστηριότητας, από ουδέτερα έως αλκαλικά ρευστά, όπως υποδεικνύουν τα συνοδά ορυκτά που περιλαμβάνουν αδουλάριο, ασβεστίτη, σμεκτίτη, σερικίτη, χλωρίτη, σιδηροπυρίτη, ζεόλιθους και πιο σπάνια βαρίτη, αλίτη, επίδοτο και φθορίτη. Συνήθεις μορφές εμφάνισης περιλαμβάνουν κολλοειδείς και ζωνώδεις δομές σε εναλλαγές με χαλκηδόνιο η/και ανθρακικά ορυκτά. Μελέτες ρευστών εγκλεισμάτων και ορυκτολογικών παραγενέσεων, υποδεικνύουν θερμοκρασίες σχηματισμού μεταξύ 174-246°C (Σάπες), 100-175°C (Κίρκη-Κορνοφωλιά) και 223-234°C (Λέσβος), κάτω από οξειδωτικές συνθήκες. Παρατηρείται μίξη μετεωρικού ή θαλασσινού νερού (όπως υποδηλώνει η παρουσία αλίτη και βαρύτη) με ανερχόμενα υδροθερμικά ρευστά. Είναι σημαντικό να αξιολογηθεί το δυναμικό των παραπάνω εμφανίσεων αμέθυστου, για πιθανή χρήση τους ως πολύτιμοι λίθοι.
Λέξεις κλειδιά: *αμέθυστος, εξαλλοιώσεις ηφαιστειακών πετρωμάτων, πολύτιμοι λίθοι.*

1. Introduction

Amethyst is a quartz variety often used in jewellery and occurs in varying shades of violet colors (Lieber, 1994). Its name comes from the ancient Greek words "*a*" (not) and "*methustos*" (intoxicated), a reference to the belief that the stone protected its owner from drunkenness. The colors of amethyst range from light pinkish to dark mauve/blue and are due to irradiation, iron impurities (in some cases in conjunction with transition element impurities), and the presence of trace elements, which result in complex crystal lattice substitutions. Amethyst was firstly used as a gemstone by the ancient Egyptians. Later, the ancient Greeks and Romans wore amethyst and made drinking vessels of it, in the belief that it would prevent them from intoxication, while medieval European soldiers wore amethyst amulets as protection in battle believing that amethysts heal people and keep them cool-headed. Nowadays, amethysts are used very often in jewellery, in spite of its relatively low price, which came as a result of the discovery of huge amethyst deposits, mainly in South America (Brazil) and elsewhere. Brazil is the main amethyst producer today, counting more than ten very important deposits. Other amethyst producing countries are Mexico, Uruguay, South Korea, Russia, Zambia and India, but the best varieties of amethysts come from Siberia and Sri Lanka. Amethyst is also found in several other minor localities worldwide, mainly associated to volcanic rocks. Amethyst can be formed in igneous, metamorphic and sedimentary rocks as well as in hydrothermal veins, metasomatic and hot spring deposits. Well-formed crystals occur filling druses in various igneous rocks, such as granites, in gneisses or volcanic rocks, mainly lavas. In metamorphic rocks, amethyst is a quite common mineral in the so-called alpine-type fissures. Greece includes several areas with major and minor occurrences of amethyst deposits (Voudouris and Katerinopoulos, 2004; Voudouris et al., 2004; Melfos, 2005; Maneta and Voudouris, 2010). These deposits are associated with magmatic-hydrothermal (e.g. skarns, volcanic rocks) and metamorphic environments of various ages. This study focuses on five amethyst deposits which are related to the Tertiary volcanic rocks of Greece. Three amethyst-bearing areas are located at Northern Greece (Sapes, Kirki, Kornofolia), while the rest two occur in Lesvos and Milos islands in the Aegean Sea. Host rocks for the studied amethyst occurrences are lavas and pyroclastics of calc-alkaline to shoshonitic composition and Oligocene to Pleistocene age. This work presents results on the local geology, mineralogy and the depositional environment of the five studied amethyst deposits.

2. Regional Geology

In the Aegean region, continuous subduction of both oceanic and continental lithosphere beneath the Eurasian plate since Early Cretaceous resulted to a series of magmatic arcs from the north (Rhodope massif) to the south (Active South Aegean Volcanic Arc) (Jolivet and Brun, 2010). The progressive southward migration of the magmatic centers from the Oligocene magmatic belts in the Rhodope massif, through the Miocene Aegean Islands (e.g. Limnos, Lesvos Island) to the Active South Aegean Volcanic Islands (e.g. Milos, Nisyros, Santorini) has been attributed to slab rollback following the continent-continent collision (Fytikas et al., 1984). In the Rhodope Massif, Late Cretaceous-Tertiary exhumation of metamorphic rocks along detachment faults resulted in the formation of metamorphic core complexes, post-collisional extensional collapse, and Late Eocene to Early Miocene calc-alcaline, high-K alkaline and shoshonitic magmatism (Innocenti et al., 1984; Christofides et al., 2004; Marchev et al., 2005). Geochemical data suggest that the Oligocene to Miocene plutonic rocks in Northern Greece (Rhodopes and Lesvos Island), are derived from sub-continental lithospheric mantle and/or the lower crust, with a minimal contribution from the crust (Pe-Piper and Piper, 2002). In addition, slab break-off and/or slab delamination were the principal mechanism for the generation of extensive post-collisional Oligocene magmatism in the broad Rhodope-Limnos area (Pe-Piper and Piper, 2002). On Lesvos Island, thick successions of early Miocene calc-alkaline to shoshonitic lavas and pyroclastics and basic to acid composition occupy large parts of the island (Pe-Piper and Piper, 2002). On Milos Island, calc-alkaline volcanic activity spans a period from ~3.5 Ma to the present and originated from several emergent eruptive centers characterized by both explosive and effusive activity (Fytikas et al., 1986; Stewart and McPhie, 2006; Alfieris et al., 2013). All amethyst-bearing areas are host of porphyry- and/or epithermal style of mineralization. They are characterized by intense hydrothermal alteration of the volcanic rocks, among them silicification which is closely related to the formation of amethyst-bearing quartz veins.

3. Local Geology

3.1. Northeastern Greece (Sapes, Kirki and Kornofolia)

The presence of amethyst in Sapes area has already been described by Voudouris (1993). Host rocks are hydrothermally altered lavas and pyroclastics of the Sapes stratovolcano. Amethyst occurs within colloform and crustiform banded epithermal quartz-chalcedony veins crosscutting mostly sericitic- and K-feldspar (adularia) altered volcanic rocks (Figure 1a). The amethyst veins are often accompanied by gangue adularia (Figure 2a). Amethyst-bearing veins also crosscut advanced argillic-altered volcanic rocks, resulting in an obliteration of adularia and replacement by aluni within the veins. Massive deep-violet amethyst veins occur within the "Silver Hill" formation, which is a phreatomagmatic conglomerate, probably within Maar-diatreme (Shawh and Constantinides, 2001). Amethyst in the "Silver Hill" formation, also form idiomorphic prismatic crystals (up to 3cm in length), sometimes developed atop a lower part composed of smoky quartz.

In Kirki area unaltered-to-propylitized lavas of dacitic composition and Early Oligocene age are the host rocks of chalcedony-amethyst bearing veins (Figure 1b). The veins are related to NNW-trending fault zones crosscutting the dacitic rock. Open spaces within the veins are filled by up to 1cm long amethyst crystals and/or milky quartz. Zeolites (analcime, heulandite, chabazite) predate (Figure 2b), whereas calcite postdates the deposition of the amethyst. Calcite has a platy habit, an indication of deposition by boiling hydrothermal fluids (according to Simmons and Browne, 2001).

Similarly to Kirki area, the amethyst in Kornofolia is hosted within unaltered to propylitized lavas of dacitic composition (Figure 1c). The quartz veins are banded with an external layer of chalcedony and inner open spaces filled by idiomorphic prismatic amethyst crystals. In some veins amethyst is missing and vugs are filled by botryoidal or stalactitic chalcedony with light pinkish

colors. Smectite, zeolites and calcite are present as accessory minerals both within the veins and in the wall rocks (Figure 2c).

3.2. Lesvos Island

Amethyst in Lesvos is related to N-trending epithermal quartz veins and associated fault zones that crosscut propylitic- or sericitic altered lavas in the northern part of the Island. The veins are banded and brecciated and consist of quartz, carbonate and fluorite with minor chlorite or sericite. Idiomorphic amethyst crystals up to 10cm in length mostly occur in the centers of the veins (Figure 1d). Sceptered and window amethyst (Figure 1e, f) is common and their habit (Muzo-type) resembles amethysts from Mexico (Voudouris and Katerinopoulos, 2004; Maneta and Voudouris, 2010).

Figure 1 - Fieldphotos and hand specimens of volcanic-hosted amethyst in Greece. (a) alternations of dark violet amethyst with chalcedony from Sapes area; (b) veinlets of amethyst and calcite crosscutting propylitic lavas in Kirki area; (c) amethyst crystals overgrown on chaclcedony within a cavity of dacite, Kornofolia area (field of view 10cm); (d) amethyst crystals and calcite in a cavity of propylitic andesite lavas, Lesvos island (photo is from Voudouris and Katerinopoulos, 2004); (e,f) Scepter and window habits of prismatic amethyst from Lesvos island; (f) Short prismatic violet amethyst crystals from Milos island (field of view 10cm).

3.3. Milos Island

On Milos Island, amethyst is present in two localities namely the Chondo Vouno and the Vani area. In both areas amethyst is found within banded quartz-chalcedony barite veins crosscutting sericitic- and adularia altered pyroclastics (Chondro Vouno) and propylitic lavas of dacitic composition (Vani). The veins display typical epithermal features (colloform-crustiform banding) and reach thickness of up to 2 m and length of several tens of meters. Similarly to the Kirki and Kornofolia areas, chalcedonic quartz is deposited first in the veins and is followed by the formation of amethyst crystals in the vein centers (Figure 1g). Amethyst in Vani area is overgrown by late botryoidal aragonite. Radial aggregates of lepidocrocite included in amethyst, and related to various colourations ranging from light pink to dark violet.

4. Materials and Methods

Thirty-five thin and ten thin-and-polished sections of amethyst-bearing veins and host rocks were studied respectively by optical and a JEOL JSM 5600 scanning electron microscope, equipped with back-scattered imaging capabilities, at the Department of Mineralogy and Petrology, University of Athens. The operating conditions were: accelerating voltage 20 kV, beam current 0.5 nA, time of measurement 60 sec and beam diameter 1-2 μm. The spectra were processed using the ZAF program (3 interactions).

5. Mineralogy and Mineral Chemistry

A detailed mineralogical and mineral chemical study of the amethyst-bearing material revealed various mineralogical association suggestive specific conditions of crystallization. The most abundant minerals in all assemblages are quartz and chalcedony, while carbonates, barite, zeolites, chlorite, adularia, sericite, pyrite and in minor amounts halite, goethite and lepidocrocite are present (Figure 2). Electron microprobe analyses are presented in Table 1 and the data are ploted in binary and ternary diagrams (Figure 3).

5.1. Adularia

Adularia is a common constituent in the Sapes amethyst deposit. Along with quartz, adularia usually replaces plagioclase, clinopyroxene and amphibole of the host rock, which is a silicified dacite-andesite. Adularia forms idiomorhic rhombohedral crystals (Figure 2a), overgrowing amethyst crystals, or can be present as tiny inclusions in chalcedony and amethystine quartz. EPMA data, revealed a stoichiometric composition for the adularia from Sapes area, with some Ba up to 0.69 wt%, corresponding to 0.01 apfu, substituting for K (which ranges from 0.97-1.01 apfu). A small percentage of Na_2O (0.20-0.32 wt %), corresponding to 0.02 apfu, also substitutes for K (Table 1).

5.2. Zeolites

Zeolites are significant accessory minerals in both Kornofolia and Kirki amethyst deposits. Clinoptilolite-Ca and heulandite-Ba (Kornofolia) and analcime (Kirki) usually form euhedral crystals that fill both quartz- and carbonate-rich veins. Deposition in the Kirki veins starts with alternations between analcime and calcite layers, followed by chalcedony and finally by amethyst, which forms short prismatic crystals in the center of the veins (Figure 2b). In the Kornofolia locality a chalcedony layer overgrowths zeolitized wallrocks, and is succeeded by deposition of amethyst, and then by clinoptilolite-Ca and finally calcite (Figure 2c). Heulandite-Ba (Coombs et al., 1998; Larsen et al., 2005) forms euhedral crystals present as inclusions in clinoptilolite-Ca. Electron microprobe analyses revealed that clinoptilolite has an almost stoichiometric composition, with relatively elevated contents of Ca and K corresponding up to 2.16 and 1.35 apfu respectively. The analyzed heulandites revealed variable cation contents with K (up to 2.7 apfu) substituting for Na and relatively high Ba contents (BaO up to 15.97 wt. %), corresponding up to 3.24 apfu. Chemical analyses of analcime from both Kirki and Kornofolia amethyst deposits, revealed stoichiometric compositions, with a stable (K+Na)/(K+Na+Ca) ratio close to 1, whereas the Si/Al ratio shows a small variance between 2-2.4 (Figure 3a,b).

5.3. Chlorite

Chlorite is a common alteration mineral of the volcanic rocks hosting amethyst-bearing veins at Lesvos island. In this locality the propylitic altered lavas contain pyroxene and hornblende phenocrysts pseudomorph after chlorite, calcite and sericite. The later minerals also occur within the amethyst veins. Electron microprobe analyses of chlorite are presented in Table 1 and the data are ploted in terms of Fe_{tot} vs Si (Figure 3d). The Lesvos chlorites are classified as pycnoclorites and diabantites (Figure 3d).

5.4. Sericite

Sericite together with chlorite replaces plagioclase, amphibole and clinopyroxene of the propylitic andesites, in the Lesvos amethyst deposit. It is also present as part of the sericitic alteration zones surrounding amethyst-bearing veins in Sapes area. Electron microprobe analyses revealed minor amounts of Mg, Fe, Na, Ca, Sr and Ti in the structural formula (Table 1).

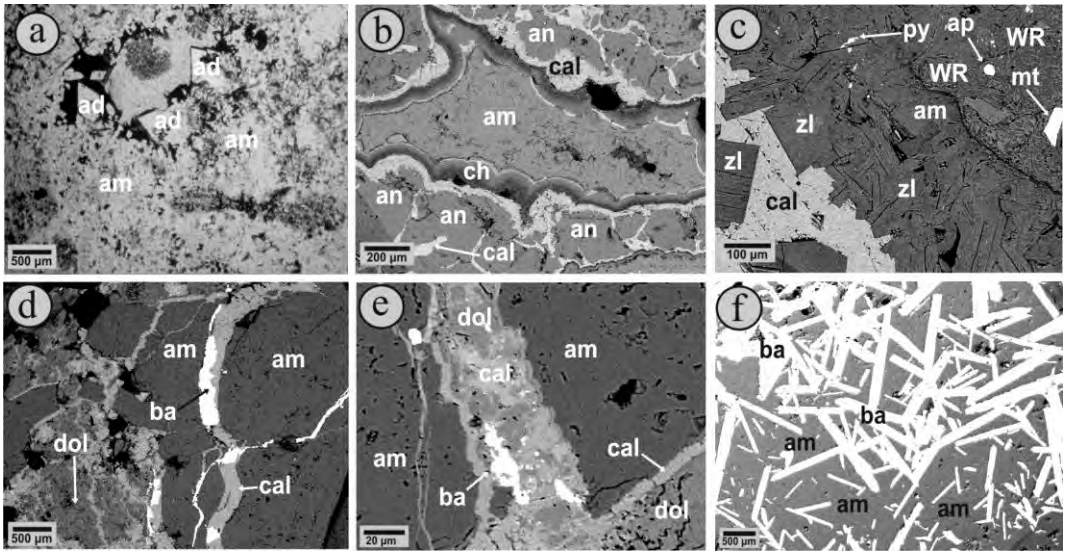

Figure 2 - Microphotographs demonstrating mineralogical assemblages of amethyst-bearing veins (a) adularia (ad) in association with amethyst (am) from Sapes area (reflected light, plane polarized); (b) cavity filled with analcime (an), then calcite (cal), which is rimmed by chalcedony (ch) with final deposition of amethyst (am), Kirki area (SEM-BSE image); (c) clinoptilolite-Ca (zl) and calcite (cal) that overgrow amethystine quartz (am) are filling cavities of dacitic lavas characterized by plagioclase (pl) and disseminated crystals of apatite (ap) and magnetite (mt), Kornofolia area (SEM-BSE image); (d,e) amethyst (am) is rimmed or crosscut by calcite (cal), dolomite (dol) and barite (bar), Lesvos island (SEM-BSE images); (i) intergrowth of barite (bar) and amethyst (am) at Milos island (SEM-BSE image) .

5.5. Calcite – Dolomite

Carbonate minerals, mainly calcite and less commonly dolomite-calcite solid solution, accompany amethyst at Kirki, Kornofolia and Lesvos Island (Figure 3c). Dolomite is absent at Kirki, Kornofolia and the amethyst pre- and/or postdates calcite in vein cavities (Figure 2b, c). In Lesvos Island, amethyst crystals are overgrown and crosscut by calcite-dolomite solid solution and calcite. Initial deposition of calcite-dolomite solid solution was followed by deposition of calcite and barite (Figure 2d, e). Electron microprobe analyses indicated up to 18.6 wt. % MgO and 4.6 wt. % FeO substituting for Ca. Minor amounts of Mn (MnO up to 1.05 wt %) and Sr (SrO up to 0.28 wt %), are detected in calcite from Lesvos.

5.6. Barite

Barite is very abundant in Milos amethyst deposits and also occurs in minor amounts in the Sapes and Lesvos occurrences. The Milos amethyst is accompanied by idiomorphic barite crystal reaching sizes of up to 10cm in length. Barite can also be found as inclusions in amethyst and chalcedony (Figure 2f), or postdates amethyst deposition. Its chemical composition is close to stoichiometry, with minor amounts of SrO (up to 3.41wt %), substituting for Ba in the structure.

Table 1 - Representative electron microprobe analyses of minerals that accompany amethyst.

	1	2	3	4	5	6	7	8	9	10	11	12
SiO_2	66.43	65.76	54.05	56.46	56.45	55.78	66.56	65.61	50.08	50.79	30.39	29.94
Al_2O_3	11.69	12.10	14.23	14.53	20.88	21.04	18.65	17.78	29.51	30.05	18.43	18.66
FeO	0.22	0.21	0.65	0.30	0.12	0.04	-	-	2.95	3.10	19.84	18.97
TiO_2	-	-	-	-	-	-	-	-	0.21	0.26	-	-
MgO	0.12	0.18	0.06	0.01	bd	bd	-	-	1.73	1.80	16.99	19.04
MnO	0.05	bd	bd	bd	bd	bd	-	-	0.08	Bd	0.42	0.46
CaO	3.82	4.01	0.91	0.80	0.03	0.11	bd	bd	0.04	0.13	0.37	0.43
Na_2O	0.71	0.82	0.66	0.87	11.45	11.35	0.32	0.21	0.59	0.46	0.66	0.70
K_2O	2.43	2.13	2.45	1.39	0.05	0.00	15.71	16.09	9.48	9.14	0.15	0.10
SrO	1.81	1.39	1.16	1.13	0.76	0.55	-	-	1.10	1.08	0.91	0.75
BaO	0.44	0.32	14.57	15.97	0.14	bd	0.69	0.57	0.02	Bd	-	-
Total	87.72	86.92	89.21	91.77	89.88	88.89	100.92	100.17	95.79	96.81	88.30	89.07
Si	29.61	29.43	27.00	27.36	33.60	33.48	3.00	3.00	6.68	6.66	6.16	6.02
Al	6.12	6.39	8.37	8.28	14.64	14.88	1.00	1.00	4.65	4.66	4.45	4.44
Fe	0.09	0.09	0.27	0.09	0.00	0.00	-	-	0.33	0.33	3.40	3.19
Ti	-	-	-	-	-	-	-	-	-	-	-	-
Mg	0.09	0.09	0.09	0.00	0.00	0.00	-	-	0.34	0.36	5.18	5.71
Mn	0.00	0.00	0.00	0.00	0.00	0.00	-	-	0.00	0.00	0.07	0.70
Ca	1.80	1.89	0.45	0.45	0.00	0.12	0.00	0.00	0.00	0.00	0.07	0.11
Na	0.63	0.72	0.63	0.81	13.2	13.20	0.02	0.03	0.17	0.11	0.25	0.28
K	1.35	1.17	1.53	0.90	0.00	0.00	0.92	0.95	1.62	1.54	0.03	0.04
Sr	0.45	0.36	0.36	0.36	0.24	0.24	-	-	0.08	0.08	0.11	0.05
Ba	0.09	0.10	2.88	3.06	0.00	0.00	0.01	0.01	0.00	0.00	-	-
1-2 clinoptilolite-Ca, 3-4 heulandite-Ba, 5-6 analcime, 7-8 adularia, 9-10 sericite, 11-13 chlorite, bd=below detection limit												

6. Discussion and Conclusions

Amethyst can be formed in a great variety of geological environments. In Greece, amethyst has been found in well-formed crystals within extensional alpinotype fissures in metamorphic core complexes, which are related to tectonic exhumation of the Rhodope- and Attico-Cycladic massifs (Voudouris et al., 2004). Excellent amethyst crystals are also found in the skarn of Serifos Island, where amethyst occur as sceptre on prase quartz crystals. However the above occurrences are of minor compared to the volcanic-rock hosted occurrences described in this study, which can be also considered as potential deposits for possible future exploitation.

The volcanic-hosted amethyst deposits described in the present study, are genetically related to the development of epithermal systems, during the waning stages of Oligocene to Pleistocene volcanic activity. In all studied occurrences the amethyst occurs distally, and is probably genetically related to the evolution of major Cu-Mo porphyry and associated high-sulfidation epithermal mineralization (Voudouris and Katerinopoulos, 2004). Mineralogical and geological information indicates that amethyst formation is late in respect to the above mineralization, and took place mainly from near neutral-pH to alkaline fluids and in the stability field of adularia, calcite and zeolites. The presence of sericite in some amethyst veins at Sapes, suggest slighty acid conditions during amethyst formation. All the studied amethyst occurrences are related to intermediate- to low-sulfidation epithermal veins with a well developed hydrothermal alteration zoning (e.g. silicic alteration grading outward to adularia and/or sericitic alteration, then to argillic-, propylitic-, zeolitic alteration and finally to fresh volcanic rock). Amethyst occurs in quartz veins crosscutting all the above alteration zones.

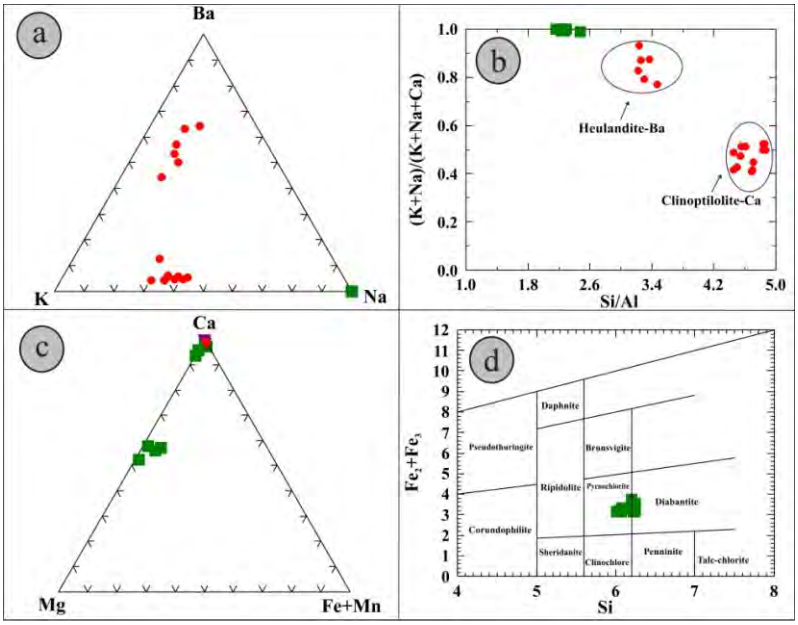

Figure 3 - (a) ternary Ba-K-Na plot of zeolites; (b) binary plot [(K+Na)/(Ca+Na+K)] versus (Si/Al) of zeolites (squares = analcime from Kirki area and circles = zeolites from Kornofolia area); (c) ternary Ca-Mg-Mn plot for calcites and dolomites from Kirki (triangles), Kornofolia (circles) and Lesvos island (squares); (d) binary Fe_{total}-Si classification diagram of chlorites from Lesvos amethyst deposit (after Hey, 1954).

The mineralogical data presented in this study as well as published fluid inclusion data were used to estimate the crystallizing conditions of the studied amethyst: In Kirki area the coexistence of laumontite, analcime, heulandite and smectite suggests maximum temperatures of 175ºC. Similar

temperatures of formation can be assumed through the coexistence of heulandite and clinoptilolite, accompanying amethyst in Kornofolia area. Temperatures in the range from 100-175ºC are compatible with the presence of chalcedony in the studied occurrences (Fournier, 1985). Application of the chlorite geothermometer after Cathelineau (1988) suggested temperatures of amethyst formation in the range 223-234 ºC. The Lesvos amethyst is intergrown with calcite-dolomite, barite (and locally fluorite and epidote) suggesting deposition from near neutral pH and SO_4^{2-} and F^- bearing solutions. In Milos island, fluid inclusion data from the Vani and Chondro Vouno occurrences by Kilias et al. (2001, 2007) and Naden et al. (2005) demonstrate temperatures in the range from about 100º to 230 ºC, boiling conditions, and involvement of seawater in addition to meteoric water for the amethyst deposition. A significant contribution of seawater during amethyst formation is also indicated by the presence of halite inclusion in the zeolites from the studied Kirki and Kornofolia occurrences. Fluid inclusion data for Sapes amethyst indicate homogenization temperatures in the range from 174 to 289 ºC and salinities from 0.5 to 3.5 wt. % NaCl equiv. demonstrating probable contribution of meteoric waters in their formation (Voudouris, 1993; Melfos, 2005). It is suggested that amethyst requires oxidizing conditions to obtain its colour, and this may be resulted by either mixing of oxidized meteoric and/or seawaters with upwelling hydrothermal fluids or boiling processes (Fournier, 1985). Both processes are considered to have caused amethyst formation in the studied areas as indicated by the mineralogical and existing fluid inclusion data. Boiling processes are responsible for the crystallization of amethyst together with adularia at Sapes and platy calcite at Kirki areas (according to Simmons and Browne, 2001). Shallow submarine conditions are most likely to have prevailed in all areas, Sapes being probably under subaerial conditions. The volcanic-hosted amethysts in Greece are of gemstone quality. Ongoing geological and gemmological work aims to evaluate their potential for future explotation.

7. Acknowledgments

Prof. Dr. Georgia Pe-Piper and Prof. Dr. E. Manoutsoglou are greatly acknowledged for their helpful and constructive comments, which improved the initial manuscript.

8. References

Alfieris D., Voudouris P. and Spry P.G. 2013. Shallow submarine epithermal Pb-Zn-Cu-Au-Ag-Te mineralization on western Milos Island, Aegean Volcanic Arc, Greece: Mineralogical, Geological and Geochemical constraints, *Ore Geol. Rev*., 53, 159-180.

Cathelineau M. 1988. Cation size occupancy in chlorites and illites as a function of temperature, *Clay Minerals*, 23, 471-485.

Christofides G., Soldatos T., Eleftheriadis G. and Koroneos A. 1998. Chemical and isotopic evidence for source contamination and crustal assimilation in the Hellenic Rhodope plutonic rocks, *Acta Vulcanol*., 10, 305-318.

Christofides G., Pecskay Z., Soldatos T., Eleftheriadis G. and Koroneos A. 2004. The Tertiary Evros volcanic rocks (Greece): Petrology, K/Ar geochronology and volcanism evolution. *Geol. Carp*., 55, 397-409.

Coombs D.S., Alberti A., Armbruster T., Artioli G., Colella C., Galli E., Grice J.D., Liebau F., Mandarino J.A., Minato H., Nickel E.H., Passaglia E., Peacor D.R., Quartieri S., Rinaldi R., Ross M., Sheppard R.A., Tillmanns E. and Vezzalini G. 1998. Recommended nomenclature for zeolite minerals: Report of the Subcommittee on Zeolites of the Mineralogical Association, Commision on New Minerals and Mineral Names, *Eur. J. Mineral.*, 10, 1037-1081.

Fournier R.O. 1985. The behaviour of silica in hydrothermal solutions. In Berger, B.R., and Bethke, P.M., eds., Geology and geochemistry of epithermal systems, *Rev. Econ. Geol.*, 2, 45-61.

Fytikas M., Innocenti F., Manneti P., Mazzuoli R., Peccerillo A. and Villari L. 1984. Tertiary to Quaternary evolution of volcanism in the Aegean region, in Dixon, J.E., and Robertson,

A.H.F., eds., The geological evolution of the eastern Mediterranean, *Geol. Soc. Spec. Publ.*, 17, 687-699.

Fytikas M., Innocenti F., Kolios N., Manneti P., Mazzuoli R., Poli G., Rita F. and Villari L. 1986. Volcanology and petrology of volcanic products from the island of Milos and neighbouring islets, *J. Volcanol. Geotherm. Res*., 28, 297–317.

Hey M.H. 1954. A new review of the chlorites, *Mineral. Mag*., 30, 277-292.

Innocenti F., Kolios N., Manetti O., Mazzuoli R., Peccerillo G., Rita F. and Villari L. 1984. Evolution and geodynamic significance of the Tertiary orogenic volcanism in northeastern Greece, *Bull. Volcanol*., 47, 25-37.

Jolivet L. and Brun J.P. 2010. Cenozoic geodynamic evolution of the Aegean region, *Int. J. Earth. Sci.*, 99, 109-138.

Kilias S.P., Naden J., Cheliotis I., Shepherd T.J., Constandinidou H., Crossing J. and Simos I. 2001. Epithermal gold mineralisation in the active Aegean volcanic arc: the Profitis Ilias deposit, Milos island, Greece, *Mineral. Deposita*, 36, 32-44.

Kilias S.P., Detsi K., Godelitsas A., Typas M., Naden J. and Marantos Y. 2007. Evidence of Mn-oxide biomineralization, Vani Mn deposit, Milos, Greece, *Proc. of the ninth Biennial SGA Meeting*, Dublin, 1069-1072.

Larsen A.O., Nordrum F.S., Döbelin N., Armbruster T., Petersen O.V. and Erambert M. 2005. Heulandite-Ba, a new zeolite species from Norway, *Eur. J. Mineral*., 17, 143-153.

Lieber W. 1994. *Amethyst: Geschichte, Eigenschaften, Fundorte*, Christian Weise Verlag, München, 188 pp.

Maneta V. and Voudouris P. 2010. Quartz megacrysts in Greece: Mineralogy and environment of formation, *Bull. Geol. Soc. Greece*, XLIII, 685-696.

Marchev P., Kaiser-Rohrmeier M., Heinrich Ch., Ovtcharova M., von Quadt A. and Raicheva R. 2005. Hydrothermal ore deposits related to post-orogenic extentional magmatism and core complex formation: the Rhodope Massif of Bulgaria and Greece, *Ore Geol. Rev*., 27, 53-89.

Melfos V. 2005. Study of fluid inclusions in amethysts from areas of Macedonia and Thrace: Sapes, Soufli, Nevrokopi, *2nd Congress of the Economic Geology Committee, Mineralogy & Petrology (GSG)*, Thessaloniki, October 2005, 219-228. (in Greek)

Naden J., Kilias S.P. and Darbyshire D.B.F. 2005. Active geothermal systems with entrained seawater as analogues for transitional continental magmato-hydrothermal and volcanic-hosted massive sulfide mineralization: the example of Milos Island, Greece, *Geology*, 33, 541-544.

Pe-Piper G. and Piper D.J.W. 2002. The Igneous rocks of Greece - The anatomy of an orogeny, Gebruder Borntraeger, 30, 573 pp.

Rykart R. 1995. Quarz-Monographie, Ott Verlag Thun, 461 pp.

Shawh A.J., and Constantinides D.C. 2001. The Sappes gold project, *Bull. Geol. Soc. Greece*. 34, 1073-1080.

Simmons S.F. and Browne P.R.L. 2001. Hydrothermal minerals and precious metals in the Broadlands-Ohaaki geothermal system: implications for understanding low-sulfidation epithermal environments, *Econ. Geol*., 95, 971-999.

Stewart A.L. and McPhie J. 2006. Facies architecture and Late Pliocene-Pleistocene evolution of a felsic volcanic island, Milos, Greece, *Bull. Volcanol*., 68, 703-726.

Voudouris P. 1993. Mineralogical, geochemical and fluid inclusion studies on epithermal vein type gold-silver mineralizations at Kassiteres/Sapes, (NE- Greece). PhD Thesis, Univ. Hamburg, 218 pp (in German).

Voudouris P. and Katerinopoulos A. 2004. New occurences of mineral megacrysts in Tertiary magmatic-hydrothermal and epithermal environments in Greece, *Documenta Naturae*, 151, 1-21.

Voudouris P., Katerinopoulos A. and Melfos V. 2004. Alpine-type fissure minerals in Greece, *Documenta Naturae* 151, 23-45.

Δελτίο της Ελληνικής Γεωλογικής Εταιρίας, τομ. XLVII , 2013
Πρακτικά 13ου Διεθνούς Συνεδρίου, Χανιά, Σεπτ. 2013

Bulletin of the Geological Society of Greece, vol. XLVII 2013
Proceedings of the 13th International Congress, Chania, Sept. 2013

A NEW OCCURRENCE OF PYROPHANITE FROM THE AMPHIBOLITE-HOSTED SKARN IN WESTERN KIMMERIA, XANTHI, NORTHERN GREECE

Voudouris P.[1], Xinou A.[2], Kanellopoulos C.[1], Kati M.[1], Mavrogonatos C.[1], and Lyberopoulos P[1].

[1,] National and Kapodistrian University of Athens, Faculty of Geology and Geoenvironment, Department of Mineralogy and Petrology, voudouris@geol.uoa.gr, ckanellopoulos@gmail.com, kmavrogon@geol.uoa.gr, *kati@geol.uoa.gr,*

[2] TITAN AE, Athens, xinouk@titan.gr

Abstract

A new occurrence of pyrophanite ($MnTiO_3$) in Greece is described from the garnet-clinopyroxene-wollastonite exoskarn of western Kimmeria. Hostrock of the pyrophanite-bearing skarn is amphibolite (retrogressed eclogites) of the Nestos suture zone in the Rhodope massif. In addition endo- and exo-skarns occur both in the Xanthi granodiorite and the surrouding marbles and consinst of diopside-vesuvianite-quartz and wollastonite-garnet-calcite-quartz respectively. Pyrophanite formed in the prograde stage, together with garnet, pyroxene, wollastonite, titanite, zircon, rutile, thorite and ouranothorianite. Retrograde minerals are quartz, epidote, calcite, hematite, and sulfides. Chlorite-geothermometry revealed temperatures in the range from 300 to 350 ^oC for the retrograde event. Calcic garnets (andradite-grossular solid solutions) from the prograde amphibolite-hosted skarn are chemically zoned with either isotropic or anisotropic cores surrounded by non-cubic anisotropic rims, thus suggesting chemical disequilibrium or disordering phenomena during crystal growth. The pyrophanite crystals are included in titanite and are accompanied by U-rich thorium minerals (uranothorianite, thorite) and by rutile. Electron microprobe analyses indicate that the studied pyrophanites are solid solutions between end-member pyrophanite and ilmenite, with isomorphous substitution of Mn^{2+} by Fe^{2+}. No Mg has been detected (geikielite end-member). The alteration of pyrophanite and rutile to titanite suggests an increase of fO_2 values of the fluids, probably due to increased incursion of meteoric waters to the system. The assemblage thorite, uranothorianite, pyrophanite and zircon indicates a magmatic contribution from the Xanthi granodiorite.

Key words: *pyrophanite, thorite – uranothorianite, skarn, Kimmeria, Rhodope.*

Περίληψη

Αμφιβολιτικό exoskarn στα δυτικά Κιμμέρια φιλοξενεί την δεύτερη εμφάνιση πυροφανίτη ($MnTiO_3$) στην Ελλάδα. Ο πυροφανίτης σχηματίστηκε στο πρόδρομο στάδιο μεταμόρφωσης μαζί με γρανάτες, πυρόξενους, βολλαστονίτη, τιτανίτη, ζιρκόνιο, θορίτη και ουρανιοθοριανίτη. Ανάδρομα ορυκτά είναι ο χαλαζίας, επίδοτο, ασβεστίτης, αιματίτης και σουφλίδια. Βάσει υπολογισμών με γεωθερμόμετρο χλωρίτη, οι θερμοκρασίες του ανάδρομου σταδίου υπολογίστηκαν περίπου στους 300-350 ^oC. Οι

ασβεστούχοι γρανάτες (στερεό διάλυμα ανδραδίτη-γροσσουλάριου) από το πρόδρομο στάδιο, παρουσιάζουν χημική ζώνωση με ισότροπους ή ανισότροπους πυρήνες, που περιβάλλονται από μη-κυβικές ανισότροπες περιφέρειες. Τα φαινόμενα αυτά υποδηλώνουν χημική ανισορροπία ή φαινόμενα αταξίας κατά την ανάπτυξη των κρυστάλλων. Οι κρύσταλλοι πυροφανίτη εγκλείονται εντός τιτανίτη και συνοδεύονται από ουρανιούχα ορυκτά του θορίου (ουρανιοθοριανίτης, θορίτης) και ρουτίλιο. Μικροαναλύσεις έδειξαν ότι οι πυροφανίτες είναι στερεό διάλυμα πυροφανίτη-ιλμενίτη, με ισόμορφη υποκατάσταση Mn^{2+} από Fe^{2+}. Η αντικατάσταση πυροφανίτη και ρουτίλου από τιτανίτη υποδηλώνει αύξηση των τιμών fO_2 στο διάλυμα, πιθανότατα λόγω συμμετοχής μετεωρικού νερού στο μαγματικό σύστημα. Η παραγένεση θορίτη, ουρανιοθοριανίτη ζιρκόνιου και πυροφανίτη είναι ενδεικτική μαγματικής συμμετοχής, από τον γρανοδιορίτη της Ξάνθης.
Λέξεις κλειδιά: *πυροφανίτης, θορίτης – ουρανοθοριανίτης, skarn, Κιμμέρια, Ροδόπη.*

1. Introduction

Pyrophanite with ideal formula $MnTiO_3$ is a relatively rare mineral and member of the ilmenite group (Zaccarini et al., 2004). It crystallizes in the trigonal system and is one end member of the rhombohedral phases in the quaternary system $FeTiO_3$-$MgTiO_3$-$MnTiO_3$-Fe_2O_3 (ilmenite-geikielite-pyrophanite-hematite). Pyrophanite as a manganese titanium oxide mineral is the Mn-rich analogue of ilmenite. Pyrophanite crystals occur as subhedral aggregates or microscopic grains. They are black, opaque, and have metallic luster. Pyrophanite was originally described by Hamberg (1890) who first found the mineral in drusy cavities of manganese ore at the Harstig mine, Pajsberg, Sweden. The associated minerals are garnet, ganophyllite, and calcite. Until 1940, only other two occurrences of pyrophanite were known, in Brazil and Wales. Pyrophanite can be present in a wide range of environments ranging from gneisses, granitic rocks, alkaline complexes and karbonatites, to serpentinite and even in meteorites. It can be also associated with epithermal and hydrothermal manganese deposits, metamorphic deposits rich in zinc and manganese and occasionally with banded iron formations (BIF) (Zaccarini et al., 2004). In Greece, pyrophanite has been described for the first time from Mn-bearing metasedimentary rocks in Ikaria Island (Iliopoulos, 2005).

Amphibolites (retrogressed eclogites) within the Nestos Suture Zone (Krenn et al. 2008) of the Rhodope metamorphic complex (western Kimmeria), host a garnet-clinopyroxene-wollastonite exoskarn. The mineralogical study of the exoskarn revealed a complex mineralogical composition and among the other minerals, the occurrence of pyrophanite ($MnTiO_3$). The mineralization contains U-rich thorium minerals (uranothorianite, thorite) and calcic garnets (andradite-grossular solid solution). The aim of the present paper is to study the mineralogy and mineral chemistry of the garnet-clinopyroxene-wollastonite exoskarn of western Kimmeria, highlighting the second occurrence of pyrophanite in Greece.

2. Regional Geological Setting

The Hellenides, part of the Alpine-Himalayan orogen, can be considered an accretionary orogen, where a late Precambrian to late Jurassic evolution was marked by the opening and closure of ocean basins and continental crust formation in the accompanying subduction zones (Papanikolaou 1984; Reischmann and Kostopoulos, 2007). A Permo-Carboniferous igneous event (known from the Pelagonian Zone, the Rhodope Massif and the Attico-Cycladic Zone) documents an active continental margin evolution in the Precambrian-Silurian basement of the Hellenides (Reischmann and Kostopoulos, 2007). After the closure of the Vardar Ocean, shortening and syn-orogenic exhumation of HP-LT rocks occurred during the late Cretaceous-Eocene, before an acceleration of slab retreat changed the subduction regime and caused the collapse of the Hellenic mountain belt

and the thinning of the Aegean Sea from the middle Eocene/late Oligocene to the present (Jolivet et al. 2010). During this post-orogenic episode large-scale detachments formed, which exhumed metamorphic core complexes, in a back-arc setting (Cyclades and Rhodope) (Gautier and Brun, 1994). Turpaud and Reischmann (2010) subdivided the central Rhodope Massif into the upper Thracia Terrane, dominated by Permo-Carboniferous orthogneisses and Triassic marbles, and the lower Rhodope Terrane, consisting of Late Jurassic orthogneisses. These two terranes can be interpreted as lower and upper continental plates, which were tectonically superimposed during Alpine N-S directed continent-continent collision and subsequent SW directed nappe stacking (Ricou et al. 1998; Krenn et al. 2010). The two terranes are separated by the Nestos Suture Zone, which is well exposed north of the SW-directed thrust fault (Nestos thrust, Papanikolaou and Panagopoulos 1981; Barr et al. 1999). The rocks within the suture zone experienced HP to UHP metamorphism with subsequent high-grade amphibolite-facies overprint, as recorded in metasediments and mafic rocks (Mposkos annd Kostopoulos, 2001; Liati and Seidel, 1996; Mposkos and Krohe, 2006). Recent studies on metamorphic zircons from the suture zone give ages of 171 Ma related to a post-eclogite facies metamorphic stage and an age of 79 Ma attributed to amphibolite-facies metamorphism (Bauer et al. 2007). The eclogite-facies metamorphic event took place at 19 kbar and 700 °C (Liati and Mposkos, 1990), and was followed by granulite facies- (P>15 kbar, T>800 °C) and amphibolite-facies overprint (8-11 kbar and 580-690 °C) as recorded from relict kyanite-eclogites (Liati and Seidel, 1996). Ultramafic rocks occur a boudins associated with amphibolites (Barr et al., 1999). In the Rhodope Massif (Bulgaria and Greece), late Cretaceous-Tertiary exhumation of deep metamorphic rocks along detachment faults, resulted in the formation of metamorphic core complexes, supra-detachment sedimentary basins, and widespread Late Eocene to Early Miocene basic to felsic magmatism (Marchev et al., 2005).

3. Local Geological Setting

The Oligocene age, I-type, Xanthi plutonite (Del Moro et al., 1988) penetrates marbles, gneisses and amphibolites of both the Thracia and Rhodope terranes, as well as of the Nestos Suture Zone. Its petrological composition varies significantly, but the most common petrographic types are granodiorite, monzonite and in smaller percentage gabbroic rocks (Sergi, 1997). The Xanthi plutonite is also characterized by many aplitic and pegmatitic veins that crosscut the igneous body in various locations. The granodioritic bodies consist of quartz, feldspars, hornblende and biotite with minor epidote, apatite, zircon and magnetite. The monzonite contains feldspars, quartz, biotite and pyroxene, while gabbros are characterized by plagioclase, pyroxenes and some olivine.

A thermo-metamorphic halo of considerable thickness is present around the contact of Xanthi plutonite and the surrounding rocks (e.g. marbles, gneisses and amphibolites). Estimated maximum P-T conditions are about 750 °C and 3 kb (Liati, 1986; Georgiadis et al. 2012). The studied skarn outcrop occurs about 3 km NW of the Kimmeria village and is hosted within amphibolites (and marbles) of the Nestos Suture Zone (Figure 1). Both prograde and retrograde minerals are present and include calc-silicate minerals (e.g. garnet, epidote, wollastonite, diopside, actinolite, scapolite), sulfides (e.g. chalcopyrfigite, pyrite), oxides (e.g. magnetite, hematite, scheelite), as well as secondary phases like azurite, malachite and limonite.

4. Materials and Methods

Fourty-five thin and polished sections of skarn samples and the host rock were studied ny optical and a Jeol JSM 5600 scanning electron microscope, equipped with back-scattered imaging facilities, at the Department of Geology and Geoenvironment, University of Athens. The operating conditions were as follows: accelerating voltage 20 kV, beam current 0.5 nA, time of measurement 50 sec and beam diameter <2 μm. The spectra were processed using the ZAF program (3 interactions). The microprobe analyses were conducted on polished sections of the samples after carbon coating.

Figure 1 - (a) Wollastonitic-garnetitic skarn developed in amphibolites (and marbles) in the vicinity of the granodiorite. (b) Hand specimen of amphibolite-hosted skarn with euhedral crystals of green garnet and quartz.

5. Analytical Data

5.1. Mineralogy and Mineral Chemistry

Garnet group minerals are major constituents of the amphibolite-hosted wollastonitic skarn of Kimmeria. Garnets occur in idiomorphic light green-yellowish to emerald-colored rhombic dodecahedral crystals (Figure 1b). Initial deposition of garnet with wollastonite, clinopyroxene, titanite, pyrophanite and thorium-bearing phases during the prograde stage, was followed by the deposition of a retrograde assemblage consisting of quartz, epidote, chlorite and calcite (Figure 2). The garnets are chemically zoned with individual zones ranging in composition between andradite and grossular (Table 1; Figures 1a,b; 3a). Mn (up to 0.4 apfu) substitutes for Mg and Fe in the structure. Isotropic domains in the cores of the crystals and non-cubic anisotropic rims and vice-versa are common features.

Clinopyroxene and **wollastonite** accompany garnets in the prograde skarn assemblage (Figure 2a, d-f). Representative microanalyses of clinopyroxene are presented in Table 1 and ploted in Figure 3b. The analyzed clinopyroxenes are solid solutions between diopside-hedenbergite (Figure 3b).

Epidote group mineral in euhedral crystals, reaching length of up to 10cm, with dark green color and intense lustre, is a common constituent in the Kimmeria skarn. Epidote is a retrograde mineral postdating wollastonite and garnet and clinopyroxene and is associated with other retrograde phases as quartz, actinolite and calcite (Figure 2e). The REE-bearing allanite contains up to 7.63 wt. % La_2O_3 and up to 12.5 wt. % Ce_2O_3. Representative microanalyses of allanite are presented in Table 1.

Chlorite in characteristic radiating aggregates with intense green color replaces garnet (Figure 2b). Representative microanalyses are presented in Table 1 and the data are ploted in Figure 3c. The Kimmeria chlorites are classified as Fe-clinochlores (Figure 3c). In order to obtain crystallization temperatures of the studied chlorites we applied the geothermometer of Cathelinau (1988), which correlates temperature with chlorite chemical composition based on the relationship T (°C) = -61.92 + 321.98 (Al^{IV}). According to this geothermometer the formation temperatures of studied chlorites range from 292° to 340 °C.

Chromite occurs is contact to uranothorianite as small euhedral crystals included in garnets (Figure 2c).

Chalcopyrite accompanies pyrophanite, rutile being part of the prograde mineral assemblage (Figure 2f).

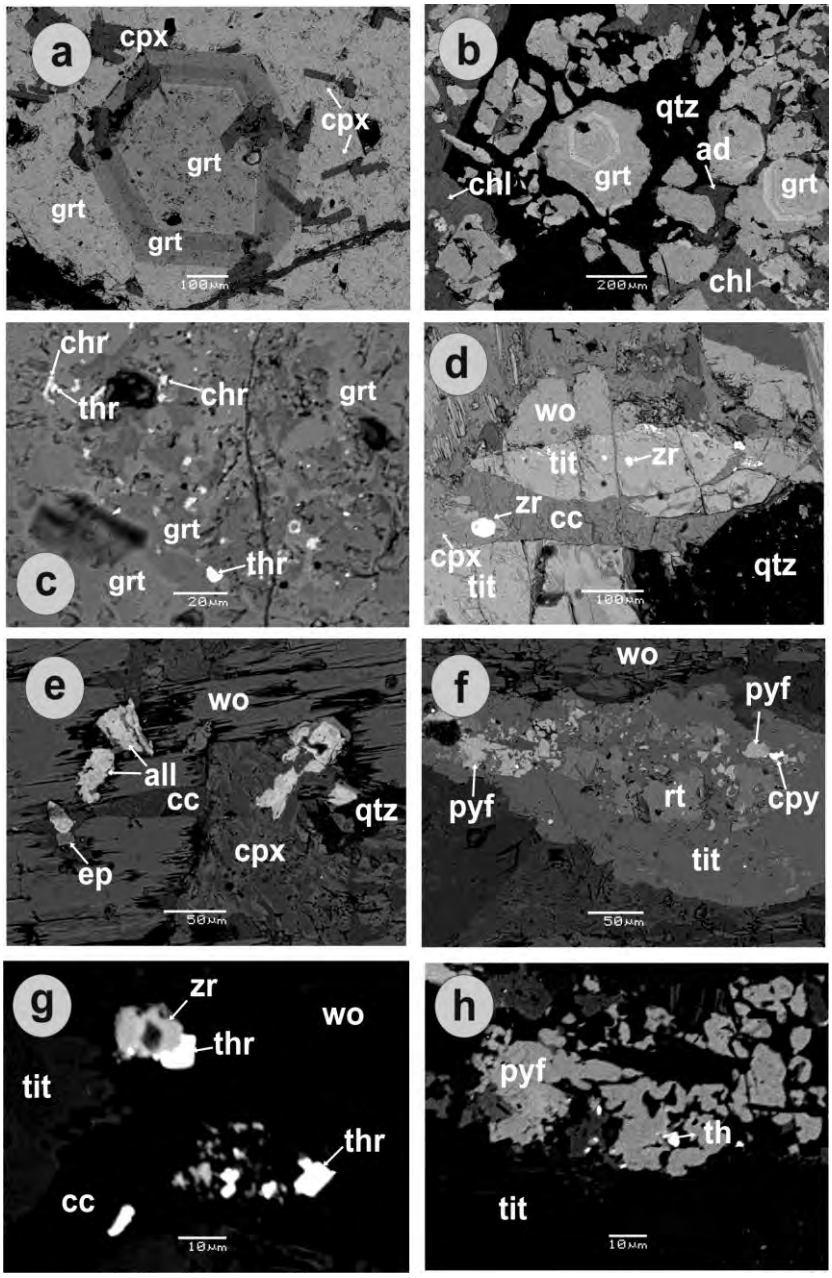

Figure 2 - Microphotographs demonstrating mineralogical assemblages of the Kimmeria skarn (SEM-BSE images). (a) Idiomorphic zoned garnet crystal (gnt) intergrown with clinopyroxene (cpx). (b) Garnets (gnt) replaced by retrograde quartz (qtz), chlorite (chl) and adularia (ad). (c) Chromite (chr) and uranothorianite (thr) included in garnet (gnt). (d) Titanite (tit) including zircon (zr) replaced by calcite (cc). Wollastonite (wo) and clinopyroxene (cpx) are also present. (e) Allanite (all), epidote (ep), quartz (qtz) and calcite (cc) postdate wollastonite (wo) and clinopyroxene (cpx). (f) Titanite (tit) crystal with inclusions of pyrophanite

(pyf), rutile (rt) and chalcopyrite (cpy) replacing wollastonite (wo). (g) Uranothorianite (thr) and zircon (zr) associated with calcite (cc) and titanite (tit) postdating wollastonite (wo). (h) Enlargement of Figure 2f (left part): pyrophanite (pyf) and thorite (th) included in titanite (tit).

Titanite in idomorphic crystals up to 300 μm in length is intergrown with garnets and includes pyrophanite and rutile (Figure 2d).

Scheelite, hematite, scapolite and **adularia**, the hydrothermal variety of K-feldspar (Dimitriadis and Soldatos, 1978; Figure 2b), are additional retrograde minerals of the Kimmeria skarn (Skarpelis and Liati 1991).

Table 1. Representative microanalyses of garnet (1-3), chlorite (4-6), pyroxene (7-8) and REE-bearing epidote (9-10).

Wt%	1	2	3
SiO_2	39.77	37.73	36.95
TiO_2	0.03	2.86	3.22
Al_2O_3	20.21	6.02	9.09
FeO	3.68	19.28	14.56
Cr_2O_3	0.05	0.73	0.33
MnO	1.15	0.10	0.07
MgO	bd	0.23	0.51
CaO	34.55	33.59	34.06
Na_2O	bd	0.26	0.16
Total	99.43	100.80	98.95
	24(O)	24(O)	24(O)
Si	3.039	3.001	2.952
Ti	0.002	0.171	0.194
Al^{IV}	-	-	0.048
Al^{VI}	1.819	0.564	0.807
Fe^{3+}	0.092	1.085	0.855
Cr	0.003	0.046	0.021
Fe^{2+}	0.143	0.197	0.118
Mg	-	0.027	0.061
Mn	0.074	0.007	0.005
Ca	2.828	2.862	2.915
Na	0.000	0.040	0.025
Alm	-	-	-
And	4.79	64.00	49.37
Gross	92.47	31.95	46.91
Pyr	0.00	1.07	2.34
Spes	2.59	0.27	0.18
Uva	0.15	2.71	1.20

Wt%	4	5	6
SiO_2	28.42	27.31	23.81
TiO_2	0.04	0.03	0.01
Al_2O_3	18.69	19.66	18.32
FeO	21.57	25.84	33.49
Cr_2O_3	0.12	bd	0.22
MnO	1.43	1.25	1.63
MgO	17.95	14.77	7.42
CaO	0.03	0.16	0.19
Na_2O	bd	0.01	bd
K_2O	0.02	bd	0.14
Total	88.27	89.03	85.23
	28(O)	28(O)	28(O)
Si	5.845	5.694	5.508
Ti	0.006	0.005	0.002
Al^{IV}	2.155	2.306	2.492
Al^{VI}	2.372	2.521	2.499
Cr	0.019	-	0.040
Fe^{2+}	3.710	4.506	6.479
Mn	0.249	0.221	0.319
Mg	5.503	4.591	2.559
Ca	0.007	0.036	0.047
Na	-	0.004	-
K	0.005	-	0.041
T (°C)	285	309	339

Wt%	7	8
SiO_2	52.35	50.45
TiO_2	bd	0.00
$Al2O_3$	bd	0.57
FeO	8.44	13.10
Fe_2O_3	bd	bd
Cr_2O_3	0.29	0.31
MnO	7.33	bd
MgO	7.52	13.10
CaO	23.20	21.77
Na_2O	0.29	bd
Total	99.42	99.29
	6(O)	6(O)
Si	2.044	2.031
Al^{IV}	-	-
Ti	-	-
Al^{VI}	-	0.027
Fe^3	-	-
Cr	0.009	0.010
Fe^{2+}	0.276	0.151
Mn	0.243	0.056
Mg	0.437	0.786
Ca	0.970	0.939
Na	0.022	-
K	-	-
Wo	50.38	48.61
En	22.72	40.69
Fs	26.90	10.70

Wt%	9	10
SiO_2	34.08	33.76
TiO_2	0.41	0.11
Al_2O_3	12.93	13.51
Fe_2O_3	15.65	14.58
Cr_2O_3	4.19	4.92
MnO	0.64	0.24
MgO	0.24	0.31
CaO	13.32	13.94
La_2O_3	7.02	7.63
Ce_2O_3	9.86	9.05
Total	98.34	98.05
	12.5(O)	12.5(O)
Si	3.145	3.118
Al	1.405	1.469
Fe^{3+}	1.086	1.012
Mg	0.033	0.043
Ca	1.317	1.379
La	0.239	0.260
Ce	0.333	0.306
Cr	0.141	0.166
Mn	0.021	0.008
Ti	0.013	0.004

Table 2. Representative microanalyses of pyrophanite (1-4), uranothorianite (5), and thorite (6,7). bd: below detection; (-) not analyzed.

wt%	1	2	3	4	5	6	7
SiO_2	-	-	-	-	0.36	16.09	16.35
Al_2O_3	-	-	-	-	bd	bd	bd
FeO	11.53	14.58	9.6	10.12	0.14	0.2	-
CaO	0.54	0.74	0.66	0.61	0.75	1.33	0.66
TiO_2	52.12	54.12	52.89	53.1	-	-	-
MnO	33.95	30.52	36.44	35.7	-	-	-
MgO	bd	bd	0.25	bd	-	-	-

Cr_2O_3	-	-	-	-	bd	bd	bd
ThO_2	-	-	-	-	76.52	75.32	77.94
UO_3	-	-	-	-	23.11	7.97	5.25
Total	98.14	99.96	99.84	99.53	100.88	100.91	100.2

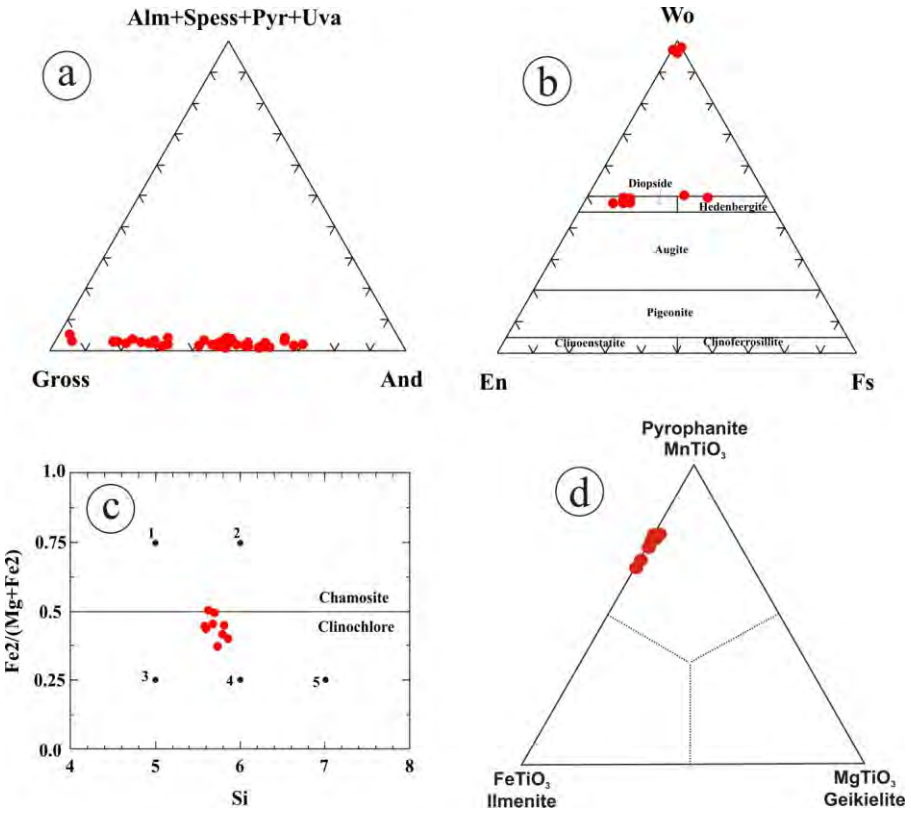

Figure 3 - (a) Ternary Gross-(Alm+Spess+Pyr+Uva)-And diagram demonstrating composition of garnet group minerals; (b) Plot of clinopyroxenes in the ternary Wo-En-Fs diagram; (c) Classification of chlorite in the binary (Fe^{2+}+Fe^{3+}) vs Si diagram after Mc Leod and Stanton (1984) (1: Mg-Al chamisite; 2: Mg-chamosite; 3: Fe-Al-clinochlore; 4: Fe-clinochlore; 5: Fe-Si-clinochlore); (d) Compositions of pyrophanite from the Kimmeria skarn plotted in the $MnTiO_3$-$FeTiO_3$-$MgTiO_3$ diagram.

Pyrophanite forms hypidiomorphic crystals with size of up to 60μm and is usually enclosed in garnet or titanite crystals (Figure 2f,h). Representative microanalyses are presented in Table 2. The analyzed pyrophanites contain 52.1-54.1 wt.% TiO_2, 9.6-14.6 wt.% FeO, 30.5-36.4 wt% MnO with minor CaO content (0.5-0.7 wt%) and are characterized as solid solution between pyrophanite-ilmenite (Figure 3d).

Zircon is included in titanite, wollastonite and garnets, forming isolated grains and/or intergrown with uranothorianite (Figure 2c, d, g).

Thorite with formula (Th,U)SiO_4, is an accesory mineral in the Kimmeria skarn, that crystallizes in the tetragonal system. It is the most common mineral of thorium and is nearly always strongly radioactive. In the Kimmeria skarn, thorite occurs as microscopic inclusions in titanite crystals (Figure 2E). Representative microanalyses are presented in Table 2 indicating that thorite contain 75.3-77.9 wt. % ThO_2, 5.2-7.9 wt.% UO_3 and minor CaO (up to 1.3 wt.%).

Uranothorianite with formula $(Th,U)O_2$ is a thorium oxide mineral, which crystallizes in the cubic system. Uranium and REE substiture for Th in the structure. In the Kimmeria skarn the uranothorianite occurs as microscopic inclusions in garnet and titanite crystals, associated with zircon (Figure 2g). A single microanalyses is presented in Table 2. The analyzed uranothorianite contain 76.5 wt. % ThO_2 and 0.75 wt. % CaO and 23.1 wt. % UO_3 substituting for Th.

6. Discussion and Conclusions

Using the orthopyroxene-clinopyroxene- and the plagioclase-amphibole geothermometers, Liati (1986) estimated temperatures during the prograde skarn evolution of Kimmeria at about 725° to 750 °C. The retrograde evolution took place at much lower temperatures (at about 300-350 °C), as indicated by the chlorite geothermometry (this study) and resulted in the deposition of quartz, sheelite, epidote, allanite, calcite, hematite and sulfides. Among the prograde skarn minerals of Kimmeria (e.g. garnet, pyroxene, wollastonite, titanite), pyrophanite is a rarity, accompanying U-bearing thorium minerals, as well as rutile and chromite.

Garnets have either anisotropic cores and isotropic periphery or the opposite, suggesting changes either in mineral chemistry or in crystallization conditions. Optical anisotropy in garnets is common in Ca-rich garnets elsewhere, especially those related to contact metamorphism and hydrothermal metasomatism. According to Allen and Buseck (1988), several hypotheses have been proposed for optical anisotropy, but none of them is totally acceptable. These hypotheses include plastic deformation and crystal lattice deformation (Lessing and Standish, 1973; Kitamura and Komatsu, 1978). Other researchers suggest that anisotropic areas in garnets may be attributed to the existence of Al and Fe^{3+} in octahedral sites (Takouchi et al., 1982) or the presence of OH in cubic coordination (Rossman and Aines, 1986).

In the Kimmeria skarn, pyrophanite occurs as a minor constituent included in garnet and titanite accompanying U-bearing thorium minerals (uranothorianite, thorite) and rutile. This suggests that pyrophanite forms part of the prograde assemblage of Kimmeria skarn. In the studied pyrophanites, a substitution of Mn^{2+} by Fe^{2+} was observed, corresponding to a significant ilmenite component (about 20-30%). The Mn, which is necessary for the formation of pyrophanite, is probably of magmatic origin and/or may have been derived from the amphibolite host-rocks. The alteration of pyrophanite and rutile to titanite (hematite and chalcopyrite) indicates a trend towards more oxidizing conditions, since pyrophanite similarly to ilmenite mostly occurs in reducing assemblages (Nayak and Mohapatra, 1998; Iliopoulos 2005) and titanite is indicative for more oxidizing conditions (e.g. Xyrouchakis and Lindslay, 1998; Broska et al., 2007). Moderate fO_2-fS_2 conditions have been also suggested by Skarpelis and Liati (1991) based on the coexistence of chalcopyrite-bornite-wollastonite-andradite in the prograde skarn paragenesis at Kimmeria. Increasing values of fO_2 in the fluid, probably due to increasing participation of meteoric water in the retrograde skarn evolution at Kimmeria skarn, may have caused deposition of hematite and major introduction of sulfides, in common to other skarn ores elsewhere (Meinert et al., 2005). The presence of thorium-bearing minerals (e.g. uranothorianite and thorite) and zircon accompanying pyrophanite are indicative of a magmatic contribution. Thorite and uranothorianite from the Kimmeria skarn contain significant amounts of UO_3 (up to 23 wt. %) substituting for thorium in the structure. This study verifies previous work by Karavassili et al. (2005) who measured high radioactivity values in fresh monzodiorites of Kimmeria and related them to the presence of thorium minerals in the granitoid body.

7. Acknowledgments

An anonymous reviewer and Prof. Dr. E. Manoutsoglou are greatly acknowledged for their helpful and constructive comments, which improved the initial manuscript.

8. References

Allen F. and Buseck P. 1988. XRD, FTIR, and TEM studies of optically anisotropic grossular garnets, *Am. Mineral*., 73, 568-584.

Barr S.R., Temperley S. and Tarney J. 1999. Lateral growth of the continental crust through deep level subduction-accretion: a reevaluation of central Greek Rhodope, *Lithos*, 46, 69–94.

Bauer C., Rubatto D., Krenn K., Proyer A. and Hoinkes G. 2007. A zircon study from the Rhodope metamorphic complex, N-Greece: Time record of a multistage evolution, *Lithos* 99, 207-228.

Broska I., Harlov D., Tropper P. and Siman P. 2007. Formation of magmatic titanite and titanite–ilmenite phase relations during granite alteration in the Tribec Mountains, Western Carpathians, Slovakia, *Lithos*, 95, 58-71.

Cathlelineau M. 1988. Cation size occupancy in chlorites and illites as a function of temperature, *Clay Minerals*, 23, 471-485.

Del Moro A., Innocenti F., Kyriakopoulos C., Manetti P. and Papadopoulos P. 1988. Tertiary granitoids from Thrace (Northern Greece): Sr isotopic and petrochemical data, *N. Jb. Mineral. Abh.* 159, 113-135.

Dimitriadis S. and Soldatos K. 1978. Optical and structural properties of adularia from Xanthi and Ouranoupolis, Greece, and their interpretation, *N. Jb. Miner. Abh.*, 133, 88-105.

Gautier P. and Brun J.P. 1994. Ductile crust exhumation and extensional detachments in the central Aegean (Cyclades and Evia Islands), *Geod. Acta* 7, 57-85.

Georgiadis I.K., Tzamos E., Kantiranis N., Papadopoulou L., Tsirambidis A. and Filippidis A. 2012. On the mineralogy of the wollastonite from Xanthi-Kimmeria (Thrace, Greece), *Soldatos Special Vol*., Aristotle Univ. Thessaloniki, 101, 17-21.

Hamberg A. 1890. Uber die Manganophylle von der Grube Harstigen bei Pajsberg in Vermland, *Geol. For. Forh*., Stockholm, 133, 567-579.

Iliopoulos I. 2005. Petrogenesis of metamorphic rocks at Ikaria island, *Unpub. Ph.D. thesis*, Univ. Patras, 592 pp (in Greek).

Jolivet L. and Brun J.P. 2010 Cenozoic geodynamic evolution of the Aegean region, *Int. J. Earth. Sci*., 99, 109-138.

Karavasili E., Christofides G., Papastefanou C., Koroneos A. and Stoulos S. 2005. Mineralogy, Petrography and Radioactivity of Greek Granites, *Proceedings of the 2nd Congress of the Committee of the Econ. Geol., Mineral. & Geochem. of the Geol. Soc. Greece*, Thessaloniki, 123-132.

Kitamura K., and Komatsu H. 1978. Optical anisotropy Associated with growth striation of yttrium garnet, *Kristallographie and Technik*, 3, 811-816.

Krenn K., Bauer C., Proyer A., Mposkos E., Hoinkes G. 2008. Fluid entrapment and reequilibration during subduction and exhumation: A case study from the high-grade Nestos shear zone, Central Rhodope, Greece, *Lithos*, 104, 33–53.

Lessing P. and Standish R.P. 1973. Zoned garnet from Crested Butte, Colorado, *Am. Mineral*., 58, 840-842.

Liati A. 1986. Regional metamorphism and overprinting contact metamorphism of the Rhodope zone, near Xanthi (N. Greece). Petrology, Geochemistry, Geochronology: *Unpub. Ph.D. thesis*, Univ. Braunschweig, 186 pp.

Liati A. and Seidel E. 1996. Metamorphic evolution and geochemistry of kyanite-eclogites in central Rhodope, northern Greece, *Contrib. Mineral. Petrol*. 123, 293-307.

Marchev P. Kaiser-Rohrmeier, M.; Heinrich, Ch.; Ovtcharova, M.; von Quadt, A.; Raicheva, R. 2005. Hydrothermal ore deposits related to post-orogenic extentional magmatism and core complex formation: the Rhodope Massif of Bulgaria and Greece, *Ore Geol. Rev*., 27, 53-89

Mc Leod R.L. and Stanton R.L. 1984. Phyllosilicates and associated minerals in some Paleozoic stratiform sulfide deposits of southern Australia, *Econ. Geol*. 79, 1-22.

Meinert L.D., Dipple G.M. and Nicolescu S. 2005. World skarn deposits, *Econ. Geol*., 100, 299-336.

Morimoto N., Fabries J., Ferguson A.K., Ginzburg I.V., Ross M., Seifert F.A., Zussman J., Aoki K. and Gottardi G. 1988. Nomenclature of pyroxenes, *Am. Mineral.,* 73, 1123-1133

Mposkos E.D. and Kostopoulos D.K. 2001. Diamond, former coesite and supersilicic garnet in metasedimentary rocks from the Greek Rhodope: a new ultrahigh-pressure metamorphic province established, *Earth Plan. Sci. Lett*., 192, 497–506.

Mposkos E. and Krohe A. 2006. Pressure-temperature-deformation paths of closely associated ultra-high-pressure (diamond-bearing) crustal and mantle rocks of the Kimi complex: implications for the tectonic history of the Rhodope Mountains, northern Greece, *Can. J. Earth Sci*., 43, 1755-1776.

Nayak B.R. and Mohapatra B.K. 1998. Two morphologies of pyrophanite in Mn-rich assemblages, Gangpur Group, India, *Mineral. Mag.* 62, 847-856.

Papanikolaou D. 1984. The three metamorphic belts of the Hellenides: A review and a kinematic interpretation, *Spec. Publ. Geol. Soc. London*, 17, 551-561.

Papanikolaou D. and Panagopoulos A. 1981. On the structural style of southern Rhodope, *Geol. Balcan*., 11, 13-22.

Rossman G.R. and Aines R.D. 1986. Spectroscopy of a birefringent grossular frorn Asbestos, Quebec, Canada, *Am. Mineral*., 71, 779-780.

Reischmann T. and Kostopoulos D. 2007. Terrane accretion in the internal Hellenides, *Geoph. Res. Abstracts*, Vol. 9.

Ricou L.-E., Burg J.P., Godfriaux I. and Ivanov Z. 1998. Rhodope and Vardar: the metamorphic and the olistostromic paired belts related to the Cretaceous subduction under Europe, *Geod. Acta* 11, 285-309.

Sergi A. 1997. Mafic microgranular enclaves from the Xanthi pluton (Northern Greece): An example of mafic-felsic magma interaction, *Mineral. Petrol*, 61, 97-117.

Skarpelis N. and Liati A. 1991. Wollastonite and associated copper mineralization in the contact metamorphic aureole fo Kimmeria, Xanthi, N. Greece, *Bull. Geol. Soc. Greece*, 25/2, 369-377.

Takouchi Y., Haga N, Umizu S., and Sato G. 1982. The derivative structure ofsilicate garnets in grandite, *Zeitschrift Kristallographie*, 158, 53-99.

Turpaud P. and Reischmann T. 2010. Characterisation of igneous terranes by zircon dating: implications for UHP occurrences and suture identification in the Central Rhodope, northern Greece, *Int. J. Earth Sci*., 99, 567–591.

Zaccarini F., Garuti G., Ortiz-Suarez A. and Carugno-Duran A., 2004. The paragenesis of pyrophanite from Sierra de Comechingones, Córdoba, Argentina, *Can. Mineral*. 42, 155-168.

Xyrouchakis D. and Lindsley D.H. 1998. Equilibria among titanite, hedenbergite, fayalit, quartz, ilmenite, and magnetite: Experiments and internally consistent thermodynamic data for titanite, *Am. Mineral*., 83, 712-725.